Cen - H01764 - 41 - P024464

UCM

AJR

41

American Journal of Roentgenology

September 1992

Leading medical imaging technology into the next generation

We're not waiting for the future of medical imaging, we're creating it. So far, we like what we see. Laser-fast networks that set new standards for performance, productivity and patient care. Advanced electronics that make next generation systems more reliable and more powerful than ever. And brilliant color output that lets you see images in a whole new light.

This innovative new world of medical imaging isn't far away. And getting there is easy. All you have to do is follow the leader. 3M.

3M Medical Imaging Systems Division, Building 223-2S-03, St. Paul, MN 55144-1000. 1-800-328-1684, Ext. 340. 3M Canada Inc., P.O. Box 5757 Terminal A, London, Ontario, Canada N6A 4T1.

Innovation working for you™

3M

Official Journal of the American Roentgen Ray Society

AJR

American Journal of Roentgenology
Diagnostic Imaging and Related Sciences

Editor-In-Chief Robert N. Berk, *La Jolla, California*
University of California, San Diego
School of Medicine and Medical Center

Editor Emeritus Melvin M. Figley, *Seattle, Washington*

P 24,464

Associate Editor Karim Valji, *San Diego, California*

Consulting Editors A. James Barkovich, *San Francisco, California*
Edward A. Sickles, *San Francisco, California*

Statistician Charles C. Berry, *San Diego, California*

Editorial Board

Mark E. Baker
Lawrence W. Bassett
Michael A. Bettmann
Ethan M. Braunstein
Felix S. Chew
Horacio R. D'Agostino
Gerald D. Dodd III
N. Reed Dunnick
David K. Edwards
Allen D. Elster
Ronald G. Evens
Sandra K. Fernbach
Richard H. Gold
Edward G. Grant
John R. Hesselink
Emanuel Kanal
Ray F. Kilcoyne
Carolyn Kimme-Smith
Melvyn T. Korobkin
Mark J. Kransdorf
Faye C. Laing
Thomas L. Lawson
Robert G. Levitt
Martin J. Lipton
Bruce L. McClennan
Richard P. Moser
Jeffrey H. Newhouse
Sven J. K. Paulin
David M. Paushter
Vassilios Raptopoulos
Donald L. Resnick
Charles A. Rohrmann, Jr.
Peter M. Ronai
Stuart S. Sagel
Sanjay Saini
Stefan C. Schatzki
William P. Shuman
Barry A. Siegel
M. Leon Skolnick
Edward T. Stewart
Murali Sundaram
Ruedi F.-L. Thoeni
Robert D. Tien

Director of Publications: Susan Brown Cappitelli **Editorial Staff:** Barbara Rose, *managing editor*; Katie L. Spiller, Barbara L. Halliburton, and Janine Anderson, *manuscript editors*; Nancy Rydbeck, *office manager*; Sheri Smith, *administrative assistant*; Linda J. Waggoner, *administrative secretary*

AJR, AMERICAN JOURNAL OF ROENTGENOLOGY (ISSN 0361 803X) is published monthly by the American Roentgen Ray Society, 1891 Preston White Dr., Reston, VA 22091. Annual dues include $50 for journal subscription. Second-class postage paid at Baltimore, MD, and at additional mailing offices. **POSTMASTER**, send address changes (Form 3579) to Subscription Fulfillment, AJR, 428 E. Preston St., Baltimore, MD 21202. Subscription rates $125 ($180 foreign); institutions $135 ($190 foreign); in training $25 ($80 foreign); single copy $18 ($22 foreign). The GST number for Canadian subscribers is 123394371. Airmail rates furnished on request. Indexed by *Current Contents* and *Index Medicus*. Copyright © 1992 by American Roentgen Ray Society.

0361–803X/92$3.00

THE *OMNI*℠ REIMBURSEMEN

CLEARIN

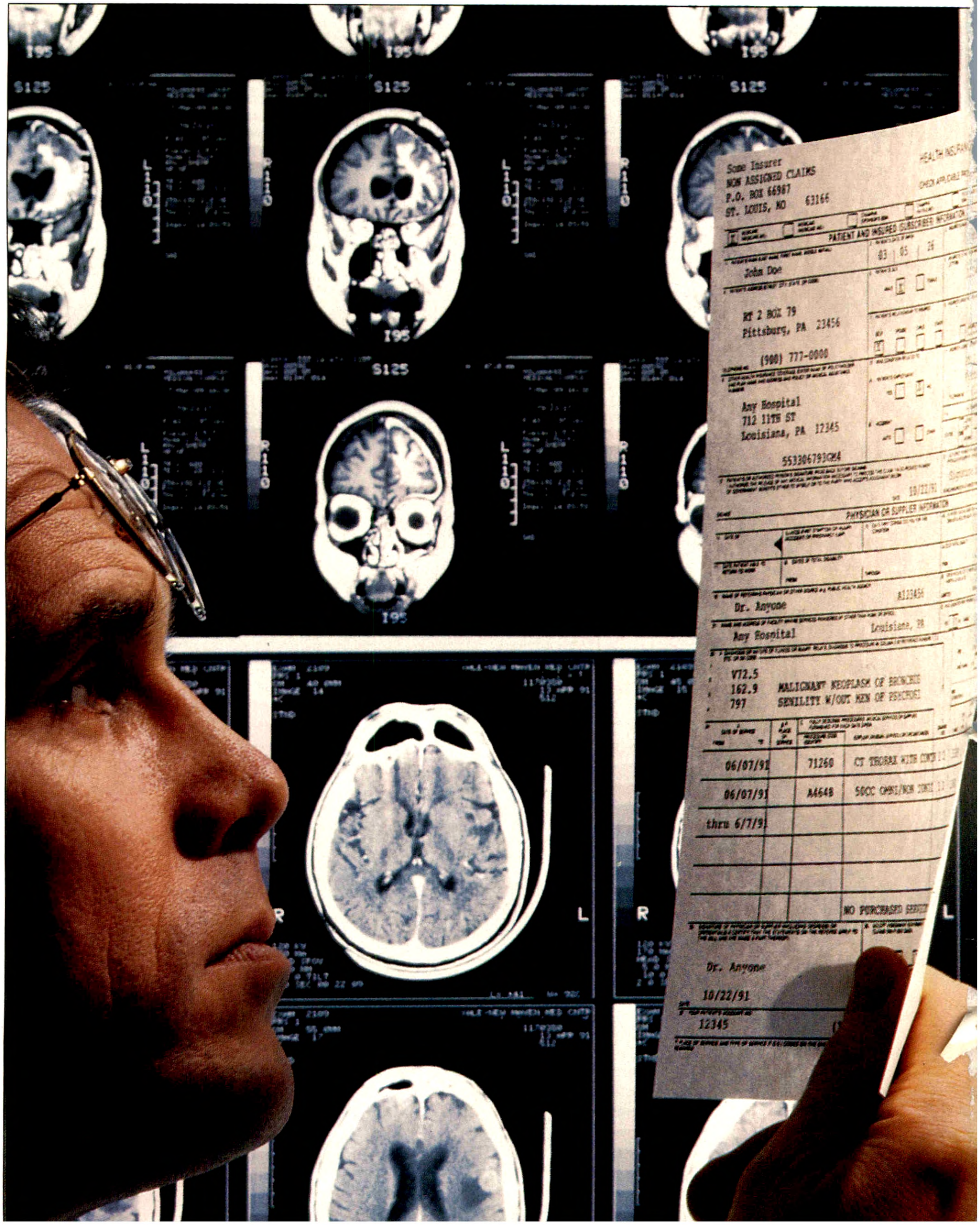

INFORMATION PROGRAM

THE WAY

Because you have more important things to read.

The *OMNI*℠ Reimbursement Information Program is dedicated to helping you obtain maximum reimbursement with minimal investment of your valuable time. Sponsored by the leader in nonionic contrast media support, the *OMNI* range of services includes:

1-800-767-*OMNI* Reimbursement Hot Line
for informed answers on claim submissions and expert guidance on resubmissions and appeals.

Policy Update Bulletins
on up-to-the-minute changes that affect your billings.

Payer Advocacy Efforts
that urge insurers to maintain competitive levels of payment and service.

Special Programs
for more in-depth analysis at your facility are also available.

Enroll your facility today.
Because insurers' policies are ever changing, timely information is the key to maximum payment. We're here to help. So call the *OMNI* Reimbursement Hot Line — 1-800-767-6664 — to enroll your facility. It could be the most rewarding decision you make today.

sanofi WINTHROP

LEADERSHIP IN NONIONIC CONTRAST MEDIA *REIMBURSEMENT*

© 1992 Sanofi Winthrop Pharmaceuticals
66-1212D

AJR Business and Subscriber Information

The American Roentgen Ray Society

AJR, American Journal of Roentgenology, is published monthly to disseminate research on current developments in the radiologic sciences and commentary on topics related to radiology. It is published by the American Roentgen Ray Society (ARRS), 1891 Preston White Dr., Reston, VA 22091; (703) 648-8992. Address inquiries regarding Society business, the annual ARRS meeting, and membership to the Society to the above address.

Correspondence regarding editorial matters should be addressed to Editorial Office, AJR, 2223 Avenida de la Playa, Ste.103, La Jolla, CA 92037-3218; telephone 1-800-348-4257 or (619) 459-2229; FAX (619) 459-8814. For information on manuscript submission, see Guidelines for Authors.

Subscriber Information

ARRS annual dues include $50 for journal subscription. Nonmember subscription rates are as follows: $125/year ($180 foreign); institutions, $135 ($190 foreign); in-training, $25 ($80 foreign). Single copies of the Journal may be purchased for $18 ($22 foreign). Airmail rates will be furnished on request. The GST number for Canadian subscribers is 123394371.

Call toll-free, 1-800-638-6423 (in Maryland call 1-800-638-4007), with subscription inquires or problems. Please have the mailing label from your latest issue available when you call.

Report changes of address to Subscription Fulfillment, AJR, 428 E. Preston St., Baltimore, MD 21202. Damaged or unreceived issues must be reported within 60 days of publication (90 days for foreign subscribers) for replacement.

Advertising Information

All advertising is subject to approval by the publisher. Acceptance of advertising does not indicate endorsement of the products or services advertised or the claims made. For display advertising information, contact Gary Walchli, National Sales Representative, AJR, 428 E. Preston St., Baltimore, MD 21202, (410) 528-4291.

For classified advertising information, contact the Publications Department, ARRS, Attn: Terry Fitterer, 1891 Preston White Dr., Reston, VA 22091; telephone (703) 648-8992; FAX (703) 264-8863.

Copyrights, Permissions, and Reprints

Contents of the *AJR* are copyrighted by the ARRS. No part of this publication may be reproduced without permission. Requests for such permission should be addressed to the Publications Department, ARRS, Attn: Terry Fitterer, 1891 Preston White Dr., Reston, VA 22091. For reprints of a particular article, please contact the author designated in the footnotes for that article.

Indexes

The *AJR* provides volume and yearly indexes (subject and author) in the June and December issues. *AJR* articles are also indexed in *Current Contents*, *Index Medicus*, and the cumulative index published by *Radiology*.

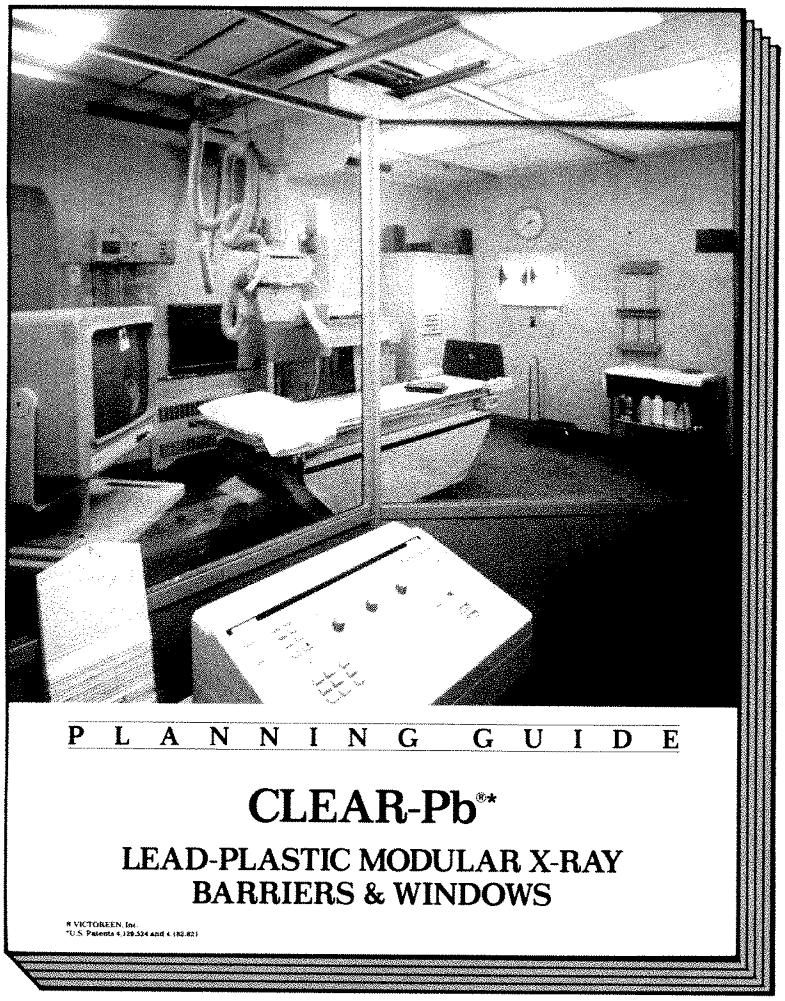

PLANNING GUIDE

CLEAR-Pb®*

LEAD-PLASTIC MODULAR X-RAY BARRIERS & WINDOWS

® VICTOREEN, Inc.
*U.S. Patents 4,129,524 and 4,182,821

We Wrote the Book on X-Ray Room Shielding...

Ask for Your **FREE** Copy!

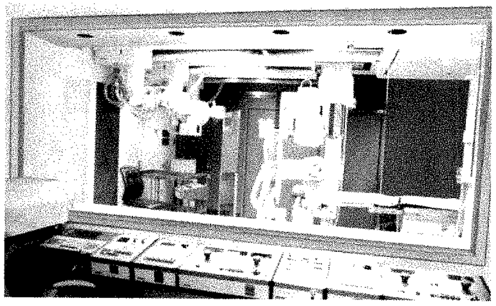

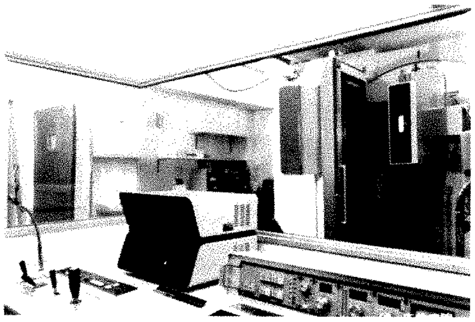

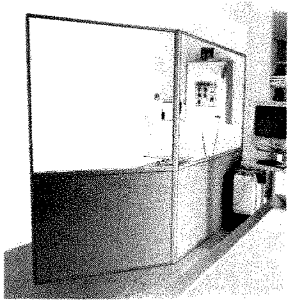

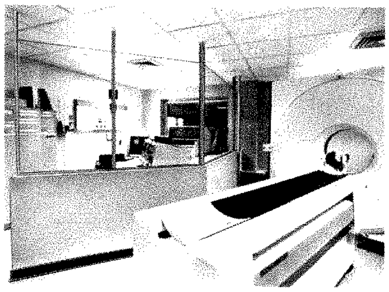

Our FREE PLANNING GUIDE shows how CLEAR-Pb® Transparent, Lead-Plastic Modular Barriers and Windows solve shielding problems in x-ray, CT and special procedures rooms in hospitals and therapy centers.

CLEAR-Pb is a lead-impregnated transparent plastic that is shatter-resistant. Available in 200 stock sizes up to 6 x 8', and in lead equivalences from 0.3 to 2.00 mm.

Phone (516) 741-7717,
FAX (516) 741-5414, or write for your FREE CLEAR-Pb X-Ray Room Planning Guide 3186-44

NUCLEAR ASSOCIATES

VICTOREEN

Division of VICTOREEN, INC.
100 VOICE ROAD • P.O. BOX 349
CARLE PLACE, NY 11514-0349 U.S.A.
(516) 741-7717
FAX (516) 741-5414

® Victoreen, Inc. U.S. Patents 4,129,524 and 4,182,821

NUCLEAR ASSOCIATES...
THE RADIATION
SHIELDING SPECIALIST

Academic Neuroradiologist

Long Island Jewish Medical Center, an 825-bed tertiary care hospital, has opening in the Division of Neuroradiology. Three neuroradiologists in the division. Technology includes state-of-the-art CT scanners, digital angiography and a magnetic resonance center. Successful candidate will be board certified radiologist with fellowship training in neuroradiology. Experience in interventional neuroradiology preferred. Academic rank and salary commensurate with experience.

Forward CV in confidence to: Peter G. Herman, MD, Chairman, Department of Radiology, LIJ, New Hyde Park, NY 11042, or call (718) 470-7175. *An Equal Opportunity Employer.*

LIJ

Long Island Jewish
Medical Center

The Long Island Campus for the
Albert Einstein College of Medicine

FACULTY POSITION

ANGIOGRAPHY/INTERVENTIONAL RADIOLOGY

The Department of Radiology at The George Washington University Medical Center, Washington, D.C. is seeking a Board Eligible or Certified Radiologist to join the Section of Angiography/Interventional Radiology, as a full-time, non-tenure track faculty member at the Assistant or Associate Professor level. Candidates must have completed a minimum of one year Fellowship training in Interventional Radiology. The section performs 800 procedures/year, and is well staffed. Salary and academic rank are commensurate with experience. Review of applications will commence on October 1, 1992, and continue until the position is filled. Letters of inquiry must be accompanied by a CV and should be sent to: David O. Davis, M.D., Professor and Chairman, Department of Radiology, The George Washington University Medical Center, 901 23rd St. N.W., Washington, D.C. 20037.

The George Washington University is an Affirmative Action/Equal Opportunity Employer.

Fellowships In Diagnostic Radiological Research.

The Diagnostic Radiology Research Program of the National Institutes of Health is accepting applications for two-year fellowship positions beginning in July 1993 and July 1994. This program provides an excellent opportunity for individuals who plan an academic career in radiological sciences.

The fellowship training program emphasizes basic research in all aspects of imaging and image processing. Fellows will have no clinical responsibilities unless they are related to their project. The imaging laboratories of the Diagnostic Radiology Research Program include: state-of-the-art 0.5 and 1.5 Tesla MR units; a newly developed image analysis program with hardware support; ultrafast CT; and an experimental angiography suite. The facilities in the *In Vivo* NMR Research Center, the PET and monoclonal antibody programs of the Nuclear Medicine Department, and other laboratories on the NIH campus will be made available to the fellow, providing an opportunity to develop expertise in areas related to imaging research. Basic research in functional or metabolic imaging, contrast agents, biochemistry, biology, chemistry, immunology, physics and physiology will be encouraged. Laboratories are being developed which will include "hot" and "cold" wet labs and tissue culture facilities. Collaboration with other scientists on the NIH campus will be encouraged.

Applicants should hold the MD or PhD degree and should have completed training in diagnostic radiology, nuclear medicine or related fields. Applications from individuals currently in US residency programs may also be considered for research fellowship positions. US citizenship or permanent residency is required for this full-time appointment.

Candidates should submit a Curriculum Vitae, at least three letters of reference and a preliminary statement concerning their research interest to Dr. Joseph A. Frank, Acting Director.

National Institutes Of Health

Diagnostic Radiology Research Program

9000 Rockville Pike, Building 10, Room B1N256, Bethesda, MD 20892 • FAX 301-402-3216

Equal Opportunity Employer

Keep It All Together

Easily and Conveniently With
Bound Volumes of the
American Journal of Roentgenology

Keeping up with scientific and technological advances in radiology is more important than ever, and that's why each issue of the *American Journal of Roentgenology* is packed with up-to-the-minute information crucial to you and your practice. **Keep this important resource together for easy reference in convenient and attractive bound volumes.**

Each edition is imprinted with the year and volume number and contains six issues filled with the kind of vital research, commentary and analysis you've come to expect in the AJR.

For ordering information, contact AJR Subscription Fulfillment Department, 428 E. Preston St., Baltimore, MD 21202-3993, or call toll-free **1-800-638-6423.**

Change of Address?

You won't miss a single issue if you notify us at least eight weeks in advance. Send your mailing label or account number along with your new address and the date the change is to take effect to:

AJR Subscription Fulfillment Dept.
428 East Preston Street
Baltimore, MD 21202-3993
or call TOLL-FREE
1-800-638-6423

E-Z-EM® Double contrast studies with single-patient bottles of Liquid HD™ give you more than excellent visualization of the upper GI tract. You get convenience and economy too. Unit-dose packaging simplifies stocking and inventory while eliminating the mess and waste of hand mixing – just shake, drink and throw away. All this and a consistent suspension every time. Look into Liquid HD in single-patient bottles. Call your E-Z-EM Distributor or one of our Customer Service Specialists at 1-800-544-4624.

E-Z-EM, Inc.
717 Main Street
Westbury, NY 11590
Tel: 1-800-544-4624
Fax: 516-333-8278

E-Z-EM INTEGRITY • E-Z-EM DEDICATION • E-Z-EM INNOVATION • 30 Years of Quality and Service to Radiology E-Z-EM®

MORE THAN MEETS THE EYE.

E-Z-EM stock is publicly traded on the NASDAQ National Market System under the symbol EZEM. For financial information, contact Investor Relations at 1-800-544-4624, ext. 345.

© E-Z-EM, Inc., 1992

Subject: Technology

Point of view: Radiologist

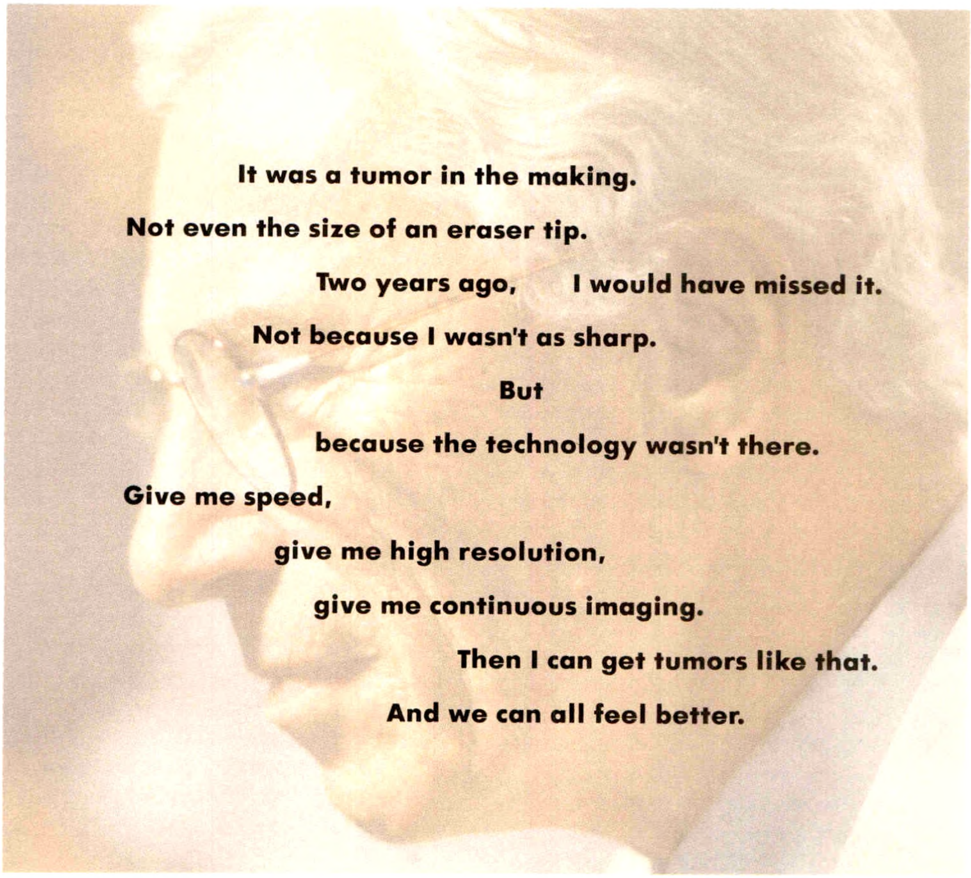
It was a tumor in the making.
Not even the size of an eraser tip.
Two years ago, I would have missed it.
Not because I wasn't as sharp.
But
because the technology wasn't there.
Give me speed,
give me high resolution,
give me continuous imaging.
Then I can get tumors like that.
And we can all feel better.

Picker technology is not just born of research. It's born of innovation. Like our PQ-2000™ CT system. With 4,800 solid state detectors. Continuous Slip Ring Rotation. And Advanced Dynamic Scanning (ADS). It provides the sharpest edge definition and most sensitive contrast resolution possible in a single scan with known technology.

PICKER
MORE THAN IMAGES. INSIGHT.

© 1991 Picker International, Inc. For reprints of this ad, or for more information, call us at 1-800-323-0550.

AJR Guidelines for Authors

Address new and revised manuscripts and correspondence to the Editor:

AJR Editorial Office
2223 Avenida de la Playa, Suite 103
La Jolla, CA 92037-3218
Telephone: (619) 459-2229; FAX: (619) 459-8814

Inquiries regarding classified ads, reprints, or permission to republish *AJR* material should be addressed to the publisher:

ARRS Publications Department
1891 Preston White Dr., Reston, VA 22091

The *AJR* publishes original contributions to the advancement of medical diagnosis and treatment. Submitted manuscripts should not contain previously published material and should not be under consideration for publication elsewhere.

Manuscript decisions are based on peer review. Reviewers receive manuscripts without title pages to ensure an unbiased review. Statements made in the article, including changes made by the Editor or manuscript editor, are the responsibility of the author and not of the *AJR* or its publisher. Authors will be sent the edited manuscript, galley proof, and proofs of illustrations. If the corresponding author will be unavailable to review galleys, arrangements should be made for a coauthor or colleague to read and return the proof.

The following guidelines are based on instructions set forth in the **Uniform Requirements for Manuscripts Submitted to Biomedical Journals** (*Ann Intern Med* **1988;**108:258–265). Articles will be edited, however, to conform to the individual style of *AJR*.

General Guidelines for Major Papers

Abstract. Clearly state (in 250 words or fewer) the purpose, methods, results, and conclusions of the study. Include actual data.

Introduction. Briefly describe the purpose of the investigation and explain why it is important.

Methods. Describe the research plan, the materials (or subjects), and the methods used, in that order. Explain in detail how disease was confirmed and how subjectivity in observations was controlled.

Results. Present results in a clear, logical sequence. If tables are used, do not duplicate tabular data in text, but do describe important trends and points.

Discussion. Describe the limitations of the research plan, materials (or subjects), and methods, considering both the purpose and the outcome of the study. When results differ from those of previous investigators, explain the discrepancy.

AUTHOR'S CHECKLIST

For priority handling, complete the following checklist, sign the copyright form on the reverse side of this page, and include both with the manuscript.

________ Two copies of the manuscript (the original and a photocopy) and two complete sets of figures are submitted. One copy has been retained by the author.

________ If appropriate, *AJR* Guidelines for case reports, technical notes, pictorial essays, or letters to the Editor have been followed. (See page A12.)

________ The manuscript, including references, figure legends, and tables, is typed double-spaced on 8½ × 11 in. (21.6 × 27.9 cm) *nonerasable* paper. Right-hand margins are not justified.

________ All manuscript pages are numbered consecutively beginning with the abstract. Authors' names do not appear on the manuscript pages.

________ The manuscript is organized as follows: title page, blind title page (title only), abstract, introduction, methods, results, discussion, acknowledgments, references, tables, figure legends, and figures.

________ Informed consent has been obtained from patients who participated in clinical investigations. If experiments were performed on animals, authors complied with NIH guidelines for use of laboratory animals.

________ Use of unfamiliar acronyms and abbrevations is kept to a minimum. When abbreviations are used they are defined at first mention, followed by the abbreviation in parentheses.

________ Metric measurements are used throughout, or the metric equivalent is given in parentheses.

________ Names and locations (city and state only) of manufacturers are given for equipment and nongeneric drugs.

________ Upon acceptance, final version is submitted on a 5 1/4-in. DOS-compatible diskette in Wordperfect or ASCII format.

Title Page

________ The following information is given: title of article; names and complete addresses (including zip code) of all authors; current addresses of authors who have moved since study; acknowledgment of grant or other assistance. The corresponding author is clearly identified, and a current address, phone number, and FAX number are given.

________ A blind title page is included in each copy of the manuscript, giving only the title (without the authors' names) for use in the review process.

Abstract

________ An abstract of approximately one and one-half typewritten pages is organized into the following paragaphs.

Objective. In one or two sentences, indicate the specific goal or purpose of the article, and indicate why it is worthy of attention. Explain the hypothesis to be tested, the dilemma to be resolved, or the deficiency to be remedied. The objective stated here must be identical to the one given in the title and introduction of the paper.

Subjects (or materials) and methods. Describe succinctly the methods used to achieve the objective explained in the first paragraph, stating what was done, how it was done, how bias was controlled, what data were collected, and how the data were analyzed.

Results. The findings of the procedures described in the preceding paragraph are presented here. All results should flow logically from the methods described and not stray from the specific objective of the paper. Include as many specific data as possible within the overall length limitation of one typewritten page.

Conclusion. In one or two sentences, present the take-home message to be remembered when all else is forgotten. Describe the conclusion of the study, based solely on the data provided in the body of the abstract. Conclusions must relate directly to the objective of the paper as defined in the title and first paragraph of the abstract.

________ No abbreviations or reference citations are used.

References

________ References (not to exceed 35) are typed double-spaced starting on a separate page and are **numbered consecutively in the order in which they appear in the text**.

________ All references are cited in the text and are enclosed in brackets and typed on line with the text (not superscript).

________ Unpublished data are not cited in the reference list, but are cited parenthetically in the text, for example, (Smith DJ, personal communication), (Smith DJ, unpublished data). This includes papers submitted, but not yet accepted, for publication.

________ Papers presented at a meeting are not cited in the reference list, but are cited parenthetically in the text (e.g., Smith DJ et al., presented at the American Roentgen Ray Society meeting, May 1990). After first mention, use (Smith DJ et al., ARRS meeting, May 1990).

________ Inclusive page numbers (e.g., 333–335) are given for all references.

________ Journal names are abbreviated according to *Index Medicus*.

________ Style and punctuation of references follow the format illustrated in the following examples (all authors are listed when six or fewer; when seven or more authors, the first three are listed, followed by "et al."):

Journal article

1. Long RS, Roe EW, Wu EU, et al. Membrane oxygenation: radiographic appearance. *AJR* **1986**;146:1257–1260

Book

2. Smith LW, Cohen AR. *Pathology of tumors*, 6th ed. Baltimore: Williams & Wilkins, **1977**:100–109

Chapter in a book

3. Breon AJ. Serum monitors of bone metastasis. In: Clark SA, ed. *Bone metastases*. Baltimore: Williams & Wilkins, **1983**:165–180

Tables

________ Each table is typed double-spaced on a separate page without vertical or horizontal rules; each has a short, descriptive title. Tables do not exceed two pages in length and contain at least four lines of data.

________ Tables are numbered in the order in which they are cited in the text.

________ Abbreviations are defined in an explanatory note below each table.

________ Tables are self-explanatory and do not duplicate data given in the text or figures.

________ All arithmetic (percentages, totals, differences) has been double checked for accuracy, and tabular data agree with data given in the text.

Figures and Legends

________ Two complete sets of original figures are submitted unmounted in labeled envelopes.

________ Figures are clean, unscratched, glossy prints, uniform in size and magnification, with **white borders.** A separate print (not larger than 5 × 7 in.) is submitted for each figure *part*.

________ All figure parts relating to one patient have the same figure number.

________ Each figure is labeled on the back with the figure number and an arrow indicating "top." For black-and-white figures, labeling is done on a gummed label, which is then affixed to the back of the print. **Never** use labels on **color** figures, but write figure number on the back lightly in pencil. *Never* use ink on front or back of any figures.

________ Authors' names are *not* written on the backs of figures.

________ Only removable (rub-on) arrows and letters are used on the figures. Symbols are uniform in size and style and are not broken or cracked.

________ Line drawings are done in black ink on a white background. They are professional in quality, and all use the same size type. (Only glossy prints are acceptable.)

________ Written permission has been obtained for use of all previously published illustrations (and copies of permission letters are included), and an appropriate credit line is given in the legends.

________ Legends are typed double-spaced, and figure numbers correspond with the order in which the figures are cited in the text.

________ Legends are written in accordance with *AJR* style (refer to any issue and follow format).

Transfer of Copyright Agreement, Conflict of Interest Acknowledgment, Certification of Coauthors, and Exclusive Publication Statement

Complete copyright to the article entitled: ____

____

is hereby transferred to the American Roentgen Ray Society (for United States government employees to the extent transferable), effective if and when the article is accepted for publication in the *American Journal of Roentgenology*. In the case of the authors who are officers or employees of the United States government, the American Roentgen Ray Society recognizes that works prepared by officers or employees of the United States government as part of their official government duties are in the public domain.

Authors reserve all proprietary rights other than copyright, such as patent rights and the right to use all or part of this article in future works of their own. The authors retain the right of replication, subject only to crediting the original source of publication and receiving written permission from the publisher.

Authors guarantee that this manuscript contains no matter that is libelous or otherwise unlawful, invades individual privacy, or infringes any proprietary rights.

Authors understand that they will receive no royalty or other compensation from the American Roentgen Ray Society.

Authors guarantee that the editor has been or will be informed of any proprietary or commercial interest or conflicts of interest the authors may have that relate directly or indirectly to the subject of this article.

All authors certify that they have made substantive and specific intellectual contributions to the article and assume public responsibility for its content.

Finally, the authors certify that none of the material in this manuscript has been published previously or is currently under consideration for publication elsewhere.

------------------------ First author/date	------------------------ Second author	------------------------ Third author
------------------------ Fourth author	------------------------ Fifth author	------------------------ Sixth author

This agreement must be signed by all authors in order for the manuscript to be published.

Case Reports

A case report is a brief description of a special case that provides a message that transcends the individual patient.

Format. There is no abstract. The introduction should be a short paragraph giving the general background and the specific interest of the case. No more than one case should be described in detail (similar ones can be mentioned briefly in the discussion). Emphasis should be on the radiologic aspects; clinical information must be limited to that necessary to provide a background for the radiology. The discussion should be succinct and should focus on the specific message and relevance of radiologic methods. A review of the literature is not appropriate.

Length. Maximum of five double-spaced, typewritten pages, including the references but not the title page or figure legends.

References. Maximum of eight.

Figures. Maximum of four, unless the text is shortened accordingly. Legends must not repeat the text.

Tables and Acknowledgments. Not appropriate in case reports.

Pictorial Essays

A pictorial essay is an article that conveys its message through illustrations and their legends. Unlike other *AJR* articles, which are based on original research, pictorial essays serve primarily as teaching tools, like exhibits at a scientific meeting. They are not encyclopedic book chapters. The abstract should be a short, introductory paragraph.

Length. Maximum of four double-spaced, typewritten pages, including the references but not the title page or figure legends.

References. Maximum of four.

Figures. Maximum of 30 figure *parts.* Number should be as few as necessary to convey the message of the paper.

Tables and Acknowledgments. Not appropriate in pictorial essays.

Opinions, Commentaries, and Perspectives

Opinions, commentaries, and perspectives are special articles dealing with controversial topics or issues of special concern to radiologists.

Format. Include a title page but no abstract. Headings may be used to break up the text.

Length. Maximum of five double-spaced, typewritten pages.

References. Maximum of five.

Tables and Figures. Maximum of four.

Technical Notes

A technical note is a brief description of a specific technique or procedure, modification of a technique, or equipment of interest to radiologists.

Format. No abstract, headings, or subheadings are required. If headings are used, they should be a combination of "Case Report," "Materials and Methods," "Results," and "Discussion." A brief one-paragraph introduction should be included to give the general background. Discussion should be limited to the specific message, including the uses of the technique or equipment. Literature reviews and lengthy case reports are not appropriate.

Length. Maximum of five double-spaced, typewritten pages, including the references but not the title page or figure legends.

References. Maximum of eight.

Figures. Maximum of two, unless the text is shortened accordingly.

Tables and Acknowledgments. Not appropriate in technical notes.

Letters to the Editor and Replies

Letters to the Editor and Replies should offer objective and constructive criticism of published articles. Letters may also discuss matters of general interest to radiologists. Material being submitted or published elsewhere should not be duplicated in letters, and authors must disclose financial associations or other possible conflicts of interest.

Format. All letters should be typed double-spaced on nonletterhead paper, with no greeting or salutation. Titles for letters should be short and pertinent. The title for a reply is simply "Reply." Do not use abbreviations in the title or the text. Authors' names and affiliations should appear at the end of the letter. Do not end a letter with a hand-written signature.

Number of authors. Maximum of four.

Length. Maximum of two double-spaced, typewritten pages, including references.

References. Maximum of four.

Figures. Maximum of two figures *or* one figure with two parts.

Tables and Acknowledgments. Not appropriate in Letters to the Editor and Replies.

Computer Page Articles

Articles published on the computer page deal with practical computer applications to radiology.

Format. Include a title page and an abstract.

Length. Maximum of eight double-spaced, typewritten pages.

References. Maximum of five.

Figures and Tables. Maximum of five. Computer printouts are not acceptable. Figures must be submitted as 5 × 7 in. glossy prints.

All submissions to the *AJR* must be accompanied by a completed copy of the Author's Checklist and the signed Copyright agreement.

S&S X-Ray Presents

ENLIGHTENED ILLUMINATION

At S&S we realize that every customer's needs and tastes are different. That's why we offer a full range of illuminators. There is an illuminator in our catalog ideally suited to the needs of your hospital, office or lab. The choice is yours - The pleasure of serving you is all ours.

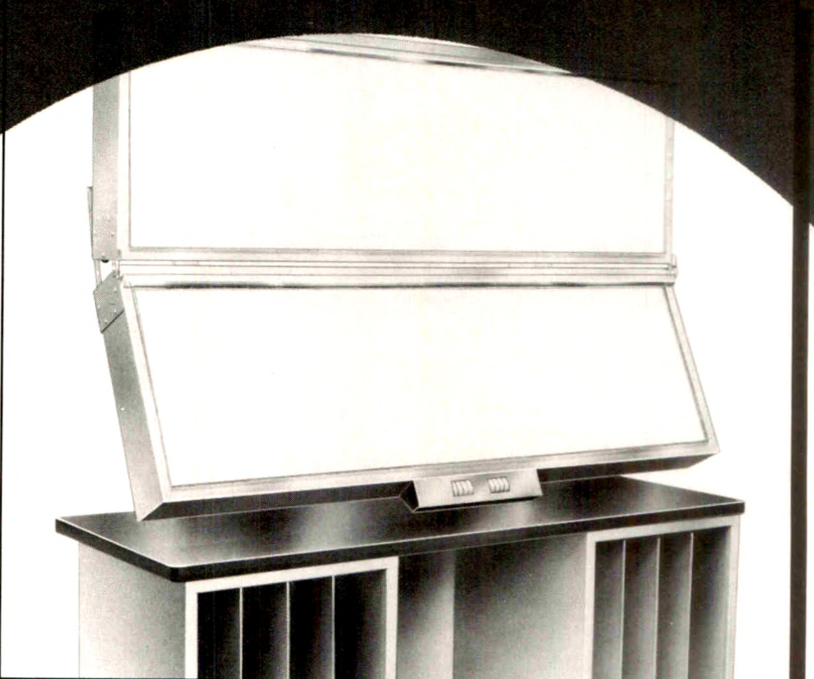

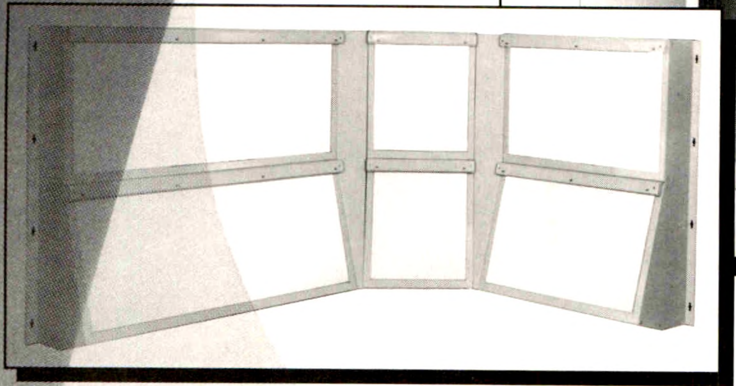

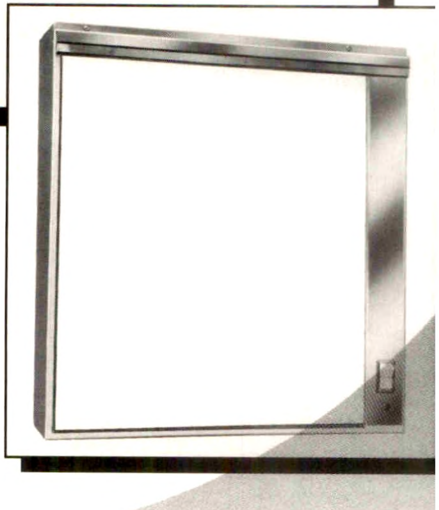

The S&S Catalog Also Includes The Following Other Featured Players:

- Motorized Viewers
- X-Ray Protection
- Darkroom Equipment
- X-Ray Accessories
- File Cabinets & Supplies
- And Much More
- For a FREE copy of our fully illustrated, 100+ page catalog, contact S&S directly or your local x-ray dealer.

S&S X-RAY PRODUC

1101 LINWOOD STREET
BROOKLYN, NY 11208
1-800-347-XRAY • Fax: 718-257-021

ELEMA SCHONANDER

Reliable, Comfortable, Fast & Easy Viewing...

Rolloscope II™

There are no strings to obstruct viewing, and you get greater convenience and increased efficiency.

RELIABLE OPERATION

Here's the most thoughtfully designed motorized multiple filmviewer available. Engineering excellence with an emphasis on simplicity, reliability and fast convenient film reading. View an entire library of radiographs and examine them completely with no distracting strings to obscure your view.

COMFORTABLE VIEWING

The slanted display area helps eliminate fatigue during film interpretation. Eight independently controlled light frames eliminate glare from surrounding frames.

The viewing area is large enough to allow examination of any two adjacent rows.

RAPID, ACCURATE SCROLLING

Slow belt start-up assures easy single row identification. You can also move quickly with the belt-driven transport that can scroll one film row per second—up or down.

Holds up to 200, 14″x17″ films—larger capacity with smaller films.

CONVENIENT CONTROLS FOR EASY OPERATION

Switches on each end of the large 15″x67″ work surface control the lights, while a foot pedal or the touch switch next to the viewing area controls scrolling. Also includes a footswitch for optional hot light.

For complete information on the ROLLOSCOPE II, contact your local X-ray distributor, or:

Elema-Schonander
2360 North Palmer Drive
Schaumburg, IL 60173-3887
Phone: (708) 397-5931
Fax: (708) 397-5058

Review Article

MR Measurement of Blood Flow in the Cardiovascular System

Gerhard H. Mostbeck,[1] Gary R. Caputo, and Charles B. Higgins

Methods for measurement of blood flow with MR were devised many years ago but have been used for diagnosis in only the past few years. The two methods of measurement that have been used most extensively are based on the principles of *time of flight* and *phase shift.* A number of factors can influence the accuracy of MR measurements of blood flow. In vitro studies using flow phantoms have verified the accuracy of the phase-shift technique for measuring flow velocities exceeding 5 m/sec, which for practical purposes, encompasses the peak flow encountered in cardiovascular disorders. The flow measurements have been used to quantify valvular heart disease, congenital heart disease, pulmonary arterial disease, thoracic aortic disease, and peripheral vascular disease.

Historically, a change in MR signal strength due to moving spins with different degrees of magnetization in the region of measurement was reported as far back as 1951 [1]. Time-of-flight effects on the signal in MR imaging were regarded as confusing artifacts at the early stages of clinical imaging. However, it has become evident that this signal can be quantitatively analyzed to obtain precise measurements of the velocity and volume of blood flow. From such measurements of flow, important hemodynamic information can be derived.

MR measurements of flow are based either on the effect of flow on the signal intensity of the longitudinal magnetization (time-of-flight techniques) or on the influence of flow on the phase of the transverse magnetization (phase-shift techniques). Singer and Crooks [2] were the first to apply a time-of-flight technique in vivo to measure blood flow in the internal jugular vein in humans. Today, time-of-flight effects combined with saturation methods are used to measure blood-flow velocities [3–10]. By measurement of the distance traveled by a labeled bolus over time, velocity can be calculated as distance divided by time.

Use of phase-shift techniques to quantify flow velocity became possible after the application of bipolar velocity-encoding pulses to conventional sequences by Moran in 1982 [11]. Refinement of this technique with the use of velocity-compensated gradient waveforms and applying repetitive gradient- or field-echo imaging for temporal resolution of phasic blood flow over the cardiac cycle permitted the measurement of venous and arterial flow in the heart and major vessels of humans [12].

This review describes the basic principles of MR techniques used to measure blood flow and discusses current clinical applications of these techniques. In addition, potential uses of flow measurements in cardiovascular diagnosis based on expected technological advances are proposed.

MR Techniques for Flow Measurement

Time-of-Flight Techniques

The time-of-flight effect is related to the replacement of partially saturated spins in an imaging plane by fresh, fully

---

Received January 31, 1992; accepted after revision April 1, 1992.

This work was supported in part by a postdoctoral research exchange grant from the Max Kade Foundation, Inc., and in part by the Ludwig Boltzmann Institute for Radiologic Tumor Research, Vienna.

[1] All authors: Department of Radiology, Box 0628, Rm. L308, University of California, San Francisco, 505 Parnassus St., San Francisco, CA 94143. Address reprint requests to C. B. Higgins.

***AJR* 159:453–461, September 1992** 0361–803X/92/1593–0453 © American Roentgen Ray Society

unsaturated spins of the adjacent tissue (i.e., blood in the vessel) and/or to the washout of excited spins during the time of the pulse sequence [13, 14]. The mechanisms by which intraluminal signal is variably altered by flowing blood in relation to flow velocity and imaging parameters have been described in detail [13–15].

Several investigators [3–10] have used time-of-flight effects to measure the velocity of blood flow. Most of these techniques are variants of the so-called bolus-tracking method (Fig. 1). In principle, the bolus-tracking method relies on the detection of the displacement of a labeled bolus of spins with the blood flow within a vessel of interest. The motion of the labeled bolus is imaged at multiple time points during the cardiac cycle by using a cine gradient-recalled echo (GRE) sequence. When the initial position of the tagged or labeled bolus is known and the displacement is recognized on subsequent images, velocity can be calculated by dividing the displacement distance of the bolus by the time interval between tagging and readout.

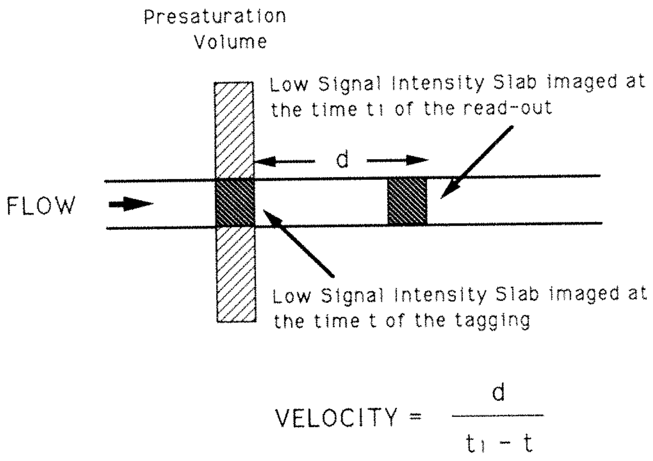
Presaturation Volume
Low Signal Intensity Slab imaged at the time t₁ of the read-out
d
FLOW
Low Signal Intensity Slab imaged at the time t of the tagging
VELOCITY = d / t₁ - t

Fig. 1.—Diagram shows time-of-flight bolus-tracking technique with a GRE sequence. A 90° pulse flips longitudinal magnetization into transverse plane, where it is dispersed by a spoiler gradient pulse. At time t_1 of readout, low-signal intensity bolus is displaced with blood flow over a distance d. Imaging plane is in vessel's longitudinal axis. t = time of tagging.

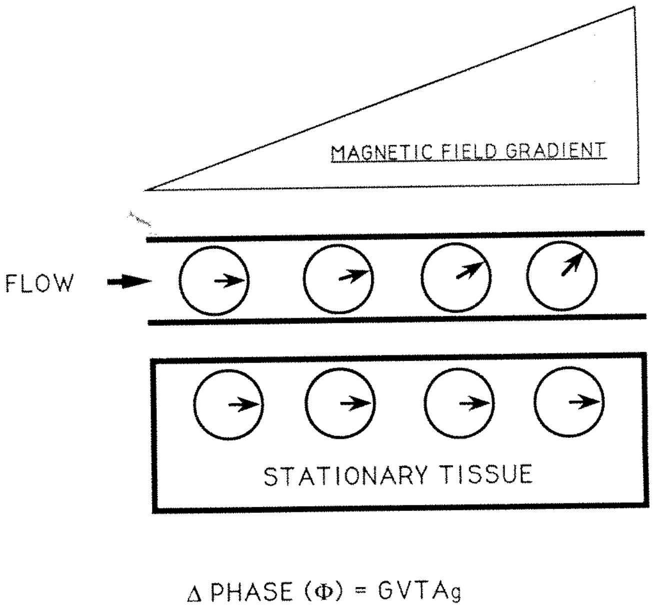

Fig. 2.—Diagram shows phase-shift technique used to measure flow velocity. Protons in stationary tissue experience no phase shift when a bipolar gradient is applied, whereas spins moving from left to right accumulate a net phase shift through imaging experiment.

Phase-Shift Techniques

Spin-phase phenomena were first studied by Carr and Purcell in 1954 [16]. In 1961, Hahn [17] used flow-induced phase shifts to measure motion of seawater. Phase-shift techniques are based on the accrued phase shift of spins moving along a magnetic field gradient (Fig. 2). In general, the phase shift used to reconstruct the MR image is proportional to the gradient times the position along the gradient direction. For moving protons, the position changes over time. When a unipolar gradient is applied, thus varying the strength of the magnetic field in one direction, both stationary and moving spins accumulate a phase shift in their transverse magnetization. When a second gradient with equal magnitude and opposite direction is applied, the phase shift of stationary spins cancels out. However, spins moving during the application of such a bipolar gradient accumulate a net phase shift Φ according to the equation:

$$\Phi = GVTA_g,$$

where G is the gyromagnetic ratio, V is the velocity, T is the interval (time) between the centers of the two gradient lobes, and A_g is the area of one lobe of the bipolar gradient pulse [18]. This net phase shift is basically proportional to velocity, the square of the echo delay time, and higher terms of motion like acceleration and jerk. In order to suppress the signal from the stationary background and to correct for phase shifts due to inhomogeneities of the static magnetic field, two bipolar gradient pulses can be applied with the same strength but opposite direction. Subtraction of these two data sets yields the phase image that is used for measurement of velocity.

Introduced by Bryant et al. in 1984 [19], the use of velocity-compensated gradient waveforms and a field-echo sequence permits the creation of velocity maps with multiple measurements during the cardiac cycle in major vessels of the body [12]. Similar techniques are now in clinical use consisting of GRE, repetitive, short-TE, first-order, flow-compensated sequences that create magnitude (modulus) and phase images [20, 21].

From the phase-shift GRE data set, the velocity can be measured for each pixel, or the average velocity within one region of interest (ROI) encircling the entire or parts of a vessel's cross-sectional area can be assessed. Thus, measurement of spatial average velocity, spatial peak velocity, temporal average velocity, and temporal peak velocity are possible [22]. The vessel cross-sectional area can be measured by applying an ROI on the magnitude image. When the same ROI is applied on the corresponding phase image, spatial mean velocity is measured. Multiplication of these data gives the instantaneous flow volume for the specific time frame of the cardiac cycle. Integration of all instantaneous flow volumes throughout the cardiac cycle (usually ≥ 16) gives the volume flow per heartbeat. Flow direction can easily be assessed by using binary images (e.g., antegrade flow = white signal and retrograde flow = black signal) and flow volume in either direction can be quantified [23–28].

In Vitro and In Vivo Validation of MR Measurements of Flow

The time-of-flight bolus-tracking technique has been used to measure constant flow velocities in nonstenotic [5, 9, 10] and stenotic flow phantoms [10]. A correlation was found between MR bolus tracking and Doppler sonographic measurements of peak velocities in the abdominal aorta ($r = .98$, $y = 0.65x + 29$, standard error of estimate [SEE] = 8.9 cm/sec) [29] and the portal vein ($r = .85$, $y = -0.9 + 1.07x$) [10].

Phase-shift GRE measurements of flow in vivo have been validated in normal subjects by showing equivalency of the stroke volumes of the left and right ventricles using flow data from the ascending aorta and main pulmonary artery, respectively [25]. Additionally, correlations between left and right ventricular stroke volumes measured by using phase-shift GRE and left ventricular stroke volumes obtained by summing the areas of multiple transverse or short-axis MR slices in systole and diastole have been reported ($r = .98$, SEE = 3.7 ml; $r = .95$, SEE = 4.8 ml, respectively) [28, 30]. The sum of the stroke flows in the right pulmonary artery and left pulmonary artery measured in nine volunteers equaled the stroke flow volume in the main pulmonary artery [31].

Factors Influencing the Accuracy of Phase-Shift Techniques for Measurements of Flow

Various studies [19, 20, 25, 27, 30–38] have evaluated the accuracy of phase-shift MR techniques for quantifying flow. At very high velocities or with disturbed flow, measurement of blood flow can be complicated, but high velocities associated with poststenotic jets can be assessed accurately by using MR. This makes it possible to calculate pressure gradients across valvular and vascular stenoses by using the modified Bernoulli equation [39]. It has been proposed that the signal loss associated with high-velocity disturbed flow increases as the TE increases. Kilner et al. [36] have shown that by reducing the TE of a field even-echo sequence to 3.6 msec and using modified gradient coils in a 0.5-T MR system, jet velocities of up to 600 cm/sec can be measured accurately in vitro and in vivo. Studies with a conventional 1.5-T system and a stenosed flow phantom provided accurate measurement of jet velocities exceeding 600 cm/sec with TEs ranging from 7.1 to 9.0 msec [37]. Thus, in high-magnetic-field imaging systems, the effect of high-flow-velocity signal loss might be less pronounced at the same TE because of the larger net magnetization as compared with a low-field system.

Aliasing of velocity data is due to the cyclic nature of phase, such that the maximum range of phases that can be measured without aliasing is 2π radians. The gradients of the velocity-encoding acquisition must be chosen to keep the phase shifts less than 180° ($<\pi$). For pulsatile flow in arteries, the maximum velocity-encoded value must be higher than peak systolic velocity, Thus, the predicted highest velocity in the vessel of interest has to be estimated before the data acquisition. This possibly leads to a decreased sensitivity to the lower flow velocities in diastole. A pulse sequence design with variable maximum-velocity encoding over one cardiac cycle has been demonstrated to decrease this small error of flow measurements in pulsatile arterial flow [40].

Misalignment between the true direction of flow and the direction of flow encoding influences the measurement of flow velocity as determined by the equation $V_{meas} = V_{true} \cos\Phi$, where Φ is the angle between flow encoding and flow direction and V_{meas} and V_{true} are measured and true velocities, respectively [35, 38]. The cosine relationship results in small errors for small values of Φ; for example, a misalignment of 20° produces an error of only 6% [35]. Moreover, experiments with flow phantoms and a circular tube showed that with cosine correction, true and measured velocities were closely related over a range of +40° to −40° [31]. Although the problem of misalignment is overcome by applying oblique velocity-encoding gradients in the true flow direction and oblique imaging planes perpendicular to the flow direction [31], others [41] have argued that the error of oblique flow are canceled by opposite variations in cross-sectional areas when measuring volume flow. When imaging planes not coinciding with the true direction of flow (e.g., imaging the heart chambers) are used, three-dimensional phase encoding in the slice-select, phase-encode, and read-gradient directions can be used to derive accurate velocity profiles [42].

Partial volume averaging of phase data might be a source of error in flow measurements in relatively small vessels. The error depends on the T1 and T2 of the surrounding tissue and the TR, TE, and flip angle of the imaging sequence and increases with increasing slice thickness [35].

Signal misregistration is due to movement of spins between the times of slice selection, phase encoding, and frequency encoding [35]. The signal from oblique moving spins can be displaced outside the vessel into adjacent stationary tissue.

Subtraction of phase data from two interleaved acquisitions does not completely compensate for errors. Firmin et al. [35] showed that decreasing TE minimized these errors.

Clinical Applications of MR Measurements of Flow

Valvular Heart Disease

Phase-shift GRE imaging can be used to measure aortic regurgitation in two different ways [43]. First, for isolated aortic regurgitation, the difference between the left ventricular stroke volume measured in the ascending aorta and the right ventricular stroke volume measured in the main pulmonary artery is the regurgitant volume. Second, net antegrade and retrograde flow can be measured directly from the aortic flow phase data, where the retrograde flow over one cardiac cycle is a direct measurement of aortic regurgitation even in the presence of additional valvular diseases (Fig. 3). When the latter technique was used in 15 patients with isolated aortic regurgitation, a correlation was shown between the regurgitant volume measured by using phase-shift GRE and volumetric measurements of the differences in stroke volumes between the two ventricles derived from a three-dimensional stack of MR images encompassing the ventricles ($r = .99$, $y = 1.6 + 0.8x$, SEE = 3.2 ml) [43]. Another advantage is the excellent interstudy and interobserver reproducibility for the measurement of regurgitant volume in aortic regurgitation (Dulce MC, unpublished data), which makes this technique useful for drug intervention and follow-up studies.

Recent studies that used small numbers of patients [36, 44] have shown the feasibility of using phase-shift GRE techniques in patients with valvular and great-vessel stenoses to measure peak velocity across stenotic regions for calculating pressure gradients by using the Bernoulli equation. Peak systolic jet velocities up to 5.6 m/sec and 2.4 m/sec have been measured in patients with aortic stenosis and mitral stenosis, respectively [44]. These estimates of gradients by phase-shift GRE have correlated roughly with Doppler flow and catheter measurements.

Blood flow across the mitral valve has been measured by using phase-shift GRE techniques [36, 44, 45]. The normal mitral flow pattern with two positive peaks was observed in 10 volunteers; the pattern was altered in patients with severe mitral valve stenosis [45]. Instead of the biphasic antegrade flow, these patients had reversed flow in the pulmonary veins during systole. The velocity pattern in the pulmonary veins has been used to quantify the severity of mitral regurgitation [45, 46].

Congenital Heart Disease

MR measurements of flow allow noninvasive quantification of shunt volumes and assessment of flow across various

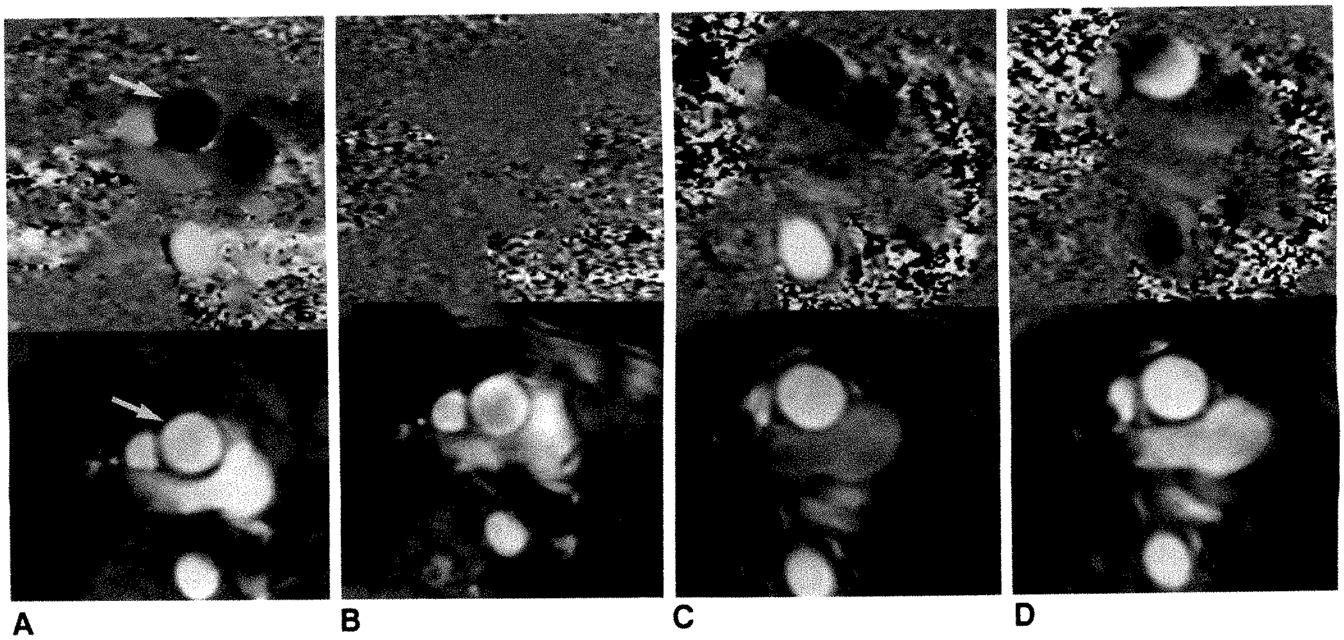

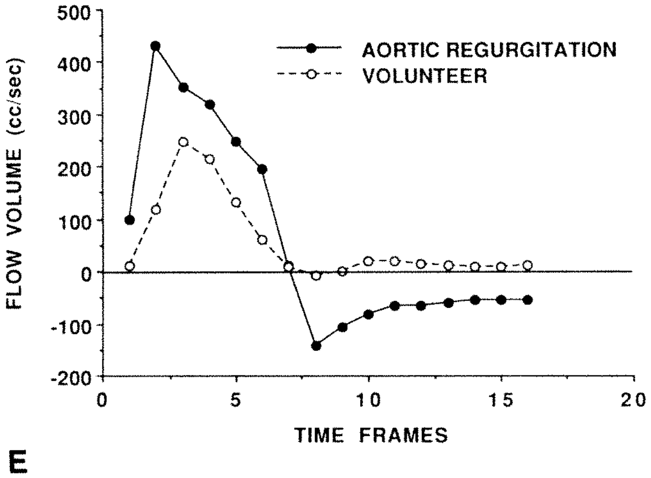

Fig. 3.—*A–D*, Peak systolic (*A* and *C*) and mid diastolic (*B* and *D*) phase (*top*) and magnitude (*bottom*) MR images in a plane perpendicular to ascending aorta (*arrow*) in a volunteer (*A* and *B*) and in a patient (*C* and *D*) with aortic regurgitation (regurgitant fraction, 42%). In both volunteer and patient, ascending aorta shows dark signal in systole, indicative of antegrade flow (*top* in *A* and *C*). In diastole, lack of signal in ascending aorta of volunteer indicates nearly zero flow (*B*). By contrast, white signal in ascending aorta during diastole in patient indicates retrograde flow (*D*).

E, Flow profiles of volunteer and of patient with aortic regurgitation shows retrograde flow (below zero line) throughout diastole in patient but not in volunteer. Regurgitant volume is calculated as area under curve for retrograde diastolic flow.

surgical shunts [36, 47–50]. Shunt volumes can be assessed easily by calculating the stroke volumes of the left and right ventricles by using phase-shift GRE technique in the ascending aorta and main pulmonary artery (Fig. 4), respectively; this was initially shown in seven patients with a variety of shunts [47]. Another study (Brenner LD, unpublished data) compared the pulmonary-to-systemic flow ratio (Q_p/Q_s) measured by using phase-shift GRE technique with oximetric measurements of Q_p/Q_s in 11 patients with atrial septal defects and found an excellent correlation ($r = .91$, $y = 0.63 + 0.79x$, SEE = 0.346).

Another application in congenital heart disease is the noninvasive measurement of blood flow in the right and left pulmonary arteries, especially in patients with pulmonary branch stenoses and after creation of surgical shunts [36, 48, 50]. In contrast to the findings in volunteers, in whom 55% of the right ventricular stroke volume perfused the right lung and 45% the left lung [31], a large disparity existed in differential blood flows in the right and left pulmonary arteries in some patients with complex congenital heart diseases (Fig. 5) [50]. Other investigators [36, 48] showed the feasibility of using MR to measure flow velocities and calculated obstructive gradients in ventriculopulmonary and Fontan conduits, which correlated with measurements obtained by using Doppler imaging.

Great Vessels

Pulmonary artery. Recent studies [23, 51] showed that phase-shift GRE technique could be used to depict the flow pattern in the main pulmonary artery in volunteers and in patients with pulmonary arterial hypertension. In volunteers, retrograde flow accounted for 2% of total flow in the main pulmonary artery, whereas in four patients with pulmonary arterial hypertension it accounted for 26% [23]. Kondo et al. [51] also showed a substantial amount of retrograde flow in the main pulmonary artery in 10 patients with pulmonary arterial hypertension. In this study, a correlation was shown between the natural logarithm of the percentage of regurgitant flow and total pulmonary resistance (Rp, derived from Doppler studies), cross-sectional area (CSA) of the main pulmonary artery and the product (Rp × CSA) of these two, respectively. However, more experience is needed in order to define the sensitivity and specificity of this abnormal flow pattern for the identification of pulmonary arterial hypertension and to assess its severity.

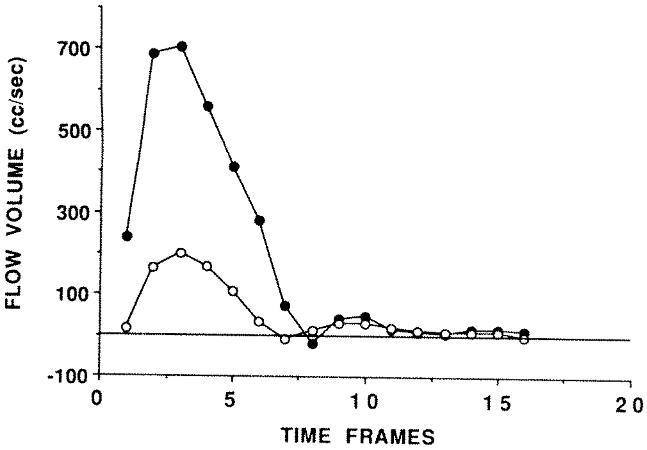

Fig. 4.—Flow profiles of pulmonary artery (PA) and ascending aorta (AO) in a patient with atrial septal defect and pulmonary-to-systemic flow ratio (Qp/Qs) of 3.9:1.0 shows difference in systolic flow in PA (*filled circles*) and AO (*open circles*). Area between two flow curves represents shunt volume.

Flow and distensibility in the main, right, and left pulmonary arteries of nine volunteers and 12 patients with single lung transplants were evaluated in another study [52]. The pulsatility index (peak forward flow plus peak backward flow divided by the time-averaged flow) of the main pulmonary artery in the 12 patients was higher in the arteries of the native lungs than in the arteries of transplanted lungs (7.4 ± 2.4 vs 2.8 ± 0.8, $p < .001$) [52]. The mean ratio between flow to the transplanted lung and the native lung was 3.0, probably reflecting differences in vascular resistance [52].

Thoracic aorta. MR is a reliable method for the diagnosis of aortic dissection [53]. Usually velocity in the false channel is slow, leading to flow signal on spin-echo images. The calculation of T2 relaxation times [54], the effect of even-echo rephasing [15, 55], and phase images [54, 56] can be helpful for distinguishing between slow flow and thrombus in the false channel. In three patients with aortic dissection, use of the phase-shift GRE technique enabled the calculation of flow in the true and in the false channel [57]. In another study [22], average spatial velocity and peak systolic velocity measured by using phase-shift GRE technique were higher in the true than in the false channel in six patients with type B aortic dissections. Thus, the phase-shift GRE technique can be used to monitor the hemodynamic alterations in aortic dissection. Monitoring the velocity of flow in the false channel may be a method for predicting the likelihood of thrombosis of the false channel. Better prognosis in aortic dissection has been related to thrombus of the false channel.

Recent studies [36, 58, 59] in patients with aortic coarctation showed a correlation between peak pressure gradients as defined by using Doppler sonography peak velocity or catheter-gradient measurements and measurements of velocity obtained by using phase-shift GRE technique. Another approach to quantify the hemodynamic changes in coarctation has been pursued by Mohiaddin et al. [60], who evaluated the flow pattern in the ascending aorta and descending aorta 1 cm distal to the coarctation in patients and in volunteers. Flow volume, peak flow rate, and mean flow rate in the descending aorta of patients were significantly reduced compared with the rates in volunteers [60]. The value of these new parameters in the preoperative evaluation and postoperative follow-up in coarctation has to be established.

Blood-flow patterns in the ascending aorta of 24 volunteers have been investigated [25]. Near end-systole and during diastole, a channel of reversed, retrograde flow in the amount of 6.3% of the antegrade flow occurred at the posterior wall of the ascending aorta and proximally entered the region of the sinuses of Valsalva [25]. In a recent study [24], the same group described reduced or abnormal reversed flow in the ascending aorta of 17 patients with coronary artery disease.

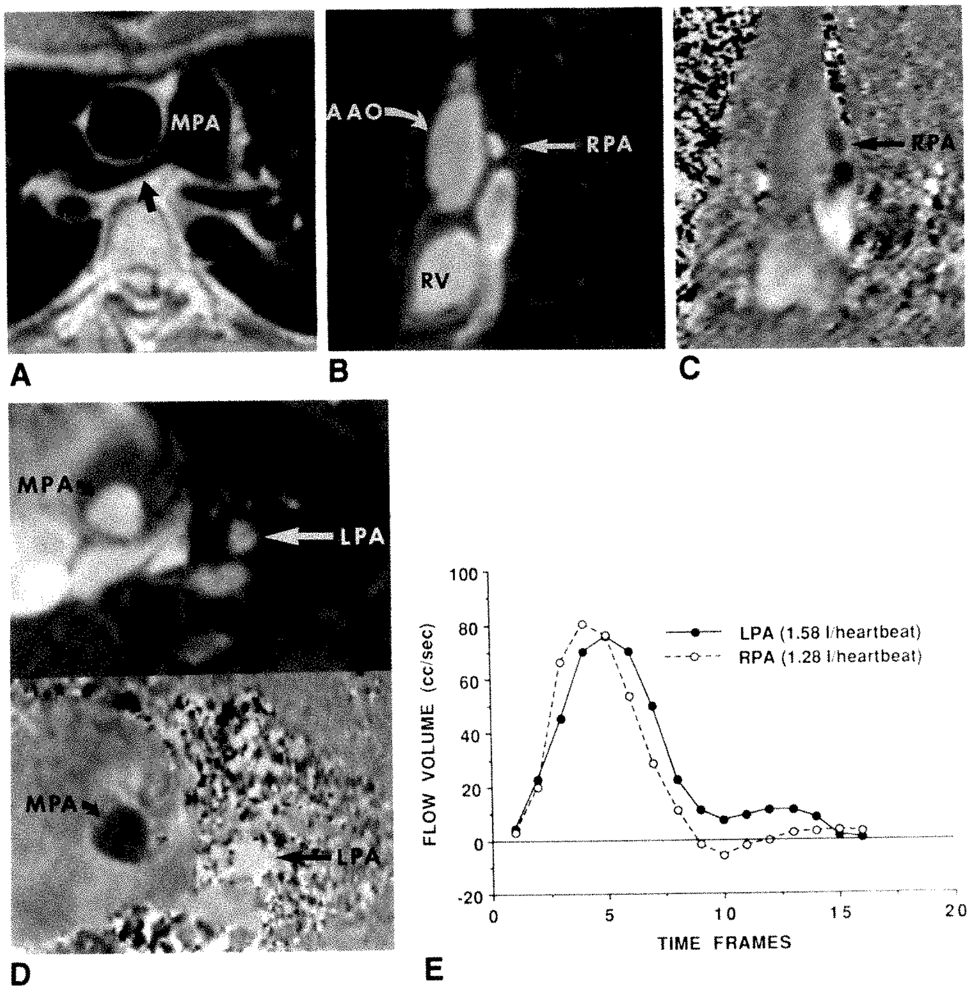

Fig. 5.—Axial T1-weighted SE (*A*), magnitude (*B*), and phase (*C*) MR images in a plane perpendicular to right pulmonary artery (RPA); magnitude (*top* in *D*) and phase (*bottom* in *D*) MR images in a plane perpendicular to left pulmonary artery (LPA); and flow profiles (*E*) of RPA and LPA in a 15-year-old patient after surgical repair of a partial transposition of great vessels. Whereas SE image clearly shows a stenosis of RPA (*arrow* in *A*), disparity between blood flow in LPA and flow in RPA is small. MPA = main pulmonary artery, RV = right ventricle, AAO = ascending aorta.

Additionally, these 17 patients had decreased aortic compliance compared with values found in volunteers and a group of trained athletes [24, 61]. Thus, besides coronary artery stenosis, abnormal aortic function and blood flow might be a second source of decreased myocardial perfusion [24].

Abdominal aorta. Blood flow in the abdominal aorta has been measured by using MR techniques: good correlations have been shown for measurements of flow velocities and flow volume obtained by using MR and Doppler sonography [27, 29]. The ability of phase-shift GRE techniques to provide two-dimensional velocity maps with good temporal resolution over the cross-sectional area of a vessel has focused attention in investigation of flow patterns in various segments of the abdominal aorta. Arterial sites subjected to retrograde flow at boundary layer separations are low-shear-stress regions thought to be at higher risk for the development of atherosclerotic plaques [62]. In this regard, the flow patterns at five different locations in the abdominal aorta of volunteers were characterized by using phase-shift GRE technique. A substantial amount of backflow at end-systole and diastole was observed at each level of the abdominal aorta; the net percentage of retrograde flow increased from 1.1% proximally to 14.4% below the origin of the renal arteries (Fig. 6) (Mostbeck GH, unpublished data). Retrograde flow was observed at the posterior wall of the abdominal aorta opposite the origin of the visceral arteries, an area with a high predilection for atherosclerotic plaques [62]. These results indicate the potential applicability of using phase-shift GRE MR imaging to investigate and monitor flow patterns in vivo and to correlate these patterns with the distribution of atherosclerosis.

Peripheral Arteries

A correlation was found between velocities and pulsatility indexes in the popliteal arteries of volunteers and patients with occlusive disease determined by using phase-shift GRE MR imaging and duplex Doppler sonography [63]. Morphologic and functional information can be acquired by combining MR angiographic images with phase-shift GRE techniques in the same subject [63]. Koch et al. [64] showed the effects of percutaneous transluminal angioplasty on mean velocity and the pulsatility index determined by using MR measurements of velocity. Phase-shift GRE imaging has been used to show

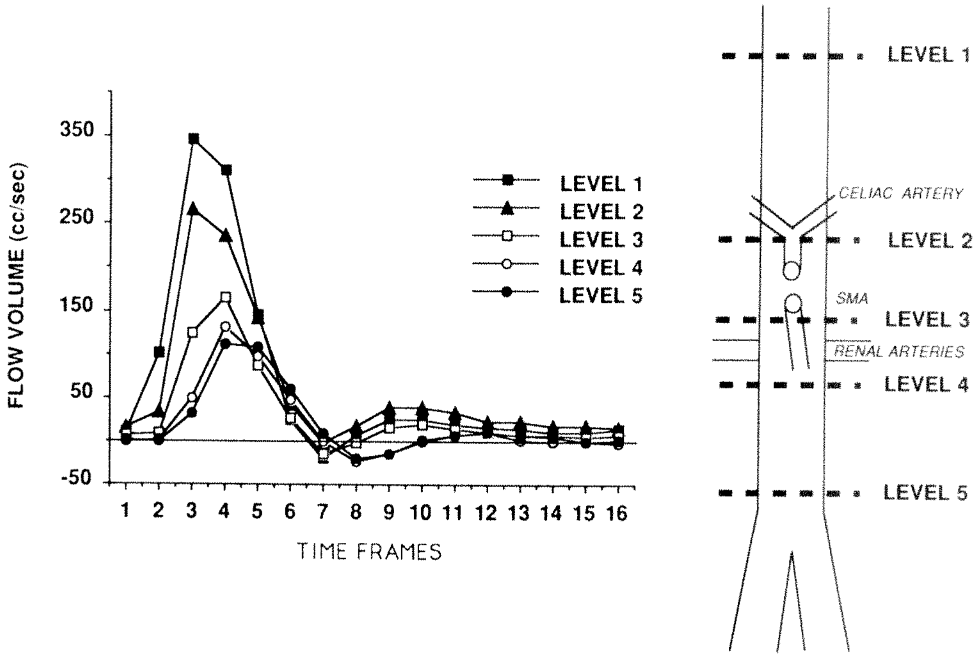

Fig. 6.—Diagram (*right*) of levels of measurements of flow in abdominal aorta and flow profiles (*left*) in a volunteer. Substantial net retrograde flow in early diastole occurs at each level. Note decrease in blood flow from proximal to distal levels due to visceral and renal perfusion.

the increase in flow in the anterior tibial artery after exercise of the anterior calf muscle [65]. However, only early preliminary data concerning MR measurements of blood flow in the peripheral arteries are available, and the clinical issues of these techniques have to be established.

Coronary Arteries and Bypass Grafts

Underwood and coworkers [49, 66] measured flow velocities in four aortocoronary bypass grafts in two patients. Peak diastolic velocities ranged from 2.0 to 31.6 cm/sec, the latter high velocity was measured in a graft connected to a large anterior descending artery [49, 66]. The small size of the coronary arteries and cardiac and respiratory motion create imposing difficulties for measurements of flow. The combination of flow-velocity mapping and echoplanar imaging might make it possible to measure flow in the coronary arteries [67].

Portal Vein

Duplex Doppler sonography is the primary noninvasive method for assessing hemodynamics in the portal vein and collateral vessels [68, 69]. Measurements of flow velocity and flow direction in the portal vein obtained by using bolus-tracking MR and assessment of hemodynamic responses to physiologic and pharmacologic interventions have been shown to be correlated with measurements obtained by using Doppler sonography [6, 8]. Volume flow in the portal vein of five volunteers, measured by using a phase-shift GRE technique, ranged from 0.71 to 1.12 l/min and increased by as much as 111% after food intake [70].

Future Directions

The full application of the phase-shift GRE technique for estimating gradients across valvular and great-vessel stenoses may require the use of short TEs, which cannot be achieved by conventional MR systems. Such short TE values depend on the use of higher magnetic gradients. To date, the gradients of most MR systems are in the range of 10 mT/m, whereas that required to achieve such short TEs might be 20 mT/m or more. Improvements in spatial resolution and the combination of velocity mapping and ultrafast imaging techniques such as echoplanar imaging may make it feasible to measure flow in small and mobile vessels such as the coronary arteries and coronary artery bypass grafts [67].

The ability to measure flow velocities across the atrioventricular valves at several time points makes it possible to estimate filling parameters of the left and right ventricle. Although this technique has not been used to assess diastolic function of the left and right ventricle, this is clearly a potential application. In contrast to Doppler sonography, phase-shift GRE MR imaging might be able to provide not only velocity measurements but also flow-volume data of left and right ventricular filling through the atrioventricular valves (Fig. 7). Because the velocities of regurgitant jets can potentially be measured, it is possible that measurements of the tricuspid regurgitant jet velocity can be used to estimate pulmonary arterial pressure in patients with pulmonary arterial hypertension.

Recently, real-time interactive color flow imaging has been applied with MR flow techniques, creating images akin to those of color Doppler sonography but lacking some of the drawbacks such as the inability to penetrate bones and air [71]. Further studies will define the ultimate role of MR flow

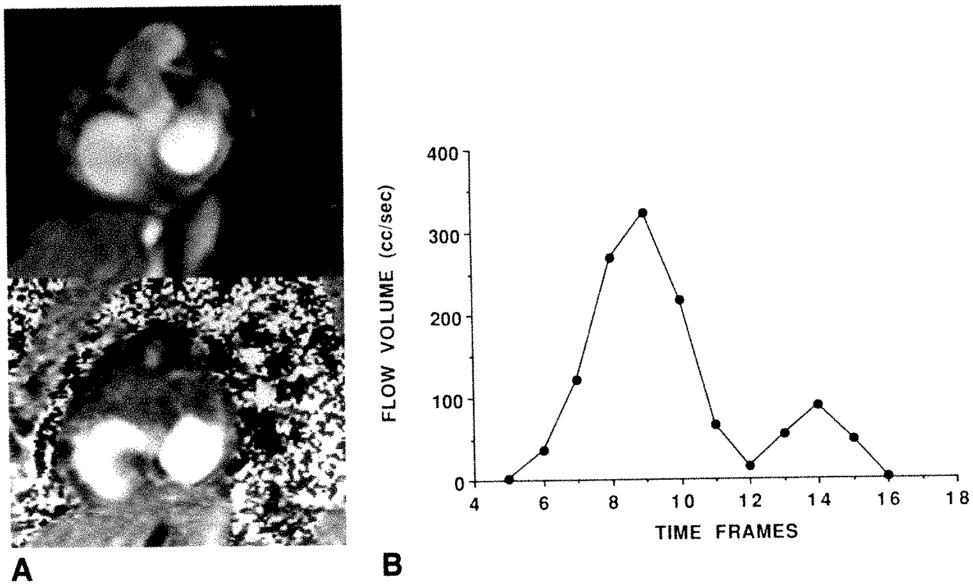

Fig. 7.—*A*, Magnitude (*top*) and corresponding phase (*bottom*) MR images in early diastole obtained in a double oblique imaging plane in the mitral valve annulus. Phase encoding was in slice-select direction. Inflow of blood from left atrium to left ventricle is seen as white signal on phase image. Mitral valve area and spatial mean velocity at each diastolic time frame were measured by tracing a region of interest on phase image.

***B*, Flow profile for mitral valve shows two flow peaks in early and late diastole similar to velocity profiles obtained by using Doppler sonography.**

techniques in the assessment of diseases affecting the cardiovascular system.

REFERENCES

1. Suryan G. Nuclear resonance in flowing liquids. *Proc Indian Acad Sci [A]* **1951**;33:107–111
2. Singer JR, Crooks LE. Nuclear magnetic blood flow measurements in the human brain. *Science* **1983**;221:654–656
3. Wehrli FW, Shimakawa A, MacFall Jr, Axel L, Perman W. MR imaging of venous and arterial flow by a selective saturation-recovery spin echo (SSRSE) method. *J Comput Assist Tomogr* **1985**;9:537–545
4. Wehrli FW, Shimakawa A, Gullberg GT, MacFall Jr. Time-of-flight MR flow imaging: selective saturation recovery with gradient refocusing. *Radiology* **1986**;160:781–785
5. Shimizu K, Matsuda T, Sakurai T, et al. Visualization of moving fluid: quantitative analysis of blood flow velocity using MR imaging. *Radiology* **1986**;159:195–199
6. Tamada T, Moriyasu F, Ono S, et al. Portal blood flow: measurement with MR imaging. *Radiology* **1989**;173:639–644
7. Feinberg DA, Crooks L, Hoenninger J, Arakawa M, Watts J. Pulsatile blood velocity in human arteries displayed by magnetic resonance imaging. *Radiology* **1984**;153:177–180
8. Edelman RR, Zhao B, Liu C, et al. MR angiography and dynamic flow evaluation of the portal venous system. *AJR* **1989**;153:755–760
9. Axel L, Shimakawa A, MacFall J. A time-of-flight method of measuring flow velocity by magnetic resonance imaging. *Magn Reson Imaging* **1986**;4:199–205
10. Edelman RR, Mattle HP, Kleefield J, Silver MS. Quantification of blood flow with dynamic MR imaging and presaturation bolus tracking. *Radiology* **1989**;171:551–556
11. Moran PR. A flow velocity zeugmatographic interlace for NMR imaging in humans. *Magn Reson Imaging* **1982**;1:197–203
12. Nayler GL, Firmin DN, Longmore DB. Blood flow imaging by cine magnetic resonance. *J Comput Assist Tomogr* **1986**;10:715–722
13. Axel L. Blood flow effects in magnetic resonance imaging. *AJR* **1984**;143:1157–1166
14. Wehrli FW. Time-of-flight effects in MR imaging of flow. *Magn Reson Med* **1990**;14:187–193
15. Bradley WG, Waluch V. Blood flow: magnetic resonance imaging. *Radiology* **1985**;154:443–450
16. Carr HY, Purcell EM. Effects of diffusion on free precession in NMR experiments. *Phys Rev* **1954**;94:630–638
17. Hahn EL. Detection of sea water motion by nuclear precession. *J Geophys Res* **1961**;65:776–783
18. Walker MF, Souza SP, Dumoulin CL. Quantitative flow measurement in phase contrast MR angiography. *J Comput Assist Tomogr* **1988**;12:304–313
19. Bryant DJ, Payne JA, Firmin DN, Longmore DB. Measurement of flow with NMR imaging using a gradient pulse and phase difference technique. *J Comput Assist Tomogr* **1984**;8:588–593
20. Meier D, Maier S, Boesiger P. Quantitative flow measurements on phantoms and on blood vessels with MR. *Magn Reson Med* **1988**;8:25–34
21. Pelc NJ, Shimakawa A, Glover G. Phase contrast cine MR (abstr). In: *Book of abstracts: Society of Magnetic Resonance in Medicine 1989*. Berkeley, CA: Society of Magnetic Resonance in Medicine, **1989**:101
22. Chang J-M, Friese K, Caputo GR, Kondo C, Higgins CB. MR measurement of blood flow in the true and false channel in chronic aortic dissection. *J Comput Assist Tomogr* **1991**;15:418–423
23. Bogren HG, Klipstein RH, Mohiaddin RH, et al. Pulmonary artery distensibility and blood flow patterns: a magnetic resonance study of normal subjects and of patients with pulmonary artery hypertension. *Am Heart J* **1989**;118:990–999
24. Bogren HG, Mohiaddin RH, Klipstein RK, et al. The function of the aorta in ischemic heart disease: a magnetic resonance and angiographic study of aortic compliance and blood flow patterns. *Am Heart J* **1989**;118:234–247
25. Bogren HG, Klipstein RH, Firmin DN, et al. Quantification of antegrade and retrograde blood flow in the human aorta by magnetic resonance velocity mapping. *Am Heart J* **1989**;117:1214–1222
26. Bogren HG, Buonocore MH, Gu W-Z. How blood flows in the aorta and other major arteries (abstr). In: *Book of abstracts: Society of Magnetic Resonance in Medicine 1991*. Berkeley, CA: Society of Magnetic Resonance in Medicine, **1991**:968
27. Maier SE, Meier D, Boesiger P, Moser UT, Vieli A. Human abdominal aorta: comparative measurements of blood flow with MR imaging and multigated Doppler US. *Radiology* **1989**;171:487–492
28. Kondo C, Caputo GR, Semelka R, Shimakawa M, Higgins CB. Right and left ventricular stroke volume measurements with velocity encoded cine NMR imaging: in vitro and in vivo evaluation. *AJR* **1991**;157:9–16
29. Matsuda T, Shimizu K, Sakurai T, et al. Measurement of aortic blood flow with MR imaging: comparative study with Doppler US. *Radiology* **1987**;162:857–861
30. Firmin DN, Nayler GL, Klipstein RH, Underwood SR, Rees RSO, Longmore DB. In vivo validation of MR velocity imaging. *J Comput Assist Tomogr* **1987**;11:751–756

31. Caputo GR, Kondo C, Masui T, et al. Right and left lung perfusion: in vitro and in vivo validation with oblique-angle, velocity-encoded cine MR imaging. *Radiology* **1991**;180:693–698
32. Martin AJ, Drake JM, Lemaire C, Henkelman RM. Cerebrospinal fluid shunts: flow measurements with MR imaging. *Radiology* **1989**;173: 243–247
33. Wedeen J, Rosen BR, Chesler D, Brady TJ. MR velocity imaging by phase display. *J Comput Assist Tomogr* **1985**;9:530–536
34. Didier D, Schouman-Claeys E, Breton E, Vignon P, Frija G. Quantitative assessment of average velocity in inferior vena cava by phase-display MR imaging: pulsed Doppler correlation. *J Comput Assist Tomogr* **1989**;13: 94–100
35. Firmin DN, Nayler GL, Kilner PJ, Longmore DB. The applications of phase shifts in NMR for flow measurements. *Magn Reson Med* **1990**;14: 230–241
36. Kilner PJ, Firmin DN, Rees RSO, et al. Valve and great vessel stenosis: assessment with MR jet velocity mapping. *Radiology* **1991**;178:229–235
37. Mostbeck GH, Caputo GR, Madjumdar S, Dulce M, Shimakawa A, Higgins CB. Assessment of vascular stenoses with MR jet phase velocity mapping at 1.5 T: in vitro validation (abstr). In: *Works in progress: Society of Magnetic Resonance in Medicine 1991*. Berkeley, CA: Society of Magnetic Resonance in Medicine, **1991**:1272
38. Caputo GR, Kondo C, Higgins CB. Quantification of blood flow using magnetic resonance imaging. In: Higgins CB, Hricak H, Helms CA, eds. *Magnetic resonance imaging of the body*. New York: Raven, **1992**: 339–349
39. Holen J, Aaslid R, Landmark K, Simonsen S. Determination of pressure gradient in mitral stenosis with a non-invasive ultrasound Doppler technique. *Acta Med Scand* **1976**;199:455–460
40. Buonocore MH, Gao L, Bogren H, Shimakawa A. Flow measurement with variable maximum velocity encoded in the RR interval (abstr). In: *Works in progress: Society of Magnetic Resonance in Medicine 1991*. Berkeley, CA: Society of Magnetic Resonance in Medicine, **1991**:804
41. Wolf RL, Ehman RL. Determinants of accuracy and precision in MR flow volumetry (abstr). In: *Works in progress: Society of Magnetic Resonance in Medicine 1991*. Berkeley, CA: Society of Magnetic Resonance in Medicine, **1991**:1157
42. Kilner P, Wann LS, Firmin D, Longmore D. Three directional magnetic resonance flow imaging of the human heart. *Dynam Cardiovasc Imaging* **1989**;2:104–109
43. Funari M, Caputo GR, Steiman D, Foster E, O'Sullivan M, Higgins CB. Quantification of aortic regurgitation by velocity encoded cine MR (abstr). In: *Book of abstracts: Society of Magnetic Resonance in Medicine 1991*. Berkeley, CA: Society of Magnetic Resonance in Medicine, **1991**:342
44. Sondergaard L, Thomsen C, Stahlberg F, et al. Quantification of flow through the mitral and aortic valves by magnetic resonance phase mapping (abstr). In: *Book of abstracts: Society of Magnetic Resonance in Medicine 1991*. Berkeley, CA: Society of Magnetic Resonance in Medicine, **1991**:341
45. Mohiaddin RA, Amanuma M, Kilner PJ, Pennell DJ, Manzara C, Longmore DB. MR phase-shift velocity mapping of mitral and pulmonary venous flow. *J Comput Assist Tomogr* **1991**;15:237–243
46. Galjee MA, Rossum ACv, Kamp O, Visser FC, Hofman M, Valk J. Reversed pulmonary venous flow measured by magnetic resonance phase velocity mapping: a marker of mitral insufficiency severity (abstr). In: *Book of abstracts: Society of Magnetic Resonance in Medicine 1991*. Berkeley, CA: Society of Magnetic Resonance in Medicine, **1991**:339
47. Rees S, Firmin D, Mohiaddin R, Underwood R, Longmore D. Applications of flow measurements by magnetic resonance velocity mapping to congenital heart disease. *Am J Cardiol* **1989**;64:953–956
48. Rebergen SA, Doornbos J, Guit GL, et al. Quantification of blood flow in the pulmonary arteries and Fontan conduits with velocity phase mapping (abstr). In: *Book of abstracts: Society of Magnetic Resonance in Medicine 1991*. Berkeley, CA: Society of Magnetic Resonance in Medicine, **1991**:338
49. Underwood SR, Firmin DN, Klipstein RH, Rees RSO, Longmore DB. Magnetic resonance velocity mapping: clinical application of a new technique. *Br Heart J* **1987**;57:404–412
50. Brenner LD, Steiman D, Caputo GR, Mostbeck GH, Cheitlin MD, Higgins CB. Velocity-encoded cine MRI measurement of left-to-right shunts and pulmonary blood flow in patients with congenital heart disease (abstr). In: *Book of abstracts: Society of Magnetic Resonance in Medicine 1991*. Berkeley, CA: Society of Magnetic Resonance in Medicine, **1991**:992
51. Kondo C, Caputo GR, Masui T, et al. Pulmonary hypertension: pulmonary flow quantification and flow profile analysis. *Radiology* **1992**;183:751–758
52. Mohiaddin RH, Hasegawa M, Rolleston S, Theodoropolous S, Underwood SR, Longmore DB. Pulmonary flow pulsatility and pulmonary arterial distensibility measured non-invasively by magnetic resonance velocity mapping in patients with single lung transplantation (abstr). In: *Book of abstracts: Society of Magnetic Resonance in Medicine 1991*. Berkeley, CA: Society of Magnetic Resonance in Medicine, **1991**:376
53. Amparo EG, Higgins CB, Hricak H, Sollitto R. Aortic dissection: magnetic resonance imaging. *Radiology* **1985**;155:399–406
54. von Schulthess GK, Augustiny N. Calculation of T2 values versus phase imaging for the distinction between flow and thrombus in MR imaging. *Radiology* **1987**;164:549–554
55. von Schulthess GK, Higgins CB. Blood flow imaging with MR: spin-phase phenomena. *Radiology* **1985**;157:687–695
56. Rumancik WM, Naidich DP, Chandra R, et al. Cardiovascular disease: evaluation with MR phase imaging. *Radiology* **1988**;166:63–68
57. Bogren HG, Underwood SR, Firmin DN, et al. Magnetic resonance velocity mapping in aortic dissection. *Br J Radiol* **1988**;61:456–462
58. Kilner PJ, Firmin DN, Manzarra CC, et al. Aortic coarctation assessed by magnetic resonance jet velocity mapping. *Circulation* **1990**;82-III[suppl]:63
59. Coulden RA, Jenkins JPR, Watson Y, Isherwood I. MRI and coarctation of the aorta: imaging structure and function (abstr). In: *Book of abstracts: Society of Magnetic Resonance in Medicine 1991*. Berkeley, CA: Society of Magnetic Resonance in Medicine, **1991**:980
60. Mohiaddin RH, Killner PJ, Firmin DN, Rees RSO, Underwood SR, Longmore DB. Characterization of flow by cine magnetic resonance velocity mapping in the thoracic aorta of patients with aortic coarctation (abstr). In: *Book of abstracts: Society of Magnetic Resonance in Medicine 1991*. Berkeley, CA: Society of Magnetic Resonance in Medicine, **1991**:340
61. Klipstein RH, Firmin DN, Underwood SR, Rees RSO, Longmore DB. Blood flow patterns in the human aorta studied by magnetic resonance. *Br Heart J* **1987**;58:316–323
62. Nguyen N, Haque A. Effect of hemodynamic factors on atherosclerosis in the abdominal aorta. *Atherosclerosis* **1990**;84:33–39
63. Caputo GR, Masui T, Chang JM, Gooding GA, Kondo CL, Higgins CB. MR angiography and blood flow measurements in the popliteal artery and trifurcational arteries. *Circulation* **1990**;82-III[suppl]:124
64. Koch M, Maier SE, Baumgartner I, et al. Magnetic resonance angiography and flow quantification in peripheral vessel disease before and after transluminal angioplasty (PTA) (abstr). In: *Book of abstracts: Society of Magnetic Resonance in Medicine 1991*. Berkeley, CA: Society of Magnetic Resonance in Medicine, **1991**:137
65. Meyer RA, Foley JM, Harkema SJ, Fisher MJ. MR angiographic study of peripheral vascular dynamics after acute exercise (abstr). In: *Book of abstracts: Society of Magnetic Resonance in Medicine 1991*. Berkeley, CA: Society of Magnetic Resonance in Medicine, **1991**:135
66. Underwood SR, Firmin DN, Klipstein RH, Rees RSO, Longmore DB. The assessment of coronary artery bypass grafts using oblique magnetic resonance imaging and velocity mapping (abstr). In: *Book of abstracts: Society of Magnetic Resonance in Medicine 1986*. Berkeley, CA: Society of Magnetic Resonance in Medicine, **1986**:47–48
67. Firmin DN, Klipstein RH, Hounsfield GL, Paley MP, Longmore DB. Echo-planar high-resolution flow velocity mapping. *Magn Reson Med* **1989**;12:316–327
68. Mostbeck GH, Wittich GR, Herold C, et al. Hemodynamic significance of the paraumbilical vein in portal hypertension: assessment with duplex US. *Radiology* **1989**;170:339–342
69. Ohnishi K, Saito M, Nakayama T, et al. Portal venous hemodynamics in chronic liver disease: effects of posture change and exercise. *Radiology* **1985**;155:757–761
70. Thomsen C, Stahlberg F, Henriksen O. Effect of food intake on portal vein volume flow (abstr). In: *Book of abstracts: Society of Magnetic Resonance in Medicine 1991*. Berkeley, CA: Society of Magnetic Resonance in Medicine, **1991**:809
71. Riederer SJ, Wright RC, Ehman RL, et al. Real-time interactive color flow MR imaging. *Radiology* **1991**;181:33–39

P24 464

Conquerors of Yellow Fever

Stefan C. Schatzki[1]

It was 1900. The Spanish American War had ended 2 years previously, and American soldiers were stationed in Cuba, where yellow fever had killed thousands of them, many more than were felled by Spanish bullets. As soldiers continued to become ill and die from this poorly understood disease, it became clear that action was required. This crisis led to one of the most extraordinary dramas of modern medicine.

That same year, a 49-year-old Army surgeon, Major Walter Reed, was appointed to head the Yellow Fever Commission, which was sent to Havana. Joining him on the commission was the bacteriologist Dr. Jesse W. Lazear, the Army surgeon and bacteriologist James Carroll, and the Cuban surgeon Aristides Agramonte, who served as the commission's pathologist. Long before 1900, Dr. Carlos Finlay, a Cuban physician, had argued strongly that the mosquito was the vector that carried the disease. No one had listened to Dr. Finlay until the commission, having no other plausible theories to test, decided to examine his hypothesis. Dr. Lazear injected Dr. Carroll with an infected mosquito. Dr. Carroll contracted the disease, but recovered. However, shortly thereafter, Lazear was bitten accidentally by a mosquito, contracted the disease, and died within 2 weeks.

All participants in the experiments were quarantined. Humans were needed as subjects because animals were not susceptible to yellow fever. Pvt. John Kissinger and John Moran volunteered to be bitten by several infected mosquitos. Kissinger contracted yellow fever and survived; Moran remained well. Because the disease was thought by many to be spread directly from patients and their contaminated surroundings, three volunteers, Dr. Robert Cooke and Pvts. Levi Folk and Warren Jernegan, agreed to live in a dirty building and to wear and use infected clothing and bedding from patients who had died. They did not become ill. Why did Moran not get ill? Was there natural immunity? Moran again volunteered. He moved to a clean, isolated building that contained infected mosquitos. This time the yellow murderer struck. Moran became ill, but recovered. Within a few months, Reed and his team proved conclusively Finlay's hypothesis that yellow fever was transmitted by the mosquito. Shortly after, the mosquito was eradicated from Cuba and the epidemic stopped. Dr. William Gorgas was then able to use this discovery to eradicate yellow fever from the Canal Zone, making it possible to build the Panama Canal.

In 1939, Dean Cornwell (1883–1960), one of the country's best known illustrators, was commissioned by Wyeth Laboratories to produce a series of paintings called *Pioneers of American Medicine*. Cornwell's work had regularly appeared in most of America's popular periodicals. He had illustrated books by Somerset Maugham, Pearl Buck, Ernest Hemingway, A. J. Cronin, and Edna Ferber, and painted many important murals for public buildings. To prepare for the painting that he entitled *Conquerors of Yellow Fever*, Cornwell extensively studied government records, interviewed surviving participants, and obtained authentic uniforms and military equipment to help him complete his task.

The painting depicts Dr. Jesse Lazear inoculating Dr. James Carroll with an infected mosquito. Standing at the head of the table, all in white, is the leader of the commission, Walter Reed. To the left behind Lazear in civilian clothes and with white mutton-chop whiskers stands Dr. Carlos Finlay. At his side is Dr. Agramonte. The other figures include General Leonard Wood, Governor General of Cuba, who provided the funding for the research of the commission; Dr. Cooke, Pvt. Jernegan, Pvt. Kissinger, Moran, and some of the Army physicians stationed in Cuba. Although Cornwell's picture illustrates a group of people who were never together in one place at any time, the painting commemorates the extraordinary scientific acumen and courageous volunteer efforts of the men who conquered the devastating disease of yellow fever. Their heroism, and particularly the wisdom of their leader, was recognized by the United States Army when it named its leading medical center after Walter Reed.

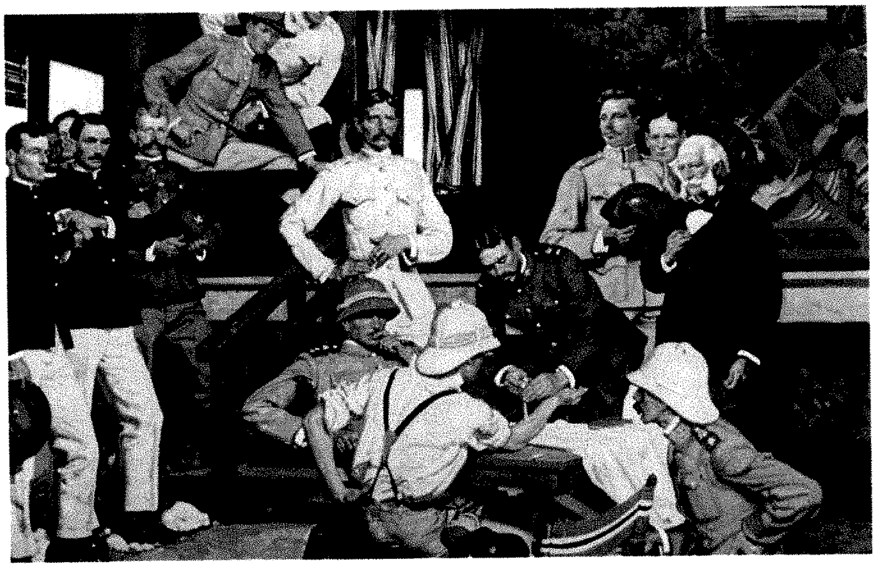

Dean Cornwell (1883–1960). *Conquerors of Yellow Fever*, 1939. Oil on canvas, 65 × 58 in. Courtesy of Wyeth-Ayerst Laboratories, Philadelphia, PA.

---

[1] Department of Radiology, Mount Auburn Hospital, 330 Mount Auburn St., Cambridge, MA 02238.

AJR **159:462, September 1992** 0361-803X/92/1593-0462 © American Roentgen Ray Society

Diagnosis of Bronchiolitis Obliterans in Heart-Lung Transplantation Patients:

Importance of Bronchial Dilatation on CT

Daniel Lentz[1]
Colleen J. Bergin[1]
Gerald J. Berry[2]
Christopher Stoehr[3]
James Theodore[3]

OBJECTIVE. The purpose of this study was to evaluate the significance of bronchial dilatation identified on high-resolution CT scans obtained after heart-lung transplantation. Bronchial dilatation has been identified on pathologic specimens and on high-resolution CT scans of patients with severe bronchiolitis obliterans after lung transplantation, but this finding has not previously been systematically studied as a manifestation of this complication.

MATERIALS AND METHODS. We studied the high-resolution CT scans of 16 patients who had had heart and lung transplantation at least 1 year before, and compared the percentage of dilated bronchi with evidence of small airways disease shown on pulmonary function tests.

RESULTS. We found a close correlation between the percentage of bronchi in the lower lobes that were dilated and the percent predicted forced expiratory volume in 1 sec, forced vital capacity, and forced expiratory flow between 25% and 75% of vital capacity. No other feature identified on high-resolution CT scans correlated with pulmonary function abnormalities.

CONCLUSION. We conclude that dilatation of the lower lobe bronchi is a good indicator of bronchiolitis obliterans in this population, and that the percentage of dilated bronchi generally increases with increasing pulmonary dysfunction.

***AJR* 159:463–467, September 1992**

Since 1981, more than 85 patients have undergone heart-lung transplantation at Stanford University Medical Center. Of the patients receiving transplants before 1990, approximately 65% survived longer than 1 year, and one patient is alive 9 years after transplantation.

Early detection and treatment of infection and organ rejection are critical in decreasing morbidity and mortality from these complications of transplantation. In 1984, Burke et al. [1] reported the occurrence of bronchiolitis obliterans in long-term survivors of heart-lung transplantation. The cause of this relatively rapid, progressive form of small airways disease remains unclear, but it may be related to organ rejection [2]. Early aggressive treatment has stabilized respiratory function in some patients [1, 3–5]. Therefore, prompt detection of bronchiolitis obliterans in minimally symptomatic or asymptomatic heart-lung transplantation patients is important. Although pulmonary function tests are sensitive in detecting diminishing airway function, they can be nonspecific. Transbronchial biopsy may show specific histologic abnormalities, but in a patchy process such as bronchiolitis obliterans, this relatively invasive test may lack sensitivity (Kramer MR, unpublished data). The chest radiograph is useful for detecting infection and acute lung rejection, but provides no specific findings of bronchiolitis obliterans [1, 6–8].

High-resolution CT is more sensitive than chest radiography is in detecting pulmonary abnormalities, and it is the most sensitive noninvasive test for detecting bronchial dilatation [9]. Bronchiectasis has been reported in lung and heart-lung

Received February 14, 1992; accepted after revision March 23, 1992.

[1] Department of Radiology, S068A, Stanford University Medical Center, 300 Pasteur Dr., Stanford, CA 94305-5105. Address reprint requests to C. J. Bergin.

[2] Department of Pathology, Stanford University Medical Center, Stanford, CA 94305-5105.

[3] Department of Medicine, Division of Respiratory Medicine, Stanford University Medical Center, Stanford, CA 94305-5105.

0361-803X/92/1593-0463
© American Roentgen Ray Society

transplantation patients with bronchiolitis obliterans [10, 11], but the relationship between bronchial dilatation and bronchiolitis obliterans has not been systematically studied. The objective of our study, therefore, was to evaluate the significance of bronchial dilatation and to assess the diagnostic value of high-resolution CT in detecting features predictive of bronchiolitis obliterans.

Materials and Methods

All patients who underwent heart-lung transplantation between 1982 and 1989 in whom high-resolution CT and pulmonary function tests were performed during routine posttransplantation evaluation were considered for this study. These studies were not performed to evaluate specific signs and symptoms. Because acute infection can influence lung function and CT findings, patients with clinical or radiologic evidence of pneumonia were excluded. In addition, to avoid early postoperative complications including acute lung rejection, we included only those studies done 1 year or more after transplantation. These criteria allowed inclusion of 16 heart-lung transplant recipients who had evaluations 12–88 months after transplantation. Since high-resolution CT scans were not obtained in the early 1980s, patients included in this study were generally those in whom transplantation was performed in the latter part of the decade. Routine evaluations included pulmonary function tests, high-resolution CT scans, chest radiographs, and, in many cases, bronchoscopy with transbronchial biopsy. Of these patients, seven had signs, symptoms, and results of pulmonary function tests consistent with the diagnosis of bronchiolitis obliterans. In six patients, including five with clinical bronchiolitis obliterans, two high-resolution CT studies were performed 8–16 months apart.

High-Resolution CT Scans

All high-resolution CT scans were obtained with a GE 9800 scanner (General Electric, Milwaukee, WI). Images were obtained at end-inspiration with 1.5-mm collimation, 140 kVp, 170 mAs, and 2–3 sec scan time, and were reconstructed with a high-spatial-resolution algorithm (bone algorithm). Each study consisted of 12 images, six with the patient supine and six with the patient prone, with three above and three below the carina. High-resolution CT scans were obtained within 1 week of the pulmonary function tests and within 2 days of the chest radiographs. The high-resolution CT scans were reviewed by two radiologists who did not know the patient's respiratory status. For each high-resolution CT scan, bronchial wall dilatation was evaluated on the two slices showing the greatest number of bronchi in cross section, one slice above and one slice below the carina. In each patient, supine and prone high-resolution CT scans were evaluated together. By visual examination, and with the use of calipers in subtle cases, bronchi that were greater in diameter than their accompanying vessels were considered dilated. The number of dilated bronchi was recorded as a proportion of the total number of bronchi viewed in cross section on each slice. Bronchial wall thickening, pleural thickening, septal lines, parenchymal bands, nodules, and air-space abnormalities also were noted.

Chest Radiographs

Frontal and lateral views of the chest obtained within 2 days of the corresponding high-resolution CT scan were reviewed by two radiologists. The radiographs were examined for air-space or interstitial abnormalities, bronchiectasis, bronchial wall thickening, and pleural thickening.

Pulmonary Function Tests

Spirometry included measurement of percent predicted forced expiratory volume in 1 sec (FEV_1); forced vital capacity (FVC); forced expiratory flow between 25% and 75% of vital capacity (FEF_{25-75}), also known as the maximal midexpiratory flow; and flow-volume loops. The gold standard that we accepted for clinical bronchiolitis obliterans was persistent (>3 months), irreversible small airways disease in the absence of pulmonary infection together with the presence of characteristic symptoms such as increasing dyspnea. The pulmonary function test that was considered to be most consistent with the diagnosis of bronchiolitis obliterans was an FEF_{25-75} persistently less than 30% of the predicted value with caving of the expiratory flow pattern [2]. FEF_{50}/FVC had to be less than or equal to 0.7 to correct for lung volume reduction. These pulmonary function test criteria have been predictive of bronchiolitis obliterans found at autopsy (Theodore J, unpublished data). Given the irregular distribution of bronchiolitis obliterans and the resultant sampling error in transbronchial biopsy, histologic confirmation of bronchiolitis obliterans was not required to make the diagnosis. Imaging studies were not performed to establish the diagnosis of bronchiolitis obliterans, but rather to exclude the presence of infection. The Spearman rank correlation test was used to evaluate the relationship between the high-resolution CT findings and each measurement of pulmonary function (percent predicted FEV_1, FVC, and FEF_{25-75}).

Bronchoscopy and Transbronchial Biopsy

Thirteen of the 16 patients, including the seven patients with clinical bronchiolitis obliterans, had bronchoscopy and transbronchial biopsy at the time of their routine evaluations. Bronchoscopy was performed with a fiberoptic bronchoscope under fluoroscopic control. Multiple transbronchial lung biopsies were performed bilaterally, usually randomly from the lower lobes.

Results

High-resolution CT scans of the seven patients who had clinical bronchiolitis obliterans showed only one consistent finding that was identified on both prone and supine images: bronchial wall dilatation relative to the size of adjacent vessels, predominantly in the lower lobes (Fig. 1). Six of these seven patients had this finding; the other patient had no bronchial dilatation until 10 months after the clinical diagnosis of bronchiolitis obliterans was made. The percentage of dilated lower lobe bronchi in these patients varied from 50% to 100%. High-resolution CT scans of the nine patients without clinical bronchiolitis obliterans showed no evidence of lower lobe bronchial dilatation (Fig. 2). The percentage of dilated lower lobe bronchi correlated with the severity of bronchiolitis obliterans as measured by the pulmonary function tests: FEV_1 ($r = -.735$, $p = .001$), FEV_1/FVC ($r = -.756$, $p = .001$), and FEF_{25-75} ($r = -.600$, $p = .01$).

Dilated upper lobe bronchi were noted in five patients with clinical bronchiolitis obliterans, but also were noted in five patients without bronchiolitis obliterans. More upper lobe bronchi were dilated in patients with clinical and functional evidence of bronchiolitis obliterans (0–100%; mean, 50%) than in patients without clinical bronchiolitis obliterans (0–40%; mean, 35%).

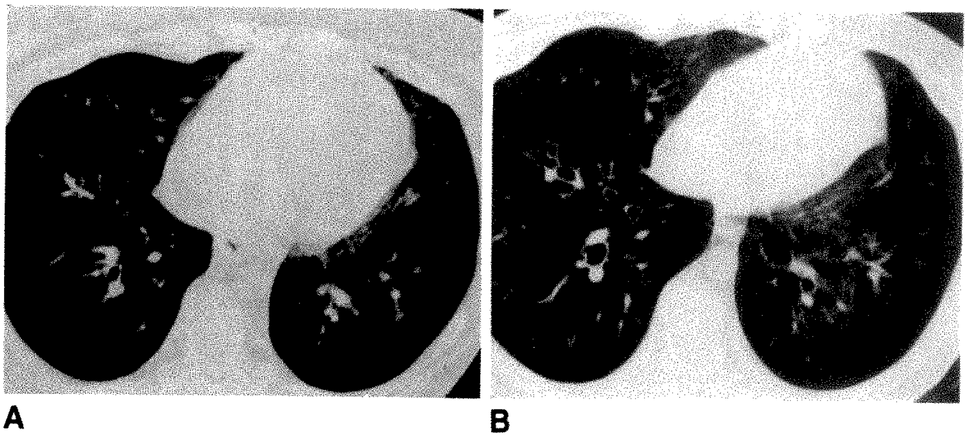

Fig. 1.—*A* and *B*, High-resolution CT scans of a 39-year-old woman before (*A*) and after (*B*) onset of clinical bronchiolitis obliterans show development of bronchial dilatation in lower lobes during a 7-month interval.

The bronchi visible in cross section were primarily segmental and subsegmental branches, although in patients with severe bronchiolitis obliterans, dilatation appeared to affect all bronchial structures. The percentage of dilated lower lobe bronchi increased with time in four of the five patients with bronchiolitis obliterans in whom two sequential high-resolution CT scans were obtained 8–16 months (mean, 11 months) apart; in the fifth patient, all lower lobe bronchi were dilated on the initial scan (Fig. 3). Although bronchi enlarged, there was no measurable interval change in size of lower lobe vessels in this group of patients.

Other high-resolution CT findings, such as bronchial wall thickening, septal lines, and parenchymal bands, were occasionally noted, but they did not correlate with the presence of bronchiolitis obliterans.

None of the chest radiographs obtained at the time of pulmonary function tests and high-resolution CT scans showed evidence of active infection. Radiographs of two patients with clinical bronchiolitis obliterans showed dilated bronchi in the lower lobes. Extensive bronchial dilatation was visible on the high-resolution CT scans. The remainder of the radiographs showed only stable postsurgical changes and minimal chronic pleural thickening.

Transbronchial biopsy was performed on 10 occasions in the seven patients with clinical bronchiolitis obliterans, but only one of the biopsies in this group showed histologic findings characteristic of bronchiolitis obliterans. The remainder showed acute and chronic bronchitis. Transbronchial biopsies obtained on six occasions in the patients without clinical evidence of the disease showed no histologic evidence of bronchiolitis obliterans; one biopsy revealed mild nonspecific chronic inflammatory infiltrates. Two of the patients with clinical bronchiolitis obliterans have subsequently died, and examination at autopsy showed findings characteristic of bronchiolitis obliterans in both cases.

Discussion

Bronchiolitis obliterans is a nonspecific reaction of the lung to airway injury that has been reported after pulmonary damage caused by inhalation of toxic agents, infection (especially viral), ischemia, and autoimmune diseases [12–14].

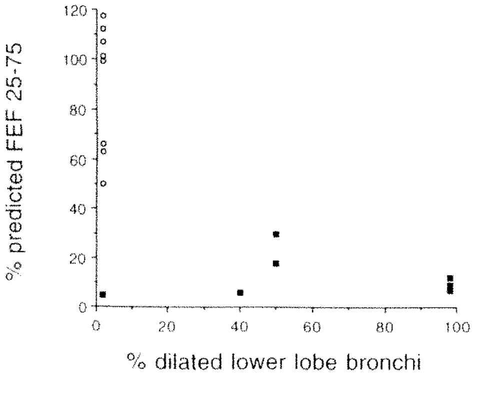

Fig. 2.—Relationship between percent predicted forced expiratory flow between 25% and 75% of vital capacity (FEF 25-75) and percentage of dilated lower lobe bronchi. For patients who had more than one high-resolution CT examination, only data from initial scans are included. Note that lower lobe bronchi are not dilated in patients without clinical bronchiolitis obliterans (*circles*), but in one patient with clinical bronchiolitis obliterans (*squares*), bronchial dilatation was not visible on initial high-resolution CT scan.

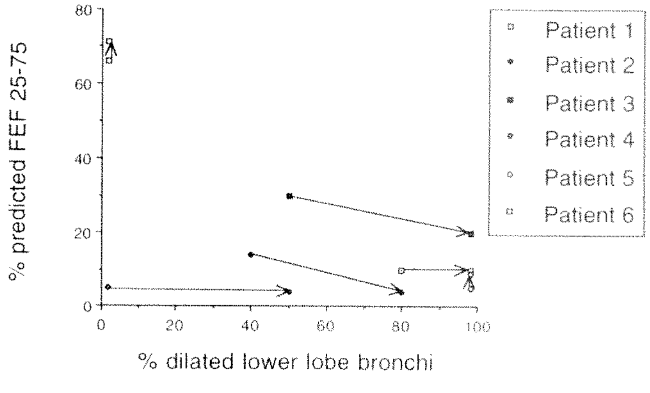

Fig. 3.—Change in percent predicted forced expiratory flow between 25% and 75% of vital capacity (FEF 25-75) correlated with change in percentage of dilated lower lobe bronchi in six patients who had two high-resolution CT examinations. Proportion of dilated lower lobe bronchi increased in all patients with bronchiolitis obliterans except one in whom all bronchi were dilated on initial scan.

Bronchiolitis obliterans also occurs in bone marrow transplantation patients with chronic graft-vs-host reaction [15]. Histologic sections of lung biopsies in patients with bronchiolitis obliterans show postinflammatory fibrosis with plugs of granulation tissue and debris within terminal and respiratory bronchioles. The resultant pulmonary impairment is obstructive with a coexistent, but less prominent, restrictive component. Bronchiolitis obliterans as a late complication of heart-lung transplantation was first reported by Burke et al. [1] in 1984, and is known to affect 30–50% of heart-lung transplant recipients [16, 17]. The onset of bronchiolitis obliterans in this population is insidious, occurring months to years after transplantation, and frequently is heralded by nonspecific pulmonary signs and symptoms. With delayed diagnosis and treatment, deterioration of pulmonary function can be rapid and fatal.

The cause of bronchiolitis obliterans in heart-lung transplantation patients is unclear, but some evidence suggests a possible relationship with chronic or repeated subacute rejection [2]. Sporadic success has been reported in reversing or stabilizing deteriorating pulmonary function in patients with bronchiolitis obliterans by early treatment with high doses of corticosteroids [1, 2, 4, 5]. The prevalence of this disease also has been shown to decrease with the addition of azathioprine to the immunosuppressive regimen [2]. As effective treatment depends on early detection, frequent tests, including pulmonary function tests, transbronchial lung biopsies, and radiologic examinations, are performed on heart-lung transplantation patients in an effort to detect this complication at an early stage.

The clinical diagnosis of bronchiolitis obliterans is made when dyspnea and irreversible obstructive small airways disease develop in the absence of infection 3 or more months after transplantation. A decrease in the percent predicted FEF_{25-75} is a measure of small airways disease and is a particularly sensitive indicator of bronchiolitis obliterans. In the appropriate clinical setting, an FEF_{25-75} remaining less than 30% predicted is a strong clinical indicator of the disease. Unfortunately, changes in pulmonary function alone, especially in the early stages, are not specific, and therefore additional studies are often performed to confirm the diagnosis. Radiographic findings are generally nonspecific. Radiographic findings that have been reported include patchy peribronchial and interstitial opacities and pleural thickening [1, 7–9]. Transbronchial biopsy also is used at some institutions to establish a diagnosis, but we and others have found this to be insensitive, presumably because of sampling error.

Previous studies have noted bronchial dilatation on high-resolution CT scans, chest radiographs, and pathologic specimens of lung transplantation patients with bronchiolitis obliterans [1, 7, 12, 16]. Hruban et al. [10] described bronchial dilatation that was visible on high-resolution CT scans of lung specimens obtained from heart-lung transplantation patients. Morrish et al. [11] also reported peripheral bronchiectasis on high-resolution CT scans of lung transplant recipients with bronchiolitis obliterans. However, neither of these studies showed a definite relationship between dilated bronchi and posttransplantation bronchiolitis obliterans.

Our results suggest a strong association between high-resolution CT evidence of lower lobe bronchial dilatation and the development of bronchiolitis obliterans. In addition, in patients in this series, the percentage of dilated lower lobe bronchi increased with time and severity of pulmonary dysfunction. Interestingly, Hruban et al. [10] also noted that bronchial dilatation was prominent in the lower lobes with relative sparing of the upper lobes in one patient. In our study, lower lobe bronchi were not dilated in patients without clinical evidence of bronchiolitis obliterans. One patient had pulmonary function evidence of bronchiolitis obliterans before bronchial wall dilatation developed, suggesting that pulmonary function tests may be more sensitive than high-resolution CT in detecting bronchiolitis obliterans. However, we have subsequently also observed the reverse situation in a patient who had bronchial dilatation on high-resolution CT scans 3 months before deterioration in pulmonary function. High-resolution CT may thus provide a noninvasive method for corroborating a suspected diagnosis of bronchiolitis obliterans after heart-lung transplantation. Our results indicate that high-resolution CT findings of bronchial dilatation correlate more closely with pulmonary function evidence of bronchiolitis obliterans than either chest radiographic abnormalities or histologic specimens obtained by transbronchial biopsy.

Because this was a retrospective study involving relatively few patients, we have not definitively determined if high-resolution CT evidence of bronchial dilatation is an early or late finding in bronchiolitis obliterans. However, we have shown that bronchial dilatation is reliable in predicting the disease, except when there is active pulmonary infection. In two of the patients excluded from this study because of concurrent infection, high-resolution CT scans showed bronchial dilatation that resolved with successful treatment of acute pulmonary infection. The reliability of using bronchial dilatation as an indicator of bronchiolitis obliterans depends on consistency in the size of vessels over time. This may not always be a valid assumption in this population of patients; however, in the small group of patients who had more than one high-resolution CT scan, we found no measurable change in the size of the lower lobe vessels over time. More patients need to be evaluated to determine the consistency of pulmonary vessel size.

We prefer *bronchial dilatation* to *bronchiectasis* when referring to heart-lung transplantation patients to avoid confusion with the clinical entity of bronchiectasis. In addition to bronchial dilatation, bronchial wall thickening and peripheral pulmonary vascular attenuation have been noted in lung transplantation patients with bronchiolitis obliterans [18]. We also observed these features in patients after heart-lung transplantation, but because of the current lack of standard criteria for determining abnormal bronchial thickening and peripheral vascularity, we did not systematically evaluate these features.

We conclude that in heart-lung transplantation patients, high-resolution CT evidence of lower lobe bronchial dilatation in the absence of infection is more sensitive in predicting the presence of bronchiolitis obliterans than are chest radiographs or transbronchial biopsy.

REFERENCES

1. Burke CM, Theodore J, Dawkins KD, et al. Post-transplant obliterative bronchiolitis and other late lung sequelae in human lung transplantation. *Chest* **1984**;86:824–829
2. Theodore J, Starnes VA, Lewiston NJ. Obliterative bronchiolitis. *Clin Chest Med* **1990**;11:309–321
3. Allen WD, Burke CM, McGregor CGA, Baldwin JC, Jamieson SW, Theodore J. Steroid responsive bronchiolitis after human heart-lung transplantation. *J Thorac Cardiovasc Surg* **1986**;92:449–451
4. Glanville A, Baldwin J, Burke CM, Theodore J, Robin ED. Obliterative bronchiolitis after heart-lung transplantation: apparent arrest by augmented immunosuppression. *Ann Intern Med* **1987**;107:300–304
5. McCarthy P, Starnes V, Theodore J, Stinson EB, Oyer PE, Shumway NE. Improved survival following heart-lung transplant. *J Thorac Cardiovasc Surg* **1990**;99:54–60
6. Skeens JL, Fuhrman CR, Yousem SA. Bronchiolitis obliterans in heart-lung transplantation patients: radiologic findings in 11 patients. *AJR* **1989**;153:253–256
7. Gosink BB, Friedman RJ, Liebow AA. Bronchiolitis obliterans: roentgenologic-pathologic correlation. *AJR* **1973**;117:816–832
8. Holland SA, Hutton LC, McKenzie FN. Radiologic findings in heart-lung transplantation; a preliminary experience. *Can Assoc Radiol J* **1989**;40: 94–97
9. Lynch DA, Brasch RC, Hardy KA, Webb WR. Pediatric pulmonary disease: assessment with high resolution ultrafast CT. *Radiology* **1990**;176: 243–248
10. Hruban RH, Ren H, Kuhlman JE, et al. Inflation-fixed lungs: pathologic-radiologic correlation of lung transplantation. *J Comput Assist Tomogr* **1990**;14:329–335
11. Morrish WF, Herman SJ, Weisbord GL, Chamberlain DW. Bronchiolitis obliterans after lung transplantation: findings at chest radiography and high-resolution CT. *Radiology* **1991**;179:487–490
12. Ramirez RJ, Dowell AR. Silo filler's disease: nitrogen-oxide induced lung injury. *Ann Intern Med* **1971**;74:569–576
13. Epler GR, Snider GL, Gaensler EA, Cathcart ES, Fitzgerald MX, Carrington CB. Bronchiolitis and bronchitis in connective tissue diseases. *JAMA* **1979**;242:528–532
14. King TE. Bronchiolitis obliterans. *Lung* **1989**;167:69–93
15. Ralph DD, Springmeyer SC, Sullivan KM, et al. Rapidly progressive airflow obstruction in marrow transplant recipients. *Am Rev Respir Dis* **1984**;129:641–644
16. Griffith BP, Hardesty RL, Trento A, et al. Heart-lung transplantation: lessons learned and future hopes. *Ann Thoracic Surg* **1987**;43:6–16
17. Yousem SA, Burke CM, Billingham ME. Pathologic pulmonary alterations in long-term human heart-lung transplantation. *Hum Pathol* **1985**;16: 911–923
18. Herman SJ. Radiologic assessment after lung transplantation. *Clin Chest Med* **1990**;11:333–346

Book Review

High-Resolution CT of the Lung. By W. Richard Webb, Nestor L. Müller, and David P. Naidich. New York: Raven, 176 pp., 1992. $79

This book is the first devoted to examination of the lung with high-resolution images. The authors have been active contributors to the pulmonary radiology literature in general and to the literature on high-resolution lung CT in particular. The book is augmented by illustrations of gross and histologic specimens provided by a surgical pathologist.

The book has 10 chapters. Chapters on technique, normal anatomy, and basic high-resolution CT findings are followed by ones on specific diseases grouped according to their high-resolution CT patterns. The final chapter deals with clinical usefulness. The book has more than 250 illustrations and more than 500 references, which include material published in 1991.

Chapter 2, on high-resolution CT technique, deals with the parameters that will provide optimal images. Artifacts are discussed, and scanning protocols are given. Chapter 3, "Normal Lung Anatomy," emphasizes the secondary lobule and relates the anatomy to findings on high-resolution CT scans. Scans of patients and pathologic specimens, drawings, and text are used effectively. Chapter 4, on high-resolution CT findings in lung disease, is the longest chapter. The basic findings in lung disease are illustrated. The origin of signs and differential diagnosis are emphasized. Sections on reticular opacities, nodular opacities, increased opacity, and decreased opacity and a section on the distribution of lung abnormalities review the findings of interstitial, air-space, and airway disease. Each of these patterns later becomes the subject of a chapter on the high-resolution CT findings of individual diseases that produce that pattern. Chapter 5, "Diseases Characterized Primarily by Reticular Opacities," considers the interstitial pneumonias, collagen diseases, and asbestosis. The use of high-resolution CT in diagnosis, planning of biopsy sites, and evaluation of stage and extent of disease is detailed. Chapter 6, "Diseases Characterized Primarily by Reticulonodular or Nodular Opacities," deals with lymphangitic metastases, sarcoidosis, silicosis, and pneumoconiosis of coal workers. Chapter 7, "Diseases Characterized Primarily by Increased Lung Opacity," deals with extrinsic alveolitis, chronic eosinophilic pneumonia, bronchiolitis obliterans with organizing pneumonia, alveolar proteinosis, and diffuse infections. Chapter 8, "Diseases Characterized Primarily by Cystic Abnormalities, Lung Destruction, or Decreased Lung Opacity," considers histiocytosis X, lymphangiomyomatosis, emphysema, bronchiectasis, and bronchiolitis obliterans. Chapter 9, on high-resolution CT of the normal and abnormal pleura, reviews the normal pleural and chest wall anatomy and then discusses pleural plaques. The final chapter, on the clinical usefulness of high-resolution CT, discusses the correlation of high-resolution CT findings with findings from conventional CT, chest radiography, pulmonary function studies, gallium scanning, and bronchoalveolar lavage. The book ends by summarizing situations (occult disease, diagnosis without histologic conformation, determination of disease activity, selecting optimum biopsy sites) in which the authors have found high-resolution CT valuable. A short glossary of terms precedes an index.

This book was a pleasure to read. The style of writing is uniform, clear, and concise from beginning to end. The arrangement of subjects is logical and easy to follow. Diagrams and pathologic illustrations are well chosen and enhance discussions throughout the book. The CT illustrations are of uniformly high quality, and the illustrated anatomy and pathologic changes are clearly visible and labeled well. The book is practical and emphasizes clinical applications. The high-resolution CT findings of individual diseases are summarized in tables that highlight the most important findings.

Thin-collimation CT scans reconstructed with an edge-enhancing algorithm have been used to examine the lung since the mid 1980s, but only more recently has high-resolution CT come to be used widely. This is probably related to advances in CT hardware, more experience in and documentation of specific uses of this imaging technique, and increasing familiarity with the anatomy as displayed on high-resolution CT scans.

Lung morphology is shown in more detail by high-resolution CT than by any other imaging method. In addition, as the authors of this book say in their introduction, "It can take years to learn to accurately diagnose interstitial lung disease on chest radiographs (and some of us are still struggling to learn), or to teach others how to do it, but experience with a relatively small number of HRCT scans can allow you to make some diagnoses with a high degree of confidence." *High-Resolution CT of the Lung* will provide a superb foundation for anyone who is beginning to use this imaging technique and will be a valuable resource for experienced radiologists and pulmonologists as well. This outstanding textbook should be available to all radiology residents because of the anatomy and the pathologic changes that are presented.

Terrence C. Demos
Loyola University Medical Center
Maywood, IL 60153

Hypersensitivity Pneumonitis:
Sensitivity of High-Resolution CT in a Population-Based Study

David A. Lynch[1]
Cecile S. Rose[2]
Deborah Way[1]
Talmadge E. King, Jr.[2]

OBJECTIVE. Hypersensitivity pneumonitis refers to a group of pulmonary disorders caused by inhalation of organic or inorganic particulates by sensitized persons. The diagnosis relies on a constellation of findings: exposure to an offending antigen, characteristic signs and symptoms, abnormal chest findings on physical examination, and abnormalities on pulmonary function tests and radiographic evaluation. In population-based studies, the sensitivity of chest radiography for detection of this disease is relatively low. The aim of this study was to determine the sensitivity of high-resolution CT (HRCT) for detection of hypersensitivity pneumonitis diagnosed in a population of swimming-pool employees.

SUBJECTS AND METHODS. Thirty-one symptomatic employees of a recreation center who were referred because of possible hypersensitivity pneumonitis were examined by using chest radiography, HRCT, and fiberoptic bronchoscopy with bronchoalveolar lavage and transbronchial biopsy. Hypersensitivity pneumonitis was diagnosed in subjects who had two or more work-related signs or symptoms, abnormal results on transbronchial biopsies, and abnormal lymphocytosis as shown by examination of bronchoalveolar lavage fluid. The chest radiographs and HRCT scans were interpreted by consensus by two observers who were unaware of the clinical diagnosis.

RESULTS. Only one of 11 subjects with a diagnosis of hypersensitivity pneumonitis had abnormal findings on a chest radiograph. Five had abnormal HRCT findings. The abnormality in each case consisted of small, poorly defined centrilobular nodules with variable profusion. No subject without the disease had abnormal HRCT findings. Those who had granulomas shown by lung biopsy were more likely to have abnormal HRCT findings than were those who had more subtle histologic abnormalities.

CONCLUSION. The sensitivity of HRCT for the detection of hypersensitivity pneumonitis in a population-based study is greater than that of chest radiography. The finding of poorly defined centrilobular nodules on HRCT scans should prompt consideration of this disease.

AJR 159:469–472, September 1992

Hypersensitivity pneumonitis refers to a group of pulmonary disorders caused by inhalation of organic or inorganic particulates by sensitized persons [1]. The clinical manifestations are frequently nonspecific and appear to vary depending on host factors, the type and concentration of inhaled antigen, and the duration of exposure to the antigens causing the disease. Histologically, the disease is characterized by perivascular accumulations of lymphocytes and plasma cells, noncaseating granulomas, and bronchiolitis with or without bronchiolitis obliterans. Findings on the chest radiograph may be normal in up to 87% [2] of patients. A recent metaanalysis [3] of published reports of outbreaks of hypersensitivity pneumonitis shows that chest radiographic findings are more likely to be normal when a population-based, epidemiologic approach to the diagnosis of the disease is undertaken than when a case-based descriptive study is performed.

High-resolution CT (HRCT) appears to be more sensitive than chest radiography for the detection of "early" interstitial lung disease [4, 5]. The HRCT appearances

Received December 27, 1991; accepted after revision April 1, 1992.

This work was supported by SCOR grant no. HL-27353 from the National Heart, Lung and Blood Institute.

[1] Department of Radiology, National Jewish Center for Immunology and Respiratory Medicine, 1400 Jackson St., Denver, CO 80206 and University of Colorado Health Sciences Center, 4200 E. Ninth Ave., Denver, CO 80262. Address reprints to D. A. Lynch at the Department of Radiology, Box A030, University of Colorado Health Sciences Center.

[2] Department of Medicine, National Jewish Center for Immunology and Respiratory Medicine, Denver, CO 80206 and University of Colorado Health Sciences Center, Denver, CO 80262.

0361-803X/92/1593-0469
© American Roentgen Ray Society

in subjects with different patterns of hypersensitivity pneumonitis have been described [6, 7]. However, no population-based study of patients with hypersensitivity pneumonitis has been done to determine the sensitivity and specificity of HRCT for detection of this disorder. If the sensitivity of HRCT is high enough, this imaging technique might be useful for the early diagnosis of this disease. An outbreak of hypersensitivity pneumonitis in employees at a local swimming pool provided an opportunity to evaluate the sensitivity of HRCT in a well-defined cohort.

Subjects and Methods

Study Group

An outbreak of hypersensitivity pneumonitis occurred among employees at a local swimming pool [8]. Extensive investigation showed that the granulomatous pneumonitis was due to inhalation of respirable bioaerosols from pool-water sprays and fountains.

The study population consisted of 31 symptomatic swimming-pool employees who were referred for examination for possible hypersensitivity pneumonitis. Sixteen of the subjects were women, and 15 were men. One patient smoked tobacco. The mean age was 24 years (range, 16-59). The protocol for HRCT was approved by our institutional review board, and informed consent was obtained from each patient.

All patients answered questionnaires designed to provide information about work-related respiratory and constitutional signs and symptoms. All the patients in this study reported two or more work-related signs or symptoms (including cough, chest tightness, dyspnea, and fever). Each patient had a complete physical examination, resting and exercise pulmonary function testing, chest radiography, HRCT, and fiberoptic bronchoscopy with bronchoalveolar lavage and transbronchial lung biopsies [9, 10].

For purposes of our study, a subject was considered to have hypersensitivity pneumonitis if he or she had two or more work-related signs or symptoms and fulfilled both of the following criteria: (1) greater than 33% lymphocytes in recovered bronchoalveolar lavage fluid (this is above the 95% confidence level for the percentage of lymphocytes in normal healthy nonsmokers) [11] *and* (2) transbronchial biopsies showing noncaseating granulomas, bronchiolitis, peribronchial or perivascular mononuclear cell aggregates, or interstitial fibrosis [12].

Radiologic Evaluation

All patients had posteroanterior and lateral chest radiographs. In two patients seen at the start of our study, comprehensive chest CT scans were performed by using a GE 9800 scanner (GE Medical Systems, Milwaukee, WI). In these subjects, the protocol included contiguous 10-mm scans through the chest with the subject supine and then 1.5-mm scans at 2-cm intervals with the subject supine and at 4-cm intervals with the subject prone. In the remaining 29 subjects, screening HRCT was performed with a Picker 1200 SX CT scanner (Picker International, Cleveland, OH). The settings were 140 kV and 130 mA; the scan time was approximately 4 sec, and 1-mm-thick slices were obtained at 4-cm intervals through the lungs, first with the subjects prone and then with the subjects supine. Ultra-high-resolution collimation was used. Reconstruction was with a high-resolution algorithm.

The intervals between removal from the pool environment and clinical evaluation varied. The median time between removal and HRCT was 12 days (range, 3-400 days). All 25 subjects who were working at the pool at the time of the outbreak had HRCT within 6 weeks of removal from the pool environment. In six subjects, exposure to the pool environment had ceased for as long as 15 months before they had HRCT. Twenty-three subjects had HRCT before they had bronchoscopy. The mean interval between CT and bronchoscopy in these 23 patients was 48 days (range, 1-165 days). Eight subjects had HRCT after bronchoscopy (mean interval, 24 days; range, 1-90 days).

The chest radiographs were interpreted independently of the HRCT scans by two observers, one of whom is a B reader certified by the International Labor Office (ILO) [13]. A modification of the ILO radiographic scoring system was used [14]. Chest radiographs were considered normal when the ILO score was 0/1 or less. The same two observers scored the HRCT scans independently of each other. Discrepancies between the observers were resolved by consensus. Findings of special interest included interstitial changes (septal thickening, nodules, vascular and pleural irregularity, and honeycombing), air-space opacification (hazy increased density or consolidation), and airway abnormalities (thickening of the bronchial wall and bronchial dilatation). For scoring for the presence of nodules, scans were classified as normal, equivocal, or abnormal. A scan was classified as equivocal when the presence of lung nodules was questionable, but not definite. The HRCT findings were not made available to the clinicians until after the study had been completed, and no clinical decisions were based on the HRCT results.

Results

Hypersensitivity pneumonitis was diagnosed in 11 of the 31 symptomatic pool employees who were evaluated in this study. Examination of material obtained by bronchoalveolar lavage showed lymphocytosis in these 11 patients. Five had granulomas on biopsy, and six had perivascular mononuclear aggregates. Only one subject had abnormal findings on a chest radiograph, which showed small, irregular opacities with profusion of 1/0 and size and shape classified as s/s according to ILO criteria. This subject also had abnormal HRCT findings and granulomas on lung biopsy.

HRCT findings were abnormal in five subjects and equivocal in two. In each case, the abnormality consisted of fine (2- to 3-mm), ill-defined centrilobular nodules. The extent of abnormality ranged from subtle nodularity (Fig. 1) to moderately profuse nodules (Fig. 2A). No lobar predominance was seen. These nodules were not apparent on 10-mm sections in one patient (Fig. 2B). Hazy increase in lung density was not present, and no other type of HRCT abnormality was seen. Four of the five subjects who had well-formed granulomas detected on transbronchial lung biopsy had abnormal HRCT findings. In contrast, HRCT findings were abnormal in only one of the six subjects who had perivascular mononuclear aggregates (Fig. 1).

Of the 11 subjects with hypersensitivity pneumonitis, five had abnormal HRCT findings (sensitivity, 45%), and the remaining six had normal findings (including one patient who had a comprehensive CT examination). In 20 subjects without the disorder, two had equivocal findings, and 18 had normal HRCT results (specificity, 100%). The interval between removal from the pool environment and HRCT was not related to the presence or absence of an abnormality on HRCT scans. One subject had HRCT findings indicative of hypersensitivity pneumonitis 14 weeks after removal from the pool environment; the six false-negative HRCT scans (normal findings on HRCT scans in subjects with hypersensitivity pneumonitis) were obtained between 2 and 9 weeks after the subjects

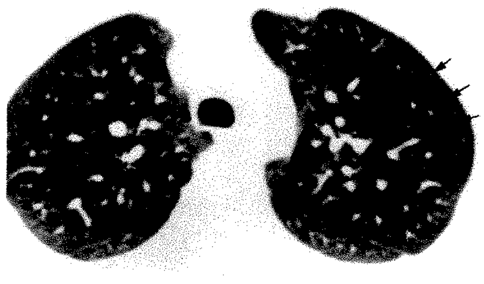

Fig. 1.—High-resolution CT scan in a subject with hypersensitivity pneumonitis but without granulomas on biopsy shows scattered ill-defined centrilobular nodules (*arrows*).

stopped working at the pool. Although one HRCT scan was performed the day after bronchoscopy, detail was not obscured by postbronchoscopy fluid.

Discussion

The apparent decline in sensitivity of chest radiography for the detection of hypersensitivity pneumonitis is probably due to several factors, including a higher index of suspicion for the disease, which leads to earlier diagnosis; increased sensitivity of other diagnostic techniques (especially bronchoscopy); and the emergence of population-based studies [3]. Abnormal findings on a chest radiograph should no longer be regarded as a major diagnostic criterion for this disease.

Two of the roles of HRCT in interstitial lung disease are detection and characterization of disease in subjects whose chest radiographic findings are normal. The prevalence of normal chest radiographic findings in subjects with interstitial lung disease is at least 10% [15]. We know of no reports of normal HRCT findings in subjects with biopsy-proved idiopathic pulmonary fibrosis, pulmonary histiocytosis X, lymphangiomyomatosis, or lymphangitic spread of carcinoma. However, five of 58 recently reported patients with pulmonary sarcoidosis had normal HRCT findings [16–18]. Many of the subjects included in previous studies of HRCT in interstitial lung disease had relatively advanced disease and abnormal chest radiographic findings. Our study confirms that subjects who have pathologic evidence of interstitial lung disease may also have normal HRCT findings.

The sensitivity of HRCT for detection of hypersensitivity pneumonitis in our study was 45%. This relatively low sensitivity has several possible causes. First, abnormalities might have been present but missed on our initial scoring of the HRCT scans. However, retrospective review of the HRCT scans of patients who had the disease showed no abnormalities not detected previously. Second, the interval between removal from the pool environment and HRCT might have been sufficient to allow regression of some of the radiologic changes of hypersensitivity pneumonitis. On the other hand, the characteristic abnormalities were still apparent at the time of biopsy and lavage, which were usually performed after HRCT.

Third, it is clear that this population-based study led to the detection of relatively mild disease. Pulmonary function was either normal or minimally abnormal in all cases. Thus, our population differs considerably from that in most previously reported studies of HRCT in interstitial disease, which primarily describe patients with more severe functional abnormalities. The only previous study that evaluated HRCT abnormalities in subjects who had normal chest radiographic findings was the one by Staples et al. [19], who evaluated HRCT as a screening technique in a group of subjects who had been exposed to asbestos. In this population, the patients with normal radiographic and abnormal HRCT findings had significantly reduced vital capacity and diffusing capacity when compared with the group who had normal HRCT findings. In our study, by contrast, those with abnormal HRCT findings did not differ significantly in pulmonary function from those who had hypersensitivity pneumonitis and normal HRCT findings, suggesting that in subjects with this disease, subtle changes may be detected on HRCT scans before significant physiologic impairment occurs.

Finally, a 4-cm CT slice interval was used in this study, so some focal areas of granulomatous inflammation might have been missed because of sampling error. The HRCT technique we used is similar to the screening protocol for interstitial lung disease recommended by Klein and Gamsu [20]. However, others [21] have found that smaller intervals are necessary for detection of micronodules. The 4-sec scan time might

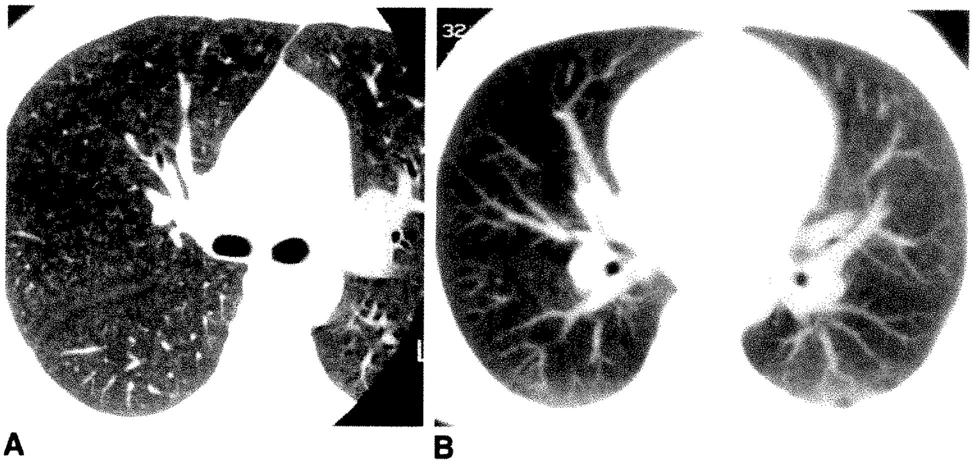

Fig. 2.—*A* and *B*, High-resolution CT scans in a subject with hypersensitivity pneumonitis show fine, ill-defined centrilobular nodules on 1.5-mm scan (*A*). Nodules are not apparent on 10-mm scan (*B*).

have caused some image degradation due to motion. Perhaps retargeting of the lung images by using a 25-cm field of view might have increased the sensitivity of HRCT by increasing resolution [22]. However, one subject in our study who had a comprehensive examination with 2-cm slice interval and retargeted reconstruction had false-negative findings on HRCT. Collimation of 10 mm may sometimes be more useful than thin sections for detection of nodules [23, 24]. However, very fine nodules may be obscured on 10-mm sections because of volume averaging, as was seen in one of our cases (Fig. 1). Consequently, it is unlikely that the technique used in this study can entirely explain the low sensitivity of HRCT.

HRCT showed nodules in four of the five subjects who had granulomas on biopsy and in only one of the six in whom more subtle perivascular mononuclear cell aggregates were the only histologic abnormality. In five of these six, the perivascular interstitial changes presumably did not induce sufficient bronchovascular thickening or irregularity to be apparent on CT. The centrilobular nodules seen in our study may represent peribronchovascular granulomas. Similar nodules were a prominent finding in the cases of subacute and chronic hypersensitivity pneumonitis described in previous studies [6, 7]. Centrilobular nodules (usually coarser than those seen in our study) may be seen in other granulomatous diseases such as sarcoidosis [16, 23], pulmonary histiocytosis X [25], and tuberculosis [26]. Other possible causes of centrilobular nodules include pneumoconioses [27] and small-airway diseases such as cystic fibrosis [28] and panbronchiolitis [29]. Importantly, the finding of fine centrilobular nodules in a patient with a history suggestive of hypersensitivity pneumonitis lends strong support to this diagnosis and should prompt further investigation. Other studies [6, 7] of HRCT in hypersensitivity pneumonitis have emphasized the finding of hazy increase in lung density and have suggested that this may be an early HRCT feature of this disorder. This finding was not seen in our subjects, perhaps reflecting a different antigenic exposure or different stage of disease.

The diagnosis of hypersensitivity pneumonitis is inferential, based on a history of exposure to an offending antigen, compatible clinical signs and symptoms, abnormal lymphocytosis shown by examination of bronchoalveolar lavage fluid, and abnormal findings on transbronchial biopsy [30]. Although HRCT is more sensitive than chest radiography in detecting subtle, early changes of pneumonitis, our findings suggest that the low sensitivity of HRCT limits its usefulness in screening for hypersensitivity pneumonitis. However, the finding of fine centrilobular nodularity on HRCT scans should suggest this disease as a diagnostic possibility. These centrilobular nodules are associated with the presence of granulomas on transbronchial biopsy.

REFERENCES

1. Stankus R, deShazo R. Hypersensitivity pneumonitis. In: Schwarz M, King TE Jr, ed. *Interstitial lung disease*. Philadelphia: Decker, **1988**:111
2. Fink J, Schleuter D, Sosman A, et al. Clinical survey of pigeon breeders. *Chest* **1972**;62:277-281
3. Hodgson M, Parkinson D, Karpf M. Chest x-rays in hypersensitivity pneumonitis: meta-analysis of a secular trend. *Am J Ind Med* **1989**;16:45-53
4. Akira M, Yokoyama K, Yamamoto S, et al. Early asbestosis: evaluation with high-resolution CT. *Radiology* **1991**;178:409-416
5. Schurawitzki H, Stiglbauer R, Graninger W, et al. Interstitial lung disease in progressive systemic sclerosis: high-resolution CT versus radiography. *Radiology* **1990**;176:755-759
6. Hansell D, Moskovic E. High-resolution computed tomography in extrinsic allergic alveolitis. *Clin Radiol* **1991**;43:8-12
7. Silver S, Muller N, Miller R, Lefcoe M. Hypersensitivity pneumonitis: evaluation with CT. *Radiology* **1989**;173:441-445
8. Rose C, Newman L, Martyny J, et al. Outbreak of hypersensitivity pneumonitis in an indoor swimming pool: radiographic, pathologic, lavage and environmental findings. *Am Rev Respir Dis* **1990**;141:A315
9. Watters L, Schwarz M, Cherniack R, et al. Idiopathic pulmonary fibrosis: pretreatment bronchoalveolar lavage cellular constituents and their relationship with lung histopathology and clinical response to therapy. *Am Rev Respir Dis* **1987**;135:696-704
10. Wilcox M, Kervitsky A, Watters L, King T. Quantification of cells recovered by bronchoalveolar lavage: comparison of cytocentrifuge preparations to the filter method. *Am Rev Respir Dis* **1988**;183:74-80
11. BAL Cooperative Group. Bronchoalveolar lavage constituents in healthy individuals, idiopathic pulmonary fibrosis, and selected comparison groups. *Am Rev Respir Dis* **1990**;141:S169-S202
12. Hammar S. Extrinsic allergic alveolitis. In: Dail D, Hammar S, eds. *Pulmonary pathology*. New York: Springer-Verlag, **1987**:384-391
13. *Guidelines for the Use of ILO International Classification of Radiographs of Pneumoconioses*, revised ed. 1980. Occupational Safety and Health Series no. 22 (rev.). International Labour Office, **1980**
14. McLoud TC, Carrington CB, Gaensler EA. Diffuse infiltrative lung disease: a new scheme for description. *Radiology* **1983**;149:353-363
15. Epler G, McLoud T, Gaensler E, et al. Normal chest roentgenograms in chronic diffuse infiltrative lung disease. *N Engl J Med* **1978**;298:934-939
16. Lynch D, Webb W, Gamsu G, Stulbarg M, Golden J. Computed tomography in sarcoidosis. *J Comput Assist Tomogr* **1989**;13:405-410
17. Bergin C, Bell D, Coblentz C, et al. Sarcoidosis: correlation of pulmonary parenchymal pattern at CT with results of pulmonary function tests. *Radiology* **1989**;171:619-624
18. Muller N, Mawson J, Mathieson J, Abboud R, Ostrow D, Champion P. Sarcoidosis: correlation of extent of disease at CT with clinical, functional, and radiographic findings. *Radiology* **1989**;171:613-618
19. Staples CA, Gamsu G, Ray CS, Webb WR. High resolution computed tomography and lung function in asbestos-exposed workers with normal chest radiographs. *Am Rev Respir Dis* **1989**;139:1502-1508
20. Klein J, Gamsu G. High resolution computed tomography of diffuse lung disease. *Invest Radiol* **1989**;24:805-812
21. Remy-Jardin M, Beuscart R, Sault MC, Marquette CH, Remy J. Subpleural micronodules in diffuse infiltrative lung diseases: evaluation with thin-section CT scans. *Radiology* **1990**;177:133-139
22. Mayo J, Webb W, Gould R, et al. High-resolution CT of the lungs: an optimal approach. *Radiology* **1987**;163:507-510
23. Muller NL, Kullnig P, Miller RR. The CT findings of pulmonary sarcoidosis: analysis of 25 patients. *AJR* **1989**;152:1179-1182
24. Remy-Jardin M, Remy J, Deffontaines C, Duhamel A. Assessment of diffuse infiltrative lung disease: comparison of conventional CT and high-resolution CT. *Radiology* **1991**;181:157-162
25. Moore A, Godwin J, Muller N, et al. Pulmonary histiocytosis X: comparison of radiographic and CT findings. *Radiology* **1989**;172:249-254
26. Murata K, Itoh H, Todo G, et al. Centrilobular lesions of the lungs: demonstration by high-resolution CT and pathologic correlation. *Radiology* **1986**;161:641-645
27. Akira M, Higashihara T, Yokoyama K, et al. Radiographic type P pneumoconiosis: high-resolution CT. *Radiology* **1989**;171:117-123
28. Lynch D, Brasch R, Hardy K, Webb W. Pediatric pulmonary disease: assessment with high-resolution ultrafast CT. *Radiology* **1990**;176:243-248
29. Akira M, Kitatani J, Yong-Sik L, et al. Diffuse panbronchiolitis: evaluation with high-resolution CT. *Radiology* **1988**;168:433-438
30. Rose CS, King TE Jr. Controversies in hypersensitivity pneumonitis. *Am Rev Respir Dis* **1992**;145:1-2

Pulmonary Sarcoidosis: Changes on Follow-up CT Examination

Jean Murdoch[1]
Nestor L. Müller

OBJECTIVE. To determine serial changes in the pattern, distribution, and extent of disease over time, and to determine if any specific findings could be used to predict prognosis in patients with pulmonary sarcoidosis, we reviewed the CT scans of 18 patients with pulmonary sarcoidosis.

MATERIALS AND METHODS. The study included 18 patients with biopsy-proved sarcoidosis and pulmonary abnormalities who had two serial high-resolution CT examinations (1.5-mm collimation, high-spatial-frequency reconstruction algorithm) 4–49 months apart. Initial and follow-up CT scans were evaluated independently and then directly compared with each other by two observers. Scans were assessed for the presence, extent, and severity of ground-glass, nodular, and irregular linear opacities; interlobular septal thickening; cystic air spaces; and architectural distortion. If a finding was predominant, it was noted.

RESULTS. Reversible findings included ground-glass, nodular, and irregular linear opacities and septal thickening. Irreversible findings included cystic air spaces and architectural distortion. Follow-up CT showed overall improvement in 12 of 18 patients, progression in five, and no change in one. A predominant pattern of disease could be determined for each patient. Fourteen patients had predominant nodular opacities; of these, 11 had improved by follow-up. Four had predominant irregular linear opacities; of these, three showed progression of disease on follow-up. The presence of any other specific abnormalities, including ground-glass opacities, was not helpful in predicting improvement or worsening of disease on the follow-up examination.

CONCLUSION. In pulmonary sarcoidosis, ground-glass, nodular, and irregular linear opacities and interlobular septal thickening represent potentially reversible disease, while cystic air spaces and architectural distortion are irreversible findings. Follow-up CT usually shows improvement in patients with predominant nodular opacities, while disease tends to progress in patients with predominant irregular opacities.

***AJR* 159:473–477, September 1992**

Sarcoidosis is a disease of unknown cause characterized by the presence of noncaseating granulomatous inflammation. The radiologic and CT findings of pulmonary sarcoidosis have been well described [1–5]. Several studies have shown that high-resolution CT (HRCT) is superior to chest radiography in the diagnosis of pulmonary sarcoidosis, in the assessment of disease pattern and extent, and in the early recognition of pulmonary fibrosis [3–8].

Although the HRCT findings have been described, only limited information is available about the change in the CT pattern of disease over time or the value of CT in distinguishing reversible parenchymal abnormalities from irreversible fibrosis [4].

The aim of the present study was to determine how the pattern, distribution, and extent of disease changed over time on serial HRCT scans and to identify CT findings that might be helpful in predicting the prognosis of the disease.

Received February 11, 1992; accepted after revision March 24, 1992.

[1] Both authors: Department of Radiology, University of British Columbia and Vancouver General Hospital, 855 W. 12th Ave., Vancouver, B.C., Canada V5Z 1M9.

0361–803X/92/1593–0473
© American Roentgen Ray Society

Materials and Methods

The CT scans of 18 patients with biopsy-proved sarcoidosis and pulmonary parenchymal abnormalities were assessed retrospectively. Diagnosis was based on bronchial or transbronchial biopsy ($n = 14$), mediastinal biopsy ($n = 2$), or peripheral nodal biopsy ($n = 2$). All patients had two CT examinations 4–49 months apart. The patients were 27–66 years old (mean, 43 years); nine were men and nine were women. The need for the second CT examination was dictated exclusively by clinical criteria.

CT scans were obtained with a 9800 scanner (General Electric Medical Systems, Milwaukee, WI). Scans were obtained at end-inspiration and photographed at window levels appropriate for pulmonary parenchyma (mean, −600 to −700 H; width, 1000–2000 H) and mediastinum (mean, 30–50 H; width, 350–500 H). Of the 36 examinations in the 18 patients, 24 were performed with 10-mm collimation at 10-mm intervals through the lungs, complemented with HRCT (1.5-mm collimation, high-spatial-frequency reconstruction algorithm) at three levels: aortic arch, tracheal carina, and 1 cm above the dome of the right hemidiaphragm. Twelve examinations were performed with HRCT at 10-mm intervals without concomitant conventional CT.

The initial and follow-up CT scans in each patient were initially assessed independently by two observers. The two observers then assessed the scans together to reach a decision by consensus as to the degree of change between examinations. The CT scans were evaluated for the presence, distribution, and extent of ground-glass, nodular, and irregular linear opacities; thickening of interlobular septa; cystic air spaces (honeycombing); and architectural distortion. Ground-glass opacities were defined as areas of increased attenuation without obscuration of the underlying vessels and bronchi. Nodular opacities were defined as localized round areas of soft-tissue attenuation 1–10 mm in diameter; they could be smoothly or irregularly marginated. Irregular linear opacities were defined as linear opacities 1–3 mm thick that were distinct from interlobular septa, bronchovascular bundles, and nodular opacities. These could be seen in an intralobular location or could extend through several adjacent lobules. Cystic air spaces were defined as localized areas of decreased attenuation with well-defined walls. Architectural distortion was considered present when fissures and hila were displaced or the secondary pulmonary lobule, bronchi, or vessels were distorted. These definitions are similar to those previously described [3–5].

Extent of involvement was assessed independently for each of three zones of each lung. Each zone corresponded to approximately one third of the scans from the lung apices to 1 cm below the dome of the diaphragm. The CT score in upper, middle, and lower lung zones was determined by visually estimating the extent of disease in each zone. The score was based on the percentage of lung parenchyma that showed evidence of abnormality and was estimated to the nearest 5% of parenchymal involvement. Overall percentage of involvement was obtained by averaging the six lung zones. Additional findings that were assessed included enlargement of mediastinal lymph nodes, calcification of lymph nodes, and pleural effusions.

The medical charts of all patients were reviewed to determine whether corticosteroids or other treatment had been given in the interval between examinations.

Results

The extent of disease seen on the initial CT scans ranged from 5% to 90% of the lung parenchyma (mean, 45%). The extent of disease on follow-up scans ranged from less than 5% to 80%. Follow-up CT showed a decrease in the extent of disease in 12 (67%) of the 18 patients, no change in one (5%), and an increase in five (28%). In 14 patients (78%), the initial CT scans showed predominant nodular opacities. Of these, 11 patients (79%) had improved by the second scan, one (7%) was unchanged, and two (14%) had progression. Four of 18 patients (22%) had predominant irregular linear opacities. Of these, follow-up CT showed improvement in one and progression of disease in three. The overall pattern of disease varied between patients but remained constant in a given patient on follow-up scans, even though severity and extent changed (Table 1).

Reversible HRCT findings included ground-glass, nodular, and irregular linear opacities and interlobular septal thickening (Table 1, Fig. 1). Ground-glass opacities were seen in 15 patients. Follow-up scans showed an increase in three, a decrease in six, and no change in six. Irregular linear opacities distinct from interlobular septa were seen in 13 cases (72%). These had increased in six, decreased in one, and were unchanged in six cases on follow-up. Interlobular septal thickening not related to nodular opacities was seen in 16 cases (89%). Follow-up CT scans showed an increase in five, decrease in eight, and no change in three.

Cystic air spaces (honeycombing) were present in seven (39%) of 18 patients, and architectural distortion was present in nine (50%). Both of these aspects of disease either stayed constant or progressed (Table 1, Fig. 2).

Enlarged hilar or mediastinal lymph nodes were seen in 17 (94%) of 18 cases. Follow-up scans showed further enlargement of lymph nodes in one case, reduction in size of lymph nodes in five, and no change in 11 cases. Calcified mediastinal and hilar lymph nodes were seen in eight patients (Fig. 3). In four of these eight, calcification was seen on the first scan and increased in the 7–10 months between scans. In the other four, calcification was seen on the follow-up scan only (5–29 month scan interval). None of these patients had any clinical or radiologic evidence of concomitant disease such as tuberculosis, histoplasmosis, or silicosis.

Pleural thickening was seen on both initial and follow-up CT in two patients. Pleural effusion was seen on initial CT in two and on follow-up CT in three patients.

TABLE 1: Parenchymal Opacities Seen on High-Resolution CT at Presentation and Follow-up in 18 Patients with Sarcoidosis

Finding	No. (%) with Finding at First CT Study	Follow-up Examination		
		Same	Worse	Better
Ground-glass opacities	15 (83)	6	3	6
Nodular opacities				
Along bronchovascular bundles	18 (100)	2	4	12
Subpleural	18 (100)	3	4	11
Interlobular septa	16 (89)	3	7	6
Irregular linear opacities	13 (72)	6	6	1
Interlobular septal thickening	16 (89)	3	5	8
Cystic air spaces	7 (39)	5	2	0
Architectural distortion	9 (50)	4	5	0

Note.—Intervals between first and follow-up CT examinations ranged from 4 to 49 months.

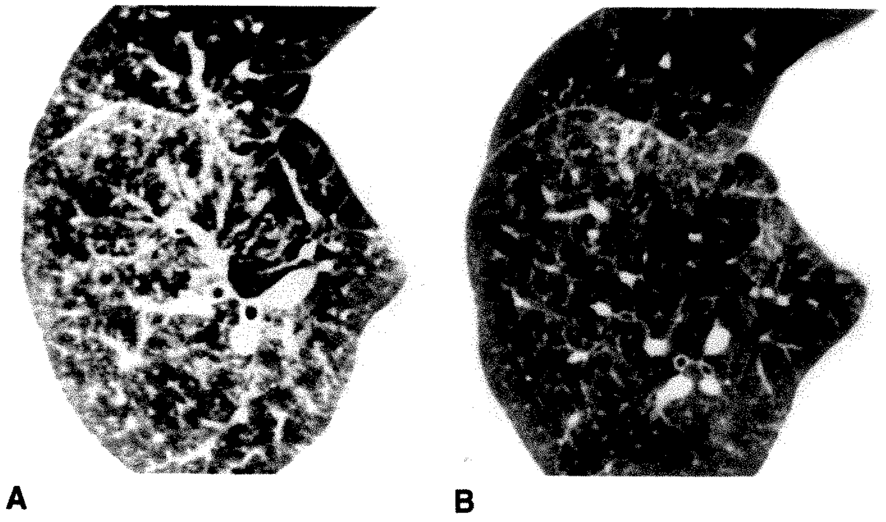

Fig. 1.—27-year-old man with sarcoidosis and dyspnea for 2 months before first high-resolution CT study.

A, Initial high-resolution CT scan shows a mostly nodular disease pattern with moderate ground-glass opacities (overall 70% parenchymal involvement).

B, At the time of the second CT scan, obtained 15 months after *A*, the patient was taking oral corticosteroids and was less dyspneic. This scan shows marked reversibility of both ground-glass and nodular opacities.

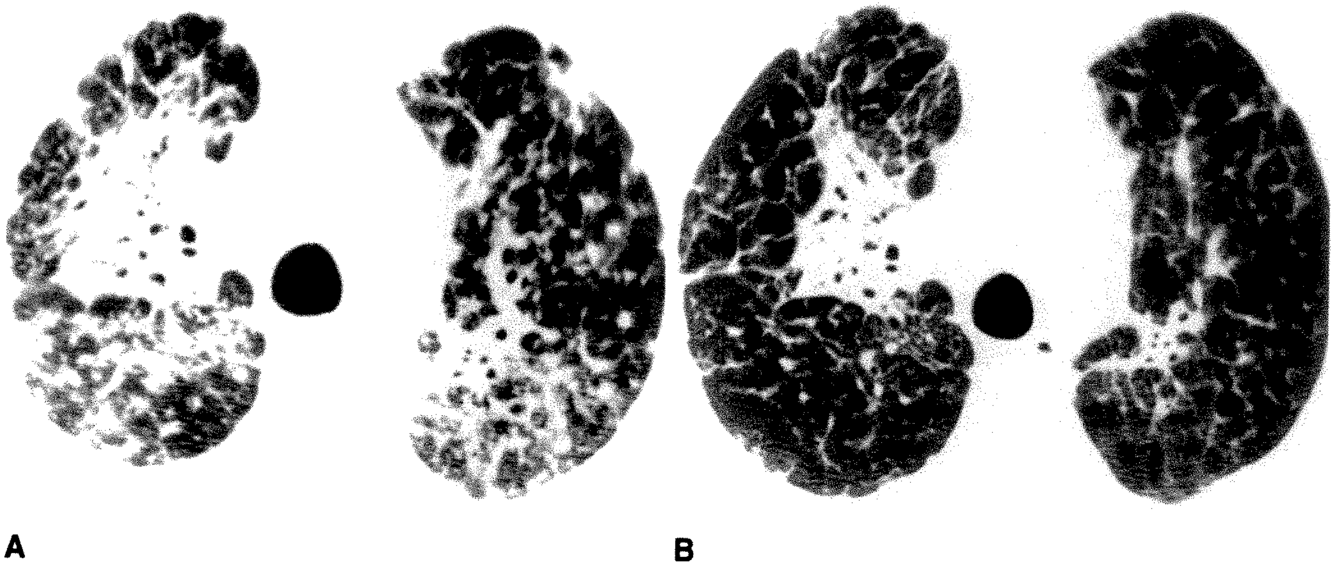

Fig. 2.—47-year-old man who had cough, dyspnea, and malaise 1 year before first CT scan.

A, Initial CT scan shows dense peribronchovascular nodularity with fibrosis and traction bronchiectasis.

B, When follow-up CT scan was obtained 7 months after *A*, the patient was taking oral corticosteroids. Scan shows reversibility of nodular opacities, while components of architectural distortion and traction bronchiectasis are not reversible.

Eleven (61%) of the 18 patients were treated with corticosteroids. These included eight (67%) of the 12 patients in whom improvement was seen on follow-up and three (60%) of the five patients in whom disease progressed.

Discussion

The CT manifestations of pulmonary sarcoidosis have been described [3–7] and include ground-glass opacities; nodular opacities along bronchovascular bundles, interlobular septa, and subpleural lung regions; and irregular linear opacities. Hilar and mediastinal lymphadenopathies are common; pleural thickening and pleural effusions are uncommon. Calcification of lymph nodes, previously reported in 2–4% of cases [2], was seen in more than 40% of cases in the present study. The apparent increased prevalence of nodal calcification presumably is due to the increased sensitivity in the detection of calcification with the use of HRCT and the increased prevalence of calcification on follow-up scans.

The most consistent pulmonary parenchymal abnormality seen in sarcoidosis is the presence of nodular opacities [3–5]. In the present study, nodular opacities were seen in all patients. These nodular opacities have been shown to represent coalescent noncaseating sarcoid granulomata [3]. Our results indicate that they represent a potentially reversible

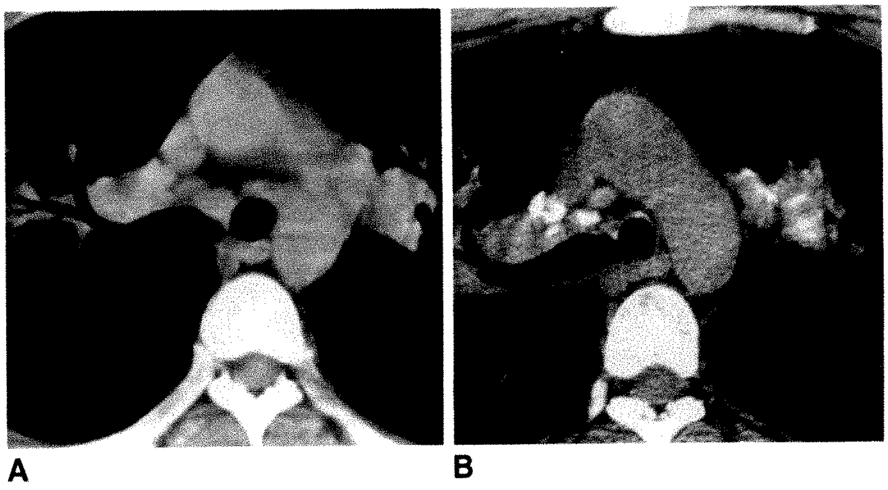

Fig. 3.—34-year-old man.

A, Initial high-resolution CT scan shows mediastinal lymphadenopathy. Faint early calcification is present.

B, Follow-up CT scan obtained 29 months after *A* shows increase in lymph node calcification. No treatment was given in interval between *A* and *B*, and parenchymal disease had progressed. The patient was asymptomatic between scans.

stage of disease and also may have prognostic significance. Patients in whom nodular opacities were the predominant finding were usually seen to have improvement on follow-up CT scans.

Areas of ground-glass opacification are seen in 16–60% of patients with sarcoidosis [4, 5]. Ground-glass opacities are seen more commonly at presentation than in patients with long-standing disease [5]. The pathologic correlate of areas of ground-glass opacities in sarcoidosis is not known. They could represent areas of active alveolitis or widespread microscopic interstitial granulomas [4]. It is thought that alveolitis is the initial abnormality in sarcoidosis and that alveolitis rather than granuloma formation leads to the development of fibrosis [4, 9–12]. Lynch et al. [4] have shown that areas of ground-glass opacity on CT correlate with disease activity as assessed by gallium-67 scanning. In their study, follow-up HRCT scans in two patients with improvement after prednisone therapy showed a decrease in the areas of ground-glass and nodular opacities. Our study confirmed that areas of ground-glass opacities represent potentially reversible lung disease. However, the presence of areas of ground-glass opacity did not have any prognostic significance.

Irregular linear opacities are seen in 30–50% of cases of pulmonary sarcoidosis [3, 5]. In the present study, in three of four patients with predominant irregular linear opacities, follow-up CT scans showed progression of disease; only one of the four had improved. Patients with predominant irregular linear opacities therefore seem to have a worse prognosis than do patients with predominant nodular opacities. Müller et al. [6] also have shown that as a group, patients with irregular linear opacities have significantly greater impairment in lung function than do patients with predominant nodular opacities. However, irregular linear opacities do not necessarily imply irreversible fibrosis. In one of our patients with irregular linear opacities, the follow-up CT scan showed improvement. Fibrosis can be diagnosed only when irregular linear opacities are associated with architectural distortion, as shown by distortion of the secondary pulmonary lobule, retraction of hila and fissures, cyst formation, and traction bronchiectasis. Cyst formation and distortion of lung parenchyma represent irreversible disease [8] and are seen in patients with long-standing sarcoidosis [5].

One of the limitations of the present study is the small number of patients. However, the results are comparable to those recently described by Brauner et al. [13] in 20 patients. They reviewed the serial CT scans of 20 patients with pulmonary sarcoidosis who had clinical improvement. Similar to our study, they found that nodules and alveolar or pseudoalveolar consolidation (ground-glass opacity) were always reversible, while lung distortion, honeycomb cysts (cystic air spaces), and traction bronchiectasis were irreversible. However, in their study, septal or nonseptal lines (irregular linear opacities) appeared to be irreversible lesions, whereas in our patients they were shown to be potentially reversible abnormalities.

Because the CT scans were obtained for clinical reasons, the patients studied had more severe disease than is usual for sarcoidosis. This is corroborated by the fact that 11 of the 18 patients received corticosteroids. However, it is in patients with more severe disease that CT is most likely to be helpful. Because of cost and radiation exposure, CT is not warranted in the routine assessment of sarcoidosis. Finally, while this study shows which HRCT findings are potentially reversible and which are not, it does not prove the clinical value of HRCT in the assessment of these cases. This will require comparison of the HRCT findings with findings on chest radiographs and gallium scans, clinical symptoms, and results of pulmonary function tests.

We conclude that in patients with sarcoidosis, findings of ground-glass, nodular, and irregular linear opacities and interlobular septal thickening on CT scans represent potentially reversible disease while cystic air spaces and architectural distortion are irreversible findings. The presence of mainly nodular opacities tends to indicate improvement will be seen on subsequent CT examination. Ground-glass opacities are not helpful in predicting improvement in sarcoidosis. Irregular linear opacities may resolve, indicating that they do not necessarily represent irreversible fibrosis. However, patients with predominant irregular linear opacities tend to have progression of disease.

REFERENCES

1. McLoud TC, Epler GR, Gaensler EA, Burke GW, Carrington CB. A radiographic classification for sarcoidosis: physiologic correlation. *Invest Radiol* **1982**;17:129-138
2. Hamper UM, Fishman EK, Khouri NF, Johns CJ, Wang KP, Siegelman SS. Typical and atypical manifestations of pulmonary sarcoidosis. *J Comput Assist Tomogr* **1986**;10:928-936
3. Müller NL, Kullnig P, Miller RR. The CT findings of pulmonary sarcoidosis: analysis of 25 patients. *AJR* **1989**;152:1179-1182
4. Lynch DA, Webb WR, Gamsu G, Stulbarg M, Golden J. Computed tomography in pulmonary sarcoidosis. *J Comput Assist Tomogr* **1989**;13:405-410
5. Brauner MW, Grenier P, Mompoint D, Lenoir S, de Crémoux H. Pulmonary sarcoidosis: evaluation with high-resolution CT. *Radiology* **1989**;172:467-471
6. Müller NL, Mawson JB, Mathieson JR, Abboud R, Ostrow DN, Champion P. Sarcoidosis: correlation of extent of disease at CT with clinical, functional and radiographic findings. *Radiology* **1989**;171:613-618
7. Mathieson JR, Mayo JR, Staples CA, Müller NL. Chronic diffuse infiltrative lung disease: comparison of diagnostic accuracy of CT and chest radiography. *Radiology* **1989**;171:111-116
8. Bergin CJ, Bell DY, Coblentz CL, et al. Sarcoidosis: correlation of pulmonary parenchymal pattern at CT with results of pulmonary function tests. *Radiology* **1989**;171:619-624
9. Rosen Y, Athanassides TJ, Moon S, Lyons HA. Nongranulomatous interstitial pneumonitis in sarcoidosis. *Chest* **1978**;24:122-125
10. Thomas PD, Hunninghake GW. Current concepts of the pathogenesis of sarcoidosis. *Am Rev Respir Dis* **1987**;135:747-760
11. Dawete RP, Rossman MD, Kern JA, et al. Pathogenesis of sarcoidosis. *Chest* **1986**;89[suppl]:1745-1775
12. Hunninghake GW, Garrett KC, Richerson HB, et al. Pathogenesis of granulomatous lung diseases. *Am Rev Respir Dis* **1984**;130:476-496
13. Brauner MW, Lenoir S, Grenier P, Cluzel P, Battesti J-P, Valeyre D. Pulmonary sarcoidosis: CT assessment of lesion reversibility. *Radiology* **1992**;182:349-354

AJR to Use Diskettes Instead of Hard-Copy Manuscripts for Editing and Printing

Beginning with the January 1993 issue, accepted papers to be published in the *AJR* will be edited and printed by using computer diskettes rather than hard copies of the manuscripts. This change will expedite the editing and publication process and result in less delay between submission of manuscripts and their appearance in the Journal. Also, with the new system, authors will receive page proofs rather than galleys before publication. This will enable them to see exactly what their final article will look like.

Effective immediately, upon *acceptance* of manuscripts for publication, authors will be asked to send a copy of their revised manuscript on a 5¼-inch DOS-compatible diskette in WordPerfect or ASCII format along with the hard copy of the revision. Articles will be edited directly on the diskettes. Changes will be highlighted electronically; as before, a hard copy of the edited manuscript and figure proofs will be mailed to authors for approval before publication. Note that hard copies of manuscripts will still be required for the peer-review and revision processes.

The *AJR* already takes great pride in the speed with which the peer-review process is accomplished (mean time, 3.4 weeks) and in the amount of time between submission of manuscripts and their final appearance in print (6 months). This is nearly twice as fast as many other journals. With the new system, these intervals will be even shorter. Authors will see their work in print faster, and the timeliness of the Journal will be greater than ever.

Robert N. Berk
Editor-in-Chief

Book Review

Atlas of Radiology of the Chest. Edited by Margaret Turner-Warwick, Margaret E. Hodson, Bryan Corrin, and Ian H. Kerr. New York: Gower Medical, 168 pp., 1991. $70

The stated purpose of the book is to provide an atlas of chest radiographs of a wide range of conditions; it is intended to be of interest to consultant radiologists, chest physicians, trainees, and those studying for examinations. The book consists of nine chapters, including ones on the normal chest, chest masses, airways, infections and allergy, vascular and systemic diseases, occupational diseases and chest wall abnormalities, mediastinum, and injuries.

A wide variety of diseases is illustrated with chest radiographs, drawings, and, occasionally, CT scans accompanied by brief descriptions. The illustrations in chapters 1-3 are of good quality. Some of the radiographs and CT scans in the remainder of the book are of only fair quality, and a few are poor.

An advantage of the book is that it is brief. The illustrations and legends can be perused in an hour or so, and the entire book can be read in an evening. Chapters 1 and 2 could be used as a quick introduction to chest radiology by medical students. Chapter 6, on vascular and systemic diseases and diseases of unknown cause, and chapter 9, on injuries, serve as reasonable introductions in their respective areas. However, in my opinion, the book has several problems and undesirable features.

First, many diseases are illustrated, but the discussion of each disease is extremely brief. The comments frequently include short descriptions of the clinical findings and treatment, and these are too short to be useful. I think that the limited text could have been better allocated to more radiologic description.

Second, the book has almost no supporting data. In several chapters, the text is "loose" and contains obvious comments: "Ultrasound and CT demonstrate effusions well," and "CT is of immense help in mediastinal lesions."

Third, the format may be misleading for a student. The tendency is to illustrate unusual entities and to give them attention equal to or even greater than that given to common diseases. Examples of endobronchial lesions include a leiomyoma and a papilloma. The example of small-cell carcinoma is a cavitary lesion. *Pneumocystis carinii* pneumonia in an 8-year-old child with leukemia (described as an "interstitial" process) and bubonic plague are examples of pneumonia. A disproportionate amount of space is devoted to allergic bronchopulmonary aspergillosis. The initiate may be misled because the book has little comment on whether the entities are common or rare and whether the radiologic findings are typical or atypical.

Fourth, the lack of a differential diagnostic approach makes the book of little value for looking something up. That is, it cannot be used to answer what are perhaps the most common questions for students of chest radiology: Given a certain radiographic appearance or pattern, what are the common causes and what features can be used to differentiate one entity from another?

Fifth, the terminology is occasionally inconsistent. Carcinoids are variously referred to as carcinoid, carcinoid adenoma, and bronchial adenoma. Several statements offered as fact are questionable, including ones that say the diagnosis of lymphoma (and hamartoma) requires surgical resection of the tumor, alveolar cell carcinoma is 100 times less common than bronchial cancer, and the only way to diagnose emphysema is at surgery or autopsy.

I am not sure that this book will be very useful to its intended audience. In my opinion, it is too elementary and is not current enough to be of much interest to radiologists, radiology residents, and chest physicians. For the student, I think better introductory books are available.

Jack L. Westcott
Hospital of Saint Raphael
New Haven, CT 06511

Case Report

Anomalous Left Brachiocephalic (Innominate) Vein: MR Demonstration

Kiminori Fujimoto,[1] Toshi Abe,[1] Tsutomu Kumabe,[1] Naofumi Hayabuchi,[1] and Yoshimi Nozaki[2]

The normal left brachiocephalic (innominate) vein extends from the confluence of the left internal jugular and subclavian veins to the right brachiocephalic vein and the superior vena cava. It runs obliquely downward and to the right, passing superior and anterior to the aortic arch and anterior to the left subclavian, left common carotid, and brachiocephalic arteries. Rarely, this vein follows an anomalous course. This is described as the anomalous left brachiocephalic vein. This anomaly was first described in 1888 [1], but the MR characteristics have not previously been described.

We report a case of an anomalous left brachiocephalic vein shown by MR imaging.

Case Report

A 54-year-old asymptomatic woman underwent MR imaging of the thorax because "buckling" of the aortic arch seen on a routine chest radiograph was suggestive of an aortic aneurysm.

MR images (1.5-T Magnetom 15H unit, Siemens, Iselin, NJ) were obtained at the level of the aortic arch, at 1-cm intervals with 1-cm slice thickness, while the patient was supine. Axial and coronal T1-weighted images were obtained with an ECG-gated technique. On axial MR images, a round area of signal void was present lateral to the aortic arch (Fig. 1A). This signal void passed downward and lateral to the aortic arch and entered the aorticopulmonary window, crossing the mediastinum to the right, posterior to the ascending aorta and anterior to the trachea (Figs. 1B and 1C). It then entered the superior vena cava inferior to the insertion of the azygos vein (Fig. 1D). The left brachiocephalic vein was not seen in its normal course. Coronal T1-weighted MR images showed that this signal void extended from the junction of the left internal jugular and subclavian veins (Fig. 1E). It passed downward to the right, inferior to the aortic arch, and entered the superior vena cava (Fig. 1F). A diagnosis of anomalous left brachiocephalic vein was made on the basis of these findings.

Because the patient had no cardiovascular malformations or anomalies, she was discharged without treatment.

Discussion

Embryologically, the primordia of the systemic veins first appear as paired anterior and posterior cardinal veins that unite on each side to form a common cardinal vein (or duct of Cuvier) that opens into the primitive sinus venosus. The anterior cardinal veins extend cephalad to the junctions of the internal jugular veins and subclavian veins on either side [2]. In an embryo with a crown-rump length of about 22 mm (eighth week), the right and left anterior cardinal veins communicate through an oblique cross channel, the precardinal (intercardinal, transversal) anastomosis, which passes the blood from left to right. As a result of its diversion, the left anterior cardinal vein proximal to the anastomosis atrophies and loses its connection with the left common cardinal vein. The right common cardinal vein and the anterior cardinal vein as far as the precardinal anastomosis become the superior vena cava. The precardinal anastomosis itself and the left anterior cardinal vein distal to the confluence of the veins from the upper limb become the left brachiocephalic vein [3]. Normally, the precardinal anastomosis occurs anterior to the aortic trunk. When the anastomosis occurs posterior to the aortic trunk, the left brachiocephalic vein runs posterior to the

---

Received January 28, 1992; accepted after revision March 9, 1992.

[1] Department of Radiology, Kurume University School of Medicine, 67 Asahimachi Kurume, Fukuoka 830, Japan. Address reprint requests to K. Fujimoto.

[2] Department of Radiology, Saint Mary's Hospital, 422 Tsubukuhonmachi Kurume, Fukuoka 830, Japan.

AJR 159:479–480, September 1992 0361–803X/92/1593–0479 © American Roentgen Ray Society

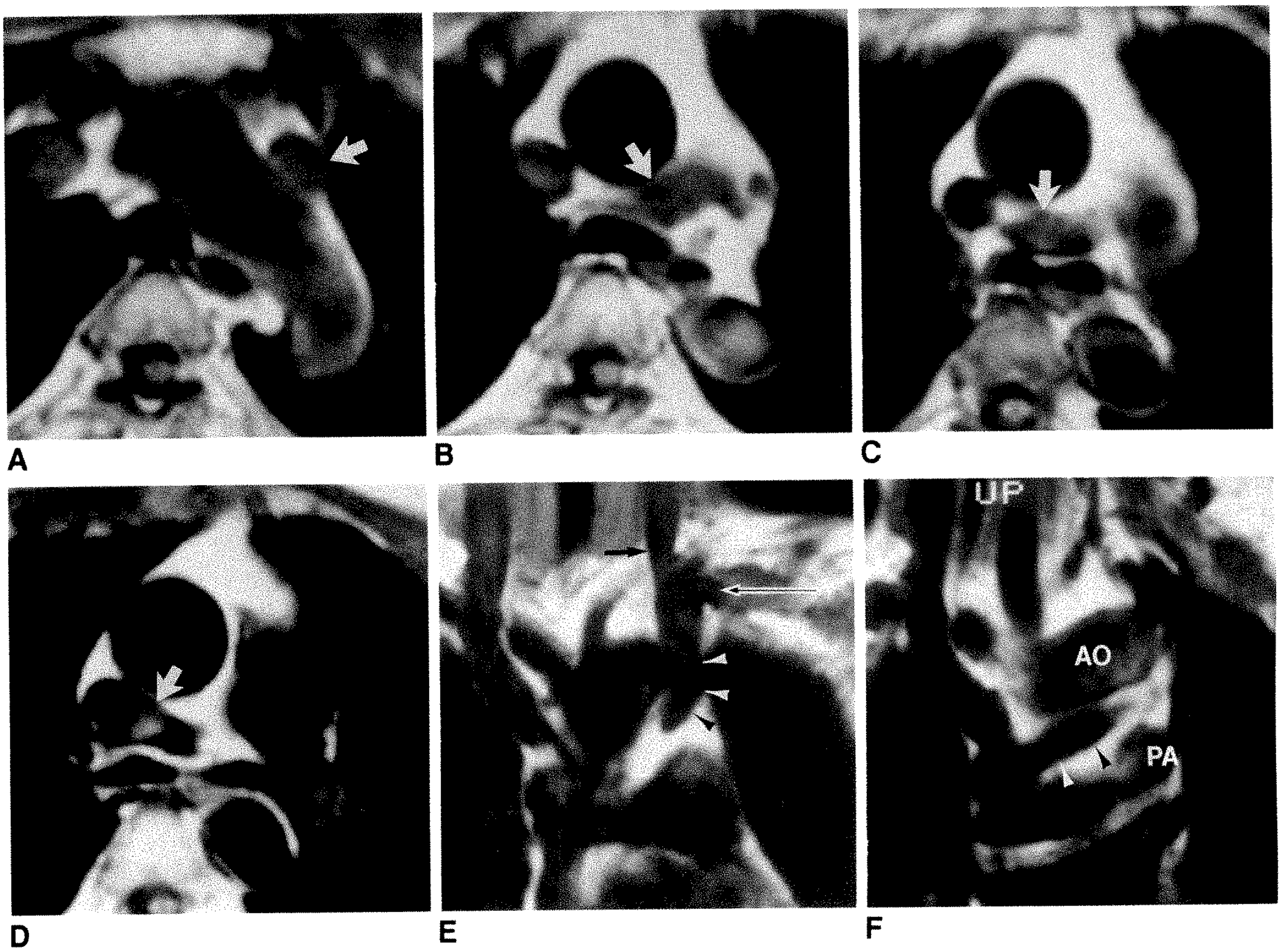

Fig. 1.—Anomalous left brachiocephalic vein in a 54-year-old woman.

A–D, **Axial T1-weighted MR images (920/15) show signal void (*arrows*) passing downward and lateral to aortic arch (*A*) and crossing mediastinum to right (*B*), posterior to ascending aorta and anterior to trachea (*C*). It then enters superior vena cava (*D*).**

E* and *F, **Coronal T1-weighted MR images show signal void (*arrowheads*) extending from confluence of left internal jugular vein (*short arrow*) and left subclavian vein (*long arrow*). It passes downward to right, inferior to aortic arch (AO) and superior to left pulmonary artery (PA), and enters superior vena cava.**

ascending aorta after birth. It has been called the anomalous left brachiocephalic vein. As the left brachiocephalic vein ran inferior to the aortic arch and superior to the pulmonary artery in our case, it was suggested that the precardinal anastomosis might have been present posterior to the aortic trunk at the level between the third and the fourth branchial arch arteries, or at the sixth branchial arch artery, in the embryonic stage [3].

The anomalous left brachiocephalic vein was first described by Kerschner [1] in 1888. The angiographic findings of this anomaly were first described by Roberts et al. [4] in 1951, echocardiographic findings by Cloez et al. [5] in 1982, and CT findings by Webb et al. [6] in 1982, but MR findings have not previously been reported. Although an anomalous left brachiocephalic vein may be adequately shown with CT or angiography, MR imaging has the advantage of a multiplane format, and neither contrast enhancement nor the use of ionizing radiation is needed.

We conclude that MR imaging clearly showed the anomalous left brachiocephalic vein. Because this anomaly may be shown with various types of medical imaging, radiologists should be aware that it is a possible finding.

REFERENCES

1. Kerschner L. Zur Morphologie der Vena cava inferior. *Anat Anz* **1888**;3:808–823
2. Gerlis L, Ho SY. Anomalous subaortic position of the brachiocephalic (innominate) vein: a review of published reports and report of three new cases. *Br Heart J* **1989**;61:540–545
3. Yoshida Y, Seki Y, Yasutaka S. A case of the left brachiocephalic vein passing behind the ascending aorta in man. *Kaibogaku Zasshi* **1984**;59:168–176
4. Roberts JR, Dotter CT, Steinberg I. Superior vena cava and innominate veins: angiographic study. *AJR* **1951**;66:341–352
5. Cloez JL, Ravault F, Marcon F, Pernot C. Thonc veineux innomine en position sous-aortique: interet de l'echocardiographie de contraste par voie suprasteinale. *Arch Mal Coeur Vaiss* **1982**;75:939–943
6. Webb WR, Gamsu G, Speckman JM, et al. Computed tomographic demonstration of mediastinal venous anomalies. *AJR* **1982**;139:157–161

Case Report

Value of MR Imaging in Detecting a Peanut Causing Bronchial Obstruction

Toshihiro O'Uchi,[1] Aya Tokumaru,[1] Ichiro Mikami,[2] Tatuya Yamasoba,[3] and Shigeru Kikuchi[3]

Bronchial obstruction due to aspirated foreign bodies is usually seen in children less than 5 years old [1, 2]. In 48–62% of cases in Japan [1] and the United States [2], the foreign body is a peanut. Because peanuts cannot be directly visualized on plain radiographs, the diagnosis is usually made on the basis of bronchoscopic findings [1, 2]. We report a case in which MR imaging was useful in detecting a peanut as the cause of bronchial obstruction.

Case Report

A 1½-year-old boy had progressive wheezing and fever for 1 week. He had no history of aspirating a peanut, but he ate peanuts daily. A chest radiograph showed overinflation of the right lung, mediastinal shift from right to left on expiration, and atelectasis of the right middle lobe.

MR was performed at the request of an otolaryngologist to localize the peanut. T1-weighted images, 600/15 (TR/TE), were obtained. A transverse image (Fig. 1A) showed a 5-mm area of high signal intensity in the right main bronchus.

At bronchoscopy, a peanut was detected in the right main bronchus near the carina, and an attempt was made to remove it. However, the patient's wheezing continued. A second MR examination showed that the area of high signal intensity in the right main bronchus had disappeared, but a focus of medium-intensity signal persisted around the narrow right bronchus. This was thought to represent granulation tissue. Atelectasis of the right middle lobe persisted. An area of high signal intensity less than 5 mm in diameter was seen in the left lower bronchus, suggesting that not all of the peanut had been removed at bronchoscopy and had moved to the contralateral side because of coughing (Figs. 1B and 1C).

Bronchoscopy was performed again, and a 5-mm fragment of peanut was removed from the left lower bronchus. The right main bronchus was narrowed by granulation tissue.

Discussion

MR is useful in detecting a peanut in the airway. Peanuts have high signal on T1-weighted images, and the surrounding air in the lung has low signal, allowing high contrast between the lesion and air in the lung. A peanut has a short T1 value because of its high fat content, and MR can show the location of the peanut in the trachea or bronchus.

The peanut is the most common foreign body found in the airway in children, especially those less than 5 years old. The highest rate of foreign body aspiration occurs in children less than 3 years old [3]. Often, there is no history of respiratory distress. In our patient, aspiration of a peanut was not obvious clinically. Radiographs showed the signs of well-developed obstructive emphysema: increased radiolucency of the involved lung segment, decreased vascular pattern, shift of mediastinal structures toward the normal lung during expiration, and decreased motion and depression of the diaphragm on the ipsilateral side [2]. However, inspiratory-expiratory

---

Received November 25, 1991; accepted after revision April 5, 1992.

[1] Department of Radiology, Kameda Medical Center, 929 Higashi-cho, Kamogawa, Chiba 296, Japan. Address reprint requests to T. O'Uchi.
[2] Department of Pediatrics, Kameda Medical Center, Chiba 296, Japan.
[3] Department of Otolaryngology, Kameda Medical Center, Chiba 296, Japan.

AJR 159:481–482, September 1992 0361–803X/92/1593–0481 © American Roentgen Ray Society

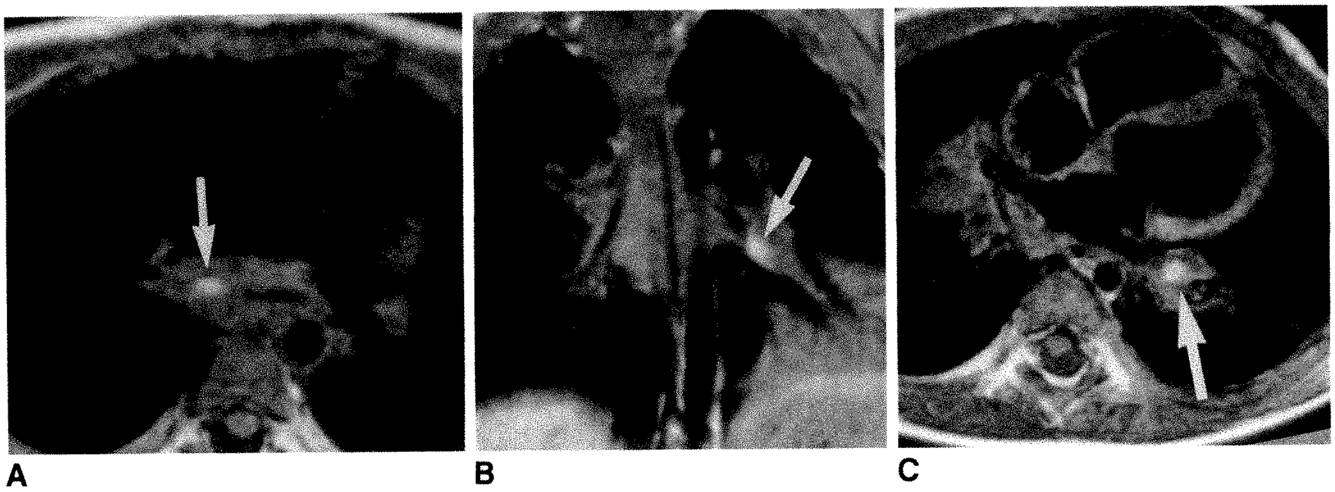

Fig. 1.—1½-year-old boy who had wheezing and fever for 1 week.

A, T1-weighted MR image shows high signal in right main bronchus caused by a piece of peanut (*arrow*).

B and *C*, Axial (*B*) and coronal (*C*) MR images obtained 5 days after *A* show area of high signal intensity in left bronchus (*arrows*) suggesting movement of peanut.

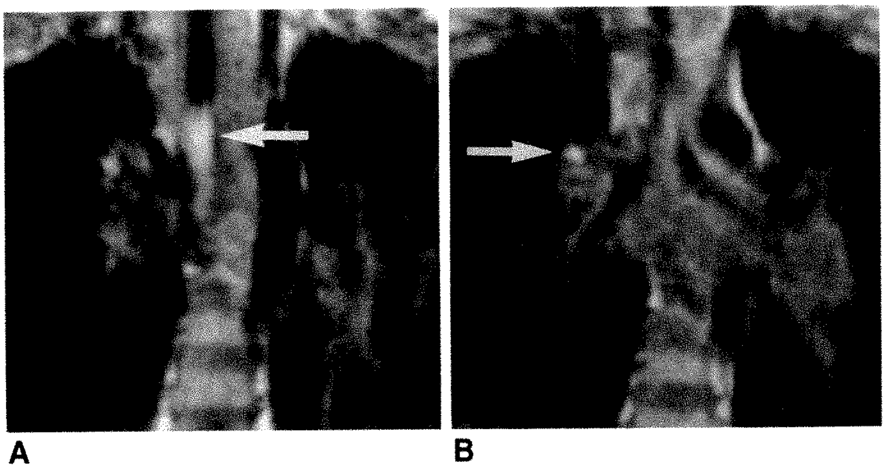

Fig. 2.—3-year-old girl who began wheezing while eating peanuts. Wheezing persisted and dyspnea developed. Chest radiograph at admission showed no obvious mediastinal shift on expiration and inspiration. At bronchoscopy, performed the next day, whole peanut located at carina was removed. Pus was seen in right upper bronchus, but expected piece of peanut was not found. A small piece of peanut, which was removed by suction, was detected in right lower lobe, suggesting movement of peanut because of coughing.

A, T1-weighted MR image shows a 10-mm area of high signal intensity (*arrow*) filling trachea at carina.

B, T1-weighted MR image shows a 3-mm area of high signal intensity (*arrow*) in right upper bronchus.

abnormalities were seen in only 27% of the cases studied by McGuirt et al. [3]. We had another patient with no signs of an inspiratory-expiratory abnormality because a whole peanut lodged at the carina (Fig. 2A). As many other reports have concluded [1-4], bronchoscopy was the most reliable diagnostic and therapeutic method.

Knowledge of the precise location of the peanut in the bronchus before bronchoscopy reduces the chances that small pieces of the peanut or peanut fragments (Fig. 1C) might be missed.

REFERENCES

1. Saijo S, Tomioka S, Takasaka T, et al. Removal of foreign bodies in the airway by means of the ventilation bronchoscope: analysis of 100 cases. *Nihon Kikan Shokudo Kaiho* **1977**;28:211-233
2. Gay BB Jr. Radiologic evaluation of the nontraumatized child with respiratory distress. *Radiol Clin North Am* **1978**;16:91-112
3. McGuirt WF, Holmes KD, Feehs R, et al. Tracheobronchial foreign bodies. *Laryngoscope* **1988**;98:615-618
4. Blumhagen JD, Wesenberg RL, Brooks JG, et al. Endotracheal foreign bodies: difficulties in diagnosis. *Clin Pediatr* (Phila) **1980**;19:480-484

Ductal Carcinoma In Situ of the Breast: Correlation Between Mammographic Calcification and Tumor Subtype

Paul C. Stomper[1]
James L. Connolly[2]

OBJECTIVE. Histologic subtypes of ductal carcinoma in situ of the breast have been correlated with disease progression after local excision only. This study was undertaken to determine how the predominant type of calcification seen on mammography correlates with the predominant histologic tumor subtype, knowledge that could aid in the development of clinical criteria for selecting patients for appropriate local treatment.

MATERIALS AND METHODS. A prospective double-blind study was performed to correlate the mammographic and histologic findings in 66 consecutive cases of ductal carcinoma in situ, or ductal carcinoma in situ associated with small invasive foci ($n = 11$), in which microcalcifications seen on mammograms were found in the ductal carcinoma during histologic evaluation of excisional biopsy specimens. Microcalcifications were categorized as predominantly linear or granular and were correlated with the predominant histologic subtype of ductal carcinoma in situ in the tissue containing the calcifications seen on mammograms.

RESULTS. Predominantly linear calcifications were present in 47% (18/38) of ductal comedocarcinomas in situ compared with 18% (5/28) of cribriform, solid, or papillary subtypes ($p = .01$). Predominantly granular calcifications were present in 53% (20/38) of comedocarcinomas compared with 82% (23/28) of the noncomedo types ($p = .01$). In 94% (16/17) of cribriform ductal carcinomas in situ, granular microcalcifications were seen on mammograms. Seventy-eight percent (18/23) of linear calcifications in ductal carcinoma in situ were associated with the comedo subtype, whereas 53% (23/43) of the granular calcifications were associated with noncomedo subtypes.

CONCLUSION. We conclude that the comedo subtype of ductal carcinoma in situ is more likely to be accompanied by linear calcifications than are the noncomedo subtypes, and noncomedo ductal carcinoma in situ is more likely to be associated with granular calcifications than is the comedo subtype when microcalcifications are seen on mammograms. However, there is considerable overlap, and the predominant histologic subtype cannot be predicted on the basis of the microcalcification type with a high degree of accuracy.

***AJR* 159:483-485, September 1992**

Ductal carcinoma in situ (DCIS), a lesion that was diagnosed less frequently before mammography, now accounts for 22–45% of breast cancers detected in patients undergoing biopsy for clinically occult lesions seen on mammography [1–4]. At a time when breast conservation in invasive carcinoma is becoming increasingly accepted, mastectomy remains the most common therapy for DCIS, with survival rates approaching 100% in several large series [5–7]. Demand for breast conservation is increasing among patients with DCIS, and some retrospective studies indicate that some subsets of patients may be adequately treated without mastectomy [8–10]. Recently, Lagios et al. [11] have shown a correlation between histologic subtypes of DCIS and the frequency of breast cancer recurrence during a short follow-up period after treatment consisting of local excision alone. Comedo-type DCIS was associated with a greater local recurrence rate than were the micropapillary or nonnecrotic cribriform subtypes. This prospective double-blind

Received January 28, 1992; accepted after revision March 31, 1992.

[1] Department of Diagnostic Radiology, Dana-Farber Cancer Institute, Harvard Medical School, Boston, MA 02115. Present address: Department of Diagnostic Radiology, Roswell Park Cancer Institute and School of Medicine and Biomedical Sciences, State University of New York at Buffalo, Elm and Carlton Sts., Buffalo, NY 14263. Address reprint requests to P. C. Stomper.

[2] Department of Pathology, Beth Israel Hospital, Harvard Medical School, Boston, MA 02115.

0361-803X/92/1593-0483
© American Roentgen Ray Society

study was undertaken to determine the correlation between mammographic microcalcification types, predominantly granular or linear, and histologic subtypes of DCIS.

Materials and Methods

This prospective double-blind study was performed to correlate the mammographic and histologic findings in 66 consecutive cases of DCIS, or DCIS associated with small invasive foci (n = 11), in which microcalcifications seen on mammograms were found to be present in the DCIS during histologic evaluation of excisional biopsy specimens. The median age of the patients was 50 years (range, 31–71).

Mammograms were obtained with different high-resolution film-screen systems from several centers. Mammograms consisted of craniocaudal and oblique projections. Accessory views, including magnification techniques in 27 patients, were performed at the discretion of the mammographer. Specimen radiographs were obtained to confirm excision of the microcalcifications and guide the histologic examination. All mammograms were prospectively reviewed and categorized by one radiologist without knowledge of the histologic findings. Mammographic microcalcifications were categorized as predominantly granular or linear, as described in the mammographic literature [12, 13]. Clusters of calcifications consisting of predominantly granular calcifications with a few linear calcifications were categorized as granular (Fig. 1).

Histologic material was stained with hematoxylin and eosin. Histologic assessment was made with knowledge of the presence and location of mammographic microcalcifications, so that specific anatomic correlation could be made, but without knowledge of the specific category of mammographic microcalcification in each case. Histologic subtypes of DCIS included comedo and noncomedo subtypes: cribriform, solid, and small papillary. The predominant histologic subtype in each case was recorded.

For the purposes of this analysis, the comedo subtype was compared with the noncomedo subtypes. The p values were determined by using χ^2 analysis [14].

Results

Fifteen percent of the mammographic calcification clusters measured 40 mm or greater in extent, and 35% measured 20 mm or less.

Overall, 65% (43) of the microcalcification clusters associated with DCIS were predominantly granular; 35% (23) were predominantly linear. Linear calcifications were present in 47% (18/38) of predominantly comedo DCIS and 18% (5/28) of predominantly cribriform, solid, or papillary DCIS (p = .01, Table 1). Predominantly granular calcifications were present in 53% (20/38) of comedo DCIS and 82% (23/28) of the noncomedo types (p = .01). The cribriform subtype of DCIS nearly always (94%, 16/17) was associated with granular calcifications.

Seventy-eight percent (18/23) of linear calcifications associated with DCIS were in comedo DCIS, as compared with 47% (20/43) of granular calcifications (p = .01). Fifty-three percent (23/43) of granular microcalcifications associated with DCIS were in noncomedo DCIS, as compared with 22% (5/23) of linear calcifications (p = .01).

The microcalcifications associated with the comedo type of DCIS were usually found during histologic evaluation to represent amorphous deposits within necrotic debris. Microcalcifications in the noncomedo types, especially in cribriform, were usually well-defined deposits within round spaces.

Discussion

The observation that a majority (65%) of microcalcifications associated with DCIS were of the granular type is similar to that in a previous report of the mammographic features of DCIS [13]. In our study, granular calcifications were associated with comedo DCIS and the noncomedo subtypes of DCIS in similar percentages of patients, 47% and 53%, respectively. DCIS of predominantly cribriform subtype showed the greatest correlation of any of the histologic subtypes with a mammographic microcalcification type; 94% had granular microcalcifications.

Although linear calcifications were more likely to be associated with comedo DCIS (78%), there was a significant overlap of association between histologic subtypes and linear calcifications: 22% of linear calcification clusters were in predominantly noncomedo DCIS. Also, comedo DCIS was as-

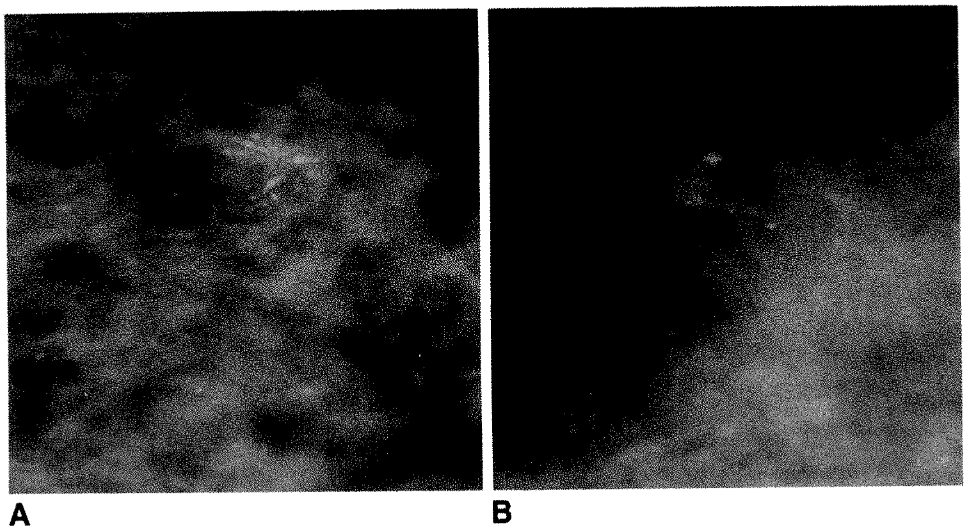

Fig. 1.—*A* and *B*, Predominantly linear (*A*) and granular (*B*) calcifications in ductal carcinoma in situ.

TABLE 1: Correlation of Mammographic Microcalcification Type with Predominant Histologic Subtype of Ductal Carcinoma In Situ

Predominant Histologic Subtype	No. of Cases by Microcalcification Type (%)		
	Linear	Granular	Total
Comedo	18 (78)	20 (47)	38 (47)
Noncomedo			
Cribriform	1	16	17
Solid	2	5	7
Small papillary	2	2	4
Subtotal	5 (22)	23 (53)	28
Total	23 (100)	43 (100)	66 (100)

sociated with linear and granular microcalcification types in similar percentages, 47% and 53%, respectively.

Our data are similar to those included in the mammographic-pathologic correlations of Holland et al. [15], who observed mammographic linear microcalcifications alone or mixed with the granular type in 85% (40/47) of the predominantly comedo DCIS with mammographic microcalcifications, as compared with 29% (5/17) of the predominantly micropapillary or cribriform tumors with mammographic microcalcifications. Their study also showed that the mammographic microcalcifications associated with the micropapillary and cribriform subtypes were more likely to be found in only part of the tumor and, therefore, underestimated the histologic extent of tumor, as compared with mammographic microcalcifications associated with predominantly comedo DCIS, which when present more accurately reflected the size of the tumor [15]. Their observation will be helpful in the identification of the extent of DCIS in the breast and may help in the selection of patients for breast-conserving therapy.

These data are compatible with the mechanisms of microcalcification pathogenesis described in the literature [12, 13, 15–18]. The linear calcifications may represent not only coalescence of well-formed dystrophic calcification of intraluminal cellular debris seen with standard histologic preparation but also a high concentration of calcium in adjacent necrotic cells that is not often visible to the pathologist unless specific calcium stains are used. Granular calcifications represent either foci of dystrophic calcifications in necrotic tumor cells that have not coalesced to form linear casts or calcified secretions or mucin found in the spaces of histologic subtypes other than comedocarcinoma, such as the cribriform pattern.

Dystrophic calcifications in necrotic debris of comedocarcinoma that have not coalesced to form linear casts most likely account for the smaller percentage of comedo DCIS cases that are associated with granular calcifications. A smaller percentage of linear microcalcifications is seen in noncomedo DCIS, probably because there is less necrotic debris in noncomedo DCIS. Also, as several histologic subtypes of DCIS are often present in a single case, some mammographic microcalcifications may be contributed by nonpredominant histologic subtypes.

We conclude that, in DCIS associated with mammographic microcalcifications, the predominant histologic subtype cannot be predicted on the basis of the microcalcification type with a high degree of accuracy. However, comedo DCIS is more likely to be accompanied by linear calcifications than is noncomedo DCIS, and noncomedo DCIS is more likely to be accompanied by granular calcifications than is comedo DCIS. Increased knowledge of the mammographic-pathologic correlations in DCIS will improve our understanding of DCIS and may aid in the development of clinical criteria for the selection of patients for appropriate local treatment.

ACKNOWLEDGMENTS

We thank Barbara Silver for data management, Okhee Suh for statistical analysis, Christine Kuznicki for assistance in manuscript preparation, and Jay Harris and Stuart Schnitt for manuscript review.

REFERENCES

1. Meyer JE, Kopans DB, Stomper PC, Lindfors KK. Occult breast abnormalities: percutaneous preoperative needle localizations. *Radiology* **1984**;150:335–337
2. Ciatto S, Cataliotti L, Distante V. Nonpalpable lesions detected with mammography: review of 512 consecutive cases. *Radiology* **1987**;165:99–102
3. Hall FM, Storella JM, Silverstone DZ, Wyshak G. Nonpalpable breast lesions: recommendations for biopsy based on suspicion of carcinoma at mammography. *Radiology* **1988**;167:353–358
4. Meyer JE, Eberlein TJ, Stomper PC, Sonnenfeld MR. Biopsy of occult breast lesions: analysis of 1261 abnormalities. *JAMA* **1990**;263:2341–2343
5. Ashikari R, Huvos AG, Snyder RE. Prospective study of non-infiltrating carcinoma of the breast. *Cancer* **1977**;35:435–439
6. Sunshine JA, Moseley HS, Fletcher WS, Krippaehne WW. Breast carcinoma in situ: a retrospective review of 112 cases with a minimum 10 year follow-up. *Am J Surg* **1985**;150:44–51
7. Farrow JH. Current concepts in the detection and the treatment of the earliest of the early breast cancers. *Cancer* **1970**;25:468–477
8. Schnitt SJ, Silen W, Sadowsky NL, Connolly JL, Harris JR. Ductal carcinoma in situ (intraductal carcinoma of the breast). *N Engl J Med* **1988**;318:898–903
9. Rosen PP, Braun DW Jr, Kinne DW. The clinical significance of pre-invasive breast carcinoma. *Cancer* **1980**;46:919–925
10. Page DL, Dupont WD, Rogers LW, Landenberger M. Intraductal carcinoma of the breast: follow-up after biopsy only. *Cancer* **1982**;49:751–758
11. Lagios MD, Margolin FR, Westdahl PR, Rose MR. Mammographically detected ductal carcinoma in situ: frequency of local recurrence following tylectomy and prognostic effect of nuclear grade on local recurrence. *Cancer* **1989**;63:618–624
12. Tabar L, Dean PB. *Teaching atlas of mammography*, 2nd ed. New York: Thieme-Stratton, **1985**:138–139
13. Stomper PC, Connolly JL, Meyer JE, Harris JR. Clinically occult ductal carcinoma in situ detected with mammography: analysis of 100 cases with radiologic-pathologic correlation. *Radiology* **1989**;172:235–241
14. Fisher RA. *Statistical methods for research workers*. Edinburgh: Edinburgh University, 1934
15. Holland R, Hendriks JHCL, Verbeek ALM, Mravunac M, Schuurmans Stekhoven JH. Clinical practice: extent, distribution, and mammographic/histological correlations of breast ductal carcinoma in situ. *Lancet* **1990**;335:519–522
16. Ahmed A. Calcifications in human breast carcinomas: ultrastructural observations. *J Pathol* **1975**;117:247–251
17. Levitan LH, Witten DM, Harrison EG. Calcification in breast disease: mammographic-pathologic correlation. *AJR* **1964**;92:29–39
18. Egan RL, McSweeney MB, Sewell CW. Intramammary calcifications without an associated mass in benign and malignant disease. *Radiology* **1980**;137:1–7

Book Review

Screen Film Mammography. Imaging Considerations and Medical Physics Responsibilities. Proceedings of SEAAPM Spring Symposium, April 6, 1990, Columbia, South Carolina. Edited by Gary T. Barnes and G. Donald Frey. Madison, WI: Medical Physics Publishing, 242 pp., 1991. $40

This book of proceedings is the result of a mammography symposium held in Columbia, SC, in April 1990. The organizers considered that a need existed for dissemination of information on appropriate physics measurements and responsibilities in mammography, and the symposium was designed to provide attendees with the best available and most current mammography physics information.

The book is divided into nine subject areas, each written by different authors: a technical overview of screen-film mammography by A. Haus; design of mammography X-ray generators by D. M. Gaunt; measurement of mammography X-ray tube characteristics by G. T. Barnes; contrast and grid performance by A. J. Wagner; screen-film selection, film exposure, and processing by C. Kimme-Smith; breast dosimetry by X. Wu; equipment acceptance testing and quality control by G. D. Frey; documentation and reports by G. T. Barnes and G. D. Frey; and American College of Radiology (ACR) accreditation program and physics responsibilities by R. L. Tanner and R. E. Hendrick.

Haus provides a fine overview of the interactions of the various elements in screen-film mammography that are elaborated on, including working practices, in later sections. The section on X-ray generators describes the philosophy behind recent advances in generator engineering and contains information rarely found in the radiologic literature on circuits and equipment specifications. The chapter titled "Tube Potential, Focal Spot, Radiation Output and HVL Measurements" gives details on how these parameters can be measured and includes state-of-the-art specifications and typical measured values.

The next section, on contrast and grid performance, presents modeling concepts and a discussion of the interplay between subject contrast and patients' exposure to radiation as a function of grid performance. It concludes that, for the present, acceptance testing and quality control of grids is limited to checking for grid lines and grid artifacts and gives brief advice on these subjects. The section on screen-film selection, film exposure, and processing is excellent. Summary discussions of instrumentation and steps in quality assurance inspection and audit and common sources of problems are supplemented by good references. The section also contains some iconoclastic ideas on combining film and screens from different manufacturers for optimum speed and resolution and a discussion of "push processing."

The section on breast dosimetry reviews the conventional method of computing the average glandular dose from the breast entrance skin exposure and from tables published by the Food and Drug Administration. The dated nature of the tables (too wide a range of half-value layers, wrong waveform for current practice) is indicated, and alternative tables requiring less interpretation are provided, ones based on more sophisticated calculations that use data on current X-ray spectra. Sensible suggestions are offered to reduce the ambiguities regarding maximum acceptable dose.

The section on equipment acceptance testing and quality control follows, with many practical hints and tips, checklists, and ranges of normal values. A clear and useful distinction is made between the number and frequency of measurements for acceptance testing and for routine quality control. Some ideas on the performance of older equipment are included. Documentation of the aforementioned measurements and the form and content of such documents is detailed in the succeeding section, together with public relations hints.

The volume concludes with an account of the origin and operation of the ACR-sponsored voluntary mammography screening program. The results from participating centers show little correlation between the patient's dose of radiation and the quality of the image. This implies variations in equipment performance, film processing, and judgment of the techniques to be used. The first two items are certainly in the purview of physicists, and this volume is an effort to increase physicists' expertise.

The publication is on good paper with adequate and clear tables and figures. I found only two editorial errors that were easily corrected by the reader from the contents. This is a how-to book, not an academic sourcebook. Consulting physicists and new employees of mammography screening centers will find it of immediate practical use.

Peter Wootton
University of Washington
Seattle, WA 98195

Solitary Breast Papilloma:

Comparison of Mammographic, Galactographic, and Pathologic Findings

E. R. Woods[1]
M. A. Helvie[1]
D. M. Ikeda[1]
S. H. Mandell[2]
K. L. Chapel[3]
D. D. Adler[1]

OBJECTIVE. Our purpose was to determine the mammographic/galactographic features of solitary breast papillomas and to correlate these features with the pathologic findings.

MATERIALS AND METHODS. Retrospective review of pathology files revealed 72 women in whom breast biopsy reports described a solitary papilloma. All patients with additional pathologic abnormalities were excluded from this study. Patients meeting the pathologic criteria and for whom mammograms, galactograms, or both were available and had been obtained within 6 months before biopsy were included. Twenty-four women met these criteria and form the basis of this study. Presenting clinical signs and symptoms were reviewed. Abnormal mammographic/galactographic findings were correlated with pathologic features.

RESULTS. Nipple discharge was present in 21 (88%) of 24 patients, two (8%) of 24 patients had abnormal findings on screening mammography, and one patient had a palpable mass that was visible on mammograms. Eight (42%) of 19 mammograms had abnormal findings, including dilated duct(s) in five cases (26%), nodules in two cases (11%), and microcalcifications in one case (5%). All technically adequate galactograms (13/15) had abnormal findings, with 12 (92%) of 13 showing an intraluminal filling defect. The other technically adequate galactogram (8%) showed only a solitary obstructed duct. Ductal dilatation was greatest at or central to the papilloma on 12 (92%) of 13 galactograms. Imaging features correlated well with the histologic findings.

CONCLUSION. Patients with solitary papillomas most commonly have nipple discharge, normal mammographic findings, and a galactographic filling defect. Galactography is useful for localizing papillomas.

AJR 159:487-491, September 1992

Solitary intraductal papilloma of the breast is a common benign mammary neoplasm and is the most common neoplasm associated with nipple discharge in women [1-7]. Women with solitary papillomas have a 1.5-2.0 times increased risk of invasive carcinoma developing [8]. Despite the frequency of solitary breast papillomas and the extensive analysis of papillary breast neoplasms in the pathologic literature [1, 3, 5, 9-18], little has been written about the radiologic features of this lesion. We report the results of a retrospective study performed to determine the mammographic/galactographic features of solitary breast papillomas and to correlate these results with the pathologic findings.

Materials and Methods

On review of our hospital pathology files for the period between February 1975 and February 1991, we found 72 women in whom the breast biopsy report described a solitary papilloma. Solitary papilloma was diagnosed on the basis of the standard description by Azzopardi [3] and Page and Anderson [11]. Twelve (17%) had an associated carcinoma in the same biopsy specimen. All patients with additional pathologic abnormalities (i.e., cyst, atypical hyperplasia, fibrosis, fibroadenoma, and/or carcinoma) were excluded from this study. Patients meeting the pathologic criteria and for whom diagnostic imaging studies were

Received February 7, 1992; accepted after revision March 24, 1992.

[1] Department of Radiology, Room 2910 Taubman Center, University of Michigan Hospitals, 1500 E. Medical Center Dr., Ann Arbor, MI 48109-0326. Address reprint requests to M. A. Helvie.

[2] Department of Pathology, Room 2G332, University of Michigan Hospitals, 1500 E. Medical Center Dr., Ann Arbor, MI 48109-0326.

[3] School of Medicine, University of Michigan, 1301 Catherine, Ann Arbor, MI 48109

0361-803X/92/1593-0487
© American Roentgen Ray Society

available and had been done within 6 months before the biopsy were included. Twenty-four women (average age, 49 years; age range, 19-81 years) met these criteria and were included in this study. Generally the patients returned every 12-24 months for mammography after biopsy of the papilloma, enabling clinical and mammographic follow-up to be done by reviewing each patient's breast imaging file.

The presenting clinical situation (serous or serosanguineous nipple discharge, palpable mass, or asymptomatic with abnormal findings on a screening mammogram) was obtained from breast imaging files. The method of localization of the papilloma for surgical biopsy was recorded as either mammographic wire localization or guidance by complementary galactography and clinical findings. When the surgical biopsy was not guided by mammographic wire localization, the surgeon identified the discharging duct, inserted a lacrimal gland probe into the offending duct (via the duct orifice), and then excised a 4- to 5-cm wedge of retroareolar tissue surrounding the probe.

Dedicated screen-film mammographic equipment was used, including 500-T or 600-T (General Electric CGR, Milwaukee, WI) and Mamex DC Mag (Technomed USA, Bayshore, NY) units. A few studies were performed at outside institutions with dedicated equipment of unknown type. Galactography was done by using standard technique [4]. Craniocaudal and mediolateral views with mild compression were obtained after contrast injection. Magnification views were obtained when indicated. A second injection followed by repeated radiographs was done routinely. All mammograms and galactograms were reviewed individually by three radiologists. Differences of opinion regarding the imaging features were settled by consensus.

Mammograms were evaluated for the presence of dilated duct(s), circumscribed masses, clustered calcifications, architectural distortion, and developing or asymmetric densities. The location of mammographic abnormalities and their distance from the nipple were recorded.

Galactograms were assessed for the presence of filling defect(s), obstructed duct(s), or dilated duct(s). The distance of the only or dominant filling defect from the nipple was measured. The maximum diameter of the duct was measured, and its location relative to the only or dominant filling defect was recorded.

All histologic slides and mammograms/galactograms for each patient were jointly reviewed by a pathologist and a radiologist, and imaging features were correlated with pathologic findings.

Results

Of the 24 patients included in this study, 21 (88%) had nipple discharge (associated with a palpable mass in one patient). The discharge was sanguineous in 19 (91%) of 21 patients. Two patients (9%) had only serous discharge. In the 21 patients with nipple discharge, the location of the surgical biopsy was based on clinical and/or galactographic findings. Two additional patients were asymptomatic, but a suspicious mammographic abnormality (a circumscribed round mass and clustered microcalcifications) was seen on screening mammograms. These two patients had biopsies with wire localization. The final patient had a palpable mass that was visible on mammograms. The mass was not successfully removed during palpation-directed biopsy, but a small papilloma was incidentally discovered in the biopsy specimen.

Nine patients had mammography only, five patients had galactography only, and 10 patients had both studies. Results were normal in 11 (58%) of the 19 patients who underwent mammography. Mammographic findings were abnormal in eight (42%) of 19 patients; these included single (three patients, Fig. 1) and multiple (two patients) dilated ducts in five patients (26%), a solitary benign-appearing circumscribed mass (8 and 7 mm in diameter) in two patients (11%), and a suspicious cluster of four or five irregular microcalcifications (Fig. 2) associated with multiple dilated ducts in one patient (5%). All masses and calcifications were located less than 5 cm from the nipple.

Findings on all 13 of the technically satisfactory galactograms were abnormal, with 12 (92%) of 13 showing either solitary (nine patients, Figs. 3 and 4) or multiple (three patients) intraluminal filling defects. Two of the patients with a solitary filling defect also had an associated adjacent obstructed duct, and one patient had multiple dilated ducts associated with a solitary filling defect. In one patient, a single obstructed duct was the sole galactographic finding. Two galactographic studies were nondiagnostic because cannulation of the discharging duct was unsuccessful.

The filling defects were a median of 3 mm in diameter, with an intraductal fingerlike projection of variable length measuring up to 20 mm long. In four cases the largest or only filling defect was more oval and was associated with focal dilatation of the duct. The two largest filling defects were 16 × 7 mm (Fig. 3) and 12 × 10 mm. The filling defects seen on the galactograms were on average 22 mm from the nipple (range, 5-40 mm). Filling defects that were proved to be due to a solitary papilloma commonly had irregular margins.

The mean maximum ductal diameter was 5 mm (13 cases), with a range of 3-10 mm. The widest diameter of the duct was at (four cases) or central to (toward the nipple, eight cases) the largest filling defect in 92% of cases. The widest part of the duct was peripheral (proximal) to the largest filling defect in only one patient (8%).

Only three of the eight patients with abnormal mammographic findings were imaged with galactography also. Two of these patients had multiple dilated ducts in the same location shown by mammography and galactography. One of the dilated ducts in one patient contained three filling defects (maximum diameter, 7 mm), while one duct in the other patient had two filling defects (maximum diameter, 9 mm). Mammographically, the third patient had a solitary dilated duct that

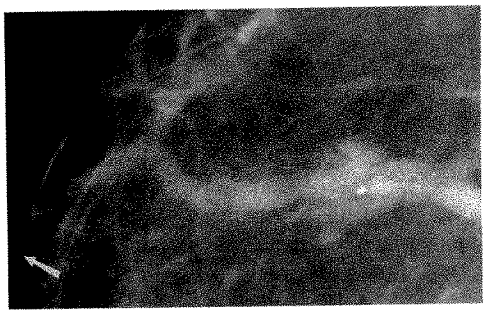

Fig. 1.—Mammogram of a solitary dilated duct in a patient who had a clinically directed biopsy that revealed a solitary papilloma. *Arrow* points toward immediately adjacent nipple (*not shown*).

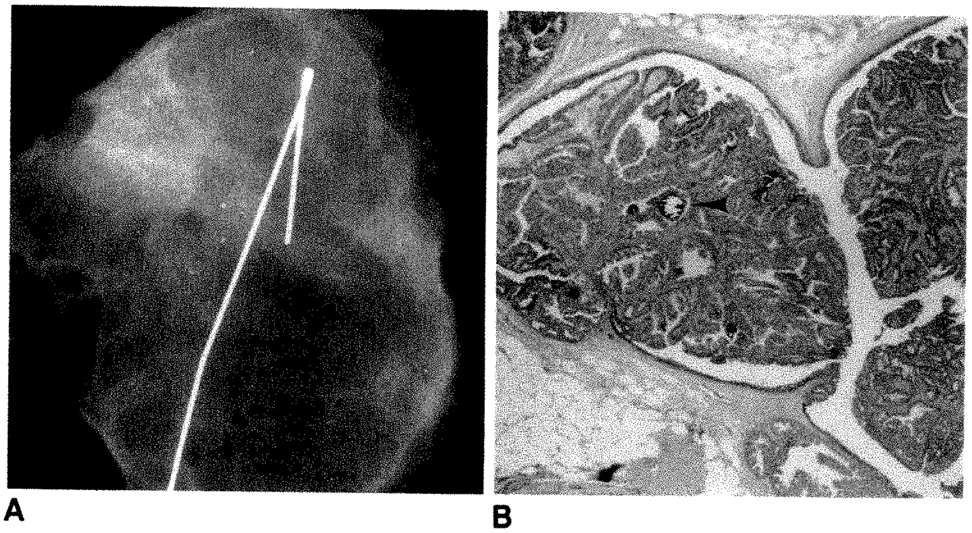

Fig. 2.—Microcalcifications directly correlated with solitary papilloma on screening mammogram.

A, Specimen radiograph shows a cluster of four or five slightly heterogeneous, rounded microcalcifications associated with nonspecific soft tissue, adjacent to embedded localization wire.

B, Photomicrograph of biopsy specimen shows solitary papilloma with apocrine features and microcalcifications (*arrowhead*). Calcifications are present in epithelial and stromal locations. (H and E, original magnification ×20)

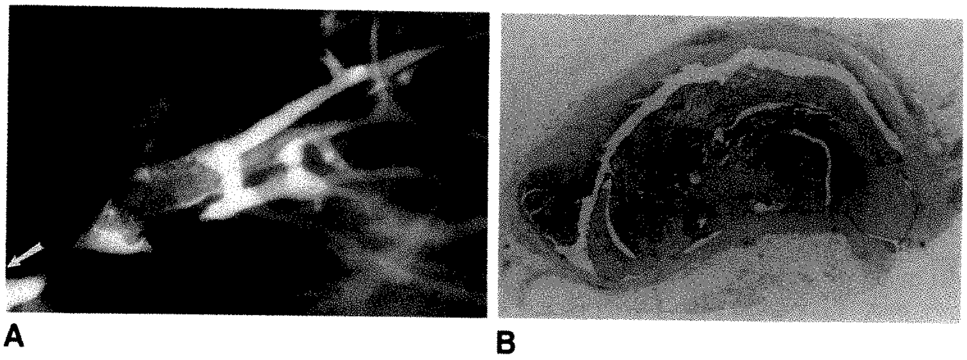

Fig. 3.—Galactographic filling defect directly correlated with a solitary papilloma.

A, Magnified galactogram shows an oval filling defect in retroareolar region of irregularly dilated duct. *Arrow* points toward immediately adjacent nipple (*not shown*).

B, Low-power photomicrograph of ectatic duct filled by an oval, focally sclerotic papilloma. (H and E, original magnification ×10)

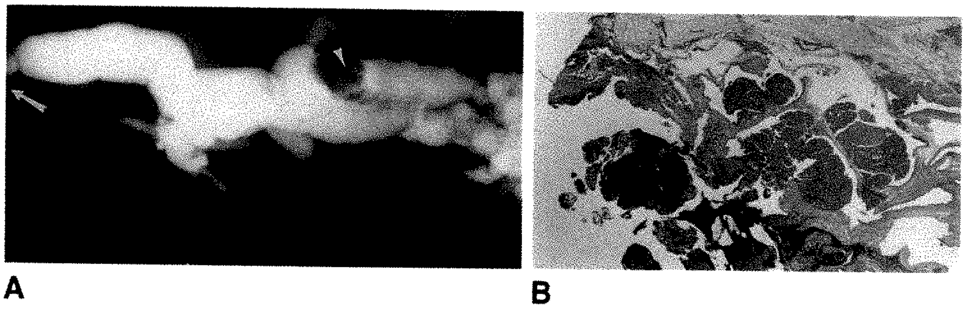

Fig. 4.—Galactographic filling defect directly correlated with a solitary papilloma.

A, Magnified galactogram shows a rounded filling defect within a grossly dilated duct. Curvilinear tracks of contrast material are seen extending into interstices of lesion (*arrowhead*). *Arrow* points toward immediately adjacent nipple (*not shown*).

B, Low-power photomicrograph of biopsy specimen shows cross section of ectatic, tortuous duct filled with papilloma. This papilloma displayed focal fibrosis. Overall pattern correlates well with appearance on galactogram (H and E, original magnification ×6)

correlated both in appearance and location with an ectatic duct (containing a 2-mm filling defect) seen galactographically.

Imaging features correlated directly with the size and appearance of the papilloma at pathologic examination in 15 (83%) of 18 cases. A papilloma was present in all surgical specimens at the site of needle localization or at the site of a galactographic filling defect. In three patients, two or three filling defects were seen at galactography, but only one papilloma was identified in the initial pathologic examination and in the retrospective review. Histologic correlation was not possible in the two cases in which the galactogram was technically inadequate and the four cases in which the mammographic findings were normal and no galactogram was obtained. Moderate to marked density of the breast tissue may have obscured the papilloma (maximum diameter of the largest papilloma, 11 mm) in these four cases. The most common associated pathologic finding was ductal ectasia, which was seen in 11 (46%) of 24 patients.

In an average clinical and mammographic follow-up of 18 months (range, 0–70 months), breast carcinoma did not develop in any patient.

Discussion

Solitary breast papillomas are grouped in the general category of papillary neoplasms of the breast (including papilloma, multiple papillomas, and papillary carcinoma). Most solitary papillomas occur centrally in the large subareolar ducts. The consensus opinion of the College of American Pathologists [8] is that solitary papillomas are associated with a slightly increased risk of breast carcinoma, but this relationship remains controversial [1, 3, 10, 11, 13–18]. Pathologically [1, 3, 5, 11, 14, 15, 17], a breast papilloma is a masslike projection that consists of arborescent fronds attached to the inner mammary duct wall by a stalk containing a fibrovascular core. These typically measure 2–3 mm in diameter, with variable extension along the duct [1, 3, 11, 17]. Ductal ectasia is associated with solitary papillomas [14, 15] and was seen in almost 50% of our patients.

Nipple discharge of less than 6 months' duration is the most common and dominant clinical sign associated with breast papillomas, and is seen in 64–88% of patients [1, 2, 15, 16]. Typically this discharge is sanguineous, but various studies have shown that a significant percentage (29–48%) of patients have only serous discharge [1, 2, 4, 19]. In our study, 88% of patients had nipple discharge, and 9% of these patients had only serous discharge. Our finding of a lower percentage of patients with nonbloody discharge may be related to strict selection of patients with solitary papillomas.

Papillomas are typically not seen on mammograms because of their small size, lack of associated calcification or fibrosis, and intraductal location [5, 17, 18]. Almost 60% of our patients had normal mammographic findings, in accord with the results of Cardenosa and Eklund [16]. Mammographic findings that may be present [5, 16–18] include benign-appearing circumscribed masses of various sizes (typically retroareolar in location), a solitary dilated retroareolar duct, and rarely, calcifications. Mammographically identified calcifications within a papilloma may be rounded, crescentic, or eggshell-like but can have other appearances indistinguishable from clustered microcalcifications seen in malignant lesions [5, 17, 18]. All these mammographic findings were observed in our study group, including solitary dilated ducts (16%), multiple dilated ducts (11%), nodules (11%), and a suspicious cluster of microcalcifications (5%).

Galactography has been advocated as the diagnostic procedure of choice in patients with nipple discharge [2, 4, 6, 7, 17, 20]. Typically, a papilloma will cause either a smooth filling defect or a complete obstruction to retrograde flow of contrast material. Galactographic findings suggestive of carcinoma include irregular filling defect(s), ductal abnormalities (irregularity, distortion, displacement, and/or stenotic encasement), complete obstruction to retrograde flow of contrast material, and/or contrast extravasation [6, 17, 20, 21]. Because of the significant overlap in galactographic findings, one cannot reliably differentiate between carcinoma and benign papillomas [17, 20, 21]. In particular, we commonly noted irregular margins of filling defects that were later proved to be due to a solitary papilloma.

Galactography has been shown to be useful in identifying and localizing abnormalities of the discharging duct and therefore is potentially useful to the breast surgeon [2, 4–7, 17, 18, 20, 21]. Our breast surgeons have differing opinions concerning the utility of galactography in the investigation of nipple discharge. Some consider galactography a procedure complementary to duct excision guided by intraoperative cannulation of the discharging duct with a probe and therefore routinely obtain preoperative galactograms. Others generally do not obtain a galactogram before surgical excision of a bloody discharging duct and reserve galactography for selected cases of nonbloody nipple discharge. Theoretically, a galactogram could show the rare peripheral abnormality that might be missed by a "blind" retroareolar biopsy guided only by cannulation of the duct with a probe. The offending duct is still generally excised in those rare cases when a galactogram is obtained preoperatively for bloody nipple discharge and the galactographic findings are normal.

All technically satisfactory galactograms in our study showed abnormalities, with 92% showing filling defect(s). The filling defect was solitary in 75%, usually retroareolar, and was generally 2–3 mm in diameter with various degrees of intraductal extension. In three patients, two or three filling defects were seen at galactography, but only one papilloma was identified pathologically. Intraductal debris or clot adjacent to the papilloma most likely explains this discrepancy, but it cannot be stated with certainty that the multiple filling defects did not originally represent multiple papillomas and that the surgical specimen included only one of the papillomas. Complete obstruction of retrograde flow of contrast material was seen in only three of 13 diagnostic studies, and this finding was the only galactographic abnormality in one patient.

Cardenosa and Eklund [16] found abnormalities on 32 (91%) of 35 galactograms obtained to investigate problems subsequently proved to be due to solitary papillomas. Ten cases (29%) showed expansion or distortion of the duct, 10 ducts (29%) were completely obstructed, eight cases (23%) had filling defects, three had irregularity of the duct wall (including one with associated obstruction), and one case showed ductal ectasia. Our results were somewhat different. In particular, we observed filling defect(s) on 92% of diagnostic galactograms, four times the frequency noted in their study. This discrepancy may be due to our strict exclusion of cases of solitary papillomas associated with other abnormalities.

The ductal system was generally dilated in all the satisfactory galactographic studies. Most filling defects (92%) were at or peripheral to the widest portion of the ductal system, even in those cases in which the papilloma was clearly obliterating most of the duct's lumen. One might expect that the ductal system would be most dilated "upstream" to a significant obstructing papilloma, but this was seen in only one case. The explanation for this finding is unclear, but possibilities would include "downstream" dilatation of the ducts due to chronic discharge, distension of the duct due to pressure of injection, and underlying ductal ectasia.

In conclusion, most patients with a solitary papilloma had sanguineous nipple discharge. The papilloma was typically mammographically occult and appeared on galactograms as a filling defect, or less commonly an obstructed duct. Other mammographic findings such as circumscribed masses, single dilated ducts, or calcifications were observed occasionally. As galactography does not allow accurate differentiation of benign from malignant lesions, excisional biopsy should be considered whenever galactographic findings are abnormal. In light of the consensus that solitary papillomas are associated with a slightly increased risk of breast carcinoma and our pathologic review finding of 17% of cases of solitary papillomas associated with carcinoma, close clinical and mammographic follow-up of these patients is recommended.

REFERENCES

1. Haagensen CD. *Diseases of the breast*, 3rd ed. Philadelphia: Saunders, **1986**:136–149
2. Ciatto S, Bravetti P, Berni D, Catarzi S, Bianchi S. The role of galactography in the detection of breast cancer. *Tumori* **1988**;74:177–181
3. Azzopardi J. *Problems in breast pathology*. Philadelphia: Saunders, **1979**:150–155
4. Tabár L, Dean PB, Péntek Z. Galactography: the diagnostic procedure of choice for nipple discharge. *Radiology* **1983**;149:31–38
5. Peters ME. Benign masses. In: Peters ME, Voegeli DR, Scanlan KA, eds. *Handbook of breast imaging*. New York: Churchill Livingstone, **1989**: 141–162
6. Tabár L, Marton Z, Kadas I. Galactography in the examination of secretory breasts. *Am J Surg* **1974**;127:282–286
7. Muller JW. Pathological secretion of the breast. *Diagn Imaging* **1982**;51:62–68
8. Cancer Committee of the College of American Pathologists. Is "fibrocystic disease" of the breast precancerous? *Arch Pathol Lab Med* **1986**;110: 171–173
9. Ohuchi N, Abe R, Invahashi T, Tezuka F. Origin and extension of intraductal papillomas of the breast: a three-dimensional reconstruction study. *Breast Cancer Res Treat* **1984**;4:117–128
10. Ohuchi N, Abe R, Kasai M. Possible cancerous change of intraductal papillomas of the breast. *Cancer* **1984**;54:605–611
11. Page DL, Anderson TJ. *Diagnostic histopathology of the breast*. New York: Churchill Livingstone, **1987**:104–119
12. Haagensen CD, Bodian C, Haagensen DE. *Breast carcinoma: risk and detection*. Philadelphia: Saunders, **1981**:146–237
13. Carter D. Intraductal papillary tumors of the breast. *Cancer* **1977**;39: 1689–1692
14. Murad TM, Swaid S, Pritchett P. Malignant and benign papillary lesions of the breast. *Hum Pathol* **1977**;8:379–390
15. Murad TM, Contesso G, Mouriesse H. Papillary tumors of large lactiferous ducts. *Cancer* **1981**;48:122–133
16. Cardenosa G, Eklund GW. Benign papillary neoplasms of the breast: mammographic findings. *Radiology* **1991**;181:751–755
17. Kopans DM. *Breast imaging*. Philadelphia: Lippincott, **1989**:274–277
18. Paulus DD. Benign diseases of the breast. *Radiol Clin North Am* **1983**;21:27–50
19. Fung A, Rayter Z, Fisher C, King DM, Trott P. Preoperative cytology and mammography in patients with single-duct nipple discharge treated by surgery. *Br J Surg* **1990**;77:1211–1212
20. Nishida M, Johno N, Murakami T, Suzuki T, Morioka H, Imai Y. Usefulness of galactography for minimal noninvasive ductal carcinoma of the breast. *Nippon Geka Hokun* **1989**;58:250–256
21. Diner WC. Galactography: mammary duct contrast examination. *AJR* **1981**;137:853–856

Book Review

Film-Screen Mammography. An Atlas of Instructional Cases. By Lawrence W. Bassett, Reza Jahanshahi, Richard H. Gold, and Yao S. Fu. New York: Raven, 318 pp., 1991. $130

Film-Screen Mammography is a learning-interactive text that challenges the reader while presenting case after case illustrated with high-resolution mammograms. This is a tour of the authors' experience, carefully and meaningfully arranged to guide the radiologist to a more focused approach.

Here is how the book works: True-to-size images, matched for right and left, virtually fill two adjacent pages, so that you are looking at the mammograms just as you would if the images were laid out for you to review. You can almost hear the breathing of the technologist behind you—the patient's lawyer is not far from earshot either. A brief history is provided, such as, "This patient had a 1 month history of a lump in the left breast." Coordinates or letters and numbers are given so you can target the area you think may need excision or other consideration. Then, the following pages describe the radiologic and pathologic findings, often with a radiograph with arrows and a section of the pathologic specimen.

Because the test mammograms are "life-sized" and free of indicating arrows or other marks that would lead you to the abnormal area (so obvious to an expert's eyes), this text is truly an innovative and risk-free venture into "virtual reality" of high-volume, high-risk breast evaluation. The book opens and closes in traditional fashion. The first chapter describes the technique of mammography, some aspects of sonography, fine-needle biopsy, and localization and includes an overview of breast disease. The book ends with an extensive list of helpful references.

It is obvious that the authors have done a great deal of collaborative work in evolving this beautifully produced text. The principal author is well known to all radiologists involved with breast imaging, and his coauthors have supplemented this field with expertise in pathology. In summary, this is an excellent book. It should be a part of every teaching program and in every radiologist's library, staff members and residents alike.

Michael Crade
Long Beach Memorial Medical Center
Long Beach, CA 90801-1428

Mammography in Women with Axillary Lymphadenopathy and Normal Breasts on Physical Examination: Value in Detecting Occult Breast Carcinoma

A. Jill Leibman[1]
Marjorie B. Kossoff[1, 2]

OBJECTIVE. The purpose of this study was to determine the value of mammography in detecting occult carcinoma in patients with axillary adenopathy and normal breasts on physical examination.

MATERIALS AND METHODS. We analyzed the results of mammography performed in 17 patients; all women had palpable axillary lymphadenopathy of unknown origin and all had normal breasts on physical examination.

RESULTS. In 10 of the 17 patients, mammographic findings were abnormal. The mammographic finding of axillary adenopathy in seven patients was inconsequential because the nodes were evident on physical examination. Three patients had abnormal mammographic findings that were potentially significant, including one with a poorly defined mass suggestive of breast carcinoma, one with a subcutaneous nodule, and one with parenchymal breast edema. Two of 17 patients had an occult breast cancer. In only one of the patients was the cancer detected on mammography. The other patient had undergone prior left mastectomy and was thought to have metastases to the right axilla from the contralateral breast. Mammographic findings in this latter patient were normal.

CONCLUSION. While occult breast carcinoma was relatively common in our series (two of 17 patients), the ability to detect the tumor with mammography was disappointing (one of two patients). This may be explained by the fact that one postmastectomy patient with occult carcinoma had metastatic disease to the contralateral axilla and a normal remaining breast, which was pathologically confirmed at mastectomy. Our experience suggests that mammography is valuable in patients with normal breasts on physical examination who have primary carcinoma involving ipsilateral axillary lymph nodes. The procedure should be included in the diagnostic evaluation of patients with axillary adenopathy in order to detect the unusual case of occult breast carcinoma.

AJR 159:493–495, September 1992

The ability to detect occult breast cancer with mammography has not been determined in patients who have axillary adenopathy of unknown origin and normal breasts on physical examination. Previous studies suggest the primary tumor (whether from breast or extramammary in origin) is infrequently occult when metastases to axillary nodes become evident [1, 2]. We reviewed the records of 17 patients with normal breasts on physical examination who were referred for mammography because of axillary lymphadenopathy to determine whether mammography is useful in detecting an occult carcinoma.

Prior studies have reported the results in patients who underwent axillary lymph node biopsy to determine the cause of adenopathy; however, mammography was not performed in all patients included in these studies [3, 4]. To our knowledge, this study represents the first report of a group of patients who all had mammography and whose physical examinations all revealed normal breasts and palpable axillary adenopathy of unknown origin.

Received December 2, 1991; accepted after revision March 30, 1992.

[1] Department of Radiology, Emory University School of Medicine, and Section of Radiology, Emory University Clinic, 1365 Clifton Rd., N.E., Atlanta, GA 30322. Address reprint requests to A. J. Leibman.

[2] Present address: Kingsway Diagnostic Centre, 729 Pittwater Rd., Dee Why 2099, Sydney, NSW, Australia.

0361-803X/92/1593-0493
© American Roentgen Ray Society

Materials and Methods

Between November 1989 and March 1991, 17 patients with palpable axillary adenopathy of unknown origin were referred for mammography. All of the patients had a normal breast on physical examination. The clinical histories, mammographic findings, and pathologic results were reviewed.

Pathologic correlation was available in 11 (65%) of the 17 patients. Fine-needle aspiration biopsy of nodes was done in three patients. Benign nodal hyperplasia was diagnosed in four patients. In one patient, the palpable axillary mass was a lipoma at biopsy. One patient who had had prior augmentation mammoplasty underwent lymph node biopsy, which showed a silicone granuloma. One patient had a pathologic diagnosis of diffuse hyperplasia consistent with dermatopathic origin, but further workup was not performed. In one patient with axillary and supraclavicular adenopathy, the diagnosis of lung carcinoma was made by biopsy of the supraclavicular node. In one patient who had previously had a left mastectomy, a right axillary node biopsy was performed and showed breast carcinoma. A right mastectomy was subsequently performed, and no malignant tumor was found. The tumor in the right axillary nodes was thought to be metastastic from the original contralateral breast tumor. In one patient with a suspicious breast mass on mammography, biopsy of the mass revealed an infiltrating duct carcinoma. The remaining patient had biopsy-proved small lymphocytic lymphoma.

In six of the 17 patients, the final diagnosis was based on clinical history and laboratory results. These included patients who were HIV positive ($n = 2$), or had a clinical diagnosis of lymphadenitis ($n = 1$), dermatopathic enlargement of nodes (associated with severe contact dermatitis) ($n = 1$), or collagen vascular disease ($n = 1$). In the remaining patient, no cause could be found for the adenopathy, and it had resolved by the time of physical examination 3 months later. These patients were followed up clinically for an average of 15 months, and other causes for adenopathy were not detected.

Mammography in all patients was performed with dedicated screen-film mammographic units (Diagnostic U-M, Philips, Shelton, CT, or Senograph 600T, General Electric CGR, Milwaukee, WI). Standard craniocaudal and 45° mediolateral oblique views were obtained of each breast. Images were evaluated by one of four experienced mammographers.

Results

Mammographic findings were abnormal in 10 of the 17 patients studied. Seven mammograms showed enlarged axillary nodes, one showed a mass suggestive of breast carcinoma, and one showed edema of the parenchyma. One patient with metastatic lung cancer had a benign-appearing breast mass on mammography that was considered an incidental finding and not sampled by biopsy.

Mammographic findings appeared normal in seven patients. Five of these patients underwent biopsy of an axillary lymph node, including three patients diagnosed with benign nodal hyperplasia, one patient with a lipoma, and one patient with metastatic disease from a contralateral breast carcinoma. One patient had axillary adenopathy that had resolved on subsequent physical examination 3 months later. The remaining patient had severe contact dermatitis, and the adenopathy resolved after treatment of the dermatitis.

Lymph node biopsy in four patients showed cancer. One patient with enlarged axillary nodes on mammography underwent lymph node biopsy, which showed lymphoma. Lung carcinoma was diagnosed in another patient. One asymptomatic postmastectomy patient had normal mammographic results, and an axillary node biopsy revealed breast carcinoma. The patient underwent mastectomy of the remaining breast and no tumor was found, so the adenopathy was thought to be metastatic from the contralateral breast. The other asymptomatic patient with a breast mass on mammography and biopsy-proved breast cancer represents the one true case of occult primary breast carcinoma detected with mammography in the study.

Discussion

Most women who have axillary adenopathy due to metastatic disease have an obvious primary tumor, either in the breast or elsewhere [1, 2]. Some women with this finding will have an occult breast carcinoma [5].

In our study, axillary adenopathy occurred as the first sign of breast cancer in two of 17 patients, a lower frequency than previously reported [3, 6]. A series from the Memorial Sloan-Kettering Cancer Center reported 48 patients with adenopathy that was proved by biopsy to contain adenocarcinoma consistent with breast origin. Mammography was performed after nodal biopsy in 37 of 48 patients and showed an impalpable lesion that was suggestive of carcinoma in nine patients (24%) [6]. A study from Roswell Park Cancer Institute reported 29 asymptomatic patients with axillary adenopathy. Mammography was performed in only 17 patients and showed a suspicious lesion in eight [3]. In both these series, biopsies of the axillary mass in all patients showed metastatic adenocarcinoma consistent with a breast primary tumor; only some patients had mammography. This is in comparison with our study in which all patients had mammography, the cause of the axillary adenopathy was unknown at the time mammography was done, and both benign and malignant causes were included in the final diagnosis.

Seventy-two patients in whom adenopathy was detected without any known cause underwent biopsy at the Mayo Clinic in a study reported by Pierce et al. [4]. In 55 (76%) of these 72 patients, causes of the adenopathy were nonspecific, and included hyperplasia and inflammatory changes. These findings are similar to the results of our study, in which benign or infectious causes of adenopathy were found in 13 of 17 patients.

Breast cancer metastasis to axillary nodes was an uncommon cause of adenopathy in our study, found in two (12%) of 17 patients. In the study by Pierce et al. [4], the source was determined to be in the breast in three (4%) of 72 patients. The difference between these two studies in the prevalence of occult breast carcinoma may be related to the design of our study, in which all patients had mammography.

The series by Pierce et al. [4], in contrast, reported results of patients in whom no cause could be found on routine examinations, and mammographic results were not reported.

In asymptomatic patients, benign or infectious causes of adenopathy should be initially considered and evaluated clinically or by laboratory testing. In the absence of any detectable cause, mammography should be included in the diagnostic workup to detect the unusual case of occult breast carcinoma found before axillary node biopsy. When the clinical or mammographic search for a cause is exhausted, fine-needle aspiration or formal biopsy of the axillary node is usually necessary to establish a definitive diagnosis for axillary adenopathy.

REFERENCES

1. Feuerman L, Attie JN, Rosenberg B. Carcinoma in axillary nodes as an indicator of breast cancer. *Surg Gynecol Obstet* **1962**;114:5–8
2. Kopans DB. Specific, nonspecific and supporting signs of malignancy. In: Kopans DB, ed. *Breast imaging*. Philadelphia: Lippincott, **1989**:115–133
3. Patel J, Nemoto T, Rosner D, Dao TL, Pickren JW. Axillary lymph node metastases from an occult breast cancer. *Cancer* **1981**;47:2923–2927
4. Pierce EH, Gray HK, Dockerty MB. Surgical significance of isolated axillary adenopathy. *Ann Surg* **1957**;145:104–107
5. Vilcoq JR, Calle R, Ferme F, Veith F. Conservative treatment of axillary adenopathy due to probable subclinical breast carcinoma. *Arch Surg* **1982**; 117:1136–1138
6. Rosen PP, Kimmel M. Occult breast carcinoma presenting with axillary node metastases: a follow-up study of 48 patients. *Hum Pathol* **1990**;21: 518–523

LIST OF BOOK REVIEWS

468 **High-Resolution CT of the Lung.** *Webb WR, Müller NL, Naidich DP*
478 **Atlas of Radiology of the Chest.** *Turner-Warwick M, Hodson ME, Corrin B, Kerr IH, eds*
486 **Screen Film Mammography. Imaging Considerations and Medical Physics Responsibilities. Proceedings of SEAAPM Spring Symposium.** *Barnes GT, Frey GD, eds*
492 **Film-Screen Mammography. An Atlas of Instructional Cases.** *Bassett LW, Jahanshahi R, Gold RH, Fu YS*
496 **Advances in Gastrointestinal Radiology, Vol. 1.** *Herlinger H, Megibow AJ, eds*
502 **Practical Doppler Ultrasound for the Clinician.** *Powis RL, Schwartz RA*
508 **Endoscopic Retrograde Cholangiopancreatography. Technique, Diagnosis, and Therapy.** *Siegel JH*
514 **Clinical Sonography. A Practical Guide, 2nd ed.** *Sanders RC, ed*
572 **Skeletal Radiology. The Bare Bones Teaching Collection.** *Chew FS*
580 **Diagnostic Imaging of AIDS.** *Reeders JWAJ, Binkhuysen FHB, Bartelsman JFWM*
608 **Cerebral Blood Flow Measurement with Stable Xenon-Enhanced Computed Tomography.** *Yonas H, ed*
622 **Imaging Anatomy of the Newborn.** *Richter E, Lierse W*
638 **Interventional Cardiology. Clinical Applications of New Technologies.** *White CJ, Ramee SR, eds*

Book Review

Advances in Gastrointestinal Radiology, Vol. 1. Edited by Hans Herlinger and Alex J. Megibow. St. Louis: Mosby–Year Book, 197 pp., 1991. $69.95

This small book is the first in a series of volumes that will focus on current topics in gastrointestinal radiology. The series is to be edited by 16 international experts. The initial volume, edited by Hans Herlinger and Alex Megibow, is composed of 10 short chapters covering a wide variety of topics.

A detailed, well-written chapter by Stevenson discusses the current concepts and controversies in screening, diagnosis, and staging of carcinoma of the colon. In particular, Stevenson clearly addresses the efficacy of fiberoptic endoscopy vs barium radiography, concluding that both play an important role and that flexible sigmoidoscopy should serve as a "signpost" for directing radiologic imaging. His review of current literature indicates that although CT staging of colorectal carcinoma offers minimal benefit to the patient, it has an important role in detection of early recurrence, particularly hepatic metastases, as suggested by recent surgical and chemotherapeutic advances in treatment of metastatic disease.

A chapter by Rubesin and Bronner reviews the pathologic basis for the morphologic abnormalities of Crohn's disease as depicted by barium radiography and CT. This chapter is beautifully illustrated and will be helpful for anyone who deals with the difficulties of radiologic diagnosis and differentiation of inflammatory bowel disease. I only wish that more CT scans had been included.

Increasing interest by gastroenterologists in anorectal dysfunction has not been met by parallel interests by radiologists. The chapters by Shorvon and Henry on defecography and by Bartram and Law on anal endosonography can serve as an introduction to this topic for practicing radiologists. Both chapters succinctly deal with techniques of examination, normal anatomy, and pathologic changes and contain current references for further and more detailed reading. The subject is not glamorous, but patients afflicted with anorectal disease, and the gastroenterologists who must deal with them, nevertheless need our help.

The role of CT in evaluation of patients with acute abdominal disease continues to expand, particularly in evaluation of diverticulitis and appendicitis. The chapters by Cho (CT of colonic diverticulitis) and Balthazar, Megibow, Bernbaum, and Gordon (CT of acute appendicitis) discuss the CT techniques required for a good examination and the typical findings in both diseases. Difficulties in differential diagnosis, particularly perforated carcinoma of the colon and inflammatory bowel disease, are clearly presented, and findings that help in making a correct diagnosis are offered. Both chapters are nicely illustrated.

A long, detailed chapter deals with histomorphometric analysis of contrast distribution in the liver and in hepatic masses. This is an interesting subject and describes a technique (histomorphometric analysis) that is not widely used or understood by radiologists. It will be of interest only to more academic radiologists who are interested in contrast dynamics. It contains little in the way of an important clinical message.

Many radiology departments have purchased or are considering purchase of equipment for digital or computed radiography. Sorting through the manufacturers' literature and claims is a frustrating pursuit. The chapter by Megibow and colleagues presents a scientific comparison of computed radiography vs conventional double-contrast gastrointestinal examinations. Although neither system is superior, the authors conclude that computed radiographic systems probably would not be efficient in small practices or private offices, but may offer some advantages in large hospitals.

Except for the chapters on lithotripsy and liver contrast distribution, I strongly recommend this book to radiologists who do gastrointestinal and abdominal imaging. The chapters contain a great deal of clinically useful information on techniques of examination; insight into interpretation; and practical, relevant applications for a routine clinical radiology practice.

Patrick C. Freeny
University of Washington School of Medicine
Seattle, WA 98195

Pictorial Essay

Left-Lobe Hepatic Transplants: Spectrum of Normal Imaging Findings

Kathleen H. Caron,[1] Janet L. Strife,[1] Diane S. Babcock,[1] and Frederick C. Ryckman[2]

The limited availability of suitable size-matched donor whole organs has been a major cause of morbidity and mortality in infants and children requiring liver transplantation. Techniques for transplanting segments of the liver have successfully addressed this problem. The surgical anatomy of the left hepatic lobe transplant is unique in three primary respects: the cut edge, the presence of an enteric Roux loop for biliary drainage, and the alteration in the position and number of hepatic vessels. The spectrum of normal imaging findings in 17 left-lobe allografts is illustrated.

The successful use of orthotopic liver transplantation for treatment of both acute and chronic liver failure at a growing number of transplant centers has led to a relative scarcity of donor organs. Nowhere has this shortage been felt more acutely than in infants and children, among whom previously 20–50% of transplantation candidates died while waiting for a suitable donor [1]. Transplantation of segments of the liver (most commonly the left lobe) has been introduced to address this need. The technique is currently in use at a number of transplant centers, including our own, where deaths associated with a scarcity of donor organs have virtually been eliminated [2, 3].

Imaging (particularly sonography, and CT to a lesser degree) and clinical and biochemical tests play important roles in the assessment of graft function and complications after transplantation. The altered anatomy of the left-lobe hepatic allograft used is reflected on cross-sectional imaging.

This essay illustrates the unique imaging features of this allograft in children.

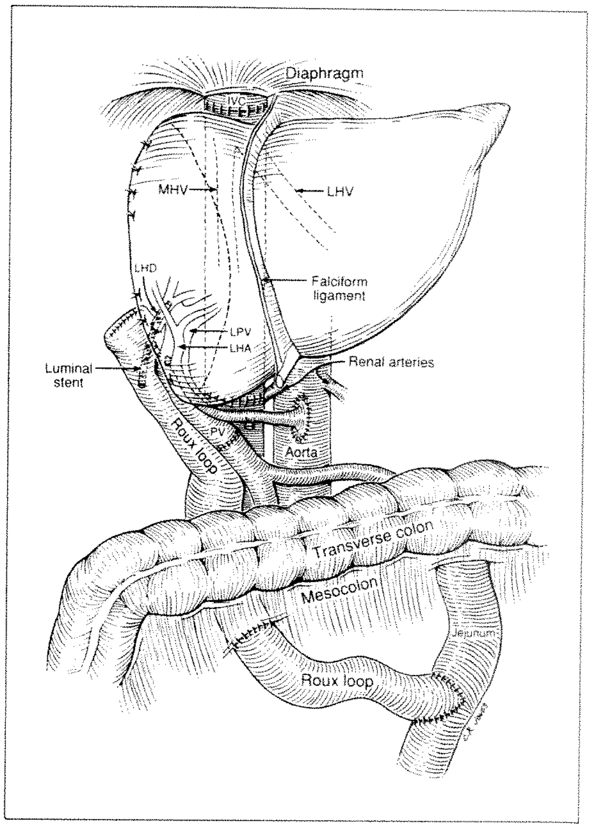

Fig. 1.—Diagram shows unique features of transplantation of left-lobe hepatic allograft: right lateral position of "porta hepatis," Roux-en-Y loop for biliary drainage, arterial end-to-side anastomosis of donor celiac artery to recipient infrarenal aorta, and presence of only two hepatic veins (see text for details). IVC = inferior vena cava, MHV = middle hepatic vein, LHV = left hepatic vein, LHD = left hepatic duct, LPV = left portal vein, LHA = left hepatic artery, PV = portal vein.

Materials and Methods

Initially, we retrospectively reviewed all posttransplantation sonograms and CT scans of 34 infants and children who had received 43

Received February 18, 1992; accepted after revision March 30, 1992.
Presented in part at the annual meeting of the Society for Pediatric Radiology, Cincinnati, April 1990.

[1] Department of Radiology, Children's Hospital Medical Center, Elland and Bethesda Aves., Cincinnati, OH 45229. Address reprint requests to K. H. Caron.
[2] Division of Pediatric Surgery, Children's Hospital Medical Center, Cincinnati, OH 45229.

AJR **159:497–501, September 1992** 0361–803X/92/1593–0497 © American Roentgen Ray Society

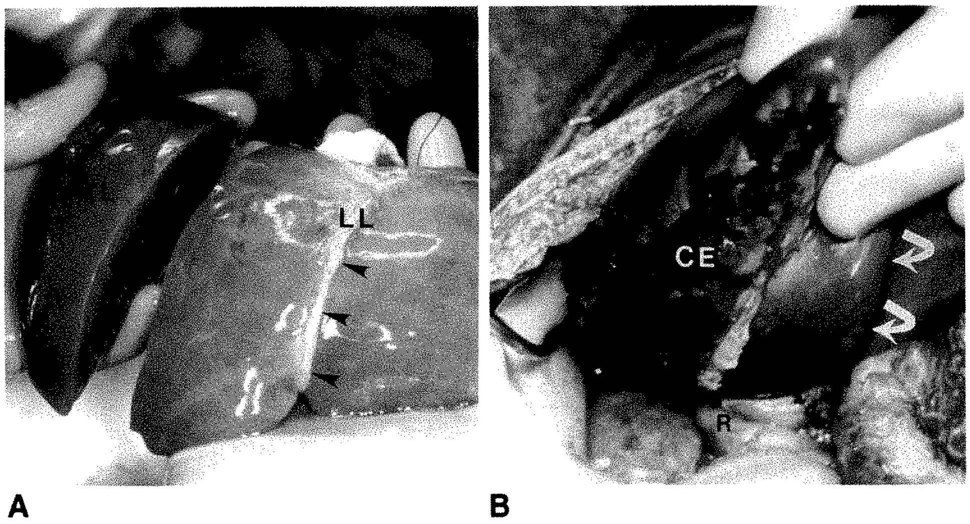

Fig. 2.—*A*, Plane of cut margin of resected donor liver viewed anteriorly. RL = right lobe, LL = left lobe, *arrowheads* = falciform ligament.

B, Transplanted left lobe in vivo as viewed from below after vessels are unclamped. Note cut edge (CE) posteriorly on patient's right. Roux loop (R) is adjacent to cut edge. *Arrows* show rightward position of falciform ligament.

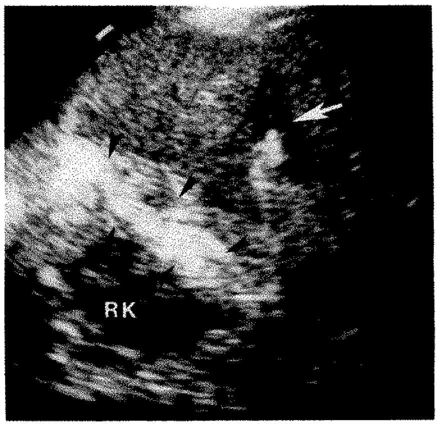

3

Fig. 3.—Transverse sonogram of patient with transplanted left-lobe allograft shows a rind of echogenic material (*arrowheads*) along cut edge. Note fluid along falciform ligament (*arrow*). RK = right kidney.

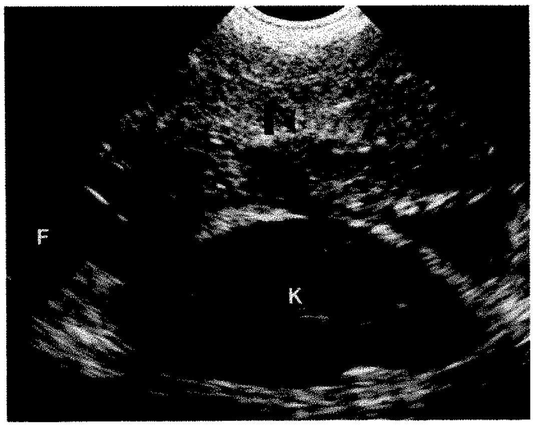

4

Fig. 4.—Longitudinal sonogram of right upper quadrant of patient with transplanted left-lobe allograft shows heterogeneous echogenicity (*arrows*) of cut surface. Note fluid collection (F) above right kidney (K).

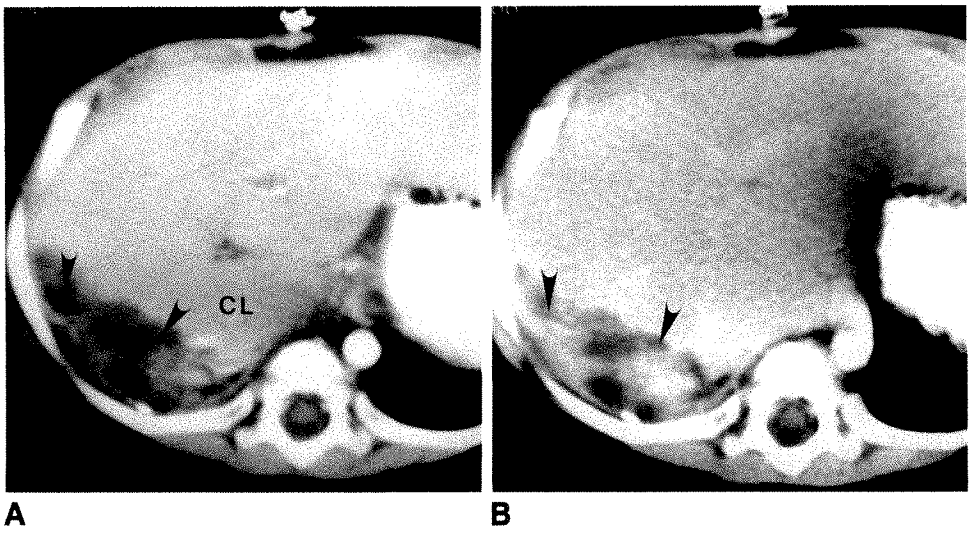

Fig. 5.—*A* and *B*, CT scans of transplanted left-lobe allograft obtained immediately (*A*) and 9 min after (*B*) injection of contrast material show delayed enhancement of portions of cut surface (*arrowheads*). CL = caudate lobe.

liver transplants at our institution between July 1986 and November 1989. Twenty-four whole-liver grafts were given to 20 patients (12 girls and eight boys). The remaining 14 patients (seven girls and seven boys) received 17 left-lobe grafts. Two of the left-lobe recipients were given emergent transplants within 1 week after failure of an initial whole graft. Since July 1988, when segmental grafting techniques were started at our institution, 59 transplantations have been performed, and all but 18 of these involved segmental transplants.

Of the children in the study group who received left-lobe grafts, 64% (9/14) were less than 3 years old and 71% (10/14) weighed 15 kg or less. In contrast, only 35% (7/20) of those who received whole-liver transplants were less than 3 years old and only 30% (6/20) weighed 15 kg or less. The numbers underscore the applicability of this technique to smaller patients, who are a high-risk population.

The major indication for transplantation in both groups was biliary atresia.

Surgical Technique

The surgical techniques of transplanting left-lobe hepatic allografts have been described (Fig. 1). Discussion of their differences compared with standard whole-liver allografts is

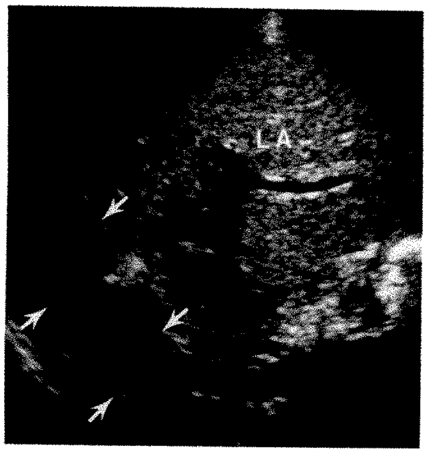

Fig. 6.—Transverse sonogram of right upper quadrant in patient with transplanted left-lobe hepatic allograft shows fluid-filled Roux loop (*arrows*) along posterolateral aspect of allograft (LA).

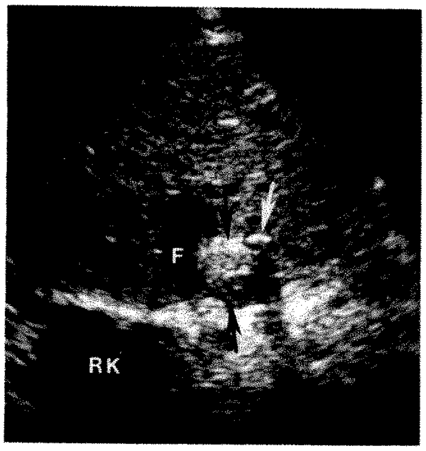

Fig. 7.—Transverse sonogram of patient with transplanted left-lobe hepatic allograft shows Roux loop (*black arrows*), which appears to be collapsed and echogenic with surrounding fluid (F). Stent (*white arrow*), a visible echogenic structure directed into loop, has posterior acoustical shadowing. RK = right kidney.

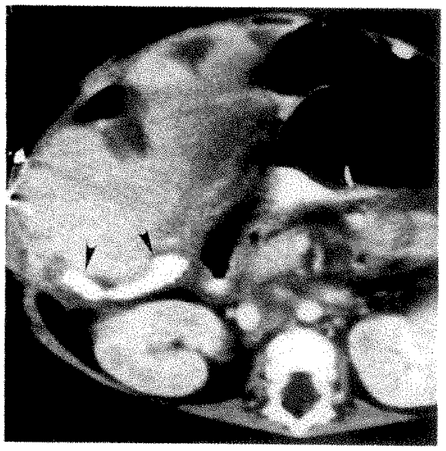

Fig. 8.—Contrast-enhanced CT scan of transplanted left-lobe hepatic allograft shows position of Roux loop because enteric contrast material (*arrowheads*) has refluxed.

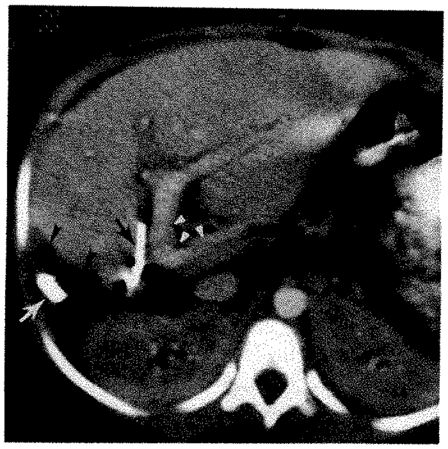

Fig. 9.—Contrast-enhanced CT scan of transplanted left-lobe hepatic allograft shows right posterolateral location of porta hepatis and angled course of portal vein (*white arrowheads*). Note radiopaque biliary stent (*black arrow*) and hypodense cut surface (*black arrowheads*) of graft. A radiopaque surgical drain (*white arrow*) is present adjacent to cut edge.

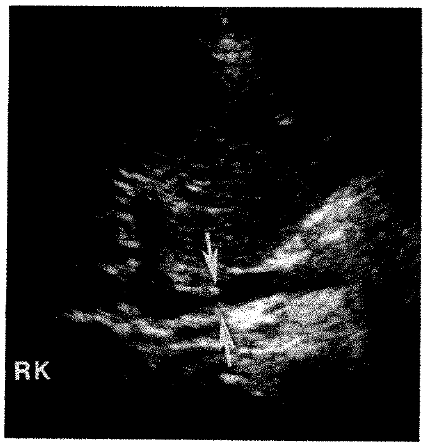

Fig. 10.—Oblique sonogram parallel to portal vein in patient with transplanted left-lobe hepatic allograft shows typical change in diameter and luminal narrowing of portal venous anastomosis (*arrows*), which may be confused with a thrombus. RK = right kidney.

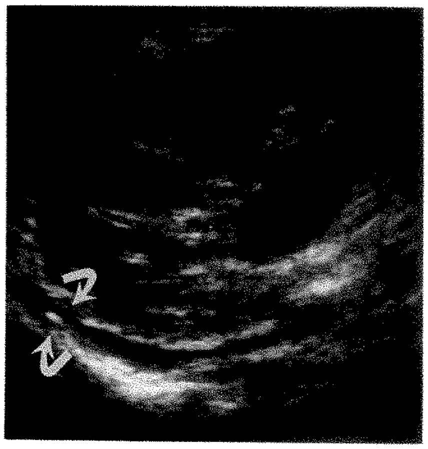

Fig. 11.—Longitudinal sonogram parallel to inferior vena cava in patient with transplanted left-lobe hepatic allograft shows normal location of suprahepatic inferior vena cava anastomosis with typical luminal narrowing (*arrows*).

warranted. Figure 1 is a diagram of the anatomy of a left-lobe transplant.

During the initial development of the procedure, the left lobe of the liver was resected ex vivo (Fig. 2A) by using sharp dissection, and major vessels and biliary radicles along the raw cut surface were individually ligated. Mattress sutures were placed along the cut margin to provide additional hemostasis. This technique, however, has been revised because of concerns about devitalizing the margin of the allograft. Blunt parenchymal fracture by means of a hemostat and then individual ligature of vessels and bile ducts are now performed sequentially to resect the left lobe. Several coats of fibrin glue are then applied to seal the cut surface after hemostasis is achieved in the transplanted allograft. The anterior portion of the caudate lobe is usually resected, leaving the caval portion in place.

In order to achieve biliary drainage, a Roux-en-Y choledochojejunostomy is performed, with a multifenestrated internal radiopaque stent bridging the anastomosis. The stent is secured with dissolving suture material and usually is passed in the gastrointestinal tract approximately 1 month after placement. The Roux loop (35 cm long) is placed through the mesocolon and posteriorly adjacent to the cut edge (Fig. 2B).

Two hepatic veins (left and middle) are present in the left-lobe allograft. The donor inferior vena cava is secured via end-to-end anastomosis to both the infra- and suprahepatic recipient inferior vena cava. The right portal vein orifice is oversewn during graft preparation, and an end-to-end anastomosis is performed between the donor and recipient main portal veins. The arterial anastomosis is end-to-side between the donor celiac axis and the recipient infrarenal aorta. The intervening arterial branches of the donor celiac trunk up to the left hepatic artery (splenic, left gastric, gastroduodenal, and right hepatic arteries) are ligated during harvesting of the graft.

Imaging Findings

The unique imaging features of left-lobe allograft as compared with standard whole-liver allografts relate primarily to three aspects: the cut edge of the graft, the position of the Roux-en-Y loop, and the altered vascular anatomy.

The cut surface of the graft typically has a rind of tissue that may be uniformly echogenic on sonograms (Fig. 3). More frequently it is heterogeneously echogenic (Fig. 4). Seepage of blood, bile, lymph, and serous fluid may contribute to the altered appearance of the cut edge. On CT with bolus IV contrast infusion, this rind typically has low attenuation relative to normal liver parenchyma. On delayed CT scans, the area may partially fill in with contrast material (Fig. 5), suggesting relative ischemia as a partial cause of the changes in echogenicity and density.

Fluid collections adjacent to the cut surface occur frequently and were present in 12 (71%) of 17 left-lobe allografts as shown by sonography. Distinguishing a sterile seroma from an abscess collection on the basis of imaging findings often is not possible. Percutaneous aspiration and Gram's staining and culture of the fluid is usually necessary in recipients of left-lobe allografts who have any clinical indication of infection. The prevalence of fluid collections adjacent to the cut surface has decreased noticeably now that sharp dissection of the allograft has been abandoned and fibrin glue is applied to the cut surface.

The Roux-en-Y loop is positioned posterolaterally adjacent to the cut edge and if fluid-filled may simulate an abnormal fluid collection (Fig. 6). The loop may appear collapsed and

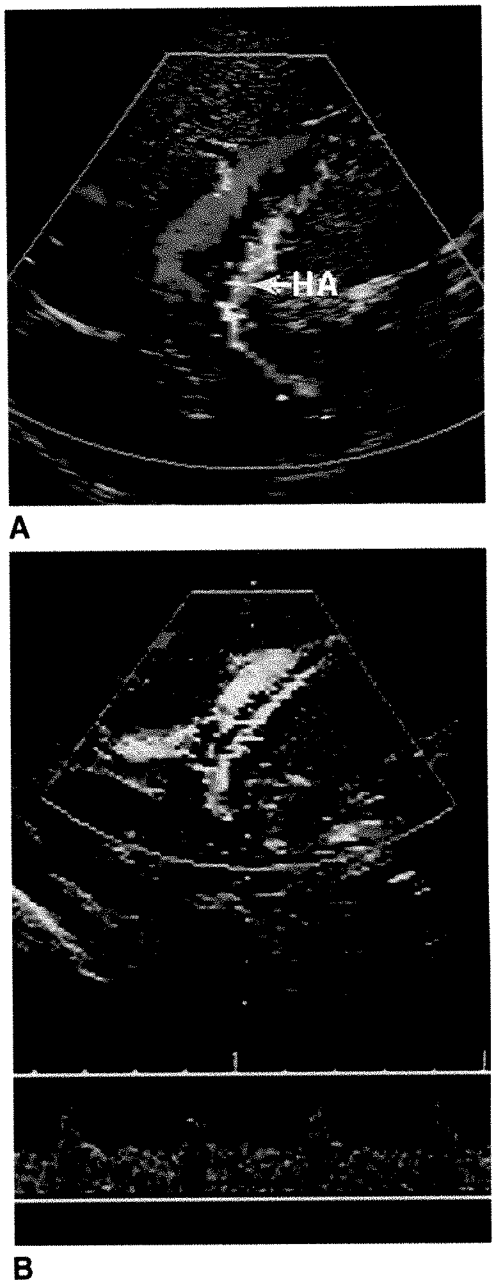

Fig. 12.—*A* and *B*, Transverse color Doppler images alone (*A*) and in conjunction with duplex analysis (*B*) in patient with transplanted left-lobe hepatic allograft show hepatic artery (HA) running parallel to portal vein in porta hepatis.

echogenic, sometimes with surrounding fluid (Fig. 7). Detection of an inner echogenic margin (corresponding to the mucosa/submucosa of the bowel loop), the tubular nature of the loop, and the echogenic (radiopaque) stent help in distinguishing the Roux loop from an abnormal fluid collection. Reflux of enteric contrast material into the loop is helpful for detection of the loop on CT scans (Fig. 8). Once the stent has passed into the gastrointestinal tract and if no enteric contrast material is refluxed, a fluid-filled loop may be difficult to distinguish from an abnormal fluid collection on imaging studies.

The left-lobe allograft typically fills the anatomic space previously occupied by the diseased native liver. The porta hepatis is located eccentrically along the right inferolateral aspect of the allograft close to the cut surface. This is evident in the axial plane, where the portal vein has a moderately angled course and extends more laterally to the right than in the whole liver (Fig. 9). The hepatic artery parallels this course, but it is more difficult to trace because of its smaller size. The normal sites and sonographic appearance of the portal venous and inferior vena cava anastomoses must be recognized. Typically, mild to moderate luminal narrowing occurs that may mimic nonobstructive clot (Figs. 10 and 11). Duplex and color flow Doppler sonographic examination of these vessels is an integral part of postoperative follow-up in these patients to confirm vascular patency (Fig. 12).

REFERENCES

1. Broelsch CE, Emond JC, Thistlethwaite JR, et al. Liver transplantation, including the concept of reduced-size liver transplants in children. *Ann Surg* **1988**;208:410–420
2. Ryckman FC, Flake AW, Fisher RA, Tchervenkov JI, Pedersen SH, Balistreri WF. Segmental orthotopic hepatic transplantation as a means to improve patient survival and diminish waiting-list mortality. *J Pediatr Surg* **1991**;26:422–428
3. Emond JC, Whitington PF, Thistlethwaite JR, Alonso EM, Broelsch CE. Reduced-size orthotopic liver transplantation: use in the management of children with chronic liver disease. *Hepatology* **1989**;10:867–872

Book Review

Practical Doppler Ultrasound for the Clinician. By Raymond L. Powis and Robert A. Schwartz. Baltimore: Williams & Wilkins, 187 pp., 1991. $55

This book is intended to provide the basic principles that underly a variety of clinical applications of Doppler ultrasound in a number of diagnostic settings. Hypothesizing that preconceptions and misinformation about Doppler sonography are the main source of error in the interpretation of Doppler images and the cause of misuse of the technique, the authors emphasize aspects of Doppler physics that, if understood, can help avoid diagnostic errors and result in a greater awareness of clinical situations in which Doppler ultrasound can be most advantageous.

The first chapter provides a clinical perspective and describes how sonography continues to change the practice of clinical medicine. The second chapter provides an overview of the widespread existence of the Doppler effect in everyday life. Perhaps as an attempt to overcome what they believe is a negative emotional response to the term "Doppler physics," the authors provide a delightful discussion of the mustache bat's use of the Doppler effect to locate its dinner. Later in this chapter, they present goals for the application of Doppler sonography. This is a somewhat abstract and philosophical section in which they attempt to separate source, form, frequency, and direction. This seems a somewhat artificial separation. For example, they choose to separate the source of Doppler flow (i.e., the cardiovascular system) from the form of flow that they say is pulsatile. These two features seem to be inseparably linked. Furthermore, both the frequency and direction of blood flow is a direct function of variations affecting the source of the blood flow. The final section of this chapter discusses problems common to all ultrasound applications; however, it does not discuss some of the unique features of Doppler imaging, which are discussed in greater detail in chapter 3. In fact, the last paragraph in chapter 2 really appears to belong in chapter 3, which describes tissue/ultrasound interactions and provides a global view of ultrasound physics that is not significantly different from that provided in numerous other books on Doppler imaging, such as *Clinical Applications of Doppler Ultrasound* by Taylor, Burns, and Wells; *Duplex Doppler Ultrasound* by Taylor and Strandness; and *Color Doppler Flow Imaging* by Foley.

Chapter 4 is dedicated to a discussion of fluid dynamics and blood-flow modeling. Although this is a well-written chapter, such information is available in numerous textbooks, including *Doppler Ultrasound Physics: Instrumentation and Clinical Applications* by Evans, McDicken, Skidmore, and Woodcock. Chapter 5 discusses the Doppler equation and some of the basic concepts involved in the Doppler effect. The critical nature of the Doppler angle and its potential role in erroneous diagnoses is stressed. Chapters 6 and 7 deal with Doppler signal processing, in continuous- and pulsed-wave Doppler systems. Schematic diagrams show how the Doppler signal is acquired and processed to produce both audible and visible spectral information. Zero crossing detectors are compared with current state-of-the-art fast Fourier transform devices for frequency analysis. The importance of fast Fourier transformation to Doppler signal analysis is stressed. The final part of chapter 7 deals with the concept of complex numbers and fast Fourier transformation, showing how this allows detection of a wider range of Doppler frequencies without aliasing.

Chapter 8 summarizes the current state of Doppler instrumentation. Duplex techniques and color Doppler imaging are presented. The benefits of the latter are only briefly and incompletely discussed in this section. Chapter 9, "Linking Doppler Display with Physical Events," seems to reiterate much of the information presented in previous chapters. Further limitations of Doppler signal processing are presented, and the importance of sample-volume geometry is stressed. Chapter 10 discusses quantitative Doppler measurements used in clinical practice. The emphasis is on cardiovascular quantitative estimations of valvular pressure gradients and valve areas. Formulas used to estimate the extent of vascular disease in carotid arteries are presented, as are potential applications for the use of pulsatility and resistivity indexes to detect vascular disease. No mention of velocity calculations for peripheral arterial disease is made.

This book's primary focus is the importance of relating the principles of Doppler physics to the Doppler phenomenon observed in the course of a clinical examination. The book has numerous useful illustrations, which, if they do not "stimulate the imagination," at least clarify some of the physical concepts and principles they describe. Many chapters repeat information contained in others, leaving the impression that the text is composed of a series of individual lectures tied together by transitional paragraphs. The text is delightfully written and presents the potentially threatening topic of Doppler physics in a comprehensive fashion.

The authors are to be congratulated for their ability to present Doppler physics in such a readable fashion and to illustrate the potential value of understanding the underlying principles of the Doppler phenomenon in the day-to-day clinical practice. The price of $55 is certainly reasonable. For those who do not already own a book that discusses Doppler physics, this text would be a reasonably priced and useful addition to the library.

Barbara A. Carroll
Duke University Medical Center
Durham, NC 27710

Malignant Biliary Obstruction:
Efficacy of Thin-Section Dynamic CT in Determining Resectability

David J. Gulliver[1]
Mark E. Baker[1]
Christine A. Cheng[2]
William C. Meyers[2]
Theodore N. Pappas[2]

OBJECTIVE. Several authorities advocate the use of preoperative angiography to determine the resectability of pancreatic and periampullary tumors, claiming that CT alone is not sufficiently accurate for this purpose. Our objective was to assess the value of CT in predicting surgical resectability in patients with malignant biliary obstruction.

MATERIALS AND METHODS. We performed a retrospective analysis of 380 consecutive cases of malignant biliary obstruction spanning a 4-year period. Most patients (230) were treated nonoperatively. Sixty-seven patients had surgery, pathologic confirmation of malignancy, and preoperative CT scans available for review. The CT scans were assessed for surgical resectability of tumor by an interpreter who did not know the patient's history.

RESULTS. Forty-two patients had pancreatic adenocarcinoma, six had ampullary carcinoma, seven had cholangiocarcinoma, and 12 had other malignant neoplasms. Of 47 patients with tumors thought to be unresectable on the basis of CT findings, 42 had tumors that were found to be unresectable at surgery (positive predictive value, 89%). Of 20 patients with tumors thought to be resectable, 16 had tumors that were surgically resectable (positive predictive value, 80%). CT did not show metastases to duodenal lymph nodes ($n = 2$), portal vein infiltration ($n = 1$), and small hepatic metastases ($n = 1$). Visualization of most of these at angiography would not be expected. The CT finding of infiltration of the periarterial fat around the celiac or superior mesenteric arteries was reliable for predicting surgical unresectability. Lymphadenopathy and infiltration of nonperivascular fat planes were less reliable predictors of unresectability.

CONCLUSION. Although some findings on CT that suggest unresectability are less reliable than others, the accuracy of CT compares favorably with reports on the accuracy of angiography for assessing tumor resectability in cases of malignant biliary obstruction. The addition of angiography to the examination of patients with potentially resectable lesions is not justified when high-quality, thin-section dynamic CT has been performed.

***AJR* 159:503-507, September 1992**

The value of CT in the preoperative examination of patients with carcinoma of the head of the pancreas or other causes of malignant biliary obstruction has been studied by several investigators, frequently with different results [1-5]. In particular, recent reports [1-3] have advocated adding angiography to the workup of all patients with pancreatic and periampullary tumors that are being considered for resection.

The purpose of this study was to determine if CT findings alone can be used to predict surgical resectability and, in conjunction with clinical findings, enable appropriate triage of patients for surgical or medical therapy.

Materials and Methods

Findings in 380 patients with malignant biliary obstruction who were seen at our institution during a 4-year period were reviewed retrospectively. The cases were gathered by reviewing

Received January 21, 1992; accepted after revision March 24, 1992.

[1] Department of Radiology, Box 3808, Duke University Medical Center, Erwin Rd., Durham, NC 27710. Address reprint requests to D. J. Gulliver.

[2] Department of Surgery, Duke University Medical Center, Durham, NC 27710.

0361-803X/92/1593-0503
©American Roentgen Ray Society

TABLE 1: Findings of Tumor Unresectability on CT in 47 Patients

Finding	Percentage of Patients
Lymphadenopathy	57
Fat plane invasion	49
Encasement or occlusion of superior mesenteric or celiac artery	36
Involvement of superior mesenteric vein or portal vein	32
Liver metastases	28
Invasion of adjacent organs	6
Ascites or peritoneal spread of malignant neoplasm	4

records of surgical procedures covering this period. Biliary obstruction was defined as elevated levels of bilirubin or alkaline phosphatase or biliary dilatation seen on CT scans or both.

Criteria for inclusion in the study were surgical exploration, pathologic confirmation of malignancy, and preoperative CT scans available for review. The majority of patients (230) were treated nonoperatively; 67 patients (33 men and 34 women) fulfilled the selection criteria. The age range of patients was 39–83 years (mean, 62 years). CT scans were interpreted by a single observer who had no knowledge of the patients' records. The observer determined if the tumor was resectable or unresectable on the basis of CT criteria, and findings of unresectability were recorded. Criteria for unresectability were hepatic or distant metastases; lymphadenopathy (short-axis dimension more than 7 mm for portal nodes, 10 mm for portacaval nodes, 9 mm for paraaortic nodes, and 8 mm for gastrohepatic ligament nodes [6]); involvement of perivascular fat planes or encasement or occlusion of superior mesenteric artery or vein, celiac artery, or portal vein; invasion of adjacent organs or peripancreatic fat planes (excluding perivascular fat); ascites; and peritoneal metastases.

Nearly all CT scans were obtained at one institution (63 of 67 cases), and all scans were obtained with IV contrast material given as a bolus. Most CT scans (48 of 67 cases) were obtained by using a dedicated pancreatic protocol: 3- or 5-mm scans at 5-mm intervals from the third part of the duodenum to just above the porta hepatis, with 10-mm contiguous scans through the remainder of the liver and from the third part of the duodenum to the iliac crests. Dynamic contrast-enhanced studies were used; usually 150 ml of iopamidol was given IV via an automated injector at 2.5 ml/sec for 20 sec, then at 1.2 ml/sec for the remaining volume. Scans times were 2.0 sec with a 7-sec interscan delay, and 120 mA and 170 kVp were used.

Surgery was performed by either of two biliary surgeons. The surgical findings were reviewed in all cases to determine if the tumors were considered resectable or unresectable. Resectability was determined as follows: First, the liver and peritoneum were palpated to detect metastatic nodules. Then, biopsy specimens from any regional lymph nodes visible (whether normal sized or enlarged) were obtained for frozen-section slides, and cholecystectomy was performed. In cases of carcinoma of the pancreatic head, the pancreatic head was mobilized to ensure that it did not adhere to retroperitoneal structures or fat planes, and the portal vein was examined to ensure that a plane of separation existed between this vessel and the pancreatic head. A diagnosis of malignancy was made before proceeding. Finally, the superior mesenteric and celiac arteries were examined, but usually only after the pancreatic head had been removed (in cases of carcinoma of the pancreatic head) because of access difficulties before tumor resection.

For unresectable tumors, the reasons for unresectability were recorded. In cases of disagreement between the assessment of resectability based on CT findings and the surgical findings, the radiologic, surgical, and pathologic findings were analyzed further to investigate the discrepancy.

When both CT and surgical findings indicated the tumors were unresectable, the features of unresectability were not compared because surgical data were potentially incomplete. For example, a surgeon finding liver metastases would not then proceed to look for lymphadenopathy or invasion of the portal vein. Therefore, we stress that CT findings that suggested unresectability could be assessed only for their value in predicting surgical resectability. Thus, a CT finding that suggested unresectability (e.g., encasement of the celiac artery) could be correct in predicting unresectability without that finding being seen at surgery. However, in patients with resectable tumors, each CT finding that suggested unresectability was correlated with surgical findings.

Results

Of 67 patients, 42 had pancreatic carcinoma; six had ampullary carcinoma; seven had cholangiocarcinoma; and three each had duodenal carcinoma, gallbladder carcinoma, portal lymph node metastases, and other tumors (one mucinous cystic neoplasm of the pancreas, one islet cell tumor,

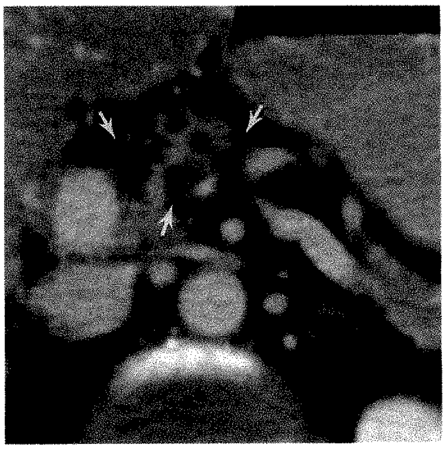
1

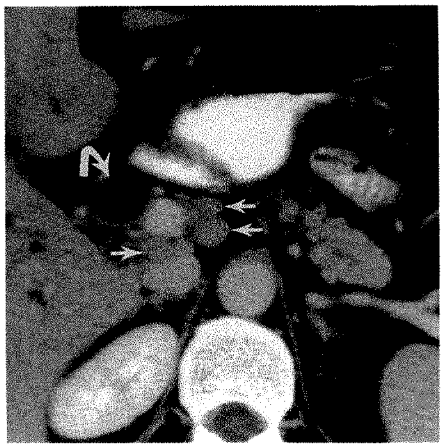
2

Fig. 1.—Tumor falsely diagnosed as unresectable on the basis of CT findings. CT scan shows increased density in peripancreatic fat (*arrows*), suggesting tumor invasion in a patient with a small (1.8 cm) pancreatic adenocarcinoma. At surgery, this tumor was resectable.

Fig. 2.—Malignant lymphadenopathy falsely diagnosed as unresectable on the basis of CT findings. CT scan shows hepatoduodenal ligament and portacaval lymphadenopathy (*straight arrows*), which led to diagnosis of unresectability in patient with pancreatic adenocarcinoma. At surgery, a solitary 1.1-cm bile duct lymph node was found and removed but was tumor-free on pathologic examination. Extrahepatic bile duct is dilated (*curved arrow*).

and one hepatocellular carcinoma). The three patients with metastases in portal lymph nodes had no known history of malignant neoplasm.

Of 47 patients thought to have unresectable tumors on the basis of CT findings, 42 had unresectable tumors at surgery (positive predictive value, 89%). Of 20 patients with tumors thought to be resectable on the basis of CT findings, 16 had resectable tumors at surgery (positive predictive value, 80%).

In the 47 patients thought to have unresectable tumors on the basis of CT findings, the average number of findings indicating unresectability was two (Table 1).

Five patients (three with pancreatic carcinoma, one with ampullary carcinoma, and one with cholangiocarcinoma) were thought to have unresectable tumors on the basis of CT findings, but at surgery these tumors were found to be resectable. Three were thought to have invasion of peripancreatic fat (not including perivascular fat) on the basis of CT findings (Fig. 1), three had lymphadenopathy, and one was thought to have early liver metastases. All three patients with lymphadenopathy had lymph node biopsies at the time of surgery; in two of the three, enlarged portal or portacaval nodes were visible surgically (Fig. 2), but none had malignant lymph nodes found on biopsy. One of the three patients in whom CT appeared to show invasion of fat planes had had ERCP the day before. In the patient thought to have early liver metastases, no palpable liver abnormality was found at surgery.

Four patients who had tumors thought to be resectable on the basis of CT findings had unresectable tumors at surgery. Two of the four had pancreatic carcinoma, and two had ampullary carcinoma. At surgery, two of the four had duodenal lymph nodes that biopsy showed were positive for tumor, one had infiltration of the portal vein (Fig. 3), and one had multiple small hepatic metastases. The interval between CT and surgery in these four patients was 5–32 days (mean, 15 days).

In this study, involvement of the celiac or superior mesenteric artery (Fig. 4) was a totally reliable indication of unresectability; unresectability was surgically confirmed in all 17 patients in whom this finding was present on CT scans, and involvement of the superior mesenteric artery or celiac artery was not found in any patients in whom it was not seen on CT. Invasion of adjacent organs, ascites, and peritoneal spread of malignant tumors also were completely reliable indications, but they were seen in fewer patients.

Of the 67 patients in this study, only four had preoperative angiography. All four had surgically unresectable tumors. Although angiography suggested tumor unresectability in only two of these four, this group is clearly not large enough for useful conclusions to be drawn.

Discussion

The long-term prognosis in patients with malignant biliary obstruction remains poor, despite advances in diagnosis and therapy [7, 8]. However, progress has been made in lowering surgical mortality rates and in determining which patients are most likely to benefit from surgery [7–11].

Only 5–20% of patients with malignant biliary obstruction have surgically resectable tumors at the time of diagnosis [7, 8, 12–15]. Patients with pancreatic adenocarcinoma who have surgical resection live longer than patients who do not (mean survival, 10–20 months vs 3–4 months, respectively [8, 14, 15]); however, the extent of this advantage is uncertain, as clearly a selection bias exists. Despite this, surgery will continue to be performed in patients thought to have localized disease, as surgery is the only chance for cure in these persons [15].

Patients with unresectable tumors causing biliary obstruction were previously treated with surgical biliary bypass. Preoperative assessment was focused on diagnosis, as staging could be performed surgically. The advent of percutaneous and endoscopic biliary stenting has created a need for accurate noninvasive staging, as most patients with unresectable tumors can now be treated nonoperatively, with no adverse effect on survival rates [4, 16–18].

However, some patients will still have surgery despite the knowledge that there is no hope for cure. This may be done, for example, to obtain a specimen for pathologic examination

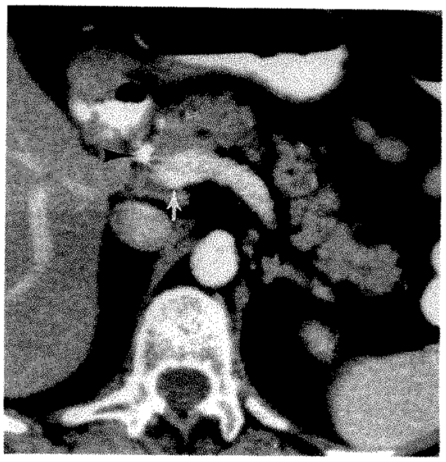

3

Fig. 3.—Tumor falsely diagnosed as resectable on the basis of CT findings. CT scan in patient with pancreatic carcinoma shows no CT features of unresectability, but tumor was unresectable at surgery owing to portal vein infiltration. This section shows lower end of portal vein (*arrow*). Endoscopically placed stent is seen in bile duct (*arrowhead*).

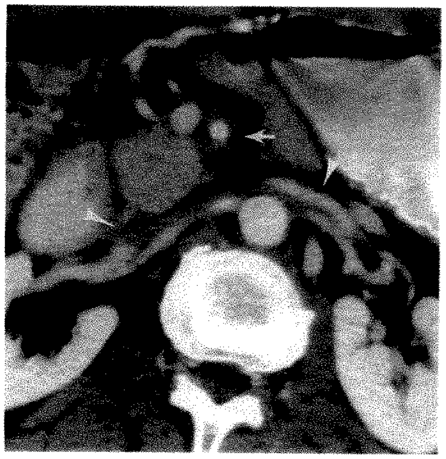

4

Fig. 4.—Tumor correctly diagnosed as resectable on the basis of CT findings. CT scan in patient with pancreatic adenocarcinoma shows complete encasement of superior mesenteric artery (*arrow*). In this series, periarterial fat involvement was completely reliable in predicting unresectability. Tumor infiltration also is seen in peripancreatic fat and around left renal artery and vein (*arrowheads*).

after diagnosis could not be made on the basis of percutaneous biopsy or to provide palliation after unsuccessful endoscopic or percutaneous biliary stenting. The role of imaging is to assist in diagnosis and to provide an accurate assessment of surgical resectability.

In this study, we dealt with malignant biliary obstruction as a clinical and radiologic entity for two reasons. First, initial management decisions (such as surgical vs endoscopic therapy) are frequently made without knowledge of the precise pathologic findings. Second, we have found the tissue of origin of adenocarcinomas arising in the region of the distal bile duct may be uncertain, even after pathologic examination of a resected specimen. By contrast, most previous studies have dealt with patients with a specific diagnosis (based on pathologic finding), placing limitations on the comparison of results of our study with those of others [1-4, 15]. A potential criticism of our article is that a single observer was used to evaluate the CT findings. We think that the use of multiple observers may have resulted in difficulties achieving consensus regarding resectability or unresectability and the presence of each CT finding of unresectability.

In our study, 89% of patients thought to have unresectable tumors on the basis of CT findings had unresectable tumors at surgery, and 80% of 20 patients thought to have resectable tumors on the basis of CT findings had resectable tumors at surgery. Studies by Freeny et al. [4, 19] and Nesbit et al. [20] included patients who had surgery for pancreatic adenocarcinoma and cholangiocarcinoma, respectively. In these studies, CT findings that suggested unresectability were correct in 100% and 78% of cases, respectively, whereas findings that suggested resectability were correct in only 78% and 44%, respectively.

In contrast to the studies of Freeny et al. [4, 19], we had several patients in whom the CT findings that suggested unresectability were false-positive. Three patients with lymphadenopathy had lymph node biopsies at surgery, and the results did not show tumor. The problem of enlarged benign lymph nodes is well recognized on CT [20-22], and these findings support that concern. In three patients, CT showed invasion of the fat planes that was not confirmed surgically. We think that this finding is not as reliable as others in indicating unresectability, particularly if the patient has recently had ERCP [23], has pancreatitis due to occlusion of the pancreatic duct, or has some other cause of strands in peripancreatic fat. In one patient, a heterogeneous liver was suggestive of early metastases, but this was not confirmed surgically.

Four patients thought to have resectable tumors on the basis of CT findings had unresectable tumors at surgery, owing to tumor in duodenal lymph nodes, infiltration of the portal vein, or small hepatic metastases. These findings reinforce those reported by others [1, 3, 4, 24] that CT findings that suggest a tumor is resectable are more likely incorrect than findings that suggest the tumor is unresectable. Tumor spread to normal-sized lymph nodes is a well-recognized problem with current imaging techniques [20-22]. Detection of hepatic metastases smaller than 1-2 cm is a similar problem [25].

Recent articles [1-3] in the surgical literature have advocated adding angiography to the preoperative workup in patients thought to have resectable tumors on the basis of CT findings. Warshaw et al. [1], Dooley et al. [2], Roos et al. [3], and Ross et al. [24] studied findings in patients with pancreatic cancer and periampullary tumors and found that positive predictive values of CT findings that suggested resectability were 45%, 60%, 15%, and 38%, respectively. Positive predictive values of CT findings that suggested unresectability were 92%, no result, 85%, and 93%, respectively (the study of Dooley et al. included only patients thought to have resectable tumors on the basis of CT findings).

However, these studies have a number of problems. They give little or no details of CT technique, only Ross et al. [24] attempted to review CT findings retrospectively, and the study by Dooley et al. [2] had incomplete surgical data. For these reasons, we disagree with the conclusions of Warshaw et al. [1], Dooley et al. [2], and Ross et al. [3] that CT is inadequate for the preoperative assessment of potentially resectable pancreatic and periampullary tumors.

Warshaw et al. [1], Dooley et al. [2], and Mackie et al. [26] have investigated the value of angiography in predicting surgical resectability in patients with pancreatic and periampullary tumors. The positive predictive values for tumors thought to be resectable on the basis of angiographic findings were 54%, 77%, and 59%, and positive predictive values for those thought to be unresectable were 96%, 79%, and 80%, respectively.

Savader et al. [27] described CT angiography for staging pancreatic and periampullary tumors. Results were promising in this small series, but more work needs to be done before this technique can be recommended routinely.

In our study, if the 20 patients thought to have resectable tumors on the basis of CT findings had had angiography, the four patients with unresectable tumors at surgery potentially could have benefited. However, among these four patients, two had spread of tumor to the duodenal lymph nodes, one had multiple small hepatic metastases, and one had infiltration of the portal vein (Fig. 3). Angiography is unlikely to show small hepatic metastases [26], so of the 20 patients only the patient with infiltration of the portal vein would have benefited from having angiography, and it is arguable whether this finding would have been detected.

We conclude that thin-section dynamic CT findings are highly accurate for predicting resectability of tumors in patients with malignant biliary obstruction, with the caveat that some CT findings are less reliable than others. Infiltration of the celiac and superior mesenteric arteries, although recognized as a nonspecific finding of pancreatic adenocarcinoma [28-30], was reliable in predicting unresectability in our study. By contrast, spread to lymph nodes and invasion of nonperivascular fat planes were somewhat less reliable indications of unresectability.

Although angiography was not performed in the patients in our study whose tumors were assessed as resectable on the basis of CT findings, the results of other authors [2, 26] indicate that angiography may falsely suggest that a significant number of resectable tumors are unresectable. Angiog-

raphy may be of value in providing a preoperative vascular road map [19, 26], but the addition of angiography for staging is not justified in all patients thought to have resectable tumors on the basis of CT findings.

ACKNOWLEDGMENT

We thank Priscilla R. Trotter for research assistance.

REFERENCES

1. Warshaw AL, Gu Z, Wittenberg J, Waltman AC. Preoperative staging and assessment of resectability of pancreatic cancer. *Arch Surg* **1990**; 125:230-233
2. Dooley WC, Cameron JL, Pitt HA, Lillemoe KD, Yue NC, Venbrux AC. Is preoperative angiography useful in patients with periampullary tumors? *Ann Surg* **1990**;211:649-655
3. Roos WK, Welvaart K, Bloem JL, Hermans J. Assessment of resectability of carcinoma of the pancreatic head by ultrasonography and computed tomography: a retrospective analysis. *Eur J Surg Oncol* **1990**;16:411-416
4. Freeny PC, Marks WM, Ryan JA, Traverso LW. Pancreatic ductal adenocarcinoma: diagnosis and staging with dynamic CT. *Radiology* **1988**; 166:125-133
5. Jafri SZH, Aisen AM, Glazer GM, Weiss CA. Comparison of CT and angiography in assessing resectability of pancreatic carcinoma. *AJR* **1984**;142:525-529
6. Dorfman RE, Alpern MB, Gross BH, Sandler MA. Upper abdominal lymph nodes: criteria for normal size determined with CT. *Radiology* **1991**; 180:319-322
7. Michelassi F, Erroi F, Dawson PJ, et al. Experience with 647 consecutive tumors of the duodenum, ampulla, head of the pancreas, and distal common bile duct. *Ann Surg* **1989**;210:544-556
8. Merrick HW, Dobelbower RR. Aggressive therapy for cancer of the pancreas: does it help? *Gastroenterol Clin North Am* **1990**;19:935-962
9. Crist DW, Sitzmann JV, Cameron JL. Improved hospital morbidity, mortality, and survival after the Whipple procedure. *Ann Surg* **1987**;206: 358-365
10. Dunn E. Impact of technology and improved perioperative management upon survival from carcinoma of the pancreas. *Surg Gynecol Obstet* **1987**;164:237-244
11. Grace PA, Pitt HA, Tompkins RK, DenBesten L, Longmire WP. Decreased morbidity and mortality after pancreatoduodenectomy. *Am J Surg* **1986**; 151:141-149
12. Kalser MH, Barkin J, MacIntyre JM. Pancreatic cancer: assessment of prognosis by clinical presentation. *Cancer* **1985**;56:397-402
13. Speer AG, Russell RCG, Hatfield ARW, et al. Randomised trial of endoscopic versus percutaneous stent insertion in malignant obstructive jaundice. *Lancet* **1987**;2:57-62
14. Lea MS, Stahlgren LH. Is resection appropriate for adenocarcinoma of the pancreas? A cost-benefit analysis. *Am J Surg* **1987**;154:651-654
15. Warshaw AL, Swanson RS. Pancreatic cancer in 1988. *Ann Surg* **1988**;208:541-551
16. Cotton PB. Endoscopic methods for relief of malignant obstructive jaundice. *World J Surg* **1984**;8:854-861
17. Huibregtse K, Katon RM, Coene PP, Tytgat GNJ. Endoscopic palliative treatment in pancreatic cancer. *Gastrointest Endosc* **1986**;32:334-338
18. Seigel JH, Snady H. The significance of endoscopically placed prostheses in the management of biliary obstruction due to carcinoma of the pancreas: results of nonoperative decompression in 277 patients. *Am J Gastroenterol* **1986**;81:634-641
19. Freeny PC. Radiologic diagnosis and staging of pancreatic ductal adenocarcinoma. *Radiol Clin North Am* **1989**;27:121-128
20. Nesbit GM, Johnson CD, James EM, MacCarty RL, Nagorney DM, Bender CE. Cholangiocarcinoma: diagnosis and evaluation of resectability by CT and sonography as procedures complementary to cholangiography. *AJR* **1988**;151:933-938
21. Balfe DM, Mauro MA, Koehler RE, Lee JKT. Gastrohepatic ligament: normal and pathologic CT anatomy. *Radiology* **1984**;150:485-490
22. Morehouse HT. Nodes or no nodes: CT of adenopathy. *Crit Rev Diagn Imaging* **1986**;25:177-207
23. Thoeni RF, Fell SC, Goldberg HI. CT detection of asymptomatic pancreatitis following ERCP. *Gastrointest Radiol* **1990**;15:291-295
24. Ross CB, Kaufman AJ, Sharp KW, Andrews T, Williams LF. Efficacy of computerized tomography in the preoperative staging of pancreatic carcinoma. *Am Surg* **1988**;54:221-226
25. Heiken JP, Weyman PJ, Lee JKT, et al. Detection of focal hepatic masses: prospective evaluation with CT, delayed CT, CT during arterial portography, and MR imaging. *Radiology* **1989**;171:47-51
26. Mackie CR, Lu CT, Noble HG, et al. Prospective evaluation of angiography in the diagnosis and management of patients suspected of having pancreatic cancer. *Ann Surg* **1979**;189:11-17
27. Savader BL, Fishman EK, Savader SJ. Comparison of CT angiography and routine angiography in assessing resectability of pancreatic tumors (abstr). *Radiology* **1990**;177(P):192
28. Baker ME, Cohan RH, Nadel SN, Leder RA, Dunnick NR. Obliteration of the fat surrounding the celiac axis and superior mesenteric artery is not a specific CT finding of carcinoma of the pancreas. *AJR* **1990**;155:991-994
29. Baker ME. Pancreatic adenocarcinoma: are there pathognomonic changes in the fat surrounding the superior mesenteric artery? *Radiology* **1991**; 180:613-614
30. Schulte SJ, Baron RL, Freeny PC, Patten RM, Gorell HA, Maclin ML. Root of the superior mesenteric artery in pancreatitis and pancreatic carcinoma: evaluation with CT. *Radiology* **1991**;180:659-662

Book Review

Endoscopic Retrograde Cholangiopancreatography. Technique, Diagnosis, and Therapy. By Jerome H. Siegel. New York: Raven, 432 pp., 1992. Book, $159; correlating slide set, $225

In the past 15 years, ERCP has advanced remarkedly into therapeutic interventions in both the biliary and pancreatic duct systems. An endoscopist who has been most active and innovative in these interventions is the author of this text: Jerome H. Siegel. He has actively contributed to the literature on ERCP and endoscopic retrograde sphincterotomy, and many of his technical innovations, papillotomy techniques, and devices have become standards in the practice of biliary and pancreatic interventional endoscopy. At the time this text was written, he had performed approximately 7500 ERCPs and more than 5000 sphincterotomies and other biliary and pancreatic therapies in an endoscopic career of more than 15 years. It is from this base of vast experience and productive writing that Dr. Siegel has come to produce a comprehensive state-of-the-art reference text for specialists and primary care members of the diagnostic-therapeutic team who deal with disorders of the pancreaticobiliary systems.

This is essentially a one-author text; only one chapter was written by invited contributors. The book is written lucidly in the first person, reflecting the personal experiences and opinions of the author in a conversational style. His opinions on management of patients and on technique are well represented, and, as can be expected, he is a strong advocate for the endoscopic approach to diagnosis and therapy. These opinions, however, are appropriately tempered with advice to serve the patient's interest in the best manner possible: If in a particular institution or locale the radiologist has more experience in diagnosis and intervention than does the endoscopist, radiologic approaches should be used.

The text provides both review of radiologic diagnosis and endoscopic technique. Approximately 30% of the text is devoted to interpretation of radiographs. The remainder is devoted to a combination of endoscopic technique, interpretation of endoscopic images, and description of endoscopic therapeutic approaches. The book has 780 illustrations, of which 230 are endoscopic photographs. The remainder are either radiographs that show normal findings or pathologic correlation with the radiographs. The endoscopic photographs are of spectacular quality, and the supplementary legends make the findings easily appreciated. The quality of the radiographs is in some cases excellent, but without the drawings and appropriately placed arrows, dark technique and unsharpness would have made some of the radiographic illustrations of limited value.

The text has three major sections. The first, a discussion of endoscopic technique, is relatively brief and includes indications for ERCP, expected success, and a brief overview of instrumentation. The second section deals with diagnosis and includes mostly radiographic information, categorized as to general interpretation; normal biliary and pancreatic duct systems and their variations; assessment of intrahepatic abnormalities; extrahepatic cholestasis (obstructive jaundice); and evaluation of pancreatic inflammatory, congenital, and malignant conditions. This section contains most of the radiographs that instruct the reader in cholangiographic and pancreatographic interpretation. The final section deals with therapeutic endoscopy and describes techniques for endoscopic sphincterotomy, extraction of stones, placement of stents and catheters, decompression techniques that use nasobiliary catheters and endoprostheses, balloon dilatation of strictures, and placement of stents to treat stenosis of the pancreatic duct. A final chapter describes potential interventions, including intraluminal radiation treatment, bipolar sphincterotomy, retrograde cannulation of the cystic duct for stone extraction and perfusion therapies, cholangioscopy, pancreatoscopy, and laser therapy.

The text is a monument to the technical skill and innovative therapeutic prowess of the author. The technique sections should not be overlooked by the nonendoscopist, as these chapters offer valuable insights into the accomplishments and potential of expert interventional endoscopy. This is a readable and extensively illustrated book, and it provides essential technical and interpretive information both for endoscopists and radiologists and for other physicians with whom they work.

Charles A. Rohrmann, Jr.
University of Washington
Seattle, WA 98195

Review Article

Chronic Biliary-Type Pain in the Absence of Gallstones: The Value of Cholecystokinin Cholescintigraphy

R. Kloiber,[1] C. P. Molnar,[1] and E. A. Shaffer[2]

Radiologic criteria for the diagnosis of gallbladder disease largely rest on the detection of calculi. Surgeons are reluctant to do a cholecystectomy in patients with symptoms of gallbladder disease if the results of sonography or cholecystography are normal. Consequently these patients are often left with no satisfactory treatment. Such patients may have chronic acalculous cholecystitis, partial obstruction of the cystic duct, or gallbladder dyskinesia. Increasing evidence indicates that at least some of these patients have decreased gallbladder emptying in response to a stimulus such as a test meal or cholecystokinin. Impaired emptying shown by cholecystokinin cholescintigraphy may be useful for predicting which patients with typical biliary-type pain but no evidence of calculi will be cured by cholecystectomy.

Most patients with biliary-type pain are initially examined with sonography, a procedure that has a sensitivity approaching 98% for detecting calculi [1]. However, sonographic findings are normal in a subset of patients with typical biliary-type pain. Detection of abnormal gallbladder emptying may be an indication of which of these patients will be cured by cholecystectomy even though they had no stones. In this review, we describe the technique used to perform cholecystokinin-stimulated cholescintigraphy, the limitations of the procedure, and the results of various clinical studies.

Cholescintigraphy

Radiopharmaceuticals

Analogues of ^{99m}Tc-iminodiacetic acid (^{99m}Tc-IDA) are the most frequently used radiopharmaceuticals for hepatobiliary imaging. After IV injection, these organic anions are taken up by hepatocytes in a fashion similar to bilirubin and rose bengal. The anions are secreted into bile canaliculi without conjugation. The radiopharmaceutical is uniformly mixed with bile and transverses the biliary system; part fills the gallbladder, and the remainder exits into the duodenum. No significant intestinal reabsorption or enterohepatic recycling occurs [2]. The ideal agent has a high extraction efficiency (>80%) by the liver, rapid transit, and high concentration in bile.

Gallbladder Filling

In healthy fasting patients, the gallbladder is usually visualized within 15 min after a bolus injection of the radiopharmaceutical and almost always within 60 min. Time-activity curves generated from the filling phase of the gallbladder vary and may show either a progressively rising curve, a stepwise rising curve, or spontaneous decreases caused by contraction that is probably associated with the migratory myoelectric complex. This spontaneous contractile wave originates in the lower esophagus or gastric antrum and sweeps down the small intestine during the interdigestive period about every 120 min in humans.

After a bolus injection, the concentration of ^{99m}Tc-IDA within bile peaks and then declines slowly. The rate of rise, peak, and rate of decline vary with different ^{99m}Tc-IDA analogues. Externally detected changes in radioactivity within the gallbladder are consequently not proportional to the volume of

---

Received October 21, 1991; accepted after revision March 23, 1992.

[1] Department of Radiology, Foothills Hospital and University of Calgary, 1403 29th St. N.W., Calgary, Alberta, Canada T2N 2T9. Address reprint requests to R. Kloiber.

[2] Department of Medicine, Foothills Hospital and University of Calgary, Calgary, Alberta, Canada, T2N 2T9.

AJR 159:509–513, September 1992 0361–803X/92/1593–0509 © American Roentgen Ray Society

bile entering the gallbladder. The concentration of bile and dilution of the radiopharmaceutical by existing unlabeled bile within the gallbladder are additional variables that negate using cholescintigraphy to directly measure gallbladder volume. The best use of the filling phase is to confirm patency of the cystic duct.

Gallbladder Emptying

Although externally detected radioactivity is independent of absolute volume as described, radioactivity is proportional to relative volume so long as no additional bile enters the gallbladder. It is also independent of the gallbladder's shape and geometry. Time-activity curves reflecting relative volume can be generated from a region of interest over the gallbladder on digitized dynamic images from the emptying phase. Background correction is done by subtracting radioactivity detected in a region of interest adjacent to the gallbladder region from the gallbladder time-activity curve after normalizing the area of the regions. Decreasing radioactivity of the ^{99m}Tc-IDA due to decay also must be corrected for.

The most commonly used single measurement that reflects the degree of emptying is the ejection fraction, which represents the percentage of initial volume or activity evacuated with contraction of the gallbladder. Although measurements at only two discrete time points are required for the calculation, generation of a time-activity curve is desirable to ensure that maximum and minimum volumes were selected. Algorithms to calculate the ejection fraction are available on most dedicated nuclear medicine computer systems and are done according to the formula: $EF = [(A - Bg_a) - (B - Bg_b)]/(A - Bg_a)$, where EF = ejection fraction, A = initial gallbladder radioactivity from a region of interest on a digitized image, Bg_a = background normalized to the initial gallbladder region of interest (A), B = decay-corrected gallbladder radioactivity after stimulated contraction, and Bg_b = decay-corrected background radioactivity normalized to the postcontraction gallbladder region of interest (B).

This method assumes complete mixing of the radiopharmaceutical with bile; the ejection fraction can be overestimated if sludge or abundant stones are present. ^{99m}Tc-IDA does not adhere to either calculi or the wall of the gallbladder [3]. This method has been validated in vitro and is simple, accurate, reproducible, and operator-independent in clinical use [4]. Other factors such as emptying rates can be calculated from the time-activity curves but have not been studied extensively.

Stimulus for Contraction

For clinical purposes, gallbladder contraction can be initiated by either a test meal or infusion of cholecystokinin or its synthetic active octapeptide (sincalide [Kinevac], Squibb Canada Inc., Montreal, Canada). The variety of protocols used by investigators complicates comparisons of different studies. It can be argued that the test meal is more physiologic and therefore is the preferred approach when information is sought about the function of the gallbladder in the overall digestive process. The meal, however, introduces additional variables. The composition of the meal will affect the endogenous release of cholecystokinin from the duodenal mucosa directly and indirectly because meals of different composition have different rates of emptying from the stomach. Furthermore, impaired gastric emptying will blunt or delay the response, as will pancreatic insufficiency [5] or mucosal diseases, such as sprue [6].

Administration of cholecystokinin provides control of the dose, resulting in a more reproducible measure of gallbladder contractility. Cholecystokinin has been administered by either bolus injection or slow IV infusion. With slow infusion (more than 5 min as a minimum), gallbladder response is dose-dependent above a threshold and reaches a plateau above which higher doses do not further enhance emptying [7, 8]. Rapid bolus injection results in submaximal emptying and can produce abdominal discomfort [9, 10]. The optimized slow-infusion rate of cholecystokinin octapeptide is 0.020 μg/kg per hour. Maximal gallbladder emptying and maximal ejection fraction are reached around 1 hr after the infusion is begun. With the slow-infusion technique that we use, subjects rarely experience pain, whether they are control subjects, patients with stones who are being examined for medical dissolution therapy, or patients with noncalculous biliary-type pain, even if their symptoms subsequently decreased after cholecystectomy. Pain reproduction is therefore a poor indicator of disease and should not be used as a criterion.

Effects of Medications and Nonbiliary Diseases

Because of the complex neural and humoral control of gallbladder contractility, many medications and physiologic states can alter the results. Morphine in particular and opiates in general cause impaired gallbladder emptying because they induce spasm of the sphincter of Oddi [11]. Endogenous opiates secreted after major upper abdominal surgery may contribute to impaired contraction [12]. Truncal vagotomy results in increased gallbladder volume and decreased contractility [13, 14]. Atropine inhibits [15] and cholinergic stimulation enhances gallbladder emptying [16]. Calcium channel blockers reduce contractility, presumably by interfering with the calcium-mediated contraction of smooth muscle [17]; emptying is enhanced by hypercalcemia [18]. In animals, stimulation of histamine$_2$ receptors also can be inhibitory [19]. Considering the wide variety of medications with similar actions, great care must be exercised to ensure accurate results. Systemic diseases also may have an effect on an intrinsically normal gallbladder. Decreased contractility and increased gallbladder volume have been described in diabetic patients who have advanced neuropathy [20, 21], in patients with sickle cell hemoglobinopathy [22], and in large persons [23]. A generalized smooth muscle abnormality with impaired cholecystokinin response has been shown in patients with irritable bowel syndrome [24]. Gallbladder contraction in response to a test meal appears to be unaffected by the age of the patient. In older patients, contraction may be maintained by an exaggerated endogenous cholecystokinin release in response to food [25], and therefore contraction in response to a standardized cholecystokinin infusion may be subnormal. Progesterone has been shown to impair gallbladder emptying [26], but differences in gallbladder ejection fraction due to the sex of the patient, phases of the menstrual cycle, and use of oral contraceptives have been inconsistent. Many of these factors have not been accurately defined but may account in part for the lack of consistency shown in clinical studies of gallbladder disease.

The Significance of Reduced Contraction

Some patients with histologically proved acalculous cholecystitis have impaired contraction [27]. These patients may be at an earlier stage of a process that leads eventually to calculous disease. The mechanism of reduced emptying could be related to an inherent impairment of contractility that contributes to stone formation [28, 29]. A direct effect of lithogenic bile on contractility has been shown even before stone formation in animal models [30] and patients [31]. Cholesterol crystals in bile are considered a precursor of stone formation, and symptomatic patients with crystals have been shown to have a lower ejection fraction than those without crystals [32]. The release of endogenous cholecystokinin also may be impaired after a meal [33]. In late stages, defective emptying could be caused by fibrosis and thickening of the gallbladder wall associated with chronic inflammation.

Impaired contraction does not appear to be related to the presence of stones themselves [34]. In one series, only 24% of 67 patients with proved chronic calculous cholecystitis had impaired gallbladder contraction [35]. It is reasonable to assume that a significant number of patients with acalculous cholecystitis will have normal emptying. Impaired gallbladder contraction also may exist in the absence of symptoms: in one study of chronic calculous gallbladder disease in which cholecystectomy was not performed, only 18% of patients had symptoms during 15 years of follow-up [36].

Cystic duct syndrome with partial noncalculous obstruction of the cystic duct [37] and gallbladder dyskinesia also have been proposed to explain biliary pain. The standard selected for confirming an abnormality is therefore problematic. Histologic evidence of chronic cholecystitis will be absent if the pain is caused by dyskinesia alone. A small cystic duct, adhesions, or kinking may be difficult to confirm, even at surgery. Pain relief after surgery may be a more appropriate indicator but is not reliable unless the clinical trial is well controlled with a long follow-up because of the placebo effect of surgery.

It is therefore not surprising that different investigators have had different results and different opinions on the value of gallbladder motility studies.

Results of Clinical Studies

The degree of gallbladder evacuation measured by cholecystography after a bolus injection of cholecystokinin showed wide variation (ejection fraction of 10–90%) in a series of control subjects in the study of Nathan et al. [38]. In a trial by Dunn et al. [39] in which three radiologists had no knowledge of which subjects had symptoms, between 10% and 36% of control subjects were considered to have abnormal cholecystographic findings of decreased contraction and asymmetric spasm after bolus injection of cholecystokinin. This was not statistically different from findings in patients who had biliary colic or dyspepsia. High interobserver variability of up to 28% also was found. These results did not help predict histologic abnormalities or relief of symptoms after cholecystectomy. The failure of cholecystokinin-stimulated oral cholecystography can be attributed to the nonphysiologic method and subjective criteria for interpretation.

Gallbladder emptying as measured by scintigraphy with cholecystokinin stimulation is quantitative. Nevertheless, nonphysiologic, rapid infusions of cholecystokinin also will cause incomplete contraction of the gallbladder even in control subjects, leading some authors to conclude that the degree of contraction "cannot be used to indicate presence of chronic acalculous cholecystitis" [40]. Abnormal contraction cannot be used to accurately predict histologic evidence of chronic inflammation [40, 41], as would be expected if pain also could result from a motility disorder.

Others [42–44], who also used a rapid injection of cholecystokinin (less than 5 min), have taken a more positive view of the value of the procedure on the basis of a high rate of clinical response (93–100%) in patients with reduced emptying who had surgery. Indeed, all series [41–44] showed favorable response rates (69–100%) comparable to those in patients who had surgery for calculi [45, 46].

All the studies were retrospective and primarily involved patients with abnormal emptying, yet by no means did all the patients with abnormal emptying have surgery. It is also likely that of the patients with abnormal emptying, those with more typical or more severe symptoms had cholecystectomy. Surgeons generally do not operate on the basis of symptoms alone, yet in one series [42], five of five patients who had normal evacuation also had pain relief with subsequent cholecystectomy. With the lack of a histologic basis, the vagaries of clinical assessment, the selection bias, and the small number and proportion of patients who have surgery, it is impossible to calculate meaningful sensitivity and specificity figures.

For future investigation, standardization of the method of cholecystokinin cholecystography is essential. Patients should be eating normally up to a minimum of 2 hr to no more than 24 hr before the study to ensure that gallbladder filling will occur. Ideally, all medications should be discontinued. Infusion of cholecystokinin at a physiologic dose rate is preferable to a test meal unless gastric emptying is measured simultaneously. Patients with advanced diabetes, liver disease, pancreatitis, irritable bowel syndrome, or previous upper gastrointestinal surgery should not have the procedure.

Although it is unlikely that a prospective study randomizing patients to have surgery regardless of their ejection fractions will be done, a recent study by Yap et al. [47] sheds additional light on the question. The gallbladder ejection fraction was calculated in 103 patients 1 hr after the beginning of a 45-min cholecystokinin-octapeptide infusion at 0.020 μg/kg per hour. An ejection fraction of less than 40% (3 SD less than the mean ejection fraction of the control group) was arbitrarily defined as abnormal. Twenty-one patients with a reduced ejection fraction were randomized to have surgery, and of the 11 operated on, 10 became asymptomatic and one had partial relief of symptoms. The patients who did not have surgery remained symptomatic. Of the 82 patients with normal ejection fractions, 50 were asymptomatic on follow-up and 10 were symptomatic without specific treatment for biliary disease. Fourteen others had cholecystectomy, and eight of these became asymptomatic. Eight patients were not available for follow-up. All patients in the group with a low ejection fraction had evidence of chronic cholecystitis, muscle hypertrophy, or a narrowed cystic duct. Similar findings were seen in six of the normally contracting gallbladders that were removed. These results suggest that an abnormal ejection fraction is a good predictor of a favorable response to surgery, but eight patients with normal ejection fractions also benefited from cholecystectomy. If it is assumed that all 21 patients with low ejection fractions would have improved with surgery and it is known that at least eight with normal ejection fractions responded favorably to surgery, the maximum sensitivity of low ejection fractions as an indicator of the desirability of surgery is 72% (21/29). Of the 74 patients with a normal ejection fraction and complete follow-up, eight are known to have responded to surgery and 10 remain symptomatic without specific treatment. The specificity of the ejection fraction therefore lies between 89% (66/74) and 76% (56/74). Given sensitivity and specificity values in that range, cholecystokinin-stimulated cholescintigraphy should be used only in a highly selected population of patients with chronic pain typical of biliary disease. It remains to be confirmed whether the positive clinical response in patients who have had surgery reflects the inherent value of cholescintigraphy or the clinical judgment in the selection of patients for surgery from the group with low ejection fractions.

ACKNOWLEDGMENT

We thank Jean Nyhus for secretarial assistance.

REFERENCES

1. Cooperberg PL, Gibney RG. Imaging of the gallbladder, 1987. *Radiology* **1987**;163:605–613
2. Loberg MD, Nunn AD, Porter DW. Development of hepatobiliary imaging agents. In: Freeman LM, Weissman HS, eds. *Nuclear medicine annual.* New York: Raven, **1981**:1–33
3. Pomeranz IS, Logan KJ, Shaffer EA. The adherence of ^{99m}Tc-DISIDA to gallstones and gallbladder wall. *J Nucl Med Allied Sci* **1984**;28:181–184
4. Krishnamurthy GT, Bobba VR, Kingston E. Radionuclide ejection fraction: a technique for quantitative analysis of motor function of the human gallbladder. *Gastroenterology* **1981**;80:482–490
5. Masclee AAM, Jansen JBMJ, Corstens FHM, Lamers CBHW. Reversible gallbladder dysfunction in severe pancreatic insufficiency. *Gut* **1989**; 30:866–872
6. Maton PN, Selden AC, Fitzpatrick ML, Chadwick VS. Defective gallbladder emptying and cholecystokinin release in celiac disease: reversal by gluten-free diet. *Gastroenterology* **1985**;88:391–396
7. Spellman SJ, Shaffer EA, Rosenthall L. Gallbladder emptying in response to cholecystokinin: a cholescintigraphic study. *Gastroenterology* **1979**; 77:115–120
8. Maton PN, Selden AC, Fitzpatrick ML, Chadwick VS. Infusion of cholecystokinin octapeptide in man: relation between plasma cholecystokinin concentrations and gallbladder emptying rates. *Eur J Clin Invest* **1984**;14: 37–41
9. Sarva RP, Shreiner DP, Van Thiel D, Yingvorapant N. Gallbladder function: methods for measuring filling and emptying. *J Nucl Med* **1985**;26:140–144
10. Hopman WPM, Jansen JBMJ, Rosenbusch G. Gallbladder contraction induced by cholecystokinin: bolus injection or infusion. *BMJ* **1986**; 292:375–376
11. Worobetz LJ, Baker RJ, McCallum JA, Wells G, Sullivan SN. The effect of naloxone, morphine, and an enkephalin analogue on cholecystokinin octapeptide-stimulated gallbladder emptying. *Am J Gastroenterol* **1982**; 77:509–511
12. Takahashi T, Yamamura T, Yokoyama E, et al. Impaired contractile motility of the gallbladder after gastrectomy. *Am J Gastroenterol* **1986**;81: 672–677
13. Parkin GJS, Smith RB, Johnston D. Gallbladder volume and contractility after truncal, selective and highly selective (parietal cell) vagotomy in man. *Ann Surg* **1973**;178:581–586
14. Baxter JN, Grime JS, Critchley M, Jenkins SA, Shields R. Relationship between gastric emptying of a solid meal and emptying of the gallbladder before and after vagotomy. *Gut* **1987**;28:855–863
15. Gullo L, Bolondi L, Priori P, Casanova P, Labo G. Inhibitory effect of atropine on cholecystokinin-induced gallbladder contraction in man. *Digestion* **1984**;29:209–213
16. Fisher RS, Rock E, Malmud LS. Cholinergic effects on gallbladder emptying in humans. *Gastroenterology* **1985**;89:716–722
17. Crochelt RF, Peikin SR. Effect of nifedipine and extracellular calcium on spontaneous and potassium-stimulated bovine gallbladder muscle contraction (abstr.). *Gastroenterology* **1987**;92:1799
18. Malagelada JR, Holtermuller KH, Sizemore GW, Go VLW. The influence of hypercalcemia on basal and cholecystokinin-stimulated pancreatic, gallbladder, and gastric functions in man. *Gastroenterology* **1976**;71:405–408
19. Waldman DB, Zfass AM, Makhlouf GM. Stimulatory (H_1) and inhibitory (H_2) histamine receptors in gallbladder muscle. *Gastroenterology* **1977**;72: 932–936
20. Mitsukawa T, Takemura J, Ohgo S, et al. Gallbladder function and plasma cholecystokinin levels in diabetes mellitus. *Am J Gastroenterol* **1990**; 85:981–985
21. Kronert K, Gotz V, Reuland P, Luft D, Eggstein M. Gallbladder emptying in diabetic patients and control subjects assessed by real-time ultrasonography and cholescintigraphy: a methodological comparison. *Ultrasound Med Biol* **1989**;15:535–539
22. Everson GT, Nemeth A, Kourourian S, et al. Gallbladder function is altered in sickle hemoglobinopathy. *Gastroenterology* **1989**;96:1307–1316
23. Vezina WC, Paradis RL, Grace DM, et al. Increased volume and decreased emptying of the gallbladder in large (morbidly obese, tall normal and muscular normal) people. *Gastroenterology* **1990**;98:1000–1007
24. Kellow JE, Miller LJ, Philips SF, Zinsmeister AR, Charboneau JW. Altered sensitivity of the gallbladder to cholecytokinin octapeptide in irritable bowel syndrome. *Am J Physiol* **1987**;253:G650–G655
25. Khalil T, Walker JP, Wiener I, et al. Effect of aging on gallbladder contraction and release of cholecystokinin-33 in humans. *Surgery* **1985**;98:423–428
26. Shaffer EA, Taylor PJ, Logan K, Gadomski S, Corenblum B. The effect of a progestin on gallbladder function in young women. *Am J Obstet Gynecol* **1984**;148:504–507
27. Raptopoulos V, Compton CC, Doherty P, et al. Chronic acalculous gallbladder disease: multiimaging evaluation with clinical-pathologic correlation. *AJR* **1986**;147:721–724
28. Thompson JC, Fried GM, Ogden WD, et al. Correlation between release of cholecystokinin and contraction of the gallbladder in patients with gallstones. *Ann Surg* **1982**;195:670–675
29. Fisher RS, Stelzer F, Rock E, Malmud LS. Abnormal gallbladder emptying in patients with gallstones. *Dig Dis Sci* **1982**;27:1019–1024
30. Fridhandler TM, Davison JS, Shaffer EA. Defective gallbladder contractility in the ground squirrel and prairie dog during the early stages of cholesterol gallstone formation. *Gastroenterology* **1983**;85:830–836
31. Behar J, Lee KY, Thompson WR, Biancani P. Gallbladder contraction in

patients with pigment and cholesterol stones. *Gastroenterology* **1989**;97:1479–1484
32. Brugge WR, Brand DL, Atkins HL, Lane BP, Abel WG. Gallbladder dyskinesia in chronic acalculous cholecystitis. *Dig Dis Sci* **1986**;31:461–467
33. Masclee AAM, Jansen JBMJ, Driessen WMM, Geuskens LM, Lamers CBHW. Plasma cholecystokinin and gallbladder responses to intraduodenal fat in gallstone patients. *Dig Dis Sci* **1989**;34:353–359
34. Pomeranz IS, Shaffer EA. Abnormal gallbladder emptying in a subgroup of patients with gallstones. *Gastroenterology* **1985**;88:787–791
35. Raymond F, Lepanto L, Rosenthall L, Fried GM. Tc-99m IDA gallbladder kinetics and response to CCK in chronic cholecystitis. *Eur J Nucl Med* **1988**;14:378–381
36. Gracie WA, Ransohoff DF. The natural history of silent gallstones: the innocent gallstone is not a myth. *N Engl J Med* **1982**;307:798–800
37. Cozzolino HJ, Goldstein F, Greening RR, Wirts CW. The cystic duct syndrome. *JAMA* **1963**;185:920–924
38. Nathan MH, Newman A, Murray DJ. Normal findings in oral and cholecystokinin cholecystography. *JAMA* **1978**;240:2271–2272
39. Dunn FH, Christensen EC, Reynolds J, Jones V, Fordtran JS. Cholecystokinin cholecystography: controlled evaluation in the diagnosis and management of patients with possible acalculous gallbladder disease. *JAMA* **1974**;228:997–1003
40. Davis GB, Berk RN, Scheible FW, et al. Cholecystokinin cholecystography, sonography, and scintigraphy: detection of chronic acalculous cholecystitis. *AJR* **1982**;139:1117–1121
41. Westlake PJ, Hershfield NB, Kelly JK, et al. Chronic right upper quadrant pain without gallstones: does HIDA scan predict outcome after cholecystectomy? *Am J Gastroenterol* **1990**;85:986–990
42. Pickleman J, Peiss RL, Henkin R, Salo B, Nagel P. The role of sincalide cholescintigraphy in the evaluation of patients with acalculous gallbladder disease. *Arch Surg* **1985**;120:693–696
43. Fink-Bennett D, DeRidder P, Kolozsi W, Gordon R, Rapp J. Cholecystokinin cholescintigraphic findings in the cystic duct syndrome. *J Nucl Med* **1985**;26:1123–1128
44. Topper TE, Ryerson TW, Nora PF. Quantitative gallbladder imaging following cholecystokinin. *J Nucl Med* **1980**;21:694–696
45. Rhind JA, Watson L. Gall stone dyspepsia. *BMJ* **1968**;1:32
46. Gunn A, Keddie N. Some clinical observations on patients with gallstones. *Lancet* **1972**;2:239–241
47. Yap L, Wycherley AG, Morphett AD, Toouli J. Acalculous biliary pain: cholecystectomy alleviates symptoms in patients with abnormal cholescintigraphy. *Gastroenterology* **1991**;101:786–793

New Format for Abstracts

Beginning immediately, the *AJR* will publish abstracts of articles in a different format, much like the ones recently adopted by the *New England Journal of Medicine* and the *Journal of the American Medical Association*. The purpose of the new design is to have abstracts present the essential elements of articles more clearly and concisely. The contents, organization, and length of the abstracts will be the same as before; however, rather than being all one paragraph except for the conclusion, abstracts will now be divided into four paragraphs, each with a title: objective, subjects (or materials) and methods, results, and conclusion.

The *AJR* Guidelines for Authors, which appears at the front of every issue of the Journal, has been revised to help you write abstracts in this new format. Authors should familiarize themselves with these guidelines and incorporate them into all manuscripts submitted for publication.

Robert N. Berk
Editor-in-Chief

Book Review

Clinical Sonography. A Practical Guide, 2nd ed. Edited by Roger C. Sanders. Boston: Little, Brown, 557 pp., 1991. $47.50, softcover

Clinical Sonography is an ultrasonic travel guide through the body that provides a cornucopia of useful information in a terse and well-organized manner. The book is designed primarily for sonographers, although it can be quite useful for residents during their initial experience with sonography. It emphasizes a practical approach to the clinical applications of this imaging technique. Chapters are organized mainly by clinical problems rather than by disease or organ. This approach encourages readers to think in terms of differential diagnoses. Some of the medical terminology is simplified, more suited for a neophyte sonographer than for a physician.

This soft cover volume is organized into many brief chapters. Each begins with a definition of terms, continues with a description of the clinical problem, the anatomy, and the pathologic findings, and closes with differential diagnostic considerations, scanning tips, and pitfalls. The initial chapters cover the physics of sonography (including Doppler sonography), instrumentation, "knobology," and basic principles of scanning. Then, gynecologic (infertility, pelvic masses, vaginal bleeding, pelvic pain) and obstetric (bleeding, uncertain or abnormal size for dates, fetal anomalies and death) problems are discussed. Problems of the abdomen not associated with pregnancy constitute another large group of chapters. Topics include pain, fever, jaundice, renal failure, masses, hematuria, renal transplants, and disorders of the reproductive tract in males. Miscellaneous clinical topics are discussed next, including breast lesions, pain and swelling in the extremities, fluid or masses in the chest, joint symptoms in the shoulder in adults and in the hip in infants, neonatal intracranial and spinal abnormalities, techniques of sonographically guided aspiration, and artifacts. An extensive index provides many tables of obstetric measurements.

This second edition is a significant expansion of the first. Real-time scanning is now emphasized; previously the emphasis was on contact scanning. Chapters on Doppler imaging; sonography of the prostate, shoulder, hip, and spine; imaging studies in infertility; and fetal echocardiography are new, and those on the carotid arteries, fetal anomalies, abdominal pain, renal transplants, first-trimester bleeding, and uncertain dates are considerably expanded.

A major attraction of this book is its illustrations, especially those relating plane of scan to global organ or regional anatomy. These drawings rapidly orient the reader to the location of the scan section, which is particularly useful in real-time scanning in which the displayed image has a small field of view. Clinical sonograms are mainly presented as drawings, an unusual departure from the common practice of using photographs. Although most of the drawings are representational of sonograms, those produced by computer (as distinguished from those drawn by hand) are more stylized and may present some difficulties for the neophyte sonographer.

Unfortunately, Doppler sonography, particularly color Doppler imaging, is given less coverage than I think it warrants, especially in abdominal imaging. This technique is becoming routine in many examinations to help characterize masses, distinguish ducts from vessels, and evaluate blood flow in organs beyond transplants. A discussion of color does not necessarily require color illustrations, which the author may not wish to use for reasons of cost. Another entire topic not covered is nonfetal echocardiography. As a number of sonographers perform both echocardiography and abdominal sonography, information on nonfetal echocardiography would make the book complete.

These relatively minor criticisms aside, this book is an excellent companion for the beginning sonographer and a good quick reference manual for more experienced examiners when they are performing studies that they do not frequently do.

M. Leon Skolnick
Presbyterian University Hospital
University of Pittsburgh School of Medicine
Pittsburgh, PA 15213

Membranous Obstruction of the Inferior Vena Cava: Comparison of Findings at Sonography, CT, and Venography

Jae Hoon Lim[1]
Jae Hyung Park[2]
Yong Ho Auh[3]

OBJECTIVE. Membranous or segmental obstruction of the inferior vena cava is one of the common causes of chronic Budd-Chiari syndrome. In this study, the venographic findings are compared with the results of sonography and CT in order to ascertain their role in the management of these cases.

MATERIALS AND METHODS. Fifteen patients with membranous ($n = 8$) or segmental ($n = 7$) obstruction of the inferior vena cava who had been examined with sonography and CT were studied retrospectively. Diagnosis was made at surgery ($n = 3$) or by venacavography ($n = 12$). Sonographic findings were analyzed on the basis of the initial report, and CT findings were reviewed retrospectively with knowledge of the sonographic findings.

RESULTS. Sonography showed membranous obstruction ($n = 5$), segmental cordlike obstruction ($n = 3$), and unspecified obstruction ($n = 5$) of the inferior vena cava, while CT showed a flap of the membrane ($n = 1$) and segmental narrowing or obstruction of the inferior vena cava ($n = 7$). In the remaining cases, the inferior vena cava either appeared normal ($n = 6$) or was not visualized ($n = 1$) on CT or was not described in the sonographic report ($n = 2$). In nine cases, CT showed one or several tiny calcific foci in the inferior vena cava. Sonography showed obliteration of at least one hepatic vein ($n = 8$) and of intrahepatic collateral vessels ($n = 12$), whereas CT was less sensitive in evaluating obliteration of intrahepatic veins ($n = 4$) and collateral vessels ($n = 7$). Sonography and CT both showed hepatic masses ($n = 6$), evidence of liver cirrhosis and portal hypertension ($n = 14$), hepatomegaly ($n = 14$), enlargement of the caudate lobe ($n = 9$), and intraabdominal ($n = 11$) and abdominal wall ($n = 15$) collateral vessels.

CONCLUSION. Sonography was superior to CT in delineating pathologic venous anatomy of the inferior vena cava and hepatic veins whereas CT was better in evaluating hepatic cirrhosis and tumor. We believe that these techniques are useful complements to venography in the diagnosis and management of these cases.

AJR 159:515–520, September 1992

Whereas Budd-Chiari syndrome in Western countries is most often due to thrombotic obstruction of the hepatic veins or the inferior vena cava (IVC) resulting from systemic diseases or malignant tumors, membranous or segmental obstruction of the IVC is a common cause of chronic Budd-Chiari syndrome in Korea, Japan, India, and South Africa, resulting in chronic liver disease and formation of portosystemic collateral vessels [1–8]. Several investigators regard membranous obstruction of the IVC as a congenital anomaly [2, 6], although patients usually present in adulthood [3, 5, 6].

Because the disease can be treated with bypass grafts, membranotomy, membranectomy, or radiologic intervention, depending on the pathologic type, accurate diagnosis is important. Although inferior venacavography and hepatic venography have been considered the gold standard in the diagnosis of Budd-Chiari syndrome, these procedures are somewhat invasive and time consuming. Sonographic detection of membranous obstruction of the IVC has been considered a simple and

Received January 17, 1992; accepted after revision March 18, 1992.

[1] Department of Diagnostic Radiology, Kyung Hee University Hospital, 1 Hoeki-dong, Dongdaemun-ku, Seoul 130-702, Korea. Address reprint requests to J. H. Lim.

[2] Department of Diagnostic Radiology, Seoul National University Hospital, 28 Yeongun-dong, Chongro-ku, Seoul 110-744, Korea.

[3] Department of Diagnostic Radiology, Asan Medical Center, Ulsan University Medical College, 388-1, Poongnap-dong, Songpa-ku, Seoul 138-040, Korea.

0361–803X/92/1593–0515
© American Roentgen Ray Society

accurate alternative to venography [7-9]. Although several studies of the use of CT in Budd-Chiari syndrome have been done [10-14], these reports have dealt largely with secondary Budd-Chiari syndrome, that is, hepatic venous occlusion due to systemic disease or tumors. We report the results of sonography, CT, and venography in 15 patients with membranous obstruction of the IVC and discuss the roles of these techniques in the evaluation and management of such cases.

Materials and Methods

Fifteen patients (12 men, three women; 17-54 years old) with membranous obstruction of the IVC who had both sonography and CT were identified at three hospitals. Eight patients were from Kyung Hee University Hospital (among the 21 patients with this problem seen between May 1986 and October 1991), five patients were from Seoul National University Hospital (among the 13 cases seen during the past 4 years), and two patients were from Asan Medical Center (among the five cases seen during the past 2 years). Clinical symptoms were nonspecific and included abdominal distension, pain in the right upper quadrant of the abdomen, indigestion, and varicosity of the abdominal wall or legs.

Three cases were diagnosed by venacavography and confirmed surgically; at surgery a 1.0- to 1.5-mm-thick membrane was found in the hepatic segment of the IVC and membranotomy or membranectomy was performed. The other 12 cases were diagnosed on the basis of results of venacavography. Of those 12, three patients had bypass surgery, four patients had balloon dilatation with or without local urokinase infusion in the radiology departments, and the remaining five patients were treated medically for liver disease and its complications.

CT scans were obtained with CT/T 9800 or CT/T 8800 scanners (GE Medical Systems, Milwaukee, WI; $n = 13$) or with other com-

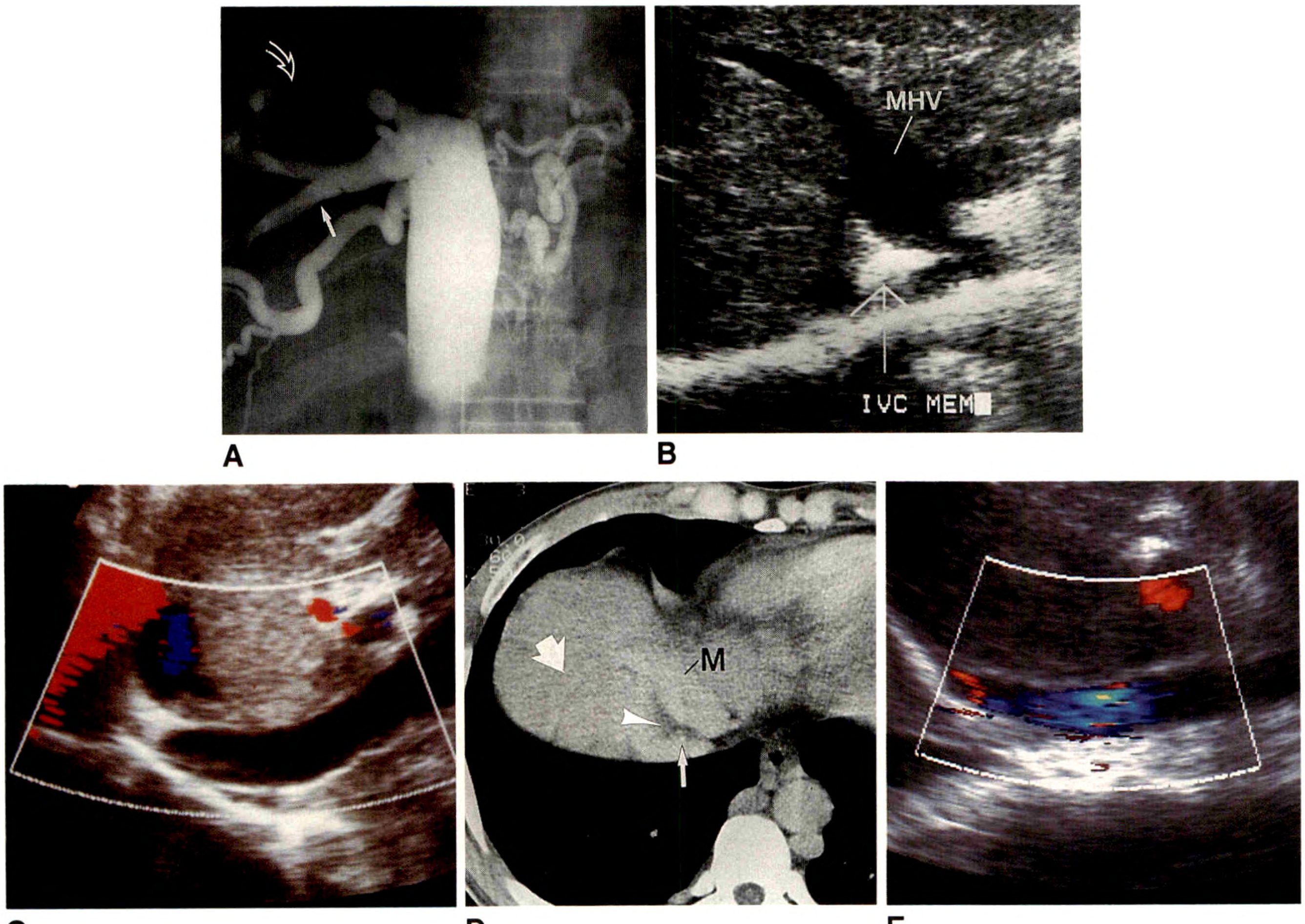

Fig. 1.—Membranous obstruction in 52-year-old man who had memory disturbance for 4 days.

A, Inferior venacavogram shows abrupt termination of inferior vena cava (IVC) just above right hepatic vein (*solid arrow*), which drains into middle hepatic vein through collateral (*open arrow*). Right atrium is faintly opacified via systemic collaterals.

B, Transverse sonogram shows crescent-shaped echogenic focus (IVC MEM), representing membrane that divides IVC above and below middle hepatic vein (MHV). Blood in right hepatic vein drains into middle hepatic vein through intrahepatic collateral (*not shown*).

C, Color Doppler sonogram of hepatic segment of IVC does not show any flow.

D, Contrast-enhanced CT scan shows collateral vessel (*large arrow*) connecting right hepatic vein and middle hepatic vein (M). Wedge-shaped area of low density (*arrowhead*) represents flap of membrane in IVC. Note tiny calcific focus (*small arrow*), which was confirmed when membranous specimen was examined.

E, Follow-up color Doppler sonogram after membranectomy shows flow through hepatic portion of IVC.

mercially available third-generation scanners ($n = 2$). Five patients were examined both before and after contrast administration, and the other 10 patients were examined only after contrast administration. Contrast-enhanced images were obtained after bolus injection of 150 ml of iodinated contrast medium (iodine content, 28%). Most images were obtained during the equilibrium stage between maximal vascular and parenchymal enhancement. Contiguous scans with a 1-cm collimation ($n = 9$), or 5-mm collimation with 2-mm interslice gap ($n = 6$) were obtained through the entire liver and pancreas. Sonographic examinations were performed with commercially available scanners (ATL Ultramark 9, Acuson 128, Toshiba SAL-55A, SSA-90A, and Aloka SSD-710) with either 3.5- or 5.0-MHz sector or linear transducers. Six patients had color Doppler sonography. Venacavography was performed using film-screen techniques. In seven patients, two catheters were inserted, one below and the other above the obstruction. In the other eight patients, venacavography was performed only below the obstruction. In those patients, the vena cava superior to the obstruction was visualized via transhepatic or systemic collaterals ($n = 2$), through the residual caval lumen ($n = 2$), or after balloon dilatation ($n = 2$); in the two remaining cases, the IVC above the obstruction was not visualized.

Sonography was performed before CT in 13 patients and after CT in two patients. Venacavography was always performed after sonographic and CT studies. Sonographic findings were analyzed on the basis of the initial report. CT findings were reviewed retrospectively for this study by one observer who knew the sonographic findings.

Results

Inferior Vena Cava

Inferior venacavography showed complete obstruction of the hepatic segment of the IVC in 13 cases and incomplete obstruction in two cases. The obstruction was abrupt (Fig. 1) in six cases of membranous obstruction and conically tapered (Fig. 2) in seven cases of segmental obstruction, in which the segment was from 1.0 to 5.0 cm long. In the remaining two cases, the shape of obstruction was obscured by thrombus; in one case, membranous obstruction was found during surgery; in the other case, CT and sonography showed segmental obstruction. Thrombus was present in the IVC in five patients, three with membranous obstruction and two with segmental obstruction.

Sonography showed a membrane in the hepatic IVC in five of the eight patients with membranous obstruction. The membrane measured 5–8 mm thick because of the oblique or tangential plane of imaging (Figs. 1B and 3). The membrane was noted to block the IVC completely or partially; complete and incomplete obstruction could be differentiated by Doppler examination (Fig. 1E). In three of seven patients with segmental obstruction, a variable length of the hepatic IVC was obliterated, resulting in a thick, echogenic cordlike structure (Fig. 2B) 5–10 mm thick and 2–5 cm long. The hepatic IVC appeared obstructed but the type of obstruction was not identified in five cases, and in the remaining two cases the IVC was not described in the sonographic report. Of the five patients with venographically proved IVC thrombosis, sonography revealed IVC thrombosis in four patients. Because of the presence of thrombus in these patients, venography did not show the type of obstruction, while sonography showed a membrane in one patient and an echogenic cord in another patient.

Of the eight patients with membranous obstruction, CT showed the flap of the membrane in the IVC (Fig. 1D) in one case. In six patients, the IVC appeared normal, and in the remaining case, the hepatic IVC was not visualized (this patient had thrombus in the IVC shown by venacavography). Of the seven patients with segmental obstruction, the IVC was narrowed and obliterated segmentally (Fig. 2C) in six patients (the segment was from 1 to 4 cm long) and normal in one patient. Thrombus was seen on CT scans in two

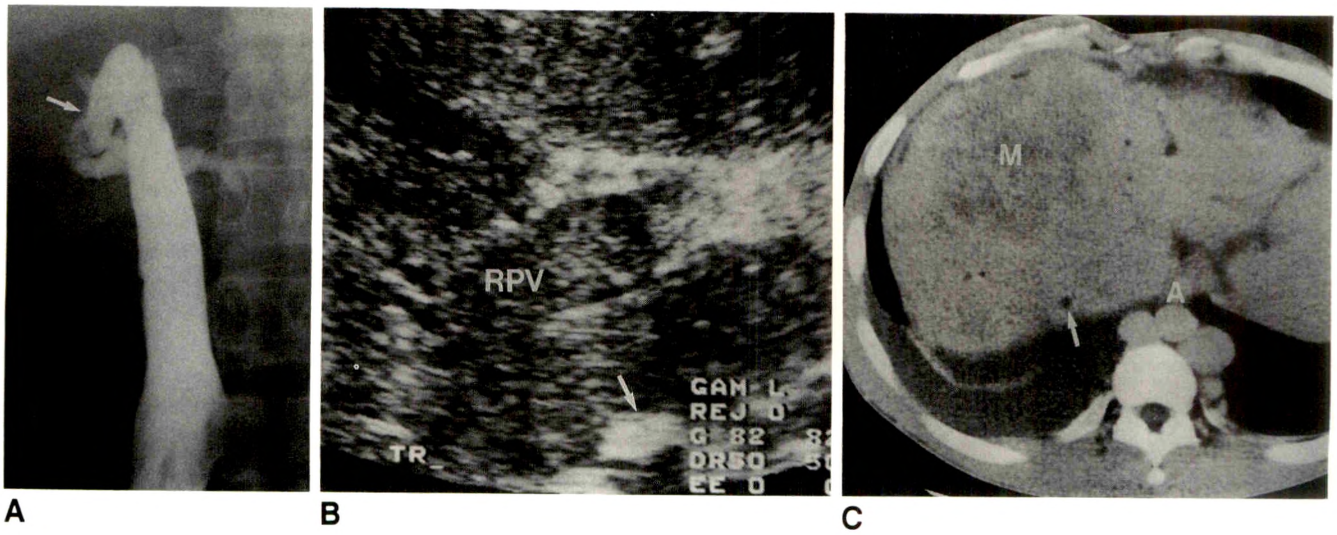

Fig. 2.—Segmental obstruction in 38-year-old man who had jaundice and varicosity of veins in legs.

A, Inferior venacavogram shows complete obstruction of hepatic portion of inferior vena cava (IVC) with smoothly tapering proximal end. *Arrow* = inferior right hepatic vein.

B, Transverse sonogram shows IVC, segmentally replaced by echogenic cord (*arrow*). Right branch of portal vein (RPV) is filled by thrombus.

C, Contrast-enhanced CT scan shows poorly defined mass (M) in liver, right-sided pleural effusion, and dilated azygos, hemiazygos, and subcostal veins. Fine-needle aspiration of mass revealed hepatocellular carcinoma. A = thoracic aorta, *arrow* = IVC.

patients with membranous obstruction and in two patients with segmental obliteration. Of the 15 patients, six patients had tiny focal (Fig. 1D) or curvilinear (Fig. 3D) calcification at the level of obstruction, presumably at the site of the membrane (Fig. 1D) or the obliterated segment. In three other cases, calcification was seen at the margin of thrombus or along the wall of the IVC distant from the level of obstruction.

Hepatic Veins

Inferior venacavography showed retrograde filling of the main right hepatic vein in all eight cases of membranous obstruction (Figs. 1A and 4A) and of the inferior right hepatic vein in five of seven cases of segmental obstruction (Fig. 2A). Selective hepatic venography was not attempted in these patients, as the primary concern was the obstruction of the IVC.

Obliteration of one or two hepatic veins was noted on sonograms in eight cases (Figs. 3C and 4B). The patterns of involvement were isolated occlusion of the middle hepatic vein ($n = 4$, Fig. 4B). Isolated occlusion of the right hepatic vein ($n = 3$, Fig. 3C), and occlusion of the middle and left hepatic veins ($n = 1$). The length of the obliterated segment from the IVC varied from 1 to 3 cm. In the remaining seven cases, the hepatic veins were normal.

Sonography showed intrahepatic collateral vessels connecting the patent portion of the obliterated hepatic vein with a normal hepatic vein (Fig. 4B) in 12 cases. Doppler examination revealed that the direction of the blood flow through the intervenous communication varied depending on the level of the membrane or obliterated segment of the IVC and the hepatic veins. For example, when the membrane was above the orifice of a right hepatic vein and below a middle hepatic vein or left hepatic vein, the blood in the right hepatic vein flowed through the interconnecting intrahepatic collaterals into the middle or left hepatic vein, which then drained into the IVC above the obstruction. When the whole hepatic segment of the IVC was obliterated, as in segmental obstruction, blood from the liver flowed largely through intrahepatic collaterals into the inferior right hepatic vein, which then drained into the suprarenal segment of the IVC and in turn, toward the retroperitoneal, vertebral, intercostal, and azygos veins.

Contrast-enhanced CT showed intrahepatic collaterals (Figs. 1D and 4C) in seven cases and obliterated segments of the hepatic vein in four cases.

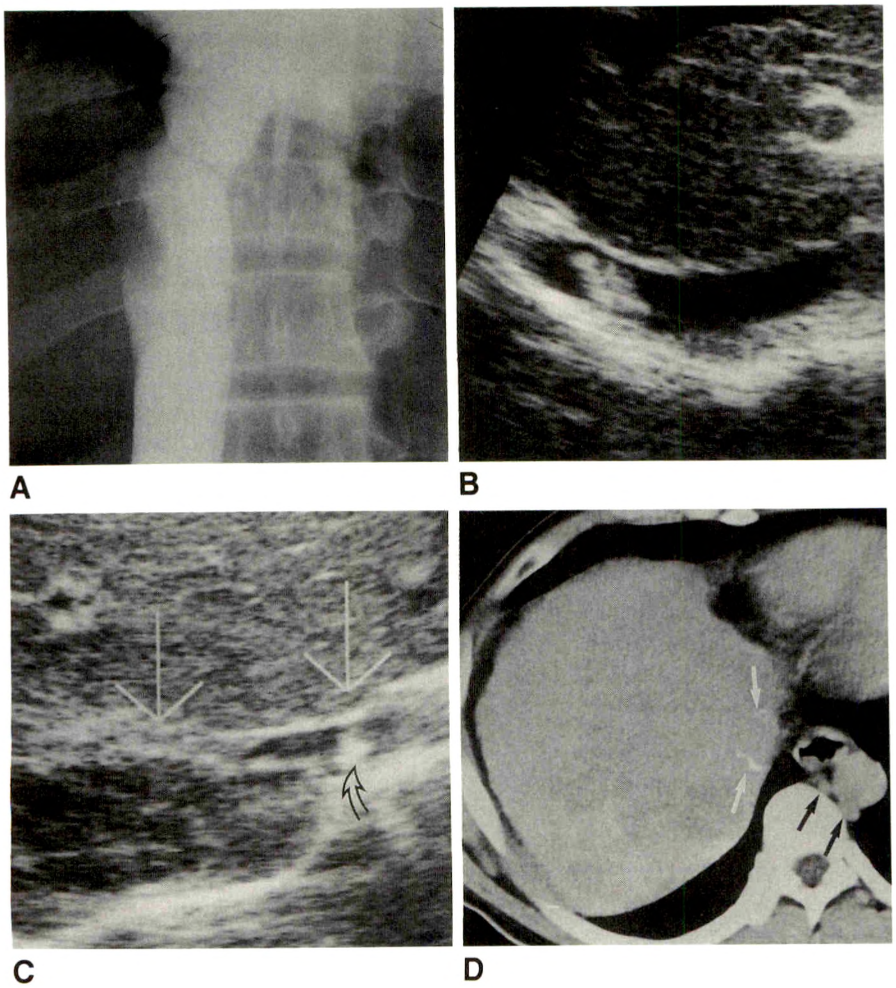

Fig. 3.—Incomplete membranous obstruction in 45-year-old man who tired easily and had abnormal results of liver function tests.

A, Inferior venacavogram shows thin membrane and flow into right atrium, indicating incomplete membranous obstruction. Note defect in flow below membrane caused by right hepatic vein.

B, Longitudinal sonogram shows thick echogenic membrane in hepatic segment of inferior vena cava (IVC). Discrepancy between thicknesses of membrane shown on sonogram and on venacavogram can be explained by oblique or tangential imaging of membrane on sonogram.

C, Transverse sonogram of liver shows obliteration of right hepatic vein (*white arrows*). Note echogenic membrane at diaphragmatic level of IVC (*black arrow*). Middle and left hepatic veins were patent, and right vein drained into middle hepatic vein.

D, Contrast-enhanced CT scan shows curvilinear calcification (*white arrows*) in wall of IVC. Several poorly defined low-density masses in right lobe of liver represent hepatomas, confirmed as hypervascular masses with angiography. *Black arrows* denote dilated azygos and hemiazygos veins. Note undulating margin of liver due to cirrhosis.

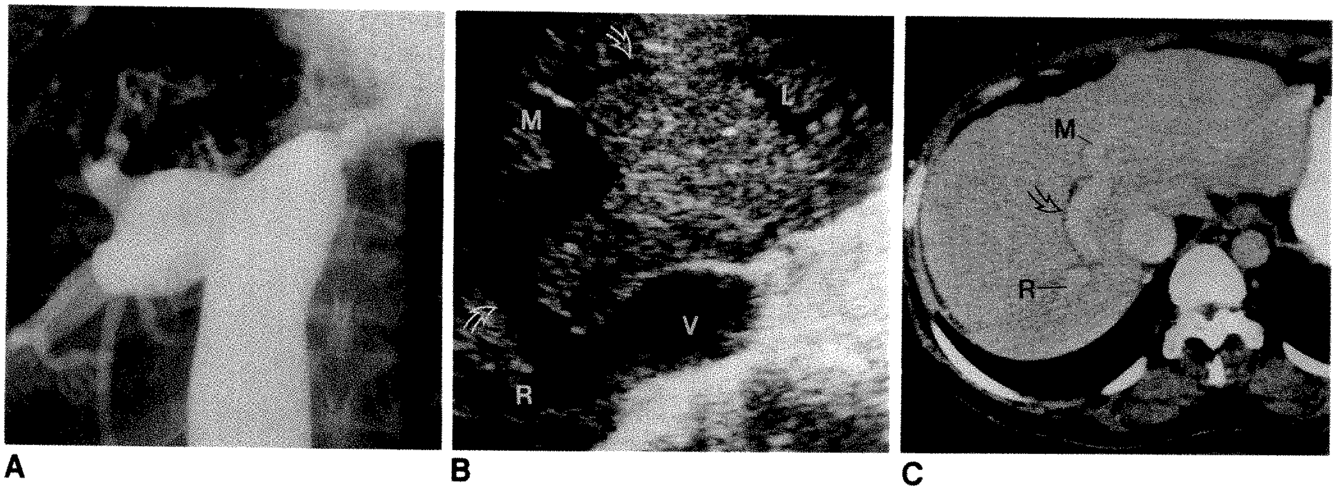

Fig. 4.—Incomplete segmental obstruction in 48-year-old woman who had general weakness for 3 months.
A, Inferior venacavogram shows segmental narrowing (1.5 cm long) with central fenestration.
B, Transverse sonogram shows tortuous collateral channel (*arrows*) connecting right hepatic vein (R) and partially obliterated middle hepatic vein (M) and left hepatic vein (L). Hepatic segment of inferior vena cava (IVC) appeared obstructed, but Doppler examination revealed flow through IVC(V), indicating incomplete obstruction.
C, CT scan shows collateral vessel (*arrow*) between right (R) and middle (M) hepatic veins. Note fine venous collateral vessels in abdominal wall.

Liver and Systemic Collaterals

On the basis of subjective grading, CT and sonography showed moderate to severe hepatic enlargement in 11 cases and mild enlargement in three cases. The size of the liver was normal in one case. The caudate lobe was enlarged in nine cases and normal in six cases. In all but one case, liver cirrhosis and portal hypertension were suggested by an undulated or serrated hepatic margin ($n = 13$, Figs. 3D and 4C), splenomegaly ($n = 13$), or intraabdominal collateral vessels ($n = 11$). A small amount of ascites was present in two cases. Hepatic masses, presumably hepatomas, were found at CT in six of the 15 cases (Figs. 2C and 3D). Hepatocellular carcinoma was diagnosed in five of these patients, on the basis of needle aspiration cytology in one case, the presence of a hypervascular mass at arteriography in two cases, iodized oil (Lipiodol, Guerbet, Aulnay-sous-Bois, France) CT in one case, and increased α-fetoprotein level in one case. Contrast-enhanced CT showed parenchymal inhomogeneity in the right hepatic lobe in four cases. In all cases, CT showed systemic collateral vasculature (Figs. 1D, 2C, and 3D): the most constant and prominent vessels were dilated azygos and hemiazygos veins ($n = 14$). Frequently, the veins along the anterior and lateral abdominal wall also were dilated ($n = 9$, Fig. 4C). Less frequently, the internal mammary veins or pericardiacophrenic veins were dilated ($n = 2$). None of these collaterals could be detected on sonograms.

Discussion

In membranous obstruction of the IVC, the hepatic segment of the IVC is obstructed by a fibromuscular membrane or replaced by a cordlike fibrous tissue [5]. The IVC is either occluded or retains a small opening. Membranous obstruction affects both the IVC and the hepatic veins in 72% of cases, the IVC alone in 18%, and the hepatic veins alone in 10% [15]. Simson [2] described three types: In type I, a thin membrane is present in the IVC, typically between the connections of the right and middle hepatic veins to the IVC, and is easily perforated during either surgery or autopsy or even by a catheter during venacavography. In type II, a segment of the IVC of variable length (but >1 cm) is replaced by a fibrous cord. In type III, a variable segment of the IVC below the membranous or segmental obstruction is filled with thrombus. In our series, eight cases were type I, and seven cases were type II; among them, five cases involved thrombus in the IVC.

Sonography easily depicts the echogenic membrane or the fibrous cord in the IVC [7–9]. The relationship of the hepatic vein, either obliterated or patent, to the membrane or obliterated segment of the IVC is usually depicted clearly. Thrombus in the IVC also is easily seen with sonography [8]. In our study, sonography showed the presence and type of hepatic venous obstruction or obliteration and showed any intrahepatic collateral vessels [7, 8] connecting the hepatic veins and the IVC above and below the obstruction. Doppler examination showed blood flow through the interconnecting vessels and the presence or absence of hepatic venous obliteration [7, 8]. Sonography was not helpful in the evaluation of systemic collaterals [8].

The CT findings in secondary Budd-Chiari syndrome have been described as central patchy or fan-shaped enhancement with a hypodense liver periphery, enlargement of the liver, enlargement of the caudate lobe, lack of visualization of hepatic veins or direct visualization of hepatic venous thrombosis, and ascites [10–14]. However, the CT findings of membranous obstruction of the IVC have not been previously reported. In our cases, CT was not useful in showing membranes, but obliterated segments of the IVC were shown relatively clearly. CT might have been more valuable if the contrast material had been injected through the foot rather than through the arm to enhance opacification of the IVC. One advantage of CT over sonography was that it showed calcific foci in the membrane or the wall of the IVC, which may be a sign of obstruction of the IVC. Kobayashi et al. [16] reported two cases of membranous obstruction of the IVC with membrane calcification, as seen in one of our cases (Fig. 1D). Mural calcification also may represent calcification of thrombus, as seen in one of our cases.

CT was relatively insensitive for delineating hepatic venous obliteration or intrahepatic collateral vessels, probably because of use of inadequate technique for visualization of the hepatic veins. In some cases, the obliterated hepatic vein was not visualized whereas the intrahepatic venous collateral vessels were directly visualized. No cases showed central patchy or fan-shaped enhancement: we believe patchy enhancement is encountered only in acute obstruction of the hepatic veins due to systemic diseases. Instead, localized parenchymal inhomogeneity was present in three cases. Usually, the liver was moderately or markedly enlarged and evidence of liver cirrhosis and portal hypertension was seen. The caudate lobe frequently was enlarged. The association of liver cirrhosis and hepatoma with membranous obstruction of the IVC as seen in our series has been previously described [2, 4, 6-8]. CT showed prominent systemic collaterals, such as azygos, hemiazygos, pericardiacophrenic, internal mammary, and superior and inferior epigastric veins and other superficial veins of the abdominal wall. This type of systemic collateral circulation has not been reported in secondary Budd-Chiari syndrome.

In summary, sonography was superior to CT in delineating the IVC membranes, in showing the relationship between the obstructed segment of the IVC and the pathologic hepatic venous anatomy, and in showing intrahepatic venous collaterals and the direction of the venous flow. Sonography was useful in showing intrahepatic collateral vessels (a sign of IVC obstruction in patients with chronic liver disease), in determining the type of IVC obstruction in patients with combined IVC thrombosis, and in follow-up after treatment (Fig. 1E). CT was superior to sonography and venography in showing calcification of the IVC, in evaluating pathologic anatomy of the liver, in detecting hepatomas, and in showing extrahepatic collateral vasculature.

Knowledge of the morphologic type of obstruction of the IVC is important for choosing appropriate therapy [3, 5, 9, 17]. If a membrane is present, with or without fenestration, radiologic intervention can be attempted. If a segment of the IVC is replaced by a fibrous cord, treatment can be tailored to the length of the involved segment [17]. In cases of diffuse narrowing or obliteration of the hepatic and suprarenal segments of the IVC, graft surgery is needed. Sonography and CT will provide important information because venacavography will show obstruction of the IVC and formation of collaterals, but may not show the pathologic anatomy of the liver and may not allow distinction of the various types of obstruction in patients with thrombosis. Thus, sonography and CT are important complements to venacavography in these patients.

ACKNOWLEDGMENT

The authors sincerely thank Young Ran Park for her secretarial assistance.

REFERENCES

1. Mitchell MC, Boitnott JK, Kaufman S, Cameron JL, Madrey WC. Budd-Chiari syndrome: etiology, diagnosis, and management. *Medicine* **1982**;61:199-218
2. Simson IW. Membranous obstruction of the inferior vena cava and hepatocellular carcinoma in South Africa. *Gastroenterology* **1982**;82:171-178
3. Espana P, Figuera D, de Miguel JMF, Anaya A, Mendez J, Durantez A. Membranous obstruction of the inferior vena cava and hepatic veins. *Am J Gastroenterol* **1980**;73:28-32
4. Okuda K. Membranous obstruction of the inferior vena cava: etiology and relation to hepatocellular carcinoma. *Gastroenterology* **1982**;82:376-379
5. Kimura C, Matsuda S, Koie H, Hirooka M. Membranous obstruction of the hepatic portion of the inferior vena cava: clinical study of nine cases. *Surgery* **1972**;72:551-559
6. Yamamoto S, Yokoyama T, Takeshige K, Iwatsuki S. Budd-Chiari syndrome with obstruction of inferior vena cava. *Gastroenterology* **1968**; 54:1070-1084
7. Makuuchi M, Hasegawa H, Yamazaki S, Moriyama N, Takayasu K, Okazaki M. Primary Budd-Chiari syndrome: ultrasonic demonstration. *Radiology* **1984**;152:775-779
8. Park JH, Lee JB, Han MC, et al. Sonographic evaluation of inferior vena caval obstruction: correlative study with vena cavography. *AJR* **1985**;145:757-762
9. Huberman RP, Gomes AS. Membranous obstruction of the inferior vena cava. *AJR* **1982**;139:1215-1216
10. Harter LP, Gross BH, St. Hilaire J, Filly RA, Goldberg HI. CT and sonographic appearance of hepatic vein obstruction. *AJR* **1982**;139:176-178
11. Becker CD, Scheidegger J, Marincek B. Hepatic vein occlusion: morphologic features on computed tomography and ultrasonography. *Gastrointest Radiol* **1986**;11:305-311
12. Murphy FB, Seinberg HV, Shires GT, Martin LG, Bernardino ME. The Budd-Chiari syndrome: a review. *AJR* **1986**;149:9-15
13. Vogelzang RL, Anschutz SL, Gore RM. Budd-Chiari syndrome: CT observations. *Radiology* **1987**;163:329-333
14. Mathieu D, Vasile N, Menu Y, Beers BV, Lorphelin JM, Pringot J. Budd-Chiari syndrome: dynamic CT. *Radiology* **1987**;165:409-413
15. Nakamura T, Nakamura S, Aikawa T, et al. Obstruction of the inferior vena cava in the hepatic portion and the hepatic veins. *Angiology* **1968**;19: 479-500
16. Kobayashi A, Matsui O, Takashima T, et al. Calcification in caval membrane causing primary Budd-Chiari syndrome: CT demonstration. *J Comput Assist Tomogr* **1988**;12:401-404
17. Yamada R, Sato M, Kawabata M, Nakatsuka H, Nakamura K, Kobayashi N. Segmental obstruction of the hepatic inferior vena cava treated by transluminal angioplasty. *Radiology* **1983**;149:91-96

Acute Lower Gastrointestinal Hemorrhage: Treatment by Superselective Embolization with Polyvinyl Alcohol Particles

Gregory E. Guy[1]
P. C. Shetty
Rajinder P. Sharma
Matthew W. Burke
Thomas H. Burke

OBJECTIVE. The major risk of transcatheter embolotherapy for acute hemorrhage in the lower gastrointestinal tract is irreversible intestinal ischemia. The authors studied the efficacy and safety of superselective transcatheter embolization with polyvinyl alcohol particles in arresting acute hemorrhage in the lower gastrointestinal tract.

SUBJECTS AND METHODS. All patients with clinical or scintigraphic evidence of acute hemorrhage in the lower gastrointestinal tract were considered for superselective embolization. The nine patients with angiograms that showed active hemorrhage in the lower gastrointestinal tract underwent the procedure. Superselective embolization was done through a 3-French catheter and was accomplished by using 100- to 590-μm polyvinyl alcohol particles. The segments of the intestinal tracts involved in the embolizations were examined for the presence of ischemia by endoscopy ($n = 7$) or histologic evaluation of a surgical specimen ($n = 2$) 2–44 days (mean, 11 days) after embolization or by clinical evaluation ($n = 1$).

RESULTS. The lesions treated by this method were located in the colon ($n = 8$) and jejunum ($n = 1$). Immediate hemostasis was achieved in every case. Three patients had recurrent lower gastrointestinal hemorrhage 1–24 days (mean, 9 days) after initial embolization. Two of these patients had surgery, while one had a successful second embolization. Two asymptomatic patients were found endoscopically to have small areas of ischemia involving only the mucosa. Only one patient was shown to have severe mucosal ischemia; this involved the colon in a distribution that suggested it was not caused by the embolization.

CONCLUSION. Ten superselective embolization procedures that used polyvinyl alcohol particles successfully controlled hemorrhage in the lower gastrointestinal tract in nine patients. In no case was intestinal infarction induced by the procedure, and only two endoscopically proved cases of asymptomatic mucosal ischemia occurred.

AJR 159:521–526, September 1992

Since the initial report of selective arterial infusion of vasopressin to control acute hemorrhage in the lower gastrointestinal tract [1], transcatheter methods have gained wider acceptance as a primary means of therapy. This is largely due to the significant perioperative mortality rates reported with emergent surgery [2–4]. Selective arterial infusion of vasopressin is considered effective in stopping acute hemorrhage in these patients [5, 6]; however, hemorrhage may recur [5, 6], and vasopressin therapy has potential complications [7]. Transcatheter embolization has been suggested as a more definitive means of treating patients with lower gastrointestinal hemorrhage [8–19]. The most significant risks of transcatheter embolization are intestinal ischemia and infarction, the latter occurring in up to 20% of cases [11–13, 15, 16, 20–22].

In response to these observations, some interventional radiologists have advised extreme caution in the use of these methods, and many advocate a relatively proximal site for embolization and the use of temporary occluding agents to minimize the risk of infarction [13, 15, 16, 18, 23]. We recently undertook transcatheter treatment of acute gastrointestinal bleeding with these methods: (1) a

Received December 26, 1991; accepted after revision March 3, 1992.

[1] All authors: Department of Diagnostic Radiology, K-3, Division of Vascular and Interventional Radiology, Henry Ford Hospital, 2799 W. Grand Blvd., Detroit, MI 48202. Address reprint requests to G. E. Guy.

0361-803X/92/1593-0521
© American Roentgen Ray Society

selective catheterization technique, with a relatively peripheral site of embolization reached by a small-caliber (3-French) catheter; (2) the use of a permanent embolic agent (polyvinyl alcohol [PVA]) to achieve hemostasis; and (3) an objective assessment (by endoscopy, surgery, or both) of the intestinal mucosa after embolization. We evaluated the efficacy and safety of our superselective PVA embolization procedure by clinical follow-up and objective assessment of the bowel wall after embolization.

Subjects and Methods

From August 1988 to October 1990, nine consecutive patients in whom active hemorrhage in the lower gastrointestinal tract was shown on arteriograms underwent 10 transcatheter arterial embolization procedures to stop the hemorrhage. These five men and four women were 19–81 years old (mean, 57 years). Patients were considered for intraarterial infusion of vasopressin or emergency surgery if embolization could not be performed, and for emergency surgery if embolization was performed but was not successful.

Selective diagnostic arteriograms were obtained with standard angiographic catheters in each case. When an active bleeding site was seen, superselective catheterization was done with a Tracker-18 catheter (Target Therapeutics, San Jose, CA) and a 0.014-in. (0.036-cm) platinum-tipped guidewire; the goal was catheterization of the arteria recta supplying the site of hemorrhage. In each case, superselective arteriograms through the Tracker catheter were obtained to delineate further the local arterial anatomy. PVA particles (Ivalon, Ingenor, Paris; and Contour, Interventional Therapeutics Corp., South San Francisco, CA) ranging in size from 100 to 590 μm were suspended as follows: one vial of particles in 50 ml of Omnipaque 300 contrast medium (Winthrop Pharmaceuticals, New York, NY) and 10 ml of normal saline. Particles were delivered to the site of embolization via the Tracker catheter by means of a 3-ml syringe. Injections were done with as few particles as were necessary to achieve hemostasis. In all but two cases, 250- to 355-μm Contour particles were used for embolization. Each patient was examined after embolization for signs and symptoms (abdominal pain or tenderness, nausea, diarrhea, fever, peritoneal signs, marked change in bowel sounds) or laboratory evidence (leukocytosis) indicative of intestinal ischemia. The eight patients who had colonic embolization were examined for evidence of mucosal ischemia by the following methods: endoscopy alone, six patients; endoscopy followed by surgery, one patient; and surgery alone, one patient (interval after embolization, 2–44 days; mean, 11 days). In the two patients who had surgery, the resected specimens were examined for histologic evidence of ischemia. The patient who had embolization to arrest a jejunal anastomotic hemorrhage was followed up by clinical means alone. The range of clinical follow-up for the seven patients treated solely by transcatheter arterial embolization (six colonic lesions, one jejunal lesion) was 41–791 days (mean, 205 days).

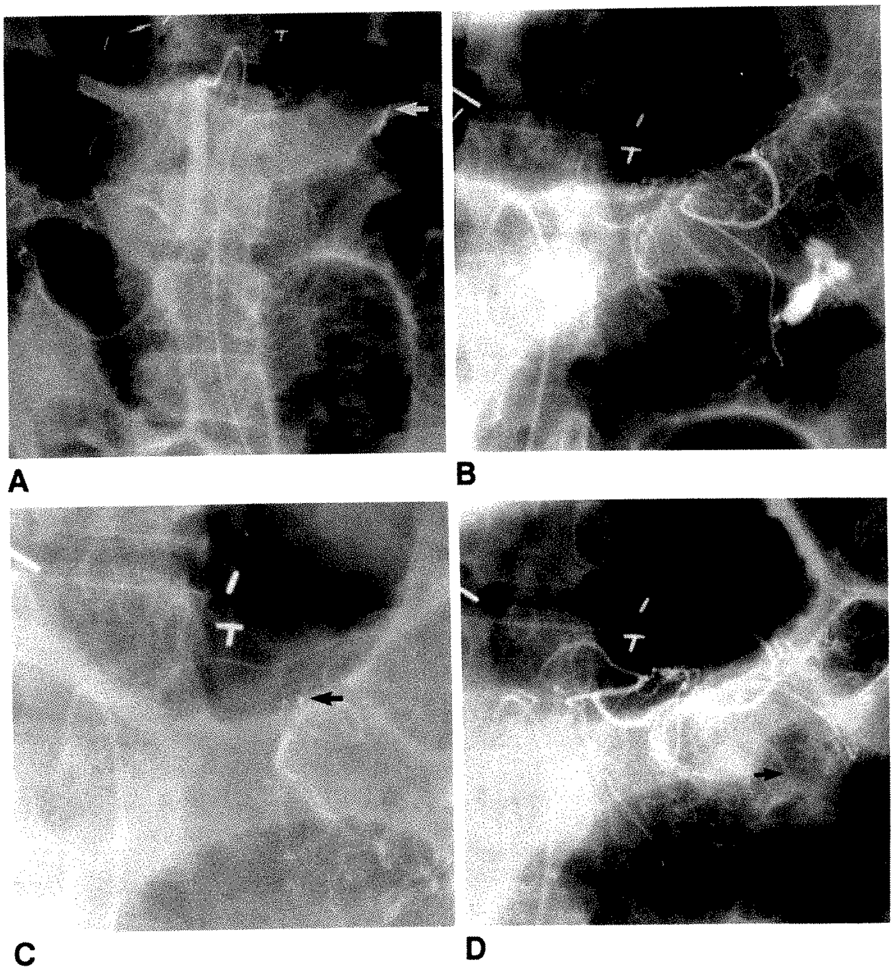

Fig. 1.—59-year-old woman who had loss of bright red blood through the rectum 3 days after right hemicolectomy for cecal ischemia.

A, Superior mesenteric arteriogram shows active hemorrhage in distal part of transverse colon (*arrow*).

B, Arteriogram obtained after coaxial advancement of Tracker catheter into left branch of middle colic artery shows active hemorrhage at this site more clearly.

C, Arteriogram shows further advancement of Tracker catheter (*arrow*), after which embolization was performed.

D, Arteriogram obtained after embolization shows occlusion of bleeding left branch (*arrow*) of middle colic artery only and no further extravasation. Endoscopy performed 2 weeks after embolization revealed normal mucosa.

Results

Bleeding was found in the distribution of the superior mesenteric artery in five patients and in the distribution of the inferior mesenteric artery in four patients: jejunal branch (*n* = 1), ileocolic branch (*n* = 2), right colic branch (*n* = 1), middle colic branch (*n* = 1), left colic branch (*n* = 2), sigmoidal branch (*n* = 1), and superior hemorrhoidal branch (*n* = 1). One patient had a lesion in the jejunum. Eight patients had large-bowel lesions in the following distribution: cecum (*n* = 2), ascending colon (*n* = 1), transverse colon (*n* = 1), descending colon (*n* = 2), sigmoid colon (*n* = 1), and rectum (*n* = 1). The causes for bleeding in the colon were diverticular disease (*n* = 4), angiodysplasia (*n* = 2), anastomotic leakage (*n* = 1), and unknown (*n* = 1).

Immediate hemostasis was achieved in every case (Fig. 1). Hemorrhage recurred in the lower gastrointestinal tract in three patients 1–24 days (mean, 9 days) after embolization. One of these patients subsequently had a successful second embolization 2 days after the initial embolization of a hemorrhage in the left colic artery (Fig. 2). The other two patients required surgery to control bleeding. One of these patients bled again the day after successful embolization of a branch of the superior hemorrhoidal artery (Fig. 3). Endoscopy revealed bleeding in a location proximal to the site of embolization. This patient subsequently had resection of the sigmoid colon and a descending colostomy. The other patient who required surgery had recurrent hemorrhage in the lower gastrointestinal tract 24 days after embolization of actively bleeding cecal angiodysplasia, which was accompanied by other

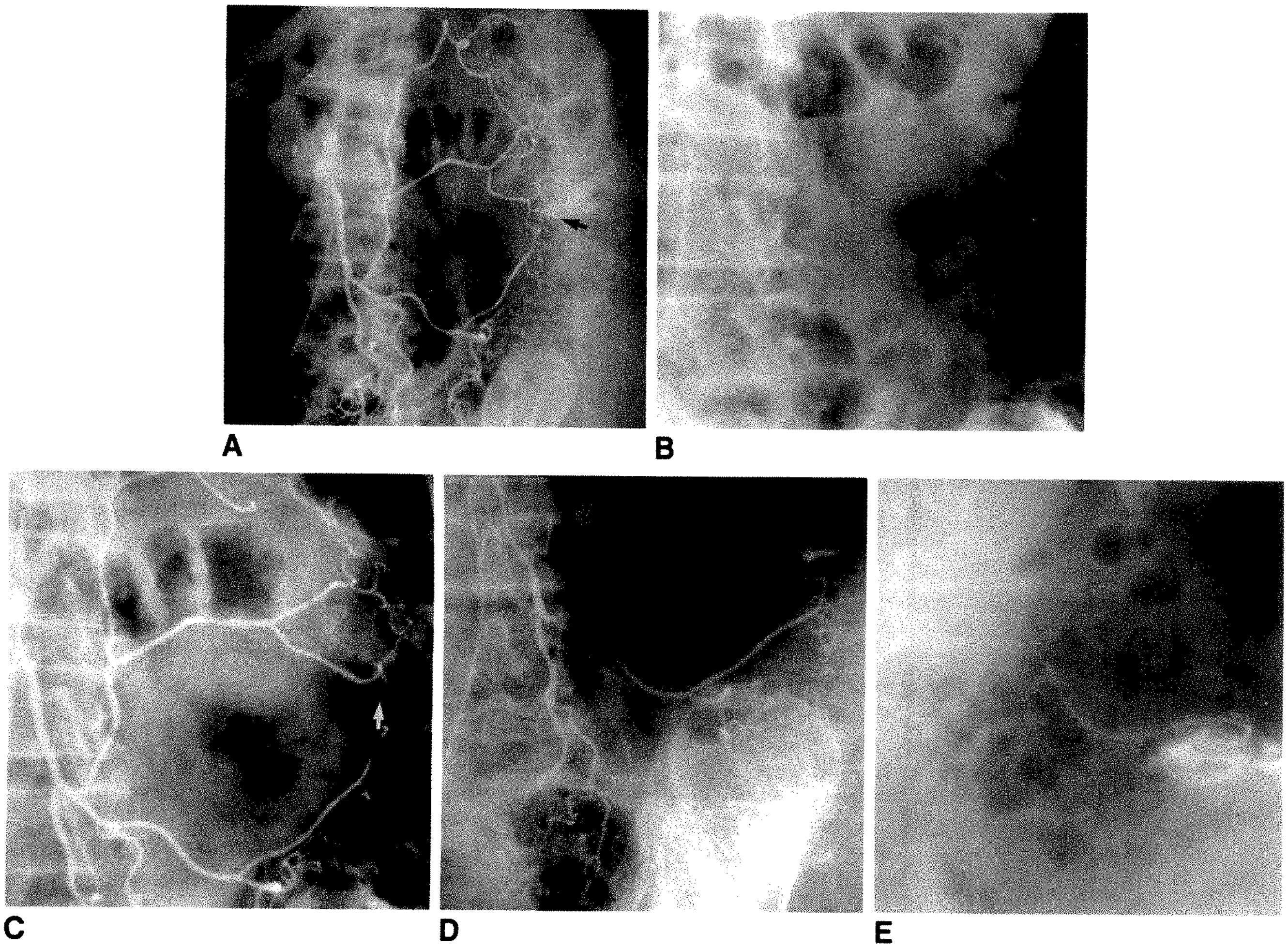

Fig. 2.—74-year-old woman with acute hemorrhage in lower gastrointestinal tract.

A, Inferior mesenteric arteriogram shows active hemorrhage (*arrow*) in distribution of left colic artery.

B, Arteriogram shows Tracker catheter advanced coaxially over platinum-tipped guidewire into distribution of active hemorrhage.

C, Inferior mesenteric arteriogram obtained after embolization with polyvinyl alcohol (PVA) particles shows no further active hemorrhage. *Arrow* denotes site of particle delivery.

D, 2 days later, hemorrhage in lower gastrointestinal tract has recurred. Scintigram (*not shown*) showed progressive accumulation of radionuclide in left side of abdomen. Arteriogram shows active hemorrhage near previously embolized vessel.

E, Tracker catheter was advanced to site of bleeding. A more selective arteriogram again shows active hemorrhage from a branch other than that previously embolized. After embolization with PVA, inferior mesenteric arteriogram (*not shown*) showed embolized vessels to be occluded and no further active hemorrhage. On endoscopy done 6 days later, mucosal ischemia was evident at embolized site. Biopsies of area showed no submucosal involvement or gangrene.

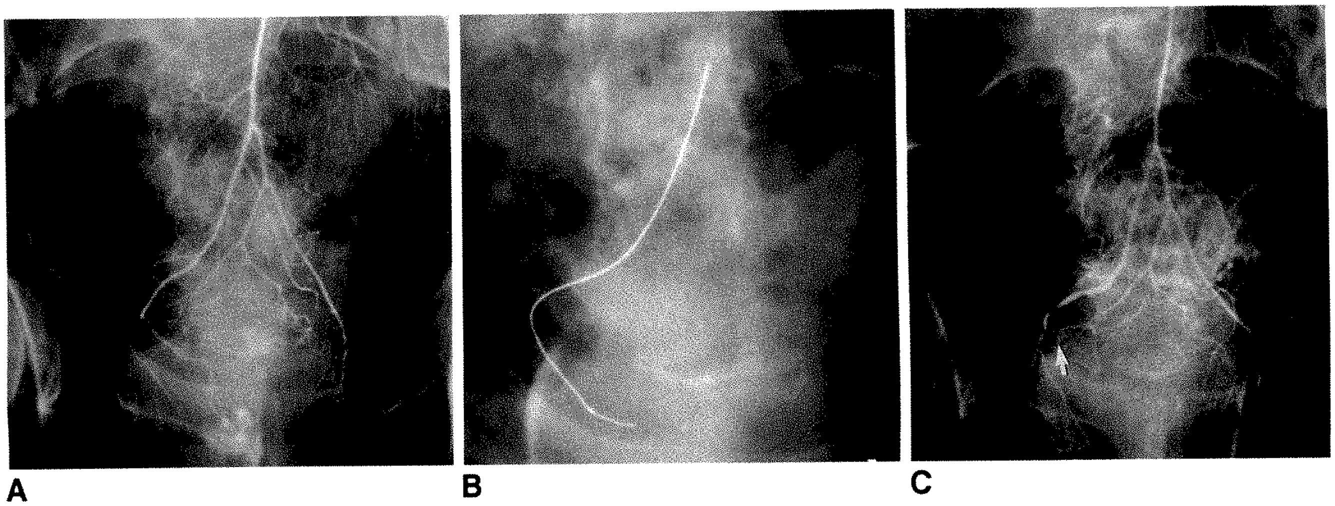

Fig. 3.—53-year-old man with numerous medical problems, including loss of bright red blood through the rectum.

A, Inferior mesenteric arteriogram shows active hemorrhage from solitary branch of superior hemorrhoidal artery.

B, Arteriogram shows coaxial advancement of Tracker catheter over a steerable platinum-tipped wire into branch supplying hemorrhage, after which embolization was performed with polyvinyl alcohol particles.

C, Inferior mesenteric arteriogram obtained after embolization shows no further hemorrhage and residual stump of occluded vessel (*arrow*). The patient's condition deteriorated, and diffuse colonic ischemia developed owing to sepsis and hypotension. He died 21 days after embolization.

right-sided colonic angiodysplasias. An arteriogram obtained at the time of the recurrent bleeding again showed multiple cecal angiodysplasias, revealed no recanalization of the embolized vessel, and did not show a site of active hemorrhage. This patient subsequently had a right hemicolectomy with ileotransverse colostomy.

Endoscopy was the sole means of evaluating the intestinal mucosa after embolization in six patients. Findings included mild mucosal ischemia (small linear ulcers and fibrinopurulent debris without necrosis) in two patients and no mucosal abnormalities in four. Each of these patients was and has remained asymptomatic. One patient (the one with cecal angiodysplasia) had surgical follow-up only; the specimen resected during right hemicolectomy in this patient had no mucosal or submucosal findings of ischemia. The patient who had embolization of a branch of the superior hemorrhoidal artery (Fig. 3) was examined with endoscopy 4 days after embolization, and then required surgery the next day because of hypotension and persistent hemorrhage in the lower gastrointestinal tract. Endoscopy showed hemorrhage at a location proximal to the embolization site, but no findings of mucosal ischemia were noted. At exploratory laparotomy, a perforation of the sigmoid colon was found that necessitated a rectosigmoid resection with rectal stapling and a descending colostomy. Postoperatively, the patient's condition continued to deteriorate, and he died 16 days after surgery (21 days after embolization). The resected rectosigmoid specimen revealed submucosal vascular congestion and focal areas of submucosal hemorrhage. Autopsy revealed mucosal hemorrhagic necrosis involving the descending colostomy and rectal stump, which also was perforated. The small bowel and the remainder of the colon had findings suggestive of pseudomembranous change. The patient who had transcatheter embolization to stop bleeding from a jejunal anastomosis had no clinical evidence of ischemia during 26 months' follow-up.

Four patients had further arteriography 12 hr to 26 days (mean, 10 days) after their original embolization. Two of these patients were reexamined for recurrent hemorrhage in the lower gastrointestinal tract that ultimately required surgery or additional transcatheter embolization. One of these two patients (Fig. 2) had active bleeding in the descending colon at the site that had been embolized 2 days earlier. The branches that had been embolized previously led to the bleeding site from a caudal direction and were occluded when the second angiogram was obtained. The bleeding site was now being supplied from more cephalad branches, and these were successfully embolized. The arteriograms in the remaining three patients did not show an active bleeding site; one of the patients underwent an emergent right hemicolectomy for persistent bleeding. In none of these four patients was recanalization of previously embolized vessels noted.

Discussion

The emergent treatment of patients with acute hemorrhage in the lower gastrointestinal tract remains a difficult clinical problem. Although surgery is still the foundation of treatment, perioperative morbidity and mortality rates for hemicolectomy approximate 50% and 30% [2–4], respectively. Even limited bowel resection is associated with a mortality rate of 15–20% [24, 25] in the best series. Transcatheter intervention has evolved since the initial description of selective arterial infusion of vasopressin by Nusbaum et al. [1] in 1967. Vasopressin infusion achieves hemostasis in up to 90% of cases [5, 6], and recurrent bleeding rates on discontinuing this therapy of about 20% have been reported [5]. Other authors, however, report significantly lower success rates in achieving hemostasis [25] and higher rates of rebleeding on discontinuing infusion [6]. Additionally, the complication rate associated with this method has been reported to be as high as 43% [7].

In 1977, Goldberger and Bookstein [26] described gelatin sponge embolization of diverticular bleeding in two patients. A later amplification of this experience [9] and other series [11-13, 15, 16, 18] and case reports [10, 14, 17, 19] have subsequently been published. Immediate hemostasis has been reported in nearly all cases, and the prevalence of recurrent hemorrhage requiring surgery is 10-20%. The hallmarks of this collective experience have been the relatively proximal site of embolization (with reference to the marginal artery of Drummond) and the use of a temporary embolic agent (mostly gelatin sponge). The major concern in performing embolization in the lower gastrointestinal tract, especially the colon, is that of producing irreversible ischemia. The significant potential for colonic infarction is based on the relatively sparse and poorly anastomosing mural arterial network of the colon [27, 28]. In the literature, the prevalence of postembolic colonic infarction has ranged from 0% to 20% [11-13, 15, 18], with the collective rate approximating 15%. Although most of these patients had successful surgical resection of the infarcted segment, it was advised to reserve embolization for those cases in which vasopressin has failed [15, 23]. More recently, newer small-caliber angiographic catheters have enabled more peripheral superselective catheterization of distal vessels, permitting more selective vascular intervention. The Tracker catheter has been a useful adjunct in transcatheter therapy elsewhere in the body [29, 30]; use of the Tracker catheter for gastrointestinal hemorrhage has been reported only in the setting of a bleeding Meckel's diverticulum [19]. Our strategy was founded on evidence suggesting that injection of particles 100 μm or larger into the inferior mesenteric arterial distribution produces reversible ischemic changes in the colon at worst [31] and on the belief that an extremely selective site of embolization would produce a very limited area for potential ischemia.

Although the study group is small, our results suggest that embolization of lower gastrointestinal hemorrhage can be safe and effective. Our success at achieving hemostasis, the prevalence of recurrent hemorrhage, and the number of patients requiring subsequent surgery compare favorably with other series. Our initial intent was to provide hemostasis in a group of patients in whom vasopressin therapy was relatively contraindicated. Transcatheter embolization was considered a preoperative stabilizing measure in these cases. However, seven of the nine patients were treated successfully with transcatheter embolization without the need for subsequent surgery. In an eighth patient, surgery was postponed until the patient was hospitalized for recurrent hemorrhage. We now believe that transcatheter embolization may be considered a primary mode of treatment for acute hemorrhage in the lower gastrointestinal tract. At our institution, intraarterial infusion of vasopressin or surgical resection is considered only when embolization cannot be performed. If embolization has been performed and is unsuccessful in achieving hemostasis, we recommend surgery. We strongly discourage vasopressin infusion after embolization because of the compounded risk of intestinal infarction.

The frequency of postembolic bowel ischemia seen in this series is greater than the collective rate of other series (22% vs 15%, respectively) [11-13, 15, 18]. However, included in our series were asymptomatic patients with endoscopically proved ischemic changes. It is not unexpected that we would identify bowel ischemia more frequently by routine use of postembolization endoscopy than by clinical signs and symptoms alone. In fact, several patients in other series had signs and symptoms attributable to intestinal ischemia after embolization [9, 11, 16, 18] but did not have strictures or infarction. Similarly, bowel ischemia after aortic reconstruction is detected more frequently with endoscopy of the lower intestine than by clinical criteria [32, 33]. In these studies, reversible colonic ischemia was not manifested clinically in many cases. Our experience is similar in this regard, as neither of the two patients who appeared to have mucosal ischemia at endoscopy had symptoms or signs of irreversible ischemia. One patient had catastrophic colonic ischemia that was temporally related to the embolization procedure. However, the sigmoid colonic perforation discovered at laparotomy was removed from the site of particle delivery in the rectum, and the diffuse distribution of ischemia far exceeded that which would be expected from embolization of a solitary branch of the superior hemorrhoidal artery. It was determined by autopsy that sepsis and hypotension were the likely causes of the colonic ischemia and subsequent death in this patient.

The use of a permanent embolic agent in this setting deserves further comment. Although PVA has been used for embolization of hemorrhage in the lower gastrointestinal tract [14], its use in a series of patients has not been reported. The choice of PVA was based on the desire to produce more permanent vascular occlusion [34] and the compatibility of particulate agents with the small-diameter catheters. Despite the increased risk of ischemia from distal embolization, evidence shows that particles 100 μm or larger may be injected from a proximal site and produce minimal or no change in the involved intestinal distribution [31]. We hypothesized that embolization at an extremely selective site would be even less likely to cause mural damage than would proximal delivery of particles. Additionally, we used the minimum number of particles necessary to achieve hemostasis in the target vessel. Our results, which indicate few ischemic sequelae and no recanalization of embolized vessels on follow-up arteriograms, support our approach.

In summary, 10 transcatheter embolization procedures with PVA particles were performed at the level of the arteria recta in nine patients with hemorrhage in the lower gastrointestinal tract. In no case was intestinal infarction induced by the procedure, and only two endoscopically proved incidents of asymptomatic mucosal ischemia occurred. Although further work needs to be done in this area, this procedure offers a practical alternative to currently accepted modes of therapy.

REFERENCES

1. Nusbaum M, Baum S, Sabiyalak P, Blakemore WS. Pharmacologic control of portal hypertension. *Surgery* **1967**;62:299-310
2. Behringer GE, Albright NL. Diverticular disease of the colon: a frequent cause of massive rectal bleeding. *Am J Surg* **1973**;125:419-423
3. Griffin JM, Butcher HR Jr, Ackerman LV. Surgical management of colonic diverticulitis. *Arch Surg* **1967**;94:619-626
4. Olsen WR. Hemorrhage from diverticular disease of the colon: the role of emergency subtotal colectomy. *Am J Surg* **1968**;115:247-263

The Density, Contour, and Thickness of the Pancreas in Diabetics: CT Findings in 57 Patients

Jean-Paul Gilbeau[1]
Vincent Poncelet[1]
Ernest Libon[1]
Geneviève Derue[2]
Francis R. Heller[2]

Insulin has a trophic effect on pancreatic acinar tissue, so the pancreas might be expected to atrophy in persons who have diabetes. Accordingly, we analyzed the density, contour (smooth or lobulated), and thickness of the pancreas on CT scans of diabetic patients and compared the results with those in control subjects. The prevalence of pancreatic lobulation (incisurae deeper than 2 mm) and its correlation with age in diabetic and control subjects were determined. The thickness of the pancreas was measured at three levels (head, body, tail). Three groups of diabetic patients were examined: 20 insulin-dependent patients, 25 patients not treated with nor dependent on insulin, and 12 patients treated with but not dependent on insulin. A control group included 57 nondiabetic patients. The ages of the control subjects were similar to those of the diabetic patients. The statistical significance of the differences between groups of diabetic patients and control subjects was estimated by using Student's t test for the values of density and thickness and the χ^2-test for the prevalence of pancreatic lobulation. The density of the pancreas in diabetic patients and control subjects was not statistically different. Diabetic patients had increased lobulation of the pancreas. All parts of the pancreas tended to be smaller in diabetic patients, but the degree of reduction varied. It was modest in the patients not treated with insulin, pronounced in insulin-dependent patients, and intermediate in non-insulin-dependent, insulin-treated patients. Moreover, the size of the body was significantly reduced in all three groups, whereas the size of the pancreatic head was preserved in patients not treated with insulin.

In conclusion, CT of the pancreas shows that although density in diabetic patients is normal, lobulation is increased. Reduction in size involves the body of the pancreas more than other parts of the gland and is more pronounced in insulin-treated diabetic patients. CT of the pancreas might be useful to predict which diabetic patients will require insulin therapy.

***AJR* 159:527-531, September 1992**

The pancreas contains endocrine cells in discrete clusters (islets) within the exocrine parenchyma (acinar tissue). A functional relationship between endocrine and exocrine tissue is suggested by the high prevalence of exocrine pancreatic dysfunction in insulin-dependent diabetic patients [1]. As the islets are only 1-2% of the pancreatic mass, atrophy of the exocrine component of the gland might be expected in patients with diabetes, with consequent reduction in the size of the gland. Despite the high prevalence and the severity of diabetes, relatively few morphologic studies of the pancreas in diabetic patients have been done. Until recently, the only material available came from autopsies of diabetic patients [2]. To our knowledge, except for a sonographic study [3] and one CT study in insulin-dependent diabetic patients [4], no studies have been done of the pancreas in living subjects who have diabetes.

On clinical grounds, two types of diabetes mellitus are distinguished: insulin-dependent diabetes mellitus, which affects mostly young persons and is characterized by low or no secretion of insulin, and non-insulin-dependent diabetes

Received November 7, 1991; accepted after revision March 9, 1992.

[1] Department of Radiology, Hôpital de Jolimont, Rue Ferrer, 7100 Haine Saint Paul, Belgium. Address reprint requests to J-P. Gilbeau.

[2] Department of Internal Medicine, Hôpital de Jolimont, 7100 Haine Saint Paul, Belgium.

0361-803X/92/1593-0527
©American Roentgen Ray Society

mellitus, which occurs in older obese persons and is characterized by insulin resistance of the target organs and normal or increased secretion of insulin. Data on the morphology of the pancreas in these two types of diabetes are scanty.

The aim of the present work was to study the density, contour, and thickness of the pancreas of diabetic patients with CT and to compare the results in three different groups of diabetic patients: non-insulin-dependent diabetic patients who need diet or diet and hypoglycemic drugs for their treatment, non-insulin-dependent diabetic patients who require insulin for good glycemic control, and insulin-dependent diabetic patients.

Subjects and Methods

Fifty-seven diabetic patients were included in the study. They belonged to one of three groups. The 20 insulin-dependent patients included 10 men and 10 women 23 - 72 years old (mean ± standard error of the mean [SEM], 48.0 ± 3.9 years). Duration of diabetes was 9.4 ± 2.9 years. The 25 non-insulin-dependent diabetic patients whose treatment consisted of adherence to an appropriate diet or adherence to a diet and use of oral hypoglycemic agents included nine men and 16 women 44–86 years old (mean ± SEM, 61.7 ± 2.2 years). Duration of diabetes was 6.6 ± 1.8 years. The 12 non-insulin-dependent diabetic patients who required insulin treatment included three men and nine women 51–83 years old (mean ± SEM, 63.5 ± 9.9 years). Duration of diabetes was 11.2 ± 3.4 years. Patients with diabetes caused by or associated with chronic pancreatitis, malignant neoplasm, or other endocrinopathies were not included. Fifty-seven patients (27 men and 30 women) were used as control subjects. They were 27–83 years old (mean ± SEM, 60.5 ± 20 years). They were not obese (body mass index less than 25 kg/m^2) and were not taking any drugs known to be diabetogenic (e.g., glucocorticoids, thiazides). They were scheduled to undergo abdominal CT as part of a medical workup for evaluation of unexplained abdominal pain or hepatomegaly. Results of an oral glucose tolerance test were normal in these patients, and examination of their clinical records confirmed the absence of exocrine or endocrine pancreatic dysfunction.

Abdominal CT was performed with a CR-Siemens unit (Erlangen, Germany). Serial transverse scans with 8-mm-thick contiguous slices were obtained. The patient was supine and was asked to take a deep breath and hold it. Iodinated contrast medium (Micropaque scanner, Nicholas, Brussels) was given orally for better delineation of the outline of the pancreatic head. Determinations of the size of the pancreas may be more accurate when IV contrast material is used because the vessels are defined better. However, we did not use IV contrast material because of the risk of renal failure in diabetic patients who receive it. The density of the pancreas was measured at the level of the tail, thus avoiding the beam-hardening effect, caused by the presence of oral contrast medium in the proximal duodenum, that occurs when measurements are made in the body or in the head of the pancreas. The contour of the pancreas was defined as smooth or lobulated on the basis of the presence of incisurae deeper than 2 mm at the surface of the gland. Analysis of the pancreatic contour was done by following the technique described by Heuck et al. [5] for normal subjects. The thickness of the pancreas was measured at three levels (head, body, and tail), also according to the method of Heuck et al. Thickness was measured on the right side of the mesenteric vessels for the head, in the extension of a line drawn from the left border of the vertebral body for the body, and from the internal border of the left kidney for the tail. The interpreters for the CT scans were not aware of the clinical diagnosis.

In order to look for an eventual effect of age or duration of diabetes on pancreatic size, correlations were calculated between these parameters and the thickness of the different parts of the pancreas in control subjects and diabetic patients. Levels of C peptide were analyzed to evaluate residual insulin secretion in diabetic patients. Measurement was made by radioimmunoassay of serum samples obtained after the patient had fasted overnight. In normal subjects, basal levels of C peptide are 1.0–3.5 ng/ml. The statistical significance of a difference between the means of the different groups was estimated by using Student's t test or the χ^2-test, and the correlation between parameters was analyzed by calculating Spearman's correlation coefficient.

Results

The density of the pancreas did not differ significantly between control subjects (40 ± 2.0 H [mean ± SEM]) and the different groups of diabetic patients: insulin-dependent, 37 ± 4.6 H; non-insulin-dependent, non-insulin-treated, 36 ± 3.2 H; and non-insulin-dependent, insulin-treated, 41 ± 3.8 H.

Heuck et al. [5] showed that lobulation of the pancreas increases progressively in healthy persons 20–80 years old. In our study (Table 1), the percentage of pancreatic lobulation was higher in control subjects more than 40 years old than in those less than 40 years old. For the age ranges 41 to 60 years and 61 to 90 years, diabetic patients had a significantly higher lobulation of the pancreas than did control subjects.

When compared with control subjects, non-insulin-treated diabetic patients had a significant reduction in the size of the body of the pancreas ($p = .035$). The sizes of the head and tail were not significantly smaller. All parts of the pancreas were smaller in insulin-treated diabetic patients than in control subjects. The difference was significant in insulin-dependent patients (head, $p < .03$; body, $p < .001$; and tail, $p < .005$) and in non-insulin-dependent diabetic patients (head, $p < .0001$; body, $p < .0005$; and tail, $p < .02$). When compared with non-insulin-dependent diabetic patients who received no insulin, insulin-treated patients had a reduction in the size of the head of the pancreas ($p < .02$), whereas the sizes of body and tail were not significantly different (Figs. 1 and 2).

TABLE 1: Prevalence of Pancreatic Lobulation by Age Range in Control Subjects and Diabetic Patients

Group	No. with Lobulation/Total No. in Age Group (%)		
	20–40 Yr	41–60 Yr	61–90 Yr
Control subjects	0/8 (0)	7/21 (33)	9/28 (32)
Insulin-dependent diabetic patients	1/10 (10)	4/5 (80)[a]	4/5 (80)[a]
Non-insulin-treated, non-insulin-dependent diabetic patients	0/0	8/11 (73)[b]	11/14 (79)[c]
Insulin-treated, non-insulin-dependent diabetic patients	0/0	4/5 (80)[a]	5/7 (71)[a]

[a] Statistically different from control subjects in the same age range at a level of $p = .05$.

[b] Statistically different from control subjects in the same age range at a level of $p = .0013$.

[c] Statistically different from control subjects in the same age range at a level of $p = .0045$.

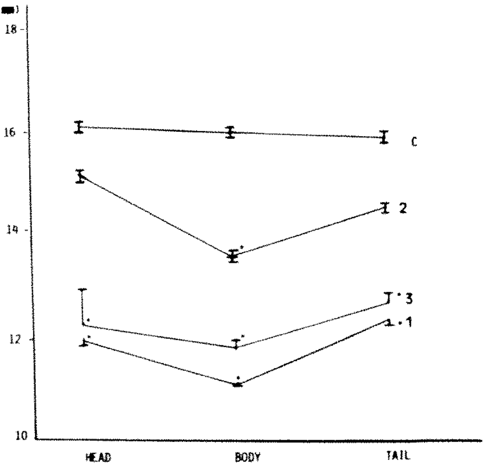

Fig. 1.—Graph gives mean (plus or minus standard error of mean) thickness of pancreas at level of head, body, and tail in different groups of patients: C = control subjects, 1 = insulin-dependent diabetic patients, 2 = non–insulin-treated, non–insulin-dependent diabetic patients, and 3 = insulin-treated, non–insulin-dependent diabetic patients. *Asterisk* indicates that values are significantly different from those in control subjects.

The size of the tail of the pancreas correlated significantly with the duration of diabetes in the whole group of diabetic patients (r = .27, p = .03). The size of the body of the pancreas correlated significantly with age in non–insulin-dependent, non–insulin-treated patients (r = −.43, p = .01) and in non–insulin-dependent, insulin-treated patients (r = −.51, p = .04). Age was not correlated with pancreatic size in control subjects. Basal serum levels of C peptide were significantly lower in insulin-dependent diabetic patients (0.83 ± 0.35 ng/dl [mean ± SEM]) than in non–insulin-dependent, non–insulin treated diabetic patients (4.12 ± 0.61 ng/dl, $p < .0001$) and in non–insulin-dependent, insulin-treated diabetic patients (2.86 ± 0.46 ng/dl, $p < .003$). Non–insulin-dependent, insulin-treated patients had lower concentrations of C peptide than did non–insulin-dependent, non–insulin-treated patients, but the difference was not significant (p = .27).

Discussion

From autopsy data, it is known that the pancreas in patients with insulin-dependent diabetes is smaller than the pancreas

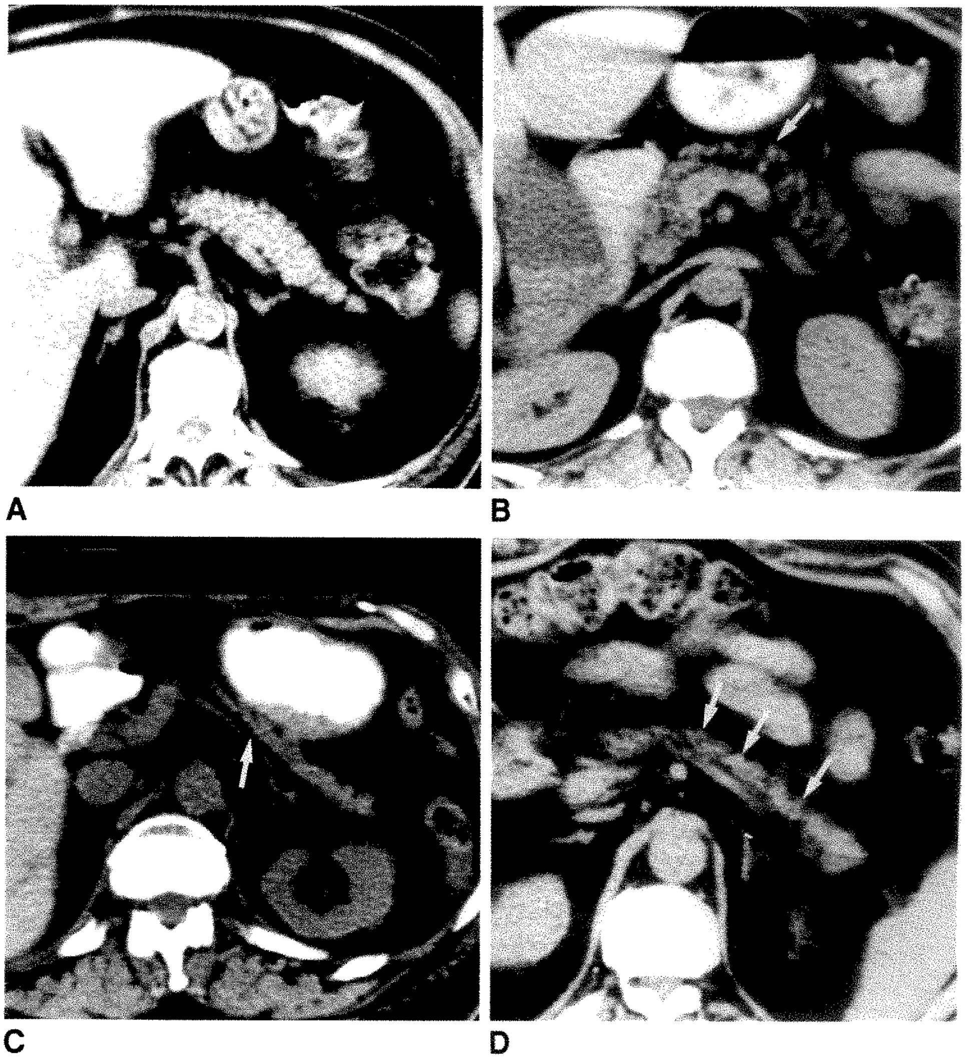

Fig. 2.—CT scans of pancreas in control subjects and three different groups of diabetic patients.

***A*, Control subject.**

***B*, Non-insulin-treated, non-insulin-dependent diabetic patient. Lobulation and atrophy of body of pancreas (*arrow*) are clearly seen.**

***C*, Insulin-treated, non-insulin-dependent diabetic patient. Marked atrophy of body of pancreas (*arrow*) is seen.**

***D*, Insulin-dependent diabetic patient. Marked atrophy of body and tail of pancreas (*arrows*) is seen.**

in persons without diabetes [2]. The pancreas appears to be slightly smaller in non-insulin-dependent diabetic patients than in persons without diabetes [6] and larger in obese patients (Ibrahim MM, Rahier J, unpublished data), whether or not the patients are diabetic [7]. The results of these studies, particularly those done in patients dying of diseases other than diabetes, may have been influenced by the effects of the underlying disease on pancreatic function and morphology.

To our knowledge, only two studies have analyzed the pancreas in living diabetic patients. Fonseca et al. [3] used sonography to study the head and body of the pancreas in diabetic patients and showed that both parts of the pancreas were smaller in patients with insulin-dependent, non-insulin-dependent, and insulin-requiring diabetes mellitus than in control subjects. The pancreas was the smallest in the first group of diabetic patients, largest in the second group, and intermediate in the third group. Compared with sonography, CT has the advantage of accurately showing all parts of the pancreas, including the tail. In our study, all parts of the pancreas tended to be smaller in diabetic patients than in the control subjects. The reduction was most prominent in insulin-dependent patients and in insulin-treated, non-insulin-dependent patients and least pronounced in non-insulin-treated, non-insulin-dependent patients. The body of the pancreas was significantly smaller in the three groups of diabetic patients. The head and tail of the pancreas were significantly smaller in insulin-treated diabetic patients only, whether they had insulin-dependent or non-insulin-dependent diabetes. In a CT study of insulin-dependent diabetic patients by Brunova et al. [4], only the sizes of the pancreatic body and tail were below the lower limit of normal.

Although Fonseca et al. [3] found no correlation between the size of the pancreas and duration of diabetes, our results suggest that the sizes of the tail and body of the pancreas tend to decrease with duration of diabetes or age. This process seems to be related to the disease itself more than to the patient's age because no correlation was found between the size of the pancreas and age in control subjects. Similarly, Brunova et al. [4] found that insulin-dependent diabetic patients who had had diabetes longer than 10 years had a smaller pancreatic body than did patients who had been diabetic fewer than 10 years. It is unclear why the reduction in size affects the body more than the other parts of the pancreas in diabetic patients. However, Rahier et al. [8] have shown that the decrease in the weight of the pancreas in patients with long-term insulin-dependent and non-insulin-dependent diabetes is not caused by diffuse atrophy. Indeed, the pancreatic polypeptide-rich lower part of the head region of the pancreas (derived from the embryologic ventral primordium) is entirely preserved, and the atrophy is limited to the pancreatic polypeptide-poor lobe derived from the dorsal primordium [8]. This could explain why the size of head of the pancreas in diabetic patients is reduced less than the size of the body is. Rahier et al. [8] have speculated that atrophy of the exocrine pancreas due to the disappearance of the trophic local effect of insulin on acinar tissue does not occur in the pancreatic polypeptide-rich lobe of the pancreas, as pancreatic polypeptide also could have a trophic effect on acinar cells. This is in accordance with our findings on the serum levels of C peptide which reflect insulin secretion in the different groups of diabetic patients. Insulin-treated patients who had insulin-dependent or non-insulin-dependent diabetes had both the most prominent reduction in pancreatic size and the lowest concentrations of C peptide, whereas non-insulin-treated patients with non-insulin-dependent diabetes had the least pronounced reduction in pancreatic size and normal concentrations of C peptide. These data also agree with those of Brunova et al. [4], who found that the only patients who had a smaller pancreas were those with insulin-dependent diabetes who had the lowest serum levels of C peptide.

Some non-insulin-dependent diabetic patients eventually require insulin for equilibration because their disease is not adequately controlled by oral hypoglycemic agents alone. This has been attributed to a loss of insulin secretion. On the average, beta-cell mass has not been shown to be reduced in non-insulin-dependent diabetic patients. However, a high variability exists [6]. Our data are consistent with the hypothesis of progressive exhaustion of the endocrine pancreas in some non-insulin-dependent diabetic patients. Indeed, compared with those who did not require insulin for glycemic control, those who did had both a reduction in the size of the pancreas and low serum concentrations of C peptide. Interestingly, the best discriminant parameter between these two groups of non-insulin-dependent diabetic patients was the size of the head of the pancreas.

Pathologic examination of the pancreas has shown that insular fibrosis together with atrophic islets is usual in patients with long-term insulin-dependent diabetes and that fat infiltration or increased fibrotic tissue may be observed in patients with non-insulin-dependent diabetes, but the latter findings are far from constant [2]. On CT scans, fat has a low coefficient of attenuation and fibrosis has a high one. Thus, it is not surprising that the density of the pancreas is not different in control subjects and in diabetic patients on one hand and in the different groups of diabetic patients on the other hand.

Lobulation of the pancreas increased with age in our control subjects, a finding in accord with the work of Heuck et al. [5]. The cause of this age-related process is not known. When the age of the subjects is considered, diabetic patients have increased lobulation of the pancreas. This suggests that the process is accelerated by diabetes mellitus.

CT examination of the pancreas in diabetic patients leads to several conclusions. First, the pancreas is smaller in diabetic patients than in control subjects, in accordance with previous reports of autopsy findings. The reduction in size is more pronounced in insulin-treated than in non-insulin-treated diabetic patients. This finding together with the results of the C peptide determinations suggests a loss of insulin secretion in insulin-treated patients. Second, the body of the pancreas appears to be the most affected part of this organ. Third, a requirement for insulin in non-insulin-dependent diabetic patients seems to be associated with reduction in size of the head of the pancreas. This finding suggests that in non-insulin-dependent diabetic patients, pancreatic atrophy is an evolving process affecting first the body and then the entire pancreas, with the head being the last involved. At this stage,

insulin se
insulin is
gitudinal
confirm th
help dete
(atrophy c
dependen
insulin the

REFEREN

1. Frier BM
on exoc
tologia 1
2. Rahier
Pipeleer

Pictorial Essay

Pancreatic Disease: Findings on State-of-the-Art MR Images

Donald G. Mitchell,[1] Marcelle Shapiro,[1] Alan Schuricht,[2] Donna Barbot,[2] and Francis Rosato[2]

Recent technical innovations have made MR imaging a useful technique for imaging the pancreas. The potential impact of MR imaging on the management and outcome of cases can be determined only by controlled prospective comparative studies; however, these cannot be performed adequately until the normal and abnormal appearances of the pancreas on state-of-the-art MR images are understood. This pictorial essay is presented to further this intermediate goal.

Imaging Techniques

For evaluation of the pancreas, conventional T1- and T2-weighted spin-echo (SE) techniques have generally been used, but results can be improved with technical advances that have been introduced recently. Imaging protocols designed to differentiate normal from abnormal pancreatic tissue and to define the extent of pancreatic disease and the presence or absence of vascular complications were devised on the basis of the following observations.

Conventional T1-weighted images (e.g., SE 400/12 [TR/TE]) are dominated by the high signal of fat, compressing the acquired and displayed dynamic range of nonfatty tissues and exacerbating artifacts. These limitations can be reduced by suppressing the signal of fat [1]. On these images, the high signal of normal pancreas becomes more obvious (Figs. 1 and 2), even in patients whose glands are marbled with fat. Currently, the most widely used method of fat suppression for T1-weighted images involves saturating triglyceride magnetization via frequency-selective excitation and spoiling. Fat suppression via saturation/spoiling is far more effective on opposed-phase images, where signals from triglyceride and olefinic fatty acids interfere with each other [1].

Conventional T2-weighted images require a long TR, which prevents the acquisition of more than two signal averages. The signal-to-noise ratio and resolution are usually limited on images with long TRs and TEs. Additionally, "long" TRs of less than 3000 msec do not allow complete recovery of magnetization of tissues that have an especially long T1, such as bile and intestinal secretions. These limitations can be corrected by acquiring as many as 16 phase-encoding views per excitation, as accomplished by the multiecho conjugate (e.g., "fast SE") techniques [2]. The dramatic increase in speed can be "traded in" for longer TRs, smaller pixels, and more averages (Figs. 2 and 3). TRs as long as 6000 msec minimize T1 "contamination" of these T2-weighted images, making bile and intestinal secretions more conspicuous.

Breath-hold images with adequate tissue contrast can be obtained (Figs. 4 and 5), but the signal-to-noise ratio is limited unless newly developed phased-array coils are used (Fig. 6). Single-slice gradient-echo techniques are useful to improve confident depiction of blood flow, showing vascular anatomy and occlusion or encasement of vessels.

Although several compounds are potentially useful as oral contrast agents, we have been using approximately 300 ml of Kaopectate (Upjohn Co., Kalamazoo, MI) to improve depiction of the stomach and duodenum for pancreatic imaging. Kaopectate is a clay (currently attapulgite) that acts as a

---

Received December 26, 1991; accepted after revision April 1, 1992.

[1] Department of Radiology, The Thomas Jefferson University Hospital and Jefferson Medical College, 10th Floor, Main Bldg., Philadelphia, PA 19107. Address reprint requests to D. G. Mitchell.

[2] Department of Surgery, The Thomas Jefferson University Hospital and Jefferson Medical College, Philadelphia, PA 19107

AJR 159:533-538, September 1992 0361-803X/92/1593-0533 © American Roentgen Ray Society

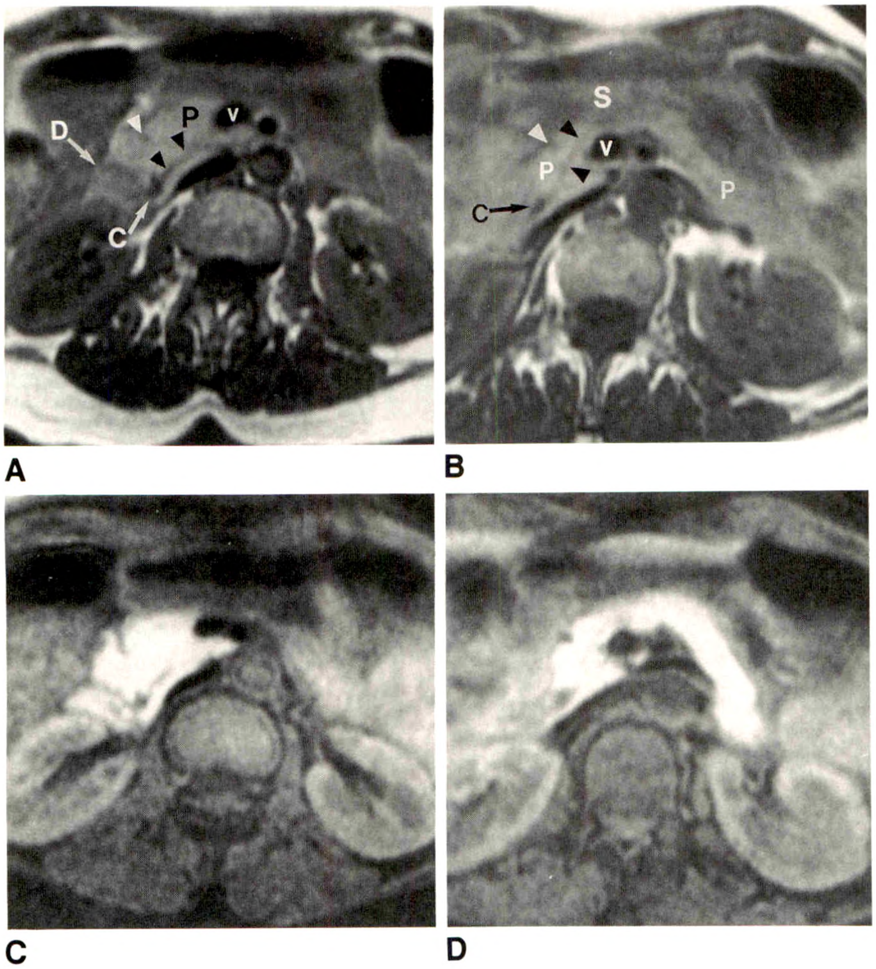

Fig. 1.—Normal pancreas with slightly prominent pancreatic head.

A–D, T1-weighted MR images without (SE 400/12, *A* and *B*) and with (SE 400/14, *C* and *D*) fat suppression (combined saturation and opposed-phase techniques) at three representative levels. *A* and *C* are at inferior portion of pancreatic head and *B* and *D* are at superior portion of head and body. *Black arrowheads* = pancreatic duct, *white arrowheads* = gastroduodenal artery, C = common bile duct, D = duodenum, P = pancreas, V = superior mesenteric vein, S = stomach. Pancreas has higher signal than do liver and other nonfatty tissues on all images, but tissue contrast and artifact suppression are improved with fat suppression.

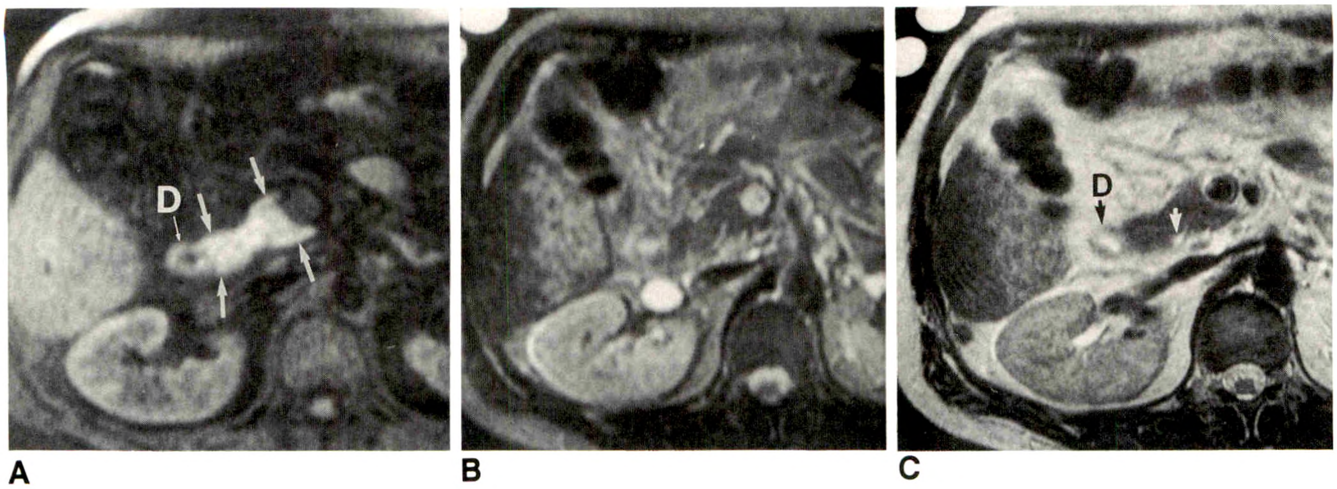

Fig. 2.—Irregular pancreatic head: normal variant.

A, Fat-suppressed MR image (SE 450/13, combination of saturation and opposed-phase techniques) shows pancreatic head with irregular shape (*arrows*). Signal intensity is well within normal limits, excluding a mass lesion as cause for irregular shape. D = duodenum.

B, Axial T2-weighted MR image (SE 2500/100) shows poor delineation of pancreas. Liver has abnormal signal heterogeneity owing to acute hepatitis.

C, T2-weighted conjugate (fast SE) MR image (SE 6000/102, 512 × 256 matrix, four signals averaged, 19 images obtained in 6 min 24 sec) shows delineation of pancreas better than that in *B*. D = duodenum, *arrow* = common bile duct.

Fig. 3.—Moderately differentiated carcinoma arising from superior surface of pancreas, with normal signal intensity of tail.

A, T2-weighted conjugate (fast SE) MR image (SE 7000/102, 512 × 256 matrix, four signals averaged, 21 images obtained in 7 min 28 sec) shows mass (M) and nodes (N) as higher signal than pancreatic tail (P). *Arrow* = hepatic metastasis, A = hepatic artery, I = inferior vena cava, V = portal vein.

B, Fat-suppressed SE 500/11 image (in phase) reveals low-signal mass (M) adjacent to pancreatic tail (P), which has normal signal intensity. *Arrow* indicates inferior vena cava. Nodes are isointense with fat.

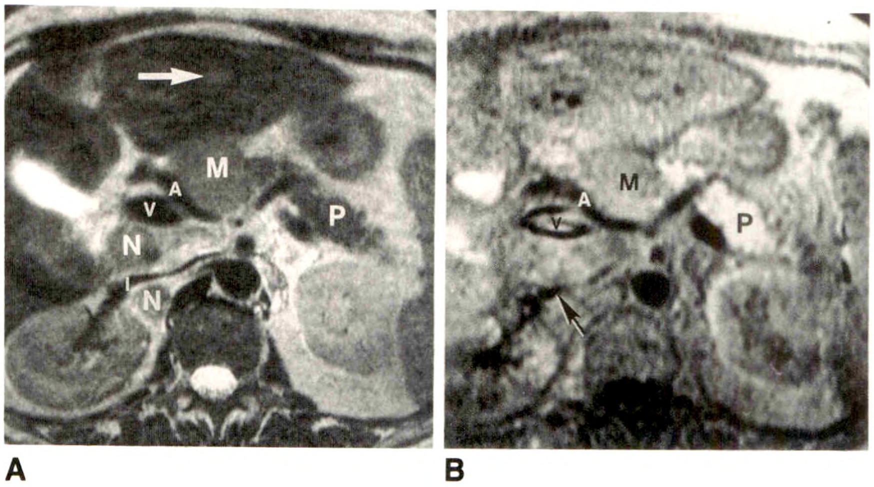

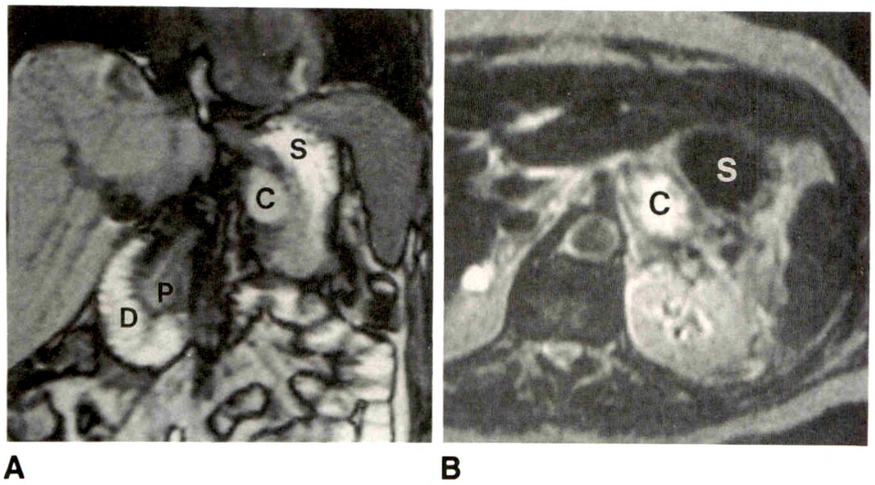

Fig. 4.—MR images obtained in a patient with pancreatic pseudocysts after acute pancreatitis. Kaopectate was administered as oral contrast material.

A, On coronal T1-weighted gradient-echo MR image (101/2.3/90° flip angle), Kaopectate within stomach (S) and duodenum (D) has high signal, allowing clear depiction of mural folds of both structures. High-signal pseudocyst (C) is adjacent to but separate from lesser curvature of stomach. Pancreatic head (P) is slightly prominent. Minor susceptibility artifact from metallic clips is visible in gallbladder fossa. (Reprinted with permission from Mitchell et al. [3].)

B, Axial SE 2500/100 MR image reveals signal void within stomach (S). Pseudocyst (C) has high signal that is heterogeneous peripherally.

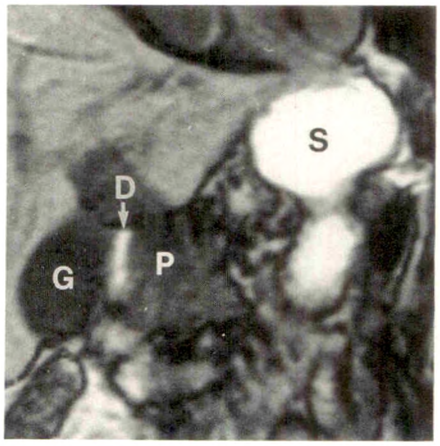

Fig. 5.—Coronal T1-weighted gradient-echo MR image (101/2.3/90° flip angle) shows low-signal-intensity pancreatic carcinoma (P) compressing duodenum (D), which has high signal intensity because of administered Kaopectate. G = gallbladder, S = stomach.

Fig. 6.—MR images in a healthy subject show potential of phased-array coil for imaging pancreas. (Acquired as a cooperative venture by investigators from the Hospital of the University of Pennsylvania, Thomas Jefferson University Hospital, and General Electric Medical Systems.)

A, Snapshot inversion-recovery MR image with flexible phased-array body coil (14.5/3.5/30° flip angle, TI = 550 msec with centric phase order, 256 × 256 matrix, 24-cm^2 field of view, two signals averaged, 8-sec acquisition time). D = duodenum, *arrow* = common bile duct, V = confluence of splenic and superior mesenteric veins.

B, SE 400/11 MR image with standard body coil (256 × 192 matrix, 36-cm^2 field of view, two signals averaged, nine images obtained in 2 min 43 sec).

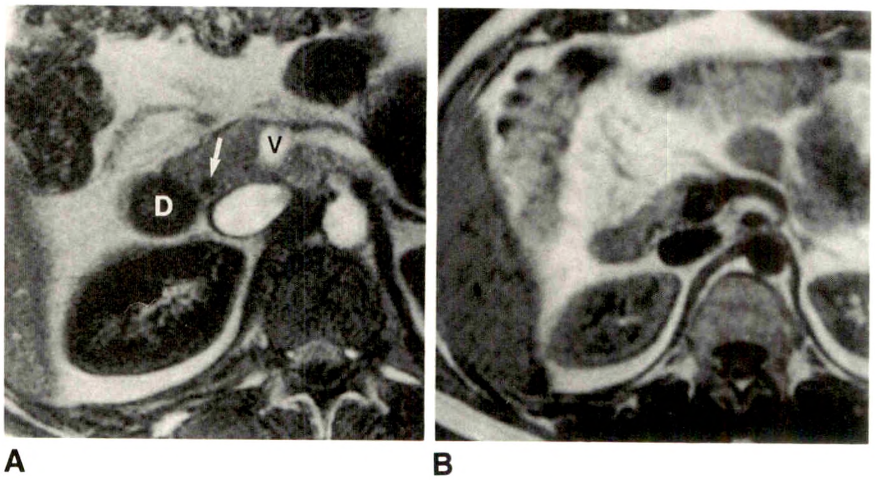

biphasic agent on MR images, causing high signal when diluted or when TE is less than 5 msec and low signal when TE is long [3] (Figs. 4 and 5).

All images illustrated in this article were acquired on a 1.5-T unit (Signa; General Electric Medical Systems, Issaquah, WI). Slices were 7 or 8 mm thick with a 1- or 2-mm interslice gap. Image matrix was 256 × 128 for T2-weighted, gradient-echo, and fat-suppressed images and most T1-weighted images; 256 × 192 for some T1-weighted images; 256 × 256 for image acquired with phased-array coil; and 512 × 256 for multiecho conjugate (fast SE) images. Motion artifact was suppressed by using respiratory-ordered phase encoding and spatial presaturation for all SE images, gradient-moment nulling for "bright blood" gradient-echo and T2-weighted SE images, and suspended respiration for all gradient-echo images.

Appearance of Abnormal Pancreas

If a pancreatic adenocarcinoma can be detected, diagnosis can be made by using guided biopsy. Signs of unresectability include hepatic or lymphatic metastases or invasion of major vessels. Imaging is useful for planning palliative surgery and intraoperative irradiation.

On T1-weighted images with fat suppression, adenocarcinoma is depicted as a low-signal mass, with intensity similar to that of the spleen and most hepatic metastases. The pancreas has even higher signal than the liver does on T1-weighted images, so T1 contrast between tumor and normal parenchyma could be even greater for the pancreas than for the liver (Fig. 3).

Adenocarcinomas in the pancreatic head are often associated with atrophy of the body and tail. In such cases the

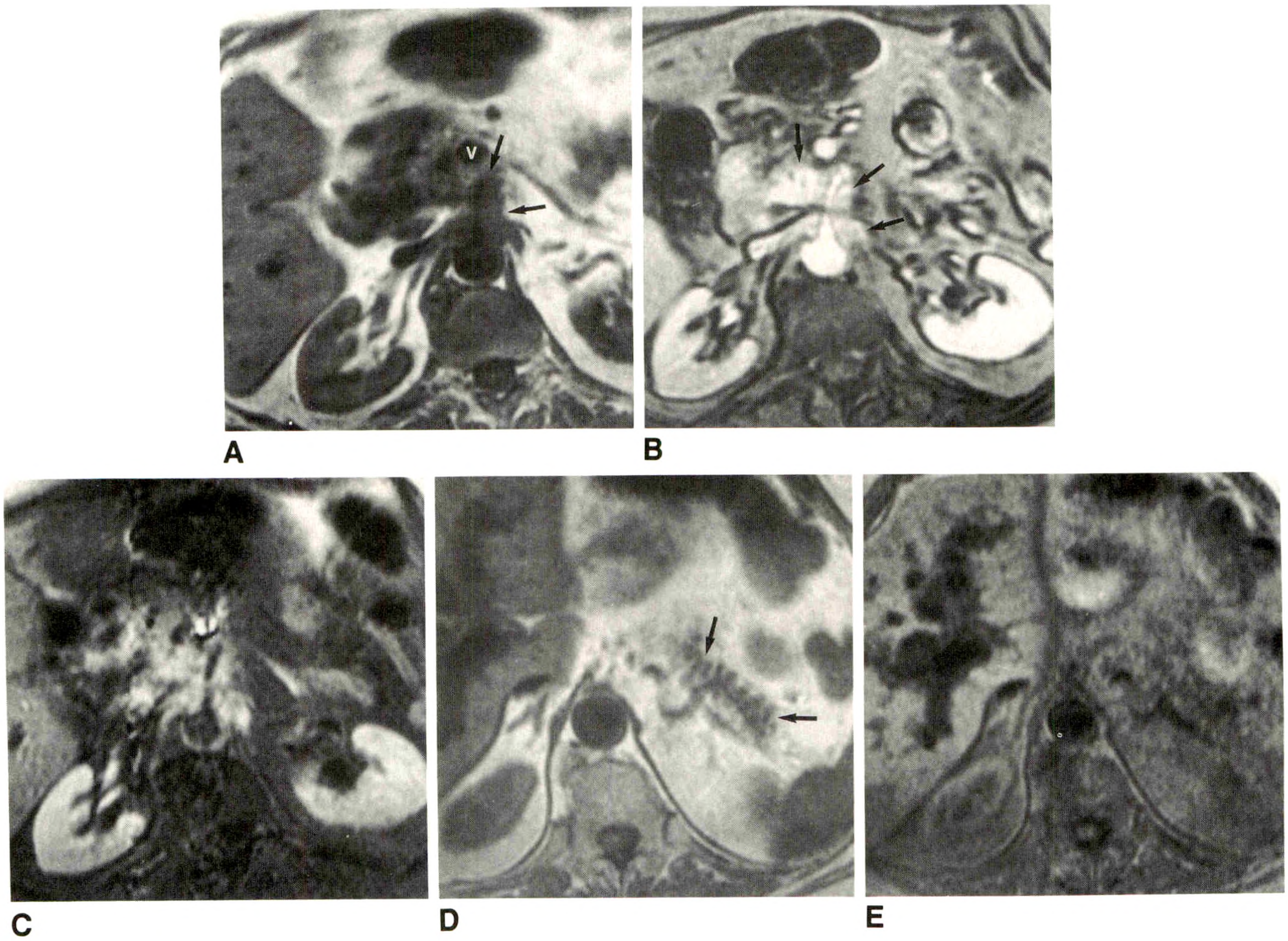

Fig. 7.—Carcinoma of pancreatic head encasing superior mesenteric artery, with signal abnormality of tail. Tumor enhances markedly.

A, SE 500/11 MR image shows abnormal low-intensity tissue encasing origin of superior mesenteric artery (*arrows*). V = superior mesenteric vein.

B, Gradient-echo MR image (102/2.3/90° flip angle) acquired less than 1 min after administration of gadopentetate dimeglumine shows enhancement of tumor (*arrows*).

C, SE 500/11 MR image with fat suppression obtained 5 min after contrast material was administered depicts persistent hyperintensity of tumor.

D, At a higher level, SE 500/11 MR image shows low signal intensity but otherwise normal-appearing pancreatic tail (*arrows*).

E, SE 500/11 MR image with fat suppression (in phase) shows abnormally low signal of pancreatic tail, which is isointense with fat.

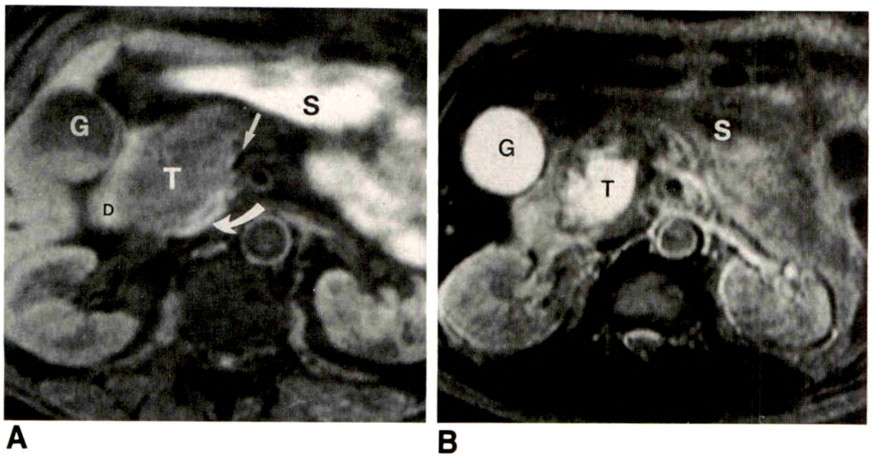

Fig. 8.—Pancreatic carcinoma with encasement of superior mesenteric vein and MR evidence of necrosis. Kaopectate, diluted with gastric secretions, has produced "positive" contrast on T1-weighted MR images and "negative" contrast on T2-weighted MR images.

A, T1-weighted MR image (SE 500/14) with fat suppression (combined saturation and opposed-phase techniques) depicts tumor (T) as much less intense than liver. Posterior portion of uncinate process (*curved arrow*) has normal signal intensity. Superior mesenteric vein is encased (*straight arrow*). D = duodenum, G = gallbladder, S = stomach.

B, T2-weighted MR image (SE 2500/100). Much of tumor (T) appears necrotic.

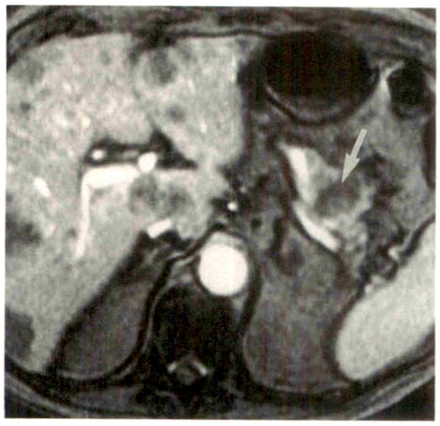

Fig. 9.—Carcinoma of pancreatic tail with metastases to liver. Spoiled gradient-echo MR image (9.5/2.6/30° flip angle) 30 sec after administration of gadopentetate dimeglumine. Mass (*arrow*) enhances less than adjacent pancreatic parenchyma.

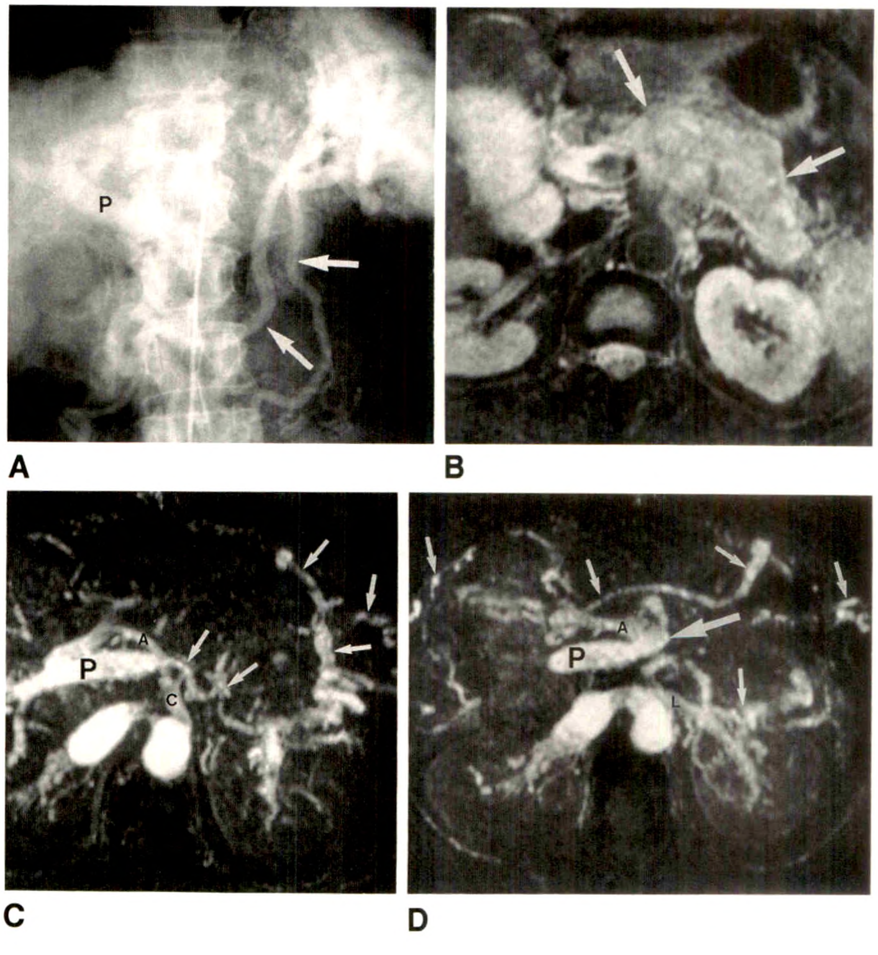

Fig. 10.—Carcinoma in body of pancreas obstructing splenic vein.

A, Venous phase of angiogram after splenic artery injection. Blood from spleen drains toward portal vein (P) via dilated gastroepiploic veins (*arrows*).

B, Axial T2-weighted MR image (2500/50) with fat suppression (in phase) shows mass (*arrows*).

C and *D*, Axial composite MR angiograms at (*C*) and inferior to (*D*) level of portal bifurcation, from contiguous 7-mm-thick gradient-echo images (27/7.4/20° flip angle). Mass is not delineated well, but obstruction of splenic vein (*large arrow*) is shown. *Small arrows* = collateral veins, A = hepatic artery, C = celiac trunk, P = main portal vein, L = left renal vein.

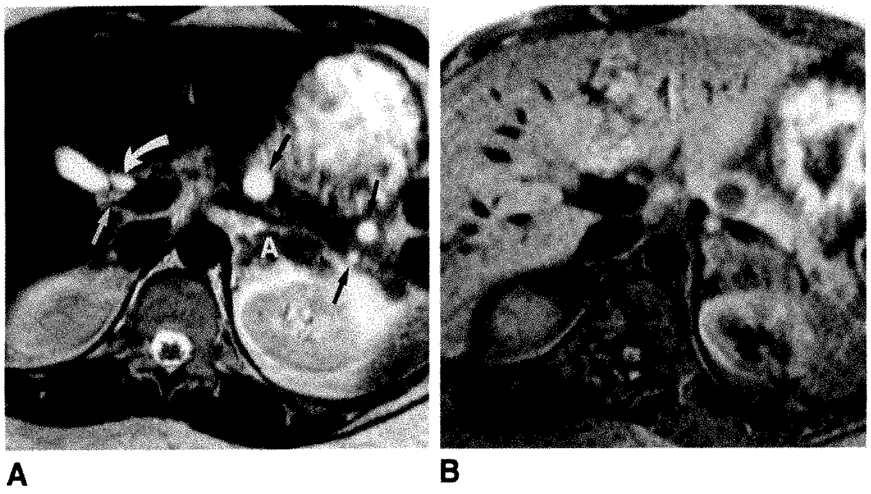

Fig. 11.—Multiple gastrinomas in a patient with multiple endocrine neoplasia, type I. CT and arteriography (*not shown*) each showed only one pancreatic lesion.

***A*, T2-weighted MR image obtained by using multiecho conjugate (fast SE) technique (SE 5000/102, 16-echo train, 512 × 256 matrix, four signals averaged) shows three lesions (*straight black arrows*) that are as intense as fluid. Four additional lesions were seen in adjacent section. *Curved arrow* = common hepatic duct, *straight white arrow* = cystic duct, A = nodular hypertrophy of left adrenal gland.**

***B*, Fat-suppressed SE 500/11 MR image (in phase) shows lesions as low-signal-intensity masses. Lesions enhanced after administration of contrast material (*not shown*).**

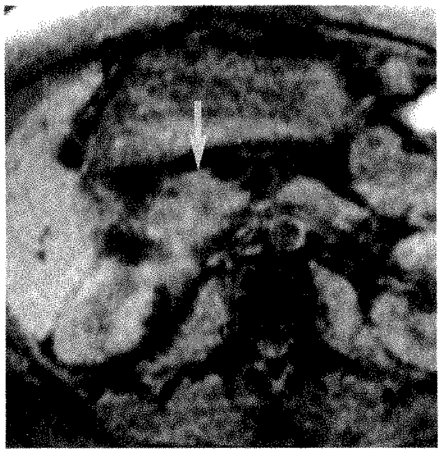

Fig. 12.—Chronic calcific pancreatitis. SE 400/16 MR image with fat suppression (combined saturation and opposed-phase techniques). Pancreatic head (*arrow*) has abnormally low signal intensity, less than that of liver. CT scan (*not shown*) showed dense pancreatic calcifications.

signal intensity of the noncancerous pancreas is abnormally low on T1-weighted images (Fig. 7). A small amount of residual pancreatic tissue with normal signal may be seen at the posterior aspect of the uncinate process (Fig. 8). Even if a focal mass is not delineated, pancreatic disease should be suspected if the signal intensity of the pancreas is less than that of the liver on high-field fat-suppressed T1-weighted images.

On T2-weighted images, adenocarcinoma has variable signal intensity relative to pancreatic parenchyma. Necrotic areas within pancreatic tumors have T1 and T2 relaxation times longer than those of solid tissue and can be readily distinguished from solid pancreatic or cancerous tissue (Fig. 8). Imaging immediately after injection of gadopentetate dimeglumine may improve contrast between pancreas and tumor on T1-weighted images [4] (Fig. 9), although some adenocarcinomas enhance greatly on MR images (Fig. 7). Vascular patency, encasement, or occlusion by pancreatic carcinoma is shown well by MR imaging (Figs. 7, 8, and 10).

Islet cell tumors have exceptionally long relaxation times, resulting in greater conspicuity than most adenocarcinomas on T1- and T2-weighted images. The long relaxation times may be due to marked edema of the stromal tissue separating nests of endocrine cells (Fig. 11).

Pancreatitis, like cancer, causes decreased signal on fat-suppressed T1-weighted MR images (Fig. 12). CT is more sensitive and specific for depicting pancreatic calcifications, so it is probably more effective in distinguishing between cancer and chronic pancreatitis with focal enlargement. Pseudocysts usually have low signal intensity on T1-weighted images and high signal intensity on T2-weighted images, but hemorrhagic pseudocysts may have high signal intensity on T1-weighted images (Fig. 4).

REFERENCES

1. Mitchell DG, Vinitski S, Saponaro S, et al. The liver and pancreas: improved spin-echo T1 contrast by shorter TE and fat suppression at 1.5 tesla. *Radiology* **1991**;178:68–71
2. Melki PS, Mulkern RV, Panych LP, Jolesz FA. Comparing the FAISE method with conventional dual-echo sequences. *J Magn Reson Imaging* **1991**;1:319–326
3. Mitchell DG, Vinitski S, Haidet K, Rifkin MD. Comparison of Kaopectate with barium for negative and positive enteric contrast at MR imaging. *Radiology* **1991**;181:475–480
4. Chezmar JL, Nelson RC, Small WC, Bernardino ME. Magnetic resonance imaging of the pancreas with gadolinium-DTPA. *Gastrointest Radiol* **1991**;16:139–142

Diagnosis of Acute Appendicitis in Pregnant Women: Value of Sonography

Hyo Keun Lim[1]
Sang Hoon Bae
Gwy Suk Seo

OBJECTIVE. The diagnosis of acute appendicitis in pregnant women often is difficult to make on the basis of clinical findings, and radiologic examination is limited because of the potentially hazardous effects of radiation. This study was done to assess the value of sonography in the diagnosis of acute appendicitis in pregnant women.

SUBJECTS AND METHODS. We obtained sonograms in 45 pregnant women with clinically suspected acute appendicitis. Our sonographic technique included graded-compression scanning. The left lateral decubitus position was used in the third trimester of gestation. The sonographic criterion for the diagnosis of acute appendicitis was visualization of an incompressible appendix with a maximal diameter greater than 7 mm. We correlated the sonographic findings with the surgical findings in 22 cases and with the results of clinical follow-up in 23 cases.

RESULTS. Sonography could not be used to make the diagnosis in three (7%) of 45 patients because the size of the gravid uterus prevented use of the graded-compression technique. These three patients were in the third trimester of pregnancy (>35 weeks' gestation). Sonographic findings were used as a basis for diagnosis in 42 cases. Acute appendicitis was diagnosed on the basis of sonograms in 16 patients, and in all but one of these patients, acute appendicitis was confirmed by surgical and pathologic findings. In the 42 cases in which the imaging findings indicated the diagnosis, the overall sensitivity of sonography was 100%, the specificity was 96%, and the accuracy was 98%.

CONCLUSION. Our experience suggests that graded-compression sonography is a valuable procedure for detecting acute appendicitis in pregnant women despite technical difficulty in performing it during the third trimester of pregnancy.

AJR 159:539–542, September 1992

Acute appendicitis in pregnant women, particularly when perforation, peritonitis, or both occur, has been associated with increases in premature labor and fetal and maternal death. The myriad of abdominal problems that are common in pregnant women and anatomic changes that include altered location of the appendix and loss of elasticity in abdominal muscles are factors that contribute to the difficulty in diagnosis [1, 2].

Radiologic imaging in pregnant women thought to have acute appendicitis is limited because of the potentially hazardous effects of radiation. Real-time high-resolution sonography with the graded-compression technique allows direct visualization of the acutely inflamed appendix. Several reports [3–6] have suggested that high-resolution sonography is fairly accurate in the diagnosis of acute appendicitis. To our knowledge, the value of sonography in the diagnosis of acute appendicitis in pregnant women has not been reported in the English-language literature except for one case report by Coady et al. [7]. This study was done to assess the value of graded-compression sonography for the diagnosis of acute appendicitis in pregnant women.

Received February 24, 1992; accepted after revision April 1, 1992

Presented at the World Congress in Ultrasound, Copenhagen, September 1991.

[1] All authors: Department of Radiology, Kangdong Sacred Heart Hospital, Hallym University, 445 Kil-dong Kangdong ku, Seoul 134-701, Korea. Address reprint requests to H. K. Lim.

0361-803X/92/1593-0539
©American Roentgen Ray Society

Subjects and Methods

During a 48-month period, we obtained sonograms in 45 pregnant women with clinically suspected acute appendicitis. The patients were 21-40 years old (mean, 25 years). Twenty-eight were in the first trimester of pregnancy (up to 13 weeks), 10 were in the second trimester (14-27 weeks), and seven were in the third trimester (28 weeks or more). All patients had abdominal pain: 34 (76%) in the right lower quadrant, nine (20%) in the right flank, and two (4%) in the right upper quadrant. The patients initially consulted their obstetricians, who determined if any abnormality was present in the fetus, uterus, or placenta. Patients with any abnormality in these areas and with no possibility of acute appendicitis were not included in the study. After the obstetrician's evaluation, a general surgeon examined the patients and requested sonography for the assessment of acute appendicitis.

All sonograms were obtained with a 5-MHz linear-array transducer (UM-4 unit, Advanced Technology Laboratories, Seattle, WA). The method of examination was similar to the graded-compression technique introduced by Puylaert [3]. However, because of the size of the gravid uterus, it was difficult during the late second trimester or the third trimester of pregnancy to perform the graded-compression technique when the woman was supine. Consequently, we were unable to use sonography for diagnosis in the first three women in the study. Therefore, for women in the late second trimester or third trimester, we imaged the cecum and appendix with the patient in the left lateral decubitus or left posterior oblique position.

The sonographic criterion for diagnosis of acute appendicitis was visualization of an incompressible appendix with a maximal diameter greater than 7 mm. The presence of a loculated periappendiceal fluid collection with an inflamed appendix indicated appendiceal perforation. We considered the sonographic findings nondiagnostic if the cecum could not be adequately visualized or compressed. If the inflamed appendix could be seen, the presence of complications such as a fluid collection in the peritoneal cavity, suppurative areas of inflammation, and abscess formation was determined. After the appendix was evaluated, we checked for disease of the pelvic cavity and for fetal well-being. For evaluation of the pelvic cavity, the patient's bladder was partially full and a 3.5-MHz transducer was used. At the time of sonographic examination, we had no knowledge of clinical findings, laboratory findings, or the surgeon's opinion. Our diagnosis was based on sonographic findings only. All patients with sonographic findings indicative of acute appendicitis and continuous or progressive signs and symptoms during and after the sonographic examination immediately had surgery. Other patients who had no indicative sonographic findings and who had improvement in signs and symptoms were clinically followed up with close observation until the signs and symptoms completely resolved. If signs and symptoms progressed during clinical follow-up, the patient had surgery. The sonographic findings were correlated with the surgical results in 22 cases and the results of clinical follow-up in 23 cases. Clinical follow-ups were performed while the patient was being treated conservatively, with close observation until symptoms and signs completely resolved. The final diagnosis of acute appendicitis was made on the basis of pathologic findings in the patients who had surgery. The diagnosis of appendicitis in patients whose sonograms showed no evidence of appendicitis was based on clinical findings: complete resolution of signs and symptoms during close clinical observation for more than 1 week.

Results

Sonography was nondiagnostic in three (7%) of 45 patients in our series. In one patient, adequate visualization and compression of the cecum were not possible because the gravid uterus was markedly enlarged. Surgery confirmed acute appendicitis. Sonograms in the other two patients were nondiagnostic for similar reasons; these two patients were clinically followed up, and their signs and symptoms resolved completely after 1 and 2 days. All three patients with nondiagnostic studies were in the third trimester (37 weeks' gestation in two cases, 36 weeks' gestation in one case). In 16 (38%) of the other 42 patients, sonographic findings indicated a diagnosis of acute appendicitis. The maximal diameter of the appendix in these patients was 8-16 mm (mean, 12 mm). In 15 (94%) of these 16 patients, acute appendicitis was surgically confirmed (Fig. 1). One of these 15 patients had a perforated appendix, and a localized abscess formation seen sonographically (Fig. 2) was confirmed at surgery. Sonographic findings were false-positive for the diagnosis of acute appendicitis in one patient who had a sonographically visible incompressible appendix with maximal diameter of 8 mm (Fig. 3). The patient's signs and symptoms had subsided by the time of sonographic examination, and surgery was not performed. In 26 (62%) of 42 patients, no evidence of a visible

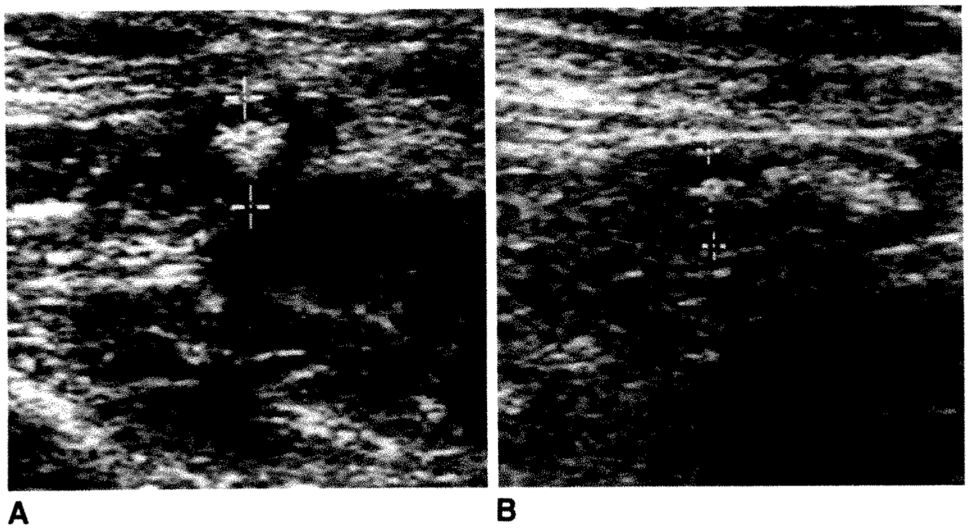

Fig. 1.—Acute appendicitis in a 27-year-old pregnant woman (8 weeks' gestation).

***A* and *B*, Transverse (*A*) and sagittal (*B*) sonograms show an inflamed appendix (between *cursors*). Surgery showed acute suppurative appendicitis without perforation.**

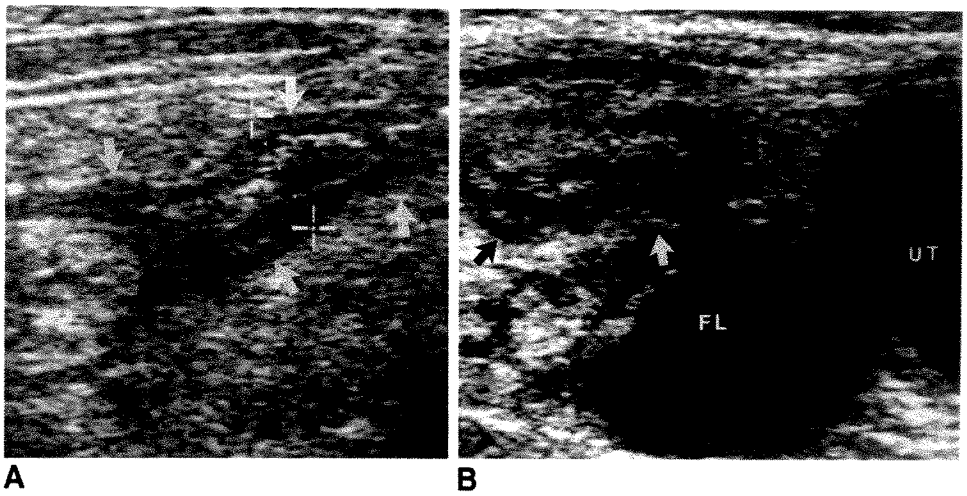

Fig. 2.—Perforative appendicitis in a 29-year-old pregnant woman (20 weeks' gestation).

***A* and *B*, Transverse (*A*) and sagittal (*B*) sonograms of right lower quadrant of abdomen show a markedly inflamed appendix (*arrows*) and a loculated, septated fluid collection (FL) in superior aspect of gravid uterus (UT). Surgery showed perforated appendix with periappendiceal abscess.**

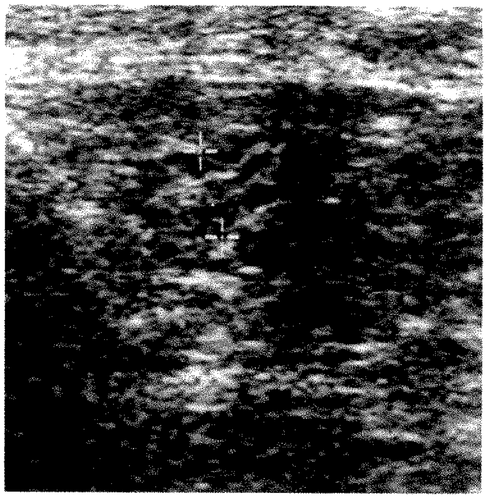

3

Fig. 3.—False-positive sonogram in a 25-year-old pregnant woman (20 weeks' gestation). Transverse sonogram of right lower quadrant of abdomen shows an incompressible, tubular structure with maximal outer diameter of 8 mm (a sonographic finding usually indicative of acute appendicitis). Patient's symptoms and signs had subsided by time of examination and spontaneously resolved during hospitalization; surgery was not performed. This case was considered false-positive because of clinical course, despite sonographic findings.

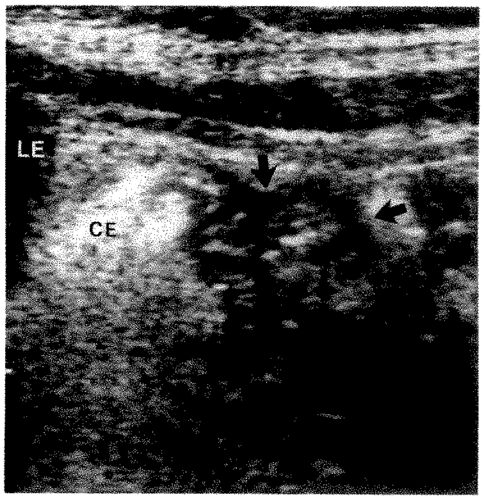

4

Fig. 4.—Acute appendicitis in a 28-year-old pregnant woman (29 weeks' gestation). Graded compression technique could not be used with this patient supine because of large gravid uterus; therefore, sonogram was obtained with patient in left posterior oblique position. Right flank was used as an acoustic window. Oblique sonogram of right flank shows an inflamed appendix (*arrows*) and cecum (CE). Surgery confirmed acute suppurative appendicitis without perforation, and cecum and appendix were in right upper quadrant of abdomen. LE = edge of liver.

incompressible appendix was seen on sonograms. Twenty of these did not have surgery, and no evidence of acute appendicitis was seen at clinical follow-up 1 week to 2 months later (mean, 3 weeks). In one of these patients, a distal ureteral stone with mild hydronephrosis of the right kidney was seen on the initial sonogram; the stone passed spontaneously after 1 day, and signs and symptoms resolved completely. This was confirmed by follow-up sonography 2 days later. In the remaining six patients, diagnoses based on sonographic findings included complicated ovarian cyst in five and hollow viscus perforation in one. At surgery, the diagnosis of complicated ovarian cyst were confirmed as torsion of ovarian cyst, and the diagnosis of hollow viscus perforation was verified as perforation of a duodenal ulcer with generalized peritonitis. All six of these patients had a normal appendix. For the 42 cases in which the sonographic findings indicated the correct diagnosis, the sensitivity of sonography was 100%, the specificity was 96%, and the overall accuracy was 98%. The positive predictive value was 94%, and the negative predictive value was 100%.

In our series, clinical follow-up until delivery showed no maternal deaths, one spontaneous abortion, and one premature delivery. The patient with a spontaneous abortion was confirmed at surgery as having acute appendicitis without perforation, and the patient with premature delivery had no evidence of appendicitis on follow-ups performed until the time of delivery. We found no relationship between acute appendicitis and suboptimal outcome; however, it was not our intent to make this comparison, and the small number of cases precluded it.

Discussion

Acute appendicitis is the most common surgical emergency occurring during pregnancy [8]. Delayed diagnosis, particularly when perforation, peritonitis, or both occur, has been associated with increases in premature labor and fetal and maternal death [2, 9]. As the appendix is pushed progressively higher by the growing uterus, containment of the infection by the omentum becomes increasingly unlikely, and appendiceal rupture causes generalized peritonitis [10].

The diagnosis of acute appendicitis is difficult to make in pregnant women. Signs and symptoms, findings on physical examination, and laboratory findings may be obscured or altered by the presence of a gravid uterus [11]. The location of the appendix varies. As the uterus enlarges, the appendix commonly moves upward and outward toward the flank, so that pain and tenderness may not be prominent in the right lower quadrant. In this study, this was true in patients with surgically proved acute appendicitis. Eleven patients had pain in the right lower quadrant of the abdomen among 16 patients with surgically proved acute appendicitis: nine (90%) of 10 patients in the first trimester of gestation, two (50%) of four patients in the second trimester, and none of two patients in the third trimester.

The reported accuracy of clinical assessment alone in the preoperative diagnosis of acute appendicitis during pregnancy is as low as 58–68%. The overall fetal mortality after removal of the appendix has been reported as 20%, and fetal mortality seems to be related to the severity of the disease [12–14]. Saunders and Milton [14] reported that diagnostic laparotomy, including unnecessary maneuvers such as removing a normal appendix, increased the premature labor and fetal mortality rates. In the 42 cases in our series in which it was used successfully, the diagnostic accuracy of graded-compression sonography was high: 100% sensitivity, 96% specificity, and 98% overall accuracy. The sensitivity and specificity rates in previous studies were 75–89% and 95–100%, respectively [3–6]. The overall results in our study are similar to those of others, despite the difficulty of performing graded-compression sonography during the third trimester of gestation.

Graded-compression sonography has been of value in the diagnosis of acute appendicitis [3–6]. However, use of this technique with the patient supine is difficult during the late second trimester and third trimester of pregnancy because the large size of the gravid uterus does not allow adequate compression. This caused three sonographic examinations to be nondiagnostic in our series. Since then, for women in the late second trimester or third trimester, we place the patient in the left posterior oblique or left lateral decubitus position, which allows displacement of an enlarged uterus and use of the graded-compression technique without difficulty. Using this technique, we successfully examined the next four patients who were in the third trimester of pregnancy (Fig. 4). Several authors have indicated the disease is most prevalent in the first two trimesters [15, 16], so the use of this alternative technique usually should be unnecessary.

One perplexing pitfall in diagnosis is that displacement of the appendix by the gravid uterus moves the somatic component of pain and the point of maximal tenderness to a higher and more lateral position in the abdomen. In 1932, Baer et al. [16] described the changes in the position and direction of the appendix as pregnancy advanced in a large series of pregnant women with surgically confirmed acute appendicitis. If we had difficulty locating the cecum and appendix, we referred to the findings of Baer et al.

Although a large-scale study would be required for confirmation, it appears the number of nondiagnostic studies can be reduced by using the graded-compression technique with the patient in the left posterior oblique or left lateral decubitus position. Our results show that sonography can be a valuable procedure for detecting acute appendicitis in pregnant women. The results are accurate despite difficulty performing the procedure during the third trimester of pregnancy, and no radiation is involved.

REFERENCES

1. Schwartz SI, Shires GT, Spencer FC. Principles of surgery. In: Schwartz SI, ed. *Appendix.* New York: McGraw-Hill, **1988**:1321–1324
2. Cunningham FG, McCubbin JH. Appendicitis complicating pregnancy. *Obstet Gynecol* **1975**;45:415–420
3. Puylaert JBCM. Acute appendicitis: US evaluation using graded compression. *Radiology* **1986**;158:355–360
4. Jeffrey RB Jr, Laing FC, Lewis FR. Acute appendicitis: high-resolution real-time US findings. *Radiology* **1987**;163:11–14
5. Puylaert JBCM, Rutgers PH, Lalisang RI, et al. A prospective study of ultrasonography in the diagnosis of appendicitis. *N Engl J Med* **1987**;317:666–669
6. Abu-Yousef MM, Bleichen JJ, Maher JW, Urdaneta LF, Franken EA Jr, Metcalf AM. High-resolution sonography of acute appendicitis. *AJR* **1987**;149:53–58
7. Coady DJ, Snyder JR, Subramanyam B. Appendiceal abscess in pregnancy: diagnosis by ultrasound. *JCU* **1986**;14:70–71
8. Gomez A, Wood M. Acute appendicitis during pregnancy. *Am J Surg* **1979**;137:180–183
9. Masters K, Levine BA, Gaskill HV, Sirinek KR. Diagnosing appendicitis during pregnancy. *Am J Surg* **1984**;148:768–771
10. Cunningham FG, Macdonald PC, Gant NF. *Williams obstetrics,* 18th ed. Englewood Cliffs, NJ: Prentice-Hall, **1989**:832
11. Bailey LE, Finley RK Jr, Miller SF, et al. Acute appendicitis during pregnancy. *Am Surg* **1986**;52:218–221
12. Priddle HD, Hesseltine HC. Acute appendicitis in the obstetric patient. *Am J Obstet Gynecol* **1951**;62:150–155
13. Bryan WM. Surgical emergencies in pregnancies and in the puerperium. *Am J Obstet Gynecol* **1955**;70:1204–1213
14. Saunders P, Milton PJD. Laparotomy during pregnancy: an assessment of diagnostic accuracy and fetal wastage. *BMJ* **1973**;3:165–167
15. Brant HA. Acute appendicitis in pregnancy. *Obstet Gynecol* **1967**;29:130–138
16. Baer JL, Reis RA, Arens RA. Appendicitis in pregnancy with changes in position and axis of normal appendix in pregnancy. *JAMA* **1932**;98:1359–1364

Case Report

Pipestem Appearance of Small Bowel in Strongyloidiasis Is Not Pathognomonic of Fibrosis and Irreversibility

L. Santiago Medina,[1] Jay P. Heiken,[1] and Richard Palmer Gold[2]

Strongyloidiasis is a common parasitic infection of the gastrointestinal tract that is associated with a variety of radiologic findings. Rigidity and narrowing of the duodenum, jejunum, or both, with complete effacement of the valvulae conniventes, is seen in some patients with severe small-bowel infection. This "pipestem" or "ribbon bowel" appearance has been associated with fibrosis of the small bowel by some investigators, who consider this appearance to be an irreversible stage of the disease [1, 2]. We report a case of *Strongyloides* infection in which the pipestem appearance of the small bowel persisted for 4 years. The appearance on radiographs returned to normal after several treatments with thiabendazole.

Case Report

A 64-year-old male immigrant from the Dominican Republic had a 3-month history of abdominal discomfort, diarrhea, and an 18-kg weight loss. Physical examination showed mild epigastric tenderness. Laboratory results included intermittent guaiac-positive stools, mild anemia, and a normal WBC count. Stool examination revealed *Strongyloides stercoralis* larvae. An upper gastrointestinal and small-bowel examination showed narrowing and rigidity of the duodenum and proximal jejunum with loss of the folds in the affected areas (Fig. 1A). Results of gastroduodenoscopy with biopsy were normal. A jejunal biopsy showed partial villous atrophy. The patient was treated with thiabendazole for 2 days but was then lost to follow-up. He was seen 1 year later with abdominal bloating and constipation. Stool examination at that time again showed *S. stercoralis* larvae. An upper gastrointestinal and small-bowel examination showed no change since the prior study. The patient was treated with thiabendazole for 2 days with subsequent clearing of *Strongyloides* from his stool. He was again lost to follow-up and presented 2 years later with diarrhea, weight loss, anorexia, and lower abdominal pain. On physical examination, he was cachectic and had no abdominal tenderness. Blood studies showed no eosinophilia and his stool was guaiac negative. Another upper gastrointestinal and small-bowel examination showed decreased gastric motility and progressive narrowing of the duodenum and jejunum since the previous examination (Fig. 1B). The valvulae conniventes were effaced, and the small bowel had a rigid appearance. Stool examination again revealed *S. stercoralis* larvae.

In the subsequent 6 months, the patient was monitored closely and treated with three 7-day cycles of thiabendazole. After the first two cycles, *Strongyloides* reappeared in the stool. The last treatment was successful, and two subsequent stool studies were negative for parasites. A final upper gastrointestinal and small-bowel examination was normal (Fig. 1C).

Discussion

Strongyloidiasis is a common parasitic disease in tropical and subtropical countries and is also endemic in the southern United States [3]. The organism has been found in 3–4% of rural Kentucky schoolchildren and in 4% of college students from the Appalachian highlands [4]. Strongyloidiasis is caused by infestation of the duodenum and jejunum with the nematode *Strongyloides stercoralis*. Filiform larvae from the soil penetrate the skin, thus initiating the direct cycle within the human body. The larvae subsequently migrate through the veins or lymphatics to the right side of the heart to reach the lungs. The larvae then ascend the tracheobronchial tree, from

---

Received February 7, 1992; accepted after revision March 24, 1992.

[1] Mallinckrodt Institute of Radiology, Washington University School of Medicine, 510 S. Kingshighway, St. Louis, MO 63110. Address reprint requests to J. P. Heiken.

[2] Department of Radiology, St. Luke's/Roosevelt Hospital Center, Columbia University College of Physicians and Surgeons, 428 W. 59th St., New York, NY 10019.

AJR 159:543–544, September 1992 0361-803X/92/1593-0543 © American Roentgen Ray Society

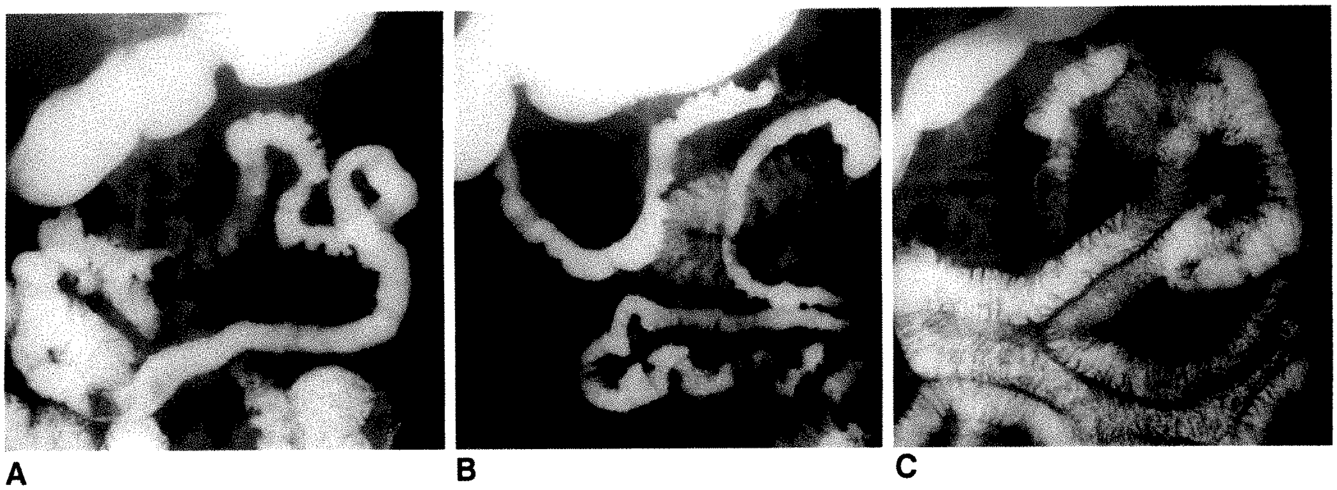

Fig. 1.—*A*, Upper gastrointestinal and small-bowel examination at presentation shows narrowing and fold effacement involving duodenum and proximal jejunum.

B, Barium examination 3½ years later shows progressive narrowing of duodenum and jejunum.

C, Follow-up barium examination after successful treatment with thiabendazole (9 months after *B*) shows normal appearance of proximal small bowel.

which they are swallowed, finally settling in the duodenum and proximal jejunum, where the adult worms develop. The female worms deposit ova that hatch into noninfectious rhabdoid larvae, which are subsequently excreted in the feces. These are transformed into infective filariform larvae in the soil during the free life cycle of the parasite outside the human body. Within the intestinal wall, the rhabdoid larvae can be transformed into infective filariform larvae, thus producing a cycle of autoinfection [5].

Many infections with *S. stercoralis* are either trivial or asymptomatic and remain unnoticed for years while being sustained by a process of autoinfection [5]. Some infections produce nonspecific signs and symptoms such as abdominal pain, diarrhea, and weight loss [6]. Changes in the host-parasite relationship can convert chronic, asymptomatic parasitosis into a debilitating and even lethal infection [5]. Hyperinfection with massive invasion of the tissues by *S. stercoralis* has been described in patients with leukemia, lymphoma, systemic lupus erythematosus, and malnutrition, as well as in elderly persons and in patients being treated with steroids or other immunosuppressive agents [6, 7]. Interestingly, hyperinfection is rare in patients with AIDS [8].

The pathologic findings in intestinal strongyloidiasis have been divided into three stages [9]. The first is catarrhal enteritis, characterized by mucosal congestion and abundant mucus secretion. Mucosal hemorrhage and microulceration also may be present. Edematous enteritis, the second stage, is characterized by edema of the intestinal wall with tumefaction of folds followed later by flattening and atrophy of the overlying mucosa.

With mild *Strongyloides* infection, the upper gastrointestinal tract may appear completely normal on radiographs [5]. Early abnormal fluoroscopic and radiographic findings associated with the first two phases of intestinal strongyloidiasis include small-bowel irritability, excess fluid, and rapid peristalsis. Dilatation and fold thickening of the duodenum and jejunum due to edema are also common findings [1, 2]. With progressive infestation, the thickened small-bowel folds may take on a bizarre coarse appearance [10]. It is generally agreed that at this stage, the radiographic abnormalities are reversible with appropriate therapy [1, 2, 5].

The third stage of intestinal strongyloidiasis has been called ulcerative enteritis and is characterized by fibrosis, mucosal atrophy, and macroscopic ulcerations within the intestinal wall [9, 10]. Long-standing disease may produce irreversible mural fibrosis [9]. The radiographic changes associated with this stage of disease are marked hypotonia and rigidity of the involved small-bowel segments [1, 2]. In the most severe cases, the small-bowel lumen is narrowed and the mucosal folds are flattened or effaced, producing the classic pipestem appearance, which is thought by some authors to be irreversible [1, 2]. However, as demonstrated in this case, the pipestem appearance may be reversible with appropriate therapy, even in patients with long-standing disease. Reversibility of this late radiographic finding has been documented by other authors [5]. Thus, the rigid pipestem appearance of the small bowel in this condition is not pathognomonic of small-bowel fibrosis and should not be equated with irreversible disease.

REFERENCES

1. Reeder M, Palmer P. Infections and infestations. In: Margulis A, Burhenne J, eds. *Alimentary tract radiology*, 4th ed. St. Louis: Mosby, **1989**:1522–1524
2. Reeder M, Palmer P. Strongyloidiasis. In: Reeder M, Palmer P, eds. *The radiology of tropical diseases*. Baltimore: Williams & Wilkins, **1981**:451–472
3. Berkmen YM, Rabinowitz J. Gastrointestinal manifestations of the strongyloidiasis. *AJR* **1972**;115:306–311
4. Berk SL, Verghese A, Alvarez S, Hall K, Smith B. Clinical and epidemiologic features of *Strongyloides*: a prospective study in rural Tennessee. *Arch Intern Med* **1987**;147:1257–1261
5. Dallemand S, Waxman M, Farman J. Radiological manifestations of *Strongyloides stercoralis*. *Gastrointest Radiol* **1983**;8:45–51
6. Yoshida T, Nozaki F, Tanaka K, Ebihara H, Shimayama T, Kutsuki T. *Strongyloides stercoralis* hyperinfection: sequential changes of gastrointestinal radiology after treatment with thiabendazole. *Gastrointest Radiol* **1981**;6:223–225
7. Scowden EB, Schaffner W, Stone WJ. Overwhelming strongyloidiasis: an unappreciated opportunistic infection. *Medicine* (Baltimore) **1978**;57:527–544
8. Lucas SB. Missing infections in AIDS. *Trans R Soc Trop Med Hyg* **1990**;84[suppl 1]:34–38
9. De Paola D, Braga-Diaz L, Rodrigues da Silva J. Enteritis due to *Strongyloides stercoralis*. *Dig Dis Sci* **1962**;7:1086–1098
10. Louisy CL, Barton CJ. The radiological diagnosis of *Strongyloides stercoralis* enteritis. *Radiology* **1971**;98:535–541

Case Report

Multiple Smooth-Muscle Tumors of the Colon and Adrenal Gland in an Adult with AIDS

D. Randall Radin[1] and Milton Kiyabu[2]

As the second decade of the AIDS epidemic begins, new diseases associated with HIV infection continue to be recognized. In 1990, three children with AIDS and multiple tumors of smooth-muscle origin involving the lungs, gastrointestinal tract, or both were reported [1]. An adult with HIV infection and multiple smooth-muscle tumors of the colon and adrenal gland is the subject of this report.

Case Report

A 28-year-old man with watery diarrhea was seen 18 months earlier, when he had cutaneous herpes zoster infection and tested positive for antibodies to HIV. Barium enema examination showed approximately two dozen sessile polyps less than 1 cm in diameter, many with central ulceration, scattered throughout the colon (Fig. 1A). Multiple colonoscopic biopsy specimens showed submucosal gastrointestinal stromal tumors of relatively uniform histologic appearance. The tumors were composed of fascicles of spindle cells with eosinophilic fibrillary cytoplasm and minimal nuclear atypia and mitotic activity. No neoplastic involvement of the overlying mucosa was present. Immunohistochemical and electron microscopic studies supported a smooth-muscle origin. Stool examination showed many *Isospora belli* oocysts and *Hymenolepis nana* ova. Esophagogastroduodenoscopy showed no abnormality. A 3-cm round, well-circumscribed right adrenal mass with central necrosis and a thin enhancing rim or capsule was seen on abdominal CT examination (Fig. 1B). Percutaneous fine-needle aspiration biopsy showed a monomorphic population of spindle cells with minimal nuclear atypia. The pathologic diagnosis was mesenchymal neoplasm morphologically consistent with smooth-muscle origin.

During the 16 months after the barium enema examination, the patient remained relatively well, although he had intermittent diarrhea and episodes of oral candidiasis and genital herpes. Follow-up CT examination at 10 months showed a 50% increase in diameter of the right adrenal mass. Follow-up barium enema examination at 15 months showed no change in the size or number of colonic polyps. Findings on chest radiographs have remained normal.

Discussion

To our knowledge, this is the first report of multiple smooth-muscle tumors in an adult with HIV infection. Four children with AIDS and smooth-muscle tumors have been reported [1, 2]. In a 5-year-old boy, multiple pulmonary leiomyomas were found at autopsy. A 2-cm leiomyosarcoma of the colon and multiple pulmonary nodules, one of which was proved to be a leiomyoma by bronchoscopic biopsy, were present in an 8-year-old girl. Autopsy of a 4-year-old girl showed 40 leiomyosarcomas, 0.5–3.5 cm in diameter, in the stomach, small bowel, and colon with mesenteric, pulmonary, and cerebral metastases. An isolated hepatic leiomyosarcoma was found in a 9-year-old child. Because smooth-muscle tumors are rare in childhood, it is likely that the association with AIDS is not coincidental [1]. Similarly, the presence of dozens of small colonic smooth-muscle tumors in our adult patient is remarkable and probably related to HIV infection. Although smooth-muscle tumors have not been reported as a complication of AIDS in adults, multiple nodules of leiomyosarcoma were

---

Received March 13, 1992; accepted after revision April 10, 1992.

[1] Department of Radiology, University of Southern California School of Medicine, Los Angeles County–University of Southern California Medical Center, 1200 N. State St., Los Angeles, CA 90033-1084.

[2] Department of Surgical Pathology, University of Southern California School of Medicine, Los Angeles County–University of Southern California Medical Center, Los Angeles, CA 90033-1084.

AJR 159:545–546, September 1992 0361-803X/92/1593-0545 © American Roentgen Ray Society

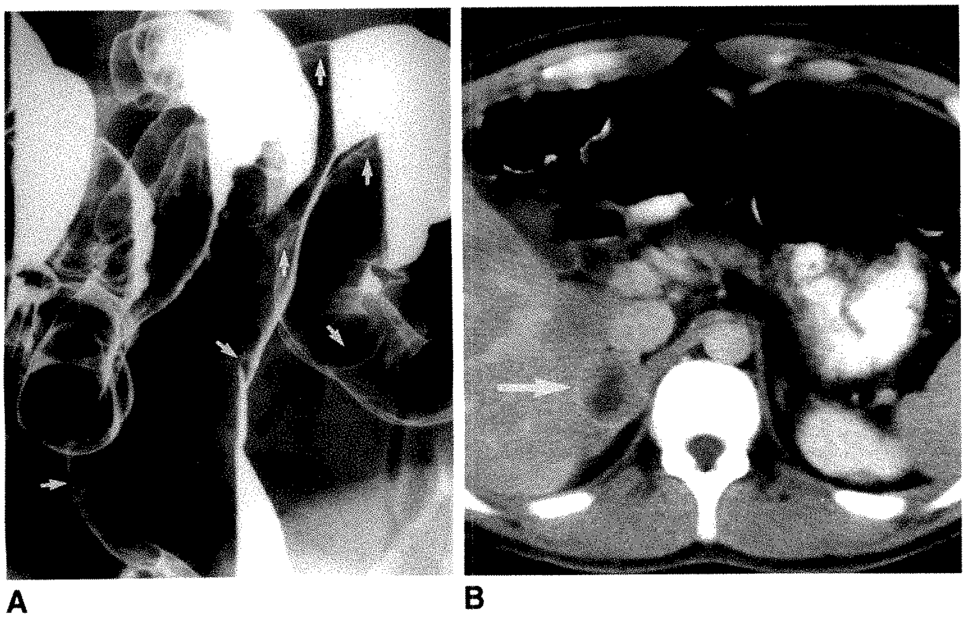

Fig. 1.—*A*, Radiograph of distal sigmoid colon and proximal rectum shows several small sessile polyps (*arrows*), some with central ulceration.

***B*, CT scan shows 3-cm round, sharply circumscribed right adrenal mass with central necrosis and a thin enhancing rim or capsule (*arrow*).**

found in the jejunum, ileum, pancreas, and liver in an adult after 4 years of immunosuppressive therapy for renal transplantation; the primary lesion was thought to be a 2-cm tumor in the ileum [3]. We have seen one other patient with HIV infection and smooth-muscle tumor. However, the occurrence of a large solitary high-grade leiomyosarcoma of the stomach in this 56-year-old man may have been unrelated to HIV seropositivity.

It is interesting that smooth-muscle tumors associated with HIV infection have been reported first in children, especially as the vast majority of patients with HIV infection are adults and the prevalence of AIDS-related lymphoma and Kaposi's sarcoma is far greater in adults than in children [2]. It has been suggested that both Kaposi's sarcoma and smooth-muscle tumors might arise from a common stem cell under the influence of some unknown factor produced during HIV infection [1]. Perhaps adults and children tend to respond differently. The distribution and multiplicity of small benign or low-grade malignant smooth-muscle tumors in some of these patients suggest a multicentric origin. Disseminated or multicentric rhabdomyosarcoma involving the gallbladder, colon, small bowel, abdominal lymph nodes, spleen, and spine has been reported in a 3-year-old girl with AIDS [4].

The radiologic findings in our patient were consistent with but not specific for smooth-muscle tumors. The differential diagnosis of multiple sessile colonic polyps, with or without ulceration, in a patient with HIV infection includes Kaposi's sarcoma and lymphoma. In our experience, an adrenal mass shown by CT in a patient with AIDS is almost always due to lymphoma. Although we have seen autopsy proof of adrenal involvement by Kaposi's sarcoma or opportunistic infections such as cytomegalovirus and *Mycobacterium tuberculosis* in many patients with AIDS, abdominal CT examinations done less than a week before death in a number of these patients showed no adrenal abnormality. Bilateral low-density adrenal masses have been reported in one patient with AIDS and disseminated histoplasmosis [5]. In another patient with HIV infection, a huge adrenal mass represented a malignant peripheral nerve sheath tumor arising in a ganglioneuroma [6].

In the small number of cases reported, the distribution and biologic behavior of smooth-muscle tumors associated with HIV infection have been varied. As more patients are encountered, the clinical significance and spectrum of radiologic findings of this interesting, newly recognized AIDS-related disease should become clearer.

REFERENCES

1. Chadwick EG, Connor EJ, Hanson ICG, et al. Tumors of smooth-muscle origin in HIV-infected children. *JAMA* **1990**;263:3182–3184
2. Horowitz ME, Friedman HS, Magrath IT. Malignancies in children with HIV infection. In: Pizzo PA, Wilfert CM, eds. *Pediatric AIDS: the challenge of HIV infection in infants, children, and adolescents*. Baltimore: Williams & Wilkins, **1991**:438–454
3. Pritzker KPH, Huang SN, Marshall KG. Malignant tumours following immunosuppressive therapy. *Can Med Assoc J* **1970**;103:1362–1365
4. Scully RE, Mark EJ, McNeely BU. Case records of the Massachusetts General Hospital: case 9-1986. *N Engl J Med* **1986**;314:629–640
5. Radin DR. Disseminated histoplasmosis: abdominal CT findings in 16 patients. *AJR* **1991**;157:955–958
6. Chandrasoma P, Shibata D, Radin R, Pinter Brown L, Koss M. Malignant peripheral nerve sheath tumor arising in an adrenal ganglioneuroma in an adult male homosexual. *Cancer* **1986**;57:2022–2025

Case Report

Inadvertent Barium Hysterosalpingography

Sandra E. Carlsen,[1] Amy S. Thurmond,[2,3] Richard M. Scanlan,[4] and Phillip E. Patton[3]

Inadvertent vaginal insertion of barium sulfate is an uncommon complication of a barium enema examination. In the few reported cases, venous embolization of barium occurred and usually resulted in death [1–4]. We report a case of vaginal insertion of the enema catheter in a young woman, resulting in barium in the uterus and fallopian tubes but not in the veins. In this premenopausal patient, future fertility was the main concern.

The effect of tubal barium on fertility is not known. Therefore, we injected barium into the fallopian tubes of four rabbits to gain a better understanding of the possible effects.

Case Report

A 26-year-old woman who had never been sexually active was referred to us after a barium enema was performed for evaluation of mild anemia and a 6-week history of bright red blood per rectum. Inadvertent vaginal placement of the enema tip by the X-ray technologist had resulted in inflow of barium into the uterus and fallopian tubes (Fig. 1A). Because of concern that a colonic-vaginal fistula was present, a Gastrografin (Squibb, Princeton, NJ) enema was then performed, the results of which were normal.

The patient was asymptomatic immediately after the examination. Findings on physical examination were normal and no significant damage of the vaginal mucosa was seen. She was hospitalized for hydration and antibiotic prophylaxis with IV Vibramycin and cefotetan. Fluoroscopically guided fallopian tube catheterization to clear the tubes of barium was considered; however, it was elected to continue noninterventional management.

Approximately 4 hr after the event, the patient had progressive nausea, vomiting, and lower abdominal pain. Approximately 12 hr after the examination, peritoneal signs were noted, accompanied by a temperature of 101.2°C and a WBC count of 15,000/mm^3 (increased from the admission value of 9000/mm^3). A plain radiograph of the abdomen showed less barium in the fallopian tubes and uterus, but more barium in the peritoneal cavity (Fig. 1B).

Twenty-four hours later, the patient felt better and abdominal tenderness had decreased. Her temperature and WBC count had decreased to 100.8°C and 9600/mm^3, respectively. A plain film of the abdomen showed no significant change in residual barium. IV antibiotics were continued for a total of 5 days; at this time the patient was asymptomatic, afebrile, had a WBC count of 7400/mm^3, and was discharged with 5 days of oral Vibramycin.

A plain film of the abdomen 1 month later was essentially unchanged, revealing trace barium in the fallopian tubes and a small amount of peritoneal cavity barium.

The patient had regular follow-ups with her gynecologist. Her menstrual period immediately following the event was delayed 10 days and was accompanied by painful cramping, which was unusual for her. At 18 months following the event she was asymptomatic and had not required treatment. She had been sexually active but had used contraception, and she had declined a follow-up hysterosalpingogram.

Materials and Methods

Four virgin adult female New Zealand Cross rabbits received an injection of 0.5 ml of barium sulfate (E-Z-EM, Inc., Westbury, NY) into one fallopian tube via fluoroscopically guided fallopian tube catheterization [5]. The other fallopian tube was used as a control. Barium was injected into the fallopian tube until free peritoneal spill could be documented, which was approximately 1 ml (Fig. 2A). Two rabbits were euthanized 24 hr afterward and two rabbits were euthanized 2

Received January 30, 1992; accepted after revision March 23, 1992.

[1] Department of Radiology, H-1307, School of Medicine, Stanford University, 300 Pasteur Dr., Palo Alto, CA 94305.

[2] Department of Diagnostic Radiology, Oregon Health Sciences University, 3181 S.W. Sam Jackson Park Rd., Portland, OR 97201. Address reprint requests to A. S. Thurmond.

[3] Department of Obstetrics and Gynecology, Oregon Health Sciences University, Portland, OR 97201.

[4] Department of Pathology, Meridian Park Hospital, 19300 S.W. 65th Ave., Tualatin, OR 97062.

AJR 159:547–549, September 1992 0361–803X/92/1593–0547 © American Roentgen Ray Society

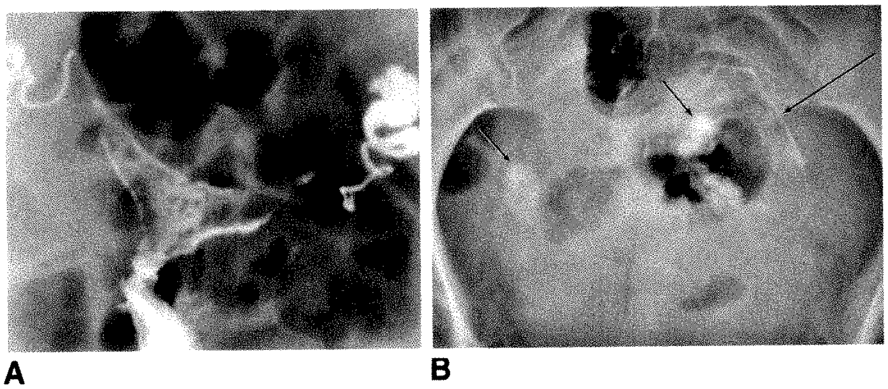

Fig. 1.—*A*, Radiograph obtained after inadvertent introduction of barium into vagina of a 26-year-old woman shows barium in uterus and fallopian tubes.

B, Radiograph of pelvis 24 hr later shows barium in peritoneal cavity (*long arrow*) and some barium in ampullary portions of both fallopian tubes (*short arrows*).

weeks after barium salpingography. At autopsy, a biopsy was done on peritoneal abnormalities and they were fixed in formalin; the right and left uteri with attached fallopian tubes and ovaries were fixed separately in formalin and examined by the pathologist. The pathologist did not know the side of barium instillation or time elapsed since barium placement. The peritoneal biopsy specimens and fallopian tubes were embedded, sectioned longitudinally, stained with hematoxylin and eosin, and examined with light microscopy.

Results

In all four rabbits, the four control fallopian tubes showed no evidence of inflammation or other abnormalities.

The two fallopian tubes of the two rabbits that received intratubal barium and were sacrificed 24 hr later showed mild to moderate acute inflammation throughout the tube (Fig. 2B). Peritoneal biopsies in both these animals revealed acute inflammatory fibrinous peritonitis surrounding particulate barium.

The two fallopian tubes of the two rabbits that received intratubal barium and were sacrificed 2 weeks later showed trace residual barium in the tube with no evidence of acute inflammation. In both animals, several fibrous adhesions were noted next to the uterine serosa and in the peritoneal cavity (Fig. 2C).

Discussion

Erroneous placement of an enema catheter tip into the vagina is not rare but is usually corrected after the patient detects the error. However, in some patients, presumably because they are too ill to communicate or because of decreased sensation from atrophic vaginal changes, barium may flow into the vagina. In all previously reported cases, involving nine patients, vaginal rupture and various degrees of venous intravasation followed, resulting in seven deaths [1–4]. It has been proposed that catheter insertion alone is sufficient to lacerate the mucosa and muscularis of an atrophic vagina, and that subsequent balloon inflation and the hydrostatic pressure of the barium column results in venous intravasation [1]. Apparently the vaginal trauma in our healthy premeno-

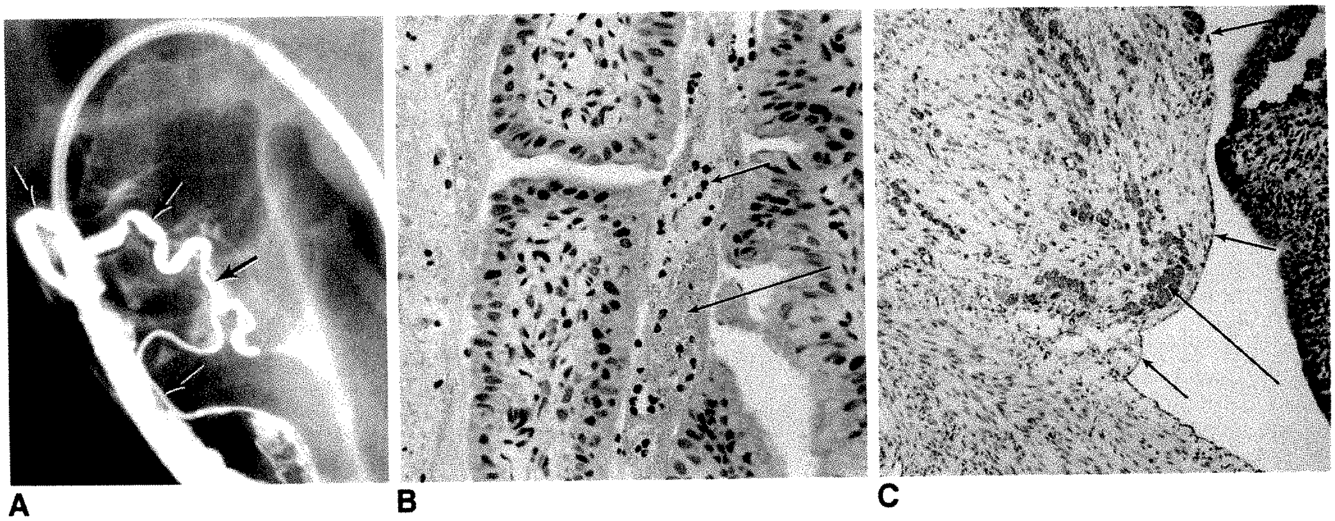

Fig. 2.—*A*, Radiograph shows barium in fallopian tube of a rabbit. Right side of uterus and right fallopian tube have been catheterized under fluoroscopic guidance (catheter tip is marked by a radiopaque bead; barium in fallopian tube is indicated by *arrows*).

B and *C*, Photomicrographs of fallopian tube show histologic changes after barium administration. By 24 hr after injection (*B*), barium is noted in tubal lumen (*long arrow*), surrounded by large numbers of polymorphonucleocytes (*short arrow*) indicative of acute inflammation. After 2 weeks (*C*), acute inflammation in tube has subsided, but adhesions are present in peritoneal cavity. In this case, serosal surface of uterus has a protuberance that consists of barium (*long arrow*) surrounded by an organizing fibrous adhesion (*short arrows*).

pausal patient was minimal, and barium went instead into the uterus and fallopian tubes.

The unique clinical question in our case is that of the treatment options that would best preserve fertility. When barium peritonitis occurs after rectal laceration, it has been well shown that there is rapid migration of leukocytes and large amounts of fluid into the peritoneal cavity [6]. This process may be quite marked within 2 hr with coating of the barium particles by fibrin. The rapidity of the evolution of the peritonitis and its severity are a function not only of the volume of the contaminating barium, but also of the volume and source of the enteric content, with most authors believing that the latter is the more important component. When barium peritonitis occurs via a rectal laceration, antibiotics, fluid replacement, and surgery are recommended. Surgical repair of the rectal tear is the primary procedure, with lavage and removal of as much barium as possible. The utility of lavage has not been clearly demonstrated, as even with immediate surgery the barium particles can be difficult to remove [7].

In our patient, there was no abnormal communication with the peritoneal cavity that required repair; the contamination of the peritoneal cavity with barium occurred through the fallopian tubes. This, combined with the fact that the amount of barium estimated to be in the peritoneal cavity was small, indicated to us that the risks of surgery or tubal flushing outweighed the benefits. It was hypothesized that with adequate hydration the normal ciliary action of the fallopian tubes would clear most of the barium.

The rabbit model has been used before to determine the effects of various contrast agents on the fallopian tubes [5]. The acute inflammatory salpingitis that developed in the two rabbit fallopian tubes within 24 hr of barium instillation, and the complete resolution of the inflammation in the two rabbits 2 weeks after barium instillation, reflect the responses reported with a variety of water-soluble contrast agents [8]. Two differences were noted, however. Barium in the tubes resulted in inflammation throughout the entire tube, whereas water-soluble agents tended to cause inflammation in the proximal tube only, closer to the site of injection. Barium instilled in the tubes also resulted in serosal fibrous adhesions, which were not present after instillation of water-soluble agents into the tubes.

Certain limitations must be kept in mind when interpreting this study. The sample size was small, a compromise between adequate experimental design and the lack of justification for use of a larger group of animals for a rare entity. Thus, it is possible that testing of a larger number of rabbits would reveal different findings. Second, although the rabbit has been used extensively for reproductive biology studies, the human fallopian tube is a complex structure that may have subtle differences that preclude the extrapolation of findings from a rabbit model. Also, the fertility of the patient has not been tested, and we cannot say with certainty that her fertility was not compromised by our approach of nonintervention.

Nonetheless, the spontaneous resolution of inflammation in the rabbit fallopian tubes by 2 weeks after barium instillation, combined with the rapid resolution of mild acute peritonitis in the woman who received barium in the fallopian tubes, indicates to us that hydration and antibiotics are a reasonable approach in the treatment of patients who experience this unusual complication of barium enema.

REFERENCES

1. David R, Berekesky IK, Bohlman M, et al. Fatal barium embolization due to incorrect vaginal rather than colonic insertion. *Arch Pathol Lab Med* **1983**;107:548–551
2. Rimarenko S, Finkel L, Taff ML, et al. Fatal complications related to diagnostic barium enema. *Am J Forensic Med Pathol* **1988**;9:78–84
3. Bonte W, Spring R. Lethal barium sulfate embolism after accidental vaginal application. *Z Rechtsmed* **1980**;86:71–78
4. TenKate RW, Kalsbeek F. Non-fatal intravasation of the barium enema accidentally introduced into the vagina. *Tijdschr Gastroenterol* **1978**; 21:277–280
5. Thurmond AS, Rosch J, Ross PL, Uchida BT, Scanlan RM, Patton PE. Transvaginal fallopian tube catheterization in an animal model. *Invest Radiol* **1988**;23:818–821
6. Grobmyer AJ III, Kerlan RA, Peterson CM, Dragstedt LR II. Barium peritonitis. *Am Surg* **1984**;50:116–120
7. Gnanaprakasam D, Sivasubramanian SV, Rangabashyam N. Barium peritonitis: a case report and review of literature. *Am J Proctol Gastroenterol Colon Rectal Surg* **1981**;32:16–20
8. Thurmond AS, Hedgpeth PL, Scanlan RM. Selective injection of contrast media: inflammatory effects on rabbit fallopian tubes. *Radiology* **1991**; 180:97–99

Photo Page

Kidney Treble

Myrosia M. Tomiak,[1] Jordan D. Rosenblum, and Jeffrey A. Leef

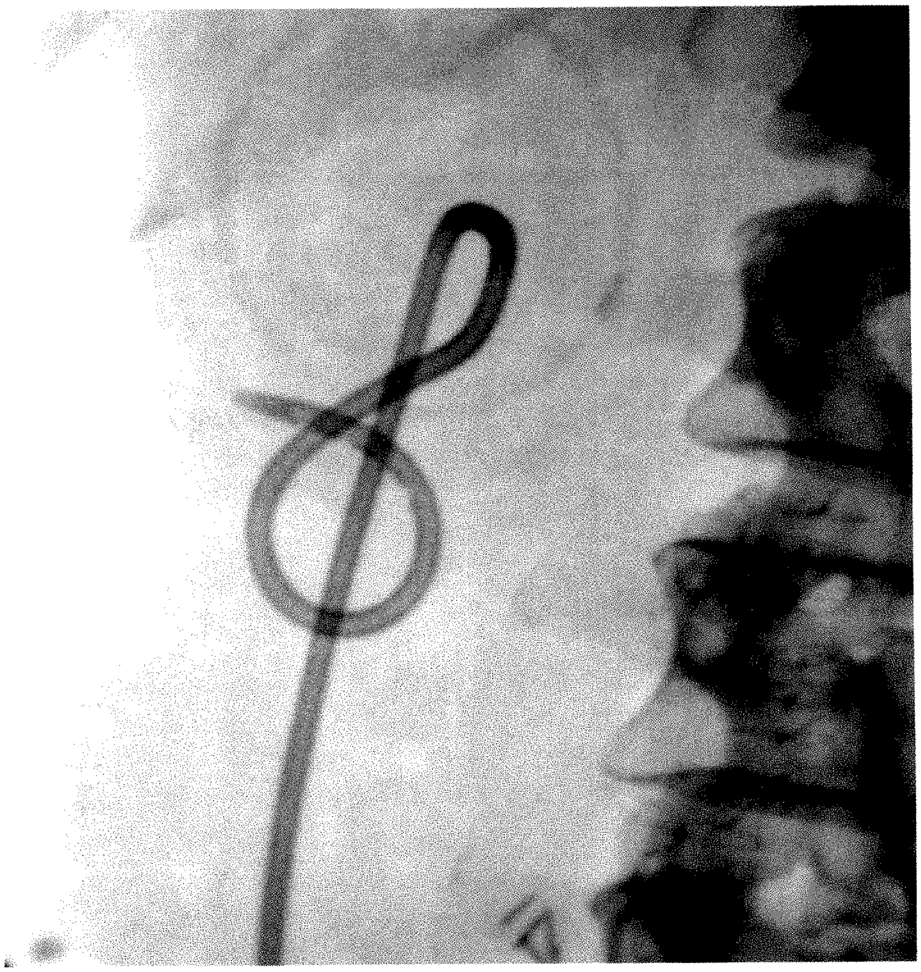

---

[1] All authors: Department of Radiology, The University of Chicago Hospitals, 5841 S. Maryland Ave., Chicago, IL 60637.

***AJR* 159:550, September 1992** 0361-803X/92/1593-0550 © American Roentgen Ray Society

Pictorial Essay

Renal Diseases in Patients with AIDS: Sonographic Findings

Chester J. Kay[1]

This essay illustrates the spectrum of sonographic findings of various renal manifestations of AIDS. The most common renal abnormality in patients with AIDS is nephropathy, which is manifested by deterioration of renal function and proteinuria. Acute tubular necrosis, intrarenal infections, focal nephrocalcinosis, hydronephrosis, and neoplasms also may occur.

Renal involvement in patients with AIDS was recognized in early descriptions of the entity. Rao et al. [1] described a nephropathy manifested by deterioration of renal function and proteinuria. They found 100% mortality 6 months after the onset of uremia. The nephropathy may also occur in HIV-infected patients and in those with AIDS-related complex. In addition, acute tubular necrosis, intrarenal infections, focal nephrocalcinosis, hydronephrosis, and interstitial nephritis may occur [2].

This essay illustrates the spectrum of sonographic findings of various renal manifestations of AIDS. The diagnosis of AIDS was based on the Centers for Disease Control surveillance criteria, including positive serologic tests for HIV and the presence of an AIDS-defining condition, which includes Kaposi's sarcoma; *Pneumocystis carinii* pneumonia, a serious opportunistic infection; and other miscellaneous changes.

Enlarged Kidneys

Most patients with AIDS nephropathy have normal-sized kidneys. Renal enlargement is a nonspecific sign of parenchymal disease. When the kidneys enlarge, they may have normal or increased echogenicity [3]. Enlargement may be related to swelling caused by toxic or hemodynamic factors in these seriously ill patients, or to a variety of renal histologic abnormalities, which are described in the next section. No constant factor causing nephromegaly, broadly defined here as kidneys longer than 13 cm, has been defined (Fig. 1).

Increased Echogenicity

In one series [3], 42% of patients with AIDS and deteriorating renal function had normal renal sonograms. The balance had cortical echogenicity equal to or greater than that of the liver (Fig. 2). The cause of the increased echogenicity is not clear. On pathologic examination, glomerular lesions, particularly focal glomerulosclerosis, are dominant. Other glomerulopathies include diffuse mesangial hypercellularity, diffuse proliferative glomerulonephritis, and membranous glomerulonephritis. No correlation between the nature and severity of glomerular diseases and cortical echogenicity has been found. Acute tubular necrosis, focal interstitial nephritis, nephrocalcinosis, and tubular atrophy have also been described. Tubular changes including focal dilatation of the tubules with infolded walls of flattened epithelium and proteinaceous casts have been noted [4]. Tubular dilatation was considered the main factor responsible for increased echogenicity, but glomerular lesions may also play some role [4]. Tubular interstitial changes have also been correlated with increased cortical echogenicity.

Received December 2, 1991; accepted after revision March 16, 1992.

[1] Department of Radiology, St. Luke's/Roosevelt Hospital Center, 428 W. 59th St., New York, NY 10019. Address reprint requests to C. J. Kay.

AJR 159:551–554, September 1992 0361–803X/92/1593–0551 © American Roentgen Ray Society

Sonographic Evidence of Pyelonephritis

The prevalence of acute and recurrent urinary tract infection may be as much as 50% in patients with AIDS [5]. The causative organisms are usually the common ones that affect the urinary tract in other patients. Sonograms in patients with acute pyelonephritis may show swollen kidneys with localized areas of increased or decreased echogenicity (Fig. 3). Complications such as intrarenal and perinephric abscesses may occur.

Focal Echogenic Densities

In patients with AIDS, focal areas of increased echogenicity may develop in the cortex and medulla. Some of these densities are sharp; others are less defined. The lesions vary in size, and in a few cases develop fairly rapidly. Punctate, and occasionally coarse, calcifications are observed in some cases. Lesions such as these have been reported in AIDS patients who have *Pneumocystis carinii* disease, *Mycobacterium avium-intracellulare* infection (Figs. 4 and 5), or histo-

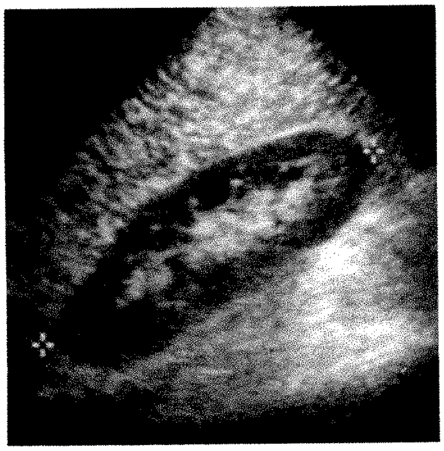

Fig. 1.—Nephromegaly. Sonogram shows symmetrically enlarged but otherwise normal kidneys. Cause of enlargement (length = 13.4 cm) in this patient with azotemia was not clear. Renal enlargement in AIDS has been noted with and without azotemia.

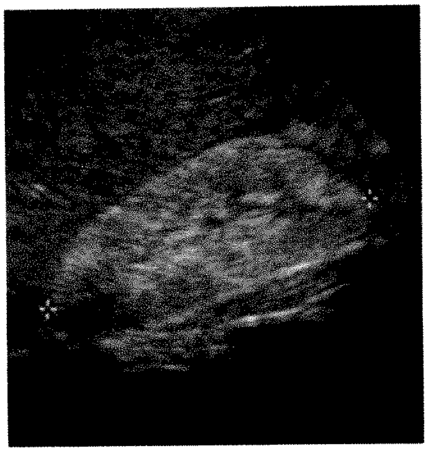

Fig. 2.—Echogenic kidney. Sonogram shows renal cortical echogenicity greater than that of liver and almost equal to that of renal sinus. Ascites is present. Increased echogenicity has been associated with dilated tubules and glomerular lesions in AIDS, but may be seen with numerous causes of medical renal disease, including heroin nephropathy without AIDS. Renal size may be normal or large with altered echogenicity.

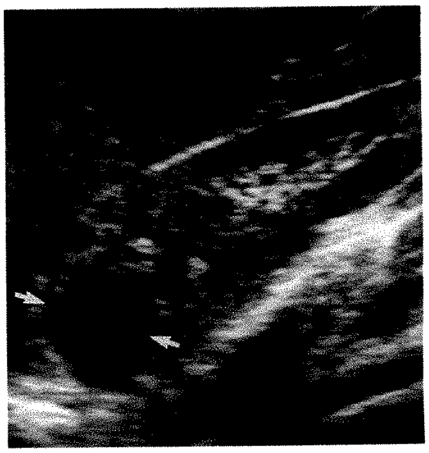

Fig. 3.—Pyelonephritis. Sonogram shows enlarged, mildly echogenic kidney with swollen upper pole that contains a hypoechoic area (*arrows*), findings consistent with pyelonephritis. Acute urinary tract infection in this patient resolved with therapy.

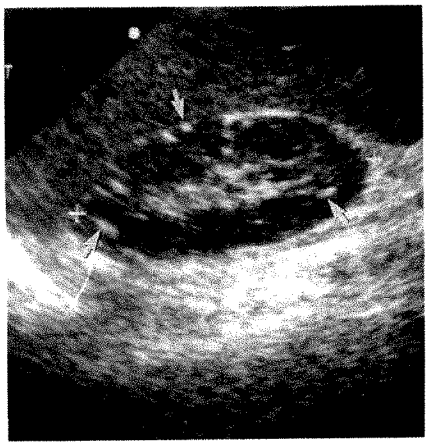

Fig. 4.—*Mycobacterium avium-intracellulare* infection. Sonogram shows focal areas of increased cortical echogenicity (*arrows*). Some of these areas appeared calcified on CT. *M. avium-intracellulare* was cultured from blood and kidney biopsy specimen.

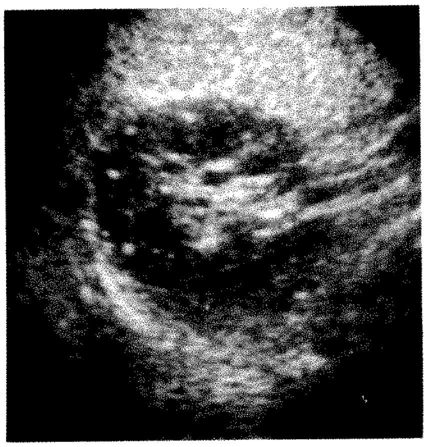

Fig. 5.—*Mycobacterium avium-intracellulare* infection. Axial sonogram of kidney shows multiple cortical and medullary areas of increased echogenicity. *M. avium-intracellulare* was cultured from blood.

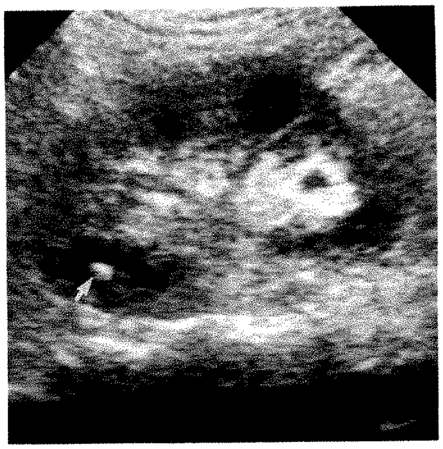

Fig. 6.—Renal histoplasmosis. Longitudinal sonogram of right kidney shows area of increased echogenicity (*arrow*) in upper pole. *Histoplasma* was cultured from bone marrow, a bronchus, and liver. Multiple nonshadowing echogenic areas were scattered throughout liver, spleen, and pancreas. These lesions varied widely in size from almost sandlike specks to large nodular areas.

plasmosis (Fig. 6). These echogenic renal densities may be associated with lesions in the liver, spleen, pancreas, and adrenal glands. None of the organisms cause specific sonographic abnormalities.

Inflammatory Masses

Extrapulmonary manifestations of *Mycobacterium tuberculosis* infection are more common in patients with AIDS.

Fig. 7.—Tuberculoma. Sonogram of right kidney shows a hypoechoic 1-cm lesion in lower pole without distal acoustic enhancement. CT scan also showed areas of decreased attenuation in liver as well as retroperitoneal adenopathy. Combination of changes is more typical of *Mycobacterium avium-intracellulare* infection, but a liver biopsy was positive for *M. tuberculosis*.

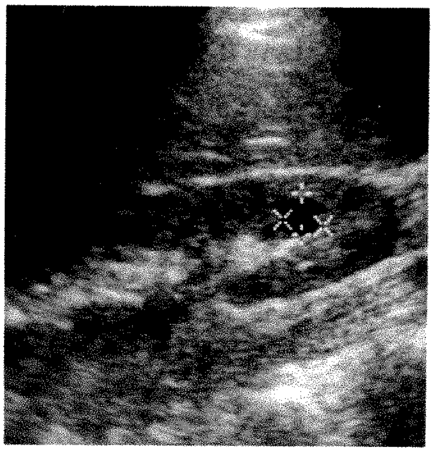

7

Fig. 8.—Renal aspergillosis. Sonogram shows multiple hypoechoic lesions (*arrows*). Lymphoma could produce these findings. Biopsy of kidney showed aspergillosis.

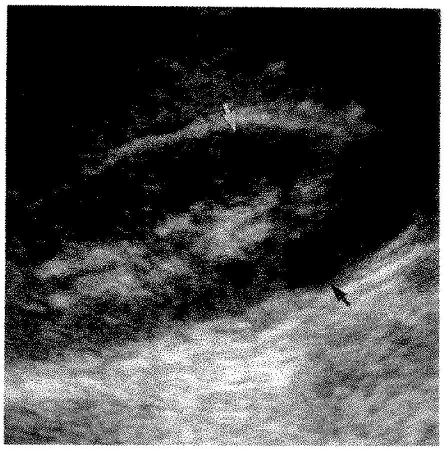

8

Fig. 9.—Candidiasis.

A, Sonogram shows 14.5-cm echogenic right kidney with dilatation of intrarenal collecting system due to mass in pelvis (*arrow*). *Candida* was cultured from urine obtained during a percutaneous nephrostomy.

B, Sonogram in another patient shows fungus ball (*arrow*) in right collecting system. *Candida* was cultured from blood and urine. Obstruction was in mid ureter. Candidiasis may also produce small echogenic renal masses similar to those seen in Figs. 4–6.

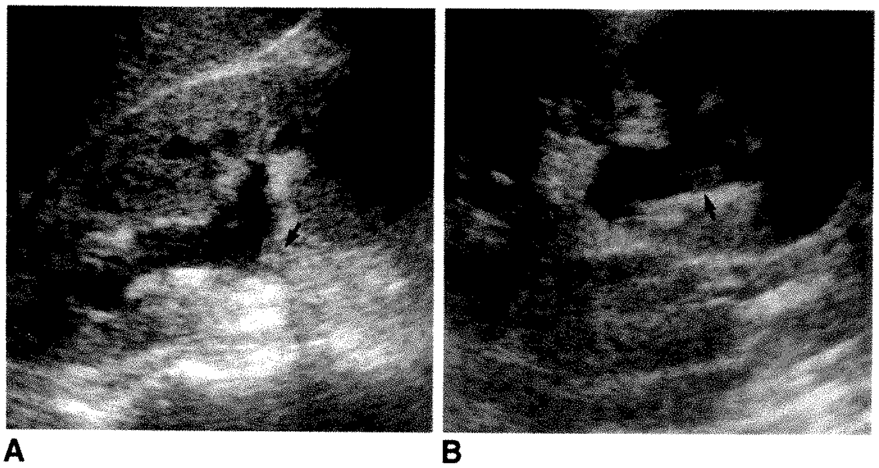

Fig. 10.—Renal lymphoma. Sonogram shows that right kidney is relatively echogenic. A solid hypoechoic mass (*arrow*) is present laterally. CT scan confirmed presence of mass and showed retroperitoneal adenopathy. Biopsy of this lesion showed non-Hodgkin's lymphoma. Biopsy and culture are necessary to differentiate these lesions from inflammation. Note similarity to case of renal tuberculosis (Fig. 7). Renal involvement is usually multiple and is detected with imaging in 6–11% of patients with AIDS and lymphoma, although itis found much more often on pathologic examinations.

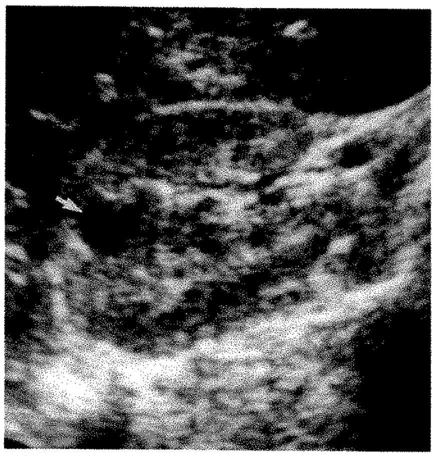

10

Fig. 11.—Hyperplastic lymph nodes. Longitudinal sonogram shows enlargement of retroperitoneal lymph nodes (*arrows*) located near renal hilum in a patient with *Mycobacterium avium-intracellulare*. Such adenopathy can mimic lymphoma.

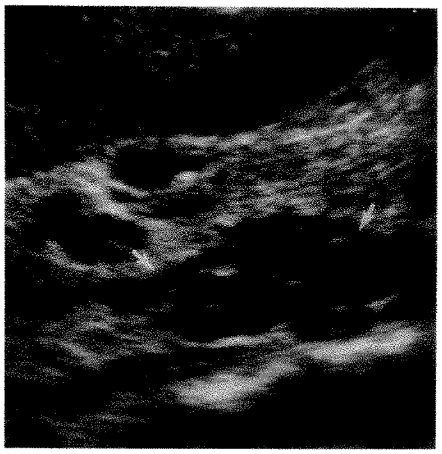

11

Figure 7 shows a renal tuberculoma. Multiple hypoechoic masses in the kidney were seen in a patient with aspergillosis (Fig. 8).

Hydronephrosis

Hydronephrosis may occur in association with ureteral reflux or obstruction. Figure 9 shows *Candida* fungus balls in a dilated renal pelvis. Hydronephrosis in patients with candidiasis may be caused by more distal obstruction of the ureter by a fungus ball.

Neoplasms

Patients with AIDS are at increased risk for non-Hodgkin's lymphoma and Kaposi's sarcoma. In AIDS, these diseases have a predilection for extranodal sites such as the kidney, liver, spleen, brain, and gastrointestinal tract.

One or more renal masses may be present (Fig. 10). The kidney may be enlarged and diffusely infiltrated, or invasion of the capsule from the outside may occur. Adenopathy can displace the kidney or ureter and cause hydronephrosis. Markedly enlarged hyperplastic lymph nodes near the renal hilum may simulate lymphoma (Fig. 11).

Kaposi's sarcoma affects 27% of patients with AIDS. The sarcoma has been found in the adrenal glands, bladder, seminal vesicles, prostate, and penis. Microscopic renal lesions occur when the disease is disseminated, but are not commonly detected by imaging techniques before autopsy. However, retroperitoneal adenopathy may be quite prominent. One case of renal carcinoma in a relatively young AIDS patient has been reported.

REFERENCES

1. Rao TKS, Fillipone EJ, Nicastri AD, et al. Associated focal and segmental glomerulosclerosis in the acquired immunodeficiency syndrome. *N Engl J Med* **1984**;310:669–673
2. Kuhlman JE, Browne D, Shermak M, Hamper UM, Zerhouni EA, Fishman EK. Retroperitoneal and pelvic CT of patients with AIDS: primary and secondary involvement of the genitourinary tract. *RadioGraphics* **1991**;11:473-483
3. Miles BJ, Melser M, Farah R, Markowitz N, Fisher E. The urological manifestations of the acquired immunodeficiency syndrome. *J Urol* **1989**;142:771–773
4. Hamper UM, Goldblum LE, Hutchins GM, et al. Renal involvement in AIDS: sonographic-pathologic correlation. *AJR* **1988**;150:1321–1325
5. Vaziri ND, Barbari A, Licorish K, Cesatio T, Gupta S. Spectrum of renal abnormalities in acquired immune-deficiency syndrome. *J Natl Med Assoc* **1985**;77:369–375

Submucosal Uterine Leiomyomas:
Diagnosis of Prolapse into the Cervix and Vagina Based on MR Imaging

Ellen Panageas[1]
Ruben Kier
Thomas R. McCauley
Shirley McCarthy

OBJECTIVE. We describe the MR appearance, signs and symptoms, and pathologic findings in five patients with submucosal leiomyomas that prolapsed into the cervical or vaginal canal.

SUBJECTS AND METHODS. During the past 3 years, five women aged 33–53 years (mean, 43 years) were identified prospectively at MR imaging as having prolapsing uterine leiomyomas. The diagnosis was confirmed by surgical pathology. MR imaging was performed on a 1.5-T unit, using both T1- and T2-weighted spin-echo or fast spin-echo sequences. The images were analyzed for signal intensity, presence of a stalk, and caudal extent of the prolapsed leiomyoma.

RESULTS. These leiomyomas, the presence of prolapse, and the caudal extent of prolapse were detected prospectively on MR images in all five cases. Prospective localization of the stalk in two cases aided subsequent hysteroscopic resection. MR imaging correctly indicated the presence of hemorrhage in one, degeneration in a second, and the absence of these complications in two others. In the fifth case, a hemorrhagic focus in the distal tip of the leiomyoma was not detected on MR images obtained 3 days before surgery.

CONCLUSION. MR imaging is useful for the diagnosis and characterization of uterine leiomyomas that have prolapsed into the cervical or vaginal canal.

AJR 159:555–558, September 1992

Leiomyomas are the most common tumors of the uterus; they occur in 20–30% of women more than 30 years old [1]. Submucosal leiomyomas, which constitute 5% of uterine leiomyomas, may be pedunculated and may be expelled from the uterine cavity [2, 3]. In a recent study [4] of 1785 women undergoing abdominal surgery for uterine leiomyomas, the prevalence of prolapsing submucosal leiomyomas was 2.5%. As the MR appearance of prolapsed leiomyomas has not been reported, we describe five surgically confirmed cases that were diagnosed prospectively on the basis of MR findings.

Subjects and Methods

From January 1989 to December 1991, 916 women had pelvic MR imaging at our institution. In five of these patients, a prolapsed uterine leiomyoma was diagnosed prospectively on the basis of the MR findings. The age range of the five patients was 33–53 years (mean, 43 years). Signs and symptoms included vaginal bleeding (four patients), vaginal discharge (three patients), fever (two patients), and pain in the lower abdomen (one patient). Four of the five patients were anemic, with hematocrits of 29–33% (0.29–0.33). Additionally, four of the five were nulliparous; two of these had previously had spontaneous abortions, one was infertile, and one had not attempted to become pregnant. Pelvic sonography, performed in three patients within 1 week (average, 5 days) before MR imaging, did not allow prospective diagnosis of the prolapse. In two of the five patients, a prolapsed leiomyoma was detected on physical examination before MR imaging, one in the cervix and one in the vagina. Final diagnosis was established by surgery in all five cases. Two patients had total abdominal

Received February 6, 1992; accepted after revision April 10, 1992.

[1] All authors: Department of Diagnostic Radiology, Yale University School of Medicine, 333 Cedar St., New Haven, CT 06510. Address reprint requests to E. Panageas.

0361-803X/92/1593-0555
© American Roentgen Ray Society

hysterectomy and bilateral salpingo-oophrectomy, two patients had hysteroscopic resection, and one had transvaginal removal with curettage.

MR imaging was performed on a 1.5-T unit (Signa, GE Medical Systems, Milwaukee, WI). All patients were studied with T1-weighted spin-echo (400–700/13–20 [TR/TE]) images in either axial or coronal plane. T2-weighted spin-echo (1500–2000/20, 80) or fast spin-echo (2900–4983/126) images were obtained in both sagittal and axial planes in five patients and in the coronal plane in four. Conventional spin-echo images were acquired by using a 128 × 256 matrix, two excitations, and 5- to 7-mm slice thickness. Fast spin-echo images [5] were acquired by using a 256 × 256 matrix, four excitations and 4- to 5-mm slice thickness. All sequences included spatial presaturation superior and inferior to the imaging volume, respiratory compensation, and 50% interslice gaps. A body coil was used with three patients to obtain a 28- to 32-cm field of view, and a pelvic phased-array coil was used with two patients to obtain a 20-cm field of view.

Images were evaluated prospectively for size, signal intensity on T1- and T2-weighted images, the presence or absence of an identifiable stalk, and caudal extent of the prolapsed leiomyoma. MR signal features were correlated with pathologic findings.

Results

In all five cases, MR imaging clearly showed a uterine leiomyoma prolapsing into either the endocervical canal (three cases) or the vaginal canal (two cases). Surgery confirmed the accuracy of MR imaging in defining the caudal extent of the leiomyomas. The leiomyomas, including the stalk and attachment site, were well circumscribed and were delineated best on T2-weighted images (Fig. 1A). The stalk and its uterine attachment was detected in two of the five cases (Figs. 1B and 2).

The diameter of the tumors was 2–8 cm. The three smaller leiomyomas (diameters of 2, 2, and 3 cm) were homogeneous and had low or intermediate signal intensity on both T1- and T2-weighted images (Figs. 1–3). Pathologic examination showed whorls of smooth muscle without degeneration. Pathologic examination of the 3-cm leiomyoma also showed a hemorrhagic focus in the distal tip of the tumor that was not seen on MR imaging (Fig. 3). The larger leiomyomas (diame-

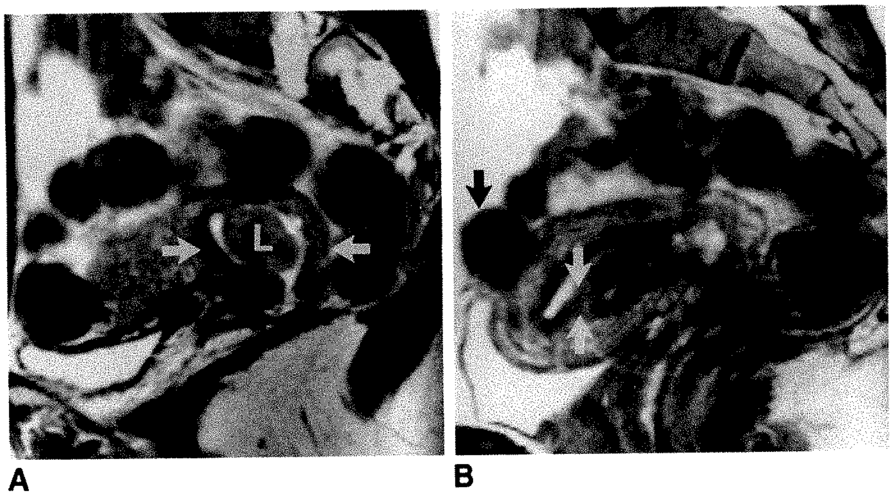

Fig. 1.—Leiomyoma prolapsing into endocervical canal, not detected on physical examination, in 33-year-old woman with heavy vaginal bleeding and anemia.

A, Sagittal T2-weighted (4500/126) fast spin-echo MR image shows well-circumscribed 2-cm leiomyoma (L) with homogeneous low signal intensity within endocervical canal (*arrows*).

B, Sagittal T2-weighted (4500/126) fast spin-echo MR image shows stalk (*white arrows*) arising from anterior fundal myometrium. Detection of stalk permitted hysteroscopic resection. Submucosal leiomyoma (*black arrow*) also is present.

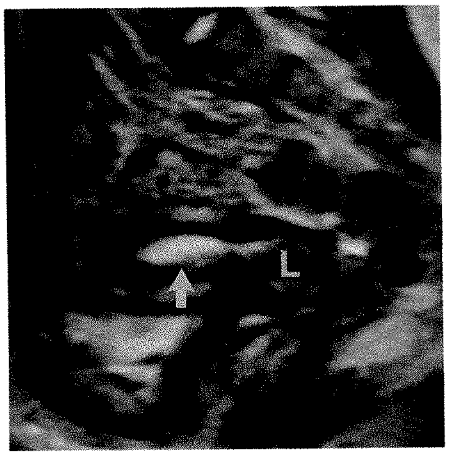

2

Fig. 2.—Unsuspected prolapsing leiomyoma in 42-year-old woman with infertility, chronic anemia, and heavy vaginal bleeding. T2-weighted (1700/80) sagittal MR image shows 2-cm pedunculated leiomyoma (L) with homogeneous low signal intensity within cervical canal. Stalk (*arrow*) and its myometrial origin were detected prospectively, which enabled hysteroscopic resection.

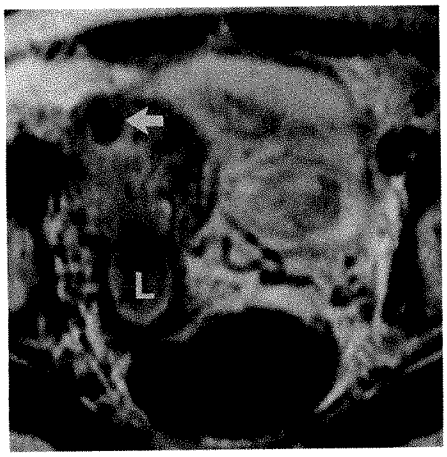

3

Fig. 3.—Leiomyoma prolapsing into endocervical canal, detected on physical examination, in 53-year-old perimenopausal woman with irregular bleeding, clear vaginal discharge, and fever. Axial T2-weighted (2000/80) MR image shows 3-cm leiomyoma (L) with homogeneous intermediate signal intensity in endocervical canal. Intramural leiomyoma (*arrow*) also is shown.

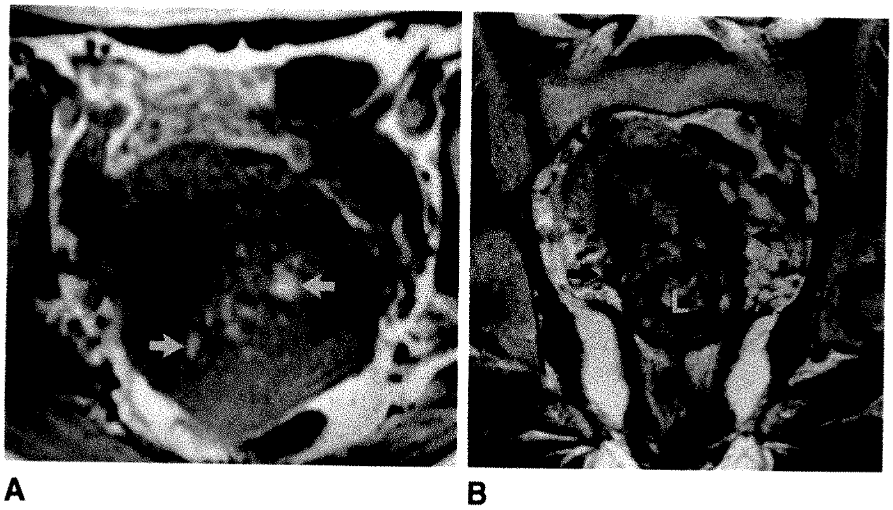

Fig. 4.—Hemorrhagic leiomyoma prolapsing into vaginal canal, detected on physical examination, in 50-year-old woman with heavy vaginal bleeding and anemia.

A, Axial T1-weighted (500/11) MR image shows focal areas (*arrows*) of increased signal intensity within 6-cm leiomyoma that represent hemorrhage.

B, Coronal T2-weighted (3017/126) fast spin-echo MR image shows heterogeneous areas of increased signal intensity within leiomyoma (L) corresponding to hemorrhage. External cervical os (*arrows*) is dilated.

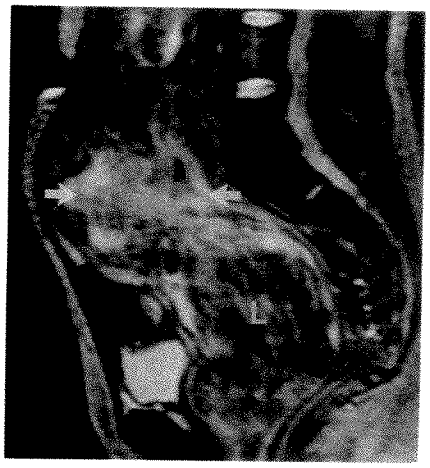

Fig. 5.—Degenerated leiomyoma prolapsing into upper vaginal canal in 37-year-old woman who had curettage 1 month earlier because of demise of fetus at 16 weeks' gestation due to leiomyomas. Patient had pelvic pain, purulent vaginal discharge, fever, and anemia. Prolapsing leiomyoma was not detected on physical examination performed 1 day before MR imaging. Sagittal T2-weighted (1700/80) MR image shows heterogeneous areas of increased signal intensity within leiomyoma (L) corresponding to degeneration. Debris within endometrial cavity (*arrows*) represents pyometria.

ters of 6 and 8 cm) had heterogeneous signal intensity on MR imaging. The 6-cm leiomyoma had mostly low signal intensity on T1- and T2-weighted images, with focal areas of increased signal intensity on both pulse sequences (Fig. 4) corresponding to pathologic evidence of hemorrhage. The 8-cm leiomyoma had low signal intensity on T1-weighted images and high signal intensity on T2-weighted images (Fig. 5), corresponding to degeneration and infarction observed at pathologic examination.

Discussion

MR imaging is useful in the evaluation of pelvic disorders [6–8], especially in the detection and localization of leiomyomas [9–11]. A pedunculated leiomyoma is usually detected on physical examination once the tumor has prolapsed into the vaginal canal. Before prolapse through the external cervical os occurs, it may be difficult to diagnose the tumor on the basis of physical findings [3]. We had one patient with a leiomyoma prolapsing into the upper vaginal canal that was not seen on physical examination performed 1 day before MR imaging. The leiomyoma may have advanced into the vaginal canal during the interval. The longer the pedunculated submucosal leiomyoma is unsuspected, the higher is the prevalence of infarction and pyometria caused by twisting of the leiomyoma around its pedicle and impairment of its blood supply [2]. Frequently the patients are also anemic because of prolonged vaginal bleeding [2, 4]. In our small series, sonography was not useful for the prospective diagnosis of prolapse. MR imaging, however, can be instrumental in the early detection of a prolapsed leiomyoma. In three of our five patients, the diagnosis of prolapse was established initially on the basis of MR findings.

MR imaging can further delineate the prolapsing leiomyoma by showing the stalk and its uterine attachment. This provides important clinical information that can help in determining the surgical approach and thus decrease the length of the procedure. In two of our patients, detection of the stalk on MR images facilitated subsequent hysteroscopic removal of the leiomyoma. The surgical procedure performed is determined by the size of the leiomyoma; presence or absence of a stalk; and the patient's age, desire to preserve fertility, and clinical condition [3].

On MR images, most leiomyomas are uncomplicated, have dense spindle muscle cells, and have homogeneous low signal intensity on all pulse sequences [11, 12]. In our series, the absence of degeneration or hemorrhage in two prolapsing leiomyomas was predicted correctly on the basis of MR findings of low or intermediate signal intensity on all pulse sequences. In a third case, pathologic examination showed a small focus of hemorrhage that was not detected 3 days earlier on MR images and that may have been related to surgical manipulation or focal bleeding after the MR study. Complications, including degeneration and hemorrhage, usually show various degrees of heterogeneity with high signal intensity on T2-weighted images [13]. The type of degeneration, including hyaline, myxomatous, fatty, mucinous, or malignant, cannot be differentiated [11–13]. Hemorrhage produces variable MR appearances depending on imaging sequences used and the duration of the bleeding. Areas of hemorrhage within a leiomyoma can have high signal intensity on both T1- and T2-weighted images [13]. However, mucinous cystic degeneration [11] and lipoleiomyoma [14] can have similar signal. We accurately predicted (1) the presence of focal hemorrhage in the 6-cm prolapsing leiomyoma that had focal areas of increased signal intensity on T1- and T2-weighted images and (2) degeneration in the 8-cm leiomyoma that had heterogeneous areas of increased signal intensity on T2-weighted images.

We could not determine the sensitivity for the diagnosis of prolapsing uterine leiomyomas because not all patients undergoing MR imaging have surgery. The specificity in our small series is high (100%), because all five patients with an MR-based diagnosis of prolapse had surgically confirmed prolapsing leiomyoma. Although cervical carcinoma or endocervical extension of endometrial carcinoma may be detected as masses extending into the cervix or vagina, the mostly low signal intensity and well-circumscribed margin of prolapsing leiomyoma should allow differentiation.

In conclusion, MR imaging enables prospective detection of leiomyomas prolapsing into the cervical or vaginal canal. Prolapse into the cervix may be undetectable by physical examination and thus prolapse may be diagnosed earlier by MR imaging. Identification of a stalk can influence how the prolapse is treated.

REFERENCES

1. Silverberg SH. *Principles and practice of surgical pathology*. New York: Wiley, **1983**:1323–1327
2. Riley P. Treatment of prolapsed submucous fibroids. *S Afr Med J* **1982**;62:22–24
3. Dicker D, Feldberg D, Dekel A, Yeshaya A, Samuel N, Goldman JA. The management of prolapsed submucous fibroids. *Aust NZ J Obstet Gynecol* **1986**;26:308–311
4. Ben-Baruch G, Schiff E, Menashe Y, Menczer J. Immediate and late outcome of vaginal myomectomy for prolapsed pedunculated submucous myoma. *Obstet Gynecol* **1988**;72:858–861
5. Smith RC, Reinhold C, McCauley TR, Kier R, McCarthy S. Comparison of conventional and fast spin-echo body coil MR imaging of the female pelvis. *Radiology* (in press).
6. Lee JKT, Gersell DJ, Balfe DM, Worthington JL, Picus D, Gapp GV. The uterus: in vitro MR—anatomic correlation of normal and abnormal specimens. *Radiology* **1985**;157:175–179
7. Hricak H. MRI of the female pelvis; a review. *AJR* **1986**;146:1115–1122
8. McCarthy S. MR imaging of the uterus. *Radiology* **1989**;171:321–322
9. Weinreb JC, Barkoff ND, Megibow A, Demopoulos R. The value of MR imaging in distinguishing leiomyomas from other solid pelvic masses when sonography is indeterminate. *AJR* **1990**;154:295–299
10. Zawin M, McCarthy S, Scoutt LM, Comite F. High-field MRI and US evaluation of the pelvis in women with leiomyomas. *Magn Reson Imaging* **1990**;8:371–376
11. Hricak H, Tscholakoff D, Heinrichs L, et al. Uterine leiomyomas: correlation of MR, histopathologic findings, and symptoms. *Radiology* **1986**;158: 385–391
12. Dudiak CM, Turner DA, Suresh KP, Archie JT, Silver B, Norusis M. Uterine leiomyomas in the infertile patient: preoperative localization with MR imaging versus US and hysterosalpingography. *Radiology* **1988**;167: 627–630
13. Hamlin DJ, Pettersson H, Fitzsimmons J, Morgan LS. MR imaging of uterine leiomyomas and their complications. *J Comput Assist Tomogr* **1985**;9:902–907
14. Dodd GD III, Lancaster KT, Moulton JS. Ovarian lipoleiomyoma: a fat-containing mass in the female pelvis. *AJR* **1989**;153:1007–1008

Temporomandibular Joint:

Relationship Between MR Evidence of Effusion and the Presence of Pain and Disk Displacement

Per-Lennart Westesson[1]
Sharon L. Brooks[1,2]

OBJECTIVE. The purpose of this study was to correlate MR evidence of joint effusion in the temporomandibular joint with symptoms of joint pain and the presence of disk displacement and arthrosis.

SUBJECTS AND METHODS. The temporomandibular joints of 379 patients with clinical symptoms of temporomandibular joint disorders and 11 asymptomatic volunteers were imaged bilaterally. Sagittal and coronal proton density-weighted and T2-weighted images were obtained. Imaging findings of joint effusion were correlated with the presence of disk displacement and arthrosis and the symptom of pain.

RESULTS. MR showed effusion in 7% of the joints with normal superior disk position, 40% of the joints with disk displacement with reduction, 50% of the joints with disk displacement without reduction, and 27% of the joints with arthrosis. Two of the control subjects had disk displacement with reduction; MR did not show joint effusion in any of the control subjects. A strong association was seen between joint effusion and joint pain. Joint effusion was seen in 46% of the joints on the more painful side and in 13% of the joints on the less painful side.

CONCLUSION. The results show that temporomandibular joint effusions primarily occur in joints with disk displacement and are strongly associated with joint pain.

AJR 159:559–563, September 1992

Disk displacement and arthrosis are the most common findings on MR images of the temporomandibular joint (TMJ) in patients with signs and symptoms of a TMJ disorder [1–9]. Disk displacement is defined as an abnormal relationship between the disk and mandibular condyle involving an anterior, medial, or lateral displacement of the disk from its normal position superior to the condyle. These abnormalities are often but not always associated with pain. Clinically, we have noted that MR evidence of joint effusion is frequently present in painful joints with disk displacement but rarely in normal joints. If a strong association between the presence of joint effusion and an abnormal and painful joint could be established, this could be the basis for valuable additional diagnostic information from MR imaging of the TMJ. The purpose of this study was to systematically correlate MR findings of joint effusion with different stages of disk displacement, arthrosis, and the clinical symptom of pain.

Subjects and Methods

We studied the left and right TMJs of 390 subjects; 379 were patients referred for MR imaging because of signs and symptoms of TMJ disorders, and 11 were asymptomatic control subjects. Before the MR imaging, each patient indicated which side of the jaw was the more painful. Twenty-two patients had a similar degree of pain in both left and right joints. In these 22 patients, both joints were classified as "more painful." The asymptomatic control subjects were all free of pain.

MR imaging was performed on a 1.5-T Signa MR scanner (General Electric, Milwaukee,

Received February 18, 1992; accepted after revision April 10, 1992.

This work was supported by the Torsten and Ragnar Söderbergs Foundations, Stockholm, Sweden.

[1] Department of Radiology, University of Rochester School of Medicine and Dentistry, 601 Elmwood Ave., Rochester, NY 14642-8694. Address reprint requests to P-L. Westesson.

[2] Present address: Department of Oral Medicine/Pathology/Surgery, University of Michigan School of Dentistry, Ann Arbor, MI 48109 and Department of Radiology, University of Michigan School of Medicine, Ann Arbor, MI 48109.

0361-803X/92/1593-0559
©American Roentgen Ray Society

WI) with bilateral 6 × 8 cm surface coils. Four pulse sequences were obtained: (1) axial localizer (300/16 [TR/TE], 0.5 excitations, 18-cm field of view [FOV], and a 256 × 128 matrix), (2) sagittal closed-mouth (2000/20, 80, 0.5 excitations, 10-cm FOV 256 × 192 matrix), (3) sagittal open-mouth (1500/20, 80, 0.75 excitations, 10-cm FOV, 256 × 128 matrix), and (4) coronal closed-mouth (2000/20, 80, 0.5 excitations, 10-cm FOV, 256 × 192 matrix). The joints were classified as (1) normal when the disk was located superior to the condyle, (2) disk displacement with reduction when the disk was displaced at the closed-mouth position and in the normal position in the open-mouth images, (3) disk displacement without reduction when the disk was displaced in both the closed- and open-mouth positions, and (4) arthrosis when osseous changes such as flattening, osteophytosis, or erosions of the condyle or temporal components were present. No distinction was made between anterior, lateral, and medial displacements. After the closed-mouth image was obtained, the patient was instructed to open the mouth as wide as possible to obtain reduction of a displaced disk. Then the patient was asked to close slightly to a comfortable degree of mouth opening. A syringe wrapped in wet gauze was given to the patient before going into the scanner. This syringe was placed between the upper and lower teeth by the patient while in the scanner to stabilize the lower jaw for the open-mouth scans. Different size syringes (5, 10, and 20 ml) were used according to what was a comfortable degree of mouth opening in the individual patients.

On T2-weighted images (2000/80), joint effusion was identified as an area of high signal intensity in the region of the upper or lower joint spaces. We regarded the images as showing no effusion when no area of high signal (Fig. 1) or a line of high signal along the articular surface (Fig. 2) was seen on T2-weighted images. When more than a line of high signal was present, we regarded this as joint effusion (Fig. 3).

Results

In nine of the 11 asymptomatic control subjects, the joints were classified as normal. In the other two, one showed unilateral disk displacement with reduction and one had bilateral disk displacement with reduction. None of the control subjects had MR evidence of joint effusion. In the rest of the results, the MR findings of the control subjects and the patients were combined according to the MR diagnosis.

MR showed joint effusion in 7% of the 261 joints with normal superior disk position, 40% of the 216 joints with disk displacement with reduction, 50% of the 221 joints with disk displacement without reduction, and 27% of the 82 joints with arthrosis. An example of a joint with disk displacement

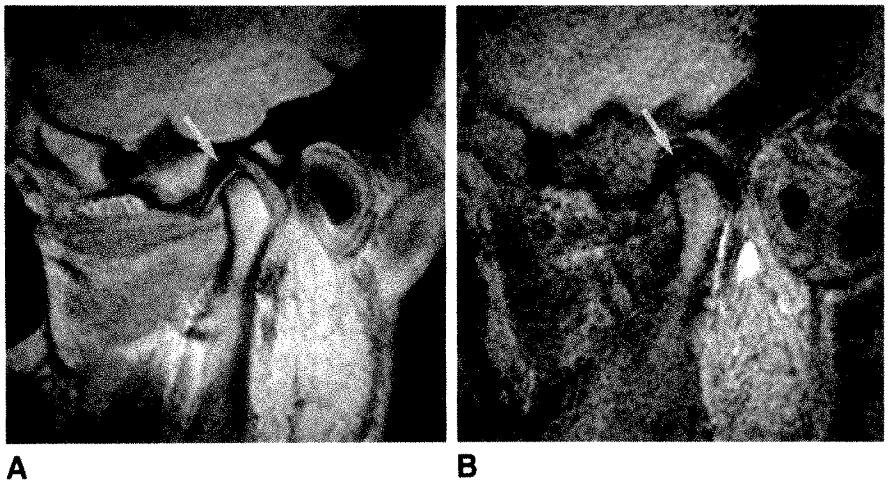

Fig. 1.—*A* and *B*, Proton density-weighted (2000/20, *A*) and T2-weighted (2000/80, *B*) sagittal MR images show normal temporomandibular joint with no evidence of joint effusion. *Arrow* = posterior band of disk. For optimal image quality, *B* shows tissue layer 3 mm more lateral than *A*.

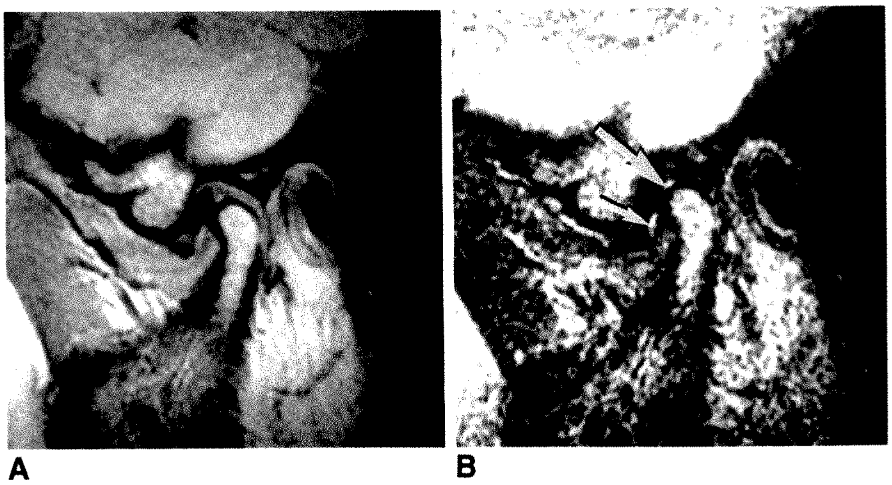

Fig. 2.—*A* and *B*, Proton density-weighted (2000/20, *A*) and T2-weighted (2000/80, *B*) sagittal MR images at closed-mouth position show minimal anterior disk displacement and lining of joint effusion (*arrows* in *B*). This lining of high signal was not classified as joint effusion.

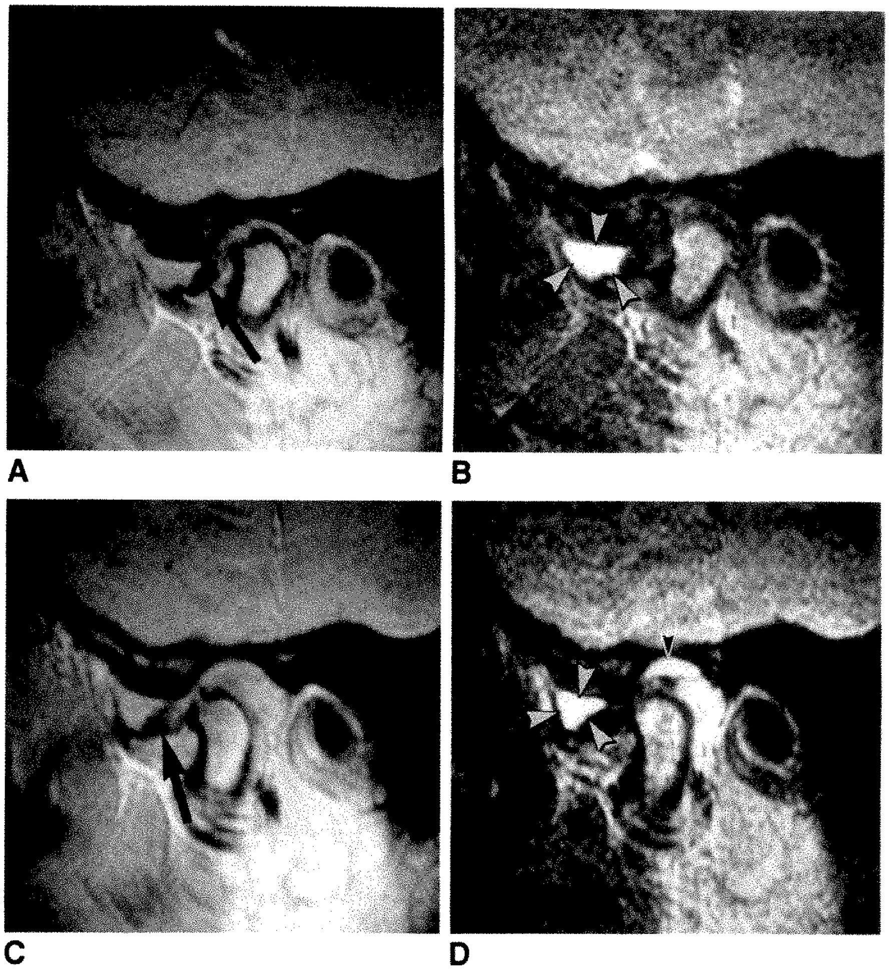

Fig. 3.—*A–D*, Proton density-weighted (2000/20, *A* and *C*) and T2-weighted (2000/80, *B* and *D*) sagittal MR images at closed (*A* and *B*) and open-mouth position (*C* and *D*) show anterior disk displacement without reduction and joint effusion. Disk (*arrow* in *A* and *C*) is anteriorly displaced both at closed- (*A* and *B*) and open-mouth (*C* and *D*) positions. Joint effusion (*arrowheads*) is visible in anterior recess of upper joint space (*B* and *D*). At open-mouth position, joint effusion in anterior recess (*large arrowheads* in *D*) is slightly decreased and a second collection is seen in posterior recess of upper joint space (*small arrowhead* in *D*).

without reduction and joint effusion is seen in Figure 3. A joint with arthrosis and no joint effusion is seen in Figure 4.

Three-hundred sixty-eight joints were on the less painful side and 412 were on the more painful side. A strong association was seen between MR evidence of joint effusion and pain ($p < .001$). Thus 46% of the more painful joints had areas of high signal in the region of the joint spaces on the T2-weighted images compared with 13% of the less painful joints. The T2-weighted images also were helpful in evaluating perforations of the posterior attachment because of the arthrographic effect of joint effusion (Fig. 5).

Discussion

We found MR evidence of joint effusion in about 30% of joints in a consecutive series of patients referred for MR imaging of the TMJ because of signs and symptoms of TMJ disorders. The association between MR evidence of joint effusion and joint pain was highly significant. The percentage of joints with joint effusion was greater in patients with the more advanced stages of disk displacement (displacement without reduction) than in those with the earlier stage (disk displacement with reduction). The prevalence of joint effusion was even lower in joints with arthrosis. These results indicate that joint effusion is associated with painful disk displacement. The results are in accordance with those of previous studies [6–8], although a systematic correlation between different stages of disk displacement and pain has not been reported earlier.

We did not quantify the amount of joint effusion. Instead, we subjectively determined the presence or absence of joint effusions. Collections of fluid in the joint as shown in Figure 3 were classified as joint effusion, but small amounts of high-signal material lining the articular surfaces (Fig. 2) were seen in normal joints also and were classified as no effusion. A lining of fluid on the articular surface is probably of no clinical significance and cannot be used to distinguish painful from asymptomatic joints. It would be preferable to quantify the amount of joint effusion, but this technology was not available. Seven percent of the normal joints had MR evidence of joint effusion. Although joint effusion was seen in a few normal joints, none of these joints had significant collections like those seen in some of the joints with disk displacement (Fig. 3). We think that quantification of the amount of joint effusion would have shown a stronger association between joint effusion, joint pain, and disk displacement.

The prevalence of joint effusion was lower in joints with arthrosis than in those with disk displacement. This is con-

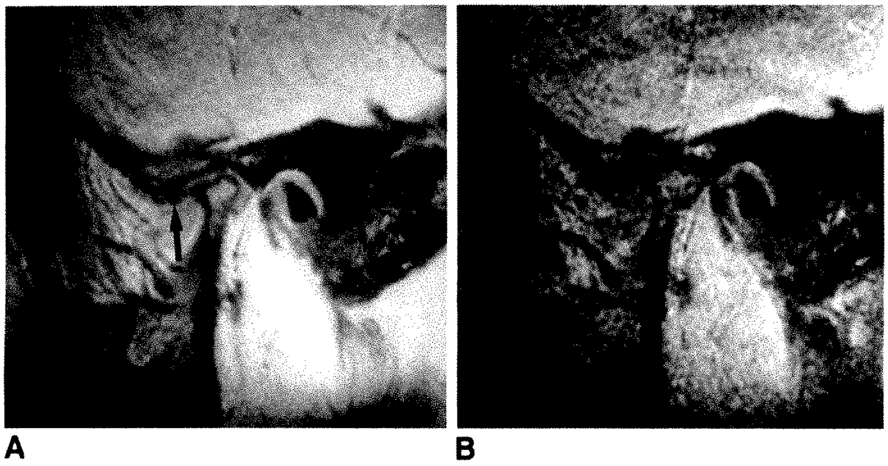

Fig. 4.—*A* and *B*, Proton density-weighted (2000/20, *A*) and T2-weighted (2000/80, *B*) sagittal MR images at closed-mouth position show arthrosis and no joint effusion. Condyle is flattened with an anterior osteophyte, articular eminence is flattened, and disk (*arrow* in *A*) is anteriorly displaced.

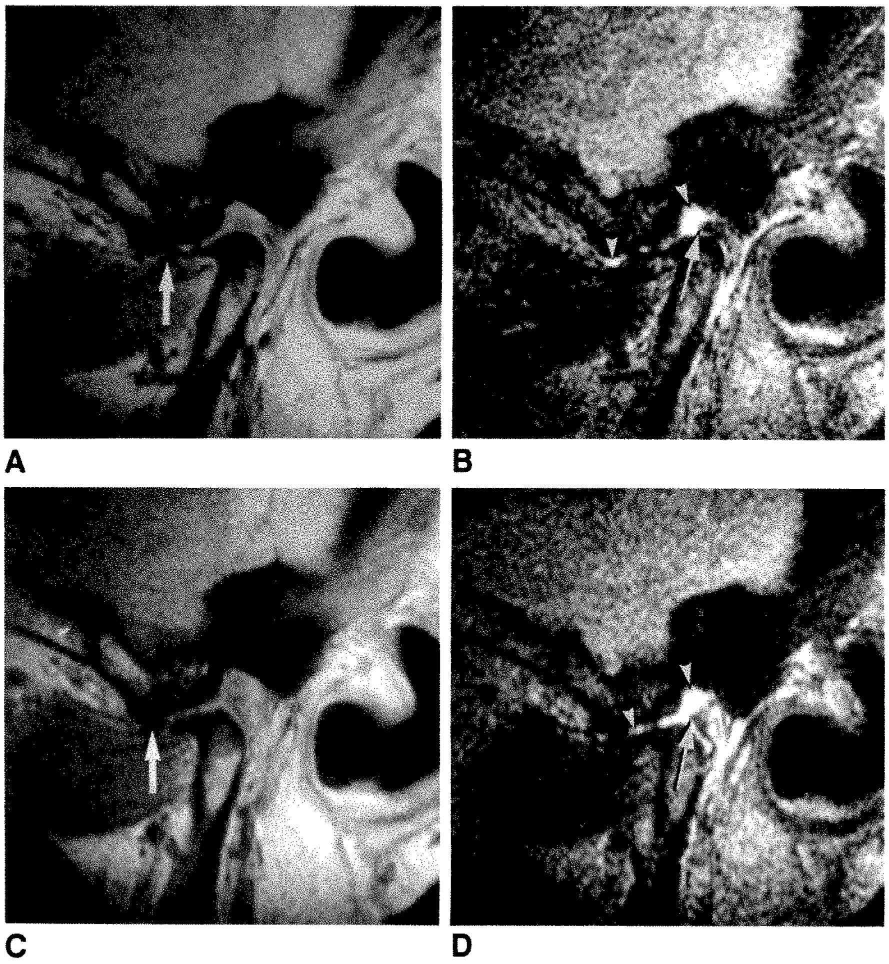

Fig. 5.—*A*–*D*, Proton density-weighted (2000/20, *A* and *C*) and T2-weighted (2000/80, *B* and *D*) sagittal MR images at closed- and open-mouth positions show arthrosis, joint effusion, and perforation of posterior disk attachment. Condyle shows anterior osteophyte, articular eminence is irregular, and disk (*arrow*) is anteriorly displaced and severely deformed. Joint effusion (*arrowheads* in *B* and *D*) is present in glenoid fossa and along articular eminence. Edge (*arrow* in *B* and *D*) of a perforation of posterior disk attachment is detected as a result of arthrographic effect of joint effusion.

sistent with observations in other joints that indicated that most effusions are seen before arthrosis develops. It also is consistent with the clinical experience that patients usually had the most symptoms with disk displacement. Symptoms are frequently less prominent when arthrosis has developed.

The results of the study further emphasize that MR imaging is a valuable tool for imaging abnormalities of the TMJ in patients who have clinical signs and symptoms of disk displacement. The high prevalence of joint effusion and the strong association between effusion and joint pain make the diagnostic information obtained with the use of MR imaging valuable. Thus, if joint effusion is seen in an abnormal joint, it appears likely that this joint has some degree of pain. This information is valuable to both the clinician and the radiologist for confirming that the joint is abnormal. For these reasons, it seems wise to routinely include T2-weighted images in an MR study of the TMJ. On T2-weighted images, the arthrographic "effect" caused by joint effusion occasionally helped in defining the extent of a perforation of the posterior disk attachment (Fig. 5). This is another reason to obtain T2-weighted images.

Before the advent of MR imaging, only a few reports [10–12] described joint effusion in the TMJ. For obvious reasons, these were related to larger collections of fluid in the joint. MR imaging has clearly shown that joint effusion is more prevalent than previously thought; in one study [6, 7] 88% of patients with painful TMJs had MR evidence of joint effusion.

Although its cause is unknown, joint pain has four probable sources: (1) compression of the highly vascularized and innervated posterior disk attachment, (2) stretching and pulling in the capsule and disk attachment, (3) inflammatory changes in the joint capsule with synovitis, and (4) distension of the joint space due to large joint effusions.

In this study, we obtained both sagittal and coronal T2-weighted images. We found that these two planes are complementary, and we routinely obtain T2-weighted images in both planes in all patients. In many cases, joint effusion was seen in both projections, but in several instances, it was seen in only one of the two planes. For this reason, we suggest that both sagittal and coronal T2-weighted images be obtained. In the past, obtaining T2-weighted images was time-consuming, and these images were not used routinely. However, the increased signal-to-noise ratio associated with the use of smaller surface coils and upgrades of the MR scanner make it possible now to obtain high-quality T2-weighted images of the TMJ in less than 4 min. Attempts have been made to use gradient-recalled acquisition in steady state (GRASS) imaging, but this has not been as successful as regular T2-weighted images [6]. We do not routinely obtain T1-weighted images of the TMJ. We believe that T1-weighted images offer no significant advantage over proton density–weighted images (2000/20).

In conclusion, this study has shown a strong association between joint pain and evidence of joint effusion. Furthermore, joint effusions were seen more often in joints with more advanced stages of disk displacement than in normal joints or in joints with earlier stages of disk displacement. Joint effusion probably represents an inflammatory response to the dysfunction of the displaced disk. The presence of joint effusion is valuable diagnostic information because it confirms that the joint is abnormal and sometimes helps delineate the anatomy. For these reasons, T2-weighted imaging is recommended as a routine part of MR imaging of the TMJ.

REFERENCES

1. Harms SE, Wilk RM, Wolford LM, Chiles DG, Milam SB. The temporomandibular joint: magnetic resonance imaging using surface coils. *Radiology* **1985**;157:133–136
2. Katzberg RW, Schenck J, Roberts D, et al. Magnetic resonance imaging of the temporomandibular joint meniscus. *Oral Surg Oral Med Oral Pathol* **1985**;59:332–335
3. Katzberg RW, Bessette RW, Tallents RH, et al. Normal and abnormal temporomandibular joint: MR imaging with surface coil. *Radiology* **1986**;158:183–189
4. Roberts D, Schenk J, Joseph P, et al. Temporomandibular joint: magnetic resonance imaging. *Radiology* **1985**;155:829–830
5. Katzberg RW, Westesson P-L, Tallents RH, et al. Temporomandibular joint: MR assessment of rotational and sideways disk displacements. *Radiology* **1988**;169:741–748
6. Schellhas KP, Wilkes CH. Temporomandibular joint inflammation: comparison of MR fast scanning with T1- and T2-weighted imaging techniques. *AJR* **1989**;153:93–98
7. Schellhas KP, Wilkes CP, Baker CC. Facial pain, headache, and temporomandibular joint inflammation. *Headache* **1989**;29:229–232
8. Schellhas KP, Wilkes CH, Omlie MR, et al. The diagnosis of temporomandibular joint disease: two-compartment arthrography and MR. *AJR* **1988**;151:341–350
9. Paesani D, Westesson P-L, Hatala M, Tallents RH, Kurita K. Prevalence of internal derangement in patients with craniomandibular disorders. *Am J Orthod Dentofac Orthop* **1992**;101:41–47
10. Cooksey DE, Girard K. Temporomandibular joint synovitis with effusion in familial Mediterranean fever. *Oral Surg Oral Med Oral Pathol* **1979**;47:123–126
11. Wenneberg B. Inflammatory involvement of the temporomandibular joint: diagnostic and therapeutic aspects and a study of individuals with ankylosing spondylitis. *Swed Dent J Suppl* **1983**;20:1–54
12. Kopp S, Wenneberg B, Clemensson E. Clinical, microscopical and biochemical investigation of synovial fluid from temporomandibular joints. *Scand J Dent Res* **1983**;91:33–42

Plural Effusions

Peter M. Ronai[1]

George Orwell, in an essay entitled "Why I Write," commented, "Writing a book is a horrible, exhausting struggle, like a long bout of some painful illness" [1]. Surely, writing a good medical paper may be no less agonizing. For most persons, writing well is *very* difficult. What is good writing?

Good writing is succinct, accurate, clear, and unambiguous. It grabs the attention, conveys a message, elicits a response. Writing well is hard work. It takes much longer than does writing badly. Perhaps that is why so few scientists write well—they simply do not have the time. Many scientists write so poorly that "scientific literature"—like "military intelligence"—has become an oxymoron. It may be scientific, but it certainly is not literature. (Indeed, some of it is so badly written, it is no longer even scientific.)

Why is it important to write well?

> Careless words are costly. Friendships have been severed, elections lost, fortunes dissolved, marriages disrupted, men murdered, and peaceful international relations exploded by verbal bungling. Yet most of us continue to treat language indifferently or casually . . . . Careless language is particularly hazardous in scientific disciplines, where precision is paramount. Yet scientists who work tirelessly to perfect a laboratory or clinical technic sometimes neglect the medium through which they communicate their observations and discoveries to the world [2].

Why is it so difficult to write well?

> A large part of the problem is inherent to language. Language is the subtlest of all tools, and its effective use requires the skill of a master craftsman. The English language, in particular, is almost limitless in its richness and complexity. It holds many pitfalls for the unwary, the careless, the ignorant, the inept [3].

One of these pitfalls is the correct use of plurals.

Plural Effusions

Because medicine has so many words of Greek or Latin origin, medical writers frequently have trouble with plurals. The following errors are commonly found in radiologic journals: the contrast *media was* injected, the *data was* analyzed, *a criteria*, *a phenomena*, *septae*, *diverticulae*. Media is a plural noun: one contrast medium, several contrast media—hence, the contrast *medium was* injected. Similarly, one datum, several data—hence, the *data were* analyzed. Criterion and phenomenon are singular, criteria and phenomena are plural—hence, *a criterion*, *a phenomenon*. Septum and diverticulum are singular, septa and diverticula plural. *Septae and diverticulae are not real words*. Some writers get the plural right but get the facts wrong: one author referred to the corpora spongiosa of the penis. Excellent Latin, terrible anatomy: there are two corpora cavernosa, but only one corpus spongiosum.

Consistency in plural forms is important. If you use the Latin or Greek form of the plural, do not mix it with the anglicized form: femora and tibiae or femurs and tibias, but not femurs and tibiae.

The biggest problem with plurals for most authors is mismatch between subject and verb. The following examples are taken from the recent radiologic literature: "Both the number and complexity increases"; "The CT findings and potential role of CT in . . . has not been described"; and this unusual example of the reverse mismatch: "A small amount of ascites were also found." A singular subject requires the singular form of the verb, and a plural subject requires the plural form. If the subject is "x and y," a plural verb is needed even if both x and y are singular, hence: "Both the number and complexity increase." If the subject is "x or y" (or "neither x nor y") and both x and y are singular, use a singular verb; if one is singular and the other plural, the verb matches the closer subject, for example: "Neither the potential role of CT nor the CT findings have been described." Units of measure (grams, liters) are used in a collective sense and take the singular form of the verb: "One hundred milliliters of contrast medium was infused." If you use a plural subject with a singular verb or vice versa, you may send your reader on a search for another subject, with fruitless or—worse—erroneous results.

Even authors who know these rules can get into trouble when they write long, complex sentences in which subject(s) and verb become widely separated. Clearly, subject-verb congruence is much easier to control in short sentences.

Future vignettes in this series will address more of the commonly encountered problems in medical writing.

REFERENCES

1. Orwell G. England your England: why I write. Quoted in: Muir F. *An irreverent and thoroughly incomplete social history of almost everything.* New York: Stein and Day, **1976**:103
2. DeBakey L. Every careless word that men utter. I. The English language. *Anesth Analg* **1970**;49:567–574
3. I'm afraid I made this up myself.

---

[1] Department of Imaging, Salem Hospital, P. O. Box 14001, Salem, OR 97309.

Editor's note.—This is the first of several vignettes, which will appear periodically in *AJR*, examining some of the common pitfalls of medical writing. The intent is to help authors communicate their observations and discoveries clearly and in accordance with accepted grammatical style.

***AJR* 159:564, September 1992** 0361–803X/92/1593–0564 © American Roentgen Ray Society

Injuries of the Superior Portion of the Glenoid Labrum Involving the Insertion of the Biceps Tendon:
MR Imaging Findings in Nine Cases

Juerg Hodler[1,2]
Sevil Kursunoglu-Brahme[3,4]
Bonnie Flannigan[3]
Stephen J. Snyder[5]
Ronald P. Karzel[5]
Donald Resnick[1]

The goal of this investigation was to describe the MR appearance of traumatic fraying or detachment of the superior portion of the glenoid labrum including the insertion of the tendon of the long head of the biceps. This condition is caused either by an acute injury or by repeated overhead motion during participation in sports. In nine patients with such a lesion, the arthroscopic report and MR images were available for review. These patients were 22-64 years old (mean, 38). In four patients only fraying was noted during arthroscopy, in four patients the superior part of the labrum was detached together with the insertion of the biceps tendon, and in one case there was a bucket-handle tear of the superior portion of the labrum. The MR images were retrospectively evaluated by three osteoradiologists in conference. Signal changes within the labrum and detachment of the labrum were noted, and the findings were compared with the results of arthroscopy. MR imaging did not allow recognition of simple fraying. In two of the five cases with arthroscopic findings of detachment of the superior labrum from the glenoid rim, differentiation between complete and partial labral detachments was not possible even with MR arthrography. However, in these cases the patient's age and history led to the correct diagnosis.

We conclude that early traumatic abnormalities of the superior portion of the labrum cannot be detected with MR imaging. Complete detachment, however, can be demonstrated if the patient's age and history are taken into consideration.

***AJR* 159:565-568, September 1992**

Most imaging investigations of the glenoid labrum describe anteroinferior lesions in patients with anterior dislocations and, less commonly, posterior labral lesions in those with posterior instability [1-4]. The analysis of the superior portion of the labrum has received less attention. However, detachment of this portion of the labrum and the insertion of the long head of the biceps tendon can cause significant disability [5]. This injury occurs mainly in young and occasionally in middle-aged patients. It may be caused by an acute injury, such as a fall on the outstretched abducted and slightly forward-flexed arm with compression of the superior glenoid structures, by excessive traction either with a sudden pull of the biceps tendon, or by repeated overhead motion during participation in sports. We describe the MR appearances of nine such arthroscopically proved injuries.

Materials and Methods

Thirteen patients with injuries of the superior labrum and the insertion of the biceps tendon came to the attention of one of the authors. From these 13 patients, nine were selected because their arthroscopic reports and MR hard copies were available for review. These patients were 22-64 years old (mean, 38 years) and included eight men and one woman.

In four patients, only fraying of the labrum was noted during arthroscopy; in four other patients, the superior part of the labrum was detached together with the insertion of the biceps tendon. In one case there was a bucket-handle tear of the superior portion of the labrum. Arthroscopic findings associated with these injuries included lesions of the rotator

Received December 30, 1991; accepted after revision February 24, 1992.

[1] Department of Radiology, Veterans Affairs Medical Center, 3350 La Jolla Village Dr., San Diego, CA 92161.

[2] Present address: Department of Radiology, University Hospital, Raemistr. 100, CH-8091 Zurich, Switzerland.

[3] Department of Radiology, Valley Presbyterian Hospital, 15107 Vanowen St., Van Nuys, CA 91405.

[4] Present address: San Diego Diagnostic Radiology Medical Group, 8008 Frost St., Suite 106, San Diego, CA 92123. Address reprint requests to S. Kursunoglu-Brahme.

[5] Southern California Orthopedic Institute, 6815 Noble Ave., Van Nuys, CA 91405-3730.

0361-803X/92/1593-0565
© American Roentgen Ray Society

cuff in five patients (four had a partial rotator cuff tear and one had a full-thickness tear), a humeral head fracture in one patient, and anterior instability in four patients.

MR imaging was performed on a GE Signa 1.5-T scanner (General Electric Medical Systems, Milwaukee, WI). Coronal oblique (oriented in a plane perpendicular to the glenoid fossa) T2-weighted images, 2000/20, 80 (TR/TE), were available for our retrospective review in eight patients. Axial T2- or T2*-weighted spin-echo images were available in seven patients. Two of these patients had spin-echo images (2000/20, 80), and five had gradient-echo images (MPGR [multiplanar gradient-recalled echo]) with a 100/15/10° flip angle sequence in four patients and a 450/15/25° flip angle sequence in one patient. MR arthrography was performed in eight of the nine patients. The use of intraarticular gadopentetate dimeglumine was approved by the investigational review board at Valley Presbyterian Hospital, Van Nuys, CA. In each patient, informed consent was obtained before the examination. Technical details have been described in an earlier report [6]. Both T1-weighted axial and T1-weighted coronal oblique sequences (500–600/20–25) after the injection of 10–15 ml of diluted gadopentetate dimeglumine (Magnevist, Berlex, Wayne, NJ) [6] were obtained. The field of view was 16 cm (20 cm for the MPGR sequences), the slice thickness was 3–4 mm (5 mm in two cases), the interslice gap was 1 mm, the number of excitations was one or two (four for the MPGR images), and the matrix was 128 × 256 or 192 × 256.

Three experienced osteoradiologists simultaneously reviewed the hard copies from MR imaging in conference with regard to signal changes and detachment of the superior labrum. These findings were compared with the arthroscopic reports.

Results

Arthroscopically proved labral fraying as found in four shoulders could not be demonstrated on standard or arthrographic MR images. In two of these shoulders, increased signal was found within the substance of the labrum. This finding was seen best on standard proton-density images. As these patients were 54 and 64 years old, however, it was not certain if the abnormal signal within the labral substance was related to trauma or normal aging (Fig. 1). In two of these cases with labral fraying, contrast medium extended beneath the central attachment of the superior portion of the labrum. The separation of the labrum from the glenoid rim was not complete on these images and was considered normal in view of the patients' ages (54 and 60 years old, respectively). The differential diagnosis from total detachment of the labrum was difficult to determine on the basis of standard proton-density images, however (Figs. 2 and 3).

One of the four cases of complete detachment of the superior portion of the labrum was correctly diagnosed on the basis of the coronal oblique MR arthrographic images by the penetration of contrast medium through the entire base of the labrum. In another patient for whom MR arthrographic images were unavailable, the coronal oblique standard T2-weighted images depicted complete detachment by the presence of joint fluid (Fig. 4). In the last two shoulders with complete detachment of the superior portion of the labrum, fluid penetrated into the base of the superior labrum but did not separate it completely from the glenoid rim. Although the definitive diagnosis of complete detachment could not be made on the basis of these images, such a lesion was suspected because of the incomplete separation, which normally should not be present in relatively young patients (22 and 32 years old) (Fig. 3).

The labral detachment in the single case of a bucket-handle tear of the superior portion of the labrum was readily visible on MR images. However, the intact insertion of the tendon of the long head of the biceps was not depicted.

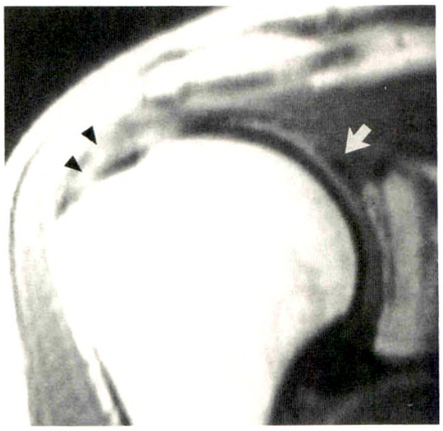

Fig. 1.—Fraying of superior portion of labrum in a 54-year-old woman. Coronal oblique MR image (2000/20) does not depict this finding; however, normally hypointense labrum shows increased signal (*arrow*). This alteration can be due to age-related degenerative changes. Partial tear of supraspinatus tendon involves both articular and bursal surfaces (*arrowheads*).

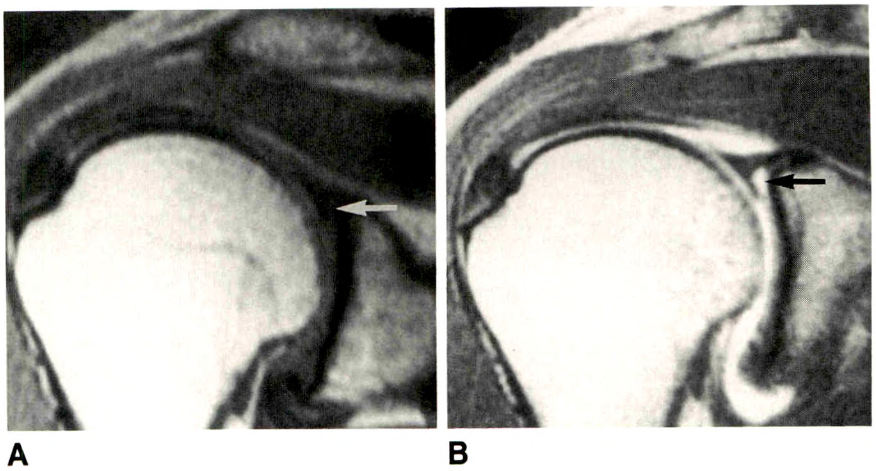

Fig. 2.—Coronal oblique images in a 60-year-old man with fraying of superior portion of labrum.

***A*, MR image (2000/20). Signal at base of labrum corresponds in part to partial detachment of labrum and is caused in part by articular cartilage extending beneath labrum (*arrow*), which appears normal.**

***B*, MR arthrogram (600/20) confirms partial central detachment (*arrow*), which probably is normal in this age group. No labral fraying is visible.**

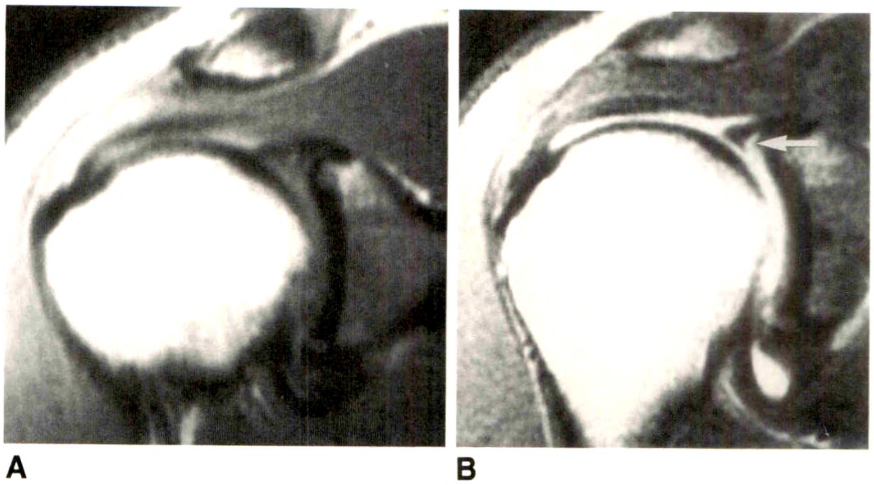

Fig. 3.—Coronal oblique images in a 32-year-old man with complete detachment of superior portion of labrum.

A, MR image (2000/20). Findings are similar to those seen in Fig. 2. During arthroscopy, however, a completely detached labrum was found.

B, MR arthrogram (600/20) confirms partial central detachment (*arrow*). Separation of superior aspect of labrum and proximal portion of biceps tendon from glenoid rim cannot be diagnosed solely on the basis of these MR images, but requires attention to patient's age and clinical history.

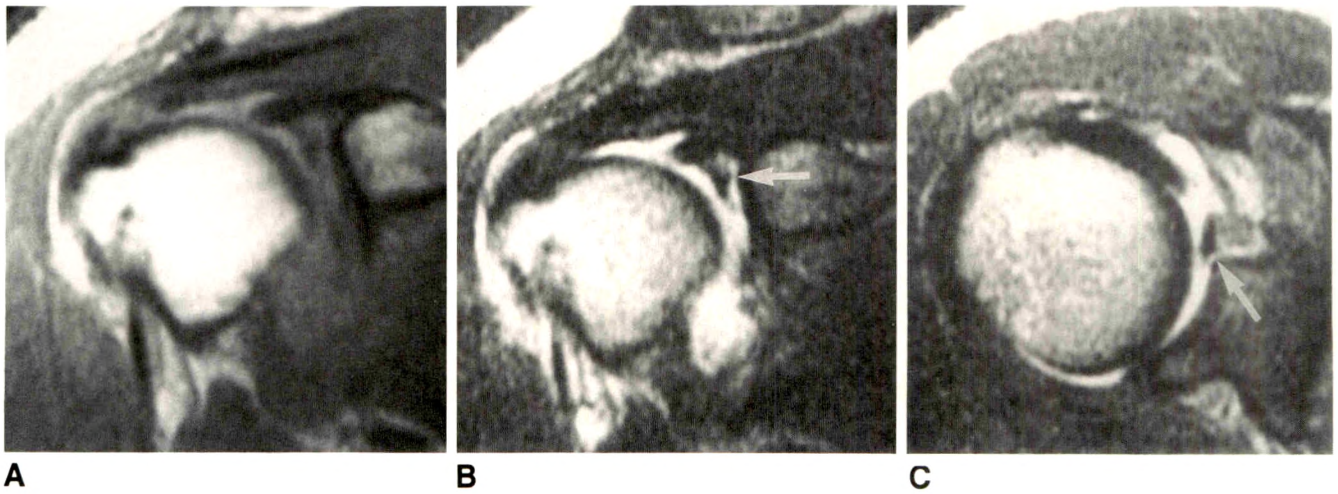

Fig. 4.—25-year-old man with complete detachment of superior portion of labrum.

A, Coronal oblique MR image (2000/20). Diagnosis cannot be made unequivocally on the basis of this image alone.

B, Coronal oblique MR image (2000/80). Presence of joint effusion enhances demonstration of nearly complete labral detachment, which cannot be considered normal in this age group (*arrow*).

C, Axial MR image (2000/80). Complete detachment of superior labrum is clearly shown (*arrow*).

Discussion

In this investigation, we describe a specific pattern of injury to the superior portion of the labrum including the insertion of the biceps tendon. This previously has been designated as a SLAP (superior labrum, anterior and posterior) injury [5]. In early stages, it consists of fraying of the labrum. In more severe cases there is complete detachment of the labrum and the biceps tendon, or a bucket-handle tear of the labrum alone or including part of the biceps tendon [5]. All these injuries may occur after acute trauma with a fall on the outstretched (abducted and slightly forward flexed) arm. They can also be related to traction either by a sudden pull of the biceps tendon or by overhead motion of the arm during sporting activities. Some patients have no history of trauma, however [5]. Because the capsulolabral apparatus is rigid, posterior subluxation of the humeral head may play a role as well [7]. Hurley and Anderson [8] emphasized the association between superior labral tears and the impingement syndrome in a population of athletes, and the possibility was raised that impingement was caused by instability.

The increasing interest that has been directed to superior labral injuries, mainly in the arthroscopic and sports medicine literature, indicates that radiologists have to be more concerned with these specific abnormalities. Our results indicate that MR imaging is not able to show early injury consisting only of fraying of the superior labrum. As suggested by the examination of a single bucket-handle tear, it also may be impossible to differentiate between complete detachment of the superior labrum and biceps tendon and the detachment of only parts of these structures. This differentiation, however, is not important clinically, because each injury requires arthroscopic treatment [5]. Another difficulty with the MR diagnosis of these injuries is the sometimes incomplete depiction of the separation of the labrum from the glenoid rim. Because incomplete central separation of the labrum has been reported as a normal variant [9] or as normal in the aging process [10], consideration of the patient's age and a history of a fall or repeated overhead motion in sports are important for correct diagnosis.

MR imaging is crucial for the depiction of other commonly occurring abnormalities of the shoulder joint that accompany injuries of the superior portion of the labrum. In their investigation of 27 patients with this injury, Snyder et al. [5] found that 26% had a partial rotator cuff tear, 15% had a full-thickness rotator cuff tear, 15% had anterior instability, 15% had chondromalacia or an impression fracture of the humeral head, and 11% had acromioclavicular joint osteoarthritis.

To our knowledge, the present investigation is the first description addressing the MR appearance of detachment of the superior portion of the labrum involving the insertion of the biceps tendon, with the exception of a recently published abstract [11]. Legan et al. [12] mentioned that, after anterior lesions, the superior labral quadrant was the second most commonly damaged part of the labrum demonstrated with MR imaging. They did not mention the position of these injuries with regard to the biceps tendon, however.

We conclude that early traumatic abnormalities of the superior portion of the labrum cannot be detected with MR imaging. Complete detachment, however, can be demonstrated if the patient's age and history are considered during evaluation.

REFERENCES

1. Rafii M, Firooznia H, Bonamo JJ, Minkoff J, Bonamo J, Golimbu C. Athlete shoulder injuries: CT arthrographic findings. *Radiology* **1987**;162:559–564
2. Seeger LL, Gold RH, Bassett LW. Shoulder instability: evaluation with MR imaging. *Radiology* **1988**;168:695–697
3. Rafii M, Minkoff J, Bonamo J, Firooznia H, Jaffe L, Golimbu V. Computed tomography (CT) of shoulder instabilities in athletes. *Am J Sports Med* **1988**;16:352–361
4. Kieft GJ, Bloem JL, Rozing PM, Obermann WR. MR imaging of recurrent anterior dislocation of the shoulder: comparison with CT arthrography. *AJR* **1988**;150:1083–1087
5. Snyder S, Karzel RP, Del Pizzo W, Ferkel RD, Friedman MJ. SLAP lesions of the shoulder. *Arthroscopy* **1990**;6:274–279
6. Flannigan B, Kursunoglu-Brahme S, Snyder S, Darzel R, Del Pizzo W, Resnick D. MR arthrography of the shoulder: comparison with conventional MR imaging. *AJR* **1990**;155:829–832
7. Andrews JR, Carson WG, McLeod WD. Glenoid labrum tears related to the long head of the biceps. *Am J Sports Med* **1985**;13:337–341
8. Hurley JA, Anderson TE. Shoulder arthroscopy: its role in evaluating shoulder disorders in the athlete. *Am J Sports Med* **1990**;18:480–483
9. Detrisac DA, Johnson LL. *Arthroscopic shoulder anatomy*. Thorofare, NJ: SLACK Inc., **1986**:71–83
10. DePalma AF. *Surgery of the shoulder*, 3rd ed. Philadelphia: Lippincott, **1983**:211–241
11. Otto RJ, Sakover R. MR imaging of the glenoid labrum SLAP (superior labrum, anterior and posterior) tear (abstr). *Radiology* **1991**;181(P):154
12. Legan JM, Burkhard TK, Goff WB, et al. Tears of the glenoid labrum: MR imaging of 88 arthroscopically confirmed cases. *Radiology* **1991**;179: 241–246

Value of Unenhanced Spin-Echo MR Imaging in Distinguishing Between Synovitis and Effusion of the Knee

Rolando D. Singson[1]
Fernando M. Zalduondo

OBJECTIVE. We performed a study to determine if unenhanced spin-echo MR imaging can be used to differentiate effusion from synovitis of the knee joint.

MATERIALS AND METHODS. Unenhanced spin-echo MR imaging examinations of 1051 consecutive patients referred for evaluation of internal derangement of the knees were reviewed. Twelve of 550 knees with significant joint effusion also had thickened or irregular synovium. Of these, the cause of synovitis was proved in 10 patients. In the other two, the cause was unknown.

RESULTS. Thickened synovium was of intermediate signal intensity on T1-weighted MR images compared with the lower signal intensity of joint effusion. In eight cases, the thickened synovium had an intermediate signal intensity on T2-weighted images relative to the high signal of the joint effusion. MR images in the other four cases showed increased signal intensity indistinguishable from that of joint effusion.

CONCLUSION. Our experience suggests that unenhanced spin-echo MR images can be used to distinguish synovitis from effusion in the knee joint.

AJR 159:569–571, September 1992

Most authorities consider it difficult if not impossible to differentiate inflamed synovium from joint effusion on T1- and T2-weighted MR images [1, 2]. Therefore, contrast-enhanced MR images are often used to make this distinction [2–5]. To determine if this is necessary, we studied the value of unenhanced spin-echo MR images of the knee in distinguishing synovitis from synovial effusion.

Materials and Methods

We reviewed MR images of the knee in 1051 patients examined to evaluate internal derangement of the knee. MR images were made with a 1.5-T MR unit with whole-volume coils. All studies included sagittal T1-weighted (500/20 [TR/TE]) and sagittal and coronal T2-weighted (2000/30,80) spin-echo images. Axial T1-weighted MR images through the patellofemoral joint also were obtained.

Five hundred fifty patients with joint effusion were further examined for the presence of a thickened synovium or irregularity along the suprapatellar bursa and/or popliteal cyst. Twelve of the 550 patients were found to have a thickened or irregular synovium. Synovitis resulted from a proved cause in 10 of these patients and was confirmed clinically and by histology. These 10 patients included two with rheumatoid arthritis, three with Lyme arthritis, two with septic arthritis, one with psoriatic arthritis, one with calcium pyrophosphate deposition disease, and one with hyperplastic synovitis from a nonspecific cause histologically. All 10 patients had acute symptomatology when first seen. The remaining two patients had chronic signs and symptoms of unknown origin. Plain films, however, demonstrated degenerative joint disease.

Results

Unenhanced MR imaging showed an effusion and a thickened (2–15 mm) or irregular synovium in 12 patients. In all cases, the thickened synovium had inter-

Received December 19, 1991; accepted after revision March 26, 1992.

[1] Both authors: Department of Radiology, Columbia College of Physicians and Surgeons, St. Luke's/Roosevelt Hospital Center, 428 W. 58th St., New York, NY 10019. Address reprint requests to R. D. Singson.

0361–803X/92/1593–0569
© American Roentgen Ray Society

mediate signal intensity compared with the lower signal intensity of joint effusion on T1-weighted images (Figs. 1 and 2A). In eight of these 12 cases, synovial thickening and irregularity had an intermediate signal intensity on T2-weighted images relative to the high signal intensity of joint effusion (Fig. 2B). At times, the synovial thickening extended centrally and filled up the distended suprapatellar bursa (Fig. 3). The other four cases showed increased signal intensity of both thickened synovium and joint effusion, which thus could not be distinguished (Fig. 4).

Discussion

Although various investigators have reported that synovial fluid cannot be distinguished from synovial thickening on unenhanced MR images, they describe intermediate-signal synovial wall thickening along the margins of the suprapatellar bursa [1-4]. We believe that this synovial thickening, as we have seen in various patients, represents synovitis. Our study had some limitations. It was impossible to determine the number of false-negative findings. The diagnosis of synovitis is frequently made on clinical grounds; also, the contrast and spatial resolution limitations of MR imaging may prevent detection of subtle or early changes in the synovium. The two cases of thickened synovium in which no known cause of synovitis existed are presumed to be false-positives. However, plain film findings showed degenerative joint disease, in which synovitis is known to occur.

Chronic synovial hypertrophy has been reported to have an intermediate signal on T2-weighted spin-echo MR images, probably because of hemorrhage or fibrosis or both [1, 5]. In acute inflammation, the synovial signal is expected to be high on T2-weighted images, owing to the water content of the inflamed synovium [6]. We observed that when the synovial proliferation was relatively thin on T1-weighted images, the thickened synovium was not apparent on T2-weighted images (Fig. 4). Whether this type of synovium represents acute

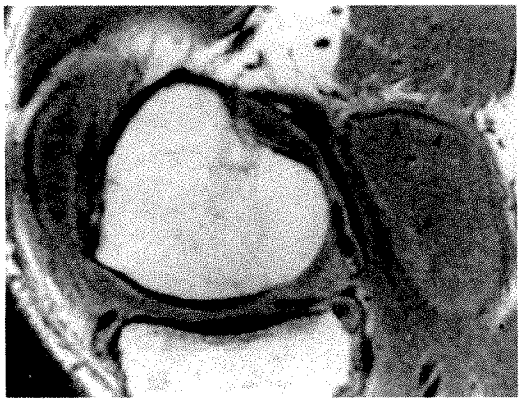

Fig. 1.—Psoriatic arthritis. T1-weighted MR image shows intermediate-signal synovial thickening (*arrowheads*) outlining bursa, popliteal cyst, tendons, and articular surfaces.

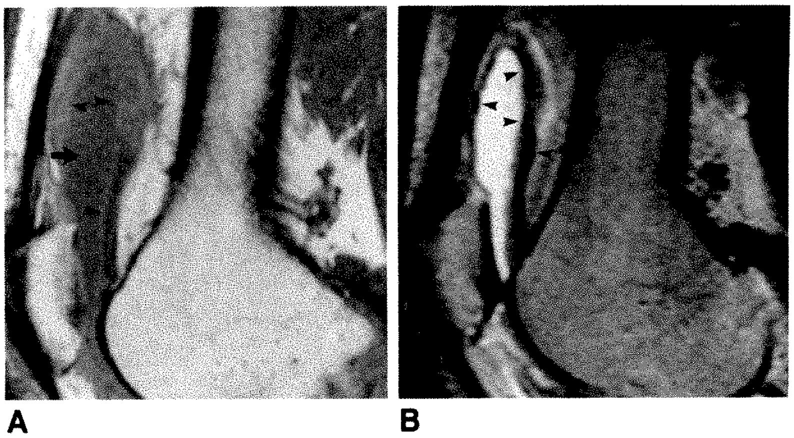

Fig. 2.—Lyme arthritis.

***A*, Sagittal T1-weighted MR image shows intermediate signal and irregular outline of thickened synovium (*arrowheads*) differentiated from lower signal intensity of joint effusion (*arrow*).**

***B*, T2-weighted MR image shows increased signal intensity of effusion outlining irregular, thickened synovium (*arrowheads*). Low signal intensity represents fibrosis and/or hemosiderin deposits.**

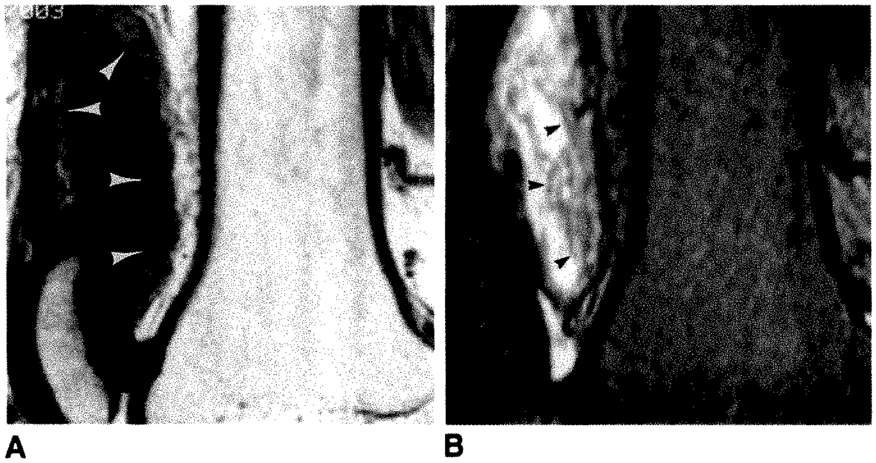

Fig. 3.—Histologically proved hyperplastic synovitis from nonspecific cause.

***A*, Sagittal T1-weighted MR image shows thickened synovium (*arrowheads*).**

***B*, T2-weighted MR image shows proliferative synovium (*arrowheads*) extending throughout bursal space, interspersed between increased signal intensity of effusion. Suprapatellar bursa has a heterogeneous and smudged appearance.**

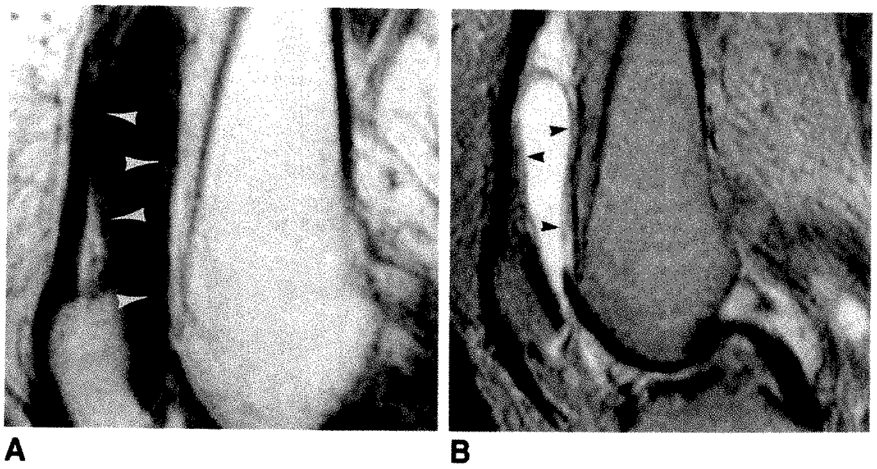

Fig. 4.—Rheumatoid arthritis.

***A*, Sagittal T1-weighted MR image shows a relatively thin synovial wall of intermediate signal intensity (*arrowheads*), as compared with Fig. 1.**

***B*, T2-weighted MR image shows an indistinct separation (*arrowheads*) between synovium and effusion.**

inflammation or whether it is simply a function of thickness obscured by the increased signal of adjacent effusion cannot be ascertained. Our objective was not to attempt to differentiate acute from chronic inflammatory synovitis. This differentiation has been reported with contrast-enhanced MR imaging [7, 8].

Synovitis can be differentiated from joint effusion by the appearance of thickened synovium. This is a finding that can be seen on unenhanced spin-echo MR images.

REFERENCES

1. Beltran J, Caudill JL, Herman LA, et al. Rheumatoid arthritis: MR imaging manifestations. *Radiology* **1987**;165:153–157
2. Kursunoglu-Brahme S, Riccio T, Weisman MH, et al. Rheumatoid knee: role of gadopentetate-enhanced MR imaging. *Radiology* **1990**;176: 831–835
3. Reiser MF, Bongartz GP, Erleman R, et al. Gadolinium-DTPA in rheumatoid arthritis and related diseases: first results with dynamic magnetic resonance imaging. *Skeletal Radiol* **1989**;18:591–597
4. Adam G, Dammer M, Bohndorf K, et al. Rheumatoid arthritis of the knee: value of gadopentetate dimeglumine-enhanced MR imaging. *AJR* **1991**; 156:125–129
5. Muirden KD, Senator GB. Iron in the synovial membrane in rheumatoid arthritis and other joint diseases. *Ann Rheum Dis* **1986**;27:38–48
6. Terrier F, Hricak H, Revel D, et al. Magnetic resonance imaging and spectroscopy of the periarticular inflammatory soft-tissue changes in experimental arthritis of the rat. *Invest Radiol* **1985**;20:813–823
7. Bjorkengren AG, Geborek P, Rydholm U, et al. MR imaging of the knee in acute rheumatoid arthritis: synovial uptake of gadolinium-DOTA. *AJR* **1990**; 155:329–332
8. Konig H, Sieper J, Wolf K. Rheumatoid arthritis: evaluation of hypervascular and fibrous pannus with dynamic MR imaging enhanced with Gd-DTPA. *Radiology* **1990**;176:473–477

Book Review

Skeletal Radiology. The Bare Bones Teaching Collection. By Felix S. Chew. St. Paul, MN: Image PSL, 276 pp., 1991. Book and videodisc, $635

If you visited the infoRAD '91 exhibits at the Radiological Society of North America annual meeting last year in Chicago, you had the opportunity to try videodisc learning. I am truly a novice in this arena; that was my first experience with this new-age technology for teaching. Felix Chew from the Massachusetts General Hospital had three bone radiology videodisc exhibits at that fair. Much of the material was from his excellent book, *Skeletal Radiology: The Bare Bones* (Aspen, 1989; reviewed in *AJR* January 1991).

He has now put the entire pictorial content of the book plus additional cases on videodisc. The 12-in. (30.5-cm) disc is sold in a package with a barcode workbook that includes the textual material. A copy of the original book is also included in the package. Not included in the purchase price is a videodisc player, video monitor, and barcode reader required to use the material. These are sold separately as a learning station package by the publisher for $1800 (13-in. (33-cm) monitor) to $2600 (19-in. (48-cm) monitor). Also not included is a separate software package to link this material to a computer with the full text of the barcode manual available on line.

The barcode manual is divided into three sections. The first is, by far, the largest and the site of all written text. This section is divided into seven subsections, which include trauma, tumors, articular disease, congenital and developmental conditions, metabolic and hematologic disease, and postsurgical imaging. The disc stores about 2500 images from 650 cases collected at the Massachusetts General Hospital and State University of New York Health Science Center at Syracuse. This is about the same number of figures in Edeiken's two-volume *Diseases of Bone*. The written material in the barcode manual is virtually the same as that in the original book, slightly rearranged in places and with a few additions (e.g., Lyme disease).

The second section simply reproduces the figures from the original text for viewing on a video monitor. A few additional images are included for closer detail of some part or an arrow for specific identification. The third section is seven self-evaluation tests, each 20 cases concentrating on an anatomic area. The diagnosis is given after two images are viewed. There is no discussion.

Image PSL, the producers of the videodisc (called an ImageDisc), uses a patented technology to produce high-resolution and sharp edge definition images. The videodisc collection of the American College of Radiology was produced by the same company. Most of the images are good to excellent. The few poorer images are, I suspect, due to poor original films such as underpenetrated plain films and reconstructed CT scans. The images are mostly plain films and close-up views, but other studies are included where appropriate, such as arthrograms, nuclear scans, CT scans, and MR images and even single-positron emission computed tomographic images, sonograms, and cine cardiac angiograms.

I found it slightly inconvenient to read text in the barcode manual and then look up to the video screen to see the associated figure. It's like having to flip three or four pages forward to see the referenced figure in a standard text. I suspect I would find the computer software attachment that can bring the text on line with the images more to my liking. I also missed having captions for the figures, especially some of the MR images and other specialty images. The closest the video images come to captions is an image with an arrow added after the bare image. Otherwise, the purposes of the author—to illustrate pathology and pathophysiology of bone with a great variety of good-quality images—is more than adequately accomplished, as it was in the original book. However, be aware that 650 cases cannot cover everything; for example, cancellous stress fractures, wrist instabilities, and spinal tuberculosis are not included.

My residents and I found the self-evaluation section an enjoyable and efficient type of review. In fact, if two persons use the equipment, one can bring up images from any subsection of the main workbook to quiz the other.

This videodisc, at more than $600, is 10 times more costly than the same material in the book. As an emerging technology, it is fun and exciting to use. I think it may be both useful and cost-effective in radiologic, orthopedic, and other learning libraries where videodisc players may already be in place and the material will attract many residents and medical students as users. I do have some concern about the useful life of the pages used for the barcodes. They are not plasticized as the front and back cover are, and some users do press the barcode reader harder against the page than is required. We have had some damage to our American College of Radiology barcode book, which is printed on similar paper and used by many.

Stanley P. Bohrer
Bowman Gray School of Medicine
Winston-Salem, NC 27157-1088

Technical Note

Intraarticular Sonography for Imaging the Knee Menisci: Evaluation in Cadaveric Specimens

Charles H. McDonnell III,[1] R. Brooke Jeffrey, Jr., Ann G. Björkengren, and King C. P. Li

Sonographic evaluation of the knee has proved to be useful for demonstrating meniscal tears as well as other abnormalities, such as cruciate and collateral ligament injuries [1, 2]. Intraarticular sonography may be useful as an adjunct to arthroscopic evaluation of meniscal tears. We describe the application of catheter-based sonography, originally designed for intravascular use, in the intraarticular evaluation of menisci in a cadaveric model.

Materials and Methods

An intravascular sonographic system (Cardiovascular Imaging Systems, Sunnyvale, CA) was used with an 8-French, 20-MHz transducer. The transducer produces images perpendicular to the transducer catheter and 360° around it. The transducer was introduced into a single cadaveric knee joint via an anterior incision, and the knee was filled with degassed water in order to obtain images of the normal menisci. The knee joint was then opened, and the menisci were dissected out. Discrete 3–5 mm horizontal, vertical, and bucket-handle tears were created with a scalpel. The menisci were submerged in a water bath and rescanned in an attempt to show the tears known to be present.

Results

The catheter-based probe was easily manipulated throughout the knee joint. The normal menisci were well visualized in their entirety and were moderately echogenic. Other structures visualized within the knee joint included the echogenic cruciate ligaments and the smooth surface of the articular cartilage. In the water bath, all three types of surgically created tears were also easily detected as long as fluid was within the tears (Fig. 1).

Discussion

Sonographic evaluation of menisci and meniscal tears has been a subject of recent interest. Cadaveric menisci with surgically created tears were first imaged in a water bath with a 5-MHz probe by Selby et al. [1] in 1987. The noninvasiveness, wide availability, relatively low cost, and patients' acceptance of sonography have prompted many investigators to explore its use in the evaluation of knee injuries [2–6]. As a result, dynamic transcutaneous sonography of the knee has become popular in some centers, particularly in Europe [7, 8]. Nevertheless, MR imaging and arthroscopy continue to be the diagnostic methods of choice for evaluating meniscal injuries because of their greater sensitivity and accuracy.

With the intent to combine arthroscopy with sonographic techniques, we have shown the feasibility of a new intraarticular application of catheter-based sonography. We think this technique has potential value as an adjunct to arthroscopy. Although it has not yet been performed on a patient, the 8-French transducer could easily be introduced and maneuvered through an arthroscopic trocar. This could allow more thorough intraoperative evaluation of the menisci, particularly of the difficult-to-reach posterior horn of the lateral meniscus and its undersurface. Furthermore, with arthroscopy only the surface of menisci can be visualized. Sonography has the

---

Received January 15, 1992; accepted after revision March 9, 1992.

[1] All authors: Department of Diagnostic Radiology and Nuclear Medicine, Stanford University Medical Center, Stanford, CA 94305-5105. Address reprint requests to C. H. McDonnell III.

AJR 159:573–574, September 1992 0361–803X/92/1593–0573 © American Roentgen Ray Society

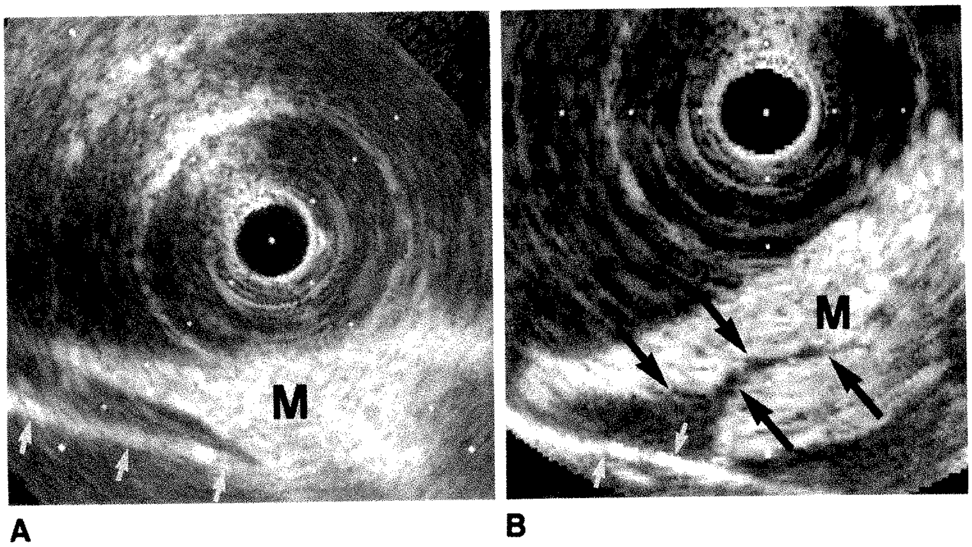

Fig. 1.—Sonograms through posterior horn of ex vivo cadaveric medial meniscus. Catheter-based transducer is parallel to free edge of meniscus and imaging plane is perpendicular (anatomically sagittal).

***A*, Normal meniscus (M) is seen against offset pad surface (*arrows*) with transducer centrally. Note homogeneous echogenicity of fibrocartilaginous tissue of meniscus.**

***B*, Surgically created horizontal tear (*large arrows*) in a meniscus (M) is seen against offset pad surface (*small arrows*).**

potential to improve the intraarthroscopic diagnosis of intrasubstance meniscal tears. Such enhanced arthroscopic evaluation could result in more appropriate use of meniscus-sparing surgical procedures rather than complete resection. Furthermore, this technique may reveal more subtle injuries or abnormalities involving other structures, such as the cruciate ligaments, which could be overlooked on direct arthroscopic examination.

Clinical evaluation of this technique and correlation with preoperative MR imaging and arthroscopic findings are necessary to evaluate its sensitivity and specificity.

REFERENCES

1. Selby B, Richardson ML, Nelson BD, Graney DO, Mack LA. Sonography in the detection of meniscal injuries of the knee: evaluation in cadavers. *AJR* **1987**;149:549-553
2. Tomasella G, Turra S, Olmeda A, Soliman A, Brunino LG. Ultrasonography in the study of lesions of the menisci and the collateral ligaments of the knee: findings in 48 surgically treated patients. *Radiol Med* (Torino) **1991**;81:822-826
3. Friedl W, Glaser F. Dynamic sonography in the diagnosis of ligament and meniscal injuries of the knee. *Arch Orthop Trauma Surg* **1991**;110:132-138
4. Casser HR, Sohn C, Kiekenbeck A. Current evaluation of sonography of the meniscus: results of a comparative study of sonographic and arthroscopic findings. *Arch Orthop Trauma Surg* **1990**;109:150-154
5. Teitz CC. Ultrasonography in the knee: clinical aspects. *Radiol Clin North Am* **1988**;26:55-62
6. Richardson ML, Selby B, Montana MA, Mack LA. Ultrasonography of the knee. *Radiol Clin North Am* **1988**;26:63-75
7. Fusting M, Casser HR. Dynamic examination technique in meniscus sonography (in German). *Sportverletz Sportschaden* **1991**;5:27-36
8. Fenkl R, Barth P. Techniques for ultrasound imaging of meniscus lesions: experimental principles (in German). *Unfallchirurgie* **1991**;94:63-68

Elastofibroma: MR and CT Appearance with Radiologic-Pathologic Correlation

Mark J. Kransdorf[1,2]
Jeanne M. Meis[3]
Elizabeth Montgomery[3]

OBJECTIVE. The purpose of our study was to determine the MR and CT appearances of elastofibroma and correlate the imaging features with the underlying pathologic findings.

MATERIALS AND METHODS. We reviewed retrospectively the MR and CT findings in five cases of elastofibroma. All patients had a soft-tissue mass; one patient also complained of pain. The mean age of the patients was 71 years (range, 63–79 years). Four lesions occurred in the subscapular region, and one occurred in the thigh. In addition, we reviewed and compared the demographic data of 72 histologically proved cases for which we had archival data.

RESULTS. Three of four lesions evaluated with spin-echo MR imaging were approximately isointense with skeletal muscle and contained areas with a signal intensity similar to that of fat; these corresponded to areas of dense collagen and interspersed fat, respectively. In the fourth case, the MR appearance was nonspecific. In one case, MR imaging with gadopentetate dimeglumine showed areas with and without enhancement. Three of four lesions evaluated with CT had variable margins, with tissue attenuation similar to that of the adjacent soft tissue as well as scattered areas of decreased attenuation, suggesting fat within the lesion. In one case, the lesion was well defined and relatively homogeneous with an attenuation less than that of skeletal muscle.

CONCLUSION. The MR and CT features of elastofibroma are different from those of most other soft-tissue tumors, reflecting entrapped fat within a predominantly fibrous mass. Although these features are not pathognomonic, their presence in a subscapular lesion in an older patient suggests a presumptive diagnosis of elastofibroma.

***AJR* 159:575–579, September 1992**

Elastofibroma is a slowly growing, fibroelastic pseudotumor, thought to result from mechanical friction between the scapula and chest wall; hence, it is considered reactive rather than neoplastic [1, 2]. Originally described at the 12th Congress of Scandinavian Pathologists by Järvi and Saxén in 1959, and subsequently reported in 1961 [1, 2], elastofibroma has received little attention in the radiologic literature and is considered a rare lesion. However, it is not uncommon and was found in 24% of women and 11% of men in one autopsy series of patients who were more than 55 years old [3]. In this autopsy study, lesions were 3 cm or less in size, suggesting that most elastofibromas are clinically occult, accounting for the perception that they are rare.

As the indications for computerized imaging expand, elastofibroma will probably be seen more frequently. Consequently, radiologists should be familiar with the imaging and clinical characteristics of this entity. This knowledge may make a correct presumptive diagnosis possible and prevent unnecessary radical surgery. We describe the CT and MR appearances of five elastofibromas and correlate the imaging features with the histologic findings. In addition, we review the demographic data of another 72 patients.

Received February 24, 1992; accepted after revision April 1, 1992.

The opinions or assertions contained herein are the private views of the authors and are not to be construed as official or as reflecting the views of the Department of the Army, the Department of Defense, or the Uniformed Services University of the Health Sciences.

[1] Department of Radiologic Pathology, Armed Forces Institute of Pathology, Washington, DC 20306-6000. Address reprint requests to M. J. Kransdorf.

[2] Department of Radiology and Nuclear Medicine, Uniformed Services University of the Health Sciences, Bethesda, MD 20814.

[3] Department of Soft Tissue Pathology, Armed Forces Institute of Pathology, Washington, DC 20306-6000.

0361–803X/92/1593–0575

Materials and Methods

We reviewed retrospectively the MR images and CT scans of five patients with elastofibroma, all of whom were imaged for the evaluation of a soft-tissue mass (one patient also complained of increasing pain). This group consisted of four men and one woman 63–79 years old (mean, 71 years). In addition, we reviewed the archival demographic data from another 72 cases of elastofibroma. The entire group of 77 lesions occurred in 75 patients 36–81 years old (mean, 69 years); two patients had bilateral subscapular masses. The combined groups included 42 men and 32 women; the sex was unknown in one case. Seventy-three lesions occurred between the tip of the scapula and the chest wall, two occurred in the thigh, one occurred in the region of the hip attached to the fascia lata femoris, and one occurred in the second web space of the foot. The size of the lesion was known in 63 cases and ranged from 1.5 to 20.0 cm in greatest dimension (mean, 8 cm). The size was unkown in 14 cases. Thirty-five cases involved the right side, and 25 involved the left; the side involved was unknown in 17.

In four patients, MR images of the lesions were obtained with a variety of systems. Field strength was 1.5 T in three cases and unknown in one. Images included spin-echo T1-weighted (300–767/20–30) and T2-weighted (2000–2090/90) pulse sequences. One patient's lesion was evaluated by using short TI inversion recovery (STIR) (200/45/165) and gradient-refocused echo (GRE) (317/15/20°) MR images rather than T2-weighted images. In one patient, gadopentetate dimeglumine–enhanced MR images were obtained in addition to standard T1- and T2-weighted images. All lesions were imaged in at least two orthogonal planes. Four patients had axial CT scans, two with and two without contrast material.

In all cases, the diagnosis of elastofibroma was verified histologically according to criteria previously described [1–3]. Sections stained with hematoxylin and eosin were reviewed without previous knowledge of each lesions's radiologic appearance; they were then correlated with each patient's MR and CT findings.

Results

MR Findings

In three of four cases, all tumors in the subscapular region, spin-echo MR images showed relatively well defined, moderately inhomogeneous lesions, with no surrounding soft-tissue edema. On T1-weighted images, the lesions had approximately the same signal intensity as skeletal muscle, with interspersed linear and curvilinear areas of high signal intensity. On corresponding T2-weighted images, the lesions also had a signal intensity approximately the same as that of skeletal muscle, with linear and curvilinear areas that appeared similar to fat in a distribution like that seen on the T1-

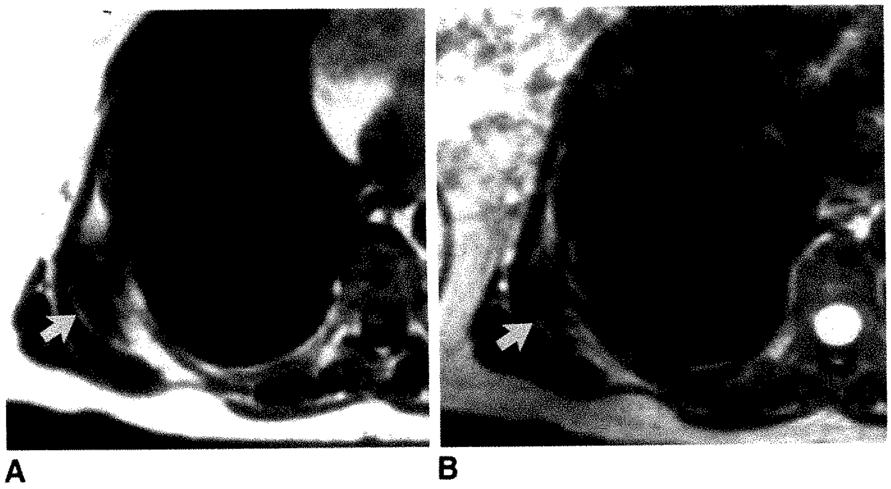

Fig. 1.—Subscapular elastofibroma in 64-year-old woman.

***A* and *B*, Corresponding axial T1-weighted (550/22) (*A*) and T2-weighted (2000/90) (*B*) SE MR images show a relatively well defined, inhomogeneous mass (*arrows*) between chest wall and scapular tip. Most of mass has a signal intensity approximately equal to that of surrounding skeletal muscle. Interspersed within mass are linear and curvilinear areas with increased signal intensity approximately the same as that of subcutaneous fat.**

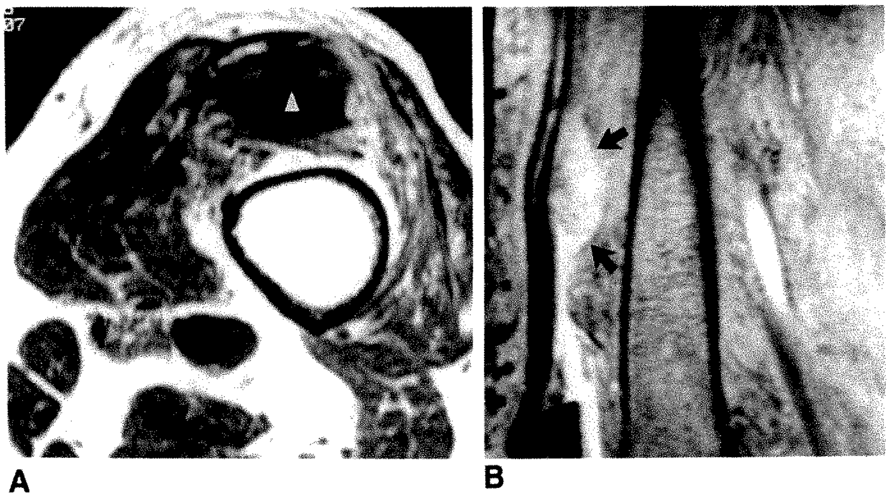

Fig. 2.—Elastofibroma in anterior thigh of 73-year-old man.

***A*, Axial T1-weighted (300/20) SE MR image shows a mass (*arrowhead*) with relatively homogeneous region centrally, with only a few small globular areas of increased signal intensity, surrounded by a region that has several interspersed areas with signal intensity similar to that of fat. Lesion is poorly delineated from adjacent tissue.**

***B*, Sagittal GRE MR image (317/15/20°) shows a relatively inhomogeneous nonspecific mass (*arrows*) with a signal intensity greater than that of fat.**

weighted images (Fig. 1). Gadopentetate dimeglumine–enhanced MR images in one case showed areas with and without enhancement. A single lesion in the thigh was poorly defined on T1-weighted images. It had a relatively homogeneous region centrally and a few small globular areas of increased signal intensity surrounded by a region with several interspersed areas of high signal intensity. GRE images in this case showed the lesion was a relatively well defined inhomogeneous nonspecific mass with a signal intensity greater than that of fat (Fig. 2). STIR images showed a poorly defined inhomogeneous mass.

CT Findings

Axial CT scans of four lesions, all in the subscapular region, showed variable margins. In three of four cases, the mass was well outlined laterally by fat, but was not separable from the muscles of the chest wall anteromedially. The tissue attenuation of the lesion was approximately the same as that of the adjacent soft tissue, with some scattered areas of decreased attenuation (Fig. 3). In one case, the lesion was relatively homogeneous, with an attenuation less than that of skeletal muscle (Fig. 4). In no case was an underlying osseous abnormality detected.

Histologic Findings

Microscopically, all lesions were composed primarily of hyalinized collagen with scattered fibroblasts and entrapped islands of mature adipose tissue. In all cases, variable numbers of characteristically enlarged, hypereosinophilic, refractile elastic fibrils were present. They resembled a pipe cleaner in longitudinal sections and an asterisk or a flower in cross sections, particularly with the stain for elastic tissue (Verhoeff–van Gieson stain for elastic fibrils) (Fig. 5).

Discussion

Elastofibroma is not a true neoplasm and is generally considered to be a fibroblastic pseudotumor; it probably arises from periosteal fibroblasts with deranged elastic fibrillogenesis [4]. Lesions typically occur on the back and are thought to be related to repeated mechanical friction between the chest wall and the tip of the scapula. Patients often have an occupational history of manual labor such as farming; however, this may be a coincidence [1, 2, 5, 6] in view of the number of elastofibromas found at autopsy and the presumed occult clinical nature of this entity [3]. Other types of trauma,

Fig. 3.—Subscapular elastofibroma in 68-year-old man. Axial noncontrast CT scan shows large subscapular mass (*arrows*). Note subtle areas of decreased attenuation within mass. Although well outlined by fat laterally, lesion cannot be separated from intercostal muscles.

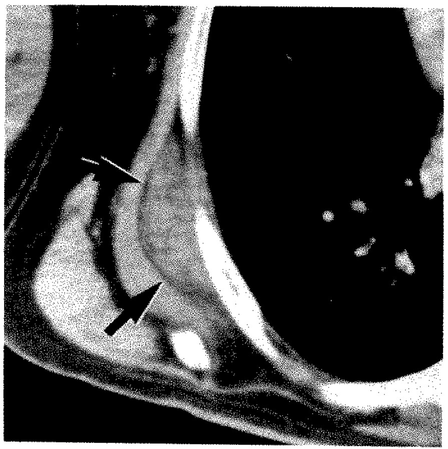

3

Fig. 4.—Subscapular elastofibroma in 79-year-old man. Axial noncontrast CT scan shows large homogeneous subscapular mass (*arrows*) with tissue attenuation less than that of skeletal muscle and greater than that of subcutaneous fat.

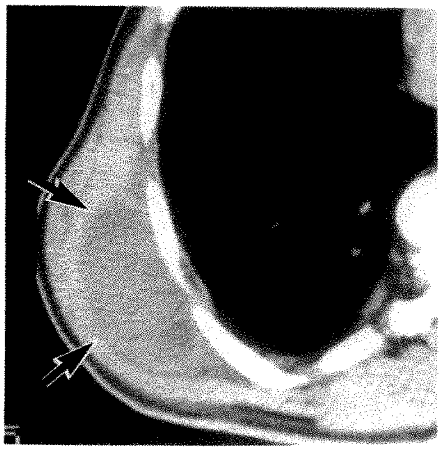

4

Fig. 5.—Histologic features of elastofibroma. *A*, Low-power photomicrograph shows lesion, composed primarily of hyalinized collagen with scattered fibroblasts and entrapped islands of mature adipose tissue, infiltrating adjacent adipose tissue. (H and E, original magnification ×75)
B, High-power photomicrograph shows characteristic serrated fibrils, which resemble a pipe cleaner in longitudinal sections and an asterisk or a flower in cross sections. (Verhoeff–van Gieson elastic stain, original magnification ×300)

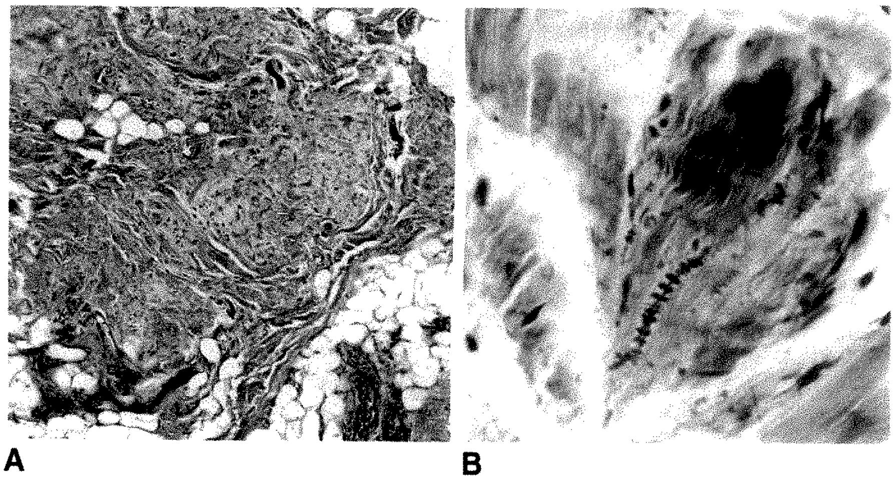

mechanical stress, chronic irritation, and nutritional derangement have also been suggested as etiologic factors [3, 7], but these factors alone may not explain the development of elastofibroma. Some patients may also have a genetic predisposition, as suggested by a study by Nagamine et al. [5] of 170 cases of the lesion in Okinawa in which one third of the patients had a family history of elastofibroma. Barr [8] postulated that "the lesion results from elastic degeneration of collagen following trauma and friction in individuals who possibly have some inherited enzymatic defect related to connective tissue metabolism." However, recent in situ hybridization and immunoelectron microscopic studies indicate that active synthesis of elastic fibrils is occurring within elastofibromas and that elastic fibrillogenesis is abnormal rather than a degenerative phenomenon [4]. Ultrastructurally, elastofibroma consists of (1) fibroblasts scattered among closely packed bundles of normally formed collagen fibrils and (2) aggregates of abnormally formed elastic fibrils of various diameters and shapes [1].

The location between the chest wall and inferior scapular tip is most characteristic of elastofibroma; it was the site of the lesion in 99% of reported cases [5]. Bilateral lesions are common and are seen in 10–66% of patients [2, 3, 5, 6, 8]. Synchronous infraolecranon lesions are also common. Nagamine et al. [5] found that this area was involved in approximately 16% of patients. They also noted isolated synchronous lesions in the thoracic wall and in the area of the ischial tuberosity. One patient had lesions in seven different anatomic locations. Elastofibromas in other locations such as the hand [9], foot [10], regions overlying the greater trochanter and ischial tuberosity [8, 11], deltoid region [7], temporal bulbar conjunctiva [12], and cervical epidural space [13] have also been reported.

Most patients are older adults. The mean age of patients is approximately 70 years [5], although elastofibroma has been reported in children as young as 6 years [6]. More than half the patients are asymptomatic [5, 6]. The most common symptom is stiffness, which is seen in approximately one fourth of patients [5]. Pain is relatively uncommon and is the presenting symptom in another 10% [5]. Large lesions may ulcerate [14]. The disorder has a female predominance, usually estimated to be 2:1 [3, 7]; however, it may be as high as 13:1 [5].

Our series had an unusually high percentage of men, which is partially explained by a biased referral pattern. Fourteen patients in our series were referred from federal (military or veterans administration) hospitals; 11 of these were men, two were women, and for one the sex was unknown. If only cases referred from civilian sources are considered, the group included 30 men and 31 women, which is still a higher percentage of men than reported in the literature.

Lesions may be as large as 20 cm and may be manifested as a soft-tissue mass; however, elastofibroma may also produce a thickened and indurated area of the thoracic fascia or a "streak in the fascia" detected on histologic examination [3, 15]. The great discrepancy between the prevalence of elastofibroma in autopsy series vs the prevalence of clinically apparent mass lesions is likely related to the lesion's great variability in size. Cystic change within the lesion has been reported [2, 5], as have bursalike areas [3, 9]. Lesions may be stable or may grow slowly over many years [5, 6]. Surgery is considered curative; rare recurrences are probably due to incomplete excision. Five (7%) of the patients in our study had recurrences 2–17 years after surgery.

On CT, elastofibroma is a poorly defined inhomogeneous soft-tissue density with attenuation approximately the same as that of skeletal muscle and containing linear low-density streaks [6, 15, 16]. Three of our four cases had this appearance. In the fourth case, the lesion was relatively homogeneous, with an attenuation less than that of muscle; this was somewhat similar to the findings reported by Marin et al. [6].

Gould et al. [17] described the MR findings in a patient with bilateral elastofibromas of the scapula. On both T1- and T2-weighted images, the lesion was a lenticular well-defined mass with an intermediate signal intensity approximately equal to that of skeletal muscle; interlaced areas had a signal intensity similar to that of fat. This appearance is similar to the appearance of the three chest wall lesions we report. The areas of increased signal intensity presumably correspond to adipose tissue within the lesion, whereas the areas of relatively decreased signal intensity correspond to areas of dense fibrous connective tissue, which predominate. The origin of the fat within the lesion could not be determined; however, we speculate that it is entrapped mature adipose tissue. Although factors governing enhancement on MR images obtained with gadopentetate dimeglumine are not completely understood, we note that similar enhancement has been seen in other densely fibrous lesions [18].

The differential diagnosis of lesions that have increased signal intensity on T1-weighted MR images is limited. All of these contain either fat or blood and in addition to elastofibroma include lipoma, liposarcoma, hemangioma, hematoma, and intralesional hemorrhage [19]. Similarly, the differential diagnosis of lesions with decreased or relatively decreased signal intensity on both T1- and T2-weighted MR images is limited. This includes densely mineralized masses as well as those that are hemosiderin-laden, such as pigmented villonodular synovitis, or those that are relatively acellular with large amounts of collagen, as in some cases of musculoaponeurotic fibromatosis or desmoid [19]. Decreased signal intensity on all spin-echo MR pulse sequences has been reported in malignant fibrous histiocytoma and in other malignant tumors and is not specific for any diagnosis; it simply reflects the morphologic features of a lesion [19, 20].

The imaging features of elastofibroma are different from those of most other soft-tissue tumors, reflecting entrapped fat within a predominantly fibrous mass. Although these features are not pathognomonic, their presence in a subscapular lesion in an older patient suggests a presumptive diagnosis of elastofibroma.

ACKNOWLEDGMENT

We thank Sheela Rao for her untiring research assistance in the preparation of this manuscript.

REFERENCES

1. Järvi OH, Saxén AE. Elastofibroma dorsi. *Acta Pathol Microbiol Scand* **1961**;144[suppl 51]:83–84
2. Järvi OH, Saxén AE, Hopsu-Havu VK, Wartiovaara JJ, Vaissalo VT. Elastofibroma: a degenerative pseudotumor. *Cancer* **1969**;23:42–63
3. Järvi OH, Länsimies PH. Subclinical elastofibromas in the scapular region in an autopsy series: additional notes on the aetiology and pathogenesis of elastofibroma pseudoneoplasm. *Acta Pathol Microbiol Scand [A]* **1975**;83:87–108
4. Kumaratilake JS, Krishnan R, Lomax-Smith J, Cleary EG. Elastofibroma: disturbed elastic fibrillogenesis by periosteal-derived cells? An immunoelectron microscopic and in situ hybridization study. *Hum Pathol* **1991**;22:1017–1029
5. Nagamine N, Nohara Y, Ito E. Elastofibroma in Okinawa: a clinicopathologic study of 170 cases. *Cancer* **1982**;50:1794–1805
6. Marin ML, Perzin KH, Markowitz AM. Elastofibroma dorsi: benign chest wall tumor. *J Thorac Cardiovasc Surg* **1989**;98:234–238
7. Mirra JM, Straub LR, Järvi OH. Elastofibroma of the deltoid. *Cancer* **1974**;33:234–238
8. Barr JR. Elastofibroma. *Am J Clin Pathol* **1966**;45:679–683
9. Kapff PD, Hocken DB, Simpson RHW. Elastofibroma of the hand. *J Bone Joint Surg [Br]* **1987**;69-B:468–469
10. Cross DL, Mills SE, Kulund DN. Elastofibroma arising in the foot. *South Med J* **1984**;77:1194–1196
11. Waisman J, Smith DW. Fine structure of an elastofibroma. *Cancer* **1968**;22:671–677
12. Austin P, Jakobiec FA, Iwamoto T, Hornblass A. Elastofibroma oculi. *Arch Ophthalmol* **1983**;101:1575–1579
13. Prete PE, Henbest M, Michalski JP, Porter RW. Intraspinal elastofibroma: a case report. *Spine* **1983**;8:800–802
14. Schwarz T, Opplzer G, Duschet P, Brückler B, Gschnait F. Ulcerating elastofibroma dorsi. *J Am Acad Dermatol* **1989**;21:1142–1144
15. Ghiatas AA, Armstrong S, Fermin OT. Case report 583 (Elastofibroma dorsi). *Skeletal Radiol* **1989**;18:619–622
16. Berthoty DP, Shulman HS, Miller HAB. Elastofibroma: chest wall pseudotumor. *Radiology* **1986**;160:341–342
17. Gould ES, Javors BR, Morrison J, Potter H. Case report. MR appearance of bilateral periscapular elastofibromas. *J Comput Assist Tomogr* **1989**;13:701–703
18. Hawnaur JM, Jenkins JPR, Isherwood I. Magnetic resonance imaging of musculoaponeurotic fibromatosis. *Skeletal Radiol* **1990**;19:509–514
19. Sundaram M, McLeod RA. MR imaging of tumor and tumorlike lesions of bone and soft tissue. *AJR* **1990**;155:817–824
20. Sundaram M, McGuire MH, Schajowicz F. Soft-tissue masses: histologic basis for decreased signal (short T2) on T2-weighted MR images. *AJR* **1987**;148:1247–1250

Book Review

Diagnostic Imaging of AIDS. Edited by J. W. A. J. Reeders, F. H. Barneveld Binkhuysen, and J. F. W. M. Bartelsman. New York: Thieme Verlag, 144 pp., 1992. $79, softcover

The aim of this book, as stated in the preface, is "to give the radiologist and the clinician treating the patient a clear insight into what radiologic and endoscopic research currently have to offer with regard to AIDS." The book contains 14 chapters and is divided into four main sections. The first section discusses the epidemiology, pathology, clinical classification systems, and microbiology of AIDS. The remaining sections detail the clinical and radiologic findings of AIDS in the nervous system, chest, and gastrointestinal tract. Two chapters also describe nuclear medicine procedures in AIDS and prevention of HIV transmission during diagnostic procedures.

The title page lists 19 contributing authors, all but one from the Netherlands. The text is uniformly clear and succinct, and the translation of the Dutch manuscripts by B. S. Vollers-King is excellent. The orderly arrangement of chapters is helpful to the reader.

The printing and paper are of high quality. The book contains 146 beautiful illustrations, 30 of which are in color (in the chapters on pathology and gastrointestinal endoscopy). Numerous concise tables supplement the text. The soft cover and small pages make the book easy to handle.

Although information about AIDS continues to increase rapidly, all sections of this book appear up-to-date. The only omission is that the book does not have a separate chapter on the clinical and radiologic manifestations of AIDS in children (AIDS in children is discussed briefly in the chapter on radiology of the gastrointestinal tract). Also, genitourinary and musculoskeletal abnormalities are mentioned only in passing and are not illustrated.

The book fulfills its intended purposes of familiarizing physicians with the radiologic and clinical findings in AIDS and of helping them to choose from among the various imaging methods available. Similar textbooks on this subject are *Radiology of AIDS* (Raven, 1988), edited by Michael P. Federle, Alec J. Megibow, and David P. Naidich, and *CT of the Immunocompromised Host* (Churchill Livingstone, 1990), edited by Janet E. Kuhlman. *Radiology of AIDS* contains 172 pages and 310 illustrations and costs $99. *CT of the Immunocompromised Host* contains 194 pages and 239 illustrations and costs $54. Although all three books are excellent, *Diagnostic Imaging of AIDS* contains the most current information and references. I recommend it as a useful guide to all radiologists and radiologists-in-training.

A recently published and similarly titled book, *Imaging of AIDS* (Mosby–Year Book, 1991), by P. M. Trotot, contains 301 pages and 328 illustrations (45 of which are in color) at a cost of $89. As this book is not yet available in my institutional library, I do not know how its text compares with that of *Diagnostic Imaging of AIDS*.

Philip Goodman
University of Texas Medical Branch
Galveston, TX 77550-2780

Review Article

Neoplastic Diseases Affecting the Central Skull Base: CT and MR Imaging

Lawrence E. Ginsberg[1]

Modern imaging techniques play a vital role in the diagnostic evaluation and follow-up of patients with neoplastic disease affecting the skull base. Many of these lesions have a high rate of recurrence if surgical removal is not complete. Newer, more aggressive surgical approaches can have a maximal effect only if the full extent of a lesion is known preoperatively. CT and MR imaging provide the surgeon with detailed information about every site of tumor involvement. Although these lesions are not common in clinical radiologic practice, the radiologist must be prepared to offer a reasonable differential diagnosis and a full evaluation of the extent of disease. This review presents some of the more commonly encountered tumors that can affect the skull base and describes their radiologic features, with emphasis on CT and MR imaging.

The central skull base, generally considered to include the clivus, sella, parasellar region, and greater wing of the sphenoid bone, is the site of a variety of tumors, both primary and secondary. Radiologists are often asked to suggest the possible nature of and evaluate the extent of such lesions. Although a definitive preoperative diagnosis is not always possible, the site of a lesion and its imaging characteristics often limit the diagnostic possibilities. Certain tumors have a strong predilection for specific anatomic locations in the skull base. Imaging characteristics such as CT appearance, MR signal intensity, tissue homogeneity, and enhancement pattern further aid in narrowing the diagnostic possibilities. The extent of neoplastic involvement can be assessed accurately n all cases. This review describes the imaging features of some of the more common skull base tumors and discusses strategies for establishing a differential diagnosis. Not included are the congenital (encephalocele, arachnoid cyst, craniosynostosis), traumatic, infectious (otogenic skull base osteomyelitis), or tumorlike (Paget's disease, fibrous dysplasia) conditions that can affect the central skull base. Tumorlike conditions should, however, be considered in the differential diagnosis of lesions of the skull base as imaging features can overlap.

Rhabdomyosarcoma

Rhabdomyosarcoma is a mesenchymal malignant tumor that occurs most often in children. This lesion constitutes 4–8% of all malignant tumors in children less than 15 years old [1] and is the most common soft-tissue sarcoma in children [2]. Although rhabdomyosarcoma is less common in adults, Nakhleh et al. [3] reported a series of 12 patients, 18–36 years old, who had either embryonal or alveolar rhabdomyosarcoma of head and neck origin. Therefore, this diagnosis probably should be considered in a young adult who has a mass in the appropriate location. Forty percent of rhabdomyosarcomas arise in the head and neck [1, 2]. The orbit and nasopharynx are affected most often; next are the paranasal sinuses and middle ear. The Intergroup Rhabdomyosarcoma Study [1, 4, 5] divides head and neck rhabdomyosarcomas by site of origin into three groups: (1) orbital, (2) parameningeal, and (3) other head and neck sites. The

---

Received December 19, 1991; accepted after revision February 28, 1992.

[1] Department of Radiology, Bowman Gray School of Medicine, Medical Center Blvd., Winston-Salem, NC 27157-1088. Address reprint requests to L. E. Ginsberg.

AJR 159:581–589, September 1992 0361–803X/92/1593–0581 © American Roentgen Ray Society

parameningeal group includes those tumors closely adjacent to the skull base meninges: middle ear, posterior nasopharynx and posterior paranasal sinuses, and nasal cavity and anterior paranasal sinuses [1]. This subgroup of rhabdomyosarcomas has the poorest prognosis because invasion of the skull and intracranial spread are likely. CT shows an enhancing soft-tissue mass and areas of bone destruction. Meningeal enhancement representing tumor involvement indicates a poor prognosis [6]. Foraminal destruction can be detected. Rhabdomyosarcomas generally appear as a bulky soft-tissue mass with a signal intensity similar to that of muscle on T1-weighted MR images (e.g., 750/16 [TR/TE]) and hyperintensity on T2-weighted images (e.g., 2000/70) [2] (Fig. 1). Heterogeneity may be seen on T2-weighted images in many cases [2]. In a study by Yousem et al. [2], seven (100%) of seven cases showed contrast enhancement. Signal characteristics alone are not sufficient to distinguish between the histologic subgroups of rhabdomyosarcoma (embryonal and alveolar) [2]. Destruction of the skull base and intracranial involvement should be readily detected on MR images, especially with contrast enhancement. In particular, involvement of the cavernous sinus is common and should be ruled out, as it may result in cranial nerve palsies and is a grave prognostic sign [7] (Fig. 1). As with other lesions in this region, perineural spread is possible and may contribute to intracranial involvement. Recent work [8] indicates improved prognosis for non-orbital head and neck rhabdomyosarcoma when multiagent chemotherapy, surgery, and radiation therapy are used.

Juvenile Angiofibroma

Juvenile angiofibroma is an uncommon, highly vascular tumor that affects adolescent boys. Though benign, it is aggressive. In their series of 30 patients with juvenile angiofibroma, Lloyd and Phelps [9] found an average age of onset of 15.5 years. Opinions differ, but the site of origin is probably in the region of the nasopharynx, posterior nares [7, 10], or, as suggested by Lloyd and Phelps [9], the sphenopalatine foramen. This lesion accounts for 0.5% of head and neck neoplasms and is the most common benign tumor of the nasopharynx [7]. Clinical presentation is related to common sites of tumor extension. Nasal obstruction, epistaxis, and, occasionally, facial deformity are the initial signs and symptoms. At the time of presentation, extensive spread beyond the site of origin is common. Involvement of the nasal cavity, sphenoidal sinus, and pterygopalatine fossa is likely; involvement of the pterygopalatine fossa results in the classic anterior bowing of the posterior wall of the maxillary sinus (Fig. 2). With involvement of the pterygopalatine fossa, extension into the infratemporal fossa via the pterygomaxillary fissure is facilitated. The tumor can gain access into the orbit via the inferior orbital fissure and then into the middle cranial fossa via the superior orbital fissure. Extension into the sphenoidal sinus is encountered in two thirds of cases at presentation. Posterior invasion into the clivus and cavernous sinuses is possible and must be sought radiologically. Because of the vascular nature of this lesion, biopsy is hazardous, and the diagnosis generally depends on the clinical presentation, age and sex of the patient, and radiologic features.

CT shows a homogeneously enhancing soft-tissue mass in the nasopharynx and adjacent spaces. Involvement of the pterygopalatine fossa is generally accompanied by anterior remodeling of the posterior wall of the maxillary sinus (Fig. 2). Loss of normal infratemporal fossa fat suggests tumor involvement at that site. This neoplasm has low to intermediate signal intensity on T1-weighted MR images (Fig. 3), and is variably hyperintense on T2-weighted images. Internal foci of punctate or serpiginous low signal intensity represent tumor vessels and are present on both T1- and T2-weighted studies and after administration of contrast material. As expected,

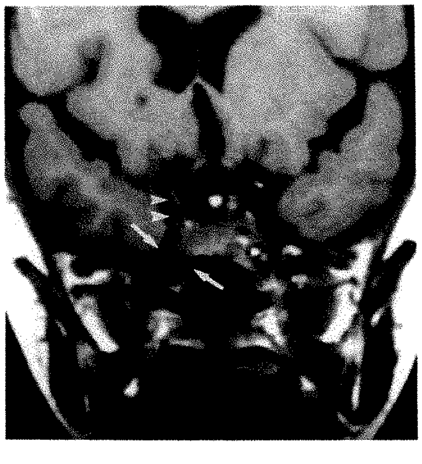

Fig. 1.—Nasopharyngeal rhabdomyosarcoma in a 10-year-old boy. Coronal T1-weighted MR image (750/16) shows mass in right nasopharynx extending intracranially through foramen ovale (*arrows*). Absence of normal internal carotid flow void (*arrowheads*) represents occlusion.

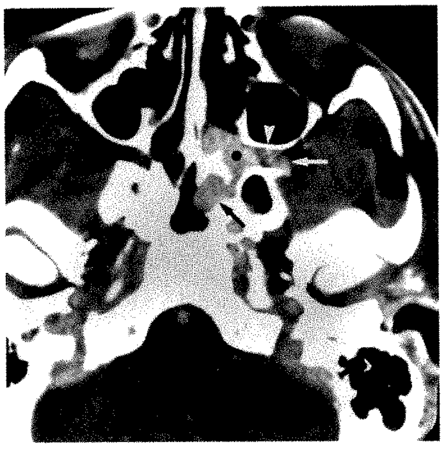

Fig. 2.—Juvenile angiofibroma in a 16-year-old boy. Contrast-enhanced axial CT scan shows mass with widening of left pterygopalatine fossa (*white arrow*) and slight anterior bowing of posterior wall of left maxillary sinus (*arrowheads*). Widening of left sphenopalatine foramen establishes tumor in this location (*black dot*). Note involvement of sphenoidal sinus (*black arrow*).

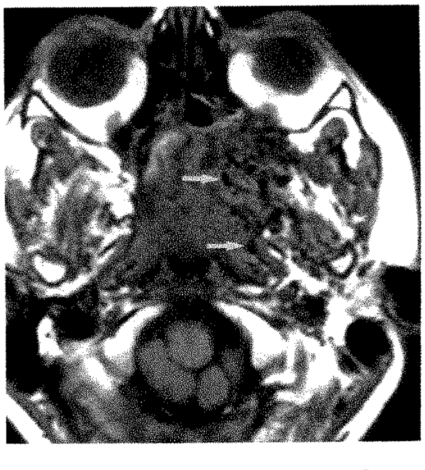

Fig. 3.—Juvenile angiofibroma in a 12-year-old boy. Axial T1-weighted MR image (650/20) shows a large isointense nasopharyngeal mass. Left aspect of lesion shows prominent flow voids corresponding to tumor vessels (*arrows*). This finding need not always be present, especially in smaller or less vascular lesions.

this vascular neoplasm enhances brightly with gadopentetate dimeglumine. As with other skull base processes, CT is better suited for detection of bone changes, and MR imaging is better for evaluating the overall extent of involvement. Arteriography is often used to provide detailed information about the vascular supply to this tumor and to facilitate preoperative embolization.

Chondrosarcoma

Chondrosarcoma, a slow-growing, malignant cartilaginous tumor, constitutes 11% of malignant bone tumors and affects the head and neck in approximately 6% of cases [11, 12]. Chondrosarcomas account for approximately 6% of all skull base lesions. They can arise in cartilage; endochondral bone; or primitive mesenchymal cells in the brain, meninges, membranous bone, or soft tissue [10, 13]. Secondary chondrosarcoma can occur in diseased bone (fibrous dysplasia, Paget's disease, osteochondroma). As the skull base is derived from cartilage, the presence of chondrosarcoma at this site is predictable; in fact, three fourths of all cranial chondrosarcomas are located in the skull base [14]. Specific sites of involvement include the parasellar region, cerebellopontine angle, and facial region, especially the sphenoethmoid, maxillary, and posterior nasal-subsphenoid regions [7, 13]. These tumors spread by local invasion. The parasellar and facial lesions can cause extensive destruction of the skull base [7, 13]. Systemic metastases are uncommon, and prognosis is related to histologic grade, site, and extent of involvement. Prognosis also may be affected by the occasional difficulty in distinguishing histologically among chondrosarcoma, benign chondroma, and the so-called chondroid chordoma. Many lesions have mixed histologic features [14]. Presentation depends on location, but typically it is manifested by insidious onset of single or multiple cranial neuropathies [14].

CT and MR play complementary roles in the imaging of chondrosarcomas. CT is useful in evaluating the calcified matrix so characteristic of this lesion (Fig. 4A). Lee and Van Tassel [13] found a mineralized tumor matrix in all 15 of their cases. The calcification varies in appearance but can be stippled and amorphous, not unlike the chondroid calcifications seen with extracranial chondrosarcomas. Careful evaluation of the calcifications is necessary to avoid confusion with other lesions such as osteosarcoma, chondroma, osteochondroma, or chordoma. Other CT findings include bone erosion and destruction, an enhancing soft-tissue mass, and a sharp zone of transition to normal tissue [13, 14]. MR imaging is generally less specific and is better suited for evaluating extent of disease. The tumor is hypointense relative to brain on T1-weighted images and hyperintense on T2-weighted images. Heterogeneous internal areas of decreased signal represent calcifications. Enhancement is seen with gadopentetate dimeglumine and may be heterogeneous for the same reason (Fig. 4B).

Chordoma

Chordomas are rare, slow-growing neoplasms of embryonic notochordal derivation. They account for less than 1% of all intracranial tumors [10] and only 3–4% of primary bone tumors [15]. Approximately 35% affect the skull base [7, 16], and most involve the clivus. Petrous apex chordomas are rare [17]. Although by strict criteria chordomas are histologically benign, their aggressive behavior and nearly 100% recurrence rate despite radical surgery account for the poor prognosis associated with these tumors. Chordomas are also radioresistant [7]. Histologic malignancy or distant metastases are rare, and metastases appear to be more likely with sacrococcygeal chordomas [18]. The most common age at onset is 20–40 years, and men and women are affected equally. Intracranial chordomas are rare in children, but Handa et al. [19] reported this condition in a 9-year-old boy and reviewed 11 other cases in the literature. Presenting signs and symptoms include cranial neuropathies, headache, vision disturbances, and otolaryngologic symptoms such as nasal obstruction and epistaxis [7, 20].

Radiologically, chordomas appear as enhancing soft-tissue masses with bone destruction. Chordomas are often quite large, extending into the epidural space and causing compression of the vertebrobasilar system and brainstem (Fig. 5). CT

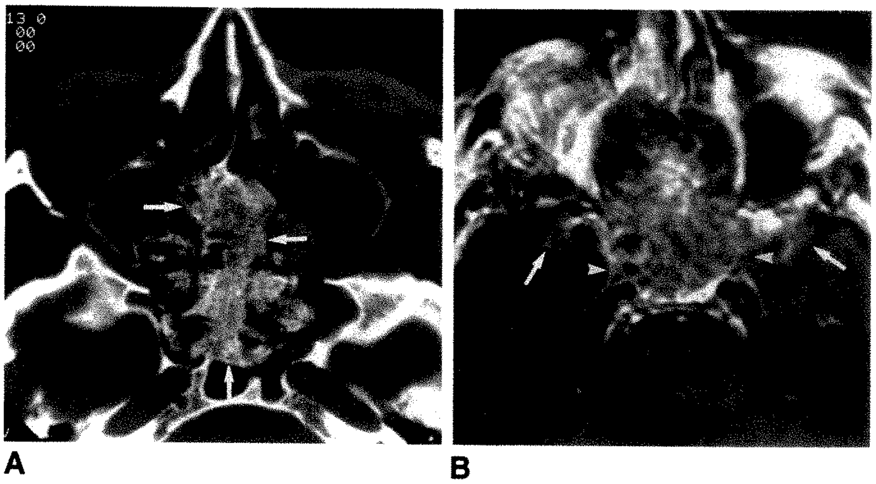

Fig. 4.—Chondrosarcoma in a 55-year-old woman.

A, Axial CT scan (bone algorithm) shows large mass arising in nasoethmoid region. Matrix calcifications are well seen (*arrows*). Sphenoidal sinus is obliterated by tumor.

B, Contrast-enhanced axial T1-weighted MR image (533/20) shows enhancement; marked heterogeneity represents matrix calcification. Note enhancement representing tumor involvement anteriorly in both middle cranial fossae (*arrows*) and both cavernous sinuses (*arrowheads*).

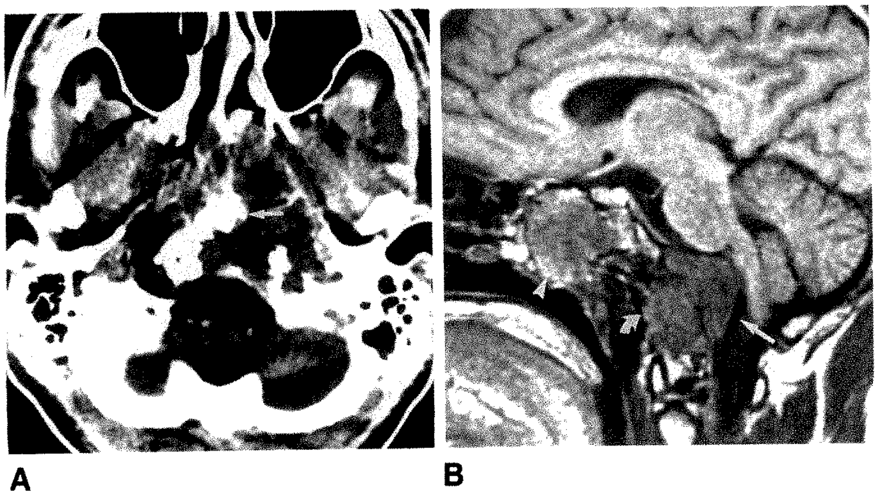

Fig. 5.—Clival chordoma in a 19-year-old man.
***A*, Axial CT scan shows large clival mass with large bone fragment centrally (*arrow*).**
***B*, Sagittal T1-weighted MR image (400/20) shows large heterogeneous, hypointense mass destroying clivus and extending posteriorly to compress medulla. Vertebral artery is seen draped posteriorly (*straight arrow*). Note involvement of sphenoidal sinus anteriorly (*arrowhead*). Inferior extension involves anterior lip of foramen magnum and dens (*curved arrow*).**
(Courtesy of G. Sze, New Haven, CT.)

shows areas of calcification, many of which are actually fragments of destroyed bone [15, 21] (Fig. 5A). In their studies of chordoma, Sze et al. [16] and Oot et al. [21] agreed on the MR appearance of these lesions. Chordomas are isointense to slightly hypointense on T1-weighted MR images (Fig. 5B) and hyperintense on T2-weighted images; they also may contain areas of decreased signal intensity corresponding to calcification. Cystic areas can be detected [16]. Enhancement occurs with contrast administration. CT and MR are equally reliable in detecting this tumor, but MR imaging is considered superior for evaluating extent of disease, especially displacement or encasement of vascular structures and degree of intracranial involvement [16].

Chondroid chordomas, a subset of chordomas, appear to be associated with a considerably better prognosis. Although Oot et al. [21] found no differentiating features on MR imaging, Sze et al. [16] found less hyperintensity on T2-weighted MR images and shorter T1 values with this variant when it was compared with typical chordomas. However, the findings depended on window setting and photography, and therefore may be of little practical value. Although chordoma has no specific radiologic sign, this tumor should be considered whenever a destructive clival lesion is detected in a middle-aged person.

Invasive Pituitary Adenoma

Most pituitary neoplasms in adults are adenomas. These lesions are generally slow growing, histologically benign, and confined to the sella or suprasellar cistern. They can extend laterally into the cavernous sinus or inferiorly into the sphenoidal sinus and skull base. Such extension can make it difficult to distinguish pituitary adenoma from other skull base lesions such as sphenoidal sinus carcinoma, chordoma, or superior extension of nasopharyngeal carcinoma [7]. Invasive pituitary adenomas may not have a suprasellar component and may grow only inferiorly (Fig. 6). Except for absence of the sellar floor, the sella itself may be relatively intact, and this finding should not be used to eliminate pituitary adenoma from consideration when an infrasellar mass is found in the appropriate clinical setting.

CT typically shows an enhancing soft-tissue mass and, as expected, shows bone destruction accurately. T1-weighted MR images show an isointense to slightly hypointense mass that enhances after administration of gadopentetate dimeglumine. The extent of infrasellar and skull base involvement is particularly well shown on coronal and sagittal MR sequences (Fig. 6).

Meningioma

Meningiomas are common benign intracranial tumors that arise from arachnoid cells on the inner surface of the dura mater. They account for approximately 15% of primary CNS tumors and are more common in women than in men [7]. Although the parasagittal and cerebral convexities are more common sites of occurrence, one large series [22] demonstrated a 33% frequency in the skull base. Most of these involved the wings of the sphenoid bone. According to Leonetti et al. [23], 20% of all intracranial meningiomas involve the sphenoid ridge. Therefore, this lesion is seen relatively frequently. Meningiomas of the wings of the sphenoid bone are often subclassified into middle, medial, and hyperostosing en plaque varieties. Hyperostosing en plaque meningiomas grow along the lateral aspect and often a large portion of the greater wing of the sphenoid bone (Fig. 7). An intense hyperostotic bony response indicates invasion of the sphenoid bone by tumor, unlike the typical reactionary hyperostosis associated with other meningiomas [22, 24, 25] (Fig. 7A). This bone invasion contributes both to the difficulty in achieving total resection and to the likelihood of recurrence [22]. Extension through the lateral orbital wall is common and accounts for the classic clinical presentation of this lesion: slowly progressive, painless unilateral exophthalmos and decreased visual acuity [22, 24]. CT shows the hyperostosis, although it also can be seen on MR images (Fig. 7B). Kim et al. [25] noted the potential for confusing this hyperostosis with such bone conditions as fibrous dysplasia, and suggested differentiating features; however, the patient's age, the presentation, and the presence of a soft-tissue mass with meningiomas should lead to the correct diagnosis.

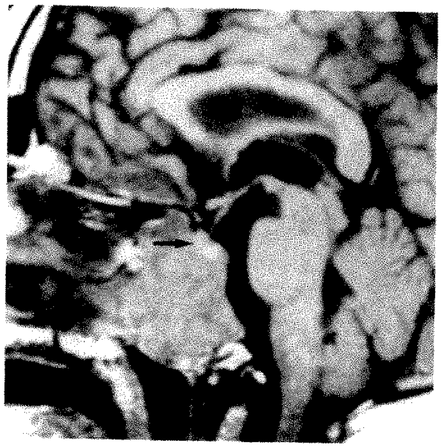

Fig. 6.—Invasive pituitary adenoma in a 65-year-old man. CT bone windows showed extensive bone destruction. Contrast-enhanced sagittal T1-weighted MR image (500/20) shows large enhancing mass occupying sphenoidal sinus and replacing clivus. Absence of thin hypointense cortical bone at sellar floor indicates destruction. Intrasellar contents are preserved. Note differential signal intensity between pituitary gland (*arrow*) and relatively less enhancing mass below it.

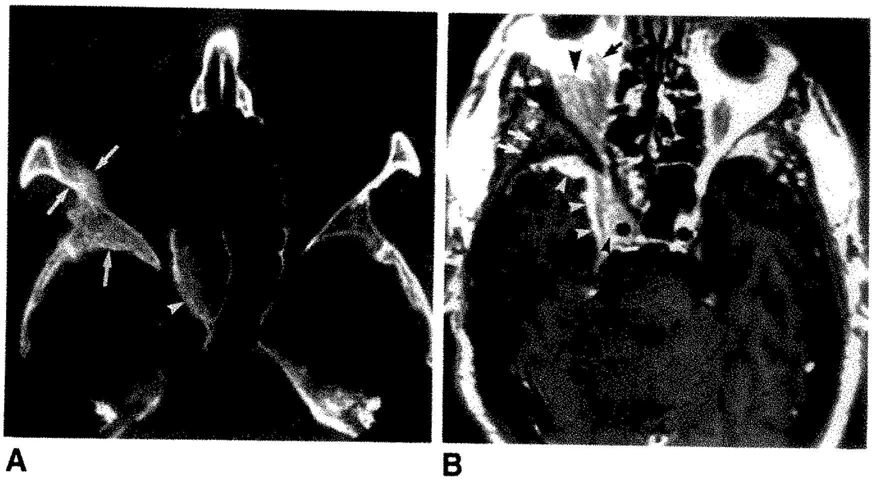

Fig. 7.—Hyperostosing en plaque meningioma involving wing of sphenoid bone in a 66-year-old man.

A, Axial CT scan (bone window) shows intense hyperostosis (*arrows*) along greater wing of sphenoid bone and lateral orbital wall on right and hyperostosis (*arrowhead*) of lateral wall of right sphenoidal sinus.

B, Axial T1-weighted MR image (600/20) after contrast administration shows enhancing tumor involving right cavernous sinus (*small black arrowhead*) and extending along parasellar region and anterior aspect of middle cranial fossa (*white arrowheads*). Bone disease can be detected by replacement of normal marrow signal of right wing of sphenoid bone by minimally enhancing, relatively hypointense tumor (*white arrows*). Note normal marrow fat on left side. Right orbital mass (*large black arrowhead*) causes medial displacement of optic nerve (*black arrow*).

Any of the meningiomas of the sphenoid ridge can extend extracranially. Extension can occur via skull base foramen or by destruction and direct extension through the floor of the middle cranial fossa [7]. Medial extension to involve the sphenoidal and ethmoidal sinuses may also occur. When involvement of the skull base is extensive, diagnostic considerations should include other neoplasms such as nasopharyngeal tumors or chordoma (Fig. 8).

CT findings include bone hyperostosis and a hyperdense, enhancing mass. On T1-weighted MR images, meningiomas are generally isointense or slightly hypointense relative to gray matter (Fig. 8A). On T2-weighted images, approximately 10% are hypointense, 50% remain isointense, and 40% become hyperintense relative to brain [26]. Bright homogeneous contrast enhancement is generally observed (Fig. 8B). Again, MR imaging is ideally suited for determining extent of disease.

Metastatic Disease

Although hematogenous metastases to the skull base occur infrequently, they are more common than primary neoplasms of the skull base [27]. The most likely primary sites of such metastases are prostate, lung, breast, and kidney; lymphomas are less likely. Most of these metastatic lesions are seen as areas of lytic bone destruction on CT, except for prostatic metastases, which are usually osteoblastic. The tumor may have a soft-tissue component. On T1-weighted MR images, the hallmark of metastatic disease is replacement of normal bone marrow with material of decreased signal intensity (Fig. 9). On T2-weighted images, metastases are generally hyperintense relative to adjacent normal bone marrow. With contrast material, bone and soft-tissue components usually show enhancement. Encroachment on neural foramina (Fig. 9A) and spread to vital structures such as Meckel's cave or the cavernous sinus may occur (Fig. 9B). In patients with no history of underlying malignant disease, imaging alone often does not allow differentiation between primary and metastatic neoplasms. The presence of other sites of metastatic disease in the calvaria are of course helpful in the diagnosis (Fig. 9B).

Invasive Nasopharyngeal Carcinoma

The most common primary malignant lesion that involves the skull base is squamous cell carcinoma, usually arising in the nasopharynx [27]. In their review of patterns of spread of nasopharyngeal carcinoma, Sham et al. [28] found that 82 (31%) of 262 cases had erosion of the skull base. Despite the much higher prevalence of this lesion in China, invasion of the skull base by nasopharyngeal carcinoma is common in the United States. CT shows an enhancing soft-tissue mass. Nasopharyngeal carcinoma is isointense relative to skeletal muscle on T1-weighted MR images (Fig. 10) and hyperintense on T2-weighted images. It enhances with gadopentetate dimeglumine. Invasion of the skull base is quite common and is readily detected with CT bone windows (Fig. 11). With T1 weighting, MR imaging also shows bone invasion as replacement of normal marrow with lower signal intensity tumor (Fig. 10). Involvement of the skull base can result in foraminal destruction, with consequent cranial neuropathy, vascular compromise, or both [29] (Figs. 10 and 11). Intracranial spread can occur via direct extension from the skull base or by perineural spread, generally affecting branches of the fifth cranial nerve. The diagnosis of nasopharyngeal carcinoma

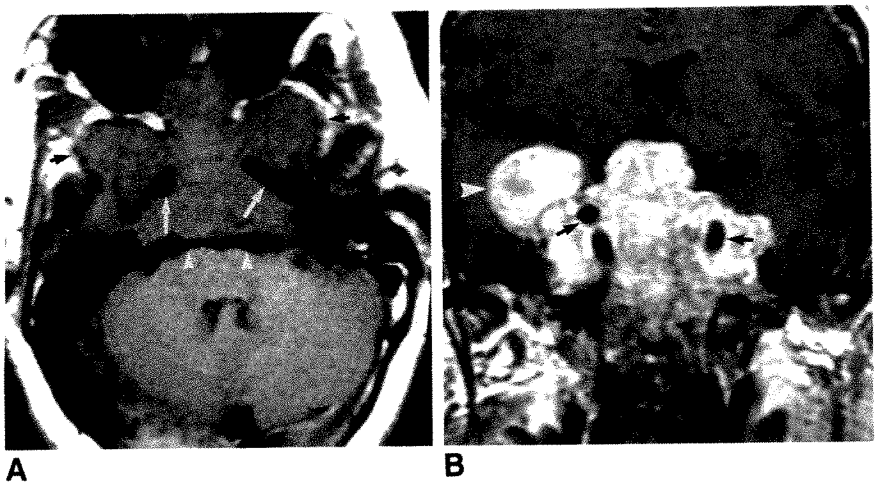

Fig. 8.—Meningioma in a 56-year-old woman. Lesion was initially thought to be a chordoma.

A, Axial T1-weighted MR image (550/20) shows large mass, slightly hypointense relative to brain, extensively infiltrating skull base and replacing clivus. Note bilateral encasement of internal carotid arteries (*white arrows*) and brainstem compression caused by extension into prepontine cistern (*arrowheads*). Pterygoid plates and masticator space are also involved bilaterally (*black arrows*).

B, Coronal T2-weighted MR image (550/20) after contrast administration shows intense tumor enhancement. Carotid arteries are clearly encased by tumor (*arrows*). Note large right middle cranial fossa tumor component (*arrowhead*).

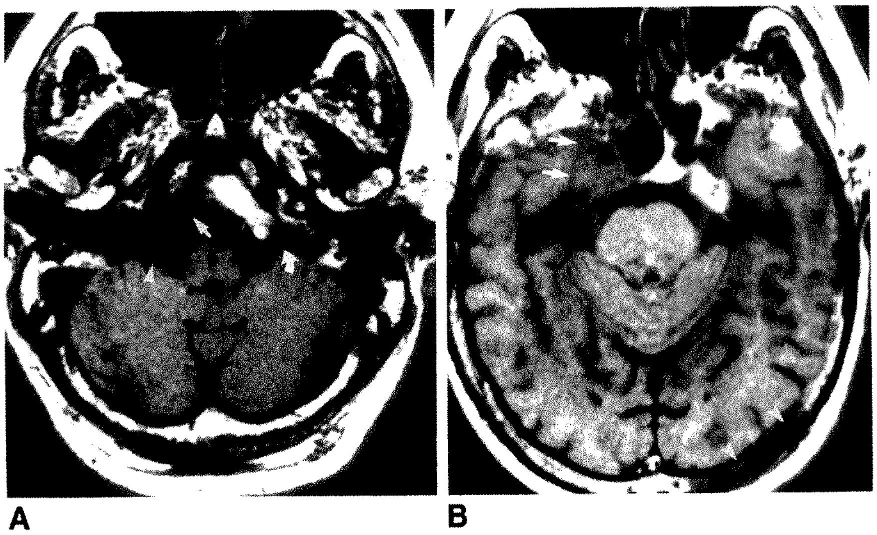

Fig. 9.—Metastatic lung carcinoma in an 84-year-old man who had right-sided cranial neuropathies. Initial CT scan (*not shown*) was interpreted as normal.

A, Axial T1-weighted MR image (550/20) shows marrow replacement in right half of clivus (*straight arrow*). Tumor respects midline and extends into region of right jugular foramen and probably compromises exiting ninth and tenth nerve roots (*arrowhead*). Note normal nerve roots on left (*curved arrow*).

B, Axial T1-weighted MR image (550/20) cephalad to *A* shows tumor infiltrating right cavernous sinus and Meckel's cave (*arrows*). Cavernous carotid artery is slightly narrowed. Additional focus of metastatic disease is seen in left occipital bone (*arrowheads*).

may not be known before imaging. The nasopharyngeal component may be small and must be carefully sought. In the absence of an identifiable nasopharyngeal origin, imaging findings may be nonspecific, and other diagnoses should be considered. Metastases, lymphoma, and primary bone neoplasms can cause destruction of the skull base and a soft-tissue mass in the nasopharynx. Opacification of the mastoids or middle ear, often seen in nasopharyngeal carcinoma as a result of obstruction of the orifice of the eustachian tube, also can be caused by direct invasion of the eustachian tube by any process and therefore is nonspecific.

Sinonasal Carcinoma

Carcinomas arising in the nasal cavity or paranasal sinuses are uncommon; they account for only 3% of head and neck tumors [30]. Histologically, squamous cell and undifferentiated carcinoma are the main cell types. The maxillary sinus is involved either directly or by extension in 80% of cases [30]. The site of origin is the nasal cavity in 25–35% of cases, the ethmoid complex in 10%, and the sphenoidal and frontal sinus in only 1% [30]. These tumors have a strong tendency to destroy bone; therefore, lesions in the posterior nasoethmoid region or sphenoidal sinus are a potential source of direct tumor spread to the skull base (Fig. 12). Differentiation from sinus extension of primary tumors of the skull base may not be possible. Sinonasal carcinomas typically have low to intermediate signal intensity on T1-weighted MR images and intermediate signal intensity on T2-weighted images [31]. This appearance often allows important differentiation between tumor involvement in a sinus and obstructive or inflammatory change. Inflammatory tissue or obstructed secretions, because of higher water content, typically have a higher T2 signal intensity [31].

Discussion

The anatomy of the central skull base is extremely complex. The sphenoid bone is the foundation of the skull base and is involved in virtually every process affecting the central skull

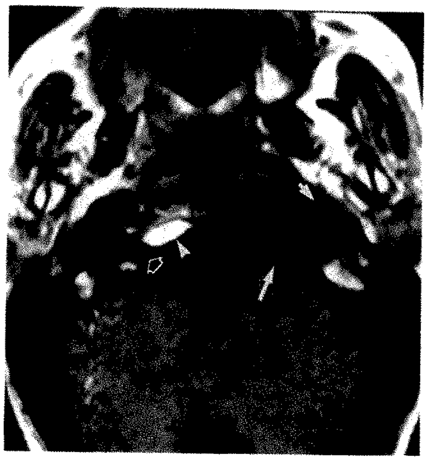

Fig. 10.—Nasopharyngeal carcinoma in a 70-year-old man. Axial T1-weighted MR image (600/16) shows a large left-sided nasopharyngeal mass that has extended posteriorly to invade skull base. Left anterior foramen magnum shows replacement of marrow by tumor. Note normal marrow on right (*arrowhead*) and normal right hypoglossal canal (*open arrow*). Left hypoglossal canal is replaced by tumor (*long solid arrow*). Note encasement of left carotid artery (*short solid arrow*).

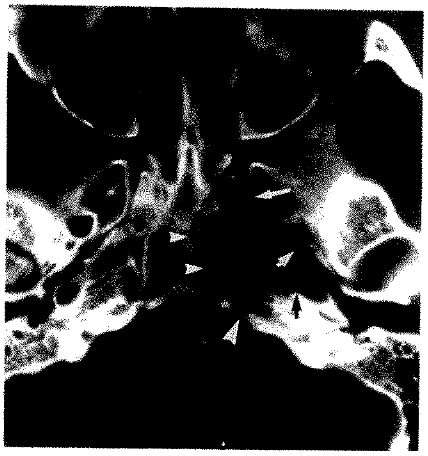

Fig. 11.—Nasopharyngeal carcinoma in a 68-year-old woman. Axial CT scan (bone window) shows extensive left-sided destruction of skull base. Left vidian canal (*long white arrow*), left carotid canal (*black arrow*), left aspect of clivus (*small arrowheads*), and left petrous apex (*large arrowhead*) are destroyed. Bone margins of left foramen ovale and spinosum probably are eroded (*short white arrow*).

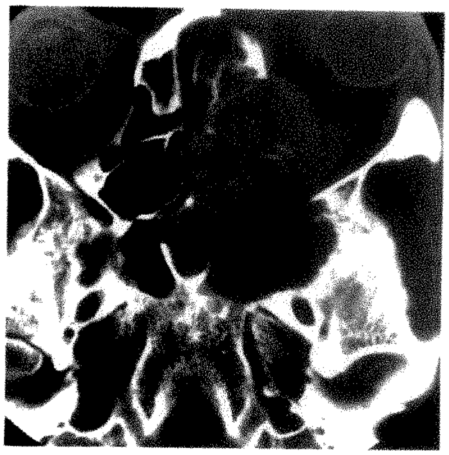

Fig. 12.—Poorly differentiated sinonasal carcinoma in a 73-year-old man. Axial CT scan shows a very destructive sinonasal mass. Left ethmoidal air cells and sphenoidal sinus are obliterated by tumor. Orbital fissures, orbital apex, foramen rotundum, and anterior floor of left middle cranial fossa are destroyed.

base and most of the pathologic conditions discussed in this article. The sphenoid bone contains most of the important foramina and fissures of the skull base, constitutes the floor and anterior wall of the middle cranial fossa, contains the pituitary gland within the sella turcica, and forms part of the clivus. The body of the sphenoid bone contains the paired sphenoidal sinuses. Therefore, to a large extent, imaging the central skull base means imaging the sphenoid bone.

A large variety of primary and secondary pathologic processes can affect the central skull base. To some extent, the radiologic features of many lesions of the skull base are nonspecific. For example, an enhancing soft-tissue mass replacing the clivus that is hypointense on T1-weighted images and hyperintense on T2-weighted images could be chordoma, meningioma, chondrosarcoma, metastasis, or even pituitary adenoma. However, when the features of the more common lesions are considered systematically, some diagnostic possibilities can be eliminated or placed lower on the list, and others become more likely. In this regard, CT and MR imaging are complementary in their capacity to help the radiologist predict the histologic diagnosis of skull base tumors. With meningioma or chondrosarcoma, for example, the presence of characteristic bone changes can narrow the differential diagnosis substantially. CT generally shows bone changes or destruction better than MR does. Once a lesion in the skull base has been fully imaged, the list of possibilities can be reduced. Still, it is often not possible to predict a tumor's histologic diagnosis with certainty because of the similarity of these lesions on CT and MR, and because of their ability to extend from one anatomic location to another.

Probably the most important role of imaging, however, is in evaluating the extent of disease. What aspects of the skull base are involved? Is foraminal destruction present? Is perineural spread present? Are the cavernous sinuses intact? Is vascular compromise present? Is there intracranial extension or compression of brain parenchyma? Answers to these questions ultimately may be more important than precise diagnosis because they provide the information needed for complete surgical excision. They may also save a patient with extensive disease from lengthy, disfiguring, and ultimately unsuccessful surgery.

With MR imaging, extent of disease can be precisely outlined in virtually every case. Occasionally, the findings on contrast-enhanced images can be inconclusive if a tumor component enhances to an intensity similar to that of adjacent fat. In these cases, unenhanced T1-weighted MR imaging or the recently developed fat-suppression techniques (after enhancement) can be used to solve specific problems [32, 33].

After the extent of a tumor has been determined, the challenge remains to make a predictive histologic diagnosis on the basis of the imaging findings. Despite some nonspecificity, clinical and imaging features often suggest the correct diagnosis.

In children less than 10 years old, a nasopharyngeal or sinus mass associated with destruction of the skull base is likely a rhabdomyosarcoma. Less likely considerations include metastatic disease from a remote primary neoplasm or the rare melanotic neuroectodermal tumor of infancy. In a poorly controlled diabetic or immunocompromised patient, opportunistic infection is a possible diagnosis. In adolescent boys, juvenile angiofibroma has a characteristic presentation and radiologic features (Figs. 2 and 3). In particular, widening of the pterygopalatine fossa and sphenopalatine foramen secondary to slow growth of this tumor and flow voids on MR studies facilitate diagnosis of juvenile angiofibroma. In equivocal cases, angiography shows the typical vascular blush associated with this lesion.

Meningiomas often can be diagnosed on the basis of imaging characteristics. Typical features such as en plaque growth along the wings of the sphenoid bone and hyperostosis of the sphenoid bone are highly suggestive. If these bone changes are associated with an orbital mass and a history of painless exophthalmos, the diagnosis is almost certain. If, however, these features are lacking, or if extracranial spread into the sinonasal region is extensive, findings are less specific and other diagnoses must be considered.

Pituitary adenoma should be considered when evidence of endocrine dysfunction is found. If imaging is done before laboratory tests or in patients without physical stigmata of endocrinopathy, an intrasellar mass with infrasellar or parasellar extension suggests the possibility of invasive pituitary adenoma. However, there need not be a discernible intrasellar component (Fig. 6). In such cases, only a differential diagnosis can be offered, and the clinical history must be reviewed and correlated with imaging findings.

Imaging of chondrosarcoma can be specific if the mineral matrix is seen on CT (Fig. 4A). This lesion also has a predilection for the parasellar and sphenoethmoid/vomer region [13]. Of course, when chondrosarcoma occurs in an atypical location or in the absence of characteristic tumor calcification, radiologic findings are less specific.

Nasopharyngeal carcinoma frequently is accompanied by destruction of the skull base. A nasopharyngeal origin usually is detected easily with CT or MR imaging. Smaller lesions are more easily detected on MR because of MR's superior soft-tissue contrast resolution. In addition to causing destruction of the skull base by direct extension, this tumor has a strong tendency to spread via a perineural mechanism. Branches of the fifth cranial nerve are affected most often. This condition can be detected on coronal MR images well before CT scans show foraminal erosion. Fat-suppressed contrast-enhanced T1-weighted MR images are useful for this purpose. Perineural spread is considered a poor prognostic sign. Isointense thickening of a cranial nerve such as V_3 on unenhanced T1-weighted images indicates perineural tumor involvement (Fig. 1). Enhancement after administration of gadopentetate dimeglumine can help show any associated intracranial component. Denervation atrophy of the masticatory muscles also may follow as a result of perineural spread. Because of the proximity of the nasopharynx to the skull base, intracranial involvement also can result from spread through the foramen lacerum. Tumor also can spread along the carotid canal, gaining access to the cavernous sinus without destroying bone, and can result in neuropathies of cranial nerves III, IV, V_1, V_2, and VI. Vascular thrombosis generally can be detected with routine spin-echo MR imaging. In difficult cases there may be a role for gradient-echo sequences or MR angiography.

Sinonasal carcinomas are uncommon, and most involve the maxillary sinus or nasal cavity. Unfortunately, these lesions are often quite large at presentation, causing extensive destruction. The site of origin cannot always be determined (Fig. 12). Involvement of the skull base and pterygopalatine fossa no longer signifies unresectable disease. Indeed, newer, aggressive surgical techniques are being used not only for cure but, in the case of cranial nerve involvement, for palliation. Wide dural or cavernous sinus involvement probably would be unresectable for cure. Although more posterior sphenoid-based or intracranial lesions can spread anteriorly to involve the sinonasal region, any mass predominantly centered about the paranasal sinus/nasal region should suggest that location as the primary source. In adults, other diagnostic considerations include minor salivary gland tumors (adenoid cystic, mucoepidermoid carcinoma), melanoma, malignant schwannoma, lymphoma, plasmacytoma, fibrosarcoma, metastases, chondrosarcoma, and fibroosseous lesions (osteosarcoma, osteoblastoma, osteoma) [30]. Esthesioneuroblastoma also should be considered for a more anteriorly situated ethmoidal lesion with intracranial spread. These do not generally involve the central skull base. Diabetic or immunocompromised patients with a destructive sinonasal process may have an opportunistic infection such as mucormycosis or aspergillosis. Less common considerations include Wegener's granulomatosis and lethal midline granuloma.

Hematogenous metastases to the skull base, although uncommon, occur more frequently than primary tumors of the skull base. Therefore, such metastases should always be considered when an adult has a clival mass. The tumor may have a soft-tissue component. Although CT is generally superior to MR in the detection of bone disease, MR imaging is preferable when the bone is infiltrated rather than completely destroyed (Fig. 9), in which case only minimal changes may be noted on CT. If a high-resolution bone algorithm is not used, tumor infiltration of the skull base can be overlooked. Differentiation between chordoma and skull base metastases may be impossible. Chordoma generally manifests as a large destructive mass (Fig. 5) with fragments of destroyed bone centrally (Fig. 5A). However, when the lesion is smaller or no fragmentation of bone occurs, differentiation from metastatic disease may be impossible. In our patient who had multiple skull base metastases, the diagnosis was facilitated not only by the knowledge of underlying lung carcinoma but also by evidence of disease involving other calvarial sites (Fig. 9B).

Conclusions

Although not encountered on a daily basis, neoplastic involvement of the central skull base can be seen by any radiologist affiliated with a busy otolaryngology or neurosurgery service. The role of the radiologist is to evaluate the extent of disease and to offer a reasonable differential diagnosis. When all aspects of a case are considered, these objectives can be accomplished readily. Although imaging results are sometimes nonspecific, the combination of CT and MR imaging is invaluable in assessing the extent of disease and in the treatment and follow-up of patients with neoplastic disease of the central skull base.

ACKNOWLEDGMENTS

I thank Julianne Berckman and Donna S. Garrison for manuscript preparation.

REFERENCES

1. Latack JT, Hutchinson RJ, Heyn RM. Imaging of rhabdomyosarcomas of the head and neck. *AJNR* **1987**;8:353–359
2. Yousem DM, Lexa FJ, Bilaniuk LT, Zimmerman RI. Rhabdomyosarcomas in the head and neck: MR imaging evaluation. *Radiology* **1990**;177: 683–686
3. Nakhleh RE, Swanson PE, Dehner LP. Juvenile (embryonal and alveolar) rhabdomyosarcoma of the head and neck in adults: a clinical, pathologic, and immunohistochemical study of 12 cases. *Cancer* **1991**;67:1019–1024
4. Raney RB Jr, Donaldson MH, Sutow WW, Lindberg RD, Maurer HM, Tefft M. Special considerations related to primary site in rhabdomyosarcoma: experience of the Intergroup Rhabdomyosarcoma Study, 1972–76. *NCI Monogr* **1981**;56:69–74
5. Tefft M, Fernandez C, Donaldson M, Newton W, Moon TE. Incidence of meningeal involvement by rhabdomyosarcoma of the head and neck in children: a report of the Intergroup Rhabdomyosarcoma Study (IRS). *Cancer* **1978**;42:253–258
6. Feldman BA. Rhabdomyosarcoma of the head and neck. *Laryngoscope* **1982**;92:424–440
7. Braun IF, Nadel L. The central skull base. In: Som PM, Bergeron RT, eds. *Head and neck imaging*, 2nd ed. St. Louis: Mosby, **1991**:875–924
8. Anderson GJ, Tom LWC, Womer RB, Handler SD, Wetmore RF, Potsic WP. Rhabdomyosarcoma of the head and neck in children. *Arch Otolaryngol Head Neck Surg* **1990**;116:428–431
9. Lloyd GAS, Phelps PD. Juvenile angiofibroma: imaging by magnetic resonance, CT and conventional techniques. *Clin Otolaryngol* **1986**;11: 247–259
10. Laine FJ, Nadel L, Braun IF. CT and MR imaging of the central skull base: Part 2. Pathologic spectrum. *RadioGraphics* **1990**;10:797–821
11. Dahlin DC, Unni KK. *Bone tumors*, 4th ed. Springfield, IL: Thomas, **1986**:227–259
12. Pritchard DJ, Lunke RJ, Taylor WF, Dahlin DC, Medley BE. Chondrosarcoma: a clinicopathologic and statistical analysis. *Cancer* **1980**;45: 149–157
13. Lee Y-Y, Van Tassel P. Craniofacial chondrosarcomas: imaging findings in 15 untreated cases. *AJNR* **1989**;10:165–170
14. Kveton JF, Brackmann DE, Glasscock ME III, House WF, Hitselberger WE. Chondrosarcoma of the skull base. *Otolaryngol Head Neck Surg* **1986**;94:23–32
15. Krol G, Sundaresan N, Deck M. Computed tomography of axial chordomas. *J Comput Assist Tomogr* **1983**;7:286–289
16. Sze G, Uichanco LS III, Brant-Zawadzki MN, et al. Chordomas: MR imaging. *Radiology* **1988**;166:187–191
17. Brown RV, Sage MR, Brophy BP. CT and MR findings in patients with chordomas of the petrous apex. *AJNR* **1990**;11:121–124
18. Krol G, Sze G, Arbit E, Marcove R, Sundaresan N. Intradural metastases of chordoma. *AJNR* **1989**;10:193–195
19. Handa J, Suzuki F, Nioka H, Koyama T. Clivus chordoma in childhood. *Surg Neurol* **1987**;28:58–62
20. Mills RP. Chordomas of the skull base. *J R Soc Med* **1984**;77:10–16
21. Oot RF, Melville GE, New PFJ, et al. The role of MR and CT in evaluating clival chordomas and chondrosarcomas. *AJR* **1988**;151:567–575
22. Ojemann RG. Meningiomas: clinical features and surgical management. In: Wilkins RH, Rengachary SS, eds. *Neurosurgery*, vol. 1. New York: McGraw-Hill, **1985**:635–654
23. Leonetti JP, Reichman OH, Smith PG, Grubb RL, Kaiser P. Meningiomas of the lateral skull base: neurotologic manifestations and patterns of recurrence. *Otolaryngol Head Neck Surg* **1990**;103:972–980
24. Pompili A, Derome PJ, Visot A, Guiot G. Hyperostosing meningiomas of the sphenoid ridge—clinical features, surgical therapy, and long-term observations: review of 49 cases. *Surg Neurol* **1982**;17:411–416
25. Kim KS, Rogers LF, Goldblatt D. CT features of hyperostosing meningioma en plaque. *AJR* **1987**;149:1017–1023
26. Curtin HD, Hirsch WL Jr. Base of the skull. In: Atlas SW, ed. *Magnetic resonance imaging of the brain and spine*. New York: Raven, **1991**: 669–707
27. Whelan MA, Reede DL, Meisler W, Bergeron RT. CT of the base of the skull. *Radiol Clin North Am* **1984**;22:177–217
28. Sham JST, Cheung YK, Choy D, Chan FL, Leong L. Nasopharyngeal carcinoma: CT evaluation of patterns of tumor spread. *AJNR* **1991**;12: 265–270
29. Teresi LM, Lufkin RB, Vinuela F, et al. MR imaging of the nasopharynx and floor of the middle cranial fossa: Part II. Malignant tumors. *Radiology* **1987**;164:817–821
30. Som PM. Tumors and tumorlike conditions. In: Som PM, Bergeron RT, eds. *Head and neck imaging*. 2nd ed. St. Louis: Mosby, **1991**:169–227
31. Som PM, Shapiro MD, Biller HF, Sasaki C, Lawson W. Sinonasal tumors and inflammatory tissues: differentiation with MR imaging. *Radiology* **1988**;167:803–808
32. Barakos JA, Dillon WP, Chew WM. Orbit, skull base, and pharynx: contrast-enhanced fat suppression MR imaging. *Radiology* **1991**;179:191–198
33. Tien RD, Hesselink JR, Chu PK, Szumowski J. Improved detection and delineation of head and neck lesions with fat suppression spin-echo MR imaging. *AJNR* **1991**;12:19–24

Radiology Outreach Foundation

The Radiology Outreach Foundation (ROF) is a nonprofit corporation whose goal is to help disadvantaged countries improve their health care by providing radiology equipment, books, consultation, education, and training to their practitioners. This assistance is on an application basis that is independent of political, ethnic, or religious orientation of the grantee. It depends on the need of the people and the ability of the ROF to meet that need. The ROF is approved by the U.S. Internal Revenue Service as a tax-exempt organization. It is endorsed by the following radiologic societies:

American Association of Women Radiologists
American College of Radiology
American Roentgen Ray Society
Association of University Radiologists
Radiological Society of North America
Society of Chairmen of Academic Radiology Departments
Society for Pediatric Radiology
European Society of Pediatric Radiology

All donations to the ROF are tax deductible. Persons who would like to contribute financially to the ROF, would be interested in being a visiting professor, would like to send books or journals to any of the institutions supported by the ROF, or would like further information about the ROF should write to

Charles A. Gooding, M.D.
President
Radiology Outreach Foundation
3415 Sacramento St.
San Francisco, CA 94118 USA

Review Article

Diffusion MR Imaging: Clinical Applications

Denis Le Bihan,[1] Robert Turner,[2] Philippe Douek,[3] and Nicholas Patronas[1,4]

Water self-diffusion, a recently discovered source of contrast on MR images, has already shown promise for some clinical applications. Most studies have been of the brain, essentially for technical reasons. Diffusion is useful in distinguishing the different components of brain tumors (cystic regions, edema, necrosis) from the tumor core itself. Recent studies have shown that diffusion is anisotropic in brain white matter (i.e., dependent on the fiber tract's orientation in space), offering new insights into myelin disorders. Diffusion is also dramatically altered in the minutes following ischemic injury in the cat brain, which may have tremendous impact for the diagnosis and management of hyperacute stroke. With ultrafast acquisition schemes, diffusion imaging has also been used outside the CNS, for instance, in the eye and kidney. Future applications include diffusion-localized spectroscopy and temperature imaging. This article reviews recent progress in this field and suggests potential applications.

With the introduction of diffusion MR imaging, water movement and transport in biological tissues have become attractive topics for in vivo MR imaging investigations [1]. Studies of molecular displacements over distances comparable to a cell's dimensions can be expected to provide information about the geometry and spatial organization of the tissue compartments, as well as some functional insights about water exchanges between these compartments in various normal or disease states [2]. Although diffusion MR imaging is a recently developed technique, some studies have already shown the clinical value of the method. Most of these clinical studies were of the CNS. Besides beings of compelling clinical interest, the CNS has the advantages of consisting of relatively immobile tissues and of having favorable MR characteristics, such as long T1 and T2 relaxation times. Body studies are far more difficult, although preliminary results of diffusion imaging of the kidneys have been reported and are shown here. Also, the possibility of applying to perfusion imaging techniques similar to those used in diffusion imaging has been suggested [2, 3]. However, technical difficulties have limited application of such perfusion imaging. Also, the feasibility of using diffusion imaging in vivo was not demonstrated overnight. The initial technique, based on spin-echo two-dimensional Fourier transform (2DFT) imaging [4, 5], was slow, sensitive to motion artifacts, and implemented on MR units with imperfect gradient systems, so that some researchers expressed justifiable concerns about the meaning of the measurements [6]. Since then, important technical improvements (e.g., the amazing capability of determining molecular displacements in the micrometer range from images that have a millimeter resolution and depict organs that may move with an amplitude of several millimeters) have occurred that have proved the feasibility of diffusion imaging in vivo. The basic principles of diffusion imaging are reviewed only briefly, as the main object of this article is to survey the current and potential clinical applications of this technique.

Background

Principles of Diffusion MR Imaging

The principles of diffusion MR imaging have been outlined recently in several review articles [2, 7] and are only sum-

---

Received July 15, 1992; accepted after revision February 28, 1992.

[1] Diagnostic Radiology Department, Bldg. 10, Rm. 1C660, The Warren G. Magnuson Clinical Center, National Institutes of Health, Bethesda, MD 20892. Address reprint requests to D. Le Bihan.

[2] National Heart, Lung and Blood Institute, National Institutes of Health, Bethesda, MD 20892.

[3] Biomedical Engineering and Instrumentation Program, National Institutes of Health, Bethesda, MD 20892.

[4] Department of Radiology, Georgetown University Hospital, 3800 Reservoir Rd. N.W., Washington, DC 20007.

AJR 159:591-599, September 1992 0361-803X/92/1593-0591 © American Roentgen Ray Society

marized here. Diffusion imaging is based on the natural sensitivity of MR to motion, which serves, for instance, as the basis of MR phase-contrast angiography. In the presence of a magnetic field gradient, protons carried by moving water molecules undergo a phase shift of their transverse magnetization (Fig. 1). As diffusion is characterized by the random (brownian) displacements of molecules, these phase shifts are widely dispersed, interfering with each other and finally resulting in attenuation of the MR signal. This attenuation directly depends on the amplitude of the molecular displacements (related to the diffusion coefficient) and on the intensity of the magnetic field gradient.

Diffusion effects are extremely small and are usually invisible on conventional MR images. In practice, diffusion-weighted images are obtained by incorporating strong magnetic field gradient pulses within any imaging pulse sequence (Fig. 2). The degree of diffusion weighting is set by the strength and duration of the gradient pulses (integrated in the so-called gradient factor [2, 7]), as the degree of T2 weighting in a spin-echo sequence is defined by the echo time. In a diffusion-weighted image (Fig. 3A), structures with fast (large) diffusion are dark, because they are subject to greater signal attenuation, whereas structures with slow (low) diffusion are bright. Calculated (quantitative) diffusion images can also be generated from a series of diffusion-weighted images by using adequate software. In those images (Fig. 3B), diffusion is the only variable responsible for the contrast (and not T1 and T2). Usually, contrast is such that structures with high (fast) diffusion are bright, and those with low (slow) diffusion are dark. Calculated diffusion images are somewhat dependent on postprocessing power. They generally have a noisier appearance than diffusion-weighted images, and therefore may be preferred for clinical use. However, only calculated images provide the quantitative information necessary for validation of new results. Moreover, as other kinds of intravoxel incoherent motion (IVIM), such as capillary perfusion, may produce effects similar to those of true diffusion, the term apparent diffusion coefficient (ADC) has been suggested to describe quantitatively the results of diffusion imaging experiments in vivo [3, 5].

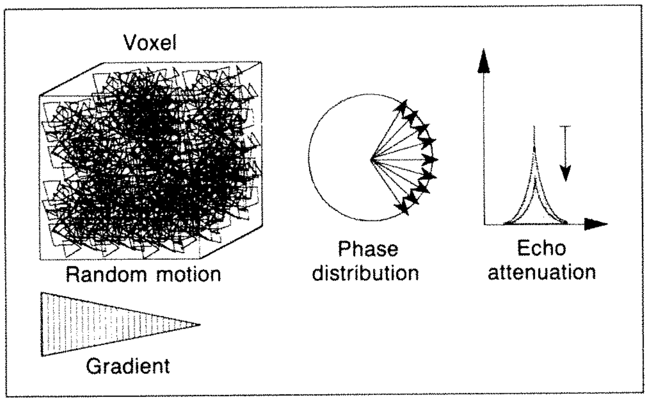

Fig. 1.—Intravoxel incoherent motion and signal attenuation. For a population of randomly moving molecules, as in diffusion, motion along the direction of the magnetic field gradient is different for each molecule, resulting in a distribution of phase shifts that reflects distribution of molecular motion. In the case of diffusion, the average phase shift is zero, because the average molecular displacement is zero. Dispersion of the phase shifts depends on the variance of the displacements (square of the diffusion distance), which is related to the diffusion coefficient. This dispersion of phase shifts finally results in an attenuation of the signal amplitude, which depends on the diffusion coefficient and the gradient waveform.

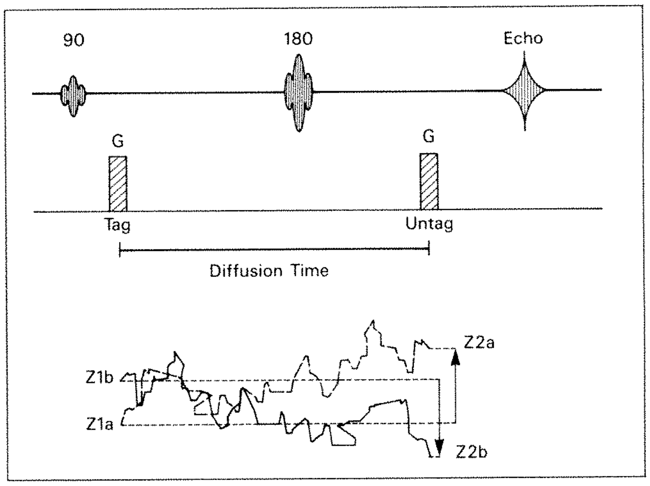

Fig. 2.—Principles of diffusion MR imaging. Effects of motion and diffusion become visible when an MR sequence, such as spin echo, is sensitized by magnetic field gradients. Suppose Z1a and Z1b are positions of two molecules when first (tagging) gradient pulse G is applied. Because of this pulse, molecules in time will acquire a phase shift that is a function of their position with respect to the gradient. After a given interval (diffusion time), a second (untagging) pulse is applied. For "static" molecules, the second phase shift is identical to that produced by the first pulse, so that pulses cancel each other out (initial phase shift is reversed by 180° RF pulse). For diffusing molecules, position changes between the two pulses (Z2a and Z2b). A net phase shift is then observable, a function of displacement, Z2 − Z1, of the molecules during diffusion time. Phase shifts acquired by all molecules interfere with each other, resulting in imperfect refocusing of echo (i.e., attenuation of an echo depends directly on molecular mobility rate [diffusion coefficient]).

Clinical use of diffusion MR imaging has been limited by the technique's high sensitivity to motion artifacts and by available hardware on conventional MR systems. Diffusion imaging has benefited from recent technical improvements. Among these are the use of shielded gradient coils [8–10], which reduce eddy currents generated by the switching of the diffusion-sensitizing gradient pulses, and the use of small dedicated low-inductance coils, which allow rapid switching of large gradient amplitudes. This latter innovation has also enabled implementation of echoplanar imaging [11–14], from which diffusion imaging has benefited enormously. The use of such a single-shot technique has greatly reduced the risk of motion artifacts and has increased the accuracy of the measured diffusion coefficients, because many differently sensitized diffusion images can now be obtained in short intervals compatible with a clinical protocol (Fig. 4).

Diffusion in Biological Tissues

Many diffusion studies in isolated biological tissues were conducted in the 1970s [15–19]. The diffusion coefficient of water in tissues was found to be two to 10 times less than

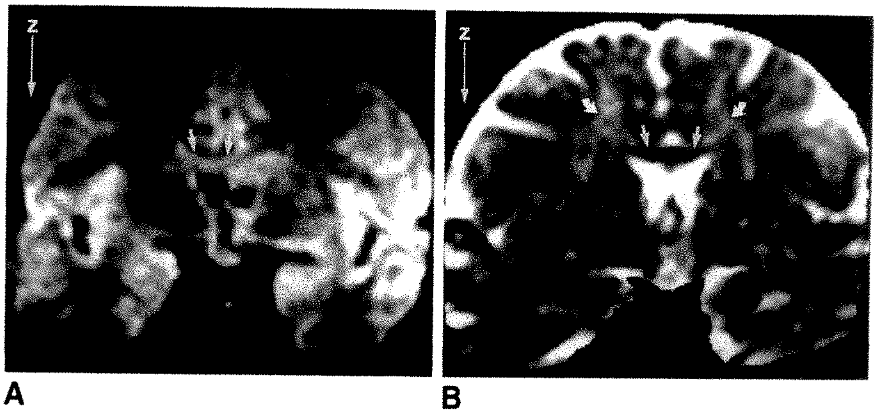

Fig. 3.—*A*, Coronal diffusion-weighted MR image (50-msec acquisition time, 10-mm slice thickness, 2.5 mm^2 in-plane resolution, 100-msec TE) was obtained directly by using echoplanar imaging sequence sensitized to diffusion by additional gradient pulses. Gradient pulses (20-msec duration, 30 mT/m amplitude) were set along z axis (superior-inferior). White matter tracts where fibers are perpendicular to the z axis, as in corpus callosum (*arrows*), present lower diffusion and therefore less signal attenuation than gray matter and white matter tracts parallel to z axis and appear brighter than these structures. Contrast between gray matter and parallel white matter is otherwise poor: Diffusion in gray matter is less than in parallel white matter, but T2 is longer in gray matter, so that diffusion and T2 effects cancel each other.

B, Calculated diffusion MR image was obtained from a set of eight different diffusion-weighted images acquired as in *A*, while amplitude of gradient pulse was varied from 0 to 38 mT/m. Brightness of each pixel is now directly proportional to diffusion coefficient and depends only on this variable. Fiber tracts perpendicular to z axis now appear dark (corpus callosum, *straight arrows*); tracts parallel to z axis are bright (*curved arrows*). Excellent contrast is achieved, because T1 and T2 effects have been removed.

that of pure water (Table 1). This is understandable, given that water molecules must move tortuously around obstructions presented by fibers, intracellular organelles, and macromolecules [20]. In addition, a continual exchange occurs between free water molecules and water molecules that spend some of their time associated with the much more slowly moving macromolecules [21, 22]. Diffusion coefficients are thus expected to vary according to a tissue's microstructure or physiologic state, a potential source of tissue contrast for characterization or functional studies. As the diffusion range of water during typical MR diffusion times (100 msec) is on the order of a few micrometers, in the size range of many cells, microdynamic studies can be done at a scale that is much smaller than the resolution of current MR images. By comparing diffusion measurements obtained with sufficiently short and sufficiently long diffusion times, it may be possible to estimate cell diameters, provided diffusion is restricted by cell membranes. This effect has been shown in vegetable tissues, in which the cell wall is essentially impermeable to water transport [19], or by measuring diffusion of metabolites that remain inside the intracellular compartment [23]. In living animal tissues, cell membranes are permeable to water [24], and rapid exchanges occur between different compartments, such as intra- and extracellular spaces. The result is that diffusion is expected to be more likely "hindered" by random

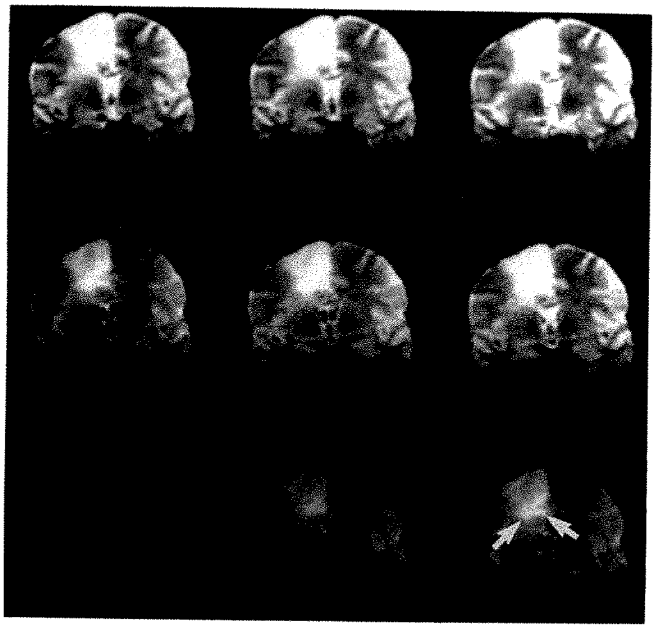

Fig. 4.—Set of eight diffusion-weighted echoplanar MR images (diffusion gradient pulses along z axis; gradient factor is 0–800 sec/mm^2 from *upper left* to *bottom right*). Signal attenuation is important in structures containing CSF (ventricular cavities, subarachnoid spaces), because of fast diffusion and CSF circulation. Note changes in gray/white matter contrast between first and last images. White matter in upper frontal lobe becomes much darker on heavily diffusion-weighted images, because of faster diffusion along myelin fiber in direction parallel to z axis. In tumor, attenuation is less at bottom (core of tumor, *arrows*) than in remaining part, which contains more free water (edema).

TABLE 1: Diffusion Coefficients of Water in Some Excised Rat Tissues, Normalized to Pure Water, at Room Temperature

Tissue [Ref.]	$\text{Diffusion}_{\text{tissue}}/\text{Diffusion}_{\text{water}}$ Ratio
Muscle [17]	
Parallel to fibers	0.61
Perpendicular to fibers	0.44
Liver [15]	0.25–0.30
Brain [18]	
20-msec diffusion time	0.45
60-msec diffusion time	0.10
Heart [15]	0.34–0.37

obstacles than strictly "restricted" in closed spaces by walls. In these conditions, MR diffusion measurements could be used to determine the permeability of cell membranes to water [15]. This new possibility of evaluating molecular displacements in vivo, without compromising tissue integrity, metabolism, and function, has given an impulse to clinical MR diffusion imaging. Some discrepancies may be expected with results obtained about 20 years ago with excised, dead tissues at room temperature and with older hardware.

Diffusion Imaging in the CNS

Diffusion in the Normal Brain; Anisotropic Diffusion in White Matter

Diffusion of water was measured previously in excised brain tissue [18]. Recent in vivo studies have shown that the diffusion coefficient of water in the normal brain does not vary much among subjects, if measurements are made with great care [7]. Diffusion of water in CSF is similar to the diffusion of pure water at the same temperature (Table 2). Indeed, the apparent diffusion coefficient in some locations, such as the foramina of Monro or the fourth ventricle, sometimes may be surprisingly larger (3–6 × 10^3/mm^2/sec), which seems physically impossible, but which is understandable considering that CSF is flowing incoherently in some locations. In MR imaging (Fig. 1), the distribution of velocities in a voxel will produce a signal attenuation (flow-void effect) that is similar to that of diffusion but larger (Fig. 4). This finding has been used to map and evaluate CSF [5, 25]. In gray matter, diffusion is isotropic and roughly 2.5-fold lower than in pure water at the same temperature (Table 2). In white matter, diffusion apparently is extremely variable. Indeed, the value of the diffusion coefficient directly depends on the relative orientation of the fibers and the magnetic field gradients; this is known as anisotropic diffusion.

It is expected that, in some tissues, hindrance or restriction in molecular water motion may not be the same for different directions of motion, so that the measured diffusion coefficients may vary according to the direction of measurement. Examples have been shown in muscle [17] and more recently in the white matter of cat [26] and human [12, 27, 28] brains. Water diffusion in gray matter is not anisotropic [26, 28] and is not completely restricted by impermeable walls [28, 29]. By contrast, diffusion in white matter is extremely anisotropic; the results of the measurements depend on the respective orientation of the myelin fiber tracts and the gradient direction at each different image location. It appears that diffusion coefficients are significantly decreased when the myelin fiber tracts are perpendicular to the direction of the magnetic field gradient used to measure molecular displacements (Fig. 3).

TABLE 2: Diffusion Coefficients of Water in Human Brain

Tissue	Diffusion Coefficient ($\times 10^{-3}$ mm^2/s)
CSF	2.94 ± 0.05
Gray matter	0.76 ± 0.03
White matter	
Corpus callosum	0.22 ± 0.22
Axial fibers	1.07 ± 0.06
Transverse fibers	0.64 ± 0.05

Note.—Direction of fibers refers to z axis (vertical). Experimental parameters are given in [12].

This has been clearly demonstrated with diffusion-weighted MR images (Fig. 3A). White matter structures in which fibers are perpendicular to the diffusion-gradient direction appear bright on such images, because diffusion is slow in this direction, as compared with diffusion in other brain structures. On calculated diffusion images (Figs. 3B and 5), contrast is opposite: Fibers that are perpendicular to the gradient direction have low diffusion coefficients and now appear dark, and fibers parallel to the gradient direction are bright. Color-coded maps of the myelin fiber orientation can be generated on the basis of diffusion anisotropy [30].

Although there is no doubt that diffusion is anisotropic in white matter, controversies about the origin of this anisotropy remain. Techniques that use radiotracers or ion-selective microelectrodes [21] have shown that slow and anisotropic diffusion of compounds in extracellular spaces could occur because of the tortuosity of the diffusion pathways between tissue microscopic substructures, such as myelin fibers. However, most MR-visible water is in the axons. A simple model would be to consider that water molecules are enclosed in the axonal spaces and that water diffusion outside the axons is prevented by the myelin sheath [26–31]. When diffusion measurements are made parallel to the direction of the fibers, diffusion is not restricted, resulting in higher measured diffusion coefficients. Indeed, the situation is more complex, as it has been shown by MR dispersion studies that the myelin sheath is somewhat permeable to water [32]. In recent diffu-

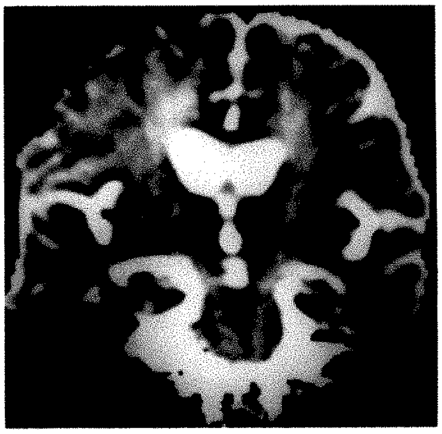

Fig. 5.—Anisotropic diffusion in white matter. Calculated diffusion MR image from a set of eight different diffusion-weighted images was acquired as in Fig. 4; amplitude of gradient pulse was varied from 0 to 38 mT/m. Brightness of each pixel is now directly proportional to diffusion coefficient and depends only on this variable. Fiber tracts perpendicular to z axis appear dark; tracts parallel to z axis are bright. Excellent contrast is achieved, because T1 and T2 effects have been removed. Corpus callosum and temporal white matter fibers, which are horizontal, are dark; vertical corona radiata frontal fibers and internal capsule fibers are bright. In brainstem, vertical fast-conducting motor and somatosensory tracts are also bright. These orientation patterns correlate well with anatomy.

sion experiments [28, 29], no restricted diffusion pattern could be observed in white matter. In particular, the diffusion coefficient remained constant with the variations in diffusion time and did not decrease as would be expected in the case of restricted diffusion in one direction. The reduced value of the diffusion coefficient across myelin fibers thus likely reflects a decreased water mobility through the successive lipid layers [28] or water exchanges limited to nodes of Ranvier. The low permeability of myelin to water apparently does not prevent water molecules from being exchanged between axons within a rather short time. Such diffusion studies could provide an estimation of the permeability of myelin to water [33]. Another possible explanation is that water in myelin sheaths is in a liquid crystalline environment in which anisotropic, but free, diffusion can be observed. On the other hand, the enhanced value of diffusion measured parallel to the axoplasm could arise from a facilitated transport favored by the highly oriented intraaxonal microstructures, such as microtubules or microfilaments, in relation to axoplasmic transport [28]. This transport is not a diffusional process, but could be seen as an incoherent motion at the voxel scale. The measurement of anisotropic diffusion in white matter offers exciting potential applications. Mapping the orientation of myelin fibers might be useful for a better understanding of white matter diseases such as multiple sclerosis, wallerian degeneration, or delayed white matter myelination in neonates [34, 35]. The coupling between the degree of diffusion anisotropy and the degree of white matter myelination during CNS maturation [35] is also an argument to justify that diffusion anisotropy in white matter is related to the myelin sheath.

Diffusion Imaging in Brain Ischemia

Subacute and chronic ischemia.—At the stage of subacute ischemia, when findings on conventional MR images appear abnormal (showing an increase in T2), the diffusion coefficient in white matter increases about two- or threefold above its normal value [36]. This is probably because of the presence of vasogenic edema, in which bulk water motion in the extracellular space is an important phenomenon. Earlier work [5] showed that edema could be easily recognized on diffusion images. Typically, vasogenic edema is visible as a large homogeneous area that has an increased diffusion coefficient (Fig. 6).

In some instances of chronic ischemia, abnormalities in brain parenchyma (low diffusion) have been seen on diffusion images, although conventional T1- or T2-weighted images appeared normal [3]. Diffusion may also help detect encephalomalacic cysts, which have a diffusion coefficient similar to that of pure water.

Acute Ischemia.—The most promising application of diffusion imaging in stroke has been suggested by the finding that diffusion imaging can be used to detect brain ischemia at an early stage. Recently, MR diffusion imaging in a cat brain model of ischemia showed that the diffusion coefficient of water is significantly decreased within minutes after an ischemic injury, a time when all other imaging techniques, including conventional MR, do not show any change (Fig. 7) [37]. The mechanism of this decrease in water mobility is still unclear. It is unlikely that this finding is related to nondiffusion phenomena, such as a decrease in bulk tissue pulsatility caused by the microcirculatory arrest. The decrease in diffusion is not instantaneous; it appears progressively within the first hour [37]. It is also difficult to explain on the basis of a decrease in temperature. A 30% decrease in the diffusion coefficient would imply a temperature decrease of about 10° C [38], which is unrealistic. This decrease in diffusion more likely reflects a modification of the water balance or transport between tissue compartments, such as intra- and extracellular spaces. It is known that ischemia is responsible for the massive entry of ions and accompanying water into the intracellular space, accompanied by an increase in osmolarity [39]. A modern, but still under debate, theory of cytotoxic edema is that the calcium channels open because of the excitation of *N*-methyl-D-aspartate receptors by the release and accumulation of neurotoxic dicarboxylic amino acids, such as glutamate, in the extracellular spaces [39]. Cytologic changes in terms of microvacuolation are visible as early as 20 min after complete ischemia. This results in the cell release of potassium ions and the massive entry of sodium ions,

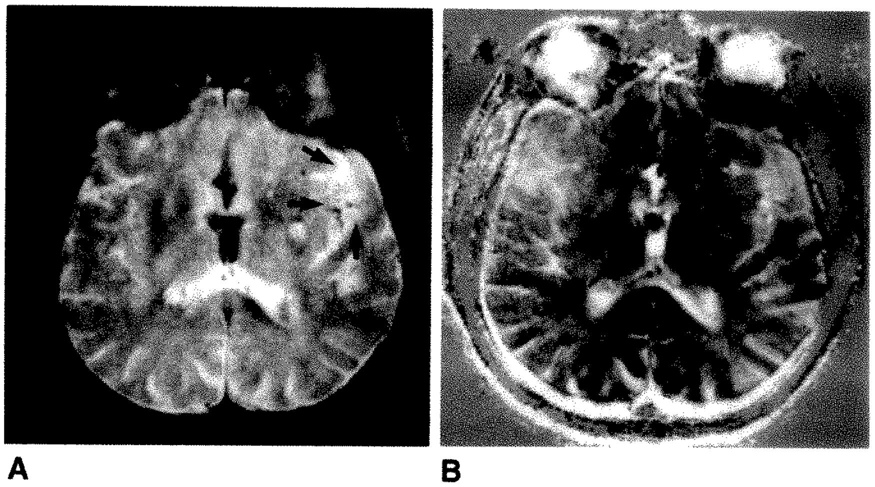

Fig. 6.—Diffusion in subacute stroke.

***A*, T2-weighted MR image (1799/140 [TR/TE]) shows small infarcted area (*arrows*) in left temporal lobe.**

***B*, Calculated diffusion MR image shows infarcted area has a large diffusion coefficient similar to that found in ventricles. This high water mobility typically accompanies vasogenic edema, in which water diffusion is relatively free and additional microscopic motion may occur.**

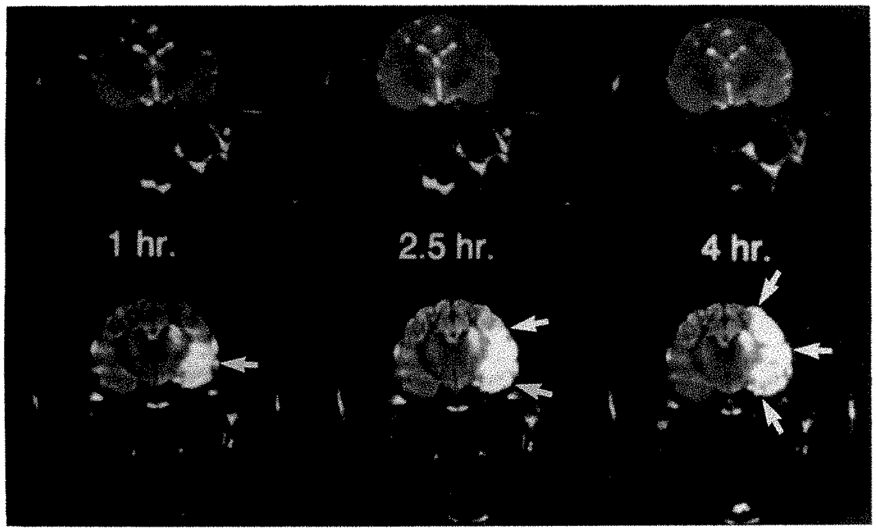

Fig. 7.—Diffusion in hyperacute cerebral ischemia. MR images obtained on a 2-T CSI unit 1, 2.5, and 4 hr after occlusion of middle cerebral artery of a cat brain. (Courtesy of M. E. Moseley, San Francisco).

Top row, T2-weighted images (gradient factor = 0 sec/mm^2) show no evidence of abnormality, even 4 hr after occlusion.

Bottom row, Diffusion-weighted images (gradient factor = 1413 sec/mm^2) dramatically show ischemic territory as a bright area, indicating decreased water mobility as soon as 1 hr after occlusion. Ischemic area is clearly enlarging with time (*arrows*).

which quickly overtake the capacity of the ionic transmembrane pumps. An interesting finding in favor of this mechanism is that calcium blockers prevent or lessen the decrease in diffusion [40]. Furthermore, artificially induced cytotoxic edema in animals also produces a decrease in the diffusion coefficient [41]. Diffusion imaging could also reflect various intracellular active transport mechanisms that cease operating when energy metabolites are no longer available.

Diffusion imaging thus offers the unique opportunity to address, noninvasively and in a clinical setting, fundamental issues about the response of brain tissue to ischemia at different stages that may not be possible with other techniques, including conventional MR and MR spectroscopy [42]. Early detection of stroke, at a stage when tissue damage is still reversible, may provide justification for more aggressive and controversial reperfusion or other therapies designed to protect CNS tissues. It will be of extreme interest to find out if diffusion can be used as a reliable marker of tissue damage and of its potential reversibility.

Brain Tumors

So far, only modest results have been obtained with the use of diffusion imaging in a clinical context [3, 5, 43–45]. The most pertinent finding is that diffusion coefficients are significantly higher in structures in which diffusion is free, such as cysts (where the diffusion coefficient is close to that of pure water, depending only slightly on the viscosity of the cystic fluid [46]). This feature becomes clinically useful when, because of a high paramagnetic protein content, T1 and T2 are not as long as expected for a liquid, so that some complicated cystic lesions have the same T1 and T2 appearances as a solid tumor [47]. In these cases, diffusion imaging clearly shows the liquid nature of the lesion [2, 5] (Fig. 8). On the other hand, the extension of the concept of diffusion to other kinds of IVIM can be clinically valuable, at least in some situations. For instance, the ADC is different between solid tumors, such as epidermoid tumors, and pulsatile cisternal CSF or even static fluid collections. Diffusion imaging, or rather IVIM [3, 5] imaging, has been found useful in improving the detection, characterization, and therapeutic management of extraaxial brain tumors [43].

Perfusion-sensitized images of the brain have also been obtained in clinical practice by applying the IVIM concept [2, 3]. With IVIM imaging, microcirculatory flow in the capillary network is considered to be random at the voxel level. Microcirculation can thus be modeled as a type of macroscopic pseudodiffusion and imaged by using diffusion imaging techniques. Use of echoplanar MR imaging eliminates the risk of motion artifacts and allows collection in a short interval of numerous images in order to separate microcirculation from bulk water diffusion in the tissues [7, 12]. However, the small fraction of normal brain occupied by flowing blood (typically a few percent) makes this separation difficult, requiring high signal-to-noise ratios. Therefore, the accuracy and sensitivity of the method are limited, especially in the low perfusion range [48]. Furthermore, the link between the information provided by IVIM measurements and actual blood flow requires some modeling [49, 50]. It remains that, with IVIM imaging, highly perfused tumors have been detected because they have patterns different from those of poorly perfused tumors or tissues. Potentially, distinction between tumor recurrence and radiation damage in patients previously irradiated for brain tumors could be made. IVIM images show high perfusion in tumor recurrence, whereas radiation damage causes low perfusion and apparently decreased diffusion [51]. These results are well correlated with those obtained from metabolic data produced by positron emission tomography with ^{18}F-fluorodeoxyglucose [52]. Diffusion/perfusion images have also shown abnormalities that regular T1- and T2-weighted images have not shown [3]. Work remains to be done to characterize the way capillary microcirculation is depicted when gradient sensitization techniques are used and how such results correlate with measurements of actual blood flow and to establish the reliability of diffusion/perfusion images for obtaining accurate, reliable, and reproducible data.

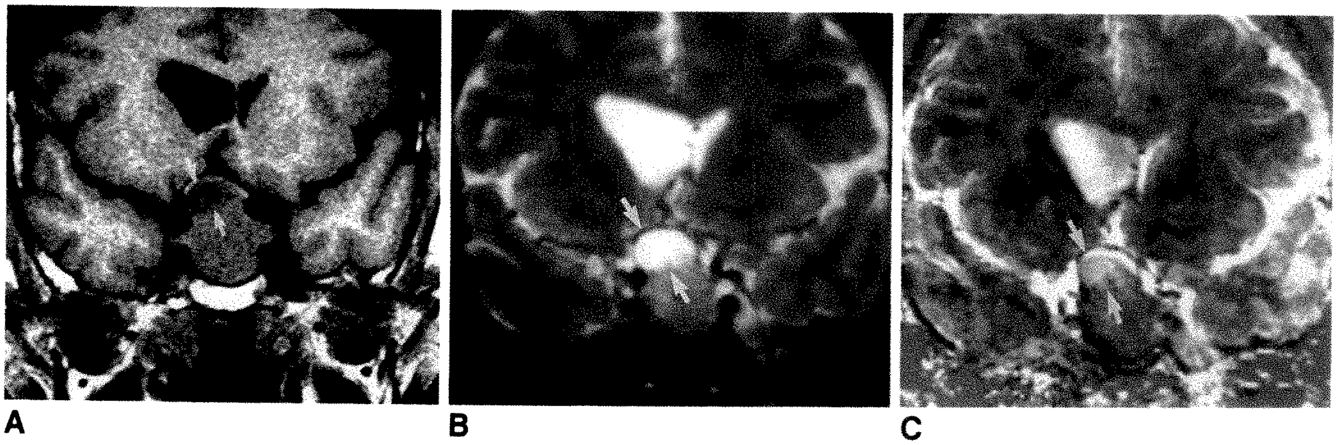

Fig. 8.—Diffusion in a cystic lesion.

A and *B*, Coronal T1-weighted (400/26 [TR/TE]) and T2-weighted (1000/140) MR images show a lesion (*arrows*) at upper extremity of a pituitary adenoma. T1 and T2 values are nonspecifically elevated, but are not as high as in CSF.

C, Intravoxel incoherent motion MR image of same slice strongly suggests lesion (*arrows*) is cystic, because of its high apparent diffusion coefficient, similar to diffusion coefficient of free water, as found in nearby ventricular cavities. (In some parts of ventricles, apparent diffusion coefficient is even higher, because of CSF flow). Using diffusion MR images to distinguish solid from cystic lesions is more reliable than using T1 or T2 images because diffusion is insensitive to proteins or other paramagnetic substances in cystic fluid. Such substances may alter T1 and T2, and cause cysts to have appearance of solid lesions.

Diffusion Imaging Outside the CNS

Diffusion Imaging of the Eye

Many eye diseases involve disorders in fluid circulation in different parts of the eye (glaucoma) or in blood microcirculation in the choroid (diabetes, uveitis). Therefore, diffusion and pseudodiffusion imaging of the eye could be extremely useful. Unfortunately, these studies are not easy owing to the mobility of the eye in vivo.

High-resolution diffusion-weighted images obtained in anesthetized rabbits [53] have shown some anatomic structures, such as the lens and the choroid, that otherwise are barely visible with conventional MR imaging (Fig. 9). In human subjects, ultrafast imaging techniques, such as echoplanar MR imaging, are required, because the direction of gaze must be kept constant during acquisition of the MR images. Unfortunately, without high-performance digitization hardware, high spatial resolution is not possible with echoplanar imaging, and, owing to the vulnerability of echoplanar imaging to susceptibility artifacts, the shape of the eye and internal structures may be distorted. Further improvements include the use of surface coils to increase the signal-to-noise ratio and a smaller field of view. These preliminary results have shown the feasibility of using diffusion imaging of the eye in vivo. Besides its clinical potential, this method also could be used to study animal models of eye disease.

Imaging of the Kidney

Diffusion imaging in the body is a challenge. The main difficulties are related to organ and respiratory motion, to which diffusion imaging is sensitive, and to the relatively short T2 values of body tissues, which require much shorter echo times than brain tissues do. By "freezing" motion in a single shot, echoplanar MR imaging has broadened the scope of application of diffusion imaging. The kidney is an interesting organ for diffusion/perfusion imaging, because of the important contribution of perfusion and the crucial role of water exchanges between the different segments of the nephron and interstitial tissue. Encouraging results have been obtained in the dog kidney [54] with a spin-echo 2DFT diffusion imaging

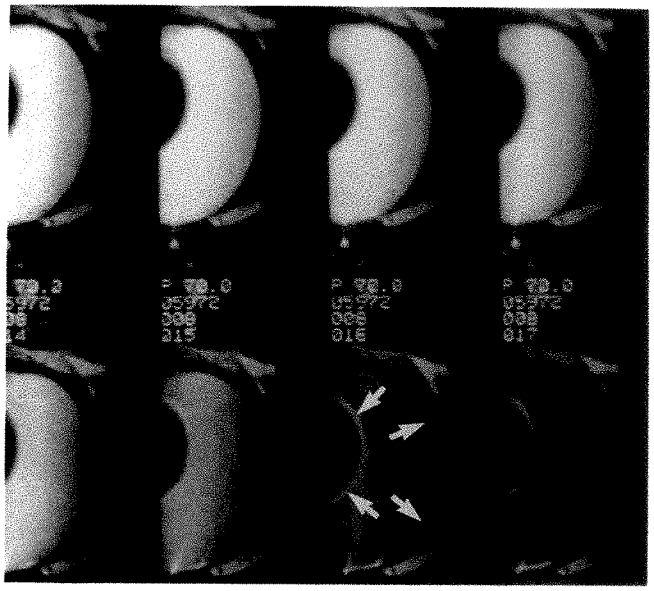

Fig. 9.—Diffusion-weighted MR images (1000/46 [TR/TE]) of a rabbit eye were obtained in vivo by using a 4.7-T CSI instrument and a two-dimensional Fourier transform spin-echo diffusion imaging sequence (4-mm slice thickness, 230-μm in-plane resolution; gradient factors = 14, 32, 89, 128, 227, 355, 511, and 600 sec/mm^2. Some structures, such as cortex of lens and choroid, are more visible on heavily diffusion-weighted images (*arrows*).

sequence, in rabbit kidneys (Fig. 10), and in human volunteers [55] with echoplanar imaging.

Future Developments

Diffusion Spectroscopy

Recent progress in in vivo localized MR spectroscopy allows the extension of diffusion measurements to molecules other than water. MR can resolve different nuclear species because of the species' different Larmor frequencies, such as phosphorous-31, fluorine-18, hydrogen-2, or carbon-13. For a given species, the chemical shift can be used to determine the diffusion coefficients of the different compounds in complex mixtures [56]. Diffusion of phosphocreatine, for instance, can be studied by using ^{31}P spectroscopy [23, 57]. Measurement of phosphocreatine is a true probe of intracellular space; in contrast to phosphocreatine, water does not diffuse across cell membranes, so true restricted diffusion can be observed. Phosphocreatine (or *N*-acetyl aspartate in neurons, which can be studied by using ^{1}H spectroscopy) can be used to provide exclusive information on the intracellular medium, such as its viscosity or geometry. Monitoring of exchanges of metabolites or drugs through cell membranes could also benefit from similar techniques designed to measure molecular flow [58].

Interventional MR Imaging

It is premature to describe the future role of MR imaging in interventional radiology, but some pioneering results have been encouraging and are worth reporting. These results are based on the sensitivity of diffusion to temperature. Temperature changes induced within the magnet bore when a dedicated hyperthermia device or laser beams are used have been shown and measured with diffusion MR imaging [38, 59, 60]. Combined with fast imaging, temperature-diffusion imaging may play a significant role in the real-time monitoring of interventional or neurosurgical procedures performed within the magnet bore, especially by giving information on tissues not directly visible.

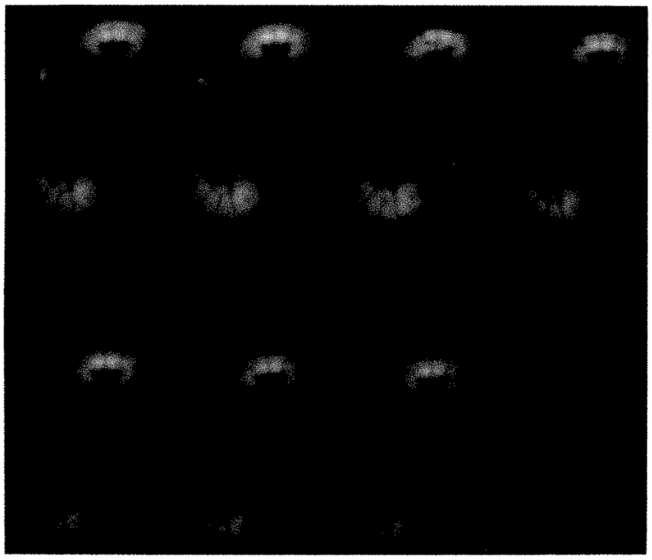

Fig. 10.—Series of diffusion-sensitized echoplanar MR images (4000/70 [TR/TE]) of rabbit kidneys (128 × 64 pixels, 5-mm thickness, 50-msec acquisition time per image, gradient factors of 0–550 sec/mm²) shows good-quality high-resolution intravoxel inherent-motion–sensitized echoplanar images can be obtained in body. No motion artifact or blurring is visible. Note that cortex has a greater signal attenuation than medulla when amplitude of diffusion gradient pulses is increased (higher diffusion/perfusion rate). (Obtained in collaboration with P. Choyke, J. A. Frank, and M. Girton, Bethesda, MD.)

Conclusions

Diffusion appears to be a promising source of contrast for MR imaging. No correlation exists between the diffusion coefficient and T1 and T2 relaxation times. T1 and T2 may be normal or elevated in diseased states while diffusion is lowered, as shown in early brain ischemia. Whereas T1 and T2 essentially provide anatomic pictures in the context of a long history of clinical imaging techniques, the information brought by diffusion has no real clinical antecedents, so diffusion MR imaging falls into a new territory in the field of radiology. Furthermore, diffusion is not simply an MR parameter; it has a much wider significance independent of MR. However, MR imaging is the only available method for evaluating diffusion in vivo with good accuracy and spatial resolution. With improvements in gradient hardware to produce very large gradient strengths, and continued regard for safety concerns, significant improvements in diffusion accuracy may be expected. It remains that diffusion imaging is not an easy technique. Good immobilization and cooperation of the patient, and sometimes cardiac gating, are essential, even when echoplanar imaging is used, to avoid misregistration problems. The gradient unit must be of excellent quality to avoid eddy currents or instability-related artifacts. Plenty of work remains to understand fully the meaning and usefulness of this phenomenon for clinical applications.

REFERENCES

1. Le Bihan D. Diffusion/perfusion MR imaging of the brain: from structure to function. *Radiology* **1990**;177:328–329
2. Le Bihan D, Turner R, Pekar J, Moonen CTW. Diffusion and perfusion imaging by gradient sensitization: design, strategy and significance. *J Magn Reson Imaging* **1991**;1:7–28
3. Le Bihan D, Breton E, Lallemand D, Aubin ML, Vignaud J, Laval-Jeantet M. Separation of diffusion and perfusion in intravoxel incoherent motion (IVIM) MR imaging. *Radiology* **1988**;168:497–505
4. Le Bihan D, Breton E, Syrota A. Imagerie de diffusion par résonance magnétique nucléaire. *C R Acad Sci [III]* **1985**;301:1109–1112
5. Le Bihan D, Breton E, Lallemand D, Grenier P, Cabanis EA, Laval-Jeantet M. MR imaging of intravoxel incoherent motions: application to diffusion and perfusion in neurologic disorders. *Radiology* **1986**;161:401–407
6. Merboldt KD, Bruhn H, Frahm G, Gyngell ML, Hanicke W, Deimling M. MRI of "diffusion" in the human brain: new results using a modified CE-FAST sequence. *Magn Reson Med* **1989**;9:423–429
7. Le Bihan D. Molecular diffusion nuclear magnetic resonance imaging. *Magn Reson Q* **1991**;7:1–28
8. Turner R, Bowley RM. Passive screening of switched magnetic field gradients. *J Phys E Sci Instrum* **1986**;19:876
9. Mansfield P, Chapman B. Active magnetic screening of gradient coils in NMR imaging. *J Magn Reson* **1986**;66:573–576
10. Roemer PB, Edelstein WA, Hickey JS. Self-shielded gradient coils (abstr).

In: *Book of abstracts: Society of Magnetic Resonance in Medicine 1988*. Berkeley, CA: Society of Magnetic Resonance in Medicine, **1986**:1067

11. Avram HR, Crooks LE. Effect of self-diffusion on echo-planar imaging (abstr). In: *Book of Abstracts: Society of Magnetic Resonance in Medicine 1988*. Berkeley, CA: Society of Magnetic Resonance in Medicine, **1988**:80
12. Turner R, Le Bihan D, Maier J, Vavrek R, Hedges LK, Pekar J. Echo-planar imaging of intravoxel incoherent motions. *Radiology* **1990**;177:407–414
13. Turner R, Le Bihan D. Single-shot diffusion imaging at 2.0 tesla. *J Magn Reson* **1990**;86:445–452
14. McKinstry RC, Weisskopf RM, Cohen MS. Instant MR diffusion/perfusion imaging. *Magn Reson Imaging* **1990**;8[suppl]:401
15. Cooper RL, Chang DB, Young AC. Restricted diffusion in biophysical systems. *Biophys J* **1974**;14:161–177
16. Chang DC, Rorschach HE, Nichols BL, Hazelwood CF. Implications of diffusion coefficient measurements for the structure of cellular water. *Ann NY Acad Sci* **1973**;204:434–443
17. Cleveland GG, Chang DC, Hazelwood CF. Nuclear magnetic resonance measurement of skeletal muscle: anisotropy of the diffusion coefficient of the intracellular water. *Biophys J* **1976**;16:1043–1053
18. Hansen JR. Pulsed NMR study of water mobility in muscle and brain tissue. *Biochim Biophys Acta* **1971**;230:482–486
19. Brownstein KR, Tarr CE. Importance of classical diffusion in NMR studies in biological cells. *Physiol Rev* **1979**;19:2446–2453
20. Nicholson C, Phillips JM. Ion diffusion modified by tortuosity and volume fraction in the extracellular microenvironment of the rat cerebellum. *J Physiol* (Paris) **1981**;321:225–257
21. Wang JH. Theory of the self-diffusion of water in protein solutions: a new method for studying the hydration and shape of protein molecules. *J Am Chem Soc* **1954**;76:4755–4763
22. Clark ME, Burnell EE, Chapman NR, Hinke JAM. Water in barnacle muscle. IV. Factors contributing to reduced self-diffusion. *Biophys J* **1982**;39:289
23. Moonen CTW, Van Zijl PCM, Le Bihan D, DesPres D. In vivo NMR diffusion spectroscopy: ^{31}P application to phosphorus metabolites in muscle. *Magn Reson Med* **1990**;13:467–477
24. Finkelstein A. *Water movement through lipid bilayers, pores, and plasma membranes: theory and reality*. New York: Wiley, **1987**
25. Le Bihan D, Breton E, Aubin ML. Study of cerebrospinal fluid dynamics by MRI of intravoxel incoherent motions (IVIM). *J Neuroradiol* **1987**;14:388-395
26. Moseley ME, Cohen Y, Kucharczyk J, et al. Diffusion-weighted MR imaging of anisotropic water diffusion in cat central nervous system. *Radiology* **1990**;176:439–446
27. Chenevert TL, Brunberg JA, Pipe JG. Anisotropic diffusion within human white matter: demonstration with NMR techniques in vivo. *Radiology* **1990**;177:401–405
28. Le Bihan D, Turner R, Douek P. Is water diffusion restricted in human brain? (abstr). In: *Book of abstracts: Society of Magnetic Resonance in Medicine 1990*. Berkeley, CA: Society of Magnetic Resonance in Medicine, **1990**:377
29. Moonen CTW, de Vleeschouwer MHM, DesPres D, van Zijl PCM, Pekar J. Restricted and anisotropic displacement of water in healthy cat brain and in stroke by NMR diffusion imaging (abstr). In: *Book of abstracts: Society of Magnetic Resonance in Medicine 1990*. Berkeley, CA: Society of Magnetic Resonance in Medicine, **1990**:1121
30. Douek P, Turner R, Pekar J, Patronas N, Le Bihan D. Myelin fiber orientation color mapping. *J Comput Assist Tomogr* **1991**;15:923–929
31. Hajnal JV, Doran M, Hall AS. MR imaging of anisotropically restricted diffusion of water in the nervous system: technical, anatomic, and pathological considerations. *J Comput Assist Tomogr* **1991**;15:1–18
32. Koenig SH, Brown RD, Spiller M, Lundbom N. Relaxometry of brain: why white matter appears bright in MRI. *Magn Reson Med* **1990**;14:482–495
33. Le Bihan D, Douek P, Turner R. On the permeability of myelin to water in vivo in the human brain (abstr). In: *Book of abstracts: Society of Magnetic Resonance in Medicine 1991*. Berkeley, CA: Society of Magnetic Resonance in Medicine, **1991**:377
34. Sakuma H, Nomura Y, Takeda K, et al. Adult and neonatal human brain: diffusional anisotropy and myelination with diffusion-weighted MR imaging. *Radiology* **1991**;180:229–233
35. Rutherford MA, Cowan FM, Manzur AY, et al. MR imaging of anisotropically restricted diffusion in the brain of neonates and infants. *J Comput Assist Tomogr* **1991**;15:188–198
36. Le Bihan D, Berry I, Gelbert F, et al. MR imaging of intravoxel incoherent motions in ischemic and malformative cerebral diseases. *Radiology* **1987**;165(P):303
37. Moseley ME, Kucharczyk J, Mintorovitch J, et al. Diffusion-weighted MR imaging of acute stroke: correlation with T2-weighted and magnetic susceptibility-enhanced MR imaging in cats. *AJNR* **1990**;11:423–429
38. Le Bihan D, Delannoy J, Levin R. Non-invasive temperature mapping using magnetic resonance imaging of molecular diffusion: application to hyperthermia. *Radiology* **1989**;171:853–857
39. Garcia JH, Anderson ML. Physiopathology of cerebral ischemia. *Crit Rev Neurobiol* **1989**;4:303–324
40. Kucharczyk K, Mintorovitch J, Asgari H, Derugin N, Sevick R, Moseley ME. Ischemic brain damage is reduced by a novel sodium/calcium ion channel modulator RS-87476 (abstr). In: *Book of abstracts: Society of Magnetic Resonance in Medicine 1990*. Berkeley, CA: Society of Magnetic Resonance in Medicine, **1990**:651
41. Sevick RJ, Tsuruda JS, Kanda CA, et al. Diffusion-weighted MR imaging of cytotoxic brain edema. *Radiology* **1991**;181(P):239
42. Baker LL, Kucharczyk J, Sevick RJ, Mintorovitch J, Moseley ME. Recent advances in MR imaging/spectroscopy of cerebral ischemia. *AJR* **1991**;156:1133–1143
43. Tsuruda JS, Chew WM, Moseley ME, Norman D. Diffusion-weighted MR imaging of the brain: value of differentiating between extraaxial cysts and epidermoid tumors. *AJNR* **1990**;11:925–931
44. Chien D, Buxton RB, Kwong KK, Brady TJ, Rosen BR. MR diffusion imaging of the human brain. *J Comput Assist Tomogr* **1990**;14:514–520
45. Rosen BR, Belliveau JW, Chien D. Perfusion imaging by nuclear magnetic resonance. *Magn Reson Q* **1990**;5:263–281
46. Sigal R, MR imaging for diagnosis of central nervous system cystic lesions: correlation with biochemical data. *Radiology* **1988**;169(P):423
47. Haimes A, Zimmerman R, Morgello S, et al. MR imaging of brain abscesses. *AJNR* **1989**;10:279–291
48. Pekar J, van Zijl PCM, Moonen CTW. Signal to noise requirements for quantitative measurements of diffusion and capillary perfusion in brain using IVIM-MRI. *Magn Reson Med* **1991**;23:122–129
49. Henkleman RM. Does IVIM measure classical perfusion? *Magn Reson Med* **1990**;6:470–475
50. Le Bihan D, Turner R. The capillary network: a link between IVIM and classical perfusion. *Magn Reson Med* (in press)
51. Le Bihan D, Turner R, Patronas N, Douek P. Intravoxel incoherent motion echo-planar imaging and magnetic susceptibility induced, contrast-enhanced EPI: comparison of two approaches to real-time brain perfusion MR imaging. *Radiology* **1990**;177(P):120
52. Di Chiro G. Positron emission tomography using [^{18}F]fluorodeoxyglucose in brain tumors: powerful diagnostic and prognostic tool. *Invest Radiol* **1987**;22:360–371
53. Le Bihan D, Turner R, de Smet M, Nussenblatt RB. IVIM echo-planar imaging of the eye. *J Magn Reson Imaging* **1991**;2:203
54. Lorentz CH, Pickens DR, Puffer DB, Price RR. Diffusion-perfusion phantom experiments. In: *Syllabus of the meeting on Future Directions in MRI of Diffusion and Microcirculation*. Berkeley, CA: Society of Magnetic Resonance in Medicine, **1990**:123
55. Turner R, Le Bihan D, Maier J, Vavrek R, Baich J. Echo-planar IVIM imaging of the body: application to kidney (abstr). In: *Book of abstracts: Society of Magnetic Resonance in Medicine 1990*. Berkeley, CA: Society of Magnetic Resonance in Medicine, **1990**:1136
56. James TL, McDonald GG. Measurement of the self-diffusion coefficient of each component in a complex system using pulse-gradient Fourier transform NMR. *J Magn Reson* **1973**;11:58–61
57. Yoshizaki K, Seo Y, Nishikawa H, Morimoto T. Application of pulsed-gradient ^{31}P NMR on frog muscle to measure the diffusion rates of phosphorus compounds in cells. *Biophys J* **1982**;38:209–211
58. Van Zijl PCM, Moonen CTW, Kaplan O, Faustino P, Cohen JS. Complete separation of intracellular and extracellular information in NMR spectra of perfused cell cultures (abstr). In: *Book of abstracts: Society of Magnetic Resonance in Medicine 1990*. Berkeley, CA: Society of Magnetic Resonance in Medicine, **1990**:851
59. Delannoy J, Le Bihan D, Hoult D, Levin R. Hyperthermia system combined with an MRI unit. *Med Phys* **1990**;17:855–860
60. Jolesz FA, Higuchi N, Bleier AR, Jakab P. MRI of laser effects on tissue. *Magn Reson Imaging* **1990**;8(P):156

Radiologic-Pathologic Conferences of the Massachusetts General Hospital

Sacral Neurofibroma

Daniel P. Barboriak, S. Mitchell Rivitz, and Felix S. Chew[1]

A 26-year-old woman presented with low back pain. MR imaging showed a left S1 nerve root mass enlarging the neural foramen and extending extradurally into the presacral soft tissues. The mass had intermediate signal intensity on T1-weighted MR images and bright intensity on T2-weighted MR images, with slight enhancement after IV administration of gadopentetate dimeglumine. Postmyelography CT scans showed the mass to be noncalcified, with no invasion of bone at the enlarged neural foramen (Fig. 1). Subsequently, a well-circumscribed soft-tissue mass that contained Schwann cells, fibroblasts, and nerve fibers was resected. The final pathologic diagnosis was neurofibroma.

Neurofibromas are benign fibroblastic neoplasms of peripheral nerves whose consistency and histologic appearance vary from myxoid to fibrous according to the differentiation of the neoplastic elements [1]. The bulk of the tumor volume consists of intercellular collagen fibrils in a nonorganized myxoid matrix. The imaging characteristics depend on the relative amounts of fibrous and myxoid material. Of nerve sheath origin, they occur as a fusiform rather than eccentric enlargement of the nerve, and neural fibers are dispersed within the lesion. Neurofibromas are slow growing and noninvasive, and their soft and elastic consistency permits them to be shaped by the adjacent bone structures; the bone reacts by remodeling around the lesions. They rarely calcify, and frequently have a bilobed "dumbbell" appearance. On MR imaging, neurofibromas tend to be isointense with muscle on T1-weighted images and show marked brightening on T2-weighted images. They may be inhomogeneous [2].

Although small cutaneous neurofibromas may be solitary, when multiple or deep, neurofibromas occur as a manifestation of neurofibromatosis. They are the most common masses of the spinal canal, accounting for 16–30% of such lesions, and are typically intradural and extramedullary [3]. The most common signs and symptoms are pain and radiculopathy due to compression of the affected nerve root. The primary treatment for neurofibromas is surgical resection. The neurologic outcome is related to the tumor bulk and to whether the adjacent nerve root can be spared [4, 5]. Malignant degeneration to neurofibrosarcoma occurs in 4–11% of patients with neurofibromatosis [3].

REFERENCES

1. Harkin JC, Reed RJ. *Tumors of the peripheral nervous system.* Washington, DC: Armed Forces Institute of Pathology, **1969**:51–97
2. Breidahl WH, Khangure MS. MRI of lumbar and sacral plexus nerve sheath tumours. *Australas Radiol* **1991**;35:140–144
3. Zimmerman RA, Bilaniuk LT. Imaging of tumors of the spinal canal and cord. *Radiol Clin North Am* **1988**;26:965–1007
4. Feldenzer JA, McGauley JL, McGillicuddy JE. Sacral and presacral tumors: problems in diagnosis and management. *Neurosurgery* **1989**;25:884–891
5. Benzel EC, Morris DM, Fowler MR. Nerve sheath tumors of the sciatic nerve and sacral plexus. *J Surg Oncol* **1988**;39:8–16

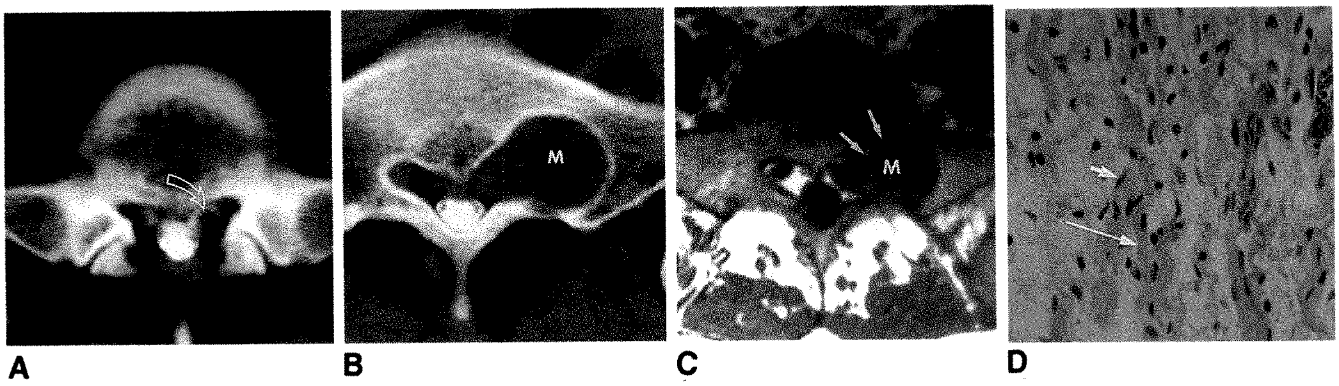

Fig. 1.—Sacral neurofibroma.
***A* and *B*, Postmyelography CT scans show intradural left S1 nerve root mass (*curved arrow*, M) expanding neural foramen but preserving bony cortex.**
***C*, On T1-weighted MR image, mass (M) is isointense with opposite nerve root and extends into soft tissues (*arrows*).**
***D*, Photomicrograph shows wirelike bundles of collagen (*long arrow*) and spindle cells (*short arrow*) with abundant intercellular myxoid matrix (H and E, high power).**

From the weekly radiologic-pathologic correlation conferences conducted by Jack Wittenberg. Pathology editor: Andrew E. Rosenberg. Radiology editors: Felix S. Chew, Daniel P. Barboriak, William E. Palmer, Daniel I. Rosenthal.

[1] All authors: Department of Radiology, Massachusetts General Hospital and Harvard Medical School, 32 Fruit St., Boston, MA 02114. Address reprint requests to F. S. Chew.

AJR 159:600, September 1992 0361-803X/92/1593-0600 © American Roentgen Ray Society

Pictorial Essay

Cystic Masses of the Head and Neck: Pitfalls in CT and MR Interpretation

Michael B. Miller,[1] Vijay M. Rao, and Barry M. Tom

The purpose of this essay is to illustrate the CT and MR findings of a variety of cystic masses of the head and neck. These masses are interesting not only because they are uncommon but because they may mimic other cystic lesions. Given the varied radiologic appearance of such lesions, the radiologist should refrain from being dogmatic about their diagnosis. The clinical presentation in combination with a knowledge of the various compartments of the head and neck can often help the radiologist establish the diagnosis or limit the differential diagnosis. Familiarity with the embryology of the head and neck may provide further clues.

Branchial Cleft Cysts

The failure of complete obliteration of an embryonic branchial cleft at the eighth to ninth week of fetal development results in a branchial cleft cyst. Ninety-five percent of branchial cleft cysts derive from the remnant of the second branchial cleft [1, 2].

Second Branchial Cleft Cysts

Second branchial cleft cysts usually manifest in the young adult as a mass near the mandibular angle. The cysts can, however, occur anywhere along the residual cleft tract extending from the supraclavicular region to the tonsillar fossa. The classic second branchial cleft cyst is a cystic, oval to round mass that displaces the sternocleidomastoid muscle posteriorly or posterolaterally, the carotid artery and internal jugular vein medially or posteromedially, and the submandibular gland anteriorly [2] (Fig. 1).

Atypically, second branchial cleft cysts originate from the pharyngeal portion of the embryologic tract, manifesting as a mass in the parapharyngeal space (Fig. 2). Second branchial cleft cysts arising from the pharyngeal end of the tract also may manifest as nasopharyngeal cysts (Fig. 3).

Second branchial cleft cysts may rarely be located posteromedial to the sternocleidomastoid muscle, displacing the carotid artery and internal jugular vein anteromedially (Fig. 4). In this location, these lesions may mimic other posterior triangle cysts; in particular, cystic hygromas. Salazar et al. [4] noted that if the cyst can be seen extending between the internal and external carotid arteries, as does the embryologic cleft tract, the lesion is likely to be a branchial cleft cyst. One of our cases of a second branchial cleft cyst in the posterior triangle extended into the supraclavicular region (Fig. 5), the most caudal extent of the residual tract of the second branchial cleft.

Infection of branchial cleft cysts is not rare. In these instances, they may mimic abscesses and/or lymphadenopathy both clinically and radiologically (Figs. 6 and 7). Conversely, a necrotic lymph node or tumor may appear radiologically as a branchial cleft cyst (Fig. 8).

Other cervical lesions that may mimic a second branchial cleft cyst include necrotic neural tumors, submandibular gland

---

Received January 21, 1992; accepted after revision March 3, 1992.

[1] All authors: Department of Radiology, Division of ENT/Neuroradiology, Thomas Jefferson University Hospital, 1092 Main Bldg., 10th and Sansom Sts., Philadelphia, PA 19107. Address reprint requests to M. B. Miller.

AJR 159:601-607, September 1992 0361-803X/92/1593-0601 © American Roentgen Ray Society

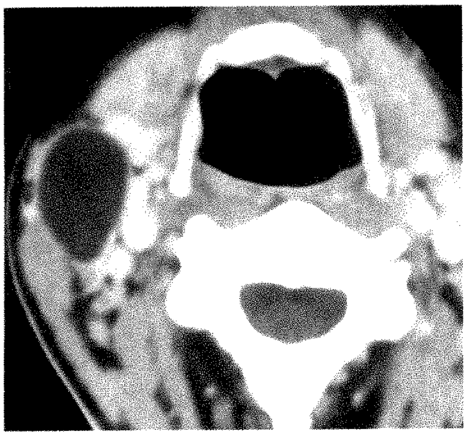

1

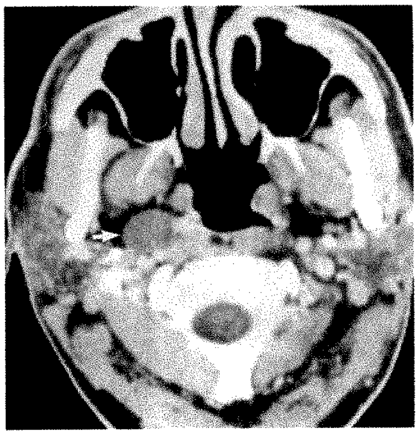

2

Fig. 1.—Typical CT appearance of second branchial cleft cyst. Contrast-enhanced CT scan shows second branchial cleft cyst to have homogeneous low attenuation and a thin rim. It displaces sternocleidomastoid muscle slightly posteriorly, carotid artery and internal jugular vein medially, and submandibular gland anteriorly.

Fig. 2.—Contrast-enhanced CT scan shows an atypical second branchial cleft cyst (*arrow*) within right parapharyngeal space, imparting no significant mass effect on surrounding structures (more inferior images showed cyst to be intimately associated with palatine tonsil, the most cephalad extent of the embryologic tract of second branchial cleft). Clinically, these lesions may mimic parotid lesions, and correct identification of their location may alter surgical approach.

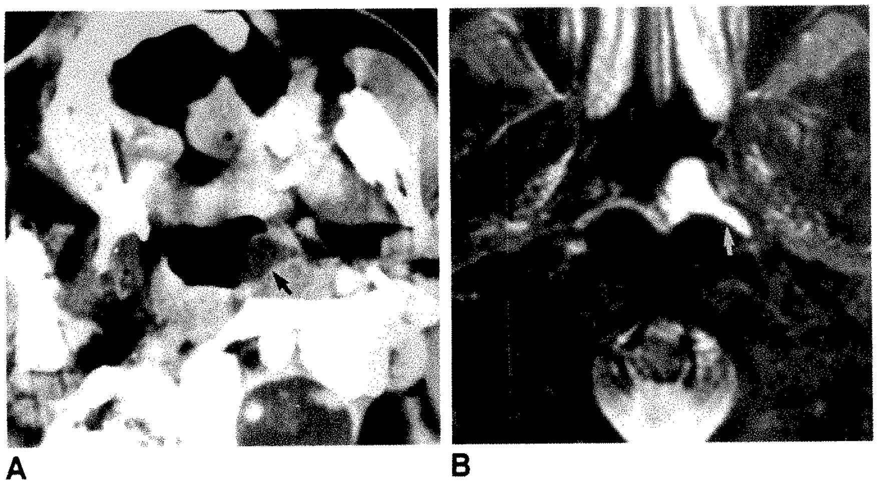

Fig. 3.—Second branchial cleft cyst manifesting as a nasopharyngeal cyst.
A, Contrast-enhanced CT scan shows a lateral nasopharyngeal cyst (*arrow*) protruding into airway (more inferior images again revealed cyst to involve palatine tonsil).
B, Axial MR image (2400/80) shows cyst to involve Rosenmuller's fossa (*arrow*). Lateral nasopharyngeal cysts are usually of branchiogenic origin [3].

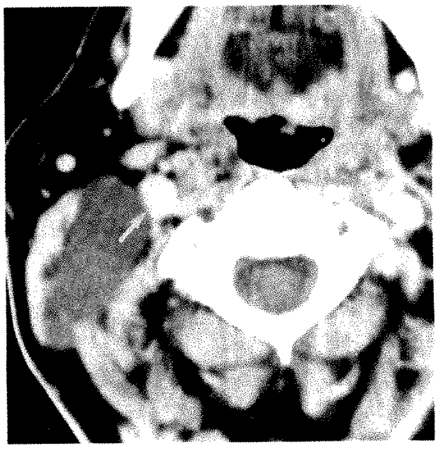

Fig. 4.—Second branchial cleft cyst in posterior triangle. Contrast-enhanced CT scan shows cyst displacing internal jugular vein anteromedially (*arrow*). Such a position is often throught to preclude a branchial cleft cyst. Patient's age (59 years old) and unilocular nature of cyst made cystic hygroma a less likely differential consideration. If cyst can be shown to extend between internal and external carotid arteries, as does embryologic tract (not shown here), this would strongly suggest a second branchial cleft cyst.

cysts, cystic lymphangiomas, necrotic metastases, and dermoid and epidermoid tumors of the submandibular and parapharyngeal spaces [1, 2].

First Branchial Cleft Cysts

First branchial cleft cysts arise along the residual embryologic tract extending from the submandibular triangle to the external auditory canal, coursing through the parotid gland [2]. These cysts can involve the superficial or deep portion of the parotid gland or be extraparotid. Classically, they manifest as enlarging masses near the lower pole of the parotid gland (Fig. 9) or as a mass within the external auditory canal.

Any cystic mass of the parotid gland can mimic the CT or MR appearance of a first branchial cleft cyst [1, 2] (Fig. 10). Retention cysts are the most common parotid cysts and those of branchial cleft origin are the second most common. Benign parotid tumors such as Warthin's tumor (papillary cystadenoma lymphomatosum) and more malignant parotid lesions, including mucoepidermoid carcinoma and necrotic metastases, may manifest as or mimic a parotid cyst. Posttraumatic sialoceles (Fig. 11) and ganglions of the temporomandibular joint (Fig. 12) also may manifest as parotid or periparotid cysts and mimic first branchial cleft cysts. Other entities in the differential diagnosis of first branchial cleft cysts include necrotic lymphadenopathy, cystic lymphangiomas, sebaceous cysts, and benign lymphoepithelial parotid cysts, which sug-

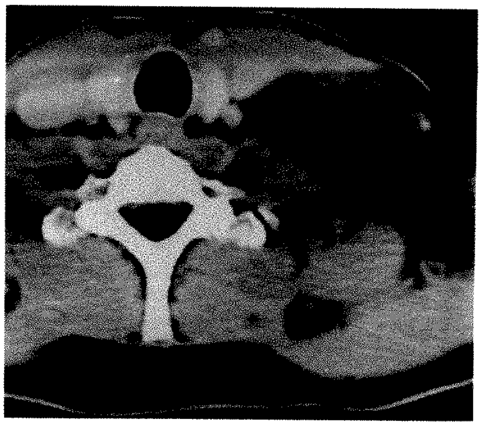

5

Fig. 5.—Second branchial cleft cyst in posterior triangle. Contrast-enhanced CT scan shows this unusual second branchial cleft cyst is within posterior triangle and extends well into supraclavicular region. Other cystic lesions such as cystic hygroma could have a similar appearance. Most caudal extent of residual tract of second branchial cleft is supraclavicular region.

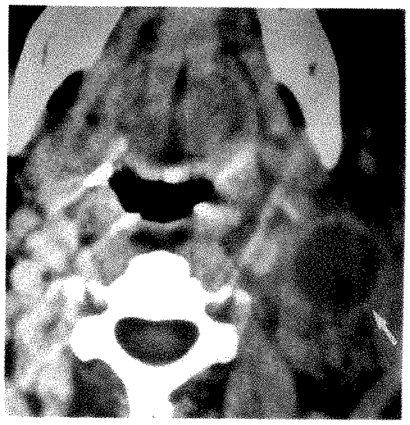

6

Fig. 6.—Infected second branchial cleft cyst. This 14-year-old girl had a low-grade fever, a tender mass in left side of neck, and a history of a recent upper respiratory infection. Contrast-enhanced CT scan reveals a slightly thick-walled cystic mass (*arrow*) posterior to angle of mandible with infiltration and obscuration of surrounding soft-tissue planes. Recognition of this as possibly an infected second branchial cleft cyst rather than a frank abscess is important to the surgeon because these cysts are closely related to ninth, 11th, and 12th cranial nerves and to the carotid arteries (an extension of the cyst may pass through the carotid bifurcation). When infected, dissection may be made difficult.

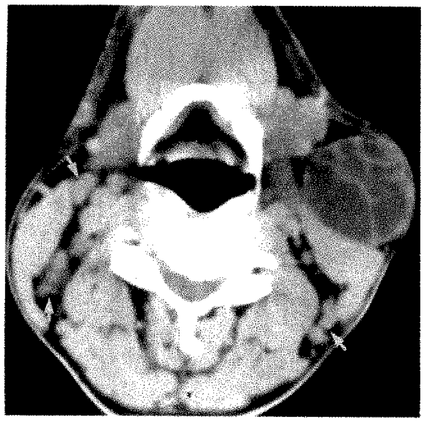

Fig. 7.—Infected branchial cleft cyst. This 27-year-old HIV-positive patient had a recurrent mass in left side of neck that was relatively resistant to antibiotic therapy. Contrast-enhanced CT scan shows a large, septated cystic mass in left anterior triangle. Lymphadenopathy (*arrows*) is bilateral. Clinically and radiologically, patient was thought to have lymphoma. Recognition that this is a common location for branchial cleft cysts should prevent the radiologist from being dogmatic about this diagnosis.

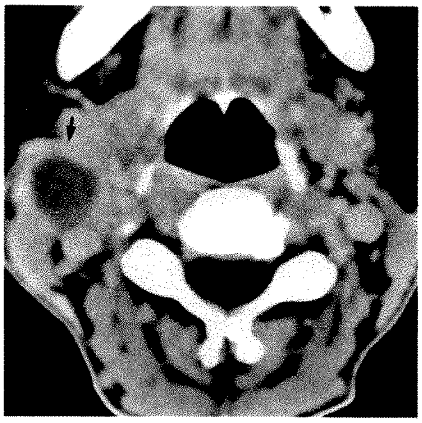

Fig. 8.—Well-differentiated squamous cell carcinoma. Contrast-enhanced CT scan shows a 2-cm, thick-walled cystic mass (*arrow*) in right anterior triangle. Differential diagnosis would include a necrotic neoplasm, abscess, or second branchial cleft cyst (probably infected). Clinical findings and history were important in this case in establishing diagnosis.

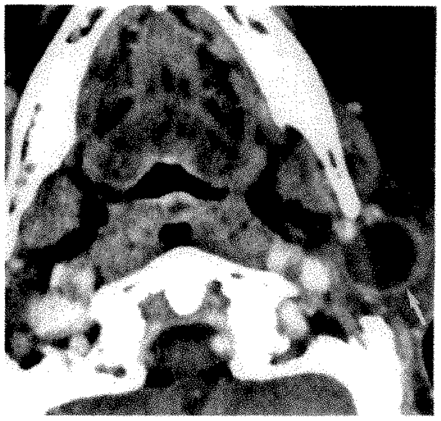

Fig. 9.—First branchial cleft cyst. Contrast-enhanced CT scan shows a 2-cm cystic lesion with a thin enhancing rim (*arrow*) within midportion of left parotid gland. Here and within external auditory canal are typical locations for first branchial cleft cysts.

gest an HIV-positive status when seen in combination with hyperplastic cervical adenopathy [1, 2, 5].

Nasopharyngeal Cysts

Nicolai et al. [3], in their recent review of nasopharyngeal cysts, classify these cysts with regard to whether they are midline or lateral and further subdivide them into congenital and acquired categories.

Congenital midline cysts originate from the pharyngeal bursa (Tornwaldt's bursa) or from Rathke's pouch. Tornwaldt's cysts (Fig. 13) occur in approximately 3% of adults and are due to persistence of the embryologic pharyngeal bursa [3]. These cysts are asymptomatic unless infected, in which case the patient may have foul breath, postnasal discharge, and muscle spasm. The advent of MR imaging has increased the radiologic detection of this lesion. Cysts originating from Rathke's pouch are extremely rare.

Acquired midline cysts, even more common than the congenital variety, are retention cysts (Fig. 14), usually arising from the median recess of the pharyngeal tonsil. Histologically, these cysts may appear similar to Tornwaldt's cysts. Retention cysts, however, often will have many lymphoid follicles in their walls, as opposed to Tornwaldt's cysts [3]. Radiologically, it may be impossible to determine whether a

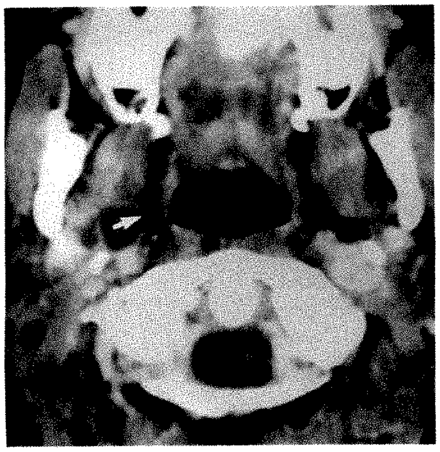

Fig. 10.—Inflammatory cyst of deep lobe of parotid gland. Contrast-enhanced CT scan shows a 1.5 × 1.0 cm cyst involving deep lobe of right parotid gland, bowing parapharyngeal fat slightly medially (*arrow*). Pathologic findings revealed a chronically inflamed cyst. Defining such a lesion as within parotid space rather than within parapharyngeal space is important to the surgeon because it alters the surgical approach.

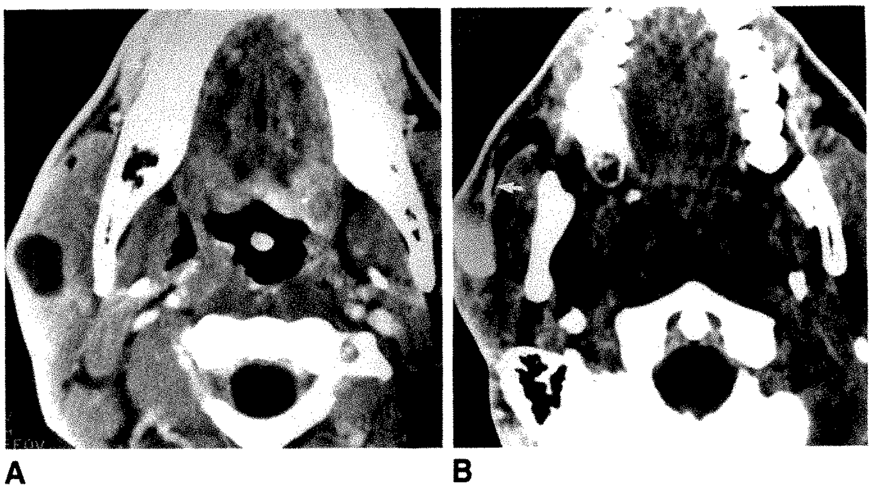

Fig. 11.—Posttraumatic sialocele.

A, Contrast-enhanced CT scan shows a 2.0 × 1.5 cm cyst in anterolateral aspect of right parotid gland.

B, CT scan after injection of contrast material into Stensen's duct (*arrow*) shows that cyst opacifies. Posttraumatic sialoceles occur when excretory ducts draining a portion of parotid gland are interrupted.

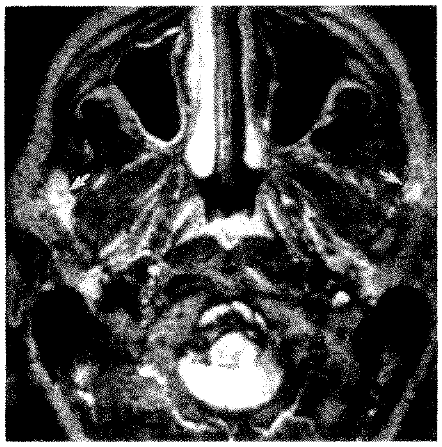

Fig. 12.—Bilateral ganglionic cysts of temporomandibular joint. Axial T2-weighted (2400/80) MR image shows bilateral cystic lesions (*arrows*) just anterior to mandibular condyles. Cysts abutted parotid glands superiorly. Temporomandibular joint arthrography revealed opacification of a cystic structure anterior to right temporomandibular joint. The radiologist's impression is often very helpful to the surgeon, as clinically these lesions frequently appear as parotid masses.

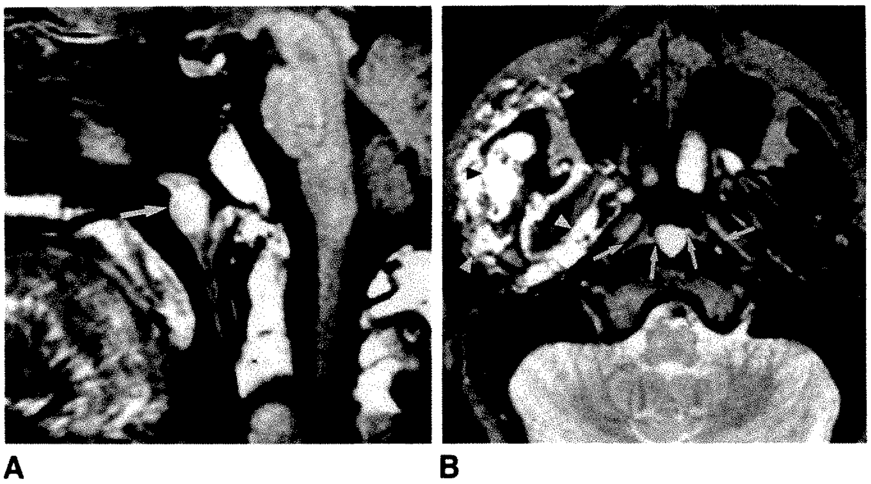

Fig. 13.—Tornwaldt's cyst.

A, Sagittal T1-weighted (600/20) MR image shows a 1-cm, high-signal intensity lesion (*arrow*) in posterosuperior angle of nasopharynx. High signal seen on T1-weighted images is due to concentrated mucus and inflammatory debris.

B, Axial T2-weighted (2400/80) MR image shows cyst to be midline and high in signal intensity. Cyst appears deep to pharyngobasilar fascia (*arrows*), consistent with a cyst arising from pharyngeal bursa (Tornwaldt's cyst). Midline retention cysts are superficial to pharyngobasilar fascia. Note also extensive hemangioma involving right masticator space, parapharyngeal space, and precarotid space (*arrowheads*).

cyst is a retention cyst or a Tornwaldt's cyst, as they may both be located in the posterosuperior angle of the nasopharynx. However, Nicolai et al. [3] state that retention cysts are superficial to the pharyngobasilar fascia and Tornwaldt's cysts are deep to it. Given this, MR imaging may be helpful in further delineating the origin of midline cysts, as the pharyngobasilar fascia can often be visualized as a signal void on MR. Furthermore, concentrated mucus and inflammatory debris often result in Tornwaldt's cysts appearing hyperintense on T1-weighted images (Fig. 13), although this is not diagnostic of the lesion. Many of the Tornwaldt's cysts seen on MR imaging may, in fact, be retention cysts.

Lateral nasopharyngeal cysts, as described earlier, may arise from persistence of the pharyngeal portion of the second

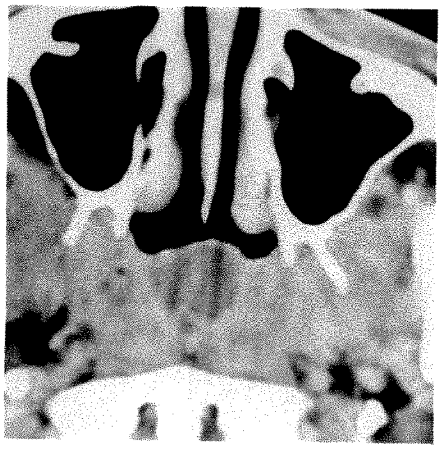

Fig. 14.—Midline nasopharyngeal retention cyst. Axial contrast-enhanced CT scan shows a 2.0 × 1.5 cm cystic mass in midline of posterior nasopharynx. Midline nasopharyngeal cysts usually are retention cysts.

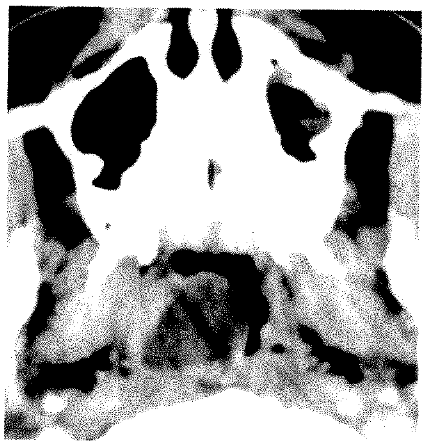

Fig. 15.—Lateral nasopharyngeal mucus retention cyst. Contrast-enhanced CT scan shows large, off-midline cyst to be markedly compromising nasopharyngeal airway. Patient had presented with sleep apnea. Radiologically and histologically it may be difficult to distinguish an acquired retention cyst from a congenital branchial cleft cyst in this location.

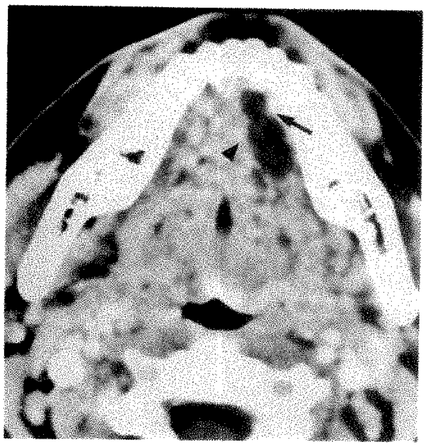

Fig. 16.—Simple ranula. Contrast-enhanced CT scan shows a 2 × 1 cm cystic lesion in left sublingual space lateral to genioglossus muscle (*arrowhead*) and medial to mylohyoid muscle (*arrow*). Differential diagnosis includes simple ranula, epidermoid, and a homogeneous dermoid cyst. MR signal characteristics can generally be used to distinguish these lesions.

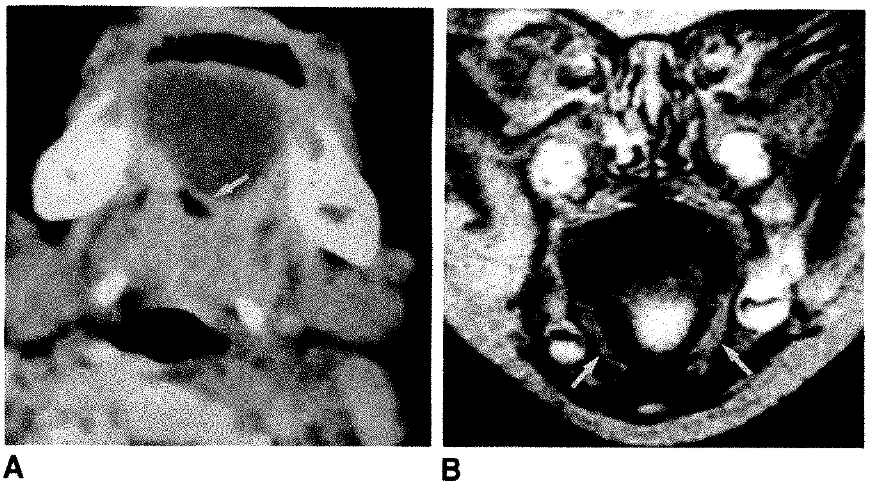

Fig. 17.—Simple ranula. This 3-month-old boy had had sublingual swelling since birth.

A, Unenhanced CT scan shows a large cystic mass in floor of mouth, deviating left genioglossus muscle to right (*arrow*).

B, Coronal T2-weighted (2400/80) MR image shows cyst clearly to be within floor of mouth, as it is superior to mylohyoid muscle (*arrows*). The somewhat midline position of this simple ranula is atypical. Differential considerations would include epidermoid and suprahyoid thyroglossal duct cyst.

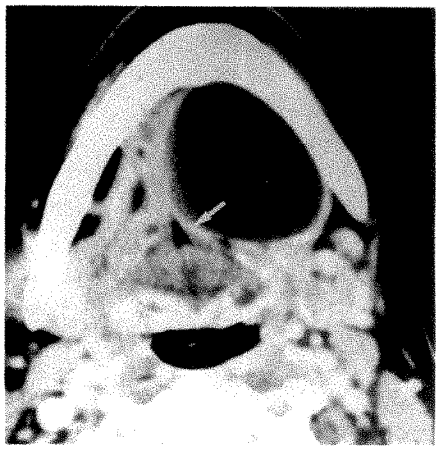

Fig. 18.—Dermoid cyst. This 15-year-old had had progressive swelling in floor of mouth for 1 year. Contrast-enhanced CT scan shows a large homogeneous cystic mass in left sublingual space, deviating genioglossus muscle to right (*arrow*). This lesion cannot be differentiated from a simple ranula or epidermoid on CT. MR should enable distinction between them. Surgical approach is the same.

branchial cleft (Fig. 3). Nicolai et al. [3] have found that lateral nasopharyngeal cysts are usually of branchial cleft origin and, as such, are usually congenital. Acquired lateral nasopharyngeal cysts are retention cysts of seromucinous glands [3] (Fig. 15) and are extremely unusual. As with midline cysts, radiologic distinction between an acquired and congenital lateral nasopharyngeal cyst may be impossible, and histologic distinction may be very difficult as well.

Cystic Masses of the Floor of the Mouth and Upper Neck

Ranulas are mucous retention cysts of the floor of the mouth resulting from obstruction of a minor salivary gland or the sublingual gland. Simple ranulas are confined to the sublingual space (Figs. 16 and 17) and are relatively distinctive lesions on CT and MR imaging. Coit et al. [6] state that "demonstration of a unilocular, cystic mass entirely within the

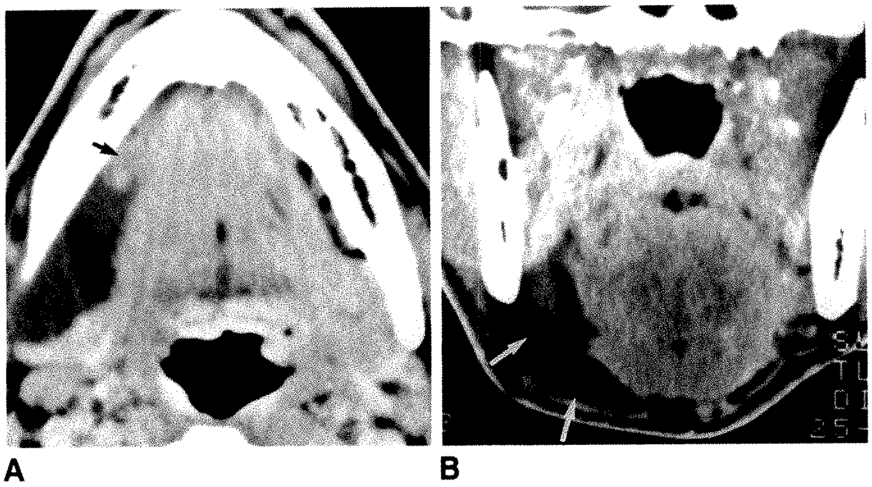

Fig. 19.—*A* and *B*, Plunging ranula. Axial (*A*) and coronal (*B*) contrast-enhanced CT scans show that ranula (*white arrows*) has dissected posteroinferiorly into submandibular space, and most of it is within submandibular space. It has dissected around mylohyoid muscle (*black arrow*), the landmark that separates floor of mouth from submandibular space and neck.

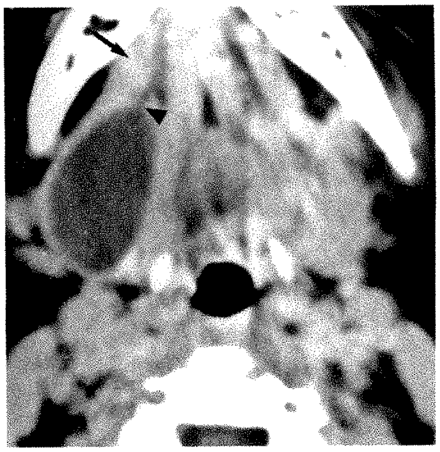

Fig. 20.—Dermoid cyst, mimicking a plunging ranula. Contrast-enhanced CT scan shows that cyst involves both sublingual space (*arrowhead*) and submandibular space, having grown around mylohyoid muscle (*arrow*). Dermoid cysts are not generally this homogeneous on CT.

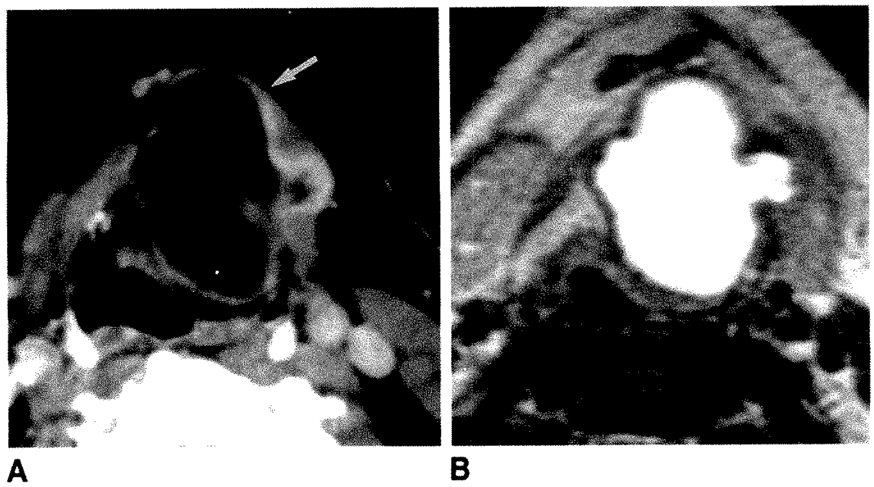

Fig. 21.—*A* and *B*, Mixed (internal and external) laryngocele. Contrast-enhanced CT scan (*A*) and axial T2-weighted (2571/80) MR image (*B*) show a well-demarcated cystic mass penetrating thyrohyoid membrane and displacing strap muscles (*arrow*) anteriorly. Other images suggested that lesion arose from laryngeal ventricle, consistent with a laryngocele. Growth through thyrohyoid membrane and position deep to strap muscles help distinguish a large fluid-filled mixed laryngocele from an infrahyoid thyroglossal duct cyst.

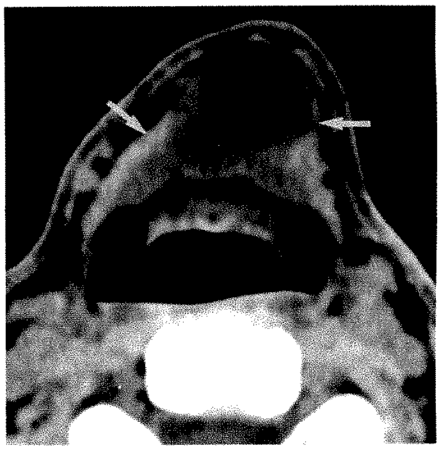

Fig. 22.—Infrahyoid thyroglossal duct cyst. Contrast-enhanced CT scan shows a 2.8 × 2.5 cm cystic mass embedded within strap muscles (*arrows*) but anterior to thyrohyoid membrane. Other cystic-appearing lesions in this location, such as necrotic lymph nodes, abscesses, and thrombosed anterior jugular veins, lie anterior to strap muscles.

sublingual space enables one to limit the differential diagnostic considerations to either a simple ranula or an epidermoid." Dermoid cysts, although usually inhomogeneous on CT, can have a relatively homogeneous fluid collection and also may mimic a simple ranula if within the sublingual space (Fig. 18). MR signal characteristics can generally be used to distinguish these lesions.

The diving or plunging ranula is a ranula that has broken through the capsule of its gland of origin, often with dissection into the submandibular or inferior parapharyngeal space (Fig. 19). Just as they can mimic simple ranulas, epidermoids and homogeneous dermoids can mimic plunging ranulas (Fig. 20). Usually, however, dermoids and epidermoids of the parapharyngeal or submandibular spaces will lack communication with the sublingual space and can be distinguished from diving ranulas [6].

Atypical cystic hygromas of the submandibular space and second branchial cleft cysts within the parapharyngeal space may, at first glance, mimic a plunging ranula. However, these lesions do not communicate with the sublingual space. Also, 20% of thyroglossal duct cysts are suprahyoid in location. Generally they are midline but up to 25% may be paramedian. In such a location, they may mimic plunging ranulas but, again, generally do not enter the sublingual space [6]. If they do extend through the mylohyoid muscle into the floor of the mouth, their midline location should suggest a thyroglossal duct cyst. As shown in Figure 17, though, ranulas may atypically appear as predominantly midline lesions. Given that suprahyoid thyroglossal duct cysts and atypical branchial cleft cysts and cystic hygromas may mimic plunging ranulas, they can, of course, also mimic dermoids and epidermoids in these locations.

Thyroglossal duct cysts arise as a result of the failure of a portion of the thyroglossal duct to involute and are classified into suprahyoid (20%), hyoid (15%), and infrahyoid (65%) cysts [1, 6]. A large fluid-filled, mixed (internal and external) laryngocele (Fig. 21) may appear similar to an infrahyoid thyroglossal duct cyst (Fig. 22) on CT and MR. Other cystic-appearing lesions such as necrotic lymph nodes, abscesses, and thrombosed anterior jugular veins may mimic an infrahyoid thyroglossal duct cyst also. Conversely, thyroglossal duct cysts can mimic certain laryngeal masses, specifically glottic and supraglottic tumors [1].

REFERENCES

1. Som PM. Cystic lesions of the neck. *Postgrad Radiol* **1987**;7:211–236
2. Harnsberger HR, Mancuso AA, Muraki AS, et al. Branchial cleft anomalies and their mimics: computed tomographic evaluation. *Radiology* **1984**;152:739–748
3. Nicolai P, Luzzago F, Maroldi R, Falchetti M, Antonelli AR. Nasopharyngeal cysts. *Arch Otolaryngol Head Neck Surg* **1989**;115:860–864
4. Salazar JE, Duke RA, Ellis JV. Second branchial cleft cyst: unusual location and a new CT diagnostic sign. *AJR* **1985**;145:965–966
5. Holliday RA, Cohen WA, Schinella RA, et al. Benign lymphoepithelial parotid cysts and hyperplastic cervical adenopathy in AIDS-risk patients: a new CT appearance. *Radiology* **1988**;168:439–441
6. Coit WE, Harnsberger HR, Osborn AG, Smoker WRK, Stevens MH, Lufkin RB. Ranulas and their mimics: CT evaluation. *Radiology* **1987**;163:211–216

Book Review

Cerebral Blood Flow Measurement with Stable Xenon-Enhanced Computed Tomography. Edited by Howard Yonas. New York: Raven, 327 pp., 1992. $80

This compact book is an edited compilation of papers presented at the First International Conference on Xenon/Computed Tomographic Cerebral Blood Flow, held in Orlando, FL, in February 1990. About three quarters of the papers presented at that meeting are included. The primary audience for this work will likely be those who attended the meeting. However, the easy availability of the book allows a quick, inexpensive "visit" for those who were unable to attend the conference or were unaware of it. It is doubtful that this book will convince centers to begin offering stable xenon–enhanced CT if they have decided not to perform it. In addition, the work does not serve as a primer on the technique. Hence, its general appeal will be limited. Certainly, every large medical library should own a copy of this book, but all radiology libraries would probably not require a copy.

The work is arranged in six parts: "Theory and Methodology, Data Presentation and Analysis;" "Normative Data;" "Neurological Applications;" "Neurosurgical Applications;" "Critical Care;" and, finally, "Problem Areas." Each part concludes with a summary of the discussion that took place at the meeting after the papers included in that part were presented. The overall quality of the printing, including line diagrams and half-tones, is good. A comprehensive index concludes the book. Extensive references are provided for each paper.

Unfortunately, the book has no abstracts. These may have been specifically excluded because of the potential availability of a scientific program. Abstracts would be useful to lead the reader into each article. No general clinical or "practical" perspective on stable xenon–enhanced CT is provided. Although such a work would not be submitted to such an international conference, this perspective could have been composed by a select group of authors. Such a perspective would rapidly orient the reader who is less well acquainted with the field. It would provide an immediate summary of the situations in which firm clinical indications exist for the technique. Ideally, such an article would include a listing of the scientific works that substantiate the indications. This would allow the reader to immediately see the weight of the evidence behind each clinical application. Such a practical perspective should then be followed by an American and European article similar to paper number 5, "Current Status of Stable Xenon-Enhanced Computed Tomography in Japan and Our Future Strategies." This work is a brief, slightly out-of-date (1989), summary of the applications of the technique in Japan. It includes tables showing the number of CT, MR, single-positron emission computed tomography, positron emission tomography, and stable xenon units operating in Japan in 1989. More such orientation and perspective articles would broaden the audience of this book.

The book has many strengths for readers interested in the technique. Outstanding articles, in addition to the Japanese article already mentioned, include "Technical Aspects," "Patient Care Considerations," "Simplified Method for Mapping Local Cerebral Blood Flow," "Experience in 450 Patients," "Interictal Regional Cerebral Blood Flow in Patients with Refractory Complex Partial Seizures," "Stable Xenon Enhanced Computed Tomography in Moyamoya Disease: A Case Study Using the Calcium Channel Blocker Nifedipine," "Correlation of Xenon-Enhanced Computed Tomography and Angiography in Patients with Intracerebral Arteriovenous Malformations and Clinical Symptoms of Steal," "Measurements in Patients with Chronic Subdural Hematoma," "Beneficial Effect of Stereotactic Hematoma Evacuation for the Small Putaminal Hemorrhage: Evaluation by Xenon-Enhanced Computed Tomography," and "Prognostic Implications of Hyperglycemia and Reduced Cerebral Blood Flow in Near Drowning in Children."

It was particularly enjoyable to see the Japanese perspective on treatment of cerebral vascular disease. Especially notable is the discussion of acute transcranial open embolectomy for emboli of the middle cerebral artery and stereotaxic evacuation of small hypertensive hemorrhages. Such works, though controversial, reflect the true international flavor of the conference. I enjoyed the summaries of the, at times, apparently lively discussions that ensued after presentation of the papers. The reader gets expert, often conflicting, opinions on preceding articles. Such discussions allow readers to feel more like they are at a small-group conference, rather than just reading a book. This is a particularly nice touch.

Stephen S. Gebarski
The University of Michigan
Ann Arbor, MI 48109-0030

CT and MR Imaging Findings in Adults with Cerebellar Medulloblastoma: Comparison with Findings in Children

Pierre M. Bourgouin[1,2]
Donatella Tampieri[1]
Stephen Z. Grahovac[1,3]
Christian Léger[4]
Raquel Del Carpio[1]
Denis Melançon[1]

The goal of this study was to determine if certain imaging features suggest the diagnosis of cerebellar medulloblastoma in adults and to determine how often the classic CT appearance seen in children is present in adults. The study included 28 adult patients with proved cerebellar medulloblastoma. The tumor was located in the cerebellar vermis in 14 patients and in a cerebellar hemisphere in 14 patients. Thirteen patients had unenhanced CT of the brain, all patients had contrast-enhanced CT, and eight patients had unenhanced MR imaging. The imaging features in adults were compared with those in children, as described in the literature. In our adult patients, all tumors were hyperdense compared with gray matter on unenhanced CT and showed a slight to moderate increase in density after injection of contrast medium. Thirteen lesions had well-defined margins, and 15 had poorly defined margins. Low-density areas consistent with cystic and necrotic degeneration were detected in 23 (82%) of the 28 tumors. By comparison, in children, medulloblastoma usually originates in the vermis. As in adults, the mass is hyperdense on unenhanced CT, but enhances markedly and homogeneously after injection of contrast medium. Usually no evidence of cyst formation or necrosis is seen, and the tumor margins are well defined. This classic CT appearance of medulloblastoma in children was identified in only three (11%) of the 28 adult patients. Medulloblastoma has a variable MR appearance in both children and adults. On T2-weighted images, lesions are hypo-, iso-, or hyperintense compared with normal gray matter.

The CT findings of medulloblastoma in adults usually differ from those of medulloblastoma in children. The tumor has a variable and nonspecific appearance in adults and should always be considered in the differential diagnosis of a mass in the posterior fossa.

AJR 159:609–612, September 1992

Cerebellar medulloblastoma most frequently occurs during childhood, when it accounts for about 15% of all brain tumors [1–3]. This neoplasm is uncommon in adults. According to the Connecticut Tumor Registry [2], medulloblastoma accounts for only 0.4% of all brain tumors in adults.

The CT appearance of cerebellar medulloblastoma in children has been well described [1–8]. A hyperdense midline mass on unenhanced CT that displays marked and homogeneous enhancement after injection of contrast medium is strongly suggestive of the diagnosis. Few reports have specifically discussed the tumor in adults [9, 10]. The goal of this study was to determine if certain imaging features strongly suggest the diagnosis in adults and how often the class CT appearance of medulloblastoma described in children is seen in adults.

Materials and Methods

This study included 28 adults, 15 men and 13 women, with histopathologically proved medulloblastoma, who were evaluated and treated at the Montreal Neurological, Notre-Dame, Ottawa General, and Ottawa Civic hospitals between 1978 and 1990. The age range was

Received October 23, 1991; accepted after revision April 10, 1992.

[1] Department of Radiology, Montreal Neurological Hospital and Institute, McGill University, Montréal, Québec, Canada H3A 2B4.

[2] Present address: Department of Radiology, Hôpital Notre-Dame, Université de Montréal, Montreal General Hospital, McGill University, 1560 Sherbrooke St. E., Montréal, Québec, Canada, H2L 4M1. Address reprint requests to P. M. Bourgouin.

[3] Present address: Department of Radiology, Ottawa General Hospital, University of Ottawa, Ottawa, Ontario, Canada K1H 8L6.

[4] Department of Computer Sciences and Operational Research, Université de Montréal, Montréal, Québec, Canada H3C 3J7.

0361–803X/92/1593–0609

©American Roentgen Ray Society

18–47 years (mean, 28 years). Seventeen patients were 18–30 years old, eight patients were 30–40 years old, and three patients were more than 40 years old. All patients had a mass in the posterior fossa.

The epicenter of the tumor was located in the cerebellar vermis in 14 patients and in a cerebellar hemisphere in 14 patients. All patients had radical excision of the tumor, followed by radiation therapy. Histopathologic studies were performed on the resected specimens to detect the presence of desmoplasia. Tissues were stained with hematoxylin and eosin and by using Gomori's reticulin method. Eight (29%) of 28 tumors showed evidence of desmoplasia. Desmoplasia was detected in three (21%) of 14 patients with vermian tumors and in five (36%) of 14 patients with hemispheric tumors. No statistical correlation between location of tumor and presence of desmoplasia was found ($p = .40$).

All patients had contrast-enhanced CT of the brain before surgery. In addition, 13 patients had unenhanced CT. Eight patients had unenhanced MR imaging. Multislice spin-echo T1-weighted images (400–600/20–30/2 [TR/TE/excitations]), proton density-weighted images (2000–2300/30–40/2), and T2-weighted images (2000–2300/80–90/2) were obtained in all patients. All studies were performed on 1.5-T systems, and images were always obtained in at least two orthogonal planes. The CT and MR examinations were reviewed by two neuroradiologists, and the following features analyzed: tumor density compared with the density of normal gray matter, before and after injection of contrast medium; signal intensity of the tumor compared with that of normal gray matter; nature of tumor margins; tumor size; and presence of cysts and necrosis, calcifications, edema, and hydrocephalus.

The imaging features of medulloblastoma in adults were compared with those of medulloblastoma in children, as described in the literature [1–8].

Results

CT Findings

All tumors were hyperdense compared with normal gray matter on contrast-enhanced CT. In the 13 patients who had unenhanced CT, all tumors were hyperdense compared with gray matter and showed mild to moderate enhancement after injection of contrast medium. Thirteen lesions had well-defined margins, and 15 had poorly defined margins. A majority (64%) of vermian tumors had well-defined margins, whereas only 29% of hemispheric lesions had well-defined margins. The mean diameter of tumors was 4.6 cm (±1.2 cm SD). Areas of low density (usually <1 cm), consistent with intratumoral cysts and necrosis, were detected in 23 patients (82%). Some tumors had multiple small cysts; others had a single large cavity. Calcifications were seen in two patients

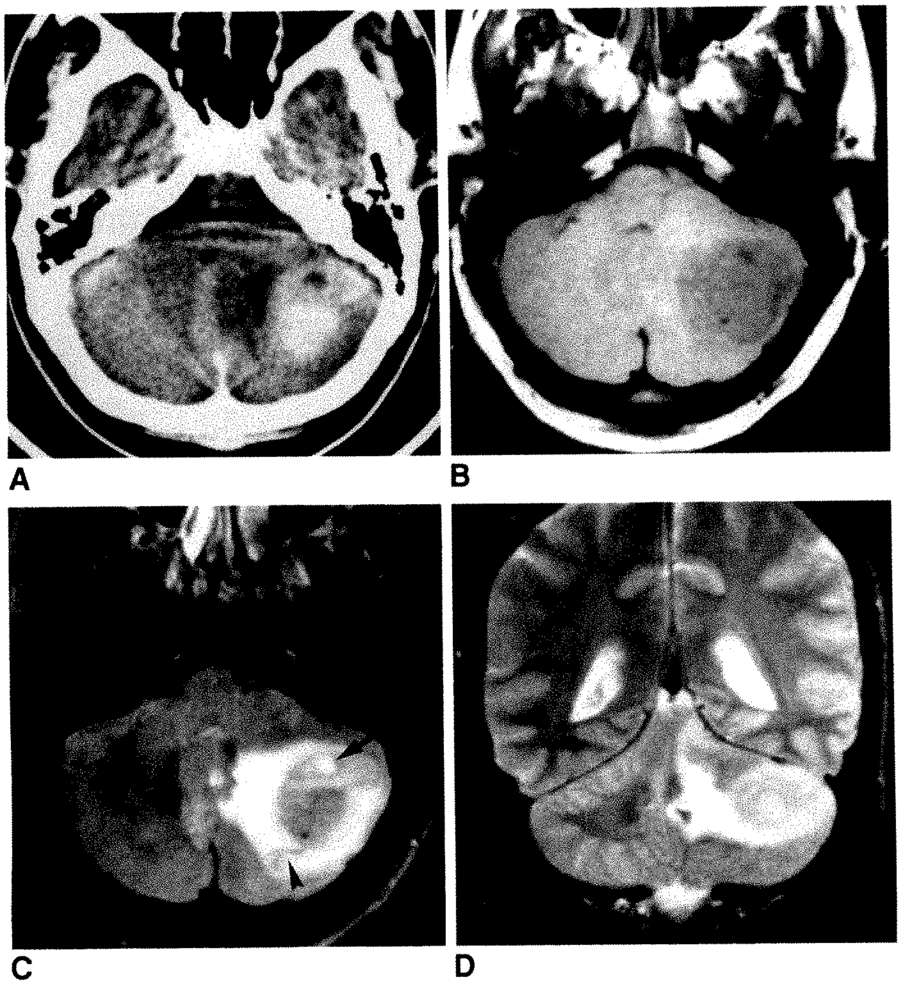

Fig. 1.—Hemispheric medulloblastoma with cyst in a 35-year-old man.

***A*, Contrast-enhanced CT scan shows a poorly defined, hyperdense mass in left cerebellar hemisphere, a small cyst inside tumor, and edema in adjacent parenchyma.**

***B*, Axial T1-weighted MR image shows a hypointense mass in left cerebellar hemisphere.**

***C*, Axial T2-weighted MR image shows tumor is isointense compared with normal gray matter. Hyperintense cyst (*arrow*) and prominent vessel (*arrowhead*) are seen inside tumor. Hyperintense edema, well differentiated from tumor and adjacent normal brain, is present.**

***D*, Coronal T2-weighted MR image shows tumor abuts left side of tentorium. Partial obliteration of tentorium's low-intensity signal was due to volume averaging. At surgery, no invasion of tentorium was found.**

(7%). A surrounding region of low density, consistent with edema, was present in 21 tumors (75%). Hydrocephalus of various degrees of severity was seen on the initial examination in 26 patients (93%).

Nine (32%) of 28 patients had a poorly defined hemispheric tumor with evidence of cystic or necrotic degeneration (Fig. 1). This was the most frequently identified pattern in our series. Six (21%) of 28 patients had well-defined vermian lesions with nonenhancing areas of low density (Fig. 2). Only three patients (11%) had a well-defined homogeneous vermian tumor, the typical appearance of medulloblastoma in children (Fig. 3).

MR Findings

Eight patients had MR imaging. On T1-weighted images, the tumors were hypointense or isointense compared with normal gray matter. On T2-weighted images, the increase in the signal intensity of tumor was variable. Some tumors were almost hypointense or isointense compared with brain, whereas others were moderately hyperintense (Figs. 1 and 4). The intratumoral cysts and necrotic foci were easily detected on T2-weighted images because of their higher signal intensity compared with that of solid tumor. In four patients, tubular areas with signal void, consistent with prominent vessels, were detected on T1- and T2-weighted images (Fig. 1). All tumors had evidence of high-signal-intensity edema, which was well differentiated from tumor and adjacent normal parenchyma on T2-weighted images. The relationship of the tumor with the fourth ventricle and brainstem was always well shown, particularly on sagittal T1- an T2-weighted images (Fig. 4). The relationship of the tumor with the tentorium was more difficult to assess. In three patients, the tumor abutted the tentorium, with partial obliteration of the tentorium's low-intensity signal, but actual invasion was found at surgery in only one patient.

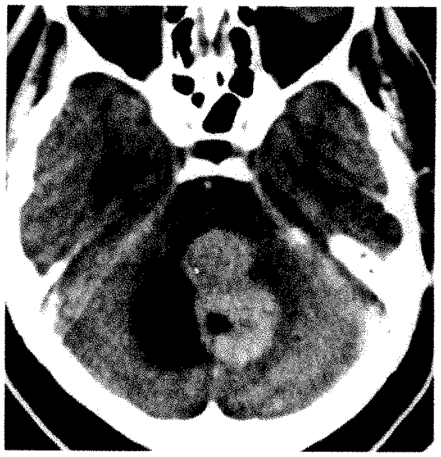

2

Fig. 2.—Vermian medulloblastoma with cysts in a 47-year-old man. Contrast-enhanced CT scan shows a well-defined mass in vermis. Cysts are present.

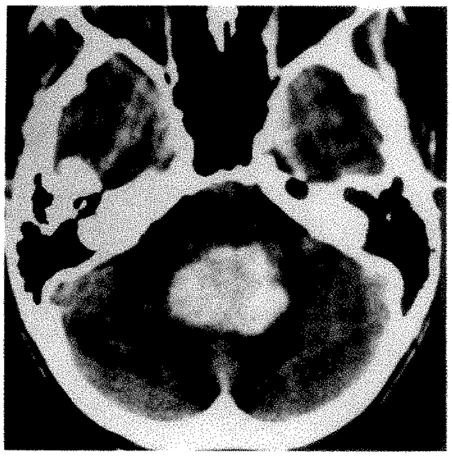

3

Fig. 3.—Vermian medulloblastoma in a 20-year-old man. Contrast-enhanced CT scan shows a hyperdense, well-defined lesion in vermis. Mass is homogeneous, without evidence of cystic or necrotic degeneration.

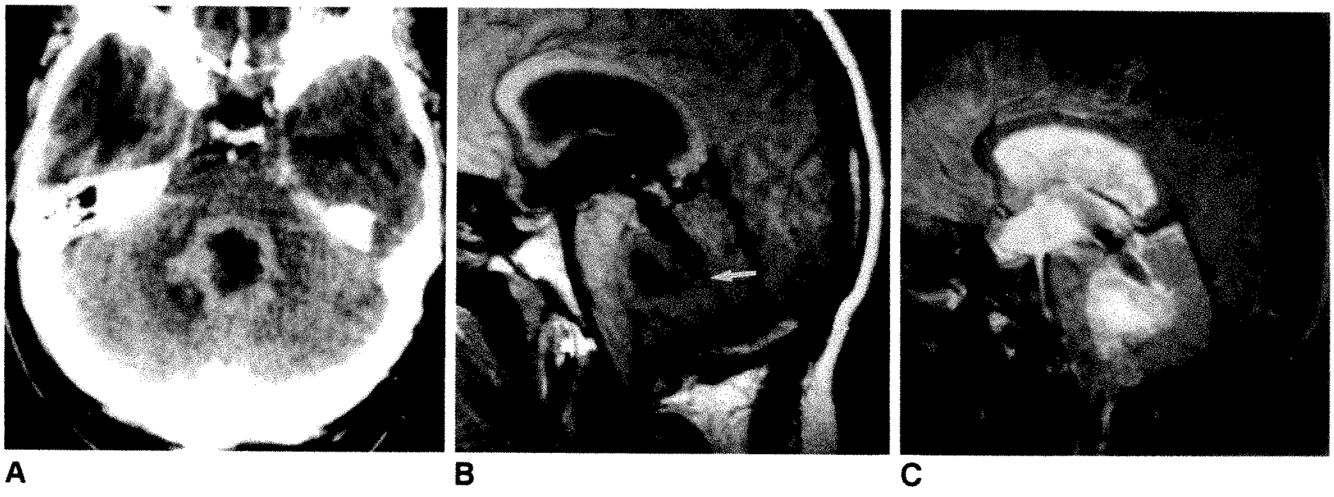

Fig. 4.—Vermian medulloblastoma in a 32-year-old woman.

***A*, Contrast-enhanced CT scan shows a hypodense mass with peripheral enhancement at level of fourth ventricle.**

***B*, Sagittal T1-weighted MR image shows mass (*arrow*) lies inferior to fourth ventricle. Peripheral solid part of mass is isointense compared with brain, whereas center is hypointense, consistent with necrosis.**

***C*, Sagittal T2-weighted MR image shows hyperintense mass with central necrosis is well delineated from brainstem, which was not invaded by tumor.**

Comparison with Medulloblastoma in Children

Medulloblastomas in children are usually located in the vermis [1–8]. The lesions are hyperdense compared with gray matter on unenhanced CT and enhance markedly after injection of contrast material. The classic appearance is that of a well-defined homogeneous tumor usually without cystic or necrotic degeneration. In a study of less common CT features of medulloblastoma in children, Zee et al. [5] found evidence of cyst formation and necrosis in only 17% of their patients. As in adults, medulloblastoma has a variable MR appearance in children [8]. On T1-weighted images, tumors are hypo- or isointense relative to cortex and on T2-weighted images, they are hypo-, iso-, or hyperintense.

By comparison with children, about half of medulloblastomas in adults originate in a cerebellar hemisphere. The tumors are hyperdense on unenhanced CT, but usually show less enhancement after injection of contrast medium. Unlike in children, medulloblastoma in adults is not homogeneous. Our study shows a high prevalence of intratumoral low-density areas caused by cystic and necrotic degeneration. Tumor margins are well defined or poorly defined in adults, whereas they are usually well defined in children. The prevalences of calcifications, edema, and hydrocephalus and the size of tumors are comparable in adults and children.

Discussion

Medulloblastoma is thought to arise from primitive or pluripotential cells found in the germinative zone of the posterior medullary velum. These cells migrate upward and laterally to form the external granular layer of the cerebellar hemispheres. Medulloblastoma can develop anywhere along the path of migration, medially or laterally [1, 3, 7, 9]. According to this hypothesis, the tumors that arise earlier in life occur close to the midline (vermis), whereas those arising later in life are located more laterally within a cerebellar hemisphere. This explains the higher prevalence of hemispheric tumors in adults than in children.

Medulloblastoma is made of compact tumor cells in a vascular stroma. This explains the hyperdensity of lesions relative to normal gray matter on unenhanced CT. Medulloblastoma in adults shows less enhancement after injection of contrast medium than does medulloblastoma in children. This is most likely because of the higher prevalence of desmoplastic lesions in adults. Desmoplastic medulloblastomas contain a large amount of reticulin fibers in their stroma [9, 11, 12]. According to Rubinstein and Northfield [12], they represent one end of the spectrum of medulloblastoma that extends from midline, classic medulloblastoma of children, through transitional forms, to lateral desmoplastic medulloblastoma seen in adults. Our study shows a high rate (82%) of cystic and necrotic degeneration. In most studies, the prevalence of cystic and necrotic degeneration ranged from 10% to 20%, although Sandhu and Kendall [13] reported 47%. The prevalence found in our study is higher because our series included only adults, and cystic and necrotic degeneration is presumably more common in this age group.

Medulloblastoma has a variable MR appearance in both adults and children. In some of our patients, the tumor was hypo- or isointense on T2-weighted images. Pomeranz [14] reported that medulloblastoma in adults had a shorter T2 relaxation time than other tumors had. He suggested that the shorter T2 relaxation time was related to a low spin density in the desmoplastic variant in adults. Contrast-enhanced MR was not used in our study. According to Latschaw et al. [15], enhancement of tumor appears to parallel that seen on contrast-enhanced CT.

A well-defined homogeneous vermian mass is the most common presentation of medulloblastoma in children. This classic CT appearance is rarely identified in adults. The CT and MR features of the tumor in adults are more variable than in children. In our adult cases, the most common presentation was that of a poorly defined hemispheric tumor with evidence of cystic and necrotic degeneration; this pattern was identified in only 32% of our patients. Because of its variable and nonspecific imaging appearance, medulloblastoma should always be considered in the differential diagnosis of a mass in the posterior fossa mass of an adult.

ACKNOWLEDGMENTS

We thank Gary Belanger for the case material contributed to the study and Rose-Mai Roy for manuscript preparation.

REFERENCES

1. Zimmerman RA, Bilanuik LT, Phalajani H. Spectrum of medulloblastomas demonstrated by computed tomography. *Radiology* **1978**;126:137–141
2. Farwell JR, Dohrmann GJ, Flannery JT. Medulloblastoma in childhood: an epidemiological study. *J Neurosurg* **1984**;61:657–664
3. Al-Nefty O, Jinkins JR, El-Senousse M, El-Shake M, Fox JL. Medulloblastomas: a review of modern management with a report on 75 cases. *Surg Neurol* **1985**;24:606–624
4. Gado M, Huete I, Mikhael M. Computerized tomography of infratentorial tumors. *Semin Roentgenol* **1977**;12:109–120
5. Zee CS, Segall HD, Miller C, et al. Less common CT features of medulloblastoma. *Radiology* **1982**;144:97–102
6. Weisberg LA. Computerized tomographic findings in medulloblastomas. *Comput Med Imaging Graph* **1982**;6:83–91
7. Naidich TP, Lin JP, Leeds NE, Pudlowski RM, Nordich JB. Primary tumors and other masses of the cerebellum and fourth ventricle: differential diagnosis by computed tomography. *Neuroradiology* **1977**;14:153–174
8. Barkovich AJ, Edwards SB. Brain tumors of childhood. In: Barkovich AJ, ed. *Pediatric neuroimaging*. New York: Raven, **1990**:149–203
9. Hubbard JL, Scheithauer BW, Kispert DB, Carpenter SM, Wick MR, Launs ER. Adult cerebellar medulloblastomas: the pathological, radiographic, and clinical disease spectrum. *J Neurosurg* **1989**;70:536–544
10. Hughes PG. Cerebellar medulloblastoma in adults. *J Neurosurg* **1984**;60:994–997
11. Kasantikul V, Shuangshoti S. Cerebellar medulloblastoma: a study of 35 cases with particular reference to cellular differentiation. *Surg Neurol* **1986**;26:532–541
12. Rubinstein LJ, Northfield DWC. The medulloblatoma and the so-called "arachnoidal cerebellar sarcoma": critical re-examination of a nasological problem. *Brain* **1964**;87:379–412
13. Sandhu A, Kendall B. Computed tomography in management of medulloblastomas. *Neuroradiology* **1987**;29:444–452
14. Pomeranz SJ. Posterior fossa, skull base, craniocervical junction. In: Pomeranz SJ, ed. *Craniospinal magnetic resonance imaging*. Philadelphia: Saunders, **1989**:248–274
15. Latschaw RE, Johnson DW, Kanal E. Primary intracranial tumors: neuroepithelial tumors, sarcomas, and lymphomas. In: Latschaw RE, ed. *MR and CT imaging of the head, neck, and spine*. St. Louis: Mosby, **1991**: 449–508

Case Report

Tortuous Vertebral Artery Shown by MR and CT

Robert Kricun,[1] Lawrence P. Levitt,[2] and H. Richard Winn[3]

Tortuosity of the vertebral artery is an uncommon cause of symptoms that can lead to imaging evaluation. We describe a patient with pain in the neck and retroauricular area in whom the diagnosis of a tortuous vertebral artery was suggested by results of both MR and contrast-enhanced CT and was confirmed by arteriography. The patient underwent a foraminotomy, which alleviated the pain.

Case Report

A 68-year-old woman had a 7-month history of pain in the left side of the neck, the occipital area, and the left retroauricular region that was exacerbated by turning of the head. The pain had increased in severity so much that it limited her lifestyle. No associated signs or symptoms of the extremities were reported. Results of neurologic examination, including sensory examination of the neck and scalp, were normal.

MR imaging of the cervical spine showed looping of the left vertebral artery at C3–C4 (Figs. 1A–1C). A CT examination showed increased soft-tissue density within the left intervertebral foramen at C3–C4 and widening of the foramen. The posterolateral aspect of the C3 vertebral body was eroded and had a sclerotic margin that was seen when the CT scan was viewed at bone window settings. After IV injection of iodinated contrast material, CT showed marked homogeneous enhancement of the prominent vertebral artery (Fig. 1D). An arteriogram was obtained and confirmed the diagnosis of a tortuous left vertebral artery (Fig. 1E).

The patient was thought to have a C4 radiculopathy due to compression by the vertebral artery. A left-sided C3–C4 foraminotomy was performed after a series of local blocks of C2, C3, and C4 relieved her pain temporarily. In the immediate postoperative period, her motor and sensory function remained normal. Six months after surgery, the patient reported that the pain in the left occipital and retroauricular regions had "improved about 80%," with only mild pain remaining.

Discussion

The vertebral artery normally originates from the subclavian artery and courses through the foramen transversarium from C6 to C2. Local tortuosity and elongation of a vertebral artery can cause pressure erosion of the adjacent vertebral body and widening of the intervertebral foramen. In a study of autopsy specimens, four of 21 specimens were reported to have a tortuous vertebral artery with adjacent bone erosions [1]. However, in clinical practice this is an unusual finding; only isolated case reports have been published. This suggests that the presence of a tortuous vertebral artery may go undetected because of the lack of symptoms. However, some patients do have symptoms, such as pain in the neck or cervicooccipital region, radicular pain, or migrainous headache [2–4]. In one unusual case, neurologic symptoms due to a tortuous vertebral artery began during pregnancy [3].

Conventional radiographs can show enlargement of an intervertebral foramen and erosion of the adjacent vertebral body and pedicle [3–8]. Typically, erosion of the vertebra is located eccentrically and involves the posterior or lateral aspect of the body [6]. A review of the literature indicates that tortuosity of the vertebral artery most often occurs at the

---

Received December 23, 1991; accepted after revision February 5, 1992.

[1] Department of Radiology, Lehigh Valley Hospital Center, 1200 S. Cedar Crest Blvd., Allentown, PA 18103. Address reprint requests to R. Kricun.

[2] Department of Neurology, Lehigh Valley Hospital Center, 1200 S. Cedar Crest Blvd., Allentown, PA 18103.

[3] Department of Neurologic Surgery, University of Washington, Seattle, WA 98104.

AJR 159:613–615, September 1992 0361–803X/92/1593–0613 © American Roentgen Ray Society

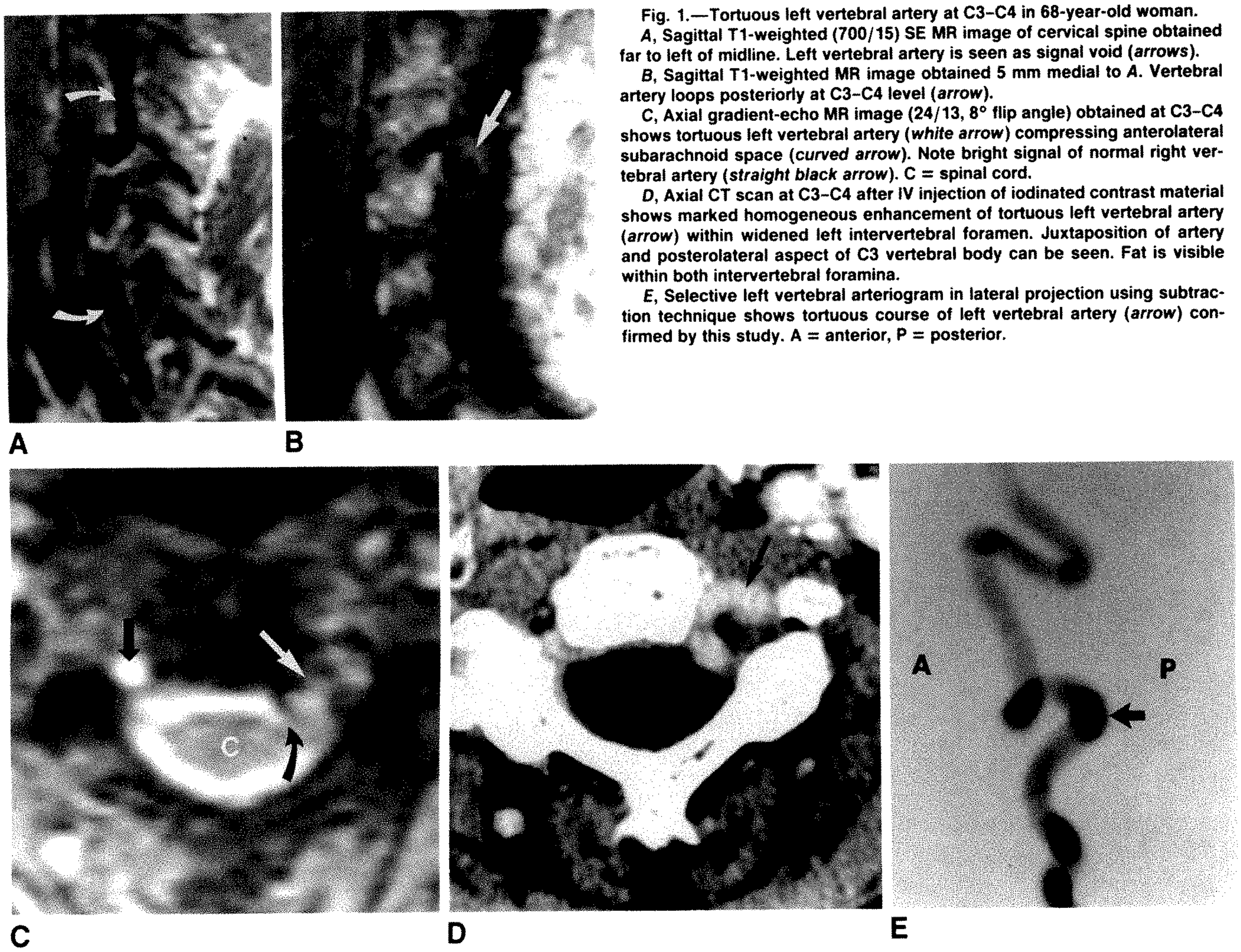

Fig. 1.—Tortuous left vertebral artery at C3–C4 in 68-year-old woman.

A, Sagittal T1-weighted (700/15) SE MR image of cervical spine obtained far to left of midline. Left vertebral artery is seen as signal void (*arrows*).

B, Sagittal T1-weighted MR image obtained 5 mm medial to *A*. Vertebral artery loops posteriorly at C3–C4 level (*arrow*).

C, Axial gradient-echo MR image (24/13, 8° flip angle) obtained at C3–C4 shows tortuous left vertebral artery (*white arrow*) compressing anterolateral subarachnoid space (*curved arrow*). Note bright signal of normal right vertebral artery (*straight black arrow*). C = spinal cord.

D, Axial CT scan at C3–C4 after IV injection of iodinated contrast material shows marked homogeneous enhancement of tortuous left vertebral artery (*arrow*) within widened left intervertebral foramen. Juxtaposition of artery and posterolateral aspect of C3 vertebral body can be seen. Fat is visible within both intervertebral foramina.

E, Selective left vertebral arteriogram in lateral projection using subtraction technique shows tortuous course of left vertebral artery (*arrow*) confirmed by this study. A = anterior, P = posterior.

C4–C5 level with osseous erosion of C4. The C3–C4 level is the second most frequent site. The left vertebral artery is involved more often than is the right vertebral artery. Rarely, bilateral or multilevel tortuosity of the vertebral arteries occurs with corresponding radiologic findings [5].

CT clearly shows foraminal enlargement and osseous erosion and may reveal a sclerotic border at the site of erosion, indicating slow expansion [5]. Preservation of a fat plane within an enlarged foramen transversarium has been described in a patient with a tortuous vertebral artery visualized with CT and is thought to suggest that a neoplasm is not present [5]. In the present case, marked homogeneous enhancement of the tortuous vertebral artery was seen within the intervertebral foramen after IV injection of iodinated contrast material.

MR imaging with spin-echo technique shows the vertebral artery as a signal void because of the rapidly flowing blood. The artery can be displayed in multiple projections and normally has a straight course that can be visualized on a single coronal or sagittal image. When the vertebral artery is tortuous, it may not be entirely displayed on a single image. Instead, evaluation of adjacent sections shows focal uncoiling of the artery. Typically, the tortuous vertebral artery loops medially and can course anteriorly or posteriorly. MR can show the arterial loop and the osseous erosion [4]. These findings can be confirmed by conventional angiography of the vertebral artery [4, 7, 8], IV digital subtraction angiography [3, 5], or MR angiography.

In some cases, MR or CT can be used to examine a patient with a widened intervertebral foramen shown on conventional radiographs. Often, widening of the intervertebral foramen is associated with a dumbbell-shaped tumor such as a neurofibroma or schwannoma. Less frequently, other tumors such as meningioma, metastases, or plasmacytoma can be associated with foraminal enlargement [6]. Congenital absence of a pedicle is an infrequent cause of widening of the intervertebral foramen [9]. A lateral meningocele can widen the foramen, especially in the thoracic spine.

An aneurysm of the extracranial vertebral artery is a rare cause of widening of the intervertebral foramen and is usually a false aneurysm associated with trauma [6]. A case of spontaneous vertebral artery aneurysm with enlargement of the foramen transversarium was reported and shown on CT scans as a homogeneous, slightly dense mass outlined by curvilinear calcifications [10]. In another report, increased caliber and tortuosity of the vertebral artery due to increased flow associated with coarctation of the aorta were described [9]. In that instance the coarctation occurred proximal to the origin of the left subclavian artery, with an anomalous origin of the left vertebral artery from the aorta proximal to the coarctation [9]. This unusual cause of tortuosity of the vertebral artery led to widening of the intervertebral foramen. MR and CT with IV contrast enhancement can be used to differentiate tumors such as neurofibroma from the less frequent vascular causes of intervertebral foraminal widening.

When a tortuous vertebral artery is imaged, clinical correlation is essential to determine whether the abnormality is responsible for the patient's signs and symptoms. If a cause and effect are not clear, conservative treatment is preferred. However, symptoms have been relieved by surgical intervention in some cases when radiculopathy is caused by nerve root compression due to the vascular anomaly [2, 6, 8], as was illustrated in our case.

REFERENCES

1. Hadley LA. Tortuosity and deflection of the vertebral artery. *AJR* **1958**;80:306–312
2. Anderson RE, Shealy CN. Cervical pedicle erosion and rootlet compression caused by a tortuous vertebral artery. *Radiology* **1970**;96:537–538
3. Glover JR, Kennedy C, Coral A. Tortuous vertebral artery: onset of symptoms during pregnancy (case report). *Clin Radiol* **1990**;41:66–68
4. Sganzerla EP, Grimoldi N, Vaccari U, Rampini PM, Gaini SM. Cervical vertebral erosion due to tortuous vertebral artery. *Surg Neurol* **1987**;28:385–389
5. Freilich M, Virapongse C, Kier EL, Sarwar M, Bhimani S. Foramen transversarium enlargement due to tortuosity of the vertebral artery: computed tomographic appearance. *Spine* **1986**;11:95–98
6. Schimmel DH, Newton TH, Mani J. Widening of the cervical intervertebral foramen. *Neuroradiology* **1976**;12:3–10
7. Slover WP, Kiley RF. Cervical vertebral erosion caused by tortuous vertebral artery. *Radiology* **1965**;84:112–114
8. Zimmerman HB, Farrell WJ. Cervical vertebral body erosion caused by vertebral artery tortuosity. *AJR* **1970**;108:767–770
9. Danziger J, Bloch S. The widened cervical intervertebral foramen. *Radiology* **1975**;116:671–674
10. Habozit B, Battistelli J-M. Spontaneous aneurysm of the extracranial vertebral artery associated with spinal osseous anomaly. *Ann Vasc Surg* **1990**;4:600–603

Memorial

Elmer G. St. John, 1906–1991

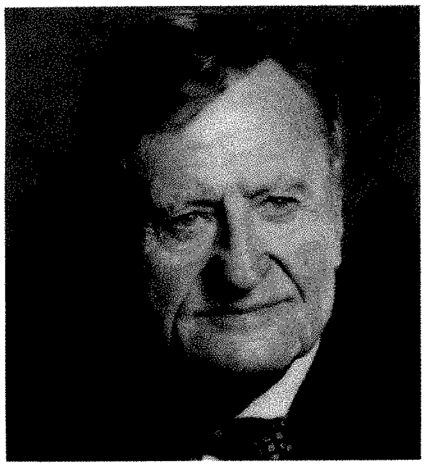

Elson-Alexandre

Elmer G. St. John died November 16, 1991, in Ormond Beach, FL, after a short illness. St. John was born in New York City and spent most of his medical career on the East Coast. He graduated from Union College, Schenectady, NY, in 1929 and from Albany Medical College, Albany, NY, in 1933. During World War II, he was a major in the Army Medical Corps.

Dr. St. John did his residency in radiology at the Johns Hopkins Hospital, Baltimore, 1946–1950, and was an associate professor of radiology at the University of Pittsburgh. He later practiced in Binghamton, NY, for 10 years and served as chief of radiology at Binghamton General Hospital. From Binghamton, he returned to Schenectady. He was on the staff at Ellis and St. Clare's hospitals in Schenectady, Child's Hospital in Albany, and Bellevue Hospital in Niskayuna, NY.

St. John was a member of the Volusia County Medical Society in Florida, an honorary member of the Schenectady County Medical Society, a member of the American Roentgen Ray Society and the Radiological Society of North America, and a fellow of the American College of Radiology.

Dr. St. John moved to Ormond Beach, FL, after his retirement. Survivors include his wife, Margaret Walker St. John.

Diagnosis of Liver Disease in Children: Value of MR Angiography

Anne M. Hubbard[1]
James S. Meyer
Soroosh Mahboubi

We retrospectively studied the clinical use of MR angiography, a gradient-echo technique susceptible to motion, in the preoperative evaluation of the hepatic vasculature in children with liver disease. Twenty imaging examinations were performed in 18 patients 3 months to 10 years old (mean, 2.3 years). Eleven patients had liver tumors and seven had cirrhosis associated with biliary atresia, cystic fibrosis, and short-bowel syndrome. Respiratory motion artifacts were present in most patients, but all MR angiographic studies were technically adequate. Comparing MR angiograms with spin-echo images, we found that vascular visualization was better with MR angiography in 12 cases (60%), equal in five (25%), and worse in three (15%). In 10 of 20 cases, MR angiography provided additional vascular information not present on spin-echo images.

MR angiography is a useful adjunct to spin-echo imaging for assessing hepatic vascular anatomy in children with liver disease.

***AJR* 159:617–621, September 1992**

MR imaging is being used increasingly in the evaluation of liver disease in adults [1]. It has also been found useful in the evaluation of childhood liver diseases, especially tumors [2, 3]. Gradient-echo pulse sequences used to study flowing blood (MR angiography) are being applied throughout the body [4–7]. MR angiography is potentially useful in the evaluation of hepatic vessels in liver tumors and in diffuse liver disease in children. In adults, good vascular definition has been obtained by using gradient-echo pulse sequences acquired in a single breath-hold [8]. Inasmuch as breath-holding by children is unreliable or impossible, this technique is usually not feasible. This study was done to evaluate the quality of MR angiograms obtained in children without breath-holding and to determine whether this technique provides additional vascular information when compared with conventional spin-echo (SE) sequences of the liver.

Materials and Methods

MR angiography was performed in 18 consecutive patients scheduled for MR imaging of liver disease. The patients ranged in age from 3 months to 10 years old (mean, 2.3 years). Eleven patients had liver tumors (three hemangioendotheliomas, five hepatoblastomas, one hepatocellular carcinoma, one embryonal cell sarcoma, and one metastatic neuroblastoma). Two patients with hepatoblastoma were imaged twice. MR images were obtained before liver transplantation in seven patients with diffuse liver disease caused by extrahepatic biliary atresia (five), cystic fibrosis (one), and short-bowel syndrome (one). All imaging was performed on a Siemens 1.5-T Magnetom unit. A knee coil was used for infants (two cases), a head coil for children weighing less than 20 kg (17), and a body coil for larger children (one). The smallest coil into which the child would fit was always chosen, because our experience indicated that this produced the best image quality on SE studies of the chest, abdomen, and pelvis. All patients less than 6 years old were sedated; those less than 18 months old received chloral hydrate (60–120 mg/kg) orally, and those between 18 months and 6 years received Nembutal (pentobarbital, 3–6 mg/kg) IV. Patients were monitored continuously in

Received December 26, 1991; accepted after revision February 19, 1992.

[1] All authors: Department of Radiology, The Children's Hospital of Philadelphia, 34th St. & Civic Center Blvd., Philadelphia, PA 19104. Address reprint requests to A. M. Hubbard.

0361-803X/92/1593-0617
© American Roentgen Ray Society

the imager via a digital pulse recorder and pulse oximeter. Coil size and sedation were the only variables in the performance of the examinations.

T1-weighted SE sequences (500/15 [TR/TE], four acquisitions, and 192 phase encodings) were obtained in the axial and coronal planes, and T2-weighted sequences (2000/90-120, two acquisitions, and 192 phase encodings) were obtained in the axial plane. Thereafter, two-dimensional sequential fast low-angle shot (FLASH) MR angiograms (25-50/10, 45° flip angle, one acquisition, and 256 phase encodings) were obtained in the axial and coronal planes. Slices were 5 mm thick with a 20% overlap. A third MR angiographic sequence was frequently used with presaturation of either the arterial or venous flow to evaluate specific vessels seen on the previous sequences. Each MR angiographic sequence took 4 min to perform, adding a maximum of 12 min to the examination time. The total examination time was 45-60 min.

The MR angiographic sequences were reviewed as raw data sets and processed after acquisition by using a maximum-intensity-projection algorithm. The SE images were reviewed first by the radiologists as a group and then used as a guide to evaluate the MR angiographic sequences. On T1-weighted images, areas of tubular flow void that connected to definitive vascular structures were identified. The major vessels supplying or draining the liver (aorta, hepatic artery, portal vein, inferior vena cava, and hepatic veins) were identified. These same areas were then evaluated on the angiographic sequences. The brightness of the signal within the vessels and the sharpness of the vessel walls were evaluated. Respiratory or motion artifacts, such as blurring of the vessels and ghosting, were noted. Visibility of the major vessels with MR angiography was graded as equal to, better than, or worse than that on the SE images. The presence of either portosystemic collateral vessels or tumor vascularity was also determined for both MR angiographic and SE techniques.

Results

Overall, visualization of major vessels (aorta, celiac artery, hepatic artery, inferior vena cava, portal vein, and hepatic veins) was better with MR angiography than with SE sequences in 12 cases (60%), equal in five (25%), and worse in three (15%). In the eight studies in which the quality of vessel visualization on MR angiograms was graded equal to or worse than that on SE images, all the patients were less than 1 year old. Additional vascular information was obtained with MR angiography in 10 of 20 cases. In two patients, this additional vascular information was obtained even though the overall quality of the MR angiograms had been rated as equal to or less than that of the SE images.

One patient with hemangioendotheliomas and congestive heart failure had an MR angiogram that showed marked dilatation of the hepatic artery and hepatic veins. The MR angiogram helped to differentiate the dilated hepatic artery from the portal vein. These large vessels could not be differentiated on SE images. An abdominal arteriogram obtained before embolization of the hepatic artery confirmed the anatomy of the major vessels seen on the MR angiogram. However, arteriography also displayed collateral vessels to the tumors from the superior mesenteric artery and intercostal arteries that were not shown by MR angiography.

MR angiography showed surgically important vascular structures in seven of 10 examinations of patients with malignant hepatic tumors. In six examinations, large vessels coursing through and around the tumor were seen on MR angiography only. MR angiography showed occlusion of major vessels in three examinations. One of these patients had preoperative arteriography, which showed the same findings (Fig. 1). One patient had cavernous transformation of the portal vein caused by tumor invasion of the porta hepatis (Fig. 2).

MR angiography was useful in two of seven examinations of patients before liver transplantation. The MR angiogram showed the presence of portosystemic collaterals (Fig. 3) in both cases and a replaced hepatic artery in one. MR angiography showed flow in the portal vein in all seven examinations.

Images obtained after processing with the maximum-intensity-projection algorithm were not beneficial because they resulted in a confusing overlap of vessels. The maximum-intensity projection was occasionally helpful when only a few contiguous slices were reformatted together. The most useful vascular information was obtained from the axial and coronal raw data images from the MR angiograms.

Respiratory and motion artifacts were present on all MR angiographic sequences and ranged from mild to severe blurring (two patients) of the vessel walls. Ghosting artifacts of the aorta were most prominent in children less than 2 years old. This was eliminated on sequences with presaturation of arterial flow. Respiratory artifacts were most prominent at the dome of the liver.

Discussion

MR is being used increasingly in the evaluation of abdominal diseases in children [9]. Liver tumors are the third most common intraabdominal neoplasms in childhood. Approximately two thirds of these tumors are malignant. The remainder are due to vascular malformations or benign tumors [10]. The primary treatment of malignant hepatic neoplasms in children is complete surgical resection of the tumor. Consequently, preoperative assessment of vascular and sectional anatomy of the liver is important. Some investigators maintain that conventional angiography is still required for presurgical planning for such patients [11]. However, MR angiography combined with SE sequences made conventional angiography unnecessary in all but one of the patients in our series. In that patient, an extremely large tumor with possible occlusion of the portal vein was found in the region of the porta hepatis, and angiography did not provide any more information than MR imaging did.

MR imaging can be useful in differentiating hepatic hemangiomas from other nonvascular tumors of the liver [12, 13]. Children with hemangioendotheliomas of the liver may have congestive heart failure caused by excessive blood flow through the tumors. Embolization of the hepatic arteries can be performed if drug and other therapies fail [14]. Although the combination of MR angiography and SE imaging can show the hepatic arterial and venous anatomy before embolization, the resolution of MR angiography is not adequate to visualize small collateral vessels. In the one child who had

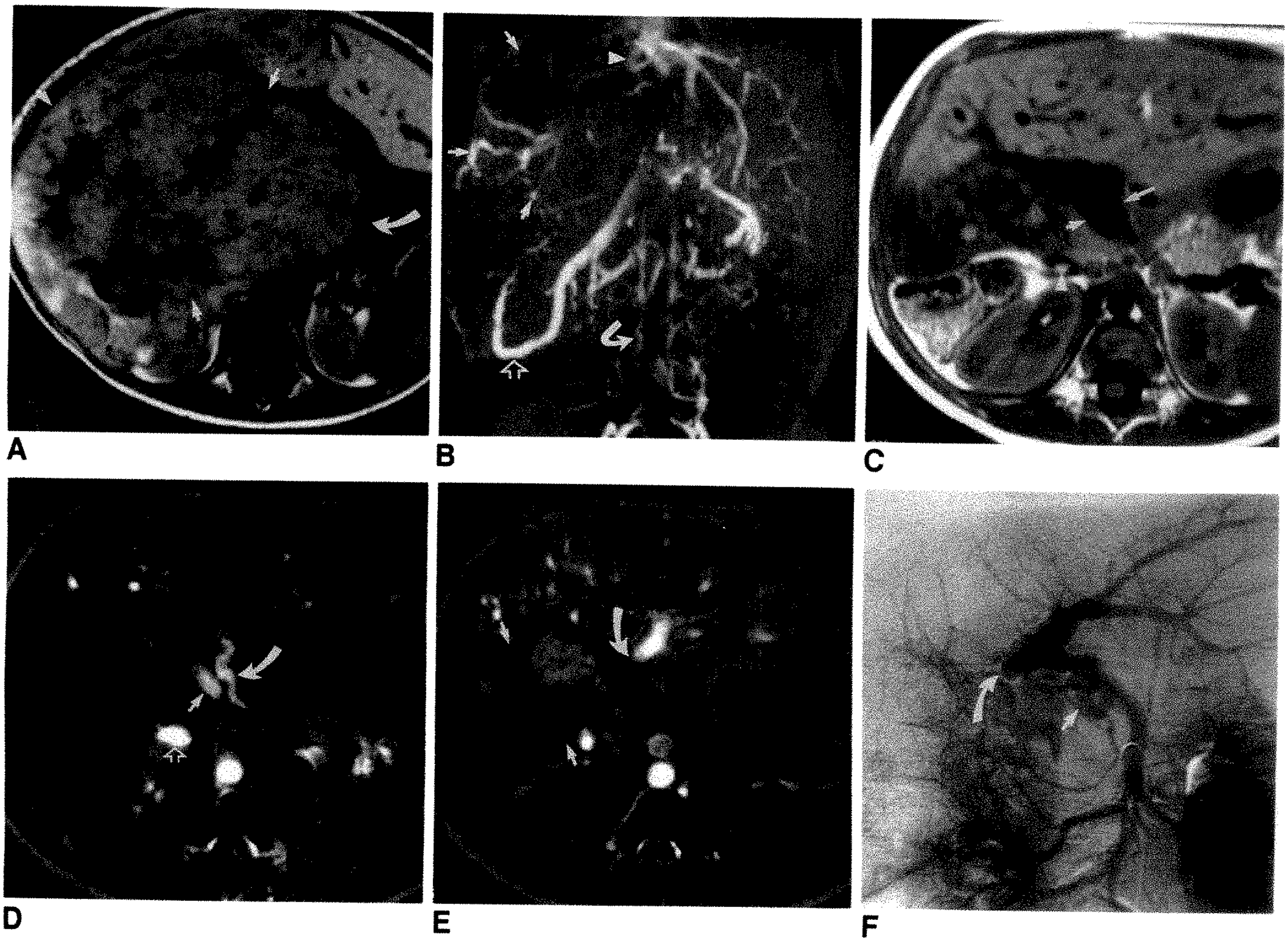

Fig. 1.—1-year-old boy with hepatoblastoma.

A, Axial T1-weighted MR image shows large hepatoblastoma (*straight arrows*) in liver displacing hepatic artery (*curved arrow*).

B, Coronal MR angiogram (maximum-intensity projection) shows occlusion of inferior vena cava (*curved arrow*), which refills via collaterals at hepatic veins (*arrowhead*). Large collateral vein (*open arrow*) on surface of tumor and multiple small collaterals (*straight solid arrows*) course around periphery of mass.

C, Axial T1-weighted MR image obtained after 6 months of chemotherapy shows clot or slow flow in inferior vena cava (*arrowhead*). Note tortuous vessel (*large arrow*) parallel to portal vein (*small arrow*).

D, Axial MR angiogram shows flow in inferior vena cava (*open arrow*) and portal vein (*straight solid arrow*). Tortuous vessel (*curved arrow*) is a collateral vein connecting portal vein and superior mesenteric vein.

E, Axial MR angiogram shows occlusion of right portal vein (*curved arrow*) by tumor (*straight arrows*).

F, Late phase of superior mesenteric digital angiogram confirms occlusion of right portal vein (*curved arrow*) and presence of a collateral vein (*straight arrow*) connecting superior mesenteric vein and portal vein.

arteriography before embolization, systemic collateral vessels from the superior mesenteric and intercostal arteries were detected that were not seen on MR angiograms or SE images. Conventional angiography is still required to plan embolization procedures in these children.

Sonography remains the primary method for evaluating the liver and its vasculature before transplantation in children [15]. Early investigational work [16] has shown that MR angiography can be useful in the examination of patients with liver disease and portal hypertension. MR angiography is accurate in showing portal vein thrombosis, varices [17], and dynamic flow within the portal system [18]. Demonstration of portal vein patency and varices is important, as is the demonstration of normal vascular anatomy [15, 19]. In children with liver disease, hepatobiliary and other congenital anomalies are common (14%) [20]. In children with extrahepatic biliary atresia, detection of a preduodenal portal vein or azygous continuation of the inferior vena cava before surgery is important. Although these vascular anomalies are no longer considered a contraindication to transplantation, knowledge of these variants allows preoperative planning of vascular grafts [21].

In two of our examinations, portosystemic collateral vessels (short gastric, coronary, gastroesophageal, and subcutaneous varices) were displayed only on MR angiography. These vessels were not observed on previous sonograms.

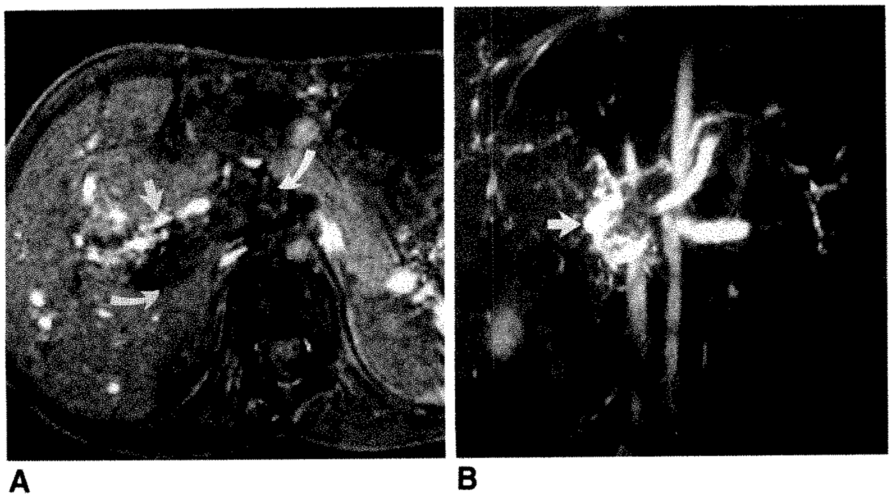

Fig. 2.—6-year-old boy with hepatocellular carcinoma, after 6 months of chemotherapy.

***A*, Axial MR angiogram shows cavernous transformation of portal vein (*straight arrow*) caused by tumor in porta hepatis (*curved arrows*).**

***B*, Coronal MR angiogram (maximum-intensity projection) also shows cavernous transformation (*arrow*) of occluded portal vein.**

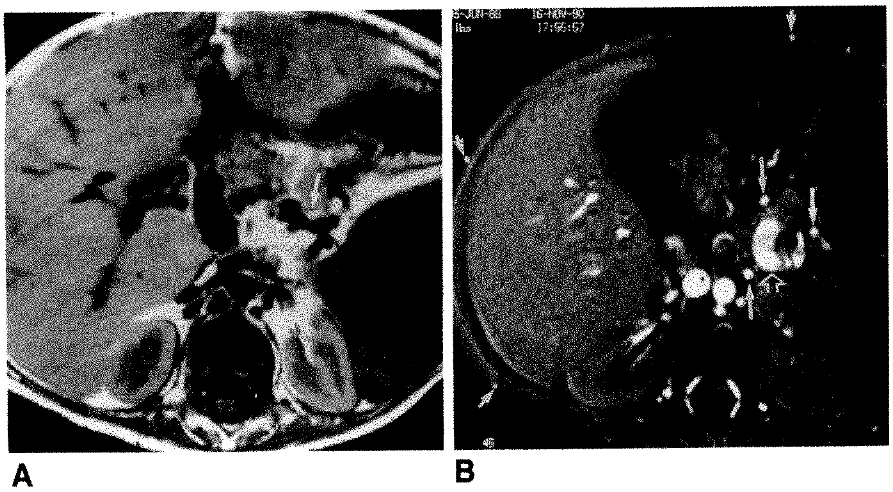

Fig. 3.—2-year-old boy with short-gut syndrome and liver failure caused by chronic hyperalimentation.

***A*, Axial T1-weighted MR image shows dilatation (*arrow*) of splenic vein.**

***B*, Axial MR angiogram shows dilated tortuous splenic vein (*open arrow*) with portosystemic (*large solid arrows*) and cutaneous collateral (*small solid arrows*) vessels not seen on SE images.**

Varices associated with portal hypertension may be difficult to see on sonograms because of overlying bowel gas. Bowel gas did not obscure the portal or mesenteric anatomy on MR angiograms in any of our patients. Preoperative knowledge of the existence of such collaterals in patients with portal hypertension or large tumor vessels in patients with neoplasms enables more careful surgical dissection.

Respiratory artifacts on the MR angiographic images were most prominent in children less than 1 year old. This probably reflects the higher respiratory rate of young children. Motion artifacts on MR angiography were most prominent at the liver dome, causing blurring of the hepatic veins and cavoatrial junction. This area of the liver was seen better on the SE images. Ghosting artifacts from pulsatile flow in the aorta were also most prominent in younger children. This artifact can be eliminated by using presaturation of arterial flow.

The method used in our study to compare the MR angiograms and SE images was not blinded, and, consequently, some bias may have been introduced. The method of grading the quality of images was quite subjective. Nonetheless, collateral vessels seen on MR angiograms were sought, but not identified, on SE images. Although sagittal scans were not obtained in this study, they may provide additional information, particularly regarding the origins of the celiac and superior mesenteric arteries.

In conclusion, although artifacts caused by respiratory motion were present on many of our MR angiographic images, these artifacts did not interfere with the diagnostic usefulness of the examinations. Additional vascular information was obtained with MR angiography in 50% of cases. As shorter TRs and TEs lead to faster imaging techniques, and as methods for motion compensation, gradient-moment nulling, and phase-encoded reordering improve, the demonstration of hepatic vasculature in children who are unable to suspend respiration will also improve.

ACKNOWLEDGMENTS

We thank Ken Fellows for editorial suggestions and academic support and Valerie Tsafos for secretarial help.

REFERENCES

1. Ferrucci JT. Liver tumor imaging: current concepts. *AJR* **1990**;155: 473-484
2. Weinreb JC, Cohen JM, Armstrong E, Smith T. Imaging the pediatric liver:

MRI and CT. *AJR* **1986**;147:785-790

3. Boechat MI, Kangarloo H, Ortega J, et al. Primary liver tumors in children: comparison of CT and MR imaging. *Radiology* **1988**;169:727-732
4. Edelman RR, Mattle HP, Atkinson DJ, Hoogewoud HM. MR angiography. *AJR* **1990**;154:937-946
5. Steinberg FL, Yucel EK, Dumoulin CL, Souza SP. Peripheral vascular and abdominal applications of MR flow imaging techniques. *Magn Reson Med* **1990**;14:315-320
6. Totterman S, Francis CW, Foster TH, Brenner B, Marder VJ, Bryant RG. Diagnosis of femoropopliteal venous thrombosis with MR imaging: comparison of four MR pulse sequences. *AJR* **1990**;154:175-178
7. Kim D, Edelman RR, Kent KC, Porter DH, Skillman JJ. Abdominal aorta and renal artery stenosis: evaluation with MR angiography. *Radiology* **1990**;174:727-731
8. Edelman RR, Wentz KU, Mattle H, et al. Projection arteriography and venography: initial clinical results with MR. *Radiology* **1989**;172:351-357
9. Boechat MI, Kangarloo H. MR imaging of the abdomen in children. *AJR* **1989**;152:1245-1250
10. Smith WL, Franken EA, Mitros FA. Liver tumors in children. *Semin Roentgenol* **1983**;18:134-148
11. Tonkin LD, Wrenn EL Jr, Hollabaugh RS. The continued value of angiography in planning surgical resection of benign and malignant hepatic tumors in children. *Pediatr Radiol* **1988**;18:35-44
12. Lombardo DM, Baker ME, Spritzer CE, Blinder R, Meyers W, Herfkens RJ. Hepatic hemangiomas vs metastases: MR differentiation at 1.5 T. *AJR* **1990**;155:55-59
13. Ohtomo K, Itai Y, Yoshida H, Kokubo T, Yoshikawa K, Iio M. MR differentiation of hepatocellular carcinoma from cavernous hemangioma: complementary roles of FLASH and T2 values. *AJR* **1989**;152:505-507
14. Fellows KE, Hoffer FA, Markowitz RI, O'Neill J. Multiple collaterals to hepatic infantile hemangioendotheliomas and arteriovenous malformations: influence on embolization. *Radiology* **1991**;181:813-818
15. Bisset GS III, Strife JL, Balistreri WF. Evaluation of children for liver transplantation: value of MR imaging and sonography. *AJR* **1990**;155:351-356
16. Torres WE, Gaylord GM, Whitmire L, Chuang VP, Bernardino ME. The correlation between MR and angiography in portal hypertension. *AJR* **1987**;148:1109-1112
17. Johnson CD, Ehman RL, Rakela J, Ilstrup DM. MR angiography in portal hypertension: detection of varices and imaging techniques. *J Comput Assist Tomogr* **1991**;15:578-584
18. Edelman RR, Zhao B, Liu C, et al. MR angiography and dynamic flow evaluation of the portal venous system. *AJR* **1989**;153:755-760
19. Day DL, Letourneau JG, Allan BT, Ascher NL, Lund G. MR evaluation of the portal vein in pediatric liver transplant candidates. *AJR* **1986**;147:1027-1030
20. Abramson SJ, Berden WE, Altman RF, Amodio JB, Levy J. Biliary atresia and noncardiac polysplenic syndrome: ultrasound and surgical considerations. *Radiology* **1987**;163:377-378
21. Hoffman MA, Celli S, Ninkov P, Rolles K, Caine RY. Orthotopic transplantation of the liver in children with biliary atresia and polysplenia syndrome: report of two cases. *J Pediatr Surg* **1989**;24:1020-1022

Book Review

Imaging Anatomy of the Newborn. By Ernst Richter and Werner Lierse. (Translated and edited by Alan E. Oestreich.) Baltimore: Urban & Schwarzenberg, 280 pp., 1991. $175

This 280-page book, written by a pediatric radiologist, Ernst Richter, and an anatomist, Werner Lierse, is an exciting and valuable addition to the diagnostic imaging literature. It correlates findings of normal perinatal and neonatal specimen anatomy and diagnostic images of variant and typically normal neonatal structures. It has been written in concise and lucid English as ably translated from the original German by Alan E. Oestreich. It provides basic and broad anatomic foundations for interpretive readings of radiographs, sonograms, CT scans, and MR images for practical clinical application.

The text is preceded by two informative forewords, one specifically for the English edition and the other translated from the German edition. The preface contains many revealing and tone-setting statements: " 'the child is not merely a small adult' is especially true for the newborn child"; "the illustrations . . . are like individual stills from a rapidly projected, highly suspenseful movie"; and "we hope our book will provide stimulation for our younger colleagues who will lead the future development of pediatric radiology."

This book's detailed coverage of prenatal anatomy and physiology aids in understanding perinatal pathologic changes. The text of the book's four chapters is supported by nine tables of summary information and 535 pertinent illustrations (line drawings, schematics, and pictures of images) combined into 334 figures. Many of the drawings and schematics are based on fetal and newborn anatomic preparations and sections. Although the postmortem arteriograms and venograms adequately show the vascular system, overfilling and superimposition sometimes limit demonstration of fine detail. Postmortem applications of contrast medium to anatomic surfaces and cavities permit various structures to become radiographically visible, to the extent of clarifying what otherwise might not be imaged. The 865 literature references are a comprehensive source for corroborative information, and a selectively appropriate index in the appendix contributes to the book's usefulness by making it easier to find a structure or subject of specific interest.

In Chapter 1, "Skull and Brain, Including Vascular System," the normal skull of the neonate, including the skull base and examples of pathologic alterations of the skull base, are described and well illustrated by patient and specimen radiographs. The extensive description of the vascular system also includes a review of the embryologic and fetal development of cerebral vasculature. Despite limitations as previously mentioned, the postmortem angiograms are informative. The material on the embryonal and fetal development of the brain is particularly well written and replete with clear and informative illustrations. The sonograms are of state-of-the-art quality and are well presented. Even more important is the excellent template offered by the coronal, axial, and sagittal sections for use not only for sonography but also for CT and MR imaging.

Chapter 2, "Face, Neck, and Thorax," is the longest chapter and the most comprehensive. The mix of illustrations has variety and balance. Functional concepts shown in precise line drawings and schematics are unique, for example, drinking from a nipple, fixed images of the swallowing mechanism, and physiologically induced morphologic patterns of the gastroesophageal junction. In chapter 3, "Abdomen and Retroperitoneal Space," radiography and sonography are again the imaging techniques features among the specimen sections and line drawings. Postmortem angiograms are limited by lack of clarity of branching because of overfilling and poor spatial resolution. The "gray box" passages of text are worthwhile "informational vignettes." The schematics of morphologic detail and sequential developmental events make this chapter vital.

Chapter 4, "Skeletal, Limbs," the shortest chapter, is no less appropriate than the other three in its content of useful information. The authors have used arthrographic examples for the imaging anatomy of the joints. Although arthrography yields useful information, more and more it is being replaced by sonography, CT, and MR imaging in defining anatomy and gross pathologic alterations of the joints. The selection of postmortem angiograms is an excellent demonstration of limb vessel anatomy.

I confidently recommend this important and excellent book for use by trainees and practitioners in neonatology, pediatrics, and radiology who perform diagnostic imaging in support of perinatal and neonatal clinical care. Frequent use of the book will increase the prevalence of knowledge on the imaging anatomy of the neonate.

Lionel W. Young
Loma Linda University Medical Center
Loma Linda University School of Medicine
Loma Linda, CA 92354

Case Report

Neonatal Hemochromatosis: Diagnosis with MR Imaging

Ailish M. Hayes,[1] Diego Jaramillo,[2] Harvey L. Levy,[3] and A. S. Knisely[4]

Neonatal hemochromatosis, also known as perinatal hemochromatosis or neonatal iron storage disease, is characterized by severe and usually fatal idiopathic liver disease of intrauterine onset. It may occur in siblings. Its hallmark is fulminant hepatic failure with siderosis of hepatocytes and of extrahepatic parenchymal cells at a variety of sites (pancreas, myocardium, thyroid gland, oral mucosa), with sparing of reticuloendothelial cells in the spleen, lymph nodes, and bone marrow [1]. Extrahepatic siderosis in this distribution is not seen in infants with liver disease of postnatal onset or in infants who do not have liver disease [2]. Neonatal hemochromatosis is not a variant presentation of human leukocyte antigen–linked (adult onset, hereditary) hemochromatosis [3] and the two entities differ in many respects [1].

The antemortem diagnosis of neonatal hemochromatosis is difficult, because neonatal liver failure may be associated with many disorders. Nonetheless, it is important to establish the diagnosis clinically. If it is recognized, plans for liver transplantation, the only effective therapy, can proceed. When neonatal hemochromatosis is suspected, liver biopsy may be hazardous owing to coagulopathy and the poor overall status of the patient. Oral mucosal biopsy, to demonstrate stainable iron in the small submucous glands of the lip, cheek, or tongue [4], has been an alternative in several instances [1], but it also is invasive.

We hypothesized that MR imaging would be a noninvasive technique for diagnosis of neonatal hemochromatosis if signal intensity could be used to detect tissue iron overload [5]. This report presents our findings with MR imaging in three neonates with neonatal hemochromatosis and a fetus whose family history indicated the fetus to be at risk for neonatal hemochromatosis.

Case Report

A singleton term female neonate manifested severe hepatic insufficiency within hours of birth. Her two siblings were well. Evaluation indicated no known heritable metabolic or infective diseases. Results of liver biopsy showed advanced cirrhosis, with large amounts of iron in hepatocytes. Neonatal hemochromatosis was considered as a possible diagnosis.

MR images were obtained when the patient was 3 weeks old. A 1.5-T system (Signa, GE Medical Systems, Milwaukee, WI) and a body coil were used. Spin-echo T1-weighted (600–800/17–30 [TR/TE]) and T2-weighted (2000–2500/20–80) images were obtained. No specific protocol was followed, and gradient-recalled-echo imaging was not used. The images were evaluated visually for the presence of iron overload according to published parameters [5]. Siderosis was diagnosed when the signal intensity of an organ or tissue on T2-weighted images was less than that of skeletal muscle. The images showed evidence of marked siderosis of the liver and pancreas but not of the spleen, consistent with the diagnosis of neonatal hemochromatosis (Fig. 1).

The patient had an orthotopic liver transplant when she was 4 weeks old. Findings in the hepatectomy and biopsy specimens were similar. MR after liver transplantation showed evidence of large amounts of iron in the pancreas and myocardium but not in the donor liver. An endomyocardial biopsy performed to evaluate poor cardiac

---

Received February 5, 1992; accepted after revision April 13, 1992.
Presented in part at the Third International Conference on Hemochromatosis, Düsseldorf, Germany, July 1991.
This work was supported in part by the Pathology Education and Research Foundation, Pittsburgh, PA.

[1] Children's Service, Massachusetts General Hospital, Boston, MA 02114.
[2] Department of Radiology, Children's Hospital, Boston, MA 02115.
[3] Neurology Service, Massachusetts General Hospital, Boston, MA 02114, and Department of Neurology, Harvard Medical School, Boston, MA 02115.
[4] Department of Pathology, Children's Hospital of Pittsburgh, 3705 Fifth Ave. at DeSoto St., Pittsburgh, PA 15213. Address reprint requests to A. S. Knisely.

AJR 159:623–625, September 1992 0361–803X/92/1593–0623 © American Roentgen Ray Society

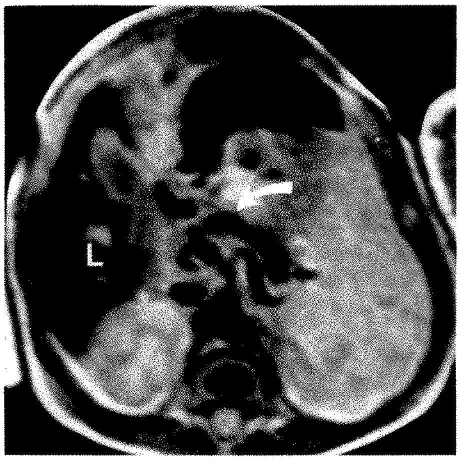

1

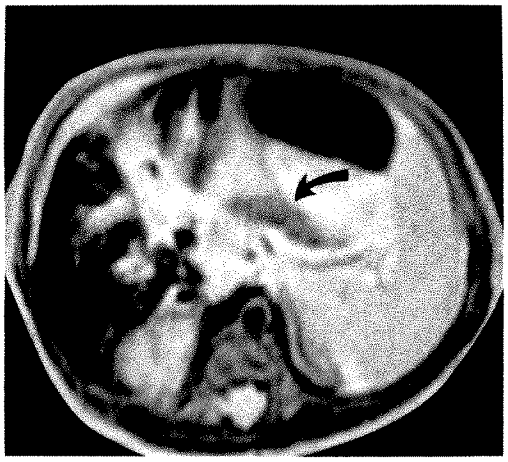

2

Fig. 1.—Neonatal hemochromatosis involving liver and pancreas in a 3-week-old girl. Axial T2-weighted MR image (2000/80) of upper abdomen shows hypointense liver (L) and pancreas (*arrow*). MR imaging after hepatic transplantation showed no evidence of signal abnormality in transplanted liver.

Fig. 2.—Neonatal hemochromatosis involving liver and pancreas in an 8-day-old girl. Axial T2-weighted image (2000/80) of upper abdomen shows signal intensity of liver is less than that of adjacent muscle. Signal intensity of tail of pancreas (*arrow*), seen ventral to splenic vessels, also is less, indicating iron deposition.

function that began after transplantation showed abundant stainable iron within myocytes, confirming the diagnosis of neonatal hemochromatosis. The patient has tolerated the liver transplant without unusual difficulty and is growing and developing normally at age 2½ years old.

The patient's sister, who is 2 years younger, manifested hypoglycemia in the first hours after birth and worsening hepatic dysfunction thereafter. The parents had refused monitoring of the pregnancy, which continued to term without complications. Liver biopsy when the neonate was 6 days old showed advanced cirrhosis, with hepatocellular siderosis, and MR imaging when she was 8 days old showed evidence of marked siderosis of the liver and pancreas (Fig. 2) without siderosis of the spleen. Neonatal hemochromatosis was diagnosed. Her hepatic dysfunction stabilized, and at age 6 months, she is being followed up as an outpatient. Liver transplantation will be indicated if her hepatic status deteriorates.

Discussion

Examination of a neonate with severe hepatic disease requires screening for infective agents and for metabolic disorders known to manifest at this age. Serologic markers of maternal infection, culture techniques, and laboratory analytic studies permit screening for many such disorders.

Although neonatal hemochromatosis is an acknowledged clinicopathologic entity, it is not clear if neonatal hemochromatosis is a single disorder or a common phenotype due to fetal liver disease from several causes [1]. Accordingly, the diagnosis is based not on laboratory results but on recognition of features of the characteristic phenotype (extrahepatic siderosis) in the appropriate clinical setting (liver failure manifest at birth). To date, this has meant an invasive procedure to obtain tissue for histopathologic examination [4].

Our results indicate that MR imaging can supplement or perhaps replace biopsy for diagnosis of neonatal hemochromatosis. Although MR findings and MR assessment of iron stores have not been reported in neonatal liver disease other than neonatal hemochromatosis, our findings in these neonates with neonatal hemochromatosis who were examined with MR imaging were consistent with hemochromatotic siderosis, as detected with MR in adults [5]. On T2-weighted images, the signal intensity was markedly diminished in the liver and pancreas and was normal in the spleen. In the patient with more severe disease, the signal intensity from the heart also was low on T2-weighted images. We speculate that the younger sister had no evidence of myocardial siderosis because her illness was less severe. Evidence for myocardial siderosis also was observed in a third neonate with neonatal hemochromatosis in whom MR images were obtained at 17 days of age (Fig. 3); that case is reported fully elsewhere [6].

Of particular value was the ability of MR images to provide information on the presence of iron overload in several organs (liver, pancreas, and heart) and on the absence of siderosis in the spleen. Histologic examination shows that the reticuloendothelial cells of the splenic cords are not siderotic in neonatal hemochromatosis [1], and this diagnostic criterion for neonatal hemochromatosis is not addressed by biopsy of oral mucosa.

It must be stressed that marked siderosis of the liver is physiologic in the perinate, and that in the absence of *extrahepatic* siderosis the diagnosis of neonatal hemochromatosis should not be made [1, 2]. Furthermore, because MR evaluation, particularly comparison of signal strength on T1- and T2-weighted images at various sites, has not been included before in diagnostic studies of neonates with liver disease, the specificity of the findings in the cases reported here may be questioned. However, extrahepatic siderosis in a hemochromatotic distribution is not seen on histopathologic examination in infants with liver disease of postnatal onset or in infants who do not have liver disease [2], so it is likely that MR evaluation of iron overload at extrahepatic sites will be of specific value.

Because neonatal hemochromatosis recurs in sibships, fetuses of a mother who has had an infant with neonatal hemochromatosis should be considered at risk for neonatal hemochromatosis [1]. Although percutaneous sampling of cord blood may provide results that can be used to diagnose neonatal hemochromatosis in an appropriate clinical setting [7], noninvasive techniques also are likely to be of value. Sonography may show abnormalities in the fetal liver or blood-

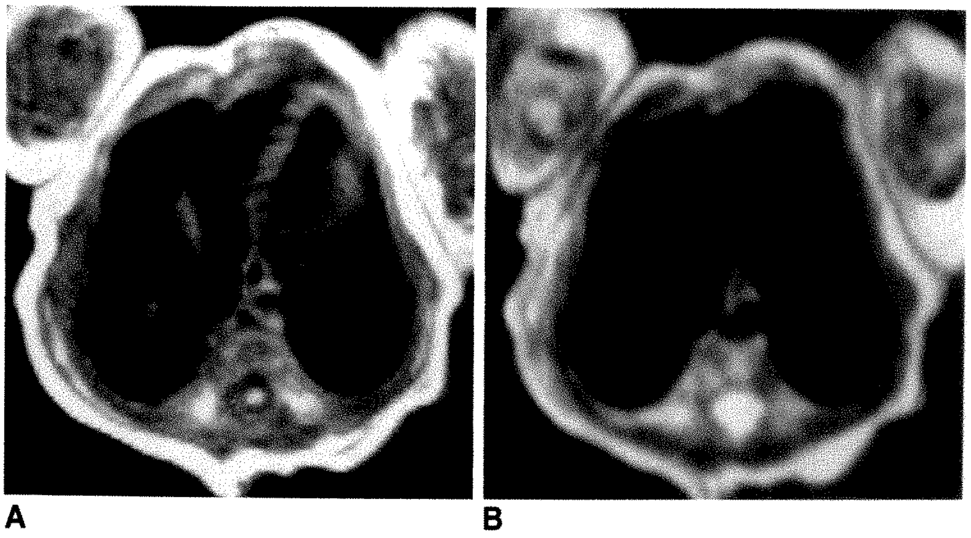

Fig. 3.—Neonatal hemochromatosis involving heart in a 17-day-old girl.

***A* and *B*, Axial T1-weighted (600/17, *A*) and T2-weighted (2500/70, *B*) MR images at level of heart show that signal of atrial and ventricular walls on T2-weighted image is decreased so much that outline of heart is barely perceptible. Myocardial siderosis was confirmed at autopsy.**

flow patterns associated with liver disease, but it will not provide information on siderosis.

We have had the opportunity prospectively to evaluate a pregnancy in a woman whose first two offspring were born prematurely and died of liver failure in the neonatal period. Autopsy in both showed neonatal hemochromatosis [8]. The parents agreed to intensive monitoring during the subsequent pregnancy. Sonography and MR imaging were performed in the 20th gestational week. Neither showed abnormalities, and no evidence of extrahepatic siderosis was found. In order to exclude liver disease of third-trimester onset, sonography and MR were repeated in the 36th gestational week. The findings again were normal. The neonatal course was unremarkable; thus, neonatal hemochromatosis was ruled out on clinical grounds. The boy has remained well for 2½ years, with normal growth and development.

We think that MR studies can be used to diagnose neonatal hemochromatosis in the neonate and to exclude neonatal hemochromatosis in the late third-trimester fetus at risk. They also may allow conclusive antenatal diagnosis of neonatal hemochromatosis. Experience with this technique in monitoring fetuses at risk will determine if it can be used for the diagnosis of neonatal hemochromatosis in the fetus, and, if so, whether pathognomonic features appear early enough in gestation for elective termination of the pregnancy.

REFERENCES

1. Knisely AS. Neonatal hemochromatosis. *Adv Pediatr* **1992**;39:383-404
2. Witzleben CL, Uri A. Perinatal hemochromatosis: entity or end result? *Hum Pathol* **1989**;20:335-340
3. Hardy L, Hansen J, Kushner JP, Knisely AS. Neonatal hemochromatosis: genetic analysis of transferrin-receptor, H-apoferritin, and L-apoferritin loci and of the HLA class I region. *Am J Pathol* **1990**;137:149-153
4. Knisely AS, O'Shea PA, Stocks JF, Dimmick JE. Oropharyngeal and upper respiratory mucosal gland siderosis in neonatal hemochromatosis: an approach to biopsy diagnosis. *J Pediatr* **1988**;113:871-874
5. Siegelman ES, Mitchell DG, Rubin R, et al. Parenchymal versus reticuloendothelial iron overload in the liver: distinction with MR imaging. *Radiology* **1991**;179:361-366
6. Knisely AS, Harford JB, Klausner RD, Taylor SR. Neonatal hemochromatosis: the regulation of transferrin-receptor and ferritin synthesis by iron in cultured fibroblastic-line cells. *Am J Pathol* **1989**;134:439-445
7. de Boissieu D, Checoury A, Barbet P, Francoual C, Rochiccioli F, Badoual J. Hémochromatose périnatale. *Arch Fr Pediatr* **1990**;47:23-28
8. Driscoll SG, Hayes AM, Levy HL. Neonatal hemochromatosis: evidence for autosomal recessive transmission (abstr). *Am J Hum Genet* **1988**; 43[Suppl]:A232

Case Report

AIDS-Related Cholangitis in Children: Sonographic Findings

Jerry A. Rusin,[1,2] Carlos J. Sivit,[1] Tamara A. Rakusan,[2,3] and Roma S. Chandra[2,4]

Biliary tract disease is recognized as a complication of AIDS in adults [1-5]. Abnormalities of the biliary tract in these patients include acalculous cholecystitis, papillary stenosis, and cholangitis [1, 3-5]. Biliary lesions have not been previously described in children who have AIDS. In this report, we describe the sonographic findings in two children who later died of AIDS and in whom cholangitis was noted at autopsy.

Case Report

A 9-year-old girl who had perinatally transmitted AIDS was admitted with recurrent varicella. Systemic manifestations of AIDS had been present for 2 years and included chronic *Cryptosporidium* enteritis and *Candida albicans* mucositis. On physical examination, the upper abdomen was tender, and the liver edge was palpable 2 cm below the right costal margin. Additionally, cervical and inguinal lymph nodes were palpable. Blood chemistry profile showed increased levels of aspartate aminotransferase, 172 U/l (normal, 9–30 U/l), and alanine aminotransferase, 161 U/l (normal, 8–32 U/l). Results of all other laboratory tests, including serum bilirubin level, were normal. Abdominal sonography showed dilatation of the intra- and extrahepatic biliary tract and hyperechoic hepatic parenchyma (Figs. 1A and 1B). The maximal diameter of the common bile duct was 8.5 mm. Thickening of the gallbladder wall also was noted; the wall measured between 4 and 7 mm. Abdominal CT performed 1 week after sonography also showed biliary dilatation. Extrinsic masses were not identified at either sonography or CT. Abdominal sonography was repeated 3 and 8 weeks after the initial study. Follow-up scans continued to show biliary tract dilatation and gallbladder wall thickening. The child did not have jaundice. She died 8 months later of cardiorespiratory arrest. At autopsy, extensive involvement of the liver by suppurative cholangitis with bacterial overgrowth and abscess formation was noted (Fig. 1C). The gallbladder and extrahepatic bile ducts were uniformly dilated owing to the cholangitis. Additionally, diffuse fatty infiltration of the liver was noted.

Discussion

A second child who had perinatally transmitted AIDS was noted to have cholangitis at autopsy. Sonographic examination at 1 year of age showed normal caliber of the biliary tract. She died of cardiorespiratory arrest following an episode of *Pneuomocystis carinii* pneumonia 4 months after sonographic evaluation. At autopsy, cholangiolar proliferation, bile plugging, and numerous periductal neutrophils were noted.

AIDS-related acalculous biliary tract disease is a newly recognized abnormality in children. No reports of cholangitis in this population have been reported. The condition may currently be underestimated, as clinical diagnosis is difficult [1, 3, 4]. Clinical features in the cases reported were nonspecific. Hepatomegaly was noted; however, that is a frequent clinical finding in children who have AIDS [6]. Jaundice was not present in either of our cases. The liver function profile of these children was variable. Transaminase levels were elevated in one child, and results of liver function tests were normal in the other. A cholestatic pattern of liver function test abnormalities, characterized by disproportionate elevation of serum levels of alkaline phosphatase and total bilirubin levels relative to transaminase levels, has been reported in many adult patients who have AIDS-related cholangitis [1, 3-5]. This pattern was not observed in either child in this report, indicating that biliary obstruction was incomplete.

Received March 9, 1992; accepted after revision April 13, 1992.

[1] Department of Diagnostic Imaging and Radiology, Children's National Medical Center and the George Washington University School of Medicine and Health Sciences, 111 Michigan Ave., N.W., Washington, DC 20010-2970. Address reprint requests to C. J. Sivit.

[2] Department of Pediatrics, Children's National Medical Center and the George Washington University School of Medicine and Health Sciences, Washington, DC 20010-2970.

[3] Department of Special Immunology, Children's National Medical Center and the George Washington University School of Medicine and Health Sciences, Washington, DC 20010-2970.

[4] Department of Pathology, Children's National Medical Center and the George Washington University School of Medicine and Health Sciences, Washington, DC 20010-2970.

AJR 159:626-627, September 1992 0361-803X/92/1593-0626 © American Roentgen Ray Society

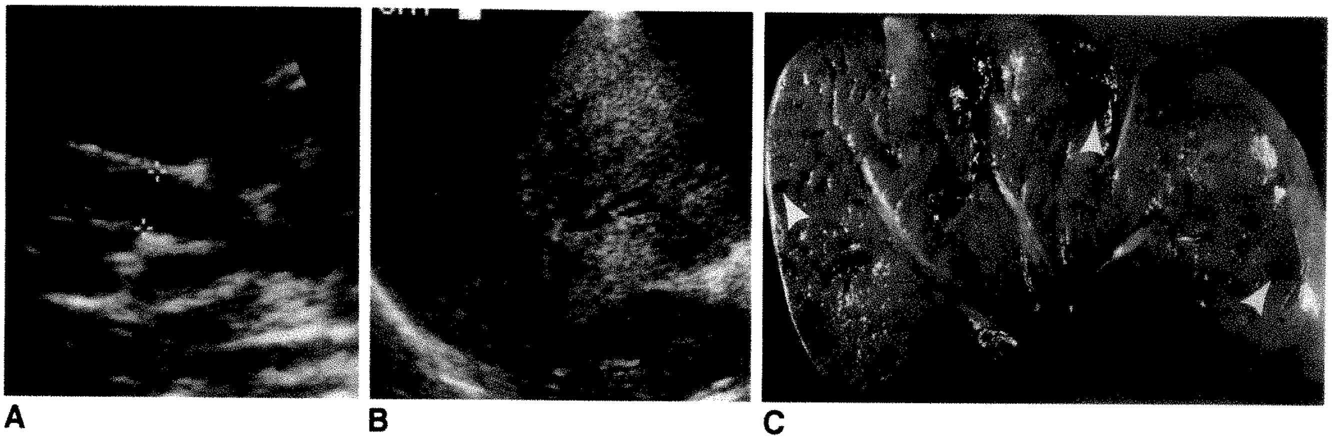

Fig. 1.—9-year-old girl with suppurative cholangitis.

***A* and *B*, Longitudinal sonograms through right upper quadrant show dilatation of common bile duct (*A*) and intrahepatic ducts (*B*). Also note hyperechoic hepatic parenchyma.**

***C*, Gross specimen of liver shows multiple abscesses with irregular contours (*arrowheads*). Dark green viscid bile was present in some.**

Proposed causes of AIDS-related biliary tract disease in adults include the following: (1) biliary inflammation due to the immune deficiency itself; (2) direct infiltration of the bile duct mucosa by HIV; and (3) secondary infection by opportunistic organisms that frequently involve the gastrointestinal tract, such as *Cryptosporidium*, cytomegalovirus, or *Candida albicans* [1–5]. *Cryptosporidium* was isolated from the stool in one of the cases presented. The underlying pathogenesis in the other child is unclear. Bile sampling was not obtained, and AIDS-specific pathogens were not isolated from the blood or stool. Histologic evidence of cytomegalovirus was not present at autopsy.

A variety of biliary tract abnormalities seen on imaging studies have been reported in adult patients with AIDS. These include dilatation, irregularity, stricture of the intra- and extrahepatic bile ducts, and dilatation and wall thickening of the gallbladder [1, 5]. Biliary dilatation and gallbladder wall thickening were noted in one of the two children with cholangitis in this report. The precise characterization of these biliary tract abnormalities usually requires cholangiography [1, 3–5], which was not done in these two cases. The biliary tract has been reported to appear uniformly dilated in patients with papillary stenosis at cholangiography, while focal strictures with intervening segments of normal and increased ductal caliber have been noted in patients who have cholangitis [1, 3–5].

Hepatic parenchymal abnormalities also have been observed at sonography in adults who have AIDS-related biliary tract disease [7, 8]. Sonographic abnormalities of the hepatic parenchyma were noted in both cases reported. Diffuse hyperechogenicity of the hepatic parenchyma was noted in one child (Figs. 1A and 1B), while periportal hyperechogenicity was observed in the other (Fig. 2). These changes may have been unrelated to cholangitis, however, as associated fatty infiltration of the liver in addition to cholangitis was noted at autopsy in both cases.

Physicians who care for children should be aware that AIDS-related cholangitis can occur in the pediatric population. Noninvasive imaging with sonography and CT, in conjunction with liver function studies, may suggest the abnormality. Functional nuclear medicine studies of the biliary tree and serial examination with sonography or CT may also be helpful in case management.

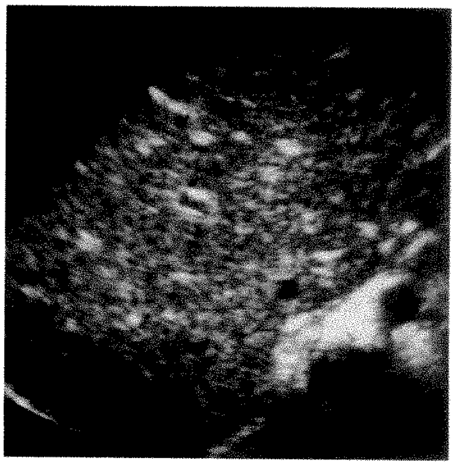

Fig. 2.—1-year-old girl with cholangitis. Transverse sonogram of liver shows diffuse periportal hyperechogenicity.

REFERENCES

1. Dolmatch BL, Laing FC, Federle MP, Jeffrey RB, Cello J. AIDS-related cholangitis: radiographic findings in nine patients. *Radiology* **1987**; 163:313–316
2. Viteri AL, Greene JF. Bile duct abnormalities in the acquired immune deficiency syndrome. *Gastroenterology* **1987**;92:2014–2018
3. Cello JP. Acquired immunodeficiency syndrome cholangiopathy: spectrum of disease. *Am J Med* **1989**;86:539–546
4. Teixidor HS, Godwin TA, Ramirez EA. Cryptosporidiosis of the biliary tract. *Radiology* **1991**;180:51–56
5. Schneiderman DJ, Cello JP, Laing FC. Papillary stenosis and sclerosing cholangitis in the acquired immunodeficiency syndrome. *Ann Intern Med* **1987**;106:546–549
6. Haney PJ, Yale-Loehr AJ, Nussbaum AP, Gellad FE. Imaging of infants and children with AIDS. *AJR* **1989**;152:1033–1041
7. Defalque D, Menu Y, Girard PM, Couland JP. Sonographic diagnosis of cholangitis in AIDS patients. *Gastrointest Radiol* **1989**;14:143–147
8. McCarty M, Choudhri AH, Helbert M, Crofton ME. Radiological features of AIDS related cholangitis. *Clin Radiol* **1989**;40:582–585

Case Report

Bile Nephrosis in a Neonate: Sonographic Findings of Rapid Kidney Enlargement and Increased Echogenicity

Michael A. Bruno,[1,2] Gerald S. Spear,[3] Rosalind B. Dietrich,[1] and Peggy A. Pugh[1,4]

The characteristic sonographic appearance of the neonatal kidney can be altered by a variety of factors, and increased echogenicity of the kidneys is often a nonspecific finding [1]. Causes include a wide variety of medical renal diseases, polycystic kidney disease, renal vein thrombosis, amyloid deposition, storage diseases, leukemia, solid tumors, and, rarely, infection [2]. We report a neonate in whom a remarkable and rapid change in the sonographic appearance of the kidneys was seen on serial sonographic examinations. Sonographic findings of rapidly enlarging, progressively echogenic kidneys proved at autopsy to be consequent to severe renal tubular ectasia with bile casts, a histopathologic lesion commonly referred to as bile nephrosis.

Case Report

A male neonate was born at 29 weeks' gestation to a 43-year-old gravida 13, para 9 woman. Prenatal sonography had revealed a large omphalocele, which was confirmed at birth, at which time features of the Beckwith-Wiedemann syndrome were identified, including coarse facies, abnormal creased ear lobules, an enlarged tongue, and enlarged fontanelles. Hypospadias and cryptorchidism also were noted. The neonate underwent a two-stage procedure for repair of the omphalocele. The first procedure, which was performed 4 days after birth, revealed malrotation of the bowel and an ileal perforation. An ileostomy and placement of a graft to close the abdominal defect were required at that time. The second procedure, performed 17 days after birth, included surgical lysis of adhesions and revision of the ileostomy.

The patient's course was complicated by cholestatic jaundice, which was initially thought to be primarily related to chronic hyperalimentation and secondary bile stasis. This was conservatively treated with phenobarbital and phototherapy, with slight gradual improvement.

Twelve days after birth, the first of three abdominal sonographic examinations was done (Toshiba Medical Systems, Irvine, CA). This revealed hepatomegaly, ascites, a hydropic gallbladder, and a large inhomogeneous mass in the posterior right lobe of the liver that was thought most likely to be a hepatoblastoma. The common bile duct appeared normal. The kidneys appeared normal, without hydronephrosis (Fig. 1A). The right kidney was 3.1 cm long and the left kidney was 2.5 cm long. A CT scan of the abdomen was obtained, which revealed a cystic area within the liver that was thought possibly to represent a choledochal cyst.

On the 29th day after birth, and 17 days after the first sonographic study, the neonate had an acute episode of severe oliguria. To evaluate this, another sonographic examination was performed. This revealed substantial and symmetric interval enlargement of both kidneys, which, in addition, had become highly echogenic, with loss of the normal echocontrast between the renal pyramids and cortex (Fig. 1B). The left kidney was 4.5 cm long and the right kidney was 5.1 cm long. To explain this remarkable change in the size and echogenicity of the kidneys, an erroneous diagnosis of bilateral renal vein thrombosis was considered. Forty-seven days after birth the neonate became anuric and subsequently hyperkalemic and uremic. A third sonogram was obtained (Fig. 1C), which demonstrated further enlargement of the kidneys. The left kidney was 5.5 cm long and the right kidney was 5.6 cm long. The kidneys remained abnormally echogenic, and, in fact, were thought to be slightly more echogenic than they appeared in the prior study. Severe ventricular arrhythmias

---

Received March 6, 1992; accepted after revision April 10, 1992.

[1] Department of Radiology, University of California, Irvine, Medical Center, 101 City Dr. S., Orange, CA 92668.

[2] Present address: Department of Radiology, Division of Neuroradiology, Box 3808, Duke University Medical Center, Durham, NC 27710.

[3] Department of Pathology, University of California, Irvine, Medical Center, Orange, CA 92668.

[4] Present address: Long Beach Medical Imaging Clinic, Long Beach, CA 90815.

AJR 159:628-630, September 1992 0361-803X/92/1593-0628 © American Roentgen Ray Society

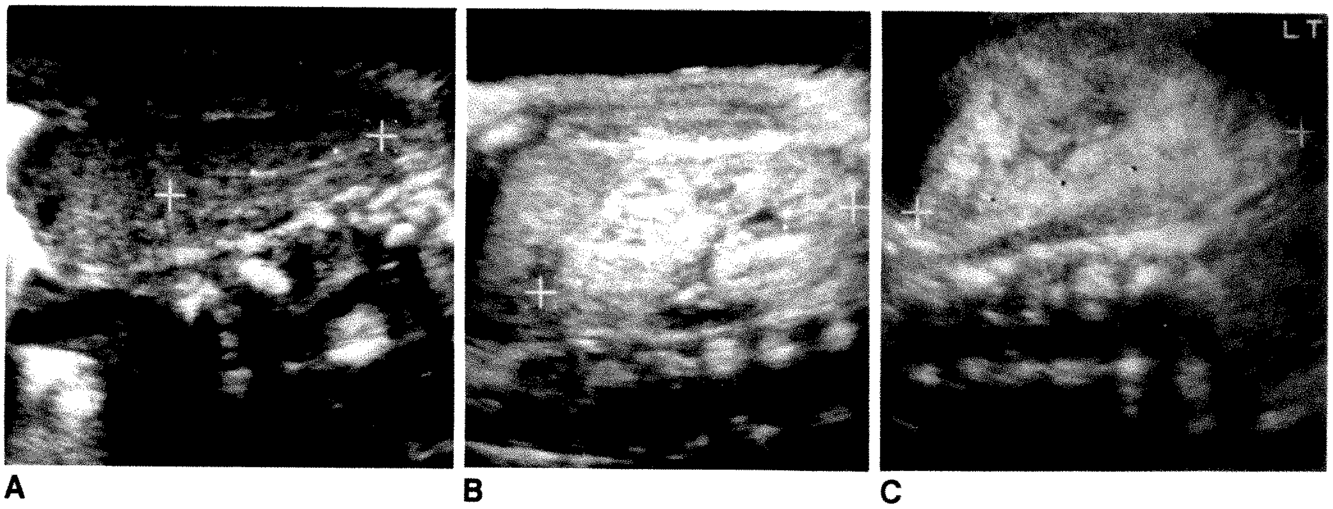

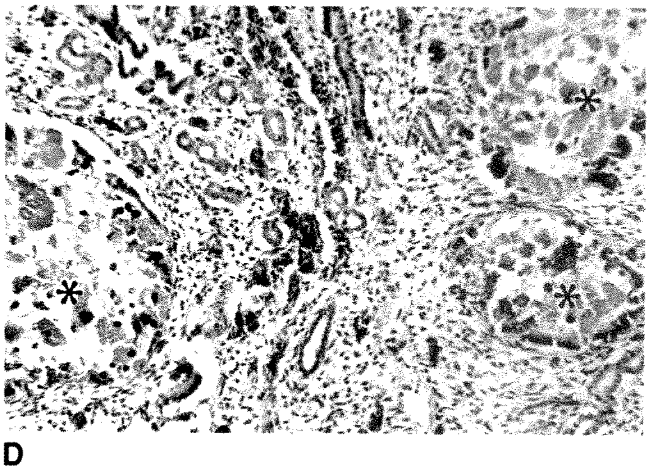

Fig. 1.—*A*, Longitudinal sonogram of right upper quadrant 12 days after birth, obtained with infant prone and use of a standoff pad, shows liver and right kidney. Kidneys appear normal.

B, Second sonogram 17 days later, obtained with infant prone and use of standoff pad. Kidneys are strikingly larger and more echogenic. Normal echo contrast between cortex and medullary pyramids is obscured.

C, Final sonogram, just before death. Kidneys show further interval enlargement and are perhaps slightly more echogenic.

D, Photomicrograph of histologic section of renal papilla at autopsy. Collecting ducts are greatly dilated, obstructed by clumps of bile (*asterisks*). (H and E, original magnification ×130)

ensued (most likely because of electrolyte imbalance and uremia), and efforts at resuscitation failed. The neonate was pronounced dead 47 days after birth.

Pathologic Findings

At autopsy, the kidneys were enlarged and bile stained. They contained normal calices, pelves, and ureters. The left kidney was 5.5 cm long and the right kidney was 5.6 cm long, which corresponded to the final sonographic measurements. Microscopic examination of the kidneys revealed extensive obstruction of distal tubules and collecting ducts by bile casts, with gross dilatation, rupture, and extravasation of bile (Fig. 1D). No evidence was seen of hemorrhage or edema, renal vein thrombosis, cellular infiltration, renal medullary dysplasia, nephroblastomatosis, or Wilms' tumor.

Autopsy also confirmed the presence of the Beckwith-Wiedemann syndrome with macroglossia, characteristic ear creases, prognathism, hepatomegaly, adrenal cytomegaly, and hypertrophy and hyperplasia of the islets of Langerhans. The liver was abnormal in shape and contained a mass of necrotic tissue and hemorrhage that proved to be a hepatoblastoma. Posteriorly, within the right lobe of the liver, was a cyst 3.0 cm in diameter with pockets of biliary epithelium, compatible with a choledochal cyst. These findings confirmed the impressions from the imaging studies. Extensive fibrous adhesions, resulting from previous surgeries, had matted the intestinal tract, and it was not possible to identify the duodenal loop, common bile duct, or ampulla of Vater.

Discussion

The neonate's first severe episode of acute renal failure, which occurred approximately 4 weeks after birth, was accompanied by a sudden, striking increase in the size and echogenicity of the kidneys as compared with a baseline sonogram obtained 17 days earlier. The underlying cause of the change remained obscure during the neonate's life, and an erroneous diagnosis of bilateral renal vein thrombosis was suggested. The process seemed to have worsened clinically on the final day of life, at which time complete anuria developed. This clinical change was associated with further sonographically evident enlargement of the abnormally echogenic kidneys, which also became slightly more echogenic.

Bile nephrosis may be defined as a condition in which bile casts are present within distal tubules and collecting ducts of the kidney in some patients with severe parenchymal or obstructive hepatic or biliary tract disease. The casts may be accompanied by epithelial necrosis and desquamation as well as dilatation, often severe, of tubular and ductular lumina. The development of bile nephrosis in this case probably was related to the underlying hepatobiliary disease, and was not related to the Beckwith-Wiedemann syndrome per se. The actual prevalence of bile nephrosis in children with hepatic tumors or in the Beckwith-Widemann syndrome is unknown.

The Beckwith-Wiedemann, or exomphalos-macroglossia-gigantism, syndrome was first described independently by Beckwith [3] in 1963 and by Wiedemann [4] in 1964. Since that time, numerous cases, with several excellent reviews of the syndrome and associated imaging findings, have been reported [5, 6]. Hepatoblastoma is commonly encountered in these series, occasionally presenting with cholestatic jaundice. Renal abnormalities are a frequent finding, with renal enlargement often reported in association with nephroblastomatosis [3, 4, 6] or abnormalities of the collecting system [7]. In this case, however, no such renal parenchymal or collecting system anomaly was present, nor were there any additional pathologic findings that might explain the rapid and remarkable changes observed. Interestingly, the sonographic appearance of the kidneys at the time of death and the pathologic correlation are similar to those previously reported to occur in cases of primary biliary atresia [8]. Our patient had a hepatoblastoma and a choledochal cyst with relatively long-standing cholestatic jaundice, but did not appear to have biliary atresia, in view of the fact that normal-appearing bile ducts were observed sonographically (the biliary ductal system could not be adequately dissected at autopsy because of extensive postsurgical fibrous adhesions).

In the absence of an alternative explanation for the sonographic findings, we believe that bile nephrosis produced both the increase in organ size and the remarkable increase in echogenicity. The exact mechanism underlying the change in echogenicity remains uncertain, although presumably it was due to increased reflectors from the bile casts and dilated tubules.

We therefore suggest that bile nephrosis should be considered in the differential diagnosis whenever renal sonographic features change suddenly, with enlargement of the kidneys and development of extremely high echogenicity, and there is significant underlying bile stasis.

ACKNOWLEDGMENT

The authors are grateful to Michael T. Gyepes for thoughtful review of the manuscript.

REFERENCES

1. Krensky AM, Reddish JM, Teele RL. Causes of increased renal echogenicity in pediatric patients. *Pediatrics* **1983**;72:846–849
2. Dietrich RB, Kangarloo H, Boechat MI, Fine RN. The significance of increased echogenicity in the detection and differentiation of pediatric disease. *Int J Pediatr Nephrol* **1985**;6(3):215–220
3. Beckwith JB. Hyperplastic fetal visceromegaly with macroglossia, omphalocele, cytomegaly of adrenal fetal cortex, postnatal somatic gigantism and other abnormalities: newly recognized syndrome (abstr). In: *Proceedings of the Annual Meeting of the American Pediatric Society, Seattle, June 16–18, 1964*. Brooklyn, NY: American Pediatric Society, **1964**:41
4. Wiedemann HR. Complex malformatif familial avec hernie ombilicale et macroglossie: un 'syndrome nouveau?' *Genet Couns* **1964**;13:223
5. Koontz WL, Shaw LA, Lavery JP. Antenatal sonographic appearance of Beckwith-Wiedemann syndrome. *J Clin Ultrasound* **1986**;14(1):57–59
6. Pettenati MJ, Haines JL, Higgins RR, et al. Wiedemann-Beckwith syndrome: presentation of clinical and cytogenetic data on 22 new cases and a review of the literature. *Hum Genet* **1986**;71(2):143–151
7. Bronk JB, Parker BR. Pyelocalyceal diverticula in the Beckwith-Wiedemann syndrome. *Pediatr Radiol* **1987**;17:80–81
8. Boechat M, Querfeld Ul, Dietrich RB, Cohen A, Kangarloo H, Vargas J. Large echogenic kidneys in biliary atresia. *Ann Radiol* (Paris) **1986**;29(8):660–666

Perspective

Strategies for Improving Power in Diagnostic Radiology Research

Craig A. Beam[1]

Research studies in diagnostic radiology often compare the diagnostic abilities of two imaging techniques. The "power" of such studies is the probability that they will detect a difference in abilities of a certain amount when, indeed, such a difference does exist. This article outlines several strategies that can be used to assess and improve the power of radiologic diagnostic studies. These strategies include selection of cases and controls, matching, use of one-tailed tests, selection of significance level, and choice of sample size.

A story told in statistical circles goes like this: There once was an investigator presenting his findings about the safety of a new compound to a scientific gathering. At one point the investigator reports to his audience, "Thirty-three percent of the rats died within 24 hr after administration of the agent, and 33% survived at least 24 hr after administration. Unfortunately, the third rat got away."

The joke, of course, is the incredulity of findings based on so small a sample and the use of "statistification" to dress things up. The fact that almost everyone who hears this story appreciates its point shows that we all somehow understand that larger sample sizes give more reliable results and that, indeed, sometimes sample sizes can be too small to arrive at sound scientific conclusions.

The reliability of a study can be viewed in two ways. In one, we consider the ability the study has to find something if, indeed, it is there to be found. This is the power of the study, and the purpose of this paper is to familiarize the radiologist with several strategies that can be used to assess and improve the power of studies that compare imaging techniques. This familiarity will promote and facilitate interaction with statisticians at the design stage of a research study. The other aspect of a study's reliability is the precision with which estimates of diagnostic ability are made. Although space limitations do not allow review of this other aspect of a study's reliability, strategies that increase the power of a study often also increase the precision of estimates. Table 1 presents some of the concepts used in the analysis of the power of diagnostic studies.

Strategies for Increasing Power

Quite often in diagnostic imaging research, studies are conducted to determine which of two techniques has better sensitivity or specificity. Power here, then, is the probability that the experiment will find a difference in the two sensitivities (or specificities) when, in fact, there is a difference of a certain amount to be found. The power of a diagnostic study depends to a large extent on its design and analysis. Accordingly, several strategies can be used to increase power via study design and analysis.

Selection of Cases and Control Subjects

One way to optimize the power to detect a difference in sensitivities is to select cases that will be neither too easy nor too difficult to diagnose. This method is based on the notion

---

Received June 24, 1991; accepted after revision February 25, 1992.

[1] Department of Radiology and Division of Biometry, Department of Community and Family Medicine, Box 3808, Duke University Medical Center, Durham, NC 27710.

AJR 159:631-637, September 1992 0361-803X/92/1593-0631 © American Roentgen Ray Society

TABLE 1: Concepts Used in Power Analysis

Null hypothesis: The statement that the two imaging techniques are equivalent in their ability to diagnose or that one technique (the "contender') is no better than the other (the "reference" technique).

p value: The probability of observing data as extreme or more extreme than those observed in the study, assuming the null hypothesis is true.

Significance level: The cutoff for deciding which *p* values lead to rejection of the null hypothesis.

Power: The probability that the study will detect a difference in diagnostic abilities of a certain amount given such a difference actually exists.

that larger differences in diagnostic performance ought to be easier to detect than smaller differences and that tests can be made to look similar in their performance if the cases selected are all too easy or too difficult to diagnose. For example, inclusion of patients who have only large lesions will make sensitivities of both tests nearly 100% and, hence, very close. Similar concerns apply to the selection of control subjects for the comparison of specificities.

Study Design

Another way to increase power is by choosing the most judicious study design and selecting the most sensitive method of analysis. Study design is often more important than the method of analysis because the latter depends on the characteristics of the data, which are often determined by the design of the study. For example, diagnostic studies in which both techniques are evaluated in the same subjects ("paired" studies) are always at least as powerful, and usually more powerful, than studies in which separate groups of subjects are used for each technique [1]. This statement is true, however, only insofar as the method of analyzing the data makes good use of the additional information that is acquired through pairing. Hence, it is essential to choose the most sensitive statistical method appropriate to the study design.

Specification of the Null Hypothesis

The null hypothesis is the position of the doubting Thomas. But, not only is the scientific Thomas a doubter, he also comes from Missouri, and the goal of the scientific experiment is often to acquire the evidence that shows the doubting Thomas he is wrong. In other words, the null hypothesis is the assumption that no differences exist until proved otherwise.

In regard to studies comparing two diagnostic techniques, the null hypothesis is either the assertion of equality in abilities between the techniques or the assertion that one of the techniques (the "contender") is simply no better than another technique (the "reference" technique).

The statistical method of hypothesis testing rejects the null hypothesis whenever the differences in the results of a study are too unlikely relative to the outcome expected by the null hypothesis. The "unlikeliness" of the data in relation to the null hypothesis is measured by the *p* value, which is the probability of observing data as extreme or more extreme than those observed in the study. This probability is computed under the assumption that the null hypothesis is true. Largely by convention, data that have *p* values less than .05 are considered too extreme and lead to rejection of the null hypothesis. But, in fact, the cutoff used to define which *p* values are too small (the "significance level" of the hypothesis test) is arbitrary and can be selected by the researcher to be a value different from the conventional 5%. The next section discusses this strategy in greater detail.

When the null hypothesis claims that the two diagnostic techniques are equivalent, more extreme data come from the performance by the contender that is either better or worse than the performance of the reference. As such, evidence against the null hypothesis is to be found in either extreme or "tail" of the probability distribution of the statistic used to compare the techniques. This type of hypothesis test has come to be known as a "two-tailed" test.

On the other hand, if the null hypothesis states that the contender is simply no better than the reference, evidence contrary to this hypothesis can come only when the contender outperforms the reference. Hence, here the evidence against the null hypothesis comes from only one extreme or "tail" of the probability distribution of the statistic used to compare the techniques. This type of hypothesis test is known as a one-*tailed* test.

One-tailed hypothesis tests are usually more powerful than two-tailed tests, and thus, another tool that we can use to influence power is our specification of the null hypothesis.

When diagnostic techniques are compared, a one-tailed hypothesis test seeks to show superiority of one particular technique over another. Thus, one-tailed tests are used when we wish to show that a new technique (the "contender") is better than a "reference" technique. In this case, the null hypothesis states that the contender is no better (could even be worse!) than the reference. If we reject this null hypothesis, we then conclude that the contender is, indeed, superior. On the other hand, if we simply seek to decide whether the two techniques differ diagnostically, then we would use a "two-tailed" hypothesis test with the null hypothesis stating that they are equal.

The investigator must be sure not to use this strategy indiscriminately, for there are situations in which the one-tailed hypothesis test is not appropriate, as in those cases in which our interest is in finding the best diagnostic technique, whichever that might be. The one-tailed test fails to be adequate here because it can provide only evidence of the superiority of one particular technique over the other and cannot demonstrate superiority the other way around. Sometimes "weeding" out inferior techniques is as important as finding better ones, and in these cases the two-tailed test is required.

Selection of Significance Level

A fourth way to influence power is by the choice of the "significance level" of our hypothesis test. The significance level defines which *p* values will be considered "too small" and acts as a cutoff to decide whether or not to reject the null hypothesis. The *p* value from the experiment is compared with this cutoff and, if it is smaller, we then declare the results too extreme, decide against the null hypothesis, and conclude that the diagnostic techniques differ.

Power and the significance level share an important relationship: as the significance level of a test increases, the power of the test increases. For example, consider increasing a significance level from 5% to 10%. In the first case only data that have less than a 5% (i.e., a one in 20) chance of occurring are considered too "unlikely" and lead to the rejection of the null hypothesis. In the second case, the data can be even more likely to occur (as likely as having a one in 10 chance of occurring) and will still be considered too "unlikely." Thus, we have an easier time rejecting the null hypothesis in the 10% case than in the 5% case and so have greater power.

Yet, although one might be tempted to use a larger significance level in order to increase the chance of finding something, the other side of the issue is that the significance level is also the probability of rejecting a true null hypothesis; that is, of making the error of declaring there is a difference when in fact none exists. Hence, although we do gain power by increasing the significance level from 5% to 10%, we also increase the probability of making a false-positive type of finding in our study from 5% to 10%.

The 5% significance level ($p < .05$) currently exists in the literature as the standard, and so the use of a different level might arouse suspicion. Nonetheless, the technique of changing the significance level should not be overlooked as a means of increasing power when designing a study in those cases in which, for example, every bit of power that can be mustered is crucial and the penalty arising from a false-positive conclusion is minimal. Of course, this alteration must be done at the study design stage, because it is not ethical to adjust the significance level after the fact in order to yield statistically "significant" results.

Finally, as is well known, one can influence the power of a study via the choice of sample size. However, use of this strategy to increase power requires a bit more in-depth consideration on our part. The next section discusses the selection of sample size to achieve desired levels of power in radiologic diagnostic studies.

Power and Sample Size When Comparing Sensitivities and Specificities

An important initial consideration in the design of studies that compare the sensitivity or specificity of radiologic techniques is whether or not both techniques will be applied to the same set of subjects. A study that uses separate groups of subjects for each imaging technique would, in standard terminology, be called an "unmatched-groups" or "independent-groups" study. A study in which both techniques are applied to the same group of subjects would be called a "matched-groups" or, more specifically, a "paired" study. Aside from ethical considerations, each type of study has its own statistical considerations that influence the choice of sample size for obtaining a certain probability, or power, to detect differences between techniques. As will be seen later, these different considerations arise from different statistical approaches to the comparison of the techniques.

A standard method for comparing sensitivities or specificities of techniques in unmatched-groups diagnostic studies is to assign separate samples of patients to be imaged by each of the two techniques and then summarize diagnostic performance in a table such as given in Figure 1. Here we have n_1 patients being imaged by the reference technique and n_2 by the contender. Proportions of correct diagnoses in the two samples of patients can then be compared statistically by using the Yates continuity-corrected χ^2 test [2].

Important assumptions underlie this statistical test. If they are not met, the results obtained will be questionable. The first assumption is that each sample of subjects represents a random sample from the same population. If this is not the case, besides invalidating the statistical properties of the test, any observed differences could be due instead to differences between the populations and not due to real differences in the diagnostic performance of the techniques. A second assumption is that the probability of correct diagnosis is the same from patient to patient within each sample. This assumption is largely met by randomly sampling each population. However, it does also require constancy and uniformity in imaging and image interpretation. For example, this statistical procedure will be invalid if learning accompanies the interpretation. A final assumption is that the images are interpreted independently; that is, how one image is interpreted in no way influences the interpretation of another. Absence of either of these two latter assumptions invalidates the estimate of variability used to form the statistic and in the calculation of its *p* value.

Casagrande and Pike [3] provide a formula to estimate the common sample size for each imaging technique required to obtain a desired level of power for the comparison of sensitivities (or specificities) in an unmatched-groups diagnostic study. This formula is presented in Table 2 and pertains to the one-tailed situation, in which we are interested in determining only if one test (the contender) is better (e.g., more

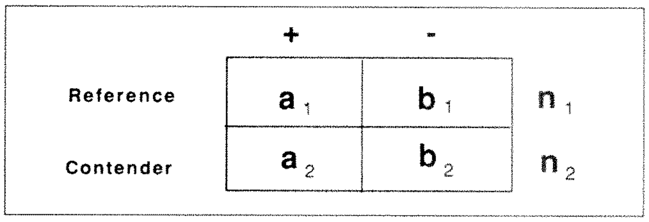

	+	-	
Reference	a_1	b_1	n_1
Contender	a_2	b_2	n_2

Fig. 1.—Typical summary of diagnostic performance in an unmatched-groups study design: n_1 patients have been imaged by the reference technique and n_2 have been imaged by the contender. Letters in squares indicate numbers of patients. If all patients have the abnormality, then the sensitivity of the reference is estimated by a_1/n_1 and that of the contender by a_2/n_2. If all patients are control subjects, then the specificity of the reference is estimated by b_1/n_1 and that of the contender by b_2/n_2.

TABLE 2: Sample Size Estimation When Comparing Sensitivities (Specificities) in the Unmatched-Groups Diagnostic Study

Data: As in Figure 1

Test: χ^2 with Yates correction (see Snedecor and Cochran [2])

Sample size: Using the method given by Casagrande and Pike [3], the sample size *for each group* is estimated to be

$$n = \frac{A \times [1 + \{1 + 4 \times (P_2 - P_1)/A\}^{1/2}]^2}{4 \times (P_2 - P_1)^2}$$

where:

P_1 = sensitivity (specificity) of the reference technique,

P_2 = sensitivity (specificity) of the contender,

$$A = [SLF \times (2 \times \bar{P} \times \bar{Q})^{1/2} + PF \times (P_1 \times Q_1 + P_2 \times Q_2)^{1/2}]^2,$$

$$\bar{P} = \frac{(P_1 + P_2)}{2},$$

$$\bar{Q} = \frac{(Q_1 + Q_2)}{2},$$

$$Q_1 = 1 - P_1, \text{ and}$$

$$Q_2 = 1 - P_2.$$

Factors: The following factors associated with the significance level and power are used in the formulas presented in this paper for estimating sample size:

Significance Level (%)	Significance Level Factor (SLF)	Power (%)	Power Factor (PF)
1	2.325	99	2.325
5	1.645	95	1.645
10	1.280	90	1.280
		80	0.840
		70	0.525

TABLE 3: Example of Sample Size Estimation in the Unmatched-Groups Diagnostic Study

Suppose we want to design our study so that there is an 80% chance of detecting a difference in the two imaging techniques when the sensitivity of the reference technique is 80% and the sensitivity of the contender is 95%.

From Table 1, the power factor (PF) for 80% power is found to be 0.840. Also, for a 5% significance level, the significance level factor (SLF) is 1.645.

The following quantities are required for the formula in Table 2: $\bar{P} = 0.875$, $Q_1 = 0.20$, $Q_2 = 0.05$, $\bar{Q} = 0.125$, and

$$\begin{aligned} A &= [1.645 \times (2 \times 0.875 \times 0.125)^{1/2} \\ &\quad + 0.840 \times (0.8 \times 0.2 + 0.95 \times 0.05)^{1/2}]^2 \\ &= 1.327 \end{aligned}$$

Then, the estimated sample size is

$$\begin{aligned} n &= \frac{1.327\ [1 + \{1 + 4(0.15)/1.327\}^{1/2}]^2}{4(0.15)^2} \\ &= 71.7 \end{aligned}$$

As we cannot have a fraction of a patient, we should round this estimate *up* to ensure our study has 80% power.

sensitive or specific) than another test (the reference). Also, although sensitivity is used in the examples, everything so developed applies equally to the analysis of specificity as well. Also note that none of the formulas introduced here can be used to compare diagnostic accuracy or predictive values, as these quantities require the additional estimation of prevalence rates, which is not typically done in these studies.

As can be seen from Table 2, the formula from Casagrande and Pike requires specification of: (a) the significance level of the hypothesis test, (b) the desired power, and (c) the sensitivities of the two techniques.

The last item required for specification shows that sample size determination depends on subjective appraisal and prior knowledge, because to use this formula we must be able to suggest values for the sensitivities of the two techniques that are not only plausible but also represent the smallest clinically important difference. Obviously, to consider implausible values is a waste of time and to consider differences too small to be of practical interest is a waste of resources.

Table 3 provides an example of the use of the Casagrande and Pike formula to estimate sample size. Here we suppose we wish to compare two techniques in which, from our experience, we expect the reference technique to have approximately 80% sensitivity. Also suppose that we are interested in the contender only if its sensitivity exceeds 95% (only then will the cost of this new procedure be worthwhile to recommend it in place of the reference). Also, suppose we wish to have at least 80% power in picking up this type of a difference between the two techniques. From the formula, we find we would need about 72 patients per technique (i.e., 144 patients total) to have an 80% chance of finding such an improvement over the reference.

Certainly this is not an encouraging result from the standpoint of practical study design. For, how often is it reasonable to expect total sample sizes to exceed 100 in those ubiquitous situations in which ethical and economic considerations severely restrict enrollment of patients? Fortunately, the matched-groups design offers an alternative that usually provides greater power per sample size than afforded by the unmatched-groups study.

In the matched-groups imaging study each patient is imaged by both techniques. A radiologist then gives two diagnoses for each patient based on separate interpretations of the two images. The resulting data from *n* patients can then be presented as in the cross-tabulation illustrated in Figure 2. An important piece of information obtainable from this table, and the reason this table should be presented whenever reporting diagnostic results from matched-groups studies, is the patterns of agreement and disagreement between the two techniques. For example, from this table we see that in (a + d) patients of the *n* patients the contender agreed with the reference. Supposing that all *n* patients had the abnormality (i.e., positives or +), then we would also observe that in the cases of disagreement, b patients were correctly clas-

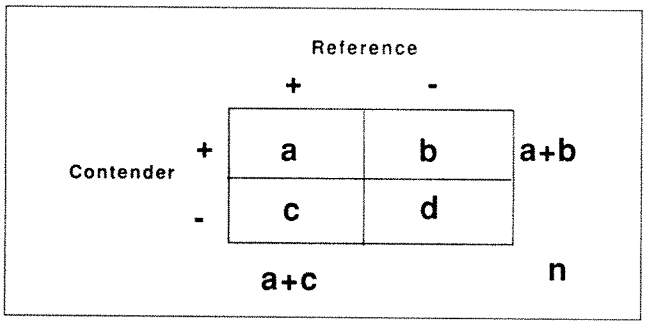

Fig. 2.—Typical summary of diagnostic performance in a matched-groups study design: *n* patients have been imaged by both techniques. Letters in squares indicate numbers of patients. If all patients have the abnormality, then the sensitivity of the reference is estimated by (a + c)/*n* and that of the contender by (a + b)/*n*. Difference in sensitivities would be estimated by (b − c)/*n*. If all patients are control subjects, then the specificity of the reference is estimated by (b + d)/*n* and that of the contender by (c + d)/*n*. Difference in specificities would be estimated by (b − c)/*n*.

sified by the contender and incorrectly by the reference. Similarly, c patients were correctly classified by the reference and not by the contender.

If all *n* patients indeed have the abnormality, then the sensitivity of the reference is estimated by (a + c)/*n*, the sensitivity of the contender is estimated by (a + b)/*n*, and the difference in sensitivities is then estimated by (b − c)/*n*. Hence, when we compare the sensitivities of these two techniques, the only useful information we have in deciding between the two resides in the instances of their disagreement. Furthermore, if the techniques really are equal, then we should expect disagreement to occur solely by chance with there being an equal chance of disagreement possible in either direction (either b or c in Figure 2). Assuming this null hypothesis to be the case, we would expect to observe about equal values for b and c in the cross-classification table when the techniques are equal. This is the idea behind the McNemar test.

The McNemar test is used for the analysis of the matched-groups imaging study and assumes that the *n* patients are a random sample from some population. As before, this study design also assumes the sensitivity or specificity of each technique is constant. Violations of these assumptions can compromise the reliability of this statistical procedure. Further discussion about the use of the McNemar test in radiologic research can be found in Dwyer [1].

Conner [4] provides a formula that can be used to estimate sample size in the matched-groups study. Although this formula can be a bit too optimistic by underestimating the sample size, those rare cases in which high power might be obtained from small sample sizes are unlikely to occur in radiologic research and can be ignored. Table 4 summarizes this formula.

In addition to specifying plausible values for the two tests' sensitivities as in the unmatched-groups case, the matched-groups design also requires specification of the probability of disagreement between the tests. In fact, our choice of sensitivities (or specificities) for the two tests determines the range of values possible for this probability. Table 4 provides a formula for the limits on the probability of disagreement.

Table 5 provides an example. For example, suppose as before that our reference test has 80% sensitivity and that we wish to detect an improvement in the contender at least as great as 95%. On the basis of these values, we know from

TABLE 4: Sample Size Estimation When Comparing Sensitivities (Specificities) in the Matched-Groups Diagnostic Study

Data: As in Figure 2

Test: McNemar (see Dwyer [1])

Sample size: Using the method given by Conner [4], the sample size for the *entire study* is estimated to be

$$n = \frac{[\mathrm{SLF} \times (\Psi)^{1/2} + \mathrm{PF} \times (\Psi - \delta^2)^{1/2}]^2}{\delta^2}$$

where, Ψ = probability of disagreement between the techniques, $\delta = P_2 - P_1$, P_1 = sensitivity (specificity) of the reference technique, P_2 = sensitivity (specificity) of the contender, SLF = significance level factor (see Table 2), and PF = power factor (see Table 2).

Bounds on the Probability of Disagreement (Ψ):
Given values for P_1 and P_2, the minimum probability of disagreement equals $P_2 - P_1$. For practical purposes, the maximum probability of disagreement is when agreement occurs solely by chance. In this case, the probability of disagreement equals $P_1 \times (1 - P_2) + (1 - P_1) \times P_2$.

TABLE 5: Example of Sample Size Estimation in the Matched-Groups Diagnostic Study

As in Table 3, suppose we want to design our study so that there is an 80% chance of detecting a difference in two imaging techniques when the sensitivity of the reference technique is 80% and the sensitivity of the contender is 95%. As in the earlier example, PF = 0.840 and SLF = 1.645. From Table 4, we see that the lowest possible probability of disagreement between the two techniques is 0.95 − 0.80 = 0.15. The greatest probability of disagreement is

$$0.80 \times (0.05) + (0.20) \times 0.95 = 0.23.$$

Assuming the lowest possible probability of disagreement, our estimated sample size is

$$n = \frac{[1.645 \times 0.15^{1/2} + 0.840 \times (0.15 - .15^2)^{1/2}]^2}{0.15^2} = 39.02.$$

Rounding up to ensure 80% power, we would estimate 40 patients would be required if there is the lowest possible level of disagreement between the two techniques.

If we assume the two techniques agree only at the level expected by chance, then, using 0.23 as the probability of disagreement, we would estimate that 62 patients would be required to ensure an 80% chance of detecting this particular difference between the two techniques.

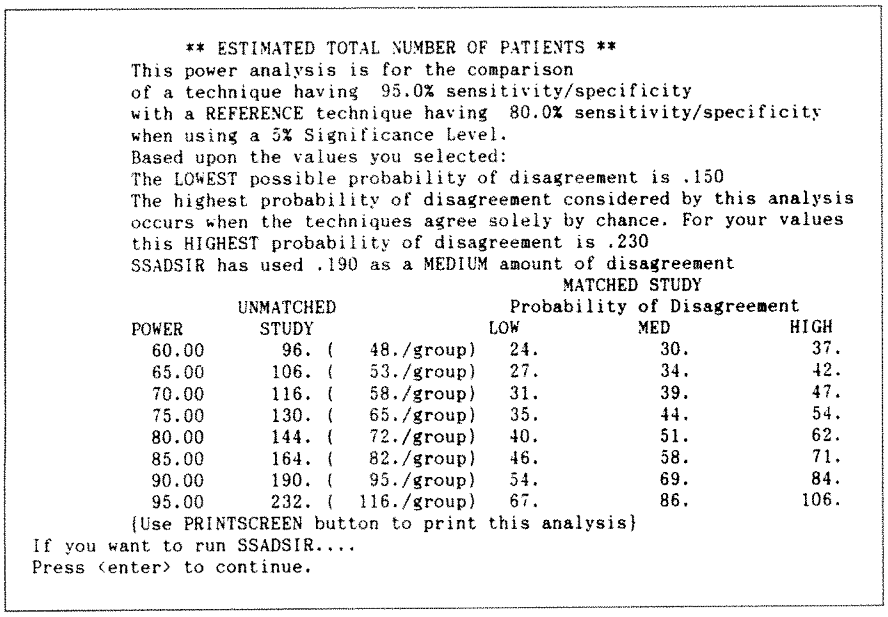

```
              ** ESTIMATED TOTAL NUMBER OF PATIENTS **
         This power analysis is for the comparison
         of a technique having  95.0% sensitivity/specificity
         with a REFERENCE technique having  80.0% sensitivity/specificity
         when using a 5% Significance Level.
         Based upon the values you selected:
         The LOWEST possible probability of disagreement is .150
         The highest probability of disagreement considered by this analysis
         occurs when the techniques agree solely by chance. For your values
         this HIGHEST probability of disagreement is .230
         SSADSIR has used .190 as a MEDIUM amount of disagreement
                                                  MATCHED STUDY
                   UNMATCHED                 Probability of Disagreement
         POWER       STUDY                 LOW            MED          HIGH
           60.00       96. (    48./group)   24.            30.           37.
           65.00      106. (    53./group)   27.            34.           42.
           70.00      116. (    58./group)   31.            39.           47.
           75.00      130. (    65./group)   35.            44.           54.
           80.00      144. (    72./group)   40.            51.           62.
           85.00      164. (    82./group)   46.            58.           71.
           90.00      190. (    95./group)   54.            69.           84.
           95.00      232. (   116./group)   67.            86.          106.
         {Use PRINTSCREEN button to print this analysis}
If you want to run SSADSIR....
Press <enter> to continue.
```

Fig. 3.—Example of output from a program that estimates sample size (SSADSIR). In the example given, the reference technique has 80% sensitivity and is being compared with a contender that has 95% sensitivity. The output shows sample size estimates for both unmatched- and matched-groups studies that are required to obtain powers ranging from 60% to 95%. The program also reports the lowest and highest probabilities of disagreement possible and reports sample sizes for these extremes as well as for a probability of disagreement halfway between the extremes.

Table 4 that the probability of disagreement ranges from a low of 15% to a high of 23%. If we assume the lowest probability of disagreement between the two techniques, then from the formula we would estimate that about 40 patients would be required to achieve 80% power. On the other hand, if we assume the highest probability of disagreement (which, for practical purposes, occurs when the techniques agree solely by chance), we would estimate that about 62 patients would be needed.

Compare these sample size requirements with those from the unmatched-groups design. There we estimated 144 patients would be required to achieve 80% power. Thus, in going to a matched-groups design we save at least 82 patients in the situation of high probability of disagreement and up to 102 patients in the very plausible situation of low probability of disagreement between the two tests. One can readily see from this example the efficiency (and economy) that can be obtained through the use of matched groups in the study design.

However, also note that although the savings to be had is in the number of patients imaged, it is not necessarily in the number of images to be interpreted. In the unmatched-groups study, 144 total images had to be interpreted. But, although fewer patients needed to be enrolled in the matched-groups study, if the probability of disagreement is "high," then 124 images (two from each patient) will have to be interpreted. Thus, ignoring the issue of patients, the major benefit to be had from the matched-groups design comes when the chance of disagreement between the tests is likely to be low. In fact, as seen in our example, if the chance of disagreement is as low as 15%, then we require 80 images (since $n = 40$) to be interpreted—still a big savings over the requirements of the unmatched-groups design.

SSADSIR

Figure 3 shows output from an interactive FORTRAN program that does the sample size estimation described in this article. This program (called SSADSIR for Sample Size Analysis of Diagnostic Studies in Radiology) asks the user to enter values for the sensitivity or specificity of the reference technique and that of the contender. The program then prints a table of sample-size estimates for both unmatched- and matched-groups studies to obtain powers ranging from 60% to 95%. The program also reports the lowest and highest probabilities of disagreement possible for the set of sensitivities or specificities specified by the user, and reports sample sizes for matched-groups studies using these extreme values as well as sample size using a value of disagreement halfway between the extremes.*

The example shown in Figure 3 continues the earlier examples with the reference technique having 80% sensitivity and the contender having 95% sensitivity. The sample sizes required for 80% power are the same as in the earlier examples. We also see in this output sample sizes for other powers. Thus, we observe that increasing our desired level of power increases our sample-size requirement. For example, going from 80% power to 95% power will cost us an additional 88 patients in the unmatched study. The same increase in power, however, costs only an additional 27 patients in the matched-groups study when the disagreement between the techniques is at the lowest possible level.

---

* A free copy of the SSADSIR program will be provided upon receipt of a formatted diskette and mailer. Please send requests to: SSADSIR, Section of Imaging Research Statistics, Box 3808, Department of Radiology, Duke University Medical Center, Durham, NC 27710.

Summary

I reviewed several strategies for an investigator to use when designing a study to optimize the chances of a successful outcome. Methods for estimating required sample size were reviewed for study situations and designs commonly reported in the radiologic literature. Other methods are available (see, for example, Snedecor and Cochran [2] and Cohen [5]).

The accuracy of estimates of sample size depends on how closely the required assumptions are met. Investigators should be aware of these assumptions. Failure to meet these assumptions does not eliminate the possibility of doing the investigation. Alternative procedures with their own methods to estimate sample size often exist for the statistical procedures I have described. In these cases, the investigator should consult with a statistician.

ACKNOWLEDGMENTS

I thank Mark E. Baker, Duke University Medical Center, for suggesting this paper and for helpful discussions. I also thank Dan Sullivan, Susan Paine, and the other reviewers of this manuscript for their suggestions.

REFERENCES

1. Dwyer AJ. Matchmaking and McNemar in the comparison of diagnostic modalities. *Radiology* **1991**;178:328–330
2. Snedecor GW, Cochran WG. *Statistical methods*, 7th ed. Ames: The Iowa State University Press, **1980**:124–125, 129–130
3. Casagrande JT, Pike MC. An improved approximate formula for calculating sample sizes for comparing two binomial distributions. *Biometrics* **1978**;34:483–486
4. Conner RJ. Sample size for testing differences in proportions for the paired-sample design. *Biometrics* **1987**;43:207–211
5. Cohen J. *Statistical power analysis for behavioral sciences*. Hillsdale, NJ: Erlbaum Associates, **1988**

Book Review

Interventional Cardiology. Clinical Applications of New Technologies. Edited by Christopher J. White and Stephen R. Ramee. New York: Raven, 264 pp., 1991. $75

This small textbook is a current, succinct, and readable review of all the various techniques and procedures that are available in interventional cardiology. The book is written by 17 different contributors, including the two editors. It is divided into two major sections; the first three chapters deal with new diagnostic techniques and the remaining seven chapters deal with new therapeutic techniques.

In the diagnostic section, the first chapter, on angioscopy, by White and Ramee, is well written. It includes excellent color illustrations and angiographic correlation. The editors set the format for the subsequent chapters. Each chapter first includes indication for use of a procedure and selection of patients and then provides a discussion on techniques, with any possible limitations and likely complications. Last, any future trends or predictions are offered. For example, the major limitations for angioscopy are the need for a bloodless field and the current difficulties in maneuvering tortuous vessels. The second chapter, on intravascular sonography, is written by three authors who are definitely leaders in the field, but it discusses only one type of catheter. The chapter also includes many excellent illustrations with angiographic correlation. The third chapter, on intercoronary blood-flow catheters, contains many graphs and diagrams on the physics of determining intercoronary blood flow. This detailed chapter may have limited practical applications.

The second half of the book deals with therapeutic techniques. The chapter on intercoronary stents is written by Dr. Schatz, a pioneer in the field. The chapter on coronary excimer laser angioplasty is written by two authors from Germany. Excimer laser angioplasty has lost favor in the United States. This chapter contains excellent histologic correlation. Rotational ablation is discussed by two authors from the University of California, San Diego. Their chapter has limited illustrations, but it does show several series of good results. The chapter on directional coronary atherectomy encompasses an excellent discussion of the technique with good angiographic illustrations and histopathologic proof. The material on assisted angioplasty encompasses all of the adjunctant techniques that are included in coronary angioplasty, from pharmacologic agents to percutaneous cardiopulmonary bypass and intraaortic balloon pumps. The final two chapters deal with balloon aortic valvuloplasty and percutaneous mitral valvuloplasty. They are exceptionally well written and include detailed references.

This textbook is a handy little reference because of its conciseness and inclusion of current techniques. Its only drawback is that some of the authors are opinionated and discuss only one school of thought. Other schools of thought (as in intravascular sonography) may have merit also. I recommend this book highly for anyone who deals with interventional techniques in cardiology. This would be especially good for beginning fellows in cardiology but also for any interventional radiologist embarking on cardiologic procedures. Much overlap occurs between the use of these techniques in cardiology and in interventional radiology.

Patricia A. Randall
State University of New York, Health Science Center at Syracuse
Syracuse, NY 13210

Meeting News

The Society of Cardiovascular and Interventional Radiology: 17th Annual Scientific Meeting, April 1992

Elizabeth Whalen[1]

The 17th annual scientific meeting of The Society of Cardiovascular and Interventional Radiology (SCVIR) was held April 4-6, 1992, at the Washington Hilton and Towers, Washington, DC. More than 2000 people attended the conference, which included the traditional plenary sessions (seven sessions, 37 lectures); presentation of more than 120 scientific papers in 23 scientific sessions, a total of 67 workshops, and three award presentations, as well as new features such as five "Controversy and Consensus" conferences, three "Special Focus" sessions, and five refresher courses. Special highlights of the meeting included the Dotter lecture (a humorous, nostalgic look at the history of coronary angiography presented by Kurt Amplatz) and the honoring of Sven Ivar Seldinger as the recipient of the 1992 Pioneer in Interventional Radiology Award. The Young Investigator Award was won by Moni Stein (Toronto, Ontario, Canada), who presented his paper "Percutaneous Facet Joint Fusion: Preliminary Experience" (see description below). Also, Senator George Mitchell (Maine), majority leader of the U.S. Senate, spoke about national health-care issues (see brief summary below).

A wide range of topics was covered in the various parts of the conference program. New technology, particularly MR angiography and use of shunts and stents, was discussed frequently in papers, plenary lectures, and workshops. Also offered was the most recent information on interventional radiology of the hepatobiliary tract, genitourinary and gastrointestinal systems, vascular structures, and spine, head, and neck. Talks were presented on new diagnostic and therapeutic techniques for treating aneurysms and abdominal malignancies.

We are unable, within *AJR* page limitations, to provide comprehensive coverage of all the excellent features of this SCVIR program. However, the following pages contain summaries of the presentations that we hope will give the reader some specific up-to-date information, as well as a general idea about the high quality of the meeting content. Included are eight presentations of original scientific research (including that given by the winner of the Young Investigator Award), two of the plenary session lectures, two of the discussions presented at one of the five "Controversy and Consensus" conferences, and Senator Mitchell's talk on legislative health care reform.

Interventional Neuroradiology

Intracerebral Embolotherapy

In a plenary lecture, Van V. Halbach (San Francisco, CA) discussed the use of platinum microcoils for intracerebral embolotherapy. Types now used include straight (0.2-1.5 cm); circular (helical, 0.3-3.0 cm); complex (flower, 2-8 mm); fibered; electrothrombotic; and custom-designed (e.g., for the vein of Galen) platinum coils. The coil can be delivered by one of several methods, such as injection or a specially designed Teflon pusher; some coils are electrolytically detachable. In the neurovascular system, possible applications of the coils

---

[1] Contributing editor, *American Journal of Roentgenology*, Ste. 103, 2223 Avenida de la Playa, La Jolla, CA 92037.

Editor's note.—"Meeting News" articles report the highlights of important national radiology meetings. The articles will not undergo the peer review usually required of *AJR* publications, nor will they offer a critique of the information provided. The sole purpose of the series is to provide Journal readers with succinct, substantive, and accurate reviews of topics of current interest, written in a readable fashion and published promptly after the meeting.

AJR 159:639-645, September 1992 0361-803X/92/1593-0639 ©American Roentgen Ray Society

include intracranial aneurysms, arteriovenous malformations, vein of Galen malformations, direct fistulas, dural fistulas, and traumatic dissections. There are several advantages to using the platinum rather than steel coils: they are more radiodense and softer; they are available in a wider range of sizes; they are nonferromagnetic and therefore MR compatible; and they can be delivered more precisely and by means of smaller catheters.

Dr. Halbach and his group have successfully used platinum transvenous coils to treat 58 patients with cavernous dural fistulas; 81% of the patients were cured and the other 19% improved. Recently, 25 aneurysms diagnosed at the University of California, San Francisco, were treated with an electrolytically detachable platinum coil (the Guglielmi detachable coil); these coils show promise because they are extremely soft and will conform to the shape of any aneurysm. As future directions for research on neuroradiologic use of platinum coils, investigators need to define better the effects of electrothrombosis, to develop thrombogenic coatings that can be added to the coils, and to produce coils that are retrievable (a snare is now being developed), larger, and both stiffer (for fistulas) and softer (for aneurysms).

Major Complications in Interventional Neuroradiologic Procedures

To investigate the causes of and lessons from complications of interventional neuroradiologic procedures, John M. Pile-Spellman (Boston, MA) and colleagues (I. Nakahara, L. Hacein-Bay, R. M. Crowell) reviewed the records from 670 procedures over a 5-year period. Major complications occurred in 20 patients (3%): seven (1%) of the patients died, two had life-threatening events that resolved without permanent damage; and 11 (2%) suffered permanent major deficits—of these 11, two survived only because of the efficient, timely responses of the staff in intensive care unit (ICU). These researchers looked for the probable cause of each of the 18 complications that led to death or permanent damage (information in parentheses is the diagnoses and outcome for the patients involved): Nine were probably caused by thrombosis (two aneurysms, seven arteriovenous fistulas; two deaths, three fair condition). Five were probably caused by hemorrhage (four aneurysms, one arteriovenous fistula; four deaths, one good condition). Emboli and low flow were the probable causes in two each of the other four major complications. Further review of the circumstances of each complication showed technical problems in nine cases, less-than-adequate management of coagulation status in five cases, and intra- or postprocedural problems in four cases. Serious complications are devastating—to the patient, to the patient's family, and to the medical team. In general, Dr. Pile-Spellman recommends a "5-C" approach when such complications occur: communicate, confess, concentrate, control, and cooperate. If reaction to a complication is not quick enough, the result is often disastrous ("it usually takes two mistakes to make a catastrophe"), so an efficient, dedicated ICU staff is absolutely critical to the successful treatment of complications from these procedures. The lessons learned from this record review included "fix what you break," "don't go anywhere you can't get back to," "the staff members in the ICU are angels," and "no one knows the patient like you do." Four specific procedural changes have occurred at Dr. Pile-Spellman's institution as a result of the study: (1) heparin is routinely used to provide anticoagulation; (2) the neurologic ICU is routinely used; (3) more celebration occurs when procedures go well; and (4) schedules are more closely controlled so that proper time and attention is given to each patient.

Thrombolytic Treatment of Dural Sinus Thrombosis

T. P. Smith (San Francisco, CA) presented another of the interventional neuroradiology scientific papers; thrombolysis as an alternative to anticoagulation or surgery for treatment of dural sinus thrombosis was investigated by Dr. Smith and his coworkers (R. T. Higashida, S. L. Barnwell, C. F. Dowd, K. W. Fraser, V. V. Halbach, G. B. Hieshima). In six patients ranging in age from 25 to 71 years old, dural sinus thrombosis was treated with a thrombolytic method. These patients had presented with headache and/or papilledema; the causes of the dural sinus thrombosis (duration, 1–24 weeks) were dural arteriovenous fistulas in three patients, postoperative complications in two, and postpartum problems in one. In all six patients, the transjugular approach was used, transfemoral angiography was performed to monitor the thrombolytic procedure, and an introducer sheath and 3-French catheter were employed for dural sinus venography. The thrombolytic agent (urokinase) was delivered directly into the dural sinus by a constant infusion (average 60,000 units/hr); two of the six patients received boluses of 100,000 and 40,000 units, respectively. All patients were anticoagulated throughout the procedure. Reasons for discontinuation of thrombolysis included evidence of complete clot lysis, antegrade blood flow, and any complication.

After the procedure, all patients received Coumadin therapy, and all underwent follow-up studies at 6 months. Four of six patients showed immediate clinical improvement after thrombolytic therapy, and the improvement was confirmed by follow-up. One patient had postprocedure surgery because of a residual dural fistula (6-month follow-up showed improvement); in the sixth patient (who underwent angioplasty after the thrombolysis), initially regarded as a "failure," 6-month follow-up showed marked improvement. Only one complication occurred in this series, an early infection at a groin injection site (before the decision had been made to consistently use the transjugular approach exclusively for infusion, as this method was easier to implement); that patient was treated with antibiotics and recovered completely. No hemorrhages occurred. In view of the controversial results of the two standard treatments (anticoagulation or surgery), this small series indicates that thrombolysis may be a safe and effective alternative treatment for dural sinus thrombosis. These researchers believe that further research is justified and that patients should be offered this treatment before undergoing surgery. Furthermore, a new—and possibly more effective—pulse-spray technique to deliver the thrombolytic agent is now being investigated.

Percutaneous Facet Joint Fusion: Preliminary Experience

The winner of the 1992 Young Investigator Award, Moni Stein (Toronto, Ontario, Canada), presented early findings on a potentially useful technique to treat facet-related back pain. His coworkers on the study were D. Elliott and J. Glen. The general problem this study addressed was low back pain, which has a lifetime prevalence of 60–90% and an annual incidence of 5%; of these cases of back pain, 95% are acute and only 5% are chronic—but the chronic cases account for most of the medical costs incurred. In only 10–20% of cases can a precise pathoanatomic diagnosis be established.

Specifically, Dr. Stein and coworkers investigated a new concept in treating one important cause of low back pain: facet disease. The facet joint is an important stabilizing structure that carries 8–30% of the total compressive load on a lumbar spine segment. To diagnose facet joint abnormalities, several imaging techniques have been used, including plain films, conventional tomography, arthrography, nuclear medicine, CT, and MR imaging, but CT has proved to be the best technique for this purpose because of the high bone resolution it provides. Previously, facet-related back pain has been treated by orthopedic surgery and a number of relatively noninvasive procedures. The surgical fusions "leave behind a lot of hardware" and involve complications that include postoperative hematoma, extradural scar, postoperative stenosis, and recurrent herniated disk. The noninvasive procedures tried so far (facet joint injection, epidural injection, and percutaneous facet joint rhizotomy) have shown better short-term than long-term success rates.

Preliminary results were presented for a new concept in treatment of facet joint abnormalities: percutaneous joint fusion of the posterior facet joints by means of a simple procedure during which radiologic guidance is used and only local anesthetic is required. Work has been done on the first two parts of the study: (1) the testing of technical feasibility by using human cadavers and (2) preliminary studies of safety and efficacy in a canine model. In the human cadaver study, a K-wire was inserted into a facet joint and, with a bone-trephine apparatus, a bone core was removed. After a 6 × 8 mm bone plug was introduced into the facet joint over the guidewire, CT was used to verify accurate placement of the bone plug. Successful use of this technique at two levels in the lumbar spine in one human cadaver was taken as proof of its technical feasibility. Next, a canine model was used to assess the technique because the facet joint of the dog is easily accessible percutaneously and anatomically, similar to the human facet joint. The researchers recognized four limitations of the dog model: orientation and size of facet joints in dogs are different from those of humans, biomechanics of the dog spine differ from those of the human spine, postprocedural behavior of dogs is difficult to control, and only fusion (not clinical impact) can be checked. The procedure in the dog study consisted of a preoperative CT to measure facet depth, followed by surgery under fluoroscopic guidance to create focal destruction in the facet and to implant a bone plug. Immediate postoperative CT verified location of the bone plug, and 4- to 6-month follow-up CT checked fusion of the joint. At 6 months after surgery, the dogs were sacrificed for histologic studies of the joints. Results of the canine study, involving seven dogs to date, showed facet depths that ranged from 8 to 12 mm, 100% successful drilling, and 86% successful insertion of the bone plug. Overall, fusion has occurred in five of 12 facets (in four of six dogs): for joints in which bone grafts were inserted successfully, four of 10 were fused; for joints in which bone grafts were not inserted successfully, one of two was fused. Complications included one death (related to anesthetic), two epidural protrusions of bone plugs (with no neurologic sequelae), one wound infection (treated successfully with antibiotics), and two seromas.

Future investigation of this technique will involve more percutaneous procedures in dogs. An important modification will involve more extensive destruction of facet joints. Dogs will be divided into three experimental groups: drilling alone, drilling plus autograft from iliac crest, and drilling plus hydroxyapatite bone plugs. Movement will be restricted postoperatively to facilitate fusion. If this percutaneous technique can be refined to minimize complications and create a high rate of fusion, it will have great potential usefulness for patients suffering from chronic low back pain caused by facet joint abnormalities.

Hepatobiliary Tract

Emergency Percutaneous Cholecystostomy for Acute Cholecystitis

P. D. Browning (Davis, CA) presented a paper on research performed by himself and coworkers (J. P. McGahan, E. O. Gerscovich) at the University of California at Davis Medical Center. In 49 hospitalized patients, 50 emergency percutaneous cholecystostomies were performed for acute cholecystitis. Patient selection criteria included sepsis, abdominal pain, elevated WBC, and abnormal sonographic findings (i.e., the gallbladder was abnormal in appearance); the procedure was performed in the ICU in 37 cases, the radiology suite in 10 cases, the ward in two cases, and the operating room in one case. In 35 cases, a trochar technique was used; in the other 15, the Seldinger technique was used. The criteria measuring response to the percutaneous cholecystostomy included defervescence, clinical improvement, loss of tenderness, and decrease in WBC.

In all 49 patients, the sonographic findings were abnormal for the gallbladder; abnormalities included sludge (42 cases), thickened wall (38 cases), "tense" gallbladder (34 cases in which the width of the gallbladder was >½ of its length), pericholecystic fluid (20 cases), and gallstones (12 cases). In 31 of 49 patients, improvement was seen after percutaneous cholecystostomy treatment. The best responses were seen in patients with sonographic findings of gallstones (92% improved), pericholecystic fluid (80% improved), and "tense" gallbladder (74% improved). Complications of the procedure included dislodgement (two), hematoma (one), and severe pain that resolved within 1 hr (two). One attempt to perform the procedure in the ICU was unsuccessful. In emergency situations, percutaneous cholecystostomy shows strong potential either to provide definitive therapy or to be a temporizing procedure until surgery can be performed, and it may save the lives of some acutely ill patients in the emergency room.

Extracorporeal Electrohydraulic Lithotripsy as an Adjunct to Percutaneous and Endoscopic Removal of Biliary Calculi

In another study concerning the hepatobiliary area, Kevin E. Burton (St. Louis, MO) and colleagues (D. Picus, M. E. Hicks, M. D. Darcy, T. M. Vesely, M. A. Kleinhoffer) studied 71 patients who underwent electrohydraulic lithotripsy for biliary and gallbladder calculi. Nonsurgical (percutaneous and endoscopic) techniques frequently fail to treat biliary stones that are impacted or very large (>1.5 cm). Currently, alternative nonsurgical methods used in these cases include mechanical fragmentation and basketing, contact dissolution, and fragmentation by lithotripsy; types of lithotripsy being used are ultrasonic (limited usefulness), laser (high cost), extracorporeal shock-wave lithotripsy, and intracorporeal electrohydraulic lithotripsy. The latter was first developed in the former Soviet Union as a mining technique to break up large rocks: the potential difference across an electrode generates a spark that produces a cavitation bubble leading to a shock wave. In intracorporeal electrohydraulic lithotripsy, it is used to generate energy (i.e., shock wave) *inside* a patient.

In the 71 patients studied, the stone removal process consisted of six steps: obtain access (via percutaneous cholecystostomy, T-tube, ERCP, intraoperative tube during common bile duct exploration, or percutaneous biliary drainage tube); dilate the tract; inspect the duct with a 15-French, 5-mm flexible choledocoscope; implement intracorporeal electrohydraulic lithotripsy treatments; extract fragments by endoscopic or percutaneous means; and use choledoscopy or cholangiography for follow-up until the patient is stone free. The number of stones removed per patient ranged from 1 to >200, and the stones were 5–40 mm in size. In 54 patients, only one session of electrohydraulic lithotripsy was required; 13 patients underwent two sessions, and four patients underwent three sessions. Of all 71 patients, 31 required further stone removal after completing the electrohydraulic lithotripsy treatments.

Results showed that 97% of all stones were fragmented and that 94% of all fragments were removed. Among the five major complications were bile peritonitis leading to death (one), subendocardial myocardial infarction (one), biloma/gallbladder necrosis (two), and pneumonia/empyema (one); minor complications included exacerbation of Alzheimer's disease, intraperitoneal bile leak, and stitch abscess (one patient each). Of all the complications, six were related to bile duct access and none were related to the intracorporeal electrohydraulic lithotripsy procedure itself. The advantages of intracorporeal electrohydraulic lithotripsy include its safety, low cost, and ready availability of equipment needed; moreover, the procedure is quick and relatively simple. These data seem to indicate that intracorporeal electrohydraulic lithotripsy is a safe and effective method to improve the success of endoscopic and percutaneous stone removal.

The Role of Renal and Biliary Tract Lithotripsy

Bruce L. McClennan (St. Louis, MO) introduced his plenary lecture with a brief chronology of the development of extracorporeal shock-wave lithotripsy (ESWL): 1948, unsuccessful attempts to fragment biliary and urinary calculi with shock waves; 1969, attempts in the former Soviet Union to use the URAT lithotriptor for bladder calculi; 1980, first use of extracorporeal lithotripsy by Chaussy and colleagues in Germany; 1992, about 10 manufacturers of lithotripsy units and 200–300 units installed in U. S. medical facilities. Although all types of ESWL units produce shock waves, controversy still rages over which type of generator is best (spark gap, piezoelectric, or electromagnetic).

Renal ESWL. Currently, renal ESWL is the preferred method for treatment of kidney and ureteral calculi. The major criterion of success is, of course, a stone-free patient, and the job of the radiologist is to inform the urologist whether the patient is stone free. The status of patients after ESWL can be assessed by conventional or digital radiography (which may overestimate stone-free rates somewhat), linear tomography (which has been considered the gold standard), sonography, CT, and nephroscopy. Studies have shown excellent results for ESWL of small solitary stones (stone-free rates of 77–85% for stones <1 cm), but stone-free rates decrease with larger stones.

Percutaneous procedures are still needed for some renal stones. Although further research is required, it appears that, for staghorn calculi, a combination of ESWL and percutaneous techniques results in a higher stone-free rate (86%) than either technique used alone. Also, percutaneous techniques are preferred to ESWL in certain other special cases, including pregnant patients and patients with cystine stones, horseshoe kidney, or ureteropelvic junction obstruction.

Renal ESWL carries certain risks; obstruction and urinary tract infection can be serious complications, and relative contraindications to the use of ESWL include preexisting renal disease, hypertension, solitary kidney, and bleeding disorders. If fragments remain after renal ESWL, they will probably grow—and infected fragments grow faster than noninfected ones. Moreover, hypertension after ESWL has become a concern; the increase in blood pressure is probably not significant, but large, long-term studies about this possible complication are under way. Other future research in this area needs to concentrate on refining extracorporeal techniques, investigating intracorporeal techniques (such as the electrohydraulic lithotripsy discussed in the previous summary), and examining cost and cost-effectiveness issues associated with renal ESWL.

Biliary ESWL. Gallstones are a medical and economic problem for today's health care providers: they annually cause 5000–8000 deaths and cost over $1.5 billion for treatment. In this environment, "doom and gloom" is the label that Dr. McClennan used to describe the technological conundrum presented by biliary lithotripsy: Is it effective enough to warrant its high cost? According to pooled data from several studies ($n > 4000$ with gallstones ranging from 16 to 20 mm in mean diameter), clearance rates 6 months after biliary ESWL were only 30–50%; 12-month and 18-month follow-up studies showed clearance rates of 50–85% and 50–80%, respectively. At present, no biliary lithotripsy is performed at Dr. McClennan's institution (Mallinckrodt Institute of Radiology) because of these relatively poor results, the pain that patients experience with gallstone clearance after biliary lithotripsy, and the need for adjuvant oral bile acid therapy. Other doom-and-gloom factors affecting the usefulness of biliary lithotripsy are the competing technologies (e.g., laparoscopic cholecystectomy); the difficulty of precise stone characterization (need for pure cholesterol stones for best results); stone recurrence rate; patient eligibility requirements; and cost/ reimbursement issues. Is there a future for biliary lithotripsy? It may play a role in treating biliary/gallbladder stones in carefully selected patients, such as high-risk, elderly individuals, those with small single stones, or those with secondary gallstones (e.g., caused by rapid weight loss diets). Researchers might investigate the use of more shocks and/or higher energy to see if a change in either parameter increases efficacy of the treatment. Interventional radiologists must look carefully at the history and fate of biliary lithotripsy and consider cautiously new alternative technologies. Expressing the take-home message of his lecture, Dr. McClennan warned his colleagues to "Beware the bearer of early results" and to remember the Tarzan Principle: "Don't let go of the first vine until the second is firmly in your grasp."

Diagnosis and Treatment of Aneurysms

Percutaneous Fenestration in Aortic Dissections

In a study designed to investigate the use of percutaneous fenestration for treating infradiaphragmatic ischemic complications of aortic dissections, D. M. Williams (Ann Arbor, MI) and colleagues (J. C. Andrews, M. V. Marx, G. D. Abrams) performed fenestration experiments on both human aortic specimens and canine specimens. In the human specimen study, the researchers performed percutaneous fenestration on seven aortic specimens (four dissections, one penetrating ulcer, one Marfan syndrome, one incidental infrarenal atherosclerosis) with 36 tears (transseptal in the four classic dissections, transmural in three; 31 unbiassed and five biassed). Tears were created in the human necropsy specimens and compared with tears created in five living dogs (subjects of an unrelated study). By using 8- and 10-mm angioplasty balloons, the investigators created transmural tears in the thoracic aorta of each dog; this transmural angioplasty caused transverse tears of the aorta that were 10% longer than the postmortem (human) tears and that were always fatal. Of the 31 unbiassed tears in the human necropsy specimens, 30 were transverse and one longitudinal; one of the biassed tears was longitudinal and one was stellate. Overall, the researchers found that percutaneous fenestration is a feasible treatment for infradiaphragmatic ischemic complications of aortic dissections and that it creates transverse tears in dissection septum; however, the results may be unpredictable in tears near grossly calcified plaques, supplemental balloon dilatation may be necessary, and careful patient selection will be required.

Use of Platinum Microcoils to Achieve Aneurysm Thrombosis in a Rabbit Model

R. A. Haas (Providence, RI) and colleagues (R. Jenkins, N. Knuckey, M. Epstein) performed a study to evaluate the usefulness of the surgically created aneurysm in a rabbit model and to examine the stability of the aneurysms after treatment with platinum microcoils. In New Zealand white rabbits, 22 aneurysms (size range, 2 × 2 mm to 11 × 25 mm) were surgically created; 13 of the aneurysms were simple and nine were complex. The aneurysms showed little tendency to thrombose spontaneously. Via a femoral artery approach, a catheter was inserted and used for selective catheter and coil placement. Complete occlusion was defined as $\geq 90\%$ occlusion; incomplete occlusion was $<90\%$ occlusion in which the neck of the aneurysm continued to fill. In these rabbits, the platinum microcoil was used to produce complete occlusion in 11 aneurysms and incomplete occlusion in the other 11. At about 6 weeks, follow-up assessments were done; in 50% of the animals, 6-month follow-up was conducted. Of the 11 "complete" occlusions, only three remained complete at follow-up; eight recanalized. One of the initially "incomplete" occlusions was judged to be "complete" at follow-up, but 10 were still incomplete. Although the rabbit model of aneurysm is a reasonable facsimile of human aneurysms in size and ease of catheterization, the failure of platinum microcoils in this study to achieve thrombosis in aneurysms appears to indicate that such coils have limited clinical applications. Further studies are needed to determine if the failure to obtain complete, stable occlusions in this study was due to some aspect of the rabbit model that is unsuitable (e.g., the known differences from humans in clotting mechanism) or due to technique or device used (e.g., their procedure always stopped short of placing the last coil down at the aneurysm neck). New retrievable coils may produce better results.

Experimental Aortic Dissections: Treatment with Vascular Stents

Aortic dissection is the most common catastrophe involving the aorta and carries a high mortality rate if not treated (30% mortality by 24 hr, 50% by 48 hr, and 90% by 3 months). Stents have been shown to be an effective treatment of dissection after percutaneous transluminal angioplasty in the peripheral arteries. This study of percutaneous stent treatment of aortic dissections surgically created in 12 dogs was presented by M.D. Dake (Stanford, CA: coauthors: L. Pelc, R. Liddell, L. Castro, M. R. Moon, J. Lukacs, M. K. Sarkisian, B. Signer, R. S. Mitchell, D. C. Miller). In these dogs, the mean aortic diameter above the dissection was 9.1 mm; the mean proximal dissection was 20.6 mm; and the mean distal dissection was 7.3 mm. Four of the dogs had extension of the dissection through visceral vessels. In evaluation of aortic dissections, intravascular sonography can precisely determine the aortic diameter; it may identify the primary tear; it clearly shows the true lumen and the compression of the false lumen; and it assesses effectively the expansion of the stent.

Nine of the 12 animals with experimental aortic dissection were stented, and the other three were used as controls. Of the nine stented dissections, the false lumen was completely obliterated in seven (there was distal persistent false lumen in six of these cases, and the researchers subsequently placed additional stents in three and observed the other three for further effects); in two, the false lumen was intentionally only partially obliterated to observe the outcome in those dogs. After the dogs were sacrificed, findings included the following: (1) all true lumens were patent without thrombosis in stented area; (2) all intercostal and visceral arteries were identified and patent; and (3) no evidence was seen of aortic rupture, stent migration, or further aortic expansion. Perhaps the most interesting results, according to Dr. Dake, was that, in the three *control* animals (no stenting), a patent lumen was found in two and partial thrombosis in one; of the nine stented animals, 75% of the seven animals in which obliteration was limited to the proximal area had patent false lumens, but no patent false lumens were seen in the two animals in which stenting was done over the entire length of the dissection. These researchers concluded that vascular stents may be useful in treating experimental acute aortic dissections; however, it is very difficult to predict how limited stenting will affect the false lumen, so follow-up intravascular sonographic studies would be very important for monitoring and assessing the results of these vascular stenting procedures.

Controversies and Consensus: Noninvasive Vascular Diagnosis

The Rationale of Noninvasive Vascular Evaluation

Kenneth S. Rholl (Alexandria, VA) stressed in his talk that the purpose of vascular assessment is to evaluate the *patient*, not the arteries—that is, to evaluate the disease and the effects of the disease on the patient. Among the functions of noninvasive vascular evaluation are the following: detecting, quantifying, and localizing disease; evaluating vascular compensation; correlating the disease with the symptoms; providing a baseline status; assisting with procedure planning; assessing the outcome of the procedure in the artery and in the *patient*; and following up after the procedure outcome is determined. The proper interpretation of noninvasive vascular assessment requires clinical correlation; the history (e.g., symptoms, risk factors, medications) and physical condition of the patient must be considered. (Dr. Rholl stated that it is "nearly criminal" to attempt interpretation of vascular studies without looking at the patient's history and physical status.)

The ideal technique for noninvasive vascular evaluation would have very high sensitivity, specificity, and reproducibility. It would be able to assess major arterial pathways, collateral arteries, and perfusion status; correlate the disease with the symptoms; and provide physiologic information. For the very ill patients in whom these techniques are often used, this ideal method would also be mobile, cost-effective, and well tolerated by the patient.

The conventional methods of noninvasive vascular evaluation include segmental limb pressures, Doppler waveform analysis, volume plethysmography, and photoplethysmography (by which the digital perfusion can be specifically assessed). Via segmental limb pressure measurements (e.g., ankle/brachial indexes), a gross estimate of perfusion pressure and segment localization can be obtained; however, these measures have limited value in calcific, noncompliant vessels (e.g., in diabetic patients), and use of these values to distinguish between stenosis and occlusion is difficult. Doppler waveform analysis can help by assessing the quality of Doppler signal, which may range from triphasic to monophasic, thus evaluating inflow and outflow, although this tends to be a gross measurement, and, once again, it is difficult to clearly separate stenosis from occlusion. Perfusion—a physiologic parameter—can be estimated by volume plethysmography; this technique does localize the abnormal segment and is reproducible, but it does not provide easy distinction between stenosis and occlusion. Photoplethysmography can assess perfusion in the digits.

Although not every patient involved in noninvasive vascular evaluation requires an exercise test, such a test plays a key role in many of the assessments. At Dr. Rholl's institution, the standard protocol involves having the patient exercise on a treadmill, after which pressure and plethysmographic measurements and the physical examination are repeated. The point of the exercise test is to evaluate physiologic response to exercise and to correlate with the patient's disease the symptoms that occur while he or she is on the treadmill. In one patient, findings on resting examinations were "close to normal" (e.g., ankle/brachial indexes were 0.81 and 0.94); however, after the patient walked for 2.5 min on the treadmill (12% grade at 1.7 miles/hr), ankle/brachial index (0.29) indicated severe ischemia. The exercise test in this case explained what had been a diagnostic problem—a patient with normal *resting* physical examination who was unable to climb the steps in his home—and angiography showed a high-grade stenosis in the iliac artery.

Newer techniques of noninvasive vascular evaluation include color duplex Doppler sonography and MR angiography. By color duplex Doppler examinations, plaque and stenosis can be detected and major arteries can be mapped; this technique also helps quantify the stenosis and show occlusions. However, the disadvantages of color duplex Doppler sonography in vascular evaluation include the accuracy being limited by depth, gas, or calcium (so that patient obesity, calcified plaque, and bowel gas interfere with interpretation); the suboptimal visualization of the aorta-iliac segment; the difficulties in evaluation of the tibial vessels, slow flow vs occlusion, and severe disease; the limited physiologic information provided; the lack of an equivalent to the *exercise* test; and the high cost. Color duplex Doppler sonography is therefore best used in special cases, such as site-specific evaluations, grafts, carotid disease, and venous disease. Dr. Rholl believes that MR angiography may, in the future, replace angiography in selected patients—the images it produces are similar to conventional angiograms, and it detects stenoses and occlusions. But MR angiography has limitations to overcome, also: it evaluates the major arteries rather than evaluating the patient; it provides limited physiologic information and no evaluation of collateral circulation; it requires a very cooperative patient and is not feasible for use in very ill patients; and, like duplex Doppler sonography, it lacks an equivalent to the powerful exercise test and it entails a very high cost. At present, MR angiography probably is best reserved for specific applications such as carotid and aortic disease.

For noninvasive vascular assessment, the conventional examinations—especially with standard exercise testing—offer physiologic information that is not available from the results of the newer methods. The conventional tests are superior to color Doppler sonography and MR angiography, especially in cases of multisegmental disease. However, color Doppler sonography and MR angiography are appropriate for specific limited applications, and conventional angiography is still the gold standard in patients for whom interventional methods are considered.

MR Angiography in Vascular Diagnosis

Because of its high cost and long examination time required (45 min to 1 hr), the usefulness of MR angiography is controversial. In this special session, one of the four speakers, E. Kent Yucel (Boston, MA) discussed the advantages of MR angiography as well as some of its limitations. Dr. Yucel sees MR angiographic technology as on a plateau from which we can realistically look at its appropriate roles, and he suggested that we may be "nearing the end of the routine [conventional] angiography era." Currently, the basic techniques of MR angiography include time-of-flight (two-dimensional ± gating/breathhold, three-dimensional, multislab three-dimensional) and phase-contrast (two-dimensional ± gating/breathhold, thick-slice two-dimensional, three-dimensional); ultrafast and echoplanar MR angiographic techniques are being developed for use in the future. Although evaluation of vascular stenosis is limited by signal loss due to intravoxel phase dispersion (IVPD), this problem can be reduced by use of flow-compensation techniques, the shortest possible echo time (<5–6 msec), and smaller voxel sizes.

Specifically, Dr. Yucel's discussion included use of MR angiography in carotid, renal, and extremity arteries. To evaluate carotid disease, two-dimensional time-of-flight (TOF) MR angiography is good for screening but tends to overestimate the length and severity of stenosis; three-dimensional TOF MR angiography provides superior resolution, but the problem with IVPD persists. "Black blood" MR angiography solves the IVPD problem and better characterizes plaque; however, the best promise for future MR angiography of carotid disease appears to lie with multislab (multiple-overlapping thin-slice acquisition, or MOTSA) three-dimensional techniques. For renal arteries, all MR angiographic techniques have been used; however, velocity sensitivity and the wide range of velocities make the phase-contrast techniques difficult to use (three flow directions are required and the study is therefore very time-consuming). Low spatial resolution limits the effectiveness of two-dimensional TOF techniques, and three-dimensional techniques are limited by penetration of signal. Once again, MOTSA three-dimensional MR angiography seems to be the optimal technique, but—for the renal arteries—two-dimensional images are needed to separate occluded vessels from slow flow.

Despite the high cost and long time needed for MR angiographic studies, Dr. Yucel thinks that MR angiography is an excellent technique to evaluate occlusions of extremity arteries. The results nicely complement those from hemodynamic studies, which are necessary in these patients, and can be effective for several important functions, including identifying candidates for percutaneous transluminal angioplasty and replacing conventional angiography in patients with such contraindications as severe renal insufficiency.

The controversial question is whether MR angiography can replace conventional angiography in routine cases, reserving the latter technique for special or presurgical cases. The current usefulness of MR angiography was the subject of many of the questions after the lectures during this session. Included in these questions were the following, which are still to be resolved by careful studies and further discussion: How is the problem with patient claustrophobia being solved? Are we using a "sledgehammer" (expensive MR angiography) to "kill a fly" (*mild* vascular disease); for example, are we using MR angiography to examine patients whose main concern is whether they will be able to play two rather than three sets of tennis each day? Why use MR angiography to screen patients with *severe* disease if these patients will have to undergo conventional angiography anyway before they go to surgery?

Health Care Reform in the United States

Senator George Mitchell (Washington, DC), majority leader of the Senate, spoke for a few minutes about the possible legislative reforms of the U. S. health care system. First, he listed "what is right" about the U. S. health care system, which he called the best in the world: superb quality, innovation, and continuing technological development. Second, he discussed the problems: the system is "best" only for those for whom it is available, and 37 million Americans have no health insurance. This failure of the system to provide access to all Americans will be compounded as medical costs continue to increase in the future. In 1960, $27 billion was spent on health care—the estimated figure for 1992 is $817 billion. Health care concerns have become an important election-year issue, and 70% of Americans surveyed now favor a government-run health care system like the one in Canada. Options to such a system are needed, and the goals of the program that Senator Mitchell proposes are threefold: providing every American access to good health care, reducing health care costs, and placing more emphasis on preventive care. In closing, the Senator encouraged the meeting participants to get involved with this decision-making process. It seems inevitable that the health care system we have now will undergo significant changes in the near future, and these changes will affect all physicians, their livelihood, and the ways in which they conduct their medical practices.

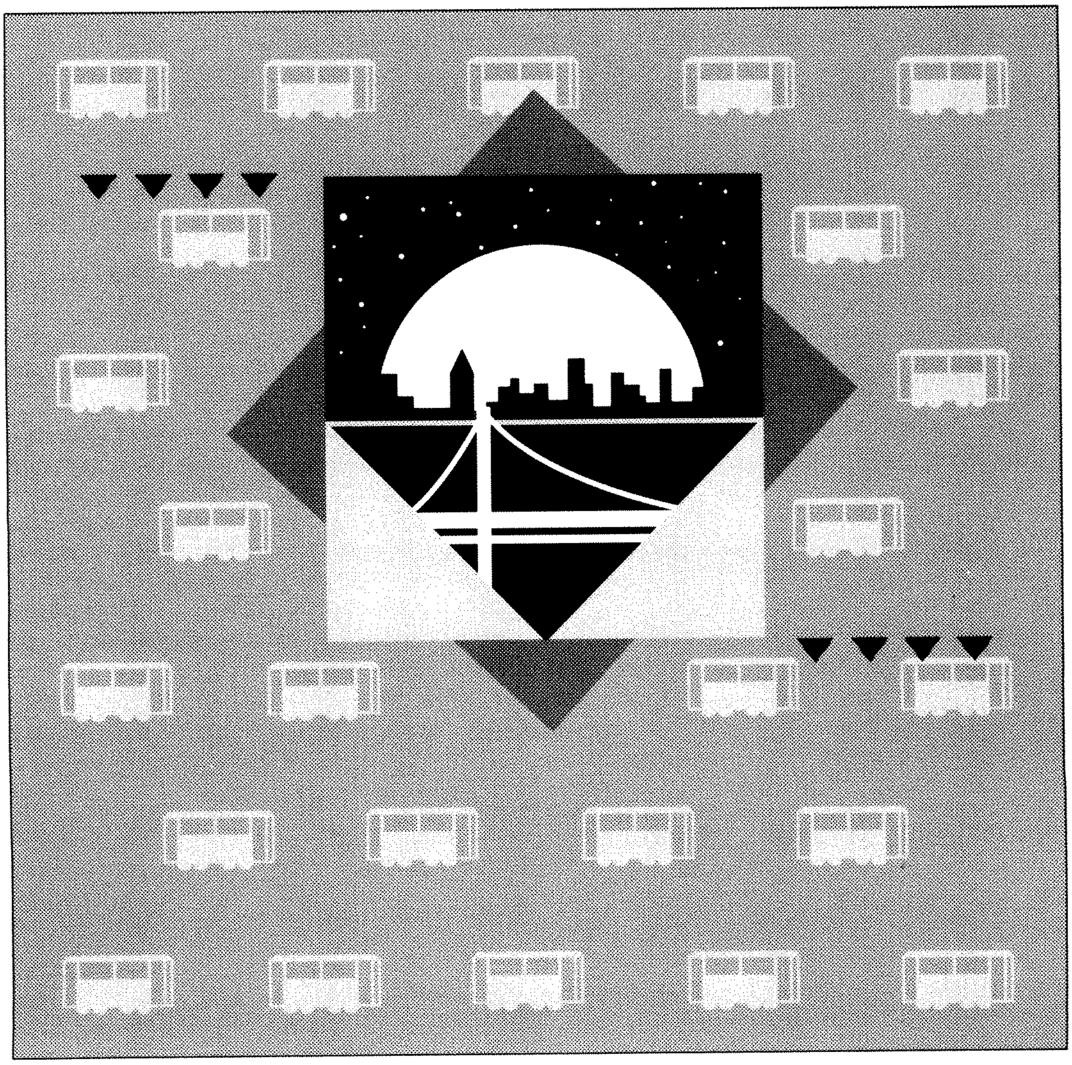

San Francisco

American Roentgen Ray Society

93rd Annual Meeting

April 25–30, 1993

San Francisco Marriott • San Francisco, CA

Meeting News

American Roentgen Ray Society, 92nd Annual Meeting, May 1992

The 92nd annual meeting of the American Roentgen Ray Society was held May 10–15, 1992, at the Marriott Orlando World Center in Orlando, FL. Approximately 200 scientific presentations, 60 instructional courses, and a large and varied selection of scientific and technical exhibits were available to the more than 2000 attendees. The topic of this year's categorical course was neuroradiology, and there were two Friday morning symposia: one, held jointly with the Society for Pediatric Radiology, was titled Stat and Urgent Problems in Pediatrics; the other was titled New Issues Forum. A very successful spouse/companion program on osteoporosis was provided also.

This review of the 1992 ARRS meeting is intended to provide the reader with a short summary of many of the papers presented in the scientific program. Unfortunately, space limitations in the Journal do not allow coverage of all presentations or an analysis of them.

Chest Radiology

J. W. Hanna and colleagues (P. L. Molina, H. S. Glazer, D. J. Anderson, S. L. Solomon, S. S. Sagel; St. Louis, MO) presented a paper comparing the rate of occurrence of postbiopsy pneumothorax and the need for chest tube placement in a study group vs control subjects. Study group patients maintained postbiopsy precautions (e.g., the biopsy site was placed in a dependent position for at least 1 hr and talking, coughing, and movement were restricted) whereas control subjects underwent lung needle biopsy without specific postprocedural precautions. No statistically significant differences in complication rates were noted between the two groups of patients.

G. Wittich and coworkers (L. Hamid, J. Lukacs, D. Lucas, C. Kusnick; Stanford, CA) reviewed the technique, results, and complications of percutaneous needle biopsy in patients who were recovering from heart or heart/lung transplantation. Percutaneous biopsy proved to be effective in differentiating malignant lesions, particularly cyclosporine-induced lymphoma, from infectious complications. Pneumothorax occurred in seven (24%) of the 29 patients studied. Simultaneous bilateral pneumothorax may occur in these patients because of a common pleural space; it may be treated with a solitary chest tube, which was required in four of these patients.

Two presentations concerned pulmonary complications in AIDS patients. In one, C. Chow and coauthors (P. A. Templeton and C. S. White; Baltimore, MD) followed the natural radiologic history of pulmonary cysts in AIDS patients who had pneumocystis carinii pneumonia (PCP). They found that 34% of 90 patients with PCP had pulmonary cysts, which were typically multiple with an upper lobe predominance. Pneumothorax developed in 32% of the patients with cysts. In most patients, follow-up chest radiographs showed the cysts had resolved or improved. In the other study, N. Seguin and coworkers (M. E. Osborne, L. Samson, R. Morisset, P. Ghadirian; Montreal, Canada) correlated the presence of

---

Editor's note.—"Meeting News" articles report the highlights of important national radiology meetings. The articles will not undergo the peer review usually required of *AJR* publications, nor will they offer a critique of the information provided. The sole purpose of the series is to provide Journal readers with succinct, substantive, and accurate reviews of topics of current interest, written in a readable fashion and published promptly after the meeting. Presenters did not have the opportunity to review this summary before publication.

I thank Dennis M. Balfe, Emil J. Balthazar, Richard L. Baron, Claire Bender, William J. Casarella, D. David Dershaw, Arthur C. Fleischer, Jay P. Heiken, Barbara S. Hertzberg, Michael Huckman, Jeremy J. Kaye, Melvyn Korobkin, Mark D. Murphey, Andrew K. Poznanski, Robert M. Quencer, Lee F. Rogers, Arina Van Breda, Kay H. Vydareny, and Stephanie Wilson for contributing to this summary.

***AJR* 157:647–656, September 1992** 0361–803X/92/1593–0647 © American Roentgen Ray Society

pleural effusion with underlying pulmonary disease in 97 patients with AIDS. In their population, a minimal or unilateral pleural effusion showed high sensitivity for mycobacterium avium intracellulare infection. PCP was the underlying cause in 20% of their patients, Kaposi's sarcoma in 10%, and tuberculosis in 8%. Intrathoracic Kaposi's sarcoma without moderate or bilateral pleural effusion was unusual. In 38% of the patients, the cause of the pleural effusion was undetermined.

Cardiac MR Imaging

Potentially the most useful study in this section was the one presented by W. A. Carpenter, R. G. Stiles, and S. K. Sheppard (Atlanta, GA). These researchers described the use of a computer to color enhance MR images after gadopentetate dimeglumine enhancement while maintaining anatomic detail. The authors used a Macintosh computer connected directly to the output of a 1.5-T MR scanner via an Ethernet network. Images were imported into a graphics program via commercially available software (Adobe PhotoShop). Using this relatively simple method, the authors were able to demonstrate in multicolor format the areas of the scan that were selectively enhanced by contrast material while retaining all the anatomic detail in the precontrast scan. This application appeared to be most useful in the analysis of postoperative spines, bone tumors, and inflammation in the musculoskeletal system.

Another paper that appears to be of clinical significance is that presented by E. Winberger and colleagues (K. S. White, D. W. Shaw, M. K. Winning; Seattle, WA). These authors used fat-saturation techniques to enhance the conspicuity of vessels with a fat interface. The use of fat-saturation sequences markedly diminished the chemical-shift artifact and positively affected vessel conspicuity. Gradient-recalled parameters with TR of 50, TE of 16–17, and a 60° flip angle with RF fat saturation were optimal for enhancing imaging of small blood vessels adjacent to fat tissue.

In a preliminary study, K. C. Seelos and coworkers (A. von Smekal, J. Gieseke, J. van Vaals, M. Reiser; Bonn, Germany) were able to characterize normal myocardium as well as six intra- or paracardiac tumors by measuring gadopentetate dimeglumine perfusion with a turbo fast-scan technique at 0.5 T. The authors demonstrated adequate time and spatial resolution in cardiac MR perfusion imaging, and they believe this particular MR pulse sequence holds promise for the evaluation of ischemic coronary artery disease.

Breast Radiology

The scientific papers presented in the breast session covered a variety of breast imaging techniques and clinical situations. M. K. Jones (other authors: D. A. Clunie, J. Szumowski, B. Webber, G. Woltering, A. S. Thurmond; Portland, OR) and K. A. Rosculet (other authors: D. M. Ikeda, M. E. Forrest, M. A. Helvie, R. O'Neal, D. O. Jeffries; Ann Arbor, MI) presented studies on imaging women to diagnose leaks in silicone prostheses. The Oregon group found that MR imaging of silicone implants was best performed with an inversion recovery sequence. Silicone leakage, including silent leaks, was often identifiable but could be mimicked by double lumen implants and capsule formation. The University of Michigan group defined the sonographic characteristics of silicone leakage as an echodense shadowing pattern and/or a hypoechoic mass.

More precise sonographic diagnosis of breast lesions was encouraged by studies from Korea and Pennsylvania. H-Y Choi and coauthors (K. Park, S. Lee, T. Kim; Seoul, Korea) evaluated 36 breast lesions with color Doppler sonography and found a low flow pattern in 83% of benign tumors and a high flow pattern in 77% of malignant tumors. M. J. Staiger and coauthors (K. M. Harris, Z. S. Ilkhanipour, M. A. Ganott, P. H. Hintz, A. B. Baratz, M. L. Skolnick; Pittsburgh, PA) found that in 25 fluid-containing masses, a thick, irregular wall was common in malignant tumors whereas other cystic or complex sonographic patterns were associated with benign lesions.

The importance of routine mammography in younger women was emphasized in papers concerned with screening. L. Liberman and coauthors (D. D. Dershaw, B. M. Deutch, B. Smolek-Lippin; New York, NY), in a study of mammographic screening in women 35–39 years old, found the rate of breast cancer equaled that of women in their 40s and suggested more aggressive screening of these younger women. T. L. Roberts and coworkers (B. S. Monsees, T. Wasserman, E. Miller, J. M. Destouet; St. Louis, MO) found an increased rate of breast cancer in women after mantle radiation for Hodgkin's disease, and encouraged screening of these women starting 10 years after their treatment, whatever their age.

Radiologists were encouraged to refine their diagnostic capabilities by A. M. Knutzen and J. J. Gisvold (Rochester, MN). These researchers noted that by appreciating clearly benign patterns as benign, fewer women will be biopsied unnecessarily. The positive predictive value for a biopsy recommendation in their series was raised to 39% by eliminating these biopsies. However, a note of caution was raised by A. S. Lev-Toaff and S. A. Feig (Philadelphia, PA), who reported on the mammographic findings of 27 women seen at their institution who had cancer despite a pattern of stable calcifications over an 8- to 63-month interval. Although most of these were due to intraductal tumors, 10% were infiltrating tumors. The overall message of the session seemed to be that while breast imagers pursue new techniques to deal with clinical problems, attempts continue to improve the usefulness of mammography, which remains the unchallenged gold standard of breast imaging.

Gastrointestinal Radiology

A variety of diseases affecting the gastrointestinal tract and the pancreas were presented and discussed during the gastrointestinal scientific session. The presentations focused on the contribution, accuracy, and pitfalls of different imaging techniques available today, including barium studies, CT, MR imaging, and sonography.

The prevalence of transpyloric extension of gastric carcinoma vs gastric lymphoma was evaluated by K. C. Cho

(Newark, NJ) and coauthors (S. R. Baker, D. D. Alterman, J. M. Fusco, S. Cho; Bronx, NY). The radiologic findings in 102 patients with gastric carcinoma and 25 patients with gastric lymphoma were correlated with the endoscopic, surgical, and pathologic findings. Transpyloric extension into the duodenal bulb occurred in 17% of the patients with carcinoma and in 28% of those with lymphoma. In this series, the transpyloric extension of gastric carcinoma is more frequent (17%) than previously stated in the literature (5%). Given the much higher prevalence of stomach carcinoma than lymphoma, and contrary to previous statements in the literature, the demonstration of transpyloric extension of tumor cannot be used in the radiologic differential diagnosis. A gastric tumor extending into the duodenal bulb is more likely to be an adenocarcinoma than a lymphoma.

K. W. Sievers and coauthors (H. J. Feldman, M. Molls, E. Lohr; Essen, Germany) presented their findings from a study in which dynamic MR imaging was used to determine the blood perfusion of pelvic neoplasms in an attempt to identify and select patients who will respond to radiation therapy. After injecting a bolus of gadopentetate dimeglumine, these researchers examined changes in signal intensity over a period of more than 3 min. Preliminary results suggest that dynamic MR imaging is able to classify high- and low-perfusion tumor as well as inhomogeneities of blood supply within the tumor itself. It is hoped that, in combination with good anatomic resolution, this MR application will play a major role in treatment planning and in determining the responses of different types of tumor.

The message of the paper presented by M. F. Levin and coauthors (A. D. Vellet, P. L. Munk, D. B. Bach; London, Ontario, Canada) was that evaluation of peripancreatic fluid collections should be performed with color Doppler sonography in addition to conventional sonography. Among the five patients diagnosed by conventional sonography as having peripancreatic fluid collections, color Doppler sonography detected the presence of pseudoaneurysm in two patients. This significant complication can be missed if color Doppler sonography is not used in the evaluation of peripancreatic fluid collections seen in patients with acute pancreatitis.

M. B. Rominger and coauthors (P. J. Kenney, D. B. Koslin, J. J. Listinsky; Birmingham, AL) correlated the accuracy of MR imaging with that of CT in the detection of pancreatic masses in 20 patients. MR imaging was performed with oral (Kaopectate) and IV (gadopentetate dimeglumine) contrast agents using multiple sequences. Contrast-enhanced CT was performed, and results were correlated with the available surgical results, biopsy findings, and follow-up studies. The investigators concluded that MR imaging is at least as accurate as CT in detecting, characterizing, and staging pancreatic masses. At present, MR imaging is most helpful for problem solving and for patients in whom iodinated contrast material is contraindicated.

CT: Abdomen

N. R. Dunnick (other authors: J. C. Gunnells, G. S. Leight, Jr., R. A. Leder, M. A. Roubidoux, E. Paulson, L. Kuryio; Durham, NC) reported on a retrospective study to determine the sensitivity and specificity of CT for the detection and localization of aldosterone-secreting adenomas. CT scans of the adrenal glands were obtained without IV contrast material by using 5- or 10-mm continuous sections. Of 27 patients with biochemically proved Conn's syndrome who were studied, 15 were found at surgery to have an aldosterone-secreting adenoma. CT identified the adenoma in 13 patients (sensitivity, 87%). The two adenomas missed by CT were 0.9 cm and 1.1 cm in diameter, respectively. None of the CT examinations produced false-positive results (specificity, 100%).

A study conducted by M. J. Lee and coworkers (S. L. Dawson, D. McLouglin, T. Kinney, S. Gazelle, S. Saini, P. L. Hahn, P. R. Mueller; Boston, MA) evaluated the usefulness of image-guided fine needle aspiration biopsy tissue carcinoembryonic antigen (CEA) determinations in the diagnosis of metastatic disease. Tissue fragments obtained from abdominal or pelvic biopsies on 45 patients who had a variety of primary malignancies were manually homogenized and centrifuged, after which immunoenzymatic CEA determinations were performed on the supernatant. Tissue CEA levels were normal (<3 ng/ml) in all patients with benign lesions or malignancies that do not produce CEA, but were markedly elevated in 11 patients with colon metastases (mean, 13,153 ng/ml) and marginally elevated in eight patients with other malignancies (mean, 16 ng/ml). CEA levels were also markedly raised in three patients with metastatic adenocarcinoma of unknown origin (mean, 2069 ng/ml). Tissue CEA levels were falsely negative in three patients with positive cytologic findings, but positive in one patient with falsely negative cytologic findings. No patients with colon carcinoma had a falsely negative tissue CEA level.

C. A. J. Granfield and coworkers (C. Charnsangavej, R. A. Dubrow, D. G. K. Varma, S. Wallace; Houston, TX) conducted a study to determine the pattern of regional nodal metastases in patients with carcinoma of the left side of the colon. These investigators reviewed the CT scans of 114 consecutive patients with intact or previously resected left colon carcinoma. Lymph nodes 1 cm or greater and clusters of three or more nodes were considered abnormal. Nodal metastases were confirmed by biopsy, surgery, progression on radiologic studies, or elevated carcinoembryonic antigen. Regional nodal metastases were identified in 31 patients (27%). The nodal groups involved by cancers other than anal were mesocolic (16%), inferior mesenteric artery (9%), and paraaortic/iliac-inguinal (6%). The paraaortic/iliac-inguinal nodes were involved by rectal or anal carcinomas, but not by any sigmoid or descending colon carcinomas.

Liver

The presentations in this session focused chiefly on the use of MR to image hepatic diseases. Two papers, one by J. A. Borrello and coworkers (J. J. Brown, M. J. Siegel, J. K. T. Lee; St. Louis, MO) and the other by K. Itoh and colleagues (M. Hosono, S. Kawakami, J. Konishi; Kyoto, Japan) addressed the usefulness of MR imaging in evaluating intrahepatic venous structures. In the paper from the St. Louis group, the authors noted that standard axial and coronal sections of the liver tend to cut obliquely through the portal vein. Using an operator-defined plane perpendicular to the long axis of the portal vein, combined with presaturation to remove hepatic artery signal, the investigators demonstrated improved detection of slow portal flow and the presence of small collateral vessels. In the paper presented by the group from Kyoto, the authors reported a series of 26 patients who were evaluated as potential liver donors; the surgical procedure involved using the lateral segment as a graft, except in cases in which an anomalous hepatic venous drainage pattern made the procedure technically difficult. The clinically relevant venous anomaly was present in three of the cases, and was correctly predicted by the preoperative MR imaging findings in two. The prediction of normal anatomy was confirmed by intraoperative sonography in the remaining cases.

J. L. Chezmar (coauthors: R. D. Redvanly, R. C. Nelson, J. M. Henderson; Atlanta, GA) reported an interesting observation regarding the venous system in liver transplant recipients. In this study, 33 patients who received transplants because of portal hypertension were followed up by CT for a mean period of 2 years. Twenty-nine of these patients had varices preoperatively; all had persistent evidence of varices after the successful transplantation (retroperitoneal and splenic hilar collaterals tended to persist longest). However, during the same follow-up interval, the splenic size in these patients tended to decrease, and in no case was the persistence of varices associated with clinical symptoms. The authors concluded that the persistence of large venous collaterals need not be construed as an ominous sign.

A. Tanimoto and coworkers (B. P. Kreft, Y. Baba, L. Zhao, J. P. Finn, D. D. Stark; Boston, MA) tested the hypothesis that hepatocyte-specific MR contrast agents would be expected to work less well in patients with hepatitis. Carbon tetrachloride was used to induce liver inflammation in rats, whose livers were imaged (in and ex vivo) before and after the hepatic insult. Noncontrast T2-weighted images showed considerable degradation of contrast-to-noise ratios because of the hepatitis, but, surprisingly, the tumor-to-liver contrast-to-noise ratios after administration of contrast agent (manganese-DPDP or superparamagnetic iron oxide) was not significantly affected by the liver inflammation.

Two papers, one by B. B. Kraus (coauthors: D. C. Rappaport, P. R. Ros, G. M. Torres; Gainesville, FL) and the other by P. F. Hahn (coauthors: S. Saini, M. S. Cohen, P. Reimer, P. R. Mueller; Boston, MA), reported on the effectiveness if various oral contrast strategies for MR imaging. In the study by the Gainesville group, five very understanding volunteers were imaged before and after ingestion of each of six agents: four barium suspensions varying from 60% to 225% weight per volume, ferric ammonium citrate, and corn oil emulsion. Corn oil, a positive contrast agent, yielded the highest subjective scores for visualizing the stomach, duodenum, pancreas, and liver. High-density barium, a negative contrast agent, was preferred in visualizing the remainder of the gut.

Increasingly, attention is being given to rapid-acquisition MR techniques, and it is likely that contrast strategies will differ for the ultrafast echoplanar sequences compared with standard spin-echo techniques. In the study by Hahn et al., the authors reported the use of a standard dilute barium preparation intended for use with CT. In this sequence, the dominant effect on signal originates from the aqueous medium, which produces intraluminal high intensity (rather than from the barium, which produces low signal intensity on longer sequences). Accordingly, the authors recommend removing the barium and using only the base material.

Genitourinary

In the Genitourinary I session, two papers concerned the use of automated biopsy guns for performing renal biopsies for diagnosis of diffuse medical renal disease. M. Sateriale and coworkers (R. Kassner and J. J. Cronan; Providence, RI) performed 58 renal biopsies on 58 patients using the automated biopsy gun with a 14-gauge needle and CT guidance. Two biopsy-related complications occurred (3% of patients). Because a previous study conducted by these investigators using a 14-gauge Vim-Silverman needle had similar diagnostic findings but a much higher rate of significant hemorrhagic complications (7.5%), the authors recommend replacing this older needle system with the newer automated biopsy gun. In a similar study, but with sonographic rather than CT guidance, K. T. Tung, M. O. Downes, P. J. O'Donnell, and M. R. C. Path (Canterbury, England) reported their results with 104 percutaneous renal biopsies with a 14-gauge biopsy needle in an automated biopsy device. Four minor complications (4% of patients) and three significant complications (3% of patients) occurred. These investigators suggested that use of the 14-gauge Biopty gun guided by real-time sonography should be the method of choice for percutaneous renal biopsy in adults.

J. H. Miller and coauthors (S. Z. H. Jafri, E. G. Bernacki, J. L. Roberts, B. L. Madrazo; Royal Oak, MI) studied the use of fine-needle aspiration biopsy of renal masses in 99 patients. Fifty-four lesions were classified as solid by imaging criteria and the remainder were cystic lesions that did not fulfill the criteria of a simple cyst. The final diagnosis of the solid lesions included renal cell carcinoma in 27, transitional cell carcinoma in three, metastasis in nine, lymphoma in one, angiomyolipoma in five, oncocytoma in five, and abscess in four. Of the ambiguous cysts, 27 proved to be simple renal cyst. There were seven hemorrhagic aspirates, of which four proved to be renal cell carcinoma and one angiomyolipoma. In 12 patients, the aspirate yielded either normal tissue or was reported as inadequate for diagnosis. Complications were minimal and included three pneumothoraces. The authors stated that fine-needle aspiration biopsies of renal masses is highly accurate and plays an integral role in the evaluation and workup of selected renal masses.

T. M. Weber and his group (N. R. Dunnick, C. N. Robertson, D. F. Paulson, R. A. Leder, M. A. Roubidoux; Durham, NC) compared the accuracy of transrectal sonography, digital rectal examination, and prostate-specific antigen in detecting prostate cancer in 153 patients. Prostate cancer was detected by sonographically guided biopsy in 48 cases (31%). The positive predictive value was greatest for prostate-specific antigen greater than 10 ng/ml (54%), followed by 38% for abnormal findings by transrectal sonography, 38% for positive findings by digital rectal examination, and 36% for prostate-specific antigen greater than 4 ng/ml. Prostate cancer was detected by random sonographically guided biopsy of the peripheral zone in 11 of 48 men (23%) who had normal findings by transrectal sonography. Cancer was also detected by sonographically guided biopsy in 14 (22%) of 64 men who had normal findings by digital rectal examination and in five (12%) of 42 men who had normal prostate-specific antigen. The authors concluded that detection rate for prostate cancer is improved by using all three diagnostic techniques. Thus, a normal transrectal sonogram does not obviate sonographically guided random biopsy of the peripheral zone in men with abnormal findings by digital rectal examination or those in whom prostate-specific antigen is elevated; similarly, a normal level of prostate-specific antigen does not obviate sonographically guided random biopsy in men with abnormal findings by digital rectal examination or by transrectal sonography.

The Genitourinary II session included a collection of papers describing various techniques—including CT, MR imaging, scintigraphy, and sonography—for imaging both native and transplanted kidneys. S. Karasick and A. S. Lev-Toaff (Philadelphia, PA) reported their findings from a comparative study of 27 patients who were imaged preoperatively for the evaluation of uterinemyomas. Although lack of standardization of the imaging examinations and the retrospective nature of the study design severely limit the reliability of these findings, MR imaging was shown to be superior to other techniques in the four patients in whom it was performed.

Preliminary, but promising, results were reported in a study by J. G. Niethammer and colleagues (K. F. Hubner, T. McDonald, G. T. Smith, H. R. Gould, E. Buonocore; Knoxville, TN) in which they evaluated ovarian cancer by positron emission tomography after IV injection of F-18 fluoro-2-D-deoxyglucose. Early results indicate that this technique is useful for differentiating benign from malignant neoplasm and for identifying occult foci of metabolically active tumor.

An interesting technical note came from S. K. Sussman and coworkers (G. Turner, F. F. Illescas, J. P. Opalacz, P. Yirga, L. C. Foley; Hartford, CT). Although their study comparing low- vs high-osmolality contrast agents in producing renal streak artifacts on abdominal CT scans did not look at the influence of artifacts on the perception of disease, the increased prevalence of renal streak artifacts with the use of low-osmolality agents is documented.

A. M. Muchow and colleagues (S. A. H. Jafri, B. L. Madrazo, A. A. Cacciarelli, R. A. Mills; Royal Oak, MI) documented the usefulness of color Doppler sonography in demonstrating hyperemia in patients with orchitis and in showing the absence of intrinsic testicular flow in patients with torsion. As differentiation of these two clinical situations has always been difficult, both producing virtually identical sonographic morphologic abnormality, this addition to the literature is most helpful.

Musculoskeletal

Identifying osteomyelitis in previously traumatized bone with internal fixation presents many diagnostic problems. In the first Skeletal session, B. Barron and coworkers (H. Tran, B. Browner, K. Lyssy, L. Lamki; Houston, TX) presented their findings in the evaluation of the use of cobalt-57 transmission and ^{99m}Tc sulfur colloid marrow scans in addition to standard bone scintigraphy and ^{111}In-WBC leucocyte images in 20 patients for diagnosis of osteomyelitis in trauma patients. Chronic metal internal fixation results in a high rate of false-positive ^{111}In-WBC studies because of bone marrow stimulation. Bone marrow ^{99m}Tc sulfur colloid images show a similar (congruent) degree of activity in these false-positive ^{111}In-WBC scans. Infection displays focal activity on bone scintigrams and ^{111}In-WBC scans, while showing diffuse (incongruent) uptake on ^{99m}Tc sulfur colloid bone marrow images. The cobalt-57 transmission images were used for improved localization of the infection site. The sensitivity in this study was 83% and the specificity 88% for detection of osteomyelitis.

M. D. Murphey and coworkers (J. L. Quale, N. L. Martin, L. Cook, M. J. Wright; Kansas City, KS) presented an observer performance comparison of conventional film-screen radiographs and phosphor plate images of the shoulder and wrist. The study involved 36 arthrograms with phosphor plate images obtained at 25-75% of exposure dose of film-screen technique. Phosphor plate images were considered superior to conventional film-screen images at all exposure doses with statistical significance ($p < .05$) at 25% and 50% exposure dose. Improvement in contrast resolution and wide dynamic range with phosphor plate technology was concluded to be the reason for the increased diagnostic accuracy.

A. Gangi and coworkers (B. Kastler, R. Allal, E. Quoix, C. Mathelin, J. L. Dietemann; Strasbourg, France) evaluated the use of percutaneous ethanol injection for pain management in 15 patients with osseous metastases. Injection was repeated after 2 weeks and no complications were reported. After therapy, tumor size decreased in 26% of patients, increased in 21%, and remained unchanged in 53%. Significant pain relief was achieved in 80% of patients, suggesting that this technique is helpful for palliative therapy.

Evaluation of long bone allograft has received only limited attention in the orthopedic and radiologic literature. H. J. Griffiths and coworkers (P. J. Amundson, R. C. Thompson, Jr., T. Detlie, L. Everson; Minneapolis, MN) presented a review of long bone allograft complications in a study of 45 patients. Complications were present in 34 patients (76%) and included resorption of graft or native bone (16), fractures (12), infection (five), nonunion (seven), fixation problems (13), and tumor recurrence (nine). Although the complication rate was high, many were minor and successfully treated. Only three allografts had to be removed. Long bone allografts continue to offer a limb-salvage alternative to amputation.

The diagnosis of anterior cruciate ligament (ACL) injuries was the subject of three presentations in the Skeletal II session. J. M. Hunt, T. N. Vahey, and D. R. Broome (Indianapolis, IN) performed a study to determine if secondary signs of ACL tears on MR images might be of value in determining the integrity of the ACL when not ideally imaged in the sagittal plane. When the ACL was disrupted, joint effusions were found in all cases; but they were nonspecific. Although the finding of buckling of the posterior cruciate ligament (PCL) had 100% specificity, it was present in only 17% of cases.

Presence of bone bruise of the tibia was highly specific (93%) and highly suggestive, and collated well with acute injury. Anterior tibial translocation greater than 5 mm was also highly specific and predictive. It was concluded that MR demonstration of anterior tibial translocation and bone bruise is highly specific and has a positive predictive value for disruption of the ACL. These secondary findings may be helpful in equivocal cases.

A second paper, by S. W. Fitzgerald (coauthors: E. Remer, H. Friedman, L. F. Rogers, R. Hendrix, M. Schaefer; Chicago, IL), addressed the value of multiplanar imaging in assessing the ACL. Sagittal MR imaging has a sensitivity of 95%, a specificity of 83%, and an accuracy of 91% in diagnosing ACL injury. Further improvement in this accuracy and specificity was obtained by acquiring views in the coronal and axial planes, which were essential to the diagnosis in 4% of patients. Multiplanar imaging proved helpful in correctly characterizing partial ACL tears and thinning and in disclosing intact ACLs. Secondary signs of ACL injury (e.g., bone marrow contusion) were better appreciated in the axial and coronal planes. It was concluded that the accuracy and confidence in the diagnosis of ACL injury is enhanced by multiplanar imaging.

In a related presentation, J. Hodler, P. Haghighi, D. Trudell, and D. Resnick (San Diego, CA) reported their findings in a study of the increased signal that is occasionally seen on MR images of the cruciate ligaments of the elderly, as well as the different appearances of signal in the ACL and PCL. These authors found no histologic basis to explain the different MR appearances, but it seemed likely that the parallel fascicles in the PCL and diverging twisted fascicles in the ACL cause secondary volume averaging artifacts. Increased MR signal within the cruciate ligaments occurring in the elderly was attributed to identifiable microscopically degenerative changes. These may simulate the findings of partial tear on MR studies.

In the Skeletal III session, M. H. De Mouy and M. E. Brunet (New Orleans, LA) presented their study of 15 patients in whom conventional shoulder MR imaging yielded inconclusive findings concerning the supraspinatus tendon or the glenoid labrum. None of the patients studied by MR after the injection of saline had significant fluid within the joint on the conventional MR examination. In cases with inconclusive findings, the authors injected 15–30 ml of normal saline into the joint and repeated oblique coronal and axial gradient-echo pulse sequences. The authors found that the MR images acquired after the injection of saline were almost uniformly helpful in resolving inconclusive findings. In particular, they were helpful for diagnosing rotator cuff tears and for evaluating the anterior glenoid labrum.

M. Yacoe, A. Ladd, and A. G. Bjorkengren (Stanford, CA) examined seven patients before surgery for Dupuytren's contractures and correlated MR findings with gross and microscopic tissue samples as well as with surgical findings of extent of disease. The authors found that MR could accurately delineate the extent of disease and the degree of displacement of adjacent structures, information that was thought to be helpful by the operating surgeon. T1- and T2-weighted pulse sequences were used in an attempt to distinguish patients with mature fibrosis from those with more cellular disease; there is a higher recurrence rate among patients with more cellular disease. In preliminary studies of these seven patients, the authors found that more signal on T2-weighted sequences correlated with greater cellularity.

D. J. Rubens and coworkers (S. M. Totterman, J. S. Blebea, R. J. Miller, J. Delsignore, M. Hooper; Rochester, NY) studied the wrists of five patients with rheumatoid arthritis before surgery by using a dedicated wrist surface coil and a high-resolution scan protocol. The authors studied the extensor compartment for the presence of fluid or pannus and for tendon infiltration, thinning, rupture, or displacement; MR findings were compared with surgical results. The authors found they were able to identify nine of 10 tendon ruptures preoperatively. One false-negative finding was reported in a patient studied 2 months before surgery. Two false-positive findings occurred in patients in whom tendons were infiltrated by pannus. Tendon displacement was accurately shown, as was pannus involvement in the extensor compartment. The authors believe that preoperative MR imaging may identify patients in need of dorsal tenosynovectomy and that preoperative MR imaging may aid in planning the timing and extent of surgery.

General CT

A presentation by L. M. Miketic, T. Chambers, and B. Lembersky (Pittsburgh, PA) reported on CT findings specific for T-cell cutaneous lymphoma. In 10 of 33 patients, CT scans showed areas of tumorous skin thickening affecting the dermal tissues but leaving the subcutaneous fat intact. When the lesions extended below the dermis, this was associated with the development of secondary squamous cell carcinoma in two patients. A pattern of peripheral adenopathy sparing the mediastinum or retroperitoneal paraaortic regions, but involving the axillary and inguinal areas, was found in seven patients. These latter findings were associated with a poor prognosis.

D. Holland and coworkers (L. E. Quint, M. Korobkin, P. N. Cascade; Ann Arbor, MI) characterized extraperitoneal hematomas occurring in 24 patients after femoral artery catheterization in association with altered hemostasis (pharmacologically induced) and in 19 patients with altered hemostasis but with no history of femoral vessel puncture. The hematomas were contiguous with punctured vessels in 18 of 24 patients after catheterization. In four cases, the hematoma was contiguous with the femoral vessels *contralateral* to the puncture site, and was contiguous with femoral vessels in 11 of 19 patients with altered hemostasis who had no history of femoral puncture. The location and extent of hematomas throughout the retroperitoneum and pelvis were not significantly different between the two patient groups. These data suggest that retroperitoneal hematomas in anticoagulated patients are often due to the anticoagulation effects rather than to a complication of the vascular catheterization itself.

The use of ultrafast CT in diagnosing pulmonary embolism was reported by D. A. Thorne, J. R. Geis, and J. Midthun (Spokane, WA), who conducted a prospective study in 14 patients, 12 of whom had no clinical signs or symptoms before imaging. CT was performed at 300–400 msec with concomitant IV contrast administration. Subsequent proof of diagnosis with pulmonary angiography within 24 hr was obtained in four patients, and confirmatory evidence of the diagnosis in five patients was provided by documenting lower extremity deep venous thrombosis. Emboli as small as 3–4 mm in diameter were illustrated in third and fourth divisions of the pulmonary arteries. Four patients with clinically suspected embolic disease were correctly diagnosed as having no emboli by ultrafast CT and confirmed at angiography. The authors suggested the need for further investigation into the use of ultrafast CT as a screen for pulmonary embolic disease.

An evaluation of the volumes of IV contrast material necessary for adequate vascular enhancement using spiral CT was reported by P. L. Molina and coworkers (J. A. Brink, J. P. Heiken, S. S. Sagel, J. J. DiCroce; St. Louis, MO). By evaluating various amounts of contrast media and administration techniques, the authors found that 70–120 ml or more of contrast material infused at 1–3 ml/sec provided adequate enhancement of the pulmonary artery branches, aorta, and aortic arch vessels in 39 of 40 cases. Of the 40 patients receiving ≤60 ml, 34 showed adequate vascular enhancement. The reason for the six inadequate enhancement cases was either an inadequate delay between contrast and scanning or too short an infusion time. The authors suggest using 60 ml or less of contrast medium with a biphasic contrast administration technique (to extend the infusion time) and a scan delay of 20 sec to achieve good vascular opacification with a minimum of contrast agent.

Sonography

The majority of papers presented in this session dealt with applications of color Doppler sonography.

J. M. Yee and E. J. Balthazer (New York, NY) investigated the role of color Doppler imaging in the differential diagnosis of the thickened gallbladder wall. Color Doppler signal was demonstrated in the gallbladder wall in 15 patients. Clinical outcomes were as follows: eight patients had acute cholecystitis, four had chronic cholecystitis, one had metastatic gallbladder carcinoma, and two patients improved on medical therapy alone. On the other hand, of 22 patients with no detectable flow in the gallbladder, four were later proved to have chronic cholecystitis and the remaining 18 had no evidence of gallbladder disease. The investigators concluded that demonstration of hyperemic flow in a thickened gallbladder wall is usually associated with acute or chronic inflammation. Conversely, absence of hyperemic changes ruled out acute cholecystitis. However, the authors cautioned that care should be used in applying this latter finding to the clinical setting, since the absence of color flow can be an operator- or equipment-dependent phenomenon.

Two presenters discussed color Doppler findings in focal hepatic lesions. M. Nino-Murcia, P. W. Ralls, R. B. Jeffrey, Jr., and M. Johnson (Palo Alto, CA) used color Doppler sonography to divide 118 focal hepatic lesions into two groups on the basis of the presence or absence of internal vascularity. Of 49 lesions with demonstrable internal vascularity, 22 were later proved to be hepatocellular carcinomas, 21 were metastases, one was a cholangiocarcinoma, and five were benign lesions. On the other hand, 68 lesions without demonstrable internal vascularity included seven hepatocellular carcinomas, 43 metastases, and 18 benign lesions. "Normal vascularity" was seen in one case of focal fatty infiltration. Thus, hepatocellular carcinomas were more likely than other lesions to show internal vascularity on color Doppler sonograms, but this finding was nonspecific.

A paper presented by E. K. Paulson (coauthors: B. S. Hertzberg, S. S. Paine, B. A. Carroll; Durham, NC) considered the question of whether color Doppler imaging can predict spontaneous thrombosis in iatrogenic postcatheterization femoral artery pseudoaneurysms. Multiple parameters—such as pseudoaneurysm volume, percentage of flow within the pseudoaneurysm, and ratio of forward to reversed flow in the pseudoaneurysm neck—were analyzed. None of the parameters tested were found to be clinically useful predictors of which pseudoaneurysms thrombose spontaneously versus which require interventional therapy.

The morphologic and hemodynamic changes occurring in patients with transjugular intrahepatic portosystemic shunts (TIPS) were discussed in a presentation by R. S. Surratt and colleagues (W. D. Middleton, M. D. Darcy, G. L. Melson, J. A. Brink; St. Louis, MO). Twenty patients were studied with gray scale and color Doppler sonography within 4 days after the TIPS procedure. Sonography successfully showed the stent connecting the portal and hepatic vein branches in all patients. Elevated venous flow velocities were detected in both the main portal vein and in the shunt after the procedure. Flow in portal vein branches reversed in 16 of 20 cases after stent placement. Lack of change in the direction of portal vein flow did not predict the onset of clinical problems, however.

S. M. Baker and W. D. Middleton (St. Louis, MO) tested the hypothesis that color Doppler sonographic detection of ureteral jets depends on differences in density between ureteral urine and bladder urine. Ten healthy volunteers were vigorously hydrated and studied by color Doppler sonography before voiding in the morning (i.e., dilute ureteral urine emptying into concentrated urine in the bladder). A second color Doppler examination was performed on each of these volunteers after two cycles of voiding and refilling the bladder (i.e., dilute ureteral urine emptying into dilute urine in the bladder). Normal ureteral jets were shown by color Doppler imaging in all subjects on the initial examination but could not be detected in any subject on the second examination, confirming that detection of ureteral jets by color Doppler sonography depends on density differences between ureteral and bladder urine.

OB/GYN Sonography

D. M. Twickler and coworkers (A. J. Satin, B. B. Little, D. A. Olsher, A. C. Soo, G. D. Wendel; Dallas, TX) presented data concerning Doppler sonographic indexes in 46 women who were chronic substance abusers. They found that the mean blood flow velocity of the fetal umbilical artery was higher in fetuses of these women than in the arteries of control group fetuses, although velocimetry of the middle cerebral artery was the same in both groups. These researchers postulated that the major effect of substance abuse is on the umbilical and/or placental vessels.

U. M. Hamper and colleagues (S. Sheth, D. Aronson, F. M. Abbas, N. B. Rosenshein, R. J. Kurman; Baltimore, MD) described their experience with endovaginal color Doppler sonography in ovarian masses. Although their data indicate some overlap of pulsatility indexes in benign and malignant lesions, benign lesions tended to have higher pulsatility indexes than did malignant lesions. The lower pulsatility indexes of malignant lesions were thought to represent changes caused by neovascularity.

A. C. Fleischer and coworkers (D. M. Kepple, W. H. Rodgers, L. C. Williams, H. W. Jones, III; Nashville, TN) described a study correlating the transvaginal and transabdominal color Doppler sonographic findings in 50 excised ovarian masses with their gross and microscopic pathologic findings. Tumors tended to have abnormal central vascularity, lower pulsatility indexes, and lacked a diastolic notch. The blood flow velocity in vessels within and surrounding the tumors was not significantly different in benign and malignant masses.

Pediatrics

S. P. Quillin and M. J. Siegel (St. Louis, MO) evaluated hepatobiliary abnormalities on sonographic studies of children with cystic fibrosis. They found that 24 (83%) of 29 patients had some sonographic abnormality in the hepatobiliary system. Eighty-three percent had abnormal hepatic echo structure, mostly increased echogenicity, although some patients had decreased hepatic echogenicity. The gallbladder was normal in 17 patients, whereas seven had abnormalities, including a microgallbladder in three, sludge in five, polyps in one, and calculi in one. The pancreas was small and echogenic in 79% of the patients. The main importance of these findings is the relatively high rate of abnormal sonographic findings in patients with cystic fibrosis.

D. J. Dovgan, O. G. Choy, and R. Herzlinger (Bridgeport, CT) reported on the radiologic assessment of complications associated with the use of surfactant in treating infants with respiratory distress syndrome (RDS). The authors analyzed the neurosonograms and chest radiographs of 50 surfactant-treated infants with RDS and those of 55 control subjects, consisting of weight-matched infants with RDS. They found that the use of surfactant decreased the rate of occurrence of pulmonary interstitial emphysema (1/50 vs 13/55), pneumothorax (2/50 vs 10/55), and intraventricular hemorrhage (7/43 vs 25/55); however, there was no apparent decrease in bronchopulmonary dysplasia, pulmonary hemorrhage, or periventricular leukomalacia with surfactant use. There does not seem to be any good reason why in spite of the decrease in many complications, such as pulmonary interstitial emphysema, the two groups showed no difference in the rate of occurrence of bronchopulmonary dysplasia.

D. I. Bulas (coworkers: M. R. Eichelberger, C. J. Sivit, C. Wright, C. Gotschall; Washington, DC) discussed the time course and technique for the follow-up CT evaluation of hepatic injuries in children resulting from blunt abdominal trauma. These researchers reevaluated 40 children with hepatic injuries at 1 week to 15 months after trauma. Some of the children had several CT scans. As expected, all mild hepatic injuries appeared healed on follow-up studies. As the injuries became more severe, residual lesions persisted. Of the severe cases, five children had persistent hepatic lesions up to 1 year after trauma. The authors found that in most cases precontrast CT scans gave the same information as postcontrast scans. Only in two of 22 cases was there some additional information available on the postcontrast studies. The authors concluded that follow-up studies of hepatic injuries are useful in determining management of these patients.

Neuroradiology

The Neuroradiology I session included papers on both neuroradiology and head and neck radiology. The paper by T. E. Wiley, III (coauthors: A. N. Hasso, J. R. Thompson, R. A. Hardesty; Loma Linda, CA) was a summary of the findings in 89 children with craniofacial anomalies who were examined by using 3-mm-thick CT sections and three-dimensional reformatting. Reformatting included "bird's eye" and "worm's eye" views. All scans were looked at with brain and bone window settings. The abnormalities examined were grouped into the following categories: primary cranial synostoses, syndromal synostoses, craniofacial anomalies, and isolated maxillary and mandibular anomalies. These examinations, commonly of interest to maxillofacial surgeons and neurosurgeons, present the radiologist with a deluge of information. Therefore, the authors developed a checklist to simplify the complete and orderly evaluation of these images. Their routine analysis consisted of examination of the following entities: sutures, head shape, brain parenchyma, ventricles, cisterns, maxilla, zygoma, mandible, sinuses, face, skull base, oropharynx, and palate.

R. B. Schwartz (coworkers: K. M. Jones, S. Mukherji, D. Chernoff; Boston, MA) presented a paper describing a technique whereby a CT scan is obtained without contrast enhancement extending from C6 through the skull base. Then, 75 ml of contrast material is injected IV at a rate of 2.5 ml/sec. After a 20-sec delay, a continuous spiral scanning of the region of the carotid artery bifurcations is begun. The scans are reconstructed using 2-mm increments. In evaluating the carotid bifurcations, the investigators found this technique yielded a 92% concordance with conventional angiography, a 97% concordance with color Doppler sonography, and a 100% concordance with MR angiography. The authors reported that one problem they encountered was difficulty in separating calcified plaque from contrast material within the lumen of vessels, because they may have similar attenuations. This problem can be overcome with considerable postprocessing.

Another study conducted by R. B. Schwartz and coworkers (S. Ahn, G. Leclercq, L. Gugino, A. Whittemore; Boston, MA) involved 15 patients who required shunting for clinical reasons during carotid endarterectomy and 15 patients who were not shunted. In all patients, the investigators particularly sought the presence of flow through anterior and posterior communicating arteries. They believed that adequate collateral flow was represented if they were able to demonstrate adequate flow from the side of the most diseased carotid bifurcation through the anterior communicating artery to the opposite side.

A commentator from the audience remarked that, in the first paper, the authors said that they were making their clinical decisions as to whether to perform carotid endarterectomy on the basis of noninvasive testing (e.g., CT angiography, MR angiography, and color Doppler sonography) whereas in the second paper they claimed that they used the pattern of collateral flow on conventional angiography as a barometer of whether shunt would be required during endarterectomy. The authors replied that the two studies were done at separate times and that they are currently investigating the patency of collateral flow by using noninvasive imaging.

The Neuroradiology II session comprised a mixture of topics. As expected, the clinical application of new and refined MR techniques held the greatest interest. MR venography has clearly become the procedure of choice in suspected dural venous sinus occlusion. K. K. Erickson and B. C. P. Lee (St. Louis, MO) compared 2D and 3D techniques to determine the optimal method for MR venography. Multislice 2D images acquired in two separate planes (coronal and sagittal) resulted in excellent image quality and overcame the potential problem of in-plane venous saturation in maximum intensity projection of acquisition if just one plane were evaluated. The use of contrast agents was not helpful in evaluating venous disease, and multislice 2D imaging was clearly superior to 3D imaging. Examples were shown where multislice 2D MR venography actually delineated more venous structures than did routine angiography. MR venography can accurately answer nearly all questions related to the dural venous sinuses, and routine angiography for major venous abnormalities is no longer necessary.

The ability to suppress the bright signal of fat in the neck and the base of the skull with specially designed MR sequences had the potential to more clearly outline abnormalities in this region. D. A. Clunie and colleagues (J. M. Talbot, J. Szumowski, J. Newcomb; Portland, OR) used two variations of fat-suppression techniques along with gadolinium in their study of the evaluation of extracranial head and neck lesions. Although no comparison was made with contrast-enhanced, thin-section, high-resolution CT, this presentation showed the advantages of fat-suppression contrast studies, particularly in perineural tumor spread and base of skull/cavernous sinus invasion. A number of lesions, particularly those in the deep neck/parapharyngeal regions either may be missed or are less well delineated if only standard spin-echo images are used. The drawbacks of fat-suppression techniques are minimal (increased magnetic susceptibility artifacts), and therefore it would seem appropriate for all MR evaluations of this region to include enhanced fat-suppression sequences.

The emergence of SPECT scanning requires that the interpreters of these studies understand the variations in radionuclide activity in different parts of the brain. L. Lemki and coauthors (H. Tran, B. Barron, W. J. Taylor; Houston, TX) pointed out these variations in their presentation. The well-known high level of activity in the normal cerebellum was reemphasized; however, additional observations suggested a lower uptake in the right vs left temporal and parietal lobes, and increased activity in the superior vs inferior portions of the frontal lobes. These variations were constant but the relationship to handedness was not clearly defined. Knowledge of these normal variations in activity is clearly important to avoid misinterpretation of these SPECT images.

Increased experience with techniques related to decreasing the time to acquire spin-echo MR images is accumulating in many centers. Advantages of these techniques (e.g., fast spin echo) relate nearly exclusively to decreased time of acquisition (four- to eightfold, depending on the number of echoes sampled). K. M. Jones and coauthors (R. V. Mulkern, R. B. Schwartz, K. Oshio, F. Jolesz; Boston, MA) spelled out some of the advantages and potential disadvantages of fast spin-echo imaging. The major signal alteration that one must become used to is the persistent high signal of fat on T2-weighted spin-echo images. This may require the addition of a fat-suppression technique in the spine so that the fat marrow signal within posterior osteophytes can be separated from the bright signal of CSF, and that vertebral body metastases can be readily identified. As these authors suggest, MR users can expect a widespread increase in the use of rapid acquisition spin-echo techniques in brain and spine imaging.

Interventional Radiology

Vascular Interventional

J. B. Selby and coworkers (G. D. Hartwell, A. H. Matsumoto, C. Tribble, I. L. Kron, C. J. Tegtmeyer; Charlottesville, VA) reported findings from a retrospective analysis of a large series of angioplasty procedures above the aortic arch. The primary indication was upper extremity ischemia; relatively few patients presented with neurologic symptoms. The overall technical success rate was 100%, and life-table analysis of long-term patency showed excellent results, with over 90% patency at average follow-up of more than 2 years. There were no significant neurologic complications, and the rate of overall complications was low. The authors concluded that aortic arch branch angioplasty was safe and effective. However, these data should not be extrapolated to the carotid circulation without further experience.

J. Cynamon and colleagues (A. Parisi, C. H. Bakal, S. Sprayregen, S. B. Epstein, F. J. Veith; Bronx, NY) reported the results of their study on balloon angioplasty in 14 patients (18 lesions) with severely diseased infrapopliteal arteries. All patients had critical ischemia with rest pain, ulcers, or gangrene. Technical success was achieved in 15 (83%) of 18 lesions or in 11 (79%) of 14 patients. All failures were due to inability to cross occlusions. Clinical results in those patients in whom there was technical success and limb survival sufficient to allow assessment of patency were excellent, with improvement in all. There was significant comorbidity due to coronary disease. These results have the potential to expand the indications and expected results with tibial angioplasty for extensive occlusive disease of the tibial arteries.

Three papers, one by P. Maquin and coauthors (H. Rousseau, J. P. Vinel, J. P. Pascal, F. Joffre, J. J. Railhac; Toulouse, France), one by B. J. Wagner and coworkers (K. Chintapalli,

P. J. Woodward, S. D. Brantley, A. E. Joseph, W. B. Maupin, J. C. Palmaz, F. J. Rivera; San Antonio, TX), and one by W. K. Chong and colleagues (C. Lind, A. C. Fleischer, M. Mazer; Nashville, TN), presented results of transjugular intrahepatic portosystemic shunts. In all three, a high (90% or greater) technical success rate was achieved with excellent initial clinical results. Long-term patency and clinical outcomes will ultimately determine the role of TIPS in the management of portal hypertension. Two of these presentations, those by the San Antonio and the Nashville groups, concentrated on postshunt assessment by using duplex sonography. In both these studies, duplex sonography was able to identify flow in patent TIPS shunts, although exact identification of flow rates and identification of technical problems related to the shunts were not uniformly successful.

Nonvascular Interventional

The very practical approach of percutaneous intraperitoneal catheter placement (PICP) for chemotherapy treatment was presented by H. B. D'Agostino and coworkers (E. vanSonnenberg, R. Sanchez, N. Chalmers, R. O'Laoide, S. Oglevie, L. Fundell; San Diego, CA). Sonography and CT-guided pneumoperitoneum-assisted PICPs were performed 45 times in 20 patients. Indications for PICP were dysfunction of a surgically placed intraperitoneal catheter, multiple adhesions, bone marrow transplant, poor surgical candidate, and refusal of surgery. Catheter size ranged from 5-French to 8.3-French, and the majority of PICPs (41/45) were inserted by trochar technique. Complications were few and included leakage around the catheter, leukocytosis, fever, and bowel puncture. This series demonstrates the ability to successfully gain access to the peritoneal cavity, even in patients with medical complications. The authors state that this is the preferred approach for chemotherapy in patients with bone marrow transplants.

P. I. Ignotus, M. Macklin, and R. R. Gray (Toronto, Canada) retrospectively assessed their performance (their learning curve) in placing percutaneous permanent hemodialysis catheters and Hickman line insertions as indicated by the rate of complications that occurred as experience increased. Overall, 324 procedures were performed, of which 35 (11%) had complications. Complication rate decreased to less than 5% when an operator had performed more than 30 procedures. Complications were defined as infection at catheter site occurring less than 1 week after insertion, pneumothorax, bleeding at puncture site, failure of catheter function, perforation of superior vena cava, malposition of catheter requiring corrective procedure, and unsuccessful procedure. The data suggest that the radiologic placement of venous access devices is a safe and effective procedure even with a minimum of experience.

The tip configurations of four different fine-needle biopsy devices (cutting needle, Franseen needle, spinal needle, and Westcott needle) were evaluated in vivo to test the individual diagnostic yield by U. M. Hamper and colleagues (W. F. Dahnert, M. H. Hoagland, Y. S. Erozan, J. C. Peirce; Baltimore, MD). Four separate passes were made with 20-gauge needles in random sequence by different operators in each of 133 patients with abdominal disease. Each specimen was evaluated by two cytopathologists for adequacy to render diagnosis and for the presence of cell block material. Biopsies were performed via sonographic or CT guidance. Adequate diagnostic material was equally well obtained by the Franseen, spinal, and Westcott needles without statistically significant differences. Use of the cutting needle resulted in the largest proportion of inadequate specimens. Material sufficient for cell blocks was obtained in 44% of all needle passes, but without significant differences between the four needles. Complications were minimal (hemorrhage, 4; pneumothorax, 1; death due to pancreatic abscess formation after biopsy, 1). The authors conclude that their results do not support the assumption that needles with an elaborate tip configuration render adequate specimens at a higher rate than do simple and less expensive spinal needles.

Early experience related to percutaneous ethanol injection of hepatic neoplasms was presented by S. L. Dawson and coauthors (M. J. Lee, J. T. Ferrucci, P. R. Mueller; Boston, MA). Fourteen image-guided alcohol treatments were performed in three patients who had unresectable hepatic neoplasms (one with hepatocellular carcinoma, two with colorectal metastases). Tumors were judged to be unresectable on the basis of location or because of underlying medical conditions, such as cirrhosis. CT was used for eight sessions, sonography for four sessions, intraoperative sonography was used twice. With the exception of one treatment, all procedures were done on an outpatient basis, and local anesthesia and conscious sedation were used. Absolute alcohol was injected through 22-gauge needles. For CT, contrast material was mixed with the alcohol in a 1 to 10 ratio. Patients were treated with divided doses, and no more than 12 ml was injected at any single session. No significant complications were noted, although one patient developed an asymptomatic small pneumothorax. The patient with hepatocellular carcinoma died of other causes after four sessions; autopsy showed no viable tumor cells. Follow-up studies in one patient with metastases showed interval growth of treated metastases. The remaining patient with metastases had no new lesions and no growth in the four treated lesions, but results of a biopsy of a lesion at 10 months were positive. The authors conclude that further evaluation is required to determine the role of alcohol ablation in metastatic liver lesions.

1992 ARRS Gold Medals

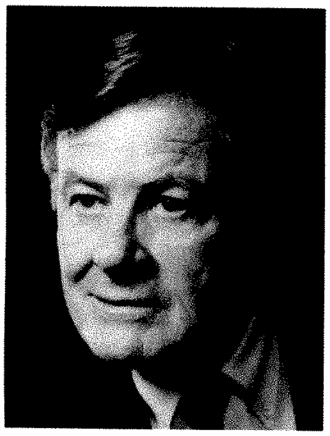

Gerald D. Dodd, Jr.

By bestowing its highest award, the Gold Medal for Distinguished Service to Radiology, upon Gerald D. Dodd, the American Roentgen Ray Society recognizes an individual who, like the society itself, has made outstanding contributions to the enhancement of our specialty and to the quality of care of our patients.

Gerald D. Dodd is a graduate of Jefferson Medical College and completed his radiology residency at Jefferson Medical College Hospital in 1950. He was chief of radiology at the U.S. Air Force Hospital, Mitchell Air Force Base, from 1951 to 1952, and in 1952 returned to Jefferson as assistant radiologist in charge of the residency program. However, in 1955 he left his alma mater to become an associate radiologist at the University of Texas M. D. Anderson Cancer Center and a consultant in radiology to the Hermann Hospital in Houston. In 1961 he returned to Jefferson and along with Albert Jutras and William Hogan was instrumental in developing a remote control fluoroscopic unit, which is still in use at Jefferson. His love of Texas, called again, however, and in 1966 Dr. Dodd became the chairman of the department of diagnostic radiology at the University of Texas M. D. Anderson Cancer Center. He held that position until 1989. In addition, from 1971 to 1974 he was chairman of the department of diagnostic radiology at Hermann Hospital, and has been a professor of radiology at the University of Texas since 1966. During this period Dr. Dodd established the radiology residency program at the University of Texas in Houston. Currently, he maintains his professorship of radiology and holds the Robert D. Moreton Chair in diagnostic radiology.

A prolific writer, Dr. Dodd has published over 100 papers, primarily dealing with the gastrointestinal tract and mammography, three monographs, a book, 12 book chapters, and innumerable editorials concerning both the science and the practice of radiology. He belongs to no less than 19 scientific societies. In each he has been an active participant and in most served in a leadership role. These include, among many others, the American College of Radiology as both chairman of the board and president, the American Roentgen Ray Society as first vice president, and the Texas Radiologic Society as president. He is currently a trustee of the American Board of Radiology and is the immediate past president of the American Cancer Society. These represent just a few of Dr. Dodd's contributions to the organizations associated with our discipline and with medicine in general.

When one looks at his curriculum vitae, the immediate question is, How can he accomplish and be involved in so much? Gerry Dodd does this because he really cares, and because he is willing to give of his time to better our specialty and the health of our patients. He is a warm and easygoing individual who finds saying "no" to his friends an impossibility.

Gerry Dodd could not have accomplished so much without the understanding and support of his wife, Glen, and their seven children. They also share in this honor, which Gerald D. Dodd has so justly earned.

Jerome F. Wiot

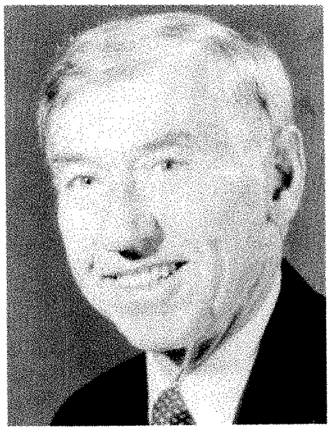

John A. Kirkpatrick, Jr.

John A. Kirkpatrick, Jr., was born in Waynesboro, PA. He graduated from Franklin and Marshall College in 1946 and Temple University School of Medicine in 1949, interned at York Hospital in York, PA, and from 1950–1952 served in the Navy Medical Corps as a lieutenant. In 1952 he entered a residency in radiology at Temple University Hospital, which was followed by a year as a volunteer assistant resident in radiology at Children's Hospital Medical Center in Boston. In 1956 he returned to Temple and to St. Christopher's Hospital for Children, where he remained until 1974, achieving the rank of professor of radiology and professor of pediatrics at Temple. In 1974 he left Philadelphia to take up the duties of professor of radiology at Harvard Medical School and radiologist-in-chief at Children's Hospital in Boston.

Professionally, John has amassed an extraordinary body of work. He has authored and co-authored 107 papers, many of them landmarks in pediatric radiology, 27 book chapters, and the book *Orthopedic Diseases* by Aegeter and Kirkpatrick, which continued successfully through four editions between 1958 and 1975. He has edited the pediatric section of the *Yearbook of Radiology* for many years.

Attesting to his skills as a speaker, he has been honored with 64 visiting professorships in North America, South America, Europe, Asia, and Australia, and has delivered 42 honorary lectures. His many honors and awards include membership in Alpha Omega Alpha, the Charles A. Janeway Award for Excellence in Clinical Teaching at Children's Hospital, and the Gold Medals of the American College of Radiology, the Society for Pediatric Radiology, and the American Roentgen Ray Society. He holds honorary membership in 22 societies, including the Society for Pediatric Radiology, of which he was a founding member. Singular honors were extended in 1991 when September 19 was designated John A. Kirkpatrick, Jr., Day by the mayors of Houston, TX, and Boston, MA. The initial meeting of the Kirkpatrick Society was held in July 1991, with a large complement of attendees. The Founders Medal of the International Skeletal Society was presented to him in September 1991, and he was elected to the Institute of Medicine of the National Academy of Sciences.

In addition to his incredible scholarly accomplishments, John has also found the time to sit on a large number of major committees at both Temple and Harvard universities, serving both the university and the hospital. He has held office in most of the major radiologic societies, served on a number of communities and commissions of the American College of Radiology, and the American Roentgen Ray Society, of which he is the immediate past president. He served as chairman of the Executive Committee of the department of Radiology at Harvard Medical School from 1980 until 1986, thus demonstrating his impressive powers as a negotiator and conciliator.

In 1988 Dr. Kirkpatrick became a member of the Board of Trustees of the American Board of Radiology, the first full-time pediatric radiologist to serve on this board. In this capacity, he has worked to establish a strong and respected section of pediatric radiology and has actively continued to further the growth of this subspecialty.

These phenomenal accomplishments form only a partial portrait of John Kirkpatrick. John and his wife, Jane, are gracious, spontaneous, down-to-earth people who recall the names, faces, personal facts, and family members of their many radiologic colleagues and trainees. They are never too busy to sit down and chat, and never too occupied to listen to a problem or concern. John's reputation as a teacher is legendary. He has a vast and infallible knowledge of radiology, the arts, and philosophy. For his students, who think of him fondly, he has been an inspiration and a source of knowledge. His own successful children are Kirk, Katie, and Ann. His larger family includes all the radiologists he has taught, encouraged, and counseled. In many ways, he has been a father to us all.

Despite his many commitments, John is a stalwart recreational partner. He has traveled widely, enjoys art and music, and is an enthusiastic fisherman and golfer. He has played all the great golf courses of the world and has mastered some of them. When he is in his office or in front of a viewbox, invariably with a smile on his face and a twinkle in his eye, John is always happy to welcome and enlighten the person who enters the room.

The members of the American Roentgen Ray Society present the Gold Medal to John A. Kirkpatrick, Jr., our immediate past president, to thank him for his wit, wisdom, vision, and constructive guidance, which have been so instrumental in our careers and in the development of radiology.

Beverly P. Wood

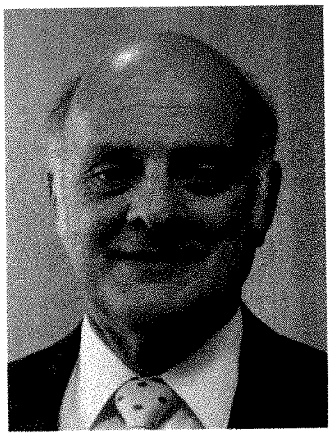

John P. Tampas

John P. Tampas is a distinguished teacher, educator, and leader in American radiology. He has dedicated his professional life to the service of the radiologic community in general, and to the American Roentgen Ray Society in particular.

John was born in Colchester, VT, raised in Vermont, educated in Vermont, took his residency in Vermont, and after short sojourns in Los Angeles and Indianapolis returned to begin a career in academic radiology at the University of Vermont. He has had a life-long interest in pediatric radiology beginning with his service as a teaching fellow at the Los Angeles Children's Hospital, followed by an NIH National Heart Institute-sponsored fellowship in cardiovascular radiology at the University of Indiana Medical Center, where he served with one of this society's recent gold medalists, Dr. Eugene C. Klatte.

Dr. Tampas served as a James Picker Scholar from 1962 until 1965. He began as an assistant professor of radiology at the University of Vermont College of Medicine in 1962, and rocketed through the ranks to become professor and chairman of the department in 1970. John is an outstanding teacher, as evidenced by teaching awards received from the university. He was the recipient of the Teacher of the Year Award in 1968 and 1974, and of the Carl Jefferson Thomas Memorial Award for excellence in teaching in 1969 and 1975. He has made many contributions to the scientific literature, chiefly related to his principal interests in pediatric and cardiovascular radiology.

With all of the above, he has still found the time and energy to devote himself to professional organizations. He was president of the Vermont Radiological Society and has served on the Board of Chancellors and several committees and commissions of the American College of Radiology, of which he was treasurer in 1983–1987 and president in 1987–1988. Dr. Tampas served on the Executive Council of the American Roentgen Ray Society in 1975–1980, and was its chairman in 1979–1980. He served as our president in 1982–1983.

Because of his dedication and ability to work with others, John was selected to be the chairman of the Radiology Centennial, Inc., a collaborative effort of essentially all national radiologic organizations. These efforts will culminate in 1995 with a centennial celebration, a year-long event celebrating a century of progress in radiology and imaging. This celebration will be the centerpiece of the American Roentgen Ray Society's 95th annual meeting in our nation's capital.

John has always brought to all his activities a sense of humor, of joy, and of pleasure that are appreciated and thoroughly enjoyed by all those with whom he comes in contact. He has a great love of music, and is an excellent singer, especially when singing duets with his lovely wife, Kathy. John is a marvelous and tireless dancer at each, every, any, and all occasions.

It is proper and fitting that the American Roentgen Ray Society recognize these outstanding contributions to all of radiology by bestowing its Gold Medal upon this distinguished American radiologist, John P. Tampas, of Burlington, VT.

Lee F. Rogers

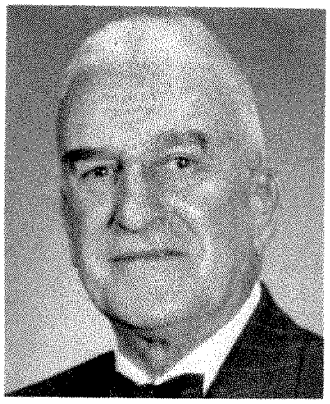

Lauriston S. Taylor

Lauriston S. Taylor, former president of the National Council on Radiation Protection and Measurement, has been a world leader in radiation protection for 65 years.

In 1927, shortly after completing his studies in physics at Stevens Institute of Technology and Cornell, Laurie Taylor joined the National Bureau of Standards as chief of the X-ray group. A year later, at the age of 26, he was involved in the establishment of what was to become the International Commission on Radiologic Protection and was named as one of the two U.S. representatives to the fledgling International Commission on Radiological Units and Measurements. He was associated with both these organizations in positions of leadership for 40 years. In 1929, building on these international initiatives in radiologic standardization and protection, Laurie became the first chairman of the National Committee in Radiation Protection and Measurements, serving in that capacity until 1964, when the committee was awarded a federal charter and became the National Council on Radiation Protection and Measurement. He served as president of the council from 1964 through 1977, when he was succeeded by Warren Sinclair. From 1927 through 1965, with the exception of interludes with the U.S. Army Air Force during World War II and later with the Atomic Energy Commission, Laurie worked at the National Bureau of Standards, leading the X-ray and radioactivity sections; these were ultimately combined into the Atomic and Radiation Physics Division. When he retired in 1965, he was an associate director of the bureau.

As this country's premier spokesman for the cause of radiation standards in measurement and protection, Laurie was called upon by many organizations for service, and has been awarded a host of honors. Among these, he chaired the ARRS Committee on X-ray Standards and Protection from 1932 through 1942 and served as an associate editor of the *American Journal of Roentgenology* for several years beginning in 1930. He received the Sylvanus Thompson Medal of the British Institute of Radiology in 1950, the Gold Medal of the Radiological Society of North America in 1955, the Janeway Medal of the American Radium Society in 1956, and the Gold Medal of the American College of Radiology in 1965. All in all, he has served 37 organizations in a meaningful capacity and received 30 important awards and citations. This degree of call to service and recognition is a measure of a man who, through intelligence, technical knowledge, conviction, and persuasion, has made the safe use of radiation in the service of humankind a reality.

S. James Adelstein

American Roentgen Ray Society:
Officers, Committees, and Membership Information

Officers

President: A. Everette James, Jr.
President-elect: Andrew K. Poznanski
1st Vice-president: George R. Leopold
2nd Vice-president: Ralph J. Alfidi
Secretary: Joseph T. Ferrucci, Jr.
Treasurer: Beverly P. Wood

Executive Council: R. J. Alfidi, R. N. Berk, M. P. Capp, W. J. Casarella, D. O. Davis, N. R. Dunnick, J. T. Ferrucci, Jr., A. E. James, Jr., J. A. Kirkpatrick, Jr., A. M. Landry, Jr., G. R. Leopold, J. E. Madewell, T. C. McLoud, A. A. Moss, A. K. Poznanski, R. J. Stanley, J H Thrall, N. O. Whitley, B. P. Wood, K. H. Vydareny, chair

Committees

Editoral Policy: R. N. Berk, E. Buonocore, M. M. Figley, R. G. Levitt, C. R. B. Merritt, K. Valji, W. J. Casarella, chair

Education and Research: G. M. Glazer, R. R. Hattery, C. B. Higgins, R. J. Stanley, W. M. Thompson, N. O. Whitley, chair

Finance and Budget: D. J. Anderson, R. K. Gedgaudas-McClees, J. E. Madewell, A. A. Moss, J. H. Thrall, chair

Nominating: M. P. Capp, C. A. Rohrmann, Jr., J. E. Madewell, chair

Publication: E. Buonocore, R. G. Levitt, C. R. B. Merritt, W. J. Casarella, chair

Membership: D. O. Davis, J. E. Madewell, T. C. McLoud, A. A. Moss, chair

Representatives to Other Organizations

American Board of Radiology: W. J. Casarella, J. A. Kirkpatrick, Jr., L. F. Rogers

American College of Radiology: J. E. Madewell, B. L. McClennan, R. J. Stanley, N. H. Messinger

American Medical Association: R. A. Gagliardi, delegate; R. G. Evens, alternate; K. L. Kidd, CPT Advisory Committee

American National Standards Institute: M. E. Haskin

National Council on Radiation Protection and Measurements: F. D. Miraldi, E. L. Saenger

Armed Forces Institute of Pathology: J. E. Madewell

Meeting Arrangements

Annual Meetings: April 25–30, 1993, San Francisco Marriott, San Francisco, CA; April 24–29, 1994, New Orleans Hilton, New Orleans, LA

Annual Meeting Committee: J. K. Crowe, N. R. Dunnick, R. R. Lukin, N. H. Messinger, R. J. Stanley, R. D. Steele, Jr., A. M. Landry, Jr., chair

Instructional Courses: B. L. McClennan, associate chair, R. J. Stanley, chair

Scientific Program: P. H. Arger, W. R. Brody, G. D. Fullerton, D. C. Kushner, W. M. Thompson, J. H. Thrall, A. K. Poznanski, chair

Scientific Exhibits: J. R. Haaga, D. S. Hartman, N. R. Dunnick, chair

ARRS Membership

Qualified applicants will be admitted quarterly. Send completed forms to American Roentgen Ray Society, 1891 Preston White Dr., Reston, VA 22091. Active members are graduates of an approved medical or osteopathic school or hold an advanced degree in an allied science. They must practice radiology or work in an associated science in the United States or Canada and be certified by the American Board of Radiology, American Osteopathic Board of Radiology, or Royal College of Physicians of Canada or otherwise adequately document training and credentials. International members are foreign radiologists or scientists who are active in radiology or an allied science. Members-in-training are residents or fellows in radiology or postgraduate students in an allied science. Application forms appear in selected issues of the Journal and can be obtained from the ARRS business office in Reston, VA.

Business Office

Paul R. Fullagar, Executive Director, American Roentgen Ray Society, 1891 Preston White Dr., Reston, VA 22091; (703) 648-8992; 1-800-438-2777.

92nd Annual Meeting of the ARRS: Secretary's Report

Joseph T. Ferrucci[1]

The second highest attendance ever was recorded at the 92nd annual meeting of the American Roentgen Ray Society held in Orlando, FL, at Marriott's Orlando World Center May 10–15, 1992. For nearly 2200 radiologists and their families, the diverse attractions of this popular area provided an enjoyable setting for the meeting. The continuing high turnouts for our annual meeting attest to its wide recognition as a splendid educational opportunity on a totally manageable scale.

The meeting began officially on Monday morning May 10, with the installation of A. Everette James, Jr., of Nashville, TN, as the 92nd president of the oldest radiologic society in North America. In a reflective presidential address, Dr. James analyzed the technologic, fiscal, regulatory, and ethical underpinnings of modern radiologic practice and noted the manner in which these influences are likely to interact in the future. The opening ceremony continued with a series of preselected scientific papers, each of which received a prestigious award. These were as follows: the Roscoe E. Miller Award of the Society of Gastrointestinal Radiology, awarded to Lars Crabo, David Conley, Daniel Graney, and Patrick Freeny for "Venous Drainage of the Pancreatic Head: Contrast-Enhanced CT Appearance"; the Society of Uroradiology Award to Heidi B. Patriquin, Michel Lafortune, Eric Demeule, Ba-Chinh Trinh, Jean-Claude Jequier, Sean O'Regan, Laurent Garel, Julie Landriault, Andre Fontaine, and Denis Filiatrault for "Doppler Sonography of Renal Artery Stenosis: Slowed Systole in the Downstream Circulation"; ARRS Executive Council Award I to Kyle K. Yu, Maythem Saeed, Michael F. Wendland, Michael W. Dae, Sarah Velasquez-Rocha, Nikita Derugin, and Charles B. Higgins for "Quantification of the Area in Jeopardy During Acute Myocardial Ischemia by T1-Enhanced and Magnetic Susceptibility Contrast Media: Comparison with ^{201}Thallium Autoradiography and Histochemical Staining"; ARRS Executive Council Award II to Nina Lundbom for "Determination of Magnetization Transfer Contrast (MTC): An Imaging Study of Brain Tumors"; and the ARRS President's Award to Avery J. Evans, H. Dirk Sostman, Mark K. Knelson, Charles E. Spritzer, Glenn E. Newman, Susan S. Paine, and Craig A. Beam for "A Prospective Comparison of Venography and Magnetic Resonance Imaging in the Detection of Deep Venous Thrombosis in 61 Consecutive Patients." The ARRS Executive Council Award papers carried a prize of $1000. The ARRS President's Award paper received $2000. The presenters of the three ARRS Award papers each received an engraved diploma.

The Scientific Program also began on Monday, having been arranged by Dr. James and the Scientific Program Committee. Two hundred eight scientific papers were presented in 20 separate sessions. The categorical course was on neuroradiology and was directed by Michael S. Huckman, with Derek C. Harwood-Nash and Glenn S. Forbes as co-directors. This was an outstanding course, with nearly 800 radiologists in attendance during a 16-hr program approved for category 1 credit. The syllabus alone was worth the cost of admission, and for those who did not attend, we urge the purchase of the syllabus while copies are still available, as it provides an excellent review of the current status of neuroradiology.

Continued special features of the meeting included a symposium for spouses on osteoporosis, organized by Kay H. Vydareny and attended by over 230 spouses and companions, and a program on research careers in radiology, which was offered to 40 preselected second-year residents from across the country in cooperation with the Radiological Society of North America and the Association of University Radiologists. The radiology residents expressed a high degree of enthusiasm for the approach and content of this program and were appreciative that so many important figures in American radiology were involved in the presentations.

Local arrangements were supervised by Lennard Greenbaum, of Orlando, and the programs were well attended. Day tours to Orlando, Church Street Station, Kennedy Space Center, Historic Winter Park/Park Avenue Shopping, Cypress Gardens, Magic of Ming, Leu Gardens/Jordan's Grove, and Universal Studios drew many eager participants.

The American College of Radiology (ACR) again cosponsored daily luncheons on socioeconomic affairs. Timely and informative topics were presented, including "Government Issues" by Gary Price, ACR Director of Government Relations; "Practice Accreditation" by Robert J. Stanley, chairman of the ACR Commission on Standards and Accreditation; "Current Legal Issues" by Thomas W. Greeson, ACR Legal Counsel; and "An Update on ACR Activities" by James M. Moorefield, chairman of the ACR Board of Chancellors.

The annual ARRS golf tournament was held at the Bay Hill Country Club in nearby Orlando. The tennis tournament was held at the Marriott Tennis Club. The Florida weather pre-

---

[1] Secretary, American Roentgen Ray Society. Department of Radiology, Massachusetts General Hospital, 32 Fruit St., Boston, MA 02114.

AJR 159:661–662, September 1992 0361–803X/92/1593–0661 © American Roentgen Ray Society

sented the participants with a warm sunny day, making an especially pleasant afternoon.

The exhibit space was the third largest ever for an ARRS meeting at 31,500 square feet and was shared by technical and scientific exhibitors. A record 381 applications for scientific exhibits were submitted and 240 were accepted. The number of front-lighted poster exhibits and computer-aided educational workstations continued to increase. Live poster discussions also were held at preselected exhibits each day. The winners of the major awards for exhibits were as follows: the gold medal was awarded to Ji-Bin Liu, D. A. Merton, and B. B. Goldberg for "Endoluminal Ultrasound"; silver medals went to Marvin H. Chasen, C. Charnsangavej, J. S. Dunnington, W. R. Richli, and G. B. Tassin for "Understanding Venous Anatomy of the Thorax: A Fundamental Approach," Fred J. Laine, W. R. K. Smoker, A. J. Kuta, and W. L. Felton III for "Cranial Nerves III, IV and VI: A New 'Look'," and Steven E. Harms, D. P. Flamig, K. L. Hesley, W. P. Evans, and W. B. Pierce for "Fat-Suppressed Three-Dimensional MR Imaging of the Breast."

On Wednesday morning, the awards session highlighted the week-long activities of the annual meeting. Four distinguished recipients were presented with the ARRS Gold Medal for outstanding contributions to radiology; they were Gerald D. Dodd, Jr. (Houston, TX), John A. Kirkpatrick, Jr. (Boston, MA), John P. Tampas (Burlington, VT), and Lauriston S. Taylor (Mitchellville, MD). These men were all cited for their special leadership roles in American radiology and service to the ARRS (see related article).

The Caldwell Lecturer was William J. Casarella, of Atlanta, GA, whose presentation was entitled "Interventional Radiology: The Radiologist as Surgeon." This was a stimulating review of the origins and current achievements of interventional radiologists, emphasizing the special promise and unique challenges to this new subspecialty of radiology.

The Friday morning imaging symposium, which has become one of the most popular segments of the ARRS meeting, was organized as a joint effort with the Society for Pediatric Radiology. The program was directed by William H. McAlister, of St. Louis, who chose the subject "Stat and Urgent Imaging in Pediatrics." This timely session was extraordinarily well received by the roughly 700 individuals attending; a crisply annotated syllabus also was provided.

An additional new feature held on Friday morning was the new issues forum. Three separate presentations on subjects of current controversy were presented, followed by lively discussion with the audience. Topics were "Economic and Political Challenges for Radiologists in the '90s" by Bruce Hillman, "The Interface of MR Imaging and Spectroscopy" by Herbert Y. Kressel, and "PACS: Overview of Clinical Importance and Technical Feasibility" by Hooshang Kangarloo and Samuel Dwyer.

At the final business meeting of the society, the following officers were elected for 1992–1993: President, A. Everette James, Jr. (Nashville, TN); President-Elect, Andrew K. Poznanski (Chicago, IL); First Vice President, George R. Leopold (San Diego, CA); Second Vice President, Ralph J. Alfidi (Cleveland, OH); Secretary, Joseph T. Ferrucci (Boston, MA); Treasurer, Beverly Wood (Los Angeles, CA); Chairman of the Executive Council, Kay H. Vydareny (Atlanta, GA); Publications Committee and Editorial Policy Committee, Robert G. Levitt (St. Louis, MO, 5-year term); Finance and Budget Committee, Dixie J. Anderson (St. Louis, MO, 3-year term); Scientific Exhibits Committee, Laurence Mack (Seattle, WA, 3-year term); Committee on Research and Education, Gary M. Glazer (Palo Alto, CA, 5-year term); and Annual Meeting Committee, Abner M. Landry (New Orleans, LA, 1-year term). David O. Davis, of Washington, DC, also was elected as a member of the Executive Council (5-year term).

At the annual business meeting, a major revision of the bylaws and constitution was adopted, bringing one of the most successful annual meetings of the ARRS to a productive close. Planning has already begun for the 1993 meeting at the new San Francisco Marriott Convention Center, April 25–30, 1993. San Francisco remains among the world's most distinctive cities and invariably rewards a revisit. We invite attendance by members and guests alike.

Mark Your Calendar Now!

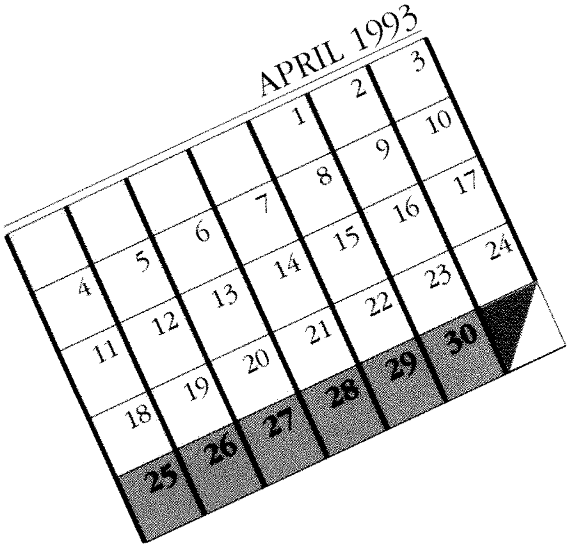

The American Roentgen Ray Society will return to San Francisco in 1993, and plans are already underway for what promises to be an educationally fulfilling and socially enjoyable week in the city by the bay. Look for the San Francisco logo in the next several issues of the *AJR* for updated meeting information.

Call for Papers

Abstracts of papers to be considered for the scientific program must be submitted by November 1, 1992. Abstract forms and instructions for submission are included in the July through October issues. The *AJR* has first rights to all papers accepted for presentation at the ARRS meeting.

Call for Scientific Exhibits

The deadline for submission of abstracts to be considered for scientific exhibits is November 1, 1992. Abstract forms and instructions for submission are included in the July through October issues.

Categorical Course

The topic of the 1993 Categorical Course is Ultrasound. A summary of topics and faculty for this course will appear in the February 1993 issue of the *AJR*.

Refresher Courses

Plans are underway to present at least 60 instructional courses on various topics of interest to the radiology community. A summary of these courses will be included in the February *AJR*. Early registration is strongly suggested, as these courses fill up quickly.

Residents' Award Papers

The society offers three cash awards for the best scientific papers prepared by residents in radiology. The President's Award has a cash prize of $2,000, and there are two Executive Council Awards with a cash prize of $1,000 each. The winners of these three awards are invited to present their papers during the opening ceremonies at the annual meeting. Papers must be submitted by February 12, 1993, for consideration in this competition. Additional information on these awards will be mailed to all residency program directors.

Local Arrangements

The San Francisco area offers many opportunities for sightseeing, shopping and entertainment. Check the February *AJR* for detailed information on local tours developed especially for ARRS meeting attendees.

Registration and Hotel Reservations

All meeting activities will take place in the beautiful new San Francisco Marriott, centrally located on Market Street. The society has negotiated special room rates for meeting attendees, and the February *AJR* will contain meeting registration and hotel reservation forms. As in previous years, early registration is strongly suggested.

Travel

The society will make arrangements with United Airlines and a major car rental firm for preferred rates for meeting attendees. Taking advantage of these special rates benefits both you and the society – you save money on your reservations, and the society receives discounts to send staff and supplies to the meeting. Plan now to check the February issue of the *AJR* for details.

RESIDENTS IN RADIOLOGY AWARDS

The American Roentgen Ray Society
sponsors the
1993 President's Award and the **Executive Council Awards**

RULES AND REGULATIONS

- Papers must be submitted on the clinical application of the discipline of radiology and radiological science.
- The event is open to residents in radiology and radiological sciences. If not the sole author, it is expected that the resident will have performed the majority of the work and be the senior author.
- The submitted manuscript should not exceed 5,000 words and 10 illustrations.
- The winners will be announced by March 16, 1993.
- The papers will be presented at the American Roentgen Ray Society 93rd Annual Scientific Meeting at the San Francisco Marriott, San Francisco, CA, April 25-30, 1993, and be submitted for publication to the *American Journal of Roentgenology*.
- Manuscripts will be returned to candidates not receiving awards.

AWARDS

- The winner of "The President's Award" will be presented a certificate and receive an honorarium of ***$2,000.***
- The two winners of "The Executive Council Award" will each receive a certificate and an honorarium of ***$1,000.***

DEADLINE

- Four copies of the paper and four packages of the illustrations should be submitted no later than **February 12, 1993** to:

Nancy O. Whitley, M.D.
Chairman, Committee on Education & Research
American Roentgen Ray Society
1891 Preston White Drive
Reston, Virginia 22091

ARRS Award-Winning Scientific Exhibits, 1992

More than 225 scientific exhibits were displayed at the ARRS 1992 meeting in Orlando, FL. The Scientific Exhibit Awards Committee selected 10 medal winners and named 40 exhibits for certificates of merit.

Elsewhere in this issue are an application form and instructions for submitting scientific exhibits for the 1993 ARRS meeting in San Francisco, CA, April 25-30.

Gold Medal Exhibit

Endoluminal ultrasound. Liu J-B, Merton DA, Goldberg BB (Philadelphia, PA).

Six and nine French catheters containing either 12.5 or 20 MHz ultrasound transducers have been used to image a variety of nonvascular lumina. Under direct or endoscopic guidance, these catheter-based transducers have been inserted into the urethra, urinary bladder, ureter, renal pelvis, endometrial canal, fallopian tube, bile and pancreatic ducts, esophagus, small bowel, bronchial tree, mediastinum, spinal canal and abdominal cavity. During the past three years over one hundred patients were evaluated using this approach. These studies have shown the feasibility of using these transducer-containing catheters for evaluation of a variety of abnormalities in various nonvascular lumina. The results obtained from both animal and human procedures will be presented.

Silver Medal Exhibits

Understanding venous anatomy of the thorax: a fundamental approach. Chasen MH, Charnsangavej C, Dunnington JS, Richli WR, Tassin GB (Houston, TX).

Radiographic images from 200 patients provide anatomical models for a comprehensive but fundamental approach to understanding venous anatomy of the thorax in normal (including variants) and pathological states.

Anatomic correlations, using multiple imaging modalities (including CT, MRI, and angiography), demonstrate how collateral vascularity in the mediastinum, chest wall, at the thoracoabdominal junction, and within the upper abdomen act in concert to maintain venous stability within the thorax at all times.

Specific topics in this teaching exhibit include:

A. Catheter position and malposition in understanding mediastinal venous anatomy.
B. The azygos-hemiazygos systems in normal and abnormal states (i.e., antegrade versus retrograde flow).
C. The importance of the anterior jugular venous system as a major collateral network.
D. The Internal Mammary-Phrenic-Diaphragm-Liver collateral venous axis in superior vena caval obstruction.

Discussions include venous variants, pathological mimics, and potential pitfalls (e.g. left superior vena cava versus partial anomalous pulmonary venous return). The concept of the "path of least resistance" is stressed throughout as part of a fundamental approach toward understanding how the thoracic venous system "works."

Cranial nerves III, IV, VI: a new "look." Laine FJ, Smoker WRK, Kuta AJ, Felton WL III (Richmond, VA).

Due to CT and MR advances, accurate identification and evaluation of cranial nerve lesions is now possible.

Cranial nerves III, IV, and VI, providing motor and sensory control of the eye, can be evaluated as a unit. In this exhibit we present an overview of the anatomy and pathology of these cranial nerves. We first illustrate their normal anatomic pathways from the brainstem to the orbit. This is followed by clinical examples of patients with a variety of isolated and complex palsies of these three cranial nerves. This is accomplished by inclusion of ocular photographs, correlative imaging studies, and by the use of diagrams.

Knowledge of the gross and imaging anatomy and the ophthalmologic manifestations of pathology affecting these three cranial nerves permits a tailored approach to their evaluation.

Fat-suppressed three-dimensional MR imaging of the breast. Harms SE, Flamig DP, Hesley KL, Evans WP, Pierce WB (Dallas, TX).

A new technique for MR imaging of the breast utilizing a fat suppressed 3D acquisition with Gadolinium administration provides improved contrast and resolution over conventional methods. A series of 56 patients with a spectrum of pathology was imaged with this technique and correlated with mammography and pathology. Results indicate improved sensitivity over mammography in detecting carcinoma. Potential uses include: 1) detection of multifocal disease in lumpectomy candidates, 2) evaluation of patients with a limited mammographic study due to dense breasts or silicone injections and implants and 3) distinction of cancer mimics such as radial scar, postoperative scar or fat necrosis from carcinoma by lack of contrast enhancement in these non-malignant lesions. Fat suppressed 3D MRI is expected to have a role in the diagnosis of breast disease in the future.

Bronze Medal Exhibits

Transjugular intrahepatic portosystemic shunt. Bancroft JW III, Becker G, Katzen B, Bennenatti J, Zemmel G (Miami, FL).

The management of variceal hemorrhage secondary to portal hypertension continues to be a significant challenge. Many forms of therapy have proven useful, however surgical portosystemic shunts are associated with the lowest frequency of rebleeding. The high morbidity and mortality associated with surgical shunting and the lack of demonstrable improvement in long-term survival prompted the search for a safer method of portal decompression. TIPSS (Transjugular Intrahepatic Portosystemic Shunt) offers a new safe and effective treatment of variceal hemorrhage. We will describe the method for creation of the intrahepatic shunt, as well as recent technical advances which decrease the risk associated with TIPSS.

Abdominal manifestations of post transplant lymphoproliferative disorders. Dodd GD III, Ledesma-Medina JJ, Baron RL, Miller WJ, Campbell WL (Pittsburgh, PA).

Post transplant lymphoproliferative disorder (PTLD) occurs in approximately 2% of transplant patients. If untreated it is almost universally fatal. However, most cases detected early and treated have a favorable outcome. In this exhibit we present the imaging spectrum of abdominal PTLD occurring in 44 patients transplanted at our institution. Abdominal CT (32), ultrasound (28), and barium studies (15) detected focal tumor lesions in 18 livers, 3 spleens, 6 kidneys, 1 pancreas, 1 esophagus, 9 stomachs, 11 small bowel, 7 colons, 4 mesenteries, 2 omentums, and in the retroperitoneal nodes of 27 patients. The appearance of the lesions varied depending on the type of organ involved. Overall, abdominal PTLD is an aggressive tumor with a strong propensity for necrosis and ulceration. Extranodal disease is more prominent than seen in other lymphomas. An awareness of the imaging characteristics of abdominal PTLD will aid in early diagnosis.

Using dual x-ray absorptiometry to calculate strength reduction in lytic lesions in cortical bone. Scott WW Jr, Chan B, Kao G, Curtis M, Bhatia D, Beck T (Baltimore, MD).

The decision to prophylactically fix a lytic bone lesion is not a simple decision. While indications exist, information about strength reduction and risk of fracture would greatly assist the process. Dual x-ray absorptiometry (DXA) is a sensitive technique for detecting small bone mineral changes and it provides cross-sectional projectional data from which the following geometric and mechanical parameters may be calculated: cross-sectional area (CSA), cross-sectional moments of inertia ^{1}ap and ^{1}ml), and polar moments (J). Various sized endosteal lesions were surgically created in one bone from each of 12 cadaveric femoral pairs. AP and ML DXA scans were obtained on a Morland X-26. The DXA projection data was then used to calculate CSA, ^{1}ap and ^{1}ml, and J. Using a material testing machine the bones were then tested to failure in torsion. The lesions caused strength reductions between 15–87%, as compared to the contralateral (nonlesion) femur. The DXA calculated strength reductions were highly correlated ($r > 0.85$) to the physically measured reductions. Therefore, we believe that orthogonal DXA scans are an accurate method of predicting actual strength reductions in cortical lytic lesions.

Acquired cystic spaces of the lung: a reappraisal of pathogenesis. Kuhlman JE, Reeves B, Hruban RH, Askin FB, Fishman EK, Siegelman SS (Baltimore, MD).

Rounded, air-filled structures within the lung are produced by a variety of different cystic spaces: blebs, bullae, cavities, pneumatoceles and dilated bronchi. Theories of morphogenesis for these various entities are reappraised based on CT findings and CT pathologic correlation of 300 inflated-fixed lungs. Five categories of acquired cystic disease are identified: 1) air-spaces due to ischemic necrosis 2) air-spaces created by retractile fibrosis 4) cystic spaces due to bronchiectasis or airway obstruction and 5) cystic lung disease due to multifactorial causes.

Advanced MRI of the pancreas. Kenney PJ, Morgan DE, Rominger NB, Listinsky JJ (Birmingham, AL).

Purpose: MRI of the pancreas has been improved by recent advances including techniques for reduction of respiratory and flow artifacts, intravenous and oral contrast agents and fat saturation. This exhibit reviews these advances in normal volunteers and patients with pancreatic disease.

Material: Fourteen normal volunteers were scanned at 1.5T with T1. proton density and T2 weighted spin echo (SE) and gradient recalled echo (SPGR45) sequences without and with fat suppression, oral contrast (Kaopectate) and intravenous contrast (GD-DTPA) to test the value of these in visualizing the pancreas. Respiratory compensation was used with SE scans and breath-holding with SPGR scans. Advantages and disadvantages of different methods are displayed. Pancreas visualization was significantly improved by Kaopectate on all sequences and by fat saturation on multiecho and SPGR sequences.

Twenty patients with suspected pancreatic masses were then examined with both MRI and CT. Final diagnosis was based on biopsy (8), surgery (5) or follow-up (6–18 months). Ten had pancreatic carcinoma, 6 other tumors, 3 pancreatitis, and 1 normal. MRI was more accurate than CT for detection and diagnosis of pancreatic tumor and equivalent in staging. MRI detected more liver metastases but CT detected more nodal disease. The combination of T1, SE, T2 FATSAT and post GD-DTPA SPGR most often clearly showed (or excluded) presence of a mass with different image characteristic compared to normal pancreas.

Conclusion: MRI of the pancreas incorporating recent advances is competitive with CT for diagnosis and staging of pancreatic neoplasm.

Neuroblastoma: usual and unusual radiologic manifestations. Day DL, Engeler CM, Carpenter BM (Minneapolis, MN).

Neuroblastoma is the most common extracranial solid tumor occurring in young children. It typically presents as a solid, calcified upper abdominal or posterior mediastinal mass. Neuroblastoma commonly spreads to adjacent nodes, grows into the spinal canal and metastasizes to the liver and bone. We will present examples of these typical findings and will also present some unusual manifestations of neuroblastoma we have encountered, including cystic neuroblastoma, IVC tumor thrombus, bilateral adrenal neuroblastomas, and intraventricular and dural metastases.

Certificate of Merit Exhibits

MR imaging of clival and paraclival lesions. Van Vleet RH, Guinto FC Jr, Crow WN, Kumar R (Galveston, TX).

Dark T2 neuropathology. Engel MR, Forbes GS, Okazaki H (Rochester, MN).

Radiologic findings in pulmonary aspergillosis. Leach JL (Cincinnati, OH).

CT findings in intestinal ischemia. Perez CM, Llauger JR, Pallardo Y, Sanchis E, Traid C (Barcelona, Spain).

CT during arterial portography: gamut of perfusion abnormalities. Nelson RC, Thompson GH, Chezmar JL, Harned RK Jr, Fernandez MP (Atlanta, GA).

Color Doppler of the scrotum: advantages compared to gray scale sonography. Muchow AM, Jafri SZH, Madrazo BL, Cacciarelli AA, Mills RA (Royal Oak, MI).

Persistent CT nephrogram: correlation with renal insufficiency. Love L, Johnson MS, Nelson JE, Olson MC, Bresler ME (Maywood, IL).

Imaging of en bloc cadaveric renal transplants in adults: normal anatomy and posttransplant complications. Memel DS, Dodd GD, Shaw A, Jordan ML, Shapiro R, Zajko A, Hakala TR (Pittsburgh, PA).

T1-weighted snapshot GRASS MR imaging of hepatic tumors: clinical evaluation. Campeau NG, Johnson CD, Riederer SJ, Bampton AE (Rochester, MN).

CT anatomy of the female pelvis: a second look. Foshager MC, Walsh JW, Anderson EM (Minneapolis, MN).

The many faces of hepatic fatty infiltration. Lantz EJ, Charboneau JW, Stephens DH (Rochester, MN).

Sonographic findings in patients with AIDS. Weingarten BJ, McKinley MG, Kellman GM (Detroit, MI).

CT and US guided FNA of renal masses. Miller JH, Jafri SH, Bernacki EG, Roberts JL, Madrazo BL (Royal Oak, MI).

The spectrum and natural history of multicystic dysplastic kidneys. Strife JL, Souza AS, Kirks DR, Bellard ET, Gelfand MJ, Wacksman J (Cincinnati, OH).

Pitfalls encountered during MR imaging of the knee. Conway WF, Hayes CW, Wirth BA, Blinder RA, Totty WG (Richmond, VA).

Pipkin fractures of the hip. Coumas JM, Marchetti M, Kelly JJ, Steinberg GG, Waite RJ (Worcester, MA).

MRI, CT-arthrography and surgical correlation of glenoid labral tears. Waite RJ, Coumas JM, Ferrari DA, Goss TP, Pappas AM (Worcester, MA).

Percutaneous placement of portocaval shunts utilizing the needle guide system. Kerns SR, Hawkin IF Jr, Akins EW, Murray KK, Garidi JG (Gainesville, FL).

Gallium staging in metastatic melanoma. Miketic LM, Brown M, Kirkwood J (Pittsburgh, PA).

Magnetic resonance imaging of Klippel-Trenaunay syndrome. Chiang KS, Stanson AW, Johnson CM, Ehman RL, Gloviczki P (Rochester, MN).

The spectrum of imaging of thromboembolic vascular disease associated with antiphospholipid antibodies. Stanson AW, Bacharach JM, Lie JT (Rochester, MN).

Computed radiographic imaging for pediatric gastrointestinal examinations. Lee KR, Harrison LA, Insana MF, Cook LT, Harvey PC, McFadden MA (Kansas City, KS).

The radiology of large neck masses. Reginella RF, Mahraj RP, Boal DKB (Hershey, PA).

Artifacts in thoracic MRI: how to recognize and avoid them. Vellet AD, Munk PL, Muller NL, Mayo JR, Levin MF (London, Ont., Canada).

Intra-abdominal hernias. Raider L, Lushington JA Jr, Brogdon BG (Mobile, AL).

Transjubular intra-hepatic porto-caval shunts (ICPS): preliminary results. Maquin P, Rousseau H, Vinel JP, Pascal JP, Joffre F, Railhac JJ (Toulouse, France).

Heterotopic gastric mucosa (HGM) in the duodenal bulb: morphological classification and differential diagnosis. Kawamoto K, Motooka M, Hirata N, Masuda K, Ueyama T (Fukuoka, Japan).

MR Imaging of hepatocellular carcinoma: effect of intra and extratumoral metallic content on signal intensity. Honda H, Onitsuka H, Kanazawa Y, Murakami J, Kaneko K (Fukuoka, Japan).

Radiology of CAPD (continuous ambulatory peritoneal dialysis). Saigh JA, Imray TJ, Leiberman R, Ochner J (Omaha, NE).

Appearance of the kidneys, liver, and spleen in paroxysmal nocturnal hemoglobinuria by magnetic resonance imaging. Robidoux MA, Weber TM, Dunnick NR (Durham, NC).

Renal streak artifact during contrast enhanced abdominal CT: a comparison of low osmolality versus high osmolality contrast. Sussman SK, Illescas FF, Opalacz JP, Turner G, Yirga P, Foley LC (Hartford, CT).

Transvaginal and transabdominal color Doppler sonography of ovarian masses: correlation with gross and microscopic pathology. Fleischer AC, Kepple DM, Rodgers WH, Williams LL, Jones HW III (Nashville, TN).

How to perform a bad mammography in 1992. Cambier L, Kamus E, Rocourt N (Lille, France).

High resolution CT of surgical breast specimen. Raptopoulos V, Baum J, Hochman M, Karellas A, Houlihan MJ, D'Orsi CJ (Boston, MA).

Grading brain tumors by amino acid PET imaging and dynamic modeling. Hubner KF, Thie JA, Stephens TS, Smith GT, Buonocore E (Knoxville, TN).

Incidence of ocontoid hypoplasia and atlantoaxial subluxation in Hurler syndrome. Carpenter BLM, Premer D, Belani KG, Day DL (Minneapolis, MN).

Tuberculosis in childhood. Wood BP, Parisi MT, Jensen MC, Chandler ND (Los Angeles, CA).

Bone scan abnormalities following bone marrow harvest in childhood neuroblastoma. Ortiz SS, Miller JH, Seeger R, Villablanca J (Los Angeles, CA).

Paget's disease: uncommon presentations. Moore TE, Kathol MH, El-Khoury GY, Walker CW (Iowa City, IA).

Radiologic evaluation of renal masses: a computer-based teaching program. Rabushka LS, Goldman SM, Fishman EK, Hennessey JG, Nixon MS (Baltimore, MD).

American Roentgen Ray Society New Members

At the 1992 annual meeting of the American Roentgen Ray Society (ARRS) in Orlando, 392 applicants were elected to active membership and 33 to international membership. Four hundred seventy applicants were added to in-training membership during the year preceding the 1992 annual meeting.

Active members of the society must be graduates in good standing of an approved medical or osteopathic school or hold an advanced degree in one of the physical, chemical, or biologic sciences. They must be board certified, active in radiology or one of its branches in the United States or Canada, and sponsored by two ARRS members.

Members-in-training are physicians in a radiology residency or in a postresidency fellowship program.

International members are physicians residing in foreign countries who are active in the science of radiology or allied sciences.

An application form is printed elsewhere in this issue or may be obtained by writing: Paul Fullagar, Executive Director, American Roentgen Ray Society, 1891 Preston White Dr., Reston, VA 22091.

Active Members

David C. Abdullah, Jacksonville, FL
Michael M. Abiri, New York, NY
Ramon D. Acosta, Mayaguez, PR
Ehsan Afshani, Williamsville, NY
Bibb Allen, Jr., Birmingham, AL
Richard A. Amato, Lynn, MA
James P. Antony, Stillwell, KS
John E. Aruny, Arlington, MA
Anh Hong Au, Van Nuys, CA
John F. AufderHeide, Oshkosh, WI
Martin Auster, Baltimore, MD
Jack C. Avalos, Westlake, OH
Behrooz Azar-Kia, Maywood, IL
David B. Bach, London, ON, Canada
Jinan O. Bahia, Harrisburg, PA
Joseph M. Bailey, Montgomery, AL
Martin K. Baker, Zionsville, IN
Amitabha Banerjee, Mississauga, ON, Canada
Arlene B. Baratz, Pittsburgh, PA
Anthony J. Barkovich, San Francisco, CA
Phillip D. Barrett, Peoria, IL
Lawrence L. Bauer, Neenah, WI
John J. Beasley, Mayfield, KY
Joseph B. Bellissimo, Harrisburg, PA
Steven R. Berg, Bridgewater, NJ
Michael A. Bettmann, Boston, MA
Christian Blais, Sherbrooke, PQ, Canada
Carl E. Blunck, III, Hammond, LA
Carol Mae Bosanko, Southfield, MI
Stephen John Brenza, Lancaster, PA
James A. Brink, St. Louis, MO
Garry M. Brown Jr., Alamogordo, NM
Thomas L. Brown, Gulf Breeze, FL
Sharon E. Byrd, Chicago, IL
James G. Caridi, Leesburg, FL
Craig M. Carpenter, Salt Lake City, UT
John Kent Chin, Winchester, MA
Haesun Choi, Houston, TX
Joseph Ciotola, Hazelton, PA
Jeffrey A. Cooper, Albany, NY
Hector L. Correa, New City, NY
Joel I. Cossrow, Pittsburgh, PA
Thomas E. Costello, Las Vegas, NV
Bret Francis Coughlin, Springfield, MA
James M. Coumas, Worcester, MA
Thomas J. Cusack, Peoria, IL
Jacob Cynamon, Suffern, NY
Barbara C. Dangman, Providence, RI
Robert H. Darwin, Columbus, OH
Robert L. Davies, Decatur, GA
Lori Ann Deitte, Johnson City, TN
Peter J. Dempsey, Birmingham, AL
Edward G. Denstman, Tolland, CT
Morris A. Diamant, Lexington, MA
Gerald D. Dodd III, Pittsburgh, PA
Steven Don, Indianapolis, IN
Anthony James Doyle, Salt Lake City, UT
Kika M. Dudiak, Rochester, MN
George S. Durisek, Loysville, PA
Edward J. Duszlak, Jr., Burlington, NC
Stephen H. Eccher, Waterville, ME
Frank M. Eggers, Memphis, TN
Allen D. Elster, Winston-Salem, NC
Fakhreddin Entezary, Cumberland, RI
Fraydoon Esfahani, Welch, WV
Eli A. Etscovitz, Newton Center, MA
Daniel W. Eurman, Grosse Pointe Farms, MI
Timothy Earl Farley, San Antonio, TX
Robert M. Faulk, Omaha, NE
Harry Feuerberg, El Paso, TX
David E. Finlay, St. Louis Park, MN
Steven W. Fitzgerald, Highland Park, IL
Michael E. Flisak, Oak Lawn, IL
Kiah T. Ford, III, Lynchburg, VA
Robert S. Francis, Nashville, TN
Rita Irene Freimanis, Winston-Salem, NC
Milton A. Friedlander, Camp Hill, PA
David Paul Friedman, Philadelphia, PA
William N. Friedman, New Haven, CT
Kee-Bun Fung, Houston, TX
Charles F. Garvin, St. Louis, MO
Hal N. Ginsberg, Randolph, NJ
Mark John Girard, Charlestown, MA
Leonard M. Glassman, Washington, DC
Lucille W. Glenn, Seattle, WA
Lawrence W. Glorioso, III, Metairie, LA
William S. Goell, Milwaukee, WI
Mahendra N. Gohil, Galveston, TX
David H. Gordon, Great Neck, NY
Edward G. Grant, Los Angeles, CA
Michael G. Gutknecht, El Paso, TX
Laurie Lynn Gutstein, Towson, MD
Harry K. Hajedemos, Cheshire, CT
Gerald T. Hanley, Oaklawn, IL
Sterling A. Harris, Jr., Athens, GA
Cosmo L. Haun, Gainesville, GA
Harvey L. Hecht, Stamford, CT
Sally Deborah Herschorn, Burlington, VT
Eric K. Hoffer, San Diego, CA
John H. Hooker, Alton, IL
Ross A. Horsley, Bradford, PA
Murray Howe, Toledo, OH
Kevin C. Hyer, Las Vegas, NV
Jill E. Jacobs, Wynnewood, PA
Jerome G. Jacobstein, Philadelphia, PA
Caren Jahre, New York, NY
Marcia C. Javitt, Washington, DC
Christopher M. Johns, Pittsburgh, PA
Daniel H. Johnson, Jr., Metairie, LA
Peter M. Jokich, Hinsdale, IL
Nolan J. Kagetsu, New York, NY
Emanuel Kanal, Pittsburgh, PA
Ira E. Kanter, Oakland, CA
Lee M. Katims, Boca Raton, FL
Gerald R. Keenan, Woodbury, NJ
Andrew S. Kerr, New York, NY
Mark D. Kettler, Portland, OR
Ducksoo Kim, Dover, MA
Carolyn M. Kimme-Smith, Los Angeles, CA
Bernadette King, Knoxville, TN
Stephen Victor Klein, Longmeadow, MA
Mark Henry Knelson, Durham, NC
Harry H. Ko, Mayfield Heights, OH
Daniel S. Krop, Clearwater, FL
David F. Lackner, Gibsonia, PA
Paul P. Lamarre, St. Jerome, PQ, Canada
Fred Lee, Jr., Madison, WI
Susanna Ming-Kim Lee, Winchester, MA
Morton H. Leonard, Jr., Galveston, TX
Jack Levenbrown, Lawrence, NY
Michael S. Levey, Columbus, OH
Richard M. Levey, Hudson, WI
Robert G. Levitt, St. Louis, MO
James M. Lieberman, Beachwood, OH
Robert T. Liscio, Hollis, NH
John P. Locksmith, Augusta, GA
Mark J. Lodespoto, Valley Stream, NY
Eric H. Loevinger, Tallahassee, FL
Richard Wilkins Lucio, II, Belleville, IL
William A. Lynch, Hartford, CT
Donald G. Majeste, Shreveport, LA
Dermot E. Malone, Hamilton, ON, Canada
Zachary B. Martin, Jr., Daytona Beach, FL
Susan B. Maurer, West Des Moines, IA
Constance Kiesler Maves, Columbia, SC
Barry M. McCook, Jacksonville, FL
Jack E. Meyer, Boston, MA
James S. Meyer, Philadelphia, PA
Moulay A. Meziane, Cleveland, OH
Michael A. Mikhael, Evanston, IL
Howard M. Miller, Morganville, NJ
Robert David Mintz, Gastonia, NC
Sasikala Mohan, Englewood, NJ
Doreen Moreira, Pelham, NY
Jeffrey S. Moulton, Englewood, CO
Michael T. Nelson, Edina, MN
Thomas Mark Niedbala, Philadelphia, PA

AJR 159:668, September 1992 0361-803X/92/1593-0668 © American Roentgen Ray Society

William H. Noble, III, Mansfield, OH
Maer B. Ozonoff, Newington, CT
William Ewing Palmer, Boston, MA
Harshad R. Patel, Williamsport, PA
Richard H. Patt, Washington, DC
Norman W. Patterson, Loudonville, NY
Rebecca G. Pennell, Lancaster, PA
Perry G. Pernicano, Ann Arbor, MI
Nicholas J. Pernice, Portland, OR
Robert S. Perret, Milwaukee, WI
Donald R. Peters, Mukilteo, WA
Mark S. Peterson, Pittsburgh, PA
David E. Phillips, Bay City, MI
Branko Plavsic, New Orleans, LA
Gerald D. Pond, Tucson, AZ
Thomas A. Powers, Nashville, TN
David Printz, Westfield, NJ
Winston S. Ramsewak, Windsor, ON, Canada
Althuru S. Reddy, Oak Brook, IL
Eashwer K. Reddy, Kansas City, KS
Martin H. Reed, Winnipeg, MB, Canada
Riley J. Reed, Eunice, LA
Laghaieh L. Rezvani, Sikeston, MO
Jerrold Reid Robins, Brookline, MA
Edward J. Robinson, Marblehead, MA
Peter M. Ronai, Salem, OR
Melissa L. Rosado-de-Christenson, Washington, DC
Edward M. Rosenblatt, Glastonbury, CT
Charles M. Rosenthal, Barrington, RI
Marilyn A. Roubidoux, Durham, NC
Glenn Allen Rouse, Loma Linda, CA
Kenneth S. Rugh, San Antonio, TX
Peter B. Sachs, University Heights, OH
Hans P. E. Sachse, Portsmouth, VA
D. Skip Sallee, Durham, NC
Eric S. Scharling, Lewisville, NC
Rovert Scharstein, Hendersonville, NC
Donald S. Schauwecker, Carmel, IN
Edward J. Schulte, Palm Desert, CA
Elizabeth Schultz, New York, NY
James A. Schuster, Rochester, NY
Francis H. Scola, Barrington, RI
William W. Scott, Jr., Baltimore, MD
Kitt Shaffer, Cambridge, MA
Chunilal P. Shah, Tampa, FL
Catherine M. Shannon, Barrington, RI
Jon D. Shanser, Mill Valley, CA
Alfred D. Shaplin, Ballwin, MO
Douglas J. Sheft, Tiburon, CA
Edward Q. Shepherd, St. George, UT
Robert Sherrier, Durham, NC
Michael A. Siegel, Portland, OR
Stuart George Silverman, Boston, MA
Martin E. Simons, Islington, ON, Canada
Rajinder P. Singh, Nashville, TN
Roy J. Siragusa, Ormond Beach, FL
Aivars Slucis, Albert Lea, MN
Stanley R. Smith, Midland, MI
Henry Dirk Sostman, Durham, NC
Howard L. Spector, Mountain Top, PA
Edgar C. Stambuk, Fullerton, CA
Elizabeth R. Stamm, Denver, CO
Marjorie W. Stein, Manhasset Hills, NY
Robert G. Stern, Philadelphia, PA
Susan Kathryn Stevens, Burlingame, CA
Paul C. Stomper, Buffalo, NY
Bradley C. Sutfflebam, Centralia, IL
Richard J. Sukov, Inglewood, CA
Billy L. Sullivan, Columbus, MS
James P. Sweeney, Colorado Springs, CO
Kenneth Earl Symington, Albuquerque, NM
Bing Tai, East Lansing, MI
Andrew J. Taylor, Milwaukee, WI
Joel Edward Tennenhouse, Thornhill, ON, Canada
M. Kristin Thorsen, Wauwatosa, WI
Jeffrey D. Towers, Pittsburgh, PA
Stanford B. Trachtenberg, Inglewood, CA
David W. Trost, New York, NY
Eugene W. Tryciecky, East Lansing, MI
Michael Vermess, Tampa, FL
Thomas M. Vesely, St. Louis, MO
Jan K. Walecki, Washington, DC
Austin Wand, Forest Hills, NY
Gerald D. Wareham, Harker Heights, TX
James W. Warren, Harrisburg, PA
Scott Alan Weaver, San Francisco, CA
Alvin J. Weber, III, Memphis, TN
Karen J. Weiss, Chicago, IL
Colin J. Wells, Seattle, WA
Sjirk Jan Westra, Los Angeles, CA
Charles Stephen White, Baltimore, MD
Debra A. Wiedmeyer, Milwaukee, WI
Claire B. Wilcox, Durham, NC
Chad R. Williams, Grand Rapids, MI
John Alan Willis, Charleston, WV
David C. Wymer, Beachwood, OH
Daniel B. Yang, Tallahassee, FL
Mark T. Yoshino, Tucson, AZ
Antoinette C. Zaepfel, Rochester, NY

Active Members (Formerly In-Training)

Nathaniel E. Adamson, Alameda, CA
Richard N. Aizpuru, Litchfield, CT
Wallace Mitchell Anderson, Tinley Park, IL
Daniel Aronson, Columbia, MD
Harold Michael Augenstein, Roslyn, NY
Sam Thomas Auringer, Winston-Salem, NC
David M. Ayoub, Springfield, IL
Zubin N. Balsara, Chula Vista, CA
Kaye Porter Barefield, Decatur, GA
Bradley P. Barnes, Lakeland, FL
Penni A. Barrett, Tulsa, OK
Eyal Barzel, Merion, PA
Susan M. Bates, Cambridge, MA
Charles Eldon Bea, Mayfield, KY
Daniel P. Berman, Groton, MA
Kostaki G. Bis, West Bloomfield, MI
Joseph A. Borrello, St. Louis, MO
Richard M. Braverman, Houston, TX
David Andrew Brink, Chesapeake, VA
Thomas S. Chang, Pittsburgh, PA
Philip W. Chao, Newark, DE
Ram P. Chaturvedi, McAllen, TX
Peter P. Chow, San Marino, CA
Steven J. Citron, Dunwoody, GA
Kathy S. Clark, Carmel, IN
Peter J. Clive, Moncton, NB, Canada
Clare A. Colombo, Rio Rancho, NM
Frederick W. Coop, Moncton, NB, Canada
Douglas P. Cutillo, Chatham, NJ
Lawrence D. Dalan, St. Louis, MO
David J. Davis, Camp Pendleton, CA
William Taylor Deeter, III, Richmond, VA
Andrea L. Desberg, Lyndhurst, OH
Francis Donahue, Miami, FL
Angela M. Fanizza-Orphanos, Fort Wayne, IN
Charles C. Ferris, Savannah, GA
Saul Finck, Irvine, CA
Ronald Mark Fletcher, Steilacoom, WA
Mary C. Frates, Sharon, MA
Ann Simpson Fulcher, Upper Marlboro, MD
Bertrand L. Gallet, Eustis, FL
Danny J. Garmer, Fort Worth, TX
Amilcare Gentili, Cleveland Heights, OH
Ari Reuben Geselowitz, State College, PA
David O. Griffith, APO AE, TX
Robert Curtice Guay, Jr., Wyomissing, PA
Ethan Joseph Halpern, Merion, PA
Polly Boren Hansen, San Antonio, TX
Ben Hugh Harmon, Carmel, IN
Linda Ann Harrison, Kansas City, KS
Ellen M. Hauptmann, Seattle, WA
Elizabeth A. Hingsbergen, Richmond, VA
Jay Glenn Hochsztein, Bergenfield, NJ
Lowrey H. Holthaus, Richmond, VA
Dean Michael Hountras, Grand Forks, ND
David L. Iles, Saint John, NB, Canada
James D. Ingram, Denver, CO
Terri Lynn Ingram, Denver, CO
Amal Adib Jabra, Catonsville, MD
Kendall Maurice Jones, Brookline, MA
Charles E. Kahn, Jr., Whitefish Bay, WI
Sheldon B. Kaplan, Ocean, NJ
Stewart Brian Karr, Washington, DC
John A. Kaufman, Lexington, MA
Mark A. Kleiwer, Durham, NC
Scott Roberts Koch, Louisville, KY
Thorsten L. Krebs, Los Angeles, CA
Mitchell P. Laks, Flushing, NY
Patrick Jerome Lanigan, Bethesda, MD
Andrew L. Laurel, APO AE, NY
Christopher F. Lawrence, Harahan, LA
David P. Lawrence, Bethesda, MD
Michael J. Lee, Boston, MA
Shlomo Leibowich, Boca Raton, FL
James S. Littman, Solon, OH
Thomas H. Magee, Bethesda, MD
Suzanne T. Mastin, Gainesville, FL
James Stephen McEvoy, Middletown, OH
William J. McGroarty, Haddonfield, NJ
Mary S. McKee, Columbia, TN
Michael Brian Miller, Philadelphia, PA
Robert M. Milman, Austin, TX
Tommy W. Mooncai, Taunton, MA
Helen R. Nadel, Vancouver, BC, Canada
Patrick Arthur Nelson, Fargo, ND
Cheng Hoon Ow, Westfield, NJ
Timothy Len Pannell, Dalzell, SC
Parag U. Parikh, Toledo, OH
Jehangir Jal Patel, Longmeadow, MA
James N. Place, Portland, ME
Leonard Scott Poirier, Napa, CA
Mark James Popovich, Tiburon, CA
April Ames Preston, Winston-Salem, NC
Charles I. Price, Ann Arbor, MI
Myra I. Rapoport, Chicago, IL
Bruce Ian Reiner, Clearfield, PA
Richard Renslo, Rancho Palos Verdes, CA
Mariela Resendes, Clovis, CA
Sandra Lea Ridings-Hesser, Tulsa, OK
Thomas Richard Rimer, Ooltewah, TN
John Rizzi, Salt Lake City, UT
Richard James Rolfes, Cincinnati, OH
William Joseph Romano, Berkley, MI
Werner Rosshirt, Bristol, CT
Richard D. Rossin, O'Fallon, IL
Michael Ian Rothman, Baltimore, MD
Gigi Blum Schemankewitz, Stone Mountain, GA
Michael Ross Schiering, Gainesville, FL
Richard C. Semelka, Winnipeg, MB, Canada
Manjul Shah, Palmdale, CA
Robin B. Shermis, Toledo, OH
Jeffrey M. Shulak, Detroit, MI
Paul B. Shyn, Fort Worth, TX
Jeffrey Michael Silverman, Woodland Hills, CA
Ruth Darr Snow, Mobile, AL
Steven John Souza, Santa Rosa, CA
Ronald A. Sparschu, Warren, MI
David Alan Staunton, Salinas, CA
Troy Farr Storey, Biloxi, MS
Pamela L. Strange, Smyrna, GA
Gary S. Sudakoff, Rensselaer, NY
Richard R. Sullivan, Pasadena, CA
Gerard Bennett Tassin, Houston, TX
Thomas Neil Thompson, Pittsford, NY
Robert L. Tyrrell, II, Springboro, OH
Lynne Voustinas, Brooklyn, NY
Craig W. Walker, Omaha, NE
Barbara Joyce Ward, Edmonton, AB, Canada
Lewis P. Warren, Jr., Wilmington, NC
Arthur S. Watanabe, Bremerton, WA
Tommy L. Weaver, Baton Rouge, LA
Therese M. Weber, Durham, NC
Gary Jacob Whitman, Boston, MA
Camelia G. Whitten, Iowa City, IA
James Jay Yaquinto, Arlington, TX
Henry Robert Zayas, Jensen Beach, FL

International Members

Johannes C. Aarts, Diepenveen, The Netherlands
Soichi Akata, Tokyo, Japan
Wolfgang Auffermann, Berlin, Germany
Mehrdad Bakhshayesh, Yazd, Iran
Roland C. Bittner, Berlin, Germany
Fernando E. Carrillo, Guatemala, Guatemala
Mario Alessandro, Cornali, Massa, Italy
Pilar Santaliestra Coscojuela, Barcelona, Spain
Dariush Etemadi, Tehran, Iran
Farivar Hashemi, Saveh, Iran
Tsutomu Hashimoto, Hyogo, Japan
Hae-Jeong Jeon, Seoul, Korea
Prasanta K. Karak, New Delhi, India
Apostolos H. Karantanas, Larissa, Greece
Il Young Kim, Chunan, Korea
Dong Ho Lee, Seoul, Korea
Sang Kil Lee, Seoul, Korea
Gin-Chung Liu, Kaohsiung, Taiwan
Pierre Maquin, Tournefeville, France
Fritz Mosshammer, Salzburg, Austria
Simon J. Ostlerg, Oxfordshire, England
Sang Kyu Park, Kang Won Do, Korea
Klaus C. Seelos, Bonn, Germany
Henri E. Schutte, Rotterdam, The Netherlands
Tiffany T. Shih, Taiwan, China
Kyung J. Suh, Taegu, Korea
Ilkka Suramo, Olku, Finland
Isabel Maria Tavora, Lisboa, Portugal
Siegfried A. Thurnher, Wien, Austria
Helmut Umek, Vienna, Austria
Ding-Kwo Wu, Taiwan, China
Itaru Yamamoto, Ishikawa, Japan
Seoung-Oh Yang, Pusan, Korea

Forthcoming Articles

CARDIOPULMONARY RADIOLOGY

MR imaging of the lungs: value of short TE spin-echo pulse sequences. *Mayo JR, MacKay A, Müller NL*

Diagnostic and therapeutic use of chest sonography: value in critically ill patients. *Yu C-J, Yang P-C, Chang D-B, Luh K-T*

Case report. Primary pulmonary artery sarcoma: diagnosis using CT, MR, and transthoracic needle biopsy. *Bressler EL, Nelson JM*

Case report. Limited thoracic periaortic lymphoma mimicking aortic dissection. *Kazerooni EA, Williams DM, Deeb GM*

Case report. Development and resolution of systemic and coronary artery aneurysms in Kawasaki disease. *Yacoe ME, Dake MD*

BREAST RADIOLOGY

Ruptured gel-filled silicone breast implants: sonographic findings in 19 cases. *Rosculet KA, Ikeda DM, Forrest ME, et al*

GASTROINTESTINAL RADIOLOGY

Review. CT of portal venous occlusion. *Marn CS, Francis IR*

Detection of malignant tumors in end-stage cirrhotic livers: efficacy of sonography as a screening technique. *Dodd GD III, Miller WJ, Baron RL, Skolnick ML, Campbell WL*

Differential diagnosis of hepatic tumors (hepatoma, hemangioma, and metastasis) with CT: value of two-phase incremental imaging. *Honda H, Matsuura Y, Onitsuka H, et al*

Influence of preoperative imaging on surgical planning in patients with hepatic metastases from colonic carcinoma: evaluation of CT portography vs sonography and dynamic CT. *Soyer P, Levesque M, Elias D, Zeitoun G, Roche A*

CT arterial portography: causes of technical failure and variable liver enhancement. *Paulson EK, Baker ME, Hilleren DJ, et al*

Stent placement for benign pancreatic diseases: correlation between ERCP findings and clinical response. *Gulliver DJ, Edmunds S, Baker ME, et al*

Complications of continuous ambulatory peritoneal dialysis: evaluation with CT peritoneography. *Hollett MD, Marn CS, Ellis JH, Francis IR, Swartz RD*

Pictorial essay. Regional lymph node metastases in carcinoma of the left side of the colon and rectum: CT demonstration. *Granfield CAJ, Charnsangavej C, Dubrow RA, et al*

Case report. Intraluminal esophageal diverticulum caused by corrosive ingestion. *Plavsic BM, Robinson AE*

Technical note. Gadopentetate dimeglumine–barium paste for opacification of the esophageal lumen on MR images. *Pavone P, Cardone GP, Cisternino S, Di Girolamo M, Aytan E, Passariello R*

Case report. Acute phlegmonous gastritis with mural abscess: CT diagnosis. *Cruz FO, Soffia PS, Del Rio PM, Fava MP, Duarte IG*

GENITOURINARY RADIOLOGY

Focal hyperdense areas in endometriomas: a characteristic finding on CT. *Buy J-N, Ghossain MA, Mark AS, et al*

Color Doppler sonography of ureteral jets in normal volunteers: importance of the relative specific gravity of urine in the ureter and bladder. *Baker SM, Middleton WD*

Technical note. Percutaneous removal of a titanium Greenfield filter. *Cynamon J, Bakal CW, Epstein SB, Gabelman G*

MUSCULOSKELETAL RADIOLOGY

Review. MR imaging of the cervical spine: techniques for two- and three-dimensional imaging. *Ross JS*

MR imaging in the evaluation of SLAP injuries of the shoulder: findings in 10 patients. *Cartland JP, Crues JV III, Stauffer A, Nottage W, Ryu RKN*

Carpal tunnel syndrome: diagnosis with high-resolution sonography. *Buchberger W, Judmaier W, Birbamer G, Lener M, Schmidauer C*

Pictorial essay. MR evaluation of spondylolysis, spondylolisthesis, and associated nerve root entrapment in the lumbosacral spine. *Jinkins JR, Matthes JC, Sener RN, Venkatappan S, Rauch R*

Pictorial essay. Lymphoma of bone, muscle, and skin: CT findings. *Malloy PC, Fishman EK, Magid D*

PEDIATRIC RADIOLOGY

Isolation of the fourth ventricle causing transtentorial herniation: neurosonographic findings in premature infants. *Hall TR, Choi A, Schellinger D, Grant EG*

MR angiography in children with cerebral neurovascular diseases: findings in 31 cases. *Vogl TJ, Balzer JO, Stemmler J, Bergman C, Egger E, Lissner J*

Sonographic diagnosis of intestinal malrotation in infants: importance of the relative positions of the superior mesenteric vein and artery. *Weinberger E, Winters WD, Liddell RM, Rosenbaum DM, Krauter D*

Pictorial essay. Sonography of the elbow in infants and children. *Markowitz RI, Davidson RS, Harty MP, Bellah RD, Hubbard AM, Rosenberg HK*

Case report. Wilms' tumor in a patient with Beckwith-Wiedemann syndrome: onset detected with 3-month serial sonography. *Andrews MW, Amparo EG*

Case report. Congenital portohepatic vein fistula in a newborn with spontaneous resolution. *Lewis AN, Aquino NM*

Case report. Aneurysm of a nonpatent ductus arteriosus in a neonate: CT findings. *Slovis TL, Meza MP, Rector FE, Chang C-H*

NEURORADIOLOGY

Primary cerebral lymphoma in patients with AIDS: MR findings in 17 cases. *Cordoliani Y-S, Derosier C, Pharaboz C, Jeanbourquin D, Schill H, Cosnard G*

Review. The ostiomeatal unit and endoscopic surgery: anatomy, variations, and imaging findings in inflammatory disease. *Laine FJ, Smoker WRK*

Relapsing-remitting multiple sclerosis: sequential enhanced MR imaging vs clinical findings in determining disease activity. *Barkhof F, Scheltens P, Frequin STFM, et al*

Evaluation of complex cystic masses of the brain: value of steady-state free-precession MR imaging. *Tien RD, MacFall J, Heinz R*

Pictorial essay. Extrapineal abnormalities of the tectal region: MR imaging findings. *Friedman DP*

Case report. Intraocular cryptococcosis: imaging findings. *Moon WK, Han MH, Song CS, Chang KH, Han MC*

CONTRAST MATERIAL

The cost-effectiveness of replacing high-osmolality with low-osmolality contrast media. *Caro JJ, Trindade E, McGregor M*

MR lymphography with iron oxide compound AMI-277: studies in ferrets with filariasis. *Tanoura T, Bernas M, Darkazanli A, et al*

SOCIOECONOMICS

Perspective. Canadian style health care: implications for radiologists. *Wesenberg RL*

RESIDENT TEACHING

Critical performance behaviors of radiology residents: evaluation of two category systems. *Smith WL, Wood PS, Altmaier EM, O'Halloran C, Franken EA Jr*

Letters

A Small Cloud on the Horizon

Radiologists may be aware that the federal government has eliminated specific fees for interpreting routine ECGs by cardiologists and other physicians [1]. Instead, most physicians are now receiving an increase of approximately $1 per visit for Medicare patients as a general compensation for interpretation of ECGs of their own patients.

Depending on the government's experience with this provision, the implications for radiologists could be considerable. Basically, the government has told all physicians that they must now interpret the ECGs they order on their patients. Of most interest to radiologists is that cardiologists are no longer paid for interpreting ECGs for other physicians, as has been the customary arrangement in many hospitals. It is not difficult to recognize that the same process applied to the interpretation of radiologic examinations could threaten the practice of radiology as currently constituted.

For years, many of our nonradiologist colleagues have been saying that they are willing and able to interpret their patients' radiologic examinations. The specialties involved include orthopedics, urology, cardiology, pulmonology, neurology, neurosurgery, cardiothoracic surgery, and emergency medicine. Cardiology and neurology already provide formal training in the performance and interpretation of radiologic studies. The others mentioned provide informal training and incorporate questions on radiology in their board examinations.

If the experiment of asking physicians to interpret their own ECGs produces no adverse consequences, the Health Care Financing Administration (HCFA) may have succeeded in demonstrating that specific fees for the interpretation of many diagnostic examinations are unnecessary. The patient's physician would be expected to interpret these examinations as part of the evaluation of the patient's condition. Any remuneration for interpretation of diagnostic examinations, as with ECGs, would be incorporated in the patient's general fee.

With the precedent set by the change in reading of ECGs, I can foresee a situation in which the HCFA tells those physicians who have wanted to interpret their own radiographs that they should do so. However, they will not receive a bonanza of fees for interpretation of radiologic studies, only a slight increase in general fees for the effort involved. As with the cardiologists, radiologists could by this means be excluded from the interpretation of most radiologic examinations. At best, the new ECG policy applied to radiology would have serious financial consequences for radiologists. At its worst, it could result in the partial disassembly of radiology as a medical specialty.

Although it is difficult to feel very sorry for the cardiologists about their loss of ECG fees, considering their efforts to divest radiology of every aspect of cardiovascular imaging, the matter exists as a storm cloud on the horizon. The pertinent question is whether it is moving in our direction.

David W. Gelfand
Bowman Gray School of Medicine
Winston-Salem, NC 27157-1088

REFERENCE

1. *Federal Register.* November 25, **1991**;56:59515

Diagnosis of Intrathoracic Goiter Based on Sonographic Findings

Intrathoracic goiters account for about 5–11% of mediastinal masses resected at thoracotomy. Although radionuclide scanning and CT can be used to detect most intrathoracic goiters, the associated exposure to radiation and the costs are disadvantages. However, sonography is useful in the evaluation of mediastinal masses, and it has certain advantages. It is inexpensive, can be used at the bedside, involves no exposure to radiation, and can be used with real-time monitoring [1–3]. We present our experience in using sonography to diagnose intrathoracic goiters.

The study included five women and one man 41–82 years old (mean, 68 years) who had histologically or cytologically proved intrathoracic goiter over a 3-year period. Cervical goiter was found by palpation of the neck in five of the six patients. All six had a normally functioning thyroid. Chest radiographs showed an anterior or a superior mediastinal mass in all six. Five patients had sonographically guided fine-needle aspiration of the mediastinal mass, and cytologic examination confirmed that the mass was an intrathoracic goiter. Two patients had thoracotomy and excision of the mediastinal mass for relief of respiratory signs and symptoms, and histologic examination showed intrathoracic goiter.

Sonograms were obtained with linear-array or convex transducers (3.5-MHz Aloka SSD-630; 3.75- or 7.5-MHz Toshiba SSA-100A) via a suprasternal, supraclavicular, or parasternal approach. The sonographic characteristics of the intrathoracic goiters were as follows: clear continuity between the mediastinal mass and the cervical thyroid (Fig. 1) in six patients, heterogeneous hyperechoic texture (Fig. 2) in six, well-defined borders in five, focal calcification manifested as hyperechoic bands or spots in four, and cystic change manifested as a hypoechoic area in four. The sonographic features of the cervical goiter were similar to those of intrathoracic goiters: well-defined borders in six patients, heterogeneous hyperechoic texture in four, focal calcification in four, and cystic changes in three.

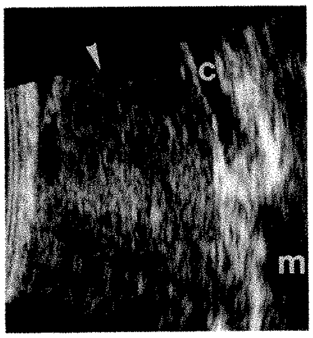

1

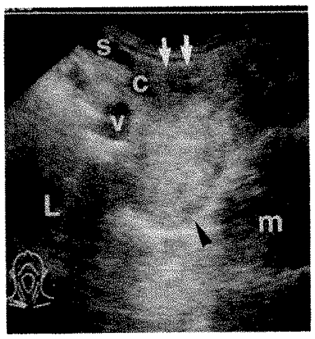

2

Fig. 1.—Longitudinal sonogram shows direct extension of cervical thyroid (*arrowhead*) into superior mediastinum (m). c = carotid artery.

Fig. 2.—Transverse sonogram shows direct connection of intrathoracic goiter (*arrowhead*) with cervical thyroid (*arrows*). Intrathoracic goiter has well-defined border with halo sign and heterogeneous hyperechoic texture. Hypoechoic area in cervical thyroid represents cystic change. c = common carotid artery, s = subclavian artery, v = innominate vein, L = lung, and m = mediastinum.

Sonography has several advantages in the diagnosis of intrathoracic goiter. It clearly shows the continuity between the cervical thyroid and the goiter and the high similarity in the echotextures of the two (e.g., calcification, cyst formation, well-defined borders, and echogenicity). In our experience, the continuity of the cervical thyroid and mediastinal mass was not found in other clinical conditions [2, 3]. Primary intrathoracic goiter, without any connection to the cervical thyroid, is rare. We have seen no such case. However, sonographically guided fine-needle aspiration may also be helpful in the diagnosis of primary intrathoracic goiter. In certain patients with a superior mediastinal mass, sonography may be the most convenient and useful technique for diagnosing intrathoracic goiter.

Dun-Bing Chang
Pan-Chyr Yang
Sow-Hsong Kuo
and colleagues
National Taiwan University Hospital
Taipei, Taiwan, Republic of China

REFERENCES

1. Wernecke K, Peters PE, Galanski M. Mediastinal tumors: evaluation with suprasternal sonography. *Radiology* **1986**;159:405–409
2. Yang PC, Chang DB, Lee YC, Yu CJ, Kuo SH, Luh KT. Mediastinal malignancy: ultrasound guided biopsy through supraclavicular approach. *Thorax* **1992**;47:377–380
3. Yu CJ, Yang PC, Chang DB, et al. Evaluation of ultrasonically guided biopsies of mediastinal masses. *Chest* **1991**;100:399–405

Bronchiolitis Obliterans with Organizing Pneumonia: Atypical Appearance on Radiographs

We report a case of biopsy-proved idiopathic bronchiolitis obliterans with organizing pneumonia in which intrapulmonary changes were confined to the right lung and were accompanied by a unilateral pleural effusion and gross mediastinal adenopathy.

A 57-year-old man had a history of cough, increasing dyspnea, chest pain, and moderate fever. Chest radiographs showed an apparent mass in the right hilum and a widening of the right paratracheal space (Fig. 1A). CT scans showed a masslike lesion within the right hilum and moderate infiltration of the right lower lobe of the lung (Fig. 1B). The paratracheal and subcarinal lymph nodes were grossly enlarged. On follow-up chest radiographs and CT scans, the size of the masslike lesion had increased rapidly, and a right-sided pleural effusion had developed. The patient had bronchoscopy twice, and the results indicated that the mass was not a tumor. A percutaneous biopsy was performed; a Tru-Cut needle (Baxter Health Care Corp., Deerfield, IL) was used to obtain a cylinder of lung tissue 1.5 cm long. Histologic examination showed plugs of connective tissue filling alveolar spaces and respiratory bronchioles. These plugs consisted of fibroblasts and a few admixed inflammatory cells in an edematous stroma, sometimes with a central capillary vessel. Some alveoli were filled with alveolar macrophages and remnants of a fibrinous exudate in organization. Interstitial changes were much less pronounced, with moderate thickening of alveolar septa due to accumulation of inflammatory cells and hyperplasia of type II pneumonocytes.

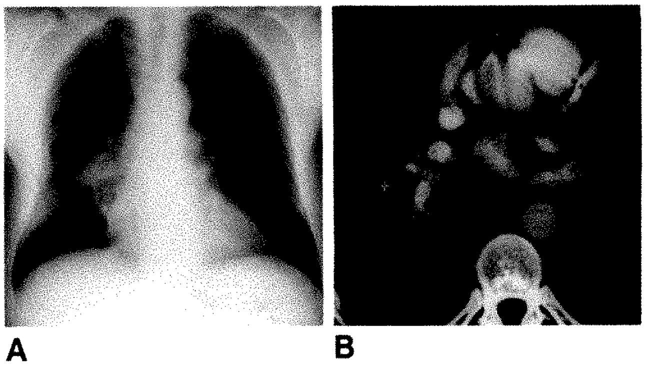

Fig. 1.—Bronchiolitis obliterans with organizing pneumonia.

***A*, Chest radiograph shows enlargement of right hilum and widening of right paratracheal space.**

***B*, CT scan obtained 2 days after admission shows an apparent mass within right hilum.**

On the basis of the histologic finding and compatible clinical signs and symptoms, idiopathic bronchiolitis obliterans with organizing pneumonia was diagnosed. However, diagnosis was delayed because of the atypical appearance on the radiographs. The unilateral masslike consolidation associated with hilar adenopathy and a pleural effusion suggested bronchogenic carcinoma, malignant lymphoma, tuberculosis, or pleuropneumonia.

McLoud et al. [1] reported findings in 29 patients with bronchiolitis obliterans with organizing pneumonia. Unilateral opacities, as seen in our patient, were present in only 4.8% of all cases. Pleural effusions were also rare (4.8%). Furthermore, pulmonary infiltrates were peripheral rather than central. Our case illustrates the diversity of radiologic findings in bronchiolitis obliterans with organizing pneumonia. To our knowledge, this is the first report of gross mediastinal adenopathy in this disease.

R. Knapp
Ch. Prior
F. Fend
D. zur Nedden
University of Innsbruck
A-6020 Innsbruck, Austria

REFERENCES

1. McLoud TC, Epler GR, Colby TV, Gaensler EA, Carrington CB. Bronchiolitis obliterans. *Radiology* **1986**;159:1–8

Breast Gas-Fluid Level on Chest Radiographs

Previously reported mammographic findings after breast biopsy include fat necrosis, oil cysts, hematomas, infection, skin thickening, contour deformity, keloid formation, architectural distortions, asymmetric parenchyma, parenchymal stellate scar, dystrophic calcification, and calcified sutures [1, 2]. Rabin and Murray [3] have described the appearance on chest radiographs of nipple shadow, mastectomy, calcified cysts, phleboliths, carcinomatous masses, dense fibroadenomas, and density caused by cystic mastitis. Additionally, radiologists are familiar with the appearance of various breast implants and prostheses on chest radiographs. We report the unusual appearance on chest radiographs of a gas-fluid level within a postbiopsy hematoma.

A 69-year-old woman had chest radiographs before undergoing a right-sided mastectomy. One week earlier, she had had incisional biopsy for an area of thickening in the right breast that showed an intraductal carcinoma with tumor extending to the specimen's margin. Posteroanterior chest radiograph (Fig. 1A) showed a gas-fluid level over the right lower part of the chest. A lateral chest radiograph (Fig. 1B) showed the cavity was within the right breast. Physical examination of the breast showed no evidence of erythema, tenderness to palpation, or fistula. Multiple superficial sutures were present in the area of incision, with satisfactory healing. A radical mastectomy was performed, and pathologic examination of the area in question showed a 5.5-cm collection of fat necrosis and clotted blood in the biopsy cavity. No residual tumor was present.

At the time of the original biopsy, no surgical drain was inserted into the biopsy cavity. Only superficial sutures were placed to allow development of hematoma and a better cosmetic result. Because the patient had no signs or symptoms of local infection, the possibility of infection by a gas-producing organism was thought to be unlikely. Although liquified fat above a hematoma could produce a radiolucent area simulating a gas-fluid collection, it was the consensus of multiple radiologists that the density on the chest radiographs was that of gas not fat.

We think the most plausible explanation in this case is that air was introduced into the breast during open incisional biopsy and sealed off by superficial closure. At the time of radiography, the gas had not yet been completely resorbed and therefore caused the gas-fluid level. In conclusion, the finding of a gas-fluid level in the breast after biopsy should suggest the possibility of retained, nonresorbed gas in addition to other diagnostic considerations such as infection with gas-producing organism or air introduced via a postoperative drain that could produce a similar finding.

Mark J. Bluth
Burton M. Gold
Winthrop-University Hospital
Mineola, NY 11501

REFERENCES

1. Tabar L, Dean PB. *Teaching atlas of mammography*. New York: Thieme-Stratton, **1985**:172
2. Stigers KA, King JG, Davey DD, Stelling CB. Abnormalities of the breast caused by biopsy: spectrum of mammographic findings. *AJR* **1991**;156: 287-291
3. Rabin CB, Murray GB. *Radiology of the chest*, 2nd ed. Baltimore: Williams & Wilkins, **1980**:183-189

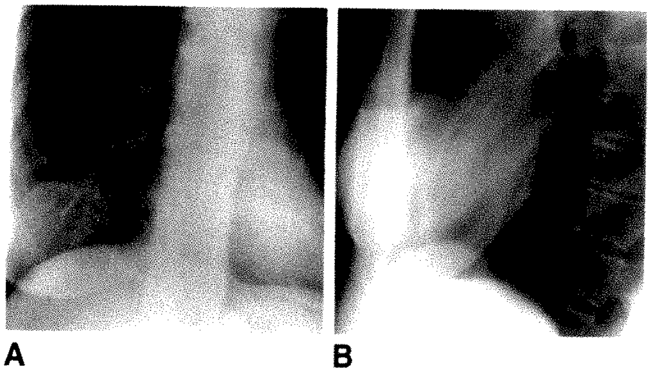

Fig. 1.—***A***, **Posteroanterior chest radiograph obtained after breast biopsy shows gas-fluid level over right lower part of chest.**

B, **Lateral chest radiograph confirms gas-fluid level is within right breast.**

Aortopulmonary Fistula Detected by CT

Although CT has been used in the diagnosis of aortopulmonary fistula [1], to our knowledge, direct detection of the fistulous connection has not been reported. We describe a patient in whom the fistula was clearly shown on CT.

A 78-year-old man with hypertension was referred to our hospital because of massive hemoptysis. Seven years before, he had had atherosclerotic aneurysm of the descending aorta, which was repaired with a synthetic graft (woven Dacron). The chest radiograph showed an enlarged thoracic aorta with homogeneous density in the upper part of the left lung. Findings on contrast-enhanced CT scans suggested a connection between the dilated aortic arch and a pulmonary hematoma (Fig. 1A). During the next few hours, hemoptysis gradually increased, and the patient died before aortography and surgery could be performed. Postmortem study showed that rupture of the thoracic aorta above the proximal anastomosis of the graft had resulted in a fistula between the aorta and a hematoma in the upper lobe of the left lung (Fig. 1B).

Although several methods have been used to detect aortopulmonary fistula [1-4], conclusive diagnosis has been difficult. In most cases, the fistula has been confirmed at surgery or autopsy. Because delay in treatment may result in catastrophic hemorrhage, early and accurate diagnosis is desirable. Aortography is useful in detecting aneurysms and in showing the adjacent structures. CT is also useful for detecting not only aortic aneurysm but also pulmonary hematoma, although it usually has not shown the true connection [1]. Thrombus formation in the fistula may prevent detection of the fistulous conti-

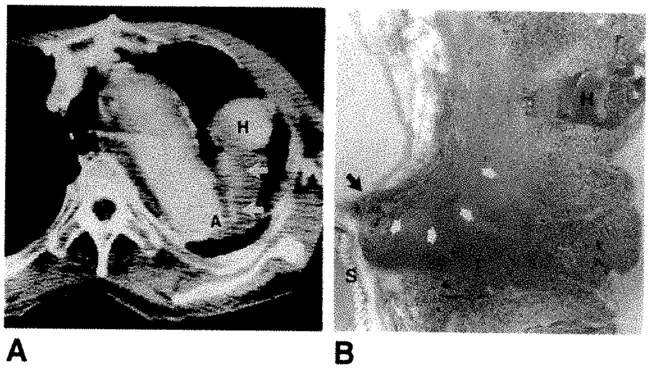

Fig. 1.—Aortopulmonary fistula.

A, **Contrast-enhanced CT scan at level of aortic arch shows contrast medium (*arrows*) connecting thoracic aorta (A) and pulmonary hematoma (H).**

B, **Autopsy specimen shows fistula (*white arrows*) from anastomosis (*black arrow*) just above synthetic graft (S) to hematoma (H) through pulmonary parenchyma.**

nuity [3, 4]. In our case, however, the reperfusion caused by thrombolysis or dislodgement, which may occur in recurrent hemoptysis [4], enabled us to visualize the connection. Mortality associated with such a CT finding is high, and surgery should be carried out as soon as possible.

Masahito Higashikawa
Junichiro Morikawa
Itsuro Nishigaki
Michio Bamba
Kohoku General Hospital
Shiga, 529-04, Japan

REFERENCES

1. Hampson S, Pepper J. Aortopulmonary fistula: role of computed tomography. *Thorax* **1987**;42:395–396
2. Demeter SL, Cordasco EM. Aortobronchial fistula: keys to successful management. *Angiology* **1980**;31:431–435
3. Coblentz CL, Sallee DK, Chiles C. Aortobronchopulmonary fistula complicating aortic aneurysm: diagnosis in four cases. *AJR* **1988**;150:535–538
4. Graeber GM, Farrell BG, Neville JF Jr, Parker FB Jr. Successful diagnosis and management of fistulas between the aorta and the tracheobronchial tree. *Ann Thorac Surg* **1980**;29:555–561

Motion Artifact Simulating Aortic Dissection on CT

Recently, Burns et al. [1] described a motion artifact simulating an aortic dissection on a CT scan obtained on a Somatom Plus system (Siemens Medical System, Iselin, NJ). We have observed the circumferential artifact, but we were unaware of the artifact simulating an intimal flap. We recently encountered a case that emphasized the importance of recognizing this artifact.

A 58-year-old man was admitted for evaluation of a possible aortic dissection. Dynamic contrast-enhanced CT scans of the thoracoabdominal aorta were obtained with a Somatom Plus system. Selective scans of the aortic arch, aortic root, and descending aorta were obtained before the administration of contrast material. Sections 1 cm thick, obtained after the IV administration of contrast material, showed a low-attenuation thin line within the posterior aspect of the ascending aorta, 1 cm above the aortic root (Fig. 1). Repeat 4-mm-thick sections obtained after a second bolus of contrast material showed persistence of the presumed flap in that same region. However, scans obtained with lung-window settings showed extension of the low-attenuation line beyond the medial wall of the ascending aorta, into the adjacent mediastinum. This artifact was in the same location as that illustrated by Burns et al.

Our experience with the Somatom Plus scanner has been similar to that of Burns et al. We have adjusted to the circumferential artifact surrounding the ascending aorta. However, this was our first experience with the artifact mimicking an intimal flap. Repeat imaging with thin sections was not particularly helpful. However, evaluation at lung-window settings was beneficial. This case emphasizes the importance of the observations made by Burns et al. and illustrates a pitfall of CT in the diagnosis of aortic dissection when the Somatom Plus system is used.

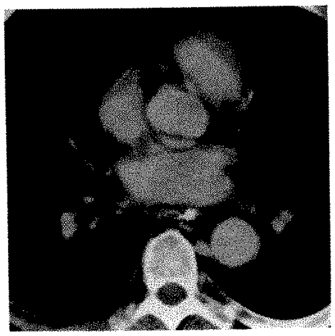

Fig. 1.—Motion artifact simulating aortic dissection. CT scan shows low-attenuation linear structure within lumen of aortic root. On closer inspection, this line extends beyond confines of aorta.

Suresh K. Mukherji
Pardeep Varma
Paul Stark
Brigham and Women's Hospital
Boston, MA 02115

REFERENCE

1. Burns MA, Molina PL, Gutierrez FR, Sagel SS. Motion artifact simulating aortic dissection on CT. *AJR* **1991**;157:465–467

Choledochal Cysts: Classification and Cholangiographic Appearance

In their article on the classification and cholangiographic appearance of choledochal cysts [1], Savader et al. do not mention clearly if they accept the concept of Babbitt [2] that dilatation of the biliary tract may be the consequence of the anomalous insertion of the common bile duct into the pancreatic duct (Fig. 1 in [1]). This concept has been widely accepted and confirmed [3–5]. Okada et al. [6] named the anomaly "common channel syndrome," but the term abnormally long common channel may be better.

In our experience, this syndrome is the most frequent cause of dilatation of the extra- and intrahepatic bile ducts in children and infants. We base our diagnosis solely on sonographic findings. Dilated biliary ducts in connection with appropriate clinical signs and symptoms are an indication for surgery. During the laparotomy, we confirm the diagnosis by using direct cholangiography. To define the anatomic changes, we carefully compress the duodenum distal to the papilla of Vater to show the common channel by retrograde filling of the common bile duct and the pancreatic duct with contrast material. We have used this approach to manage this syndrome in 21 cases, and we think that percutaneous transhepatic cholangiography and ERCP are unnecessary and not without risk.

Kl. D. Ebel
M. Gharib
Children's Hospital of the City of Cologne
5000 Köln 60, Germany

REFERENCES

1. Savader SJ, Benenati JF, Venbrux AC, et al. Choledochal cysts: classification and cholangiographic appearance. *AJR* **1991**;156:327–331
2. Babbitt DP. Congenital choledochal cyst: new etiological concept based on anomalous relationships of common bile duct and pancreatic bulb. *Ann Radiol* (Paris) **1969**;12:231–240
3. Jona ZJ, Babbitt DP, Starshak RJ, LaPorta AJ, Glicklich M, Cohen RD. Anatomic observations and etiologic and surgical considerations in choledochal cysts. *J Pediatr Surg* **1979**;14:315–319
4. Suarez F, Bernard O, Gauthier F, Valayer J, Brunelle F. Bilio-pancreatic common channel in children: clinical, biological and radiological findings in 12 children. *Pediatr Radiol* **1987**;17:206–211
5. Gharib M, Ebel Kl-D, Engelskirchen R, Bliesener JA. Abnormal choledocho-pancreatico ductal junction causative of cystic-cylindric dilatation of intra- and extrahepatic bile ducts. *Monatsschr Kinderheilk* **1982**;130:783–788
6. Okada A, Oguchi Y, Kamata S. Common channel syndrome—diagnosis with endoscopic retrograde cholangiopancreaticography and surgical management. *Surgery* **1983**;93:634–642

Reply

We thank Drs. Ebel and Gharib for their interest in our paper [1]. We wish to clarify that we do support the theory of Babbitt [2] on the mechanism of choledochal cyst formation. Babbitt has theorized that an anomalous insertion of the common bile duct into the pancreatic duct results in chronic reflux of pancreatic enzymes into the biliary tree, which leads to inflammation, dilatation, and scarring. Although this theory most likely does not account for the formation of a type III choledochal cyst (choledochocele) or a type V choledochal cyst (Caroli's disease), it does seem to explain the occurrence of the other types of choledochal cysts, as the anatomic variation of the common channel has been documented in 10–58% of cases [3]. We have also noted this anatomic variation in a large percentage of our patients with more typical choledochal cysts.

We agree with Drs. Ebel and Gharib that many diagnostic approaches can be used to evaluate choledochal cysts, and we agree that in children, the findings of dilated biliary ducts and a cystic mass in the region of the extrahepatic biliary tree, in conjunction with appropriate clinical signs and symptoms, are an indication for surgery. However, our population of patients consisted mostly of adults, many of whom had previous surgical evaluation or attempts at reconstruction. We have found that in this population, percutaneous transhepatic cholangiography provides the most thorough assessment of cyst anatomy, site of biliary origin, extent of both intra- and extrahepatic disease, and associated biliary tract anomalies. As noted in our article [1], six of our 14 patients had associated hepatobiliary disease, only one case of which (intrahepatic abscesses) was detected by using noninvasive imaging techniques. In addition, we have found that placement of a percutaneous transhepatic drain is useful during surgery for location of the common hepatic duct. This is particularly true in patients who have had previous attempts at reconstruction and who have distortions of the porta hepatis, in addition to adhesions. In regards to the risk associated with percutaneous transhepatic cholangiography, we think that when the technique is performed by an experienced radiologist, the risk should be minimal. In our group of 14 patients, the only complication associated with percutaneous transhepatic cholangiography and biliary drainage was one episode of transient bacteremia, which was effectively treated with antibiotics.

Scott J. Savader
John L. Cameron
The Johns Hopkins Hospital
Baltimore, MD 21205

REFERENCES

1. Savader SJ, Benenati JF, Venbrux AC, et al. Choledochal cysts: classification and cholangiographic appearance. *AJR* **1991**;156:327–331
2. Babbitt DP. Congenital choledochal cyst: new etiological concept based on anomalous relationships of common bile duct and pancreatic bulb. *Ann Radiol* (Paris) **1969**;12:231–240
3. Crittenden SL, McKinley MJ. Choledochal cyst: clinical features and classification. *Am J Gastroenterol* **1985**;80:643–647

Benign Schwannoma of the Pancreas

Previously described cases of benign schwannoma of the pancreas have been associated with Recklinghausen's disease. We describe the first case not associated with this disease.

A 73-year-old man had pain in the right upper quadrant. Sonograms showed gallstones and a mass in the body of the pancreas. Contrast-enhanced abdominal CT scans (Fig. 1A) confirmed a 2-cm, isodense, well-circumscribed, solid pancreatic mass without adenopathy or biliary duct dilatation. After ERCP showed pancreatic duct obstruction, angiography was performed. Injection of the superior mesenteric artery resulted in a blush in the pancreatic tail without vascular encasement (Fig. 1B). At surgery, a 2-cm mobile mass was found at the junction of the pancreatic body and tail. Pathologic examination showed a well-defined nodule with a mottled, gelatinous-appearing brownish surface when cut. Histologic examinations showed classic Antoni A and B areas of closely woven spindle cells arranged in a palisading fashion.

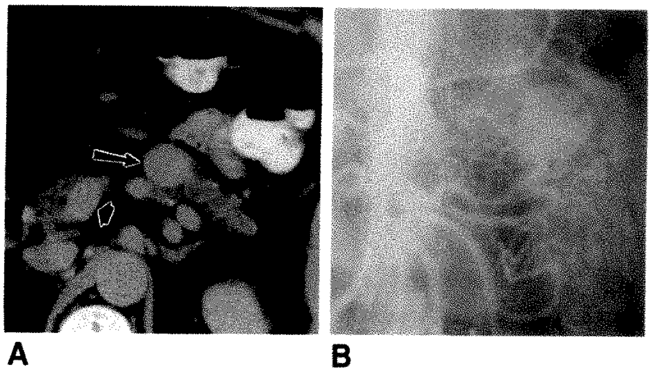

Fig. 1.—Benign schwannoma of pancreas.

***A*, CT scan at level of pancreatic tail shows a solid mass (*long arrow*) in distal part of pancreas. Portal venous confluence is clearly visible (*short arrow*).**

***B*, Aortic angiogram shows tumor blush in left upper quadrant, overlying upper pole of left kidney.**

A schwannoma, or neurilemoma, is a benign tumor that originates from the nerve sheath along the course of a peripheral nerve. Smaller tumors are solid; larger ones may undergo necrosis and hemorrhagic degeneration. These rare tumors may occur in any location, the least common of which is the retroperitoneum [1]. The association between schwannoma and Recklinghausen's disease is well described [1, 2]. Schwannomas of the retroperitoneum are mostly benign [3]. Interestingly, those associated with Recklinghausen's disease have a worse prognosis. A 5-year survival of 75% for patients who have schwannoma decreases to 30% when the patient has schwannoma associated with Recklinghausen's disease.

The differential diagnosis for such a pancreatic mass includes malignant neoplasia as well as benign vascular tumors such as islet cell tumors. Studies have shown, however, that CT and MR findings cannot be used to distinguish benign from malignant lesions [3]. CT attenuation values varied from 5 to 40 H, according to the degree of necrosis [2]. For complete evaluation of the tumor, use of multiple techniques is recommended, including sonography, CT, angiography, and, possibly, MR.

Douglas A. Burd
Girish Tyagi
David A. Bader
St. Vincent Hospital
Worcester, MA 01604

REFERENCES

1. Das Gupta TK, Brasfield RD, Strong EW, Hajdu SI. Benign solitary schwannoma (neurilemoma). *Cancer* **1969**;24:355–366
2. Kumar AJ, Kuhajda FP, Martinez CR, Fishman EK, Jezic DV, Siegelman SS. Computed tomography of extracranial nerve sheath tumors with pathologic correlation. *J Comput Assist Tomogr* **1983**;7:857–865
3. Levine E, Huntrakoon M, Wetzel LH. Malignant nerve-sheath neoplasms in neurofibromatosis: distinction from benign tumors by using imaging techniques. *AJR* **1987**;149:1059–1064

Stress-Induced Adrenal Hyperplasia Simulating Metastatic Disease: CT and MR Findings

Elevation of serum levels of adrenocorticotropic hormone and cortisol can occur in response to stress [1]. Experiments in animals have also shown that adrenal hypertrophy occurs in association with elevated levels of corticosterone in response to stress [2, 3]. To our knowledge, however, such hypertrophy has not been shown by using any imaging technique. We report the CT and MR findings in a case of adrenal hyperplasia that appeared to be stress induced and that resolved when the patient received corticosteroid therapy.

A 58-year-old man had a left radical nephrectomy, including left adrenalectomy, for stage 2 renal cell cancer. CT scans obtained 1 year later showed a nodule in the right lung and a well-defined 2-cm mass in the right adrenal gland, which was thought to represent an incidental adenoma, as it had not changed since a CT scan obtained before the nephrectomy. Over the ensuing 8 months, the nodule in the lung enlarged; it was resected 2 years after the nephrectomy. A CT scan obtained 6 months later showed that the mass in the right adrenal gland had increased to 4 cm (Fig. 1A), which suggested that it was a metastasis. The mass had high signal intensity on T2-weighted MR images (Fig. 1B), which, although nonspecific, supported the impression that it represented metastatic disease. The patient elected not to have surgery. An extensive skin rash that had developed was treated with topical and oral corticosteroids. Follow-up CT scans showed regression of the mass in the right adrenal gland; the gland eventually became normal (Fig. 1C). Follow-up T1- and T2-weighted MR images showed that the mass had decreased in size and now had a low signal intensity (Fig. 1D). Metastases, however, had appeared and were enlarging in the lung and liver.

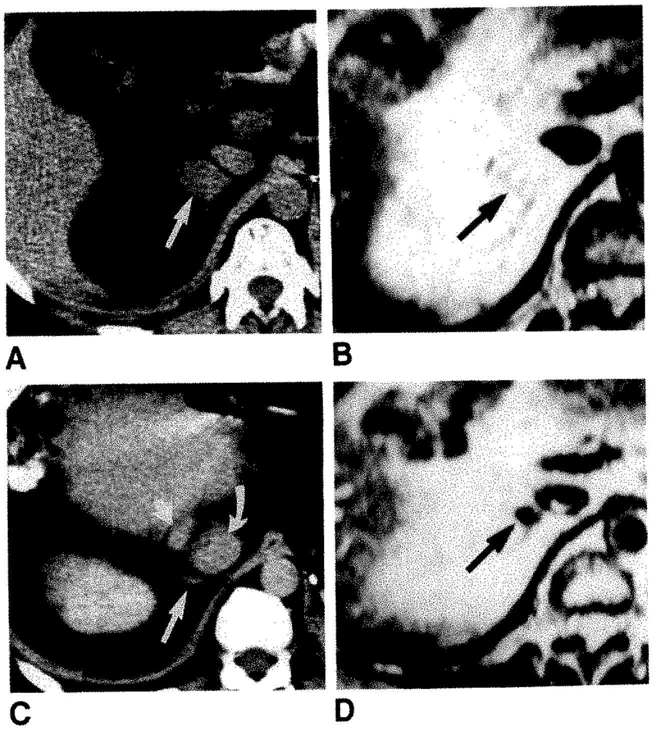

Fig. 1.—Stress-induced adrenal hyperplasia simulating metastatic disease.

***A* and *B*, CT scan (*A*) and T2-weighted MR image (*B*) obtained 2.5 years after nephrectomy and left adrenalectomy for renal cell cancer and 6 months after resection of a pulmonary metastasis show a mass (*arrows*) in right adrenal gland. Mass has high signal intensity on MR image.**

***C* and *D*, CT scan (*C*) and T2-weighted image (*D*) obtained after corticosteroid therapy and resection of right lobe of liver show normal adrenal gland (*long straight arrows*). Mass has decreased in size and now has low signal intensity on MR image. *Short straight arrow* = portal vein. *Curved arrow* = inferior vena cava.**

This adrenal mass almost certainly was an incidental adenoma, rather than metastatic disease, undergoing hyerplastic change, as it decreased in size at the same time that metastases in the lung and liver were enlarging. The stress associated with detection and treatment of a new metastatic focus in the lung presumably caused the adrenal hyperplasia we observed. The combination of topical and oral corticosteroids in our patient most likely played a role in reversing this hyperplasia [4]. This case also reemphasizes that the signal intensity of adrenal lesions on T2-weighted MR images is nonspecific. The signal intensity of the mass was high on images obtained when it was largest and low on images obtained later when it was smaller. Thus, the signal intensity of adrenal lesions may be influenced not only by the cellular composition of the lesion but also by the degree of adrenal stimulation or suppression.

Ahalya Premkumar
Catherine K. Chow
Peter L. Choyke
John L. Doppman
National Institutes of Health
Bethesda, MD 20892
Georgetown University Medical Center
Washington, DC 20007

REFERENCES

1. Ney RL, Shimizu N, Nicholson WE, Island DP, Liddle GW. Correlation of plasma ACTH concentration with adrenocortical response in normal human subjects, surgical patients and patients with Cushing's disease. *J Clin Invest* **1963**;42:1669–1677
2. Khasina EI, Kurilenko LA, Kirillov OI. Adrenal hypertrophy in rats during long-term movement restrain. *Z Mikrosk Anat Forsch* **1985**;99:603–610
3. Spencer RL, McEwan BS. Adaptation of the hypothalamic-pituitary-adrenal axis to chronic ethanol stress. *Neuroendocrinology* **1990**;52:481–489
4. Ohman EM, Rogers S, Meenan FO, McKenna TJ. Adrenal suppression following low-dose topical clobetasol propionate. *J R Soc Med* **1987**; 80:422–424

Metastatic Papillary Adenocarcinoma to the Brain Simulating Toxoplasmosis on CT in a Patient with AIDS

Neurologic disease associated with HIV infection is common, occurring in 40% of patients. It has been reported that both primary CNS lymphoma and toxoplasmosis cause ring-enhancing lesions on CT. Although lymphoma is frequently solitary, multifocal lesions occur in up to 50% of cases [1–3]. This report describes a patient with AIDS and metastatic adenocarcinoma to the brain whose CT scan was highly suggestive of toxoplasmosis or multifocal lymphoma.

A 44-year-old man who was seropositive for HIV and who was having follow-up for pulmonary tuberculosis had had diplopia, loss of motor coordination, and headaches for 3–4 weeks. He had no associated fevers, chills, weight loss, or nuchal rigidity. Physical examination showed a cranial nerve VI palsy on the left side. The titer in a test for *Toxoplasma* was less than 1:16. CT showed multiple lesions in the cerebral hemispheres, characterized by rim enhancement and modest mass effect (Fig. 1). The patient was treated with pyrimethamine and sulfadiazine for possible CNS toxoplasmosis. Despite this, the lesions enlarged, with increasing edema. A craniotomy and biopsy were performed; the pathologic findings indicated metastatic papillary adenocarcinoma. An extensive workup did not show a primary site of the carcinoma.

Evaluation of CNS mass lesions in patients with HIV infection may be complex. CT and MR imaging may be helpful in the differential diagnosis and management of these lesions. In those patients with ring-enhancing lesions, differentiation between toxoplasmosis and

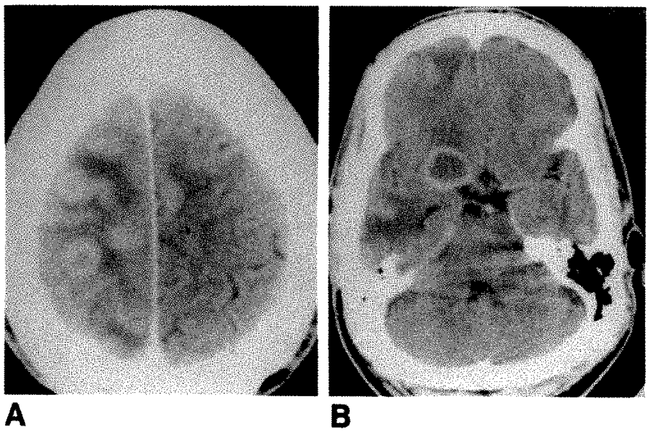

Fig. 1.—Metastatic papillary adenocarcinoma to the brain simulating toxoplasmosis in a patient with AIDS.
***A* and *B*, CT scans with contrast material show multiple lesions with ring enhancement.**

lymphoma may be difficult [4]. Increases in titers in tests for *Toxoplasma* and responses to empirical therapy may suggest toxoplasmosis. CT findings of metastatic adenocarcinoma include predisposition for gray and white matter, diffuse or ring enhancement, and moderate to marked edema. To my knowledge, metastatic adenocarcinoma mimicking the CT findings of toxoplasmosis has not been reported before.

Barry Bernstein
Medical College of Wisconsin
Milwaukee, WI 53226

REFERENCES

1. Ciricillo SF, Rosenblum ML. Use of CT and MR imaging to distinguish intracranial lesions and to define the need for biopsy in AIDS patients. *J Neurosurg* **1990**;73:720–724
2. Dina TS. Primary central nervous system lymphoma versus toxoplasmosis in AIDS. *Radiology* **1991**;179:823–828
3. Goldstein JD, Zeifer B, Chao C, et al. CT appearance of primary CNS lymphoma in patients with acquired immunodeficiency syndrome. *J Comput Assist Tomogr* **1991**;15:39–44
4. Cimino C, Lipton RB, Williams A, Feraru E, Harris C, Hirschfeld A. The evaluation of patients with human immunodeficiency virus-related disorders and brain mass lesions. *Arch Intern Med* **1991**;151:1381–1384

Tuberculosis Involving the Patella

We describe a case of tuberculous osteomyelitis in which patellar disease was the only clinical and radiologic abnormality.

A 48-year-old man had had pain on the surface of the patella for 3 months. No effusion or synovial thickening of the knee was detected. Radiographs showed an osteolytic lesion involving a large part of the patella. The surrounding bone did not show sclerosis or osteoporosis (Fig. 1A). Bone scintigrams showed an area of increased uptake of radionuclide in the right patella; no abnormal uptake was seen in the rest of the skeleton. CT scans of the right knee showed an osteolytic lesion of the patella without destruction of the articular surface (Fig. 1B). A dense focus was present inside the lytic area, suggesting a sequestrum. The preoperative diagnosis was osteoid osteoma. The anterior part of the patella was excised. Histologic examination showed necrosis and surrounding granulomata, consistent with a diagnosis of tuberculosis. Tests with Ziehl-Neelsen stain were negative. However, *Mycobacterium tuberculosis* was isolated from cultures of subcutaneous tissue obtained by puncture near the patella; the subcutaneous tissue probably was contaminated after surgery. The patient was treated with rifampicin, isoniazid, and ethambutol; a splint was put on his knee; and he was discharged from the hospital. Two months later, local signs and symptoms were greatly reduced.

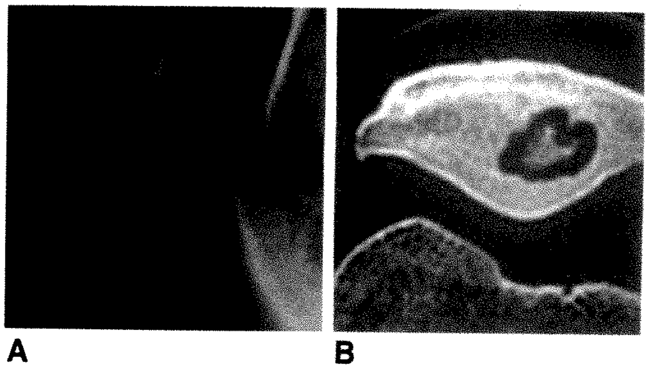

Fig. 1.—Tuberculosis involving the patella.
***A*, Lateral radiograph shows an osteolytic lesion involving large part of right patella.**
***B*, CT scan of right patella shows an osteolytic lesion with a central dense area, suggesting a sequestrum.**

Tuberculosis of the patella is rare. It has been reported in only four cases [1, 2]. In one [2], CT scans showed a lytic lesion similar to the one seen in our case; both lesions had a dense area centrally, suggesting a sequestrum. The radiologic appearance of a malignant bone tumor or a chronic infectious process can be similar to that of a benign tumor. This case highlights the importance of obtaining tissue for bacterial and pathologic analysis in order to establish a definitive diagnosis in such cases.

C. Bonnet
M. DeBandt
E. Palazzo
D. Malaizier
Bichat Hospital
Paris, France

REFERENCES

1. Hartofilakidis-Garofalidis G. Cystic tuberculosis of the patella. *J Bone Joint Surg [Am]* **1969**;51-A:582–585
2. Hernandes-Gimenez M, Tovar-Beltrann JV, Frieyro-Segui MI, Pascual-Gomez E. Tuberculosis of the patella. *Pediatr Radiol* **1987**;17:328–329

Psychogenic Urinary Retention in a Child

Tu and Scanlan [1] report findings in an 11-year-old boy who had urinary dribbling. They consider the case an example of psychogenic retention. This may be correct, but we disagree with some of their findings. The voiding cystourethrogram is described as showing "a large, trabeculated . . . , atonic bladder" and a "normal urethra." In fact, the figure shows a widening in the posterior part of the urethra and a narrow sphincter region, consistent with dyssynergia. This may be a voluntary dyssynergia, but, nonetheless, we would not regard this sphincter as normal. The authors' comment that the bladder is atonic appears to be an assumption. It is possible that the bladder, having gone through a stage of hypertrophy in reaction to the sphincteric obstruction, has now become atonic; however, without urodynamic assessment [2], it is impossible to say this. The dilatation of the upper tracts is a matter of concern. If this is due to reflux, even at low pressure, it could be harmful, and if the pressure increased, damage could be severe. Even noncontractile bladders may show an increase in pressure when they are fully distended. This is one reason intermittent self-catheterization is beneficial in such patients.

Considerable problems may arise if cystourethrographic findings in patients with neuropathic and similar disorders are interpreted without regard to the information provided by urodynamic assessment [3, 4]. Those who make therapeutic decisions on the basis of pictures alone may be putting their patients at some risk.

M. Borzyskowski
H. M. Saxton
Guy's Hospital
London, England SE1 9RT

REFERENCES

1. Tu RK, Scanlan KA. Psychogenic urinary retention (Hinman syndrome) in a child (letter). *AJR* **1992**;158:460–461
2. Saxton HM. Urodynamics: the appropriate modality for the investigation of frequency, urgency, incontinence and voiding difficulties. *Radiology* **1990**;175:307–316
3. Mundy AR, Borzyskowski M, Saxton HM. Videourodynamic evaluation of neuropathic vesico-urethral dysfunction in children. *Br J Urol* **1982**;54: 645–649
4. Mundy AR, Shah PJR, Borzyskowski M, Saxton HM. Sphincter behaviour in myelomeningocele. *Br J Urol* **1985;**57:647–651

Reply

We appreciate the letter from Drs. Borzyskowski and Saxton about our letter to the editor, "Psychogenic Urinary Retention (Hinman Syndrome) in a Child" [1]. We agree with their discussion that Hinman syndrome is not a diagnosis made exclusively on the basis of radiologic studies, and that the syndrome is a complex entity that requires thorough neurologic, urologic, and radiologic studies, which our patient indeed had.

Our patient had comprehensive uroflometric, bladder electromyographic, cranial MR, and complete spinal MR examinations in addition to those studies illustrated in our letter. We agree with Drs. Borzyskowski and Saxton that the bladder, having gone through a stage of hypertrophy in reaction to sphincteric obstruction had eventually become atonic; however, our patient did have appropriate urodynamic evaluation. In addition, we agree completely that dilated upper tracts may imply refluxive renal atrophy, and that this may be harmful. This was recognized early in our evaluation, and intermittent self-catherization by the patient was recommended.

A letter to the editor is a brief, concise format that requires pertinent details to illustrate the issue at hand; in our case, we emphasized the importance of including psychogenic causes in a differential diagnosis of urologic dysfunction. Inherent to such a format is subordination of other details, which unfortunately Drs. Borzyskowski and Saxton assumed were not considered; nothing could be further from the case. In particular, they assumed that we interpreted cystourethrographic findings *without* considering information provided by urodynamic assessments. They imply we made "therapeutic decisions on the basis of pictures alone." We assure Drs. Borzyskowski and Saxton that American radiologic consultation is indeed a corroborative team effort and that we do include all physiologic and anatomic details available.

Raymond K. Tu
Kathleen A. Scanlan
University of Wisconsin
Madison, WI 53792-3252

REFERENCES

1. Tu RK, Scanlan KA. Psychogenic urinary retention (Hinman syndrome) in a child (letter). *AJR* **1992**;158:460–461

Letters are published at the discretion of the Editor and are subject to editing.

Letters to the Editor must not be more than two *double-spaced*, typewritten pages. One or two figures may be included. Abbreviations should not be used. Limit the number of authors to four, or we will list only the first three and add "and colleagues" to the end of the list. See Author Guidelines.

Material being submitted or published elsewhere should not be duplicated in letters, and authors of letters must disclose financial associations or other possible conflicts of interest.

Letters concerning a paper published in the *AJR* will be sent to the authors of the paper for a reply to be published in the same issue. Opinions expressed in the Letters to the Editor do not necessarily reflect the opinions of the Editor.

AJR Subscription

AJR
American Journal of Roentgenology
Official Journal of the American Roentgen Ray Society

If you expect to use what you read
...Subscribe!

AJR is your best source for up-to-date coverage of clinical radiology. Our editors look for articles you can make use of in your daily work. That means lots of practical, pertinent information – the topics that interest you right now. Every month, you get original articles that are relevant to what you do. Plus time-saving review articles that bring together all the confusing or conflicting literature on a particular topic of interest and make sense of it for you. You also get case reports that help you reevaluate your own experience...technical reports that keep you on top of new techniques and give you clear pictures of the procedures used and the results obtained.
All this comes to you in one journal: **AJR**. Enter your subscription today.

Editor: Robert N. Berk, M.D., San Diego, California

YES, please start my subscription to AJR for

☐ 3 yrs. ☐ 2 yrs. ☐ 1 yr. ☐ Individual $125/yr ☐ In-training $25/yr* ☐ Institutional $135/yr

(Add $55 for postage outside the US; in Canada, also add 7% GST)

Payment options:

☐ Check enclosed (Payable to AJR)

☐ Bill me ☐ VISA ☐ MasterCard ☐ AmEx

Card # ____________________ Exp. Date ____________________

Signature ____________________

Name ____________________

Address ____________________

City/state/zip ____________________

* Residents, fellows, interns...when requesting the in-training rate to which you are entitled for 3 years, please supply training status and name of institution. MD residents please add 5% state sales tax. Subscriptions outside the U.S. must be prepaid in U.S. dollars only. Airmail rates available on request.

• *Or call us FREE ... 1-800-638-6423 from anywhere in the U.S. or Canada* •

AJR Bound Volumes

Bound Volumes ... for current subscribers!

AJR
American Journal of Roentgenology
Official Journal of the American Roentgen Ray Society

Now you can get a year's worth of articles in bound volume form – so the information you need will be at your fingertips.

Bound volumes offer the timely coverage only a journal can provide – penetrating discussions of the topics that interest you most by the brightest names in the field – with all the durability and convenience of a hardcover edition. You'll have a year's worth of vital information all arranged and indexed in one sturdy source. And each carefully crafted volume will make a handsome addition to your permanent library.

Bound volumes are available for the current year only and are in addition to the regular subscription price. The 1992 Bound Volume will be mailed in early 1993.

Yes, send me the AJR, American Journal of Roentgenology 1992 Bound Volume at $97 ($112 outside the U.S.)

☐ Check enclosed *MD residents please add 5% sales tax.*

☐ Bill me ☐ VISA ☐ MasterCard ☐ AmEx

Card Number ____________________ Expiration ____________________

Signature ____________________

Name ____________________

Address ____________________

City/state/zip ____________________

NO POSTAGE
NECESSARY
IF MAILED
IN THE
UNITED STATES

BUSINESS REPLY MAIL
FRIST CLASS PERMIT NO.724 BALTIMORE, MD

POSTAGE WILL BE PAID BY ADDRESSEE

Waverly Press
Attn: AJR
P.O. Box 23291
Baltimore, MD 21298-9533

NO POSTAGE
NECESSARY
IF MAILED
IN THE
UNITED STATES

BUSINESS REPLY MAIL
FRIST CLASS PERMIT NO.724 BALTIMORE, MD

POSTAGE WILL BE PAID BY ADDRESSEE

Waverly Press
Attn: AJR
P.O. Box 23291
Baltimore, MD 21298-9533

Review of Current Literature

Initials and addresses of corresponding authors are provided in parentheses for each article so that the reader can obtain reprints directly. Abstracts are printed verbatim from each journal.

The New England Journal of Medicine

A cohort study of transcutaneous oxygen tension and the incidence and severity of retinopathy of prematurity. Flynn JT, Bancalari E, Snyder ES, et al. (JTF, Bescom Palmer Eye Institute, P. O. Box 016880, Miami, FL 33101). *N Engl J Med* 326:1050–1054, April 1992

Background. Retinopathy of prematurity is a disease affecting the blood vessels of the retina in premature infants that may result in scarring, retinal detachment, and loss of vision. An association between this condition and the exposure of premature infants to supplemental oxygen has been postulated, but the relation between retinopathy of prematurity and blood oxygen levels has not been defined. The purpose of this study of a cohort of preterm infants was to correlate the incidence and severity of retinopathy of prematurity with the duration of exposure to different ranges of oxygen tension as measured by transcutaneous monitoring (tcPO$_2$).

Methods. One hundred one premature infants (birth weight, 500 to 1300 g) requiring supplemental oxygen had continuous monitoring of tcPO$_2$. The number of hours during which the tcPO$_2$ was 80 mm Hg or higher was tabulated for each infant during the first four weeks of life.

Results. There was a significant association between the amount of time that the tcPO$_2$ was $\geq$80 mm Hg and the incidence and severity of retinopathy of prematurity. The odds ratio for each 12-hour period in which the tcPO$_2$ was $\geq$80 mm Hg was 1.9 (95 percent confidence interval, 1.2 to 3.0) after adjustment for the following factors: birth weight $\leq$1300 g (odds ratio, 2.3 [95 percent confidence interval, 1.6 to 3.4]), five-minute Apgar score of 7 or less (odds ratio, 7.2 [95 percent confidence interval, 2.5 to 21]), and exposure to inspired oxygen at a fractional concentration $\geq$0.4 (odds ratio, 1.0 [95 percent confidence interval, 0.97 to 1.05]). The association was stronger for tcPO$_2$ values of $\geq$80 mm Hg occurring from the second through the fourth week of life; during this period, the adjusted odds ratio for a 12-hour period of such exposure was 3.1 (95 percent confidence interval, 1.6 to 6.1).

Conclusions. This study supports an association between the incidence and severity of retinopathy of prematurity and the duration of exposure to arterial oxygen levels of 80 mm Hg or higher, measured transcutaneously.

Prediction of mortality in patients with cystic fibrosis. Kerem E, Reisman J, Corey M, Canny GJ, Levison H (GJC, Pulmonary Division, Hospital for Sick Children, 555 University Ave., Toronto, Ontario, Canada M5G, 1X8). *N Engl J Med* 326(18):1187–1191, April 1992

Background. The majority of patients with cystic fibrosis die in early adulthood of lung disease. Lung transplantation is a treatment option for patients with advanced pulmonary disease, although the waiting period for organs may be as long as two years. Our purpose was to determine whether the risk of death due to respiratory failure could be predicted one or two years in advance on the basis of pulmonary function, blood gas levels, and nutritional status.

Methods. The study cohort consisted of 673 patients followed between 1977 and 1989. In each patient, pulmonary function, blood gas levels, nutritional status, and vital status were assessed between 1977 and 1987. Cox proportional-hazards regression analysis was used to compute the relative risk of death within one or two years after particular measurements. The effects of age and sex on mortality were also included in the analysis.

Results. One hundred ninety patients (28 percent) died during the study period. Overall, patients with a forced expiratory volume in one second (FEV$_1$) less than 30 percent of the predicted value, a partial pressure of arterial oxygen below 55 mm Hg, or a partial pressure of arterial carbon dioxide above 50 mm Hg had two-year mortality rates above 50 percent. Among the laboratory measurements, the FEV$_1$ was the most significant predictor of mortality, but age and sex were also significant in predicting risk. After adjustment for age and sex, the relative risk of death within two years was 2.0 (95 percent confidence interval, 1.9 to 2.2) for each decrement in the FEV$_1$ of 10 percent below the predicted value. Among patients with the same FEV$_1$, the relative risk of death was 2.0 (95 percent confidence interval, 1.5 to 2.6) in patients 10 years younger than other patients, and 2.2 (1.6 to 3.1) in female patients as compared with male patients.

Conclusions. Patients with cystic fibrosis should be considered candidates for lung transplantation when the FEV$_1$ falls below 30 percent of the predicted value. Female patients and younger patients may need to be considered for transplantation at an earlier stage.

Hypervitaminosis D associated with drinking milk. Jacobus CH, Holick MF, Shao Q, et al. (E. W. Seely, Endocrine Hypertension Division, Brigham and Women's Hospital, 221 Longwood Ave., Boston, MA 02115). *N Engl J Med* 326(18):1173–1177, April 1992

Background. Vitamin D has been added to milk in the United States since the 1930s to prevent rickets. We report the unusual occurrence of eight cases of vitamin D intoxication that appear to have been caused by excessive vitamin D fortification of dairy milk.

Methods. Medical records were reviewed and a dietary questionnaire was sent to eight patients who had unexplained hypervitaminosis D. Vitamin D analyses with high-performance liquid chromatography were performed on samples of the patients' serum, the dairy milk they drank, and the vitamin D concentrate added to the milk.

Results. All eight patients drank milk produced by a local dairy in amounts ranging from ½ to 3 cups (118 to 710 ml) daily. All had elevated serum 25-hydroxyvitamin D concentrations (mean [±SD], 731 ± 434 nmol per liter [293 ± 174 ng per milliliter]). Six of the eight patients had elevated serum vitamin D_3 concentrations. Of the eight patients, seven had hypercalcemia and one had hypercalciuria but normocalcemia (mean serum calcium, 3.14 ± 0.51 mmol per liter [12.6 ± 2.1 mg per deciliter]). Analysis of the dairy's vitamin D-fortified milk revealed concentrations of vitamin D_3 (cholecalciferol) that ranged from undetectable to as high as 232,565 IU per quart (245,840 IU per liter). An analysis of the concentrate that was used to fortify the milk, labeled as containing vitamin D_2 (ergocalciferol), revealed that it contained vitamin D_3.

Conclusions. Hypervitaminosis D may result from drinking milk that is incorrectly and excessively fortified with vitamin D. Milk that is fortified with vitamin D must be carefully monitored.

Gastroenterology

Comparative studies of esophageal function in systemic sclerosis. Klein HA, Wald A, Graham TO, Campbell WL, Steen VD (HAK, Dept. of Radiology, University of Pittsburgh School of Medicine, Pittsburgh, PA). *Gastroenterology* 102:1551–1556, 1992

Three modalities for assessing esophageal dysfunction in patients with systemic sclerosis were prospectively compared. Seventeen patients underwent (a) esophageal manometry with measurement of distal esophageal peak contraction pressure amplitude, percentage of peristaltic waves, and lower esophageal sphincter pressure; (b) cine-esophagography with scoring based on residual contrast and the character of visualized waves; and (c) esophageal transit scintigraphy with quantification of residual swallowed tracer. Highly significant correlations were found between scintigraphic residual and cine-esophagography score, between scintigraphic residual and manometric amplitude, and indeed between all pairs of measured esophageal function parameters except those involving lower esophageal sphincter pressure. In addition, scintigraphy and cine-esophagography showed comparable ability to discriminate between patients with abnormal and normal esophageal motor function. Symptoms did not significantly correlate with quantitative parameters, nor did they have diagnostic discriminating ability. Induction of Raynaud's phenomenon in a subgroup of patients had no detectable effect on esophageal function. It was concluded that these three diagnostic modalities are approximately equivalent in their ability to detect esophageal dysmotility in systemic sclerosis and measure its severity.

Reprinted with permission by the American Gastroenterological Association.

Digestive Diseases and Sciences

Spectrum of esophageal disorders in children with chest pain. Glassman MS, Medow MS, Berezin S, Newman LJ (MSG, Dept. of Pediatrics, New York Medical College, Munger Pavilion, Rm. 101, Valhalla, NY 10595). *Dig Dis Sci* 37(5):663–666, May 1992

The charts of 83 children with chest pain who underwent esophageal manometry followed by esophagogastroscopy were reviewed. Forty-seven (57%) had normal esophageal histology and normal motility (group I). Esophagitis and normal motility were demonstrated in 15 children (group II), normal esophageal histology and esophageal dysmotility in 13 (group III), and both esophagitis and abnormal motility in 8 (group IV). Diffuse esophageal spasm and achalasia were the most common motility disorders identified (in seven and four patients, respectively). The presence and duration of symptoms, the age, and the gender were not different among the four patient groups. After six months of H_2-receptor blockade, 12 of 15 group II patients were asymptomatic, whereas a significantly smaller percentage (five of 18) of patients with abnormal esophageal motility responded to esophageal dilation or treatment with calcium channel blockade, H_2-receptor antagonist, and/or prokinetic agents ($P < 0.01$). These data suggest that the evaluation of children with chest pain should include esophageal motility testing and esophagoscopy, even in the absence of other gastrointestinal-associated symptoms, and that while treatment of esophagitis results in resolution of symptoms, motility disorders were relatively refractory to therapy.

The Journal of Bone and Joint Surgery

Osteogenesis imperfecta: radiographic classification, natural history, and treatment of spinal deformities. Hanscom DA, Winter RB, Lutter L, Lonstein JE, Bloom B, Bradford DS (DAH, Ste. 1600, 1229 Madison St., Seattle, WA 98104). *J Bone Joint Surg [Am]* 74(4):598–616, April 1992

The natural history of the radiographic changes associated with osteogenesis imperfecta was recorded for sixty-four patients. Detailed clinical data regarding spinal deformities were available for forty-three patients. The patients could be placed in six well defined groups on the basis of a cluster of radiographic changes.

The radiographic criteria used to classify patients who had osteogenesis imperfecta included the shape, dimensions, and appearance of the long bones; the presence of a trefoil pelvis and protrusio acetabuli; and the shape of the vertebrae. Patients can be classified more accurately if the dynamic nature of the radiographic changes is appreciated.

Patients who had Type-A disease, a mild form of osteogenesis imperfecta, maintained the contours of the vertebrae. Most had straight long bones except for five patients who had mild bowing. Patients who had Type-B disease had bowed long bones with wide cortices. The pelvis had a normal contour. The vertebral bodies were biconcave, and kyphosis and scoliosis developed. Patients who had Type-C disease had thin, bowed long bones, and protrusio acetabuli developed around the age of ten years. Patients who had Type-D disease had the same findings as those who had Type-C disease, with the additional finding of cystic changes around the knee by the age of five years. The physes closed early, and the cysts disappeared around the age of fifteen. Patients who had Type-C or D disease had development of severe spinal deformities. Patients who had type-E disease were totally dependent functionally, and spinal deformities developed at a very early age. The long bones appeared to have no cortex. Patients who had Type-F disease had complete disruption of the ribs, which was incompatible with survival.

The natural history of scoliosis in the patients who had Type-B, C, D, or E disease was one of progression of the curve. Bracing used in the treatment of scoliosis in one patient who had Type-E disease and five patients who had Type-C disease was unsuccessful. Arthrodesis of the spine prevented progression of the spinal deformities in patients who had Type-A disease, but the results of the operation were variable in the remaining types of the disease.

The Journal of Urology

Increasing role of angiography and segmental artery embolization in the management of renal stab wounds. Heyns CF, van Vollenhoven P (CFH, Dept. of Urology, Tygerberg Hospital, Tygerberg, South Africa). *J Urol* 147:1231–1234, May 1992

During a 5-year period 93 patients with stab wounds involving the upper urinary tract were treated. Of these patients 79 were treated initially at our department (group 1) and 14 were referred with complications after initial treatment elsewhere (group 2). In group 1, 26 patients (33%) were selected for surgery on the basis of signs of severe blood loss or associated intra-abdominal injury, or major abnormality on the excretory urogram. At operation, a major renal injury and/or associated intra-abdominal laceration was found in 23 patients (88%) and nephrectomy was required in 7 (27%) of them. Nonoperative management was selected in 53 patients (67%) in group 1 and secondary hemorrhage occurred in 8 (15%). Of the patients in group 2, 4 had undergone an operation elsewhere and 10 had been managed nonoperatively. Renal arteriography was performed in 14 patients who had been managed nonoperatively (6 from group 1 and 8 from group 2) and demonstrated a traumatic pseudoaneurysm in 6, an arteriovenous fistula in 5 and no large vessel injury in 3. Selective embolization of the involved segmental artery was successful in 9 of 11 patients (82%) when angiography showed a vascular lesion. This study demonstrates the increasingly important role of renal angiography and selective embolization in the selective nonoperative management of patients with stab wounds of the kidney.

The Journal of Pediatrics

Long-term treatment with growth hormone of children with short stature and normal growth hormone secretion. Moore WV, Moore KC, Gifford R, Hollowell JG, Donaldson DL (WVM, Dept. of Pediatrics, University of Kansas Medical Center, 39th and Rainbow, Kansas City, KS 66103). *J Pediatr* 120:702–708, 1992

Children with short stature but normal growth rate and/or normal growth hormone response to sleep and secretagogues were treated with recombinant methionyl human growth hormone, 0.3 mg/kg per week. In each year of treatment, about 80% of the subjects maintained an increase in growth rate greater than the defined limit (>1 cm/yr above pretreatment growth rate) for continuation of human growth hormone treatment. Comparison of the group that continued to respond to human growth hormone with the group that did not maintain an accelerated growth rate did not reveal differences in bone age delay, sleep or secretagogue-stimulated human growth hormone secretion, degree of short stature either absolute or relative to target height, and somatomedin C concentration before or after initiation of therapy. The group that failed to respond to the human growth hormone treatment in the first year of treatment was younger and had a higher pretreatment growth rate. Review of the longitudinal growth curves revealed five patterns of response to human growth hormone treatment: (1) failure to increase growth rate in two subjects with height SD scores within 1 SD of target height, (2) failure to increase growth rate in five subjects with height SD scores > 1 SD less than the target height, (3) acceleration in growth rate in three subjects that was not maintained until achievement of a height within 1 SD of the target height, (4) acceleration of growth rate in five subjects that was maintained until achievement of a height within 1 SD of the target height, and (5) acceleration in growth rate that was maintained during the 3 years of treatment in 15 subjects who had not attained a height within 1 SD of the target height. We conclude that human growth hormone treatment of some but not all short children with "normal" growth hormone secretion will result in sustained acceleration of growth rate and attainment of prepubertal heights that are closer to but do not exceed their genetic height potential. A clinical trial of human growth hormone may be necessary to determine which subjects will benefit from the treatment.

Surgery, Gynecology & Obstetrics

Significance of sludge and thickened wall in ultrasound evaluation of the gallbladder. Jennings WC, Drabek GA, Miller KA (WCJ, 1145 S. Utica, #202, Tulsa, OK 74104). *Surg Gynecol Obstet* 174(5):394–398, May 1992

Ultrasonography is reliable in detecting the presence of cholelithiasis. Isolated findings of a thickened gallbladder wall or intraluminal sludge (echogenic bile), or both, are regarded as less reliable in the diagnosis of primary gallbladder pathologic factors and are often thought to be indicators of some other pathologic or physiologic process. A retrospective analysis of 72 patients with isolated findings of sludge or thickened wall was performed. Thickened wall remains a nonspecific finding. The presence of sludge on ultrasound, when coupled with normal liver function and amylase test results and right upper quadrant pain, correlated with a significant incidence of intrinsic pathologic findings of the gallbladder.

Journal of Ultrasound in Medicine

Milk of calcium in renal cysts: new sonographic features. Yeh H-C, Mitty HA, Halton K, Shapiro R, Rabinowitz JG (H-CY, Dept. of Radiology, Box 1234, Mount Sinai Medical Center, One Gustave L. Levy Pl., New York, NY 10029-6574). *J Ultrasound Med* 11:195–203, May 1992

Milk of calcium (MOC) in a small renal cyst or calyceal diverticulum is quite common. Ninety-one small renal cysts with MOC in 61 patients were found within a period of 4 years and 7 months. The main sonographic features are echogenic material layering in the dependent portion of a cyst, associated with reverberation echoes without shadowing. Shadowing was seen when MOC was present in larger amounts. Because MOC is usually asymptomatic and requires no treatment, differentiation from other lesions such as calculi or angiomyolipomas is important for proper patient management. MOC is detected more readily by ultrasonography than by radiography or CT.

Reprinted with permission by the American Institute of Ultrasound in Medicine.

News

Visiting Fellowships in Interventional Radiology

The Cardiovascular Diagnostic Laboratory Section, Dept. of Radiology and Radiological Sciences, The Johns Hopkins Medical Institutions, is offering 5-day visiting fellowships, by appointment only, in interventional radiology. The program is designed for radiologists who wish to update their techniques and observe new technologies. The course will include basic and advanced principles of interventional radiology and will be tailored to the needs of each fellow. Fellows will participate in morning conferences, patient rounds, and laboratory observations. A wide range of interventional procedures will be covered, including angiography, angioplasty, percutaneous atherectomy, use of thrombolytic agents, embolization of varicoceles and arteriovenous malformations, intravascular sonography, caval filters, percutaneous placement of central venous catheters, urologic and biliary interventional procedures, and percutaneous biliary endoscopy. Category 1 credit: 40 hr. Fee: $1200. Information: Program Coordinator, The Johns Hopkins Medical Institutions, Office of Continuing Education, Turner Bldg., 720 Rutland Ave., Baltimore, MD 21205; (410) 955-2959.

Preceptorships in Ultrasound

The Division of Ultrasound, Dept. of Radiology, The Johns Hopkins Hospital, is offering visiting preceptorships by appointment only, in ultrasound. The program is designed for physicians or sonographers who have been practicing ultrasound for at least 6 months. Participants will attend ultrasound reporting sessions and observe obstetric, gynecologic, and abdominal sonographic studies and new or unusual techniques. Category 1 credit: 40 hr. Fee: $500. Information: Program Coordinator, The Johns Hopkins Medical Institutions, Office of Continuing Education, Turner Bldg., 720 Rutland Ave., Baltimore, MD 21205; (410) 955-2959.

Magnetic Resonance Imaging 1992

The Dept. of Radiology, University of Cincinnati College of Medicine, is sponsoring Magnetic Resonance Imaging 1992: Back to the Future, Sept. 23–26, at the Omni Netherland Plaza, Cincinnati. Course directors: George S. Bisset III, Robert R. Lukin, and Jonathan S. Moulton. Guest faculty: W. G. Bradley, Jr., J. L. Chezmar, and J. V. Crues III. Category 1 credit: 23 hr. Information; Lynne K. Tiras, CMP, Conference Coordinator, International Meeting Managers, Inc., 4550 Post Oak Pl., Ste. 248, Houston, TX 77027; telephone: (713) 965-0566; fax: (713) 960-0488.

Diagnostic Ultrasound in Gynecology and Obstetrics and Abdomen

The Dept. of Radiology and Radiological Science, The Johns Hopkins Medical Institutions, is sponsoring the 21st annual Diagnostic Ultrasound in Gynecology and Obstetrics and Abdomen, Sept. 25–27, at the Stouffer Harborplace Hotel, Baltimore. The course is designed for both new and experienced practitioners. Clinical problems will be discussed by world-renown experts in diagnostic ultrasound. Category 1 credit: 16.5 hr. Fee (1/2/3 days): physicians, $400/$300/$150; sonographers, nurses, and allied health professionals, $300/$225/$125. Information: Program Coordinator, The Johns Hopkins Medical Institutions, Office of Continuing Education, Turner Bldg., 720 Rutland Ave., Baltimore, MD 21205; (410) 955-2959.

Ultrasound Update: 1992

The Office of Continuing Medical Education, University of California, Davis, School of Medicine and Medical Center, is sponsoring Ultrasound Update: 1992, Oct. 3–4, at the Red Lion Inn, Sacramento, CA. Category 1 credit: 10 hr; CME credit for ultrasound technologists, 10 hr. Information: Office of Continuing Medical Education, University of California, Davis, Medical Center, 2701 Stockton Blvd., Sacramento, CA 95817; telephone: (916) 734-5390; fax: (916) 736-0188.

AFIP Course on Radiologic-Pathologic Correlation

The Armed Forces Institute of Pathology and the American Registry of Pathology are sponsoring the 2nd annual AFIP course on radiologic-pathologic correlation, Oct. 12–16, at the Buena Vista Palace Hotel, Lake Buena Vista, FL. The course will review basic principles of and present new developments in radiologic-pathologic correlation. Each day will be devoted to one of the major organ systems and will include a display and discussion of unknown cases to illustrate contemporary concepts. Information: Alan J. Davidson, M.D., American Registry of Pathology, Armed Forces Institute of Pathology, Washington, DC 20306-6000; telephone: (202) 576-0413 or 576-0414; fax: (202) 576-0678.

Pan-Philadelphia Neurosurgery Conference

The Depts. of Neurosurgery, Hahnemann University, Medical College of Pennsylvania, Temple University, Thomas Jefferson University, and University of Pennsylvania, are jointly sponsoring Pan-Philadelphia Neurosurgery Conference: Management of Cerebrovascular Disease, Oct. 16–17, at the Ritz-Carlton Hotel, Philadelphia. The course will include current methods of medical and surgical management of carotid artery stenosis, cerebral aneurysms, and arteriovenous malformations and the newest techniques in interventional and radiosurgery therapies. Category 1 credit: 7 hr. Fee: $300. Information: Janice Ford, Manager, CME, Hospital of the University of Pennsylvania, 3400 Spruce St., Philadelphia, PA 19104; telephone: (215) 662-6904; fax: (215) 349-5925.

Computed Body Tomography for the Technologist

The Dept. of Radiology, The Johns Hopkins Medical Institutions, is sponsoring Computed Body Tomography for the Technologist: State of the Art, Oct. 22–25, at the Peabody Orlando Hotel, Orlando, FL. The course will present an integrated approach to the use of computed body tomography. Lectures will cover normal anatomy and pathologic changes, with specific emphasis on CT technique and technology. CME credits will be awarded. Fee: $425. Information: Program Coordinator, The Johns Hopkins Medical Institutions, Office of Continuing Education, Turner Bldg., 720 Rutland Ave., Baltimore, MD 21205; (410) 955-2959.

Women's Health and Breast Cancer

The Office of Continuing Medical Education, University of California, Davis, School of Medicine and Medical Center, is sponsoring Women's Health and Breast Cancer, Oct. 24, at the Cancer Center Auditorium, University of California, Davis, Medical Center, Sacramento, CA. Topics to covered include osteoporosis, nutrition, and breast and other cancers. Category 1 credit: 6 hr. Information: Office of Continuing Medical Education, University of California, Davis, Medical Center, 2701 Stockton Blvd., Sacramento, CA 95817; telephone: (916) 734-5390; fax: (916) 736-0188.

Interventional Neuroradiology

The Dept. of Radiology and Radiological Science, The Johns Hopkins University School of Medicine, is sponsoring Interventional Neuroradiology: Complications Associated with Current Techniques, Oct. 24–25, at The Johns Hopkins Medical Institutions in Baltimore. The course will focus on the knowledge necessary to understand when to treat, how to treat, and how to avoid complications. Each major topic will be introduced by lectures on anatomy, clinical presentations, and indications for treatment. Cases illustrating potential risks or complications will be presented by a panel of experts. Each case will be analyzed in detail in order to understand the reasons for the occurrence of complications and how they could have been avoided. Course director: Gerard M. Debrun. Category 1 credit: 18 hr. Fee: physicians, $400; residents, fellows, and technologists (letter required), $250. Information: Program Coordinator, The Johns Hopkins Medical Institutions, Office of Continuing Education, Turner Bldg., 720 Rutland Ave., Baltimore, MD 21205; (410) 955-2959.

Postgraduate Imaging Seminar

The University of California, San Diego, is sponsoring Postgraduate Imaging Seminar, Dec. 28, 1992–Jan. 1, 1993, at the Intercontinental Hotel, Maui, HI. Program director: David S. Feigin. Category 1 credit: 25 hr. Fee (through Dec. 16, 1992/after Dec. 16, 1992): physicians, $550/$595; residents, fellows, and technologists, $350/$395. Information: Dawne Ryals, Ryals and Associates, P. O. Box 1925, Roswell, GA 30077-1925; telephone: (404) 641-9773; fax: (404) 552-9859.

Holiday Imaging Update

Stanford University Medical Center is sponsoring Holiday Imaging Update, Dec. 28, 1992–Jan. 1, 1993, at the Ritz-Carlton Aspen, Aspen, CO. Program director: Barton Lane. Category 1 credit: 23.75 hr. Fee: physicians (Stanford alumni/nonalumni), $500/550; residents, $300. Information: Dawne Ryals, Ryals and Associates, P. O. Box 1925, Roswell, GA 30077-1925; telephone: (404) 641-9773; fax: (404) 552-9859.

The Complete MRI Course

The Dept. of Radiology, Hospital of the University of Pennsylvania, is sponsoring The Complete MRI Course, Jan. 4–8, 1993, at the Ritz-Carlton Kapalua, Maui, HI. The course will cover all areas of MR imaging, including the brain, spine, head and neck, musculoskeletal system, abdomen, chest, and pelvis. Noted authorities in the field will discuss advanced techniques such as fast scanning, MR angiography, and use of phased-coil arrays. Course director: David Yousem. Guest faculty: G. Sze. Category 1 credit: 25 hr (pending). Fee: physicians, $575; residents, $400. Information: Janice Ford, Manager, CME, Dept. of Radiology, Hospital of the University of Pennsylvania, 3400 Spruce St., Philadelphia, PA 19104; telephone: (215) 662-6904 or 662-6982; fax: (215) 349-5925.

Society of Gastrointestinal Radiologists Annual Meeting

The 22nd annual meeting and postgraduate course of the Society of Gastrointestinal Radiologists will be held Jan. 17–22, 1993, at the Scottsdale Princess, Scottsdale, AZ. Information: Lynne K. Tiras, CMP, International Meeting Managers, Inc., 4550 Post Oak Pl., Ste. 248, Houston, TX 77027; telephone: (713) 965-0566; fax: (713) 960-0488.

The American Board of Radiology Examinations

Written examinations for the American Board of Radiology (ABR) are scheduled for Oct. 1–2, 1992, and Sept. 23–24, 1993. Oral examinations will be held at the Executive West Hotel in Louisville, KY, June 7–10, 1993. The ABR will accept applications for admission to the examinations after July 1, but not later than Sept. 30, in the year *preceding* the year in which the examination is to be taken. For application forms and further information: Office of the Executive Director, The American Board of Radiology, 2301 W. Big Beaver Rd., Ste. 625, Troy, MI 48084.

Meeting and Course Review

For the reader's convenience, a summary of upcoming meetings and courses is provided. Detailed listings are given in the *AJR* issue given in parentheses.

Congress of Asian Federation of Societies for Ultrasound in Medicine and Biology, Aug. 30–Sept. 3, Seoul, Korea (Feb)

Cardiovascular and Interventional Radiological Society of Europe Annual Meeting and Postgraduate Course, Aug. 30–Sept. 3, Sitges (Barcelona), Spain (May)
Radiation, Physics, and Biology, Aug. 31–Sept. 4, New York City (May)
Ultrasound Angiography 92, Sept. 2–4, University of Southampton, United Kingdom (Feb)
Radiology in County Kerry, Sept. 6–9, Parknasilla, County Kerry, Ireland (July)
Mammography Update, Sept. 7–11, Santa Fe, NM (June)
Sonography Update, Sept. 9–11, San Diego (July)
Pacific Northwest Diagnostic Ultrasound: OB/GYN Symposium, Sept. 10–12, Seattle (May)
Cancer Prevention and Early Detection, Sept. 10–12, Chicago (Aug)
Pittsburgh Breast Imaging Seminar, Sept. 10–13, Pittsburgh (May)
Symposium on Transrectal Ultrasound, Sept. 11–13, Chicago (May)
Ultrasound and Cardiovascular Technology Review Conference, Sept. 11–13, San Diego (June)
Vancouver Imaging Update 1992, Sept. 13–17, Vancouver, B.C. (May)
Alex Norman Lectureship in Radiology, Sept. 14, New York City (Aug)
Mammographic Interpretation, Sept. 14–17 and Oct. 26–29, Boston (April)
MRI Visiting Fellowships at UCLA, Sept. 14–18, Oct. 5–9, and Dec. 7–11, Los Angeles (Sept 1991)
Organ Imaging Review 1992, Sept. 14–18, Toronto (July)
Advances in CT and MRI, Sept. 15–17, Ann Arbor (Aug)
Dose, Time, and Fractionation in Radiation Oncology, Sept. 16–19, Madison, WI (May)
Seminar in Diagnostic Ultrasound, Sept. 17–19, Ann Arbor (July)
Neurologic Complications of Pregnancy, Sept. 17–19, New York City (July)
ARDMS Exam Preparation Courses: Ultrasound and Doppler Physics, Sept. 18–19, Los Angeles; Sept. 26–27, Atlanta; and Oct. 2–3, Chicago, **OB/GYN Ultrasound,** Sept. 20, Los Angeles, and Oct. 4, Chicago; **Vascular Technology,** Sept. 20–21, Los Angeles, and Oct. 4–5, Chicago (July)
Los Angeles Conference on Musculoskeletal MR Imaging, Sept. 19–20, Los Angeles (Aug)
Radiology/92: Imaging and Intervention, Sept. 19–23, Minneapolis (Aug)
Digital Radiography and Image Management Networking Conference, Sept. 20–23, Santa Monica, CA (Aug)
Musculoskeletal and Neuroradiological MRI, Sept. 21–26, Hilton Head Island, SC (June)
Contemporary MR Imaging, Sept. 24–25, Madison, WI (Aug)
Practicum in Mammography for Technologists, beginning dates, Sept. 28 and Oct. 19, San Diego (May)
Update in Film Screen Mammography, Sept. 30–Oct. 2, Richmond, VA (May)
Western Neuroradiological Society Annual Meeting, Oct. 1–4, San Francisco (July)
International Symposium on Vena Cava Filters, Oct. 9–10, Poitiers, France (July)
Fall Foliage Imaging Seminar, Oct. 9–11, Burlington, VT (May)
International Body Imaging Congress, Oct. 10–17, Kona, HI (Aug)
MRI: Clinical State of the Art 1992, Oct. 12–14, New York City (Aug)
Practical Radiology, Oct. 12–15, Charlottesville, VA (June)
Symposium on Cardiovascular and Interventional Radiology, Oct. 13–16, Boston (Aug)
Nuclear Cardiology Symposium and Workshop, Oct. 14–16, Milwaukee (June)
Progress in Magnetic Resonance, Oct. 15–17, Locarno, Switzerland (June)
Breast Cancer Diagnosis: State of the Art, Oct. 15–17, New York City (Aug)
Chest Imaging 1992, Oct. 16, Toronto (Aug)
Course on Prostate Ultrasound, Oct. 16–17, Albany, NY (June)
Michigan Fall Radiology Conference, Oct. 16–17, Birmingham, MI (July)
Breast Imaging Seminar, Oct. 19–21, New York City (July)
Society of Radiologists in Ultrasound Postgraduate Course, Oct. 23–25, Chicago (June)
Musculoskeletal Imaging, Oct. 24–25, San Diego (July)
International Course on MR Imaging, Oct. 25–28, Riyadh, Kingdom of Saudi Arabia (March)
Postgraduate Radiology Course, Oct. 26–30, San Diego (July)
Magnetic Resonance Imaging and CT Update, Oct. 26–30, Cambridge, MA (Aug)
Interventional Radiology Course, Oct. 30–Nov. 1, San Diego (Aug)
Postgraduate Radiology, Nov. 2–6, Naples, FL (Aug)
Dysphagia Research Society Inaugural Meeting, Nov. 6–8, Milwaukee (July)
Advanced Seminars in Diagnostic Imaging, Nov. 13–15, Laguna Niguel, CA (Aug)

AJR carries announcements of courses, symposia, and meetings of interest to its readers if received a minimum of 5 months before the event. There is no charge; receipt of items by the *AJR* Editorial Office is not acknowledged. Submit items for publication typed double-spaced. Provide title, date, location, brief description, sponsor, course directors, fees, category I credit, and address and telephone number for additional information. Faculty from the host institution will not be listed. Guest faculty names will appear **only** if initials are provided. Mail news items to *AJR* Editorial Office, 2223 Avenida de la Playa, Suite 103, La Jolla, CA 92037-3218.

Classified Advertisements

Positions Available

GADSDEN RADIOLOGY ASSOCIATES is a 3-member radiology group seeking a fourth board-certified/eligible radiologist. Gadsden Radiology covers Baptist Memorial Hospital, a 250-bed hospital performing more that 55,000 radiologic exams/yr. All radiologic modalities are available, including state-of-the-art CT, SPECT, nuclear medicine, special procedures, and MRI. Gadsden Radiology Associates also covers their private office, imaging center, and a breast center. Teleradiography is used for call. Gadsden, AL, is a safe, clean city centrally located on the Coosa River approximately 1 hour from Birmingham, 90 Min. from Chattanooga, and 2 hours from Atlanta, GA. Salary and vacation are excellent. Health insurance and malpractice is paid. Interested candidates contact Homer A. Spencer, M.D., 401 Bay Street, Gadsden, AL 35999; (205) 543-3200, or fax (205) 546-7908. 7–1ap

MRI CLINICAL RESEARCH DIRECTOR—Roswell Park Cancer Institute is seeking an MRI clinical research director with interest in oncologic imaging. The radiology dept. includes a recently built GE MRI and research center linked with 2 new GE Hi-Light Advantage CT systems. This is part of an MRI, CT, SPECT Cancer Imaging and Research Center. PET collaboration with a nearby university is also possible. At this renowned comprehensive cancer center, opportunity for research and academic activity is outstanding. A faculty appointment will be at the School of Medicine and Biomedical Sciences, State University of New York at Buffalo, according to the level of professional qualifications. Please send CV to Andrew A. Gage, M.D., Deputy Institute Director, Roswell Park Cancer Institute, Elm and Carlton Streets, Buffalo, NY 14263. EOE M/F/H/V. 7–10a

BC/BE RADIOLOGIST—Busy clinic-and hospital-based practice is seeking to add additional BC/BE radiologists to its staff of 2 neuroradiologists and 7 general radiologists. Special skills or training in pediatrics, MRI, or nuclear medicine would be beneficial. Physician will join a 270-physician multispecialty group representing over 50 specialities. Fargo Clinic is affiliated with St. Luke's Hospitals, a 400-bed level III care center with a NACHRI designated Children's Hospital. Fargo-Moorhead is a tri-college community of 130,000 which supports an opera company, symphony, community theater, and various athletic events. Year-round recreational opportunities abound. Guaranteed first year salary and competitive compensatory arrangements are available. Respond to Kathleen Toft, Physician Recruitment Director, 737 Broadway, Fargo, ND 58123; (800) 437-4010, ext. 2151. 7–10xa

NEURORADIOLOGIST—Unique opportunity to join expanding N.Y.C. area practice. Board-certified radiologist with 2-yr fellowship in neuroradiology needed to head section of neuroradiology. This well-established university affiliated practice includes 9 board-certified radiologists practicing in a 487-bed teaching hospital and 2 private offices performing approximately 110,000 procedures/yr. State-of-the-art imaging equipment including 1.5-T GE Signa. Competitive salary leading to full equal partnership. Contact Jorge G. Pardes, M.D/William G. Wolff, M.D. Booth Memorial Medical Center; (718) 670-1594 or 1050. 7–10ap

COASTAL FLORIDA, IMMEDIATE OPENING FOR BC DIAGNOSTIC RADIOLOGIST to join 2-man group in single-site practice at well-equipped 110-bed hospital in small east coast community 60 miles from Orlando and Disney World. Relaxed practice includes all aspects of general radiology, including MRI. Excellent fringe benefits and early partnership. Contact Alan J. Stern, M.D. or Joseph E. Godard, M.D., P.O. Box 933, New Smyrna Beach, FL 32170; (904) 427-3401. 7–10ap

DIAGNOSTIC RADIOLOGIST—Private practice opportunity with 2 radiologists. Senior partner retiring. Excellent salary and early partnership. All imaging modalities including MRI. Angio experience desired. University community of 100,000 with abundant outdoor recreation. CV to Dan Davidson, M.D., 3000 W. Deborah Dr., Monroe, LA 71201; (318) 388-7810. 6–9ap

DIAGNOSTIC RADIOLOGIST, NORTHEAST MICHIGAN—Excellent practice opportunity available for a diagnostic radiologist to commence in the autumn of 1992. Alpena Radiology, P.C,. seeks a BC/BE radiologist to complete our 3-man group. We offer excellent income, early partnership and idyllic lifestyle. We require; a friendly, hard-working individual who will be a team player. The ability to work well with us and our excellent medical staff is a must. Alpena General Hospital is a modern 175-bed facility located on the shores of Lake Huron. The hospital provides all radiology equipment including: new R&F equipment (G.E.), Siemens CT, SPECT nuclear imaging, color flow Doppler, DSA, ACR accredited mammography. Siemens mobile MRI will commence shortly. The hospital administration is very supportive. The Alpena area is a sportsman's paradise. Sailing, boating, golf, fishing, hunting, skiing, etc. are all minutes away. Our moderate winters and Mediterranean summers are ideal. For more information please contact Steven Zweig, M.D. or James Weeks, M.D., Dept. of Radiology, Alpena General Hospital, 1501 W. Chisholm Street, Alpena, MI 49707; (517) 356-7250. 7–9ap

DIAGNOSTIC RADIOLOGY AND BREAST IMAGING—Roswell Park Cancer Institute is seeking board-certified radiologists with interests in oncologic and general radiology, CT/MRI, ultrasound, and breast imaging. The modernization of the entire Radiology and Nuclear Medicine Depts. includes a new multidisciplinary Breast Imaging Center, a new MRI Center, and new CT, ultrasound and flouroscopy suites. At this renowned comprehensive cancer center, opportunity for multimodality clinical diagnostic imaging, research and academic activity is outstanding. A faculty appointment will be at the School of Medicine and Biomedical Sciences, State University of New York, according to the level of professional qualifications. Please send CV to Andrew A. Gage, M.D., Deputy Institute Director, Roswell Park Cancer Institute, Elm and Carlton Streets, Buffalo, NY 14263. EOE M/F/H/V. 7–10a

FAIRBANKS, AK—Four diagnostic radiologists seek fifth partner for diversified practice including general radiology, ultrasound, nuclear medicine, MRI (GE 1.5-T), and CT (GE 9800). Hospital and office practice. Desirable life style advantages in a university town. Unlimited access to the outdoors. Excellent salary, benefits, retirement, and vacation. One yr to full partnership. Contact Douglas Hutchinson, M.D., 1919 Lathrop #5, Fairbanks, AK 99701; (907) 452-5092. 8–1ap

VASCULAR/INTERVENTIONAL RADIOLOGIST—Temple University Hospital and School of Medicine is seeking a board-certified vascular/interventional radiologist with fellowship training for a faculty position at the assistant professor rank in the academic yr 1992–1993. This position involves responsibilities in patient care and teaching. Additionally, those candidates with research skills would be preferred. Applicants should contact Francis J. Shea, M.D., Deputy Chairperson, Dept. of Diagnostic Imaging, Temple University Hospital, 3401 N. Broad St., Philadelphia, PA 19140. Temple University Hospital and School of Medicine is an affirmative action equal opportunity employer. 7-9a

CENTRAL WISCONSIN—Established radiology group in independent practice is seeking 2 additional radiologists for growing practice in central Wisconsin. All imaging modalities. Competitive first yr salary with full partner status available second yr. Full benefits. Excellent schools, recreation, and quality of life. Contact David E. Enerson, M.D., 900 Illinois Ave., Stevens Point, WI 54481; (715) 346-5140 or Andrew M. Lucas, M.D., 410 Dewey St., Wisconsin Rapids, WI 54495-8080; (715) 423-6060. 9xa

ISRAEL, DIAGNOSTIC RADIOLOGY—Opportunities for 3- to 4-wk or longer working vacations in a number of Israeli medical centers, on a volunteer basis. Positions varied, arrangements flexible. For information contact Jonathan H. Fish, M.D., 1844 San Miguel Dr., #302, Walnut Creek, CA 94596; (510) 947-0560. 8–10xa

PARTNERSHIP POSITION IN PALM SPRINGS, CA—Well-established, 9-member group has openings for 2 board-certified radiologists. A physician with a strong background in MRI is sought as director of the section of MRI. The other position requires a physician with mammography experience to direct imaging in the breast health section of a new comprehensive cancer center. The group covers a 350-bed hospital and 2 offices in a desirable, rapidly expanding area of southern California. MRI facilities include 1.5-T Picker Vista HPQ with MRA package, ViStar imaging computer, and 1.5-T GE Signa. Other equipment includes 3 CT, a Cemax image processor, 2 Acuson color-flow Doppler ultrasound, 4 nuclear cameras including 2 SPECT, and all other diagnostic modalities. Ground has just been broken on a new 25,000 sq. ft. radiology wing, which will be furnished with state-of-the-art equipment. New trauma center, cancer center, and rehab hospital being built. Excellent compensation and benefits package leading to full partnership. Beaches and large-city amenities of Los Angeles only 2 hr away. Yr-round sunny weather. Ample free time to enjoy southern California and the unparalleled recreational opportunities offered by the resort community of Palm Springs. Direct inquiries to Marvin J. Friedenberg, M.D., Desert Hospital, Dept. of Radiology, 1150 N. Indian Canyon Dr., Palm Springs, CA 92262. 9xa

BOSTON—Expanding private-practice group. No night or evening call. Need experience in mammography. Great lifestyle. Salary leading to equal partnership. Send letter and CV to Box E49, *AJR* (see address this section). 5–10a

DIAGNOSTIC RADIOLOGIST, ABDOMINAL IMAGING—The University of Missouri– Columbia Hospital and Clinics is seeking a radiologist with expertise in abdominal imaging (GI, CT, ultrasound, and MRI). Board-certification required. Fellowship desirable. Tenure and nontenure tracks available at assistant and associate professor levels. Address inquiries to Robert J. Churchill, M.D., Dept. of Radiology, University of Missouri—Columbia Hospital and Clinics, One Hospital Dr., Columbia, MO 65212. An equal opportunity/affirmative action employer. 5–10ap

SUPERB PARTNERSHIP POSITION IN LAS VEGAS—Rapidly expanding 7-member group practice covering 2 full-service imaging centers and a small hospital has an immediate opening. We are looking for an additional board-certified radiologist with an uncommon dedication to excellence in patient care. Our outpatient facilities include 2 MR, 2 CT, angio with a 4-bed recovery area, 5 ultrasound, 5 mammography, 3 SPECT, plus R&F. This is an excellent opportunity for a partnership position with a well-respected group in a growing community. Please send CV to Dr. Mark Winkler, SDMI, 2950 S. Maryland Pkwy., Las Vegas, NV 89109. 3–2ap

PHILADELPHIA—Full- or part-time opportunity for diagnostic radiologist at an outpatient clinic affiliated with the Medical College of Pennsylvania. Modalities include general radiology, mammography, and ultrasound. This individual would rotate through the main dept. with teaching responsibilities for the residency program. Send CV or call Mindy M. Horrow, M.D., Dept. of Radiologic Sciences at the MCP, Main Clinical Campus, 3300 Henry Ave., Philadelphia, PA 19129; (215) 842-6578. 8–9a

SAN ANTONIO, TEXAS—Large group covering multiple hospitals and outpatient facilities seeks radiologists with angiography skills. Send CV to Search Committee, M&S X-Ray Associates, P.O. Box 15920, San Antonio, TX 78212-9510. 7–12ap

SOUTH CENTRAL FLORIDA—Immediate opening for board-certified (or eligible with intention to certify), Florida licensed general diagnostic radiologist. Four radiologists are now covering 3 hospitals totaling 250 beds as well as private diagnostic office with mammography. Onsite MRI at 1 hospital and mobile unit at another. Expertise in all modalities including interventional and angiography. Competitive package including early partnership. Send CV to Lawrence S. Ross, M.D., Radiology Consultants, P.A., 114 Medical Center, Sebring, FL 33870. 9xa

CENTRAL NEW JERSEY, IMMEDIATE OPENING—Full-time and part-time radiologists with fellowship training or equivalent experience in vascular/interventional and/or in MR imaging to join 6-member group. Must be willing to do other aspects of diagnostic radiology, mammography, ultrasound, CT, and nuclear medicine. Practice includes a 340-bed community hospital, a private radiology office, and an MRI facility. Area is within a 10-mi. radius of Princeton and is near New York City and Philadelphia. Competitive salary, excellent benefits, and partnership opportunity. Send CV or call Margaret M. Beck, Business Manager, 2127 Hamilton Ave., Trenton, NJ 08619; (609) 587-9410. 9xa

MAMMOGRAPHER—Dartmouth-Hitchcock Medical Center is seeking radiologist to lead mammographic program with strong interest in new techniques and teaching. Dept. consists of 18 staff, 12 residents, 2 fellows, with a full range of modern radiologic practice. A new dept. in a new 420-bed medical center. Separate mammography section with state-of-the-art equipment. Opportunity exists to collaborate with Jack Wennberg in Outcomes Research. Seeking senior assistant, full professor level to be member of a 200-physician academic multispecialty group which forms the clinical faculty of Dartmouth Medical School. Write to Peter K. Spiegel, M.D. Chairman, Dept. of Diagnostic Radiology, Dartmouth-Hitchcock Medical Center, One Medical Center Dr., Lebanon, NH 03756. 7–9ap.

LIVE WHERE YOU CAN PLAY, THE SMOKY MOUNTAINS OF WESTERN NC—A 5-person group seeks a BC/BE diagnostic radiologist with experience in all modalities. Special interest in angio/interventional or nuclear medicine desired. Competitive salary leading to early full partnership. State-of-the-art equipment. Friendly, small-town atmosphere in 75,000+ population county. Plentiful amenities and diverse recreational activities in the immediate area. Moderate 4-season climate. Position available at this time, but would hold for suitable candidate. Send CV or call Dr. Ronald Liljedahl, Hendersonville Radiological Consultants, 807 N. Justice, Hendersonville, NC 28739; (704) 696-1046, work; (704) 697-6741, home. 6–9ap

FACULTY POSITION IN ABDOMINAL IMAGING—Dartmouth-Hitchcock Medical Center is seeking a faculty member at the senior assistant, full professor level with experience and interest in abdominal imaging. Clinical responsibility will be in an entirely new 420-bed clinical facility opening in Oct. 1991 with state-of-the-art instrumentation. Position will involve responsibility for residency training in GI/GU area. Proven record of academic performance including research and teaching with an interest in providing academic guidance for energetic staff of younger radiologists. Interested candidates write with CV to Peter K. Spiegel, M.D., Chairman, Dept. of Diagnostic Radiology, Dartmouth-Hitchcock Medical Center, Hanover, NH 03756. AA/EOE. 7–9ap

CARDIOVASCULAR RADIOLOGIST wanted for clinical care, teaching and research at the New England Deaconess Hospital (NEDH), a 450-bed adult tertiary-care hospital. NEDH is an equal opportunity/affirmative action employer and is fully affiliated with Harvard Medical School. Submit CV to Melvin Clouse, M.D., Chairman, Dept. of Radiology, New England Deaconess Hospital, 185 Pilgrim Rd., Boston, MA 02215. 8–9a

ACADEMIC BC/BE DIAGNOSTIC RADIOLOGIST wanted at the New England Deaconess Hospital (NEDH), a 450-bed adult tertiary-care hospital. NEDH is an equal opportunity/affirmative action employer and is fully affiliated with Harvard Medical School. Applicants should have training experience in body imaging, CT, MRI and ultrasound. Preference will be given to candidates who have experience in resident training and managing a teaching program. Submit CV to Melvin Clouse, M.D., Chairman, Dept. of Radiology, New England Deaconess Hospital, 185 Pilgrim Rd., Boston, MA 02215. 8–9a

CT/ULTRASOUND/MRI, VASCULAR/INTERVENTIONAL, NEURORADIOLOGISTS—The Medical College of Pennsylvania is seeking BC/BE radiologists with expertise in the above specialty areas. Responsibilities involve clinical work, teaching (resident and medical students), and research as desired. Competitive salary and benefits. Immediate full/part-time openings. Please contact Mindy M. Horrow, M.D., Dept. of Radiologic Sciences, Medical College of Pennsylvania, 3300 Henry Ave., Philadelphia, PA 19129; (215) 842-6578. 8–9a

LAKE PLACID-SARANAC LAKE, NY—Director of Radiology. State-of-the-art radiology dept. seeks BC director skilled in all imaging modalities. Angiography essential. Modern, 90-bed medical center in beautiful Adirondack region. Send CV to New England Health Search, 63 Forest Ave., Orono, ME 04473; (207) 866-5680. 8–9a

IMMEDIATE OPENING, DIAGNOSTIC RADIOLOGIST, NEW YORK STATE—Expanding, progressive and innovative 26-radiologist group seeking BC/BE university trained radiologist with experience in body CT and body MRI. Private practice opportunity in university affiliated tertiary teaching hospitals as well as smaller suburban and rural hospitals and multiple comprehensive free-standing imaging centers. Practice includes 4 MRI units, 5 CT scanners and complete range of current ultrasound, mammography, diagnostic, interventional and nuclear medicine technology. The practice is centered in an Upstate New York community of approximately 1 million with full cultural, educational and sports opportunities. Excellent compensation and job security. Send CV to Dr. Steven Herbert, 2273 South Clinton Ave., Rochester, NY 14618. 8–9a

TWO DIAGNOSTIC RADIOLOGISTS, WASHINGTON—Prominent, 100-physician multispecialty clinic in Pacific Northwest seeks both a diagnostic radiologist and an interventional radiologist. Interventional radiologist should have fellowship training and/or extensive experience in interventional radiology. Diagnostic radiologist should have general radiology experience to include all full-scope imaging services. Guaranteed salary and partnership track available. Excellent benefit package. Abundant 4-season recreational opportunities. Send CV to Fred Bockenstedt, M.D., P. O. Box 489, Wenatchee, WA 98807. 5-10ap

DIAGNOSTIC RADIOLOGIST, NUCLEAR MEDICINE—500-bed hospital Midwest-based private practice radiology group seeking applications for a BE/BC radiologist with nuclear medicine competency and interest. Successful applicant will devote 50% of their time to nuclear medicine and remaining involved in diagnostic radiology. Nuclear medicine dept. utilizes state-of-the-art SPECT and planar equipment to support a wide range of imaging studies including nuclear cardiology. Equipment includes a majority of Siemens cameras and computers as well as a Trionix Triad camera. Imaging studies available include new heart agents and monoclonal antibodies. Excellent salary, benefits, retirement and vacation. Interested candidates should send CV and references to James E. Call, M.D., Radiology Nuclear Medicine, Inc., 622 Doctors Building, 4239 Farnam St., Omaha, NE 68131. 8–10ap

THE DEPT. OF RADIOLOGY AT THE UNIVERSITY OF MASSACHUSETTS MEDICAL CENTER in Worcester has a full-time position available in the musculoskeletal division at the rank of assistant, associate or full professor beginning July 1, 1992. The medical center is a 370-bed university hospital and medical school located approximately 40 miles west of Boston. The dept. consists of 25 staff, 15 residents and 2–4 fellows and does approximately 140,000 exams/yr. The dept. is well-equipped with 2 GE 9800 HiLite CT scanners as well as 2 GE 1.5-T MRI scanners and a 2.0-T small-bore unit for animal research in a stand-alone facility. The hospital is a Level 1 trauma center maintaining a full-time trauma service and an active emergency room with an associated emergency medicine residency of approximately 36 residents. The hospital is serviced by 2 Life Flight helicopters. A strong interest in teaching and collaborative clinical research is desired. Rank and salary are commensurate with experience. For further information contact Edward H. Smith, M.D., Chairman, Dept. of Radiology, University of Massachusetts Medical Center, 55 Lake Ave. North, Worcester, MA 01655; (508) 856-3252. UMMC is an equal opportunity/affirmative action employer. 8–9ap

MUSCULOSKELETAL RADIOLOGIST—University of Arkansas for Medical Sciences, University Hospital, and McClellan Veterans Administration Hospital. This 14-person group in a large tertiary-care medical center seeks musculoskeletal radiologist. The 800-bed complex, receiving referrals from the entire state of Arkansas and from surrounding states, offers full service radiology depts., including digital fluoroscopy, nuclear medicine (with SPECT), Acuson ultrasound with color Doppler, GE 1.5-T MRI, and GE, Picker, and Phillips CT scanners. Position is for director of the musculoskeletal radiology division and includes musculoskeletal MR, CT, and interventional/biopsy cases, as well as 1 academic day per week. A 1- or 2-yr fellowship in musculoskeletal radiology is suggested; salary and academic intensity are negotiable. Little Rock is a medium-sized city in the foothills of the Ouachita Mountains with little traffic and clean air and water. Please send letters and CV to Richard E. Leithiser, Jr., M.D., Associate Professor of Radiology, University of Arkansas for Medical Sciences, 4301 West Markham, Little Rock, AR 72205. 8–10a

MAINE—BC/BE diagnostic radiologist with MRI and/or interventional skills. Join well-established multidimensional group. Associate leading to partnership. Competitive financial package. Family oriented small city. Business and cultural center. Major university. One hour to coast. Easy access to ski areas. Send CV to New England Health Search, 63 Forest Ave., Orono, ME 04473; (207) 866-5680.

DIAGNOSTIC RADIOLOGIST with skills in CT, MR, interventional, ultrasound, and nuclear medicine needed to join group of 8 board-certified radiologists. Growing practice in eastern Washington at a 228-bed hospital, a new multimodality imaging center and 1 private office. Potential for long-term practice is excellent. Top-notch school system, including 3 first-rate universities. Excellent hunting, fishing, boating and skiing. Contact Eric W. Koelsch, N. 5901 Lidgerwood, Ste. 18B, Spokane, WA 99207; (509) 487-1264. 8-1ap

PEDIATRIC RADIOLOGIST-CHILDREN'S HOSPITAL OF LOS ANGELES—Several faculty positions are available in pediatric radiology including ultrasound, MR, CT, and angiography/interventional radiology, and a position as a second pediatric neuroradiologist. CHLA is a 331-bed primary and tertiary-care hospital with pediatric and surgical programs. Faculty appointments are at the University of Southern California. The dept. is fully equipped with modern equipment including color Doppler ultrasound, CT, and a 1.5-T magnet. Approximately 100,000 radiologic studies are performed annually. Residency training and a fellowship training program are in place with an active teaching program. CHLA is a EOE/AA employer. For information write to Beverly P. Wood, M.D., Radiologist-in-Chief, Dept. of Radiology MS #81, Children's Hospital Los Angeles, 4650 Sunset Blvd., Los Angeles, CA 90027. 8–10a

PART-TIME/LOCUM TENENS DIAGNOSTIC RADIOLOGIST NEAR NORTH CAROLINA COAST—High quality, amiable, hospital-based 2-man practice seeks well-trained BC/BE radiologist. Practice encompasses all imaging modalities but expertise in all modalities not required. Work schedule flexible. One hour to beautiful beaches. Send CV, inquiries to *AJR* Box 80 (see address this section). 9ap

BOARD-CERTIFIED RADIOLOGISTS FOR OUTPATIENT MEDICAL GROUP—Located in San Juan Capistrano for late 1992, early 1993. Bristol Park Medical Group is a rapidly growing large provider of care for HMO, PPO, industrial and private patients. M–F, no call or weekends. Ultrasound, mammography and diagnostic. Quality support staff and equipment, generous benefits and incentive program. Please send CV to Arlene Barton, Bristol Park Medical Group, Inc., 3160 Redhill Ave., Costa Mesa, CA 92626, or call Arlene Barton (714) 241-6362. An equal opportunity employer. 9ap

GROWING HOSPITAL/OFFICE PRACTICE IN BEAUTIFUL COEUR D' ALENE, ID, 40 MILES EAST OF SPOKANE, WA, is seeking a general radiologist to join 5-man group. All modalities available including MRI. Experienced individuals with subspecialty preferred. Send CV to Peter Semogas, M.D., 1104 Ironwood Dr., Coeur d'Alene, ID 83814. 8-9a

FLORIDA, STAFF RADIOLOGIST—Opportunity for board-certified/eligible diagnostic radiologist with experience in reading plain films, fluoroscopy, ultrasound, CT, nuclear medicine, and some angiography, in the radiology service at this Dept. of Veterans Affairs (VA) Medical Center. Affiliation in surgery with the University of Florida. Excellent employment benefits including 30 days paid vacation and 15 days paid sick leave per yr; liberal life and health insurance benefits; malpractice insurance; and retirement program. Moving expenses paid. Lake City, Fl., is located in northern Florida with a mild climate yr- round. Extensive outdoor recreational activities, reasonable cost of living no state income tax, fine schools, local community college, and nearby universities provide opportunities for continuing education and cultural diversion. Licensure in any state acceptable. Contact or send CV to Richard Parker, M.D., Chief of Radiology, VA Medical Center, Lake City, FL 32055-5898; (904) 705-3016, ext. 2543. An equal opportunity employer. 8–9a

VASCULAR/INTERVENTIONAL RADIOLOGIST—The University of Arizona Dept. of Radiology is recruiting a fellowship-trained vascular/interventional radiologist to join the faculty at the assistant associate professor level. Facilities at the University Hospital (300-bed) and Tucson Veteran's Hospital (300-bed) are state-of-the-art. Income is based on AAMC guidelines, but is negotiable. Contact Gerald D. Pond, M.D., Head, Section of Vascular and Interventional Radiology, University of Arizona Health Sciences Center, Tucson, AZ 85724; (602) 626-6794. Women and minorities are encouraged to apply. The University of Arizona is an EEO/AA employer. Applications will be accepted until position is filled. 9xa

NW ROCKY MOUNTAINS—Highly respected 8-person group with strong subspecialty interests seeks highly qualified radiologist. Fellowship or academic experience preferred. Body imaging/MRI or nuclear medicine with boards or ABR special competency strongly desired. Position includes all aspects of radiology. Practice is located in Boise, ID , which has many recreational and cultural amenities. Reply to Paul Traughber, M.D., or J. Tim Hall, M.D., Dept. of Radiology, St. Alphonsus Regional Medical Center, 1055 No. Curtis Rd., Boise, ID 83706; (208) 378-2161. 8-1a

EXCELLENT OPPORTUNITY FOR FULL-TIME BREAST IMAGING RADIOLOGIST—The Dept. of Diagnostic Radiology of Henry Ford Hospital in Detroit is seeking a board-certified radiologist with subspecialty training or expertise and experience in breast imaging. The Henry Ford Health System in the Metropolitan Detroit area performs over 35,000 mammograms annually. The Breast Imaging Division also performs breast sonography and fine needle aspiration cytology. We are a subspecialized dept. with large residency and fellowship programs, including mammography. There is opportunity for clinical research. Eligibility for or licensure by the State of Michigan is required. Please contact Murray Rebner, M.D., Director of Breast Imaging, Dept. of Diagnostic Radiology, Henry Ford Hospital, 2799 W. Grand Blvd., Detroit, MI 48202-2689; (313) 876-1331, fax (313) 876-9134. The Henry Ford Health System is an equal opportunity institution. 8-10 ap

FACULTY POSITIONS—The University of Colorado Health Sciences Center, Denver, Colorado, is recruiting for faculty in the following positions: Angiography/interventional radiology, body imaging/ultrasound. The level of faculty appointment depends upon prior experience. Candidates interested in working in a stimulating academic and clinical environment are encouraged to send their CV to Michael L. Manco-Johnson, M.D., Professor and Chairman, Dept. of Radiology, University of Colorado Health Sciences Center, Campus Box C-277, 4200 E. Ninth Ave., Denver, CO 80262; (303) 270-7719. The University of Colorado Health Sciences Center is committed to equal opportunity and affirmative action. 8-9a

PART-TIME RADIOLOGIST—General diagnostic radiology; no call; no angiography; several half days per week; hours flexible; state-of-the-art-equipment; large community hospital, southern Chicago suburb. Interested individuals should contact Peter Kucharski, M.D., Dept. of Radiology, Ingalls Hospital, Harvey, IL 60426; (708) 333-2300, ext. 5600. 9-1lap.

MUSCULOSKELETAL RADIOLOGIST AT THE ARMED FORCES INSTITUTE OF PATHOLOGY—The Dept. of Radiologic Pathology at the Armed Forces Institute of Pathology is seeking a civilian radiologist to head its section of musculoskeletal radiology. The position will be funded through the American Registry of Pathology and the salary will be commensurate with the individual's academic rank. Any board-certified, fellowship-trained, musculoskeletal radiologist may apply by sending a letter and a copy of his or her CV to James L. Buck, M.D., Chairman, Dept. of Radiologic Pathology, Armed Forces Institute of Pathology, Washington, D.C. 20306-6000; (202) 576-2973. 9a

ASHEVILLE, NC, a beautiful mountain city, serves as the referral center for western N.C. We are a dynamic 13-person group which serves a 400-bed hospital, an active private office, and a stand-alone MRI facility. We are seeking a fellowship-trained individual to join our group. We have flexibility as to the type of fellowship. Interested candidates should contact Janet Garrett, M.D., P.O. Box. 2959, Asheville, NC 28802; fax (704) 252-1408. 9a

WASHINGTON, DC, NEURO AND MUSCULOSKELETAL MRI—Highly successful 15-person radiology group serving 1 hospital and 6 wholly owned outpatient facilities in downtown Washington, DC, and surrounding affluent suburbs has a rare opportunity for an individual to help cultivate a new MRI service. Fellowship training in MRI with at least 2 yrs of experience in neuro and musculoskeletal MRI is desirable. In addition, the successful candidate must have a strong willingness to provide service in all aspects of diagnostic radiology including ultrasound, CT, mammography, and general diagnosis. Angiography and interventional not required. Highly competitive salary and excellent fringe benefits package leading to full partnership. If interested please send CV to Ian M. Lande, M.D., 3022 Williams Dr., Ste 204, Fairfax, VA 22031. 9a

THE DEPT. OF PEDIATRIC IMAGING AT CHILDREN'S HOSPITAL OF MICHIGAN, DETROIT, MI, is recruiting academic radiologists for 2 divisions of the dept. interventional radiology and PET. The candidate for the interventional position must be certified in diagnostic radiology by the American Board of Radiology and must be eligible for active membership in the Society of Pediatric Radiology. The candidate for PET must be certified by the American Board of Nuclear Medicine. Duties for both positions include clinical service, teaching, and research. Address inquiry and CV to Thomas L. Slovis, M.D., Radiologist-in-Chief, Dept. of Pediatric Imaging, Children's Hospital of Michigan, 3901 Beaubien Blvd, Detroit, MI 48201-9985; (313) 745-5460. 9a

RADIOLOGIST—DVI Health Services Corporation, a publicly traded company on the New York Stock Exchange, has opportunities for radiologists in outpatient diagnostic imaging facilities located in various states. Immediate openings are available in Arizona and Wisconsin for individuals with extensive MRI experience and credentials and in Arizona for individuals with general radiology experience. Send resumes to Cynthia Cohn, DVI Health Services Corporation, One Park Plaza, Ste 800, Irvine, CA 92714; (714) 474-5800. Compensation commensurate with experience. 9a

BC/BE DIAGNOSTIC RADIOLOGIST—Immediate opening with a well-established 12-person private hospital-based radiology group seeking diagnostic radiologist. Group is affiliated with 710-bed teaching medical center. Hospital is a tertiary referral center and a designated trauma center. Outstanding professional, financial and lifestyle opportunities with outstanding schools are available to qualified candidate. You may call Mariann Clark, Medical Search Consultant, at (800) 882-5911 or reply to Box 90 *AJR* (see address this section) 9-10a

EASTERN VIRGINIA—Position available for BC/BE diagnostic radiologist with interest/specialty training in body imaging and MR. Experience in all modalities needed and capability for basic angiography call. Practice includes full service regional medical center, multiple satellite offices, benefit package, and partnership tract. Location offers attractive climate and diversity for recreation. Send CV with initial correspondence to D. T. Bartol, M.D., Dept. of Radiology, Riverside Regional Medical Center, J. Clyde Morris Blvd., Newport News, VA 23601. 9-10ap.

INSTRUCTOR/ABDOMINAL RADIOLOGY—The Dept. of Radiology at the University of Minnesota has 1 or 2 yr post-residency positions in abdominal radiology available at the rank of instructor (temporary, annual renewable) beginning July 1, 1994. Minimum requirements include successful completion of an accredited radiology residency and board-certification in radiology by beginning date of appointment. The position will consist of body MRI, CT and ultrasound rotations. In addition to clinical practice, responsibilities will include all facets of abdominal radiology as well as graduate and undergraduate medical instruction and assisting with related dept. research projects. Salary is negotiable and competitive and is dependent upon past scholarly productivity and post-M.D. experience. Applicants must be licensed or able to obtain a license to practice medicine in the state of MN before appointment date. Applications will be accepted through December 31, 1992. Send letters to Dr. Janis Letourneau, Professor, Dept. of Radiology Box 292 UMHC, University of Minnesota, 420 Delaware St. S.E., Minneapolis, MN, 55455. The University of Minnesota is an equal opportunity educator and employer. 9a

SUBSPECIALTY RADIOLOGY POSITIONS—An expanding 14-man subspecialized dept. has openings for fellowship-trained individuals in its section of cardiovascular and interventional radiology and its body imaging section. A broad scope of angiographic procedures, including neuroangiography, and all types of interventional procedures are currently performed by 2 full-time interventionists. Two well-equipped angiography suites are available and plans for expansion/updating are underway. An adjacent, fully staffed clinical office practice is available. Three full-time body imagers have 4 CT scanners, 7 ultrasound suites, and 2 MR scanners at their disposal. The full range of imaging procedures, including obstetrical ultrasound, are performed. Openings in other specialties are available locally as well. Physician couple applications are encouraged. Please send inquiries with CV to Box 91 *AJR* (see address this section). EOE/AAM/F/H/V. 9a

INSTRUCTOR/CARDIOVASCULAR/INTERVENTIONAL RADIOLOGY—The Dept. of Radiology at the University of Minnesota has 2-yr post-residency positions in cardiovascular/interventional radiology available at the rank of instructor(temporary, annual renewable) beginning July 1, 1994. Minimum requirements include successful completion of an accredited radiology residency, and board-certification in radiology by beginning date of appointment. In addition to clinical practice and training, responsibilities will include graduate and undergraduate medical instruction in cardiovascular/interventional radiology as well as assisting with related departmental research projects. Salary is negotiable and competitive and dependent upon past scholarly productivity and post-M.D. experience. Applicants must be licensed or able to obtain license to practice medicine in the state of MN before appointment date. Applications for these positions will be accepted through December 31, 1992. Send letters to Kurt Amplatz, M.D., Dept. of Radiology, Box 292 UMHC, University of Minnesota, 420 Delaware St. S.E., Minneapolis, MN 55455. The University of Minnesota is an equal opportunity educator and employer. 9a

OVERWORKED? Need a higher income and more vacation time? Tired of big city commuting and inner-city crime? Want a better quality of life but still want a professional challenge? We need a BC, capable, motivated radiologist qualified in all phases of diagnostic radiology but with special interest, ability and preferable fellowship training in MR to join a 7-member group of American trained, BC radiologists in 450-bed tertiary-care hospital, located in 125,000 populated city, 1 1/2 hrs from Pittsburgh and 3 1/2 hrs from DC and Baltimore. We do 100,000 exams/yr with state-of-the-art equipment. Generous starting salary and benefit package with complete and equal partnership to follow. If interested, send CV to Jon Abrahams, M.D., Chairman, Dept. of Radiology, Conemaugh Hospital, Johnstown, PA 15905; (814) 536-7226. 9-11ap

FULL-TIME BC/BE DIAGNOSTIC RADIOLOGIST needed to replace retiring senior partner in a friendly, cooperative 4-man group in south-central Idaho. 165-bed hospital with GE Signa 1.5-T MR, GE 9800 quick CT, Acuson XP, and good technical staff. General radiology including angio, interventional, and nuclear medicine. Good income and vacation schedule 1 yr to partnership. Nice community with extensive nearby skiing, hunting, fishing, etc.,80 miles from Sun Valley, 4 hrs drive from Yellowstone. Send CV and references to Dr. Evan Thomas, Southern Idaho Radiology, P.O. Box AB, Twin Falls, Idaho 83303. 9-11ap

RADIOLOGIST—Immediate opening for experienced radiologist at St. Agnes Hospital, a facility associated with New York Medical College. Candidate must be board-certified or eligible and possess a current NY State license at time of appointment. Academic rank granted by New York Medical College commensurate with expertise and experience. Excellent salary and fringe benefits. Send CV to Michael S. Tenner, M.D., Professor and Chairman, Dept. of Radiology, New York Medical College, Valhalla, NY 10595; (914) 285-8546. An equal opportunity employer. 9a

INSTRUCTOR/NUCLEAR MEDICINE—The Department of Radiology at the University of Minnesota has 1- to -2-yr. post-residency positions in nuclear medicine available at the rank of instructor (temporary, annual renewable) beginning July 1, 1994. Minimum requirements include successful completion of an accredited radiology residency and board-certification in radiology by beginning date of appointment. In addition to clinical practice and training, responsibilities will include graduate and undergraduate medical instruction in nuclear medicine as well as assisting with related departmental research projects. Salary is negotiable and competitive and dependent upon past scholarly productivity and post-M.D. experience. Applicants must be licensed or able to obtain license to practice medicine in the state of MN before appointment date. Applications for these positions will be accepted through December 31, 1992. Send letters to Robert Boudreau, M.D., Dept. of Radiology, Box 292 UMHC, University of Minnesota, 420 Delaware St. S.E., Minneapolis, MN, 55455. The University of Minnesota is an equal opportunity educator and employer. 9a

ABDOMINAL IMAGING RADIOLOGIST—Temple University Hospital and School of Medicine is seeking a board-certified radiologist with fellowship training in abdominal imaging to serve in the section of abdominal imaging. This is a faculty position at the rank of assistant professor. The candidate should have strong clinical skills in CT, MRI, ultrasound, gastrointestinal radiology and urography. The position involves major teaching responsibilities for both residents and medical students. Candidates with established research support would be preferred. Send cover letter/CV to Francis J. Shea, M.D., Professor and Deputy Chairperson, SmithKline Beecham Dept. of Diagnostic Imaging, Temple University Hospital, 3401 N. Broad St., Philadelphia, PA 19140. Temple University Hospital is an affirmative action/equal opportunity employer. 9a.

INSTRUCTOR/PEDIATRIC RADIOLOGY—The Dept. of Radiology at the University of Minnesota Hospital has 1 or 2-yr post-residency positions in pediatric radiology available at the rank of instructor (temporary, annual renewable) beginning July 1, 1994. Minimum requirements include successful completion of an accredited radiology residency and board-certification in radiology by beginning date of appointment. In addition to clinical practice and training, responsibilities will include graduate and undergraduate medical instruction in pediatric radiology as well as assisting with related dept. research projects. Seven experienced pediatric radiologists will be actively involved in the training process. The clinical experience will be equally distributed between the Minneapolis Children's Medical Center and the University Hospital. Salary is negotiable and competitive, and dependent upon past scholarly productivity and post-M.D. experience. Applicants must be licensed or able to obtain license to practice medicine in the state of MN before appointment date. Applications for these positions will be accepted through December 31,1992. Send letters to Deborah Day, M.D., Dept. of Radiology, Box 292 UMHC, University of Minnesota Hospital, 420 Delaware St. S.E., Minneapolis, MN 55455. The University of Minnesota is an equal opportunity educator and employer. 9a

DIRECTOR OF RADIOLOGY—Applications are invited for the full-time staff specialist position of director of radiology at Westmead Hospital, (Sydney, Australia) a modern 850-bed major teaching hospital of the University of Sydney with a tertiary referral population of approx. 1.5 million. The hospital is located in a pleasant setting only 16 miles from the Central Business District. Sydney enjoys a temperate climate with excellent beach and recreational facilities and has a population of nearly 4 million. The dept. offers a wide range of diagnostic services including CT, mammography, ultrasound, MRI, angiography and interventional radiology. The successful applicant will have a proven record in administration, teaching and research; the appointee will be considered by the University of Sydney for the award of an appropriate clinical academic title. There is an expectation that an additional academic post (funded by Westmead Hospital) will be created in the dept. of radiology in the near future. Initially, the appointment will be for 3 yrs; the successful applicant will the be eligible to apply for re-appointment when the position is re-advertised. Salary and conditions are in accordance with the Medical Officers, Hospital Specialists Award, and include right of private practice. Further information is obtainable from Dr. Stephen Cahill (acting director), Dept. of Radiology, Westmead Hospital, Westmead, NSW, 2145, Australia; Phone 61-2-633-6523, fax 61-2-687-2109. Closing date is 30 November 1992. An equal opportunity employer supporting a smoke-free environment. 9a

RESIDENT—Due to an unexpected vacancy, the University of Missouri-Kansas City will have an opening for a 2nd, 3rd, or 4th yr radiology resident, beginning January 2, 1993. The UMKC Radiology Residency program is an accredited program and has been in existence for approximately 7 yrs. Truman Medical Center - West is the primary teaching hospital for the program. Applicants must be eligible for Missouri licensure. Competitive salary and benefits. Please forward your CV and letter of interest to Kenneth Alfieri, M.D., Residency Program Director, Truman Medical Center, Dept. of Radiology, 2301 Holmes, Kansas City, MO 64108. 9-11a

INSTRUCTOR/MUSCULOSKELETAL RADIOLOGY—The Dept. of Radiology at the University of Minnesota has 1- to 2-yr post-residency positions in musculoskeletal radiology available at the rank of instructor (temporary, annual renewable) beginning July 1, 1994. Minimum requirements include successful completion of an accredited radiology residency, and board-certification in radiology by beginning date of appointment. In addition to clinical practice and training, responsibilities will include graduate and undergraduate medical instruction in musculoskeletal radiology as well as assisting with related departmental research projects. This appointment will encompass all aspects of musculoskeletal radiology including CT, arthrography, and MR. Salary is negotiable and competitive and dependent upon past scholarly productivity and post-M.D. experience. Applicants must be licensed or able to obtain license to practice medicine in the state of MN before appointment date. Applications for these positions will be accepted through December 31, 1992. Send letters to Harry Griffiths, M.D., Dept. of Radiology, Box 292 UMHC, University of Minnesota, 420 Delaware St. S.E., Minneapolis, MN 55455. The University of Minnesota is an equal opportunity educator and employer. 9a

INSTRUCTOR/PULMONARY RADIOLOGY—The Dept. of Radiology at the University of Minnesota has 1- or -2 yr post-residency positions in pulmonary/chest radiology available at the rank of instructor (temporary, annual renewable) beginning July 1, 1994. Minimum requirements include successful completion of an accredited radiology residency, and board-certification in radiology by beginning date of appointment. In addition to clinical practice, responsibilities will include all facets of pulmonary radiology as well as graduate and undergraduate medical instruction and assisting with related dept. research projects. Salary is negotiable and competitive, and is dependent upon past scholarly productivity and post-M.D. experience. Applicants must be licensed or able to obtain a license to practice medicine in the state of MN before appointment date. Applications will be accepted through December 31, 1992. Send letters to Dr. Christopher Engeler, Assistant Professor, Dept. of Radiology, Box 292 UMHC, University of Minnesota, 420 Delaware St. S.E., Minneapolis, MN 55455. The University of Minnesota is an equal opportunity educator and employer. 9a

THE UNIVERSITY OF OKLAHOMA HEALTH SCIENCES CENTER, DIVISION OF RADIATION THERAPY, is seeking a full-time radiation biologist. We are looking for someone willing to start a program in radiation biology as a branch of our graduate program. Teaching experience is necessary, salary will be based upon qualifications. CV to Carl R. Bogardus, Jr., M.D., Dept. of Radiological Sciences, P.O. Box 26901 Oklahoma City, OK 73190; (405) 271-5641. The University of Oklahoma is an equal opportunity/affirmative action employer. 9a

NORTHEASTERN PA, 2 1/2 HRS FROM NYC AND PHILADELPHIA, IMMEDIATE FINANCIAL EQUALITY— Two or more radiologists needed to join 2 forming new group. Interventional and nuclear medicine experience desirable. Fee for service arrangement and separate billing at 2 hospital based sites. 120-beds and 400-beds respectively. Send CV or contact Douglas W. Parrillo, M.D., Chairman, Diagnostic Imaging, Mercy Hospital, 746 Jefferson Ave., Scranton, PA 18501; (717) 348-7069. 9a

INSTRUCTOR/NEURORADIOLOGY—The Dept. of Radiology at the University of Minnesota has 2-yr post-residency positions in neuroradiology available at the rank of instructor (temporary, annual renewable) beginning July 1, 1994. Minimum requirements include successful completion of an accredited radiology residency and board-certification in radiology by beginning date of appointment. In addition to clinical practice and training, responsibilities will include graduate and undergraduate medical instruction in neuroradiology as well as assisting with related departmental research projects. Salary is negotiable and competitive and dependent upon past scholarly productivity and post-M.D. experience. Applicants must be licensed or able to obtain license to practice medicine in the state of MN before appointment date. Applications for these positions will be accepted through December 31, 1992. Send letters to Dr. Richard Latchaw, Professor, Dept. of Radiology, Box 292 UMHC, University of Minnesota, 420 Delaware St. S.E., Minneapolis, MN 55455. The University of Minnesota is an equal opportunity educator and employer. 9a

NUCLEAR MEDICINE—RADIOLOGIST—CALIFORNIA—Immediate opening for diagnostic radiologist with nuclear medicine boards or special competency in growing private practice in the San Fernando Valley 20 minutes north of UCLA. Candidate to supervise growth of nuclear medicine dept. in addition to general diagnostic radiology work. Full partnership tract with excellent salary. Practice includes hospital and imaging centers. Group consists of young enthusiastic radiologists all with fellowship training. Equipment includes Sopha Spect nuclear, GE 1.5-T MRI with angio, 2 Acuson ultrasound, Siemens Angiostar specials, and 2 Picker 1200 CT scanners. Send CV to T. Sprague M.D., Holy Cross Medical Center, 15031 Rinaldi St., Mission Hills, CA 91345;.fax (818) 898-4451. 9-2ap

PULMONARY RADIOLOGIST—The Beth Israel Medical Center, Dept. of Radiology in New York City is seeking a BC diagnostic radiologist with expertise in chest radiography and experience in mammography is desirable. The newly renovated dept. of radiology has a staff of 20 full-time radiologists. An active clinical practice, a strong teaching program as well as stimulating research opportunities are available at this 950-bed teaching hospital affiliated with the Mount Sinai School of Medicine. In addition to clinical expertise, a strong interest and ability in teaching is required. Academic rank will be commensurate with candidate's qualifications and experience. Excellent remuneration and benefits. Please send inquiries with a CV to Michael M. Abiri, M.D., Deputy Director, Dept. of Radiology, Beth Israel Medical Center, First Ave. at East 16th St., New York, NY 10003. An equal opportunity employer committed to a smoke-free environment. 9a

MAMMOGRAPHER—Large private multi-hospital group in a coastal city of Virginia seeks a radiologist with special interests in all aspects of mammography. The practice includes a tertiary-care hospital which is affiliated with both a medical school and a radiology residency training program, thereby offering the benefits of both private practice and academics. The position would include directorship of future mammography clinics. Additional aptitude in other aspects of diagnostic radiology with specialized and/or fellowship training preferred. Interested applicants please send CV or inquiries to Medical Center Radiologists, Halifax Building, Ste. 330, 6161 Kempsville Circle, Norfolk, VA 23502; (804) 466-0089. 9xa

BC/BE RADIOLOGIST needed at Bradford Regional Medical Center due to increased volume. BRMC is a full service 150-bed hospital with adjacent 100-bed nursing home. The x-ray dept. is brand new and consists of 2 fluoro, 2 plain film, 1 dedicated chest and 1 mammo room (all Siemens), Siemens Nuclear with SPECT, GE .5T mobile MR 2 days a week. Ultrasound equipment includes ATL, Diasonics, and Interspec. Excellent new Picker CT. Bradford is a university town with 15,000 population. Snow skiing, hunting, boating and fishing are close. There are groomed cross country skiing trails in the Allegheny National Forest. Bradford is 1 1/2 hrs from Buffalo, NY, and Erie, PA. Toronto and Pittsburgh are 3 to 3 1/2 hrs away. Attractive opportunity with above average compensation leading to partnership with plenty of time off and light call. Please contact Ross A. Horsley, M.D., Bradford Regional Medical Center, 116 Interstate Parkway, Bradford, PA 16701; (814) 362-8239. 9a

INTERVENTIONAL NEURORADIOLOGIST, COASTAL VIRGINIA—A 32-physician private radiology group which practices in 6 hospitals and several offices is seeking an interventional neuroradiologist who is eligible for senior membership in the American Society of Neuroradiology. The individual's clinical responsibilities would be primarily limited to a 644-bed tertiary-care center with level 1 trauma status. Diagnostic equipment includes 2 state-of-the-art Signa 1.5-T GE MR scanners (4.79 software and angio package), a DFP 60A bi-plane bi-digital 1024 matrix Toshiba DSA system (with digital stereo capabilities), and a Siemens DRH as well as a GE 9800 CT scanner. Some time would be spent at a 250-bed hospital with a Hitachi MRP-5000 0.2-T MR unit and a GE 9800 CT scanner with Hi-Light advantage software. Two (2) year fellowship trained neuroradiologists are already on staff. The practice is affiliated with a medical school and residency program which allows the pursuit of academic interests. The practice is located in a coastal resort area with a temperate climate and all water sports available. Interested persons should send a CV or contact Carl V. Bundschuh, M.D., Director of Neuroradiology and MRI, Medical Center Radiologists, Inc., 6161 Kempsville Circle, Ste. 330, Norfolk, VA 23502; (804) 466-0089. 9xa

UNIQUE, EXCITING OPPORTUNITY FOR RADIOLOGIST(S)—Touro Infirmary, a 150-yr-old respected New Orleans hospital is looking for a dynamic, motivated individual or group to provide radiology services. Great opportunities exist for increasing and expanding current business. Successful candidates must be board-certified, experienced, clinically proficient and committed to providing quality services to our medical staff. Coverage required for MRI, CT, ultrasound, nuclear medicine, mammography, interventional and basic radiology services. State-of-the-art equipment is available. If you feel you or your group is unequaled in these qualifications, please submit a CV to Meg McNally, Vice President, Ambulatory Services, Touro Infirmary, 1401 Foucher St., New Orleans, LA 70115; fax (504) 897-8769. 9a

IMMEDIATE OPENING—BC/BE diagnostic radiologist to join 8 board certified radiologist incorporated practice covering 3 hospitals with approx. 700-beds and 100+ physician multispecialty clinic. All modalities represented. Must be willing to participate in all aspects of general radiology. Excellent fringe benefit package with competitive salary leading to early shareholder status at modest buy-in. Practice located in Arkansas River Valley. Excellent public and private schools. Send CV or contact June Martin, Business Manager, Radiology Services, P.A., P.O. Box 1827, Fort Smith, AR 72902; (501) 782-5035. 9-11ap

BEAUTIFUL COAST OF MAINE—Excellent opportunity for full-or part-time BC/BE radiologist to work with established radiologist in private practice. Pleasant community, yr-round recreational area, smog free, low crime environment. Fully accredited, multispecialty acute care hospital serving 25,000. All modalities of diagnostic radiology offered. Mobile nuclear medicine and MRI currently being pursued. Approximately 15,000 exams annually. Send CV to Executive Director, Waldo County General Hospital, P.O. Box 287, Belfast, ME 04915; (207) 338-2500. 9-11a

DIAGNOSTIC RADIOLOGIST—The College of Physicians and Surgeons of Columbia University is searching for a general diagnostic radiologist for its multi-specialty private practice group located near 60th and Madison Ave. Board-certification required. Proficiency in mammography, ultrasound, CT and general diagnostic radiology is desirable. Expansion of outpatient imaging modalities planned with MRI to be added. Salary and academic rank will be commensurate with experience and qualifications. NYS medical license required; narcotics license desirable. Please send resume to Ellen F. Silverstein, M.D., Columbia Presbyterian Radiologists, 38 East 61st St., New York, NY 10021. Columbia University is an affirmative action/equal opportunity employer. 9a

INTERVENTIONAL RADIOLOGIST—An opportunity exists for an interventionalist to join a group of 12 board-certified radiologists in their hospital and private practice. Position requires fellowship-trained interventionalist with an interest in diagnostic radiology. The practice is based in a 430-bed community hospital with 2 private offices and a hospital owned satellite facility. Services include 2 MRI units, 2 CT units, 2 SPECT cameras, and a new interventional suite with an established interventional practice. Bethlehem is 1 of 3 cities situated in the Lehigh Valley which is within close proximity of NY and Philadelphia. Contact G. Edward Streubert, M.D., Bethlehem Radiologists Associates, 95 Highland Ave., Ste. 105, Bethlehem, PA 18017. 4-12ap

SOUTHEAST PENNSYLVANIA/CENTERAL NEW JERSEY—Established state-of-the-art multi-hospital and private office practice seeks diagnostic radiologist with interest in all aspects of general radiology. Also seeks individual with subspecialty expertise in angio/interventional or nuclear medicine. Full or part time position. Excellent access to Philadelphia and NYC areas. Send CV to S. Meshkov, M.D., 838 W. State St., Trenton, NJ 08618. 9-11a

DIAGNOSTIC RADIOLOGIST, COASTAL DOWNEAST MAINE—We'd rather pay recruiting fee to you than to agency. Call for details. Opening for BC/BE radiologist at progressive small rural hospital; college community. Solid financial opportunity. Will tailor arrangements to fit candidate's desire. Contact administration, Down East Community Hospital, Machias, ME 04654; (207) 255-3356. 9-12ap

TWO RADIOLOGISTS NEEDED IMMEDIATELY 1 MRI, 1 GENERAL—Large hospital and private practice, Westchester, Orange Counties, New York Region. Salary leading to partnership. Northern Metropolitan Radiology Associates, P.C., P.O. Box 199, Jefferson Valley, NY 10535; (914) 245-8935. 9a

THE FALLON CLINIC—New England's most respected physician owned and directed multispecialty group practice seeks 2 BC/BE diagnostic radiologists to join the dept. of 6 currently performing over 108,000 studies this year. Competence and interest in CT, ultrasound and mammography required. No night call. Excellent lifestyle, salary and benefits. Send CV to Stephen Patton, Recruitment Manager, 100 Central St., Worcester, MA 01608. 9-10a

VASCULAR/INTERVENTIONAL, RADIOLOGIST, FLORIDA—Staff radiologist is being sought by the University of Florida Health Science Center/Jacksonville for a full-time, tenure earning faculty position. Special interest, expertise, or fellowship training in vascular/interventional radiology is required. Additional diagnostic radiology responsibilities may be available. Technical facilities, salary and fringe benefits are excellent. An appointment will be at the academic rank of instructor/assistant professor/associate professor/professor, based on training, background and experience. Application recruiting deadline, October 1, 1992. Send CV and references to Chairman, Search Committee, Dept. of Radiology, University Medical Center, 655 W. 8th St., Jacksonville, FL 32209 AA/EOE. 9a

THE DEPT. OF RADIOLOGY AT THE ALBERT EINSTEIN MEDICAL CENTER IN PHILADELPHIA, PA, is undergoing a major expansion and is seeking to add 6 additional radiologists to our current staff of 14 including those with special interest in gastrointestinal radiology, genitourinary radiology, musculoskeletal radiology, mammography, pediatric radiology, neuroradiology, nuclear medicine, general radiology, and interventional radiology. Albert Einstein Medical Center is a 600-bed, tertiary-care, university-affiliated hospital. In addition, the dept. staffs 2 out-patient imaging centers. The dept. has a fully-accredited residency program with the capacity for 16 residents and is the major clinical affiliate of Temple University School of Medicine. The dept. maintains a 2-yr, certificate-based School of Radiologic Technology with 30 students. This is an excellent opportunity for young, bright and enthusiastic diagnostic radiologists to become involved in quality patient care, program development, teaching and research. Salary and fringe benefits are highly competitive. If interested, send CV to Henrietta Kotlus Rosenberg, M.D., Chairman, Dept. of Radiology, Albert Einstein Medical Center, 5501 Old York Rd., Philadelphia, PA 19141. 9a

SEEKING BOARD-CERTIFIED RADIOLOGIST with nuclear medicine fellowship, or with nuclear boards and recent SPECT training or experience. Excellent practice opportunity in large volume hospital practice located in Orange County, Southern California. New dual head Sopha SPECT camera offers state-of-the-art imaging. In addition to a competitive salary, you will enjoy a comprehensive benefits package that includes paid vacations, ESOP, tuition reimbursement, paid time off for CME and much more. For more information contact Jose Guijarro at (800) 336-2255 or send your CV to FHP Professional Staffing, 9900 Talbert Ave., Fountain Valley, CA 92708. 9a

IMMEDIATE OPENING FOR BC/BE DIAGNOSTIC RADIOLOGIST, NEW ENGLAND, to join a 6-member group, leading to partnership, in an active community, university-affiliated hospital. Over 100,000 exams/yr. Practice includes CT, ultrasound, nuclear medicine, MRI, angiography, and interventional. Locum needed in interval. Located in New England close to boating and skiing, 1 hr from Boston. Contact Allan M. Deutsch, M.D., Dept. of Radiology, The Miriam Hospital, 164 Summit Ave., Providence, RI 02906; (401) 331-8500, ext. 4400. 9-11ap

ST. JOSEPH'S HOSPITAL/MED. CENTER, Dept. of Radiological Sciences provides unique opportunity for highly motivated teachers, clinicians and researchers with subspecialty interest in vascular/interventional, chest/cardiothoracic, musculoskeletal, abdominal (MRI/CT/ultrasound, pediatric, residency director. Home of BN1; state-of-the-art equipment (1.5-T MRIs, PET, 9800 CTs, angio, ultrasound); only residency program in Phoenix (1 of 2 in Arizona); salary and partnership commensurate with private institution; 626-bed tertiary-care hospital. Send CV or call Burton P. Drayer, M.D., Radiologist-in-Chief, Dept. of Radiological Sciences, Barrow Neurological Institute, 350 West Thomas Rd., Phoenix, AZ 85013; (602) 285-3179 or Donald Lawson, M.D., (602) 285-3364. 9a

Fellowships and Residencies

FELLOWSHIP IN VASCULAR AND INTERVENTIONAL RADIOLOGY—The University of Arizona is sponsoring a 1-yr fellowship in vascular and interventional radiology beginning July 1, 1994. In-depth clinical experience and training in all aspects of interventional radiology will be offered. Facilities at the University Hospital (300-bed) and Tucson Veterans Hospital (300-bed) are state-of-the-art. Interested applicants should submit a current CV and 3 letters of recommendation (including one from their program director) to Gerald D. Pond, M.D., Head, Section of Vascular and Interventional Radiology, University of Arizona Health Sciences Center, Tucson, AZ 85724. For further information please contact Ruth Kneup at (602) 626-6794. 8xc

FELLOWSHIPS AT THOMAS JEFFERSON UNIVERSITY HOSPITAL—The Dept. of Radiology at Thomas Jefferson University Hospital in Philadelphia offers the following fellowship programs each yr: (1) Ultrasound/CT/MRI—Jefferson's ultrasound division is one of the largest in the world and performs all currently available exams, including obstetric, vascular, lithotripsy, invasive, and endoluminal. We also operate 4 GE 1.5-T MRI units and 3 CT scanners. Contact Barry Goldberg, M.D. regarding this program. (2) Cardiovascular/interventional—This division is housed in a new suite containing Philips angio units with DSA and performs the full range of vascular and nonvascular interventional procedures. Contact Geoffrey Gardiner, Jr., M.D. (3) Neuro/ENT radiology—very active clinical services supply a wealth of material to this division, which is housed in a neurosciences imaging center containing all imaging modalities. Contact Carlos Gonzales, M.D. (4) Breast imaging—Jefferson's new breast-imaging center performs approximately 85 studies/day including ultrasound and needle localizations. Contact Stephen Feig, M.D. (5) Chest—includes biopsies and CT. Contact Robert Steiner, M.D. (6) MRI—a dedicated body MRI program including excellent research opportunities in addition to a large clinical case load. Contact Donald Mitchell, M.D. (7) Ultrasound—a dedicated ultrasound program. Contact Barry Goldberg, M.D. (8) Musculoskeletal—includes MRI of the musculoskeletal system. Contact David Karasick, M.D. All program directors listed above can be contacted at the Dept. of Radiology, Thomas Jefferson University Hospital, Philadelphia, PA 19107. Jefferson is an equal opportunity/affirmative action employer. 8xc

VASCULAR/INTERVENTIONAL RADIOLOGY FELLOWSHIP—Temple University Hospital and School of Medicine has available a 1-yr fellowship beginning July 1, 1992. The candidate will have exposure to all areas of vascular and interventional radiology including noninvasive techniques and MRI/A. Applicants should contact, David S. Ball, D.O., Chief, Section of Vascular/Interventional Radiology, Dept. of Diagnostic Imaging, Temple University Hospital, 3401 N. Broad St., Philadelphia, PA 19140. Temple University Hospital and School of Medicine is an affirmative action/equal opportunity employer. 8xc

THE DEPT. OF RADIOLOGY AT NEW ENGLAND MEDICAL CENTER (the major teaching hospital of Tufts University School of Medicine) has a body imaging fellowship position available as of July 1, 1993. The fellowship program consists of approximately 6 months of body CT, 3 months of MRI (including neuro), and 3 months of adult ultrasound. Some elective time is being considered. Candidates must have completed an accredited diagnostic radiology residency program and be eligible for temporary licensure in MA. The radiology dept. is very active, providing a broad experience in CT, MRI, and ultrasound. Any interested candidate should send a CV and/or contact Mark Bankoff, M.D., New England Medical Center, Box 180, 750 Washington St., Boston, MA 02111; (617) 956-0043. 9a

FELLOWSHIP POSITIONS—The Dept. of Radiology of the Brigham and Women's Hospital-Harvard Medical School has 1- or 2-yr fellowship positions in the following areas: (1) cardiovascular and interventional, (2) neuroradiology, (3) CT/ultrasound/MR/interventional, (4) oncoradiology, (5) chest, (6) bone, (7) nuclear medicine, and (8) computer science. For more information, please send CV specifying your area of interest to B. Leonard Holman, M.D., Chairman, Dept. of Radiology, Brigham and Women's Hospital, 75 Francis St., Boston, MA 02115. Harvard Medical School and Brigham and Women's Hospital are equal opportunity, affirmative action employers. 5-4c

IMAGING (ULTRASOUND, BODY CT, AND MRI) FELLOWSHIP TO BEGIN JULY 1993—The Dept. of Radiology at The Western Pennsylvania Hospital (a 578-bed advanced, tertiary-care teaching hospital), Pittsburgh, PA, offers a 1-yr imaging fellowship. The fellowship emphasizes diagnostic ultrasound with rotations in body magnetic resonance imaging and computed body tomography. Examinations in all areas of sonography are performed and include obstetrics and gynecology, vascular/Doppler, abdominal, prostate, pediatrics, breast, and small parts. State-of-the-art equipment in all areas of the dept. Fellows will participate in procedures guided by ultrasound and computed tomography. Fellows have ample opportunity to participate in conference presentations and research projects, many of which culminate in publications. Inquiries should be addressed to Marcela Bohm-Velez, M.D., Director of Imaging Fellowship Program, Dept. of Radiology, The Western Pennsylvania Hospital, 4800 Friendship Ave., Pittsburgh, PA 15224. 5-12c

FELLOWSHIP PROGRAM IN INTERVENTIONAL RADIOLOGY—The fellowship offered is a 1-yr training program in interventional radiology. A high volume of studies provides excellent experience for the fellowship training program. The 1-yr appointment is intensive, supervised, and allows for graded responsibility in performance and interpretation of studies including angioplasty, atherectomy, arterial and biliary stents, and all drainage procedures. The fellowship training involves performance of interventional procedures under sonographic and CT guidance as well as fluoroscopy. Inquiries should be addressed to Gordon K. McLean, M.D., Director, Interventional Radiology, The Western Pennsylvania Hospital, 4800 Friendship Ave., Pittsburgh, PA 15224. 5–12c

ONCORADIOLOGY/MAMMOGRAPHY FELLOWSHIP—The Dept. of Radiology at the Dana-Farber Cancer Institute and Brigham and Women's Hospital, which are Harvard Medical School affiliates, offers a 1-yr fellowship position beginning July 1, 1993. All imaging modalities involved in the diagnosis, staging, and follow-up of patients with malignant disease are integrated into this program. An additional feature is a concentrated experience in the performance of interventional breast diagnostic procedures. Please contact Jack E. Meyer, M.D., Director of Diagnostic Radiology, Brigham and Women's Hospital and Dana-Farber Cancer Institute, 75 Francis St., Boston, MA 02115; (617) 732-6269. Brigham and Women's Hospital/Dana Farber Cancer Institute/Harvard Medical School is an affirmative action/equal opportunity educator and employer. 5–4c

UNEXPECTED OPENING FOR FELLOWSHIP IN CARDIOVASCULAR-INTERVENTIONAL RADIOLOGY—Available July 1, 1992, 1-yr fellowship program is available at a 750-bed teaching hospital. Extensive clinical experience involving all aspects of cardiovascular imaging, interventional vascular, and nonvascular procedures. Availability for clinical or animal research. Send CV and inquiries to Oscar H. Gulierrez, M.D., Dept. of Radiology, Box 648, University of Rochester Medical Center, Rochester, NY 14642. AA/EO/M-F employer. 8–10c

FELLOWSHIPS AT ALBANY MEDICAL CENTER—The newly-renovated and equipped Dept. of Radiology at the Albany Medical College and Center in Albany, NY, offers the following fellowship positions each yr: (1) Abdominal Imaging—This fellowship encompasses all aspects of MRI, ultrasound, CT, and other advanced techniques in imaging the abdomen. Four state-of-the-art MRI and 4 CT scanners as well as 5 color Doppler ultrasound units are utilized daily. Contact James C. Peters, M.D. regarding this program. (2) Neuroradiology—This fellowship encompasses the full range of advanced neuro imaging including MRI, CT, angiography, and myelography. Contact William A. Wagle, M.D. (3) Angiography and interventional radiology—Three advanced angiographic suites are utilized daily for a full range of vascular and interventional procedures. Contact Mohammad S. Sarrafizadeh, M.D. All program directors listed above may be contacted at the Dept. of Radiology, A-113, Albany Medical Center, Albany, NY 12208; (518) 445-3277 or contact Matthew D. Rifkin, M.D., Chairman, Dept. of Radiology, A-113, at the above address. Albany Medical Center is an equal opportunity/affirmative action employer. 1–12c

ACCREDITED FELLOWSHIPS IN PEDIATRIC RADIOLOGY AND PEDIATRIC NEURORADIOLOGY—Dept. of Radiology, Children's Hospital Medical Center, Cincinnati, OH, offers 1- or 2-yr accredited (Residency Review Committee for Radiology of ACGME) fellowships in pediatric radiology beginning July 1, 1994. A 1-yr pediatric neuroradiology fellowship program is also offered and may be taken separately or combined with 1 yr of adult neuroradiology fellowship at the University of Cincinnati Medical Center. Children's Hospital Medical Center (CHMC) is a 355-bed institution. The dept. performs over 105,000 radiological exams/yr in the largest children's hospital and ambulatory practice in the U.S. The dept. has 14 full-time faculty pediatric radiologists, 1 full-time research faculty, 7 fellows, and many resident trainees. Six pediatric radiology and 1 pediatric neuroradiology fellowship positions are available annually. Training includes all aspects of pediatric imaging neonatal radiology; neuroimaging; musculoskeletal radiology; cardiovascular and thoracic imaging; abdominal imaging; oncologic imaging; ultrasonography; nuclear medicine; computed tomography; MRI; and vascular/interventional procedures. The dept. has an active clinical service with state-of-the-art equipment as follows: digital fluoroscopy; Acuson and ATL ultrasound units with Doppler and color flow Doppler capabilities; planar SPECT gamma cameras; GE 9800 Quick CT scanner; 1.5-T GE MRI with spectroscopy, and cardiac catheterization/angiographic suite with digital vascular imaging. The fellowship provides a broad clinical experience in pediatric radiology as well as numerous opportunities to participate in both clinical and basic research. Candidates must be board-certified or board-qualified in diagnostic radiology and must obtain an Ohio medical license. Salary and fringe benefits are highly competitive. Applications are due prior to February 1993 with interviews scheduled during the fall and winter of 1992–93. There are numerous career opportunities in pediatric radiology and pediatric neuroradiology in both academic and private practice settings. To receive more information about the fellowships at CHMC or careers in pediatric radiology, please contact Director, Dept. of Radiology, Children's Hospital Medical Center, Cincinnati, OH 45229-2899; (513) 559-8058. Children's Hospital Medical Center and the University of Cincinnati College of Medicine are affirmative action/equal opportunity employers. 7–1cp

FELLOWSHIP POSITION: WOMEN'S IMAGING—High-volume breast imaging (mammography, breast ultrasound, interventional procedures) and ultrasound with emphasis on obstetrical and gynecologic sonography. State-of-the-art mammographic and sonographic equipment including stereotactic table and digital capability. Using stereotactic, ultrasound, or mammographic guidance, all breast interventional procedures are performed, including fine needle and core biopsies, cyst aspirations, presurgical localizations, and galactography. Elective time in MRI, CT, and related clinical specialties (surgery, pathology, obstetrics-gynecology). One-year fellowship to start in July 1993. Fellows also have the opportunity to participate in teaching, conference presentations, and research projects, many of which culminate in publications. Inquiries should be addressed to Ellen B. Mendelson, M.D., Chief, Mammography and Women's Imaging, The Western Pennsylvania Hospital, 4800 Friendship Ave., Pittsburgh, PA 15224. 5–12c

FELLOWSHIP IN VASCULAR/INTERVENTIONAL RADIOLOGY—The Yale University Dept. of Radiology has an unexpected opening for a third fellowship position open starting July 1993. The section has an active clinical service performing a wide range of vascular and interventional procedures including: diagnostic angiography, angioplasty, stenting, atherectomy, Infusion therapy, embolotherapy, IVC filter placement, and percutaneous renal, biliary, and abscess management. Additionally, there is an inpatient admitting service and clinic. The fellowship is for 1 yr. Please send CV and 3 letters of recommendation to Jeffrey Pollak, M.D., Section Chief, Dept. of Diagnostic Radiology, Yale University School of Medicine, 333 Cedar St., P.O. Box 3333, New Haven, CT 06510; (203) 785-4746, (203) 785-3024 fax. Yale University is an equal opportunity/affirmative action employer. Applications from women and minority group members are encouraged. 9a

MRI FELLOWSHIP—One-yr position is available in 1993 for fellow in MRI. The fellowship encompasses all phases of MR (musculoskeletal, body and neuro) as well as magnetic resonance angiography (including phase contrast, time-of-flight and magnitude phase contrast MRA). Over 12,000 MRIs are performed and interpreted annually as a part of this fellowship with direct one-on-one supervision. The fellowship also includes 20–30% CT; additionally, the option to obtain independent, full American Board of Nuclear Medicine certification is available. MR studies are divided between approximately 45% neuro and 55% body and musculoskeletal, including all joints and body parts. For further information contact Stephen J. Pomeranz, M.D.; (513) 281-3400, and ask for Chris or Jill. 7–9cp

THE DEPARTMENT OF RADIOLOGY OF THE CHILDREN'S MEMORIAL HOSPITAL, CHICAGO, offers a fellowship in pediatric radiology beginning July 1, 1994. Children's Memorial is a 265-bed institution where approximately 95,000 radiological exams are done per yr by 13 attending radiologists. Rotations will include general radiology, ultrasound, computed tomography, nuclear medicine, MRI and neuroradiology. Requirements for fellowship include completion of a radiology residency and eligibility for IL licensure. Please send CV to Andrew K. Poznanski, M.D., Radiologist-in-Chief, Children's Memorial Hospital, 2300 Children's Plaza #9, Chicago, IL 60614. For inquiries, please call (312) 880-3520. 9-10c

FELLOWSHIP IN VASCULAR/INTERVENTIONAL RADIOLOGY—The University of Maryland Medical Center has an opening for a fellow in the section of vascular and interventional radiology, beginning July 1, 1993. The medical center is an 800-bed acute-care hospital and tertiary referral center with an active and varied vascular/interventional practice. In addition, a new 324-bed VA hospital, adjacent to and connected to the medical center will be opening in November. The fellow will participate in all aspects of diagnostic vascular radiology as well as the full range of vascular and non-vascular interventional procedures. Interested persons should contact Dr. Philip A. Templeton, Acting Chairman, Dept. of Diagnostic Radiology, 22 S. Greene St., Baltimore, MD 21201. 9c

FELLOWSHIP IN IMAGING/ANGIO-INTERVENTIONAL—A 1-yr fellowship program at Lehigh Valley Hospital in Allentown, PA, is available. LVH is a 492-bed acute-care, university affiliated hospital. The fellowship program offers training in CT (head and body), ultrasound, MR, angiography, and interventional radiology. For further information contact Robert Kricun, M.D., Dept. of Radiology, Lehigh Valley Hospital, P.O. Box 689, Allentown, PA. 18105-1556. 7–9c

FELLOWSHIP IN ABDOMINAL IMAGING AND INTERVENTIONS—The dept. of radiology, Massachusetts General Hospital and Harvard Medical School, offers a 2-yr fellowship in abdominal imaging and interventional radiology beginning July 1, 1994. Training covers all aspects of abdominal imaging (fluoroscopy, ultrasound, CT and MR) and nonvascular interventions in the GI/GU tract. Ample time is made available for both clinical and laboratory research in the above areas during the second year. Candidates should be ABR-eligible or certified. Address inquiries to Peter R. Mueller, M.D., or Nicholas Papanicolaou, M.D., Dept. of Radiology, Massachusetts General Hospital, Boston, MA 02114. An equal opportunity employer. 9-11c

FELLOWSHIP IN BODY CT/MRI—Because of an unexpected opening the Dept. of Radiology of New York Medical College has an opening for a 1-yr imaging fellowship. Westchester County Medical Center is a 650-bed, tertiary-care facility offering advanced training with state-of-the-art equipment. Equipment includes 2 Siemens Hi-Q CT scanners, GE Signa, 1.5-T MR, ISG 3-D reconstruction console, and 6 ultrasound imagers (Acuson and Diasonics). Applicant must have completed an approved residency in diagnostic radiology and must be board-eligible or certified. Please contact Jessica Berkowitz, M.D., Dept. of Radiology, New York Medical College, Valhalla, NY 10595; (914) 285-8875. 9c

Tutorials/Courses

KONA, HI 1992—Seventeenth Annual International Body Imaging Congress, Oct. 10–17. CME 1. Mauni Lani Bay Hotel. Contact Medical Seminars International, Inc., 18981 Ventura Blvd., Ste. 303, Tarzana, CA 91356; (818) 774-9077, fax (818) 774-0244. 5–10d

MUSCULOSKELETAL MRI, SECOND ANNUAL LOS ANGELES CONFERENCE, SEPT. 19–20, 1992—Faculty: Drs. Bradley, Brant-Zawadzki, Dietrich, Friedman, Harms, Resnick, Schlesinger. Medical Seminars International, Inc., 18981 Ventura Blvd., Ste.303, Tarzana, CA 91356; (818) 774-9077, fax (818) 774-0244. 4–9d

CARIBBEAN CRUISE-BREAST IMAGING AT SEA—January 17–24, 1993. Presented by a renowned faculty member. CME I application. Medical Seminars International, Inc., 18981 Ventura Blvd., Ste. 303, Tarzana, CA 91356: (818) 774-9077, fax (818) 774-0244. 9d

CARIBBEAN CRUISE-NEURO IMAGING/MRI AT SEA—January 10–17, 1993. Faculty: Hervey Segall, M.D. CME I application. Medical Seminar International, Inc., 18981 Ventura Blvd. Ste. 303, Tarzana, CA 91356: (818) 774-9077, fax (818) 774-0244. 9–12d

CARIBBEAN CRUISE-MRI AT SEA—January 24–31, 1993, Faculty: Barry S. Goldberg, M.D. CME I application. Medical Seminars International, Inc., 18981 Ventura Blvd., Ste. 303, Tarzana, CA 91356: (818) 774-9077, fax (818) 774-0244. 9–12d

DIAGNOSTIC IMAGING IN ARUBA—The Dept. of Radiology, Cornell University Medical College and The New York Hospital will present the 18th annual postgraduate course, Diagnostic Imaging, January 31 – February 5, 1993 at the Hyatt Regency Hotel in Aruba. Category I credit: 30 hrs. Fee: Physicians, $495; residents, fellows and technologists $295. Information: Ms. Julia Anne Mala, Radiology, Cornell University Medical College, 1300 York Ave., New York, NY 10021; (212) 746-2522. 9-12d

New Business Office
for *AJR*

All inquires and correspondence regarding classified ads should be sent to:

***AJR* Classifieds**
1891 Preston White Drive
Reston, VA 22091

Attn: Terry Fitterer
Phone: (703) 648-8992
FAX: (703) 264-8863

No one ever said a lot of knowledge is a dangerous thing.

IN FACT, for radiologists, the only danger is not keeping up with what's new. **AJR: American Journal of Roentgenology** is your monthly guide to the latest advances, with articles that are timely, succinct, and relevant to daily practice.

AJR
American Journal of Roentgenology
Published monthly
Robert N. Berk, M.D., Editor
The University of California, San Diego

Call toll-free to order: **1-800-638-6423**
from anywhere in the U.S. or Canada.
Or clip and mail this coupon to
Waverly, Inc. ATTN: AJR

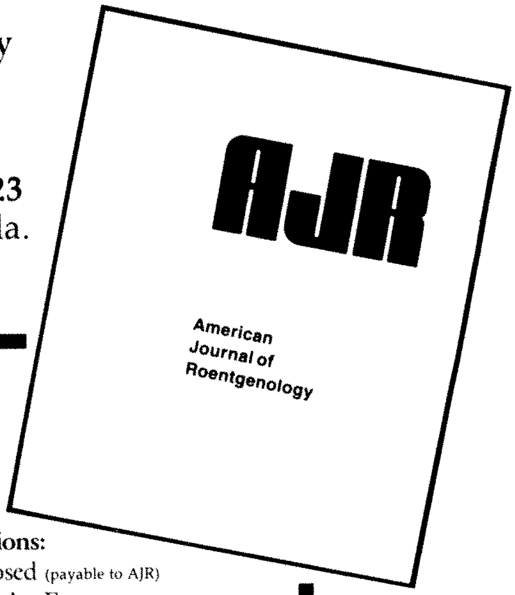

Subscribe to **AJR** now. (Current rates available for up to three years.)

☐ Individual $125/year
☐ Institutional $135/year
☐ In-training* $25/year
(Add $55/year outside the U.S.; in Canada, also add 7% GST.)

☐ 3 years ☐ 2 years ☐ 1 year

Maryland residents and 5% sales tax. Subscriptions outside the U.S. must be prepaid in U.S. dollars. Rates valid through October 31, 1992.

Name ____________________

Address ____________________

City/State/Zip ____________________

*Please specify institution and training status ____________________

____

AJR 992

Payment Options:
☐ Check enclosed (payable to AJR)
☐ Bill me ☐ AmEx
☐ MasterCard ☐ VISA

Card # ____________________ Exp. Date __________

Signature ____________________

Return coupon to:
Waverly, Inc. ATTN: AJR
P.O. Box 23291, Baltimore, MD 21203-9990

AJR: AMERICAN JOURNAL OF ROENTGENOLOGY is the official journal of the American Roentgen Ray Society.

	Final No.
Date Received	Tracking No.

Call for Scientific Papers

American Roentgen Ray Society
1993 Annual Meeting
April 25 – 30, 1993
San Francisco, CA

ADDRESS OF PRESENTING AUTHOR

Department

Institution

Street

City State Zip

Phone

Type title, authors, and abstract in the space provided below. (Instructions are on reverse side of this page. Abstract should not exceed 300 words.)

Select one category: ☐ Angio/Interventional ☐ Breast ☐ Sonography ☐ CT ☐ Gastrointestinal Tract ☐ Genitourinary Tract
☐ Neuroradiology ☐ Skeletal ☐ Chest ☐ MR ☐ Pediatrics ☐ Medical Physics

Projection Requirements: ☐ 35mm– single or double (circle one) ☐ 16mm silent film ☐ VHS (½") ☐ VHS (¾")

Has this been presented elsewhere? ☐ Yes ☐ No If yes, where? ____________

Instructions for Scientific Paper Abstracts

1. Type information single-spaced. Underline the name of the presenting author. Append as a last line of the abstract any research grant support, if applicable (e.g. Supported by USPHS Grant HE-80144). If the abstract is accepted, it will appear in the program book exactly as typed. Use the following format:

   MR IMAGING OF THE SPINE AND NECK
   F.S. Lau, M.D., A.N. Kirk, M.D., R.A. Beck, Ph.D.
   University of California, Bakersfield, Bakersfield, CA 92338

2. Abstracts should include four paragraphs devoted sequentially to the following topics: (1) object or purpose of the study; (2) materials, methods and procedures; (3) results; and (4) significance of the results and conclusions. The text should not exceed 300 words. Specific data are essential. The abstract should be a succinct summary of work done rather than a promissory note.

3. The Scientific Program Committee will grade each abstract and determine acceptance. Letters indicating acceptance or rejection will be mailed to all applicants in mid-January, together with meeting registration information.

Deadline for submission of abstracts is November 1, 1992. Mail **one** copy of abstract to

ARRS President-Elect
c/o Susan Roberts, Projects Manager
American Roentgen Ray Society
1891 Preston White Drive
Reston, VA 22091

Although mail submission is preferable, abstracts will be accepted by fax at (703) 264-8863. When faxing an application, **do not** mail a confirmation copy, as this results in unnecessary duplication of paper work.

	Final No.
Date Received	Tracking No.

Call for Scientific Exhibits

American Roentgen Ray Society
1993 Annual Meeting
April 25 – 30, 1993
San Francisco, CA

ADDRESS OF PRESENTING AUTHOR

Department

Institution

Street

City State Zip

Phone

Type title, authors, and abstract in the space provided below. (Instructions are on reverse side of this page.)

Select one category: ☐ Cardiovascular ☐ Breast ☐ Sonography ☐ Gastrointestinal ☐ Genitourinary ☐ Chest
☐ Neuroradiology ☐ Bone ☐ Pediatric ☐ Nuclear medicine ☐ Medical physics

What Type of Exhibit is Proposed? (Check one and fill in all appropriate blanks.)

__________ **Free-standing.** This is a self-contained display created in total by the exhibitor. It may be a fold-open unit, a unit shipped in cases and assembled on site, or a tabletop unit. Standard free-standing space is 10' x 10'. Indicate linear feet required________.

__________ **Poster Board (Backboard panels).** Backboard panels are 4 x 8 ft. (1.2 x 2.5m). Number of panels required ________. If two panels ar needed, there will be a ¼-in. frame separating the panels, thus requiring a separation in the presentation.

__________ **Viewbox.** Mounted materials (radiographs and other transparencies) for display on the society's illuminators. Each illuminator is 39.5 x 59.5 in. (100 x 151 cm). Number of illuminators required _______. Materials should not be glass mounted.

Instructions for Scientific Exhibit Abstracts

1. Type information single-spaced. Underline the name of the presenting author. Append as a last line of the abstract any research grant support, if applicable (e.g. Supported by USPHS Grant HE-80144). If the abstract is accepted, it will appear in the program book exactly as typed. Use the following format:

    MR IMAGING OF THE SPINE AND NECK
    F.S. Lau, M.D., A.N. Kirk, M.D., R.A. Beck, Ph.D.
    University of California, Bakersfield, Bakersfield, CA 92338

2. The abstract should be a brief paragraph that states the purpose, principal information and conclusions of the exhibit. Promissory statements are not acceptable. Brevity is desirable but not at the expense of specific information. Exhibits will be chosen on the basis of the quality of the abstract and exhibit space available. Poster board exhibits are encouraged as they do not require a viewbox or electricity.

3. The Scientific Exhibits Committee will grade each abstract and determine acceptance. Letters indicating acceptance or rejection will be mailed to all applicants in mid-January, together with meeting registration information. Exhibitors will receive instructions for exhibit preparation.

Deadline for submission of abstracts is November 1, 1992. Mail **one** copy of abstract to

N. Reed Dunnick, M.D.
Chairman, Scientific Exhibits Committee
c/o Susan Roberts, Projects Manager
American Roentgen Ray Society
1891 Preston White Drive
Reston, VA 22091

Although mail submission is preferable, abstracts will be accepted by fax at 703-264-8863. When faxing an application, **do not** mail a confirmation copy, as this results in unnecessary duplication of paper work.

PERSONAL COMPUTER/LASER VIDEODISC SYSTEM
to assist you in the
diagnosis of Skeletal Dysplasias

A unique collection of 400 Skeletal Syndromes
7000 Illustrations
including

- *X-rays*
- *Clinical pictures*
- *Chondro-osseous histology*

OSSUM

AN ILLUSTRATED DATABASE OF SKELETAL DYSPLASIAS

S
S
U
M

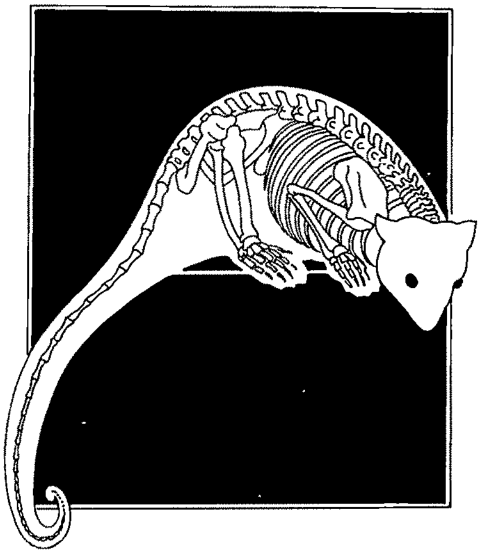

for further information contact:
Dr. Agnes Bankier – Medical Geneticist to the successful related POSSUM system.

PO Box 1100 Parkville Victoria 3052 Australia
Phone: (03) 345 5160 Fax: (03) 348 1391

Volume 159 **American Journal of Roentgenology** September 1992

REVIEW ARTICLE

453 **MR measurement of blood flow in the cardiovascular system.** *Mostbeck GH, Caputo GR, Higgins CB*

CARDIOPULMONARY RADIOLOGY

463 **Diagnosis of bronchiolitis obliterans in heart-lung transplantation patients: importance of bronchial dilatation on CT.** *Lentz D, Bergin CJ, Berry GJ, Stoehr C, Theodore J*
469 **Hypersensitivity pneumonitis: sensitivity of high-resolution CT in a population-based study.** *Lynch DA, Rose CS, Way D, King TE Jr*
473 **Pulmonary sarcoidosis: changes on follow-up CT examination.** *Murdoch J, Müller NL*
479 **Case report. Anomalous left brachiocephalic (innominate) vein: MR demonstration.** *Fujimoto K, Abe T, Kumabe T, Hayabuchi N, Nozaki Y*
481 **Case report. Value of MR imaging in detecting a peanut causing bronchial obstruction.** *O'Uchi T, Tokumaru A, Mikami I, Yamasoba T, Kikuchi S*

BREAST RADIOLOGY

483 **Ductal carcinoma in situ of the breast: correlation between mammographic calcification and tumor subtype.** *Stomper PC, Connolly JL*
487 **Solitary breast papilloma: comparison of mammographic, galactographic, and pathologic findings.** *Woods ER, Helvie MA, Ikeda DM, Mandell SH, Chapel KL, Adler DD*
493 **Mammography in women with axillary lymphadenopathy and normal breasts on physical examination: value in detecting occult breast carcinoma.** *Leibman AJ, Kossoff MB*

GASTROINTESTINAL RADIOLOGY

497 **Pictorial essay. Left-lobe hepatic transplants: spectrum of normal imaging findings.** *Caron KH, Strife JL, Babcock DS, Ryckman FC*
503 **Malignant biliary obstruction: efficacy of thin-section dynamic CT in determining resectability.** *Gulliver DJ, Baker ME, Cheng CA, Meyers WC, Pappas TN*
509 **Review. Chronic biliary-type pain in the absence of gallstones: the value of cholecystokinin cholescintigraphy.** *Kloiber R, Molnar CP, Shaffer EA*
515 **Membranous obstruction of the inferior vena cava: comparison of findings at sonography, CT, and venography.** *Lim JH, Park JH, Auh YH*
521 **Acute lower gastrointestinal hemorrhage: treatment by superselective embolization with polyvinyl alcohol particles.** *Guy GE, Shetty PC, Sharma RP, Burke MW, Burke TH*
527 **The density, contour, and thickness of the pancreas in diabetics: CT findings in 57 patients.** *Gilbeau J-P, Poncelet V, Libon E, Derue G, Heller FR*
533 **Pictorial essay. Pancreatic disease: findings on state-of-the-art MR images.** *Mitchell DG, Shapiro M, Schuricht A, Barbot D, Rosato F*
539 **Diagnosis of acute appendicitis in pregnant women: value of sonography.** *Lim HK, Bae SH, Seo GS*
543 **Case report. Pipestem appearance of small bowel in strongyloidiasis is not pathognomonic of fibrosis and irreversibility.** *Medina LS, Heiken JP, Gold RP*
545 **Case report. Multiple smooth-muscle tumors of the colon and adrenal gland in an adult with AIDS.** *Radin DR, Kiyabu M*
547 **Case report. Inadvertent barium hysterosalpingography.** *Carlsen SE, Thurmond AS, Scanlan RM, Patton PE*

GENITOURINARY RADIOLOGY

551 **Pictorial essay. Renal diseases in patients with AIDS: sonographic findings.** *Kay CJ*
555 **Submucosal uterine leiomyomas: diagnosis of prolapse into the cervix and vagina based on MR imaging.** *Panageas E, Kier R, McCauley TR, McCarthy S*

MUSCULOSKELETAL RADIOLOGY

559 **Temporomandibular joint: relationship between MR evidence of effusion and the presence of pain and disk displacement.** *Westesson P-L, Brooks SL*
565 **Injuries of the superior portion of the glenoid labrum involving the insertion of the biceps tendon: MR imaging findings in nine cases.** *Hodler J, Kursunoglu-Brahme S, Flannigan B, Snyder SJ, Karzel RP, Resnick D*
569 **Value of unenhanced spin-echo MR imaging in distinguishing between synovitis and effusion of the knee.** *Singson RD, Zalduondo FM*
573 **Technical note. Intraarticular sonography for imaging the knee menisci: evaluation in cadaveric specimens.** *McDonnell CH III, Jeffrey RB Jr, Björkengren AG, Li KCP*
575 **Elastofibroma: MR and CT appearance with radiologic-pathologic correlation.** *Kransdorf MJ, Meis JM, Montgomery E*

NEURORADIOLOGY

581 **Review. Neoplastic diseases affecting the central skull base: CT and MR imaging.** *Ginsberg LE*
591 **Review. Diffusion MR imaging: clinical applications.** *Le Bihan D, Turner R, Douek P, Patronas N*
601 **Pictorial essay. Cystic masses of the head and neck: pitfalls in CT and MR interpretation.** *Miller MB, Rao VM, Tom BM*
609 **CT and MR imaging findings in adults with cerebellar medulloblastoma: comparison with findings in children.** *Bourgouin PM, Tampieri D, Grahovac SZ, Léger C, Del Carpio R, Melançon D*
613 **Case report. Tortuous vertebral artery shown by MR and CT.** *Kricun R, Levitt LP, Winn HR*

PEDIATRIC RADIOLOGY

617 **Diagnosis of liver disease in children: value of MR angiography.** *Hubbard AM, Meyer JS, Mahboubi S*
623 **Case report. Neonatal hemochromatosis: diagnosis with MR imaging.** *Hayes AM, Jaramillo D, Levy HL, Knisely AS*
626 **Case report. AIDS-related cholangitis in children: sonographic findings.** *Rusin JA, Sivit CJ, Rakusan TA, Chandra RS*
628 **Case report. Bile nephrosis in a neonate: sonographic findings of rapid kidney enlargement and increased echogenicity.** *Bruno MA, Spear GS, Dietrich RB, Pugh PA*

STATISTICS IN RADIOLOGY

631 **Perspective. Strategies for improving power in diagnostic radiology research.** *Beam CA*

MEETING NEWS

639 **The Society of Cardiovascular and Interventional Radiology: 17th annual scientific meeting, April 1992.** *Whalen E*

ARRS 1992 ANNUAL MEETING

647 **Summary of scientific program**
657 **Gold medal recipients**
661 **Secretary's report.** *Ferrucci JT*
665 **Award-winning exhibits**
668 **New members**

OTHER CONTENT

462 **Medicine in American art.** *Schatzki SC*
495 **List of book reviews**
550 **Photo page.** *Tomiak MM, Rosenblum JD, Leef JA*
564 **Pitfalls in medical writing.** *Ronai PM*
600 **Radiologic-pathologic conference.** *Barboriak DP, Rivitz SM, Chew FS*
616 **Memorial. Elmer G. St. John**
660 **American Roentgen Ray Society information**
663 **1993 ARRS meeting information**
664 **ARRS 1993 residents' award papers information**
670 **Forthcoming articles**
671 **Letters**
679 **Review of current literature**
682 **News**
685 **Classified advertisements**
Call for papers and exhibits for 1993 ARRS meeting
A4 ***AJR* business and subscriber information**
A10 **Guidelines for authors**

AJR

American
Journal of
Roentgenology

October 1992

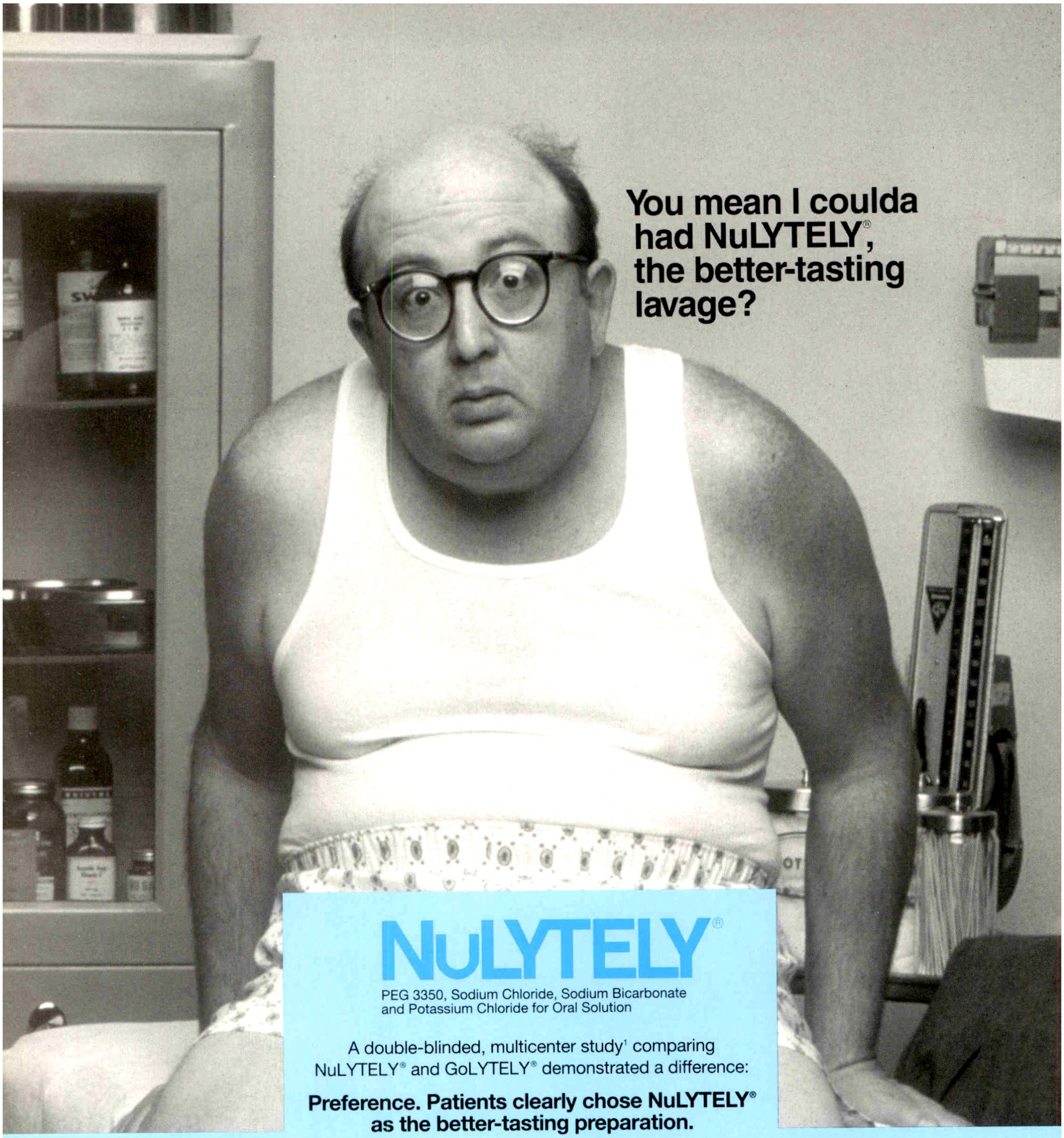
You mean I coulda
had NuLYTELY®,
the better-tasting
lavage?

NuLYTELY®

PEG 3350, Sodium Chloride, Sodium Bicarbonate
and Potassium Chloride for Oral Solution

A double-blinded, multicenter study[1] comparing NuLYTELY® and GoLYTELY® demonstrated a difference:

Preference. Patients clearly chose NuLYTELY® as the better-tasting preparation.

BRIEF SUMMARY: Before prescribing, see complete prescribing information.

INDICATIONS AND USAGE: NuLYTELY is indicated for bowel cleansing prior to colonoscopy.

CONTRAINDICATIONS: NuLYTELY is contraindicated in patients with gastrointestinal obstruction, gastric retention, bowel perforation, toxic colitis or toxic megacolon.

WARNINGS: No additional ingredients, e.g. flavorings, should be added to the solution. NuLYTELY should be used with caution in patients with severe ulcerative colitis.

PRECAUTIONS: General: Patients with impaired gag reflex, unconscious, or semiconscious patients, and patients prone to regurgitation or aspiration should be observed during the administration of NuLYTELY, especially if it is administered via nasogastric tube. If a patient experiences severe bloating, distention or abdominal pain, administration should be slowed or temporarily discontinued until the symptoms abate. If gastrointestinal obstruction or perforation is suspected, appropriate studies should be performed to rule out these conditions before administration of NuLYTELY.

ADVERSE REACTIONS: Nausea, abdominal fullness and bloating are the most common adverse reactions (occurring in up to 50% of patients) to administration of NuLYTELY. Abdominal cramps, vomiting, and anal irritation occur less frequently. These adverse reactions are transient and subside rapidly. Isolated cases of urticaria, rhinorrhea and dermatitis have been reported with a related drug (GoLYTELY®) which may represent allergic reactions.

CAUTION: Federal law prohibits dispensing without prescription.

STORAGE: Store in sealed container at 25° C. When reconstituted, keep solution refrigerated. Use within 48 hours. Discard unused portion. NDC 52268-0300-01

Manufactured for Braintree Laboratories, Inc. Braintree MA 02184 by Lyne Laboratories, Inc., Stoughton MA 02072.

Reference: 1. Data on file, Braintree Laboratories.

Braintree
LABORATORIES · INC

Official Journal of the American Roentgen Ray Society

AJR

American Journal of Roentgenology
Diagnostic Imaging and Related Sciences

Editor-In-Chief Robert N. Berk, *La Jolla, California*
University of California, San Diego
School of Medicine and Medical Center

Editor Emeritus Melvin M. Figley, *Seattle, Washington*

Associate Editor Karim Valji, *San Diego, California*

Consulting Editors A. James Barkovich, *San Francisco, California*
Edward A. Sickles, *San Francisco, California*

Statistician Charles C. Berry, *San Diego, California*

Editorial Board

Mark E. Baker
Lawrence W. Bassett
Michael A. Bettmann
Ethan M. Braunstein
Felix S. Chew
Horacio R. D'Agostino
Gerald D. Dodd III
N. Reed Dunnick
David K. Edwards
Allen D. Elster
Ronald G. Evens
Sandra K. Fernbach
Richard H. Gold
Edward G. Grant
John R. Hesselink
Emanuel Kanal
Ray F. Kilcoyne
Carolyn Kimme-Smith
Melvyn T. Korobkin
Mark J. Kransdorf
Faye C. Laing
Thomas L. Lawson
Robert G. Levitt
Martin J. Lipton
Bruce L. McClennan
Richard P. Moser
Jeffrey H. Newhouse
Sven J. K. Paulin
David M. Paushter
Vassilios Raptopoulos
Donald L. Resnick
Charles A. Rohrmann, Jr.
Peter M. Ronai
Stuart S. Sagel
Sanjay Saini
Stefan C. Schatzki
William P. Shuman
Barry A. Siegel
M. Leon Skolnick
Edward T. Stewart
Murali Sundaram
Ruedi F.-L. Thoeni
Robert D. Tien

Director of Publications: Susan Brown Cappitelli **Editorial Staff:** Barbara Rose, *managing editor*; Katie L. Spiller, Barbara L. Halliburton, and Janine Anderson, *manuscript editors*; Nancy Rydbeck, *office manager*; Sheri Smith, *administrative assistant*; Linda J. Waggoner, *administrative secretary*

AJR, AMERICAN JOURNAL OF ROENTGENOLOGY (ISSN 0361 803X) is published monthly by the American Roentgen Ray Society, 1891 Preston White Dr., Reston, VA 22091. Annual dues include $50 for journal subscription. Second-class postage paid at Baltimore, MD, and at additional mailing offices. **POSTMASTER**, send address changes (Form 3579) to Subscription Fulfillment, AJR, 428 E. Preston St., Baltimore, MD 21202. Subscription rates $125 ($180 foreign); institutions $135 ($190 foreign); in training $25 ($80 foreign); single copy $18 ($22 foreign). The GST number for Canadian subscribers is 123394371. Airmail rates furnished on request. Indexed by *Current Contents* and *Index Medicus*. Copyright © 1992 by American Roentgen Ray Society.

0361–803X/92$3.00

AJR Business and Subscriber Information

The American Roentgen Ray Society

AJR, American Journal of Roentgenology, is published monthly to disseminate research on current developments in the radiologic sciences and commentary on topics related to radiology. It is published by the American Roentgen Ray Society (ARRS), 1891 Preston White Dr., Reston, VA 22091; (703) 648-8992. Address inquiries regarding Society business, the annual ARRS meeting, and membership to the Society to the above address.

Correspondence regarding editorial matters should be addressed to Editorial Office, AJR, 2223 Avenida de la Playa, Ste.103, La Jolla, CA 92037-3218; telephone 1-800-348-4257 or (619) 459-2229; FAX (619) 459-8814. For information on manuscript submission, see Guidelines for Authors.

Subscriber Information

ARRS annual dues include $50 for journal subscription. Nonmember subscription rates are as follows: $125/year ($180 foreign); institutions, $135 ($190 foreign); in-training, $25 ($80 foreign). Single copies of the Journal may be purchased for $18 ($22 foreign). Airmail rates will be furnished on request. The GST number for Canadian subscribers is 123394371.

Call toll-free, 1-800-638-6423 (in Maryland call 1-800-638-4007), with subscription inquires or problems. Please have the mailing label from your latest issue available when you call.

Report changes of address to Subscription Fulfillment, AJR, 428 E. Preston St., Baltimore, MD 21202. Damaged or unreceived issues must be reported within 60 days of publication (90 days for foreign subscribers) for replacement.

Advertising Information

All advertising is subject to approval by the publisher. Acceptance of advertising does not indicate endorsement of the products or services advertised or the claims made. For display advertising information, contact Gary Walchli, National Sales Representative, AJR, 428 E. Preston St., Baltimore, MD 21202, (410) 528-4291.

For classified advertising information, contact the Publications Department, ARRS, Attn: Terry Fitterer, 1891 Preston White Dr., Reston, VA 22091; telephone (703) 648-8992; FAX (703) 264-8863.

Copyrights, Permissions, and Reprints

Contents of the *AJR* are copyrighted by the ARRS. No part of this publication may be reproduced without permission. Requests for such permission should be addressed to the Publications Department, ARRS, Attn: Terry Fitterer, 1891 Preston White Dr., Reston, VA 22091. For reprints of a particular article, please contact the author designated in the footnotes for that article.

Indexes

The *AJR* provides volume and yearly indexes (subject and author) in the June and December issues. *AJR* articles are also indexed in *Current Contents*, *Index Medicus*, and the cumulative index published by *Radiology*.

"IS IT TRUE THAT NUCLEAR ASSOCIATES MAKES THE ONLY HAND-HELD SCANNING DENSITOMETER WITH BUILT-IN SINGLE-POINT MEASUREMENT CAPABILITY?"

YES! AND IT'S CALLED MINISCAN.

It's a fact. MINISCAN is exactly what you've been looking for to ensure optimum image characteristics for your x-ray film processors.

Lightweight and compact, MINISCAN can be used to make single-point measurements – essential in mammography and cardiology procedures where the most stringent quality control is required. Operating as a transmission densitometer in the single-point mode, MINISCAN lets you spot-check single-point densities; a big help where non-21-step wedges are used or where spot measurements are required.

In addition to its single-point measurement capability, MINISCAN can also measure, analyze and store data for as many as 20 sets of independent strips, allowing you to read the 21 density steps as well as average gradient, relative speed, base plus fog, contrast index, speed index and maximum optical density – all by step number. This data can be converted to hard copy using an IBM™ compatible PC running on Nuclear Associates' FILM-PRO software package.

MINISCAN can be calibrated in-house, using a standard step table, eliminating a lot of down time and the possibility of erroneous calibrations by an outside service. And because MINISCAN is battery-operated, you can take your measurements at the processor site ...another time-saving plus.

When you use MINISCAN in your x-ray processor quality control program, you assure yourself of:

- getting all of the necessary data to show you that your x-ray film processor is delivering optimum image quality.
- detecting - at an early stage - changes that affect image quality, and taking the proper steps to resolve the problem.
- maintaining the highest standards of quality control, resulting in a significant reduction in repeat x-ray examinations.

Whether your format is sheet, spot or cine film, whether your requirements are for single-point measurements or scanning, the MINISCAN Densitometer can play a key role in helping maintain the high quality control standards you strive for.

For more information, request Bulletin 5013-44

IBM™, International Business Machines, Inc.

NUCLEAR ASSOCIATES

VICTOREEN

Division of VICTOREEN, INC.
100 VOICE ROAD • P.O. BOX 349
CARLE PLACE, NY 11514-0349 U.S.A.
(516) 741-6360
FAX (516) 741-5414

CARIBBEAN '93

Neuro Imaging/MRI at Sea - January 10-17, 1993
Breast Imaging at Sea - January 17-24, 1993
Ultrasound at Sea - January 24-31, 1993

Neuro Imaging/MRI at Sea will be presented by **Hervey Segall, M.D.**, Professor of Radiology and Director of Neuroradiology at the University of Southern California School of Medicine, Los Angeles, California.

Breast Imaging at Sea will be presented by **Marc J. Homer, M.D.**, Professor of Radiology, Tufts University School of Medicine and Chief, Mammography Section, New England Medical Center Hospital, Boston, Massachusetts.

Ultrasound at Sea will be presented by **Barry B. Goldberg, M.D.**, Professor of Radiology, Director, Division of Diagnostic Ultrasound, Department of Radiology, Thomas Jefferson University Hospital, Philadelphia, Pennsylvania.

Application will be made for approximately 12-15 Category 1 CME credits for each section of the program.

Registration Information:

Complete Program (2 or 3 sections):

US $695.00 to November 15, 1992, US $750.00 thereafter.

Individual Section:

Neuro Imaging/MRI or Breast Imaging or Ultrasound at Sea

US $495.00 to November 15, 1992, US $525.00 thereafter.

(Fellows, residents, interns, technicians, and nurses with letter may deduct $100.00.)

Meeting Information: Please contact **Medical Seminars International, Inc.** 18981 Ventura Blvd., Suite 303, Tarzana, CA 91356, (818) 774-9077, FAX (818) 774-0244.

Cruise and Travel Information: Please contact **Pacifica Plaza Travel Inc.**, 5839 Green Valley Circle, Suite 202, Culver City, CA 90230, Telephone: (310) 649-6677, (800) 927-4778, FAX (310) 568-0402, ATTN: Katie.

Fellowships In Diagnostic Radiological Research.

The Diagnostic Radiology Research Program of the National Institutes of Health is accepting applications for two-year fellowship positions beginning in July 1993 and July 1994. This program provides an excellent opportunity for individuals who plan an academic career in radiological sciences.

The fellowship training program emphasizes basic research in all aspects of imaging and image processing. Fellows will have no clinical responsibilities unless they are related to their project. The imaging laboratories of the Diagnostic Radiology Research Program include: state-of-the-art 0.5 and 1.5 Tesla MR units; a newly developed image analysis program with hardware support; ultrafast CT; and an experimental angiography suite. The facilities in the *In Vivo* NMR Research Center, the PET and monoclonal antibody programs of the Nuclear Medicine Department, and other laboratories on the NIH campus will be made available to the fellow, providing an opportunity to develop expertise in areas related to imaging research. Basic research in functional or metabolic imaging, contrast agents, biochemistry, biology, chemistry, immunology, physics and physiology will be encouraged. Laboratories are being developed which will include "hot" and "cold" wet labs and tissue culture facilities. Collaboration with other scientists on the NIH campus will be encouraged.

Applicants should hold the MD or PhD degree and should have completed training in diagnostic radiology, nuclear medicine or related fields. Applications from individuals currently in US residency programs may also be considered for research fellowship positions. US citizenship or permanent residency is required for this full-time appointment.

Candidates should submit a Curriculum Vitae, at least three letters of reference and a preliminary statement concerning their research interest to Dr. Joseph A. Frank, Acting Director.

National Institutes Of Health

Diagnostic Radiology Research Program

9000 Rockville Pike, Building 10, Room B1N256, Bethesda, MD 20892 • FAX 301-402-3216

Equal Opportunity Employer

GET THE BIG PICTURE

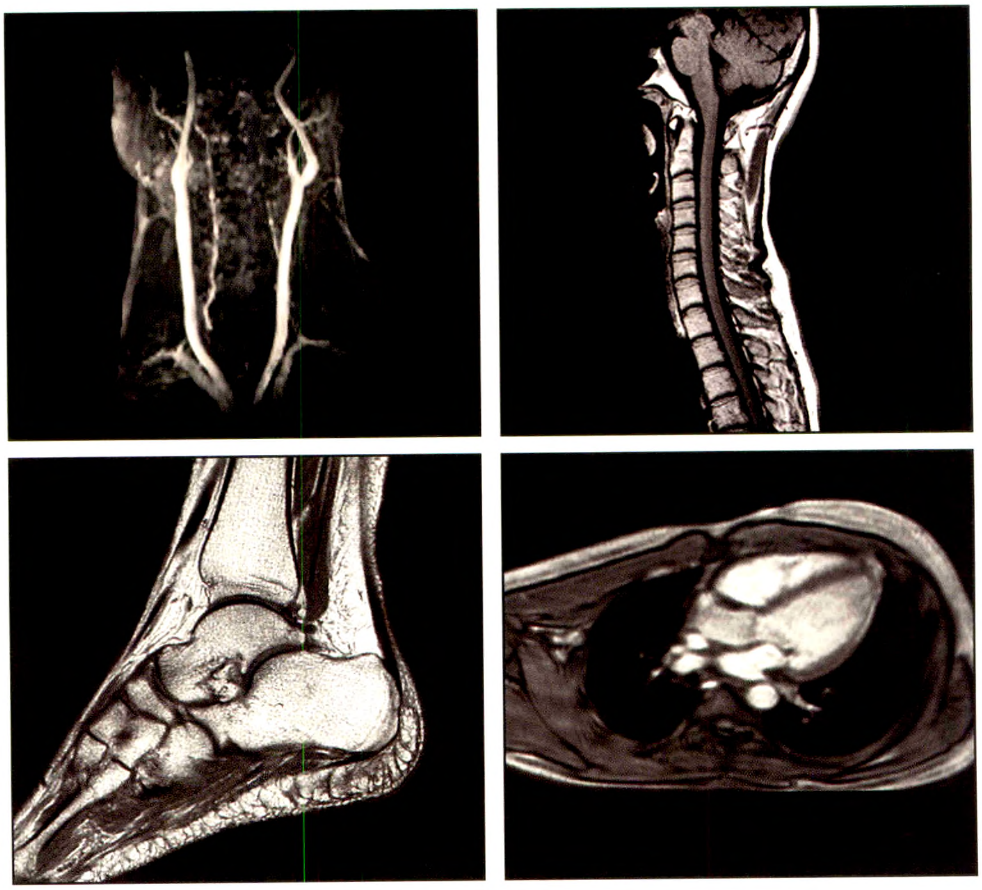

IN A SMALL SPACE.

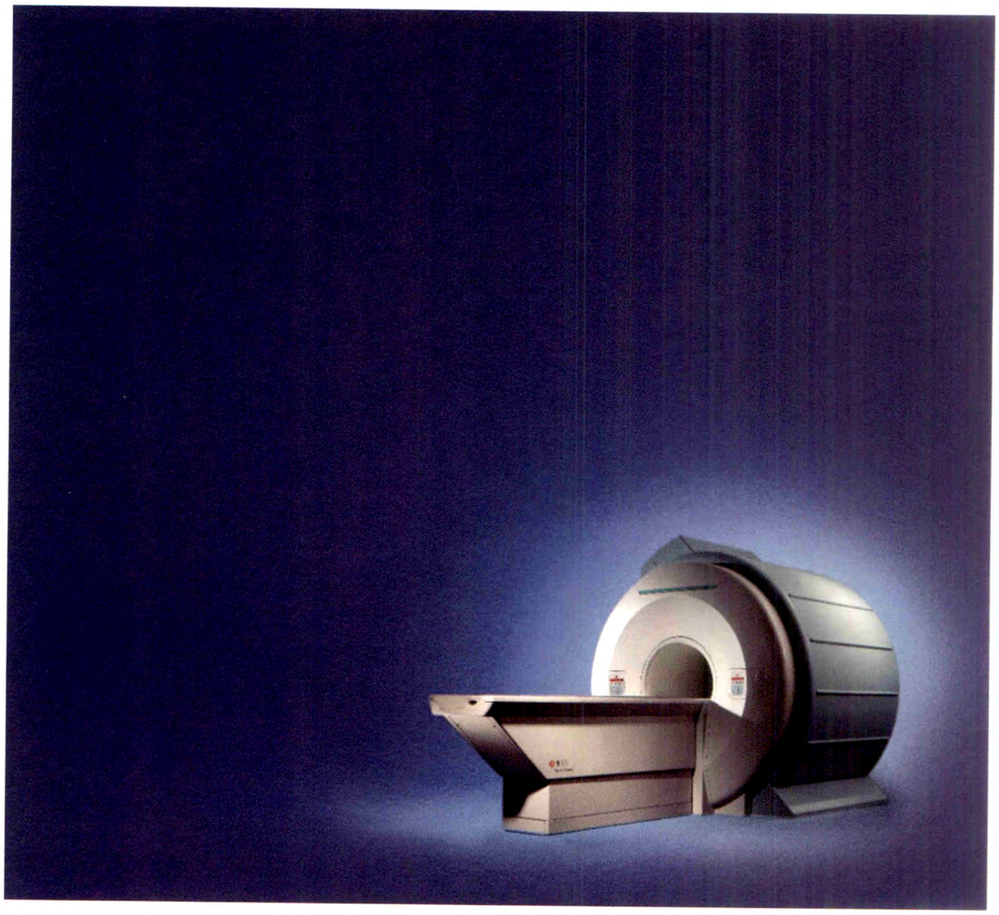

Now there's no reason to sacrifice image quality for size.

Not when the Picker Vista® Q active shield 1.0T system delivers images this clear, this detailed. Vista Q offers you the industry's highest homogeneity magnet, the only 60 cm patient aperture, and the only quadrature body and surface coils in a 1.0T MR system.

Vista Q is setting industry standards in image acquisition too – offering angio and cardiac imaging, 512^2 resolution, and volume imaging with submillimeter accuracy.

Yet with its small footprint, Vista Q is easy to site. Operating costs are low too. Vista Q's helium-only magnet requires just two refills a year.

So if you thought high field performance in an economical system was years away, think again. The Vista Q from Picker is here now.

For more information on Vista Q, call us at 1-800-323-0550. Or write Picker International, Inc., 595 Miner Road, Dept. CC, Cleveland, Ohio 44143.

PICKER

MORE THAN IMAGES. INSIGHT.

© 1992 Picker International, Inc.

When you give blood
you give another birthday,
another anniversary,
another day at the beach,
another night under the stars,
another talk with a friend,
another laugh,
another hug,
another chance.

American Red Cross

Please give blood.

Ad Council

DIRECTOR OF RADIOLOGY RESEARCH

The University of California, Davis, School of Medicine has a full-time faculty position available in the Diagnostic Division of the Department of Radiology. Appointment will be at the Associate or Full-Professor level. Candidates must possess the M.D. degree, the Ph.D. degree, or both. Candidates possessing and M.D. degree must be Board certified in either Diagnostic Radiology or Nuclear Medicine, either possess or be eligible for licensure in the State of California, and have completed clinical training in diagnostic radiology and/or nuclear medicine. Ph.D. or M.D. candidates should possess a record of successfully funded research, and have a background in teaching and research.

Please forward a curriculum vitae, a letter outlining background and interests in teaching/research, and the names and addresses of five references to: Richard W. Katzberg, M.D., Professor and Chair, Department of Radiology, University of California, Davis, Medical Center, 2516 Stockton Boulevard, TICON II Building, Sacramento, California 95817. This position will be "Open Until Filled" but not later than December 31, 1992. The University of California is an Equal Opportunity/Affirmative Action Employer and encourages applications from members of minority groups and women.

HEALTH CARE PROFESSIONALS

MONTEFIORE

RADIOLOGISTS

Major teaching hospital affiliation is expanding Computerized Tomography, Mammography and Ultrasound areas. Two full time positions are available for General Radiologists with training in CT and US. Candidates should be Board Certified. Fellowship training in CT/US preferred. Excellent salary and benefits. Please call or send CV to: **Director of Human Resources, 212-519-3727, Montefiore North Central Bronx Hospital Affiliation, 3424 Kossuth Avenue, Bronx, New York 10467.**

MONTEFIORE MEDICAL CENTER

The University Hospital
for the Albert Einstein
College of Medicine
An Equal Opportunity Employer M/F

EZEM® Single-patient bottles of Liquid E-Z-Paque® can make your routine upper GI studies more efficient, more economical and more consistent. Easy to stock and inventory, with no mess or waste, each bottle of pre-mixed Liquid E-Z-Paque gives you a consistent suspension for completely repeatable results. Make the move to single-patient liquids. Call your E-Z-EM Distributor or one of our Customer Service Specialists at 1-800-544-4624.

E-Z-EM, Inc.
717 Main Street
Westbury, NY 11590
Tel: 1-800-544-4624
Fax: 516-333-8278

E-Z-EM INTEGRITY • E-Z-EM DEDICATION • E-Z-EM INNOVATION
30 Years of Quality and Service to Radiology

LESS IS MORE.

E-Z-EM stock is publicly traded on the NASDAQ National Market System under the symbol EZEM. For financial information, contact Investor Relations at 1-800-544-4624, ext. 345.

© E-Z-EM, Inc., 1992

Subject: Technology

Point of view: Technologist

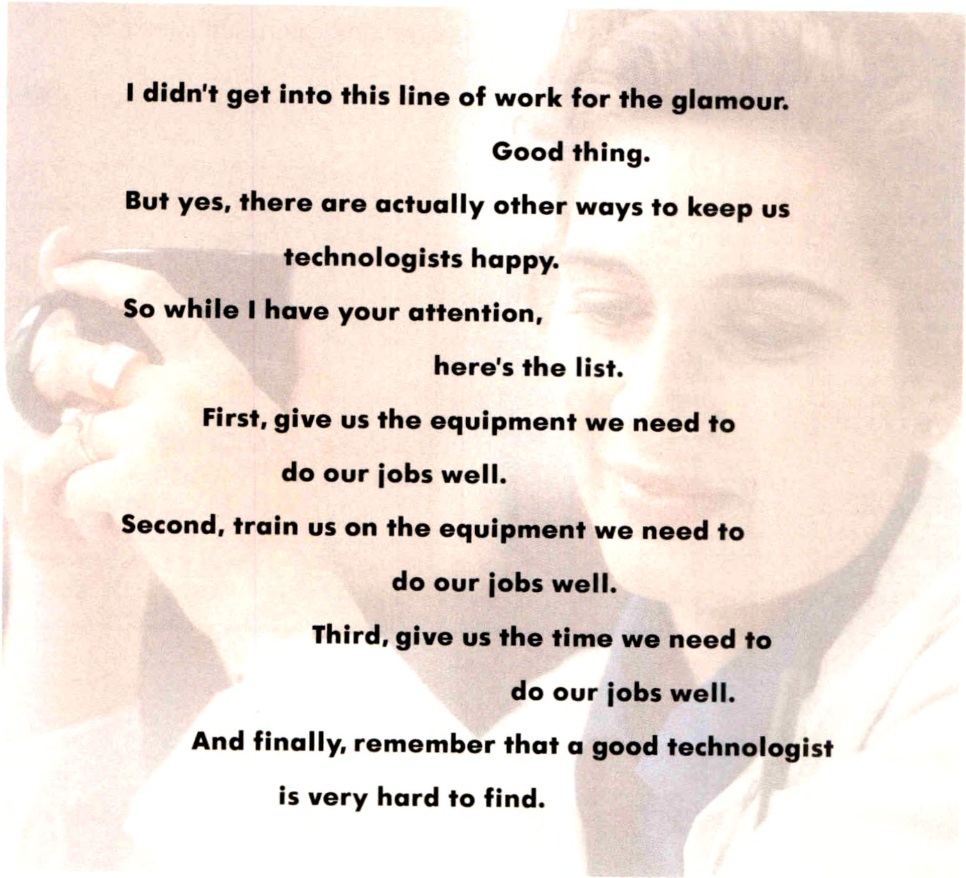

I didn't get into this line of work for the glamour.

Good thing.

But yes, there are actually other ways to keep us technologists happy.

So while I have your attention,

here's the list.

First, give us the equipment we need to do our jobs well.

Second, train us on the equipment we need to do our jobs well.

Third, give us the time we need to do our jobs well.

And finally, remember that a good technologist is very hard to find.

At Picker, our commitment is not only to developing technology. It's to developing technologists as well. Which is why our Health Care Products division created the Education Support Program to benefit the Educational Foundation of the American Society of Radiologic Technologists.

PICKER

MORE THAN IMAGES. INSIGHT.

© 1992 Picker International, Inc. For reprints of this ad or for more information, call us at 1-800-323-0550.

Visit us at RSNA Booth 4014 & 4021 - East Hall

ASSOCIATE MEDICAL DIRECTOR

RADIOLOGY

This is an exceptional opportunity to utilize your medical training with Sanofi Winthrop Pharmaceuticals, a Division of Sterling Winthrop, a world class leader in the field of ethical pharmaceuticals and diagnostic imaging agents.

The selected candidate for this high visibility position will provide a broad array of high quality clinical research data for a marketed line product utilized in radiology. Specific duties will involve: supporting the marketing, sales, regulatory, product safety and legal aspects of the assigned product by providing concise medical expertise; designing and conducting comprehensive clinical research trials; participating in developing related marketing programs and sales training materials.; providing expert medical testimony when required; and serving as medical consultant / advisor to internal support groups and outside agencies and health professionals.

To be considered, you must possess a valid U.S. medical license, 2 to 3 years of U.S. based post graduate medical training, and proven expertise in the field of Radiology. The interpersonal and communication skills to interact effectively with Senior Management and outside regulatory agencies and the ability to keep abreast of technical developments and related changes in regulatory / safety requirements are essential pre-requisites of the position.

If you're looking for a unique and rewarding environment with a dynamic industry leader forward your resume to: **Human Resources, Dept. A.M.D., Sanofi Winthrop, Div. of Sterling Winthrop, 90 Park Ave., 10th Fl, New York, NY 10016.**

sanofi WINTHROP

A Division of Sterling Winthrop

A Subsidiary of Eastman Kodak

We are an equal opportunity employer M/F/H/V

THE UNIVERSITY OF CALIFORNIA, IRVINE, Department of Radiological Sciences has fellowship positions as Clinical Instructors available commencing July, 1994 in Ultrasound/CT/MR, Vascular and Interventional, Magnetic Resonance Imaging, and research in MRI or other specialty areas. Applicants must be Board eligible in Diagnostic Radiology and possess a California license by the time they commence their training. Interested candidates should send their curriculum vitae and reference letters to:

Rosalind B. Dietrich, M.D.
Director
Radiology Fellowship Program
Department of Radiological Sciences
University of California
Irvine Medical Center
101 City Drive South
Route 140
Orange, CA 92668

The University of California is an Equal Opportunity and an Affirmative Action employer.

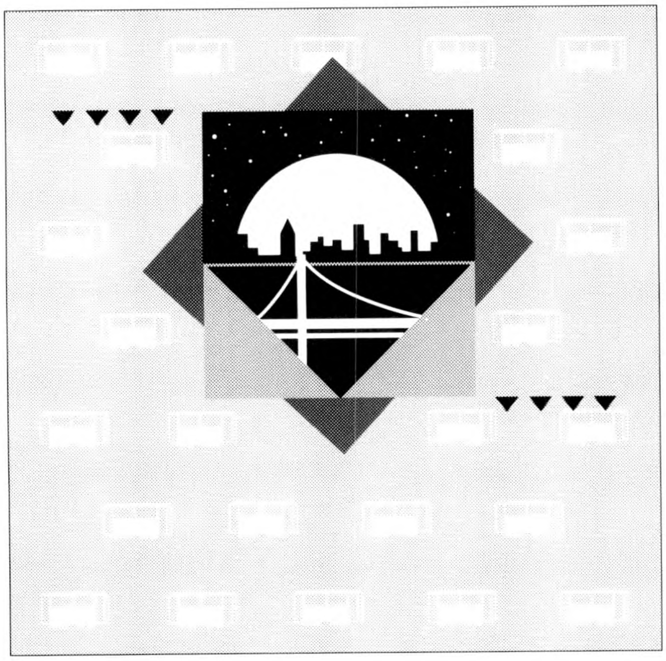

San Francisco

American Roentgen Ray Society

93rd Annual Meeting
April 25–30, 1993

San Francisco Marriott
San Francisco, CA

There are two sides to all radiology procedures.

MALLINCKRODT
Radiology

There's more to our contrast than just great pictures.

When you select Mallinckrodt Radiology contrast media, you get products that definitively meet the needs of your practice.

Quality diagnostic images, and a complete line that allows you to choose the right contrast, for the right procedure, for the right patient.

Take a closer look at Mallinckrodt and you'll also see the unique way in which we approach your business today. Greater efficiency. Time savings. Even increased productivity.

That's the type of commitment you see, and the type of value you will continue to get with products from Mallinckrodt Radiology.

The one you see.

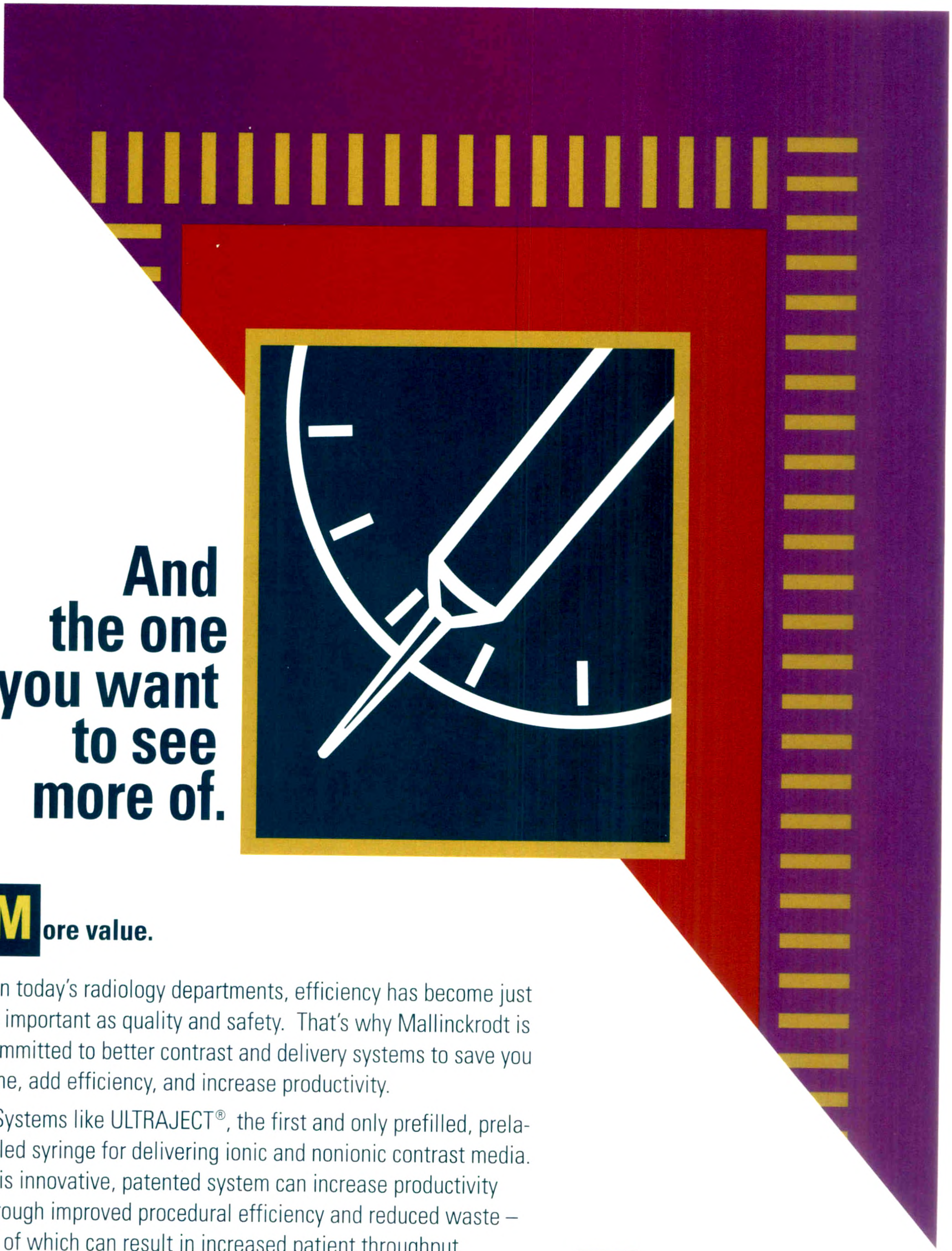

And the one you want to see more of.

More value.

In today's radiology departments, efficiency has become just as important as quality and safety. That's why Mallinckrodt is committed to better contrast and delivery systems to save you time, add efficiency, and increase productivity.

Systems like ULTRAJECT®, the first and only prefilled, prelabeled syringe for delivering ionic and nonionic contrast media. This innovative, patented system can increase productivity through improved procedural efficiency and reduced waste – all of which can result in increased patient throughput.

This is just one example of how we are combining quality and efficiency to help you get more value today. And we're committed to continue leading the way with innovative systems and programs for tomorrow.

MALLINCKRODT
Radiology

Where value is the bigger picture

There are two sides to a state-of-the-art contrast delivery system:

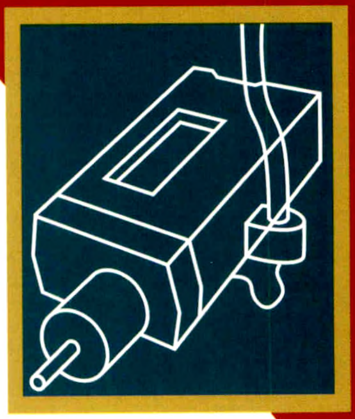

Ultraject®

Prefilled contrast media syringes

Liebel-Flarsheim™*

Power injectors

Find out how you may receive an Angiomat™* CT Power Injector at no additional capital expense.

Liebel-Flarsheim Company is a worldwide leader in power injectors. The Angiomat™ CT digital injector system is a microprocessor controlled unit with unique features and benefits for your department that no other power injector can offer.

And the fact that this premium system now accepts all sizes and concentrations of ionic and nonionic ULTRAJECT® power injector syringes makes this a complete system that helps improve the standard-of-care of contrast media delivery in any CT suite.

To hear more about how your lab may receive the premier Angiomat™ CT injector, simply call toll-free 1-800-833-4731, or contact your Mallinckrodt Radiology sales representative.

*Liebel-Flarsheim™ and Angiomat™ are trademarks of Liebel-Flarsheim Company.

MALLINCKRODT

Radiology

Where value is the bigger picture

© 1992 Mallinckrodt Medical, Inc. MI22466 Printed in U.S.A.

AJR Guidelines for Authors

Address new and revised manuscripts and correspondence to the Editor:

AJR Editorial Office
2223 Avenida de la Playa, Suite 103
La Jolla, CA 92037-3218
Telephone: (619) 459-2229; FAX: (619) 459-8814

Inquiries regarding classified ads, reprints, or permission to republish *AJR* material should be addressed to the publisher:

ARRS Publications Department
1891 Preston White Dr., Reston, VA 22091

The *AJR* publishes original contributions to the advancement of medical diagnosis and treatment. Submitted manuscripts should not contain previously published material and should not be under consideration for publication elsewhere.

Manuscript decisions are based on peer review. Reviewers receive manuscripts without title pages to ensure an unbiased review. Statements made in the article, including changes made by the Editor or manuscript editor, are the responsibility of the author and not of the *AJR* or its publisher. Authors will be sent the edited manuscript, galley proof, and proofs of illustrations. If the corresponding author will be unavailable to review galleys, arrangements should be made for a coauthor or colleague to read and return the proof.

The following guidelines are based on instructions set forth in the **Uniform Requirements for Manuscripts Submitted to Biomedical Journals** (*Ann Intern Med* **1988;**108:258–265). Articles will be edited, however, to conform to the individual style of *AJR*.

General Guidelines for Major Papers

Abstract. Clearly state (in 250 words or fewer) the purpose, methods, results, and conclusions of the study. Include actual data.

Introduction. Briefly describe the purpose of the investigation and explain why it is important.

Methods. Describe the research plan, the materials (or subjects), and the methods used, in that order. Explain in detail how disease was confirmed and how subjectivity in observations was controlled.

Results. Present results in a clear, logical sequence. If tables are used, do not duplicate tabular data in text, but do describe important trends and points.

Discussion. Describe the limitations of the research plan, materials (or subjects), and methods, considering both the purpose and the outcome of the study. When results differ from those of previous investigators, explain the discrepancy.

AUTHOR'S CHECKLIST

For priority handling, complete the following checklist, sign the copyright form on the reverse side of this page, and include both with the manuscript.

________ Two copies of the manuscript (the original and a photocopy) and two complete sets of figures are submitted. One copy has been retained by the author.

________ If appropriate, *AJR* Guidelines for case reports, technical notes, pictorial essays, or letters to the Editor have been followed. (See page A19.)

________ The manuscript, including references, figure legends, and tables, is typed double-spaced on 8½ × 11 in. (21.6 × 27.9 cm) *nonerasable* paper. Right-hand margins are not justified.

________ All manuscript pages are numbered consecutively beginning with the abstract. Authors' names do not appear on the manuscript pages.

________ The manuscript is organized as follows: title page, blind title page (title only), abstract, introduction, methods, results, discussion, acknowledgments, references, tables, figure legends, and figures.

________ Informed consent has been obtained from patients who participated in clinical investigations. If experiments were performed on animals, authors complied with NIH guidelines for use of laboratory animals.

________ Use of unfamiliar acronyms and abbrevations is kept to a minimum. When abbreviations are used they are defined at first mention, followed by the abbreviation in parentheses.

________ Metric measurements are used throughout, or the metric equivalent is given in parentheses.

________ Names and locations (city and state only) of manufacturers are given for equipment and nongeneric drugs.

________ Upon acceptance, final version is submitted on either a 5 1/4-in. or 3 1/2-in. DOS-compatible diskette in Wordperfect or ASCII format.

Title Page

________ The following information is given: title of article; names and complete addresses (including zip code) of all authors; current addresses of authors who have moved since study; acknowledgment of grant or other assistance. The corresponding author is clearly identified, and a current address, phone number, and FAX number are given.

________ A blind title page is included in each copy of the manuscript, giving only the title (without the authors' names) for use in the review process.

Abstract

________ An abstract of approximately one and one-half typewritten pages is organized into the following paragraphs.

Objective. In one or two sentences, indicate the specific goal or purpose of the article, and indicate why it is worthy of attention. Explain the hypothesis to be tested, the dilemma to be resolved, or the deficiency to be remedied. The objective stated here must be identical to the one given in the title and introduction of the paper.

Subjects (or materials) and methods. Describe succinctly the methods used to achieve the objective explained in the first paragraph, stating what was done, how it was done, how bias was controlled, what data were collected, and how the data were analyzed.

Results. The findings of the procedures described in the preceding paragraph are presented here. All results should flow logically from the methods described and not stray from the specific objective of the paper. Include as many specific data as possible within the overall length limitation of one typewritten page.

Conclusion. In one or two sentences, present the take-home message to be remembered when all else is forgotten. Describe the conclusion of the study, based solely on the data provided in the body of the abstract. Conclusions must relate directly to the objective of the paper as defined in the title and first paragraph of the abstract.

________ No abbreviations or reference citations are used.

References

________ References (not to exceed 35) are typed double-spaced starting on a separate page and are **numbered consecutively in the order in which they appear in the text.**

________ All references are cited in the text and are enclosed in brackets and typed on line with the text (not superscript).

________ Unpublished data are not cited in the reference list, but are cited parenthetically in the text, for example, (Smith DJ, personal communication), (Smith DJ, unpublished data). This includes papers submitted, but not yet accepted, for publication.

________ Papers presented at a meeting are not cited in the reference list, but are cited parenthetically in the text (e.g., Smith DJ et al., presented at the American Roentgen Ray Society meeting, May 1990). After first mention, use (Smith DJ et al., ARRS meeting, May 1990).

________ Inclusive page numbers (e.g., 333–335) are given for all references.

________ Journal names are abbreviated according to *Index Medicus*.

________ Style and punctuation of references follow the format illustrated in the following examples (all authors are listed when six or fewer; when seven or more authors, the first three are listed, followed by "et al."):

Journal article

1. Long RS, Roe EW, Wu EU, et al. Membrane oxygenation: radiographic appearance. *AJR* **1986**;146:1257–1260

Book

2. Smith LW, Cohen AR. *Pathology of tumors*, 6th ed. Baltimore: Williams & Wilkins, **1977**:100–109

Chapter in a book

3. Breon AJ. Serum monitors of bone metastasis. In: Clark SA, ed. *Bone metastases.* Baltimore: Williams & Wilkins, **1983**:165–180

Tables

________ Each table is typed double-spaced on a separate page without vertical or horizontal rules; each has a short, descriptive title. Tables do not exceed two pages in length and contain at least four lines of data.

________ Tables are numbered in the order in which they are cited in the text.

________ Abbreviations are defined in an explanatory note below each table.

________ Tables are self-explanatory and do not duplicate data given in the text or figures.

________ All arithmetic (percentages, totals, differences) has been double checked for accuracy, and tabular data agree with data given in the text.

Figures and Legends

________ Two complete sets of original figures are submitted unmounted in labeled envelopes.

________ Figures are clean, unscratched, glossy prints, uniform in size and magnification, with **white borders.** A separate print (not larger than 5 × 7 in.) is submitted for each figure *part*.

________ All figure parts relating to one patient have the same figure number.

________ Each figure is labeled on the back with the figure number and an arrow indicating "top." For black-and-white figures, labeling is done on a gummed label, which is then affixed to the back of the print. **Never** use labels on **color** figures, but write figure number on the back lightly in pencil. *Never* use ink on front or back of any figures.

________ Authors' names are *not* written on the backs of figures.

________ Only removable (rub-on) arrows and letters are used on the figures. Symbols are uniform in size and style and are not broken or cracked.

________ Line drawings are done in black ink on a white background. They are professional in quality, and all use the same size type. (Only glossy prints are acceptable.)

________ Written permission has been obtained for use of all previously published illustrations (and copies of permission letters are included), and an appropriate credit line is given in the legends.

________ Legends are typed double-spaced, and figure numbers correspond with the order in which the figures are cited in the text.

________ Legends are written in accordance with *AJR* style (refer to any issue and follow format).

Transfer of Copyright Agreement, Conflict of Interest Acknowledgment, Certification of Coauthors, and Exclusive Publication Statement

Complete copyright to the article entitled: ____

____

is hereby transferred to the American Roentgen Ray Society (for United States government employees to the extent transferable), effective if and when the article is accepted for publication in the *American Journal of Roentgenology*. In the case of the authors who are officers or employees of the United States government, the American Roentgen Ray Society recognizes that works prepared by officers or employees of the United States government as part of their official government duties are in the public domain.

Authors reserve all proprietary rights other than copyright, such as patent rights and the right to use all or part of this article in future works of their own. The authors retain the right of replication, subject only to crediting the original source of publication and receiving written permission from the publisher.

Authors guarantee that this manuscript contains no matter that is libelous or otherwise unlawful, invades individual privacy, or infringes any proprietary rights.

Authors understand that they will receive no royalty or other compensation from the American Roentgen Ray Society.

Authors guarantee that the editor has been or will be informed of any proprietary or commercial interest or conflicts of interest the authors may have that relate directly or indirectly to the subject of this article.

All authors certify that they have made substantive and specific intellectual contributions to the article and assume public responsibility for its content.

Finally, the authors certify that none of the material in this manuscript has been published previously or is currently under consideration for publication elsewhere.

------------------------------	------------------------------	------------------------------
First author/date	Second author	Third author
------------------------------	------------------------------	------------------------------
Fourth author	Fifth author	Sixth author

This agreement must be signed by all authors in order for the manuscript to be published.

Case Reports

A case report is a brief description of a special case that provides a message that transcends the individual patient.

Format. There is no abstract. The introduction should be a short paragraph giving the general background and the specific interest of the case. No more than one case should be described in detail (similar ones can be mentioned briefly in the discussion). Emphasis should be on the radiologic aspects; clinical information must be limited to that necessary to provide a background for the radiology. The discussion should be succinct and should focus on the specific message and relevance of radiologic methods. A review of the literature is not appropriate.

Length. Maximum of five double-spaced, typewritten pages, including the references but not the title page or figure legends.

References. Maximum of eight.

Figures. Maximum of four, unless the text is shortened accordingly. Legends must not repeat the text.

Tables and Acknowledgments. Not appropriate in case reports.

Pictorial Essays

A pictorial essay is an article that conveys its message through illustrations and their legends. Unlike other *AJR* articles, which are based on original research, pictorial essays serve primarily as teaching tools, like exhibits at a scientific meeting. They are not encyclopedic book chapters. The introduction should serve as an abstract: define the scope of the paper and explain its importance on one half of a double-spaced typewritten page.

Length. Maximum of four double-spaced, typewritten pages, including the references but not the title page or figure legends.

References. Maximum of four.

Figures. Maximum of 30 figure *parts*. Number should be as few as necessary to convey the message of the paper.

Tables and Acknowledgments. Not appropriate in pictorial essays.

Opinions, Commentaries, and Perspectives

Opinions, commentaries, and perspectives are special articles dealing with controversial topics or issues of special concern to radiologists.

Format. Include a title page but no abstract. Headings may be used to break up the text.

Length. Maximum of five double-spaced, typewritten pages.

References. Maximum of five.

Tables and Figures. Maximum of four.

Technical Notes

A technical note is a brief description of a specific technique or procedure, modification of a technique, or equipment of interest to radiologists.

Format. No abstract, headings, or subheadings are required. If headings are used, they should be a combination of "Case Report," "Materials and Methods," "Results," and "Discussion." A brief one-paragraph introduction should be included to give the general background. Discussion should be limited to the specific message, including the uses of the technique or equipment. Literature reviews and lengthy case reports are not appropriate.

Length. Maximum of five double-spaced, typewritten pages, including the references but not the title page or figure legends.

References. Maximum of eight.

Figures. Maximum of two, unless the text is shortened accordingly.

Tables and Acknowledgments. Not appropriate in technical notes.

Letters to the Editor and Replies

Letters to the Editor and Replies should offer objective and constructive criticism of published articles. Letters may also discuss matters of general interest to radiologists. Material being submitted or published elsewhere should not be duplicated in letters, and authors must disclose financial associations or other possible conflicts of interest.

Format. All letters should be typed double-spaced on nonletterhead paper, with no greeting or salutation. Titles for letters should be short and pertinent. The title for a reply is simply "Reply." Do not use abbreviations in the title or the text. Authors' names and affiliations should appear at the end of the letter. Do not end a letter with a hand-written signature.

Number of authors. Maximum of four.

Length. Maximum of two double-spaced, typewritten pages, including references.

References. Maximum of four.

Figures. Maximum of two figures *or* one figure with two parts.

Tables and Acknowledgments. Not appropriate in Letters to the Editor and Replies.

Computer Page Articles

Articles published on the computer page deal with practical computer applications to radiology.

Format. Include a title page and an abstract.

Length. Maximum of eight double-spaced, typewritten pages.

References. Maximum of five.

Figures and Tables. Maximum of five. Computer printouts are not acceptable. Figures must be submitted as 5 × 7 in. glossy prints.

All submissions to the *AJR* must be accompanied by a completed copy of the Author's Checklist and the signed Copyright agreement.

Keep It All Together

Easily and Conveniently with Bound Volumes of the *American Journal of Roentgenology*

Keeping up with scientific and technological advances in radiology is more important than ever, and that's why each issue of the *American Journal of Roentgenology* is packed with up-to-the-minute information crucial to you and your practice. **Keep this important resource together for easy reference in convenient and attractive bound volumes.**

Bound volumes offer the timely coverage only a journal can provide — penetrating discussions of the topics that interest you most by the brightest names in the field — with all the durability and convenience of a hardcover edition. You'll have a year's worth of vital information all arranged and indexed in one sturdy source. And each carefully crafted volume will make a handsome addition to your permanent library.

To help you keep your reference library up to date, once a year we'll send a reminder so you can order the latest bound volumes. When you send in your paid order, a set will be reserved for you, to be sent as soon as available on 30-day approval. If you do not want the volumes for any reason, simply return them within 30 days for a courteous refund. It's that easy.

Bound volumes are available to subscribers only and are in addition to the regular subscription. For ordering information, contact *AJR* Subscription Fulfillment Department, 428 E. Preston St., Baltimore, MD 21202-3993, or call toll-free

1-800-638-6423.

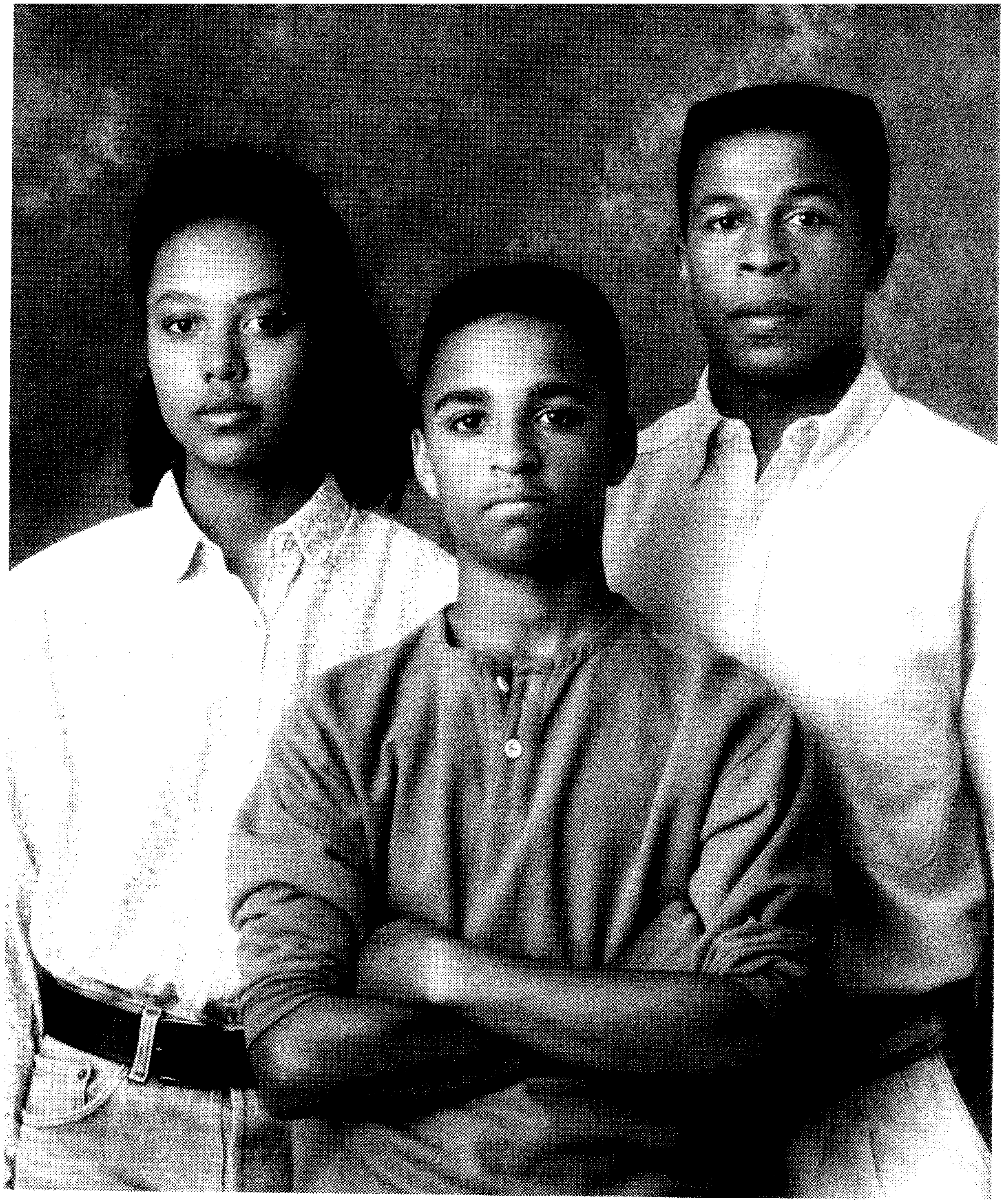

If all your children deserved to go to college, but you could only send one, how would you choose?

A better question is why should you have to choose? Why shouldn't every bright, hard-working kid get a chance to fulfill his or her dreams?

That's why your donation to the United Negro College Fund is so important. As the most experienced source in providing general operating support for historically black colleges, we've enabled thousands of deserving students to get a quality education.

But there are still thousands who urgently need your support. How can we possibly say yes to one and no to another? Send your donation to: UNCF, 500 E. 62nd St., New York, NY 10021.

UNITED NEGRO COLLEGE FUND
A Mind Is A Terrible Thing To Waste.

Ad A Public Service of
This Publication

GREAT SPIRAL IMAGES

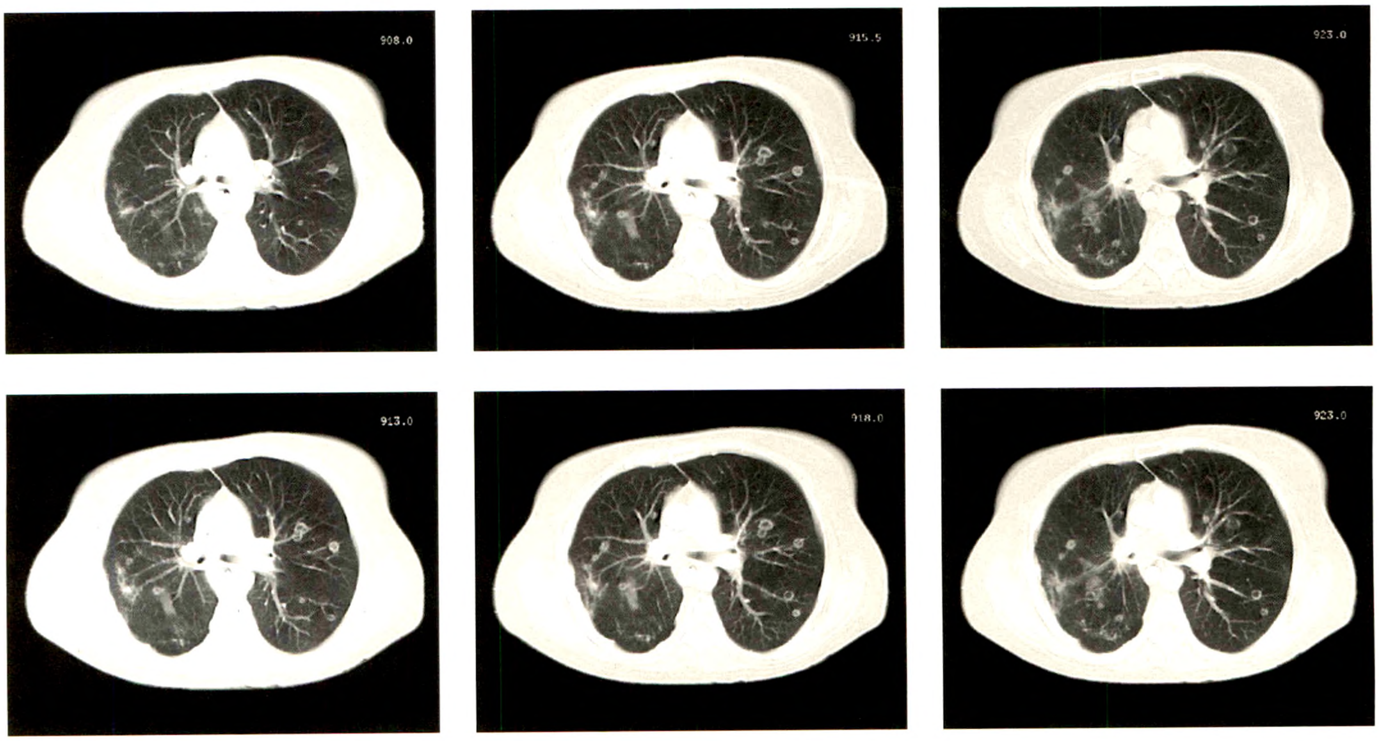

Scanning Parameters:	*120kV, 150mA*
Volume Parameters:	*15mm pitch (150% helix)* *10mm slice thickness* *7.5mm reconstruction spacing (top)* *5mm reconstruction spacing(bottom)*

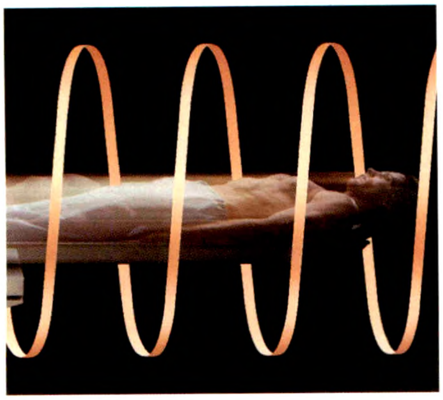

When it comes to spiral scanning, you have to know the proper protocol: **ZAP™-16 Z-Axis Protocol**–Picker's first in a series of rapidly expanding, high-speed spiral acquisitions. ZAP sets a clinical precedence as the highest resolution spiral scanning technique in CT today.

ZAP's exclusive extended helix provides up to 50% greater coverage with the same resolution you find in conventional axial scanning. That means 24-centimeter organ-specific coverage in a single 16-second breath-hold. Eliminating patient motion and slice misregistration. Improving patient compliance. And providing

ARE A MATTER OF PROTOCOL.

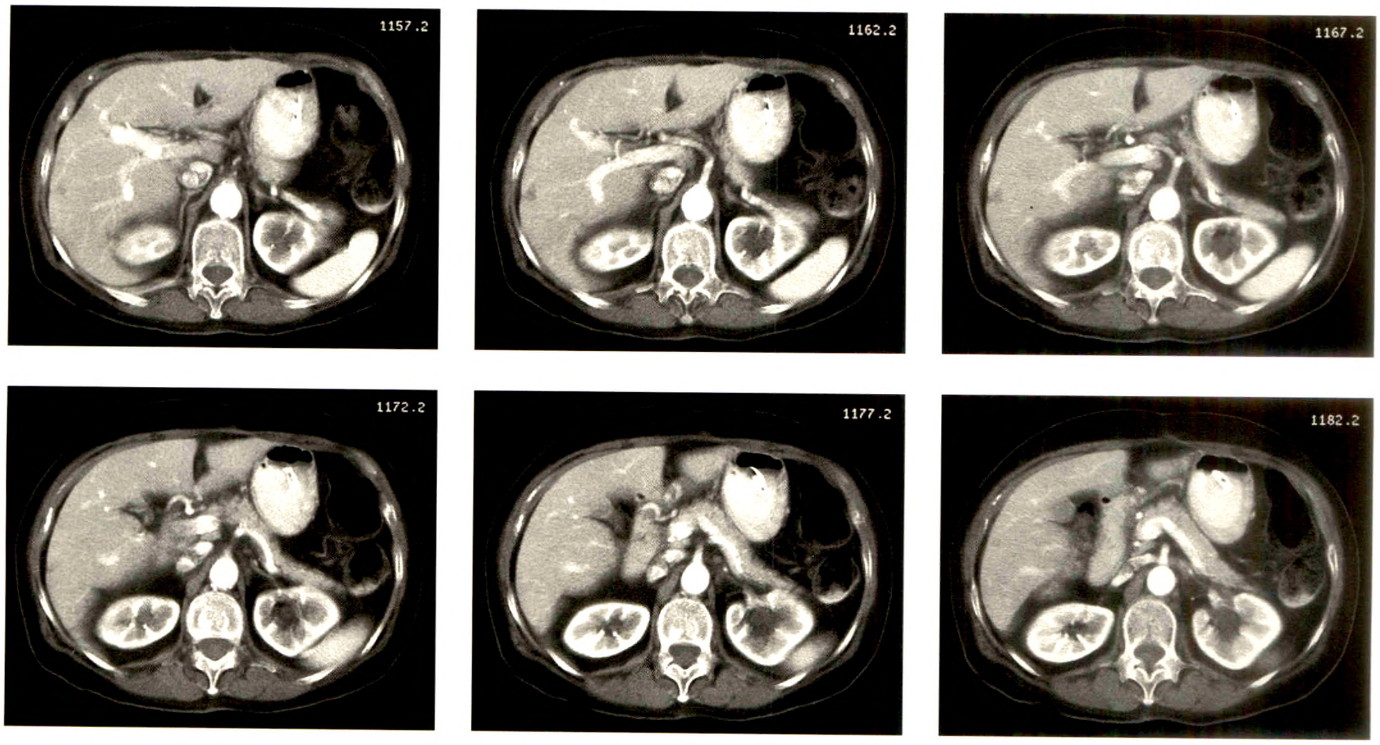

Scanning Parameters: *120kV, 150mA*
Volume Parameters: *15mm pitch (150% helix)*
10mm slice thickness
5mm reconstruction spacing

Images courtesy of The Cleveland Clinic Foundation, Cleveland, Ohio

the highest available resolution to characterize subtle lesions. And this is just the beginning. Next, ZAP capabilities combined with planned tube and computer expansions will offer you up to 100-centimeter Z-axis coverage. All to place you at the very forefront of CT.

ZAP is made possible by the powerful PQ-2000 scanner– the highest resolution CT scanner in the industry today. PQ's 4,800 microPoint™ detectors and direct uninterrupted data channels provide exceptional low contrast resolution at efficient low mAs techniques. The end result: Low noise image quality. Extended volume coverage. Enhanced tube performance. So, for expanded clinical applications and precision diagnoses in spiral scanning, you simply need to have the proper protocol: **ZAP, Z-Axis Protocol.**

PICKER
MORE THAN IMAGES. INSIGHT.

Visit us at RSNA booth 4014 & 4021·East Hall.

©1992 Picker International, Inc. For more information, call us at 1-800-323-0550.

IN THE FOREST, KINDLE YOUR SPIRIT.
NOTHING MORE.

ONLY YOU CAN PREVENT FOREST FIRES.

A PUBLIC SERVICE OF THE USDA FOREST SERVICE AND YOUR STATE FORESTERS.

X-RAY ACCESSORIES

The Difference is Clear

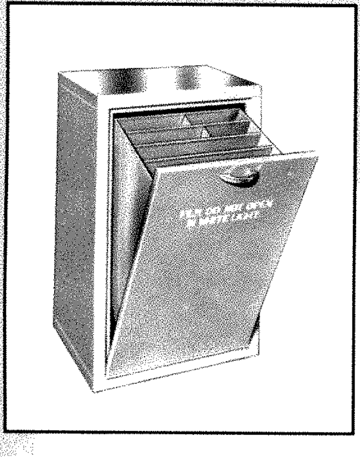

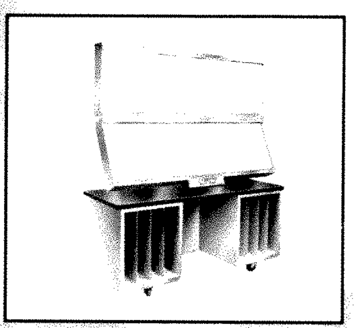

Tried, tested and trusted for over 40 years, S & S x-ray products deliver maximum proficiency and economy -- backed by quality, dependability and innovation.

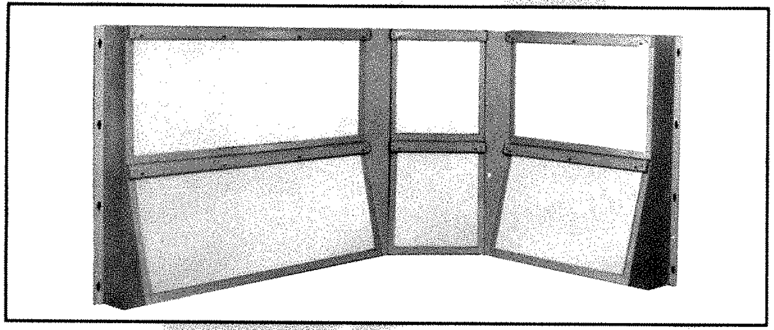

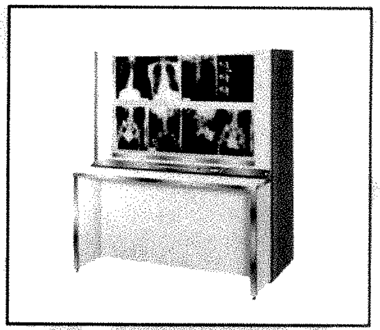

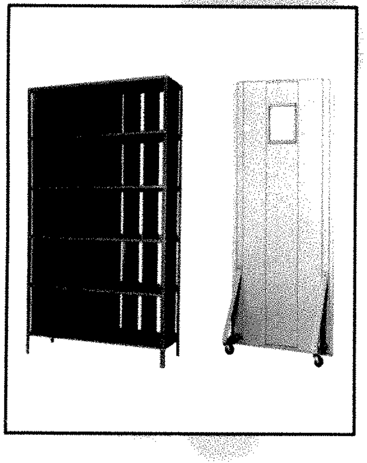

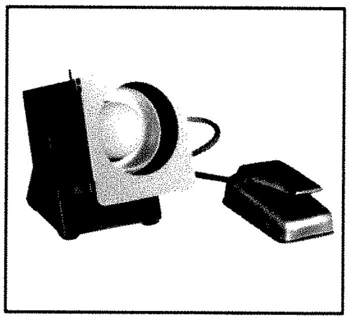

X-RAY Film Viewers ◆
X-RAY Protection ◆
X-RAY Files ◆
X-RAY Darkroom Equipment ◆
X-RAY Cabinets ◆
X-RAY Accessories ◆

For a FREE copy of our fully illustrated, 100+ page catalog, contact S & S directly or your local x-ray dealer.

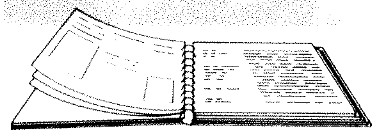

1101 Linwood Street
Brooklyn, N.Y. 11208

Phone: 718/649-8500
FAX: 718/257-0219
Toll Free: 800/347-XRAY

S&S X-RAY PRODUCTS INC

Free software and support are part of the package

3M IR Laser Imaging Film boxes are really no bigger than any others. But it seems we're able to pack a lot more into each one.

Because when you buy 3M IR Laser Imaging Films, you also get periodic software upgrades for your 3M Laser Imager. Regular inspection and fine-tuning for your medical imaging hardware. And expert service and support any time you have technical questions or concerns.

Of course, you also get reliable, high quality film designed specifically for your 3M Laser Imager. And all you pay for is the film, because as far as we're concerned, the software and support are part of the package.

For more information about 3M IR Laser Imaging Films, call 1-800-328-1684 ext. 340. Or write: 3M Medical Imaging Systems Division, P.O. Box 33050, St. Paul, MN 55133-3050. In Canada, write: 3M Canada Inc., P.O. Box 5757 Terminal A, London, Ontario, Canada N6A 4T1.

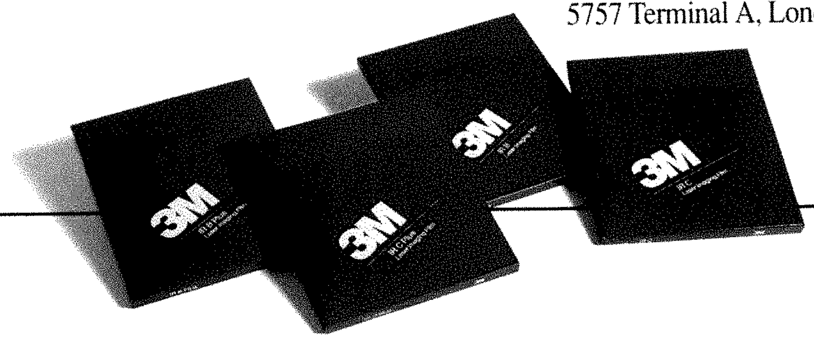

© 1992 3M

Innovation working for you™

3M

Diagnostic and Therapeutic Use of Chest Sonography: Value in Critically Ill Patients

Chong-Jen Yu[1]
Pan-Chyr Yang[1]
Dun-Bing Chang[1]
Kwen-Tay Luh[2]

OBJECTIVE. Portable chest radiography, used for critically ill patients, often fails to depict thoracic disease clearly. Chest sonography allows good characterization of pleural diseases, mediastinal lesions, and pulmonary consolidations, and provides accurate and safe guidance for interventional procedures. Accordingly, we evaluated its usefulness in the diagnosis and management of critically ill patients.

SUBJECTS AND METHODS. Sonography was used prospectively to evaluate 41 critically ill patients, when portable chest radiographs were difficult to interpret and failed to explain the clinical findings. An initial diagnosis was made on the basis of clinical and radiologic information. The final diagnosis was confirmed by thoracentesis ($n = 15$), image-guided aspiration biopsy ($n = 7$), surgery ($n = 3$), and clinical follow-up ($n = 16$). All 41 sonographic examinations were performed by a sonographer who had no knowledge of the initial diagnosis. The sonographic findings were recorded and analyzed. The usefulness of sonography in diagnosis and management was then evaluated according to the following criteria: diagnostic value—(1) made diagnosis, (2) changed diagnosis, (3) additional information, (4) no benefit; and management aid—(1) affected decision, (2) affected decision and guided thoracentesis, (3) affected diagnosis and guided aspiration, (4) no benefit.

RESULTS. Chest sonography was helpful in diagnosis in 27 (66%) of 41 patients and in treatment in 37 (90%) of 41 patients. A significant influence on treatment planning occurred in 17 (41%) of 41 patients. A diagnostic aspiration biopsy under sonographic guidance was done without complications in seven patients with occult lung tumors detected sonographically. Thoracenteses were attempted in 25 of 29 patients with pleural effusion and were successful in 24 patients (96%); a minimal pneumothorax developed in one patient (4%).

CONCLUSION. Chest sonography is a useful diagnostic tool for critically ill patients with chest diseases. This technique can be particularly helpful when CT is not available or when critically ill patients cannot be moved.

AJR 159:695-701, October 1992

Portable chest radiography is the most frequently used examination for critically ill patients in the intensive care unit or in the emergency service. These patients need an accurate and timely diagnostic procedure to provide appropriate information for subsequent management. However, portable chest radiographs have several shortcomings that make the interpretation of chest diseases difficult. One of the major problems is the difficulty in discerning the interface between pleural and parenchymal surfaces on portable chest radiographs [1, 2]; thus, it is not always possible to differentiate accurately between pleural and parenchymal opacities.

Recent advances in sonographic technology have demonstrated the multipotential capabilities of chest sonography in the diagnosis of pleural diseases [3], peripheral parenchymal lesions [4], mediastinal lesions [5], consolidation, and atelectasis [6]. Transthoracic aspiration biopsy also can be performed safely under real-time sonographic guidance to obtain specimens adequate for histologic diag-

Received February 24, 1992; accepted after revision May 5, 1992.

Supported in part by Kwang Ten Trading Co., LTD, Taipei, Taiwan, Republic of China.

[1] Department of Internal Medicine, National Taiwan University Hospital, No. 7, Chung-Shan S. Rd., Taipei, Taiwan 100, Republic of China. Address reprint requests to P.-C. Yang.

[2] Department of Clinical Pathology, National Taiwan University Hospital, No. 7, Chung-Shan S. Rd., Taipei, Taiwan 100, Republic of China.

0361-803X/92/1594-0695
©American Roentgen Ray Society

nosis [7]. The sonographic equipment is portable, and the examination can be done at the bedside if necessary. Previous study of sonography for critically ill patients has been restricted to its usefulness in guiding thoracentesis [3]. No attempt has been made to use chest sonography as a diagnostic tool in critically ill patients. Therefore, a prospective study was performed to ascertain the value of sonography in assisting the diagnosis and management of critically ill patients whose chest radiographs were difficult to interpret.

Subjects and Methods

A prospective study to assess the value of chest sonography in the diagnosis and management of critically ill patients was performed at National Taiwan University Hospital from July 1990 to April 1991. Patients were referred if: (1) their portable chest radiographs showed abnormal findings that failed to explain adequately the clinical conditions and showed radiographic opacities that were difficult to differentiate as parenchymal or pleural lesions or (2) timely diagnosis was necessary because of their critically ill condition. A total of 41 consecutive patients (31 male and 10 female; age range, 14-86 years; mean age, 56 years) were included.

Eighteen patients had respiratory failure that necessitated mechanical ventilation (eight had pneumonia, four had empyema, two had massive pleural effusion, one had flail chest, one had total lung collapse, one had esophageal cancer with cervical spine metastasis, and one had mediastinal hemangiomatosis); seven patients had respiratory distress (four had lung tumors and three had pleural effusions), seven patients had aortic aneurysm (five had aortic dissections); four patients had congestive heart failure (one had hypertensive cardiovascular disease, one had dilated cardiomyopathy, one had ischemic heart disease, and one had infective endocarditis); two patients were in a coma (one had recurrent cerebrovascular accidents and one had head injury); one patient was in a postoperative state (Caroli's disease—segmental hepatectomy); one patient had hepatic failure (fulminant hepatitis); and one patient had sepsis.

Among these 41 patients, 19 (46%) were examined in the intensive care units, 16 (39%) were examined in the wards, and six (15%) were examined in the emergency department. The radiographic patterns found in these patients included total or nearly total opacification of a hemithorax in 15 patients, cavitary lesions in three patients, mass lesions in two patients, lobar or segmental consolidation in five patients, and pleural opacities in 16 patients. The attending physicians gave each patient a tentative diagnosis based on clinical information and findings on portable chest radiographs as interpreted by a radiologist before the sonographic examination. Final diagnoses were further confirmed by thoracentesis ($n = 15$), image-guided aspiration biopsy ($n = 7$), surgery ($n = 3$), and clinical follow-up ($n = 16$).

In all patients, sonographic examination was done without knowledge of the tentative diagnosis. After viewing the chest radiographs of the patients, a sonographer performed the chest sonography with a portable sonographic machine equipped with a sector, a linear, and a convex transducer (Aloka SSD-256, and SSD-630, Aloka, Tokyo, Japan). The sonograms were recorded on Polaroid film (Polaroid, Cambridge, MA) and analyzed. The sonographic features were classified into pleural space processes (pleural effusion and pleural thickening), lung parenchymal lesions (consolidation, atelectasis, and tumor), and mediastinal lesions (tumor, cyst, and aneurysm). The sonographic patterns for various chest lesions have been described in prior studies [4-6, 8]. Consolidations are homogeneously hypoechoic, wedge-shaped parenchymal lesions, containing air or fluid bronchograms; they move with respiration. Atelectases are lesions with findings similar to those in consolidation, but with volume reduction, mainly fluid bronchograms and no air bronchograms. Pleural effusions are spaces of various echogenicities, from anechoic to homogeneously echogenic, which may contain floating strands or complex septa, located between visceral and parietal pleuras. Pleural nodules are round, hypoechoic lesions with well-defined margins located in either the visceral or parietal pleura. Pleural thickenings are arbitrarily defined as thickness greater than 3 mm. When a fluid accumulation was detected sonographically and thoracentesis also was needed, sonography was used to select a favorable site. The skin-to-target depth was measured before thoracentesis. Thoracentesis was conducted with a 21-gauge needle after local anesthesia.

For those patients found to have occult tumor within the lung parenchyma, sonographically guided aspiration biopsy was performed by using a puncture probe, with a technique as described by Izumi et al. [7].

After sonographic examinations and the interventional procedures were completed, the usefulness of sonography in assisting the diagnosis of these critically ill patients was evaluated. Sonographic examinations that met one of the following criteria were considered to have had a positive role in the diagnosis: (1) made diagnosis: a tentative diagnosis was confirmed after sonographic examination, (2) changed diagnosis: a tentative diagnosis was changed after sonographic examination, (3) additional information: provided new information to prior diagnosis. Sonographic examinations were considered to be without benefit in assisting the diagnosis if they provided no additional information. The sonographic examinations were considered to have helped management if (1) a new decision on a patient's management was made after sonographic examination; (2) thoracentesis, conducted for occult pleural effusion detected sonographically, gave rise to a new decision; (3) aspiration biopsy of the lesion detected by sonography gave rise to a new decision; (4) sonography was used to guide a thoracentesis alone. The sonographic examinations were considered to have no management benefit if the decisions concerning patients' management, already made on the basis of clinical information and chest radiographic findings, did not change because of the sonographic findings.

Results

Sonographic Features

Pleural effusion was the only finding in 19 patients. Ten patients had pleural effusions associated with other parenchymal abnormalities (three with pulmonary consolidation, four with tumors, two with consolidation and tumor, and one with atelectasis). The images of these 29 pleural effusions included 17 anechoic lesions, five complex nonseptated, five complex-septated, and two homogeneously echogenic. Sonography was very useful in the detection of pleural effusions. For two patients, originally considered on the basis of the findings on portable chest radiographs to have lobar consolidation with pleural effusion, parenchymal consolidation was the only finding detected sonographically. In one patient originally considered to have bilateral pulmonary contusions, a moderate pleural effusion was found unexpectedly with sonography (Fig. 1).

Eight patients were found to have occult tumors with sonography. Among them, seven patients had hemithoracic opacification on the chest radiographs and two patients had tumor hidden in the consolidated lungs (Figs. 2 and 3).

Atelectasis was noted in five cases. The sonogram revealed a picture of consolidation with fluid bronchograms. No air

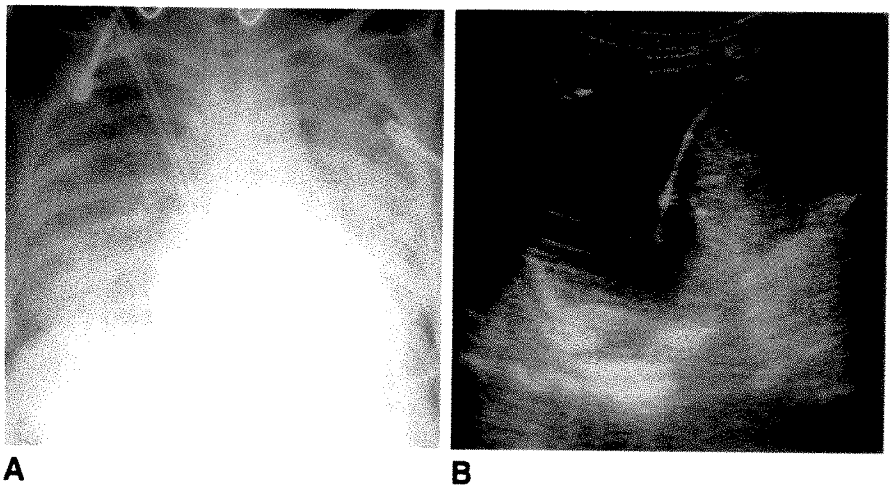

Fig. 1.—*A* and *B*, A 14-year-old boy had multiple fractures from an accident. Initial chest radiograph (*not shown*) showed possible contusion in right lung. Admitted to surgical intensive care unit, he was put on a ventilator. Follow-up chest radiograph (*A*) 4 days later showed total opacification of both lungs. Chest sonogram (*B*) disclosed bilateral small to moderate pleural effusions (only left-sided pleural effusion is shown), which were then drained. The follow-up chest radiographs showed pattern of cardiogenic lung edema, and a traumatic ventricular septal defect was diagnosed surgically.

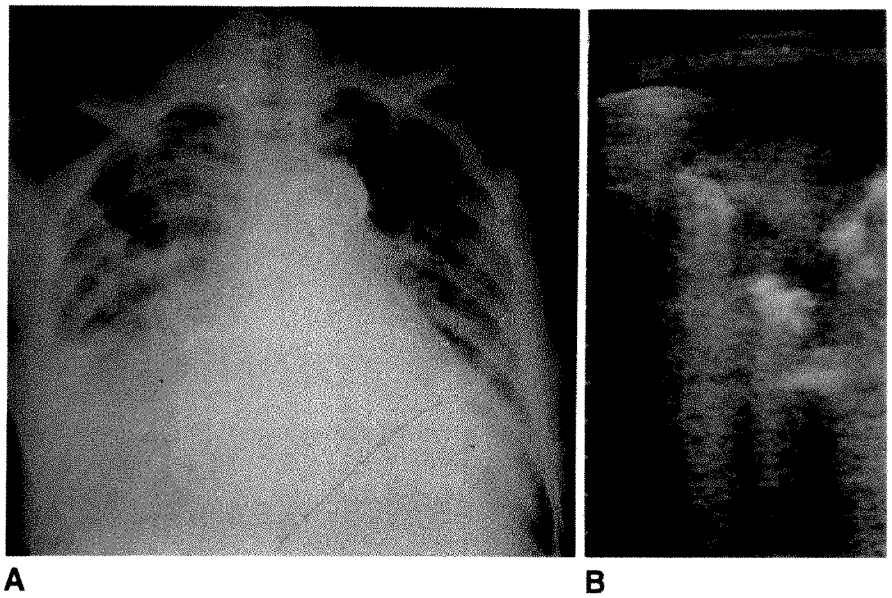

Fig. 2.—A 71-year-old woman who had had diabetes and hypertension for decades was admitted to the general ward for treatment of pneumonia with heart failure.

A, Chest radiograph taken 1 month after admission shows bilateral pleural effusions with pneumonia in right lower lobe.

B, Chest sonogram shows a central tumor within consolidated lung. Sonographically guided aspiration biopsy confirmed the diagnosis of adenocarcinoma.

movement within the involved bronchus or respiratory movement of the involved segment was visible on real-time sonography (Fig. 4).

Aortic aneurysms were diagnosed on the basis of chest sonography in two patients with chest pain. On the basis of findings on chest radiographs and clinical information, an anterior mediastinal tumor had been diagnosed in one and a lung tumor in the left upper lobe had been diagnosed in the other. Aneurysm had not been diagnosed in either patient before sonography. Sonography showed pulsating anechoic cystic lesions communicating with the aorta in both patients. The diagnoses were confirmed by aortography after the condition stabilized.

Sonography failed to provide satisfactory diagnosis for two patients. Both had bronchopleural fistulas with pleural opacities. Sonographic examination did not show whether these patients had a lung abscess or empyema with bronchopleural fistula. The diagnosis was based on results of subsequent chest CT examination.

Interventional Diagnostic Procedures After Sonographic Examinations

Of 29 patients with pleural effusions, 25 underwent thoracentesis. Twenty-four patients had successful thoracentesis (success rate, 96%); thoracentesis failed in one who had only a minimal effusion. All 14 patients undergoing thoracentesis under mechanical ventilation had successful tapping. In one patient (7%) with severe hypoalbuminemia (serum albumin level <1.8 g/dl [18 g/l]), pneumothorax developed after thoracentesis and a chest tube had to be inserted.

Of those eight patients with occult tumors within the consolidated lung, seven underwent sonographically guided aspiration biopsy at the bedside, and a confirmed diagnosis was

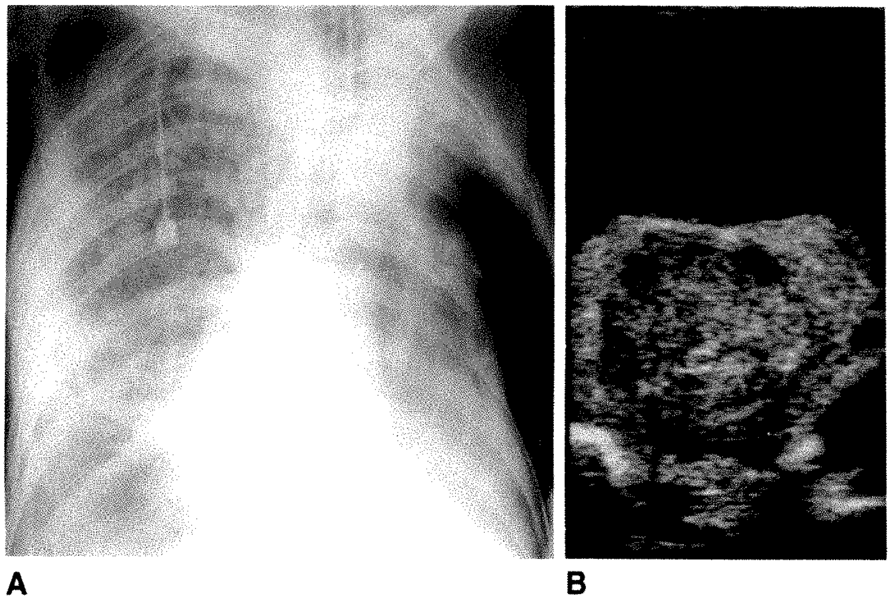

Fig. 3.—A 70-year-old man was admitted to general ward with acute respiratory failure that required ventilatory support.

***A*, Chest radiograph shows right-sided pneumonia with pleural effusion.**

***B*, Chest sonogram shows a 5 × 5 cm hypoechoic tumor with central necrosis near hilum with massive pleural effusion. Aspiration cytology showed squamous cell carcinoma, and cytologic study of pleural effusion failed to find malignant cells.**

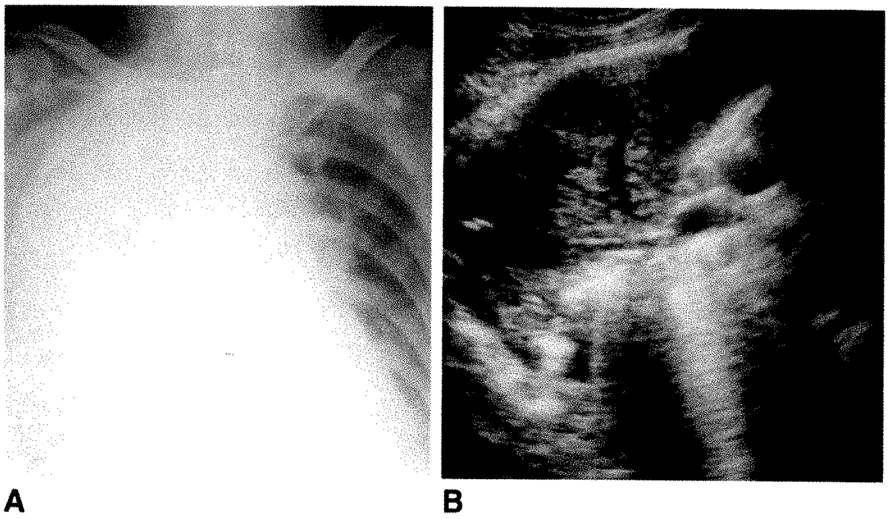

Fig. 4.—*A* and *B*, An 83-year-old woman had recurrent cerebral vascular accidents and was bedridden. She came to the emergency department after 1 day of consciousness disturbance with tachydyspnea for 1 day. Chest radiograph (*A*) shows opacification of right hemithorax without mediastinal shift; massive pleural effusion was suspected. Chest sonogram (*B*) shows consolidated lung with fluid bronchograms (*arrowhead*), which suggests atelectasis. After postural drainage, chest radiograph obtained the next day (*not shown*) showed that lung had cleared up.

thus possible. Four patients had squamous cell carcinomas; two had adenocarcinomas, and one had carcinoid tumor. One patient underwent sonographically guided aspiration biopsy successfully while he was on mechanical ventilation.

One patient with mediastinal hemangiomatosis, pleural involvement, and pleural effusion did not undergo the aspiration procedure because of a tendency to hemorrhage.

Influence of Sonographic Examinations on the Diagnosis and Management of the Patients

As shown in Table 1, sonography was considered helpful in making the diagnosis in 27 (66%) of 41 patients. Sonographic examinations allowed a definite diagnosis in 12 patients (Table 2). Prior tentative diagnosis was changed for eight patients (Table 3), and additional information was obtained for seven patients (Table 4). However, 14 patients gained no diagnostic benefit from sonographic examinations.

TABLE 1: Value of Sonography in the Diagnosis of Critically Ill Patients

Categories	No. of Patients ($n = 41$)
Assisting diagnosis	27 (66%)
Made diagnosis	12
Changed diagnosis	8
Provided additional information	7
No benefit	14 (34%)

The influence of sonography in assisting the management of critically ill patients is shown in Table 5. The sonographic examinations helped management in 37 (90%) of 41 patients, including making a new decision in 25 patients, thoracentesis

TABLE 2: Patients with Diagnoses Based on Sonographic Findings

Age (yr)	Diagnosis		
	Before Sonography	After Sonography	Final
86	?Aortic dissection, left-sided pleural effusion	Aortic dissection with leakage	Aortic dissection with leakage into pleural cavity and mediastinum
72	Pneumonia, delayed resolution	Lung cancer with pneumonia	Lung cancer with pneumonia
22	Pneumonia or pleural effusion	Pneumonia, no pleural effusion	Dilated cardiomyopathy pneumonia
19	Hemithorax opacity, right-sided	Atelectasis	Sputum impaction with atelectasis
23	Hemithorax opacity, right-sided	Mediastinal tumor, lung collapse, pleural effusion	Thymic carcinoid
54	Hemithorax opacity, right-sided	Lung cancer	Lung cancer
25	Hemithorax opacity, left-sided	Pleural mass with pleural effusion	Pleural hemangiomatosis, bloody effusion
57	Massive pleural effusion, right-sided	Lung cancer, pleural effusion, small amount	Lung cancer with pleural effusion
76	Pneumonia with pleural effusion	Lung cancer with pneumonia and empyema	Lung cancer with pneumonia and empyema
83	Hemithorax opacity, right-sided	Atelectasis, right-sided	Sputum impaction
37	Hemithorax opacity, right-sided	Pleural effusion, right-sided	Transudative pleural effusion (hypoalbuminemia)
45	Hemithorax opacity, left-sided	Lung cancer, pleural effusion	Lung cancer with pleural effusion

TABLE 3: Patients with Diagnosis Changed After Sonographic Examination

Age (yr)	Diagnosis		
	Before Sonography	After Sonography	Final
70	Pneumonia with pleural effusion	Lung cancer with pneumonia and pleural effusion	Lung cancer with pneumonia and pleural effusion
52	Massive pleural effusion, right-sided	Lung cancer, no pleural effusion	Lung cancer (tumor consolidation)
76	Pulmonary tuberculosis, massive pleural effusion	Lung cancer with massive pleural effusion	Lung cancer with pleural effusion, old pulmonary tuberculosis
44	Adult respiratory distress syndrome	Consolidation, left-sided; pleural effusion, bilateral	Pneumonia with parapneumonic effusion; transudative effusion, right-sided
14	Lung contusion	Pleural effusion, bilateral	Traumatic ventricular septal defect with heart failure
50	Lung abscess	Empyema	Empyema thoracis
30	Mediastinal tumor	Aortic aneurysm	Aortic aneurysm (aortic root)
43	Lung tumor	Aortic aneurysm	Aortic aneurysm (aortic arch)

TABLE 4: Patients in Whom Additional Information Was Obtained from Sonographic Examination

Age (yr)	Diagnosis		
	Before Sonography	After Sonography	Final
37	Subpulmonic effusion	Segmental atelectasis with effusion	Atelectasis with effusion
23	Pleural effusion, bilateral	Consolidation and pleural effusion	Pneumonia with parapneumonic effusion
62	Pleural effusion, left-sided	Pleural effusion, left-sided	Aortic dissection with leakage
60	Pleural effusion, left-sided	Pleural effusion, left-sided	Aortic dissection with leakage
34	Pneumothorax and pleural effusion, right-sided	Hemopneumothorax, right-sided	Necrotizing pneumonia with hemopneumothorax
56	Pleural effusion or pneumonia, right-sided	Empyema, right-sided	Leakage of esophageal-colonic anastomosis
55	Pleural effusion, left-sided	Pleural effusion, left-sided	Aortic dissection with leakage

and aspiration for unexpected findings in 17 patients, and guiding thoracentesis in 12 patients. A significant influence of treatment planning occurred in 17 (41%) of 41 patients, including 10 of the 12 patients who had a diagnosis made after sonographic examination and seven of the eight patients who had a diagnosis changed on the basis of sonographic findings.

One patient had fallen from a height, and radiologic examination on arrival revealed multiple rib fractures, bilateral femoral shaft fractures, pelvic fracture, and pulmonary contusion (Fig. 1). He was admitted to the intensive care unit and was put on a ventilator. Opacification of bilateral lung fields associated with impaired oxygenation was noted on a chest radiograph obtained on the fifth day after admission. Aggravating pulmonary contusion was taken into consideration. However, a chest sonogram showed bilateral pleural effusions, which were subsequently drained. Follow-up chest radiographs revealed a pattern of cardiogenic lung edema. A careful physical examination disclosed a faint cardiac murmur, and echocardiography showed a ventricular septal defect. Emergent surgery was performed to repair the posttraumatic ventricular septal defect.

Sonographic examinations were found to be of no benefit in four instances (including one case of minimal pleural effusion with unsuccessful thoracentesis, one case of atelectasis without diagnostic or management change after examination, and two cases of bronchopleural fistula with no benefit ob-

TABLE 5: Influence of Sonography on the Management of Critically Ill Patients

Categories	No. of Patients (n = 41)
Helped management	37 (90%)
Affected decision	8
Affected decision and guided thoracentesis	10
Affected decision and guided aspiration	7
Guided thoracentesis only	12
No benefit	4 (10%)

tained by sonography owing to poor penetration of the ultrasound wave).

Discussion

A timely and accurate diagnosis is needed for patients with critical medical conditions. Radiologic procedures, especially chest radiography, are frequently performed in these patients. Portable chest radiography is the most frequently used diagnostic tool in critically ill patients for assessment of the position of support equipment, evaluation of the development of parenchymal infiltrates, atelectasis, effusions, and pneumothorax; and exclusion of iatrogenic complications after interventional procedures such as placement of a central venous catheter. However, examination by this means is usually suboptimal because (1) patients are frequently too weak to sit up so that an air-fluid level will be visible, (2) patients are frequently unable to inspirate fully because of sedation, consciousness change, pain, or fatigue, (3) unrecognized rotation of body occurs during imaging, (4) mobile radiographic equipment has low power, (5) techniques and target-film distances vary between studies [1, 2]. Bedside studies have been estimated to be technically compromised in 6–37% of examinations in the intensive care setting [9]. This result also is true for patients in general wards with acute medical conditions requiring portable radiographic examinations.

Thoracic CT scans have been shown to have several advantages over portable chest films in the evaluation of thoracic diseases for critically ill patients [1]. It is useful in localizing thoracic disease, evaluating complex pleural disease, and showing mediastinal and chest wall diseases that radiographs fail to show. In a retrospective study done by Mirvis et al. [1], CT added information affecting the diagnosis and management in 71% of the studied patients. A recent report by Snow et al. [10] also showed the superiority of CT to conventional chest radiography for critically ill patients. However, the most frequently encountered problems with CT scans are the difficulty of transporting patients and the cost, which make repeating examinations inconvenient or impractical. Moreover, the lack of real-time guidance and bedside availability also makes further interventional procedures rather difficult [5].

This prospective study has shown that chest sonography also can be useful in assisting the diagnosis and management of critically ill patients, especially for those patients with portable chest radiographs that are difficult to interpret. The overall aid in diagnosis was 66% and the aid in management was 90%. These results are comparable to those achieved with chest CT [1].

Chest sonography has several advantages: (1) high sensitivity in detecting pleural lesions and differentiating pleural disease from parenchymal lesions (consolidation, abscess, or tumor), (2) consolidation can be used as a sonographic window to visualize some centrally located lesions more clearly, (3) sonographically guided aspiration biopsy and thoracentesis can be performed accurately and easily, (4) lower cost, (5) it is easily performed at bedside, (6) flexibility and short examination time as compared with compound scans [3, 11]. These advantages make chest sonography a useful diagnostic tool with great potential in assisting decision making for and management of critically ill patients.

Total or nearly total opacification of a hemithorax is the most frequent radiologic finding in the patients referred for immediate bedside sonographic examinations (15 of 41 patients). Because of the disappearance of lung aeration, the nonaerated lung with or without pleural effusion provides a sonographic window for examination of underlying lung disease [12]. In all 15 cases, sonography showed the underlying causes immediately after the examinations. The chest sonogram clearly showed massive pleural effusions, consolidation with or without pleural effusion, atelectasis, and the existence of occult tumor. Further confirming procedures such as thoracentesis, sonographically guided aspiration biopsy, and fiberoptic bronchoscopy, could be performed without delay. The influence of sonography on the diagnosis and management of this type of patient is exemplified in the following case (Fig. 4). Although an initial chest radiograph showed hemithorax opacification without mediastinal shift, thus suggesting massive pleural effusion, sonography showed a consolidated lung with fluid bronchograms and only scanty pleural effusion. A sonographic diagnosis of atelectasis was made. The atelectasis may have been due to sputum impaction. After positional changes and postural drainage, findings on a chest radiograph the next day showed that the lung had cleared.

Tumor with obstructive consolidation also provides a window for sonographic examinations. Sonography has a sensitivity similar to that of CT in the detection of central tumors [6]. In one patient originally considered to have congestive heart failure and pneumonia, chest sonograms showed a centrally located tumor subsequently proved to be a lung adenocarcinoma with obstructive pneumonia (Fig. 2). This result had a significant impact on both diagnosis and management of the patient.

Because of real-time monitoring, sonography provides a safe and accurate guiding system for either fine-needle aspiration or large-bore cutting biopsy. Aerated lung and great vessels can be avoided during biopsy, and the complication rate can be minimal [7]. The seven patients who had sonographically guided aspiration biopsy all had cytologic results that confirmed the diagnosis. In a similar way, with sonographic localization, thoracentesis also can be performed more safely and accurately. The success rate of thoracentesis in this study was 96%, comparable to that reported for a prior study [3]. The only unsuccessful case was that of a patient with minimal pleural effusion, detected during sonographic investigation for a patchy infiltration of the lung shown on chest radiographs. After sonographic examination, a mark for thoracentesis was made on the skin, but thoracentesis failed. The reason for this failure may have been malposition of the needle without real-time guidance.

Sonographic examination takes less time and is less expensive than CT. In our institute, a thorough sonographic examination of the chest by an experienced sonographer usually takes 15–30 min and will take another 10–20 min if sonographically guided interventional procedures are needed. The costs are 2000 NT (US$80) for the shorter sonographic examination and 2400 NT (US$96), for the longer sonographic examination.

Chest sonography also has several disadvantages: (1) the ultrasonic wave is easily hindered by air (either an aerated lung or an area of air accumulation such as pneumothorax or air in the cavity), (2) poor visualization of the mediastinum, hilum, and airway, (3) restricted field of view, and (4) operator dependence [11]. Two of the cases of bronchopleural fistula and empyema were not diagnosed sonographically because of a large amount of accumulated air. These shortcomings have made chest sonography a less favorable choice of examination than CT in many medical centers. However, this does not mean that all patients with chest radiographs that are difficult to interpret should undergo CT. Sonography can frequently be advantageous for many critically ill patients, especially when transport of patients is troublesome or risky. Sonography is lower in cost, less time-consuming, and available at the bedside, making repeated examinations possible.

In conclusion, our study has shown that chest sonography is valuable in assisting diagnosis and management of critically ill patients. We advise chest sonography when the portable chest radiograph is difficult to interpret, especially when use of chest CT is hampered because of problems in transport or when a thoracentesis is considered risky.

REFERENCES

1. Mirvis SE, Tobin KD, Kostrubiak I, Belsberg H. Thoracic CT in detecting occult disease in critically ill patients. *AJR* **1987**;148:685–689
2. Overfors C, Hedgecock MW. Intensive care unit radiology: problems of interpretation. *Radiol Clin North Am* **1978**;16:407–409
3. Hirsch JH, Rogers JV, Mack LA. Real-time sonography of pleural opacities. *AJR* **1981**;136:297–301
4. Yang PC, Luh KT, Sheu JC, Kuo SH, Yang SP. Peripheral pulmonary lesions: ultrasonography and ultrasonically guided aspiration biopsy. *Radiology* **1985**;155:451–456
5. Yu CJ, Yang PC, Chang DB, et al. Evaluation of ultrasound-guided biopsies of mediastinal masses. *Chest* **1991**;100:399–405
6. Yang PC, Luh KT, Wu HD, et al. Lung tumors associated with obstructive pneumonitis: US studies. *Radiology* **1990**;174:717–720
7. Izumi S, Tamaki S, Natori H, Kira S. Ultrasonically guided aspiration needle biopsy in diseases of chest. *Am Rev Respir Dis* **1982**;125:460–464
8. Lee LN, Chen CR, Yang PC, Yang GG, Kuo SH, Luh KT. Ultrasonography of thoracic lesions: analysis of 251 cases. *Taiwan I Hseuh Hui Tsa Chih* **1987**;86:838–846
9. Sheerier RH, McAdams HP. Digital processing of portable films can reduce need for repeat studies. *Diag Imag Clin Med* **1986**;8:117–118
10. Snow N, Bergin KT, Horrigan TP. Thoracic CT scanning in critically ill patients: information obtained frequently alters management. *Chest* **1990**;97:1467–1470
11. Wiener MD, Garay SM, Leitman BS, Wiener DN, Ravin CE. Imaging of the intensive care unit patients. *Clin Chest Med* **1991**;12:169–198
12. Wu HD, Yang PC, Kuo SH, Luh KT. Ultrasonography in complete chest X-ray opacification of hemithorax. *Taiwan I Hseuh Hui Tsa Chih* **1989**;88:694–699

Case Report

Primary Pulmonary Artery Sarcoma: Diagnosis with CT, MR Imaging, and Transthoracic Needle Biopsy

Eric L. Bressler[1] and Jeanne M. Nelson[2]

Primary sarcomas of the pulmonary artery are extremely rare; only 45 cases had been reported in the English literature as of 1985 [1]. The diagnosis is rarely made before surgery or autopsy because the clinical and radiologic findings are nonspecific. We describe the CT and MR imaging appearances of such a tumor and diagnosis of this lesion based on the results of transthoracic needle biopsy.

Case Report

A 75-year-old man had had slowly progressive fatigue and dyspnea on exertion for 6 months. He had a 60-pack-year history of smoking. Spirometry indicated moderate chronic obstructive pulmonary disease. The patient was treated with inhaled bronchodilators, inhaled corticosteroids, and courses of systemic corticosteroids and antibiotics. His signs and symptoms progressed without an objective change in the results of spirometry. Four months before admission, an echocardiogram showed normal left ventricular function, slight mitral and aortic insufficiency, and mild tricuspid insufficiency. Three months before admission he had anemia, but evaluation of the gastrointestinal tract and the results of bone marrow biopsy did not show any abnormalities. He was admitted for further evaluation after he reported that he had had a syncopal episode 1 week earlier and several weeks of unexplained fevers. He had no chest pain and no acute episodes of dyspnea. He had discontinued working as a mortician 3 months earlier because of fatigue and dyspnea. Physical examination showed a grade 2 systolic murmur at the apex and a trace of pedal edema. The lungs were clear to auscultation. Analysis of arterial blood indicated a pH of 7.41, P_{CO_2} of 28 mm Hg, and P_{O_2} of 51 mm Hg. In the previous 6 months, findings on several chest radiographs had been interpreted as normal except for evidence of chronic obstructive pulmonary disease. In retrospect, slight enlargement of the left main and descending left pulmonary arteries and mild oligemia of the left lung were seen.

A second echocardiogram showed right ventricular and right atrial enlargement, with an estimated pulmonary artery systolic pressure of 75 mm Hg. Ventilation and perfusion scans showed diffuse hypoventilation and complete absence of perfusion of the left lung with normal perfusion of the right lung. Dynamic CT scans with IV contrast material showed a large, irregular, completely intraluminal mass extending from the level of the pulmonic valve along the anterior aspect of the main pulmonary artery into the proximal right pulmonary artery, passing posteriorly into and occluding the left main pulmonary artery (Figs. 1A and 1B). A solitary nodule 8 mm in diameter with an attenuation like that of soft tissue was detected in the right lower lobe. MR imaging was performed to distinguish between solid tumor, thrombosis, and myxoma. Cardiac-gated T1-weighted images showed an intraluminal mass with a signal intensity only minimally higher than that of chest wall muscle (Fig. 1C). T2-weighted images showed mild hyperintensity of the mass relative to the chest wall muscles (Fig. 1D). T1-weighted images showed enhancement of the mass after gadopentetate dimeglumine was administered (Fig. 1E). Lack of high signal intensity in the mass on the T1-weighted images and contrast enhancement were most consistent with a solid tumor. Several diagnostic approaches were considered. Open biopsy was not desirable because the radiologic findings suggested that the tumor was unresectable and the patient was not a good candidate for surgery because of his severe pulmonary hypertension. A transvascular biopsy was considered technically difficult because of the dilated right ventricle and the risk of embolization of the tumor into the right pulmonary artery. After much discussion, it was decided to

---

Received March 26, 1992; accepted after revision May 8, 1992.

[1] Department of Radiology, Riverside Medical Center, 2450 Riverside Ave., Minneapolis, MN 55454.

[2] Pulmonary Medicine, Group Health, Inc., Riverside Medical Center, 2220 Riverside Ave. S., Minneapolis, MN 55454.

AJR 159:702-704, October 1992 0361-803X/92/1594-0702 © American Roentgen Ray Society

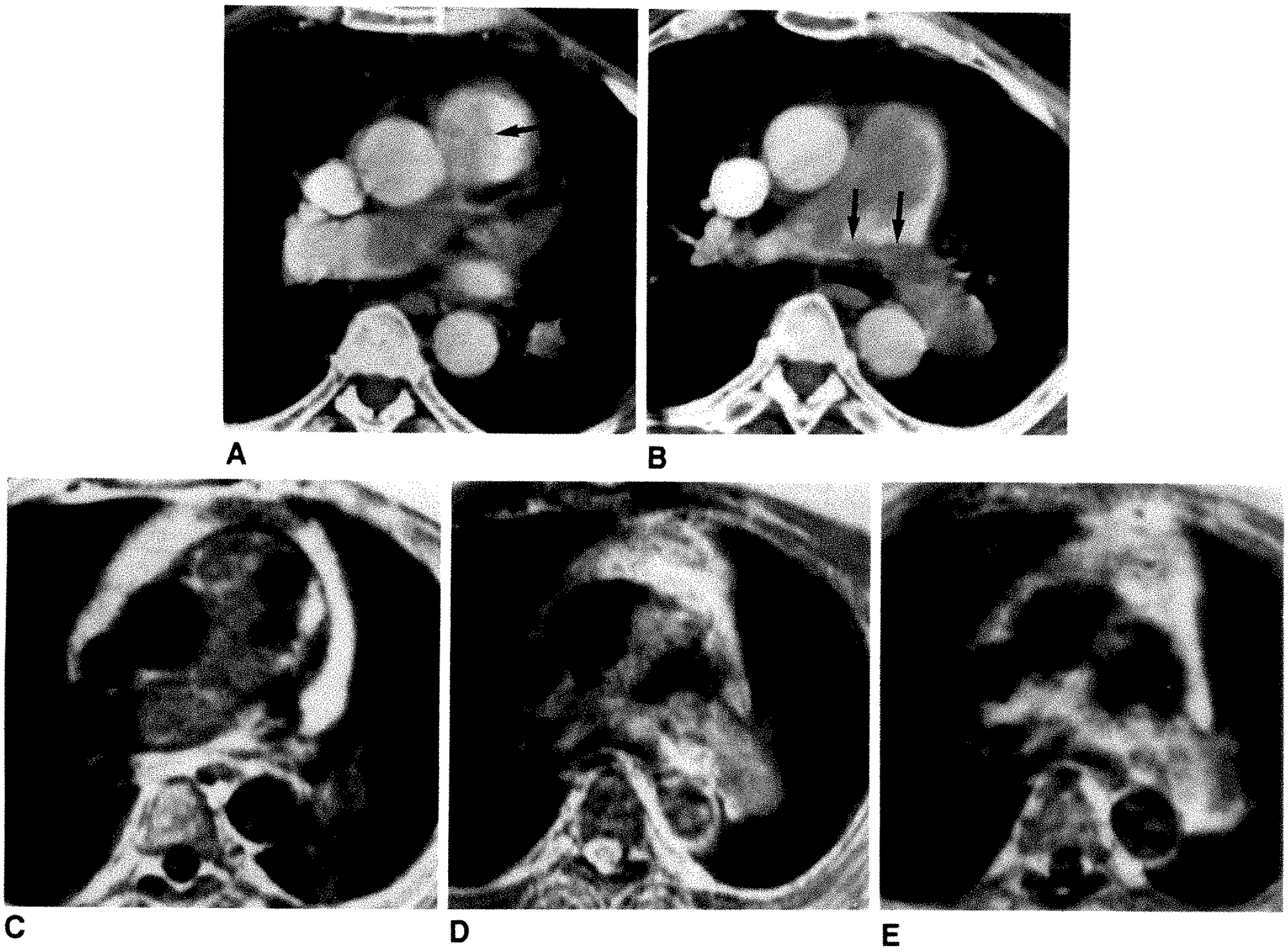

Fig. 1.—Primary pulmonary artery sarcoma in a 75-year-old man.

***A*, Contrast-enhanced CT scan shows completely intraluminal mass in main pulmonary artery and right pulmonary artery (*arrow*).**

***B*, Contrast-enhanced CT scan in plane superior to that in *A* shows mass extending from main pulmonary artery to right pulmonary artery, with a sessile component of tumor on posterior wall (*arrows*). This may represent subintimal spread of tumor to left pulmonary artery, which is occluded by mass.**

***C*, Cardiac-gated axial T1-weighted (612/25) spin-echo MR image shows mass with signal intensity slightly higher than that of chest wall muscle.**

***D*, T2-weighted (1782/60) MR image shows mass with signal intensity higher than that of muscle.**

***E*, T1-weighted (612/25) MR image after IV administration of gadopentetate dimeglumine shows definite enhancement of mass compared with *C*.**

perform a CT-directed transthoracic needle biopsy with surgical standby.

The lesion was localized after reinjection of contrast material. A 20-gauge biopsy gun was used for the procedure because sarcomas often do not fragment well enough to produce core biopsy specimens when cutting needles are used (Bressler EL, unpublished data). This approach obviated multiple needle passes, which would increase the risk of tumor embolization and bleeding. The needle was passed through the part of the mass that appeared to be attached to the anterior wall of the main pulmonary artery; the needle was placed medial to the left internal mammary artery and vein. The biopsy yielded a 2-cm-long tissue core. Histologic examination showed a sarcoma with considerable degeneration and necrosis. Immunohistochemical subtyping could not be performed because of the extensive necrosis. The patient tolerated the procedure well, with only minimal bleeding in the mediastinum from the biopsy site, which was confirmed by a CT scan obtained 20 min after the biopsy.

In accordance with the patient's wishes, he was sent to a tertiary referral center for possible surgical resection of the tumor. He had a tumor endarterectomy of the pulmonary trunk, right and left main pulmonary arteries, and all segmental pulmonary arteries on the left side. The final pathologic examination confirmed the diagnosis of leiomyosarcoma of the pulmonary artery. The patient was discharged, and clinically he was doing well at a 2-month follow-up visit. Unfortunately, 4 months after surgery he had massive recurrence of tumor in the left lung and mediastinum.

Discussion

Pulmonary artery sarcomas appear as polypoid intraluminal masses and nodular, sessile masses originating in and spreading along the pulmonary artery intima [1, 2]. In the cases reviewed by Baker and Goodwin [1], all 45 patients had involvement of either the left or right pulmonary artery, and 41 of these had involvement of the main pulmonary artery. In approximately half of the cases, the tumors remained intraluminal; in the other half, they spread transmurally into the adjacent lung, bronchial wall, or lymph nodes [1, 2]. The CT findings in our case reflect the intraluminal, subintimal type of tumor spread. The lesion most likely originated in the main pulmonary artery and spread subintimally to the right pulmonary artery and along the posterior wall of the right pulmonary artery into the left pulmonary artery, with subsequent occlusion of this last vessel. Nodular metastases are frequently found in the lungs, and distant metastases have been reported in most organs [1]. Although it was not proved, the nodule in the right lung in our case may have been a metastatic lesion.

The radiologic findings of pulmonary artery sarcoma depend on whether the tumor is large enough to distend a pulmonary artery and the extent of transmural spread into the adjacent lung. The radiologic findings in our case reflect the surgical findings, with tumor distending the left lower lobe and main pulmonary arteries, visible in retrospect as arterial dilatation with mild left-sided pulmonary oligemia. This is similar to the most characteristic appearance of a pulmonary artery sarcoma, which Moffat et al. [2] describe as a "distinctly lobulated, unilateral hilar mass projecting into the lung parenchyma in a pulmonary arterial distribution." If the mass extends into the pulmonary parenchyma, it mimics bronchogenic carcinoma. If it is entirely intraluminal and too small to distend the pulmonary artery, no abnormalities may be seen on radiographs [2]. Absence of perfusion of a lung on a lung scan has been documented [2].

Angiographic distinction of a sarcoma from thrombus is occasionally possible when the lesion is polypoid and moves during the cardiac cycle [3, 4]. However, when the tumor is sessile or partially covered with thrombus, this distinction is difficult [1].

Percutaneous transvascular biopsies have been performed for many years, and various methods are summarized in a recent textbook [5]. Previous techniques for biopsies of intravascular tumors have generally involved either aspiration biopsies using the tips of catheters or transcatheter biopsies using endobronchial biopsy brushes [5]. More recent techniques have included the use of pediatric endoscopic biopsy forceps through an intravascular sheath [6] and use of an atherectomy catheter [7]. Although CT-guided percutaneous needle biopsies of masses that extrinsically compress blood vessels are commonplace, few cases of CT-guided biopsies of completely intraluminal masses have been reported [8]. Significant bleeding is a potential complication of this technique, but this generally does not occur in patients with normal clotting, as evidenced by the safety of translumbar aortography, which uses catheters and sheaths much larger than biopsy needles.

The CT appearance of an intraluminal filling defect can be seen in embolic pulmonary thromboembolism, so the finding is not specific. On the other hand, the finding of contrast enhancement in an intraluminal mass on MR images indicates a neoplasm. A chronic clinical course without acute episodic dyspnea also should suggest the possibility of a neoplasm.

Historically, the diagnosis of pulmonary artery sarcomas has been difficult. In the review of 45 patients by Moffat et al. [2], the diagnosis was made at autopsy in 28 (62%) of the cases. The diagnosis was made at surgery in the remaining 17 patients, and four died within 12 days of surgery. The average survival after the onset of symptoms was 12 months. Only three patients survived longer than 2 years.

The CT and MR findings described in this report may facilitate the diagnosis of a pulmonary artery tumor. The surgical mortality and the grim prognosis summarized by Moffat et al. [2] make a nonsurgical diagnostic approach attractive. We think transthoracic needle biopsy of a fixed mass in the pulmonary artery is safe and can be used to make the diagnosis without resorting to surgery.

REFERENCES

1. Baker PB, Goodwin RA. Pulmonary artery sarcomas: a review and report of a case. *Arch Pathol Lab Med* **1985**;109:35–39
2. Moffat RE, Chang CHJ, Slaven JE. Roentgen considerations in primary pulmonary artery sarcoma. *Radiology* **1972**;104:283–288
3. Killebrew E, Gerbode F. Leiomyosarcoma of the pulmonary artery diagnosed preoperatively by angiocardiography: replacement with composite graft. *J Thorac Cardiovasc Surg* **1976**;71:469–471
4. Hynes JK, Smith HC, Holmes DR, Edwards WD, Evans TC Jr, Orszulak TA. Preoperative angiographic diagnosis of primary sarcoma of the pulmonary artery. *Circulation* **1982**;66:672–674
5. Kadir S, Miller SW. Percutaneous transvascular biopsy. In: Athanasoulis CA, Pfister RC, Greene RE, Roberson GH. *Interventional radiology.* Philadelphia: Saunders, **1982**:391–397
6. Withers CE, Casola G, Herba M, Viloria J. Intravascular tumors: transvenous biopsy. *Radiology* **1988**;167:713–715
7. Dake MD, Zemel G, Dolmatch BL, Katzen BT. The cause of superior vena cava syndrome: diagnosis with percutaneous artherectomy. *Radiology* **1990**;174:957–959
8. Miner DG, Cohan RH, Davis WK, Braun SD. CT-guided percutaneous aspiration of septic thrombosis of the inferior vena cava. *AJR* **1987**;148:1213–1214

Case Report

Thoracic Periaortic Lymphoma Mimicking Aortic Dissection

Ella A. Kazerooni,[1] David M. Williams,[1] and G. Michael Deeb[2]

Tumors adjacent to the descending thoracic aorta are unusual, and can mimic aortic disease, specifically aneurysm or dissection, both clinically and radiologically. Isolated tumors have been reported to mimic aortic dissection or aneurysm on chest radiographs and angiograms, and a single case of oat cell carcinoma has been reported to mimic aortic dissection on CT scans. We present a case of limited periaortic thoracic non-Hodgkin's lymphoma surrounding the lumen of the aorta and mimicking aortic dissection on CT, MR, angiography, and intravascular sonography.

Case Report

The patient is a 79-year-old asymptomatic man with a history of hypertension and mild peripheral vascular occlusive disease. At the time of routine physical examination, posteroanterior and lateral chest radiographs revealed a large left-sided pleural effusion and widening of the mediastinal contour on the left, initially thought to represent abnormal enlargement of the mid-distal portion of the descending thoracic aorta (Fig. 1A). A preliminary diagnosis of chronic aortic dissection or aortic aneurysm was made. A contrast-enhanced CT scan of the chest obtained at the referring institution revealed soft tissue surrounding the descending thoracic aorta.

The patient was referred to our institution for angiography to further explore the diagnosis of aortic dissection. Thoracic aortography showed mild narrowing of the aortic lumen at the level of the abnormal periaortic tissue. The aortic wall was normal from the level of the left subclavian artery origin to the diaphragmatic hiatus on intravascular sonography performed with a 6.2-French, 12.5-MHz transducer (Boston Scientific, Watertown, MA; Diasonics, Milpitas, CA). In particular, there was no aortic wall thickening, irregularity, or tear to suggest intramural hematoma and aortic dissection. The diagnosis of neoplastic encasement was suggested; however, in view of the possibility of aortic dissection without intimal tear [1], aortic dissection could not be excluded.

Dynamic axial CT was then repeated. Ten-millimeter-thick contiguous sections were imaged with a CT/T 9800 Advantage scanner (GE Medical Systems) after IV administration of 100 ml of 60% contrast medium (Hypaque 60, Winthrop Pharmaceuticals, New York, NY) at 2 ml/sec for 20 sec, then at 1 ml/sec with a power injector. CT revealed a rind of tissue, measuring 2–3 cm, encasing the mid and distal portion of the descending thoracic aorta for a length of 10 cm and a small left-sided pleural effusion (Fig. 1B). The soft-tissue mass had not changed in size since the CT examination 4 weeks earlier. The soft tissue was external to faint aortic wall calcification and measured 47 H in attenuation. CT-guided aspiration of the periaortic tissue was done with the patient prone. Two passes were made with a 22-gauge needle yielding 5 ml of serosanguineous fluid and 5 ml of dark red blood. No neoplastic cells were found.

To further characterize the nature of the periaortic tissue, we did an MR examination with a 1.5-T unit (Signa, GE Medical Systems, Milwaukee, WI). Coronal T1-weighted (400/20 [TR/TE]), axial T1-weighted (750/30), axial spin-density and T2-weighted (2000/40, 80) spin-echo images were obtained. An axial gradient-echo sequence (33/15/30°) also was obtained. After IV administration of 10 ml gadopentetate dimeglumine (Magnevist, Berlex Imaging, Wayne, NJ) an additional axial T1-weighted (750/30) sequence was obtained. The tissue was of intermediate signal intensity on both T1- and T2-weighted images and enhanced minimally with contrast administration (Figs. 1C and 1D). The signal characteristics were not consistent with recent hematoma and suggested the possibility of fibrosis or an unusual neoplasm, such as malignant fibrous histiocytoma or lymphoma. Although the signal characteristics of the mass were con-

---

Received March 23, 1992; accepted after revision April 16, 1992.

[1] Department of Radiology, University of Michigan Hospitals, Box 0030, 1500 E. Medical Center Dr., Ann Arbor, MI 48109. Address reprint requests to E. A. Kazerooni.

[2] Department of Surgery, Section of Thoracic Surgery, University of Michigan Hospitals, 1500 E. Medical Center Dr., Ann Arbor, MI 48109.

AJR 159:705–707, October 1992 0361-803X/92/1594–0705 © American Roentgen Ray Society

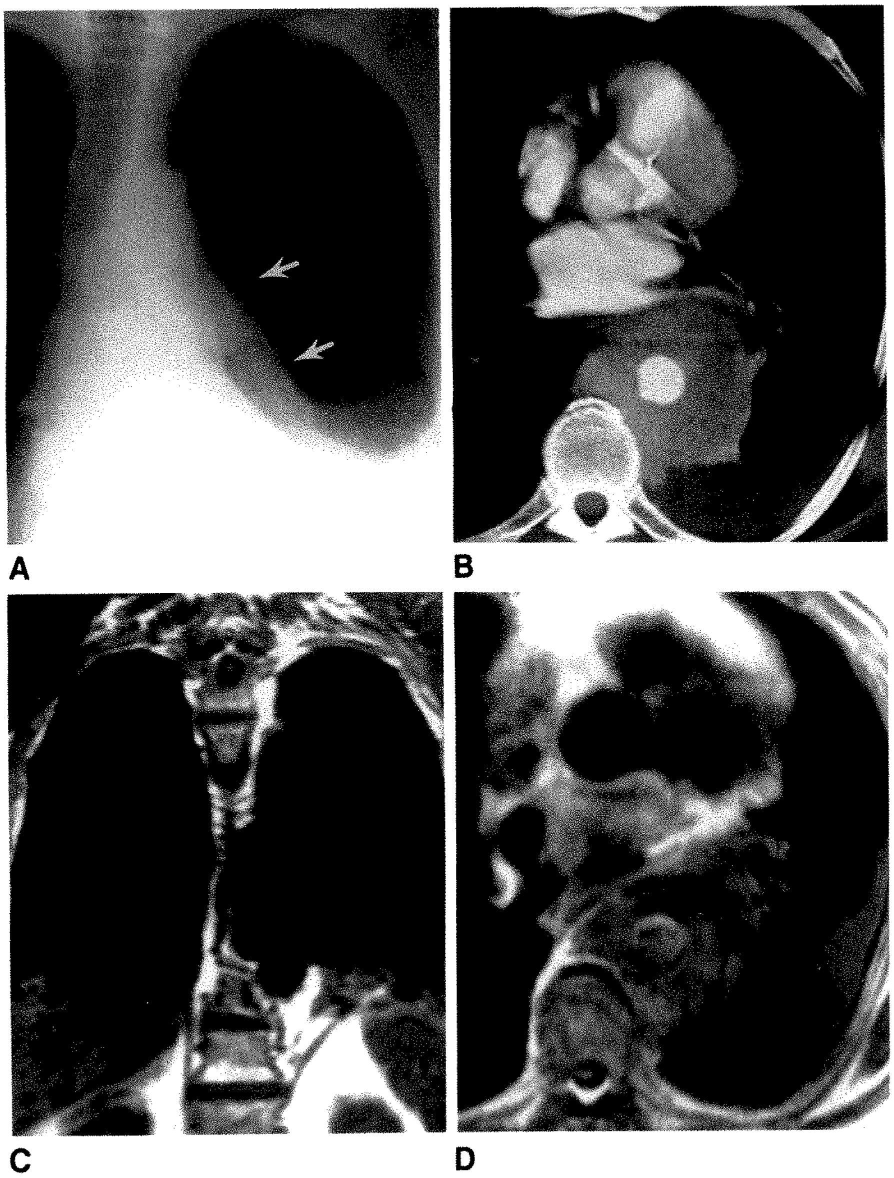

Fig. 1.—79-year-old asymptomatic man with a history of hypertension and mild peripheral vascular occlusive disease.

A, Chest radiograph shows widening of descending thoracic aortic shadow (*arrows*) and left-sided pleural effusion.

B, Contrast-enhanced CT scan shows circumferential periaortic soft tissue, with faint aortic wall calcification and a left-sided pleural effusion.

C and *D*, Coronal T1-weighted (*C*) and axial T1-weighted contrast-enhanced (*D*) MR images show periaortic soft tissue of intermediate signal intensity and a left-sided pleural effusion.

sistent with chronic hematoma, the stable size and attenuation of the mass during the 4-week period suggested that this was less likely.

A second CT-guided aspiration was performed 4 days later. Six passes were made, including two passes each with 22-, 20-, and 18-gauge needles. The specimens contained collagen and lymphoid cells. No tissue diagnosis could be made. A cytopathologist was present during both CT-guided procedures for preparation of the specimens and consultation.

At exploratory thoracotomy, gelatinous, dark, serous fluid was present in the left pleural space. The left lung was adherent to the aorta and firm, white-tan soft tissue encased the descending thoracic aorta. Two biopsy specimens were obtained. The fluid from the left lung contained 147,000 RBCs/mm^3 (0.15×10^{12}/l) and 1320 WBCs/mm^3 (1320×10^6/l). The leukocytes were 96% lymphocytes, which were mature at cytologic evaluation. Gram stain, aerobic and anaerobic cultures, fungal smear, and culture were all negative for infection. The biopsy specimens measured 1.5 × 1.0 × 0.5 cm and 1.5 × 0.8 × 0.3 cm and yielded the diagnosis of diffuse, mixed, small cleaved-cell and large-cell lymphoma with sclerosis. Staging evaluation, including abdominal and pelvic CT, and bone marrow biopsy revealed no other evidence of lymphoma. After chemotherapy the soft-tissue mass completely resolved. Ten months later, no evidence of recurrent disease was present.

Discussion

The diagnosis of both aortic dissection and lymphoma is often difficult. The clinical appearance of aortic dissection is diverse, and radiographically it may be difficult to differentiate dissection from tumor. Aortic dissection can masquerade as another disease, including tumor; and other diseases may look like aortic dissection. Patients with aortic dissection may have signs and symptoms that mimic myocardial infarction, aortic regurgitation, hypertensive crisis, pericarditis, cholecystitis, cerebrovascular accident, spinal cord ischemia, mesenteric infarction, superior vena cava syndrome, acute pulmonary disorders, or mediastinal neoplasm [2]. Conversely, in a series of 176 patients undergoing angiography for suspected aortic dissection during a period of 20 years, 55 patients had normal angiographic findings. Although four of these angiographic findings were later proved to be false-negative, 51 patients (29%) had a different disease [2]. Several mediastinal tumors have been reported to masquerade as aortic dissection on radiographs [2-5]. Conversely, aortic dissection has been reported to mimic tumor [6]. This includes patients with signs and symptoms of acute aortic dissection, as well as asymptomatic patients with abnormal findings on chest radiographs. Most of these reports describe findings on plain films and/or thoracic aortograms. In the case in which aortic dissection mimicked a lung tumor at aortography, a large mass was seen displacing the aortic arch inferiorly without opacification of a false lumen [6]. At surgery, the dissection had leaked into the lung, which contained an 8 × 10 cm hematoma. Many vascular abnormalities, including aneurysms, tortuosity, and pseudocoarctation may radiographically simulate neoplasm.

Eight cases of tumor mimicking aortic dissection or aneurysm have been reported. Eagle et al. [2] describe three patients with chest pain and normal thoracic aortograms in whom lymphoma, hemorrhagic rupture of a mediastinal cyst, and metastatic undifferentiated carcinoma mimicked aortic dissection. Cyst rupture or hemorrhage into the tumor was thought to be the cause of sudden severe pain. Other tumors, including two cases of oat cell carcinoma [3, 5] and a single case of a parathyroid adenoma with hemorrhage [4], have been reported to mimic aortic dissection; single cases of malignant schwannoma and extramedullary plasmacytoma have been reported to mimic aortic aneurysm [2]. CT was performed in both cases of oat cell carcinoma. Shin et al. [5] describe a case of metastatic oat cell carcinoma mimicking aortic dissection and imaged with contrast-enhanced CT. The abnormal soft tissue abutted a portion of the aortic wall and did not surround the aortic lumen. Additionally, the extent of the abnormality was not contiguous, with a skip area of several centimeters between two regions of abnormal periaortic tissue. In the second case of oat cell carcinoma, abnormal paraaortic soft tissue was believed to represent a thrombosed lumen of aortic dissection, as no contrast material was seen adjacent to the aortic lumen [3].

Retroperitoneal lymphoma is not rare. Circumferential encasement of the abdominal aorta is less common, and often nodular. Chrisholm et al. [7] report that 59 patients among 10,000 patients undergoing a body CT examination during a 4-year period at one hospital had circumferential paraaortic abdominal masses. Thirty-two (54%) of these patients had lymphoma. The paraaortic mass had smooth margins in 22 cases (69%) and nodular in 10 cases (31%) of lymphoma. Lymphoma may have many appearances, but in the chest it typically involves mediastinal and, to a lesser extent, hilar lymph nodes. Pulmonary parenchymal, pleural, pericardial, chest wall, and endobronchial forms are less common, seen more frequently with non-Hodgkin's lymphoma than with Hodgkin's lymphoma, and can mimic many benign and malignant diseases [8]. Although lymphoma encasing the abdominal aorta is common, and encasement of other structures such as the ureter has been reported, thoracic periaortic disease has not been described.

The workup of this patient was lengthy and expensive, applying some of the most sophisticated imaging techniques. In reviewing the alternatives in the evaluation of this patient, intravascular sonography provided the most pivotal information in the evaluation of the periaortic mass, showing an intact aortic wall, without intimal defect or intramural hematoma. Although intravascular sonography is a promising new technique for the evaluation of vascular and perivascular disease, its sensitivity is not yet known. The axial orientation of intravascular sonograms raises the possibility that a small transverse intimal tear may be missed. Consequently, the diagnosis of aortic dissection was not completely excluded.

The diagnosis of aortic dissection may be difficult, both clinically and radiographically. CT and angiography may be unable to differentiate mural from extramural disease. The attenuation on CT scans and signal characteristics on MR images of the mass in this case could not be used to distinguish chronic intramural hematoma from a malignant tumor. Although aortic dissection has been reported in the absence of an intimal tear [1], the circumferential nature of the abnormal periaortic soft tissue on CT scans and MR images, together with the lack of change in size or attenuation of the mass on CT scans in a 4-week period suggested that this was not an aortic dissection. Although our pathologists can diagnose malignant lymphoma with an 18- or 20-gauge needle aspirate, this is not always possible. A core biopsy is preferred both for diagnosis and immunohistochemical classification. Given the proximity of the mass to the aorta, and the inability to distinguish mass from aortic lumen without immediate contrast enhancement of the aorta, the physicians who did the CT-guided aspiration did not feel comfortable performing a core biopsy.

When considering the differential diagnosis of abnormal enlargement of the descending thoracic aorta on chest radiographs, either in a patient with acute/chronic pain or in an asymptomatic patient, the diagnosis of aortic aneurysm or dissection must be raised. Unusual morphology on CT scans and MR images, such as a skip area, as previously reported, or unusual circumferential encasement of the aorta, as in this case of lymphoma, should suggest a neoplasm. Additionally, the use of intravascular sonography as an adjunct to thoracic aortography should be considered in the evaluation of suspected aortic dissection when the CT or MR appearance is atypical.

REFERENCES

1. Yamada T, Shimpei T, Junta H. Aortic dissection without intimal rupture: diagnosis with MR imaging and CT. *Radiology* **1988**;168:347-352
2. Eagle KA, Quertermous T, Kritzer GA, et al. Spectrum of conditions initially suggesting acute aortic dissection but with negative aortograms. *Am J Cardiol* **1986**;57:322-326
3. Margolis JA, Cohn RA, Griffin JP, Flanagan WH, Person BY. Oat cell carcinoma presenting as a pseudoaneurysm. *South Med J* **1980**;73:1087-1088
4. Berry BE, Carpenter PC, Fulton RE, Danielson GK. Mediastinal hemorrhage from parathyroid adenoma simulating aortic dissection. *Arch Surg* **1974**;108:740-741
5. Shin MS, Ho KJ, Kirklin JW, Sears NJ. Metastatic mediastinal neoplasm masquerading as aortic dissection: a skip sign on computed tomography for their distinction. *J Comput Assist Tomogr* **1983**;9:299-303
6. Tandon AP, Lukacs LI, Cooke NJ, Ionescu MI. Dissection of the aorta mimicking lung tumour. *J Cardiovasc Surg* **1980**;21:251-252
7. Chrisholm RA, Coltart RS, Cooper P, Dixon AK. Circumferential para-aortic masses: computed tomographic observations. *Clin Radiol* **1986**;37:531-535
8. Bragg DG, Colby TV, Ward JH. New concepts in the non-Hodgkin lymphomas: radiologic implications. *Radiology* **1986**;159:289-304

Case Report

Development and Resolution of Systemic and Coronary Artery Aneurysms in Kawasaki Disease

Marshall E. Yacoe[1] and Michael D. Dake

Kawasaki disease is an acute multisystem vasculitis that primarily affects children. The clinical features include fever, conjunctival hyperemia, erythema and induration of the hands and feet, inflammation of the oral mucosa, tongue, and lips, and cervical lymphadenopathy [1]. Numerous complications can arise; the most feared are coronary artery aneurysms, which can lead to myocardial infarction, sudden death, or chronic coronary insufficiency [2]. Aneurysms of the renal, mesenteric, and other systemic arteries have been described [3-5], but are rare, and little is known of their natural history. We describe a case of Kawasaki disease that is unusual both for the extent of coronary and systemic arterial aneurysms, leading to myocardial infarction and ischemic small-bowel strictures, and for the complete angiographic resolution of the vascular abnormalities.

Case Report

The patient is a male infant who was well until 4 months of age, when a relapsing febrile illness and transient rash developed. This was initially diagnosed as otitis media and was treated with oral antibiotics without resolution. Approximately 2 weeks after the onset of symptoms, he was still intermittently febrile and was admitted for further evaluation and treatment. Cultures of blood, CSF, and urine were sterile, but elevation of erythrocyte sedimentation rate (ESR) and mild anemia were noted. Antibiotics were discontinued and he was discharged home. He continued to have daily fevers, however, and was admitted again approximately 2 weeks later because of fever of unknown origin, loss of developmental milestones, and lethargy. Physical examination revealed generalized decrease in muscle tone, but no rash, abnormal masses, or lymphadenopathy. Laboratory studies were significant for a leukocyte count of 25,500/mm^3 (25.5 $\times$ 10^9/l), a platelet count of 1000 $\times$ 10^3/mm^3 (1000 $\times$ 10^9/l), and an erythrocyte sedimentation rate of 45 mm/hr. Analysis of CSF showed 31 WBC/mm^3 (31 $\times$ 10^6/l), all of which were monocytes. Two-dimensional echocardiography showed coronary artery aneurysms. An electrocardiogram showed Q waves in leads V_4 through V_6. On the basis of the electrocardiographic abnormalities and the elevated serum levels of enzymes, acute myocardial infarction was diagnosed. Kawasaki disease was diagnosed on the basis of all these results.

Cardiac catheterization showed giant aneurysms of the left anterior descending and circumflex coronary arteries, with thrombus and multiple focal stenoses in the distal portion of the left anterior descending coronary artery and a high-grade focal stenosis of the midportion of the circumflex coronary artery (Fig. 1A). Marked apical hypokinesis, consistent with myocardial infarction, was noted. Abdominal aortograms obtained at the same time showed multiple systemic aneurysms involving the hepatic, superior mesenteric, and renal arteries (Figs. 1B and 1C).

The patient was treated with systemic anticoagulants and aspirin because of the presence of coronary artery thromboses, but otherwise received only supportive care. He was intolerant to food and had persistent vomiting during a monthlong hospitalization, which continued after he was discharged. He was readmitted several weeks later with acute small-bowel obstruction. Exploratory laparotomy revealed multiple bandlike adhesions and two focal areas of stricture in the distal jejunum and proximal ileum. The strictured segments of the small bowel were surgically resected with primary anastomosis. Pathologic examination of the resected segments of the small bowel

---

Received March 11, 1992; accepted after revision May 5, 1992.

[1] Both authors: Department of Radiology, Stanford University Medical Center, Stanford, CA 94305.

AJR 159:708-710, October 1992 0361-803X/92/1594-0708 © American Roentgen Ray Society

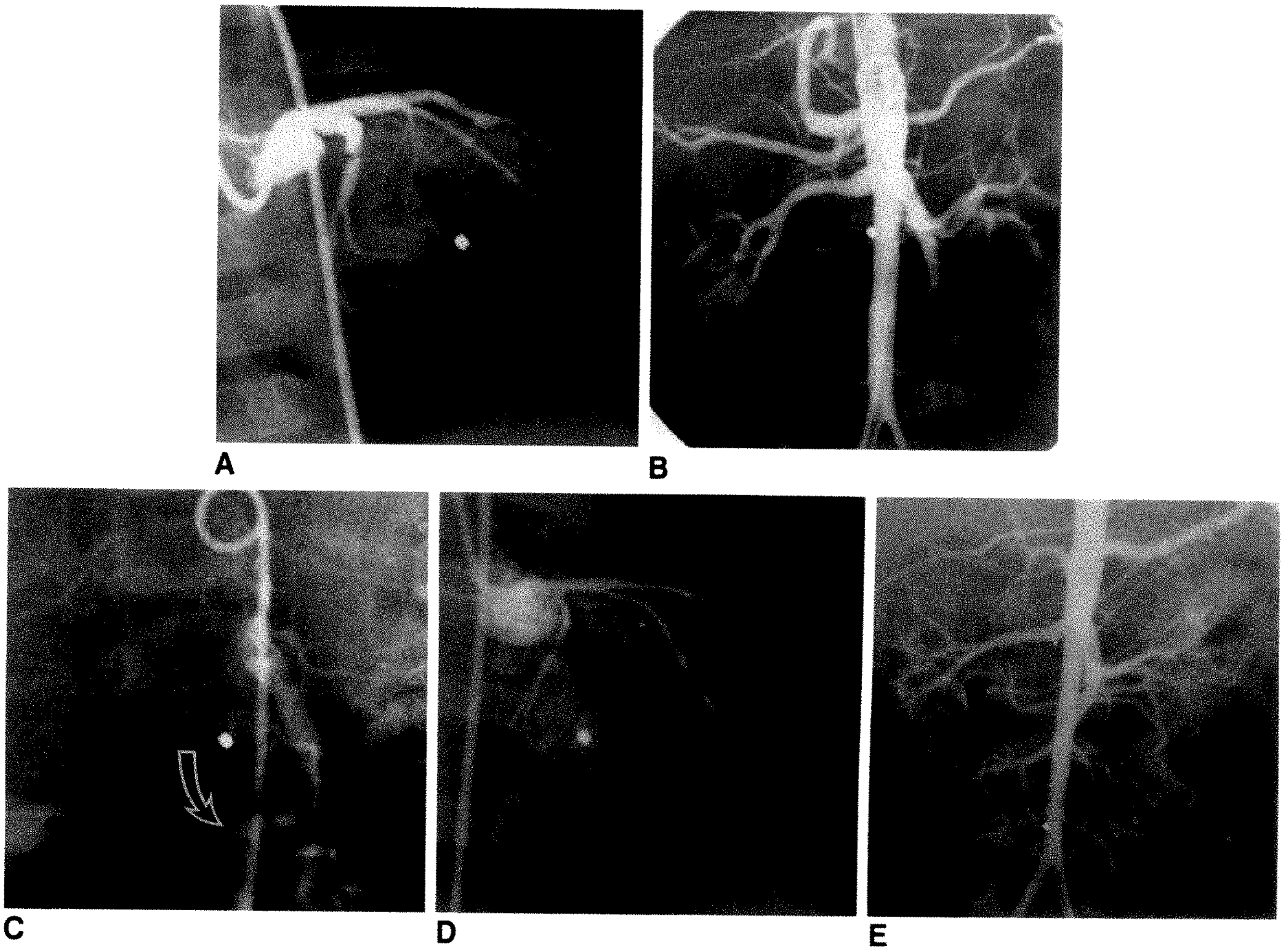

Fig. 1.—*A*, Coronary angiogram shows giant aneurysms of left anterior descending and circumflex coronary arteries. Multiple distal stenoses and irregular mural thrombus are seen in left anterior descending artery, and a high-grade focal stenosis is seen in mid circumflex artery.

B, Abdominal aortogram shows multiple systemic aneurysms. A long segmental aneurysm is seen in left hepatic artery, with focal stenosis in its midportion. Aneurysms of proximal right renal artery and superior mesenteric artery also are identified on this early arterial phase image.

C, Abdominal aortogram late in arterial phase shows contrast medium pooling in a segmental aneurysm of a superior mesenteric artery branch (*arrow*) because of distal stenosis.

D, Left-sided coronary angiogram 1 year later shows complete resolution of coronary artery aneurysms and stenoses with no residual disease.

E, Abdominal aortogram 1 year later shows complete resolution of renal, superior mesenteric, and hepatic artery aneurysms with no residual disease.

revealed acute and chronic inflammation and evidence of arteritis and vascular obstruction consistent with Kawasaki disease. The patient had an uneventful postoperative course.

Follow-up cardiac catheterization and aortography performed approximately 1 year later showed angiographically normal coronary, mesenteric, and renal arteries (Figs. 1D and 1E) and hypokinesis of a small apical segment of the left ventricle.

Discussion

Coronary artery aneurysms are a well-known complication of Kawasaki disease, occurring in up to 20% of untreated patients [2]. Early diagnosis of Kawasaki disease is critical, as IV gamma globulin given during the first week of illness reduces the likelihood of coronary abnormalities to less than 5% [1]. The natural history of coronary artery aneurysms is fairly well known. In the subacute phase, they may be complicated by myocardial infarction, as in the present case, or sudden death due to coronary thrombosis [2]. Chronic coronary insufficiency may occur as a late complication due to scarring. Most coronary artery aneurysms, however, regress spontaneously. The factors that favor resolution of these lesions include age less than 1 year at onset of symptoms, female sex, and fusiform morphology [6]. The maximal diameter of the aneurysm also affects prognosis. Giant aneurysms (>8 mm) usually remain persistently large or progress to obstructive or stenotic lesions [7]. The present case is unusual in that giant aneurysms of the left anterior descending and circumflex coronary arteries, complicated by mural thrombosis and apical infarction, showed complete resolution on follow-up angiograms 1 year later (Fig. 1D). The long-term effect of transient aneurysmal dilatation of these vessels is unknown. Some evidence suggests that these lesions may predispose patients to accelerated atherosclerosis [8].

Although Kawasaki disease has a strong predilection for the coronary arteries, it is a systemic vasculitis of medium-sized muscular arteries [2]. At autopsy, vasculitis of noncoronary arteries has been well described [2]. However, few radiographic reports of such systemic arterial aneurysms have been published [3-5]. The present case illustrates the widespread formation of aneurysms of the splanchnic and renal arteries in Kawasaki disease. The natural history of noncoronary aneurysms is unknown, but might be expected to be similar to that of coronary aneurysms, ranging from complete resolution to persistent aneurysm, stricture, or occlusion. In the present case, mesenteric vasculitis resulted in ischemic strictures of the small bowel that required surgical resection. To our knowledge this has not been reported as a complication of Kawasaki disease, although other end-organ infarctions have been reported [2, 3]. Interestingly, follow-up angiography after 1 year showed complete resolution of disease. However, the extent to which angiographically inapparent vascular disease remains and the ultimate fate of such lesions are not known.

REFERENCES

1. Melish ME, Hicks RV. Kawasaki syndrome: clinical features. Pathophysiology, etiology and therapy. *J Rheumatol Suppl* **1990**;24:2-9
2. Rose V. Kawasaki syndrome: cardiovascular manifestations. *J Rheumatol Suppl* **1990**;24:11-14
3. Lapointe JS, Nugent RA, Graeb DA, Robertson WD. Cerebral infarction and regression of widespread aneurysms in Kawasaki's disease: case report. *Pediatr Radiol* **1984**;14:1-5
4. Marks WH, Coran AG, Wesley JR, et al. Hepatic artery aneurysm associated with the mucocutaneous lymph node syndrome. *Surgery* **1985**;98:598-601
5. Nitsure MY, Hiremath MS, Grant PK, et al. Kawasaki syndrome with multiple arterial aneurysms. *Indian J Pediatr* **1988**;25:881-888
6. Takahashi M, Mason W, Lewis AB. Regression of coronary aneurysm in patients with Kawasaki disease. *Circulation* **1987**;75:387-394
7. Nakano H, Ueda K, Saito A, et al. Repeated quantitative angiograms in coronary arterial aneurysms in Kawasaki disease. *Am J Cardiol* **1985**;56:846-851
8. Tatara K, Kusakawa S. Long-term prognosis of giant coronary aneurysms in Kawasaki disease: an angiographic study. *J Pediatr* **1987**;111:705-710

Ruptured Gel-Filled Silicone Breast Implants:

Sonographic Findings in 19 Cases

Katrina A. Rosculet[1]
Debra M. Ikeda[1,2]
Maureen E. Forrest[3]
Robert M. Oneal[4]
Jonathan M. Rubin[1]
Deborah O. Jeffries[3]
Mark A. Helvie[1]

OBJECTIVE. The purpose of this study was to describe and illustrate the sonographic appearances of 19 ruptured silicone gel breast implants.

MATERIALS AND METHODS. We retrospectively reviewed the sonograms of 16 patients with 19 ruptured silicone gel implants from two institutions. The ruptured implant was confirmed at surgery in 17 cases and by mammographic and clinical findings of a ruptured implant combined with biopsy findings of a silicone granuloma in two cases. Breast sonograms were available for review in all patients. The clinical presentation of each patient was recorded. The sonograms and mammograms were reviewed, and the findings were correlated with the surgical findings. In 16 of the 19 ruptured implants, mammographic findings suggested rupture, including lobulation of the contour of the implant and/or silicone extrusion into the breast parenchyma or axilla. In two ruptured implants, mammographic findings were normal, and in one case, no mammogram was available. In those three patients, palpable masses and clinical findings were suggestive of rupture.

RESULTS. Sonography showed a unique echogenic appearance called echodense noise, in 17 of the 19 ruptured implants; in 10 of the 17, sonograms showed hypoechoic masses of extruded silicone also. In two ruptured implants, sonograms showed only the hypoechoic masses of extruded silicone gel.

CONCLUSION. Our experience suggests that echogenic noise is a unique sonographic sign of ruptured silicone gel breast implants and may be caused by phase aberration related to the speed of sound being slower in silicone than in soft tissue.

AJR 159:711-716, October 1992

Since the first breast implant was placed in 1962, approximately 1 to 2 million women in the United States have had silicone gel breast implants [1]. Rupture of silicone gel breast implants is one of the occasional complications of their use that has received a great deal of attention recently. Rupture of the breast implant is often evident clinically, usually because of sudden breast deformity, change in breast consistency, or breast size reduction. Occasionally the diagnosis is difficult such as when patients have a breast mass, pain, discomfort, or a perception that the implanted breast has changed. In these cases, mammography may be useful, but is not always conclusive. The role of sonography in the evaluation of silicone gel breast implants is not clear, although some have advocated its use [2].

We reviewed the sonographic findings in 19 ruptured implants in 16 patients.

Materials and Methods

We retrospectively reviewed our log sheets of women with silicone gel breast implants who were seen at the University of Michigan Hospital between January 1989 and January 1992 or at St. Joseph's Mercy Hospital between October 1988 and January 1992. During the periods specified, 30,748 mammograms and 2330 breast sonograms were obtained at the University of Michigan Hospital, and 7377 breast sonograms and 80,536 mammograms were obtained at St. Joseph's Mercy Hospital. Requirements for inclusion in the study were

Received February 3, 1992; accepted after revision April 14, 1992

Presented at the annual meeting of the American Roentgen Ray Society, Orlando, FL, May 1992.

[1] Department of Radiology, University of Michigan Hospitals, Box 0326, 1500 E. Medical Center Dr., Ann Arbor, MI 48109-0326.

[2] Present address: Division of Breast Imaging, Department of Radiology, Stanford University Medical Center, 300 Pasteur Dr., Rm. S-072, Stanford, CA 94304. Address reprint requests to D. M. Ikeda.

[3] Department of Radiology, St. Joseph Mercy Hospital, 5301 E. Huron River Dr., Ann Arbor, MI 48106.

[4] Department of Plastic and Reconstructive Surgery, University of Michigan Hospitals, Ann Arbor, MI 48109-0326, and Department of Plastic Surgery, St. Joseph Mercy Hospital, Ann Arbor, MI 48106.

0361-803X/92/1594-0711
© American Roentgen Ray Society

(1) a ruptured implant found at surgery (17 cases) or mammographic and clinical findings of a ruptured implant with a silicone granuloma present on biopsy (two cases) and (2) breast sonograms available for review. Sixteen women with 19 ruptured implants fulfilled the study criteria.

Mammography was performed in 15 women with state-of-the-art equipment (GE/CGR 600T or GE/CGR 500T unit, Columbia, MD, or Mammex Mag DC unit, Technomed USA, Bayshore, NY), and sonography was performed with either a Hitachi EUB400 (Tokyo, Japan; 13 women) or an Acoustic Imaging (Phoenix, AZ; three women) unit with 7.5-MHz transducers. Sonograms and mammograms were reviewed independently by three radiologists. The following data were recorded for each case from the clinical records and from review of the mammograms and sonograms: (1) reason for implant, (2) location of implant (subpectoral or retromammary), (3) clinical presentation, (4) contour of implant seen on mammograms, (5) presence or absence of silicone gel extrusion outside the implant shown on mammograms, and (6) sonographic findings (echodense noise, hypoechoic masses, or irregularity of the contour of the implant).

The 16 women were between 33 and 54 years old (average, 45 years old). The implants had been in place for 6–20 years (average, 13 years).

In 14 women (17 breasts) with suspected ruptured implants, the implant was removed. In two women (two breasts), biopsy showed a foreign body (silicone) granuloma; these two women also had mammographic and clinical findings suggestive of rupture.

Fourteen women had implants for breast augmentation and two for reconstruction after mastectomy, for a total of 16 women in whom 19 implants were found to be ruptured at surgery. Sixteen of the 19 implants that ruptured were retromammary and three were subpectoral. The patients underwent imaging for various reasons: palpable masses (seven breasts), mass and pain (one patient, two breasts), mass and breast deformity (one breast), change in breast shape (three patients, four breasts), pain (one breast), or screening mammography (three patients, four breasts).

In 16 of the 19 ruptured implants, mammographic findings suggested rupture, including a lobulated contour of the implant and silicone extrusion between the implant and fibrous capsule or between the axillary tissue planes (12 cases), extrusion into breast parenchyma (two cases), and a markedly lobulated contour (two cases). Mammographic findings were normal in two patients, and one other did not undergo mammography; palpable masses in these three patients were examined sonographically.

Results

At sonography a unique homogeneous low-level echogenic appearance, labeled echodense noise, was noted in 17 (90%) of the 19 ruptured implants. This echodense noise, which corresponded to silicone gel leakage, did not allow imaging of structures beyond it (Figs. 1 and 2). Seven ruptured implants showed this finding alone, and 10 showed hypoechoic masses (representing conglomerates of silicone gel) in conjunction with the echogenic noise (Figs. 3 and 4).

In two ruptured implants, sonography did not show echodense noise, but did show hypoechoic masses corresponding to extruded silicone gel masses either alone (one case) or in conjunction with an irregular contour of the implant (one case). The hypoechoic masses were separate from the implant, except in one patient who had a palpable mass corresponding to an irregular hypoechoic mass adjacent to the implant on sonography. Surgery confirmed that the mass contained silicone gel within a fibrous wall adherent to the implant capsule, with a communication between the mass of silicone gel and the implant (Fig. 5).

In the two patients with normal mammographic findings and palpable breast masses, echodense noise and hypoechoic masses were seen on sonograms, suggesting ruptured implants not seen on mammograms. Each patient had a surgically confirmed implant rupture at the site of the palpable mass, as detailed by the surgical report.

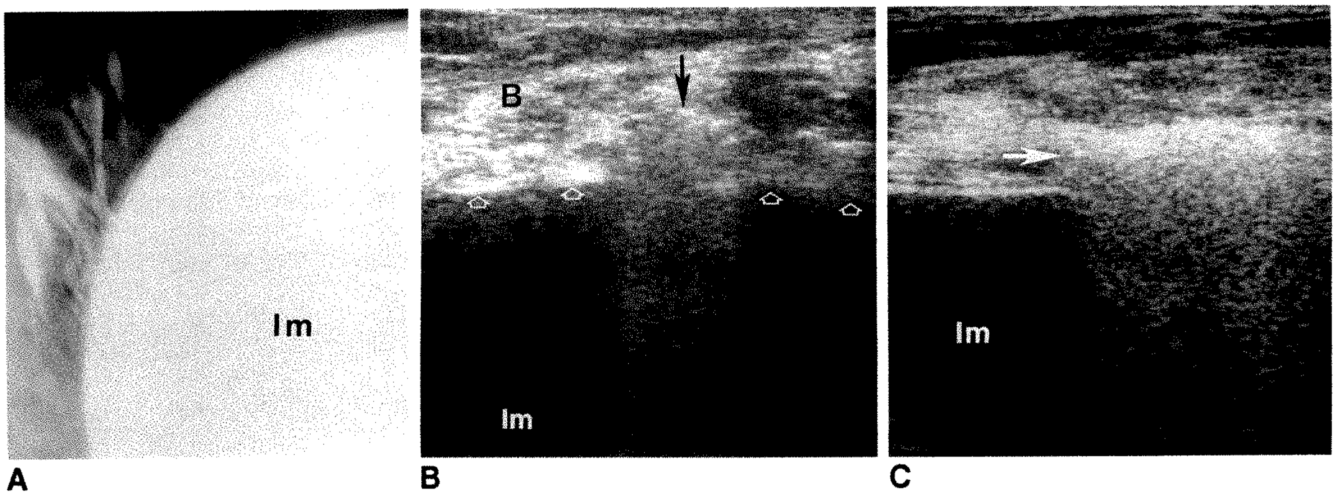

Fig. 1.—49-year-old woman with a ruptured 11-year-old implant in left breast noticed softening of the breast after a fall from a horse 10 days earlier.

***A*, Lateromedial mammogram (cropped) of left breast reveals rupture of implant (Im), with streaks of silicone gel in breast parenchyma.**

***B*, Sonogram of left breast shows echogenic noise corresponding to extruded silicone gel (*solid arrow*), breast tissue (B), and silicone gel implant (Im). Note abnormal breast-implant boundary on either side of echogenic noise (*open arrows*).**

***C*, Sonogram of another region in left breast shows distinct echogenic noise corresponding to extruded silicone gel (*arrow*). Posterior to noise, all sonographic information is lost. Hypoechoic silicone gel implant is seen adjacent to noise (Im).**

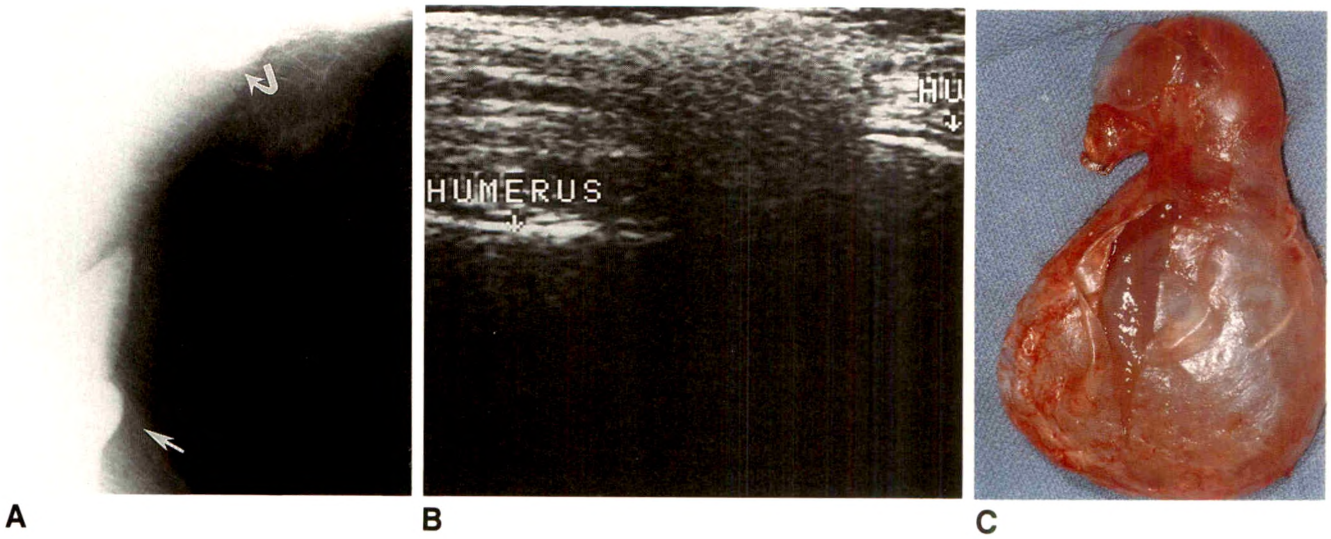

Fig. 2.—45-year-old asymptomatic woman with a ruptured 7-year-old implant in left breast.

A, Mediolateral oblique mammogram (cropped) of left breast shows extruded silicone gel (*straight arrow*). A small mass of silicone gel has migrated from implant to left upper extremity, adjacent to humerus (*curved arrow*).

B, Sonogram of silicone gel mass in left upper extremity shows focal echodense noise (silicone gel mass) that completely obscures underlying humerus.

C, Gross surgical specimen shows ruptured silicone gel implant contained in a fibrous capsule.

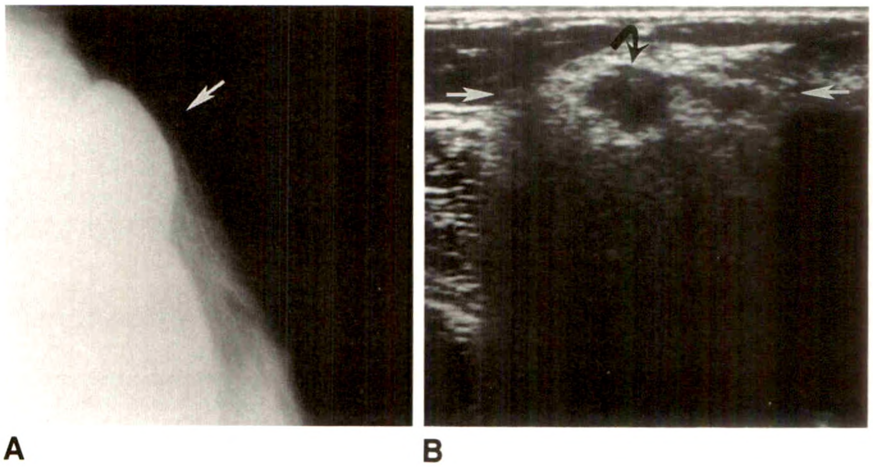

Fig. 3.—36-year-old woman with ruptured 10-year-old implants noted masses and pain bilaterally.

A, Mediolateral oblique mammogram (cropped) of left breast shows focal lobulation of superior aspect of implant (*arrow*), corresponding to a 1-cm mass in upper part of left breast.

B, Sonogram of left breast shows a hypoechoic mass (*black arrow*) with surrounding echodense noise at site of implant rupture (*white arrows*).

In eight of the nine women with a palpable mass, a sonographic abnormality (either echodense noise or hypoechoic masses of silicone) corresponded to the palpable finding. In the remaining woman with a palpable mass, areas of echodense noise indicating rupture of the implant were seen on sonograms, but no discrete lesions could be identified in the region of the palpable mass. The cause of the palpable mass could not be ascertained from the report or the medical chart, but at surgery the implant was ruptured, as suggested by echodense noise seen over other (impalpable) regions.

In one case, mammography showed a 1-cm conglomerate of extravasated silicone gel corresponding to a hypoechoic mass on sonography; aspiration under sonographic guidance yielded silicone gel (Fig. 6).

Discussion

Sonography has been used to evaluate complications of breast implants including rupture, with past reports describing sonographic evidence of rupture as linear echoes through the implants representing invaginations of the implant envelope [3, 4] and a decreased anteroposterior diameter of the ruptured implants [3]. An irregular contour of the implant was seen in only one of our cases, perhaps because our group of patients included women who had subtle or confusing clinical findings, often referred for imaging to "rule out rupture," and those in whom unsuspected silicone gel leaks were found at screening mammography.

The unique echogenic noise that is such a striking feature

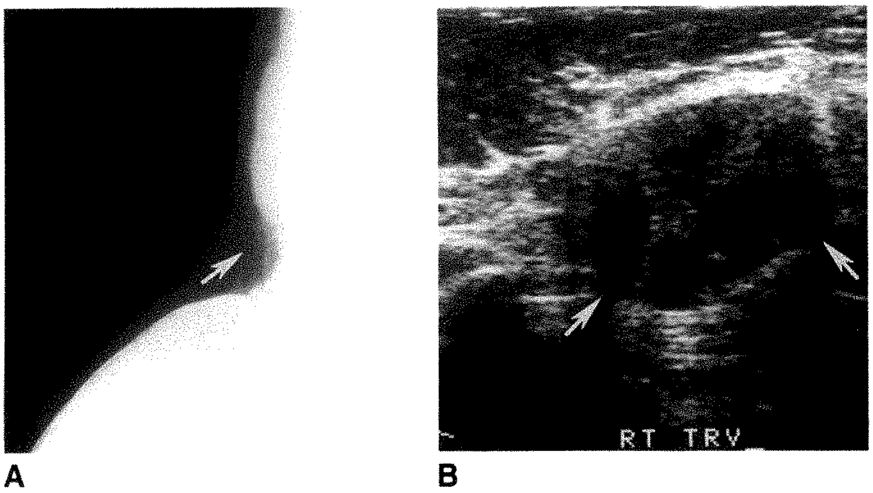

Fig. 4.—46-year-old woman with a ruptured 18-year-old implant noted nodularity in upper portion of right breast.

A, Mediolateral oblique mammogram (cropped) of right breast shows silicone gel (*arrow*) extruded from ruptured implant. Note capsular calcification.

B, Sonogram of right breast shows extruded silicone gel as a hypoechoic mass (*arrows*). Echogenic noise was noted in other regions (*not shown*).

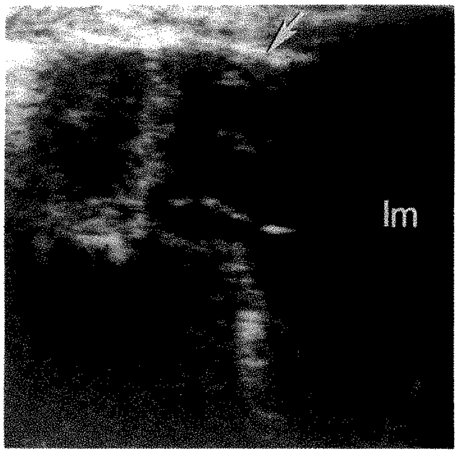

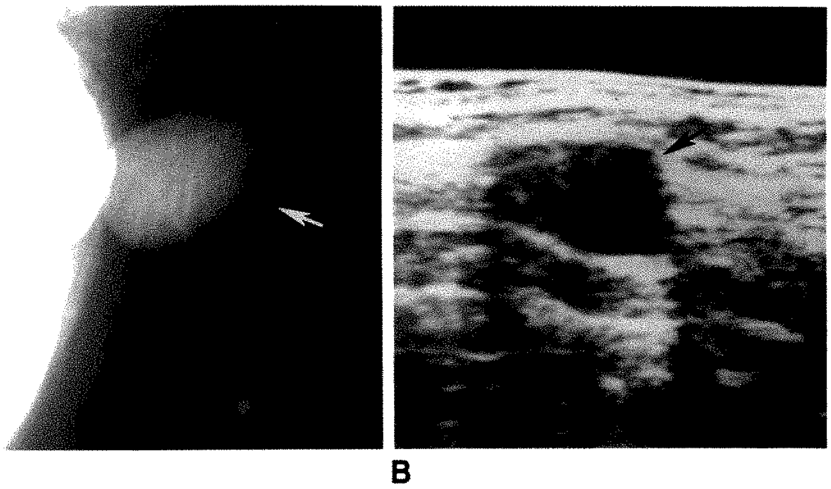

Fig. 5.—33-year-old woman with a ruptured 9-year-old implant noted a 2-cm mass in lower outer quadrant of right breast. Sonogram of right breast shows a hypoechoic mass (*arrow*) thought to be extruded silicone gel adjacent to implant (Im). At capsulectomy, a mass with macroscopic amounts of silicone gel communicated with implant and was adherent to fibrous capsule, representing a walled-off leak from the implant.

Fig. 6.—39-year-old woman with 15- to 20-year-old implants noted a 1-cm mass in upper part of left breast.

A, Lateromedial mammogram (cropped) of left breast shows lobulation of superior contour of implant and a 1-cm silicone globule (*arrow*), corresponding to mass marked by a skin marker.

B, Sonogram of left breast shows a hypoechoic mass (*arrow*), separate from implant, corresponding to both palpable mass and mass seen on mammography. Note sonographic breast structures posterior to mass. Fine-needle aspiration of mass yielded silicone. Removal of implant confirmed rupture.

of many of our cases rarely has been described in the radiologic literature. Of note, however, ours is a retrospective study of a biased population consisting only of women who had ruptured implants at surgery. Herzog [5] described two women who had small nodules with "echodense shadows" behind them that corresponded histologically to silicone granulomata and silicone lymphadenopathy [5]. Levine and Collins [4] alluded to "echogenic confusion" on sonography in a single case of a grossly ruptured implant. Harris et al. [2] have presented a preliminary report describing this unique appearance associated with ruptured breast implants.

We found this echogenic noise to be unique and different from the typical "dirty shadow" formerly ascribed to gas [6]. It is not analogous to the shadow seen behind gas or stones, because large masses of silicone gel or the intact implant clearly transmit sound (Figs. 4B and 6B). We hypothesize that the appearance is caused by aggregates of silicone with diameters on the order of a wavelength within breast parenchyma or axillary tissues. The speed of sound in silicone is significantly slower (990 m/sec) than in soft tissue (1540 m/sec) [7]. This creates large differences in speeds of sound across the ultrasound beam when it propagates across tissue impregnated with silicone. These velocity discontinuities produce focal areas in the wave that advance ahead or lag behind and are out of phase with neighboring areas, producing a loss of coherence of the beam, destroying beam focus and, ultimately, the image [8]. This is termed phase aberration [8]. We considered the possibility that this noise is due to reverberations or "multipathing" in the tissue. However, such phenomena require the presence of specular reflectors, that is, large surfaces with fluctuations that are small compared with a wavelength. The small droplets of silicone produced by a ruptured implant do not meet these criteria. In fact, because of the difference in the speed of sound in silicone vs soft tissue, these small droplets would produce large fluctuations in phase, canceling any strong reverberations.

We must then explain why some ruptured implants with obvious silicone gel extrusion on mammography do not show this sonographic appearance (noise), but manifest as irregular hypoechoic masses, which were proved at surgery to represent conglomerates of silicone gel outside the implant. When the beam encounters a large mass of silicone gel, that is, large compared with the wavelength, the sound wave reflects and refracts when the wave front is not perpendicular to the interface. The beam is bent by the boundary and propagates through the silicone gel in the wrong direction, but is still coherent. Therefore, one sees the boundary between the silicone and the breast parenchyma and structures behind the boundary, which appear normal but are actually in the wrong position. This is what happens when sound is focused behind cysts in routine clinical sonograms, but only to a greater degree [9, 10]. This explanation also accounts for bulges in implants not producing the noisy appearance, as in the walled-off leak shown in Figure 5. If the wave front is perpendicular to the silicone-breast parenchyma boundary, the sound beam is not bent but propagates much more slowly through the silicone gel and still retains coherence.

Rupture was suggested with film-screen mammography in all but two cases, in agreement with a prior study suggesting a high accuracy of mammography in showing ruptures of silicone gel implants [11]. It should be noted, however, that our population was biased as it contained only patients with ruptured implants. We speculate that the area of rupture in our two cases with normal mammographic findings and abnormal sonographic findings was not imaged on the mammogram because of the location of the rupture (upper inner quadrant in one and upper outer quadrant in the other), which may have been hidden by the dense silicone gel implant. As the woman with the implant that ruptured in the upper inner quadrant also had severe capsular formation, the region may not have been optimally imaged because of the hardness of the breast and difficulty in positioning.

Many of our other cases showed extrusion of opaque silicone gel into the surrounding tissues on mammography, a finding previously described in case reports of ruptured implants [12–15]. On the other hand, sonography showed ruptured implants (echodense noise) as the cause of palpable breast masses despite normal mammographic findings in two of our cases.

Lobulation of the contour of the implant also was seen in some of our cases. However, when a lobulated contour on mammography is the only radiologic sign suggesting an implant has ruptured, the diagnosis is not certain because false-positive diagnoses of ruptured implants can be due to herniation of the intact implant through a fibrous capsule that can form around breast implants [16]. Clinically, it may be difficult to identify ruptured implants in women with fibrous capsules forming around breast implants. The Baker classification categorizes encapsulation as follows: grade I, normal; grade II, palpable firmness with a natural appearance; grade III, firm with visible distortion; and grade IV, obvious spherical distortion [17]. In some cases, particularly those with Baker III–IV encapsulation of implants, sonography can be technically most difficult at the inframammary crease because of the inflexibility of the transducer combined with a stiff and immobile implant. We have found this can usually be overcome by turning the patient onto her side or having her raise her arm higher above her head.

Implant lobulations detected with mammography may raise the clinical question of whether the implant is lobulated, herniated, or ruptured. We speculate that sonography would be particularly valuable in these patients to show that simple implant lobulations caused by capsular formation are continuous with the rest of the intact implant, and that herniations of intact implants through the fibrous capsule are not ruptures; in either of these two scenarios involving implant contour lobulations without rupture, we speculate sonography would not show the echodense noise we described. On the other hand, it would be difficult to distinguish herniation from walled-off leaks from implants (Fig. 5).

The diagnosis of rupture of a silicone gel breast implant may be missed on mammography, as the rupture site may be hidden behind the radiodense implant or not included in the field of view. However, mammography remains critically important in the evaluation of breasts containing implants to evaluate the breast parenchyma for cancer [18]. Sonography provided valuable additional information when a ruptured implant was clinically suspected and mammographic findings were normal or when mammographic findings were equivocal, as in lobulated contours. The echodense noise produced by silicone gel dispersed in soft tissue is a valuable sonographic sign seen in most of our cases. Of note, however, all of our patients who were identified retrospectively for this investigation had either abnormal mammographic findings or clinical signs of ruptured implants and had surgical confirmation of rupture, producing sample bias into the population studied. The value of this sign in women with mammographic findings not suggestive of ruptured implants and normal findings on physical examination of the breast is yet to be determined. As the sensitivity and specificity of this sonographic sign are not known, further study of this sign is needed.

ACKNOWLEDGMENTS

We thank Cynthia E. Sims and Melanie L. Shaw for secretarial support in the preparation of this manuscript and J. Brian Fowlkes for technical consultation.

REFERENCES

1. Department of Health and Human Services. *Food and Drug Administration bulletin. Background information on the possible health risks of silicone*

breast implants (rev. February 8, 1991). Rockville, MD: Department of Health and Human Services, **1991**

2. Harris KM, Ganott MA, Shestak K, Loskin W, Tobon H. Detection of silicone implant leaks: a new sonograpic sign (abstr). *Radiology* **1991**;181(P): 134-135
3. Van Wingerden JJ, van Staden MM. Ultrasound mammography in prosthesis-related breast augmentation complications. *Ann Plast Surg* **1989**;22:32-35
4. Levine RA, Collins TL. Definitive diagnosis of breast implant rupture by ultrasonography. *Plast Reconstr Surg* **1991**;87:1126-1128
5. Herzog P. Silicone granulomas: detection by ultrasonography (letter). *Plast Reconstr Surg* **1989**;84:856-857
6. Rubin JM, Adler RS, Bude RO, Fowlkes JB, Carson PL. Clean and dirty shadowing at US: a reappraisal. *Radiology* **1991**;181:231-236
7. *Table of ultrasonic properties.* Richmond, WA: Metro Tek Inc., **1982**
8. Trahey GE, Freiburger PD, Ng G, Sullivan DC. The impact of acoustic velocity variations on target detectability in ultrasonic images of the breast. *Invest Radiol* **1991**;9:782-791
9. Robinson DE, Wilson LS, Kossoff G. Shadowing and enhancement in ultrasonic echograms by reflection and refraction. *JCU J Clin Ultrasound* **1981**;9:181-188
10. LaFollette PS Jr, Ziskin MC. Geometric and intensity distortion in echography. *Ultrasound Med Biol* **1986**;12:953-963
11. Andersen B, Hawtof D, Alani H, Kapetansky D. The diagnosis of ruptured breast implants. *Plast Reconstr Surg* **1989**;84:903-907
12. Scott IR, Muller NL, Fitzpatrick DG, Warren Burhenne LJ. Ruptured breast implant: computed tomographic and mammographic findings. *Can Assoc Radiol J* **1988**;39:152-154
13. Theophelis LG, Stevenson TR. Radiographic evidence of breast implant rupture. *Plast Reconstr Surg* **1986**;78:673-675
14. Apesos J, Pope TL. Silicone granuloma following closed capsulotomy of mammary prosthesis. *Ann Plast Surg* **1985**;14:403-406
15. Ho WC. Radiograhpic evidence of breast implant rupture (letter). *Plast Reconstr Surg* **1987**;79:1009-1010
16. Smith DS. False-positive radiographic diagnosis of breast implant rupture: report of two cases. *Ann Plast Surg* **1985**;14:266
17. Bostwick J. *Plastic and reconstructive breast surgery*. St Louis: Quality Medical Publishing, **1990**;181
18. American College of Radiology. Joint statement on mammography guidelines. *ACR Bull* **1989**;45:1, 4

AJR to Use Diskettes Instead of Hard-Copy Manuscripts for Editing and Printing

Beginning with the January 1993 issue, accepted papers to be published in the *AJR* will be edited and printed by using computer diskettes rather than hard copies of the manuscripts. This change will expedite the editing and publication process and result in less delay between submission of manuscripts and their appearance in the Journal. Also, with the new system, authors will receive page proofs rather than galleys before publication. This will enable them to see exactly what their final article will look like.

Effective immediately, upon *acceptance* of manuscripts for publication, authors will be asked to send a copy of their revised manuscript on a 3½-in. or 5¼-in. DOS-compatible diskette in Wordperfect or ASCII format along with the hard copy of the revision. Articles will be edited directly on the diskettes. Changes will be highlighted electronically; as before, a hard copy of the edited manuscript and figure proofs will be mailed to authors for approval before publication. Note that hard copies of manuscripts will still be required for the peer-review and revision processes.

The *AJR* already takes great pride in the speed with which the peer-review process is accomplished (mean time, 3.4 weeks) and in the amount of time between submission of manuscripts and their final appearance in print (6 months). This is nearly twice as fast as many other journals. With the new system, these intervals will be even shorter. Authors will see their work in print faster, and the timeliness of the Journal will be greater than ever.

Robert N. Berk
Editor-in-Chief

Review Article

CT of Portal Venous Occlusion

Charles S. Marn[1] and Issac R. Francis

Thrombosis of a portion of the portal venous system can be directly imaged by contrast-enhanced CT as a low-attenuation lesion within the involved portal venous segment with or without expansion of the vessel or enhancement at the margin of the thrombus. Collateral venous pathways are often evident, which provide supporting evidence of the occlusion. Alterations in portal venous blood flow lead to metabolic disturbances in the liver and to abnormalities in parenchymal enhancement during dynamic CT scanning, and these changes are manifested as abnormalities in hepatic parenchymal density. The detection of portal venous thrombosis or occlusion, collateral veins, or abnormal liver enhancement should initiate a search for the diseases that cause these abnormalities.

The portal venous system can be affected by a variety of neoplastic, inflammatory, hematologic, and hypertensive disorders. In many cases, the portal venous abnormality reflects pathologic processes in the liver, spleen, pancreas, or gastrointestinal tract. Abdominal CT is often used in the initial evaluation of many abdominal disorders. Recent advances, such as faster scanning times, the rapid bolus administration of contrast medium using mechanical injectors, and scanning during the portal phase of intraarterial contrast injection into the superior mesenteric artery (CT arterial portography), have significantly increased our understanding of CT patterns of hepatic contrast enhancement in normal and diseased states. This article focuses on the portal venous system as a mirror of abdominal diseases, with emphasis on the pathophysiologic conditions that affect the portal and splenic veins. The CT imaging findings typically seen in some of these conditions also are discussed and illustrated.

Technique

Much emphasis has been placed on the use of dynamic CT imaging during the bolus administration of relatively large amounts of contrast material for the detection of hepatic lesions [1]. The detection and characterization of vascular abnormalities in the abdomen also are facilitated by similar techniques. At our institution, routine contrast-enhanced abdominal CT using 100–150 ml of 60% meglumine iothalamate is performed in the vast majority of cases. Contrast medium is given by a mechanical injector at a rate of 2 ml/sec through an 18-gauge catheter placed in the antecubital fossa. Contiguous 10-mm axial sections are obtained with 2-sec scanning time and 7- to 10-sec interscan delay, depending on the patient's size. Scanning is initiated 30–45 sec (depending on age, 30 sec for patients less than 40 years old, owing to their better cardiac output) after the initiation of the bolus to ensure hepatic imaging in the portal venous phase of contrast enhancement. When this technique is used, hepatic imaging is routinely completed in 2–3 min. If necessary, single-level or limited repeated scanning during administration of an additional bolus of 50 ml of contrast medium can be used to confirm or exclude an abnormality suspected on routine scanning.

Anatomy

The portal venous system drains the stomach, spleen, pancreas, small bowel, and colon to the liver. Contrast-enhanced CT scans can show the central portions of the superior and inferior mesenteric veins, the splenic vein, main, right,

---

Received February 14, 1992; accepted after revision April 5, 1992.

[1] Both authors: Department of Radiology, Box 0030, University of Michigan Medical Center, University of Michigan Hospitals, 1500 E. Medical Center Dr., Ann Arbor, MI 48109-0030. Address reprint requests to C. S. Marn.

AJR 159:717–726, October 1992 0361-803X/92/1594-0717 © American Roentgen Ray Society

and left portal veins, and central portions of the intrahepatic portal veins. Smaller branches of more peripheral portions of the superior or inferior mesenteric veins in the mesentery or portal vein branches within the liver are not consistently shown by CT unless they contain air. An understanding of normal and collateral venous drainage of the stomach is essential to diagnose portal venous abnormalities (Fig. 1). Small venous branches along the lesser curve drain into the coronary vein, traversing the gastrohepatic ligament, a triangular space between the lesser curve of the stomach and the left lobe of the liver. The coronary vein joins the portal venous system at or near the portal confluence [3]. If vessels larger than 6 mm are present in the gastrohepatic ligament, then varices are present [4]. The greater curve of the fundus is drained toward the splenic hilum, either directly by short gastric veins or by the left gastroepiploic vein. The greater curve of the antrum is drained by the right gastroepiploic vein, which drains into the superior mesenteric vein at the level of the inferior aspect of the head of the pancreas by means of the gastrocolic trunk. Portions of the right or left gastroepiploic vein are evident in many cases, and the mean size of this vessel is 3 mm, with 6 mm or more representing pathologic enlargement [2, 5-7]. A diameter of 5 mm has been reported as a threshold value for abnormality of the gastrocolic trunk [8]. Although large vascular structures are usually present in the splenic hilum, vessels greater than 4 mm in diameter at the margin of the spleen are suggestive of short gastric varices [2].

CT Appearance of Thrombosed Veins

The CT appearance of thrombosed portions of the portal venous system has been well described [7-12]. Thrombi are identified readily on contrast-enhanced CT scans by the presence of a low-attenuation intraluminal filling defect (Fig. 2). Frequently, a high-attenuation rim representing contrast enhancement of the vessel wall is seen (Fig. 3). It has been suggested that this enhancement is a pathophysiologic response to proliferation of the vasa vasorum [7, 13]. Others have noted that vessel wall enhancement is most likely always present, but obscured by the intraluminal contrast [10]. In either case, rim enhancement accentuates the presence of intraluminal clot. This finding is much more apparent in portions of the portal venous system surrounded by mesenteric fat than in segments surrounded by enhancing pancreatic or liver tissue [10]. Unenhanced CT scans are usually noncontributory. In one study, only four of 122 patients with portal venous thrombosis had clot identified on the unenhanced study [14]. These cases had intraluminal masses that were of increased attenuation when compared with flowing blood or soft tissue (Fig. 4). It is known that hematomas change over time, with the highest density clot seen in the first 72 hr after bleeding [15]. This observation about hyperdense fresh hematoma has been extended to thrombosis to suggest that a hyperdense intraluminal abnormality represents fresh thrombus [9, 11, 14]. Enlargement of the occluded portal vein segment also has been reported in portal venous thrombosis

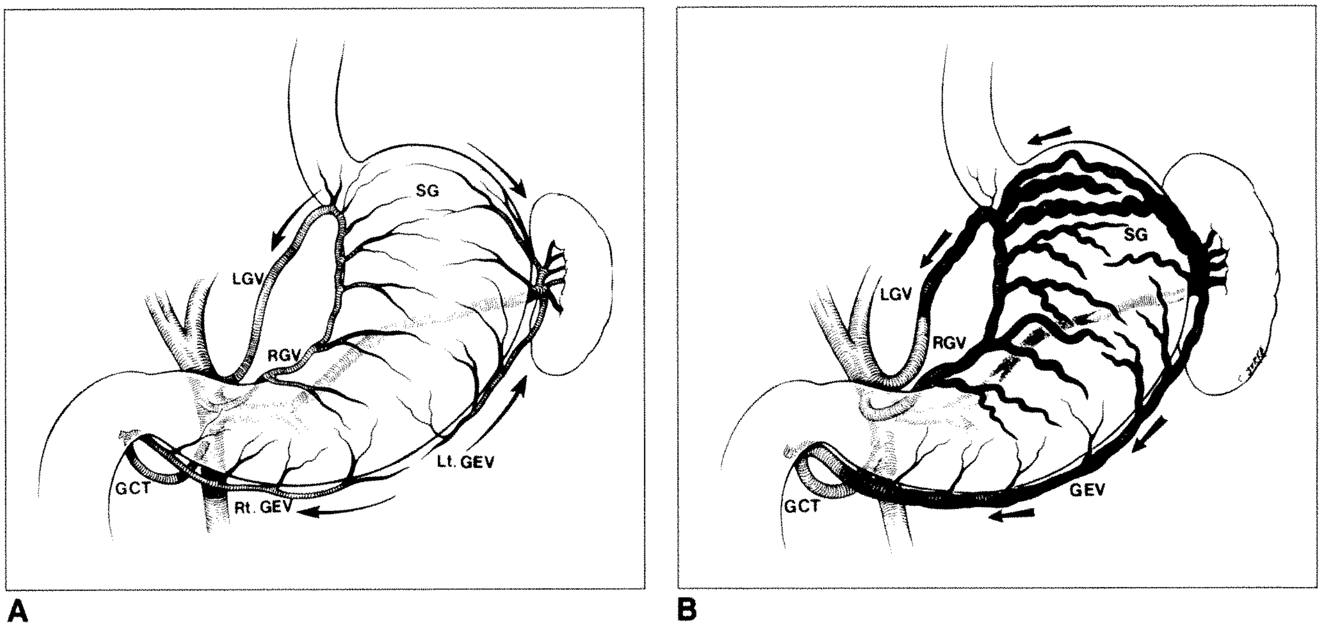

Fig. 1.—Portal venous drainage of stomach and spleen.

***A*, Normal venous drainage. Left gastric (coronary) and right gastric veins drain lesser curve of stomach. Short gastric veins drain fundus. Greater curve is drained either toward splenic hilum via left gastroepiploic vein or toward superior mesenteric vein via right gastroepiploic vein and gastrocolic trunk.**

***B*, Occlusion of splenic vein. Increased flow occurs through short gastric varices around fundus to coronary and right gastric veins, and along greater curve via gastroepiploic vein.**

SG = short gastric veins, LGV = left gastric vein, RGV = right gastric vein, GCT = gastrocolic trunk, Rt. GEV = right gastroepiploic vein, Lt. GEV = left gastroepiploic vein. Reprinted with permission from Marn et al. [2].

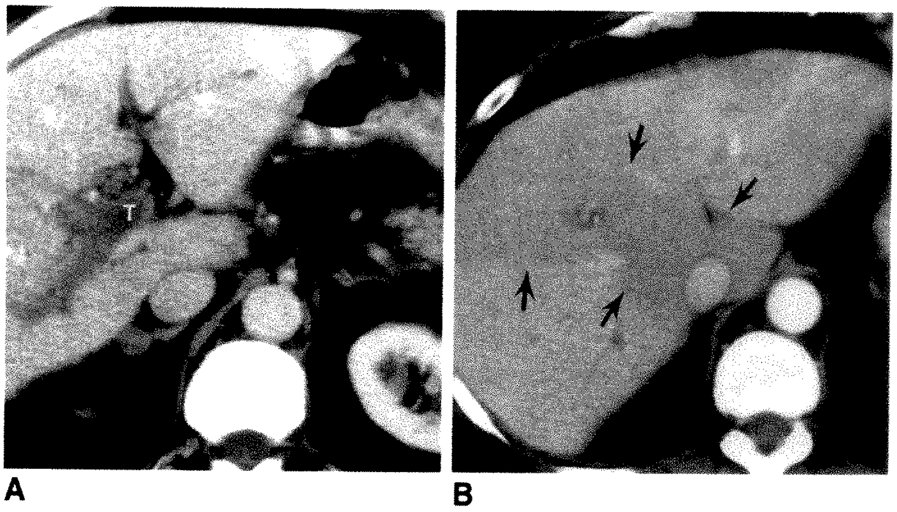

Fig. 2.—Portal venous thrombosis from diverticulitis.

A and *B*, Contrast-enhanced CT scans through level of main portal vein (*A*) and midportion of liver (*B*) show low-attenuation thrombus (T) filling central portions of portal vein. A band of low attenuation (*arrows* in *B*) representing decreased portal perfusion or fatty infiltration extends to dome of liver.

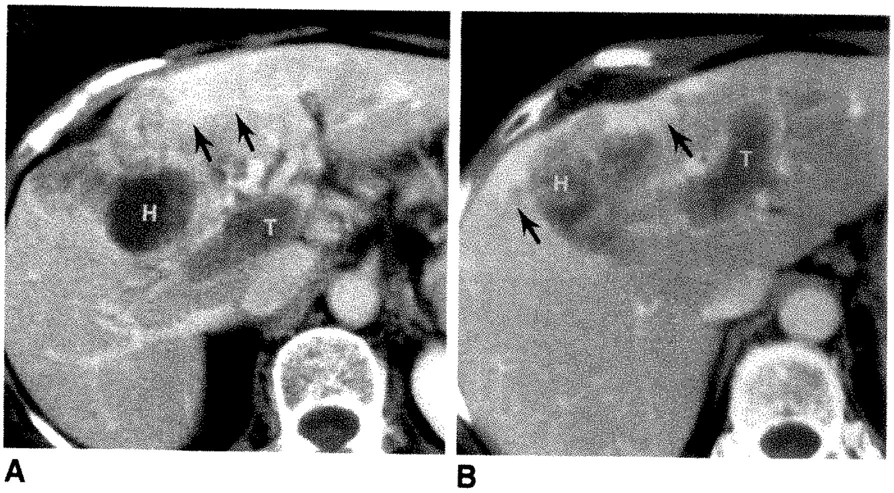

Fig. 3.—Hepatoma with portal venous thrombosis. Contrast-enhanced CT scans through level of main portal vein (*A*) and, more superiorly, through level of ascending segment of left portal vein (*B*) show a hepatoma (H) with an extensive tumor thrombus (T), which has spread from tumor into main and left portal veins. A band of increased contrast enhancement at periphery of lesion (*arrows*) is due to compensatory hepatic arterial flow in response to decreased portal flow.

[9]. This sign must be used with caution, however, because a wide range of normal values for size of various segments of the portal vein has been reported. Measurements of the portal vein change with position, respiration, and fasting, and portal hypertension alone without thrombosis can enlarge the portal vein [16]. Dilatation can be so great as to mimic other mass lesions, such as pancreatic pseudocysts [17].

The true sensitivity of contrast-enhanced CT scans for the detection of portal venous thrombosis is unknown. Igawa and colleagues [18] performed a study using drip infusion and reported a sensitivity of only 11% in 18 cases of thrombosis related to hepatocellular carcinoma (HCC). Another study from 1984, in which the presence of a positive imaging test was used to select patients for a comparison of sonography and CT in this disease, reported a CT sensitivity of 76% [7]. Other studies have properly avoided any attempt at calculation of sensitivity because of variable methods of selecting patients, small study size, or limitations in pathologic proof [12, 13, 19]. A larger study using current equipment and techniques is needed to fully address the issue of sensitivity. The specificity of contrast-enhanced CT for portal venous thrombosis is probably quite high. Numerous studies have made no reference to false-positive examinations [12, 13, 19]. One case of innumerable tiny calculi in the biliary system mimicking a calcified clot in the portal vein has been reported [17]. The same study reports a case of intrahepatic portal venous thrombosis mimicking biliary dilatation, and we also have observed one such case (Fig. 5).

Collateral Pathways in Segmental Occlusion

When segmental occlusion of the portal venous system occurs, local collateral pathways of flow arise spontaneously to bypass an obstruction. Two specific circumstances deserve mention: (a) cavernous transformation of the portal vein in response to thrombosis in the main portal vein and (b) perigastric collateral flow in response to occlusion of the splenic vein. Both these entities have specific appearances on contrast-enhanced CT scans. Recognition of these particular collateral patterns provides supporting evidence of the segmental occlusion and allows a more complete understanding of the patient's clinical status.

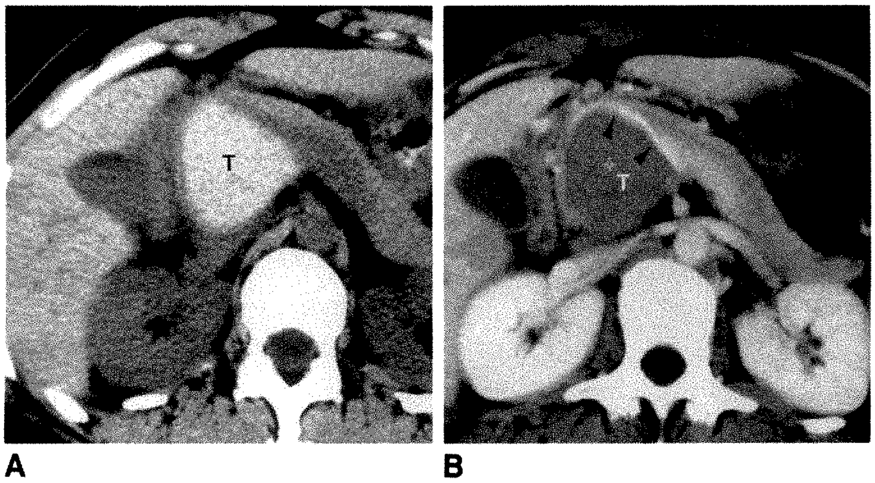

Fig. 4.—Acute thrombosis of aneurysm in portal vein.
A, Unenhanced CT scan shows high-attenuation thrombus (T), indicative of acute thrombosis.
B, CT scan during bolus administration of contrast medium shows flow at margin of thrombus (*arrowheads*).

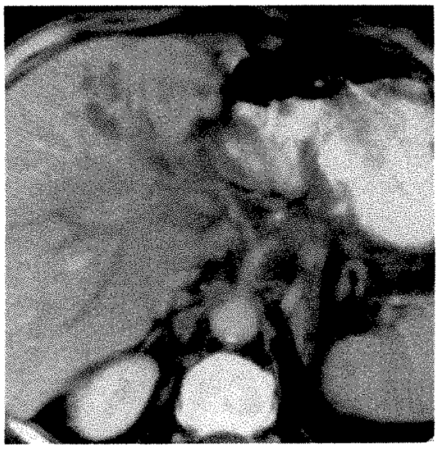

Fig. 5.—Contrast-enhanced CT scan in patient with pancreatic cancer with portal venous thrombosis mimicking biliary dilatation. Branching areas of decreased attenuation in liver were initially misinterpreted as representing dilated bile ducts. However, thrombosed portal venous system is not as low in attenuation as expected for fluid (bile), and that observation should lead to correct diagnosis of portal venous thrombosis.

Cavernous transformation of the portal vein (portal cavernoma) is defined as a masslike network of intertwined veins in the hepatoduodenal ligament and porta hepatis that provides an alternative pathway around a stenosed or occluded segment of the main portal vein or lobar branches [12, 20] (Fig. 6). Flow is maintained in the hepatopedal direction unless preexistent liver disease had already caused reversed flow [20]. The thrombosed portal segment is usually not seen, but is replaced by multiple enhancing smaller veins. This mass of abnormal vessels usually involves the main portal vein, but can extend into or be isolated to intrahepatic lobar branches [20].

Splenic venous occlusion leads to the development of well-known perigastric collateral venous pathways first defined by angiography [21, 22] (Fig. 1B). The diagnosis of splenic venous occlusion by angiography is made when all or a portion of the splenic vein is not visualized during the portal phase of a high-dose celiac injection despite the visualization of intrasplenic or splenic hilar veins and collateral vessels. These collateral vessels include gastric fundal (short gastric and coronary) varices, increased flow along the greater curve of the stomach via the gastroepiploic vein and the omental and inferior mesenteric veins [21, 22]. These same principles have been applied to CT scans in patients with splenic venous occlusion [2, 5, 6]. In most cases, the direct observation of dense contrast enhancement of the splenic vein during bolus contrast administration excludes the diagnosis of occlusion. As the splenic vein runs either parallel or slightly oblique to the axial scanning plane, occasionally a portion of the splenic vein is not well seen because of slice misregistration, motion, or distortion of the splenic vein by an adjacent mass. A careful search for the expected collateral vessels in splenic venous occlusion should then be performed. Fundal varices drain the splenic hilum with flow to the main portal vein through the coronary vein. The spleen is also drained by increased flow along the greater curve via a dilated gastroepiploic vein terminating in the gastrocolic trunk, which then drains into the superior mesenteric vein below the head of the pancreas. These observations require careful mapping over many images (Fig. 7), but can often be made with confidence unless the fat around the stomach is obliterated by pancreatitis or because of cachexia. This pattern is unique, and differentiating isolated splenic vein occlusion from generalized portal hypertension is usually possible [2]. A recent report indicates that acute pancreatic disease initially dilates only the gastroepiploic vein, while other collateral veins (short gastric, left gastric, or omental veins) tend to dilate in a chronic setting [5].

Alterations in Hepatic Attenuation Due to Portal Venous Obstruction

The normal liver derives 70–80% of its blood supply from the portal vein, with the remainder coming from the hepatic artery [23]. These two sources of blood differ in pressure and in content of oxygen and nutrients. Additionally, when contrast material is administered in a bolus during dynamic scanning, contrast-laden hepatic arterial blood directly from the aorta reaches the liver before contrast-laden portal venous blood, which must first pass through the capillary bed of the intestines and the sinusoids of the spleen. Therefore, a complex set of metabolic and vascular circumstances affect the density of the liver before, during, and after contrast administration.

Metabolic disturbances in the liver can alter the baseline hepatic attenuation before the administration of contrast me-

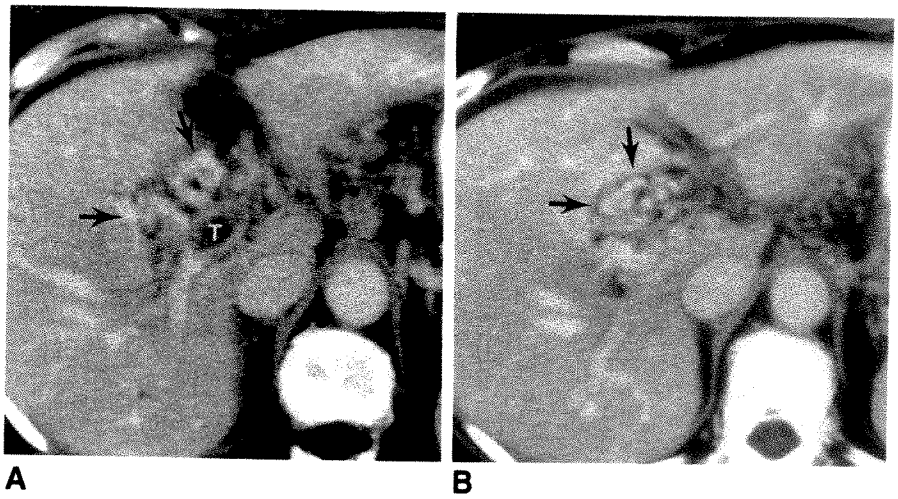

Fig. 6.—*A* and *B*, Contrast-enhanced CT scans obtained at (*A*) and immediately above (*B*) main portal vein in patient with cavernous transformation of portal vein. In this case, a thrombosed segment of main portal vein (T) is surrounded by collateral veins (*arrows*).

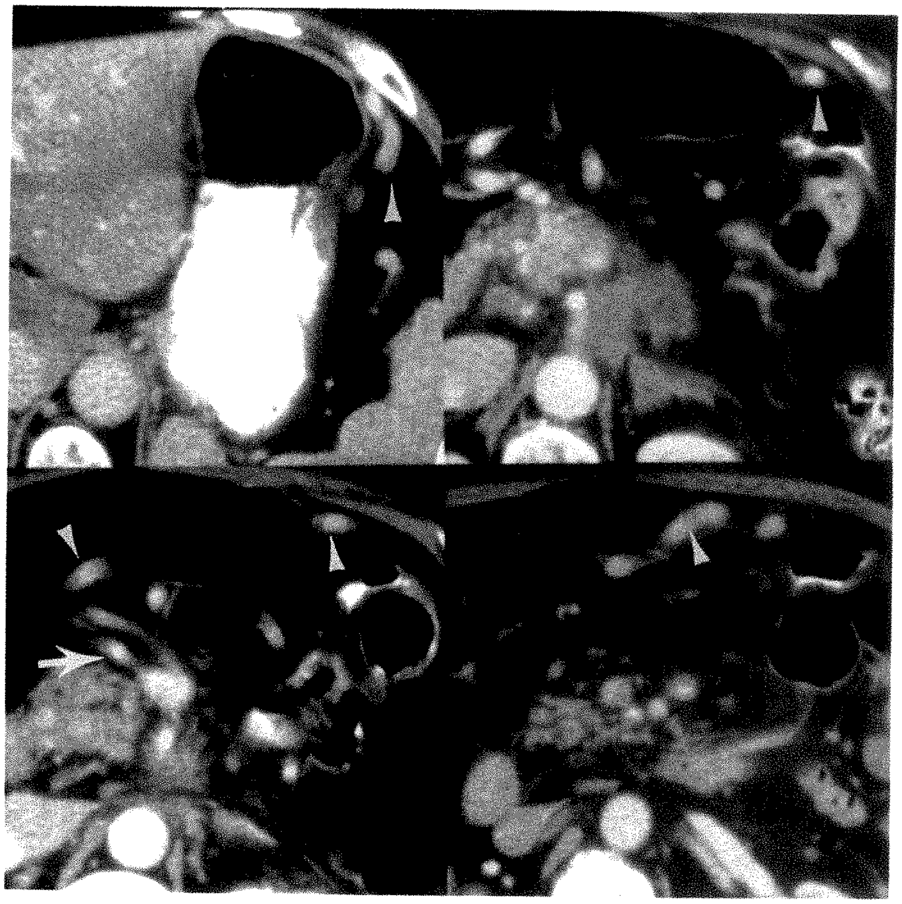

Fig. 7.—Perigastric collateral veins in splenic venous occlusion. Four noncontiguous contrast-enhanced CT scans show a large gastroepiploic vein (*arrowheads*) coursing along greater curve of stomach, terminating at superior mesenteric vein via gastrocolic trunk (*arrow*). See Fig. 1B for comparison.

dium. Because portal blood supplies absorbed nutrients to the liver, reduction of portal blood flow can alter liver density. In an animal experiment in which hepatic metabolism was altered through manipulations of diet and hormones, significant attenuation differences throughout the entire liver were reported between times when the liver was glycogen depleted and times when the liver was glycogen enriched [24]. The well-nourished, glycogen-rich liver is denser than the liver that is acutely depleted of glycogen. When chronic, glycogen depletion leads to increased deposition of fat within hepatocytes, and this effect further lowers the attenuation of nutrient-depleted liver [24]. These observations have been extended to explain low-attenuation, wedge-shaped defects on unenhanced CT scans of patients with segmental portal venous occlusion, because decreased portal flow might decrease glycogen storage in involved segments [25, 26].

These fixed, metabolic alterations provide a background against which transient changes in density during bolus contrast administration occur. A mechanical model has been advanced that explains the relationship of portal to arterial blood flow using the analogy of the interposition of a slower flowing stream (portal flow) in the path of a faster flowing stream (arterial flow) [27]. When the flow in the slower stream decreases, an increase in the flow of the faster stream occurs immediately. In patients with portal thrombosis [9] and cavernous transformation [20], increased arterial flow to portions of the liver deprived of portal venous flow can be seen in scans obtained early in the bolus administration of contrast material (Figs. 3B and 8). In the case of cavernous transformation, this enhancement occurs on the periphery of the liver, because the cavernoma most likely provides adequate flow only to the central portions of the liver [9]. More recent work with CT arterial portography provides further evidence of segmental portal ischemia in patients with focal hepatic masses [28]. In this technique, a catheter is placed via the transfemoral route into the superior mesenteric artery, and CT scans are obtained while contrast material injected in the superior mesenteric artery provides purely portal enhancement of the hepatic parenchyma. This procedure is used in limited circumstances for patients with potentially resectable liver lesions, usually colon cancer metastases or hepatoma, and is superior to routine contrast-enhanced CT in depicting the number of lesions and the relationship between the lesion and major hepatic blood vessels [29]. In more than one third of cases, a wedge-shaped defect with straight margins was evident, with tumor present at the apex of the defect (Fig. 9). Angiographic correlation proved that in most cases, stoppage of portal flow was responsible for this finding [27].

It is important to note that not every focal or segmental alteration in hepatic density or perfusion is due to an abnormality of the portal vein. Alterations in venous drainage caused by occlusion of hepatic veins (Budd-Chiari syndrome) [30] or alterations in hepatic arterial flow due to tumors [13, 31, 32] or simply focal fatty infiltration [33, 34] can produce segmental or subsegmental areas of decreased liver attenuation. In studies performed with CT arterial portography, it has been shown that not all perfusion defects are related to portal venous thrombosis or mass effect by tumor. Defects in contrast enhancement during arterial portography can be due to cirrhosis, nodular regeneration, siphoning of blood supply by vascular tumors, compression of vessels by tumor, or may occur with no known cause (Fig. 10) [35]. A well-defined oval or bandlike area of decreased attenuation in the posterior aspect of the medial segment of the left lobe is present in 14% of CT arterial portographic studies (Fig. 11) [36]. As this area is sometimes spared in fatty infiltration, it is

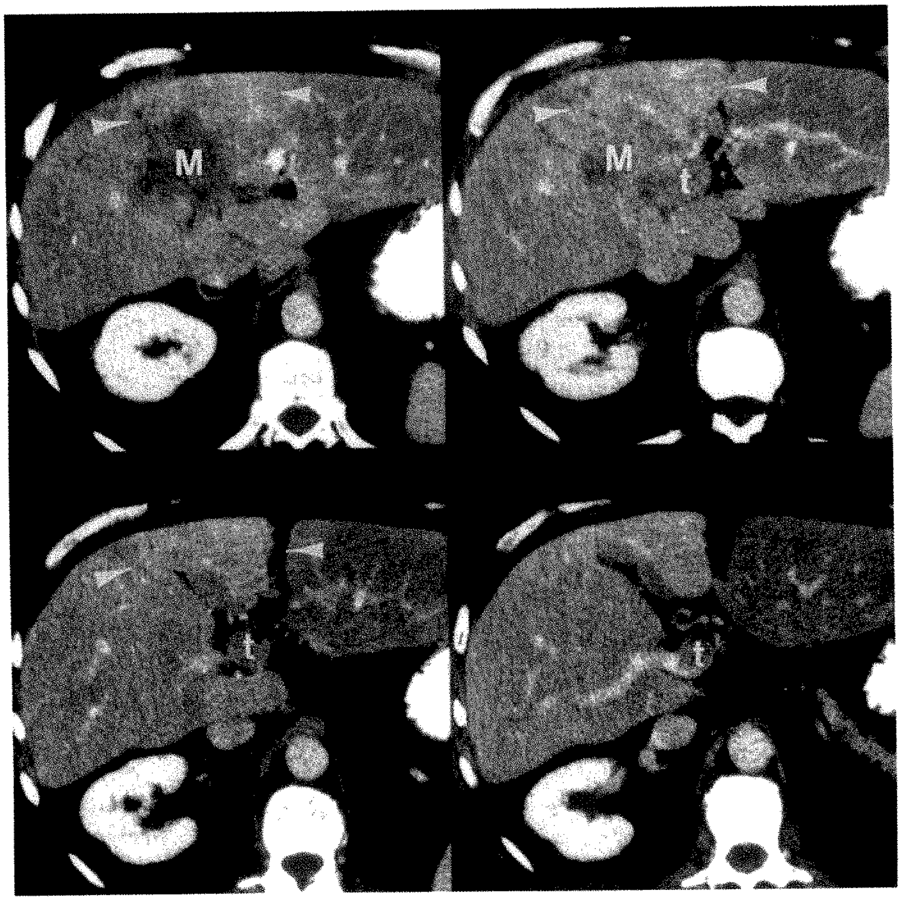

Fig. 8.—Colon cancer metastasis with portal venous thrombosis. Four contiguous CT scans show large metastasis (M) with an associated portal venous thrombus (t) that has a peripheral area of increased enhancement (*arrowheads*) early in bolus phase of study owing to compensatory increase in arterial flow.

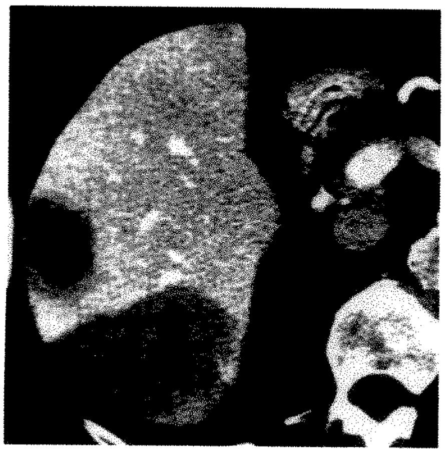

Fig. 9.—CT arterial portogram in patient with metastases from colon cancer. Two lesions are in right lobe of liver. Posterior lesion has straight margins, most likely because of interruption of portal venous flow.

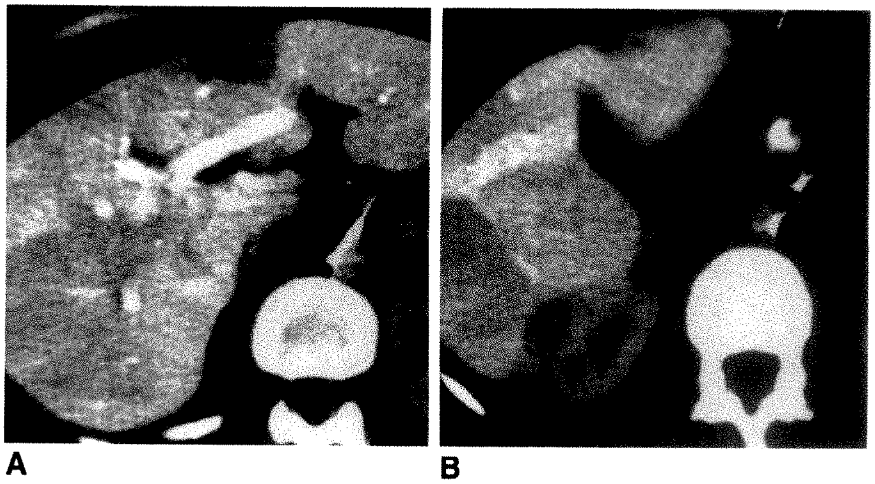

Fig. 10.—*A* and *B*, CT arterial portograms show patchy irregular areas of increased and decreased enhancement, which were artifactual in this case. Palpation and intraoperative sonography showed no lesions.

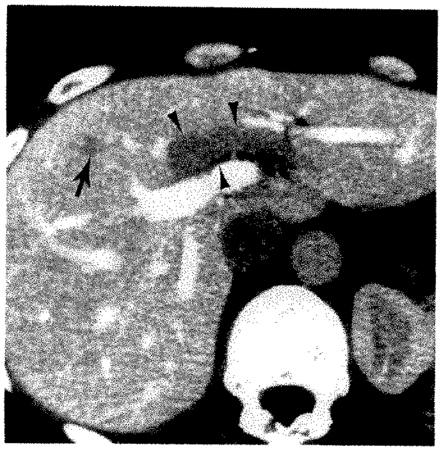

Fig. 11.—CT arterial portogram shows a well-defined ovoid pseudolesion (*arrowheads*) in posterior aspect of medial segment of left hepatic lobe, along with two small metastatic deposits (*arrows*).

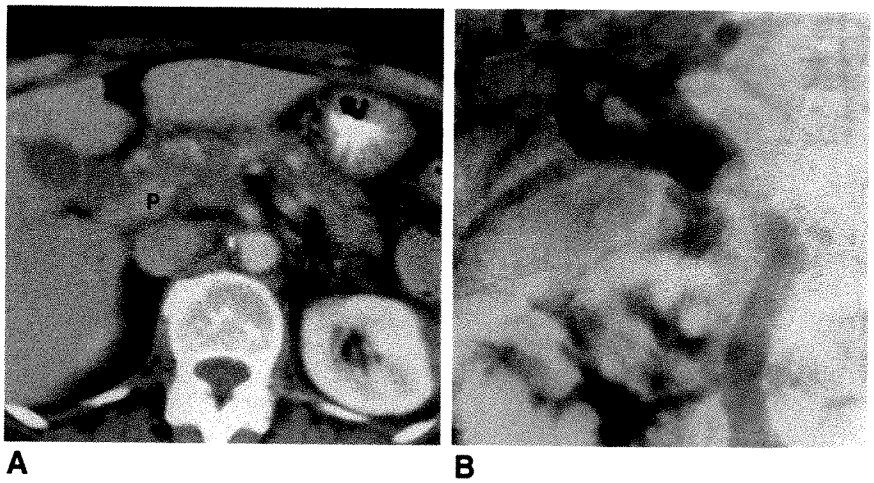

Fig. 12.—Pancreatic cancer.

A, CT scan shows vascular encasement with no collateral veins. A portion of main portal vein (P) is enhanced.

B, Angiogram of portal phase of superior mesenteric artery injection shows narrowing of main portal vein without occlusion.

postulated that some local variance in blood flow accounts for this abnormality [26, 35, 36].

Diseases Causing Segmental Occlusions of the Portal Venous System

Thrombi generally originate in the portion of the portal venous system nearest the diseased organ. HCC invades the portal venous system in the hepatic parenchyma, but often extends centrally into the main portal vein. Pancreatitis or pancreatic cancer often occludes the splenic vein along the pancreatic body, but thrombosis may propagate into the main portal vein or inferiorly into the superior mesenteric vein. These abnormalities therefore are grouped according to the portion of the portal venous system that they most commonly involve. Intrahepatic and main portal venous occlusions are usually caused by HCC, metastatic disease, and hepatic venocclusive disease (Budd-Chiari syndrome), and these are discussed first. Pancreatic cancer, pancreatitis, and splenectomy tend to predominate as causes of splenic venous occlusion, and these are discussed second. Septic thrombosis and coagulopathy can involve any portion of the portal venous system, and these are discussed last.

Hepatocellular Carcinoma

As the vast majority of HCCs are unresectable at the time of presentation, a careful preoperative clinical and imaging evaluation is necessary to select those patients who should undergo resection in the hope of surgical cure. The distribution of tumor within the liver must be carefully documented. Infiltrative or multifocal lesions are almost always unresectable, and any planned resection must not only be anatomically possible but also must leave the patient with adequate hepatic function. Extrahepatic metastatic disease with spread to nodal or peritoneal sites is common and also precludes resection. Clinical factors such as ascites, jaundice, cirrhosis, or liver failure also weigh in the decision to attempt resection. Invasion of the portal vein by tumor is a well-known manifestation of HCC, occurring in up to 70% of cases [13, 18, 19], and precludes surgery in two ways. First, involvement of the main portal vein by tumor makes resection impossible because no surgical technique allows for bypass of this critical structure [19]. Second, involvement of first or second branches of the portal vein adversely affects prognosis because of an increased risk of intrahepatic metastases (Fig. 3) [18].

The signs of portal venous involvement by HCC include an intraluminal filling defect, enlargement of the occluded segment, and the formation of a portal cavernoma, as stated earlier [13, 19]. Most thrombi in the portal venous system in patients with HCC are tumor thrombi and not bland thrombi [37]. In some instances, abnormal enhancement at the margin of the thrombus ("rail sign") or linear enhancement within the thrombus (corresponding to the angiographic "thread and streak" sign) provides further evidence of tumor thrombus [13]. The absence of these signs, however, does not mean that the thrombus is necessarily bland.

Large central thrombi in HCC are not the only manifestation of venous invasion by this tumor. The inferior vena cava and hepatic vein are sometimes invaded, but this occurs much less frequently. Smaller branches of the portal vein also can be involved and are imaged as punctate or linear low-attenuation foci adjacent to the lesion. These thrombi may be associated with rapid tumor growth and a poor clinical outcome if they occur in portal branches proximal to the tumor [38].

Abnormalities of liver attenuation both before and during contrast administration are common in HCC. Hepatic perfusion is altered by arteriovenous shunts within the tumor or shunts due to cirrhosis, along with portal venous compression or thrombosis. Abnormalities seen on unenhanced scans reflect local changes due to edema, glycogen depletion, and fatty infiltration, whereas abnormal enhancement during the bolus phase of contrast enhancement reflects changes in both arterial and portal flow (Fig. 3) [13, 25, 31, 32]. It is important to recognize these flow abnormalities, because they may lead to an overestimation of the size of the tumor and to selection of an inappropriate location for biopsy. Finally, it must be stressed that patients with cirrhosis and portal hypertension without hepatoma may have portal venous thrombosis, and the detection of a thrombosed portion of the portal vein does not necessarily imply the presence of a malignant tumor [10, 14].

Metastatic Disease

Although hepatic metastatic disease is far more common than HCC in Western countries, involvement of the portal vein is rarely shown by contrast-enhanced CT [39]. There is, however, a report of the Doppler sonographic identification of thrombi in the main, right, or left portal veins in eight of a series of 100 consecutive patients with hepatic metastatic disease [40]. Gastric and colonic cancers are the most common primary sources of hepatic metastases causing portal venous thrombosis, but cases of breast, ovarian, and bladder cancer also have been reported [39, 40].

Budd-Chiari Syndrome

Hepatic venous occlusion (Budd-Chiari syndrome) is uncommon and typically occurs with ascites, hepatomegaly, and abdominal pain. Jaundice, portal hypertension, variceal bleeding, and hepatic failure also are features of this disorder [41]. The causes of hepatic venous thrombosis include hypercoagulable states (polycythemia, leukemia, malignant tumors, or use of oral contraceptive pills) and mechanical obstruction (tumors or congenital webs), but up to two thirds of cases have no known cause [41]. The diagnosis is difficult to confirm and usually requires some combination of scintigraphy, CT, sonography, MR imaging, angiography, and biopsy for proof. The CT descriptions of this disorder have largely focused on the markedly abnormal pattern of hepatic enhancement, with dense early enhancement of the caudate lobe and portions of the left lobe [30, 41, 42]. In one report of four cases, three patients had thrombosis of intrahepatic branches of the portal vein, and one of those patients had extensive thrombosis of the main portal, splenic, and superior mesenteric veins [30]. As hepatic transplantation is now offered as one therapeutic option in these patients, portal venous thrombosis must be excluded because occlusion of the main portal vein complicates or precludes transplantation [43].

Pancreatic Cancer

Pancreatic cancer frequently becomes clinically apparent at an advanced, unresectable stage owing to local tumor extension, contiguous organ invasion, metastases to lymph nodes or liver, peritoneal carcinomatosis, and vascular involvement. In a series of 159 patients with proved pancreatic cancer [44], obstruction of the splenic vein with associated varices was present in 54 patients, and the superior mesenteric vein was obstructed in 15 cases. In this study, CT and angiography produced similar results in a vessel-to-vessel analysis for vascular encasement or occlusion. When all indicators of unresectability (arterial and venous involvement, local extension, and hepatic metastases) were used, 42 cases deemed unresectable by CT were proved unresectable at the time of surgery, whereas only three of nine cases judged resectable by CT were found to be resectable at surgery. Palliative biliary bypass did not improve the length of survival of patients with unresectable lesions. The authors conclude that angiography is not necessary for preoperative assessment and that CT alone is adequate for selecting patients for attempted resection [44]. CT can show extension of splenic or portal venous thrombosis from the pancreatic tumor with or without cavernous transformation (Fig. 6) or arterial and portal venous encasement without thrombosis (Fig. 12).

Pancreatitis

Pancreatitis in any form (acute, chronic, or complicated by abscess or pseudocyst) can have vascular complications, including portal, superior mesenteric, or splenic venous occlusion and formation of a pseudoaneurysm [2, 5, 10, 21, 22, 45, 46]. Venous occlusions are most likely due to spasm, stasis, intimal damage, and mass effect [2]. The splenic vein is very vulnerable to the effects of pancreatic inflammation because it is in direct contact with the body and tail of the pancreas over much of its course. In patients with pancreatitis, the direct visualization of a thrombosed splenic vein by CT may be difficult because of obliteration of retroperitoneal soft-tissue planes by inflammation, but the indirect evidence of splenic venous occlusion provided by the recognition of collateral flow through short gastric and gastroepiploic collateral vessels may be helpful [2]. Splenic venous occlusion can lead to bleeding gastric varices, and the differentiation of splenic venous occlusion from portal hypertension as the underlying cause is critical for selecting the appropriate surgical procedure to stop bleeding. Splenectomy usually cures bleeding from splenic venous occlusion, while a more complex procedure such as the formation of a portosystemic shunt is required to stop bleeding due to portal hypertension [2].

Septic Thrombosis

Along with pancreatitis, the portal venous system can become inflamed and thrombosed in the setting of portal bacteremia due to appendicitis, diverticulitis, inflammatory or ischemic bowel disease, cholecystitis, cholangitis, schistosomiasis, omphalitis, or sepsis [8, 20, 47–51]. In some cases, no intraabdominal process is present to explain the thrombosis, but the role of portal bacteremia is confirmed by the coexisting presence of pyogenic liver abscesses [49]. In the preantibiotic era, septic thrombosis of the portal venous system was often a fatal complication [47, 49]. However, aggressive antibiotic therapy has decreased the prevalence and severity of this entity [47, 49, 50]. Signs and symptoms are nonspecific and include fever, leukocytosis, and abdominal pain. Septic thrombosis of the portal venous system needs to be excluded in any patient in whom symptoms persist or worsen during treatment for sepsis or intraabdominal infection and inflammation. Likewise, a patient who has liver abscesses requires a careful evaluation of the portal venous system along with a search for an intraabdominal source of infection.

Miscellaneous Disorders

A wide variety of entities are occasionally seen in association with portal, splenic, or superior mesenteric venous thrombosis. Various forms of coagulopathy, including protein C deficiency, excessive factor VIII administration, and oral contraceptive use have been reported as causes of portal thrombosis [10, 49]. Although portal venous thrombosis can complicate any abdominal surgery, it is most commonly seen after splenectomy [7–9]. Hepatic arterial thrombosis is more common than portal venous thrombosis after liver transplantation [43].

Conclusions

Imaging of portal venous occlusions has been discussed in terms of the appearance of the occluded segment, the manifestations of occlusion in the development of collateral venous pathways, and the diseases that commonly lead to portal venous obstruction. The liver is affected by variations in portal venous flow, and CT scans in such patients reflect both metabolic changes and alterations in contrast enhancement. CT arterial portography is a sensitive method to show abnormalities in hepatic enhancement because this technique delivers contrast medium solely through the portal vein. Currently, Doppler sonography and CT are the main noninvasive imaging tools used for the detection of thrombosis of the mesenteric vasculature. However, MR is being used more often for this purpose [52–55] and also has been shown to be sensitive to hepatic parenchymal changes due to portal blood flow [56]. MR techniques are being developed to allow quantitative as well as qualitative assessment of portal venous flow.

REFERENCES

1. Foley WD. Dynamic hepatic CT. *Radiology* **1989**;170:617–622
2. Marn CS, Glazer GM, Williams DM, Francis IR. CT-angiographic correlation of collateral venous pathways in isolated splenic vein occlusion: new observations. *Radiology* **1990**;175:375–380
3. Little AG, Moossa AR. Gastrointestinal hemorrhage from left-sided portal hypertension. *Am J Surg* **1981**;141:153–158
4. Balfe DM, Mauro MA, Koehler RE, et al. Gastrohepatic ligament: normal and pathologic CT anatomy. *Radiology* **1984**;150:485–490
5. Moody AR, Poon PY. Gastroepiploic veins: CT appearance in pancreatic disease. *AJR* **1992**;158:779–783
6. Mori H, McGrath FP, Malone DE, Stevenson GW. The gastrocolic trunk and its tributaries: CT evaluation. *Radiology* **1992**;182:871–877
7. Subramanyam BR, Balthazar EJ, Lefleur RS, Horii SC, Hulnick DH. Portal venous thrombosis: correlative analysis of sonography, CT, and angiography. *Am J Gastroenterology* **1984**;10:773–776
8. Rosen A, Korobkin M, Silverman PM, Dunnick NR, Kelvin FM. Mesenteric vein thrombosis: CT identification. *AJR* **1984**;143:83–86
9. Mathieu D, Vasile N, Grenier P. Portal thrombosis: dynamic CT features and course. *Radiology* **1985**;154:737–741
10. Vogelzang RL, Gore RM, Anschuetz SL, Blei AT. Thrombosis of the splanchnic veins: CT diagnosis. *AJR* **1988**;150:93–96
11. Lee WB, Wong KP. CT demonstration of thrombosis of the portal venous system. *Australas Radiol* **1988**;32:360–364
12. Zirinsky K, Markisz JA, Rubenstein WA, et al. MR imaging of portal venous thrombosis: correlation with CT and sonography. *AJR* **1988**;150:283–288
13. Mathieu D, Grenier P, Larde D, Vasile N. Portal vein involvement in hepatocellular carcinoma: dynamic CT features. *Radiology* **1984**;152:127–132

14. Mori H, Hayashi K, Uetani M, Matsuoka Y, Iwao M, Maeda H. High-attenuation recent thrombus of the portal vein: CT demonstration and clinical significance. *Radiology* **1987**;163:353–356
15. Swensen SJ, McLeod RA, Stephens DH. CT of extracranial hemorrhage and hematomas. *AJR* **1984**;143:907–912
16. Goyal AK, Pokharna DS, Sharma SK. Ultrasonic measurements of portal vasculature in diagnosis of portal hypertension. *J Ultrasound Med* **1990**;9:45–48
17. Martin K, Balfe DM, Lee JKT. Computed tomography of portal vein thrombosis: unusual appearances and pitfalls in diagnosis. *J Comput Assist Tomogr* **1989**;13:811–816
18. Igawa S, Sakai K, Kinoshita H, Hirohashi K, Inoue T. Comparison of sonography, computed tomography, angiography, and percutaneous transhepatic portography in detection of portal tumor thrombus in hepatoma. *World J Surg* **1986**;10:876–883
19. LaBerge J, Laing F, Federle MP, Jeffrey RB, Lim RC. Hepatocellular carcinoma: assessment of resectability by computed tomography and ultrasound. *Radiology* **1984**;152:485–490
20. Mathieu D, Vasile N, Dibie C, Grenier P. Portal cavernoma: dynamic CT features and transient differences in hepatic attenuation. *Radiology* **1985**;154:743–748
21. Walter JF, Chuang VP, Bookstein JJ, Reuter SR, Cho KJ, Pulmano CM. Angiography of massive hemorrhage secondary to pancreatic disease. *Radiology* **1977**;124:337–342
22. Cho KJ, Martel W. Recognition of splenic vein occlusion. *Radiology* **1978**;131:439–443
23. Kadir S. *Diagnostic angiography*. Philadelphia: Saunders, **1986**:398–406
24. Dwyer A, Doppman JL, Adams AJ, Girton ME, Chernick SS, Cornblath M. Influence of glycogen on liver density: computed tomography from a metabolic perspective. *J Comput Assist Tomogr* **1983**;7:70–73
25. Doppman JL, Dwyer A, Vermess M, et al. Segmental hyperlucent defects in the liver. *J Comput Assist Tomogr* **1984**;8:50–57
26. Arai K, Matsui O, Takashima T, Ida M, Nishida Y. Focal spared areas in fatty liver caused by regional decreased portal flow. *AJR* **1988**;151:300–302
27. Ternberg JL, Bucher HR. Blood-flow relation between hepatic artery and portal vein. *Science* **1965**;150:1030–1031
28. Tyrrel RT, Kaufman SL, Bernardino ME. Straight line sign: appearance and significance during CT portography. *Radiology* **1989**;173:635–637
29. Heiken JP, Weyman PJ, Lee JKT, et al. Detection of focal hepatic masses: prospective evaluation with CT, delayed CT, CT during arterial portography, and MR imaging. *Radiology* **1989**;171:47–51
30. Vogelzang RL, Anschuetz SL, Gore RM. Budd-Chiari syndrome: CT observations. *Radiology* **1987**;163:329–333
31. Itai Y, Moss AA, Goldberg HI. Transient hepatic attenuation difference of lobar or segmental distribution detected by dynamic computed tomography. *Radiology* **1982**;144:835–839
32. Nishikawa J, Itai Y, Tasaka A. Lobar attenuation difference of the liver on computed tomography. *Radiology* **1981**;141:725–728
33. Baker MK, Wenker JC, Cockerill EM, Ellis JH. Focal fatty infiltration of the liver: diagnostic imaging. *RadioGraphics* **1985**;5:923–939
34. Marchal G, Tshibwabwa-Tumba E, Verbeken E, et al. Skip areas in hepatic steatosis: a sonographic-angiographic study. *Gastrointest Radiol* **1986**;11:151–157
35. Freeny PC, Marks WM. Hepatic perfusion abnormalities during CT angiography: detection and interpretation. *Radiology* **1986**;159:685–691
36. Fernandez MP, Bernardino ME. Hepatic pseudolesion: appearance of focal low attenuation in the medial segment of the left lobe at CT arterial portography. *Radiology* **1991**;181:809–812
37. Lim RC, Bongard FS. Hepatocellular carcinoma: changing concepts in diagnosis and management. *Arch Surg* **1984**;119:637–642
38. Imaeda T, Yamawaki Y, Hirota K, Suzuki M, Seki M, Doi H. Tumor thrombus in the branches of the distal portal vein: CT demonstration. *J Comput Assist Tomogr* **1989**;13:262–268
39. Araki T, Suka K, Sekikawa T, Ishii Y, Hihara T, Kachi K. Portal venous tumor thrombosis associated with gastric adenocarcinoma. *Radiology* **1990**;174:811–814
40. Atri M, de Stempel J, Bret PM, Illescas FF. Incidence of portal vein thrombosis complicating liver metastasis as detected by duplex ultrasound. *Ultrasound J Med* **1990**;9:285–289
41. Murphy FB, Steinberg HV, Shires GT III, Martin LG, Bernardino ME. The Budd-Chiari syndrome: a review. *AJR* **1986**;147:9–15
42. Harter LP, Gross BH, St. Hilaire J, Filly RA, Goldberg HI. CT and sonographic appearance of hepatic vein obstruction. *AJR* **1982**;139:176–178
43. Zajko AB, Bron KM, Starzl TE, et al. Angiography of liver transplantation patients. *Radiology* **1985**;157:305–311
44. Freeny PC, Marks WM, Ryan JA, Traverso LW. Pancreatic ductal adenocarcinoma: diagnosis and staging with dynamic CT. *Radiology* **1988**;166:125–133
45. Rice RP, Thompson WM, Kelvin FM, Kriner AF, Garbutt JT. Gastric varices without esophageal varices. *JAMA* **1977**;18:1976–1979
46. Matos C, Van Gansbeke D, Zalcman M, Ansay J. Mesenteric vein thrombosis: early CT and US diagnosis and conservative management. *Gastrointest Radiol* **1986**;11:322–325
47. Harch JM, Radin RD, Yellin AE, Donovan AJ. Pylethrombosis. *Arch Surg* **1987**;122:1116–1119
48. Chan SCH, Chan F, Chau EMT, Mok FPT. Portal thrombosis complicating appendicitis: ultrasound detection and hepatic computed tomography lobar attenuation alteration. *J Comput Assist Tomogr* **1988**;21:208–210
49. Lim GM, Jeffrey RB, Ralls PW, Marn CS. Septic thrombosis of the portal vein: CT and clinical observations. *J Comput Assist Tomogr* **1989**;13:656–658
50. Slovis TL, Haller JO, Cohen HL, Berdon WE, Watts FB. Complicated appendiceal inflammatory disease in children: pylephlebitis and liver abscess. *Radiology* **1989**;171:823–825
51. Castillo M, Murphy B. Septic portal vein thrombophlebitis: computed tomography appearance. *Comput Radiol* **1986**;10:289–292
52. Levy HM, Newhouse JH. MR imaging of portal vein thrombosis. *AJR* **1988**;151:283–286
53. Zirinsky K, Markisz JA, Rubenstein WA, et al. MR imaging of portal venous thrombosis: correlation with CT and sonography. *AJR* **1988**;150:283–288
54. Edelman RR, Zhao B, Liu C, et al. MR angiography and dynamic flow evaluation of the portal venous system. *AJR* **1989**;153:755–760
55. Tamada T, Moriyasu F, Ono S, et al. Portal blood flow: measurement with MR imaging. *Radiology* **1989**;173:639–644
56. Itai Y, Ohtomo K, Kokubo T, Okada Y, Yamauchi T, Yoshida H. Segmental intensity differences in the liver on MR images: a sign of intrahepatic portal flow stoppage. *Radiology* **1988**;167:17–19

Detection of Malignant Tumors in End-Stage Cirrhotic Livers: Efficacy of Sonography as a Screening Technique

Gerald D. Dodd III[1]
William J. Miller
Richard L. Baron
M. Leon Skolnick
William L. Campbell

OBJECTIVE. Patients with hepatic cirrhosis are at an increased risk of developing primary malignant tumors of the liver. If these tumors are discovered early, current therapies may be curative. We conducted a prospective study to assess the accuracy of sonographic screening for the detection of malignant tumors in cirrhotic livers as determined by correlation with resected whole livers.

SUBJECTS AND METHODS. A total of 200 prospectively interpreted preoperative sonograms from 200 patients with cirrhosis who underwent hepatic transplantation were correlated with specimens of freshly resected whole livers. The results were analyzed to determine the sensitivity and specificity of sonography in identifying patients with malignant tumors and detecting individual tumors in each patient.

RESULTS. Pathologic examination showed 80 malignant lesions in 34 patients (28 with hepatocellular carcinoma, three with cholangiocarcinoma, two with metastases, and one with non-Hodgkin's lymphoma) and three hemangiomas in two patients. Sonography correctly showed malignant tumors in 17 of the 34 patients, for a sensitivity of 50%. Sonograms were false-positive for malignant tumors in three patients, two of whom had a total of three hemangiomas. Sonography correctly showed 36 of the 80 malignant lesions, for a lesion sensitivity of 45% and specificity of 98%. Of the 44 missed lesions, 24 were 1 cm or less, 12 were between 1 and 3 cm, and eight were more than 3 cm in diameter.

CONCLUSION. Our results show that sonography is highly insensitive in the detection of malignant lesions in end-stage cirrhotic livers and thus is not a reliable screening technique. However, because of sonography's very high specificity, any sonographically identified lesion in a cirrhotic liver should be considered malignant until proved otherwise.

AJR 159:727–733, October 1992

Patients with hepatic cirrhosis are at a much greater risk of developing primary malignant tumors of the liver than is the general population [1]. If these tumors are detected early, current therapies such as hepatic resection, transplantation, or intraarterial chemotherapy and embolization offer the possibility of cure [2–5]. The early detection of these tumors is heavily dependent on hepatic imaging. However, the detection rate of hepatic tumors varies with the type of imaging technique [6–16]. While many investigations have evaluated the accuracy of the different imaging techniques in the detection of hepatic malignant tumors, inherent limitations in investigational design such as small patient populations, limited pathologic correlation, retrospective reviews, or nonscreening protocols with biases in selection of patients have produced widely varying results. One technique in particular, sonography, has at different times been reported as both an excellent and a poor imaging technique for the detection of hepatic tumors [14–16]. Our own clinical experience with sonographic screening of cirrhotic livers has yielded results far below those of recent optimistic studies. Given the importance of accurate sensitivity data, the limitations of the previous studies, and a unique opportunity at our institution to perform high-volume correlation of pretransplantation hepatic imaging with resected

Received March 20, 1992; accepted after revision April 20, 1992.

Presented at the annual meeting of the Society of Gastrointestinal Radiologists, Orlando, FL, February 1992, where it received the Memorial Award.

[1] All authors: Department of Radiology, Presbyterian University Hospital, DeSoto at O'Hara Sts., Pittsburgh, PA 15213.

0361-803X/92/1594-0727

© American Roentgen Ray Society

total hepatectomy specimens, we designed a prospective study to determine the accuracy of sonography in detecting malignant tumors in the cirrhotic liver.

Subjects and Methods

From July 1990 to November 1991, all patients undergoing evaluation for potential hepatic transplantation at our institution were entered into a prospective sonographic screening study focused on the detection of hepatic malignant tumors. All patients in the study had hepatic sonograms obtained before transplantation. In the patients who underwent subsequent hepatic transplantation, the sonographic results were directly correlated with the resected total hepatectomy specimens. For this report we evaluated the sonographic-pathologic correlative results from 200 transplant recipients with histologically proved hepatic cirrhosis. These 200 patients consisted of 122 men and 78 women, nine Asians and 191 non-Asians. Their ages ranged from 18 to 74 years (mean, 49 years). The time from sonography to transplantation varied from 1 to 343 days (mean, 63 days), with 86% of the sonograms obtained within 120 days. Biochemical assays, alpha-fetoprotein (AFP) [17] and des-gamma-carboxy-prothrombin (DCP or PIVKA II) [18], obtained as part of the pretransplantation screening process, were compared with sonography for sensitivity in identifying patients with hepatocellular carcinoma (HCC).

Each screening sonogram consisted of preliminary scanning of the liver by one of seven technologists. The livers were scanned according to protocol in both transverse and longitudinal planes with anterior and lateral intercostal and subcostal probe placement. The protocol included hard-film documentation of the liver in sequential transverse images from the dome to the caudal tip of the right lobe and sequential longitudinal images from the extreme right to the extreme left margin of the liver. All scans were obtained with similar sonographic equipment (Acuson Corp., Mountain View, CA) using 2.5- or 3.5-MHz phased-sector transducers. The technologist's results were reviewed with a staff radiologist. As per standard procedure at our institution, approximately 65% of the patients were rescanned by a radiologist for either clarification of the technologist's results or quality control. Approximately 90% of the sonograms were interpreted by two radiologists specializing in sonography. The remaining sonograms were interpreted by four radiologists from the division of abdominal imaging who routinely attend in the ultrasound service. The results of the sonograms, including the presence, number, size, and character of all abnormalities, were recorded on protocol sheets. The exact location and approximate configuration of each lesion were sketched on standardized axial diagrams of the liver to facilitate accurate correlation of the sonographic results with the resected specimens.

The sonographic criteria for the diagnosis of a possible malignant tumor consisted of identification of a discrete focal mass distinguishable from the adjacent hepatic parenchyma or a poorly marginated, focal region of heterogeneous echogenicity. Both types of abnormalities were interpreted as suggestive of malignancy regardless of their intrinsic echogenicity. Diffuse heterogeneous echogenicity was attributed to cirrhosis rather than tumor unless it was associated with mass effect on, or thrombosis of, the intrahepatic vessels. The only focal lesions considered benign and excluded from the study were those meeting the strict criteria for simple cysts.

At the time of transplantation, the results of the pretransplantation sonograms were directly correlated with serially sectioned fresh total hepatectomy specimens. For ease of correlation, all livers were sliced in the transverse plane at 1-cm intervals. Lesions were matched by location and size. Each sonographically identified lesion was either confirmed or refuted on the basis of pathologic findings. Sonographically missed lesions were recorded. Statistical analysis was performed to determine the sensitivity and specificity of sonography in identifying individual patients with tumor and detecting individual tumors in each patient. In patients with more than one tumor, each lesion up to a total of six was counted for statistical analysis. Patients with more than six lesions (eight patients) were counted as having only six lesions because of the inherent difficulties in accurately documenting excessive numbers of lesions in the same liver and to prevent one particular type (appearance) of lesion from significantly biasing the sensitivity results. In patients with pathologically proved tumor, the sonographic character (echo intensity and heterogeneity) of the liver parenchyma and visualized tumors was analyzed to determine the effect of echogenic patterns on tumor detection.

Although every attempt was made to perform screening sonography without knowledge of the possible presence of tumor (from other clinical or imaging results), because of the necessary interaction with the patients and referring clinicians, it was impossible to ensure a completely blinded study in this regard.

Results

At pathology, 34 of the 200 patients were discovered to have hepatic malignant tumors; 28 had HCC, three had cholangiocarcinomas, two had metastases, and one had non-Hodgkin's lymphoma. A total of 80 discrete tumor nodules were found in the 34 patients. In addition, two other patients

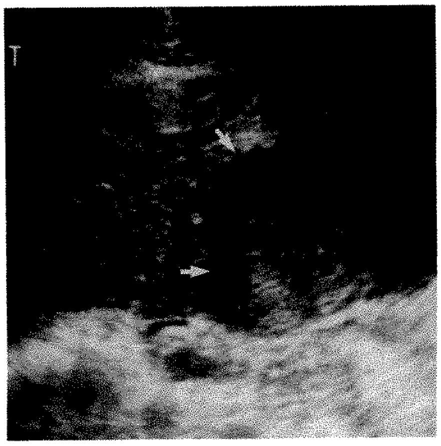

1

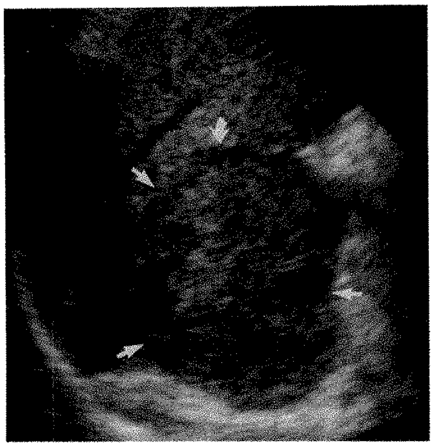

2

Fig. 1.—Hypoechoic hepatocellular carcinoma (HCC). Longitudinal sonogram through right hepatic lobe shows a large, easily seen, hypoechoic HCC tumor mass (*arrows*).

Fig. 2.—Isoechoic hepatocellular carcinoma (HCC). Longitudinal sonogram through right hepatic lobe shows a large isoechoic HCC tumor mass (*straight arrows*) that is primarily visible because of a thin hypoechoic halo (*curved arrow*). Note mildly coarse echo texture of hepatic parenchyma.

had a total of three cavernous hemangiomas. Of the 28 patients with HCC, the biochemical assays for HCC and for AFP and PIVKA II showed elevated levels in 36% (10/28) and 42% (11/26) of patients tested, respectively. The combined sensitivity of both assays for the detection of the patients with HCC was 57% (16/28). The overall prevalence of HCC in our study population of patients with cirrhosis was higher than the 5-10% commonly reported for this group because of a high referral rate of patients with HCC to our institution [14].

Only 17 of the 34 patients with malignant tumors and 36 of the 80 malignant nodules were identified with sonography, resulting in a detection sensitivity for patients and individual tumor nodules of 50% and 45%, respectively. Twelve of the 28 patients with HCC and 29 of 69 HCC tumor nodules were identified sonographically, giving a detection sensitivity for patients and individual tumor nodules of 43% and 42%, respectively. Of the total 36 sonographically shown malignant lesions, 34 appeared as discrete focal masses and two as poorly marginated focal regions of heterogeneity. The sonographically discrete tumor nodules varied in size, with 10 being 1 cm or less, nine between 1 and 3 cm, and 15 more than 3 cm in diameter. The echogenicity of the discrete lesions also varied, with 24 appearing hypoechoic, five isoechoic with either a hypoechoic or hyperechoic halo, and five hyperechoic relative to the cirrhotic hepatic parenchymal echogenicity (Figs. 1-4). The two tumors that appeared as poorly marginated focal regions of heterogeneity were proved pathologically to be diffusely infiltrating HCC (Figs. 5 and 6). The three hemangiomas appeared sonographically as discrete 1-4 cm masses, with two appearing heterogeneously echogenic and the third hyperechoic with a hypoechoic halo (Fig. 7). Because of overlap in the sonographic appearance of the hemangiomas and hepatic malignant tumors, the hemangiomas were prospectively falsely interpreted as potentially malignant. In addition, in one patient a focal region of heterogeneity was falsely interpreted as a malignant tumor. At pathology, no explanation for the focal abnormality could be identified. Statistical evaluation of the number of false-positive interpretations produced a patient and lesion specificity for malignancy of 98%.

Of the 44 sonographically missed lesions, 24 were 1 cm or less, 12 were between 1 and 3 cm, and 8 were greater than 3 cm in diameter. The largest missed lesion was 10 cm in

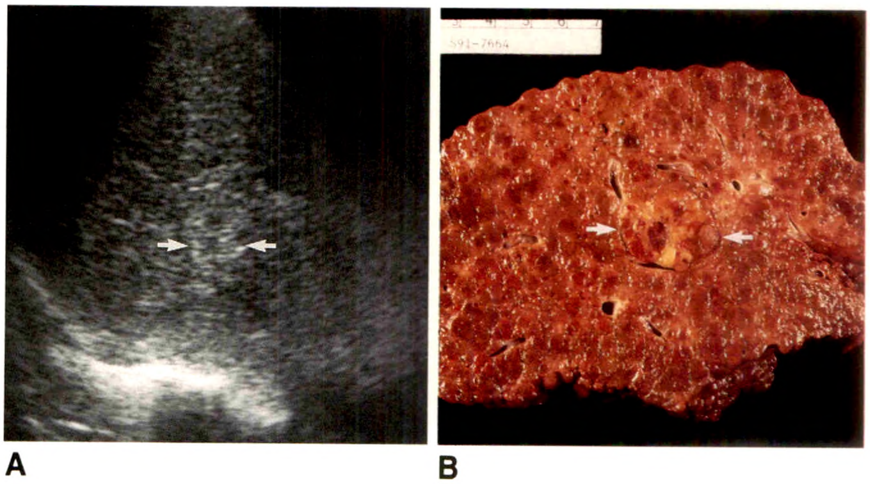

Fig. 3.—Hyperechoic hepatocellular carcinoma (HCC).

A, Transverse sonogram through dome of right hepatic lobe shows a 3-cm hyperechoic nodule (*arrows*).

B, Corresponding hepatic specimen shows mass to be an HCC tumor nodule (*arrows*).

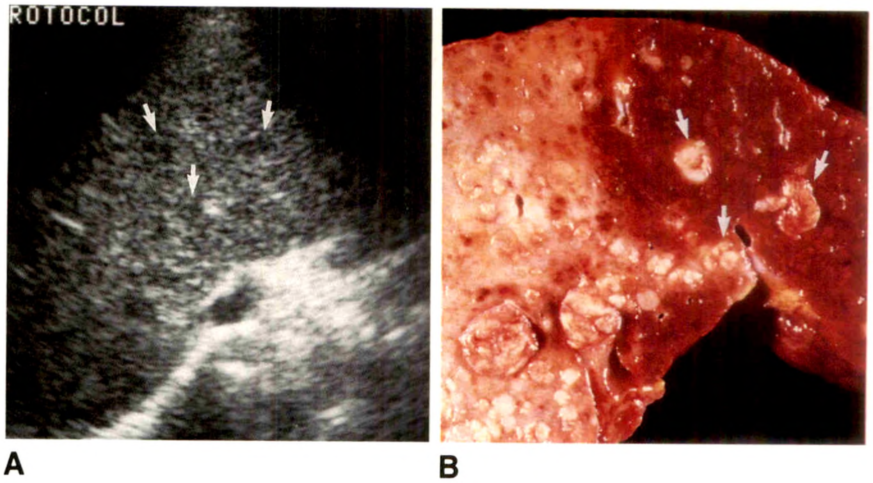

Fig. 4.—Multiple small hypoechoic hepatocellular carcinoma (HCC) tumor nodules.

A, Transverse sonogram through left hepatic lobe shows multiple subtle hypoechoic nodules (*arrows*) 1 cm or less in diameter in a moderately coarse hepatic parenchyma.

B, Corresponding hepatic specimen shows small nodules (*arrows*) to be foci of HCC and also shows a massive HCC tumor in right lobe that was poorly shown by sonography. Note multiple small regenerative nodules in nontumorous parenchyma.

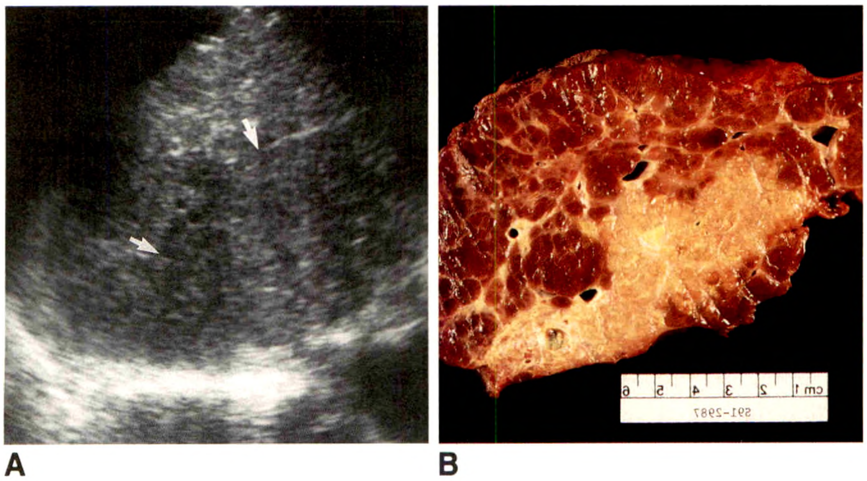

Fig. 5.—Poorly defined hepatocellular carcinoma (HCC) tumor mass.

***A*, Transverse sonogram of right hepatic lobe shows a large posterior, poorly marginated hypoechoic region (*arrows*). Note severe heterogeneity of anterior hepatic parenchyma.**

***B*, Corresponding hepatic specimen shows hypoechoic region to be a diffusely infiltrating HCC. Marked distortion of nontumorous hepatic parenchymal architecture is due to multiple large regenerative nodules and fibrosis.**

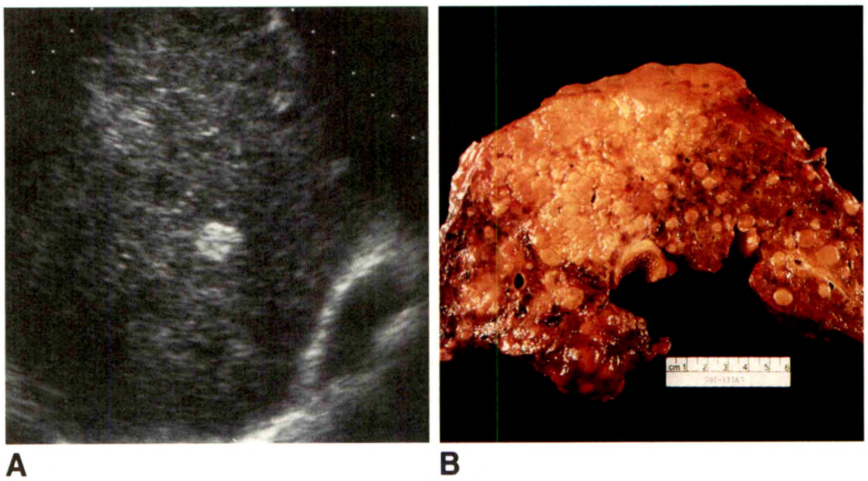

Fig. 6.—Diffusely infiltrating hepatocellular carcinoma (HCC).

***A*, Transverse sonogram of right hepatic lobe shows a diffusely coarse hepatic parenchymal echogenicity that lacks definable margins. Except for one focal hyperechoic nodule present, echo texture is quite similar to that frequently seen in macronodular end-stage cirrhotic livers.**

***B*, Corresponding hepatic specimens shows right hepatic lobe to be almost completely replaced by HCC.**

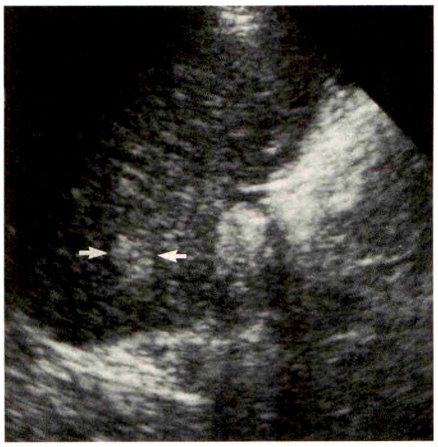

Fig. 7.—Cavernous hemangioma. Longitudinal sonogram through right hepatic lobe shows a focal 2-cm hyperechoic nodule (*arrows*) with a partial hypoechoic halo that was pathologically proved to be a cavernous hemangioma. Note similarity in appearance between this nodule and hepatocellular carcinoma nodule in Fig. 3.

diameter and located in the dome of the right lobe. The remaining missed lesions were randomly distributed throughout the liver without predilection for a specific region.

The hepatic parenchyma in the 34 patients with malignant tumors was hyperechoic in all cases. However, the echo texture of the hepatic parenchyma varied, with seven of the livers exhibiting a mildly coarse, 13 a moderately coarse, and 14 a severely coarse echo texture (Figs. 8–10). In 21 of 26 patients in whom tumor was partially or completely missed, the hepatic parenchyma exhibited either a moderately or severely coarse echo texture (Fig. 11). In six of eight patients in whom sonography showed all tumor nodules, the hepatic parenchymal echo texture was either mildly or moderately coarse. Correlation of the hepatic parenchymal echo texture with the gross pathologic liver specimens revealed that 21 of 27 patients with moderately or severely coarse hepatic parenchymal echo texture had either macronodular or mixed macro-micronodular cirrhosis with regenerative nodules measuring up to 2 cm in diameter.

Discussion

Early detection of malignant tumors arising in the cirrhotic liver requires a comprehensive screening program that uses both biochemical assays and hepatic imaging. Both techniques are necessary because neither technique is 100% sensitive and each can be used to identify patients with malignant tumors that the other missed. The two biochemical assays for HCC, AFP and PIVKA II, even when used in combination, may fail to identify 30% or more of patients with tumors [17, 18]. In patients with small HCC tumors (less than 5 cm), the results may be worse, with tumor detection sensitivities of AFP reported as low as 16% [11]. The sensitivity of hepatic imaging in the detection of liver tumors depends

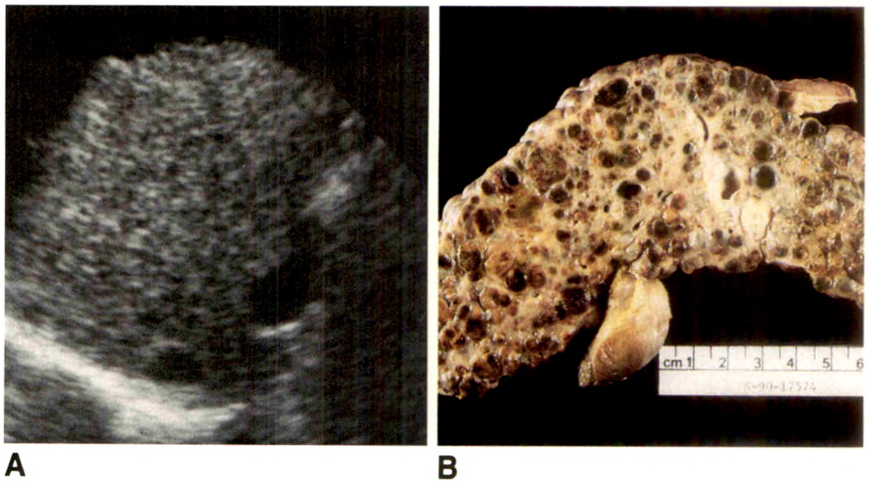

Fig. 8.—Advanced macronodular cirrhosis causing a severely coarse hepatic parenchymal echo texture.

***A*, Transverse sonogram through right hepatic lobe shows a diffuse, severely coarse echo texture of hepatic parenchyma not dissimilar from echogenicity of tumor present in Figs. 5 and 6.**

***B*, Corresponding hepatic specimen shows changes of severe macronodular cirrhosis with multiple regenerative nodules up to 2 cm in diameter. In a liver this cirrhotic, it would be exceedingly difficult to differentiate small malignant nodules from regenerative nodules.**

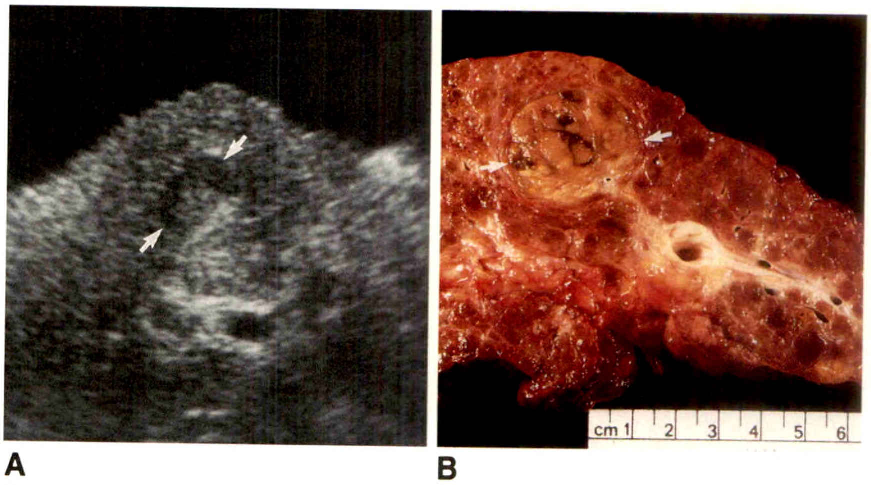

Fig. 9.—Subtle 3-cm hepatocellular carcinoma (HCC) tumor nodule in a macronodular cirrhotic liver.

***A*, Transverse sonogram through left hepatic lobe shows a subtle 3-cm hypoechoic nodule (*arrows*) that is difficult to differentiate from moderately coarse hepatic parenchymal echogenicity.**

***B*, Corresponding hepatic specimen shows hypoechoic nodule to be a discrete HCC tumor nodule (*arrows*) surrounded by numerous moderate-sized regenerative nodules.**

on the technique used. Although the more invasive techniques—intraoperative sonography, CT during arterial portography, CT during hepatic arteriography, and CT after intraarterial injection of lipiodol—are generally considered the most sensitive for hepatic tumor detection, their invasive nature limits their widespread use in screening [6–16]. Of the noninvasive techniques (transabdominal sonography, conventional dynamic bolus enhanced CT, and MR imaging) transabdominal sonography, owing to its global availability and limited expense, has received considerable attention as a tumor-screening technique.

The accuracy of transabdominal sonography in the detection of HCC in the cirrhotic liver has been investigated by several research groups [11, 14, 15]. The most recent investigation [15] found sonography capable of showing 84% of HCC tumor nodules (3 cm or smaller) occurring in 100 patients with HCC and hepatic cirrhosis. These results are remarkably better than ours; however, significant differences in investigational methods and populations of patients likely account for the disparity in results. Our investigational methods differed from those of Takayasu et al. [15] in that our study was prospective, was executed as a screening study that included patients with and without tumor, used interpretations predominantly blinded to the results of other imaging tests, and was based on pathologic correlation with the entire resected liver. The potential effect of these differences was to limit the sensitivity of sonography in our study and falsely elevate the sensitivity reported by Takayasu et al. For example, retrospective, nonscreening and nonblinded studies, through prior knowledge of the presence or location of a tumor, can significantly lower the interpretive threshold for calling a subtle abnormality suggestive of malignancy. Additionally, incomplete pathologic correlation can lead to false elevation of the sensitivity of a technique because of the failure to recognize and include in statistical analysis small incidental tumors undetectable except by complete specimen dissection.

An additional and significant difference between our study and that of Takayasu et al. [15] is the population of patients. Our patients were primarily North American and non-Asian, whereas the patients studied by Takayasu et al. were exclusively Asian. This difference in patients likely resulted in a significant difference in body habitus between the two studies, with our patients being larger and more difficult to penetrate sonographically. Hence, body type may have affected tumor detection. Furthermore, Takayasu et al. examined patients with either precirrhosis or cirrhosis, while our evaluation was

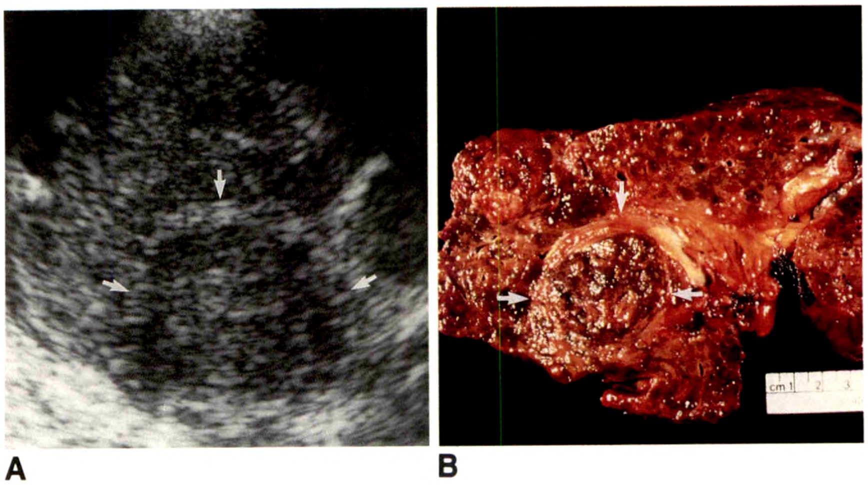

Fig. 10.—Large hepatocellular carcinoma (HCC) tumor mass in a macronodular cirrhotic liver.

A, Transverse sonogram through right hepatic lobe shows a large heterogeneous mass (*arrows*) that, except for presence of an echogenic rim, is difficult to differentiate from marked heterogeneity of remaining hepatic parenchyma.

B, Corresponding hepatic specimen shows an HCC tumor mass (*arrows*) that even at gross examination is difficult to differentiate from markedly distorted macronodular cirrhotic parenchyma.

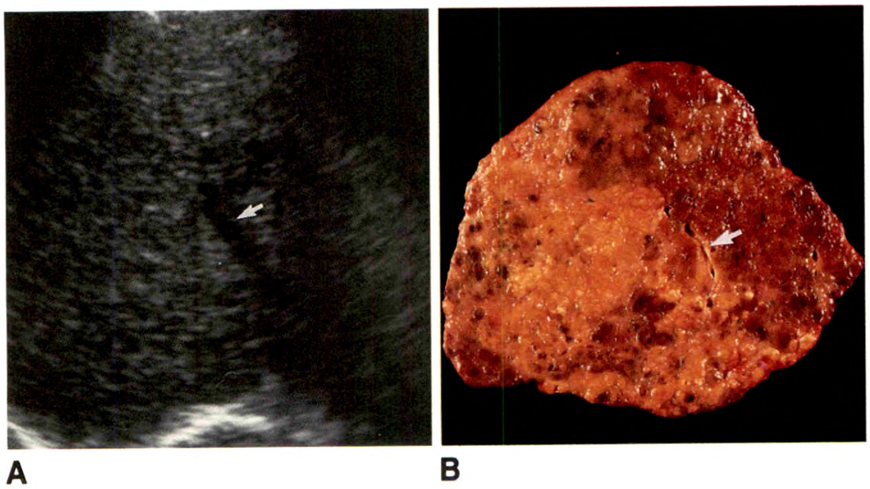

Fig. 11.—Largest sonographically missed tumor.

A, Transverse sonogram through dome of right hepatic lobe shows a diffuse coarse hepatic parenchymal echogenicity without a definable mass. Heterogeneity of hepatic parenchyma could easily be attributed to advanced cirrhosis. Note middle hepatic vein (*arrow*).

B, Corresponding hepatic specimen shows a 10-cm diffusely infiltrating tumor just lateral to middle hepatic vein (*arrow*). Even in retrospect this tumor could not be identified on hepatic sonogram.

limited to patients with end-stage cirrhosis requiring transplantation. This difference is significant because, in our experience, end-stage cirrhotic livers are often smaller and more heterogeneous than are less severely cirrhotic livers. The decreased size of the end-stage cirrhotic liver, owing to its tendency to be located high up under the diaphragm, makes it harder to image. As with excessive body size, any impediment to adequate visualization of the liver may decrease the sonographic detection of liver tumors. The increased heterogeneity of the end-stage cirrhotic liver is probably one of the most significant factors accounting for the sonographic sensitivity differences between the study by Takayasu et al. and ours. Of the patients in our study in whom tumor was partially or completely missed, most had moderately to severely coarse hepatic parenchymal echo texture that was due to advanced macronodular or mixed macro-micronodular cirrhosis. We believe the large regenerative nodules and extensive fibrosis present in these patients can hide both small and large tumor nodules.

Our study had two practical limitations. One was that technologists and physicians performing a sonographic study might have had some idea that a patient had a hepatic tumor, which may have falsely increased sonographic sensitivity in tumor detection. This limitation was imposed by the prospective nature of our study and necessary interaction with the patients and referring physicians. However, given the poor sensitivity identified in our study, any false increase in sensitivity only strengthens our conclusion that sonography is a poor screening technique for the detection of malignant tumors in the end-stage cirrhotic liver.

The other practical limitation of our study was the incomplete rescanning of all patients by a physician. Because of the large volume of sonographic studies performed at our institution, it is impractical for a physician to rescan all patients. We therefore rely on technologists to screen patients for disease, with rescanning performed as deemed necessary after review of the technologist's results. With minimal exception, this is the standard sonography practice in the United States. In contrast, outside the United States most sonography is performed by an imaging physician without the aid of a technologist. The difference in the accuracy of these two methods of practice has been debated. Unfortunately, to date no definitive studies have clearly proved one method better than the other. In our study we have tried to minimize this difference by rescanning the majority of patients. As previously stated, we rescanned all patients with sonographically suspected tumor and a significant percentage of patients without detectable tumor. Furthermore, all technologists were aware of the nature of our study before its inception and were frequently reminded of the importance of tumor detection throughout its duration. We therefore believe that our use of technologists did not degrade the validity of our results.

Although our results show sonography to be insensitive for the detection of malignant tumors in the end-stage cirrhotic liver, they also show that any sonographically detected solid lesion has a high probability of being malignant. The only lesions in our study that were falsely interpreted as malignant were three hemangiomas and one focal region of heterogeneity, the appearances of which, even in retrospect, could not be differentiated from malignant lesions. We therefore consider any reproducible focal solid lesion identified in the cirrhotic liver to be malignant until disproved by definitive imaging (such as isotope-tagged RBC scintigraphy in the case of a cavernous hemangioma) or biopsy.

In light of the poor sensitivity of sonography in tumor detection shown in our study, we do not believe that sonography can be used as the sole screening technique for the detection of malignant tumors in the end-stage cirrhotic liver. Instead, it must be realized that a hepatic sonogram with normal findings in a patient with cirrhosis does not exclude the presence of malignant tumors. At best, sonography may be used as an adjunct examination in a broader screening program that includes biochemical analysis and other imaging techniques.

ACKNOWLEDGMENTS

We thank Scharmen Confer, the technologists of our sonolaboratory, and the pathology technologists for their time and efforts in the performance of this research project.

REFERENCES

1. Okuda K. Primary liver cancers in Japan. *Cancer* **1980**;45:2663–2669
2. Franco D, Capussotti L, Smadja C, et al. Reaction of hepatocellular carcinomas: results in 72 European patients with cirrhosis. *Gastroenterology* **1990**;98:733–738
3. Okuda K, Ohtsuki T, Obata H, et al. Natural history of hepatocellular carcinoma and prognosis in relation to treatment: study of 850 patients. *Cancer* **1985**;56:918–928
4. Ringe B, Wittekind C, Bechstein WO, Bunzendahl H, Pichlmayr R. The role of liver transplantation in hepatobiliary malignancy. *Ann Surg* **1989**;209:88–98
5. Tanaka K, Okazaki H, Nakamura S, et al. Hepatocellular carcinoma: treatment with a combination therapy of transcatheter arterial embolization and percutaneous ethanol injection. *Radiology* **1991**;179:713–717
6. Hayashi N, Yamamoto K, Tamaki N, et al. Metastatic nodules of hepatocellular carcinoma: detection with angiography, CT, and US. *Radiology* **1987**;165:61–63
7. Heiken JP, Weyman PJ, Lee JKT, et al. Detection of focal hepatic masses: prospective evaluation with CT, delayed CT, CT during arterial portography, and MR imaging. *Radiology* **1989**;171:47–51
8. Nelson RC, Chezmar JL, Sugarbaker PH, Bernardino ME. Hepatic tumors: comparison of CT during arterial portography, delayed CT, and MR imaging for preoperative evaluation. *Radiology* **1989**;172:27–34
9. Igawa S, Sakai K, Kinoshita H, Hirohashi K. Intraoperative sonography: clinical usefulness in liver surgery. *Radiology* **1985**;156:473–478
10. Freeny PC, Marks WM. Hepatic perfusion abnormalities during CT angiography: detection and interpretation. *Radiology* **1986**;159:685–691
11. Kudo M, Hirasa M, Takakuwa H, et al. Small hepatocellular carcinomas in chronic liver disease: detection with SPECT. *Radiology* **1986**;159:697–703
12. Merine D, Takayasu K, Wakao F. Detection of hepatocellular carcinoma: comparison of CT during arterial portography with CT after intraarterial injection of iodized oil. *Radiology* **1990**;175:707–710
13. Yumoto Y, Jinno K, Tokuyama K, et al. Hepatocellular carcinoma detected by iodized oil. *Radiology* **1985**;154:19–24
14. Cottone M, Marceno MP, Maringhini A, et al. Ultrasound in the diagnosis of hepatocellular carcinoma associated with cirrhosis. *Radiology* **1983**;147:517–519
15. Takayasu K, Moriyama N, Muramatsu Y, et al. The diagnosis of small hepatocellular carcinomas: efficacy of various imaging procedures in 100 patients. *AJR* **1990**;155:49–54
16. Machi J, Isomoto H, Yamashita Y, Kurohiji T, Shirouzu K, Kakegawa T. Intraoperative ultrasonography in screening for liver metastases from colorectal cancer: comparative accuracy with traditional procedures. *Surgery* **1987**;101:678–684
17. Chen D-S, Sung J-L. Serum alpha-fetoprotein in hepatocellular carcinoma. *Cancer* **1977**;40:779–783
18. Fujiyama S, Morishita T, Hashiguchi O, Sato T. Plasma abnormal prothrombin (des-gamma-carboxy prothrombin) as a marker of hepatocellular carcinoma. *Cancer* **1988**;61:1621–1628

Roentgen Centennial and Reynolds Medical History Collection

Hrudaya Nath and Robert J. Stanley[1]

The approaching centennial of Roentgen's discovery of X-rays is an appropriate time for us in radiology to go back and trace its beginnings and its course of development, purveying its ups and downs, its brave aspirations after truth and finality, and also its pathetic failures. Libraries of medicine, and in particular, medical history collections serve as guidebooks and provide the mileposts. The medical history collection amassed and donated by Dr. Lawrence Reynolds, located at the University of Alabama at Birmingham, is one of the largest of its kind in the United States. The fact that Dr. Reynolds was a noted radiologist in addition to being a great bibliophile, makes this collection of greater significance to all radiologists.

Lawrence Reynolds was born into a family of physicians in Alabama on February 11, 1889. His father, Dr. Robert Davis Reynolds, a rural physician in Skipperville, had very poor eyesight, making it necessary for one of his three sons to accompany him in his horse-drawn buggy on visits to his patients around Skipperville. During these lengthy rides, each son read medical literature to his father [1]. By age 12, Lawrence Reynolds had enough knowledge of medicine to assist his father in his medical practice. He entered the University of Alabama at Tuscaloosa with the intention of becoming a lawyer, but 3 years later decided to become a physician instead. Upon completing his undergraduate studies in 1912, he joined the Medical School at Johns Hopkins University, where he became the first resident in radiology under Dr. Frederick Harry Baetjer. In 1917, Dr. Reynolds enlisted in the army to serve in World War I. In his 2 years of military service he gained invaluable experience in the use of radiology during warfare, and years later, in 1944, made this the subject of his Caldwell–Carman Lecture [2]. After the war, Dr. Reynolds was invited to be head of the X-ray department at Peter Bent Brigham Hospital and an instructor of roentgenology at Harvard Medical School.

Dr. Reynolds left Boston after 3 years to join his friends Preston Hickey and William A. Evans in a group radiology partnership in Detroit, where he practiced for almost 40 years (1922–1961). Although a dedicated private radiologist, he was also deeply committed to teaching and research as well as to radiologic journalism. He published 35 radiology articles and was president of the American Roentgen Ray Society, the American College of Radiology, and the Detroit Roentgen Ray and Radium Society. He was a distinguished editor of *The American Journal of Roentgenology and Radium Therapy* for 31 years (1928–1961) and was active in library committee memberships in Detroit, Ann Arbor, and New Haven. He served on the Advisory Board of the Yale Medical Library, which houses the Harvey Cushing Collection.

Growth of Dr. Reynolds, the bibliophile, began in earnest during his years in Boston, where he developed a friendship with Dr. Harvey Cushing. He joined the Harvey Cushing Society, an organization devoted to the acquisition and preservation of classics in medicine, and remained a member for life. Eight books in the Reynolds Collection appear to have once been part of the Cushing Collection [1]. As the years went by and he became wealthier, Dr. Reynolds' interest in book collecting became a near obsession. By the end of the 1950s he had amassed one of the world's finest collections of rare and important books in the medical sciences. As the fame of this collection spread, several universities sought to acquire it. The University of Alabama at Birmingham was fortunate in receiving the collection, partly because of Dr. Reynolds' loyalty to his alma mater and partly because of the influence of his friend, Charles C Thomas, who was for a long time the publisher of *The American Journal of Roentgenology*. The gift agreement was signed in June 1953, and on February 2, 1958, the Reynolds Historical Library was dedicated. In 1975 it was moved to a specially designed area in the newly completed Lister Hill Library of Health Sciences on the campus of the University of Alabama at Birmingham, where it remains today.

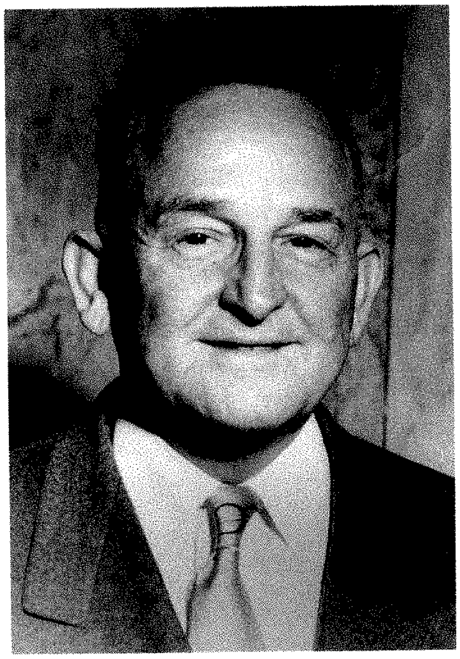

Lawrence E. Reynolds

This "handful of books" [3] Dr. Reynolds gave to the Medical Center of his alma mater is a priceless collection. It contains a group of choice medical incunabula (books printed before 1500 AD), a first edition of Vesalius' text on anatomy, Harvey's *De Motu Cordis*, in which circulation of blood was first described, and a collection of rare ivory mannequins used in anatomy instruction, which date from the 16th and 17th centuries. The library currently holds over 10,000 books, letters, and pamphlets.

REFERENCES

1. Weaver B, Britt MC. Dr. Lawrence Reynolds and his medical history collection. *Ala J Med Sciences* **1984**;21:311-447
2. Reynolds LE. History of roentgen ray in warfare. *AJR* **1945**;54:649-672
3. Handwritten copy of Dr. Lawrence Reynolds' remarks. (Reynolds File, Reynolds Historical Library)

In preparation for the 1995 centennial celebration of the discovery of the X-ray, the *AJR* will periodically publish History Pages, which deal with events leading up to and occurring around the time of the discovery.

[1] Both authors: Department of Radiology, University of Alabama at Birmingham, 619 S. 19th St., Birmingham, AL 35233. Address reprint requests to H. Nath.

***AJR* 159:734, October 1992** 0361-803X/92/1594-0734 © American Roentgen Ray Society

Differential Diagnosis of Hepatic Tumors (Hepatoma, Hemangioma, and Metastasis) with CT: Value of Two-Phase Incremental Imaging

Hiroshi Honda[1]
Yasuo Matsuura[1]
Hideo Onitsuka[1]
Junji Murakami[1]
Kuniyuki Kaneko[1]
Sadayuki Murayama[1]
Takashi Kanematsu[2]
Kouji Masuda[1]

Two-phase dynamic incremental CT is a technique in which CT scans are obtained 45 sec and 6 min after commencing the rapid bolus injection of contrast medium. We analyzed the contrast enhancement patterns of three types of hepatic tumors (72 hepatomas, 39 hemangiomas, and 28 metastases) in 139 patients to determine if any differences in the patterns are useful in the differential diagnosis of these lesions. Dynamic incremental CT scanning was performed after 100 ml of iodinated contrast material was administered IV with a power injector at a rate of 2 ml/sec. A 1-sec scanning time was used with a 1.6-sec interscan delay, which allowed table motion between scans. CT scans (eight to 16 sections) were obtained 45–110 sec (early phase) and 6–7 min (delayed phase) after commencing the injection of contrast medium. The enhancement patterns of hepatomas were as follows: 32% were totally hyperdense in the early phase and totally hypodense in the delayed phase, while 24% were totally hypodense in both phases. Most of the hepatomas (88%) appeared as totally hypodense lesions in the delayed phase. In the case of hemangiomas, 56% were peripherally hyperdense in the early phase; in the delayed phase, 36% were isodense and 31% were totally hyperdense. Most hemangiomas (85%) were not totally hypodense in the early phase, and no hemangioma was totally hypodense in both phases. In the early phase, 61% of metastases were hypodense. In the delayed phase, 57% were hypodense. Metastases most commonly were totally hypodense in both phases (43%).

We conclude that contrast enhancement patterns of hepatomas, hemangiomas, and metastases seen on two-phase dynamic incremental CT scans are useful in the differential diagnosis of these tumors.

***AJR* 159:735–740, October 1992**

Dynamic incremental CT of the liver, in conjunction with bolus intravascular administration of contrast medium, is useful in the diagnosis of liver diseases [1, 2]. Focal hepatic lesions have several distinct patterns on contrast-enhanced CT scans [3]. Differences in attenuation and enhancement reflect the tumor's vascularity, size, and histology [4]. Despite these differences, several investigators have reported overall improvement in lesion-to-liver contrast when CT is performed within 2–3 min after administering a bolus of contrast medium [5–7]. With recent improvement in CT equipment, eight to 16 sections with table incrementations are easily obtained during one suspended respiration. In addition to this dynamic incremental scanning with bolus injection, delayed CT images can be obtained to detect and define hepatic tumors.

The purpose of this study was to compare the appearances of hepatomas, hemangiomas, and metastases on dynamic incremental CT scans to determine the value of this technique in the differential diagnosis of these lesions.

Materials and Methods

We reviewed 1150 CT scans of the liver from 890 patients who had two-phase incremental CT scanning between July 1989 and December 1990. Of these patients, 139 had clinically or

Received July 11, 1991; accepted after revision March 23, 1992.

[1] Department of Radiology, Faculty of Medicine, Kyushu University, 3-1-1 Maidashi, Higashi-ku, Fukuoka 812, Japan. Address reprint requests to H. Honda.

[2] Department of Surgery II, Faculty of Medicine, Kyushu University, Fukuoka 812, Japan.

0361-803X/92/1594-0735
©American Roentgen Ray Society

TABLE 1: Number of Tumors of Each Histologic Type by Tumor Size

Histologic Type	Tumor Diameter (cm)			Total
	≤2	2–4	>4	
Hepatoma	23	25	24	72
Hemangioma	21	11	7	39
Metastasis	4	12	12	28
Total	48	48	43	139

histopathologically diagnosed hepatic tumors that were seen on early- or delayed-phase images or both. Seventy-two patients had hepatomas, 39 had hemangiomas, and 28 had metastases from various primary malignant tumors. The sizes of tumors as measured on CT scans were 2 cm or less (48 patients), 2–4 cm (48 patients), or more than 4 cm (43 patients) (Table 1).

Of the 72 patients with hepatomas, histologic proof of the lesion was obtained during surgery in 46, by direct biopsy in 21, and at autopsy in five. In the 39 patients with hemangiomas, five cases were proved by surgery and 34 were proved by sonography, MR imaging, angiography, and clinical follow-ups of at least 1 year. Of the 28 patients with hepatic metastases, nine cases were proved at surgery and five were proved by direct biopsies. Fourteen cases were diagnosed because the patients had histories of primary malignant tumors, abnormal serologic laboratory findings such as carcinoembryonic antigen for colonic carcinoma, and serial radiographic findings that showed progressive enlargement of the lesions. The most common sites of origin of metastases were carcinomas of the colon and rectum (12 cases). Other primary malignant neoplasms were carcinomas of the stomach (seven cases); gallbladder (two cases); and kidney, lung, ovary, hypopharynx, pancreas, and esophagus (one case each). One metastasis was from gastrinoma of the pancreas.

The patients with hepatomas were 33–84 years old (mean, 61 years), those with hemangiomas were 34–71 years old (mean, 52 years), and those with metastases were 43–82 years old (mean, 57 years). Fifty-six of the 72 patients with hepatomas, 20 of the 39 patients with hemangiomas, and 12 of the 28 patients with metastases were men.

Contiguous axial 1-cm-thick sections were obtained by using a Toshiba TCT-900S scanner (Tokyo, Japan). Dynamic incremental scanning was performed after 100 ml of iopamidol (61.2% iodine, 300 mg I/ml) was administered at 2 ml/sec with a power injector. In the early phase, scanning was begun 45 sec after commencing the injection. A 1-sec scanning time was used with a 1.6-sec interscan delay, which allowed table motion between scans. Eight to 16 scans were obtained in suspended respiration during 20–40 sec. Oxygen inhalation was used when necessary in five patients. When scans of the entire liver could not be obtained during the initial suspended respiration, additional scans were obtained after 10–15 sec of respirations. In the delayed phase, scanning was begun 6 min after the contrast medium was administered by using the same technique as with the early-phase images.

The two-phase images were retrospectively reviewed. The CT appearances of each tumor on each of the phased images were categorized in five groups according to the degree and pattern of enhancement in comparison with surrounding hepatic parenchyma (Fig. 1): totally hyperdense, peripherally hyperdense, centrally hyperdense, mixed density, totally isodense (undetected), and totally hypodense. When more than one tumor was present, the largest ones were selected for evaluation because they were the ones most frequently present in biopsy samples.

Angiographic findings in 39 hepatomas also were studied to clarify the characteristic CT findings. Angiography was performed via the celiac artery and selectively via the right or left hepatic artery by using iopamidol injection rates of 7 ml/sec and 3–4 ml/sec, respectively.

Results

Table 2 shows the enhancement patterns of each of the tumors on the early- and delayed-phase images. Among 29 tumors that appeared to be totally hyperdense in the early phase, 25 (86%) were hepatomas. The single metastasis that was totally hyperdense in the early phase was from a gastrinoma. Of 25 tumors that appeared to be totally hyperdense

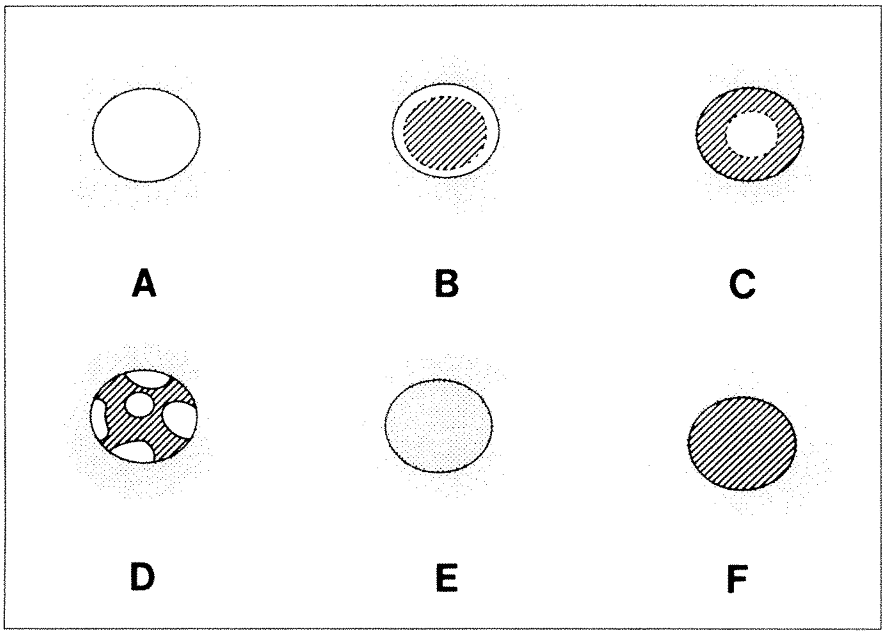

Fig. 1.—Various enhancement patterns of tumors: totally hyperdense (*A*), peripherally hyperdense (*B*), centrally hyperdense (*C*), mixed density (*D*), totally isodense (*E*), and totally hypodense (*F*).

TABLE 2: Enhancement Pattern of Each Tumor on Two-Phase Images

Phase/Pattern	No. of Findings (%)		
	Hepatomas (*n* = 72)	Hemangiomas (*n* = 39)	Metastases (*n* = 28)
Early			
Totally hyperdense	25 (35)	3 (8)	1 (4)
Peripherally hyperdense	5 (7)	22 (56)	8 (29)
Centrally hyperdense	7 (10)	5 (13)	0
Mixed density	6 (8)	2 (5)	1 (4)
Totally isodense	9 (13)	1 (3)	1 (4)
Totally hypodense	20 (28)	6 (15)	17 (61)
Delayed			
Totally hyperdense	1 (1)	12 (31)	0
Peripherally hyperdense	0	7 (18)	3 (11)
Centrally hyperdense	1 (1)	0	2 (7)
Mixed density	1 (1)	4 (10)	1 (4)
Totally isodense	6 (8)	14 (36)	6 (21)
Totally hypodense	63 (88)	2 (5)	16 (57)

in the early phase and totally hypodense in the delayed phase, 23 (92%) were hepatomas. Twenty-two (63%) of 35 tumors that were peripherally hyperdense on the early-phase images were hemangiomas. However, seven tumors that were peripherally hyperdense in the early phase and totally hypodense in the delayed phase were not hemangiomas. Of the 11 tumors that appeared to be totally isodense in the early phase, nine (82%) were hepatomas, one was a hemangioma, and one was a metastasis. Of the 26 tumors that appeared to be totally isodense in the delayed phase, six (23%) were hepatomas, 14 (54%) were hemangiomas, and six (23%) were metastases. Nine tumors (100%) that appeared to be totally isodense in the early phase and totally hypodense in the delayed phase were hepatomas. Of the 13 tumors that appeared to be totally hyperdense in the delayed phase, 12 (92%) were hemangiomas.

In the 72 hepatomas, total hyperdensity was the most common pattern in the early phase, seen in 25 (35%) of 72 cases, followed by total hypodensity in 20 (28%), total isodensity in nine (13%), central hyperdensity in seven (10%), mixed density in six (8%), and peripheral hyperdensity in five (7%). In the delayed phase, total hypodensity was the most common pattern, seen in 63 cases (88%), followed by total isodensity in six (8%), total hyperdensity in one (1%), central hyperdensity in one (1%), and mixed density in one (1%). No hepatoma appeared to have peripheral hyperdensity in the delayed phase. Total hyperdensity in the early phase and total hypodensity in the delayed phase were the most common appearances in hepatomas (Fig. 2), seen in 23 (32%) of 72 cases, followed by total hypodensity in both phases in 17 (24%). Ten (59%) of 17 hepatomas that appeared to have total hypodensity in both phases were 2 cm or less in diameter, but only four (17%) of 23 hepatomas that appeared to be totally hyperdense in the early phase and totally hypodense in the delayed phase were 2 cm or less in diameter. Forty-three (60%) of 72 hepatomas enhanced totally or partially in the early phase (totally hyperdense, peripherally hyperdense, centrally hyperdense, and mixed density). Thirty-seven (51%) of 72 hepatomas enhanced totally or partially in the early phase and showed total hypodensity in the delayed phase.

In the 39 hemangiomas, peripheral hyperdensity was the most common pattern in the early phase, seen in 22 (56%) of 39 cases, followed by total hypodensity in six (15%), central hyperdensity in five (13%), total hyperdensity in three (8%), mixed density in two (5%), and total isodensity in one (3%). In the delayed phase, total isodensity was the most common pattern, seen in 14 (36%) of 39 hemangiomas, followed by total hyperdensity in 12 (31%), peripheral hyperdensity in seven (18%), mixed density in four (10%), and total hypodensity in two (5%). The pattern of central hyperdensity was not seen in any hemangioma on delayed-phase scans.

In the 28 metastases, total hypodensity was the most common pattern in the early phase, seen in 17 (61%) of 28 cases, followed by peripheral hyperdensity in eight (29%), total hyperdensity in one (4%), mixed density in one (4%), and total isodensity in one (4%). No metastases had central hyperdensity in the early phase. In the delayed phase, total hypodensity was the most common pattern, seen in 16 (57%) of 28 metastases, followed by total isodensity in six (21%), peripheral hyperdensity in three (11%), central hyperdensity

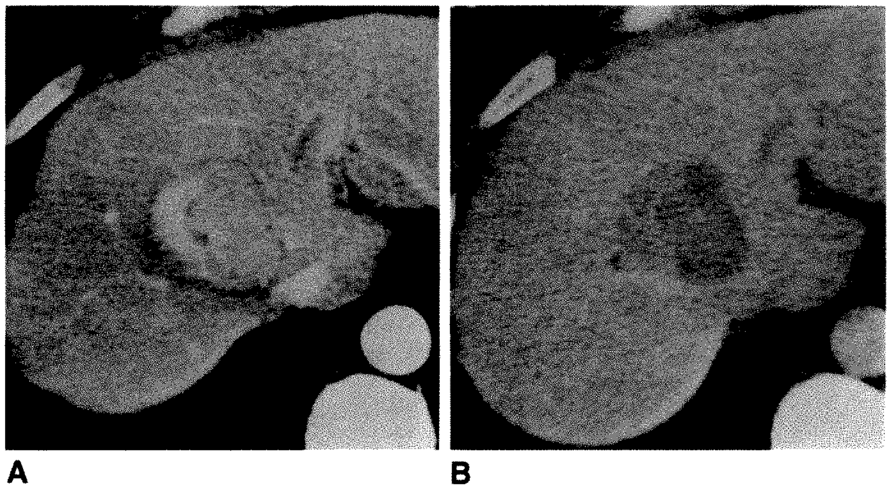

Fig. 2.—64-year-old man with hepatoma.
***A*, Early-phase incremental CT scan shows 4-cm-diameter hepatoma to be totally hyperdense.**
***B*, Delayed-phase incremental CT scan shows tumor to be totally hypodense.**

in two (7%), and mixed density in one (4%). No metastases showed total hyperdensity on delayed-phase images. Although total hypodensity in both phases was the most common appearance of metastases (12/28, 43%) (Fig. 3), 24% (17/72) of hepatomas also had that pattern in both phases (Fig. 4).

In the early phase, 8% of all tumors (11/139) were totally isodense and in the delayed phase, 19% (26/139) were totally isodense. Nine (13%) of 72 hepatomas, one (3%) of 39 hemangiomas, and one (4%) of 28 metastases were totally isodense in the early phase and seen only in the delayed phase (Fig. 5). Six (8%) of 72 hepatomas, 14 (36%) of 39 hemangiomas, and six (21%) of 28 metastases were totally isodense in the delayed phase.

Angiograms of hepatomas that showed the patterns of total hyperdensity on early-phase CT scans and total hypodensity on delayed-phase CT scans were compared with angiograms of hepatomas that showed total hypodensity in both phases. Fifteen (88%) of 17 hepatomas that were totally hypodense in both phases did not enhance on celiac angiography and 10 (59%) did not enhance even with selective angiography of the right or left branch of the proper hepatic artery. Another two hepatomas (12%) that showed enhancement on celiac angiograms were more than 4.5 cm in diameter. Angiograms were available for review in 22 of the 23 hepatomas that were totally hyperdense on early-phase CT scans and totally hypodense on delayed-phase CT scans. Twenty (91%) of the 22 hepatomas enhanced on celiac angiograms. Three of these were more than 4.5 cm in diameter. Another two enhanced on angiograms of the right branch of the proper hepatic artery.

Discussion

The evolution of techniques for contrast enhancement with CT has paralleled improvement in CT technology. As rapid CT scanning with scanning rates of eight to 16 scans per suspended respiration became possible, the rate of injection of contrast medium was increased. In this study, early-phase scanning was started 45 sec after the beginning of injection, as described previously [8]. Within 5 min after bolus injection, 80% of contrast material has already escaped from the vascular space into the interstitial space [9]. Equilibrium between the two spaces is attained within 2–5 min [7, 9, 10]. In this study, 50 sec was needed to inject 100 ml of contrast material.

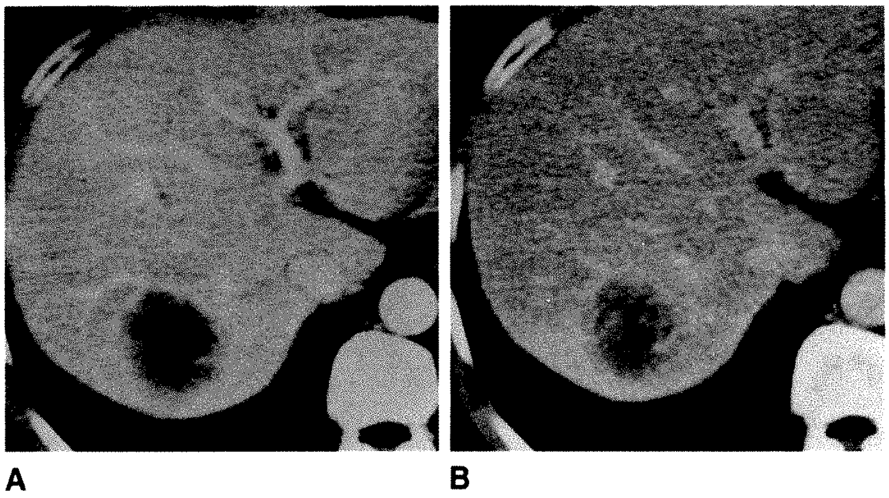

Fig. 3.—58-year-old man with metastatic tumor from colonic carcinoma.
***A* and *B*, Early- (*A*) and delayed- (*B*) phase incremental CT scans show 4-cm-diameter metastasis to be totally hypodense.**

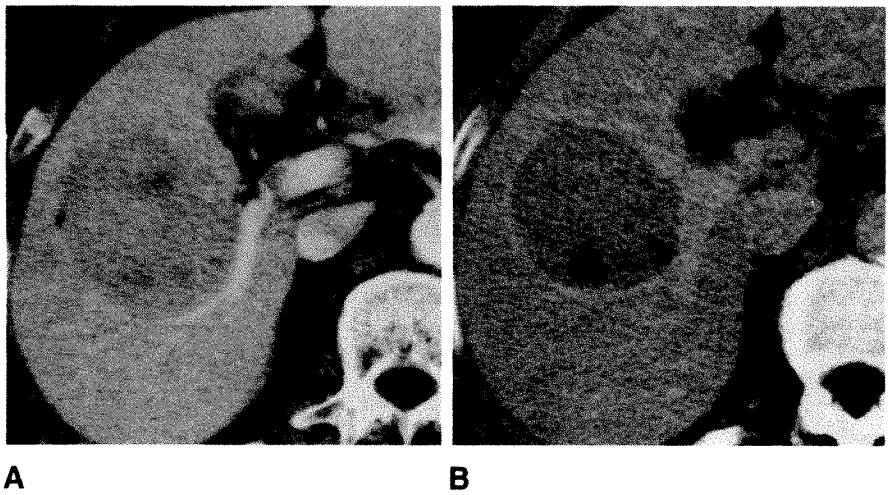

Fig. 4.—68-year-old woman with hepatoma.
***A* and *B*, Early- (*A*) and delayed- (*B*) phase incremental CT scans show 7-cm-diameter hepatoma to be totally hypodense.**

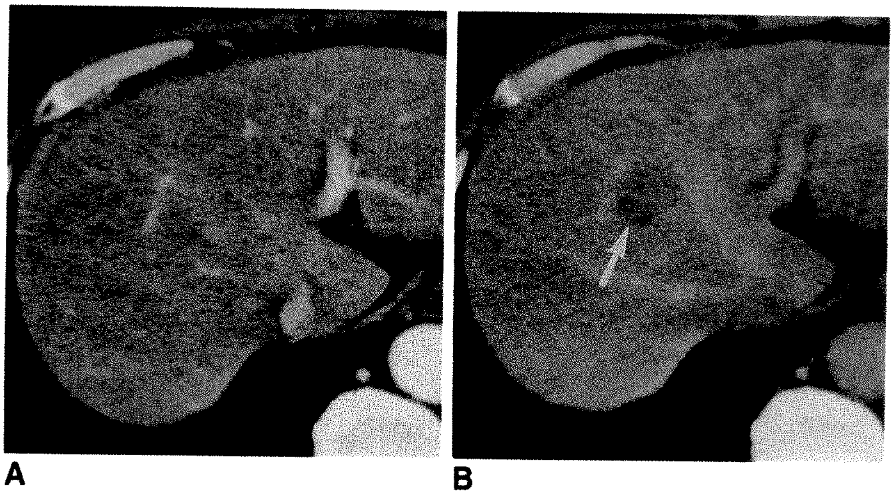

Fig. 5.—56-year-old man with hepatoma.
***A*, Early-phase incremental CT scan shows 2-cm-diameter hepatoma to be totally isodense (undetectable).**
***B*, Delayed-phase incremental CT scan shows hepatoma as totally hypodense (*arrow*).**

Accordingly, the delayed-phase images were obtained 6 min after the injection was started.

Hepatomas are known to enhance in proportion to the degree of uptake of contrast medium, and because of their hypervascular nature, they enhance earlier than the surrounding hepatic parenchyma does. Metastases, especially those from adenocarcinomas of the gastrointestinal tract, usually enhance less and take up contrast material more slowly [5, 6, 11, 12]. After the administration of iodinated contrast material as a bolus injection, dynamic CT scanning results in improved delineation of tumor vascularity, venous shunting, venous occlusion, and hepatic lobar or segmental flow abnormalities [2, 13–17]. Hepatomas, supplied by hepatic arterial branches, become maximally hyperdense during the arterial phases of dynamic scanning sequences, then rapidly become less dense as portal flow to the liver becomes dominant [8, 18, 19]. This pattern is well seen on dynamic incremental CT and delayed-phase CT scans of hepatomas. On the early-phase images in our study, 35% of hepatomas enhanced totally and 25% enhanced partially (total, 60%). In the delayed phase, 88% were less dense than the surrounding hepatic parenchyma.

However, 26% of hepatomas were less dense than hepatic parenchyma in both phases. Fifty-nine percent of the hepatomas that were hypodense in the early phase were not seen even with selective angiography. Tumors not seen on angiograms are characterized as being smaller than 2 cm and well differentiated, and as having fatty metamorphosis, severe liver cirrhosis, or necrosis [20–22]. These pathologic characteristics might cause the poor enhancement on early-phase images and poor visibility on angiograms. The hepatomas that were totally hypodense in both phases were more often (59%) small (<2 cm) than were the hepatomas that were totally hyperdense in the early phase and totally hypodense in the delayed phase (17%). Most of the hepatomas that were totally hypodense in both phases did not enhance on celiac angiography, while more than 90% of the hepatomas that were totally hyperdense in the early phase and totally hypodense in the delayed phase did enhance. This was because the hepatomas that are totally hypodense in both phases are less vascular than the hepatomas that are totally hyperdense in the early phase and totally hypodense in the delayed phase. Even when the hepatomas were hypervascular and enhanced on celiac angiograms, CT showed two relatively large hepatomas as totally hypodense in both phases. This may be because of the smaller volume of contrast material that flows into the hepatoma during CT than during angiography. During the early phase (45–90 sec after initiation of the contrast injection), the hepatic parenchyma is enhanced by portal blood flow. If the tumor is not appreciably enhanced because the volume of contrast material is less than the necessary volume to enhance the hepatoma more than hepatic parenchyma, the tumor may appear less dense than the hepatic parenchyma.

After IV administration of contrast material, all or part of the rim of hemangiomas shows an increase in density on CT, exceeding the enhancement of the normal liver. Delayed CT scans reveal progressive contrast enhancement of the central parts of the hemangioma owing to the gradual accumulation and slow washout of contrast material [23]. Hepatic hemangiomas are best distinguished from other solid hepatic masses by administering contrast material and by performing dynamic CT scanning with delayed scans at 1–4 min [24]. Although the peripherally hyperdense pattern was seen in the early phase and various patterns were seen in the delayed phase, the peripheral hyperdensity in the early phase was seen in less than 60% of hemangiomas, as has been reported [25]. The high percentage (36%) of hemangiomas that were undetected in the delayed phase reinforces the advantage of using bolus injections and incremental CT. The lower density of the tumor relative to the surrounding hepatic parenchyma in both phases strongly suggests that such a tumor is not a hemangioma.

Most secondary tumors of the liver are hypovascular. Among the primary neoplasms that tend to give rise to hypervascular metastases are carcinoids; leiomyosarcomas; choriocarcinomas; and carcinomas of renal, thyroid, adrenal, and pancreatic islet cell origins. Some metastatic melanomas and occasional metastases from carcinomas of the colon and breast also are hypervascular. In our study, the metastasis from the gastrinoma had totally hyperdense and totally hypodense patterns similar to those of hepatomas. In cases of hypervascular malignant tumors in other organs, biopsy is necessary. One of the common patterns of metastasis identified with CT after a bolus injection of contrast material is a rim of contrast enhancement around a less dense central zone. This reportedly occurs in 35% of these lesions [26]. In our study, rim enhancement was seen as peripheral hyperdensity in the early phase with similar frequency (29%). The metastases could be detected more readily in the early phase (96%) than in the delayed phase (79%). However, because the variety of metastatic origins was limited in this study, more study of hepatic metastases might be necessary.

In summary, delayed images assisted in the detection of 8% of all tumors and 13% of hepatomas. A lesion that is totally hyperdense or totally isodense on early-phase images and totally isodense on delayed-phase images is almost always a hepatoma. Even if a lesion showed peripheral hyperdensity in the early phase, total hypodensity in the delayed phase can be a sign that the lesion is not a hemangioma.

We conclude that, although bolus injection with incremental CT scanning is known to be useful for the quantitative diagnosis and detection of hepatic tumors, subsequent delayed-phase images are helpful in the differential diagnosis of hepatic tumors.

REFERENCES

1. Araki T, Itai Y, Furui S, Tasaka A. Dynamic CT densitometry of hepatic tumors. *AJR* **1980**;135:1037–1043
2. Kunstlinger F, Federle MP, Moss AA, Marks W. Computed tomography of hepatocellular carcinoma. *AJR* **1980**;134:431–437
3. Moss AA, Schrumpt J, Schnyder P, Korobkin M, Shimsshak RR. Computed tomography of focal hepatic lesions: a blind clinical evaluation of the effect of contrast enhancement. *Radiology* **1979**;131:427–430
4. Burgener FA, Hamlin DJ. Contrast enhancement of focal hepatic lesions in CT: effect of size and histology. *AJR* **1983**;140:297–301
5. Foley WD, Berland LL, Lawson TL, Smith DF, Thorsen MK. Contrast enhancement technique for dynamic hepatic computed tomographic scanning. *Radiology* **1983**;147:797–803
6. Berland LL, Lawson TL, Foley WD, Melrose BL, Chintapelli KN, Taylor AJ. Comparison of pre- and postcontrast CT in hepatic masses. *AJR* **1982**;138:853–858
7. Burgener FA, Hamlin DJ. Contrast enhancement in abdominal CT: bolus vs. infusion. *AJR* **1981**;137:351–358
8. Foley WD. Dynamic hepatic CT. *Radiology* **1989**;170:617–622
9. Kormano M, Dean PB. Extravascular contrast material: the major component of contrast enhancement. *Radiology* **1976**;121:379–382
10. Itai Y, Ohtomo K, Kokubo T, et al. CT of hepatic masses: significance of prolonged and delayed enhancement. *AJR* **1986**;146:729–733
11. Sager EM, Scheel B, Talle K. Increased detectability of liver metastases by the use of contrast enhancement in computed tomography: a comparison between the precontrast, the immediate postcontrast and the one hour postcontrast scan. *Acta Radiol* **1985**;26:369–372
12. Dean PB, Violante MR, Mahoney JA. Hepatic CT contrast enhancement: effect of dose, duration of infusion, and time elapsed following infusion. *Invest Radiol* **1980**;15:158–161
13. Tada S, Fukuda K, Aoyagi Y, Harada J. CT of abdominal malignancies: dynamic approach. *AJR* **1980**;135:455–461
14. Inamoto K, Sugiki K, Yamasaki H, Miura T. CT of hepatoma: effects of portal vein obstruction. *AJR* **1981**;136:349–353
15. Pauls CH. Ultrasound and computed tomographic demonstration of portal vein thrombosis in hepatocellular carcinoma. *Gastrointest Radiol* **1981**;6:281–283
16. Nishikawa J, Itai Y, Tasaka A. Lobar attenuation differences of the liver on computed tomography. *Radiology* **1981**;141:725–728
17. Itai Y, Moss AA, Goldberg HI. Transient hepatic attenuation difference of lobar or segmental distribution detected by dynamic computed tomography. *Radiology* **1982**;144:835–839
18. Hosoki T, Chatani M, Mori S. Dynamic computed tomography of hepatocellular carcinoma. *AJR* **1982**;139:1099–1106
19. Moss AA, Dean PB, Axel L, Goldberg HI, Glazer GH, Friedman MA. Dynamic CT of hepatic masses with intravenous and intraarterial contrast material. *AJR* **1982**;138:847–852
20. Takayasu K, Shima Y, Muramatsu Y, et al. Angiography of small hepatocellular carcinomas: analysis of 105 resected tumors. *AJR* **1986**;147:525–529
21. Sumida M, Ohto M, Ebata M, et al. Accuracy of angiography in the diagnosis of small hepatocellular carcinoma. *AJR* **1986**;147:531–536
22. Hirose J, Matsui O, Kadoya M, et al. Analysis of indefinite tumor staining on hepatic angiography in small hepatocellular carcinomas. *Nippon Igaku Hoshasen Gakkai Zasshi* **1987**;47:1413–1419
23. Barnett PH, Zerhouni EA, White RI Jr, Siegelman SS. Computed tomography in the diagnosis of cavernous hemangioma of the liver. *AJR* **1980**;134:439–447
24. Moss AA. Computed tomography of the hepatobiliary system. In: Moss AA, Gamsu G, Genant HK, eds. *Computed tomography of the body.* Philadelphia: Saunders, **1983**:599–698
25. Freeny PC, Marks WM. Hepatic hemangioma: dynamic bolus CT. *AJR* **1986**;147:711–719
26. Paushter DM, Zeman RK, Scheibler ML, Choyke PL, Jaffe MH, Clark LR. CT evaluation of suspected hepatic metastases: comparison of techniques for IV contrast enhancement. *AJR* **1989**;152:267–271

Preoperative Assessment of Resectability of Hepatic Metastases from Colonic Carcinoma: CT Portography vs Sonography and Dynamic CT

Philippe Soyer[1]
Marc Levesque[1]
Dominique Elias[2]
Guy Zeitoun[3]
Alain Roche[4]

OBJECTIVE. A retrospective study was performed to determine the influence of CT portography vs sonography and dynamic CT on the preoperative assessment of the resectability of hepatic metastases from colorectal cancer.

MATERIALS AND METHODS. Results of sonography, bolus dynamic CT, and CT portography in 28 patients who underwent surgical exploration (resection or intraarterial catheter placement) for hepatic metastases from colorectal cancer were retrospectively reviewed by two abdominal radiologists and one hepatic surgeon. For each patient, the resectability and surgical approach were decided on the basis of the results of combined sonography-bolus dynamic CT and compared with the decision made from the CT portographic results alone. The final approach suggested was compared retrospectively with the surgical procedure actually performed.

RESULTS. Sixty-nine metastases were identified at surgery and pathologically proved. Combined sonography-bolus dynamic CT and CT portography showed 52 (75%) and 64 (93%) metastases, respectively. Twelve metastases in five patients were seen only with CT portography. In four patients, CT portography depicted additional metastases, which changed the surgical approach that had been chosen on the basis of results of sonography and bolus dynamic CT. In one patient, CT portography showed four additional metastases, precluding hepatic resection.

CONCLUSION. Findings from CT portography provide vital data unattainable with sonography and bolus dynamic CT that improve the preoperative assessment of the resectability of liver metastases from colonic carcinoma.

AJR 159:741–744, October 1992

Partial hepatic resection is the best treatment currently available for hepatic metastases from colorectal cancer. Without hepatic resection, only 5% of patients with limited hepatic metastases from colorectal cancer survive for more than 2 years after the diagnosis [1]. On the other hand, the 5-year survival rates after curative resection are up to 30% [2]. Unfortunately, estimates of the percentage of patients who may undergo hepatic resection range only from 5% [3] to 10% [4]. Careful preoperative selection of patients through the use of imaging studies is crucial to avoid unnecessary surgical explorations. It is well established that CT portography (CTP) is the most sensitive preoperative imaging technique for detecting hepatic metastases from colorectal cancers [5–7]. Recent advances in hepatic oncologic surgery have made the diagnostic imaging methods [8, 9] used in such patients more critical. Hepatic resection should be attempted only in patients with four or fewer metastases [10] located in a distribution that permits resection. Thus, imaging studies are used to determine which patients have resectable metastases and to plan the operation (e.g., left or right lobe resection, segmental or multisegmental resection, or subsegmental resection). However, to our knowledge, the impact of CTP on surgical decision making has not been analyzed.

The purpose of this study was to determine the influence of CTP compared with that of sonography combined with bolus dynamic CT on the preoperative assess-

Received February 13, 1992; accepted after revision April 1, 1992.

[1] Department of Radiology, Hôpital Louis Mourier, 178, rue des Renouillers, 92701 Colombes Cedex, France. Address reprint requests to P. Soyer.

[2] Department of Surgery, Institut Gustave Roussy, Villejuif, France.

[3] Department of Surgery, Hôpital Louis Mourier, 92701 Colombes Cedex, France.

[4] Department of Interventional Radiology, Institut Gustave Roussy, Villejuif, France.

0361-803X/92/1594-0741
© American Roentgen Ray Society

ment of the resectability of hepatic metastases from colorectal cancer and on the choice of surgical approach.

Materials and Methods

During a 2-year period, 35 consecutive patients with suspected hepatic metastases from colorectal cancer were referred for CTP before possible surgical resection. Seven patients with metastases that were considered inoperable on the basis of the results of preoperative imaging techniques did not have surgery and were not included in this study. Twenty-eight patients with hepatic metastases from colorectal cancer, 16 men and 12 women 20–72 years old (mean age, 57 years), underwent surgical exploration and form the basis of this retrospective study. Twenty-five patients underwent partial hepatectomy, and three patients had a catheter surgically placed in the hepatic artery. The metastases originated from the colon in 23 patients and the rectum in five patients. Three patients referred for recurrent disease had previously had hepatic surgery (left lobectomy, $n = 1$; right lobectomy, $n = 2$). All patients underwent preoperative real-time sonography, dynamic CT after bolus injection of contrast medium, and CTP within 10 days of surgery (mean, 4 days).

All CTP examinations were performed by using the same procedure. After a 5-French end-hole angiographic catheter (Cook, Bloomington, IN) was placed in the superior mesenteric artery, the patency of the portal vein was assessed by delayed filming after injection of 30 ml of a nonionic contrast medium (30 g I/100 ml; Iopamiron 300, Schering, Berlin, Germany) at a rate of 6 ml/sec. For each patient, the interval between the beginning of the injection and the beginning of portal opacification was noted and used to plan the scan delay time for CTP. Thereafter, patients were transferred immediately to the CT scanner. CT was first performed without contrast material to identify hepatic cysts. Intraarterial injection of 40 mg of papaverine hydrochloride (Papaverive, Laboratoire Aguettant, Lyon, France) was done to increase portal blood flow [11], after which nonionic contrast medium (Iopamiron 300) was injected through the catheter with a power injector (Medrad, Pittsburgh, PA) at a rate of 2 ml/sec. Contiguous 10-mm-thick slices were obtained. The scan delay was based on the interval (mean, 12 sec) until partial venous opacification was seen angiographically. CTP was performed with either an Exel 2400 scanner (Elscint, Haifa, Israel) with a 340 × 340 matrix, 2.1-sec scan time, and 3.2-sec interscan delay or a CT Pace Plus scanner (General Electric, Milwaukee, WI) with a 512 × 512 matrix, 2-sec scan time, and 3-sec interscan delay. Approximately 11 sections per minute were obtained. The total volume of contrast medium used varied with the number of sections needed to image the entire liver and was determined by multiplying the number of sections by the cycle time and the rate of injection. The mean number of CTP sections necessary to image the whole liver was 15.5 ± 2.0, but the mean volume of contrast material used was only 147 ± 6 ml because we never injected more than 150 ml.

Sonography was performed by a medical sonographer with a real-time sonographic unit (Radius, General Electric, Milwaukee, WI; or 77 SAL-A, Toshiba, Tokyo, Japan) and a 3.5-MHz probe. Routine scan planes and hard-copy images were obtained during these examinations.

All bolus dynamic CT scans were obtained with an Exel 2400 scanner or a CT Pace Plus scanner, with 10-mm-thick contiguous sections and cycle times of 5.3 sec and 5.0 sec, respectively. Both unenhanced and enhanced CT were performed after a bolus injection of 100 ml of contrast medium containing 38 g of iodine per 100 ml (Telebrix 38, Guerbet, Aulnay-sous-Bois, France) into an antecubital vein at a rate of 2 ml/sec. Injections were administered via an 18- or 20-gauge plastic cannula either manually or through a power injector (Medrad). CT scanning was begun 40 sec after beginning contrast injection.

Intraoperative sonography was performed with either an SAL 38 (Toshiba, Tokyo, Japan) or a Scannel 300 (CGR-General Electric, Paris, France) sonographic unit and a high-resolution 5.0- or 7.5-MHz intraoperative sonographic probe. The T-shaped transducer was sterilized and placed directly on the surface of the liver. The probe was held in one hand and was applied to all accessible parts of the liver after extensive mobilization and bimanual palpation of the liver. The examination was started on the posterior surface of the right lobe. Thereafter, the probe was passed in both longitudinal and axial directions. The probe was placed laterally and moved to the left to the round ligament. The left lateral segment and the undersurface of the liver were imaged with the same technique. All intraoperative sonograms were obtained by two experienced liver surgeons who were aware of the results of sonography, bolus dynamic CT, and CTP. At the time of surgical exploration, the entire liver was inspected and bimanually examined for the presence of intrahepatic metastases. Intraoperative sonography was performed whenever a partial hepatic resection had already been planned in order to determine whether additional lesions were present. When resection was not performed, biopsy specimens from each lesion detected with intraoperative sonography were obtained with intraoperative sonographic guidance to confirm their malignant natures.

For this retrospective review, two abdominal radiologists and one experienced hepatic surgeon reviewed the sonographic, bolus dynamic CT, and CTP examinations of the 28 patients. The original interpretations rendered at the time the studies were performed were unknown to the reviewers. The radiologists and the surgeon identified all visible lesions and selected a surgical planning approach after viewing sonographic and bolus dynamic CT examinations together during a first interpretation. Two weeks later, during a second interpretation, the CTP examinations were reviewed alone and analyzed in a random manner. Lesions were identified, and a surgical approach was determined. On all CTP images, a rounded, well-delineated, low-attenuation space-occupying lesion was diagnosed as a metastasis. Triangular segments of low attenuation were considered to be artifacts of portal blood flow and were not counted as lesions. The intraoperative sonographic findings of these areas were evaluated to confirm that they reflected perfusion abnormalities rather than metastases or perfusion abnormalities associated with a more proximally located tumor. The operative approaches chosen retrospectively on the basis of the two sets of imaging findings were compared with the surgical procedures actually performed and correlated with the intraoperative findings and pathologic data obtained after examination of the resected specimens. The subsegmental location of the metastases was categorized according to the Couinaud numbering system [12]. The sizes of the metastases to the nearest millimeter were determined from measurements made by the pathologist after surgery or from intraoperative sonography when metastases were not removed. The sensitivities of the imaging techniques were statistically compared by using the McNemar test for paired data [13]. A value less than .05 was considered statistically significant.

Results

Fifty-six metastases to the liver were resected, and a total of 69 metastases were identified by means of palpation and intraoperative sonography with intraoperative biopsy or pathologic examination of the resected specimens. The mean number of metastases per patient was 2.46 (range, one to seven metastases), and the mean tumor diameter was 4.2 ± 2.9 cm (range, 0.4–11.2 cm). One biliary cyst was correctly identified with all preoperative imaging techniques and confirmed at surgery.

Sonography showed 46 of 69 metastases and bolus dynamic CT showed 49 of 69. By combining the results of sonography and bolus dynamic CT, a sensitivity of 75% in the detection of metastases (52 of 69 metastases) was achieved. Three metastases located in the left lobe of the liver were depicted with transabdominal sonography but not with bolus dynamic CT. No lesions were false-positive on the basis of either sonography or bolus dynamic CT (specificity = 100%).

The overall sensitivity for detection of metastases was 93% for CTP (64 of 69 metastases). Five liver metastases were not seen with CTP. Two of them, located deep in the parenchyma, were smaller than 5 mm in diameter, were not detected with intraoperative sonography, and were found incidentally in the resected specimens. The three other metastases measured 8, 10, and 12 mm in diameter and were located on the surface of the liver under the hemidiaphragm. These metastases, not visible with sonography or bolus dynamic CT, were detected only by palpation and intraoperative sonography. Twelve metastases (17%) in five patients were detected preoperatively with CTP alone. The mean size of these metastases was 1.4 ± 0.3 cm (range, 0.8–2.0 cm). No lesions were false-positive on the basis of CTP findings (specificity = 100%).

The difference in sensitivity between combined sonography–bolus dynamic CT and CTP was statistically significant ($p < .01$). The confidence interval of the differences in the sensitivities between CTP and combined sonography–bolus dynamic CT was 0.08–0.28, indicating that CTP can be used to detect between 8% and 28% more metastases from colorectal cancer than the combination of sonography and bolus dynamic CT can.

The operative approaches suggested on the basis of combined sonography–bolus dynamic CT and CTP are outlined in Table 1. CTP findings altered the choice of operative approach in five of 28 patients. One case was considered inoperable because four additional metastases were seen in Couinaud subsegments II, IV, V, and VIII on CTP. The initial decision was changed from left lateral segmentectomy to left lobectomy in one patient because three additional metastases were found in subsegments III and IV on CTP. The initial decision was changed from right lobectomy to trisegmentectomy in one patient because two additional metastases were detected in subsegment IV on CTP. The initial decision was changed from left lateral segmentectomy to left lateral segmentectomy with additional right inferior subsegmentectomy in one patient when two additional metastases were detected in subsegments II and VI. The initial decision was changed from left lateral segmentectomy to left lateral segmentectomy with additional wedge resection in one patient when one additional metastasis was found in subsegment VIII.

In all patients, the operative approaches chosen in retrospect on the basis of CTP findings correlated with the surgical procedures actually performed. At the time surgery was performed, findings on intraoperative sonography did not change the operative procedure selected after viewing sonographic, bolus dynamic CT, and CTP examinations simultaneously.

TABLE 1: Proposed Surgical Approaches Based on Retrospective Evaluation of Imaging Studies

Type of Resection	No. of Patients	
	Combined Sonography–Bolus Dynamic CT	CT Portography
Unresectable	2	3
Resectable		
Lobectomy		
Right sided	4	3
Left sided	5	6
Subtotal	9	9
Trisegmentectomy	6	7
Segmentectomy	4	2
Subsegmentectomy	7	8
Wedge resection	4	5
Total	26[a]	25[b]

Note.—Combined resections were performed in four[a] and six[b] patients.

Discussion

Recent advances in hepatic surgery have resulted in both an increase in the number of candidates for partial hepatic resection for metastatic disease and a decrease in operative morbidity and mortality. Nevertheless, since the number of patients who are candidates for surgery is low, a major role of imaging techniques in patients with liver metastases from colorectal cancer is to assist the surgeon in the preoperative decision regarding the feasibility of and approach to hepatic resection. It is critical that the surgeon have a clear and detailed map of the hepatic involvement with metastases. The ability to perform multisegmentectomies or multisubsegmentectomies underscores the need to accurately determine the number and segmental locations of hepatic metastases. Currently, patients with four or fewer hepatic metastases are considered candidates for resection [10]. Since resection usually is not performed if five or more metastases are present, it is vital to detect even small metastases (less than 1 cm).

Although recent advances in noninvasive imaging techniques, including sonography, bolus dynamic CT, delayed CT, and MRI imaging, have improved the detection of hepatic metastases, the detection rate still remains less than about 85% [6, 14, 15]. The sensitivities of sonography, bolus dynamic CT, and MR imaging make them unsuitable for preoperative imaging when used alone, especially when metastases are small [5, 6, 15]. Previous studies have shown that CTP is the most sensitive technique for detecting focal hepatic lesions [5–7, 14–17]. In our study, sonography did not show 23 (33%) of 69 metastases and bolus dynamic CT did not show 20 (29%) of 69 metastases; the majority of the missed lesions were around 1 cm or less in diameter. CTP did not show five metastases (7%), three of which were located at the hepatic dome. This lack of sensitivity for the detection of metastases located high in the hepatic dome is well known and probably is due to artifacts caused by respiratory motion.

CTP showed 12 metastases in five patients that were not seen with sonography or bolus dynamic CT, changing the surgical planning approach in each case. In the one case considered inoperable owing to CTP findings, the choice was changed from a complex surgical procedure with associated morbidity to a more appropriate and simple surgical procedure (intraarterial catheter placement for chemotherapy). Our study confirms that sonography and bolus dynamic CT are significantly less valuable than CTP in the preoperative management of such cases. Furthermore, in our study, the final decisions based on CTP alone were the same as the surgical decisions actually made for each patient. Since the surgical decisions actually made were based on a combination of the findings of sonography, bolus dynamic CT, CTP, and intraoperative sonography, this result suggests that CTP is the only imaging examination necessary before surgery in patients with hepatic metastases from colorectal cancer.

Recently, intraoperative sonography has been used to detect small metastases not identified by direct palpation or by preoperative imaging techniques [18, 19]. In a recent article, Charnley et al. [18] reported that intraoperative sonography was used to detect additional metastases in patients in whom findings on liver palpation were normal and changed the operative approach based on conventional imaging studies. However, none of these patients were examined preoperatively with CTP. In our study, intraoperative sonography did not show any lesions not seen on CTP that altered the surgical approach. On the other hand, in order to detect additional metastases, intraoperative sonography necessitates wide surgical exposure of the liver. This is of importance when a patient is subjected to the wide surgical exposure necessary for intraoperative sonography only to have it subsequently discovered that the metastases are unresectable and that unnecessary surgery has been performed. In such cases, detection of multiple small metastatic nodules before rather than after opening the abdomen with wide exposure of the liver is definitely to the patient's benefit. Proper preoperative assessment is important because placement of a catheter in the hepatic artery requires a smaller surgical incision and is associated with lower morbidity and mortality.

A high false-positive rate has sometimes been considered a disadvantage of CTP [6]. In accord with another series [17], we performed CTP with a higher injection rate of contrast material and with prior intraarterial injection of papaverine to increase portal blood flow [11]. Because no findings in this study were falsely positive for metastasis, the use of papaverine to improve the homogeneity of hepatic enhancement may have been beneficial in avoiding such errors in diagnosis.

In conclusion, this study shows that CTP provides vital data unattainable with combined sonography–bolus dynamic CT that improve the preoperative assessment of the resectability of hepatic metastases from colorectal cancer. Furthermore, CTP findings more accurately predict the optimal surgical approach in such patients. On the basis of our retrospective study, we recommend that sonography and bolus dynamic CT no longer be performed because CTP alone provides information sufficient for deciding to what extent the liver should be resected in patients with hepatic metastases from colorectal cancer.

REFERENCES

1. Adson MA, Van Heerden JA, Adson MH, Wagner JS, Ilstrup DM. Resection of hepatic metastases from colorectal cancer. *Arch Surg* **1984**;119:647–651
2. Morrow CE, Grage TB, Suthaland DER, Najarian JS. Hepatic resection of secondary neoplasms. *Surgery* **1982**;92:610–614
3. Fortner JG, Silva JS, Golbey RB, et al. Multivariate analysis of a personal series of 247 consecutive patients with liver metastases from colorectal cancer: I. Treatment by hepatic resection. *Ann Surg* **1984**;199:306–316
4. August DA, Ottow RT, Sugarbaker PH. Clinical perspective on human colorectal cancer metastases. *Cancer Metastasis Rev* **1984**;3:303–324
5. Matsui O, Takashima T, Kadoya M, et al. Liver metastases from colorectal cancers: detection with CT during arterial portography. *Radiology* **1987**;165:65–69
6. Heiken JP, Weyman PJ, Lee JKT, et al. Detection of focal hepatic masses: prospective evaluation with CT, delayed CT, CT during arterial portography, and MR imaging. *Radiology* **1989**;171:47–51
7. Nelson RC, Chezmar JL, Sugarbaker PH, Bernardino ME. Hepatic tumors: comparison of CT during arterial portography, delayed CT, and MR imaging for preoperative evaluation. *Radiology* **1989**;172:27–34
8. Charnley RM, Binch C, Morris DL, Hardcastle JD. Visualization of detailed hepatic anatomy by intraoperative ultrasound. *Br J Radiol* **1988**;61:769–770
9. Ravikumar TS, Kane R, Cady B, et al. Hepatic cryosurgery with intraoperative ultrasound monitoring for metastatic colon carcinoma. *Arch Surg* **1987**;122:403–409
10. Sugarbaker PH. Surgical decision making for large bowel cancer metastatic to the liver. *Radiology* **1990**;174:621–626
11. Widrich WC, Nordahl DL, Robbins AH. Contrast enhancement of the mesenteric and portal veins using intra-arterial papaverine. *AJR* **1974**;121:374–379
12. Couinaud C. Le foie. In: Couinaud C, ed. *Etudes anatomiques et chirurgicales.* Paris: Masson, **1957**
13. Dwyer AJ. Matchmaking and McNemar in the comparison of diagnostic modalities. *Radiology* **1991**;178:328–330
14. Gunven P, Makuuchi M, Takayasu K, Moriyama N, Yamasaki S, Hasegawa H. Preoperative imaging of liver metastases comparison of angiography, CT scan and ultrasonography. *Ann Surg* **1985**;202:573–579
15. Yamaguchi A, Ishida T, Nishimura G, et al. Detection by CT during arterial portography of colorectal cancer metastases to liver. *Dis Colon Rectum* **1991**;34:37–41
16. Miller DL, Simmons JT, Chang R, et al. Hepatic metastases detection: comparison of three CT contrast enhancement methods. *Radiology* **1987**;165:785–790
17. Nelson RC, Chezmar JL, Sugarbaker PH, Murray DR, Bernardino ME. Preoperative localization of focal liver lesions to specific liver segments: utility of CT during arterial portography. *Radiology* **1990**;176:89–94
18. Charnley RM, Morris DL, Dennison AR, Amar SS, Hardcastle JD. Detection of colorectal liver metastases using intraoperative ultrasonography. *Br J Surg* **1991**;78:45–48
19. Igawa S, Sakai K, Kinoshita H, Hirohashi K. Intraoperative sonography: clinical usefulness in liver surgery. *Radiology* **1985**;156:473–478

CT Arterial Portography: Causes of Technical Failure and Variable Liver Enhancement

Erik K. Paulson[1]
Mark E. Baker[1]
David J. Hilleren[1]
William P. Jones[1]
Mark H. Knelson[1]
Scott N. Nadel[1]
Richard A. Leder[1]
William C. Meyers[2]

OBJECTIVE. We studied the causes of technical failure and enhancement variability encountered during CT arterial portography.

MATERIALS AND METHODS. CT arterial portograms and digital arteriograms were obtained via the superior mesenteric artery before partial liver resection in 43 patients with malignant tumors. These studies were reviewed for causes of technical failure and variable enhancement.

RESULTS. Eleven (26%) of 43 procedures were technical failures. Causes of failure included aortic injection after catheter dislodgement (four), dense hyperenhancement associated with laminar flow in the portal vein produced by rapid venous return from a selective injection into a proximal branch vessel of the superior mesenteric artery (two), premature scanning beginning at the iliac crest (two), reflux into a replaced right hepatic artery (one), hepatic arterial enhancement via the pancreaticoduodenal arcade (one), and portal hypertension (one). Of the 32 remaining studies, 28 showed areas of parenchymal hypoenhancement or hyperenhancement. Causes of variable enhancement included impaired portal vein perfusion from mass effect of the tumor, laminar flow in the portal vein, and focal fatty infiltration.

CONCLUSION. Technical failures and enhancement variability are common in CT arterial portography. Factors leading to technical failure include catheter choice and position, portal hypertension, and operator error.

***AJR* 159:745-749, October 1992**

Aggressive surgical resection of hepatic masses has led to the need for sensitive imaging techniques, such as CT angiography and CT arterial portography [1-5], that can detect and localize these masses [6-10]. Although the technical aspects of CT angiography have been described, the technical aspects and enhancement variability of CT arterial portography have not been well described [11-13]. During our first year of experience with CT arterial portography, we frequently encountered technical failures and variable patterns of hepatic enhancement. The purpose of this study was to retrospectively review our initial experience with CT arterial portography and to determine the frequency and causes of technical failures and variable enhancement.

Materials and Methods

We reviewed 43 consecutive CT arterial portographic examinations performed in a 12-month period (February 1990 to February 1991) in patients being evaluated for hepatic resection of malignant tumors. The group included 22 men and 21 women 24-84 years old (mean age, 53 years). Twenty-eight patients had hepatic metastases, and 15 had primary liver tumors. The metastatic tumors included colonic carcinoma (22), leiomyosarcoma (three), breast carcinoma (two), and renal cell carcinoma (one). The primary liver tumors included hepatocellular cancer (12), sarcoma (one), focal nodular hyperplasia (one), and adenoma (one). Before CT arterial portography, digital subtraction angiography of the superior mesenteric artery (SMA) and celiac artery was performed. CT arterial portography was done after

Received February 12, 1992; accepted after revision April 20, 1992.

[1] Department of Radiology, Box 3808, Duke University Medical Center, Durham, NC 27710. Address reprint requests to E. K. Paulson.

[2] Department of Surgery, Duke University Medical Center, Durham, NC 27710.

0361-803X/92/1594-0745
©American Roentgen Ray Society

catheterization of the SMA. When a replaced right hepatic artery (RRHA) was identified, an attempt was made to position the catheter well beyond its origin. The following catheters were used: 5-French Mikaelsson (13), 5.5-French Chuang B (13), 5-French cobra (two), 5-French Simmons II with side holes (11), Simmons I with side holes (two), and unspecified (two).

CT arterial portography was performed with a GE 9800 HiLight or HiLight Advantage (General Electric Medical Systems, Milwaukee, WI) scanner. Before CT portography, CT scans were obtained at the level of the origin of the SMA to ensure proper catheter placement. CT arterial portograms were obtained using the following dynamic technique: contiguous 10-mm axial sections through the liver beginning at the inferior margin, 2-sec scanning time, and 6-sec interscan delay. Scanning was begun 20 sec after the start of the contrast injection. Between 150 and 200 ml iopamidol 300 was injected using a mechanical pump injector (MedRad, Pittsburgh, PA) at 2 ml/sec for 10 sec followed by 1 ml/sec for the remainder of the contrast volume. The volume of contrast medium was based on the liver's size as determined subjectively on the scanogram. Twenty-two patients received 200 ml of contrast medium. Twenty-one patients received 150 ml of contrast medium. Six-hour delayed iodine scanning was not routinely performed.

All angiograms were reviewed retrospectively by an experienced angiographer to identify possible causes of technical failure or variable enhancement. The position of the catheter within the SMA and the presence of an RRHA or collateral arterial supply to the hepatic artery from the SMA was recorded. All CT arterial portograms were reviewed retrospectively by two CT radiologists. Scans were considered technically adequate if segments unaffected by tumor were well opacified. Thus, a scan was technically adequate if areas of variable enhancement allowed the observer to detect the presence or absence of lesions with confidence. Scans were categorized as technical failures if there was failure to opacify at least one segment of the liver, hepatic arterial rather than portal venous enhancement, or if dense hyperenhancement of at least one segment hampered lesion detection. These scans were reviewed for the cause of the failure.

Technically adequate scans were evaluated for areas of parenchymal hypoperfusion or hyperperfusion. Tumor-related hypoperfusion was defined as decreased enhancement of a segment or area of the liver due to mass effect on the portal vein with shunting of opacified blood away from affected segments. Non-tumor-related hypoperfusion was defined as decreased enhancement of a segment of the liver unrelated to mass effect from tumor. Tumor-related hyperperfusion was defined as increased enhancement of a segment or area of liver caused by mass effect associated with shunting of opacified blood toward that segment. Non-tumor-related hyperperfusion was defined as increased enhancement of a segment or area unrelated to mass effect from tumor.

The digital subtraction angiograms and CT arterial portograms were evaluated to determine the cause of the variable enhancement, although a specific cause was not always identified. Scans were further evaluated for layering of contrast medium in the portal veins consistent with laminar flow.

Results

Technical Failures

Eleven (26%) of 43 procedures were technical failures. Four failures were due to injection in the aorta rather than the SMA. In two of these cases, preliminary CT scans showed the catheter in the proximal SMA, suggesting that the catheter was dislodged into the aorta during the injection. In the other two failures, no preliminary CT scans were obtained. In these cases, either the catheter was displaced during transfer from the angiography suite to the CT scanner or it was dislodged during the injection (Fig. 1).

Two technical failures were due to markedly increased enhancement of the right lobe associated with streaming of contrast material (laminar flow) in the portal vein leading to hyperperfusion of the dependent lobe (Fig. 2). In both cases, a short, curved, end-hole catheter was placed selectively into a proximal branch of the SMA. Rapid return of dense, opacified blood resulted in the streaming of contrast medium posteriorly in the main portal vein. Two technical failures were due to a technician's error. In both cases, the scanning was begun at the iliac crest rather than the inferior edge of the liver. By the time images of the hepatic domes were obtained, parenchymal and vascular opacification was unacceptable.

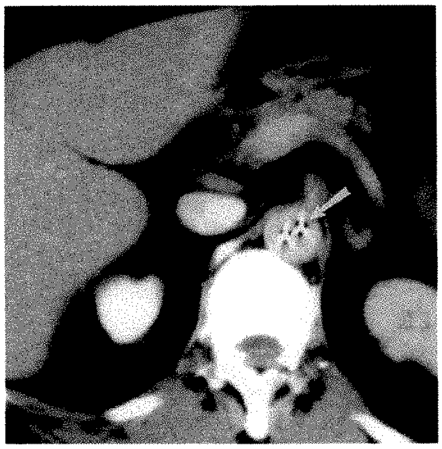

Fig. 1.—Technical failure caused by catheter dislodgement into aorta. CT arterial portogram shows catheter tip in aorta (*arrow*), renal enhancement, and minimal portal venous enhancement.

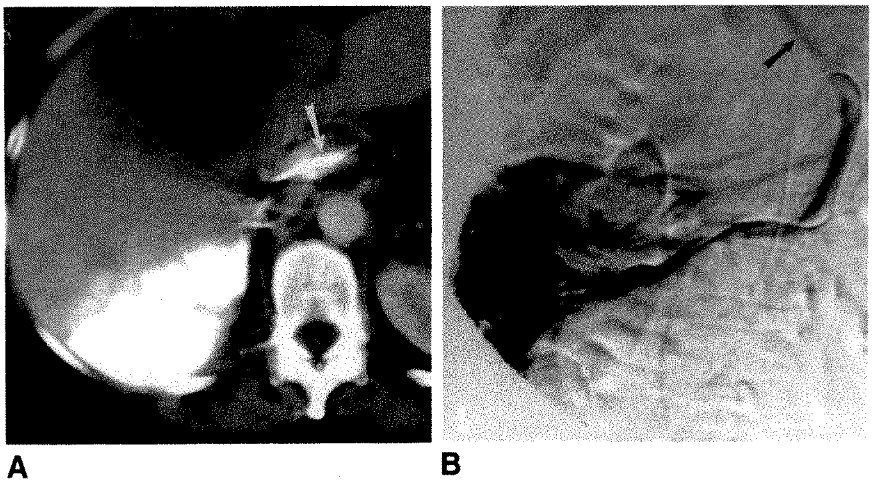

Fig. 2.—Technical failure caused by laminar flow in portal vein.

A, CT arterial portogram shows hyperenhancement of dependent posterior segment of right hepatic lobe. Note streaming of contrast medium in portal vein (*arrow*).

B, Digital subtraction angiogram shows selective injection into proximal branch of superior mesenteric artery with streaming of contrast medium in portal vein (*arrow*).

One of the technical failures was due to arterial enhancement of the right hepatic lobe due to reflux of contrast medium into an RRHA (Fig. 3). This occurred despite placement of the catheter beyond the origin of the RRHA. Either the catheter moved proximally during transport to the CT scanner or there was retrograde reflux of contrast medium into the RRHA.

In one technical failure, the catheter was initially placed into the proximal SMA, and during CT arterial portography it slipped selectively into the pancreaticoduodenal arcade. This caused retrograde opacification of the hepatic artery with dense, arterial enhancement of portions of the right lobe (Fig. 4).

One technical failure occurred in a patient with known portal hypertension. Because of hepatofugal blood flow, the parenchyma was poorly opacified (Fig. 5).

Variable Enhancement

Of the 32 technically adequate examinations, 28 showed areas of parenchymal hypoperfusion or hyperperfusion. Of these, 14 showed hypoperfusion alone, four showed hyperperfusion alone, and 10 showed both hypoperfusion and hyperperfusion. The scans were grouped into those with at least one area of hypoperfusion ($n = 24$) or hyperperfusion ($n = 14$).

Of the 24 cases that showed hypoperfusion (with or without hyperperfusion) 13 were tumor related (Fig. 6), four were associated with laminar flow in the portal vein, three were suggestive of either focal fat or hypoperfusion due to capsular collaterals along the gallbladder fossa (Fig. 7), and four had no clear cause. In the four cases of laminar flow, three examinations were performed with short, curved, end-hole catheters (two Mikaelsson and one Chuang B) and one examination was made with a proximal SMA injection.

In the 14 cases that showed hyperperfusion, six were tumor-related (Fig. 8), six were associated with laminar flow, and two were of unclear cause. In five of the six cases with laminar flow artifacts, three examinations were performed with short, curved, end-hole catheters (two Mikaelsson and one Chuang B) and two were made with proximal SMA injections.

Discussion

Many studies have shown CT arterial portography to be superior to routine dynamic CT or MR imaging for the detection of hepatic metastases [6, 7, 9, 10]. As a result, in many centers, CT arterial portography is now a routine procedure in the preoperative evaluation of patients undergoing liver resection. However, no study has specifically addressed the technical aspects of this examination; thus, the frequency and causes of technical failures are unknown. Further, only one

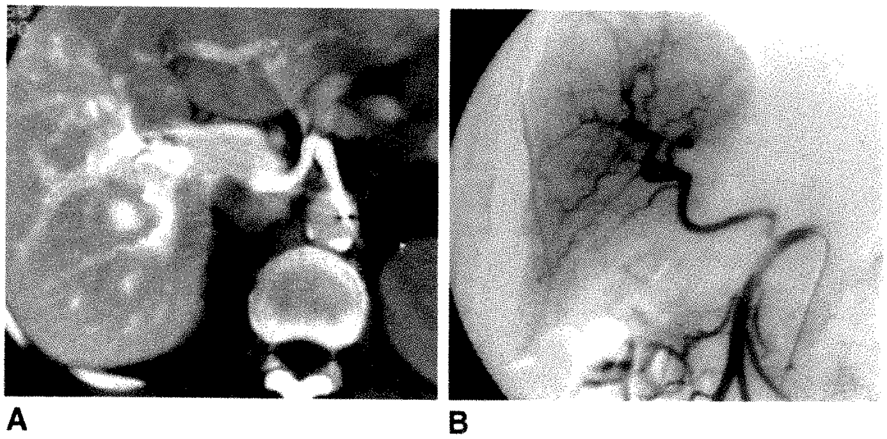

Fig. 3.—Technical failure caused by injection into a replaced right hepatic artery.

***A*, CT arterial portogram shows dense hepatic arterial enhancement with less dense portal venous enhancement.**

***B*, Digital subtraction angiogram of superior mesenteric artery shows replaced right hepatic artery.**

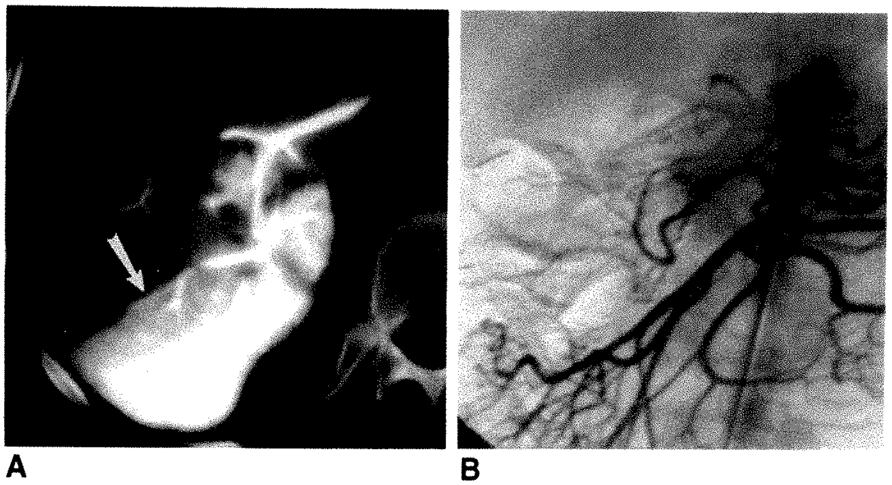

Fig. 4.—Technical failure caused by retrograde hepatic arterial enhancement via pancreaticoduodenal arcade.

***A*, CT arterial portogram shows dense arterial enhancement of portions of right hepatic lobe (*arrow*). Note enhancement of hepatic artery. CT window and level were adjusted to show enhancement to best advantage. Retroportal location of hepatic artery is a normal variation.**

***B*, Digital subtraction angiogram of superior mesenteric artery shows no replaced right hepatic artery. Digital subtraction angiogram of celiac artery (*not shown*) revealed conventional hepatic arterial anatomy.**

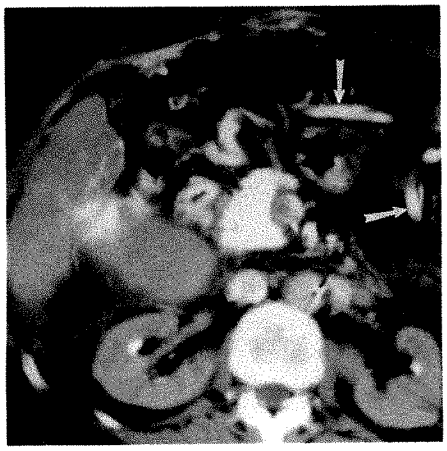

5

Fig. 5.—Technical failure due to portal hypertension with hepatofugal blood flow. CT arterial portogram shows opacified varices (*arrows*) with little opacification of portal vein.

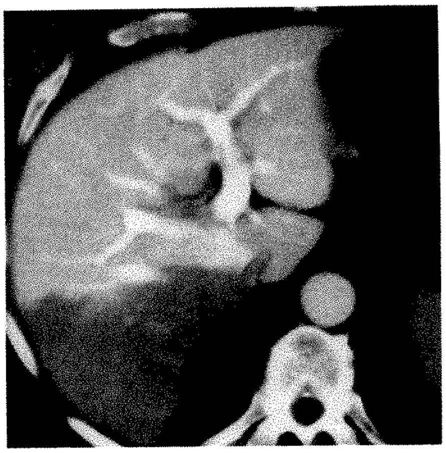

6

Fig. 6.—Tumor-related hypoperfusion. CT arterial portogram shows segmentally decreased enhancement. CT scans of other sections (*not shown*) revealed a central metastasis from colonic carcinoma.

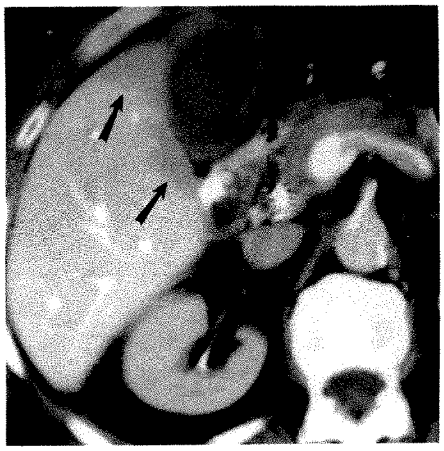

7

Fig. 7.—Non-tumor-related hypoperfusion. CT arterial portogram shows decreased enhancement adjacent to gallbladder (*arrows*). This pattern may be due to fatty infiltration or capsular collateral vessels along the gallbladder fossa.

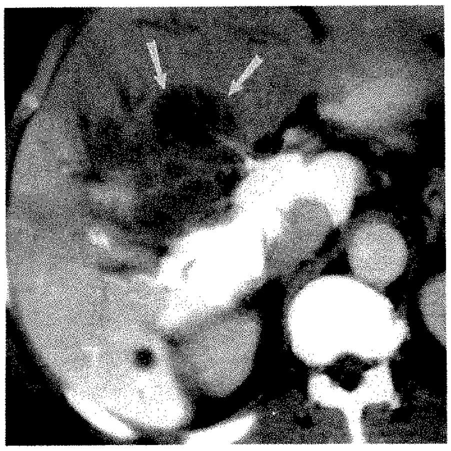

8

Fig. 8.—Tumor-related hyperperfusion. CT arterial portogram shows increased enhancement of caudate lobe and right lobe associated with a central metastasis from colonic carcinoma (*arrows*).

study has addressed the problem of variable enhancement patterns identified in patients undergoing CT arterial portography [13].

We have shown that technical failures are surprisingly common. They are due to a variety of causes, which can be separated into three categories: catheter problems (placement, dislodgement, and type), portal hypertension, and operator error. Our high rate of technical failure occurred during our initial experience with CT arterial portography. As our experience accumulates, the technical failures should decrease.

Aortic opacification was the result of either catheter dislodgement during transport or injection or reflux of significant amounts of contrast medium into the aorta from the SMA. In two such cases, preliminary CT scans showed the catheter in the proximal SMA before injection. This suggests that either dislodgement or reflux may occur with a proximal injection. However, dislodgement would be unlikely with an injection rate of 2 ml/sec.

Technical failure or enhancement variability also can result from proximal placement of catheters in the SMA via three mechanisms. First, if the right hepatic artery is replaced and the catheter is proximal or close to the takeoff of that artery, contrast-filled arterial blood can opacify the segments of the liver and obscure lesions [13]. Second, arterial enhancement of the liver can occur because of retrograde opacification of the hepatic artery via the pancreaticoduodenal arcade. Last, selective injection of proximal branches of the SMA can lead to rapid venous return of densely opacified portal blood. It is well known that contrast medium, which is more dense than blood, flows in the portal vein in a layered fashion [14–16]. With injection of contrast material into a proximal SMA branch, the densely enhanced portal blood has less time to dilute before reaching the main portal vein. When contrast medium reaches the liver, it is more likely to cause variable enhancement of segments receiving flow from dependent branches of the vein.

Many of these catheter problems may be related to the catheter type. Early in our experience, short, curved, Chuang B, or cobra catheters were used, and they tended to be seated in the proximal SMA. This proximal placement increased the possibility of catheter dislodgement during transport or reflux of contrast medium into the aorta. When these end-hole catheters slipped into a side branch during injection or transport, a selective injection occurred. As our experience evolved, long, reverse-curved catheters such as the Simmons II were preferred. Compared with the short, simple curved catheters, these were more easily placed into the distal SMA.

Side holes were punched into the distal end of the catheter to prevent direct injection into small arterial branches.

Operator error led to two technical failures, despite efforts to educate both technologists and radiologists. Thus, the technical failure rate related to the CT arterial portography itself was only nine (21%) of 43 patients. These technical failures point out the need for careful selection of scan levels from the scout view by experienced radiologists. Further, if only a few CT arterial portograms are being obtained, well-trained technologists should be performing such procedures. We did not analyze the effect of injection rate or concentration of contrast material on the technical outcome. Some difficulties could have been related to the rate of injection of contrast material, although the rate and contrast concentration used are similar to those used by other investigators [4, 7, 13, 17].

Mass effect from tumor is a major cause of enhancement variability, which results from diminished portal venous flow caused by the tumor. Although such an effect is well described, we encountered this problem more frequently than previously reported [13, 17]. This higher frequency may relate to our referral population, which may have more advanced disease than did other populations studied. Although some investigators have suggested that variable enhancement patterns may reduce the clinical utility of CT arterial portography because of high false-positive rates, we rarely found this problem to cause diagnostic difficulty [4]. It would be interesting to review routine IV enhanced CT to determine if definite lesions seen on conventional CT scans were obscured in areas of variable enhancement on CT arterial portograms. Unfortunately, the conventional CT scans in this retrospective study were obtained at outside institutions and were not available for review. During our initial experience, 6-hr delayed-iodine CT was not used when variable enhancement was encountered. Since then, we have found it useful in selected cases. We do not routinely administer additional contrast medium to result in a total dose of 60 g of iodine because 50–80 ml are given for the digital subtraction angiogram. In addition, focal areas of diminished enhancement adjacent to the gallbladder and falciform ligament that are suggestive of focal fatty infiltration or hypoperfusion due to capsular collaterals can be confirmed by delayed CT scanning, MR imaging, or surgery [18, 19]. A low-attenuation "pseudolesion" with a characteristic appearance in the posterior aspect of the medial segment of the liver has been attributed to a variation in the vascular supply to this portion of the liver [20].

Although our experience with portal hypertension is limited, patients with this problem may not be well served by CT arterial portography. If hepatofugal blood flow and varices are present, the hepatic parenchyma will not receive adequate opacified blood and enhancement will be unacceptable [21].

Conclusions

Technical failures and enhancement variability are frequently encountered during CT arterial portography. Multiple factors may contribute to these problems, including catheter choice and position, mass effect from tumor, portal hypertension, and operator error. Potential solutions include the following: (1) Careful attention to CT arterial portography technique with preliminary CT scans to verify catheter location in the SMA and close supervision of the technologist doing the scanning. (2) Distal catheter placement, to avoid injection of proximal small branches of the SMA or replaced hepatic arteries. (3) Use of catheters with reverse curves and multiple side holes rather than simple curved end-hole catheters. (4) Use of alternative imaging techniques in patients with portal hypertension. (5) Awareness of frequency of variable enhancement patterns.

REFERENCES

1. Hughes KS, Simon RM, Songhorabodi S, et al. Resection of liver for colorectal carcinoma metastases: a multi-institutional study of indications for resection. *Surgery* **1988**;103:278–288
2. Sugarbaker PH. Surgical decision making for large bowel cancer metastatic to liver. *Radiology* **1990**;174:621–626
3. Freeny PS, Marks WM. Computed tomographic arteriography of the liver. *Radiology* **1983**;148:193–197
4. Miller DL, Simmons JT, Chang R, et al. Hepatic metastasis detection: comparison of three CT contrast enhancement methods. *Radiology* **1987**;165:785–790
5. Nelson RC, Chezmar JL, Sugarbaker PH, Bernardino ME. Hepatic tumors: comparison of CT during arterial portography, delayed CT and MR imaging for preoperative evaluation. *Radiology* **1989**;172:27–34
6. Matsui O, Takashima T, Kodaya M, et al. Dynamic computed tomography during arterial portography: the most sensitive examination for small hepatocellular carcinomas. *J Comput Assist Tomogr* **1985**;9:19–24
7. Matsui O, Tsutomu T, Masumi K, et al. Liver metastases from colorectal cancers: detection with CT during arterial portography. *Radiology* **1987**;165:65–69
8. Nelson RC, Chezmar JL, Sugarbaker PH, Murray DR, Bernardino ME. Preoperative localization of focal liver lesions to specific liver segments: utility of CT during arterial portography. *Radiology* **1990**;176:89–94
9. Heiken JP, Weyman PJ, Lee JKT, et al. Detection of focal hepatic masses: prospective evaluation with CT, delayed CT, CT during arterial portography, and MR imaging. *Radiology* **1989**;171:47–51
10. Takayasu K, Moriyami N, Muramatsu Y, et al. The diagnosis of small hepatocellular carcinomas: efficacy of various imaging procedures in 100 patients. *AJR* **1990**;155:49–54
11. Freeny PC, Marks WM. Hepatic perfusion abnormalities during CT angiography: detection and interpretation. *Radiology* **1986**;159:685–691
12. Dolenz KR, Li KCP, Hawkins IF, Miles SG, Ros PR, Bland KI. Dynamic CT of hepatic masses using intra arterial enhancement: advantages and pitfalls. *Gastrointest Radiol* **1990**;15:241–244
13. Van Beers B, Pringot J, Gigot JF, Dautrebande J, Mathurin P. Nontumorous attenuation differences on computed tomographic portography. *Gastrointest Radiol* **1990**;15:107–111
14. Bron KM. Arterial portography. In: Abrams HL, ed. *Abrams angiography: vascular and interventional radiology,* 3rd ed. Boston: Little, Brown, **1983**:1609–1611
15. Moore GE, Bridenbaugh RB. Roentgen demonstration of the venous circulation in the liver: portal venography. *Radiology* **1951**;57:685–690
16. Copher GH, Dick BM. "Stream line" phenomena in the portal vein and the selective distribution of portal blood in the liver. *Arch Surg* **1928**;17:408–419
17. Tyrrel RT, Kaufman SL, Bernardino ME. Straight line sign: appearance and significance during CT portography. *Radiology* **1989**;173:635–637
18. Yoshikawa J, Matsui O, Takashima T, et al. Focal fatty change of the liver adjacent to the falciform ligament: CT and sonographic findings in five surgically confirmed cases. *AJR* **1987**;149:491–494
19. Marchal G, Tshibwabwa-Tumba E, Verbeken E, et al. "Skip areas" in hepatic steatosis: a sonographic-angiographic study. *Gastrointest Radiol* **1986**;11:151–157
20. Fernandez MP, Bernardino ME. Hepatic pseudolesion: appearance of focal low attenuation in the medial segment of the left lobe at CT arterial portography. *Radiology* **1991**;181:809–812
21. Oliver JH, Baron RL, Dodd GD, Carr BI, VanThiel D. Efficacy of CT portography in the evaluation of cirrhotic patients for hepatocellular carcinoma (abstr). *Radiology* **1991**;181:167

A Halloween Trick?

Nancy Anderson[1]

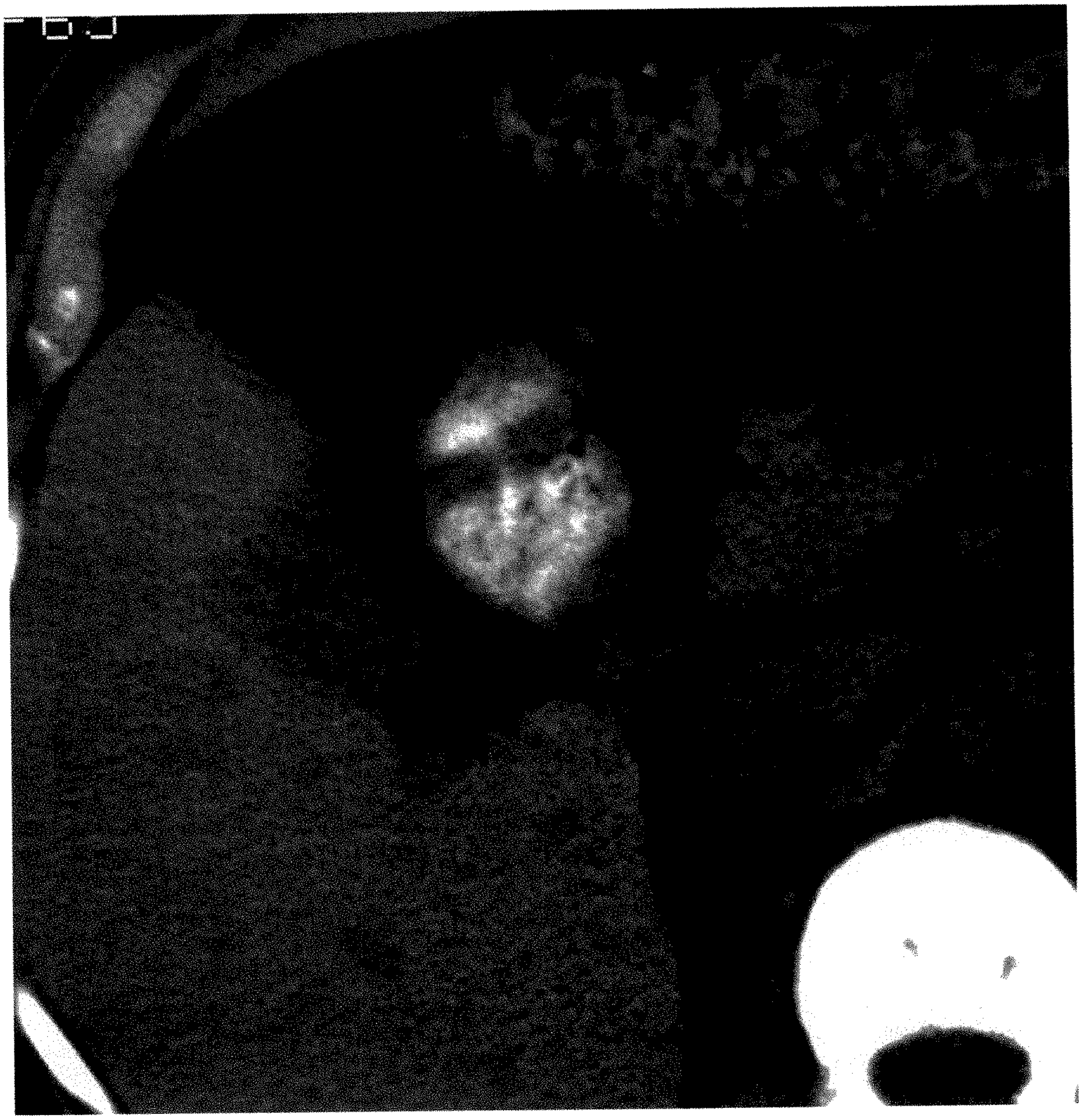

---

[1] X-ray Department, MacGregor Medical Association, 8100 Greenbriar, Houston, TX 77054.

AJR **159:750, October 1992** 0361-803X/92/1594-0750 © American Roentgen Ray Society

Stent Placement for Benign Pancreatic Diseases: Correlation Between ERCP Findings and Clinical Response

David J. Gulliver[1]
Simon Edmunds[2,3]
Mark E. Baker[1]
Susan Paine[1]
John Baillie[2]
Peter B. Cotton[2]
Reed P. Rice[1]

OBJECTIVE. We performed a study to determine if the appearance of the pancreatic duct on ERCP before and after placement of pancreatic duct stents correlates with the therapeutic response in patients treated for impaired pancreatic drainage.

MATERIALS AND METHODS. Findings in 29 consecutive patients with a variety of benign pancreatic diseases in whom pancreatic stents were placed and subsequently removed within a 3-year period were reviewed retrospectively. Early (1-5 days) and late (1-3 months) clinical outcomes after stent placement were assessed. These findings were correlated with a blinded interpretation of ERCP findings (Cambridge criteria were used) before and after stent placement.

RESULTS. ERCP findings before stent placement were normal in 10 patients. At the end of stent therapy, ERCP showed changes associated with chronic pancreatitis in all 10; five had focal narrowing at the tip of the stent. Subsequent ERCP studies in five of these 10 patients showed that ductal changes induced by stents diminished after stent removal. Of the 19 patients with abnormal findings on ERCP at the time of stent placement, ERCP at the end of stent therapy showed some improvement in seven patients, no change in eight, and deterioration in four. Changes seen on ERCP had no statistically significant correlation with clinical outcome ($p = .36$).

CONCLUSION. Our findings show that pancreatic duct stents can induce abnormalities on ERCP indicative of chronic pancreatitis. However, diminution of these abnormalities after stent removal in some patients suggests that these changes may be due to edema rather than to fibrosis. Ductal changes seen on ERCP are not a useful guide for determining the degree of response to pancreatic stents.

***AJR* 159:751-755, October 1992**

Stents are placed in the pancreatic duct in a heterogeneous group of patients thought to have occlusion of the duct or inadequate pancreatic drainage due to benign diseases. Indications for stent placement include pancreas divisum with chronic pain, disrupted pancreatic ducts, pseudocysts communicating with the pancreatic duct, and strictures of the main pancreatic duct with chronic epigastric pain or recurrent pancreatitis [1, 2]. Stents in the pancreatic duct are known to induce ductal changes consistent with chronic pancreatitis in some patients [1, 3]. This study was undertaken to determine if the appearance of the pancreatic duct system on ERCP is useful in assessing clinical response to stent placement.

Materials and Methods

We retrospectively reviewed findings in all patients in whom pancreatic endoprostheses were inserted and subsequently removed within a 3-year period. For each patient, ERCP examinations performed at the time of stent placement and removal were randomized for order, both in terms of ERCP studies done before and after stent therapy, and in terms of the order in which patients' examinations were presented. These studies were then placed side-by-side and reviewed independently by two experienced gastrointestinal radiologists who did not know the patient's name, the dates of the studies, or the timing of each ERCP

Received February 14, 1992; accepted after revision April 10, 1992.

[1] Department of Radiology, Box 3808, Duke University Medical Center, Durham, NC 27710. Address reprint requests to D. J. Gulliver.

[2] Department of Gastroenterology, Duke University Medical Center, Durham, NC 27710.

[3] Present address: Gastroenterology Unit, Royal Perth Hospital, Perth, Western Australia 6000.

0361-803X/92/1594-0751
©American Roentgen Ray Society

examination relative to stent placement. ERCP findings were graded by the observers according to the Cambridge classification of chronic pancreatitis [4]. The observers also recorded which of the two ERCP studies showed more marked changes of chronic pancreatitis. Results from the two observers were compared, and disagreements were resolved by consensus in a separate viewing session with both observers. The diameter of the pancreatic duct was measured at the junction of the head and body of the pancreas before and after stent therapy (with corrections made for magnification by multiplying measured duct diameters by known endoscope diameter, divided by endoscope diameter measured on the film).

The clinical findings in each patient were reviewed by a gastroenterologist who did not know the radiologic findings. The clinical charts of all patients were reviewed for clinical history, signs and symptoms, weight gain or loss, biochemical results (levels of amylase, lipase, albumin, alkaline phosphatase, bilirubin, and aspartate aminotransferase), hematologic results, and results of fecal fat and secretin tests if performed. Values found before stent placement and soon (1–5 days) and later (1–3 months) after removal of the endoprosthesis were recorded. On the basis of these results, early and late clinical outcomes were classified as better than, unchanged from, or worse than before pancreatic stent placement. Pain was assessed subjectively by the patient and according to the type of analgesia required to control it (simple analgesics, compound analgesics, or narcotics). Pain was weighted more strongly than other factors in the assessment of response. Early and late clinical outcomes were then correlated with the radiologic findings.

In patients in whom the ducts appeared normal on initial ERCP but ductal changes of chronic pancreatitis developed during stent therapy, the ductal changes were correlated with the location of the pancreatic stent(s) used to help determine the cause of any ductal changes induced. This correlation was performed by a radiologist not involved in interpreting the ERCP images. In these patients, the radiologic findings were compared with findings on any subsequent ERCP studies to determine the natural history of the ductal changes.

Twenty-nine patients had pancreatic stents placed and subsequently removed within the 3-year period. All patients had benign diseases. Seventeen of these had pancreas divisum, nine had chronic or recurrent pancreatitis, two had stones in the pancreatic duct, and one had a stricture of the pancreatic duct. All patients had pain; one patient also had weight loss. All stents were of the Amsterdam type, made of polyethylene with one side hole, one end hole, and one anchoring flap at each end (Wilson-Cook, Winston-Salem, NC). Twelve patients had 5-French stents and 17 had 7-French stents. We found no correlation between outcome and stent size ($p = 1.0$, Fisher's exact test). Stents were 1–15 cm long. When pancreatic stents were inserted for pancreatic ductal strictures, the stricture(s) were dilated endoscopically with a balloon at the time of stent insertion. Nineteen patients had one stent placed, and 10 had more than one stent placed sequentially during the period of stent therapy. Duration of therapy was 2 weeks to 26 months (mean, 6 months).

Results

Early clinical outcomes were less favorable than late clinical outcomes. Early findings indicated improvement in 14 patients, no change in nine, and worsening in six. However, late findings showed that only nine were better, 10 were unchanged, and 10 were worse. We found no significant difference in clinical outcome between patients with pancreas divisum and those with other diagnoses. Radiologic appearances were graded as worse after stenting in 14 patients, unchanged in eight, and better in seven.

Ten patients had normal findings on ERCP before stent placement, other than the presence of pancreas divisum in eight. The other two patients had abdominal pain associated with recurrent and chronic pancreatitis, respectively. Stents in these patients were inserted for abdominal pain, which was assessed as being possibly related to pancreas divisum and justifying a trial of stent placement. Changes associated with chronic pancreatitis developed in all 10 during stent therapy. Eight had changes associated with "moderate" or "marked" chronic pancreatitis (indicating abnormalities of the main pancreatic duct), one had mild changes, and one had equivocal changes. Of these 10 patients, five were worse clinically, two were unchanged, and three were improved despite the onset of the ductal changes. Changes induced by stents in the main pancreatic duct were seen in eight patients; these consisted of mild to moderate dilatation and irregularity of the main pancreatic duct. Five of these eight patients had focal narrowing at the site of the stent tip (Figs. 1 and 2), two patients had narrowing elsewhere along the site of the stent, and one had narrowing 4 cm proximal to the stent tip. Follow-up studies in the 10 patients in whom pancreatic ductal changes were induced by stents showed that none had further stent therapy, but five had subsequent ERCP studies 2 weeks to 33 months after stent removal (mean, 9 months). Among these five, the ductal changes resolved in one patient, became less marked in two (Fig. 2), and were unchanged in two.

Of the 19 patients in whom findings on ERCP were abnormal at the time of stent placement, the Cambridge grade did not change in 18; in one, it was downgraded from marked to moderate during the period of stent therapy.

When the late clinical outcomes in the 10 patients who had normal ducts before stent placement are compared with those in the 19 patients who had abnormal ducts before stent placement, patients in the first group did not respond to stent placement as well as those in the second group (two and seven, respectively, showed improvement). However, the numbers were not sufficient for statistical significance ($p = .50$, Fisher's exact test).

We found no significant correlation between radiologic changes during the period of stent therapy and either early or late ($p = .36$, Fisher's exact test) clinical outcome (Fig. 3). Duct diameters before and after stent therapy did not correlate with early ($p = .16$, Fisher's exact test) or late ($p = .53$, Fisher's exact) clinical outcome.

Discussion

Endoscopic placement of stents in the pancreatic duct was developed as a less invasive alternative to partial pancreatectomy, Puestow's procedure, surgical sphincterotomy, and other operative procedures [5]. The precise role of these stents has not been clearly defined, but they have been used to treat pancreas divisum or hypertensive pancreatic sphincter associated with chronic pain, disrupted pancreatic ducts, chronic pancreatitis with pseudocysts, chronic pancreatitis with ductal strictures plus chronic pain, and chronic pancreatitis with recurrent attacks of acute pancreatitis [1, 2, 5–11]. Balloon dilatation may be helpful in the management of pan-

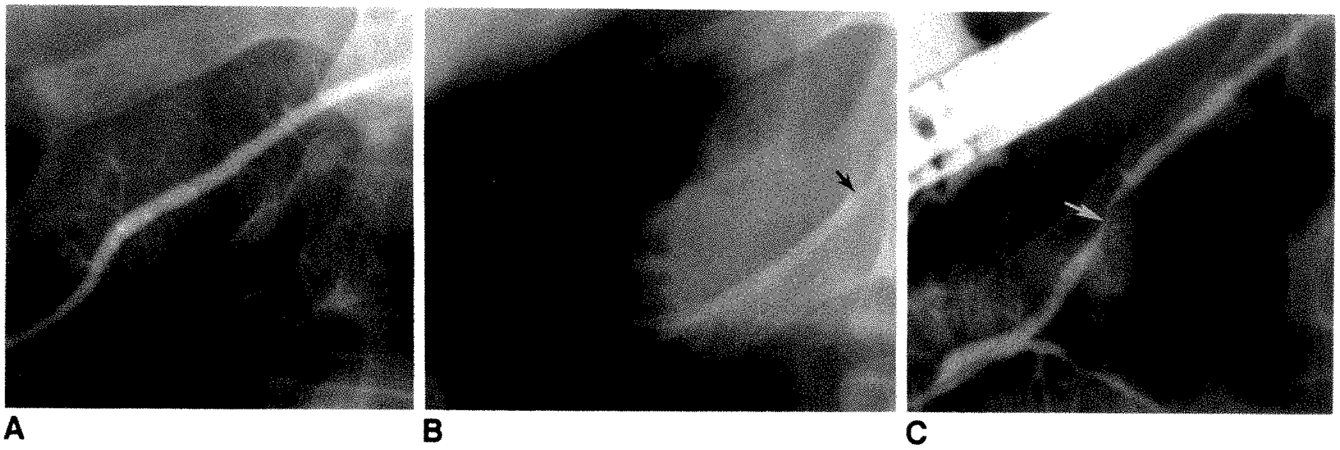

Fig. 1.—Development of pancreatic ductal narrowing at tip of pancreatic stent in patient with pancreas divisum.
A, ERCP shows dorsal pancreatic duct injected via minor papilla. Dorsal pancreatic duct otherwise appears normal.
B, ERCP shows 5-French, 5-cm stent placed in dorsal pancreatic duct. Tip (*arrow*) of stent is approximately 3 cm from minor papilla.
C, ERCP obtained at time of stent removal, 16 days after *B*, shows focal narrowing (*arrow*) at former site of stent tip, approximately 3 cm from minor papilla.

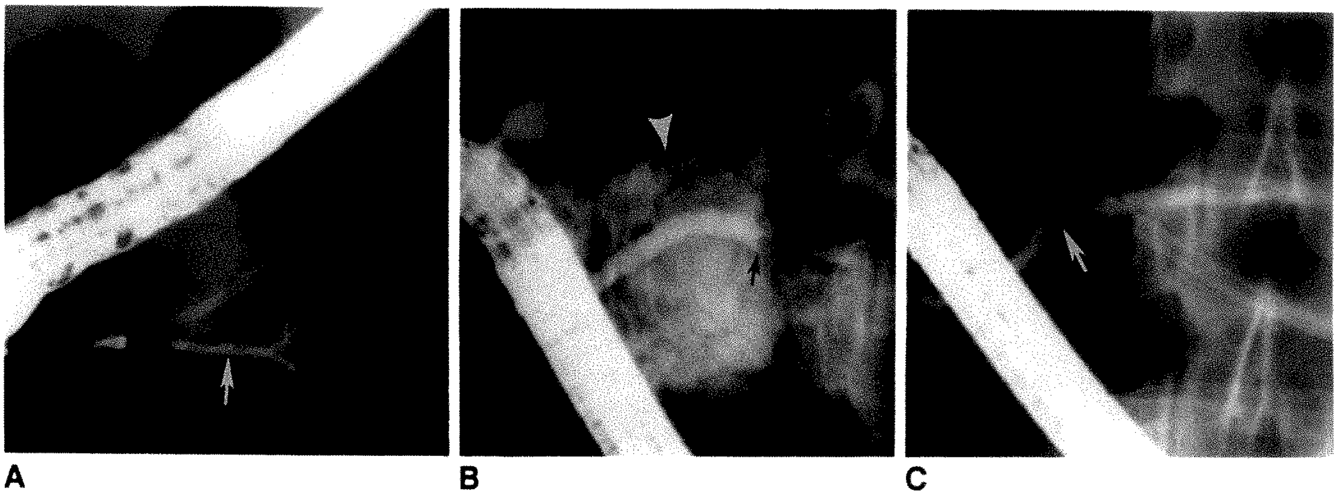

Fig. 2.—Improvement in pancreatic duct narrowing after removal of pancreatic stent in patient with pancreas divisum.
A, ERCP shows placement of stent in dorsal pancreatic duct to treat chronic abdominal pain. Ventral duct is opacified (*arrow*).
B, ERCP obtained 4 weeks later, immediately after removal of stent, shows tight focal narrowing (*arrow*) at former site of tip. Note acinar appearance (*arrowhead*) of pancreatic head.
C, ERCP obtained 2 weeks after *A* shows marked improvement in narrowing (*arrow*) of pancreatic duct.

creatic duct strictures [2, 11], but we use this technique only in conjunction with stent therapy because our experience has shown a high probability of stricture recurrence.

Others have found that stents in the pancreatic duct induce ductal changes consistent with chronic pancreatitis [1, 3], and this study confirms these findings. Narrowing in the main pancreatic duct produced during stent therapy can be focal or relatively diffuse, but in our study it usually occurred in the part of the pancreatic duct occupied by the stent, especially the stent tip (Figs. 1 and 2). In all 10 patients with normal pancreatic ducts (other than the presence of pancreas divisum in eight) at the beginning of the period of stent therapy, ERCP immediately after stent therapy showed changes associated with chronic pancreatitis. Seven of these 10 had changes associated with moderate chronic pancreatitis after stenting, indicating abnormalities in the main pancreatic duct. In another patient, ERCP showed changes associated with marked chronic pancreatitis. In addition, of these 10 patients, only two improved clinically; clinical findings became worse in five.

We have described the ductal changes seen in patients in this study as "associated with chronic pancreatitis," and the Cambridge classification of chronic pancreatitis was used to grade them. However, it must be stressed that although many of the ductal changes seen were due to chronic pancreatitis, other ductal changes were not. This is particularly true of reversible or partially reversible ductal narrowing induced by pancreatic stents, which we propose may be due, at least in part, to edema (Fig. 2).

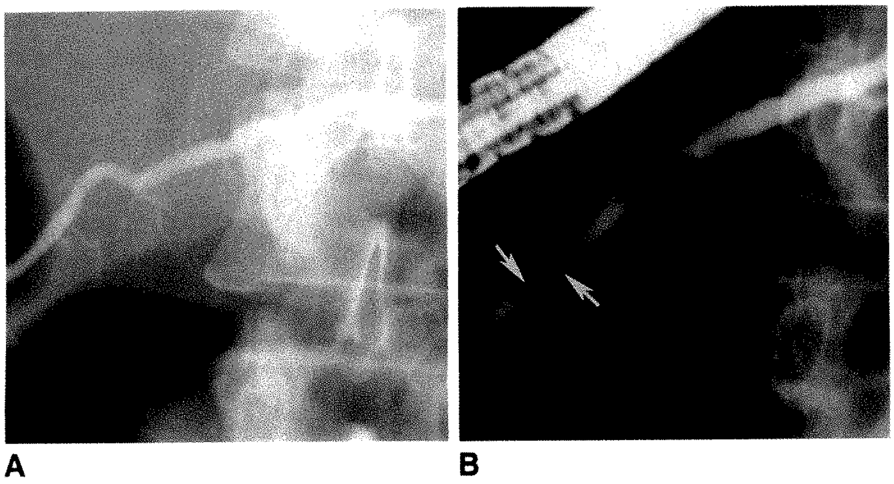

Fig. 3.—Poor correlation between clinical response and ERCP findings after placement of stent in pancreatic duct of patient with pancreas divisum.

A, ERCP shows dorsal pancreatic duct immediately before insertion of 5-French, 3-cm stent.

B, ERCP immediately after end of stent therapy shows narrowing in pancreatic duct at former site of stent (*arrows*). Despite this, the patient had improved clinically, with less pain.

A potential difficulty in studying the findings in this group of patients lies in differentiating pancreatic ductal changes induced by stents from those developing as a result of the underlying disease. Although chronic pancreatitis may have been responsible for progression of some ductal changes in our study, the appearance of ductal abnormalities during stent therapy in the 10 patients with previously normal ducts demonstrates the potential for stents to induce ductal changes. This was seen particularly in those patients in whom focal narrowing developed at the tip of the stent.

The appearance of the pancreatic duct system on ERCP was not a useful guide to the clinical outcome after stent placement. This has not been previously reported, although a study by McCarthy et al. [9] noted that two patients had symptomatic improvement despite the appearance of pancreatic ductal changes consistent with chronic pancreatitis during the period of stent therapy. In some patients in our study, clinical findings improved but radiologic findings worsened. In others, the clinical findings became worse and the radiologic findings improved. Although radiologic and clinical progression had a weak positive correlation, this did not approach clinical significance, either for early or for late clinical outcome.

In our study, clinical outcomes after placement of a stent in the pancreatic duct were less encouraging than those obtained by others [2, 8, 9, 11]. Our results did not show a positive overall clinical outcome at 1–3 months after stent placement, despite somewhat better results at 1–5 days after stent placement.

Other studies [2, 8, 9, 11] describe a collective experience of 136 patients with chronic pancreatitis, pancreas divisum, or acute relapsing pancreatitis who had stents placed in the pancreatic duct. Overall, improvement was seen in 87 patients (64%) at medium- to long-term follow-ups (3 months to 3 years). Huibregtse et al. [2] described endoscopic therapy in 30 patients with chronic pancreatitis. Of the 16 patients who had pancreatic stents as part of their therapy, 12 were thought to be improved clinically and four were worse. Cremer et al. [11] described placement of large (10-French) plastic stents in 75 patients with chronic pancreatitis and strictures of the pancreatic duct. Ninety-four percent of these patients had relief of pain immediately after stent placement. However, follow-up for a mean of 37 months showed that 11 of the 75 required pancreatojejunostomy and 22 subsequently had metal-mesh stents inserted after the plastic stent did not significantly improve the pancreatic ductal stenosis. Complications were uncommon but included stent clogging, stent migration, and cholangitis.

Kozarek et al. [8] included in their study 12 patients with acute relapsing or chronic pancreatitis treated with pancreatic stents. Eight of the 12 patients improved with stent therapy, and four were unchanged or worse; results in patients with chronic pancreatitis were better than results in those with acute relapsing pancreatitis. McCarthy et al. [9] treated 33 patients with endoscopic findings of pancreas divisum or recurrent pancreatitis with 5- or 7-French stents. Twenty-five improved symptomatically, whereas eight did not. Results were better for those with pancreas divisum than for those with recurrent pancreatitis. In this study, ductal changes of chronic pancreatitis developed in two patients during stent therapy despite symptomatic improvement.

The clinical results of our study are disappointing in comparison with the results of others, particularly with regard to the number of patients who became worse after stent placement (10 of 29 patients). Possible explanations for these differences include differences in the populations, selection of patients, and technique. More work needs to be done before the value of stent placement and the indications for its use are established, particularly in patients in whom ERCP before stent placement shows no changes associated with pancreatitis.

Increased pressure within the pancreatic duct may be a major factor in the production of pain in chronic pancreatitis [2, 5, 6, 12]. This has led to the use of pancreatic duct manometry (performed during ERCP) to predict which patients may benefit from stent placement, pancreatic sphincterotomy, or surgical decompression. Manometry is currently used in our institution to diagnose papillary stenosis in patients with recurrent idiopathic pancreatitis. However, manometry has not yet been widely used to assess the significance of pancreatic duct strictures owing to uncertainty in interpretation of the results [5, 6]. In practice, ductal strictures are usually assessed according to the degree of ductal dilatation they produce and the patient's clinical history. We do not use manometry in patients with pancreas divisum, because the minor papilla is too small to accommodate this device.

Stents in the pancreatic duct may cause ductal changes associated with chronic pancreatitis, particularly focal narrowings of the main pancreatic duct at the tip of the stent, which usually improve after stent removal. In patients with abnormal ducts at the time of stent placement, the appearance of the ductal system may improve or deteriorate during stent therapy. However, correlation with the clinical findings in patients in this study indicates that radiologic features are not a useful guide to clinical response to pancreatic stent placement.

REFERENCES

1. Kozarek RA. Pancreatic stents can induce ductal changes consistent with chronic pancreatitis. *Gastrointest Endosc* **1990**;36:93–95
2. Huibregtse K, Schneider B, Vrij AA, Tytgat GNJ. Endoscopic pancreatic drainage in chronic pancreatitis. *Gastrointest Endosc* **1988**;34:9–15
3. Derfus GA, Geenen JE, Hogan WJ. Effect of endoscopic pancreatic duct stent placement on pancreatic ductal morphology (abstr). *Gastrointest Endosc* **1990**;36:206–207
4. Axon ATR. Endoscopic retrograde cholangiopancreatography in chronic pancreatitis. *Radiol Clin North Am* **1989**;27:39–50
5. Malfertheiner P, Buchler M. Indications for endoscopic or surgical therapy in chronic pancreatitis. *Endoscopy* **1991**;23:185–190
6. Widdison AL, Alvarez C, Karanjia ND, Reber HA. Experimental evidence of beneficial effects of ductal decompression in chronic pancreatitis. *Endoscopy* **1991**;23:151–154
7. Cotton PB. Effectiveness of endoscopic drainage for pancreas divisum. *Endoscopy* **1991**;23:107–108
8. Kozarek RA, Patterson DJ, Ball TJ, Traverso LW. Endoscopic placement of pancreatic stents and drains in the management of pancreatitis. *Ann Surg* **1989**;209:262–266
9. McCarthy J, Geenen JE, Hogan WJ. Preliminary experience with endoscopic stent placement in benign pancreatic diseases. *Gastrointest Endosc* **1988**;34:16–18
10. Burdick JS, Hogan WJ. Chronic pancreatitis: selection of patients for endoscopic therapy. *Endoscopy* **1991**;23:155–160
11. Cremer M, Deviere J, Delhaye M, Baize M, Vandermeeren A. Stenting in severe chronic pancreatitis: results of medium-term follow-up in seventy-six patients. *Endoscopy* **1991**;23:171–176
12. Bradley E. Pancreatic duct pressure in chronic pancreatitis. *Am J Surg* **1982**;32:367–368

New Format for Abstracts

Beginning immediately, the *AJR* will publish abstracts of articles in a different format, much like the ones recently adopted by the *New England Journal of Medicine* and the *Journal of the American Medical Asociation*. The purpose of the new design is to have abstracts present the essential elements of articles more clearly and concisely. The contents, organization, and length of the abstracts will be the same as before; however, rather than being all one paragraph except for the conclusion, abstracts will now be divided into four paragraphs, each with a title: objective, subjects (or materials) and methods, results, and conclusion.

The *AJR* Guidelines for Authors, which appears at the front of every issue of the Journal, has been revised to help you write abstracts in this new format. Authors should familiarize themselves with these guidelines and incorporate them into all manuscripts submitted for publication.

Robert N. Berk
Editor-in-Chief

Radiologic-Pathologic Conferences of the Massachusetts General Hospital

Bronchial Carcinoid

Felix S. Chew and James H. Brown[1]

A 20-year-old man had four episodes of hemoptysis over the past year. Chest radiographs and conventional tomograms showed a mass in the left mainstem bronchus (Fig. 1). CT scan confirmed the presence of a single endobronchial lesion and revealed no extrabronchial abnormalities. The differential diagnosis included bronchial carcinoid, mucoepidermoid adenoma, adenoid cystic carcinoma, hamartoma, and mesenchymal tumor. A sleeve resection of the left mainstem bronchus was performed, and an ovoid mass arising from the mucosal surface was found. There was no invasion of the underlying cartilaginous rings. Six regional lymph nodes were sampled and found to be free of tumor. The final pathologic diagnosis was bronchial carcinoid.

The classic bronchial carcinoid, formerly called bronchial adenoma, is a low-grade malignant neoplasm that shares histologic features with Kulchitsky's cells, a neuroendocrine argentaffin cell of the bronchial and bronchiolar mucosa [1–3]. The carcinoid tumor is further characterized by an organoid growth pattern with a rich vascular stroma, minimal nuclear pleomorphism, minimal mitotic activity, and an absence of necrosis. It is the lowest grade subtype of the pulmonary neuroendocrine tumors (the others being atypical carcinoid tumor and neuroendocrine carcinoma), also called Kulchitsky-cell carcinomas (type I of three subtypes). The lesion occurs in adults and is rare in adolescents. The prognosis is favorable following surgical resection with clear margins [2, 3].

Bronchial carcinoids usually involve subsegmental or more proximal bronchi. Because the lesions grow slowly into the bronchial lumen, the typical presentation is segmental or lobar atelectasis, leading to indolent symptoms of coughing, wheezing, recurrent infections, or hemoptysis. When directly visualized, the lesions are polypoid intraluminal masses smaller than 3 cm. A more peripheral lesion will present as an asymptomatic pulmonary nodule because the region of distal atelectasis is radiologically and clinically insignificant. Even in patients with metastatic disease (10% of cases), carcinoid syndrome (intermittent diarrhea, flushing, and cyanosis) is uncommon [3].

REFERENCES

1. Forster BB, Müller NL, Miller RR, Nelems B, Evans KG. Neuroendocrine carcinomas of the lung: clinical, radiologic, and pathologic correlation. *Radiology* **1989**;170:441–445
2. Warren WH, Faber LP, Gould VE. Neuroendocrine neoplasms of the lung. A clinicopathologic update. *J Thorac Cardiovasc Surg* **1989**;98:321–332
3. McCaughan BC, Martini N, Bains MS. Bronchial carcinoids. Review of 124 cases. *J Thorac Cardiovasc Surg* **1985**;89:8–17

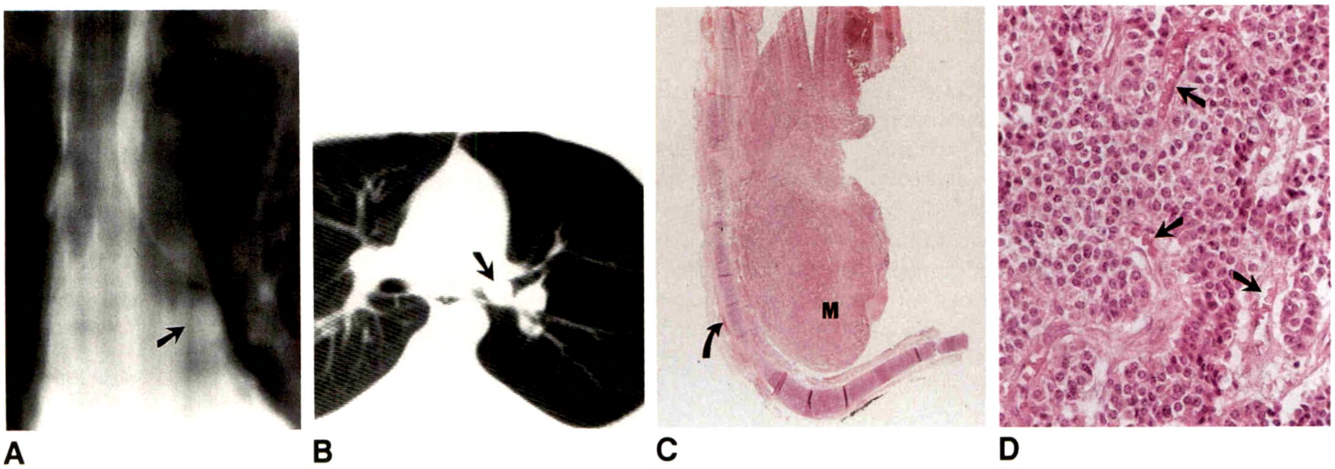

Fig. 1.—Bronchial carcinoid.
***A* and *B*, Anteroposterior linear tomogram (*A*) and CT scan (*B*) show intrabronchial polypoid mass (*arrows*) without extrabronchial extension.**
***C*, Removed segment of bronchus shows ovoid mass (M) arising from mucosal surface of left main bronchus (*arrow*).**
***D*, Photomicrograph shows cords and islands of tumor cells that have centrally placed nuclei and moderate amounts of eosinophilic cytoplasm. Numerous vessels (*arrows*) traverse the stroma.**

From the weekly radiologic-pathologic correlation conferences conducted by Jack Wittenberg. Pathology editor: Andrew E. Rosenberg. Radiology editors: Felix S. Chew, William E. Palmer, Daniel P. Barboriak, Daniel I. Rosenthal.

[1] Both authors: Department of Radiology, Massachusetts General Hospital and Harvard Medical School, 32 Fruit St., Boston, MA 02114. Address reprint requests to F. S. Chew.

***AJR* 159:756, October 1992** 0361–803X/92/1594–0756 © American Roentgen Ray Society

Pictorial Essay

Regional Lymph Node Metastases in Carcinoma of the Left Side of the Colon and Rectum: CT Demonstration

Christine A. J. Granfield,[1] Chusilp Charnsangavej,[1] Ronelle A. Dubrow,[1] Datla G. K. Varma,[1]
Steven A. Curley,[2] Nancy O. Whitley,[1,3] and Sidney Wallace[1]

Regional lymph node metastases are one of the most common routes of tumor spread in colorectal carcinoma. In the past decade, CT has been used in the staging of colorectal carcinoma. However, the accuracy of CT in detecting regional nodal metastasis has not been satisfactory, varying between 22% and 73% [1, 2]. Because of the paucity of information in the imaging literature of this subject, we review the distribution of lymph node metastases on CT scans of patients with colorectal carcinoma.

The purpose of this pictorial essay is to illustrate the CT appearance of the groups of nodes that can be the site of metastases or recurrent disease from colorectal carcinoma. The focus is on the left side of the colon (the descending colon and sigmoid colon), the rectum, and the anus.

Nodal Metastases in Carcinoma of the Left Side of the Colon and Upper Rectum

Tumors originating from the left side of the colon and upper rectum may spread to the lymph nodes via lymphatics in the mesocolon and mesorectum toward the root of the mesocolon. These lymph nodes can be classified into four groups: the epicolic nodes, the paracolic nodes, the intermediate mesocolic nodes including the left colic nodes, and the principal inferior mesenteric artery (IMA) nodes [3, 4] (Fig. 1).

The epicolic nodes lie on the wall of the colon beneath the peritoneum covering the colon. Recognizing this nodal group as a separate entity may be difficult because the nodes may be contiguous with the tumor, but in general, they lie on the antimesocolic side of the colonic wall.

The paracolic nodes lie medial to the wall of the colon along the mesocolic side (Fig. 2). They accompany the marginal vessels of the descending and sigmoid colon. The nodes can be recognized and distinguished from the vessels by their relative lack of contrast enhancement in comparison with the vessels; in addition, they cannot be traced on consecutive CT slices, whereas the vessels can be followed because of their predictable course and because they are usually smaller than the nodes.

The intermediate mesocolic nodes lie in the mesocolon farther away from the colon. The nodes follow the vessels in the mesocolon; that is, the superior hemorrhoidal arteries and veins (Fig. 3), the sigmoidal arteries and veins, and the left ascending colic arteries and veins. The left colic nodes, also considered as intermediate nodes, are located at the junction of the inferior mesenteric vein (IMV) and the left colic branch of the IMA (Figs. 4 and 5). These nodes can be distinguished from and should not be mistaken for paraaortic or common iliac nodes. By following the course of the superior hemor-

---

Received February 24, 1992; accepted after revision April 13, 1992.
Presented in part at the annual meeting of the American Roentgen Ray Society, Orlando, FL, May 1992.

[1] Department of Diagnostic Radiology, The University of Texas M. D. Anderson Cancer Center, 1515 Holcombe Blvd., Houston, TX 77030. Address reprint requests to C. Charnsangavej.

[2] Department of General Surgery, The University of Texas M. D. Anderson Cancer Center, Houston, TX 77030.

[3] Present address: Diagnostic Radiology, The University of Maryland Medical Systems Hospital, 22 S. Greene St., Baltimore, MD 21201.

AJR 159:757-761, October 1992 0361-803X/92/1594-0757 © American Roentgen Ray Society

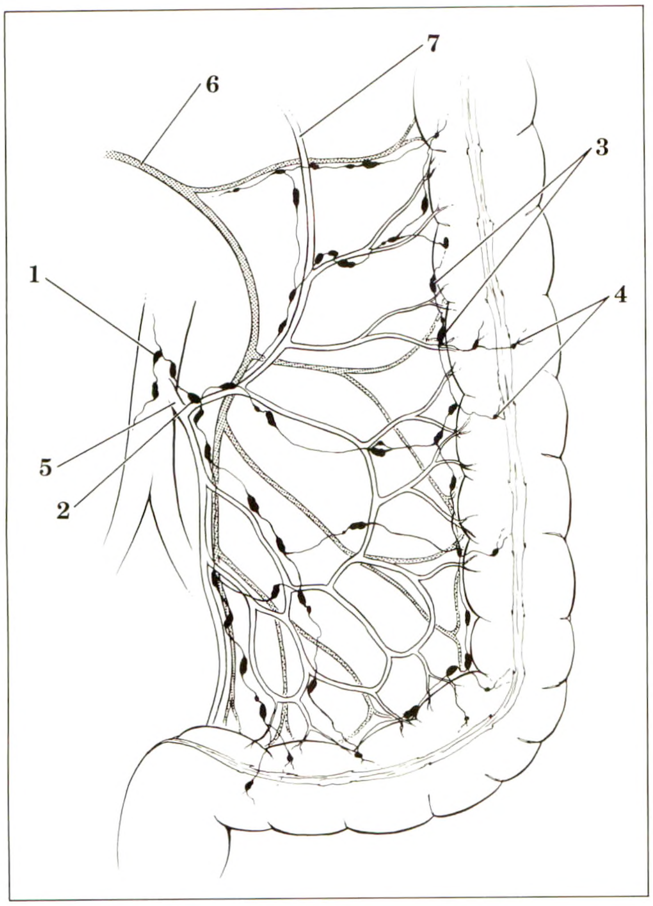

Fig. 1.—Diagram shows lymphatic drainage of descending colon, sigmoid colon, and upper rectum. 1 = principal nodes, inferior mesenteric artery nodes; 2 = left colic nodes; 3 = paracolic nodes; 4 = epicolic nodes; 5 = inferior mesenteric artery; 6 = inferior mesenteric vein; 7 = left ascending colic artery.

rhoidal vein in the sigmoid mesocolon, where it forms the IMV coursing in the cephalic direction, the IMV can generally be detected anterior and medial to the left common iliac vessels. As it ascends farther, it remains anterior but becomes lateral to the left common iliac vessels; this is where it meets the left colic branch of the IMA and where the left colic nodes are located. The adjacent anatomic landmarks are the left ureter, the left gonadal vein, and the left common iliac vessels, all of which are slightly posterior to the IMV and left colic nodes. When these nodes enlarge, they may invade and involve the left ureter and left common iliac vessels and become indistinguishable from abnormal common iliac nodes (Fig. 5).

The principal nodes for lymphatic drainage of the left side of the colon and upper rectum are the IMA nodes. This nodal group consists of several nodes around the orifice of the IMA, where it originates from the abdominal aorta. Abnormal IMA nodes can be recognized as soft-tissue nodules slightly to the left of and anterior to the abdominal aorta (Fig. 6) at about the level of the third lumbar vertebrae. Detecting the orifice of the IMA on CT should not be difficult, particularly after injection of IV contrast material, because the orifice of the IMA is quite constant.

Distribution of metastasis in these different nodal groups in the mesocolon seems to change as the location becomes farther away from the primary tumors; that is, metastases involving the IMA or left colic nodes are less common than ones that involve the paracolic nodes. Isolated involvement of the IMA or left colic nodes is rare, and when these nodes are involved, they are usually associated with hepatic metastases or peritoneal disease. Involvement of the left colic node is often associated with obstruction of the left ureter (Fig. 5) because of the proximity of the two structures.

Nodal Metastases in Carcinoma of the Lower Rectum and Anus

Tumors in the rectum can spread by two different pathways, either following the superior hemorrhoidal route (Fig. 3) toward the mesorectum and mesocolon or following the lateral pathways along the middle and inferior hemorrhoidal vessels toward the hypogastric and obturator nodes, and then to the paraaortic nodes (Fig. 7). Tumors in the anus generally spread to the superficial inguinal nodes at the sa-

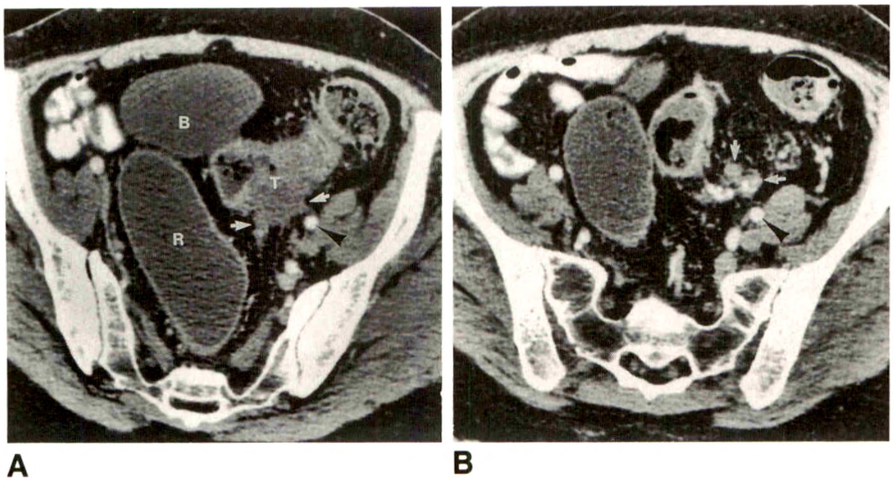

Fig. 2.—CT scans of paracolic nodes obtained during bolus phase of IV contrast enhancement. Slice thickness = 1.5 mm.

A, Primary adenocarcinoma (T) of sigmoid colon with tumor invasion (*arrows*) beyond serosa. B = bladder, R = rectum.

B, Cluster of nodes (*arrows*) in paracolic nodal group in sigmoid mesocolon.

Arrowheads = external iliac artery.

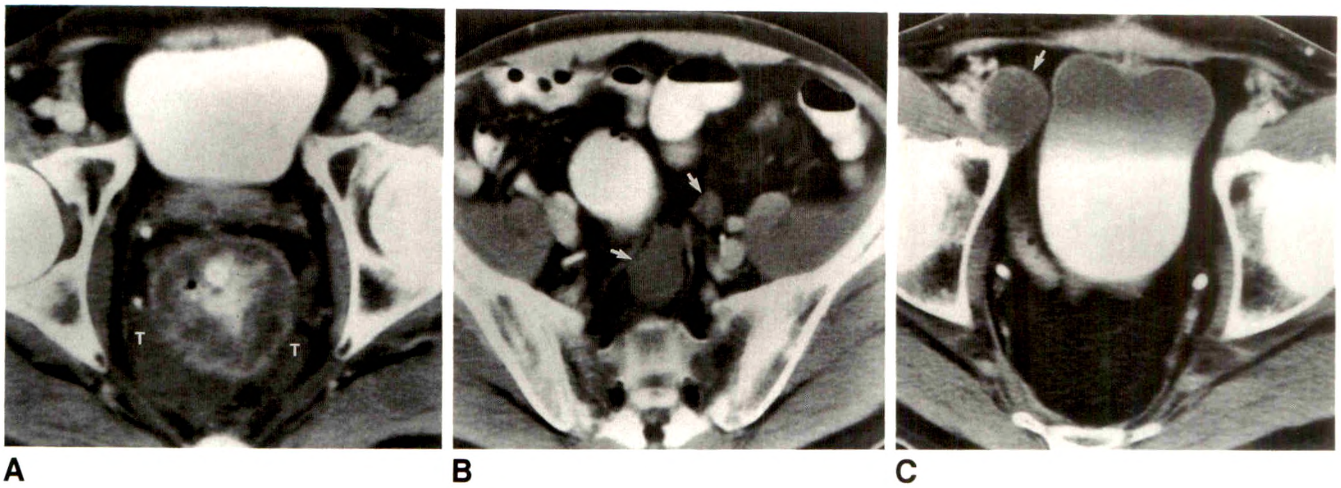

Fig. 3.—CT scans of mesocolic nodes and recurrent disease in deep inguinal node after anteroperineal resection of colorectal carcinoma.

A, Primary adenocarcinoma of rectum with apparent perirectal invasion (T).

B, Enlarged sigmoid mesocolic nodes (*arrows*) at level of mesocolon.

C, Recurrent disease (*arrow*) in right deep inguinal node after surgery.

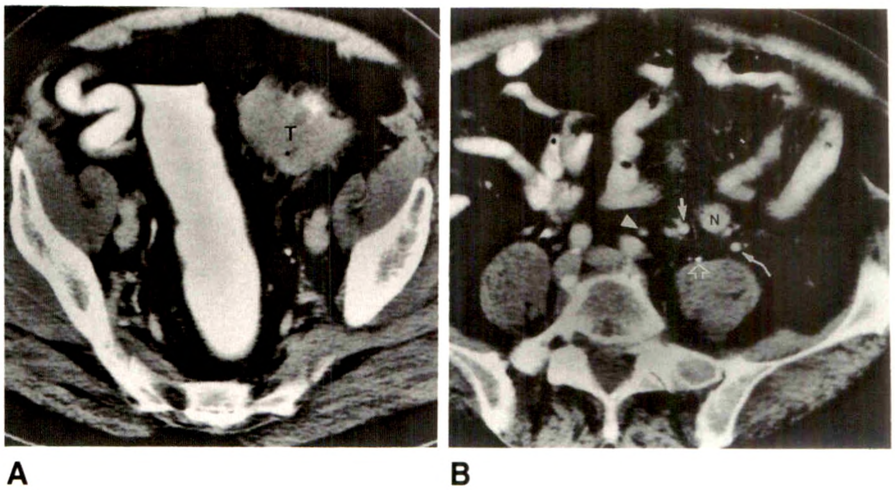

Fig. 4.—CT scans of left colic nodes obtained after bolus IV contrast enhancement. Slice thickness = 5 mm.

A, Primary adenocarcinoma (T) of sigmoid colon.

B, 2-cm node (N) at left colic nodal group. Pathologic examination of surgical specimen showed metastatic disease in this node only. *Arrowhead* = inferior mesenteric artery, *wavy arrow* = gonadal vein, *solid straight arrow* = inferior mesenteric vein, *open arrow* = left ureter.

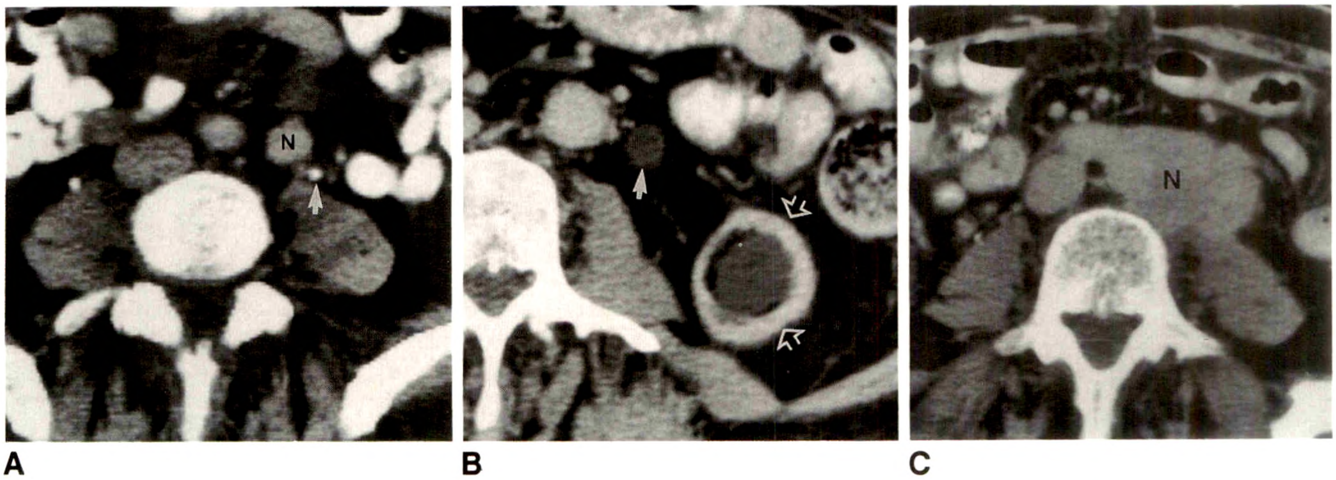

Fig. 5.—CT scans of left colic nodes with progression causing obstruction of left ureter. Patient had previously undergone resection of primary tumor, and hepatic metastases developed. Patient was referred to us for hepatic artery infusion of chemotherapeutic agents.

A, 2-cm node (N) that was not recognized at time of placement of infusion catheter. Note node anterior to left ureter (*arrow*).

B, Scan obtained 6 months after *A* shows hydronephrosis of left kidney (*open arrows*) and dilated left ureter (*solid arrow*). Hepatic metastases (not shown) responded to treatment.

C, Scan obtained at same time as *B* and 4 cm lower shows progression of left colic node (N) with invasion of retroperitoneal structures, including left ureter.

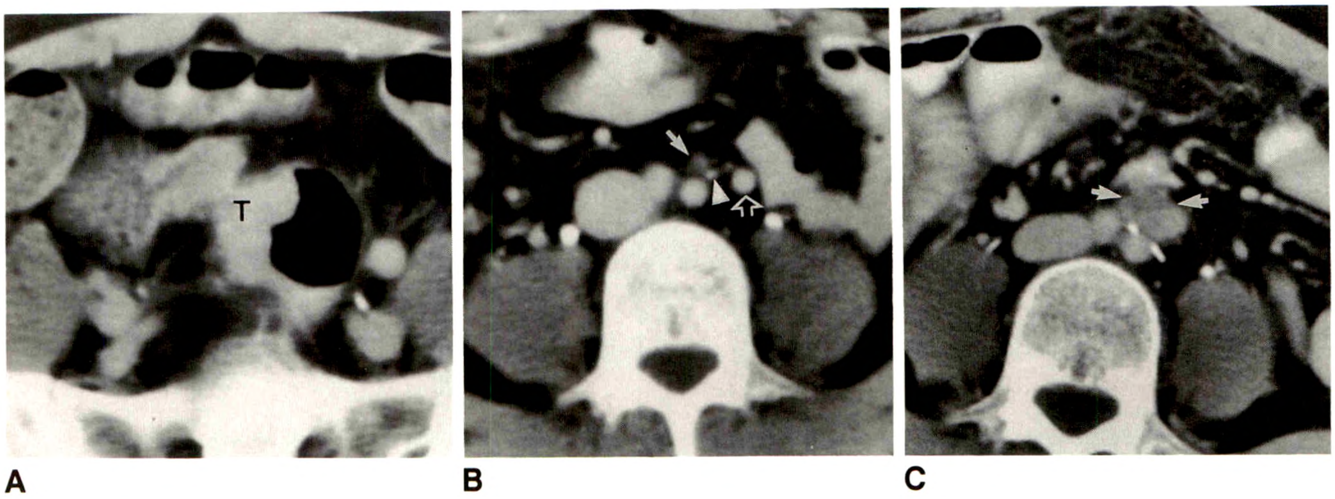

Fig. 6.—CT scans of inferior mesenteric artery (IMA) node.

A, Scan shows primary tumor (T) in sigmoid colon.

B, Scan obtained at same time as *A* at level of aortic bifurcation shows small nodule (*solid arrow*) anterior to left common iliac artery just medial to IMA (*arrowhead*). *Open arrow* = inferior mesenteric vein. At surgery, nodule was proved to be a metastatic node.

C, Scan obtained 2 years after *A* and *B* shows recurrent nodal disease (*arrows*) in IMA nodal group.

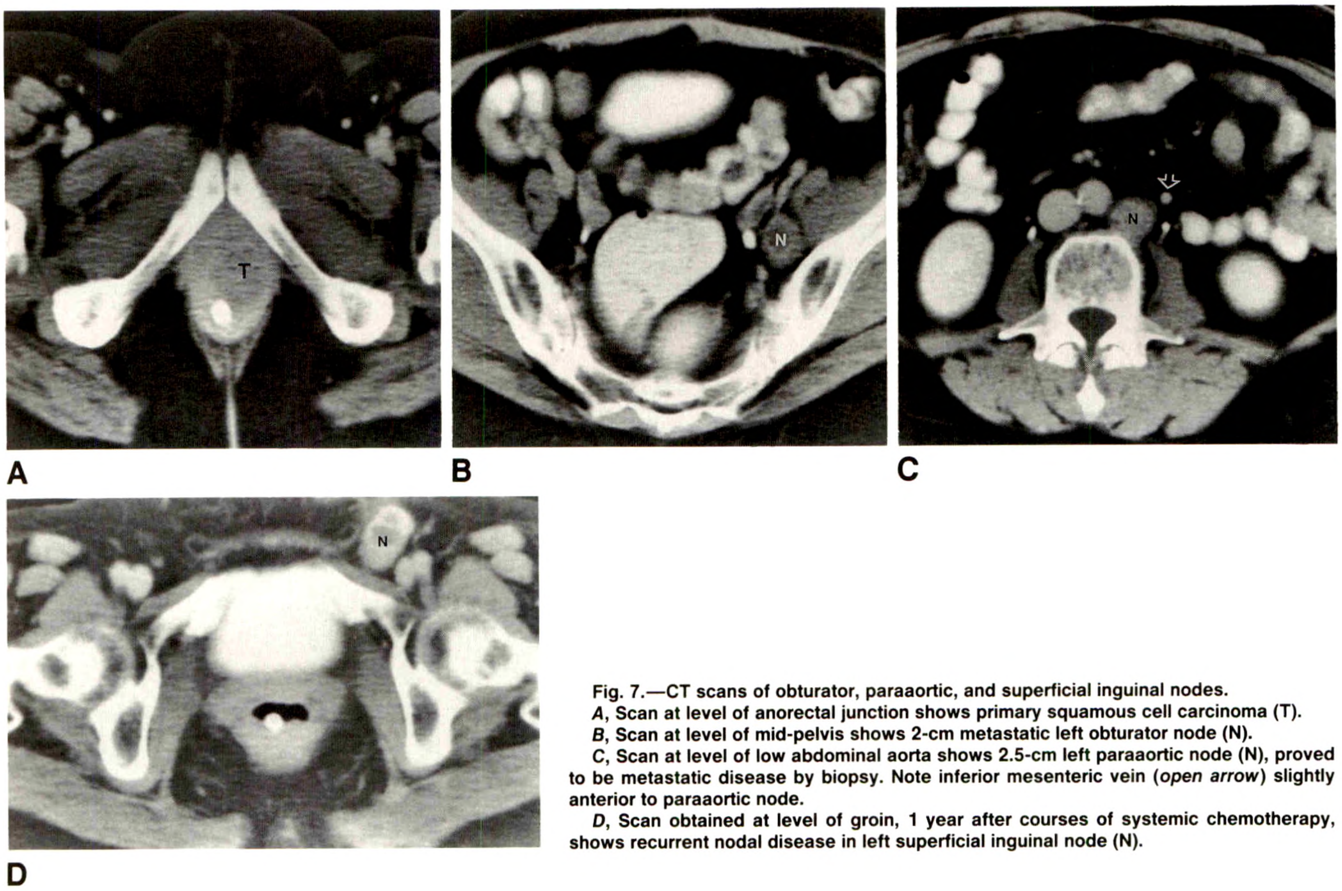

Fig. 7.—CT scans of obturator, paraaortic, and superficial inguinal nodes.

A, Scan at level of anorectal junction shows primary squamous cell carcinoma (T).

B, Scan at level of mid-pelvis shows 2-cm metastatic left obturator node (N).

C, Scan at level of low abdominal aorta shows 2.5-cm left paraaortic node (N), proved to be metastatic disease by biopsy. Note inferior mesenteric vein (*open arrow*) slightly anterior to paraaortic node.

D, Scan obtained at level of groin, 1 year after courses of systemic chemotherapy, shows recurrent nodal disease in left superficial inguinal node (N).

phenofemoral junction and then ascend along the common femoral vessels to the deep inguinal nodes and along the external iliac, common iliac, and paraaortic groups. Occasionally, after radical surgery for carcinoma of the rectum with interruption of the normal pathway of lymphatic drainage, recurrent disease may find an alternative route to the superficial and deep inguinal nodes (Fig. 3C).

Detecting abnormal nodes in the hypogastric nodal group is more difficult because of variations in size and location of the branches of the hypogastric arteries and veins, such as the uterine vessels, vesical vessels, and hemorrhoidal vessels, all of which may simulate nodes. An appropriate IV contrast enhancement technique is required to detect these abnormal nodes.

Summary

The distribution of regional lymph node metastases in carcinoma of the left side of the colon, rectum, and anus can be well shown by routine CT of the abdomen and pelvis. Recognition of the location of nodes in the mesocolic, left colic, and IMA nodal groups can help in developing a systematic approach to the detection of nodal metastasis. This can be especially important in preoperative planning for cases in which resection may be curative. In addition, an understanding of the distribution of nodal metastasis will make it possible to recognize early recurrent nodal disease, particularly with an increase in associated increase in levels of carcinoembryonic antigen, and to predict certain clinical sequences such as hydronephrosis of the left kidney associated with left colic nodal metastases.

REFERENCES

1. Thompson W, Halvorsen RA, Foster WLJ, Roberts L, Gibbons R. Preoperative and postoperative CT staging of rectosigmoid carcinoma. *AJR* **1986**;146:703–710
2. Balthazar EJ, Megibow AJ, Hulnick D, Nadich DP. Carcinoma of the colon: detection and preoperative staging by CT. *AJR* **1988**;150:301–306
3. Goligher J. *Surgery of the anus, rectum and colon,* 5th ed. Eastbourne, England: Balliere Tindall, **1984**:25–26
4. Netter FH, Oppenheimer E. Lower digestive tract. *Ciba collection of medical illustrations,* vol. 3. *Digestive system,* part 2. Summit, NJ: Ciba Medical Education Division, **1979**:75

Technical Note

Gadopentetate Dimeglumine–Barium Paste for Opacification of the Esophageal Lumen on MR Images

Paolo Pavone,[1] Gian Piero Cardone, Salvatore Cisternino, Marco Di Girolamo, Engin Aytan, and Roberto Passariello

We prepared an emulsion consisting of a mixture of gadopentetate dimeglumine and low-density barium paste and tested its value as an oral contrast agent for opacification of the esophageal lumen during MR imaging.

Materials and Methods

The contrast material used to opacify the esophageal lumen was prepared by emulsifying two different commercially available contrast agents. A high-viscosity contrast agent used for esophageal CT 3% barium paste (TAC Esofago, distributed by Bracco I. C. Milan, Italy, and produced by E-Z-EM Co. Inc., Westbury, NY), was used together with a paramagnetic MR imaging agent, gadopentetate dimeglumine (Magnevist, Schering, Berlin, Germany). We diluted 0.25 mol of gadopentetate dimeglumine (corresponding to 0.5 ml of the commercially available solution) in 3 ml of water and then emulsified it with 30 g of barium paste. No other substances were added to the mixture.

The preparation was orally administered to the patients while they were on the scanning table, immediately before the MR study was started. The MR imaging examinations were performed with a 0.5-T superconductive magnet (Esaoate Biomedica, Genua, Italy), using a body coil. In all patients, T1-weighted spin-echo images (420/16 [TR/TE] eight excitations, 128 × 256 matrix) were obtained, with a 10-mm slice thickness and a 3-mm interslice gap. No cardiac gating was used. In all patients, axial images were acquired first, followed by sagittal and coronal images, obtained with a shorter TR (260 msec). The total examination time, including image reconstruction, was 20–25 min. Fifty-three patients undergoing MR imaging were given the viscous esophageal contrast preparation. Indications for MR imaging of the chest in these patients included lung cancer (11 cases), lymphoma (six cases), primary esophageal neoplasm (16 cases), mediastinal tumors (eight cases), dissecting aneurysms (two cases), and screening for involvement of mediastinal lymph nodes (10 cases). The opacification of the esophageal lumen was evaluated on each image.

Results

In 10 of the 15 patients in whom the esophagus was normal, opacification of segments of the esophagus was noted (Fig. 1). Complete filling of the lumen on sagittal images was observed in only eight patients. In these patients, filling persisted for the entire duration of the MR (20–25 min). In all but one of the 38 abnormal cases, opacification of the esophageal lumen was seen on all axial scans. On sagittal and coronal scans, the entire opacified esophagus was visualized in only 12 and six cases, respectively. In cases of esophageal tumors, differentiation of the thickened wall of the esophagus from the esophageal lumen was possible (Fig. 2). Ulcers within the tumors were evident in three cases. The opacification permitted identification of the location of the esophagus in cases of lung cancer or mediastinal lesions (Fig. 3).

Discussion

MR imaging is considered more accurate than CT in the evaluation of esophageal and paraesophageal lesions, especially in the assessment of extraesophageal invasion of mediastinal fat [1–4]. Without contrast agents, however, it is not

---

Received February 24, 1992; accepted after revision April 21, 1992.

[1] All authors: Department of Radiology, University of L'Aquila, Ospedale SM di Collemaggio, L'Aquila 67100, Italy. Address reprint requests to P. Pavone.

AJR 159:762–764, October 1992 0361–803X/92/1594–0762 © American Roentgen Ray Society

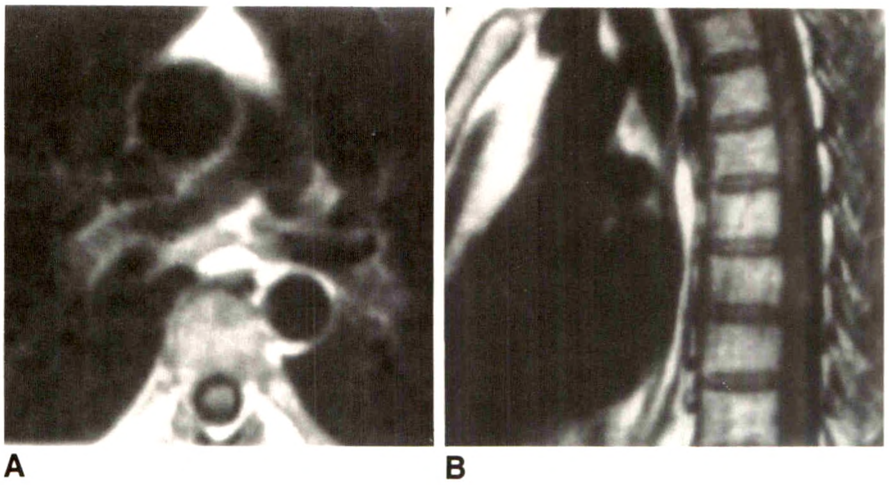

Fig. 1.—Axial (*A*) and sagittal (*B*) MR images show opacification of normal esophageal lumen.

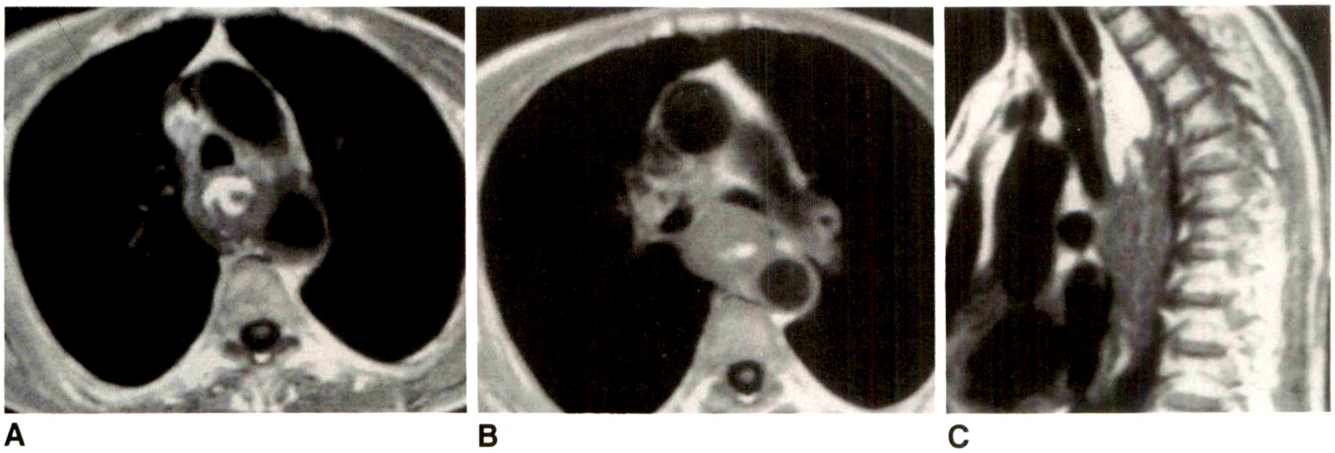

Fig. 2.—Esophageal neoplasm.
A and *B*, Axial contrast-enhanced MR images show intratumoral ulcers (*A*) and concentric neoplastic growth (*B*).
C, Sagittal MR image shows complete definition of extent of lesion, as compared with dilated opacified lumen.

possible to evaluate the wall of the esophagus in the presence of a tumor or the location of the esophagus in the presence of a mediastinal neoplasm. These limitations can be easily overcome by administration of contrast material, as has been shown in CT studies [5].

To create a specific contrast agent for the esophagus, we used two commercially available contrast agents: one, a specific esophageal contrast agent used in CT, and the other a paramagnetic agent for MR imaging. The result was a preparation that did not cause any undesirable side effects.

Most of the normal esophagi were well opacified during MR imaging (Fig. 1). Poor opacification in five normal subjects was due to the contrast medium remaining in the esophagus for too short a time because of peristalsis. This phenomenon, however, never occurred in the abnormal esophagi.

In patients with esophageal carcinoma, this contrast medium improved imaging of neoplastic wall thickening, allowing more precise distinction of the true extent of the tumor (Fig. 2), defining the relative, concentric or eccentric, neoplastic growth. Luminal irregularities and intratumoral ulcers also were evident. The sagittal plane proved to be particularly useful, because it provided contemporary visualization of the progressively stenosing lumen, as in conventional barium studies, together with the thickened neoplastic wall and surrounding structures. In other mediastinal diseases, the use of this contrast agent allowed easy depiction of the exact location of the esophagus and allowed differentiation of the esophagus from the surrounding mediastinal masses. This opacification is particularly helpful in the evaluation of the esophagus in cases of extensive mediastinal involvement (Fig. 3) or when the esophagus is displaced from its correct location.

In conclusion, this new preparation of a specific esophageal contrast agent was of great utility in the MR evaluation of normal and abnormal esophagi. Like the low-density barium paste used in chest CT, this MR contrast agent can be used in the evaluation of esophageal carcinoma, and in the examination of other mediastinal masses, to localize the esophagus properly.

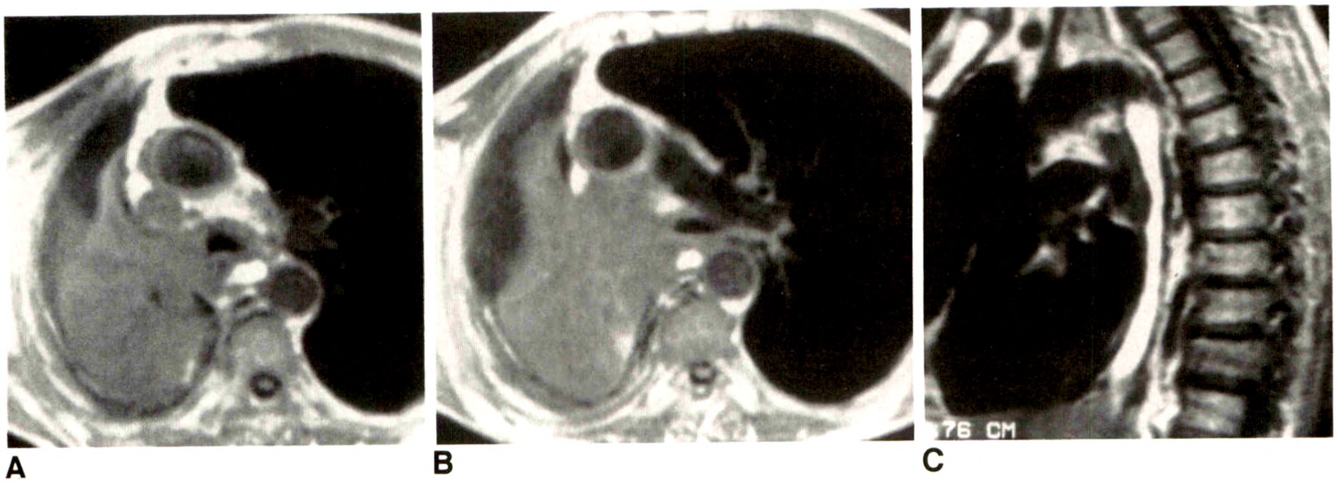

Fig. 3.—Recurrent lung cancer.
***A–C*, Axial (*A* and *B*) and sagittal (*C*) MR images show large thoracic mass extending into mediastinum, with involvement of esophagus.**

REFERENCES

1. Quint EL, Glazer MG, Orringer MB. Esophageal imaging by MR and CT: study of normal anatomy and neoplasm. *Radiology* **1985**;156:727–731
2. Schmutz GR, Jeung MY, Wihilm JM, Massard G, Chem RK, Guyen DN. CT and MR evaluation of esophageal extramucosal diseases (abstr). *Radiology* **1990**;170(P):250
3. Vellt D, Bennet G, Cassin A, Lefcoe M, Finley R, Inculet R. Comparative evaluation of CT and MR imaging in the preoperative staging of esophageal carcinoma (abstr). *Radiology* **1990**;170(P):250
4. Takashima S, Takeuchi N, Shiozaki H, et al. Carcinoma of the esophagus: CT and MR imaging in determining resectability. *AJR* **1991**;156:297–302
5. Conces DJ, Tarver CJ, Lappas CJ. The value of opacification of the esophagus by low density barium paste in computed tomography of the thorax. *J Comput Assist Tomogr* **1988**;12:202–205

Case Report

Intraluminal Esophageal Diverticulum Caused by Ingestion of Acid

B. M. Plavsic[1] and A. E. Robinson

Intraluminal esophageal diverticulum, an extremely uncommon entity, is a pouch of mucosal membrane open proximally and closed distally [1]. A double-layered mucosal intraluminal esophageal diverticulum also has been described [2, 3]. A review of the literature has disclosed no case of intraluminal esophageal diverticulum due to ingestion of a caustic agent. We report two patients in whom intraluminal esophageal diverticulum developed after they ingested a corrosive substance.

Case Report

A 36-year-old woman had ingested sulfuric acid in a suicide attempt. Dysphagia, particularly with liquids, has led to an upper gastrointestinal series 1 week later. A single-contrast esophagogram showed filling of both esophageal lumen and intraluminal esophageal diverticulum. The intraluminal esophageal diverticulum was seen intraluminally in all projections and its wall was discontinuous distally (Fig. 1). No specific therapy was instituted. Two weeks later, the intraluminal esophageal diverticulum was still evident, but the perforation could not be seen. A small mucosal tear in the proximal esophagus with redness of the mucosa was found at endoscopy after the second barium study.

Acute clinical symptoms ceased spontaneously and no further radiographic examination was requested. Upper gastrointestinal series for peptic ulcer 2 years earlier had not shown evidence of intraluminal esophageal diverticulum.

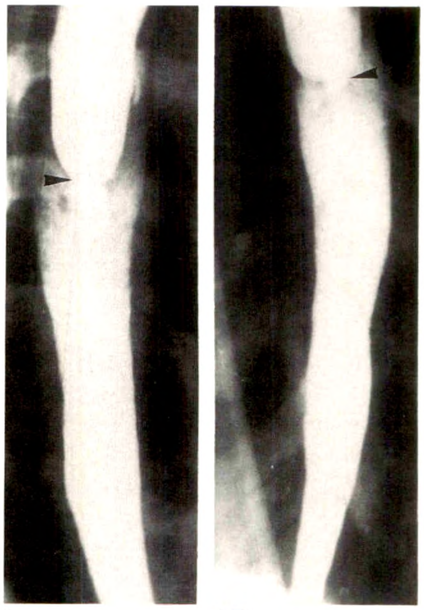

1A 1B

Fig. 1.—*A* and *B*, 36-year-old woman with an intraluminal esophageal diverticulum in proximal esophagus. Diverticulum is seen in the esophageal lumen in all projections. Rupture of distal wall of diverticulum (*arrowheads*) also is shown.

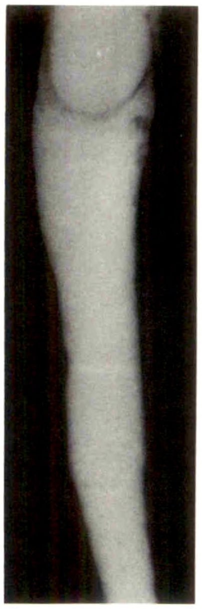

2

Fig. 2.—52-year-old man with intraluminal esophageal diverticulum. Wall of intraluminal esophageal diverticulum appears as a thin radiolucent line. Note moderate postcorrosive stenosis of distal esophagus.

Received March 19, 1992; accepted after revision April 23, 1992.

[1] Both authors: Department of Radiology, Tulane University Medical Center, 1430 Tulane Ave. (SL54), New Orleans, LA 70112. Address reprint requests to B. M. Plavsic.

AJR **159:765–766, October 1992** 0361–803X/92/1594–0765 © American Roentgen Ray Society

Discussion

A similar appearance was noted in a 52-year-old man who had inadvertently ingested 30% hydrochloric acid. Barium examination 4 weeks later showed an intraluminal esophageal diverticulum and a corrosive stricture (Fig. 2).

Increased intraluminal pressure in the postinflammatory constricted esophagus can damage the mucosa, resulting in formation of an intraluminal esophageal diverticulum [1]. In one of our patients, the distal esophagus had been moderately narrowed. Damage to the mucosa also could result from direct injury by ingested acid in caustic esophagitis.

Congenital, double-layered mucosal intraluminal esophageal diverticulum, covered on both sides with epithelium, also has been described [2]. Two other patients with acquired intraluminal esophageal diverticula had signs of advanced esophagitis and stricture [1]. A transient radiographic phenomenon resembling intraluminal esophageal diverticulum might be a sequela of esophageal dysmotility with tertiary contractions and stasis of air resulting in insufficient mixing of barium with air and secretions [4].

Intraluminal esophageal diverticulum was proved to be constant on repeated examinations. In the case described, the diverticulum had not been shown on upper gastrointestinal series 2 years earlier. Dysphagia and odynophagia also were present. Common to both patients was subacute or chronic caustic acid damage to the esophagus [5]. At esophagoscopy, a mucosal tear was shown in the proximal esophagus of one patient. This allowed submucosal dissection, which formed an intraluminal esophageal diverticulum. Because the clinical signs disappeared, spontaneous closure with healing of the mucosa most likely occurred, and no further examinations were done.

REFERENCES

1. Schreiber MH, Davis M. Intraluminal diverticulum of the esophagus. *AJR* **1977**;129:595–597
2. Funakoshi O, Soma Y, Takasugi T, Munakata A, Yoshida Y. Intraluminal esophageal diverticulum. *Gastroenterol Jpn* **1990**;25:117–121
3. Wiot TI, Spiro E. Intraluminal diverticulum: a form of duplication. *Radiology* **1963**;80:46–49
4. Agha FP. Transient intraluminal diverticulum of the esophagus: a significant flow artifact. *Gastrointest Radiol* **1984**;9:99–103
5. Muhletaler CA, Gerlock AJ, de Soto X, Halter SA. Acid corrosive esophagitis: radiographic findings. *AJR* **1980**;134:1137–1140

Case Report

Acute Phlegmonous Gastritis with Mural Abscess: CT Diagnosis

Francisco O. Cruz,[1] Pablo S. Soffia,[1] Pedro M. Del Rio,[1] Mario P. Fava,[1] and Ignacio G. Duarte[2]

Acute phlegmonous gastritis is an uncommon and serious bacterial infection of the gastric wall. It has a high mortality rate mainly because the diagnosis is usually made late [1, 2]. Most cases have been diagnosed at autopsy and occasionally at laparotomy because the clinical presentation is often confusing. A barium study or sonography may suggest the diagnosis, but the findings are not characteristic. We report a case in which a preoperative diagnosis was made by means of CT.

Case Report

A 78-year-old man was admitted after 1 week of mild abdominal pain and melena. The abdomen was diffusely tender. Endoscopy showed thickened gastric folds and a submucosal lesion in the gastric antrum. Biopsy of the antrum showed nonspecific gastritis. A sonogram showed thickening of the gastric wall. ^{99m}Tc-RBC scintigraphy revealed evidence of intermittent bleeding in the right upper quadrant. CT also showed thickening of the gastric wall and an intramural low-attenuation mass in the antrum of the stomach, thought to represent a fluid collection (Figs. 1A and 1B). A barium study showed deformity of the gastric antrum, with rigidity of the wall and effacement and thickening of the gastric folds (Fig. 1C). A gastric wall abscess due to acute phlegmonous gastritis was diagnosed. A subsequent gastrectomy with a Billroth II anastomosis was performed.

Pathologic examination of the surgical specimen (Fig. 1D) revealed that the gastric wall was markedly thickened and exuded purulent material on slight pressure. The mucosa was covered by granular exudate and many tiny perforations. Microscopic examination showed a partially necrotic mucosa and an intense polymorphonuclear infiltrate of the submucosa, also with some focal areas of necrosis. The pus cultures grew *Escherichia coli* and *Proteus mirabilis*.

Discussion

Only a few cases of acute phlegmonous gastritis have been reported, and most of these were misdiagnosed preoperatively [2]. Occasionally the diagnosis has been suggested by a barium study [3] and sonography [4, 5]. In one case the diagnosis was made by using endoscopic snare biopsy [6].

In our case, the correct preoperative diagnosis of an inflammatory process rather than linitis plastica was suggested, because in addition to gastric wall thickening, a localized fluid collection was seen in the gastric wall.

Received February 27, 1992; accepted after revision April 16, 1992.

[1] Department of Radiology, Catholic University of Chile, Clinical Hospital, Marcoleta 367, Santiago, Chile. Address reprint requests to F. O. Cruz.
[2] Department of Pathology, Catholic University of Chile, Clinical Hospital, Santiago, Chile.

***AJR* 159:767–768, October 1992** 0361–803X/92/1594–0767 © American Roentgen Ray Society

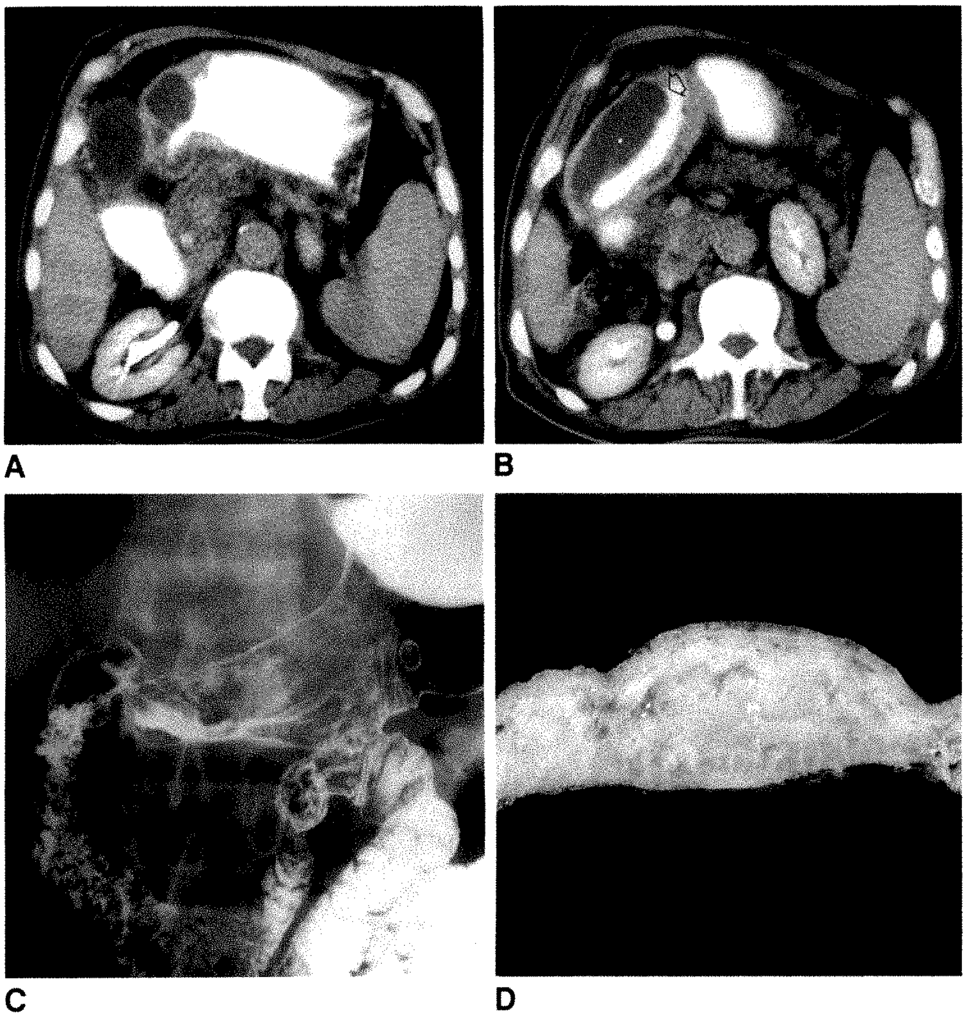

Fig. 1.—*A* and *B*, Right lateral decubitus CT scans at different levels of antrum show abrupt narrowing of antral lumen (*A*) and an intramural low-attenuation mass in gastric wall (*arrow*) with marked thickening of antral wall (*B*).

C, Upper gastrointestinal radiograph shows antral and distal body narrowing with effacement of mucosal pattern (linitis plastica pattern).

D, Pathologic specimen shows phlegmonous changes of gastric wall and an intramural abscess.

REFERENCES

1. Nevin NC, Eakins DI, Clarke SD, Carson DJL, Brit J. Acute phlegmonous gastritis. *Surgery* **1969**;56:268–270
2. Miller AL, Smith B, Rogers AI. Phlegmonous gastritis. *Gastroenterology* **1975**;68:231–238
3. Turner MA, Beachley MC, Stanley D. Phlegmonous gastritis. *AJR* **1979**;133:527–528
4. Lifton LJ, Schlossberg D. Phlegmonous gastritis after endoscopic polypectomy. *Ann Intern Med* **1982**;97:373–374
5. Tierney LM, Gooding G, Bottles K, Montgomery CK, Fitzgerald FT. Phlegmonous gastritis and *Hemophilus influenzae* peritonitis in a patient with alcoholic liver disease. *Dig Dis Sci* **1987**;32:97–101
6. Bron BA, Deyhle P, Pelloni S, Krejs GJ, Siebenmann RE, Blum AL. Phlegmonous gastritis diagnosed by endoscopic snare biopsy. *Dig Dis* **1977**;22:729–733

Focal Hyperdense Areas in Endometriomas: A Characteristic Finding on CT

Jean-Noël Buy[1]
Michel A. Ghossain[1]
Alexander S. Mark[2]
Laurent Deligne[1]
Danièle Hugol[3]
Jean B. Truc[4]
Philippe Poitout[4]
Dominique Vadrot[1]

OBJECTIVE. To assess the value of a hyperdense focus seen on CT scans of endometrial cysts in the differential diagnosis of a lesion.

MATERIALS AND METHODS. The preoperative CT scans of 328 patients with 410 ovarian masses (54 patients with 62 pathologically proved endometriomas and 274 patients with 348 pathologically proved other ovarian masses) were retrospectively reviewed in a random fashion without knowledge of the pathologic findings to determine whether a hyperdense focus was visible inside a cyst.

RESULTS. In nine of 62 endometrial cysts (sensitivity, 15%), CT scans showed a hyperdense round or crescent-shaped focus, measuring 2 to 15 mm. This focus was located close to the inner border of the cyst in eight cases and in the central part of the cyst in one case. A hyperdense focus was not seen on CT scans of 348 other ovarian masses (specificity, 100%). An in vitro CT study of two specimens showed that this hyperdense area corresponded to a blood clot next to the inner wall of the cyst. This hyperdense area appeared as a nonspecific hyperechogenic focus on sonograms in five of nine cases and as a hypointense signal on T1- and/or T2-weighted MR images in four of five cases.

CONCLUSION. The finding on CT scans of a hyperdense focus inside an ovarian cyst is suggestive of endometrioma and should help distinguish endometrioma from other pelvic masses.

***AJR* 159:769–771, October 1992**

CT has been considered to lack specificity in the diagnosis of endometriosis [1]. However, we noticed a hyperdense focus inside some endometriomas visible on CT scans. To determine the value of this finding, we reviewed a series of 410 surgically proved ovarian masses including 62 endometriomas and 348 other ovarian masses.

Materials and Methods

We reviewed the imaging findings in 328 patients with 410 ovarian masses (54 patients with 62 pathologically proved endometriomas and 274 patients with 348 pathologically proved other ovarian masses) who had preoperative CT scans between January 1985 and October 1990. All patients underwent laparotomy. Pathologic examinations of surgical specimens showed 62 endometriomas, 234 primary epithelial tumors, 81 germ cell tumors, 31 stromal and sexual cord cell tumors, and two functional cysts.

CT was performed with an Exel 1800 system (Elscint, Haifa, Israel) with a scanning time of 4.8 sec, a slice thickness of 10 mm, and a 340 × 340 matrix. The patient received 1 l of 1% Gastrografin (Schering, Lys-Lez-Lannoy, France) orally 30 min before the examination, and the patient's bladder was kept as full as possible during the examination. In all patients, initially unenhanced pelvic scans were obtained to locate a special region of interest. Then each patient received 60 ml of sodium and ioxithalamate meglumine (Telebrix 38, Guerbet, Aulnay-sous-Bois, France) injected as a bolus in 8–12 sec through a 16-gauge needle, and dynamic nonincremental CT scans were obtained. Seven scans were obtained at 10-sec

Received March 6, 1992; accepted after revision April 28, 1992.

[1] Department of Radiology, Hôtel Dieu de Paris, 1 Place du Parvis de Notre Dame, 75004 Paris, France. Address reprint requests to J-N. Buy.

[2] Department of Radiology, Washington Hospital Center, 110 Irving St. N.W., Washington, DC 20010.

[3] Department of Pathology, Hôtel Dieu de Paris, 1 Place du Parvis de Notre Dame, 75004 Paris, France.

[4] Department of Obstetrics and Gynecology, Hôtel Dieu de Paris, 1 Place du Parvis de Notre Dame, 75004 Paris, France.

0361-803X/92/1594-0769
©American Roentgen Ray Society

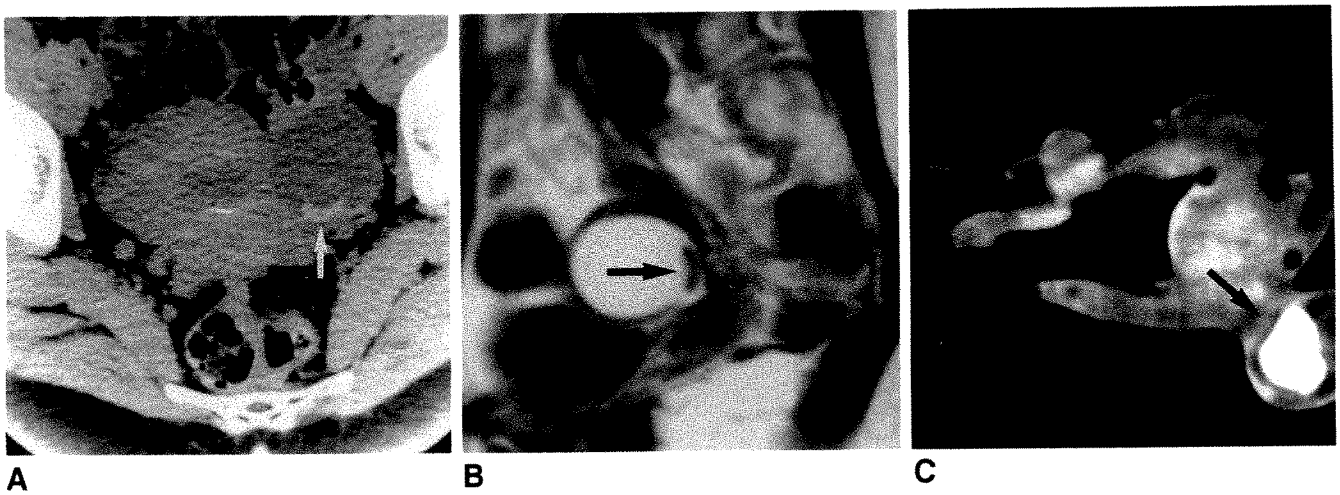

Fig. 1.—46-year-old woman with pelvic pain.

A, Unenhanced CT scan shows a small curvilinear hyperdense area (*arrow*) in dependent part of pathologically proved endometrioma in left ovary. Contrast-enhanced CT scan (*not shown*) confirmed cystic nature of mass.

B, T1-weighted (SE 400/28) MR image shows hyperdense area of A as an area of low signal intensity (*arrow*), which contrasts with high signal intensity of hemorrhagic content of cyst. In this case, the hypointense area was visualized on T2-weighted images also.

C, CT scan of surgical specimen shows hyperdense clot (*arrow*) in opened cyst.

intervals, beginning at the start of the bolus injection. Then, after a second bolus injection, a complete series of abdominopelvic CT scans was obtained in all patients.

Sonograms were obtained with an Ultramark 4 unit (ATL, Bothell, WA) using a 3.5- or 5-MHz annular array transducer in all patients and an intravaginal transducer (ADR IVT, 5-MHz 10-mm; ATL, Bothell, WA) in three patients.

MR imaging was performed in 124 patients with a 0.5-T superconducting magnet (Magniscan 5000, General Electric-CGR, Paris, France). Axial and sagittal T1-weighted spin-echo (SE) images with a repetition time of 400 msec and an echo time of 28 msec and axial and sagittal T2-weighted SE images (1800/40, 80) were obtained.

In vitro CT scans of the surgical specimens were obtained in 40 patients within 1 hr after surgery using 5-mm-thick contiguous sections.

Two radiologists independently reviewed in a random fashion all the CT scans without knowledge of the clinical and pathologic findings. In all endometrial and nonendometrial tumors, we looked for a hyperdense focus inside the cystic component of the mass on the unenhanced CT scans. When such a focus was present, we systematically analyzed it as follows: (1) size, (2) shape: round or linear, (3) location: central or peripheral (i.e., close to the inner border of the cyst), (4) density before and after IV administration of contrast material, and (5) pattern: homogeneous or containing small hypodense foci.

In all cases in which a hyperdense focus was detected on CT scans, we correlated the CT scans with the corresponding sonograms and MR images.

Results

CT Findings

A hyperdense focus (Figs. 1A and 2A) was present in nine of 62 endometriomas (sensitivity, 15%). Such a focus was not detected in any of the 348 nonendometrial tumors of our series (including eight hemorrhagic nonendometrial cysts; specificity, 100%).

The size of these nine endometriomas ranged from 2.5 to 6.0 cm (mean, 4.6 cm). Findings on noncontrast CT, dynamic CT, and delayed CT made it possible to diagnose a cystic mass in all cases.

The hyperdense focus ranged in size from 2 to 15 mm (mean, 10 mm). It was curvilinear in four cases, round in two, oval in two, and ringlike in one. It was never present in the wall of the cyst; it was next to the inner border in eight cases (in the dependent portions in six and near the lateral wall in two) and in the center of the cyst in one. Attenuation of the hyperdense area was 90–140 H. In all cases, no modification in and around the hyperdense focus was noticed on dynamic CT scans.

In Vitro CT Findings

Among the nine patients who had a hyperdense focus seen on the in vivo CT scans, in vitro CT scans of the surgical specimen were obtained in two patients. The hyperdense focus was even better documented (Fig. 1C) and correlated well with a blood clot seen at pathologic examination.

Discussion

Although CT has limits in the diagnosis of endometriomas [1], our study shows an uncommon but specific finding of endometrioma (sensitivity, 15%; specificity, 100%). Indeed, a peculiar hyperdense focus detected in nine cases was not found in any of the other 348 cases of surgically proved ovarian masses, which included eight nonendometrial hemorrhagic cysts. The round or crescent shape of this hyperdense focus, its location next to the inner border of the cyst (in eight of nine cases), and the presence of hypodense foci (in four of nine) inside this hyperdense area are seen in

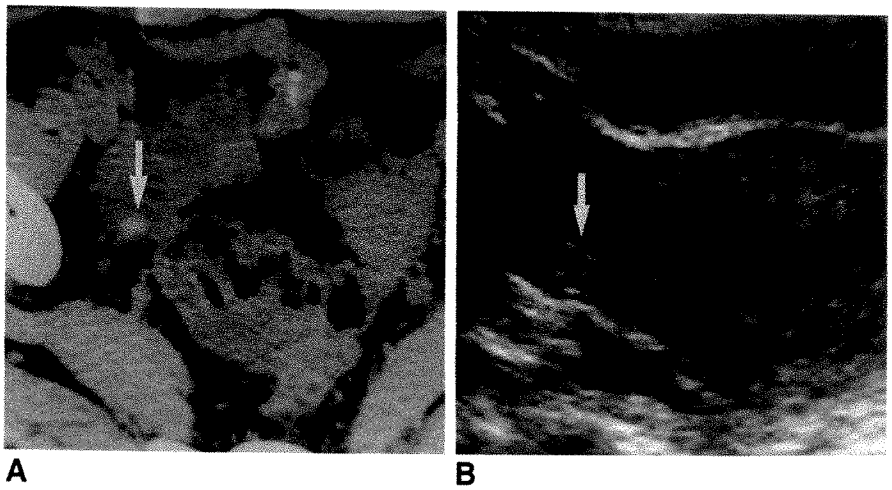

Fig. 2.—35-year-old woman with amenorrhea.

A, Unenhanced CT scan of pathologically proved endometrioma in right ovary shows a small 1-cm oval hyperdense area (*arrow*) in dependent part of cyst.

B, Sonogram shows a hyperechoic area (*arrow*) in otherwise anechoic cyst.

endometriomas only. Moreover, the hyperdense focus cannot be confused with other hyperdense areas. For example, calcifications in cystic teratomas are usually bigger, are sometimes toothlike, and are always located in the wall of the cyst, in the septa, or, more often, inside the Rokitansky protuberance [2]. They are also often associated with fat and other morphologic features that have characteristic appearances on CT such that the correct diagnosis of cystic teratoma could be made in 98% of cases [2]. Psammoma bodies, usually found with serous and papillary tumors [3], are always located in the wall or in the septa [4].

In the two surgical specimens studied in vitro, the hyperdense focus seen on CT scans (Fig. 1C) correlated well with a blood clot found on pathologic examination.

Sonographically, a hyperechogenic focus, without acoustic shadowing, was visualized retrospectively at the site of this hyperdense area in five of nine cases (Fig. 2B). This finding is neither specific nor sensitive for endometrioma. Indeed, a hyperechogenic area seen on a sonogram can correspond to a blood clot, a vegetation, a small loculus, or a Rokitansky nodule in a dermoid cyst [5, 6].

Among the nine patients who had a hyperdense focus seen on CT scans, MR imaging was performed in five. In four of these five patients, MR images showed a hypointense lesion (Fig. 1B) of the same shape and size as the hyperdense focus seen on CT scans. This hypointense lesion was visualized on both T1- and T2-weighted images in two cases (Fig. 1B) and on the T1-weighted images only in two cases.

In conclusion, the finding of a hyperdense focus, which seems to represent a blood clot on CT scans, is suggestive of endometrioma and should help distinguish endometrioma from other pelvic masses, particularly epithelial tumor or nonendometrial hemorrhagic cyst.

ACKNOWLEDGMENT

We thank Bernadette Vatin for reviewing the manuscript.

REFERENCES

1. Fishman EK, Scatarige JC, Saksouk FA, Rosenshein NB, Siegelman SS. Computed tomography of endometriosis. *J Comput Assist Tomogr* **1983**;7:257–264
2. Buy JN, Ghossain MA, Moss AA, et al. Cystic teratoma of the ovary: CT detection. *Radiology* **1989**;171:697–701
3. Czernobilsky B. Common epithelial tumors of the ovary. In: Kurman RJ, ed. *Blaustein's pathology of the female genital tract.* New York: Springer-Verlag, **1987**:560–606
4. Buy JN, Ghossain MA, Sciot C, et al. Epithelial tumors of the ovary: CT findings and correlation with US. *Radiology* **1991**;178:811–818
5. Quinn SF, Erickson S, Black WC. Cystic ovarian teratomas: the sonographic appearance of the dermoid plug. *Radiology* **1985**;155:477–478
6. Baltarowich OH, Kurtz AB, Pasto ME, Rifkin MD, Needleman L, Goldberg BB. The spectrum of sonographic findings in hemorrhagic ovarian cysts. *AJR* **1987**;148:901–905

Book Review

Diagnostic Ultrasound. Physics, Biology and Instrumentation. By Stuart C. Bushong and Benjamin R. Archer. St. Louis: Mosby–Year Book, 177 pp., 1991. $34.95

This introductory text is an interesting addition to the teaching literature on sonography. It is aimed at the most elementary level and starts from the very beginning: a discussion of basic mathematical principles (in the unfortunately mislabeled chapter, "Fundamentals of Physics") such as algebra and graphing, the elements of basic physics (e.g., motion, energy), and the fundamental principles of waves. These introductory chapters set the tone for the remainder of the book in emphasizing the *natural* way in which common physical phenomena are used for the practical application of sonography.

The process of sonography unfolds in the ensuing chapter on ultrasound power and intensity and its spatial and temporal variations and in the next chapter on the interaction of ultrasound with matter, where attenuation and reflection are covered. The next several chapters discuss the details of actual imaging, such as the transducer and quality factor, the characteristics of the beam, and resolution. This leads to the discussion of pulse-echo imaging and then real-time imaging. The discussion of A-, B-, and M-mode imaging is lumped into a single chapter on pulse-echo methods and serves as a useful introduction to the subsequent chapter on real-time imaging. The different properties of the echoes generated in real-time imaging and their manipulation by gain, delay, and slope control (among other things) lead to the chapter on image processing and display, which covers elements of the pulser and receiver, as well as scan conversion and recording and display devices. This is not the usual order of presentation, but it works quite well. Doppler sonography is covered next in a single short chapter. The last three chapters cover image artifacts, quality control, and biological effects.

The book is comparable in structure and emphasis to *Physics and Instrumentation of Diagnostic Medical Ultrasound*, by Peter Fish, though it begins at a much more elementary level of introduction and is far less detailed. To this extent, it may be considered as prefatory to this work or others of similar level, such as *Ultrasound Physics and Instrumentation*, by Hykes, Hedrick, and Starchman. A greater proportion of *Diagnostic Ultrasound* is spent on bringing the reader up to speed on very basic mathematical and physical concepts necessary to understand sonography. Readers with adequate technical facility will most likely find these chapters superfluous and indeed may find the entire book too simple. On the other hand, the book seems to provide information that is all too often missing in books on technical subjects: a clear and simple exposition of the basics.

The well-conceived overall structure of the book is persistent within the chapters themselves as well. Key concepts are highlighted in boldface type in the text, and important definitions, along with the relevant symbol and units, are delineated in gray boxes. Example calculations and solutions are presented throughout the text in order to emphasize the relevance of the various parameters as well as give the reader a feel for their order of magnitude. These are further supplemented by numerous tables that neatly summarize the order of magnitude of, and relationships between, important ultrasound quantities. The numerous technical drawings are successful in presenting clear simplifications of some difficult concepts, although they tend toward oversimplification. Reproductions of actual sonographic images are used almost exclusively to illustrate image artifacts. Unfortunately, the book also contains several ill-conceived drawings added solely for levity. Some of these drawings feature the prototypical nerd scientist amidst subservient buxom women—not exactly 1990s behavior. Further, certain cartoons appear to have been redrawn without permission from well-known published material.

That aside, the clarity and conciseness of the book allow a wide scope of material to be covered in a small space. The book is quite short, especially considering the amount of graphics it contains. What it gains in brevity is necessarily lost in detail. The content covers just the very basic concepts needed to understand sonography. The illustrations reflect this stripped-down approach and are drawn to show only the most basic concepts. Therefore, the book will primarily be useful to technologists or radiology residents with minimal mathematical or physical background, although the nicely intuitive physical way in which the ultrasound process is presented will make the book a quick and informative introduction for anyone. For readers seeking a more detailed and technical description, such as medical physics students or radiologists, Fish's book is more appropriate. The authors' willingness to present even the simplest details of mathematics reflects a refreshing lack of arrogance, and the book succeeds in expressing their desire that the reader *appreciate* ultrasound physics.

Lawrence R. Frank
University of California, San Diego, Medical Center
San Diego, CA 92103

Color Doppler Sonography of Ureteral Jets in Normal Volunteers: Importance of the Relative Specific Gravity of Urine in the Ureter and Bladder

Scott M. Baker[1]
William D. Middleton

OBJECTIVE. Sonographic visualization of ureteral jets is a well-recognized phenomenon. In vitro studies have indicated that detection of fluid flow similar to ureteral jets depends on differences in density between the moving and the stationary fluid. This study was undertaken to determine if differences in density between ureteral urine and urine in the bladder could make a significant impact on the sonographic detectability of ureteral jets in vivo.

SUBJECTS AND METHODS. Ten healthy volunteers were vigorously hydrated after an overnight fast. An initial color Doppler sonographic examination of ureteral jets was performed before voiding (while concentrated urine that had accumulated overnight was still in the bladder). A second examination was performed after two cycles of voiding and refilling the bladder (to ensure that dilute urine produced by the hydration was in the bladder).

RESULTS. In all subjects, normal ureteral jets were readily identified on the initial examination. The difference in the estimated specific gravity between bladder urine and ureteral urine during the initial examination ranged from 0.002 to 0.016 (mean, 0.008). This was a statistically significant difference ($p < .05$). On the second examination, ureteral jets were not detected from either ureter in any subject. The difference in the estimated specific gravity of bladder urine and ureteral urine during the second examination ranged from 0.000 to 0.002 (mean, 0.001). This was not a statistically significant difference ($p > .05$). There was no statistically significant difference in the diuresis rates throughout the course of the examinations. These ranged from 300 to 1218 ml/hr.

CONCLUSION. These in vivo results support the hypothesis that detection of ureteral jets depends on density differences between ureteral and bladder urine. This is important clinically, because normal ureteral jets may be undetectable, despite adequate hydration and high rates of diuresis, if the patient is allowed to completely void and refill the bladder before the examination.

***AJR* 159:773-775, October 1992**

The detection of ureteral jets as echogenic streams arising from the ureteral orifices and entering the bladder has been well described on gray-scale sonography [1]. Recently, color Doppler sonography has been used to image ureteral jets [2]. Burge et al. [2] have shown that color Doppler analysis of ureteral jets can provide a means of documenting renal obstruction. This study, conducted in a group of patients with ureteral stones demonstrated that it is possible to document readily detectable ureteral jets on the unobstructed side and an absence of ureteral jets on the obstructed side. Detection of ureteral jets on the asymptomatic side is critical in order to confirm that nondetection on the symptomatic side is not related to poor overall diuresis or improper technical factors. Therefore, if this technique is to have success, it is important to maximize the likelihood of detecting normal ureteral jets.

Previous in vitro studies have indicated that sonographic detection of fluid jets is dependent on differences in density between the fluid exiting the orifice and the fluid residing within the reservoir [3, 4]. This study was undertaken to determine if

Received February 6, 1992; accepted after revision April 16, 1992.

[1] Both authors: Mallinckrodt Institute of Radiology, Washington University School of Medicine, 510 S. Kingshighway Blvd., St. Louis, MO 63110. Address reprint requests to W. D. Middleton.

0361-803X/92/1594-0773
© American Roentgen Ray Society

this dependence on density differences could potentially affect the results of ureteral jet analysis in healthy volunteers.

Subjects and Methods

Color Doppler sonography of ureteral jets was performed in 10 healthy men (age range, 27–38 years old). On the morning of the examination, the subjects were instructed not to completely void after awakening. Partial voiding was allowed if necessary. They were vigorously hydrated orally with 2 l of water during a 1.0- to 1.5-hr interval. After hydration but before complete voiding, the first color Doppler study of ureteral jets was performed (while concentrated urine that had accumulated overnight was still in the bladder). Immediately after this first study, the subjects were allowed to void completely, and a sample was saved for measurement of specific gravity (specific gravity 1 in Table 1). The specific gravity of each of the three voided specimens was determined by using a Reichert refractometer (Baxter Diagnostics, Earth City, MO). The bladder was allowed to refill and after approximately 15–20 min, the participants voided again; a sample was saved for specific gravity (specific gravity 2 in Table 1), and the diuresis rate was documented. Diuresis rate was calculated by measuring voided urine volume and dividing by the time required to produce that volume. The bladder was allowed to refill and after 15–20 more minutes, a second color Doppler study was performed (while dilute urine produced by the hydration was in the bladder). Immediately after the second study, the subjects voided a third time, and again a sample was saved for specific gravity (specific gravity 3) and a diuresis rate was calculated. The bladder was allowed to refill one last time, and after 15–20 min, the subjects voided and a final diuresis rate was calculated.

All color Doppler sonographic examinations were performed with a commercially available unit (Ultramark-9, Advanced Technology Laboratories, Bothell, WA) with a 3-MHz phased-array transducer. A low pulse-repetition frequency (1500 Hz), moderate receiver gain, and moderate output were used to optimize visualization. The wall filter was set at 50–100 Hz. Flow toward the transducer was assigned a red color. The bladder was examined in the transverse plane at the level of the trigone (to view both jets simultaneously). All participants were scanned for 5 min, and the examination was videotaped for subsequent review.

The Friedman test was used to determine if statistically significant differences existed between the calculated diuresis rates. The Wilcoxon signed-rank test was used to determine if statistically significant differences existed between the first and second and between the second and third specific gravities.

Results

The results obtained for each participant are shown in Table 1. In all 10 subjects, normal ureteral jets were readily identified on the initial examination (Fig. 1A). The difference in specific gravity between bladder urine and ureteral urine during the initial study (estimated as the difference between specimens 1 and 2) ranged from 0.002 to 0.016 (average, 0.0075). This difference was statistically significant ($p < .05$).

On the second study, ureteral jets were not detected in any subject (Fig. 1B). The differences in the specific gravity of bladder urine and ureteral urine (estimated as the difference between specimens 2 and 3) ranged from 0.000 to 0.002 (average, 0.0005). This difference was not statistically significant ($p > .05$).

The average initial diuresis rate was 762 ml/hr (range, 390–1314 ml/hr). The average second diuresis rate was 684 ml/hr (range, 300–1104 ml/hr). The average final diuresis rate was 756 ml/hr (range, 480–1218 ml/hr). The difference in the diuresis rates was not statistically significant ($p > .05$).

Discussion

A number of potential mechanisms have been proposed as being responsible for the formation of sonographically detectable ureteral jets. Among these are microbubbles or particulate matter in the urine, turbulence or cavitation at the ureteral orifice, temperature differences between ureteral and bladder urine, and density differences between ureteral and bladder urine [1, 4–6]. Price et al. [4] provided convincing evidence that the latter mechanism is primarily responsible for the detection of fluid jets in vitro.

In this in vivo study, we attempted to manipulate the density of ureteral and bladder urine in order to determine if density differences would affect detection of ureteral jets despite high rates of diuresis. Subjects were vigorously hydrated in the morning but were instructed not to *completely* empty the bladder. Partial voiding was allowed if necessary. This ensured a situation in which bladder urine would have a high density (because it contained some concentrated urine that had accumulated overnight) while ureteral urine would have a low density (because it contained dilute urine produced after the early morning hydration). Color Doppler sonographic

TABLE 1: Individual Urine Specific Gravities and Diuresis Rates

Characteristic	Subject Number										Average
	1	2	3	4	5	6	7	8	9	10	
Specific Gravity											
1	1.007	1.008	1.010	1.012	1.012	1.004	1.009	1.004	1.014	1.018	1.0098
2	1.003	1.003	1.002	1.002	1.004	1.002	1.002	1.001	1.002	1.002	1.0023
3	1.003	1.001	1.001	1.002	1.004	1.002	1.001	1.001	1.002	1.001	1.0018
1–2	0.004	0.005	0.008	0.010	0.008	0.002	0.007	0.003	0.012	0.016	0.0075
2–3	0.000	0.002	0.001	0.000	0.000	0.000	0.001	0.000	0.000	0.001	0.0005
Diuresis (ml/hr)											
1	858	1314	390	600	624	600	798	1122	600	720	762
2	1104	876	486	300	456	504	720	822	564	1020	684
3	1218	750	498	666	480	570	882	1128	720	630	756

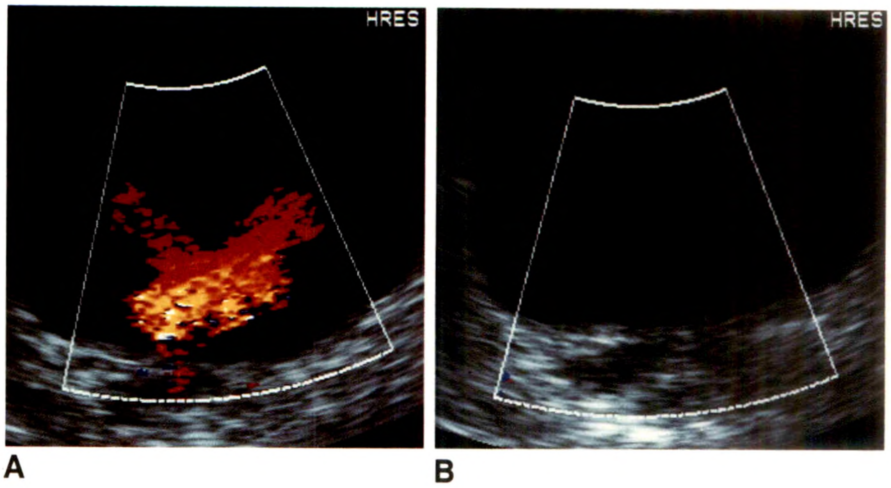

Fig. 1.—Color Doppler sonographic appearance of ureteral jets in subject 7.

***A*, Transverse image of the bladder taken during initial examination shows bilateral, easily detectable ureteral jets crossing in midline. Multiple other jets were detected bilaterally during the remainder of this 5-min examination.**

***B*, Similar image taken during second examination shows no detectable ureteral jets. No jet was detected on either side during the entire 5-min examination.**

analysis under these conditions confirmed easily detectable bilaterally symmetric ureteral jets in all subjects. Then the patients were allowed to completely void, refill, and completely void one more time in order to wash out any of the concentrated urine from the bladder. The bladder was then refilled a second time, with dilute urine exiting the ureters to ensure a situation in which density of ureteral and bladder urine would be similar. Color Doppler sonographic examinations performed under the latter circumstances failed to show ureteral jets in any subject despite documented diuresis rates that were similar throughout the study. These results confirm the contention of Price et al. [4] that density differences are the reason that ureteral jets are detectable sonographically.

In our study, one participant (subject 6) had detectable jets at an estimated density difference of 0.002 while another participant (subject 2) had no detectable jets at a similar density difference. This apparent overlap was probably due to the fact that exact density measurements of ureteral and bladder urine could not be obtained noninvasively. While the values we used were the best possible estimates, a slight underestimation of the density of bladder urine during the initial examination was unavoidable because the first specimen was constantly being diluted by nonconcentrated ureteral urine. Therefore, the actual density differences of ureteral and bladder urine during the first examination were slightly greater than what was estimated. On the basis of these results, we suspect that a density difference of slightly greater than 0.002 is required to detect ureteral jets in vivo. Interestingly, 0.002 was the minimum density difference required to visualize fluid jets in vitro [4].

Our results underscore an important technical consideration that must be taken into account when performing ureteral jet analysis in a true clinical setting. All previous reports on this subject have emphasized the need for good hydration of the patient before the examination [1, 2, 4]. This is important because it increases the frequency of ureteral jets and thus facilitates comparison of the normal and abnormal side and shortens the amount of time needed for examination. However, if the well-hydrated patient is allowed to completely void and then refill his bladder before ureteral jet analysis by color Doppler examination, then detection of ureteral jets will be extremely difficult, if not impossible. Therefore, patients should not be allowed to completely empty their bladder after hydration. If the patient becomes uncomfortable because of bladder distension, partial voiding is suggested, since this will maintain some concentrated urine in the bladder and thus ensure at least some difference in the density between bladder and ureteral urine. Alternatively, if the patient is unable to partially void and complete voiding is unavoidable, then placement of a Foley catheter and filling of the bladder with a saline solution should be considered in order to optimize ureteral jet detection. The latter procedure also may be necessary in patients with defects in renal concentrating ability.

REFERENCES

1. Dubbins PA, Kurtz AB, Darby J, Goldberg BB. Ureteric jet effect: the echographic appearance of urine entering the bladder. *Radiology* **1981**;140:513–515
2. Burge HJ, Middleton WD, McClennan BL, Hildebolt CF. Ureteral jets in healthy subjects and in patients with unilateral ureteral calculi: comparison with color Doppler ultrasound. *Radiology* **1991**;180:437–440
3. Kremer H, Dobrinski W, Mikyska M, Baumgartner M, Zollner N. Ultrasonic in vivo and in vitro studies on the nature of the ureteral jet phenomenon. *Radiology* **1982**;142:175–177
4. Price CI, Adler RS, Rubin JM. Ultrasound detection of differences in density: explanation of the ureteric jet phenomenon and implications for new ultrasound applications. *Invest Radiol* **1989**;24:876–883
5. Meltzer RS, Tickner EG, Sahines TP, Popp RL. The source of ultrasound contrast effect. *J Clin Ultrasound* **1980**;8:121–127
6. Kremkau FW, Gramiak R, Carstensen EL, Shah PM, Kramer DH. Ultrasonic detection of cavitation at catheter tips. *AJR* **1970**;110:177–183

Books Received

Receipt of books is acknowledged as a courtesy to the sender. Books considered of sufficient interest are reviewed as space permits. If the book has been reviewed in the *AJR*, the date of its review is given in parentheses.

Diagnostic Ultrasonics. Principles and Use of Instruments, 3rd ed. By W. N. McDicken. New York: Churchill Livingstone, 367 pp., 1991. $59 (7/92)

Echocardiography. Edited by Marveen Craig. (Vol. II in Diagnostic Medical Sonography. A Guide to Clinical Practice.) Philadelphia: Lippincott, 416 pp., 1991. $85 (7/92)

Ultrasound of Appendicitis and its Differential Diagnosis. By Julien B. C. M. Puylaert. New York: Springer-Verlag, 118 pp., 1990. $59 (7/92)

Cardiac Imaging in Infants, Children, and Adults. By Larry P. Elliott. Philadelphia: Lippincott, 960 pp., 1991. $150 (7/92)

The Cystic Kidney. Edited by Kenneth J. Gardner, Jr., and Jay Bernstein. Boston: Kluwer, 444 pp., 1990. $145 (7/92)

Èchographie en Pratique Obstétricale. By B. Guérin Du Masgenêt, Y. Ardaens B. Bailleux, and D. Houzé De L'Aulnoit. Paris: Masson, 196 pp., 1991. (7/92)

Head and Neck Radiology. By Arnold Noyek. Philadelphia: Lippincott, 115 pp., 1991. $49.95 (7/92)

Radiology of the Extremities. By Nancy Baker. Philadelphia: Lippincott, 125 pp., 1991. $49.95 (7/92)

The Traumatized Hand and Wrist. Radiographic and Anatomic Correlation. By Louis A. Gilula. Philadelphia: Saunders, 235 pp., 1992. $65 (7/92)

RSNA Today Video, Vol. 5, No. 6. Oak Brook, IL: The Radiological Society of North America, 1991. $55; by subscription, 6 issues annually at $185 for RSNA members and $225 for nonmembers (VHS videotape) (7/92)

A Practical Guide to Ultrasound of Fetal Anomalies. By Frederick N. Hegge. New York: Raven, 242 pp., 1992. $39 (7/92)

Pediatric Orthopedic Radiology, 2nd ed. By M. B. Ozonoff. Philadelphia: Saunders, 816 pp., 1992. $125 (7/92)

MRI Atlas of the Spine. By Kenneth R. Maravilla and Wendy A. Cohen. New York: Raven, 456 pp., 1991. $140 (8/92)

Diagnostic Ultrasound. Physics, Biology, and Instrumentation. By Stewart C. Bushong and Benjamin R. Archer. St. Louis: Mosby–Year Book, 177 pp., 1991. $34.95 (8/92)

Human Cross-sectional Anatomy. Atlas of Body Sections and CT Images. By Harold Ellis, Bari M. Logan, and Adrian Dixon. Stoneham, MA: Butterworth-Heinemann, 180 pp., 1991. $49.95 (8/92)

Radiation Protection in Nuclear Medicine and Pathology. (Report No. 63.) Edited by K. E. Goldstone, P. C. Jackson, M. J. Myers, and A. E. Simpson. York, England: The Institute of Physical Sciences in Medicine, 203 pp., 1991. £22.50 (8/92)

CT & MRI Radiological Anatomy. Edited by Samuel Merran. (Translated by Adrian Dixon.) Stoneham, MA: Butterworth-Heinemann, 304 pp., 1991. $130 (8/92)

Imaging of Orthopedic Trauma, 2nd ed. Edited by Thomas H. Berquist. New York: Raven, 916 pp., 1992. $140 (8/92)

The Esophagus. Edited by Donald O. Castell. Boston: Little, Brown, 817 pp., 1992. $150 (8/92)

Magnetic Resonance Imaging of the Body, 2nd ed. By Charles B. Higgins, Hedvig Hricak, and Clyde A. Helms. New York: Raven, 1420 pp., 1992. $169 (8/92)

Ultrasound in Ophthalmologic Diagnosis. A Practical Guide. By Rudolf Guthoff. (Translated from the German by F. C. Blodi.) New York: Thieme, 174 pp., 1991. $59 (8/92)

The Radiologists's Second Reader. By Harry W. Fischer. Available from Granville Medical Books, Granville, OH. 348 pp., 1992. $18.95, softcover (8/92)

Imaging Anatomy of the Newborn. By Ernst Richter and Werner Lierse. (Translated and edited by Alan E. Oestreich.) Baltimore: Urban & Schwarzenberg, 280 pp., 1991. $175 (9/92)

Film-Screen Mammography. An Atlas of Instructional Cases. By Lawrence W. Bassett, Reza Jahanshahi, Richard H. Gold, and Yao S. Fu. New York: Raven, 318 pp., 1991. $130 (9/92)

Practical Doppler Ultrasound for the Clinician. By Raymond L. Powis and Robert A. Schwartz. Baltimore: Williams & Wilkins, 187 pp., 1991. $55 (9/92)

Advances in Gastrointestinal Radiology, vol. 1. Edited by Hans Herlinger and Alec J. Megibow. St. Louis: Mosby–Year Book, 197 pp., 1991. $69.95 (9/92)

Atlas of Radiology of the Chest. Edited by Margaret Turner-Warwick, Margaret E. Hodson, Bryan Corrin, and Ian H. Kerr. New York: Gower Medical, 168 pp., 1991. $70 (9/92)

Screen Film Mammography. Imaging Considerations and Medical Physics Responsibilities. Proceedings of SEAAPM Spring Symposium, April 6, 1990, Columbia, South Carolina. Edited by Gary T. Barnes and G. Donald Frey. Madison, WI: Medical Physics Publishing, 242 pp., 1991. $55 (9/92)

Interventional Cardiology. Clinical Applications of New Techniques. Edited by Christopher J. White and Stephen R. Ramee. New York: Raven, 264 pp., 1991. $75 (9/92)

Clinical Sonography. A Practical Guide, 2nd ed. Edited by Roger C. Sanders. Boston: Little, Brown, 557 pp., 1991. $47.50, softcover (9/92)

High-Resolution CT of the Lung. By W. Richard Webb, Nestor L. Müller, and David P. Naidich. New York: Raven, 176 pp., 1992. $79 (9/92)

Endoscopic Retrograde Cholangiopancreatography. Technique, Diagnosis, and Therapy. By Jerome H. Siegel. New York: Raven, 442 pp., 1992. Book, $159; correlating slide set, $225 (9/92)

Diagnostic Imaging of AIDS. Edited by J. W. A. J. Reeders, F. H. Barneveld Binkhuysen, and J. F. W. M. Bartelsman. New York: Thieme Verlag, 114 pp., 1992. $79, softcover (9/92)

Cerebral Blood Flow Measurement with Stable Xenon-Enhanced Computed Tomography. Edited by Howard Yonas. New York: Raven, 327 pp., 1992. $80 (9/92)

Skeletal Radiology. The Bare Bones Teaching Collection. By Felix S. Chew. St. Paul, MN: Image PSL, 276 pp., 1991. Book and videodisc, $635 (9/92)

The Children of Atomic Bomb Survivors. A Genetic Study. Edited by James V. Neel and William J. Schull. Washington: National Academy Press, 518 pp., 119. $29.95

Oral Contraceptives and Neoplasia. By the WHO Scientific Group. Geneva: World Health Organization, 46 pp., 1992. $8.10

La Diagnostica Per Immagini Dei Traumi Chiusi Dell'Addome. By Antonio Frassineti and Francesco Musante. Reggio Emilia, Italy: Tecnograf, 343 pp., 1991.

Clinical Oncology for Students of Radiation Therapy Technology. By John A. Stryker. St. Louis: Warren H. Green, 307 pp., 1992.

Laryngeal Cancer. Edited by Carl E. Silver. New York: Thieme, 284 pp., 1991.

Technical Note

Percutaneous Removal of a Titanium Greenfield Filter

Jacob Cynamon,[1] Curtis W. Bakal,[1] Steven B. Epstein,[1] and Gary Gabelman[2]

Placement of a filter in the inferior vena cava (IVC) is accepted as standard therapy for patients at risk for pulmonary emboli in whom anticoagulant therapy is ineffective or contraindicated [1, 2]. Several types of filters are in clinical use, including the original 24-French Kimray-Greenfield filter, the new 12-French titanium Greenfield filter (Medi-tech, Watertown, MA), the Bird's Nest filter (Cook, Bloomington, IN), the Venatech LGM filter (Venatech, Chicago, IL), and the Simon Nitinol filter (Simon Nitinol, Woburn, MA). Although each type has certain advantages and disadvantages, they all share filter misplacement as a potential complication. Misplacement can be due to premature filter release or migration due to malpositioning or to a filter that is too small for the IVC lumen. Surgical or percutaneous removal has been recommended if the filter migrates to the heart because of the risk of significant morbidity and mortality [3-6]. Several 24-French stainless steel Kimray-Greenfield filters have been removed percutaneously [3-5]. We report the first retrieval of a 12-French titanium Greenfield filter.

Case Report

A 74-year-old woman presented to another hospital with shortness of breath. A ventilation and perfusion lung scan showed multiple mismatched defects, suggesting a high probability for pulmonary emboli. Duplex sonography showed deep venous thrombus extending to the common femoral vein in the right lower extremity. A modified-hook titanium Greenfield filter was placed from the left femoral approach. Because of difficulty in advancing the filter through the tortuous iliac vessels, the filter was released prematurely from its carrier (while still in the delivery sheath). When the filter was ultimately deployed, the legs did not open. The apex of the filter was then noted to migrate from L3 to T11, the level of the right atrium. The patient was then transferred to our hospital.

Two 14-French sheaths were placed: one in the right internal jugular vein and one in the left femoral vein. An inferior venacavogram showed the orientation and position of the filter within the inferior vena cava (Fig. 1A). An Amplatz gooseneck snare was introduced via the jugular sheath and one of the legs was engaged. Through the femoral sheath, a loop snare was introduced through a nontapered catheter. When the transfemoral snare wire completely surrounded all of the filter's legs, the loop was tightened by advancing the catheter over the snare (Fig. 1B). While tension was maintained at both ends of the filter, it was pulled caudally into the iliac vein and it easily slid into the femoral vein sheath and was removed from the patient (Fig. 1C). The Amplatz gooseneck snare, still tightly applied to the filter apex, followed the exiting filter. A 12-French Bird's Nest filter was then placed in the infrarenal IVC, via the sheath in the left femoral vein. The patient remained stable throughout the procedure. No significant decrease in hematocrit was noted. The patient was discharged several days later and has remained asymptomatic.

Discussion

The most common complication reported by Greenfield et al. [1] with the insertion of the original stainless steel Kimray-Greenfield filter was aberrant placement, which occurred in 7-9% of cases. The most recent communication by Greenfield and coworkers [7], describing a multicenter experience with the new modified-hook titanium Greenfield filter in 186 patients, did not address aberrant placement. Incomplete opening of the filter's legs was reported in four patients (2%), subsequently corrected by the manipulation of the guidewire;

Received April 23, 1992; accepted after revision May 8, 1992.

[1] Department of Radiology, Montefiore Medical Center, 111 E. 210th St., Bronx, NY 10467. Address reprint requests to J. Cynamon.

[2] Department of Medicine, Division of Cardiology, 111 E. 210th St., Bronx, NY 10467.

AJR 159:777-778, October 1992 0361-803X/92/1594-0777 © American Roentgen Ray Society

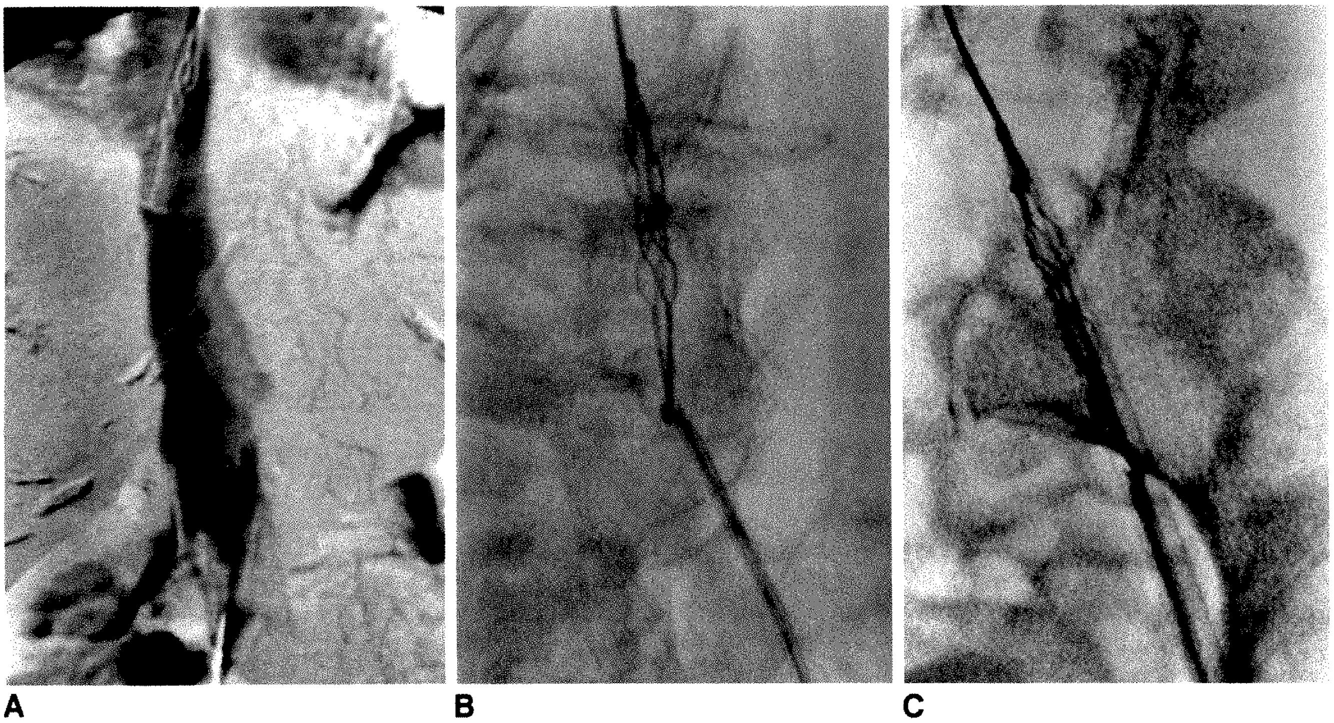

Fig. 1.—Inferior venacavograms of removal of misplaced filter.
***A*, Modified hook titanium Greenfield filter misplaced in inferior vena cava.**
***B*, Filter snared at both ends.**
***C*, Filter being removed through 14-French femoral sheath with traction on upper portion of filter.**

in addition, asymmetry of the filter's legs occurred in 10 patients (5%) [7].

Although the indications for removal of misplaced filters remain controversial, most authors agree that misplacement or migration to the right atrium mandates removal [2-5]. Percutaneous removal of misplaced filters has obvious advantages over surgical methods. Several case reports describe removal or repositioning of misplaced Kimray-Greenfield filters. The experience with the new titanium Greenfield filter is limited; the frequency of aberrant placement has not been determined; and percutaneous removal of this filter has not been reported.

Tsai et al. [4] used a beveled chest tube for removal of a Kimray-Greenfield filter via the jugular route. The angle of the hooks of a titanium Greenfield filter allows safe caudal movement of the filter after it has been collapsed by a loop snare. A collapsed titanium Greenfield filter easily fits through a 14-French sheath. A beveled sheath is not necessary if the filter is secured at both ends, as the filter can be stabilized and straightened, facilitating relatively safe movement of the filter in the right atrium and vena cava and allowing the filter to easily enter the 14-French sheath. If an Amplatz gooseneck snare is used, it may be difficult or impossible to free the snare if all of the legs are not successfully snared. We therefore prefer creating a loop snare, fashioned from a single guidewire and then advanced through a nontapered catheter, as the most suitable device for percutaneous filter retrieval.

During the initial deployment of a Greenfield filter, if the filter is accidentally released from its delivery catheter while still in the sheath, the entire sheath should be removed, hemostasis achieved, and the procedure reattempted. No attempt should be made to release the filter into the vena cava; pushing a filter through the sheath for deployment in the IVC is contraindicated. As experience with IVC filters increases, indications for removal of misplaced filters should become more defined and more widely agreed on.

REFERENCES

1. Greenfield LJ, Zocco J, Wilk J, Schroder TM, Elkins RL. Clinical experience with the Kimray-Greenfield vena cava filter. *Ann Surg* **1977**;185:692-698
2. Cohen JR, Tenenbaum N, Citron M. Greenfield filter as primary therapy for deep venous thrombosis and/or pulmonary embolism in patients with cancer. *Surgery* **1991**;109:12-15
3. Scneider PA, Bednarkiewicz M. Percutaneous retrieval of a Kimray-Greenfield vena cava filter. *Radiology* **1985**;134:1047-1052
4. Tsai FY, Myers TV, Ashraf A, Shah OC. Aberrant placement of a Kimray-Greenfield filter in the right atrium: percutaneous retrieval. *Radiology* **1988**;167:423-424
5. Yakes WF. Percutaneous retrieval of Kimray-Greenfield filter from right atrium and placement in inferior vena cava. *Radiology* **1988**;169:849-851
6. Greenfield LJ, Crute SL. Retrieval of the Greenfield vena caval filter. *Surgery* **1980**;88:719-722
7. Greenfield LJ, Kyung JC, Proctor M, et al. Results of a multicenter study of the modified hook titanium Greenfield filter. *J Vasc Surg* **1991**;14:253-257

Review Article

MR Imaging of the Cervical Spine: Techniques for Two- and Three-dimensional Imaging

Jeffrey S. Ross[1]

This review briefly describes two-dimensional (2D) and three-dimensional (3D) MR imaging of the cervical spine and focuses on the current and potential clinical usefulness of 3D sequences in the evaluation of cervical spine abnormalities. The practical advantages of 3D imaging are several, and include an increase in signal-to-noise ratio over 2D imaging, thin contiguous slices, more accurate slice thickness, and optimal computer postprocessing. Different 3D techniques can provide either high- or low-signal-intensity CSF, with excellent suppression of CSF pulsation artifacts.

MR imaging has had a tremendous impact on the evaluation of degenerative disease of the cervical spine. The high contrast between foraminal and epidural fat and between disk material and osteophyte coupled with MR's multiplanar imaging capability allows accurate assessment of disk herniations and stenosis in the cervical spine [1]. An early prospective study [2] found that MR could be used to correctly predict surgical findings in 74% of patients, CT myelography was correct in 85%, and plain film myelography was correct in 67%. In a blinded retrospective review, Brown et al. [3] studied 34 patients who had surgery of the cervical spine. Findings on MR images could be used to correctly predict 88% of the surgically proved lesions compared with 81% for postmyelographic CT, 58% for myelography, and 50% for CT. Small osteophytes were sometimes not predicted on the basis of MR findings, although these were visible on plain films. MR replaced the invasive myelographic evaluation in 32% of the patients who had surgery. These authors concluded that MR imaging, combined with plain films, is an accurate and noninvasive test for cervical radiculopathy and myelopathy.

Current protocols for MR imaging of cervical degenerative disease vary widely from institution to institution. However, the sequences usually include a T1-weighted two-dimensional (2D) spin-echo (SE) sagittal image (providing detailed anatomic findings with dark CSF), and 2D axial and sagittal images with high-signal-intensity CSF (the "CSF myelogram" effect) either with SE T2-weighted or with gradient-echo T2*-weighted imaging.

This review briefly describes the two broad categories for acquiring MR imaging data of the spine that are in use today (2D and three-dimensional [3D]), and focuses on the clinical usefulness of 3D sequences in the evaluation of spinal disease, particularly degenerative disk disease. The practical advantages of 3D imaging include an increase in signal-to-noise ratio over 2D imaging, thin contiguous slices, more accurate slice thickness, and optimal computer postprocessing. Three-dimensional techniques can provide high- or low-signal-intensity CSF, with suppression of CSF pulsation artifacts.

Two-dimensional Techniques

Two-dimensional image acquisition is currently the most common MR technique for evaluating the cervical spine for degenerative disease. In 2D imaging, a single slice is imaged by applying a series of three magnetic gradients to spatially encode the three orthogonal directions, that is, slice select, phase encoding, and frequency encoding. In 2D imaging, total imaging time is determined by the following formula: repetition

---

Received December 19, 1991; accepted after revision March 9, 1992.

[1] Cleveland Clinic Foundation, Division of Radiology, Magnetic Resonance, Desk L-10, 9500 Euclid Ave., Cleveland, OH 44195. Address reprint requests to J. S. Ross.

AJR **159:779–786, October 1992** 0361–803X/92/1594–0779 © American Roentgen Ray Society

time (TR) × number of excitations × number of phase-encoding steps. Although multiple slices are routinely obtained with 2D sequences, a space that is not imaged, the so-called gap, must generally be placed between slices. This is placed to remove interference from adjacent slices, which would degrade image quality (i.e., cause "cross-talk").

Sagittal T1-weighted SE images are excellent for showing central disk herniations, which are seen as intermediate signal outlined against the higher-signal-intensity vertebral bodies and the low-signal-intensity CSF. The herniation may be largest posteriorly, with a slight constriction at the site of ligamentous tear (the so-called toothpaste sign). The overall size of the herniation on T1-weighted SE images may be slightly underestimated because the low signal of the annulus merges imperceptibly with the low signal of the CSF. Deformity of the cord is also easily seen on these images.

Two-dimensional imaging evaluation of the neural foramina for osteophyte or lateral disk herniations is best accomplished with axial imaging. This can be achieved with CSF of either high or low signal intensity. Images on which CSF has high signal intensity are generally preferred because of the problem of visualizing low-signal-intensity ligaments or osteophytes against the dark CSF on T1-weighted images. T2-weighted SE images provide high-signal-intensity CSF and the best sensitivity for intramedullary disease. However, current imaging times for these sequences are approximately 8–12 min and require flow compensation, cardiac gating, or both to stop "ghosting" artifacts on images, which result from pulsatile motion of the CSF.

Rapid imaging of the spine with high-signal-intensity CSF (CSF myelogram effect) can be achieved with gradient-echo techniques [4, 5], in which gradient reversal in the frequency-encoded direction is used to obtain an echo, analogous to the 180° pulse used in SE imaging (Fig. 1). However, the gradient-echo sequence allows reduced imaging times. Enzmann and Rubin [6] prospectively studied 90 patients by using a partial-flip-angle gradient-echo technique to detect cervical disk disease. The parameters that were manipulated to change signal-to-noise ratio and contrast included flip angle, TR, and TE. For cervical disk disease, they recommended a small flip angle (3–8°) for the best contrast between disk, cord, and CSF. Sagittal imaging required the use of smaller flip angles (3–4°) than did axial imaging. TR should be kept as short as possible to reduce imaging time, and these sequences are sensitive to motion artifact. TE should be kept short as well, to minimize shading effects caused by field inhomogeneity and magnetic susceptibility. Hedberg et al. [7] suggested that the low-flip-angle gradient-echo technique should be the initial MR procedure of choice for evaluation of cervical radiculopathy. MR images were obtained in 130 patients with radicular complaints, with surgical correlation in 13, and CT myelographic correlation in 20. MR findings correlated with the CT findings in all cases, and with surgical findings at 29 of 30 levels. The use of both sagittal and axial gradient-echo images allowed distinction of disk herniation and osteophytes, and the best detection of extradural disease. Disk material generally showed slightly increased signal intensity on gradient-echo images, whereas osteophytes showed decreased signal intensity.

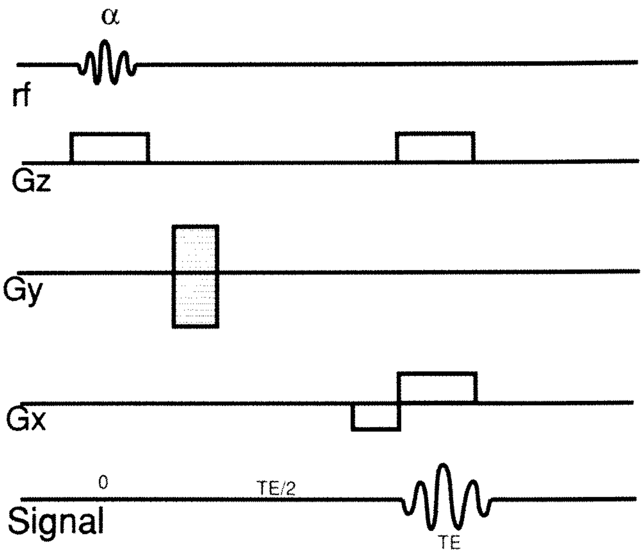

Fig. 1.—Diagram of a generic gradient-echo sequence (Gz = slice select gradient, Gy = phase-encoding gradient, Gx = frequency-encoding gradient, α = variable flip angle). Echo is generated by bipolar gradient in Gx.

Although 2D MR imaging can accurately show cervical spine disease, it is not without limitations. The major problem of present 2D MR imaging techniques for cervical disease is the failure to accurately detect foraminal disease because of long echo times, thick slices (3–4 mm), and the failure to optimally view the course of the exiting nerve roots [8]. Reduction in image slice thickness is limited by the hardware used with 2D techniques. This is because slice thickness relates to the RF pulse bandwidth and the gradient amplitude in the slice-select direction. Maximum gradient strengths on 1.5-T systems are on the order of 10 mT/m. Although overall examination times have decreased with the use of gradient-echo imaging, the length of examinations continues to be problematic. One potential solution to these problems is found in gradient-echo volume imaging (3D), which would allow short echo times with thin contiguous slices, and the ability to reformat the data in any desired viewing plane.

Three-dimensional Techniques

In 3D imaging, a volume of interest is defined by the initial RF excitation pulse rather than by a thin slice, as in 2D imaging. This volume of tissue is divided into thin contiguous partitions (slices) by an additional direction of phase encoding along the slice-select direction (Figs. 2 and 3). The in-plane phase and frequency-encoding gradients are applied as in 2D imaging. With phase encoding used in two different directions, the imaging time compared with that of 2D techniques will be proportionally increased by the number of slices selected. Imaging time is therefore equal to repetition time (TR) × number of excitations × number of in-plane phase-encoding steps × number of slices (slice-select phase encoding). Although 3D Fourier transform imaging is possible with SE sequences, for all practical purposes, the short TRs achieved by gradient-echo imaging have allowed more widespread applications [9]. For example, an axial 3D technique may typically have the following parameters: TR = 0.035 sec, one excitation, 192 in-plane phase-encoding steps, 64 slices for a

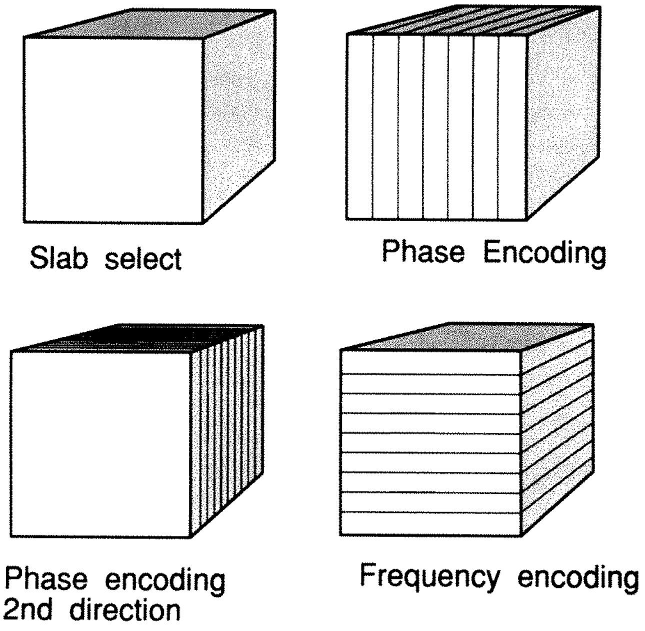

Fig. 2.—Drawing shows method of spatial encoding for a nonselective volume excitation. Three-dimensional acquisitions are differentiated from two-dimensional ones by second direction of phase encoding along slice-select direction (coronal slices in this instance).

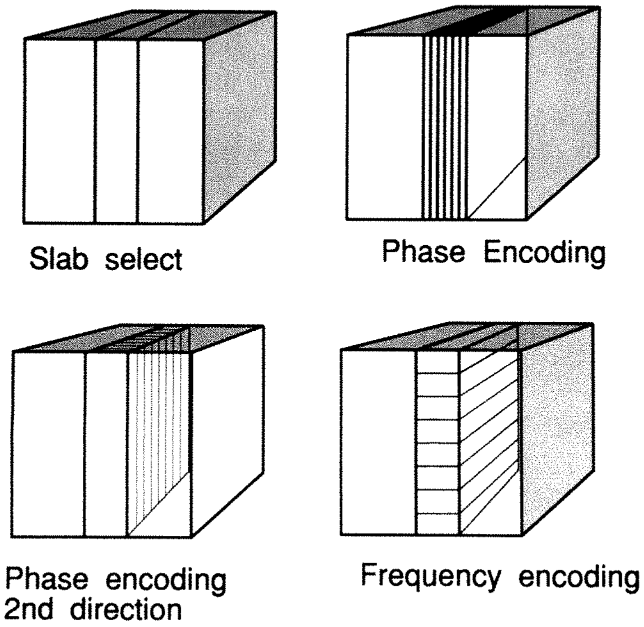

Fig. 3.—Drawing shows method of spatial encoding for a selective volume excitation. Difference between this method and a nonselective excitation is that only a small portion of active volume of coil is used.

total of 430 sec (7.2 min) of imaging time (TE = 7, 5° flip angle). Two general types of 3D imaging can be used: either the entire active volume of the surface coil can be used (nonselective) (Fig. 2) or only a smaller specific volume of tissue can be imaged within the active area of the coil (selective) (Fig. 3).

The theoretical and practical advantages of 3D imaging are several and include the following: (1) An increase in signal-to-noise ratio over 2D imaging by the square root of the number of partitions (slices) selected, as there is reexcitation of the entire volume for each partition [10, 11]. This may be considered analogous to increasing the number of acquisitions in 2D imaging. It is therefore advantageous to increase the number of slices with this technique and increase the area covered. (2) Thin contiguous slices can be obtained from the volume without the problem of cross-talk found in 2D imaging [11] (cross-talk between adjacent 2D slices will give unwanted changes in image contrast from slice to slice). Thinner slices can be achieved with 3D techniques than with 2D because slice thickness is not dependent on gradient amplitude in the slice-select direction but rather on the time the slice-select phase-encoding gradient is on. Minimum slice thickness is approximately 0.75 mm for 3D vs 2.5 mm for 2D imaging. (3) Three-dimensional techniques have a more accurate slice thickness than in 2D imaging and a reduction in susceptibility artifacts (i.e., $T2^*$ effects) [12, 13]. Slice thickness is more accurate because in 3D the slices are achieved by phase encoding as opposed to being a function of the quality of the slice profile, as in 2D imaging. Susceptibility artifacts can cause false "expansion" of bone at bone–soft-tissue interfaces, which can result in overestimation of the degree of foraminal stenosis. (4) Because a volume of data is collected, computer postprocessing allows reformatting of the data along any desired imaging plane, with minimal degradation in image quality. Different 3D techniques can provide either high- or low-signal-intensity CSF, with excellent suppression of CSF pulsation artifacts. Certain sequences provide high enough signal intensity that a computer algorithm can be used to display the CSF in a rotating 3D manner, similar to a myelogram. This 3D myelogram could provide the clinician with the global assessment of the CSF spaces that has previously been lacking with imaging techniques.

Certain problems persist with 3D imaging. Truncation artifact (Gibbs artifact) is present in the in-plane directions and in the slice-encoding direction because of finite sampling [11, 14]. Motion and ghosting artifacts are present not only along the in-plane phase-encoding directions (as in 2D imaging) but also along the additional direction of phase encoding in slice select. Motion artifacts present one of the most commonly encountered problems affecting the diagnostic quality of 3D techniques. Magnetic susceptibility effects associated with the gradient-echo technique also may cause artifactual foraminal stenosis. Tsuruda and Remley [15] showed that the overestimation of foraminal disease relates, as expected, directly to the TE, and ranged from 8% with a TE = 11 to 27% with a TE = 22 compared with CT. Additionally, RF profiles associated with selective and nonselective 3D sequences are not perfect. Although the individual slice thickness is preserved in 3D, the imperfect slice profile may result in excitation of matter outside the volume of interest with subsequent aliasing of the information into the region of interest [16]. The amount of slice-select aliasing for a fixed volume decreases as the number of partitions is increased. The imperfect slice profile also causes nonuniform distribution of the flip angle across the volume, and thus nonuniform contrast and signal-to-noise ratio from slice to slice. Although this may not be noticeable on one slice, it can degrade the quality of multiplanar reformats with a banding pattern.

T1-Weighted Three-dimensional Imaging

T1-weighted 3D imaging is accomplished by using sequences such as FLASH (fast low-angle shot) or spoiled GRASS (gradient-recall acquisition in the steady state) with flip angles greater than approximately 30°. With these techniques, residual transverse magnetization is destroyed by a spoiler gradient applied after the data are collected, or by randomly varying the phase of the RF. Because the transverse magnetization is dephased before each RF pulse, only the longitudinal magnetization reaches a steady state. This steady-state signal is dependent on T1, but not T2.

This technique allows good conspicuity of the CSF-extradural interface. Oblique reconstructions may allow improved definition of the cervical neural foramina, and in particular any hypertrophic changes that involve the uncinate processes of the vertebrae. However, improvement in tissue contrast, especially within the neural foramina, would allow increased confidence in the diagnosis of foraminal disease. Improved tissue contrast can be achieved by injection of gadopentetate dimeglumine, which will enhance the cervical epidural and foraminal plexi in a manner analogous to iodinated contrast enhancement with CT [17, 18].

Snapshot imaging can be implemented as a 3D sequence, called turbo-FLASH or MP RAGE (Magnetization Prepared Rapid Acquisition Gradient Echo) [19–21] (Figs. 4 and 5). This technique uses short TRs (<10 msec) and low flip angles (10°) for very rapid volume imaging. A 128-partition volume sequence can be completed in approximately 5 min. TEs are on the order of 2–7 msec. With the very short TR, image contrast may be a problem because little time is available between excitations for relaxation even with low flip angles. One method used to improve T1 contrast is the addition of a preparation period included before acquisition of each 3D phase-encoding cycle. To produce T1 contrast, this preparation period includes a 180° RF pulse, which inverts the spins. An inversion-recovery period that lasts a few hundred milliseconds is included to allow T1 relaxation past the zero signal point (inversion-recovery period, TI). A single enhanced T1-weighted gradient-echo volume sequence, with the appropriate reformatted images, has recently been compared with a more conventional 2D set of MR sequences for the evaluation of cervical extradural degenerative disease [22]. Sixty-one patients evaluated for extradural degenerative disease with MR were imaged with a "standard" MR examination (sagittal T1-weighted SE, axial low-flip-angle gradient-echo), and after injection of contrast material they were reimaged with either a 3D FLASH or a 3D turbo-FLASH (MP RAGE) technique, acquired as 128 contiguous 1.5-mm coronal partitions. The volume sequences were reconstructed in the axial plane and in right and left 45° oblique coronal planes. The two sets of examinations (standard vs volume) were prospectively interpreted for quality of examination and location and severity of extradural degenerative disease. No significant difference was found between the standard examination and the 3D MP RAGE for central extradural disease. Neither the 3D FLASH nor the 3D MP RAGE examinations showed any significant difference compared with the routine examination for the location and severity of lateral extradural disease. This initial study suggests that a single enhanced volume T1-weighted imaging sequence can be equivalent to a routine set of mixed SE and gradient-echo sequences taking half the imaging time. A single MR sequence serving as a screen for cervical degenerative disk disease could minimize the patient's discomfort and motion, while maximizing efficiency. Patients with a question of intrinsic cord abnormality are not presently suited for

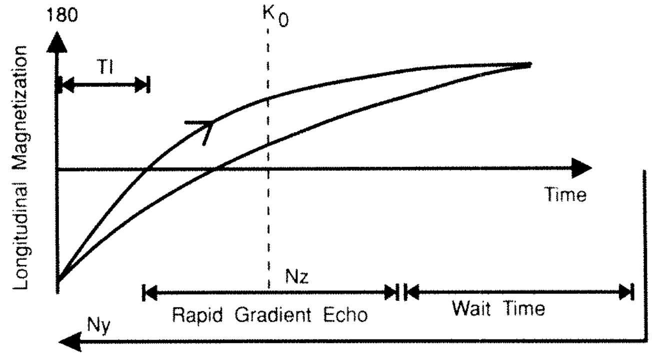

Fig. 4.—Representation of three-dimensional MP RAGE sequence. Every 180° inverting pulse is followed by an inversion time (TI), a rapid gradient-echo sequence repeated Nz times (number of slice-select phase-encoding steps, 128), and a wait time. This series is then repeated Ny times (number of in-plane phase-encoding steps, 130, 192, etc.). Effective TI is time from inversion pulse to central Fourier line (K_0), and is different from user-defined TI (defined on schematic).

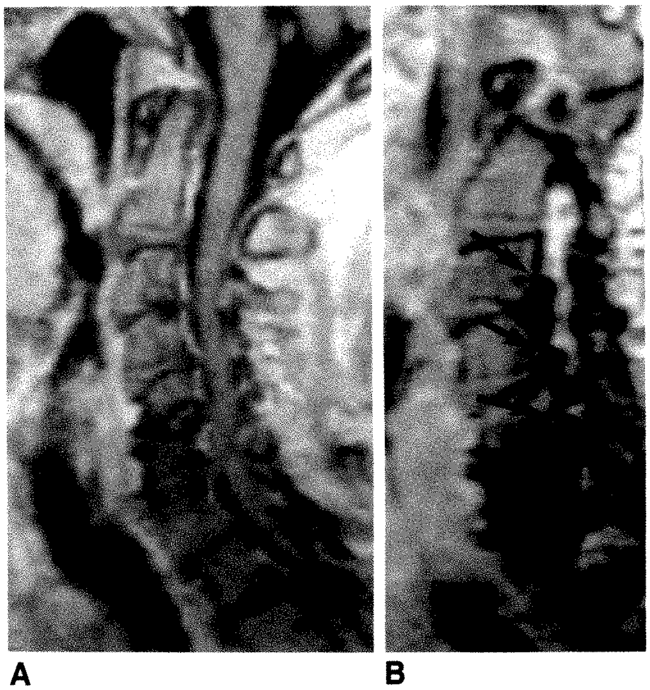

Fig. 5.—Contrast-enhanced three-dimensional T1-weighted MP RAGE MR imaging.

***A*, Sagittal reformatted image shows cervical spondylosis with multiple extradural defects and narrowing of canal.**

***B*, Oblique reformatted image through neural foramina shows osteophytes from uncinate processes of vertebrae narrowing foramina at multiple levels (*arrows*).**

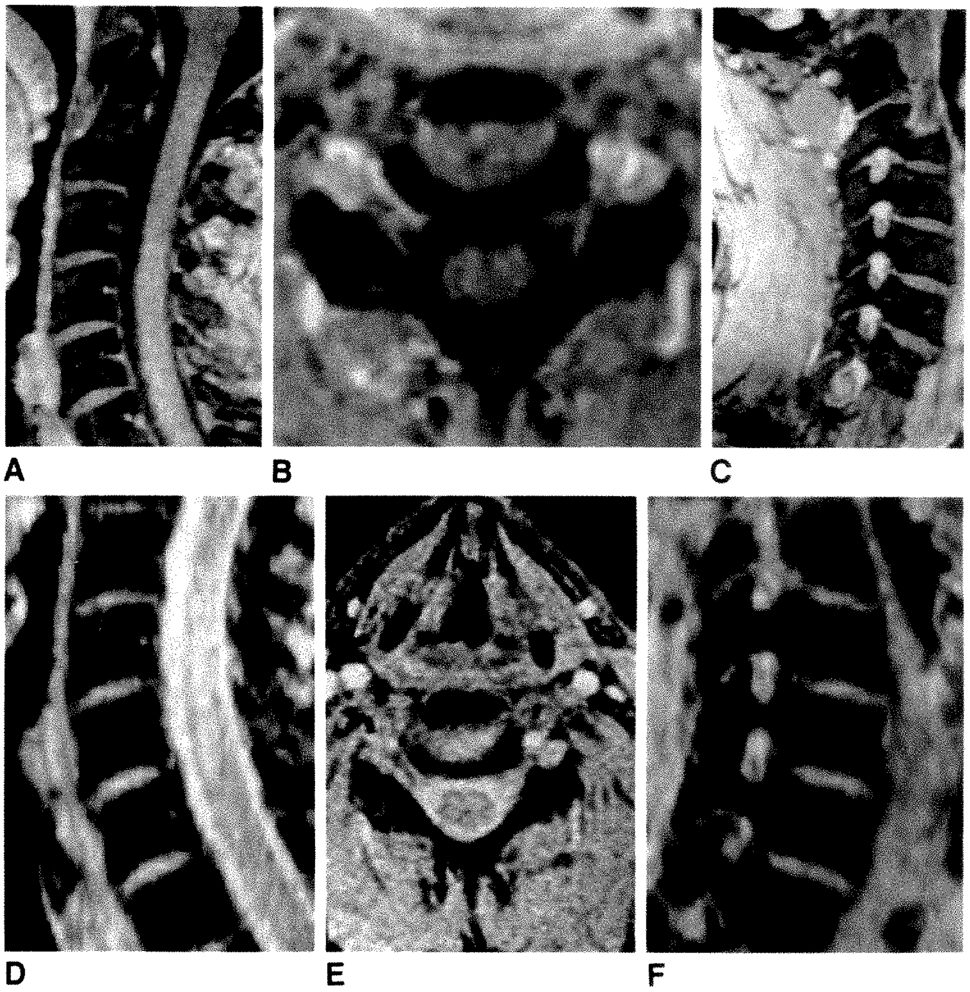

Fig. 6.—Comparison of T1-weighted turbo-FLASH (13/6/1, 12° flip angle, 128 slices, 1.2 mm thick, 192 × 256, 5.5 min) and T2*-weighted FISP (35/7/1, 5° flip angle, 64 slices, 2 mm thick, 192 × 256, 7.2 min) volume MR sequences.

***A–C*, Sagittal (*A*), axial (*B*), and oblique (*C*) reformatted images of turbo-FLASH sequence show good detail of foramina and good cord, disk, and CSF contrast.**

***D–F*, Sagittal reformatted (*D*), axial individual slice (*E*), and oblique reformatted (*F*) images of axial FISP volume.**

this technique, because the ability of 3D MP RAGE to define intrinsic cord disease is unknown.

Although the MP RAGE sequence provides T1-weighted contrast, use of the inversion preparation pulse and the wait time do not appear to be essential for the evaluation of the spine (at least for assessment of degenerative disk disease). The optimal parameters for a T1-weighted cervical 3D turbo-FLASH imaging sequence have been evaluated and include no preparatory inversion pulse and the elimination of the wait time, a flip angle of 12° (non–RF spoiled) and 15–20° (RF spoiled), a matrix of 192 × 256, and 128 1.2-mm slices acquired coronally for an overall examination time of 5 min, 21 sec [23]. This sequence provides T1-weighted contrast with good resolution, allowing quality axial, oblique, and sagittal reformats from the coronal slices. The time savings from the elimination of the wait time and the inversion preparation pulse allows the use of an in-plane matrix of 192 × 256, with little change in overall examination time (5.5 min) and a near isotropic voxel (1.2 × 1.1 × 0.9 mm) for maximum reformat quality (Figs. 6 and 7).

T2- and T2-Weighted Three-dimensional Imaging*

Low-flip-angle imaging has achieved wide acceptance because it can be used to define low-signal-intensity extradural defects and foraminal disease contrasted with the high signal intensity of the CSF. Gradient-echo techniques provide spin density–weighted contrast at low flip angles. GRASS or FISP (fast imaging with steady-state precession) imaging can use small flip angles (5–10°) to produce hyperintense CSF and the CSF myelogram effect [7] (Fig. 8). In one report (Hueftle M et al., presented at the American Society of Neuroradiology meeting, May 1988), 120 patients were examined by using a low-flip-angle 3D FLASH technique (5° flip angle), and the images were compared with sagittal and axial T1-weighted images. The 3D technique provided a good examination in 70% of cases, as compared with 90% of the T1-weighted images. This figure highlights the importance of minimizing the patient's motion with the 3D techniques, as this was the major cause of a poor examination. The 3D FLASH examinations showed improved contrast between the CSF and the extradural space because of the high-signal-intensity CSF. Axial reconstructions from the sagittal partitions allowed thin contiguous axial images through the disk levels. In an early study, Enzmann and Rubin [24] compared 2D and 3D Fourier transform (FT) techniques in cervical disease in 16 patients. They found that image contrast related to disk disease was poorer with the 3D sequence than with the 2D sequence. They concluded that the 3D technique (27/14.5/1, 6° flip angle, 2-mm thickness, 256 × 256 matrix) was not ideal for

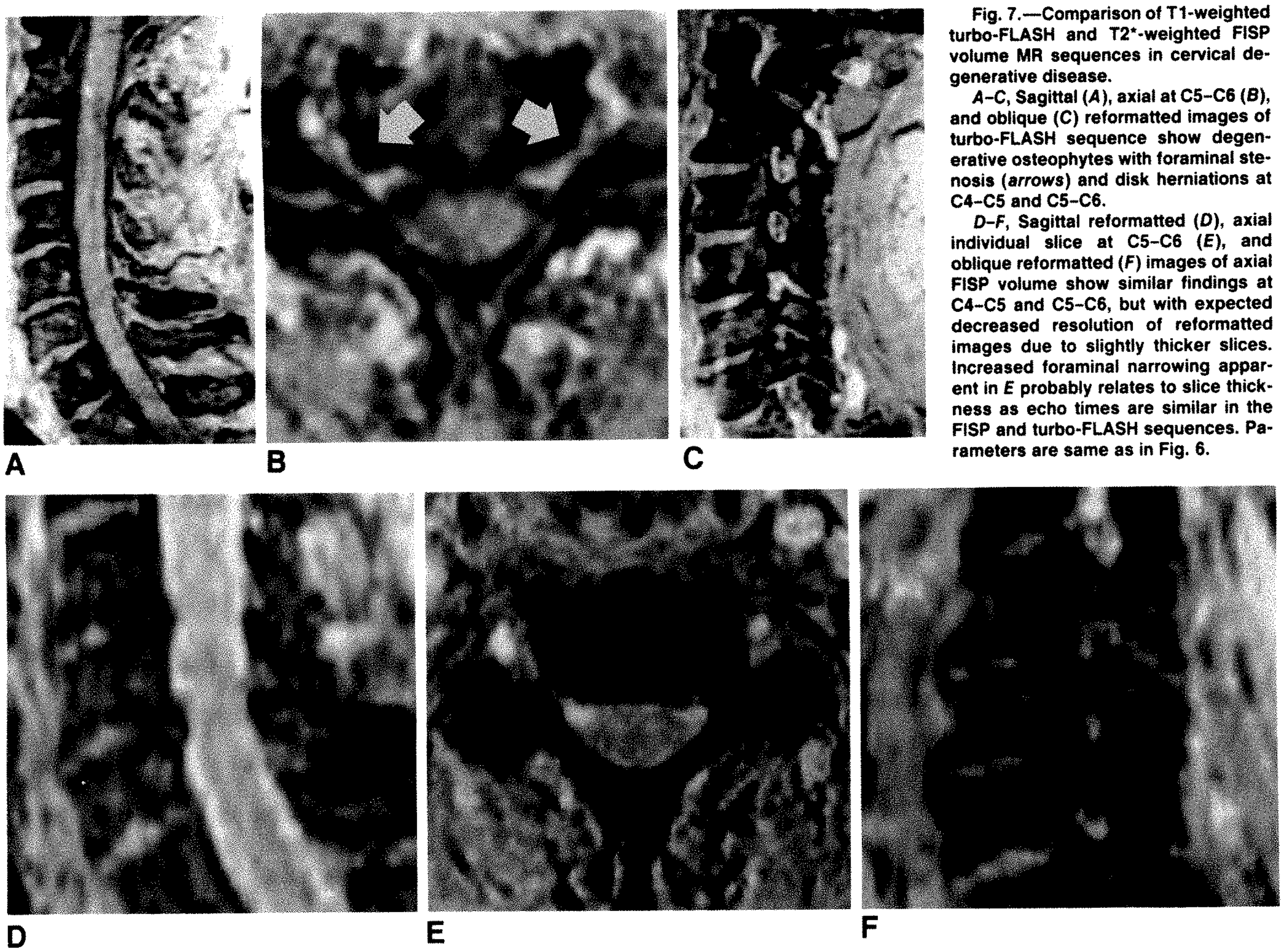

Fig. 7.—Comparison of T1-weighted turbo-FLASH and T2*-weighted FISP volume MR sequences in cervical degenerative disease.

A–C, Sagittal (*A*), axial at C5–C6 (*B*), and oblique (*C*) reformatted images of turbo-FLASH sequence show degenerative osteophytes with foraminal stenosis (*arrows*) and disk herniations at C4–C5 and C5–C6.

D–F, Sagittal reformatted (*D*), axial individual slice at C5–C6 (*E*), and oblique reformatted (*F*) images of axial FISP volume show similar findings at C4–C5 and C5–C6, but with expected decreased resolution of reformatted images due to slightly thicker slices. Increased foraminal narrowing apparent in *E* probably relates to slice thickness as echo times are similar in the FISP and turbo-FLASH sequences. Parameters are same as in Fig. 6.

evaluating degenerative disk disease. Of note, the 2D technique was acquired with eight excitations, vs one for the 3D technique. More recently, Tsuruda et al. [16] evaluated 3DFT low-flip-angle gradient-echo axial 1.5–2.0 mm slices for cervical spine imaging in 30 patients, and compared this with 2D 4-mm-thick gradient-echo MR in 10 patients. In this study, the 3D acquisition provided better details of the structure of the foramina, canal, and disk. They determined that the increased diagnostic confidence seen with the 3D technique was attributable to decreased partial volume effects. Their 3D sequence had a TR = 35, TE = 15, two excitations, 5° flip angle, 256 × 128 matrix for a total of 9 min 34 sec imaging time. Yousem et al. [25] compared axial MR images of a 3DFT gradient-echo sequence with CT myelograms for disk herniation in 19 patients. They used a 5° flip angle, 50/11–15/1 sequence with 1.5-mm slices. MR had an accuracy of 86%, which was comparable to the variation in CT myelograms interpreted blindly on different days (88% concordance). The axially acquired low-flip-angle 3D sequence has become the standard against which other 3D sequences are compared for cervical degenerative disk disease. These sequences are easily implemented, and provide 1.5- to 2.0-mm-thick contiguous axial slices for evaluation of the neural foramina.

The MP RAGE sequence previously discussed for producing T1-weighting also can be used to produce T2-weighted images. T2 weighting is produced by a driven equilibrium pulse set, such as 90°–180°–90° [26]. Although this sequence has not yet been applied to imaging of the spine to any extent, it can produce high-signal CSF images of the brain (32 2-mm slices acquired in 4.3 min) [27]. Another method of producing fast T2-weighted 3D images is with hybrid versions of RARE (rapid acquisition with relaxation enhancement) [28–30]. With this fast spin-echo technique, any one 90° pulse is followed by a series of 180° pulses (anywhere from two to 16), instead of a single 180° pulse as in conventional SE imaging. Thus, multiple phase-encoding steps are taken for any one 90° pulse, with a concomitant decrease in imaging time. Although the 2D versions of fast SE have been applied for evaluation of intra- and extradural spinal disease, the 3D technique has not yet been assessed for spinal imaging [31, 32]. Fast SE has produced a multislab T2-weighted 3D data set of the brain (80 slices, 128 × 256 matrix) in approximately 5 min [30]. Advantages of this technique over FISP or MP RAGE include decreased sensitivity to susceptibility changes and field inhomogeneities, as it is an SE technique, and higher signal-to-noise ratio, as a 90° pulse is used (instead of the low flip angle in FISP or MP RAGE).

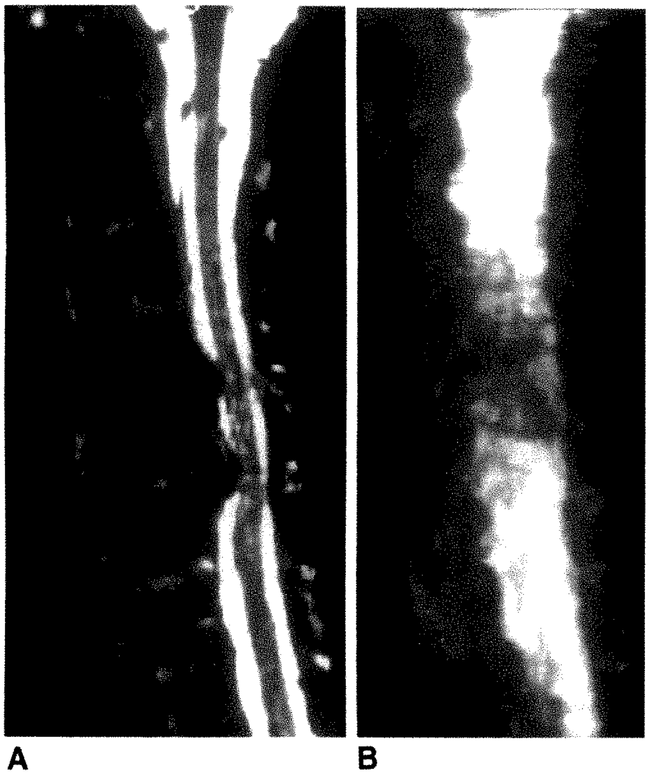

Fig. 8.—True FISP (20/11/1, 40° flip angle, 64 slices, 2-mm thick, 256 × 256 matrix) MR sequence in cervical disk disease.

A, Sagittal image from volume sequence shows CSF with very high signal intensity, defining two large herniations at C4–C5 and C5–C6 with stenosis of canal.

B, Oblique maximum intensity projection (MIP) image has appearance of a contrast myelogram, with loss of CSF signal from area of cord compression, narrowing of canal and cutoff of nerve roots.

Theoretically, FISP and GRASS imaging (with their T1/T2 contrast) should give high-signal-intensity CSF in the spine with a short TR and high flip angles. In practice, the CSF is typically of decreased signal intensity because of pulsatile motion [33–35]. This is evident in the cervical spine, where the CSF dynamics have greater impact than in the lumbar region. CSF motion acts to randomize the phases of spins in the transverse plane from cycle to cycle, which reduces the effective T2 of the spins.

Motion-related loss of signal intensity and contrast at higher flip angles in techniques such as FISP can be overcome by compensating for moving spins in the gradient structure. True FISP is a sequence in which the gradients are symmetric and balanced over each TR interval in all three orthogonal directions. This gives inherent CSF velocity compensation and high-signal-intensity CSF at higher flip angles (i.e., 70°) [36–38]. With balanced gradients, image contrast is dependent on the local static field inhomogeneities. In standard gradient-echo imaging, this dependence is eradicated by purposely including constant gradients along one or more directions. This causes the signal variations along the associated directions to be smoothed. The use of additional gradients further dephases moving spins, which increase the motion sensitivity of these standard steady-state techniques and therefore change contrast behavior. In true FISP, reduced motion sensitivity precludes use of unbalanced "smoothing" gradients (Wielopolski PA et al., presented at the Radiological Society of North America meeting, November 1989). It is impossible to obtain a true FISP image with one scan whose signal contrast is independent of static local field inhomogeneities. These field inhomogeneities are seen as dark bands traversing the image. The field inhomogeneity problem can be negated by obtaining two separate volume sequences, one with 180° phase-alternated RF and the other with non-phase-alternated RF. Areas of signal loss in one volume image will have improved signal intensity within the other volume image, and vice versa. The final product is obtained by taking the maximum signal between the two volumes on a pixel-by-pixel basis. Even though two acquisitions are required, a short TR of 40 msec results in a short overall scanning time for two true FISP acquisitions. The signal intensity of the CSF is good enough that a maximum intensity projection (MIP) algorithm can be used to display the CSF in a rotating 3D manner, similar to a myelogram (Fig. 8). This 3D myelogram could provide the clinician with the global assessment of the CSF spaces that has been previously lacking with imaging techniques. Thus, this technique could provide enough information, in the proper display, to eliminate the need for contrast myelography. This technique suffers from the problems inherent in visualizing only the CSF space, as in contrast myelography. In particular, the technique may be insensitive to anterior extradural disease if there is a large epidural space, as at L5–S1. Lateral bony or disk disease involving the nerve root distal to the root sleeve termination will not be identified. The CSF myelographic technique may be most effectively used to replace the sagittal T2*- or T2-weighted 2D sequence in a routine MR protocol, and then evaluated in conjunction with T1-weighted SE images. This would allow detection of lateral disease and subtle disease at L5–S1. The MIP images do not allow visualization of individual nerve roots. This evaluation would have to be accomplished with reformatting of the data axially or by relying on the other sequences in the imaging protocol.

Although 2D bright CSF techniques produce good image quality and reasonable correlation with surgical and CT myelographic findings for degenerative disk disease in the cervical spine, their life span is limited by the introduction of a variety of 3D techniques. The potential of advanced postprocessing techniques available for image display, such as multiplanar reconstruction, 3D MIP, or surface rendering cannot be used effectively with 2D imaging and still maintain a reasonable examination time. Three-dimensional MR techniques can alter the approach to a standard spinal examination by providing thin contiguous slices, which allow high spatial resolution, high tissue contrast, and quality multiplanar reconstructions. However, 3D techniques place increased demands on MR hardware, because of their rapid gradient switching. Further advances in imaging sequences will occur in conjunction with hardware improvements such as increased gradient strengths, shorter ramp times, and improved durability. Particular care also must be taken to minimize patients' motion, which remains the greatest routine limitation to satisfactory image quality.

REFERENCES

1. Masaryk TJ, Modic MT, Geisinger MA, et al. Cervical myelopathy: a comparison of MR and myelography. *J Comput Assist Tomogr* **1986**; 10:184–194
2. Modic MT, Masaryk TJ, Mulopulos GP, Bundschuh C, Han JS, Bohlman H. Cervical radiculopathy: prospective evaluation with surface coil MR imaging, CT with metrizamide, and metrizamide myelography. *Radiology* **1986**;161:573–579
3. Brown BM, Schwartz RH, Frank E, Blank NK. Preoperative evaluation of cervical radiculopathy and myelopathy by surface-coil MR imaging. *AJNR* **1988**;9:859–866
4. Mills TC, Ortendahl DA, Hylton NM, Crooks LE, Carlson JW, Kaufman L. Partial flip angle MR imaging. *Radiology* **1987**;162:531–539
5. Perkins TG, Wehrli FW. CSF signal enhancement in short TR gradient echo image. *Magn Reson Imaging* **1986**;4:465–468
6. Enzmann DR, Rubin JB. Cervical spine: MR imaging with a partial flip angle, gradient-refocused pulse sequence. *Radiology* **1988**;166:467–472
7. Hedberg MC, Drayer BP, Flom RA, Hodak JA, Bird CR. Gradient echo (GRASS) MR imaging in cervical radiculopathy. *AJNR* **1988**;9:145–151
8. Russel EJ. Cervical disk disease. *Radiology* **1990**;177:313–325
9. Sherry CS, Harms SE, McCroskey WK. Spinal MR imaging: multiplanar representation from a single high resolution 3D acquisition. *J Comput Assist Tomogr* **1987**;11:859–862
10. Frahm J, Haase A, Matthaei D. Rapid three-dimensional MR imaging using the FLASH technique. *J Comput Assist Tomogr* **1986**;10:363–368
11. Carlson J, Crooks L, Ortendahl D, Kramer DM, Kaufman L. Signal-to-noise ratio and section thickness in two-dimensional versus three dimensional Fourier transform MR imaging. *Radiology* **1988**;166:266–270
12. Young IR, Cox IJ, Bryant DJ, Bydder GM. The benefit of increasing spatial resolution as a means of reducing artifacts due to field inhomogeneities. *Magn Reson Imaging* **1988**;6:585–590
13. Haacke EM, Tkach JA, Parrish TB. Reduction of T2* dephasing in gradient field echo imaging. *Radiology* **1989**;170:457–462
14. Czervionke LF, Czervionke JM, Daniels DL, Haughton VM. Characteristic features of MR truncation artifacts. *AJNR* **1988**;9:815–824
15. Tsuruda JS, Remley K. Effects of magnetic susceptibility artifacts and motion in evaluating the cervical neural foramina on 3DFT gradient-echo MR imaging. *AJNR* **1991**;12:237–241
16. Tsuruda JS, Norman D, Dillon W, Newton TH, Mills DG. Three-dimensional gradient-recalled MR imaging as a screening tool for the diagnosis of cervical radiculopathy. *AJNR* **1989**;10:1263–1271
17. Ross JS, Modic MT, Masaryk TJ et al. Assessment of extradural degenerative disease with Gd-DTPA-enhanced MR imaging: correlation with surgical and pathologic findings. *AJNR* **1989**;10:1243–1249
18. Russell EJ, D'Angelo CM, Zimmerman RD, Czervionke LF, Huckman MS. Cervical disk herniation: CT demonstration after contrast enhancement. *Radiology* **1984**;152:703–712
19. Haase A. NMR imaging of the human brain using high-speed FLASH NMR. In: *Book of abstracts: Society of Magnetic Resonance in Medicine 1989*. Berkeley, CA: Society of Magnetic Resonance in Medicine, **1989**:5
20. Haase A. Snapshot FLASH NMR imaging. In: *Book of abstracts: Society of Magnetic Resonance in Medicine 1989*. Berkeley, CA: Society of Magnetic Resonance in Medicine, **1989**:364
21. Mugler JP III, Brookeman JR. Three-dimensional magnetization-prepared rapid gradient-echo imaging (3D MP RAGE). *Magn Reson Med* **1990**;15:152–157
22. Ross JS, Ruggieri P, Masaryk TJ, Tkach J, Modic MT. Gd-DTPA enhanced 3D MR imaging of cervical degenerative disease. *AJNR* **1992**;13:127–136
23. Ross JS, Tkach J, Masaryk TJ, Modic MT, Dillinger J. Optimization of 3D T1 weighted MP RAGE for cervial degenerative disease (abstr). *Radiology* **1991**;181(P):193
24. Enzmann D, Rubin JB. Short TR, variable flip angle, gradient echo scans of the cervical spine: comparison of 2DFT and 3DFT techniques. *Neuroradiology* **1989**;31:213–216
25. Yousem DM, Atlas SW, Hackney DB. Cervical spinal disk herniation: evaluation of 3D FT thin section GE MR images with post myelography CT as proof (abstr). *Radiology* **1991**;181(P):193
26. Edelman RR, Wallner B, Singer A, Atkinson DJ, Saini S. Segmented TurboFLASH: method for breath-hold MR imaging of the liver with flexible contrast. *Radiology* **1990**;177:515–521
27. Mugler JP III, Spraggins TA, Brookeman JR. T2 weighted three dimensional MP-RAGE MR imaging. *JMRI* **1991**;1:731–737
28. Henning J, Nauerth A, Friedburg H. RARE imaging: a fast imaging method of clinical MR. *Magn Reson Med* **1986**;3:823–833
29. Mulkern RV, Wong STS, Winalski C, Jolesz FA. Contrast manipulation and artifact assessment of 2D and 3D RARE sequences. *Magn Reson Imaging* **1990**;8:557–566
30. Oshio K, Melki PS, Jolesz FA. T2 weighted thin slice imaging with multislab 3D RARE. In: *Book of abstracts: Society of Magnetic Resonance in Medicine 1991*. Berkeley, CA: Society of Magnetic Resonance in Medicine, **1991**:842
31. Sze G. Fast spin echo MR imaging of the spine: evaluation of cord lesions (abstr). *Radiology* **1991**;181(P):172
32. Melki PS, Mulkern RV, Jolesz FA. How fast are fast spin echo techniques compared with spin echo sequences (abstr). *Radiology* **1991**;181(P):236
33. Hawkes RC, Patz S. Some factors that influence the steady state in steady-state free precession. *Magn Reson Imaging* **1988**;6:405–413
34. Patz S, Hawkes RC. The application of steady-state free precession to the study of very slow fluid flow. *Magn Reson Med* **1986**;3:140–145
35. Tkach JA, Haacke EM. A comparison of fast spin echo and gradient echo sequences. *Magn Reson Imaging* **1988**;6:373–389
36. Oppelt A, Graumann R, Barfuss H, Fischer H, Hertl W, Schajor W. A new fast MRI sequence. *Electromedica* **1986**;3:15–18
37. VanDyke C, Modic MT, Beale S, Amartur S, Ross JS. 3D MR myelography. *J Comput Assist Tomogr* **1992**;16:497–500
38. Haacke EM, Wielopolski PA, Tkach JA, Modic MT. Steady-state free precession imaging in the presence of motion: applications for improved visualization of the cerebrospinal fluid. *Radiology* **1990**;175:545–552

MR Imaging in the Evaluation of SLAP Injuries of the Shoulder:
Findings in 10 Patients

James P. Cartland[1]
John V. Crues III[2]
Anthony Stauffer[3]
Wesley Nottage[4]
Richard K. N. Ryu[5]

OBJECTIVE. Injuries to the superior portion of the glenoid labrum, called SLAP (superior labrum, anterior and posterior) injuries, are recently recognized injuries consisting of tears of the long head of the biceps tendon anchor/superior labral complex. The purpose of this study was to determine if the MR imaging findings in patients with surgically proved SLAP injuries correspond to the abnormalities found at arthroscopy.

MATERIALS AND METHODS. Four variants of SLAP lesions have been described; they are based on the degree of compromise of the superior portion of the glenoid labrum, biceps tendon, and labral-biceps anchor. A type I lesion has superior labral fraying in the region of the biceps anchor. A type II lesion has superior labral fraying and stripping of the superior part of the glenoid labrum and attached biceps off the underlying glenoid fossa. A type III lesion has a bucket-handle tear of the superior portion of the glenoid labrum in the region of the biceps anchor. A type IV lesion has a bucket-handle tear of the superior part of the glenoid labrum with extension of the tear into the proximal biceps tendon. Standard spin-echo MR imaging studies in 10 patients with surgically proved SLAP lesions were evaluated retrospectively. Correlations were made between MR imaging findings and the SLAP injury type determined from descriptions in the surgical report. MR imaging studies in a control group of seven symptomatic patients surgically proved not to have SLAP injuries also were evaluated.

RESULTS. MR imaging examinations of two patients with type I lesions showed irregularity of the labral contour and a slight increase in signal intensity on all imaging sequences. MR imaging examinations of two patients with type II lesions showed globular high signal interposed between the superior part of the glenoid labrum and the superior portion of the glenoid fossa. One case showed high signal in the labral-biceps anchor. The other case showed paired cleavages in the superior and inferior aspects of the superior part of the glenoid labrum at the labral-biceps anchor. MR imaging examinations of two patients with type III lesions showed superior labral tears identified as high signal intensity within the superior part of the labrum separate from the normal superior part of the labral cavity. MR imaging examinations of the four patients with type IV lesions showed diffuse high signal intensity within the superior part of the glenoid labrum with marked abnormal high signal intensity extending into the proximal biceps tendon. None of the MR imaging studies of patients in the control group showed findings seen on MR imaging studies of patients with surgically proved SLAP lesions.

CONCLUSION. Although prospective data are required to document accuracy, these preliminary data suggest that an MR examination can be useful in detecting SLAP abnormalities and establishing the type of SLAP lesion before surgery, thereby permitting better operative planning.

AJR 159:787–792, October 1992

The increasing use of shoulder arthroscopy has resulted in the discovery of injuries to the superior portion of the glenoid labrum, biceps tendon, and labral-biceps complex. These lesions, called SLAP (superior labrum, anterior and posterior) injuries, have not been well evaluated with standard radiologic techniques and usually require arthroscopy for detection [1]. SLAP lesions are injuries of the superior part of the glenoid labrum in the region of the insertion of the biceps

Received January 10, 1992; accepted after revision March 13, 1992.

[1] Department of Diagnostic Radiology, Santa Barbara Cottage Hospital, Santa Barbara, CA 93105.

[2] Cottage Community Magnetic Resonance Center, 401 Pueblo St., Santa Barbara, CA 93105. Address reprint requests to J. V. Crues III.

[3] Department of Radiology, Mission Regional Medical Center, Mission Viejo, CA 93691.

[4] 23961 Calle de la Magdalena, Ste. 229, Laguna Hills, CA 92653.

[5] Orthopedics Specialists of Santa Barbara, 536 E. Arreaga St., Santa Barbara, CA 93103.

0361–803X/92/1594–0787
© American Roentgen Ray Society

tendon [2]. Biceps tendon involvement varies. The injuries are clinically significant, causing pain, clicking, and occasionally instability of the shoulder. Arthroscopic repair can yield satisfying results [1].

Arthroscopists have classified SLAP injuries into four types. The percentage of each type of injury found in a series of 27 patients are in parentheses [1]: A type I lesion (11%) has fraying of the articulating surfaces of the superior portion of the glenoid labrum with no frank tear and with an intact biceps tendon (Fig. 1A). A type II lesion (41%) has superior labral fraying with stripping of the superior part of the glenoid labrum and attached biceps off the underlying glenoid fossa (Fig. 1B). A type III lesion (33%) has a bucket-handle tear of the superior portion of the glenoid labrum with the central portion of the tear often displaced into the joint. The periphery remains firmly attached to the glenoid fossa. There is no involvement of the biceps tendon or labral-biceps anchor in a type III lesion (Fig. 1C). A type IV lesion (15%) has a bucket-handle tear of the superior portion of the glenoid labrum similar to type III with the extension of the tear into the biceps tendon. The biceps tendon has an attached partial tear that frequently is found to migrate into the joint space (Fig. 1D).

The purpose of this study was to retrospectively evaluate MR imaging examinations of patients with surgically proved SLAP injuries and to determine if a correlation could be made between the MR imaging and arthroscopic findings.

Materials and Methods

Ten patients (eight men and two women, 19–63 years old) with arthroscopically documented SLAP lesions were included in the study. MR imaging studies in a control group of seven symptomatic patients (four men and three women 15–60 years old) surgically proved not to have SLAP injuries also were evaluated.

MR examinations were performed on 1.5-T GE Signa MR scanners (General Electric Medical Systems, Milwaukee, WI) at two different locations. Standard spin-echo sequences in an oblique coronal plane (parallel to the distal portion of the supraspinatus muscle) were made. We found images in this plane to show the anatomy better because the superior portion of the glenoid labrum is seen in cross section and not in tangent as in axial images. A specially designed shoulder coil (General Electric Medical Systems) was used to receive the signal. Before imaging in three patients, normal saline was injected into the glenohumeral joint by using a 50-ml syringe and a 22-gauge needle until a mild degree of resistance was felt. The arthroscopic surgeries

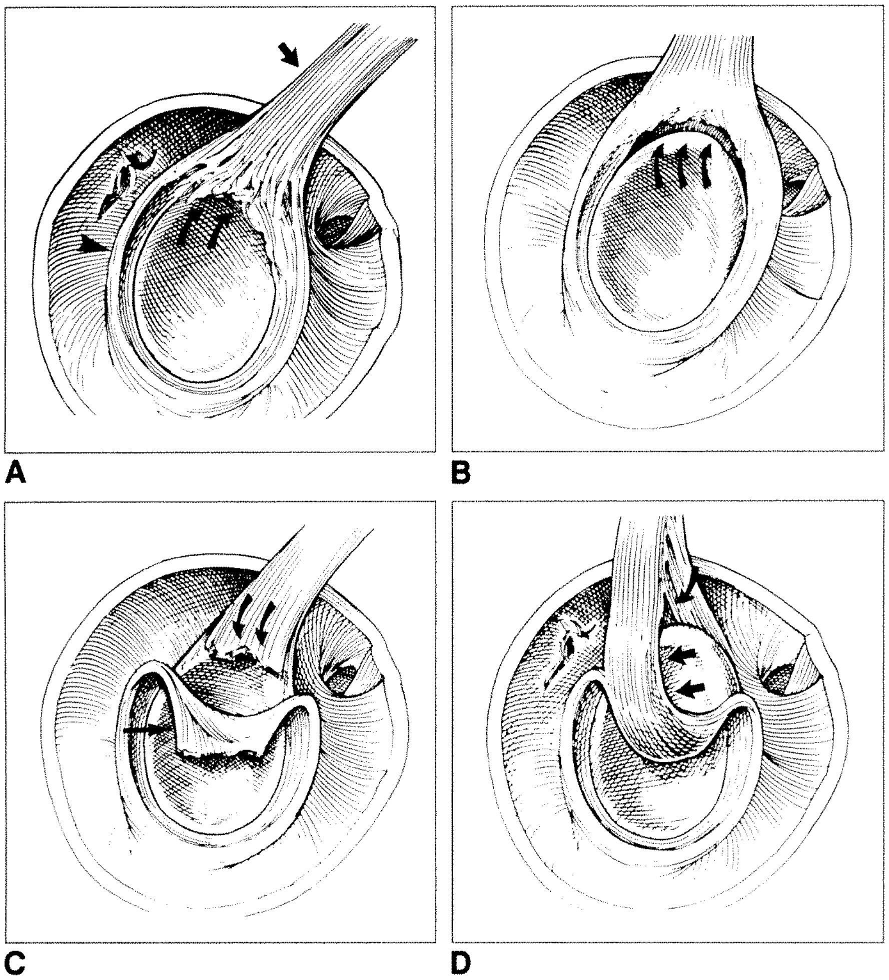

Fig. 1.—Types of SLAP lesions. (Reprinted with permission from Snyder et al. [1].)

_A_, Type I SLAP lesion. Diagram shows intact biceps tendon (_straight arrow_), glenoid labrum (_arrowhead_), and fraying of free edge of superior part of glenoid labrum (_curved arrows_).

_B_, Type II SLAP lesion. Diagram shows avulsion of labral-biceps anchor from superior portion of glenoid fossa (_arrows_).

_C_, Type III SLAP lesion. Diagram shows bucket-handle tear of superior portion of glenoid fossa (_straight arrow_) and intact labral-biceps anchor (_curved arrows_).

_D_, Type IV SLAP lesion. Diagram shows bucket-handle tear of superior portion of glenoid fossa (_straight arrows_) with extension of tear into the proximal biceps tendon (_curved arrow_).

were performed by three orthopedic surgeons with extensive experience in shoulder arthroscopy.

MR images were obtained with two different scanners (both Signa 1.5 T, General Electric Medical Systems) with different MR sequencing parameters. In five cases, 2000/70,140 (TR/TE) images were obtained. In four of these, a 16-cm field of view, 5-mm-thick slices, and 0.75 excitation on a 256 × 192 acquisition matrix were used. In one of the five cases, images were obtained with a 12-cm field of view, 5-mm-thick slices, and 1.0 excitation on a 256 × 128 acquisition matrix.

In the remaining five cases, 2000/30,80 images were acquired with a 14-cm field of view, 3-mm-thick slices, and two excitations on a 256 × 128 acquisition matrix. A display matrix of 512 × 512 was used in all examinations. Oversampling was performed in the phase- and frequency-encoded directions in these five cases, and saturation pulses were applied superiorly and inferiorly to minimize artifacts.

The images in the control group of seven patients were obtained by using image acquisition parameters identical to the 2000/30,80 technique used in acquiring images in the second group of five patients.

Three radiologists analyzed the MR images to find abnormalities in the biceps anchor/superior labral complex. Each radiologist was aware of the surgical findings. MR findings were correlated with the type of SLAP lesion determined at arthroscopy.

We found it vital to follow the course of the proximal biceps tendon carefully to the labral-biceps anchor on the superior part of the glenoid fossa (Fig. 2). Intact biceps tendons and the labral-biceps anchor are found in types I and III SLAP lesions. Disruptions of the labral-biceps anchor occur in type II SLAP lesions. Disruptions of the biceps tendon body are found in type IV lesions.

Results

Type I SLAP lesions were identified in two patients. MR examinations showed minimal irregularity of the articulating labral contours with a slight increase in signal intensity on both first- and second-echo images. The biceps tendon and the labral-biceps anchor were intact and had normal signal intensity (Fig. 3).

Type II SLAP lesions were identified in two patients. Globular high signal interposed between the superior part of the glenoid labrum and the superior part of the glenoid fossa was seen in both cases. In one case, high signal in the region of the labral-biceps anchor was seen. In the second case, paired cleavages were seen in the superior and inferior aspects of the superior section of the labrum at the labral-biceps anchor (Fig. 4). This contour should be smooth if the biceps anchor is intact. This represents a tear that is not well seen in its entirety because of limitations in spatial resolution.

Type III SLAP lesions were identified in two patients. In both, normal signal intensity and contour of the biceps tendon and labral-biceps anchor were seen. Superior labral tears were identified as areas of high signal intensity within the superior section of the labrum separate from the normal superior part of the labral recess (Figs. 5 and 6).

Type IV SLAP lesions were seen in four patients. MR images in all four patients showed diffuse high signal intensity within the glenoid labrum with marked abnormal high signal intensity extending into the proximal biceps tendons (Fig. 7).

None of the MR imaging findings seen on images of patients with SLAP lesions were seen on MR images of patients in the control group.

Discussion

Mechanism and Treatment

The most common mechanism eliciting a SLAP injury is a compressive force applied to the shoulder with the shoulder positioned in abduction and slight flexion, as may occur during a fall. This can generate a compressive force or traction on the glenoid fossa by the humeral head and pinch the biceps tendon and the superior part of the glenoid labrum. A second mechanism is sudden traction to the arm and forceful contraction of the biceps muscle, such as may occur as a result of throwing an object [1].

Patients are usually symptomatic and have shoulder pain that worsens with overhead activity [1]. Physical examination findings are neither sensitive nor specific, which makes a reliable diagnostic imaging technique desirable.

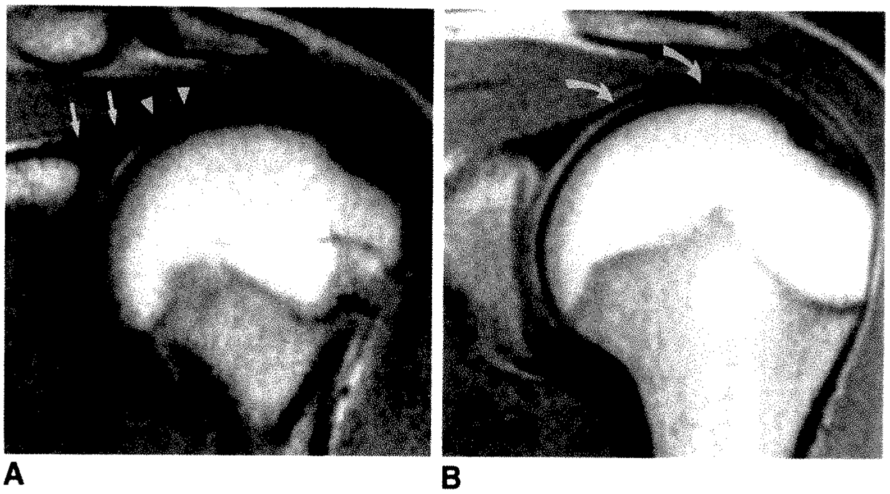

Fig. 2.—Normal superior portion of glenoid labrum and labral-biceps anchor. MR images (2000/20) are from anterior to posterior.

***A*, Superior portion of tendon of long head of biceps muscle can be seen coursing inferior to anterior aspect of supraspinatus tendon (*arrowheads*). Biceps anchor fuses with superior margin of superior portion of labrum (*arrows*).**

***B*, More posteriorly, variable appearance of superior portion of glenoid capsule (superior glenohumeral ligament) should not be mistaken for biceps tendon (*arrows*).**

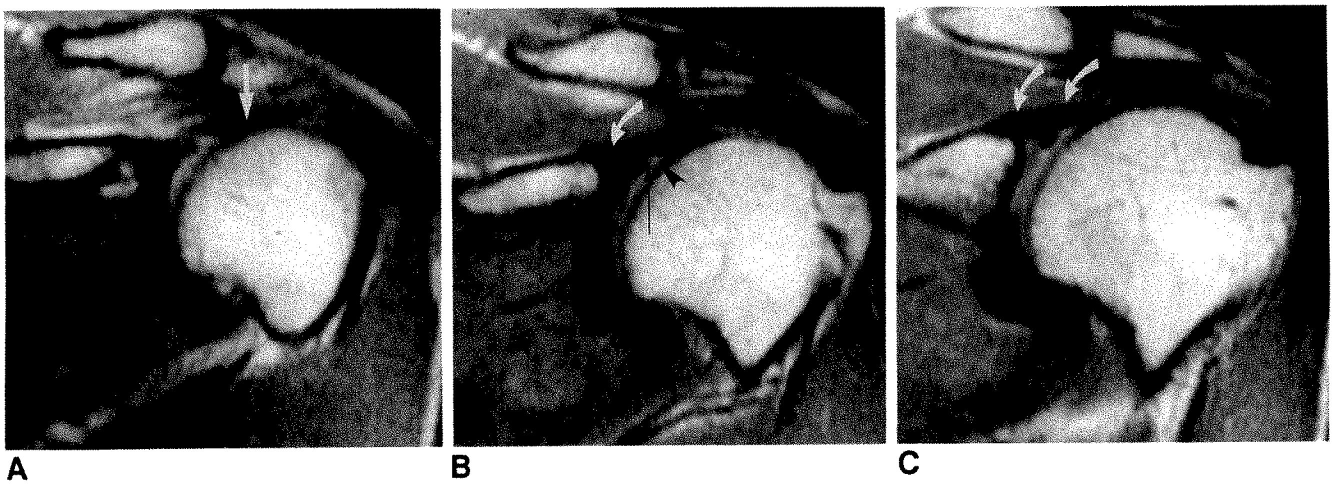

Fig. 3.—Type I SLAP lesion. MR images (2000/30) are from anterior to posterior.
A, Intact biceps tendon is seen coursing from intertubercular (biceps) groove of humerus toward superior part of glenoid fossa (*arrow*).
B and *C*, There is continuity of biceps tendon as it inserts on labral-biceps anchor (*curved arrows*). Cleavage plane of high signal may represent a normal potential space between superior portion of glenoid fossa and proximal biceps tendon (*arrowhead*). Blunting of labral margins with increased signal intensity at labral edge indicates degenerative fraying (*straight arrow*).

Treatment is surgical and usually can be accomplished arthroscopically. The prognosis is variable and depends on the type of SLAP lesion. Types I and III injuries have a favorable prognosis after surgical intervention. Types II and IV injuries have a less favorable prognosis, probably because of the disruption of the biceps tendon or labral-biceps anchor, which are intact in types I and III lesions.

Potential Pitfalls in MR Imaging of SLAP Lesions

The glenoid labrum is an ovoid rim of fibrous tissue surrounding the articulating surface of the glenoid fossa. Fibers of the long head of the biceps tendon become intertwined with the superior portion of the glenoid labrum near its insertion of the glenoid fossa. The point of insertion of the glenoid fossa is called the labral-biceps anchor.

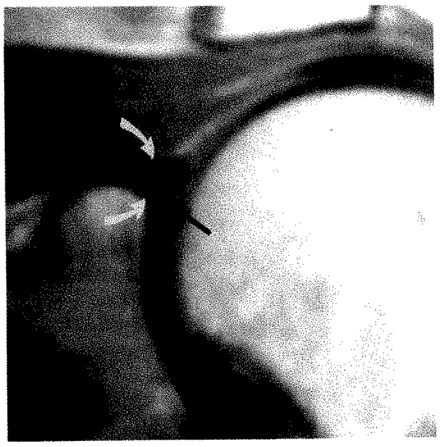

Fig. 4.—Type II SLAP lesion. MR image (2000/30) shows enlarged labral recess (*straight arrow*). Irregularity and cleavage of contour of superior and inferior surfaces at labral-biceps anchor are prominent (*curved arrows*).

Several normal configurations of labra have been described, with the profile of the superior portion of the glenoid labrum having different potential configurations. In one configuration, the superior part of the labrum has a triangular profile with a free central margin. A probe can be placed between the labrum and the articulating surface of the glenoid fossa in this type, usually with no communication between the intraarticular and extraarticular spaces. However, cases have been reported documenting a small, nonpathologic separation between the upper anterior portion of the glenoid fossa and the upper anterior aspect of the superior part of the glenoid labrum such that a probe could be placed through the separation into the extraarticular space. This normal "foramen" is anterior and inferior to the insertion of the biceps tendon [2]. A possible source of error may occur when attempting to differentiate between this normal labral variant and a pathologic avulsion of the superior part of the labrum from the glenoid fossa in a type II lesion. We realize that the thin cleavage plane that may be normally found between the superior part of the labrum and the glenoid fossa could also simulate an injury.

Studies of normal shoulders can show a linear band of high signal interposed between the proximal aspect of the biceps tendon and the superior part of the labrum (Fig. 3B). This signal is not in the appropriate plane for a SLAP lesion and is thought to represent a cleavage plane between the superior part of the labrum and the most proximal biceps tendon. This should not be confused with a superior labral tear. Liquid adjacent to the external surface of the superior part of the labrum was seen in four patients with arthroscopically documented superior labral tears (three studies were performed after saline injection). This finding may represent confined abnormal joint fluid extravasating through a tear. Its clinical

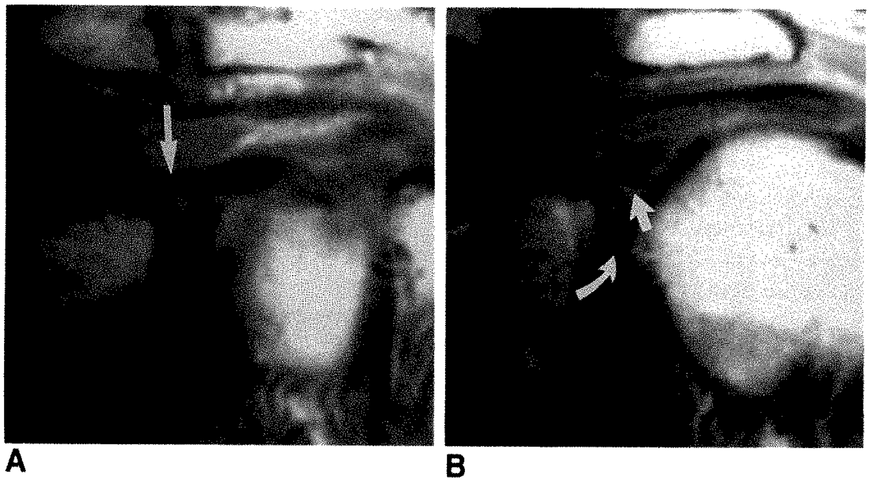

Fig. 5.—Type III SLAP lesion. MR images (2000/30) are from anterior to posterior.
A, Biceps tendon can be followed to labral-biceps anchor without disruption (*arrow*).
B, Superior labral recess is seen as a curvilinear structure adjacent to superior glenoid cortex (*curved arrow*). A second irregular region of increased signal represents a labral tear (*straight arrow*).

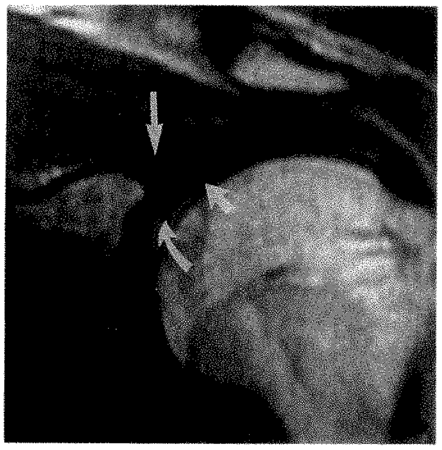

Fig. 6.—Type III SLAP lesion. MR image (2000/30) shows intact biceps tendon and labral-biceps anchor (*long straight arrow*). Superior labral recess (*curved arrow*) and separate labral tear have increased signal intensity (*short straight arrow*).

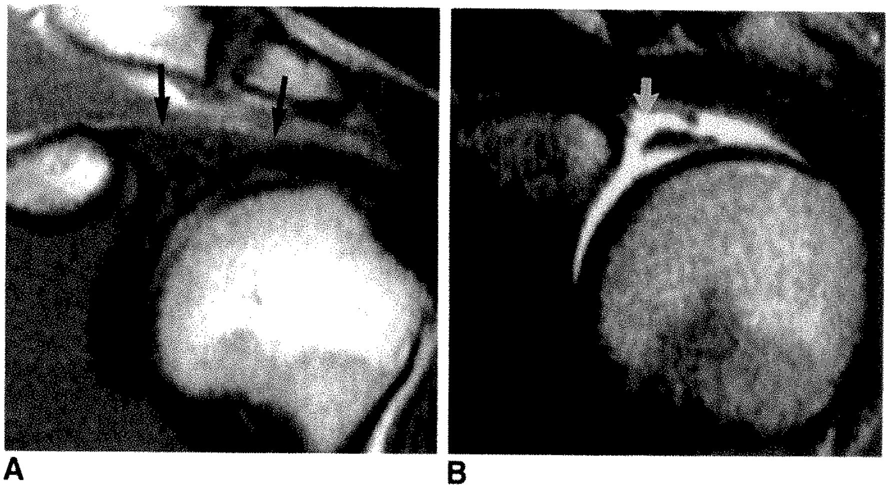

Fig. 7.—Type IV SLAP lesion.
A, MR image (2000/30) shows diffuse high signal of superior part of glenoid labrum extending into proximal biceps tendon (*arrows*).
B, MR image (2000/80) in another patient shows similar findings of high signal in proximal biceps tendon with a well-seen bucket-handle tear (*arrow*).

significance requires correlation with a larger series of prospectively examined patients.

Occasionally, it may be difficult on MR images to differentiate between injuries of types II and IV as both cause disruption of the biceps tendon or biceps tendon anchor. From a surgical standpoint, detection of the biceps injury is of greatest significance, and potential overlap in characterizing these two types is of less significance than mistyping them as type I or III.

All of the images evaluated in this study were coronal in orientation, parallel to the distal portion of the supraspinatus muscle. It is difficult at times to follow the entire course of the proximal biceps tendon in this plane. It is thought that an imaging plane parallel to the proximal long head of the biceps tendon would allow better visualization and evaluation of the proximal biceps tendon and labral-biceps anchor. This would allow easier differentiation of SLAP injury types. An approximation of this plane could be made by forming an oblique coronal plane through the line connecting the bicipital groove in the proximal humerus to the anterior aspect of the superior part of the labrum where the biceps insertion usually is found. This could be determined from axial images. Approximately 50% of the time the superior biceps tendon can be directly visualized coursing from the bicipital groove to the superior part of the labrum on an axial image. A coronal sequence with the arm in exaggerated supination also may provide the desired plane parallel to the proximal biceps tendon. An oblique sagittal short TE spin-echo sequence perpendicular to the coronal sequence can be beneficial in evaluating involvement of the biceps tendon, especially in type IV injuries.

Intraarticular injection of saline did not appear to improve visualization of SLAP lesions. This may in part be due to tension on the superior part of the labrum from the biceps tendon during MR imaging. As opposed to anterior labral tears, tension from the biceps tendon at its insertion on the superior part of the labrum might consistently separate the labral fragments, allowing easier recognition. Although the significance is unclear, abnormal fluid collections around the superior part of the labrum may be seen more consistently after intraarticular injections. The important finding of injury to the biceps anchor appears to be best detected as abnormal signal on short-TE images, rather than as abnormal locations of joint fluid.

Conclusions

Our study was preliminary in nature. Our experience was limited to a small number of retrospectively evaluated cases; therefore, no significant statistical conclusions concerning sensitivity and specificity can be made. A prospective study will be necessary to determine the value of MR imaging in evaluating SLAP lesions. Tailored spin-echo sequences along with oblique sagittal images may allow better evaluation of the proximal biceps tendon and labral-biceps anchor.

Recognition of SLAP injuries is important for patients with otherwise unexplained shoulder symptoms because surgical intervention often produces satisfactory results. MR images correlated well with surgical findings in this limited series. We hope that our discussion will promote interest in and discussion of SLAP injuries and provide a basis for improvement in recognizing and classifying these injuries to facilitate surgical planning by the arthroscopist.

REFERENCES

1. Snyder SJ, Karzel RP, Del Pizzo W, Ferkel RD, Friedman MJ. SLAP lesions of the shoulder. *Arthroscopy* **1990**;6:274–279
2. Detrisac DA, Johnson LL. *Arthroscopic shoulder anatomy: pathologic and surgical implications.* Thorofare, NJ: Slack, **1987**:71–89

LIST OF BOOK REVIEWS

772	**Diagnostic Ultrasound. Physics, Biology and Instrumentation.** *Bushong SC, Archer BR*
804	**Diagnostic Radiology. An Anglo-American Textbook of Imaging,** 2nd ed., vols. 1–3. *Grainger RG, Allison DJ, eds*
810	**Diagnostic Imaging of the Premature Infant.** *Dominques R, ed*
824	**Ultrasonography of Infants and Children.** *Teele RL, Share JC*
858	**MRI of the Brain I. Non-Neoplastic Disease.** *Bradley WE Jr, Brant-Zawadzki M, eds*

Carpal Tunnel Syndrome: Diagnosis with High-Resolution Sonography

Wolfgang Buchberger[1]
Werner Judmaier[2]
Günther Birbamer[3]
Manfred Lener[2]
Christoph Schmidauer[3]

OBJECTIVE. Carpal tunnel syndrome is characterized by typical anatomic changes that can be shown with high-resolution sonography. To determine whether these findings are reliable and can be used to establish the diagnosis, sonograms of patients with the disease were compared with sonograms obtained in patients with normal wrists. Also compared were sonograms and MR images obtained in the patients with carpal tunnel syndrome.

SUBJECTS AND METHODS. Twenty wrists in 18 consecutive patients with clinical symptoms of carpal tunnel syndrome and with abnormal nerve conduction studies were examined with real-time sonography and MR imaging. The sonograms and MR images were evaluated quantitatively by two unbiased observers with regard to the size and shape of the median nerve and the palmar bowing of the flexor retinaculum. A t test was used to compare these data with those from previous sonographic studies of 28 normal wrists. Correlation coefficients for the measurements obtained with sonography and with MR were calculated. The relative accuracies of different diagnostic criteria for the diagnosis of carpal tunnel syndrome were assessed by using receiver-operating-characteristic analytical techniques.

RESULTS. Characteristic findings on both MR and CT scans of the 20 wrists with carpal tunnel syndrome included swelling of the median nerve in the proximal part of the carpal tunnel in 16 wrists, flattening of the median nerve in the distal part of the carpal tunnel in 13 wrists, and increased palmar bowing of the flexor retinaculum in nine wrists. Comparison with the data of 28 normal wrists proved that these findings were significant ($p < .01$ to $p < .001$). Receiver-operating-characteristic analysis showed that the discrimination between wrists in normal subjects and in patients with carpal tunnel syndrome achieved with each of the three diagnostic criteria was not significantly different. Measurements of the size and flattening of the median nerve obtained from sonograms were similar to those on MR images, whereas sonography was less accurate for measuring the palmar bowing of the flexor retinaculum.

CONCLUSION. We conclude that the results of sonography are reliable, and that the diagnosis of carpal tunnel syndrome can be established on the basis of sonographic findings.

AJR 159:793–798, October 1992

Differentiation between carpal tunnel syndrome and other nerve entrapments, such as cervical root compression, thoracic outlet syndrome, or nerve entrapment in the forearm (anterior interosseous nerve syndrome), is not always possible on the basis of clinical findings alone, and the results of nerve conduction studies also may be equivocal [1, 2]. In addition, selecting treatment requires more precise information about the extent and cause of median nerve compression.

MR imaging has been used successfully for evaluating the carpal tunnel [3–5]. However, its high cost and time requirement limit its application for routine clinical use. In a preliminary study, 28 normal wrists and 28 wrists in patients with surgically proved carpal tunnel syndrome were examined with high-resolution sonography [6]. Quantitative analysis of the cross-sectional area and shape of the median nerve

Received January 29, 1992; accepted after revision April 30, 1992.

[1] Department of Radiology, University of Innsbruck, Anichstrasse 35, A-6020 Innsbruck, Austria. Address reprint requests to W. Buchberger.

[2] Institute of Magnetic Resonance Imaging and Spectroscopy, University of Innsbruck, A-6020 Innsbruck, Austria.

[3] Department of Neurology, University of Innsbruck, A-6020 Innsbruck, Austria.

0361–803X/92/1594–0793
© American Roentgen Ray Society

and of the palmar bowing of the flexor retinaculum provided information that was used to define objective criteria for the diagnosis of carpal tunnel syndrome. The present study was undertaken to determine whether these findings are reliable and can be used to establish the diagnosis and to determine the accuracy of measurements obtained on sonograms by using MR as the gold standard.

Subjects and Methods

Twenty wrists of 18 consecutive patients with carpal tunnel syndrome were studied. The 14 women and four men in this group were 23–82 years old (mean, 57 years). The right wrist was affected in nine cases and the left wrist in seven cases; two patients had bilateral carpal tunnel syndrome. All patients had pain and sensory impairment in the distribution of the median nerve, and 10 patients had paresis of the abductor pollicis brevis. Electrodiagnostic studies were done in all patients. The motor latency of the median nerve was prolonged in all wrists, and the sensory latency was abnormal in seven. In 13 wrists, no action potential could be evoked on stimulation of the afferent fibers of the median nerve.

Sonography was performed with real-time equipment (Picker LSC 9500, Hitachi Medical Corp., Tokyo, Japan) and a 7.5-MHz linear probe with a standoff. Axial images at the distal radioulnar joint, the pisiform bone, and the hook of the hamate bone and sagittal images of the flexor tendons and the median nerve were recorded with a multiformat camera. At each level, the mediolateral and anteroposterior diameters of the median nerve were measured, and the cross-sectional area was calculated (it was assumed that the area had an elliptic shape). Flattening of the median nerve was calculated as the ratio of the nerve's major to its minor axis (flattening ratio). Bowing of the flexor retinaculum was determined by drawing a straight line between its attachments to the tubercle of the trapezium bone and the hook of the hamate bone and measuring the distance from this line to the palmar apex of the ligament (palmar displacement).

MR imaging was performed with a 1.5-T superconducting system (Magnetom, Siemens, Erlangen, Germany) and a surface coil. During imaging, the patients were prone, with the arm extended overhead and the palm placed on the surface coil. A 128 × 256 matrix, two repetitions, and a 15-cm field of view were used. The imaging protocol included axial T1-weighted (450–550/15 [TR/TE]), proton density–weighted (2400/15), and T2-weighted (2400/90) spin-echo images. In addition, coronal T1-weighted images were obtained in 16 patients and sagittal T1-weighted images were obtained in four. With both the T1- and T2-weighted sequences, the section thickness was 3–4 mm, with a 0.3-mm gap. Quantitative analysis was performed as described, without knowledge of the results of the sonographic examination. All measurements were done at the viewing console; built-in computer software was used.

Measurements obtained with sonography in 20 wrists of 18 patients with carpal tunnel syndrome were compared with those in 28 previously studied normal wrists [6]. The results of quantitative analysis in both groups were compared with a t test. Carpal tunnel syndrome was diagnosed when at least one of the following findings was shown: (1) increased cross-sectional area of the median nerve at the pisiform bone and/or at the hamate bone, (2) increased flattening ratio of the median nerve at the hamate bone, or (3) increased palmar displacement of the flexor retinaculum. Quantitative measurements of the cross-sectional area and the flattening ratio of the median nerve and of the palmar displacement of the flexor retinaculum were used to calculate true-positive and false-positive percentages at different critical values on a continuous scale. Receiver-operating-characteristic (ROC) curves were obtained by using a maximum likelihood curve-fitting algorithm [7, 8]. Relative diagnostic accuracy was estimated for each single sonographic feature by using the individual area under the ROC curve [9].

Results

Sonography

In our earlier study [6] of 28 normal wrists, we found neither a significant increase in size nor flattening of the median nerve in the carpal tunnel (Fig. 1). The mean cross-sectional area of the median nerve was 7.9 mm^2 (range, 6.5–11.9 mm^2; SD, 1.1 mm^2) at the level of the distal radioulnar joint, 8.1 mm^2 (range, 6.7–12.8 mm^2; SD, 1.3 mm^2) at the pisiform bone, and 7.7 mm^2 (range, 6.3–11.6 mm^2; SD, 1.1 mm^2) at the hamate bone. The mean flattening ratio of the median nerve was 2.7 (range, 2.2–3.1; SD, 0.3) at the distal radioulnar joint, 3.0 (range, 1.7–4.0; SD, 0.5) at the pisiform bone, and 3.2 (range, 2.3–4.3; SD, 0.5) at the hamate bone. The mean palmar displacement of the flexor retinaculum was 2.1 mm (range, 0–3.1 mm; SD, 0.8 mm).

In the present study of 20 wrists in 18 patients with carpal tunnel syndrome, the mean cross-sectional area of the median nerve was 10.0 mm^2 (range, 7.2–14.8 mm^2; SD, 2.0 mm^2) at the distal radioulnar joint, 14.5 mm^2 (range, 8.8–20.5 mm^2; SD, 3.8 mm^2) at the pisiform bone, and 10.3 mm^2 (range, 5.9–15.9 mm^2; SD, 2.5 mm^2) at the hamate bone. As determined with the t test, the mean cross-sectional areas of the median nerve at the pisiform bone ($p < .001$) and at the hamate bone ($p < .01$) were significantly greater than in normal wrists. The mean flattening ratio was 2.7 (range, 2.2–3.1; SD, 0.4) at the level of the distal radioulnar joint, 2.7 (range, 2.0–3.7; SD, 0.4) at the pisiform bone, and 4.6 (range, 3.1–6.5; SD, 0.5) at the hamate bone. Compared with the normal wrists, the median nerve was significantly more flattened at the level of the hamate bone ($p < .001$). The palmar displacement of the flexor retinaculum (mean, 3.7 mm; range, 2.0–6.0 mm; SD, 1.1 mm) was significantly greater than in normal wrists ($p < .001$).

The normal range at two standard deviations of the cross-sectional area of the median nerve was calculated from the data obtained in normal wrists; it was 5.7–10.1 mm^2 at the level of the distal radioulnar joint, 5.5–10.7 mm^2 at the pisiform bone, and 5.5–9.9 mm^2 at the hamate bone. The normal range of the flattening ratio of the median nerve was 2.0–4.0 at the distal radioulnar joint and at the pisiform bone and 2.2–4.2 at the hamate bone. The normal range of the palmar displacement of the flexor retinaculum was 0.5–3.7 mm. Sixteen wrists showed swelling of the median nerve at the level of the pisiform bone (Fig. 2). In 11 cases, swelling of the median nerve also was seen at the level of the hamate bone. Thirteen wrists had increased flattening of the nerve at the level of the hamate bone, and nine wrists had increased palmar bowing of the flexor retinaculum (Fig. 3). The characteristic triad of median nerve swelling and flattening and increased bowing of the flexor retinaculum was seen in six wrists. Six other wrists showed median nerve swelling and flattening, and four others showed median nerve swelling and increased bowing of the flexor retinaculum. Swelling of the

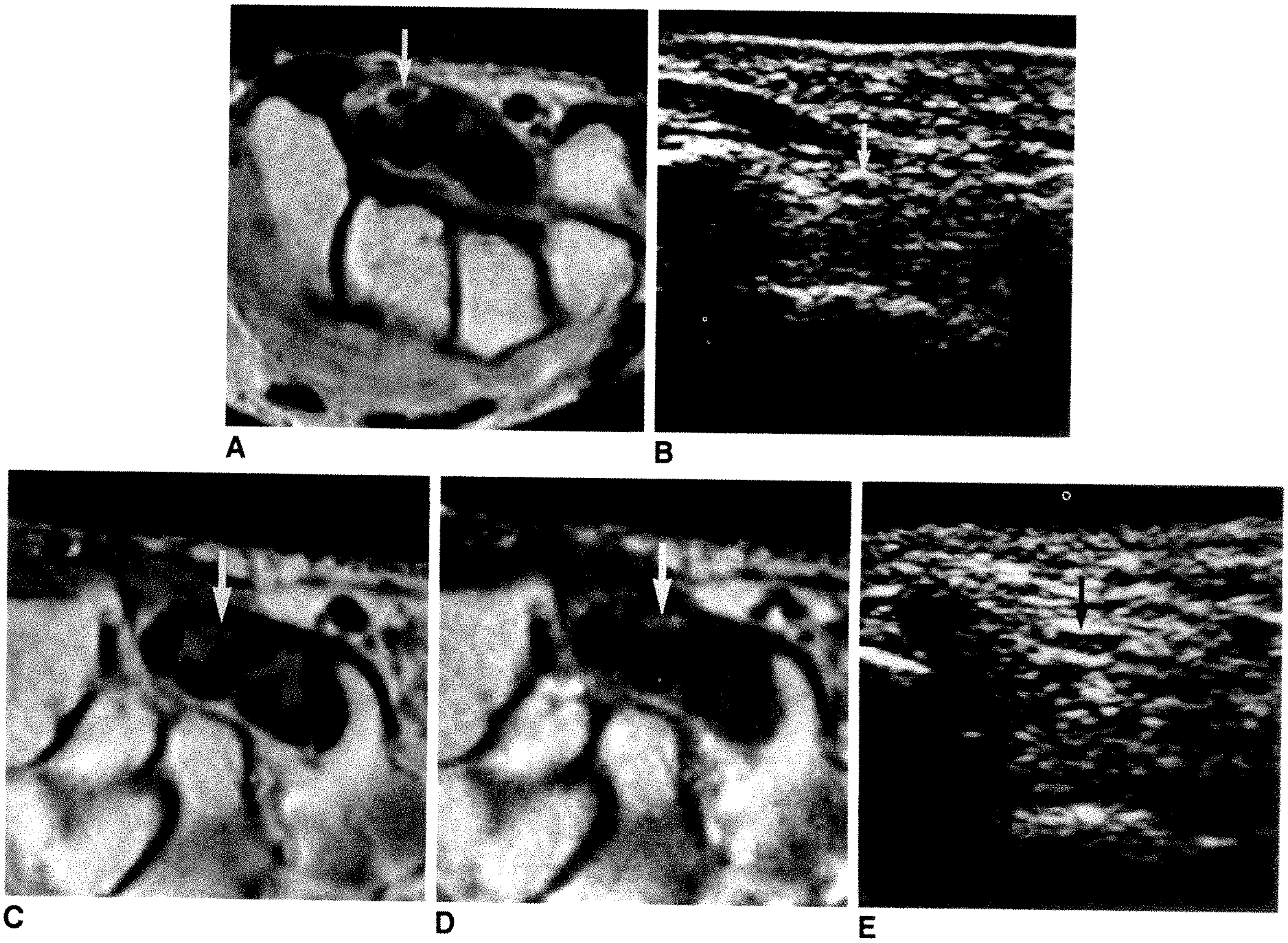

Fig. 1.—Normal carpal tunnel.

A, Axial T1-weighted (550/15) MR image of left wrist at pisiform bone shows median nerve (*arrow*) with normal size and shape.

B, Corresponding axial sonogram shows normal median nerve (*arrow*).

C, Axial T1-weighted (550/15) MR image at hamate bone shows normal median nerve (*arrow*). Only subtle flattening is seen compared with shape of nerve at pisiform bone.

D, T2-weighted (2400/90) MR image at same level shows no significant increase in signal intensity of median nerve (*arrow*).

E, Corresponding axial sonogram shows normal median nerve (*arrow*).

median nerve was the only finding in two wrists, and increased flattening of the median nerve was the only finding in one. In one wrist, the sonographic findings were normal despite clinical and electrodiagnostic evidence of carpal tunnel syndrome. The ROC curves for the cross-sectional area and the flattening ratio of the median nerve and for the palmar displacement of the flexor retinaculum are displayed in Figure 4. The individual area under the ROC curve was 0.90 for the flattening ratio, 0.86 for the swelling ratio, and 0.85 for the palmar displacement; the differences were not statistically significant.

In five wrists, the flexor tendons were separated by an unusual amount of hypoechoic tissue, probably representing proliferated synovium of the flexor tendon sheaths (Fig. 2D). In one wrist, a 10-mm anechoic structure with smooth contours was seen deep to the flexor tendons, probably representing a ganglionic cyst.

MR Imaging

In all 20 wrists, the signal intensity of the median nerve was increased on both proton density–weighted and T2-weighted images (Figs. 2C, 3B, and 5). The increased signal was more obvious on T2-weighted images and extended from the entrance of the carpal tunnel to as far distally as the metacarpal bases.

Swelling and flattening of the median nerve and increased palmar bowing of the flexor retinaculum were visualized equally as well on MR images as on sonograms (Figs. 2 and 3). Measurements of the cross-sectional area and of the flattening ratio of the median nerve on MR images were similar to those obtained with sonograms (Figs. 6A and 6B). The differences were not statistically significant ($p < .01$ to $p < .001$). Measurements of palmar displacement of the flexor retinaculum correlated less well ($p < .05$) (Fig. 6C).

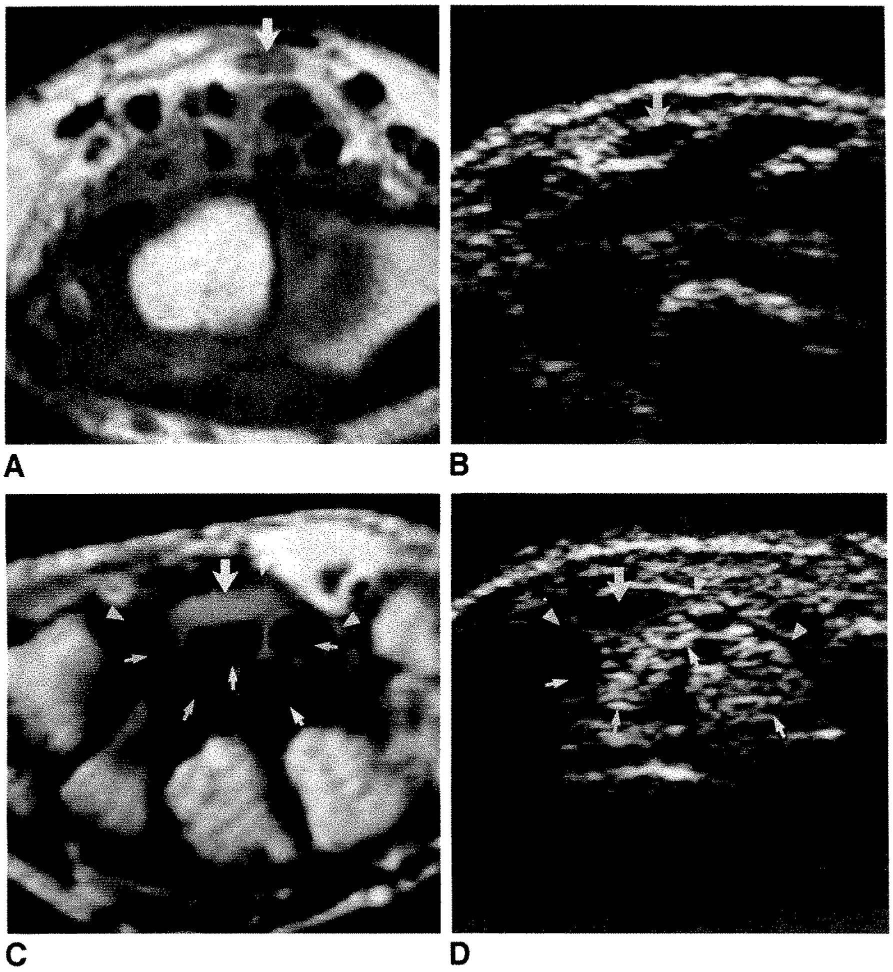

Fig. 2.—43-year-old woman with carpal tunnel syndrome.

A, Axial T1-weighted (450/15) MR image of left wrist at distal radioulnar joint shows normal size and shape of median nerve (*arrow*).

B, Corresponding axial sonogram shows normal median nerve (*arrow*).

C, Axial proton density–weighted (2400/15) MR image at pisiform bone shows enlarged median nerve (*large arrow*) with increased signal intensity. Note increased separation of flexor tendons (*small arrows*) by moderately thickened tendon sheaths and palmar bowing of flexor retinaculum (*arrowheads*).

D, Corresponding axial sonogram shows enlarged median nerve (*large arrow*) and unusual amount of hypoechoic tissue between flexor tendons (*small arrows*). Note significant bowing of flexor retinaculum (*arrowheads*).

In eight wrists, MR imaging showed obvious thickening of the flexor tendon sheaths (Fig. 2C). The signal intensity of the synovium was increased on T2-weighted images (Fig. 3B). In three wrists, the tendons had poorly defined margins, suggesting edema. Ganglionic cysts 4–10 mm in diameter were seen in another three wrists (Fig. 5).

Discussion

Because of its inherently high contrast, which allows accurate depiction of the soft-tissue structures of the hand, MR imaging has been the only imaging technique of diagnostic value in carpal tunnel syndrome. Middleton et al. [3] and Mesgarzadeh et al. [4, 5] described the normal anatomy of the carpal tunnel, as shown with MR imaging, and reported on preliminary observations in patients with carpal tunnel syndrome. Real-time high-frequency sonography has been used to diagnose soft-tissue lesions of the hand [10, 11]. The sonographic appearance of various peripheral nerves of the extremities, including the median nerve, has been described by Fornage [12]. Calleja Cancho et al. [13] described the normal anatomy of the carpal tunnel, seen on sonograms, and discussed the ability of sonography to show the median nerve on sagittal and axial scans. We found earlier that sonography can be used to detect anatomic changes in patients with carpal tunnel syndrome [6]. Consistent with the results of Mesgarzadeh et al. [5], our findings showed that, regardless of the cause, carpal tunnel syndrome included swelling of the median nerve at the entrance and in the proximal part of the carpal tunnel, flattening of the median nerve in the distal part of the carpal tunnel, and increased bowing of the flexor retinaculum.

In the present study, at least one of these diagnostic changes was shown in all wrists except one. Diffuse or localized swelling and increased flattening of the median nerve were the most common findings. Both observations are well described in the surgical literature. Rietz and Önne [2] found swelling of the median nerve in 66% of cases. Phalen [14] observed bulbous swelling of the median nerve (pseudoneuroma) in 45 of 212 wrists operated on and flattening of the median nerve beneath the flexor retinaculum in 151 of 212. Increased bowing of the flexor retinaculum was seen less frequently, and usually was associated with swelling of the median nerve.

Enlargement and flattening of the median nerve may be evident at subjective evaluation. However, in most cases, quantitative studies are necessary. The accuracy of sonographic measurements is limited by the axial and lateral

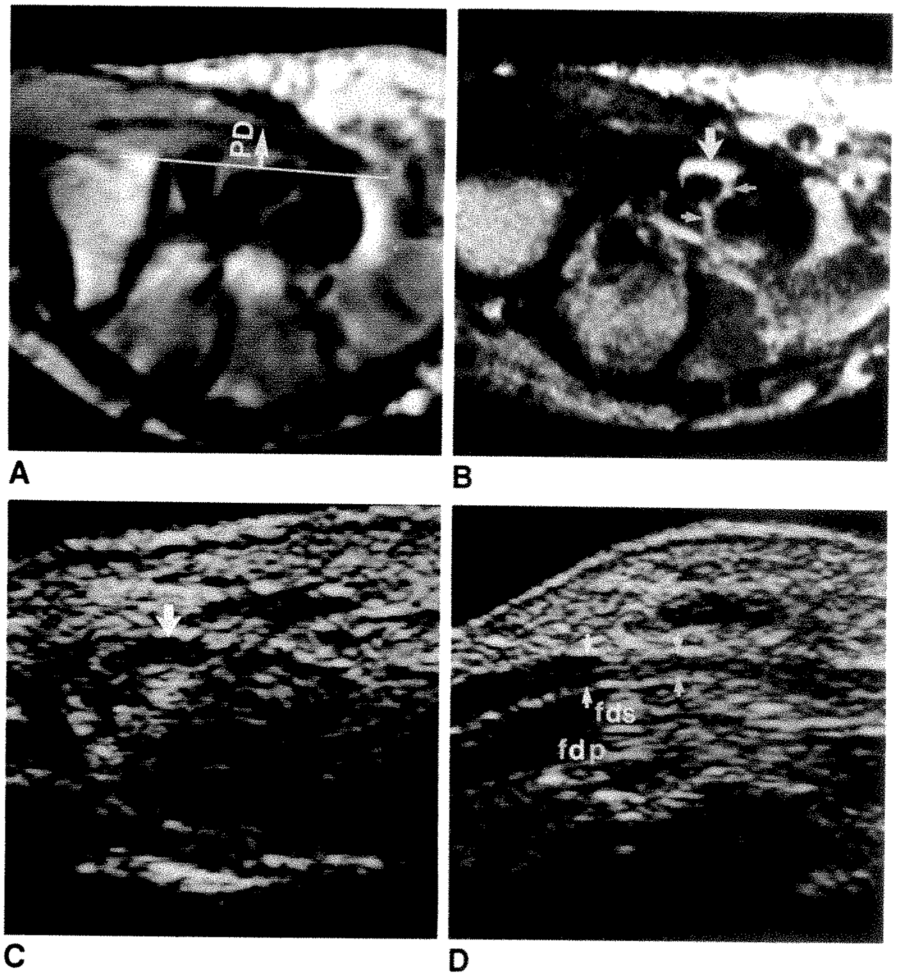

Fig. 3.—51-year-old woman with carpal tunnel syndrome.

A, Axial T1-weighted (450/15) MR image of left wrist at hook of hamate bone shows increased palmar bowing of flexor retinaculum. PD = palmar displacement.

B, Corresponding axial T2-weighted (2400/90) MR image shows increased signal of flattened median nerve (*large arrow*). Thickening and increased signal intensity of flexor tendon sheaths (*small arrows*) suggest synovitis.

C, Corresponding axial sonogram shows flattened median nerve (*arrow*).

D, Sagittal sonogram shows flattening of median nerve (*arrows*) in distal part of carpal tunnel. Tendons of flexor digitorum superficialis (fds) and profundus (fdp) are deep to median nerve.

resolution of the transducer, which, according to its manufacturer, is 0.2 mm for axial resolution and 0.5 mm for lateral resolution in the focal zone. In tissue, the effective spatial resolution depends on echo amplitude and tissue attenuation. In the carpal tunnel, the small differences in acoustic impedance between the median nerve and its surroundings and the relatively high tissue attenuation result in a low signal-to-noise ratio. Despite these restrictions, the results of quantitative studies with sonography corresponded well with the results

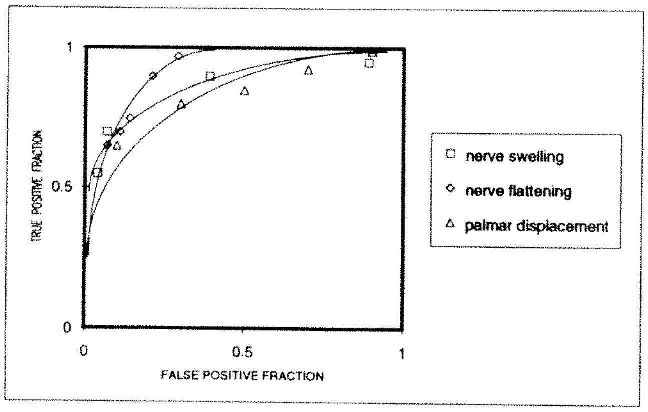

Fig. 4.—Graph shows receiver-operating-characteristic curves for different diagnostic criteria (swelling of median nerve, flattening of median nerve, and increased palmar displacement of flexor retinaculum).

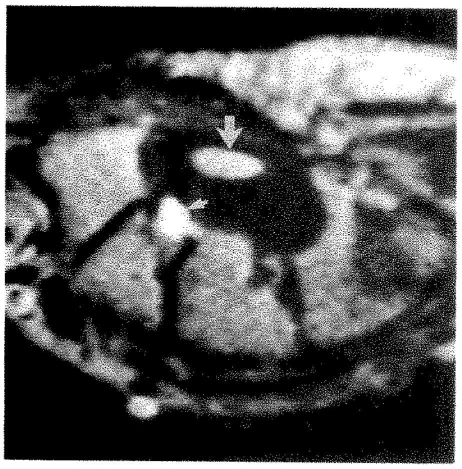

Fig. 5.—23-year-old woman with carpal tunnel syndrome. Axial T2-weighted (2400/90) MR image of right wrist at hook of hamate bone shows enlarged median nerve (*large arrow*) with increased signal intensity. Note high-signal-intensity ganglionic cyst (*small arrow*).

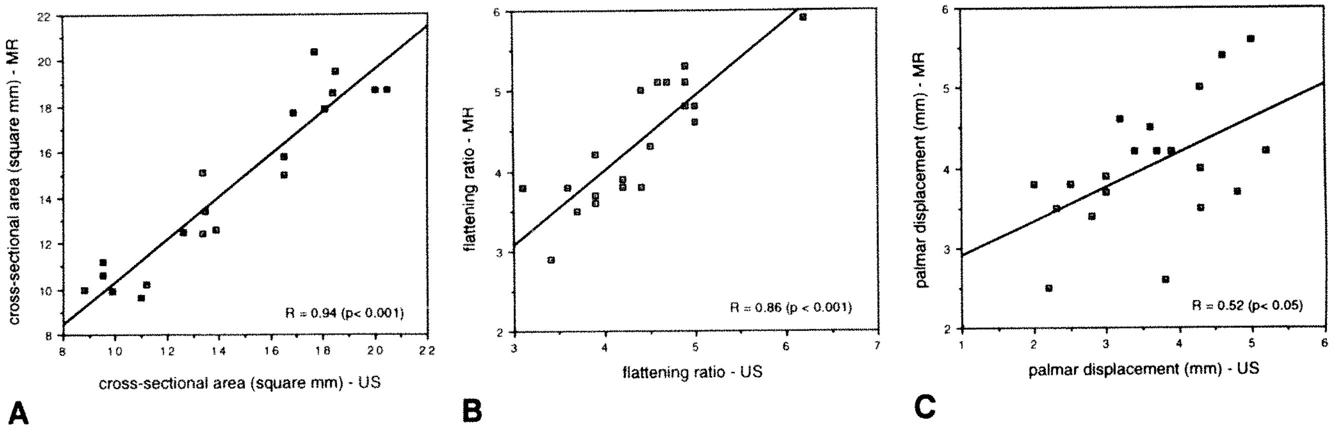

Fig. 6.—Graphs of measurements obtained from sonograms (US) and MR images in 20 wrists with carpal tunnel syndrome.
***A*, Cross-sectional area of median nerve at level of pisiform bone.**
***B*, Flattening ratio of median nerve at level of hamate bone.**
***C*, Palmar displacement of flexor retinaculum.**

of similar studies with MR imaging. Measurements of the cross-sectional area and of the flattening ratio of the median nerve were not significantly different with the two imaging techniques. Measurements of the palmar bowing of the flexor retinaculum were less accurate with sonography than with MR imaging. This was probably due to poor visualization of the carpal bones on sonograms, which made identification of the measuring points difficult.

The diagnostic performance of a screening test is best evaluated by means of an ROC analysis [7, 8]. Although complete ROC analysis could not be performed in our study, the individual ROC curves for the cross-sectional area and the flattening ratio of the median nerve and for the palmar displacement of the flexor retinaculum, obtained with sonography, suggest that the discrimination ability of these measurements is sufficiently high to establish the diagnosis.

A comparison of the efficacy of sonography and MR imaging in the diagnosis of carpal tunnel syndrome was not the purpose of our study. However, our results suggest that, because of its excellent soft-tissue contrast, MR can show mild degrees of compression of the median nerve that may be missed on sonograms. In addition, the increased signal intensity of the median nerve on proton density- and T2-weighted images, probably due to edema, is a frequent finding that facilitates the diagnosis [3, 5]. In our patients, MR imaging also was superior to sonography in the detection of etiologic findings, such as tendon-sheath thickening and ganglionic cysts. In summary, high-resolution real-time sonography has proved to be an effective method for diagnosing carpal tunnel syndrome. Its low cost, minimal time requirement, and general availability favor its use as the initial study in evaluating the carpal tunnel. The efficacy of sonography compared with MR imaging and the complementary roles of the two techniques will require further evaluation.

REFERENCES

1. Phalen GS. The carpal tunnel syndrome: seventeen years' experience in diagnosis and treatment of six hundred fifty-four hands. *J Bone Joint Surg [Am]* **1966**;48-A:211-228
2. Rietz KA, Önne L. Analysis of sixty-five operated cases of carpal tunnel syndrome. *Eur J Surg* **1967**;133:443-447
3. Middleton WD, Kneeland JB, Kellman GM, et al. MR imaging of the carpal tunnel: normal anatomy and preliminary findings in the carpal tunnel syndrome. *AJR* **1987**;148:307-316
4. Mesgarzadeh M, Schneck CD, Bonakdarpour A. Carpal tunnel: MR imaging. Part I. Normal anatomy. *Radiology* **1989**;171:743-748
5. Mesgarzadeh M, Schneck CD, Bonakdarpour A, Amitabha M, Conway D. Carpal tunnel: MR imaging. Part II. Carpal tunnel syndrome. *Radiology* **1989**;171:749-754
6. Buchberger W, Schön G. Strasser K, Jungwirth W. High-resolution ultrasonography of the carpal tunnel. *J Ultrasound Med* **1991**;10:531-537
7. Metz CE. Basic principles of ROC analysis. *Semin Nucl Med* **1978**;8:283-298
8. Lusted LB. Decision-making studies in patient management. *N Engl J Med* **1971**;284:416-424
9. Hanley JA, McNeil BJ. The meaning and use of the area under a receiver operating characteristic (ROC) curve. *Radiology* **1982**;143:29-36
10. Fornage BD, Schernberg FL, Rifkin MD. Ultrasound examination of the hand. *Radiology* **1985**;155:785-788
11. Fornage BD, Rifkin MD. Ultrasound examination of the hand and foot. *Radiol Clin North Am* **1988**;26:109-129
12. Fornage BD. Peripheral nerves of the extremities: imaging with US. *Radiology* **1988**;167:179-182
13. Calleja Cancho E, Schawe-Calleja Cancho M, Milbradt H, Galanski M. Sonoanatomy and examination technique of the normal carpal tunnel (English abstr.). *Rofo Fortschr Geb Rontgenstr Neuen Bildgeb Verfahr* **1989**;151:414-418
14. Phalen GS. The carpal-tunnel syndrome: clinical evaluation of 598 hands. *Clin Orthop* **1972**;83:29-40

Pictorial Essay

Spondylolysis, Spondylolisthesis, and Associated Nerve Root Entrapment in the Lumbosacral Spine: MR Evaluation

J. R. Jinkins,[1] J. C. Matthes, R. N. Sener, S. Venkatappan, and R. Rauch

Spondylolysis is defined as a bone defect in the pars interarticularis. Its cause is uncertain but is believed in most cases to be related to repeated stress, trauma, or both [1, 2]. Findings of spondylolysis on conventional radiographs and on CT scans have been well characterized [1, 3]. Although these imaging techniques remain effective for the diagnosis of this defect, MR imaging is increasingly used as the primary or sole imaging method in patients with lower back pain and radiculopathy. Therefore, because MR images of the lumbar spine may be interpreted in the absence of correlative CT scans or conventional radiographs, the MR features of spondylolysis and its associated findings must be recognized [4]. This essay illustrates the MR findings of lumbosacral spondylolysis and associated entrapment and direct impingement of the spinal nerve root.

Prevalence

The estimated prevalence of defects in the pars interarticularis is about 6% in adults [1, 2]. The rate of occurrence during childhood is low, thus accounting for the 5% prevalence in the population as a whole [1, 2]. In a large survey of skeletons, defects were found more often in males than in females (ratio, 3:1). At the L5–S1 level, the defect almost always occurs bilaterally. In one reported CT series [3], for example, 96% of cases had bilateral defects at L5–S1. In another CT series [1], however, unilateral defects were seen in 16% of cases. The hypothetical reason for the increased prevalence of unilateral spondylolysis was unilateral healing or union of a defect that was initially bilateral.

Pathoanatomy

Anatomically, a vertebral spondylolysis is a cleft in the pars interarticularis. As noted, this occurs bilaterally in most cases, thus dividing the vertebra into two segments [1, 3]. The anterosuperior (ventrocranial) segment consists of the vertebral body with the pedicles, the transverse processes, and the superior interarticular facets. The posteroinferior (dorsocaudal) segment consists of the inferior interarticular facet, the laminae, and the spinous process. According to most investigators, the sagittal plane is the best one for evaluating the entire pars interarticularis, because the obliquity of the pars interarticularis in this plane is minimal [4] (Fig. 1). An interruption in the continuity or intensity of the marrow signal of the pars interarticularis in cases of spondylolysis can also be best detected on sagittal MR images (Fig. 2). However, general low MR signal within the pars interarticularis relative to adjacent marrow on T1-weighted MR images may be due to several conditions unrelated to spondylolysis, including acquired benign or malignant sclerosis within the neck of the pars interarticularis itself and partial volume averaging of a degenerative spur of the facet joint slightly lateral to the pars interarticularis [4].

Segmental anteroposterior elongation of the spinal canal at the level of the defect in the pars interarticularis is seen in virtually all patients who have spondylolysis. Elongation of the canal can be caused both by anterior dislocation of the vertebral body from the neural arch associated with spondylolisthesis and by posterior displacement of the neural arch

---

Received February 18, 1992; accepted after revision April 20, 1992.

[1] All authors: Neuroradiology Section, The University of Texas Health Science Center at San Antonio, 7703 F. Curl Dr., San Antonio, TX 78284-7800. Address reprint requests to J. R. Jinkins.

AJR 159:799-803, October 1992 0361-803X/92/1594-0799 © American Roentgen Ray Society

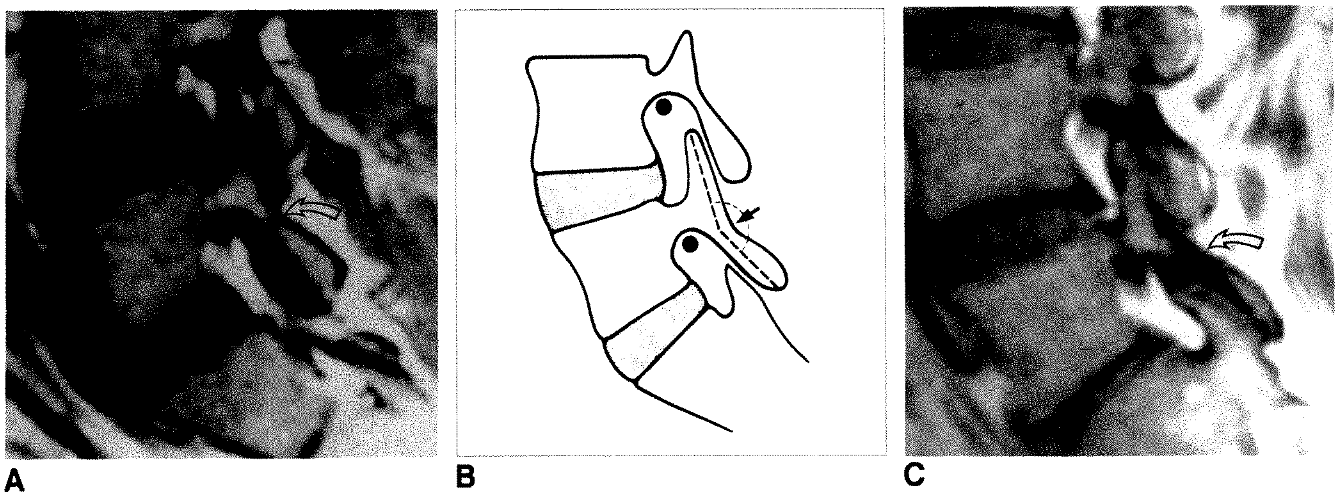

Fig. 1.—Variation in MR signal in pars interarticularis in two control subjects without spondylolysis or radicular symptoms.

A, Sagittal T1-weighted (600/20) MR image shows isointensity of marrow in pars interarticularis (*arrow*) at L5 level relative to surrounding intraosseous marrow.

B, Cutaway schematic drawing shows normal anatomy of pars interarticularis and related tissues in sagittal plane at L4–S1. Note typical interfacet angle (*dashed arc* describes angle between *dashed straight lines* running parallel to but offset from facet joints) that may be present at this level, with fulcrum falling at or near pars interarticularis (*arrow*). *Black circles* = nerve roots exiting neural foramina, *stippled areas* = intervertebral disks.

C, Sagittal T1-weighted (600/20) MR image to left of midline shows hypointensity in pars interarticularis (*arrow*) relative to surrounding marrow.

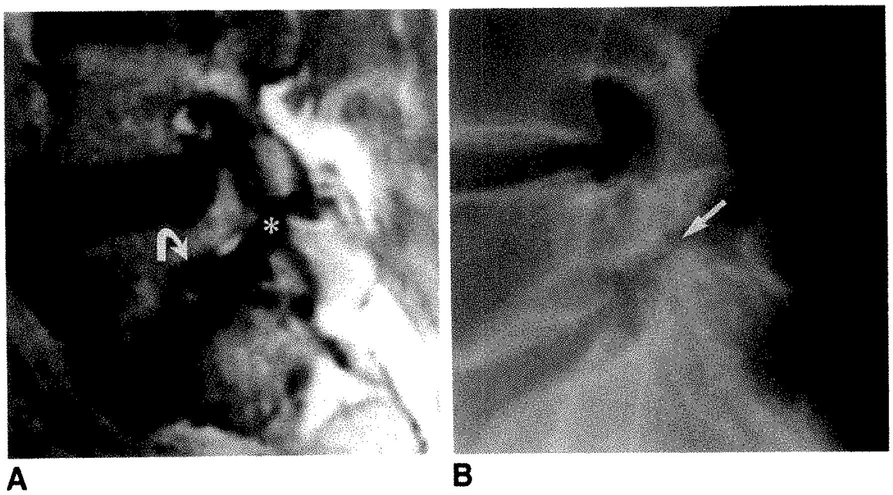

Fig. 2.—MR signal changes in pars interarticularis in patient with spondylolysis and radiating pain with paresthesias in left lower extremity.

***A*, Sagittal T1-weighted (600/20) MR image to left of midline at L5 shows an area of decreased signal intensity (*asterisk*) in pars interarticularis, representing spondylolysis. High-signal fat normally present in neural foramen at L5 (*arrow*) is obliterated.**

***B*, Conventional lateral lumbosacral radiograph confirms spondylolysis (*arrow*).**

relative to the arches of the vertebrae above and subjacent. This is visualized in the midline on routine sagittal MR images and can be used as one of the more sensitive indirect indicators of spondylolysis (Fig. 3).

Actual distraction of the dislocated bony elements at the pars interarticularis, or a step-off pattern, can be a specific indicator of spondylolysis (Fig. 4). This finding is well shown on sagittal MR images and allows unequivocal demonstration of the defect in the pars interarticularis. As often occurs, the degree of subluxation may be bilaterally unequal at the pars interarticularis, resulting in rotational dislocation of the neural arch or segmental rotatory scoliosis or both (Fig. 5).

In the absence of gross subluxation at the pars interarticularis, detection of a simple linear interruption in marrow signal still may signal the presence of spondylolysis (Fig. 6). This most likely represents a nondislocated or stress fracture of the pars interarticularis. If the defect is bilateral, little spondylolisthesis of the involved vertebral body or retroluxation of the neural arch may occur. In this situation, the primary abnormality can easily be overlooked on imaging studies.

Foraminal Encroachment and Nerve Root Entrapment

A deformity of the involved neural foramina in spondylolisthesis, described as a "flattening" on axial CT scans with multiplanar reconstruction, has been reported [1]. The orientation of the foramen becomes more horizontal rather than vertical-oblique, and the foramen assumes a bilobed appearance (Fig. 7). Direct sagittal MR imaging provides excellent visualization of the neural foramina and allows direct assessment of foraminal encroachment originating from any radial

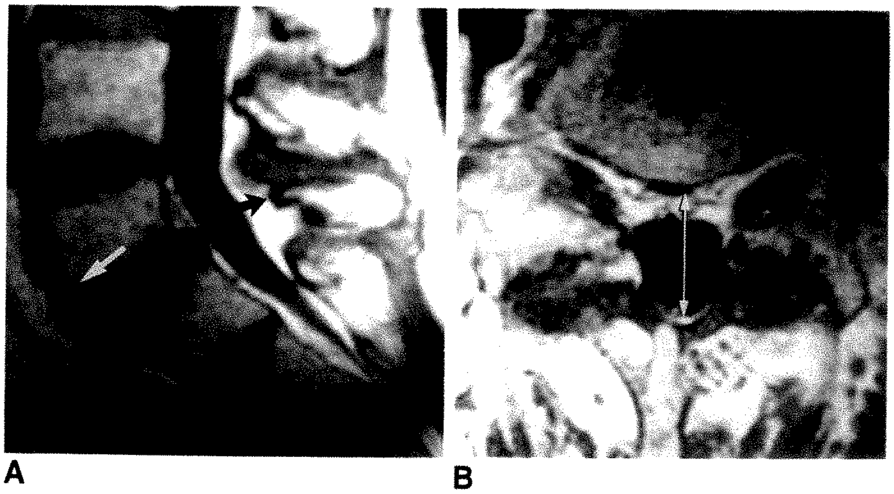

Fig. 3.—Segmental elongation of diameter of spinal canal in subjects with spondylolysis at level of defect in pars interarticularis.

A, Sagittal T1-weighted (600/20) MR image in midline shows retroluxation (*black arrow*) of neural arch of L5, producing malalignment of spinous process posteriorly relative to adjacent levels, and minor spondylolisthesis (*white arrow*) at L5–S1 (grade I:III). Together these phenomena produce an elongation of anteroposterior diameter of spinal canal at L5.

B, Axial T1-weighted (600/20) MR image at L5–S1 level shows elongation (*double-headed arrow*) of anteroposterior diameter of spinal canal.

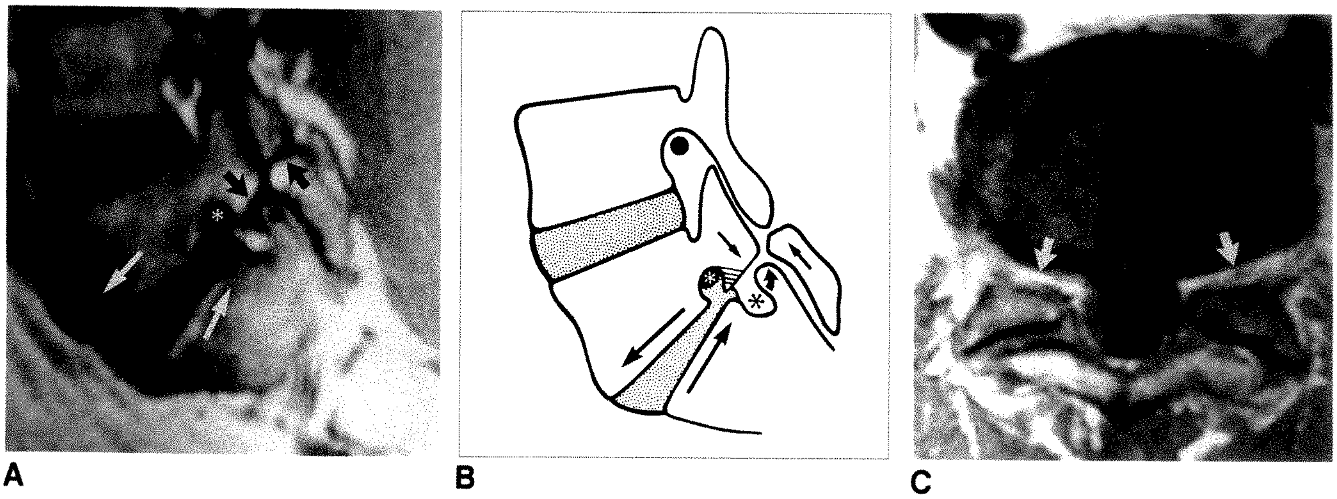

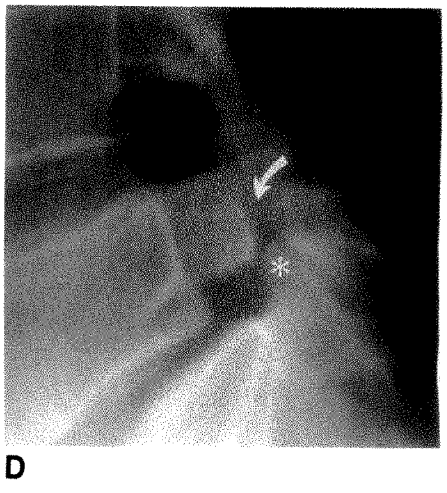

Fig. 4.—Spondylolysis and spondylolisthesis at L5–S1 with subluxation of bony elements at site of pars interarticularis defect and associated entrapment of spinal nerve root in a patient with bilateral radiating pain with paresthesias in lower extremities.

A, Sagittal T1-weighted (600/20) MR image to left of midline shows step-off or subluxation (*black arrows*) of involved bony elements at level of spondylolysis. Interposition (*black asterisk*) of superior articular facet of S1 has occurred. Note relatively angulated spondylolisthetic translation of L5 on S1 (*white arrows*) and encroachment on superior recess of neural foramen with associated entrapment (*white asterisk*) of nerve root.

B, Cutaway schematic drawing shows anatomy of spondylolysis and spondylolisthesis at L5–S1. Cranial, angulated spondylolisthetic translation of S1 relative to L5 (*long straight arrows*) results in encroachment on superior recess of neural foramen and entrapment of L5 nerve root (*white asterisk*). In many cases, the inferior recess of neural foramen (*black asterisk*) may remain patent. In this case of spondylolysis, note associated dislocation or step-off of distracted bony elements (*short straight arrows*) and interposition of superior articular facet of S1 (*curved arrow*). Some foraminal stenosis may be contributed to in certain instances by adjacent hypertrophic pseudoarthrosis induced by spondylolysis (area of *short parallel lines*). *Black circle* = nerve root exiting neural foramina, *stippled area* = intervertebral disks.

C, Axial T1-weighted (600/20) MR image angled to L5–S1 disk shows high intraforaminal signal bilaterally (*arrows*), which falsely indicates foraminal patency. However, as visualized here, hyperintensity represents only residual fat in inferior recess of neural foramina.

D, Corresponding conventional lateral lumbosacral radiograph confirms defect (*arrow*) in pars interarticularis. Interposed superior facet (*asterisk*) of S1 also is shown.

direction. Axial MR images, on the other hand, are often indeterminate or even misleading (Figs. 4 and 8). Obliteration or nearly complete loss of the high fat signal that normally borders on and often surrounds the spinal nerve root on T1-weighted images suggests actual entrapment of the nerve root within the neural foramen.

Foraminal encroachment with stenosis is detected in many patients who have spondylolysis at L5–S1. This stenosis has a characteristic configuration, namely a specific encroachment on the superior recess of the neural foramen. Such encroachment may be significant, as this is the usual anatomic location of the exiting spinal nerve root. Therefore, this en-

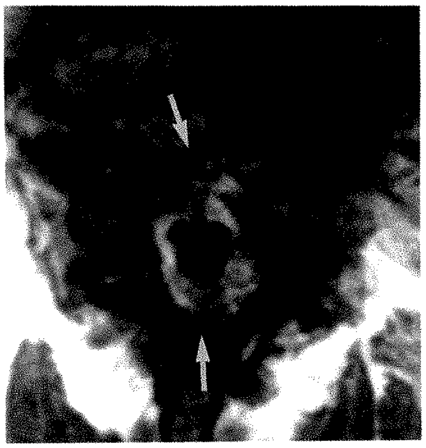

Fig. 5.—Bilateral spondylolysis with unequal subluxation of bony elements resulting in rotational dislocation of neural arch or segmental rotatory scoliosis. Axial T1-weighted (600/20) MR image at level of L5 shows rotational alteration in axis (*arrows*) between vertebral body and neural arch.

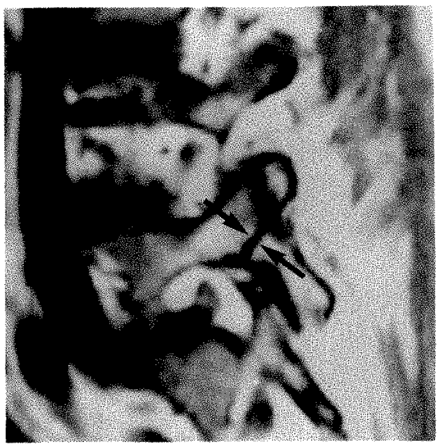

Fig. 6.—MR signal changes in pars interarticularis in patient with nondislocated or stress fracture of pars. Sagittal T1-weighted (600/20) MR image to right of midline at L5 shows simple linear area of interrupted marrow signal, without subluxation of elements of pars interarticularis (*arrows*).

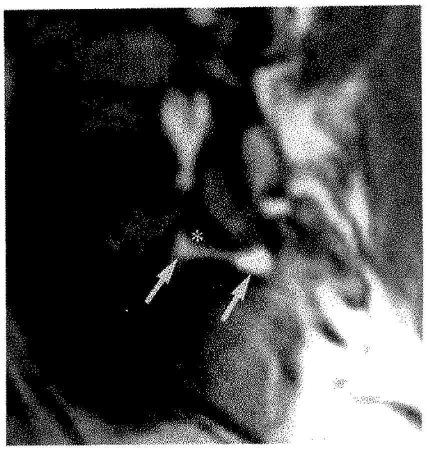

Fig. 7.—Bilobed appearance of neural foramen in L5–S1 spondylolysis and accompanying spondylolisthesis in the absence of entrapment or impingement of nerve root in patient without ipsilateral radicular symptoms. Sagittal T1-weighted (600/20) MR image to left of midline shows bilobed configuration (*arrows*) of neural foramen. Nerve root is located in posterosuperior aspect of neural foramen (*asterisk*), and no evidence of entrapment or impingement is seen.

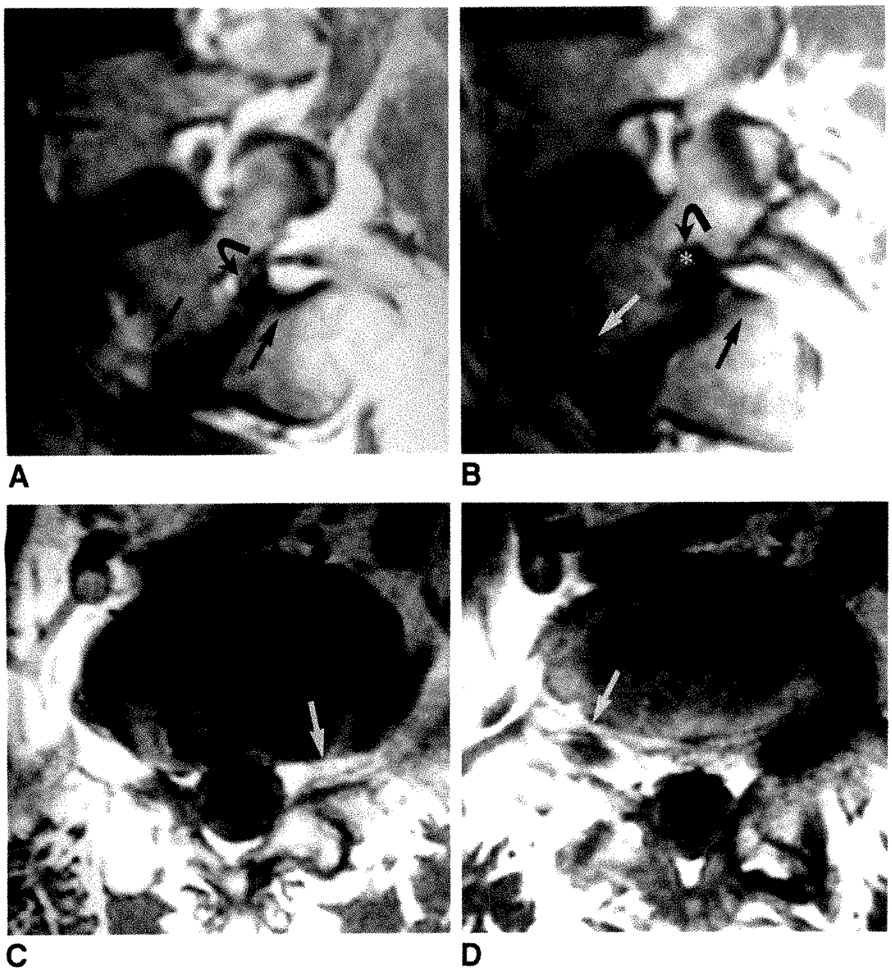

Fig. 8.—Encroachment on superior recess of neural foramen in L5–S1 spondylolysis and accompanying spondylolisthesis, with and without entrapment of spinal nerve root in patients with radiating pain with paresthesias in left lower extremity.

A, Sagittal T1-weighted (600/20) MR image to right of midline shows mild encroachment on superior recess of neural foramen on patient's right side. Note that root is still surrounded by high-intensity fat signal (*curved arrow*). Also note bilobed configuration of L5 neural foramen and angulated spondylolisthetic translation of L5 vertebral body relative to S1 (*straight arrows*).

B, Sagittal T1-weighted (600/20) MR image at left of midline shows severe left-sided encroachment (*curved arrow*) on superior recess of neural foramen by posterosuperior lip of S1 and contiguous L5–S1 intervertebral disk. Note complete loss of perineural high-signal-intensity fat (*asterisk*), indicating entrapment of nerve root. Also note angulated spondylolisthetic translation (*straight arrows*) of L5 vertebral body relative to S1 vertebral body.

C and *D*, Adjacent, contiguous oblique axial T1-weighted (600/20) MR images at L5–S1 show that the neural foramina falsely appear to be widely patent, as indicated by presence of high-signal-intensity foraminal fat (*arrows*). Foramina do not appear together on same section because of minor scoliosis.

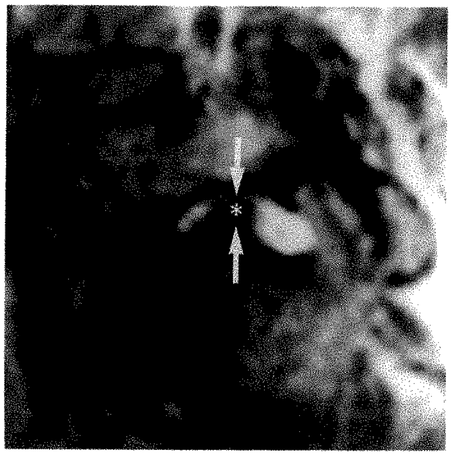

Fig. 9.—Left-sided encroachment on superior recess of neural foramen in L5–S1 spondylolysis and accompanying spondylolisthesis without frank entrapment of but with impingement of nerve root in patient with ipsilateral radiculopathy. Sagittal T1-weighted (600/20) MR image to left of midline shows that the L5 nerve root apparently is caught between encroaching vertebral elements (disk and bone) involved in spondylolisthetic translation. The L5 nerve root (*asterisk*) is impinged in a pincerlike configuration (*arrows*).

croachment can cause radicular neurologic symptoms. Sagittal MR images may show that this encroachment is not necessarily bilaterally symmetric, a finding that may not be obvious on axial images (Fig. 8).

Specific encroachment on the superior recess of the neural foramen in spondylolisthesis at L5–S1 may have a simple anatomic explanation. With forward slippage of L5, the consonant posterior displacement of S1 is angled posteriorly and cranially. Consequently, the leading posterosuperior corner of the S1 vertebral body and the associated bulging disk protrude into the superior recess of the L5–S1 neural foramen. This process takes place without a true herniation of the intervertebral disk and with only relatively minor degrees of spondylolisthesis.

Direct Nerve Root Impingement

Some patients have radicular signs and symptoms without frank circumferential entrapment of the nerve root within the superior recess of the neural foramen. Nevertheless, in these cases, sagittal MR images may show evidence of a form of foraminal encroachment in which the root is impinged between the respective bony elements of the spondylolisthesis in a pincerlike configuration (Figs. 7 and 9). Therefore, depending on the spatial location of the nerve root within its respective neural foramen relative to the components of the spondylolisthesis, early direct impingement without gross entrapment may be a clinically significant diagnostic feature on MR images.

REFERENCES

1. Rothman SLG, Glenn WV. CT multiplanar reconstruction in 253 cases of lumbar spondylolysis. *AJNR* **1984**;5:81–90
2. Grenier N, Kressel HY, Schiebler ML, Grossman RI. Isthmic spondylolysis of the lumbar spine: MR imaging at 1.5 T. *Radiology* **1989**;170:489–493
3. Teplick JG, Laffey PA, Berman A, Haskin ME. Diagnosis and evaluation of spondylolisthesis and/or spondylolysis on axial CT. *AJNR* **1986**;7:479–491
4. Johnson DW, Farnum GN, Latchaw RE, Erba SM. MR imaging of the pars interarticularis. *AJNR* **1988**;9:1215–1220, *AJR* **1989**;152:327–332

Book Review

Diagnostic Radiology. An Anglo-American Textbook of Imaging, 2nd ed., vols. 1–3. Edited by Ronald G. Grainger and David J. Allison. New York: Churchill Livingstone, 2443 pp., 1992. $450

This comprehensive three-volume textbook has two principal editors, 121 contributors (44 new contributors), and 109 chapters (18 new). Approximately 50% of the authors are from the United Kingdom and 50% from the United States, so the subtitle of the book, An Anglo-American Textbook, is an apt description.

The editors have produced an all-embracing text on radiology that is comprehensive, well-balanced, and as up-to-date as possible. The authors cover a wide range of normal and pathologic findings in an organ-related approach and incorporate standard and new radiologic techniques. As in the first edition, each section ends with a list of references and suggestions for further reading. In addition to the 18 new chapters, each of the previous chapters has been updated, and considerable emphasis has been placed on bringing the relationship of MR imaging to conventional radiologic techniques into a current perspective.

According to the authors, this text has three goals: (1) to help radiologists through all stages of their careers, (2) to aid residents who are preparing for board examinations, and (3) to serve as a reference in radiology reading rooms. To accomplish these goals, the editors have organized the three volumes into 12 sections. The first section covers techniques and imaging procedures. Subsequent sections are organized on an organ basis, except for specific chapters on angiography, interventional radiology, oncology, and AIDS. The book has little overlap from section to section, and the integration of radiologic techniques in general is excellent. Exceptions are the separate sections on the use of radionuclides and CT in the skeletal, cardiac, genitourinary, and CNS systems.

The editors and their contributors should be congratulated. They have produced an excellent book that certainly will take its place among other comprehensive radiology texts. It should be on the shelves of all major departmental teaching libraries. Volume 2 is a superior text, and the editors have incorporated a vast amount of new material without having the text grow to four volumes.

Despite the successes, some parts of the text do not work as well as they should. The depth in which the various sections cover their material varies considerably. Strong sections on respiratory disease and on the gastrointestinal, genitourinary, cardiac, and musculoskeletal systems are balanced by somewhat weak sections on the CNS, head and neck radiology, and the female reproductive system and by the technical chapters. The organization of the book could also be improved. I would prefer to have all the descriptions of techniques, including angiography, nuclear medicine, and sonography, together rather than have some presented in chapter 1 and some in chapter 11. The section on the cardiac system appears overly long, and the reticuloendothelial, mammography, liver, pancreas, and endocrine sections are too short to cover all important material. The placement of the color plates for all three volumes together in the front of volume 1 makes appropriate use of the plates extremely difficult. Information on the musculoskeletal system is split between volume 2 and volume 3, which causes an unnecessary hassle for the reader. In general, I would prefer fewer tables and lists and more state-of-the-art CT scans, sonograms, and MR images.

The authors certainly have succeeded in two of their three goals. I somehow doubt that a radiology resident will be able to spend $450 for this text, and residents probably will rely on cheaper, more appropriate review materials when preparing for board examinations. I do recommend that this book be purchased for major libraries.

Albert A. Moss
University of Washington
Seattle, WA 98195

Pictorial Essay

Lymphoma of Bone, Muscle, and Skin: CT Findings

Patrick C. Malloy,[1] Elliot K. Fishman,[1] and Donna Magid[1,2]

Lymphoma can involve any part of the musculoskeletal system. Primary musculoskeletal lymphoma is rare but can occur in bone (reticulum cell sarcoma) or in the skin and subcutaneous tissues (mycosis fungoides). Secondary involvement in the musculoskeletal system is more common and can have a variety of radiologic findings. The definitive diagnosis of musculoskeletal lymphoma, however, is difficult to make by using imaging criteria alone. Any part of the musculoskeletal system can be involved and, therefore, a wide variety of primary and secondary neoplasms or inflammatory processes may have similar radiologic findings. The main differential diagnostic considerations, depending on the age of the patient and the clinical presentation, include osteosarcoma, Ewing's tumor, metastatic disease (from breast, lung, thyroid, or renal primary lesions), as well as chronic osteomyelitis or myositis. Primary and secondary bone lymphoma can be indistinguishable radiologically and histologically, but modern imaging

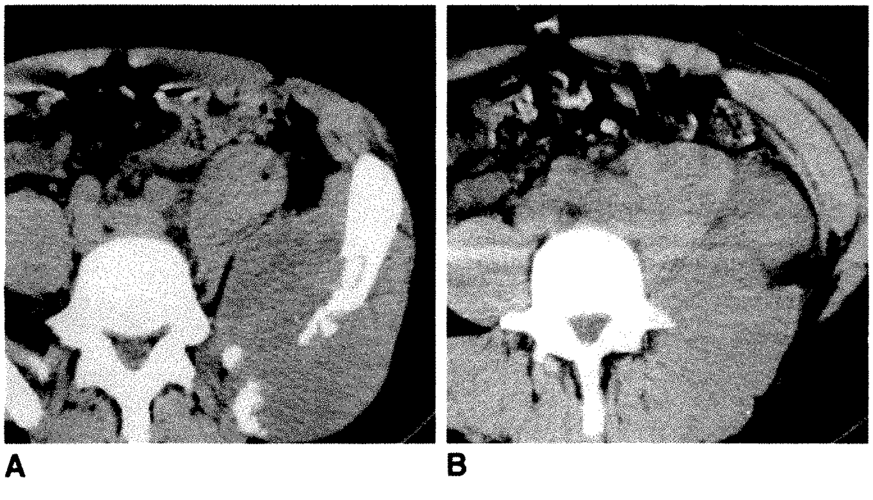

Fig. 1.—42-year-old man with biopsy-proved large-cell lymphoma.
***A*, CT scan shows a destructive, lytic, primary lesion in left ilium, with a large soft-tissue mass and no evidence of nodal disease.**
***B*, CT scan shows tumor extending superiorly to involve left iliopsoas and paraspinal musculature.**

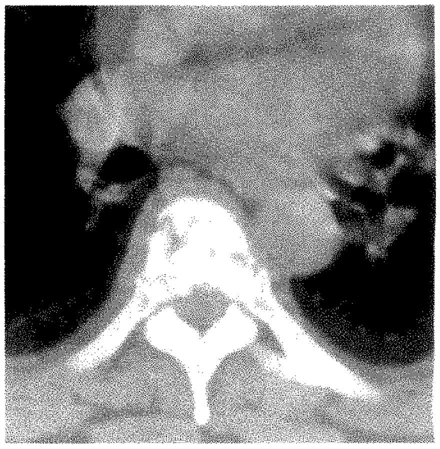

Fig. 2.—65-year-old man with diffuse histiocytic lymphoma with primary tumor above right orbit. CT scan shows infiltrative lesion of T7 vertebral body and associated paraspinal mass. Lesion is mixed lytic and blastic.

Received January 24, 1992; accepted after revision April 7, 1992.

[1] Russell H. Morgan Department of Radiology and Radiological Science, The Johns Hopkins Hospital, 600 N. Wolfe St., Baltimore, MD 21205. Address reprint requests to E. K. Fishman.

[2] Department of Orthopaedic Surgery, The Johns Hopkins Hospital, Baltimore, MD 21205.

***AJR* 159:805–809, October 1992** 0361–803X/92/1594–0805 © American Roentgen Ray Society

techniques allow more accurate differentiation of primary from secondary bone involvement. This pictorial essay illustrates the CT findings of primary and secondary lymphoma involving bone, muscle, and skin and subcutaneous tissues.

Bone

Primary lymphoma of bone is rare and accounts for approximately 5% of all primary bone tumors. In a large series of 1269 cases of lymphoma with autopsy confirmation, Rosenberg et al. [1] found that primary osseous lesions accounted for 4% of bone tumors. Most primary cases are non-Hodgkin's lymphoma, usually diffuse histiocytic lymphoma (Fig. 1). Primary bone lymphoma has the best prognosis of all primary bone malignant lesions.

Secondary involvement, however, is common in both Hodgkin's and non-Hodgkin's lymphoma. Rosenberg et al. [1] found osseous involvement in 16% of cases during the entire course of the disease. The prevalence of bone involvement is higher with lymphomas in children; approximately 25% of patients have bone lesions. Anecdotal experience at our institution suggests a higher prevalence of skeletal manifestations of lymphoma; up to 25% of patients with Hodgkin's disease and 20% of patients with widespread non-Hodgkin's

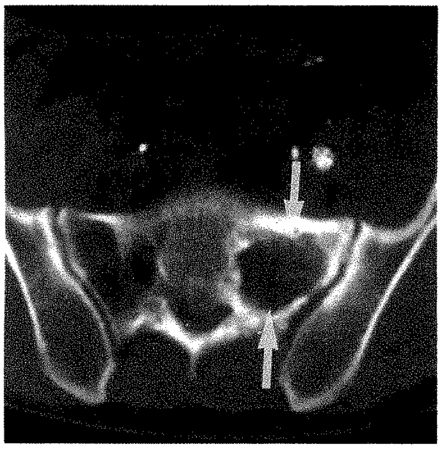

Fig. 3.—27-year-old man with Hodgkin's disease. CT scan shows lytic lesion at S1–S2 level and expansion of S1 foramen (*arrows*). Note minimal sclerosis of lesion's border.

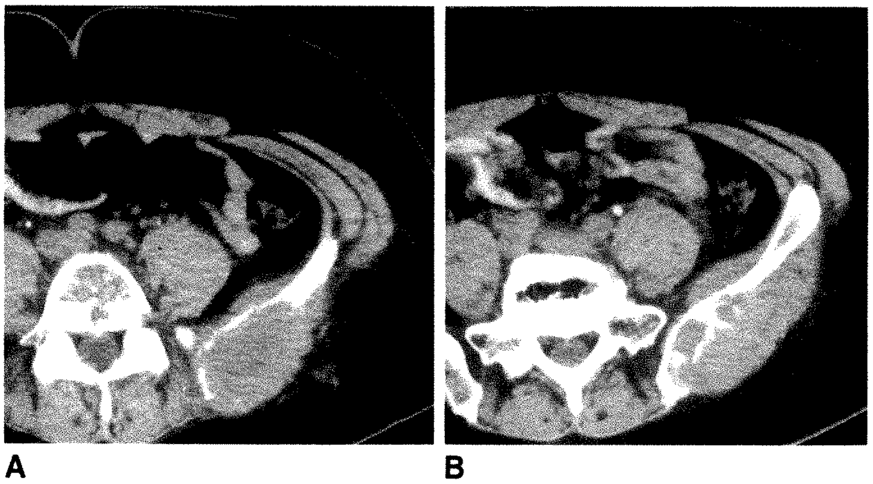

Fig. 4.—42-year-old man with Hodgkin's lymphoma.

A and *B*, CT scans show lytic lesion infiltrating left iliac bone, which has no obvious matrix, and associated soft-tissue mass infiltrating adjacent musculature.

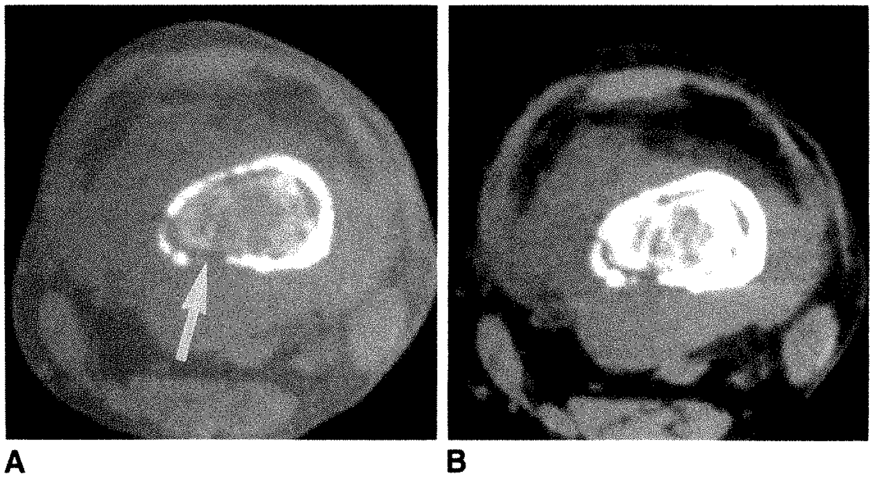

Fig. 5.—59-year-old man with primary mixed lymphocytic-histiocytic non-Hodgkin's lymphoma of left femur.

A, CT scan shows destructive lesion of left femur with pathologic fracture and infiltration of bone marrow (*arrow*).

B, CT scan shows associated soft-tissue infiltration of tumor into adjacent fat.

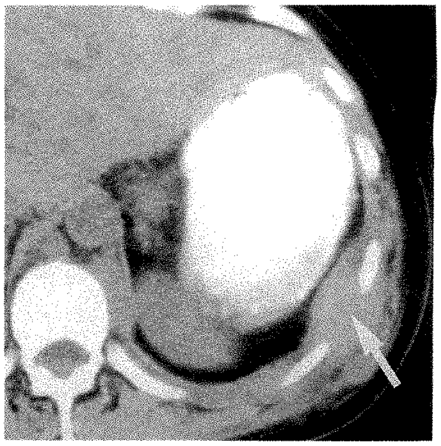

Fig. 6.—44-year-old woman with widespread Hodgkin's lymphoma. CT scan shows tumor involvement of left ninth rib, with adjacent pleural mass and chest wall extension (*arrow*). Subcrural nodes also are present.

lymphoma had skeletal involvement. The most frequent areas of metastatic involvement are the spine, pelvis, and skull (Figs. 2–4). In non-Hodgkin's disease, osteolytic lesions with permeative bone destruction are the most common radiologic findings (Fig. 5). Cortical destruction is often associated with involvement of adjacent muscle and soft tissue (Figs. 6–8). In primary non-Hodgkin's lymphoma, the most common site of occurrence is the lower extremity (Fig. 9). In Hodgkin's disease, primary osseous involvement is extremely rare, but metastatic disease is common and can involve bone by either hematogenous dissemination or contiguous spread from adjacent nodes. This is especially common in the sternum, with extension from internal mammary nodes (Figs. 10 and 11). The lesions can be either osteosclerotic, osteolytic, or of a mixed pattern; sclerotic lesions account for up to 45% of all bone lesions in Hodgkin's disease [2].

The distinction between primary and metastatic non-Hodgkin's disease is essential for accurate tumor staging. A primary bone lesion is considered stage I disease, whereas a bone lesion associated with disease in other sites is considered stage IV. Stage II disease involves nodes in more than two anatomic regions on the same side of the diaphragm; stage III involves nodes on both sides of the diaphragm. CT continues to be the imaging technique of choice for staging

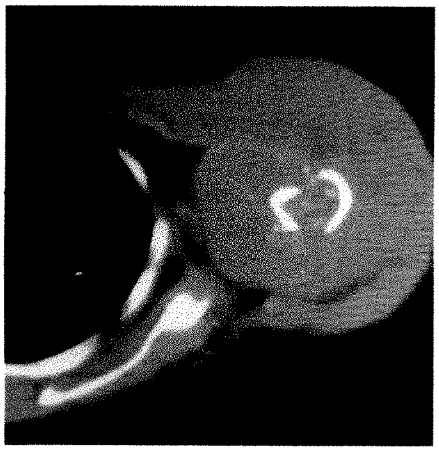

Fig. 7.—55-year-old woman with diffuse histiocytic lymphoma, large-cell type. CT scan shows destructive lesion of proximal left humerus with associated soft-tissue and muscle involvement. Pathologic fracture also is noted.

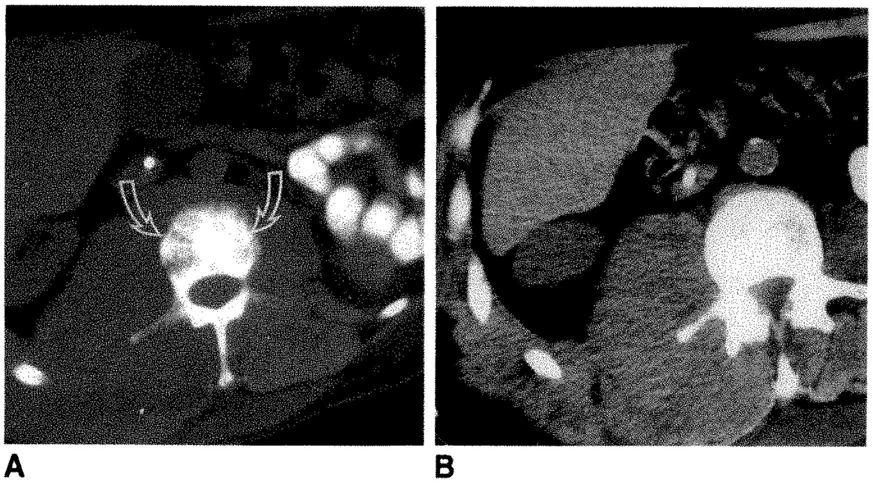

Fig. 8.—40-year-old man with recurrent nodular sclerosing Hodgkin's lymphoma.

***A* and *B*, CT scans show tumor involving right psoas and paraspinal muscles and L2–L3. Bone lesions are sclerotic with periosteal reaction (*arrows*).**

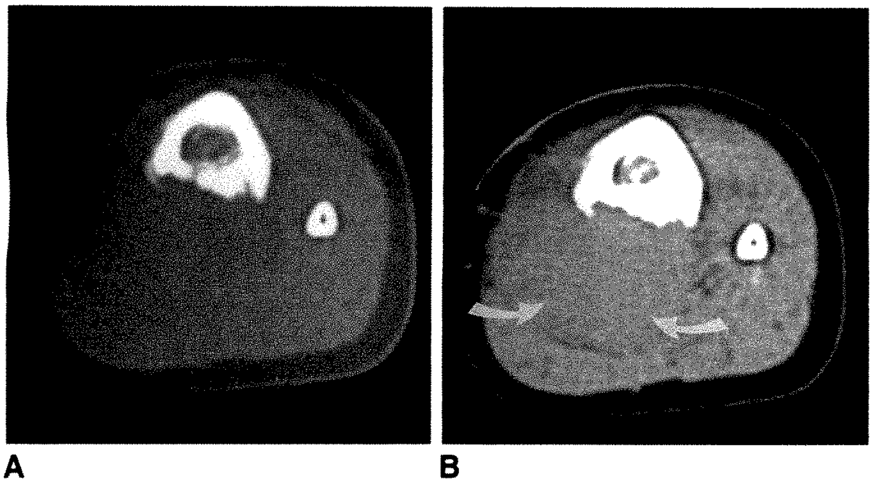

Fig. 9.—16-year-old woman with diffuse large-cell lymphoma.

***A* and *B*, CT scans show lytic lesion of left proximal tibia with associated soft-tissue mass (*arrows*).**

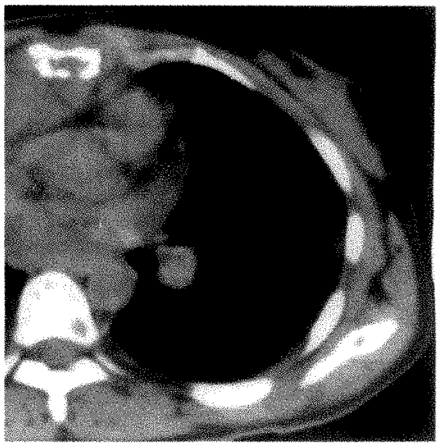

Fig. 10.—39-year-old woman with diffuse histiocytic lymphoma. CT scan shows large internal mammary nodes extending into sternum and infiltration of sternum.

lymphoma and is particularly useful in evaluating nodal disease and organ involvement.

Muscle

Lymphoma can involve muscle as either a discrete mass or diffuse tumor infiltration. In an autopsy study of 82 cases of lymphoma, Buerger and Monteleone [3] found histologic evidence of lymphomatous muscle infiltration but no gross enlargement of muscles. The site of lymphomatous infiltration of muscle may be the primary site (Fig. 12), but contiguous extension of a tumor mass into adjacent muscle is more common. In our experience, the most common radiologic finding is diffuse tumor infiltration of muscle (Figs. 13 and 14). The CT attenuation of the tumor is lower than that of normal muscle, and the distinction is magnified when contrast material is used (Fig. 15).

Occasionally, muscle enlargement in patients with lymphoma can occur without lymphatic obstruction or a distinct tumor mass. Most of these patients have bone involvement adjacent to the affected muscle. In this group, the size of the muscle rapidly returns to normal after treatment.

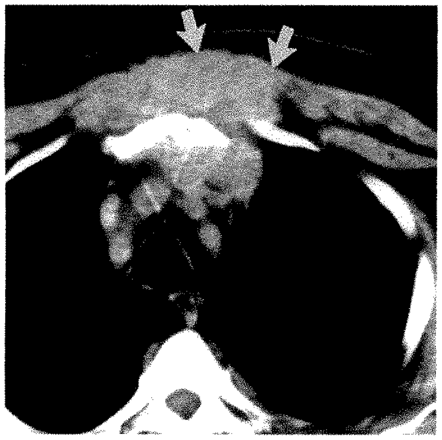

Fig. 11.—77-year-old man with a history of chest pain and a palpable mass. Malignant large-cell lymphoma was proved at biopsy. CT scan shows soft-tissue mass involving both pectoralis major muscles (*arrows*), sternum, and internal mammary nodes.

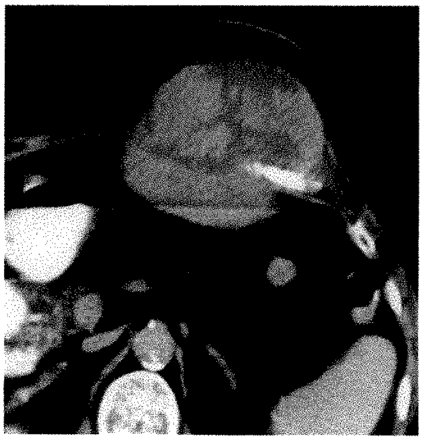

Fig. 12.—87-year-old woman with non-Hodgkin's lymphoma. CT scan shows 8-cm mass originating in musculature at anterior abdominal wall, which was the only site of tumor. Mass extends through abdominal wall with minimal involvement of adjacent rib.

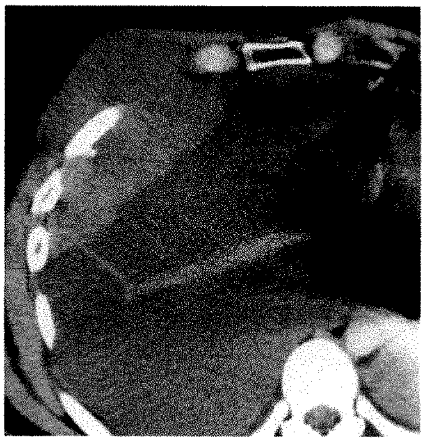

Fig. 13.—39-year-old man with recurrent sclerosing Hodgkin's disease. CT scan shows tumor infiltrating chest wall and extending into abdominal musculature. Abdominal ascites is present.

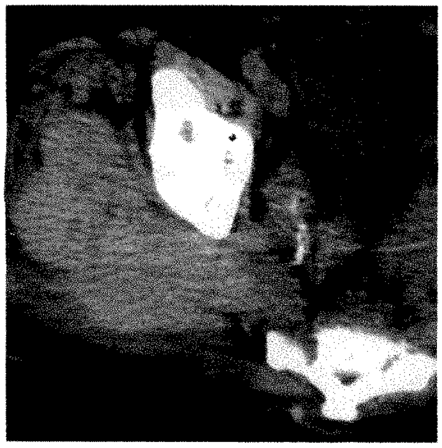

Fig. 14.—82-year-old man with history of right gluteal pain and biopsy-proved lymphoma, large-cell immunoblastic type. CT scan shows tumor infiltrating right gluteal medius and maximus muscles. Tumor extends into right sacrosciatic foramen. Pelvic adenopathy also is present.

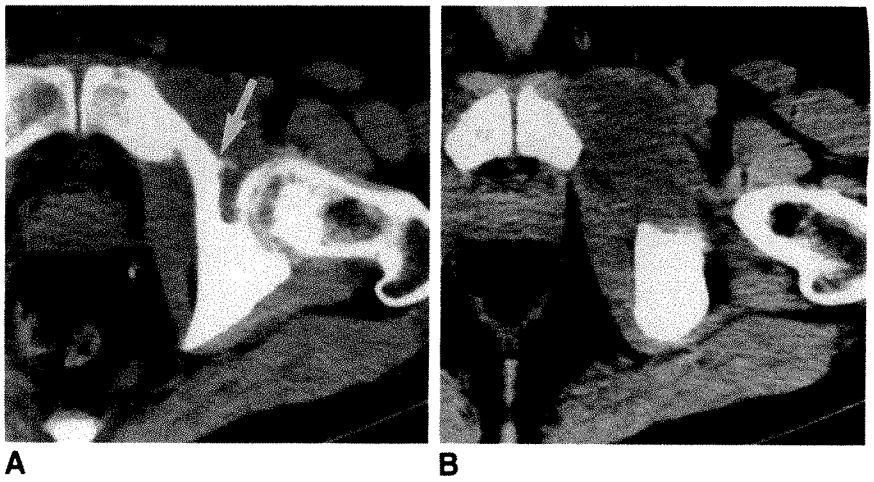

Fig. 15.—47-year-old man with nodular and diffuse large-cell lymphoma.

A and *B*, CT scans show tumor infiltrating left obturator externus and pectineus muscles. Tumor is of lower CT attenuation than normal muscle. This would be accentuated after administration of IV contrast material. Note erosion and infiltration of adjacent bone (*arrow*).

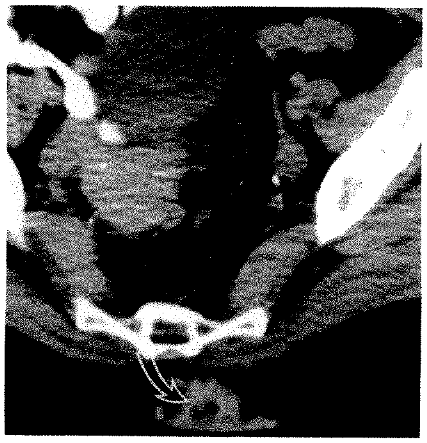

Fig. 16.—61-year-old woman with primary lymphoma of skin. CT scan shows tumor extending into subcutaneous fat (*arrow*).

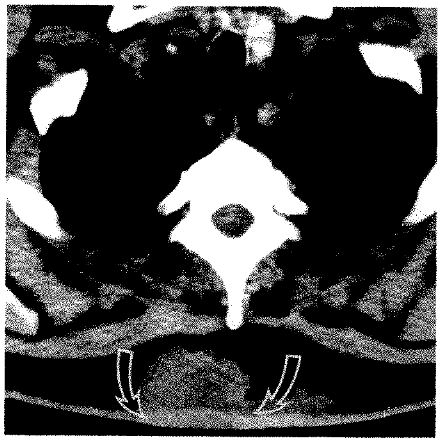

Fig. 17.—62-year-old man with primary cutaneous lymphoma on back. CT scan shows tumor extending into subcutaneous tissue but not invading paraspinal musculature. There is associated skin thickening (*arrows*).

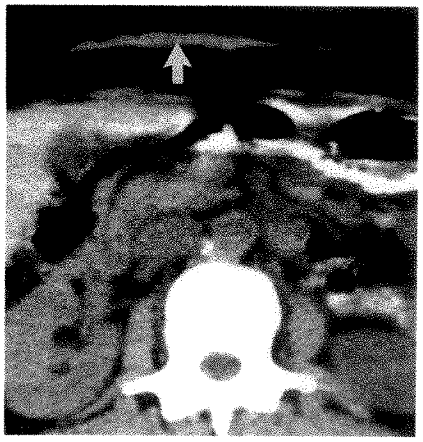

Fig. 18.—59-year-old woman with mycosis fungoides. CT scan shows infiltration of skin with apparent ulcerations (*arrow*).

Skin

Mycosis fungoides is an uncommon primary malignant T-cell lymphoma of the skin. The disease eventually spreads to internal organs and is clinically indistinguishable from primary visceral disease. The disease has three classic stages. The first is the erythematous or eczematous stage. The second is the infiltrative stage, manifested by indurated plaques, which in some cases may subside and in others lead to the development of lymphadenopathy. The third stage is most severe, with development of ulcerative lesions and rapid clinical decline. After infiltration, mean survival is usually 1 year or less. CT has been useful in staging mycosis fungoides and in defining the extent of adenopathy. Typical findings include focal skin thickening due to dermal and epidermal infiltrates (Figs. 16–18). Adenopathy indicates systemic involvement [4].

REFERENCES

1. Rosenberg SA, Diamond HD, Taslowitz B, Craver CF. Lymphosarcoma: review of 1269 cases. *Medicine* **1961**;40:31–84
2. Fishman EK, Kuhlman JE, Jones RJ. CT of lymphoma: spectrum of disease. *RadioGraphics* **1991**;11:647–669
3. Buerger LF, Monteleone DN. Leukemic-lymphomatous infiltration of skeletal muscle: systematic study of 82 autopsy cases. *Cancer* **1966**;19:1416–1422
4. Shapeero LG, Young SW. Mycosis fungoides: manifestations on computed tomography. *Radiology* **1983**;148:202

Book Review

Diagnostic Imaging of the Premature Infant. Edited by Rodrigo Dominguez. New York: Churchill Livingstone, 288 pp., 1992. $89.95

Diagnostic Imaging of the Premature Infant is a timely book. The best known previous texts, by Wesenberg and Swischuk, are both excellent but are somewhat out of date. Modern imaging methods have been increasingly adapted for use in neonatal intensive care units, and this monograph provides a good overview for the early 1990s.

The book has fewer than 300 pages, and it is physically easy to use. The quality of the print is excellent; the entire layout of the book, from the eye-catching cover onward invites frequent perusal. This is a cooperative effort, and most of the 10 authors are from Texas. The brief introduction by Swischuk skillfully reminds younger readers just how recently neonatal intensive care units came into being. The title itself was a fortunate choice, emphasizing *premature* rather than *newborn*.

The introductory chapter, by Oelberg, deals with clinical considerations regarding the premature infant. The concise, succinct approach sets the tone for the rest of the book. And yet, if I have any criticism about the writing, it pertains to this somewhat abbreviated style. For example, at the end of the first chapter, club foot is discussed in exactly eight lines. Still, the overall quality of the clinical introduction is good, and the material is most informative, especially for radiologists. The second chapter is about the risks associated with radiologic examinations in premature infants. The authors correctly stress that these small infants must be treated with special care and dispatch. The chapter also has a good discussion of the effects of ionizing radiation; both the somatic and the genetic concerns are addressed. The book continues with a chapter on the use of nuclear medicine studies in the high-risk neonate, an often neglected topic. Several of my neonatologist colleagues commented on how useful the chapter on radionuclides would be to clinicians. Conversely, the last section, on eye problems (particularly retinopathy) will be useful to radiologists.

The central parts of the book present various imaging methods and organ systems in a fairly conventional sequence. The chapter on perinatal brain pathology has a good selection of illustrations, both MR images and sonograms. The book has practically no radiographs of the skull and few CT scans—an interesting commentary on how quickly imaging technology has developed. Two chapters are on the chest: one on the heart and one on cardiac problems. The pulmonary chapter is good, and even the small illustrations are easy to appreciate visually; however, this is a relatively short discourse on a very large subject. In the chapter on cardiac imaging, the importance of the chest film is overemphasized. The few echocardiograms are adequate, but only a handful of Doppler images are included and no color flow studies. No angiograms can be found in the entire chapter. Although angiocardiography has been largely replaced by echocardiography, abnormalities of the aortic arch still require preoperative contrast studies in many cases. The chapter on gastrointestinal radiology quite correctly emphasizes the use of traditional examining methods. Interestingly, the book does not have a separate section on the genitourinary system. Instead, it has a good chapter on abdominal sonography, which includes the important aspects of renal and adrenal diseases. The next to last chapter, on musculoskeletal abnormalities, is short and far too comprehensive. It is simply not possible to cover such diverse subjects as spinal cord abnormalities and dysplasias in such a short space.

As might be anticipated, this book has a large number of illustrations, which are, by and large, quite good. I had some problem seeing finer details, such as air dissection into the bowel wall. However, this finding is somewhat difficult to appreciate even on original imaging studies. The bibliography varies from section to section. More than 150 references are listed at the end of the cardiac chapter, but only 21 at the end of the musculoskeletal overview.

This monograph-size book will be most useful for fellows in pediatric radiology, neonatology, or perinatology. It could also be used to good advantage by radiologists or pediatricians, who do not have to deal with the problems of sick premature babies all the time and who need a good, short, up-to-date reference.

Michael T. Gyepes
Miller Children's Hospital
Long Beach, CA 90801

Isolation of the Fourth Ventricle Causing Transtentorial Herniation:

Neurosonographic Findings in Premature Infants

Theodore R. Hall[1]
Anna Choi[2]
Dieter Schellinger[3]
Edward G. Grant[1]

OBJECTIVE. Significant posthemorrhagic enlargement of the fourth ventricle occurs only in a small minority of patients. Although entrapment or isolation of any ventricle can occur, the fourth ventricle is the most common site. This study was undertaken to better understand enlargement of the fourth ventricle after intraventricular hemorrhage and the neurosonographic features of isolation and transtentorial herniation.

MATERIALS AND METHODS. The sonographic records of 1535 premature neonates were reviewed for evidence of intracranial hemorrhage and ventriculomegaly. Cranial sonography was performed within the first 3 days of life in all neonates born in our hospital and within the first week of admission for transferred neonates. Follow-up sonograms were obtained at weekly intervals until discharge from the nursery. Intracranial hemorrhages were classified as severe when the hemorrhage was associated with hydrocephalus, intraparenchymal hemorrhage, or both.

RESULTS. Intracranial hemorrhage occurred in 761 (50%) of 1535 patients, with severe hemorrhages in 229. Ten had massive enlargement of the fourth ventricle with isolation in six of the 10 after shunt placement. Isolation of the fourth ventricle causing transtentorial herniation occurred in three. Of the patients with isolation of the fourth ventricle, two had associated infection and ventriculitis caused by *Klebsiella oxytoca* and one had *Candida* ventriculoencephalitis.

CONCLUSION. The early recognition of the neurosonographic features of an enlarged fourth ventricle causing transtentorial herniation has important therapeutic implications. Although isolation can occur after intraventricular hemorrhage alone, infection and ventriculitis are significant factors in the development of an isolated fourth ventricle.

AJR 159:811-815, October 1992

Numerous sonographic studies have investigated intraventricular hemorrhage [1-7] and posthemorrhagic hydrocephalus [8-10] in the premature infant. Although the sonographic manifestations of posthemorrhagic hydrocephalus can vary, the lateral ventricles are usually affected most severely [2, 10, 11]. Posthemorrhagic hydrocephalus involves the third and fourth ventricles less frequently; significant posthemorrhagic enlargement of the fourth ventricle occurs only in a small minority of patients. Occasionally, however, entrapment or isolation of a ventricle may occur. Any portion of the ventricular system can be affected, but the fourth ventricle is the most common site. Both the CT and neurosurgical literature contain descriptions of isolated fourth ventricles, but these consist of heterogeneous groups of patients [12, 13]. In most cases, CT showed the entrapped fourth ventricle several years after the patient's initial presentation. Little attention has been paid to this entity in the sonography literature. We report the neurosonographic features of an enlarged fourth ventricle in 10 premature neonates after perinatal intracranial hemorrhage.

Materials and Methods

The sonographic records of 1535 premature neonates were reviewed for the presence of intracranial hemorrhage. The authors referred to the grading system for intracranial hemor-

Received February 21, 1992; accepted after revision April 21, 1992.

Presented at the annual meeting of the Society for Pediatric Radiology, Orlando, FL, May 1992.

[1] Department of Radiological Sciences, University of California, Los Angeles, School of Medicine, 10833 Le Conte Ave., CHS B2-248, Los Angeles, CA 90024-1721. Address reprint requests to T. R. Hall.

[2] Department of Radiology, The Washington Hospital Center, Washington, DC 20010.

[3] Department of Radiology, Georgetown University Hospital, Washington, DC 20007.

0361-803X/92/1594-0811
©American Roentgen Ray Society

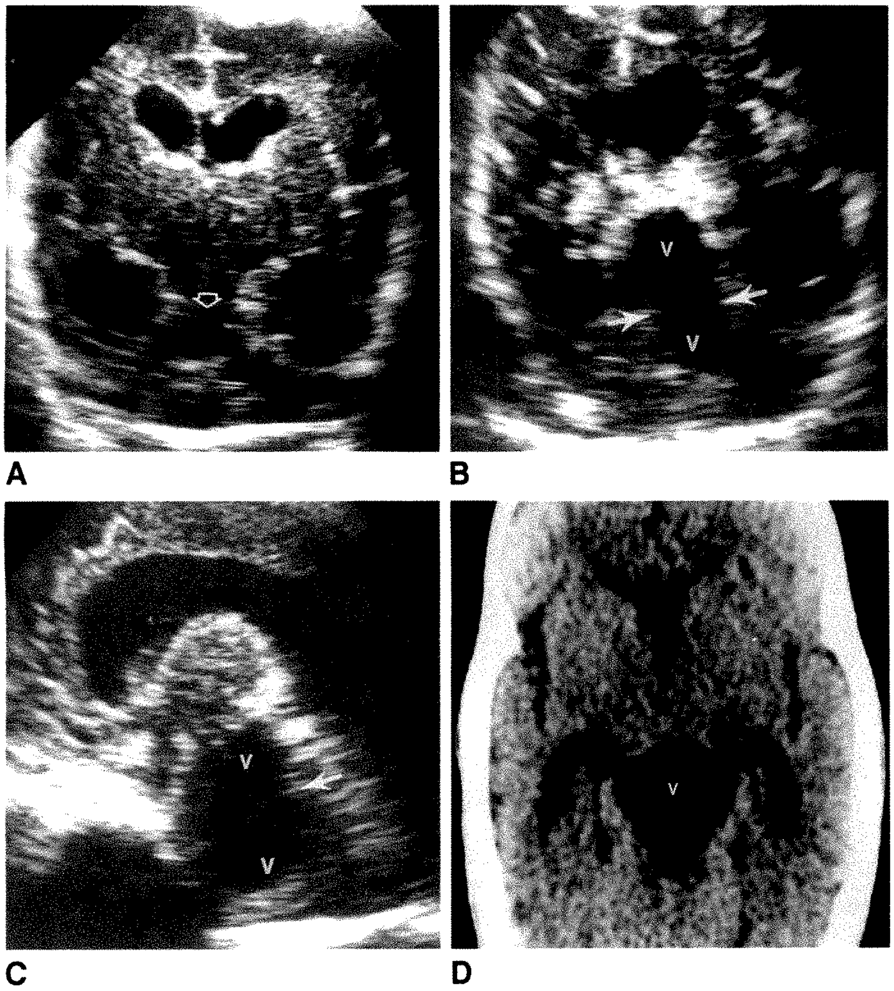

Fig. 1.—Premature infant born at 28 weeks' gestation with intraventricular hemorrhage.

***A*, Coronal sonogram at 12 days of age shows panhydrocephalus. Fourth ventricle (*arrow*) is mildly dilated.**

***B* and *C*, Sonograms obtained after placement of a shunt reservoir show incomplete decompression and asymmetry in size of lateral ventricles. Fourth ventricle (V) is disproportionately large when compared with lateral and third ventricles. Loss of triangular shape of fourth ventricle is noted with distortion caused by tentorium (*arrows*).**

***D*, CT scan obtained 3 months after placement of a ventriculoperitoneal shunt shows continued herniation with entrapment of fourth ventricle (V). Note that rest of ventricular system decompressed, consistent with isolation of fourth ventricle.**

rhage devised by Papile et al. [9] to judge severity of hemorrhage. The hemorrhage was classified as severe when it was associated with hydrocephalus, intraparenchymal hemorrhage, or both. The sonographic records of these infants were particularly screened for enlargement of the fourth ventricle. Sonograms obtained in the first week after birth revealed the fourth ventricle to be normal in all patients, eliminating any possibility of congenital lesions. Criteria for enlargement of the fourth ventricle included loss of the normal triangular configuration in the midline sagittal images and marked effacement of the surrounding cerebellar tissue.

All premature infants who were born in our hospital had a cranial sonogram obtained within the first 3 days after birth. All transferred patients had at least one cranial sonographic examination during the first week of admission. Any premature infant who subsequently had signs of an intracranial hemorrhage had a follow-up sonogram, even though the initial sonogram did not show an intracranial hemorrhage. Neonates with intracranial abnormalities other than those of congenital origin had follow-up sonograms at weekly intervals until discharge from the nursery. Sonographers scanned all infants with commercially available real-time units with either 5- or 7.5-MHz transducers. Five of the 10 neonates with enlarged fourth ventricles had correlative CT studies; one had contrast ventriculography.

Results

The infants in the study were from very large urban populations with a high prevalence of premature infant births and postnatal complications. Cranial sonography was performed in 1535 premature infants. Intracranial hemorrhage occurred in 761 patients (50%). Of those infants with hemorrhage, 229 had hemorrhages associated with hydrocephalus, intraparenchymal hemorrhage, or both. Enlargement of the fourth ventricle occurred in 10 (4%) of 229 premature infants with severe intracranial hemorrhage. The gestational ages of these 10 infants ranged from 24 to 32 weeks, with birth weights from 540 to 1780 g.

Four of the 10 infants had subependymal and intraventricular hemorrhages, with intraparenchymal hemorrhages in the remaining six. Neurosonographic findings consistent with periventricular leukomalacia were present in one of the infants with subependymal and intraventricular hemorrhage. A shunt was placed in the lateral ventricles of eight infants. The fourth ventricle remained dilated after shunt placement in six of

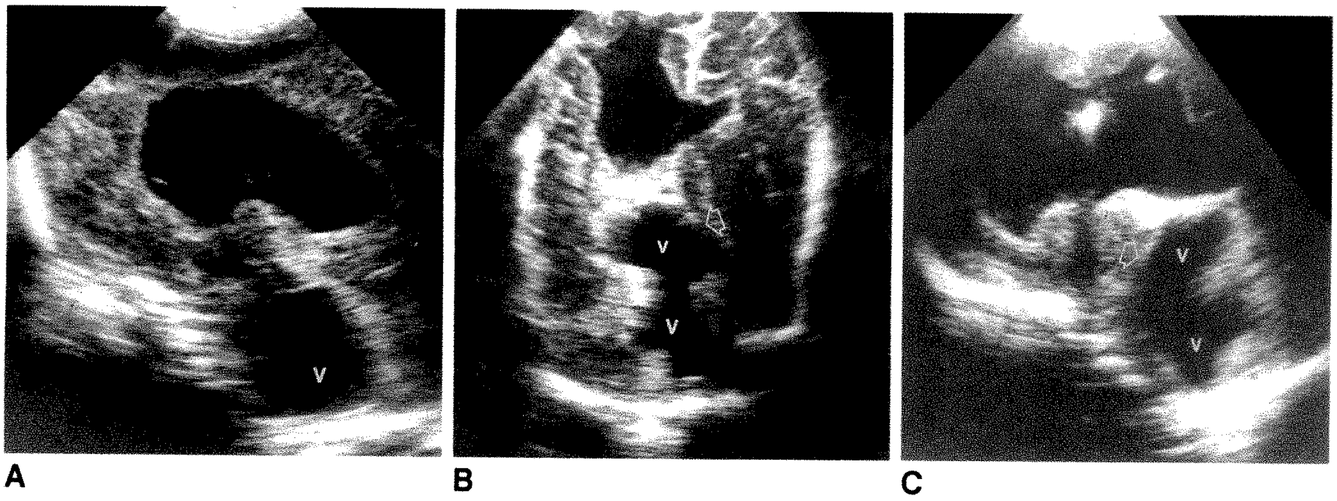

Fig. 2.—An 850-g premature infant with intraventricular hemorrhage and hydrocephalus 2 days after birth. At 3 months, severe panhydrocephalus persists.

A, Parasagittal sonogram shows marked enlargement of fourth ventricle (V).

B and *C*, After shunt placement, coronal (*B*) and sagittal (*C*) sonograms show decompressed lateral ventricles with persistent asymmetry of lateral ventricles due to porencephaly. Dilatation of fourth ventricle is disproportionate, with distortion (*arrow*) caused by transtentorium. A narrow waist is created in fourth ventricle (V) at level of tentorium.

these infants, indicating isolation of the fourth ventricle. Progressive enlargement of the fourth ventricle causing transtentorial herniation occurred in three of the six infants with isolation. No ventriculostomy was done nor was a shunt placed in two patients because of refusal in the case of one patient and death of the other. No autopsy was done on the neonate who died.

Infection and ventriculitis occurred after shunt placement in three infants who had isolation of the fourth ventricle. Of these three, CSF and blood cultures were positive for *Klebsiella oxytoca* and coliforms in two patients and for *Candida* ventriculoencephalitis in the third patient at the age of 7 weeks.

Discussion

Hydrocephalus is the most common sequela of intraventricular hemorrhage. The occurrence of hydrocephalus relates directly to the severity of the hemorrhage [10, 14]. Infants with subependymal hemorrhages that are isolated or that occur with small intraventricular hemorrhages tend not to have significant posthemorrhagic hydrocephalus. However, posthemorrhagic hydrocephalus is a frequent sequela in those infants who have subependymal hemorrhage with large intraventricular hemorrhages or in those who have subependymal hemorrhage with intraventricular hemorrhage and associated intraparenchymal hemorrhage [6]. These infants also require occasional intervention and long-term follow-up. With small hemorrhages, the trigones and occipital horns usually enlarge [9]. However, as the severity of the hemorrhage increases, diffuse enlargement of the lateral ventricles occurs. Hydrocephalus affects the lateral ventricles more commonly than it affects the third and fourth ventricles.

The pathogenesis of posthemorrhagic hydrocephalus is complex and difficult to explain by a single mechanism [10, 14]. Obstruction to CSF flow can result from a hematoma blocking the narrow passages of the ventricular system, that is, the aqueduct of Sylvius, the foramen of Monro, or the sites of CSF outflow such as the foramina of Magendie and Luschka. In addition, the presence of blood in the ventricles and subarachnoid spaces can cause an inflammatory ependymitis and arachnoiditis. Inflammation leads to fibrinous adhesions, which can block CSF outflow in the ventricular system or scar the arachnoid granulations at the site of CSF resorption. In addition to problems associated directly with intraventricular hemorrhage, the aqueduct of Sylvius can become obstructed by distortion from enlarging supratentorial and infratentorial ventricles. By combining these factors, one can see how both panhydrocephalus, isolated ventricles, or both can occur in the neonate with intraventricular hemorrhage.

Isolation of the fourth ventricle due to any cause is uncommon. The literature includes reports of ventricular isolation after intraventricular hemorrhage, neonatal meningitis, multiple shunt revisions, and myelomeningocele with Arnold-Chiari malformation [6, 11, 12, 15, 16]. In the largest series of 16 patients with entrapment of the fourth ventricle, most of the patients had shunts as neonates, and ventricular entrapment was a late diagnosis, usually several years after the initial shunt was placed [12]. A uniform clinical presentation was not found. Some patients had signs of mass effect in the posterior fossa, and others were asymptomatic. A more recent report on isolated ventricles in the premature infant after intraventricular hemorrhage postulates the role of ependymal flaps or chronic inflammatory changes to account for the membranes in isolated ventricles [11, 17]. These cases in-

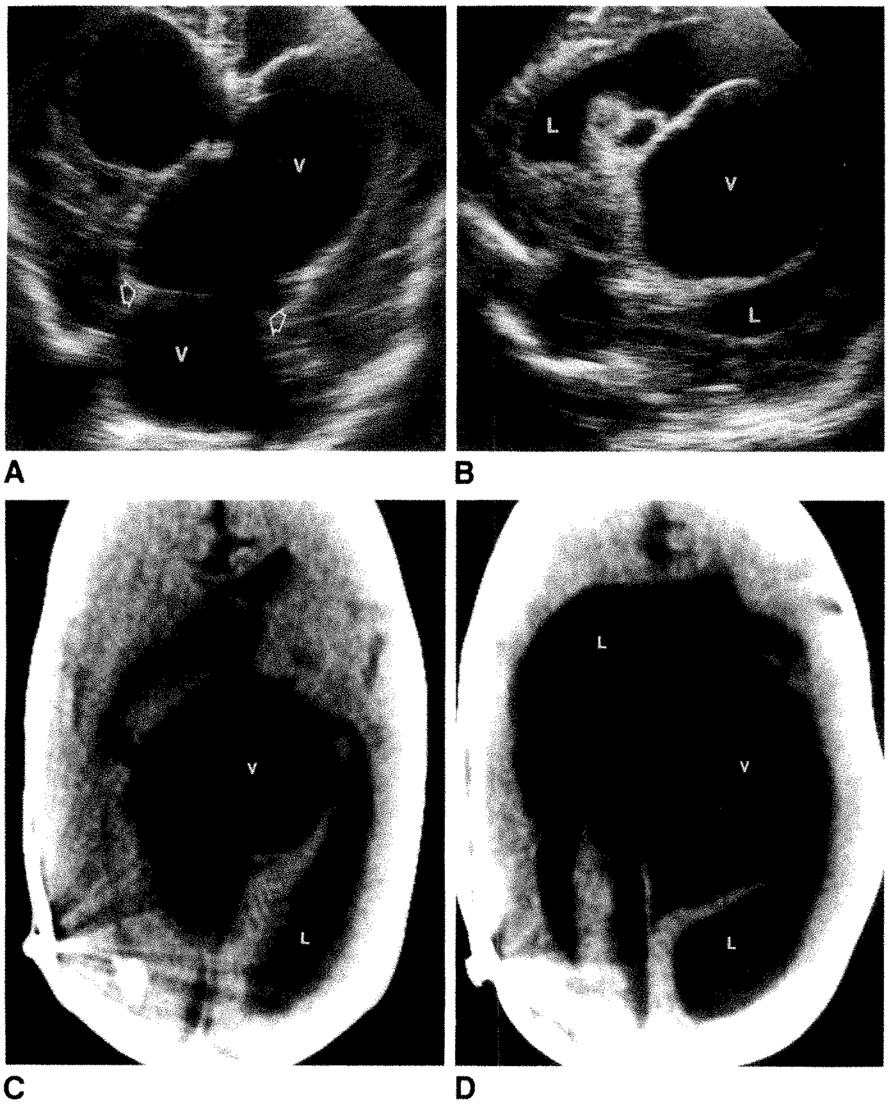

Fig. 3.—A 900-g premature infant born at 29 weeks' gestation with bilateral intraventricular hemorrhage. Cranial sonograms (*not shown*) before placement of a ventriculoperitoneal shunt showed hydrocephalus, porencephaly, and progressive transtentorial herniation.

***A* and *B*, Coronal (*A*) and parasagittal (*B*) sonograms after placement of a shunt show dilatation and distortion of both lateral (L) and fourth (V) ventricles caused by transtentorial herniation of the superior medullary velum. Note again narrow waist created in enlarged fourth ventricle (V) by tentorium (*arrow*).**

***C* and *D*, Accompanying CT scans depict similar anatomy with better definition of spatial relationships between portion of fourth (V) and lateral (L) ventricles distorted by herniation.**

volved isolated lateral and fourth ventricles. A shunt procedure was a common denominator. Infection associated with a shunt was reported in only one patient.

In our series, isolation of the fourth ventricle followed intraventricular hemorrhage in six of 10 patients with enlarged fourth ventricles. Although isolation of the fourth ventricle can occur with intraventricular hemorrhage alone, infection played a significant role in three of the patients. The postulated mechanisms for an enlarging isolated fourth ventricle include: (1) acute obstruction of the aqueduct and foramina of Luschka and Magendie by clot or debris; (2) postinflammatory adhesions from ventriculitis causing obstruction of the aqueduct and CSF outflow points or arachnoid granulations; (3) mechanical obstruction of the aqueduct from mass effect caused by the enlarged ventricles themselves in addition to outflow obstruction of the foramina of Luschka and Magendie. The third mechanism may account for the markedly enlarged fourth ventricle that returns to normal or decompresses with shunt placement.

The occurrence of transtentorial herniation with isolation of the fourth ventricle has received little attention. In patients in whom the fourth ventricle is isolated, early recognition and intervention can help to decrease morbidity. In all our patients, the enlarged fourth ventricle was an incidental finding that was discovered on routine follow-up sonograms. It was difficult to assess the effect of the enlarged fourth ventricle on the neurologic status of these very young neonates. However, the series reported by Eller and Pasternak [13] showed that it is important to identify and treat patients with isolated ventricles because of progressive enlargement, and several of our cases support this finding. Selective enlargement of the fourth ventricle may produce motor and visual deficits from compression of the brainstem and cerebellum [3, 13]. In the series of Eller and Pasternak [13], the effect of shunting the fourth ventricle was not uniform. Likewise in the series of Scotti et al. [12], successful shunting reversed progressive symptoms in the posterior fossa in some patients, but had no effect on the neurologic status of others. Findings on follow-up neurologic examinations were markedly abnormal in all 10 infants we studied.

Radiologists should be familiar with the sonographic features of an enlarged fourth ventricle and be aware of the potential for isolation of the ventricle after intraventricular hemorrhage and the increased risk of transtentorial herniation. Early recognition of cases of isolation can improve quality of care, because most of these patients will require a second shunt. Our results show that in a significant number of patients, infection with ventriculitis can be an associated factor, but that isolation of the ventricle also can result from intraventricular hemorrhage alone.

REFERENCES

1. Silverboard G, Horder MH, Ahmann PA, Lazzara A, Schwartz JF. Reliability of ultrasound in diagnosis of intracerebral hemorrhage and posthemorrhagic hydrocephalus: comparison with computed tomography. *Pediatrics* **1980**;66:507-514
2. Mack LA, Wright K, Hirsch JH, et al. Intracranial hemorrhage in premature infants: accuracy of sonographic evaluation. *AJR* **1981**;137:245-250
3. Volpe JJ. Neonatal intraventricular hemorrhage. *N Engl J Med* **1981**;304:886-891
4. Grant EG, Borts FT, Schellinger D, McCullough DC, Sivasubramian KN, Smith Y. Real-time ultrasonography of neonatal intraventricular hemorrhage and comparison with computed tomography. *Radiology* **1981**;139:687-691
5. Allan WC, Holt PJ, Sawyer LR, Tito AM, Meade SK. Ventricular dilation after neonatal periventricular-intraventricular hemorrhage: natural history and therapeutic implications. *Am J Dis Child* **1982**;136:589-593
6. Fleischer AC, Hutchison AA, Bundy AL, et al. Serial sonography of posthemorrhagic ventricular dilatation and porencephaly after intracranial hemorrhage in the preterm neonate. *AJR* **1983**;141:451-455
7. Perlamn JM, Nelson JS, McAlister WH, Volpe JJ. Intracerebellar hemorrhage in a premature newborn: diagnosis by real-time ultrasound and correlation with autopsy findings. *Pediatrics* **1983**;71:159-162
8. Hambleton G, Wigglesworth JS. Origin of intraventricular haemorrhage in the preterm infant. *Arch Dis Child* **1976**;51:651-659
9. Papile L, Burstein J, Burstein R, Koffler H. Incidence and evolution of subependymal and intraventricular hemorrhage: a study of infants with birthweight less than 1500 grams. *J Pediatr* **1978**;92:529-534
10. Levene MI, Starte DR. A longitudinal study of post-hemorrhage ventricular dilation in the newborn. *Arch Dis Child* **1981**;56:905-910
11. Fiske CE, Filly RA, Callen PW. Sonographic measurement of lateral ventricular width in early ventricular dilation. *J Clin Ultrasound* **1981**;9:303-307
12. Scotti G, Musgrave MA, Fitz CR, Harwood-Nash DC. The isolated fourth ventricle in children: CT and clinical review of 16 cases. *AJR* **1980**;135:1233-1238
13. Eller TW, Pasternak JF. Isolated ventricles following intraventricular hemorrhage. *J Neurosurg* **1985**;62:357-362
14. Larroche JC. Post-haemorrhagic hydrocephalus in infancy: anatomical study. *Biol Neonate* **1972**;20:287-299
15. Fisher RM, Lipinski JK, Cremin BJ. Ultrasonic assessment of infectious meningitis. *Clin Radiol* **1984**;35:267-273
16. Reeder JD, Sanders RC. Ventriculitis in the neonate: recognition by sonography. *AJNR* **1983**;4:37-41
17. Gaisie G, Roberts MS, Bouldin TW, Scatliff JH. Echogenic ependymal wall in intraventricular hemorrhage sonographic-pathologic correlation. *Pediatr Radiol* **1990**;20:297-300

Lyndos Widow

B. Leonard Holman[1]

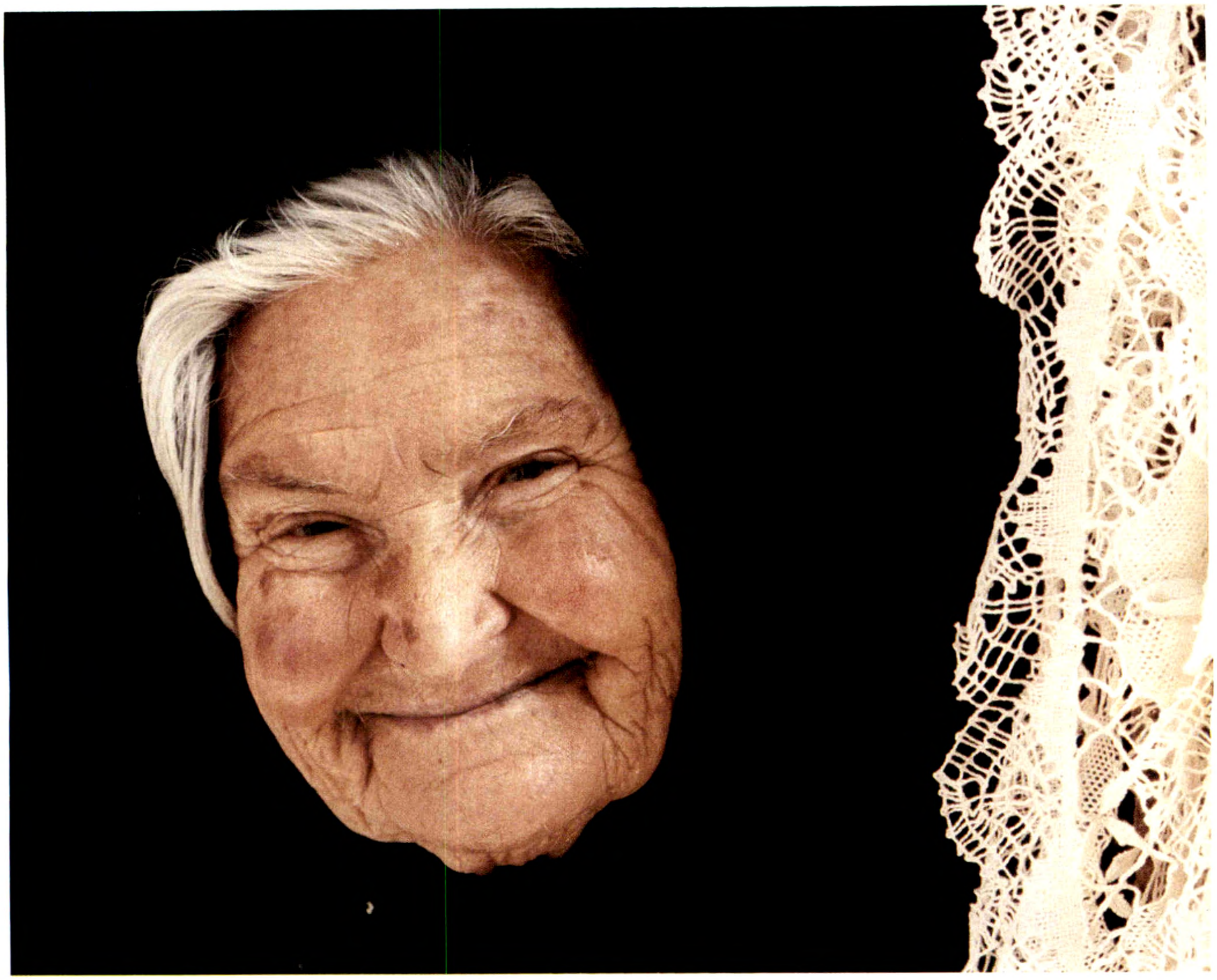

---

[1] Department of Radiology, Brigham and Women's Hospital, Harvard Medical School, 75 Francis St., Boston, MA 02115.

***AJR* 159:816, October 1992** 0361-803X/92/1594-0816 © American Roentgen Ray Society

MR Angiography in Children with Cerebral Neurovascular Diseases:

Findings in 31 Cases

Thomas J. Vogl[1]
Jörn O. Balzer[1]
Joachim Stemmler[1]
Clifford Bergman[1]
E. Egger[2]
Josef Lissner[1]

OBJECTIVE. We evaluated the suitability of MR angiography for routine use in children with suspected intracranial vascular disease.

SUBJECTS AND METHODS. Thirty-one children, 6 months to 14 years old, with intracranial lesions or clinically suspected vascular malformations were studied prospectively with conventional MR imaging and time-of-flight MR angiography. In nine cases, MR angiographic findings were verified with digital subtraction angiography or conventional angiography. All MR studies were performed on a 1.5-T MR system using a circularly polarized head coil.

RESULTS. Arterial MR angiography, performed in 24 cases, revealed congenital abnormalities of the arterial vessels in 20 cases. Vessel stenosis was observed in nine patients, and displacement of intracranial arteries due to tumors could be seen in 10 patients. Seven children had no abnormal findings. Venous MR angiography was performed in seven children, with depiction of sinus thrombosis in six cases. The comparative analysis of MR angiography and digital subtraction angiography showed equivalent results in nine patients; in one patient the degree of stenosis was overestimated with MR angiography.

CONCLUSION. MR angiography, when combined with MR imaging, reveals information about soft-tissue and vascular structures in a single setting. At this point, MR angiography can replace invasive conventional angiography or digital subtraction angiography only in selected cases because of software and hardware limitations. Arterial or venous MR angiography can be helpful as an additional scan in MR examinations of children with suspected cerebral neurovascular diseases, and its noninvasive nature makes it well suited for routine use in children.

***AJR* 159:817-823, October 1992**

Although conventional X-ray angiography and digital subtraction angiography (DSA) are the gold standards for the assessment of intracranial vessels [1-3], the invasiveness of these procedures makes them difficult to perform, particularly in children. Thus, they are not routinely available for use in children in many centers. Among the noninvasive methods of imaging blood flow, MR angiography is an attractive alternative. It can be used to evaluate vessel patency, flow magnitude, and flow direction. As an adjunct to conventional MR imaging studies, MR angiography can provide information about blood supply and vascular topography of tumors that would otherwise be available only through angiography via catheterization. MR angiography exploits the intrinsic properties of flowing blood so that catheterization and the need for contrast material are eliminated. Because of its safety, it is likely that MR angiography will play an increasingly significant role in the workup of children with suspected neurovascular disease. Nevertheless, MR angiography is still subject to a number of technical limitations, because of motion-induced artifacts and artifacts caused by alterations in flow behavior through abnormal vessels. Furthermore, it is not yet possible to consistently visualize vessels smaller than 1 mm in diameter [4, 5].

We present the MR angiographic findings in 31 children, correlate the findings

Received March 12, 1992; accepted after revision April 30, 1992.

This study was supported by a grant (no. 84-2501) of the Wilhelm Sander Foundation.

[1] Department of Radiology, University of Munich, Ziemssenstraße 1, 8000 Munchen 2, Germany. Address reprint requests to T. J. Vogl.

[2] Pediatric Hospital, University of Munich, 8000 Munchen 2, Germany.

0361-803X/92/1594-0817
©American Roentgen Ray Society

with those of conventional angiography or digital subtraction angiography, when available, and briefly summarize the examination strategies and parameters we found most useful.

Subjects and Methods

Thirty-one children 6 months to 14 years old with suspected intracranial lesions or vascular malformations seen on conventional spin-echo MR images were studied prospectively with MR angiography.

MR imaging examinations were carried out with the patient under general anesthesia in 27 cases. All MR studies were performed on a 1.5-T MR system (Magnetom SP 63, Siemens AG, Erlangen, Germany) with a circularly polarized head coil 30 cm in diameter. Conventional MR imaging was performed according to the following scheme: After a preliminary sagittal image was obtained, axial T2-weighted spin-echo images (3000/22,60,120 [TR/TE], 17 slices, slice thickness 3–10 mm, 256 × 256 matrix, one acquisition) and then T1-weighted images (600/15, 13 slices, slice thickness 3–10 mm, 256 × 256 matrix, two acquisitions) were obtained. T1-weighted coronal or sagittal images were acquired as needed to show any lesions seen on axial images. For all axial images, a saturation plane was placed below the imaging slices to eliminate motion artifacts. The total width of the field of view (FOV) was 20 cm in all cases. In 11 children with intracranial tumors, T1-weighted images were obtained after IV bolus injection of gadopentetate dimeglumine (dosage: 0.1 mmol per kilogram body weight).

MR angiography was performed by using three-dimensional (3D) Fourier transformed, rephased gradient-recalled echo sequences. Three-dimensional fast imaging with steady precession (FISP) imaging was used to depict vessels with fast blood flow, and two-dimensional (2D) or 3D fast low-angle shot (FLASH) imaging was used for vessels with slow flow. For arterial MR angiography, we used a TE of 7 msec, a TR of 40 msec, and a flip angle of 15°, which we had previously found gave the best results in visualizing fast-flowing blood with 3D FISP imaging. A TR/TE of 36/10 was best for visualizing the dural sinus system (Table 1). Presaturation slices were placed adjacent to the imaging volume in order to suppress either arterial or venous blood flow as appropriate to produce more purely venous or arterial MR angiograms, respectively.

The 3D or 2D data set was processed by using a computer ray-tracing algorithm on an integrated workstation to provide maximum intensity projection (MIP) images [6, 7]. Rotatable projections of the MR angiograms were usually calculated with a range increment of 15°. The computing time required for image reconstruction was 3–12 min, depending on range increment and resolution.

For each set of MR angiographic data and corresponding MIP images, the quality and extent of vessel visualization within the slab were ranked by a concensus of three independent observers on an ordinal scale of 0 to 3: grade 0, vessels that lay within the FOV but were not depicted on MR images; grade 1, vessels that could be detected only over a short distance; grade 2, vessels that could be visualized over a greater distance but had interruptions in flow signal; grade 3, vessels that were imaged over their entire length within the FOV and without signal interruption. The following arteries were evaluated: internal carotid, anterior cerebral, middle cerebral, anterior communicating, ophthalmic, posterior communicating, posterior cerebral, superior cerebellar, anterior inferior cerebellar, posterior inferior cerebellar, basilar, and vertebral (Table 2).

On venous MR angiography, depiction of the following segments of the sinus system was evaluated: superior sagittal sinus, inferior sagittal sinus, straight sinus, confluens of sinuses, transverse sinus, sigmoid sinus, cavernous sinus and its draining superior and inferior sinuses, the sphenoparietal sinus, and the superior bulb of the jugular vein (Table 3).

TABLE 1: Recommended Sequences and Parameters for Intracranial MR Angiography

System/Sequence	Parameters											
	TR/TE (msec)	Angle (degree)	No. of Slices	Slice Thickness (mm)	Slice Gap (mm)	3D Partitions	EST (mm)	FOV (mm)	Acquisition	Matrix	Slice Orientation	No. of Saturation Pulses
Arterial												
Fast flow: 3D FISP	40/7	15	1	40–96	0.00	64	1.5	200	1	256 × 256	Axial, coronal	2
Slow flow: 2D FLASH	36/10	60	53	3–10	−0.25	0		200	1	256 × 256	Coronal	2
Venous												
2D FLASH	36/10	60	53	3–10	−0.25	0		200	1	256 × 256	Coronal	1
3D FLASH	32/7	30	1	135	0.00	64	1.0	200	1	256 × 256	Sagittal	1

Note.—TR = repetition time, TE = echo time, EST = effective slice thickness, FOV = field of view, 3D = three dimensional, FISP = fast imaging with steady precession, 2D = two dimensional, FLASH = fast low-angle shot.

TABLE 2: Delineation of Intracranial Arteries and Evaluation of Imaging Quality on Arterial MR Angiography

Vessel[a]	Could Not Be Evaluated (%)	Grade 1 (%)	Grade 2 (%)	Grade 3 (%)
Internal carotid artery	0	15	25	60
Anterior cerebral artery	0	20	35	45
Middle cerebral artery	0	10	45	45
Posterior cerebral artery	5	20	5	70
ACA	70	20	5	0
PCA	45	25	25	5
Ophthalmic artery	90	0	10	0
Thalamostriate artery	95	5	0	0
Choroid artery	100	0	0	0
Vertebral artery	0	20	25	0
Basilar artery	0	0	25	70
Superior cerebellar artery	65	25	5	0
AICA	50	20	0	0
PICA	40	10	15	0
Abnormal vessels	0	20	10	40

Note.—24 patients were examined; 30% had no abnormalities. Grade 1 = poor visualization, grade 2 = good visualization with some flow-signal interruption, grade 3 = optimal visualization.

[a] ACA = anterior communicating artery, PCA = posterior communicating artery, AICA = anterior inferior cerebellar artery, PICA = posterior inferior cerebellar artery.

TABLE 3: Delineation of Intracranial Sinus System and Evaluation of Imaging Quality on Venous MR Angiography

Vessel	Could Not Be Evaluated (%)	Grade 1 (%)	Grade 2 (%)	Grade 3 (%)
Superior sagittal sinus	17	0	33	50
Straight sinus	0	0	0	100
Inferior sagittal sinus	17	50	17	17
Vein of Galen	0	66	17	17
Confluens of sinuses	0	0	17	83
Transverse sinus	0	0	0	100
Sigmoid sinus	17	0	0	83
Cavernous sinus	67	17	17	0
Superior petrosal sinus	83	0	17	0
Inferior petrosal sinus	83	0	17	0
Sphenoparietal sinus	13	17	53	17
Superior bulb of jugular vein	0	0	33	67
Abnormal vessels	0	0	17	50

Note.—Seven patients were examined; 14% had no abnormalities. Grade 1 = poor visualization, grade 2 = good visualization with some flow-signal interruption, grade 3 = optimal visualization.

Results

Arterial MR Angiography

Arterial MR angiography was performed in 24 children. In the nine cases in which results of angiography via catheterization were available, depiction of the vascular structures on MR angiograms compared favorably with depiction on DSA images, although vessels smaller than 1 mm in diameter could not be visualized consistently on MR angiograms (Table 2). The anterior cerebral artery could be seen as far as the high cortical segment in nine patients, the middle cerebral artery could be followed to the angular gyrus in eight patients. Excellent imaging quality could be achieved in 12 patients for the upper segments of the internal carotid artery, in 14 patients for the entire posterior cerebral and basilar artery, and in one patient for the posterior communicating artery. Smaller arteries such as the anterior communicating artery, the ophthalmic artery (Fig. 1), the superior cerebellar artery, the anterior inferior cerebellar artery (AICA), and the posterior inferior cerebellar artery (PICA) could be visualized in only a few cases.

On arterial MR angiograms, vessel stenoses were detected in eight cases involving the middle cerebral artery ($n = 4$; Figs. 2–5), the anterior cerebral artery ($n = 2$; Figs. 2 and 3), the posterior cerebral artery ($n = 1$), and the internal carotid artery ($n = 1$, Fig. 5). Correlation with DSA findings was available in four patients and confirmed the diagnosis based on MR angiographic findings in three cases (Figs. 2B and 3B). In one case the grade of stenosis was overestimated on the basis of MR angiographic findings (Figs. 4B and 4C). In a fifth patient with hemiparesis, stenosis of the middle cerebral artery, consistent with clinical findings, was seen on MR angiograms; in the remaining three patients, infarcts evident on the spin-echo images corresponded to the areas of flow-signal loss as seen on the MR angiograms. Displacements of the anterior cerebral artery by an astrocytoma in one case and of the middle cerebral artery by a large hydrocephalus in

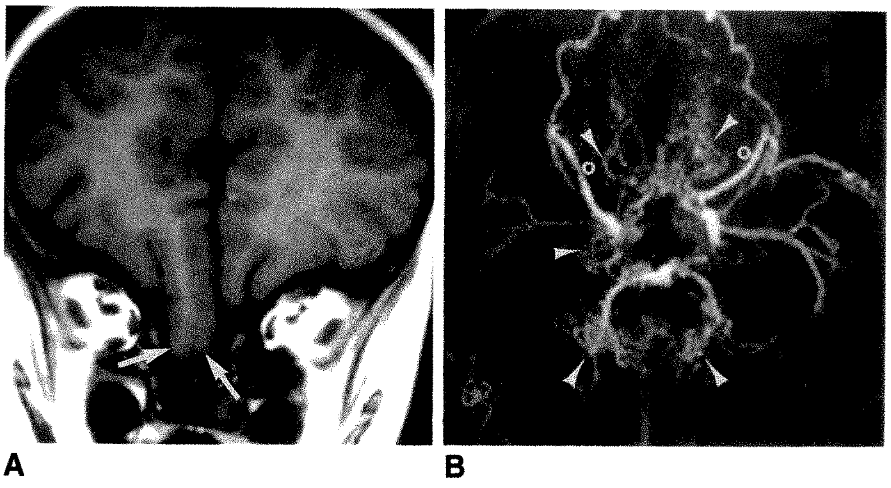

Fig. 1.—3-year-old with intracranial arteriovenous malformation and a frontoethmoidal encephalocele.

***A*, Coronal T1-weighted (600/15) MR image shows encephalocele (*arrows*) of frontal lobe.**

***B*, Axial, three-dimensional FISP (40/7, 15°) arterial MR angiogram shows a network of abnormal vessels (*arrowheads*). Ophthalmic arteries (O) can be seen because they are dilated.**

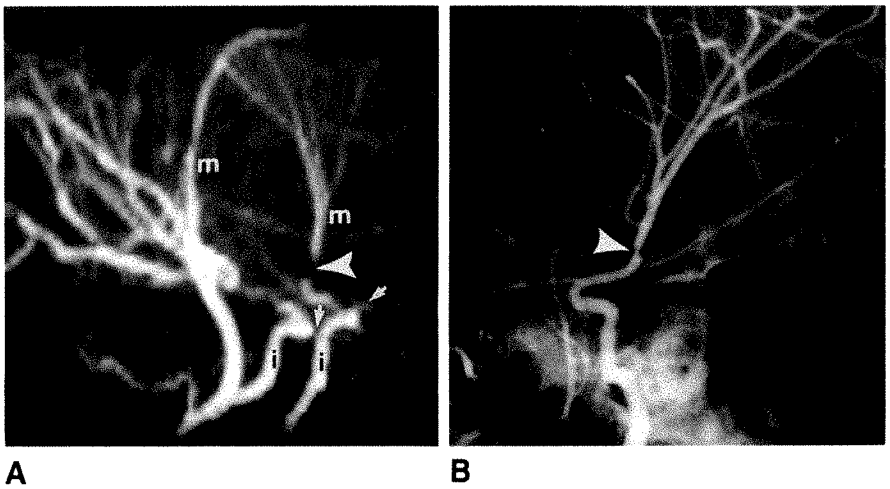

Fig. 2.—2-year-old with an astrocytoma in frontal lobe and stenoses of both anterior cerebral arteries and right middle cerebral artery.

A, Axial, three-dimensional FISP (40/7, 15°) arterial MR angiogram, rotated to a more sagittal view, reveals stenosis of right middle cerebral artery (*arrowhead*) and stenosis of anterior cerebral arteries (*arrows*). m = middle cerebral artery, i = internal carotid artery.

B, Conventional angiogram (lateral view) of right internal carotid artery verifies the diagnosis of stenosis of right middle cerebral artery made by MR angiography (*arrowhead*). Comparison of stenosis on MR angiography and conventional angiography shows that MR angiography overestimates grade of stenosis.

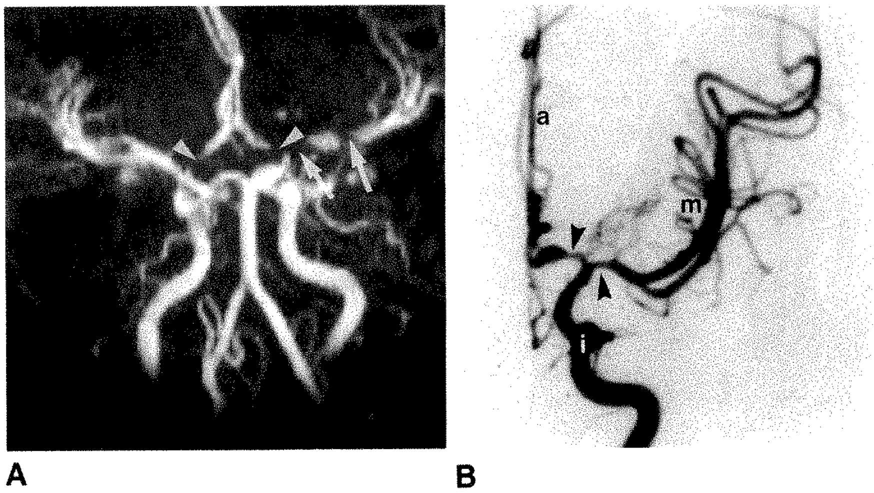

Fig. 3.—2-year-old with right-sided hemiparesis and local vascular lesion (infarct) in left internal capsule.

A, Axial, three-dimensional FISP (40/7, 15°) arterial MR angiogram. Axial > coronal −30° rotated maximum intensity projection angiogram reveals stenosis of both anterior cerebral arteries (*arrowheads*) and of left middle cerebral artery (*arrows*).

B, Digital subtraction angiogram of left internal carotid artery verifies results of MR angiography in this patient: stenosis of anterior and middle cerebral arteries (*arrowheads*). a = anterior cerebral artery, m = middle cerebral artery, i = internal carotid artery.

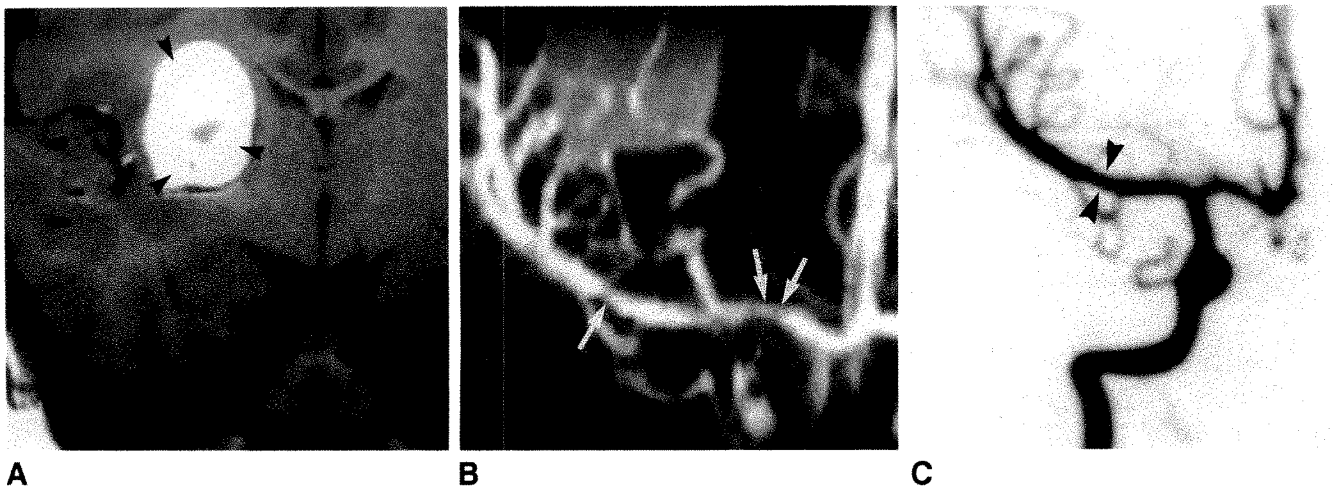

Fig. 4.—6-year-old with idiopathic hemorrhage in region of right internal capsule.

A, Coronal T1-weighted (600/15) MR image shows hemorrhagic lesion in region of right internal capsule (*arrowheads*).

B, Axial, three-dimensional FISP (40/7, 15°) arterial MR angiogram. Coronal rotated maximum intensity projection angiogram shows suspected stenosis of right middle cerebral artery (*arrows*).

C, Digital subtraction angiogram of right internal carotid artery confirms stenosis of right middle cerebral artery (*arrowheads*).

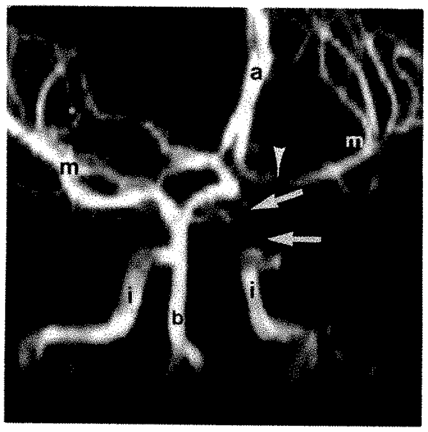

Fig. 5.—14-year-old with giant-cell arteritis (Takayasu's syndrome) and stenoses of upper segments of left internal carotid artery and origin of left anterior and middle cerebral arteries. Axial, three-dimensional FISP (40/7, 15°) arterial MR angiogram. Coronal > sagittal 30° rotated maximum intensity projection angiogram shows stenoses of upper segments of left internal carotid artery (*arrows*) and at origin of left anterior and middle cerebral artery (*arrowhead*). a = anterior cerebral artery, m = middle cerebral artery, i = internal carotid artery, b = basilar artery.

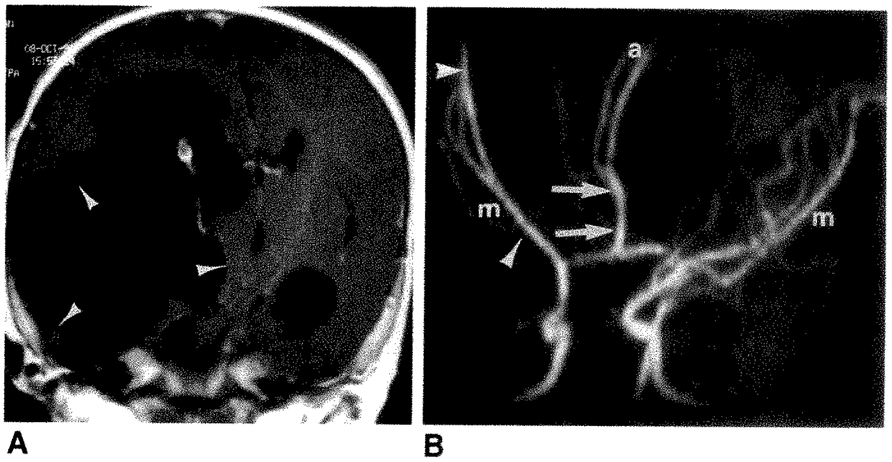

Fig. 6.—12-year-old with enlargement of right ventricle due to occlusion of foramen of Monro after bacterial meningitis, resulting in displacement of vessels.

A, Coronal T1-weighted (600/15) enhanced MR image shows an occlusive hydrocephalus in right hemisphere (*arrowheads*).

B, Axial, three-dimensional FISP (40/7, 15°) arterial MR angiogram. Coronal > sagittal −30° rotated maximum intensity projection angiogram shows displacement of right middle cerebral artery due to occlusive hydrocephalus (*arrowheads*). Additionally, a common anterior cerebral artery is detected (*arrows*). a = anterior cerebral artery, m = middle cerebral artery.

another case were clearly seen on the MR angiograms. In one case, an occlusion of both middle cerebral arteries was seen.

MR angiograms showed anatomic variations in five patients. These included primitive trigeminal arteries (three), a common anterior cerebral artery (one, Fig. 6) and kinking of the internal carotid artery (one, Fig. 7). In the patient with the occlusive hydrocephalus and a common anterior cerebral artery, a displacement with superimposition of both arteries was suggested, but this was excluded after we examined additional projections and rotated the angiograms (Fig. 6). In one patient with a frontoethmoidal encephalocele, MR angiograms showed an arterial network in the area of the anterior cerebral artery. Dilatation of both ophthalmic arteries resulted in particularly good visualization of these vessels, which otherwise are not usually seen on MR angiograms (Fig. 1). DSA findings confirmed the presence of a primitive trigeminal artery in one case and kinking of the internal carotid artery in another case (Fig. 7). In one case, the mass effect of an astrocytoma resulted in displacement of the anterior cerebral artery and occlusion of the high cortical segments of the ascending superior curvature; this was observed with MR angiography and confirmed with DSA (Fig. 2).

Venous MR Angiography

The superior sagittal, straight, transverse, and sigmoid sinuses and the bulb of the internal jugular vein were visualized in all patients (Table 3). The cavernous sinus and its draining superior and inferior petrosal sinus were in most cases ranked with grade 0 or grade 1, largely because these sinuses lay at the edge of the imaging slices. Detection of the inferior sagittal sinus and the vein of Galen was inconsistent.

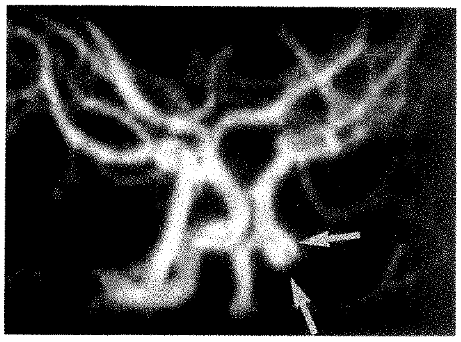

Fig. 7.—2-year-old with kinking of both internal carotid arteries and no other abnormal findings. Axial, three-dimensional FISP (40/7, 15°) arterial MR angiogram. Sagittal > coronal 30° rotated maxium intensity projection angiogram reveals kinking of left internal carotid artery (*arrows*).

Venous MR angiography was performed in seven patients with suspected sinus thrombosis and showed sinus thrombosis in six cases; collateral drainage could be seen in one. In one patient, venous MR angiography revealed no pathologic findings. Sinus thrombosis involved the transverse sinus in four of the seven cases. One patient with extensive thrombosis of the transverse and sigmoid sinuses was examined before and after treatment with heparin; venous flow improved markedly after administration of heparin (Fig. 8). Complete and partial sinus thrombosis could be differentiated by including the original MR angiographic data set in the review.

Use of gadopentetate dimeglumine in 11 children did not improve the overall imaging quality of angiography, although the relationship of tumor to adjoining vessels was better depicted in five cases. Large tumors or tumors with high

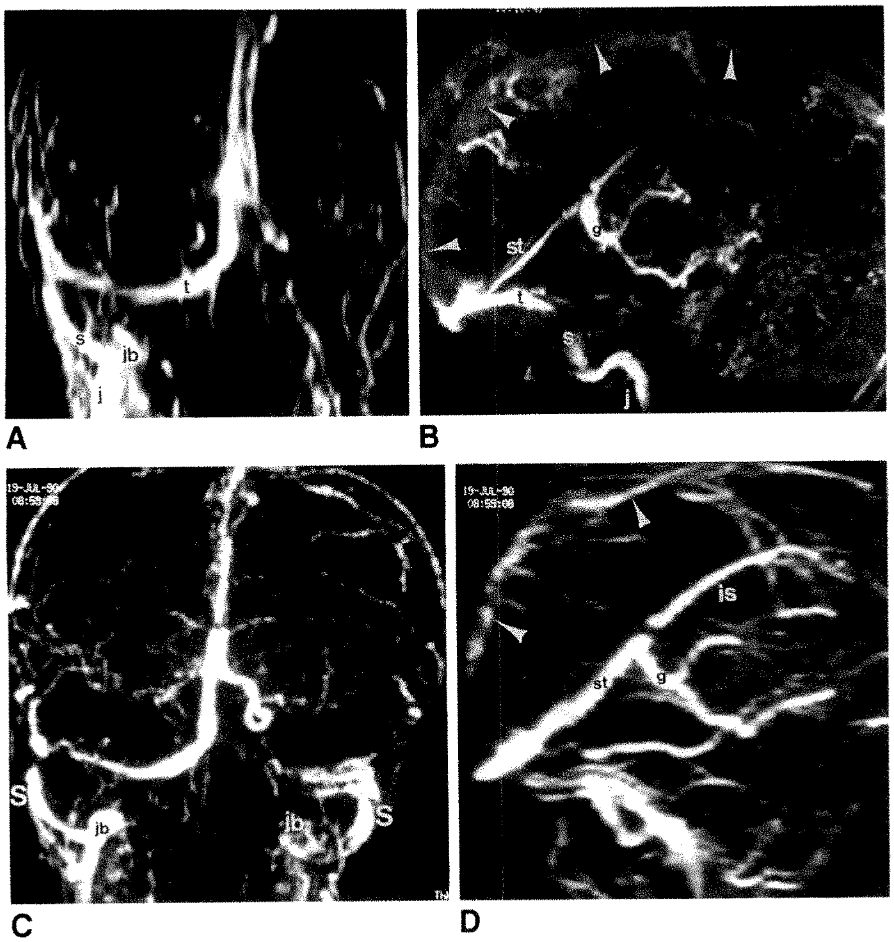

Fig. 8.—14-year-old girl under chemotherapy for acute myelogenous leukemia with sinus thrombosis before (*A* and *B*) and 1 month after (*C* and *D*) application of heparin.

A, Coronal, two-dimensional (2D) FLASH (36/10, 60°) venous MR angiogram. Coronal view shows occlusion of right transverse sinus (t), right sigmoid sinus (s), right jugular bulb (jb), and jugular vein (j).

B, Coronal, 2D FLASH (36/10, 60°) venous MR angiogram. Sagittal view shows thrombosis of superior sagittal sinus (*arrowheads*) as well. st = straight sinus, g = vein of Galen, t = transverse sinus, s = sigmoid sinus, j = jugular vein.

C, Coronal, 2D FLASH (36/10, 60°) venous MR angiogram after heparin application shows reperfusion of right sigmoid sinus (s) and jugular bulb (jb).

D, Coronal, 2D FLASH (36/10, 60°) venous MR angiogram. Sagittal view after heparin application shows imperfect reperfusion of superior sagittal sinus (*arrowheads*). is = inferior sagittal sinus, st = straight sinus, g = vein of Galen.

enhancement reduced the angiographic imaging quality in MIPs in six cases, as these lesions were superimposed on neighboring vessels. Use of contrast material slightly improved the visualization of small vessels in venous MR angiography, especially in three infants where 3D FLASH imaging was used.

We achieved the best results by using the sequence parameters for 3D FISP and 2D FLASH imaging listed in Table 1. Visualization of smaller intracranial veins, such as the great vein of Galen and the inferior sagittal sinus, was better on 3D FLASH than on 2D FLASH images.

Discussion

Time-of-flight MR angiography is a useful technique for imaging intracranial vessels, although it does have several limitations. Because it depends on the refocusing of inflowing unsaturated spins, it may suffer from increasing saturation within a large imaging volume and incomplete refocusing [2, 5, 8]. Alterations in flow dynamics can cause partial signal loss, because these spins are dephased. Dephasing results from the random, tumbling motion in areas of turbulence and from the increased duration of stay in the measuring slice. Because of signal loss induced by poststenotic turbulence, vessel stenosis cannot be graded appropriately on the basis of MR angiographic findings [5, 9]. Nevertheless, the grade of stenosis or occlusion as seen on MR angiograms could more accurately be assessed by including conventional MR images and the original 3D FISP data set in the review. Another source of error stems from the lack of signal from partially thrombosed aneurysms, which may lead to underestimation of aneurysm size [10, 11]. However, spin-echo images obtained during the same examination usually provide more information on true size and composition of the aneurysm; indeed, MR angiography together with conventional MR imaging may yield more information than DSA alone.

Progressive saturation within an imaging volume occurs sooner with slow-flowing blood (e.g., venous blood) but also depends on the vessel's course (perpendicular, oblique, or parallel to the imaging volume). Slice thickness and the RF deposition, which are operator-controlled parameters, also cause saturation effects [8, 12]. As scanning parameters depend on the T1 relaxation of blood, a variation of these parameters is possible within a narrow range only [6, 8].

Before this study, we determined optimal scanning parameters in healthy children. We found that a TR of 40 msec and a flip angle of 15–20° produced the maximum contrast-to-noise and signal-to-noise ratios. Slice thickness must be held to a minimum to decrease saturation effects; however, this also reduces the length of the vessel segment that can be imaged during a given examination [5, 8, 12–14]. A difficulty arises in positioning small axial planes in order to achieve maximum information about vessels, as slice thickness must be kept as small as possible in order to increase spatial resolution. To increase slice thickness while minimizing saturation effects, two 3D volumes can be used with half the partitions and 25% overlapping [10].

A more severe problem is the loss of visualization of small vessels in the process of acquisition and MIP reconstruction. Imaging of small vessels or reduced venous flow in partially thrombosed sinuses requires an increase of in-plane spatial resolution, which can be achieved if the FOV is kept as small as possible. The best achievable in-plane resolution in our study was 1 mm, with a loss of signal from smaller vessels. A further problem arises in image reconstruction. When a vessel's size is small compared with pixel size, small vessels may be lost completely on MIP reconstruction because of partial volume averaging and statistical fluctuations in background noise [10, 15]. This problem can be overcome by including the original MR angiographic data set in the review, as small vessels or restricted venous flow in partial sinus thrombosis is documented on these images but is eliminated by the MIP algorithm on projection angiograms.

High-resolution 3D FISP or FLASH sequences can be used to depict small intracranial vessels such as the anterior inferior cerebellar artery (AICA), posterior inferior cerebellar artery (PICA), anterior cerebral artery, and ophthalmic artery or small intracranial veins. A disadvantage of the 3D FLASH sequence is the simultaneous visualization of subcutaneous fatty tissue, which is superimposed on vessels in MIPs. This can be diminished by using echo times that induce a fat-suppressive effect (e.g., TE = 7 or 11 msec), combined with the smallest possible slice thickness and field of view.

In 89% of our healthy children and five of our patients, we found partial signal loss from the confluens of sinuses that seemed not to correlate with pathologic changes. Particularly in stenosis or sinus thrombosis, the extent of the lesion can be overestimated, because the atheromatous plaque or thrombus creates a poststenotic turbulent flow with signal loss adjacent to vessel boundaries, simulating a high-grade occlusion. It has been reported that fresh thrombus can have a high signal intensity, mimicking that of flowing blood, resulting in missed diagnosis of sinus thrombosis [13]. However, we found that in evaluating the original sections of the MR angiographic sequences, we had no difficulty in differentiating between thrombus and the laminar flow of blood.

Despite the reasonable anatomic correlation of MR angiographic findings with DSA findings, MR angiography is not likely to be sufficient for the preoperative staging of aneurysms. At the current state of the art, small vessels arising near an aneurysm, knowledge of which is crucially important in planning neurosurgical strategies, are likely to be missed [10, 14].

For the evaluation of MR angiograms, rotatable projection images in two planes are recommended, and the original data set as well as conventional MR images should be included. This reduces the risk of overestimating the degree of a stenosis or underestimating the size of an aneurysm. The cine technique facilitates detection of vessels, because superimposed vessels can be easily distinguished from one another and their identification verified by rotating the images.

Use of contrast material contributed little to the visualization of intracranial vessels in MR angiography. Whereas 3D FLASH sequences required gadopentetate dimeglumine injection for depiction of vessels, 3D FISP and 2D FLASH did not. Use of contrast material improves the depiction of vessels only in patients with an intact blood-brain barrier, that is, when contrast material remains intravascular [16]. In patients with tumor, contrast-enhanced MR angiography can be an excellent tool for visualizing the lesion and adjacent vessels, but is not applicable for tumors with strong contrast enhancement or tumors lying near the nasal cavity, as the high signal intensity of the lesion or the mucosal tissue can interfere with the vascular signal.

As a noninvasive technique, MR angiography can be added to routine MR imaging, providing additional information about intracranial vessels and soft tissues in a single setting. It may be useful as a screening method when vascular disease is suspected, as a mapping technique before surgery or catheterization of abnormal vessels, or as a method for diagnosis and follow-up of sinus thrombi [10, 17]. Additional clinical experience and improvements in flow-compensation technique will expand the role of MR imaging in the diagnosis of intracranial vascular abnormalities.

REFERENCES

1. Brown DG, Riederer SJ, Jack CR, Farzaneh F, Ehman RL. MR angiography with oblique gradient-recalled echo technique. *Radiology* **1990**;176:461–466
2. Edelman RR, Mattle HP, Atkinson DJ, Hoogewoud HM. Magnetic resonance angiography. In: *Cardiovascular imaging: ARRS categorical course syllabus*. Reston, VA: American Roentgen Ray Society, **1990**:51–60
3. Krayenbühl H, Yasargil MG. *Zerebrale Angiographie für Klinik und Praxis*. Stuttgart: Thieme Verlag, **1979**:71–211
4. Edelman RR, Wentz KU, Mattle HP, et al. Intracerebral arteriovenous malformations: evaluation with selective MR angiography and venography. *Radiology* **1989**;173:831–837
5. Edelman RR, Hesselink JR. *Clinical magnetic resonance imaging*. Philadelphia: Saunders, **1990**:110–182
6. Angiography Numaris II/Version A 2.1. In: *Magnetom SP user guide*, 5th ed. Erlangen, Germany: Siemens AG, **1990**
7. Ehricke H-H, Laub G. Integrated 3D display of brain anatomy and intracranial vasculature in MR imaging. *J Comput Assist Tomogr* **1990**;14:846–852
8. Lissner J, Seiderer M. *Klinische Kernspintomographie*. Stuttgart: Ferdinand Enke Verlag, **1990**:59–83, 570–607
9. Masaryk TJ, Modic MT, Ruggieri PM, et al. Three-dimensional (volume) gradient-echo imaging of the carotid bifurcation: preliminary clinical experience. *Radiology* **1989**;171:801–806
10. Sevick RJ, Tsuruda JS, Schmalbrock P. Three-dimensional time-of-flight MR angiography in the evaluation of cerebral aneurysms. *J Comput Assist Tomogr* **1990**;14:874–881
11. Marchal G, Bosmans H, Van fraeyenhoven L, et al. Intracranial vascular lesions: optimization and clinical evaluation of three dimensional time-of-flight MR angiography. *Radiology* **1990**;175:443–448
12. Bongartz G, Vestring TH, Fahrendorf G, Peters PE. Einsatz schneller Sequenzen bei der kraniozerebralen MR-Diagnostik. *Fortschr Röntgenstr* **1990**;153:669–677
13. Nadel L, Braun IF, Kraft KA, Fatouros PP, Laine FJ. Intracranial vascular abnormalities: value of MR phase imaging to distinguish thrombus from flowing blood. *AJNR* **1990**;11:1133–1140
14. Peters PE, Bongartz G, Drews C. Magnetresonanzangiographie der hirnversorgenden Arterien. *Fortschr Röntgenstr* **1990**;152:528–533
15. Anderson C, Saloner D, Tsuruda J, Shapeero LG, Lee RE. Artifacts in maximum-intensity-projection display of MR angiograms. *AJR* **1990**;154:623–629
16. Creasy JL, Price RR, Presbrey TH, Goins D, Partain CL, Kessler RM. Gadolinium-enhanced MR angiography. *Radiology* **1990**;175:280–283
17. Schuierer G, Laub G, Huk WJ. MR angiography of the primitive trigeminal artery: report on two cases. *AJNR* **1990**;11:1131–1132

Book Review

Ultrasonography of Infants and Children. By Rita Littlewood Teele and Jane Chrestman Share. Philadelphia: Saunders, 534 pp., 1991. $95

Drs. Teele and Share from Boston Children's Hospital have succeeded in producing an outstanding text. Problem-oriented topics include urinary tract infection, abdominal mass, abdominal pain, blunt abdominal trauma, intraabdominal infection, and liver transplantation. Anatomic topics covered are cranial and spinal sonography, intraoperative neurosonography, face and neck, chest, extremities, gastroduodenal region, spleen, and liver.

A combination of the problem-oriented approach with the traditional anatomic review has produced a text that is eminently useful and relatively complete. The logic of the problem-oriented approach makes the information in the book easier to read, understand, and retain. It is obvious that the authors are highly clinically oriented and have examined a large number of children over many years. Thus, they write with experience and wisdom. The text is filled with suggestions on how to obtain the best results technically, which anatomic regions need to be defined, and what anatomic information is needed to answer all aspects of a clinical problem.

The authors maintain a nice balance between the value of sonography and the value of other imaging techniques. A tantalizing technique is sometimes used to explore the full capability of sonography. For example, the authors acknowledge that CT is the examination of choice for a child with blunt abdominal trauma; however, the supposition is made that sonography is the only technique available. To what extent can information obtained with sonography answer the clinically relevant issues?

Criticisms of this text are minor. The color Doppler illustrations are isolated in the front of the book without accompanying text. Also it is sometimes difficult to locate specific diseases, as some of the problem-oriented chapters lack subheads.

In summary, this book is both a necessity and a luxury for any radiologist whose practice includes imaging of infants and children. I also highly recommend it to residents in training and as a reference text for pediatricians and family practice physicians.

Saskia v. W. Hilton
San Diego, CA 92106

Sonographic Diagnosis of Intestinal Malrotation in Infants:

Importance of the Relative Positions of the Superior Mesenteric Vein and Artery

Ed Weinberger[1]
William D. Winters
Robert M. Liddell
David M. Rosenbaum
Dale Krauter

OBJECTIVE. An abnormal relative position of the superior mesenteric vein and artery can be present in patients with intestinal malrotation. We undertook this retrospective study to see how often we could determine the relative position of these vessels on abdominal sonograms in infants and how often abnormal position of the vessels was associated with malrotation.

MATERIALS AND METHODS. We reviewed the radiology files and medical records of 337 infants with vomiting who were referred for sonography because of possible pyloric stenosis. We used sonograms and written reports to determine the position of the superior mesenteric vessels. The position was considered normal when the superior mesenteric vein was to the right of the superior mesenteric artery on transverse sonograms. The position was considered abnormal when the vein was directly ventral to the artery or when the vein was to the left of the artery. Sonographic findings were compared with results of upper gastrointestinal series when possible and with clinical outcome.

RESULTS. The relative positions of the superior mesenteric vein and artery were evident in 249 (74%) of the 337 patients. Abnormal orientation of the mesenteric vessels was detected in nine patients. In five patients, the superior mesenteric vein was located to the left of the artery, and all five had intestinal malrotation. In four patients, the superior mesenteric vein was directly ventral to the artery, and one of these had malrotation.

CONCLUSION. Sonographic assessment of the relative positions of the mesenteric artery and vein is an important adjunct in the examination of infants with suspected pyloric stenosis. Patients in whom sonograms show an abnormal position of the vessels should have further examination to detect malrotation.

AJR **159:825–828, October 1992**

Abnormal orientation of the superior mesenteric vessels has been reported in patients with intestinal malrotation [1–5] with the superior mesenteric vein (SMV) immediately ventral (anterior) to the superior mesenteric artery (SMA), or the SMV to the left of the SMA. During the past several years, we have included sonographic assessment of the positions of the SMA and SMV as part of our routine workup for infants having sonography because of possible pyloric stenosis. We undertook this retrospective study to see how often an abnormal orientation of the SMV and SMA could be detected in these infants and how often such an abnormal orientation was associated with intestinal malrotation. Because intestinal malrotation can become a life-threatening emergency if the common complications of obstruction by Ladd's bands or midgut volvulus are not detected and treated promptly, early diagnosis of this disorder is important.

Materials and Methods

During a 2½ year period, 343 patients at our hospital had 353 sonographic examinations because of suspected pyloric stenosis. Ten patients had two examinations (the second one

Received February 26, 1992; accepted after revision April 13, 1992.

[1] All authors: Departments of Radiology, University of Washington, School of Medicine, Seattle, WA 98195, and Children's Hospital and Medical Center, 4800 Sand Point Way, N.E., Seattle, WA 98105. Address reprint requests to E. Weinberger at Children's Hospital and Medical Center.

0361-803X/92/1594-0825
©American Roentgen Ray Society

usually after surgery for pyloric stenosis), and the results of these second examinations were excluded from our study. Six patients' sonograms or charts were unavailable for review, and these patients also were excluded. The remaining 337 sonographic studies in 337 patients formed the basis of our investigation. We follow a standard technique for sonographic examination of the abdomen [6]. We also attempt to visualize the SMV and SMA by placing the transducer ventral to the mesenteric vessels and assessing their orientation as far caudal to the confluence of the portal and splenic veins as possible. The position of the SMV was considered normal when the vein was located laterally to the right of the SMA. The position was considered abnormal when the vein was located ventral to or laterally to the left of the SMA. Patients whose sonograms showed that the positions of the vessels were abnormal then had an upper gastrointestinal series. At our hospital, an upper gastrointestinal series is the procedure of choice for an infant with suspected malrotation, volvulus, or both. Sonography is the first and usually the only imaging study done when pyloric stenosis is suspected because of clinical findings or when the clinician wants to rule out pyloric stenosis in an infant with nonbilious vomiting.

For our retrospective study, the radiology files and medical records of all 337 patients were reviewed. All of the sonograms were reviewed and compared with the written report of the study with regard to the positions of the SMV and the SMA.

The study population included 239 boys and 98 girls. Mean age of the patients was 6.6 weeks (range, 2–218 days); 127 had pyloric stenosis, and 210 did not.

Results

The relative positions of the SMV and SMA were evident from the sonograms or the written reports in 249 (74%) of 337 patients. In 56 patients (17%), bowel gas prevented adequate visualization of the vessels. In 32 patients (9%), neither the sonograms nor the written report included mention of the vessels (26 of these 32 patients had pyloric stenosis, so the examination may have been abbreviated).

Abnormal orientation of the mesenteric vessels was detected in nine of the 249 patients in whom the relationship of the vessels could be evaluated. In five of these patients, the SMV was located to the left of the SMA; all five had intestinal malrotation. One patient had had surgery for malrotation and midgut volvulus (results of an upper gastrointestinal series confirmed malrotation but without obstruction). One patient had had repair of a gastroschisis on the day of birth and had pyloric stenosis (Fig. 1). The other three patients had unsuspected intestinal malrotation confirmed by subsequent upper gastrointestinal series. Two of these had obstruction due to Ladd's bands and had immediate surgical repair (Fig. 2); one had microgastria and had malrotation without obstruction (Fig. 3).

In four of the patients, the SMV was ventral to the SMA. All four patients had upper gastrointestinal series. One of the four had malrotation and obstruction due to Ladd's bands and had immediate surgical repair (Fig. 4). (A history of bilious vomiting, not known at the time of sonography, was noted in retrospective review of this patient's medical chart.) Another had small-bowel obstruction as a result of adhesions from previous surgical repair of an inguinal hernia. The other two patients had no evidence of malrotation as shown by upper gastrointestinal series and are clinically well.

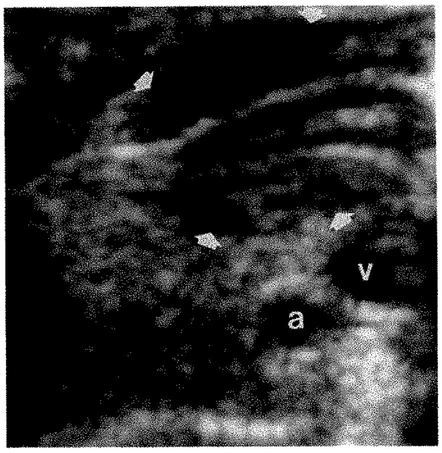

Fig. 1.—24-day-old boy who had nonbilious projectile vomiting for 36 hr. Transverse sonogram shows superior mesenteric vein (v) to left of superior mesenteric artery (a). Lumen of superior mesenteric artery can be recognized by surrounding rim of echogenicity. Note thick pyloric muscle (*arrowheads*). Patient had pyloromyotomy for pyloric stenosis. Intestinal malrotation was substantiated during surgical repair of gastroschisis on day of birth.

Of the 240 patients in whom the SMV was to the right of the SMA, 37 (15%) had upper gastrointestinal series, which showed no evidence of malrotation.

Discussion

Intestinal malrotation encompasses a wide spectrum of embryologic failures of rotation and fixation of the gut, resulting in a narrow-based attachment of the mesentery and the presence of abnormal peritoneal (Ladd's) bands that represent indirect attempts at fixation [4]. These abnormalities predispose to midgut volvulus and obstruction. Although most patients have bilious vomiting and signs of obstruction in the first few months of life [7–9], some may remain asymptomatic or have atypical clinical findings that may be misleading [4, 9]. In this last group of patients, earlier diagnosis might prevent complications of malrotation, including bowel ischemia, necrosis, and death. We were able to detect intestinal malrotation correctly on sonograms in four patients in whom this problem was not suspected, and in only one of these patients did a review of the chart suggest bilious vomiting.

In 1983, Nichols and Li [1] described three adults in whom CT showed that the SMV was located on the left ventral aspect of the SMA instead of the right ventral aspect. They termed this finding the "SMV rotation sign"; upper gastrointestinal examinations showed various degrees of intestinal malrotation in all three patients. In 1986, Blumhagen and Weinberger [2] detected the same abnormal position of the two vessels on sonograms of a 15-year-old girl with intestinal malrotation. In 1987, Gaines et al. [3] showed sonographically that the SMV was located directly anterior to or to the left of

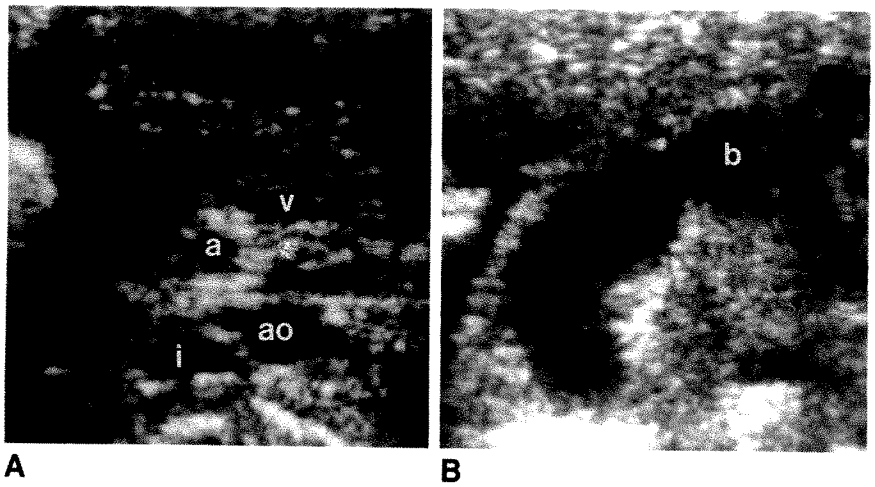

Fig. 2.—18-day-old boy who had intermittent nonbilious vomiting for 48 hr.

***A*, Transverse sonogram below level of confluence of splenic and portal veins shows superior mesenteric vein (v) at left lateral aspect of superior mesenteric artery (a). ao = aorta, i = inferior vena cava.**

***B*, Sonogram shows intermittent distension of duodenum by fluid. b = duodenal bulb.**

After upper gastrointestinal series, surgery confirmed intestinal malrotation with obstruction by Ladd's bands.

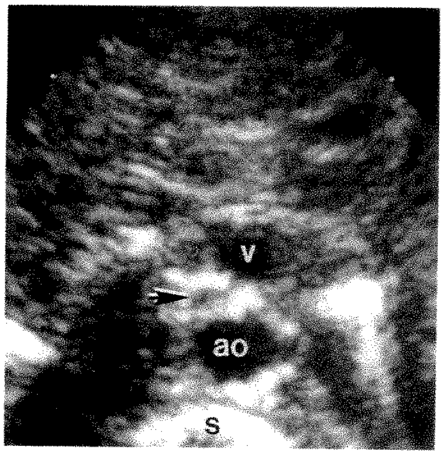

Fig. 3.—10-day-old boy with emesis. Transverse sonogram just below level of confluence of splenic and portal veins shows superior mesenteric vein (v) at left ventral aspect of superior mesenteric artery (*arrowhead*). ao = aorta, s = spine.

Upper gastrointestinal series showed malrotation and microgastria.

the SMA in three children and two adults with known malrotation, as shown by previous upper gastrointestinal series. Gaines et al. also suggested the diagnosis of malrotation on the basis of sonographic findings in an 11-year-old child in whom abnormal orientation of the mesenteric vessels was discovered during sonography done because of urinary tract infection. These studies, as well as ours, suggest that using sonography to evaluate the relationship between the SMV and the SMA may be helpful in the diagnosis of unsuspected intestinal malrotation.

Malrotation was present in all our patients in whom the SMV was located to the left of the SMA; and although this seems to be the rule [1-5], it is not always the case. Zerin and DiPietro [10] described a 20-year-old patient in whom CT scans showed that the SMV was to the left of the SMA but in whom upper gastrointestinal series did not show malrotation. Conversely, normal orientation of mesenteric vessels (SMV to the right of SMA) does not ensure normal intestinal rotation, even though this was seen in our patients who had subsequent upper gastrointestinal series. Leiberman and Haaga [11] described a patient with malrotation shown by upper gastrointestinal series in whom CT scans showed normal orientation of mesenteric vessels. Finally, the finding of the SMV directly ventral to the SMA is probably indeterminate for malrotation; one of our four patients with this vascular relationship had malrotation. If we had been able to scan farther caudally in the patients without malrotation, we might have found that the SMV was to the right of the SMA more inferiorly.

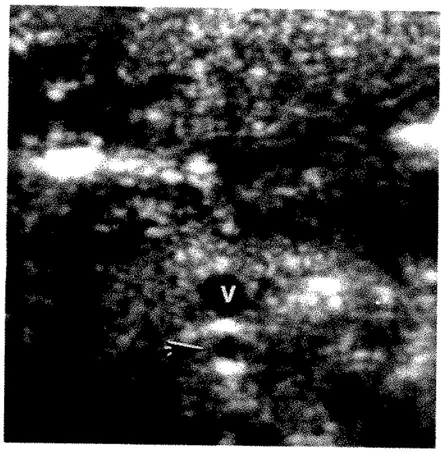

Fig. 4.—Transverse sonogram shows superior mesenteric vein (v) ventral to superior mesenteric artery (*arrowhead*). Upper gastrointestinal series showed duodenal obstruction. At surgery, malrotation with Ladd's bands was found.

Sonographic assessment of the orientation of mesenteric vessels must be done with great care. Two important points in technique are worth mentioning. First, *scanning must be* done as far caudally as possible from the confluence of the splenic and portal veins, because at this level the SMV may be almost directly ventral to the SMA, resulting in an incorrect diagnosis of abnormal orientation of mesenteric vessels. Second, the transducer must be placed in the midline directly anterior to the vessels in order to assess orientation correctly. As the vessels may be obscured by gas, it is often tempting to move the transducer to the right of midline to use the liver as an acoustic window. This, however, results in the SMV appearing to have a more leftward or clockwise orientation with respect to the SMA, resulting in an incorrect diagnosis of abnormal orientation.

We do not think that sonography should replace upper gastrointestinal examination for the diagnosis of intestinal malrotation. Rather, sonographic assessment of the relationship of the mesenteric vessels may provide useful information in patients with intestinal malrotation who are asymptomatic or have atypical signs and symptoms. Specifically, our study suggests that sonographic assessment of the relationship of the mesenteric vessels is an important adjunct in the evaluation of the young child who has signs suggestive of pyloric stenosis. When the position of the SMV with respect to the SMA is abnormal, further evaluation via an upper gastrointestinal series is warranted.

REFERENCES

1. Nichols DM, Li DK. Superior mesenteric vein rotation: a CT sign of midgut malrotation. *AJR* **1983**;141:707–708
2. Blumhagen JD, Weinberger E. Pediatric gastrointestinal ultrasonography. In: Sanders RC, Hill M, eds. *Ultrasound annual.* New York: Raven, **1986**:99–140
3. Gaines PA, Saunders AJS, Drake D. Midgut malrotation diagnosed by ultrasound. *Clin Radiol* **1987**;38:51–53
4. Loyer E, Eggli KD. Sonographic evaluation of superior mesenteric vascular relationship in malrotation. *Pediatr Radiol* **1989**;19:173–175
5. Shatzkes D, Gordon DH, Haller JO, Kantor A, DeSilva R. Malrotation of the bowel: malalignment of the superior mesenteric artery-vein complex shown by CT and MR. *J Comput Assist Tomogr* **1990**;14:93–95
6. Blumhagen JD, Maclin L, Krauter D, Rosenbaum DM, Weinberger E. Sonographic diagnosis of hypertrophic pyloric stenosis. *AJR* **1988**;150:1367–1370
7. Stewart DR, Colodny AL, Daggett WC. Malrotation of the bowel in infants and children: a 15 year review. *Surgery* **1976**;79:716–720
8. Andrassy RJ, Mahour GH. Malrotation of the midgut in infants and children: a 25-year review. *Arch Surg* **1981**;116:158–160
9. Spigland N, Brandt ML, Yazbeck S. Malrotation presenting beyond the neonatal period. *J Pediatr Surg* **1990**;25:1139–1142
10. Zerin JM, DiPietro MA. Mesenteric vascular anatomy at CT: normal and abnormal appearances. Radiology **1991**;179:739–742
11. Lieberman JM, Haaga JR. Duodenal malrotation. *J Comput Assist Tomogr* **1982**;6:1019–1020

Pictorial Essay

Sonography of the Elbow in Infants and Children

Richard I. Markowitz,[1] Richard S. Davidson,[2] M. Patricia Harty,[1] Richard D. Bellah,[1] Anne M. Hubbard,[1] and Henrietta Kotlus Rosenberg[1]

High-resolution real-time sonography of the musculoskeletal system of infants and young children is being used with increasing frequency, in part because of the inability of plain film radiography to visualize unossified cartilage. Real-time sonography now plays an important role in the evaluation of infantile hip dysplasia, as well as in the identification and aspiration of joint effusion. The purpose of this essay is to illustrate clinical situations in which sonography of the elbow is helpful.

Technique and Limitations

Sonography was performed with an Advanced Technology Laboratories (ATL) (Bothell, WA) UltraMark 5 real-time sonographic unit equipped with a 7.5-MHz linear array transducer. The elbow was studied in multiple sagittal, coronal, and transverse planes from the anterior, posterior, medial, and lateral aspects. Dynamic real-time scanning was performed with the patient's arm flexed and extended, as well as with pronation and supination of the forearm. Sonograms of the asymptomatic side were obtained for comparison.

Limitations of sonography, when compared with plain film radiography, include the planar nature of the technique, the barrier to transmission of the ultrasound beam by ossified cortical bone, operator dependency, longer examination time, and greater cost. Despite less spatial resolution than that of conventional radiography, the ability to dynamically delineate cartilage and soft tissue in detail is the single greatest advantage of sonography.

Clinical Indications

Reasons to examine a patient with sonography include pain, limitation of motion, trauma, nonspecific soft-tissue swelling, vascular malformation, and clinical suspicion of joint abnormality when findings on plain films are inconclusive. The most frequently asked clinical questions are (1) Is there a fracture or dislocation present that is not visualized on plain films? (2) Does an infection involve the joint space or deep soft tissues? (3) Why is movement of the elbow limited?

Normal Anatomy

Because of the planar nature of sonography, multiple images are necessary to show the various anatomic features of the elbow joint [1] (Figs. 1 and 2). The posterior, sagittal, midline view of the distal humerus is most useful in cases of transphyseal fracture. On this view, it is helpful to think of the posterior aspect of the distal humeral shaft as a shallow spoon containing the echogenic fat pad. The unossified cartilaginous ball of the trochlea lies just below the tip of the spoon (Figs. 2 and 3). The unossified epiphysis of the olecranon of the ulna moves in and out of the fossa as the elbow flexes and extends.

Soft-Tissue Swelling (Cellulitis)

In cases of suspected cellulitis, radiographs often show nonspecific soft-tissue swelling and normal bones. Sonogra-

---

Received January 17, 1992; accepted after revision March 11, 1992.

[1] Department of Radiology, The Children's Hospital of Philadelphia, 34th St. and Civic Center Blvd., Philadelphia, PA 19104. Address reprint requests to R. I. Markowitz.

[2] Department of Orthopedics, The Children's Hospital of Philadelphia, Philadelphia, PA 19104.

AJR 159:829-833, October 1992 0361-803X/92/1594-0829 © American Roentgen Ray Society

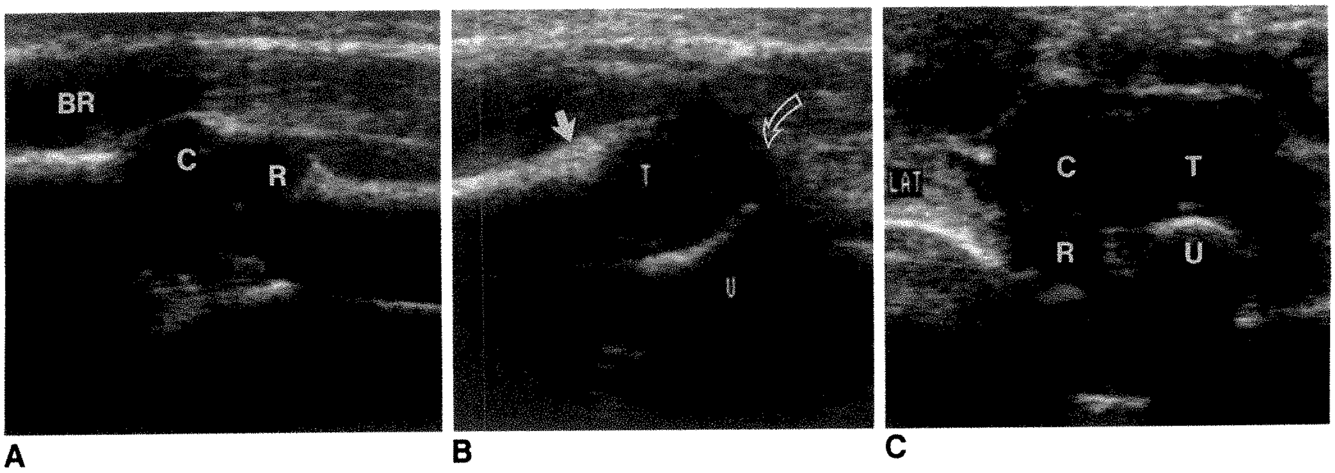

Fig. 1.—Sonograms of normal elbow in a 2-month-old girl.

A, Lateral coronal image shows brachioradialis muscle (BR) superficial to distal humerus and unossified capitellum (C), which articulates with unossified, hypoechoic radial head (R). Metaphysis and proximal shaft of radius are on right side. (All longitudinal images show proximal end on left and distal end on right.)

B, Sagittal anteromedial image shows anterior surface of distal humerus on left side to which round ball of unossified trochlea (T) is attached. A small, echogenic anterior fat pad (*solid arrow*) lies deep to pronator teres muscle. Notch of proximal ulna (U) is seen as a curved white line upon which rests unossified, hypoechoic coronoid process (*open arrow*).

C, Anterior transverse image obtained at elbow joint shows flattened, ovoid shape of unossified humeral epiphysis. Cartilaginous radial head (R) articulates with capitellum (C) and echogenic surface of ossified ulna (U) articulates with trochlea (T). Lateral aspect is on left and medial aspect is on right.

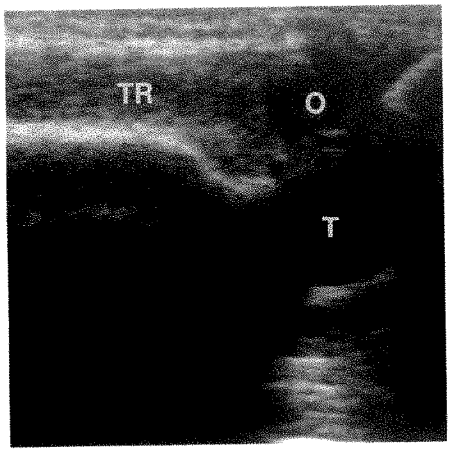

2

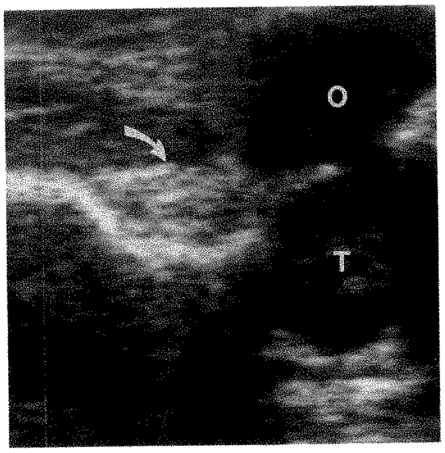

3

Fig. 2.—Sonogram of normal elbow in a newborn girl. Posterior sagittal view through midplane of extended elbow shows straight surface of distal humeral shaft leading to curved indentation of olecranon fossa in which lies echogenic posterior fat pad. Round, hypoechoic trochlea (T) lies deep to unossified olecranon (O) to which triceps muscle (TR) is attached.

Fig. 3.—Sonogram of normal elbow in a 3-month-old boy. Posterior, sagittal, midline sonogram of distal humerus shows spoonlike contour of olecranon fossa (containing echogenic fat pad, *arrow*) and unossified trochlea (T) in shape of a ball situated at tip of spoon. Note that although ultrasound beam is transmitted through unossified olecranon (O) and trochlea, signal is absent proximally owing to dense calcification of cortical bone.

phy can show extraarticular soft-tissue swelling with obliteration of the normal fascial planes and increased tissue echogenicity when compared with the adjacent normal soft tissues (Fig. 4). If the joint space and deep soft tissue next to bone appear normal, one may conclude that the patient has cellulitis and does not have a fracture, osteomyelitis, or septic arthritis. Clinical and radiographic findings on follow-up examination in such cases should be consistent with cellulitis.

The ability to distinguish superficial soft-tissue inflammation from bone or joint disease is thus helpful in making clinical management decisions. We did not study any patients with osteomyelitis, but we agree with others [2] who believe that high-resolution sonography has potential in differentiating deep from superficial inflammation. Confirming the absence of a joint effusion can spare these children unnecessary attempts at needle aspiration.

Fractures

Recognition of significant bone or joint injury in the infant or young child is limited by the inability to directly visualize the large, cartilaginous epiphyses on plain film radiographs. Figures 5 and 6 show examples of transphyseal fractures of the distal humerus in infants that either were mistaken for dislocation or were not recognized as significantly displaced and/or unstable on radiographs. We defined instability as failure to maintain satisfactory reduction and diagnosed it when unacceptable motion at the fracture site during real-

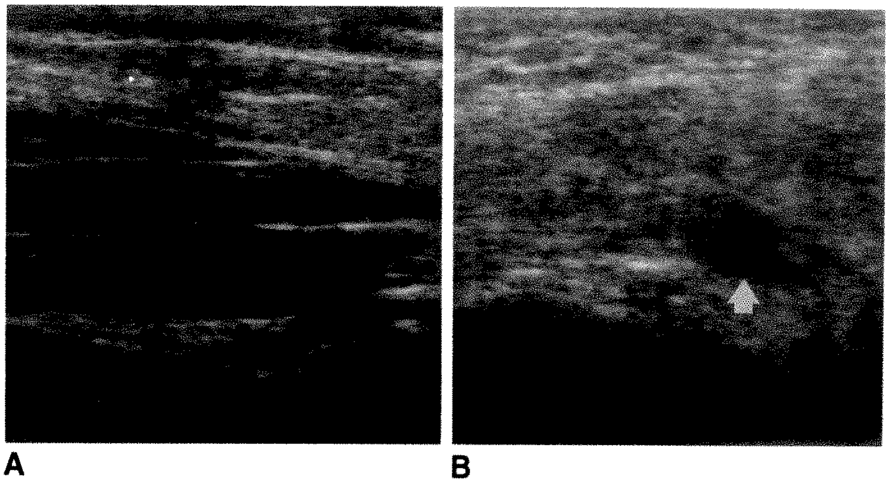

Fig. 4.—Sonograms of a 12-year-old boy with cellulitis. (Radiographs showed normal bones.)

A, Lateral coronal image shows normal deep soft tissue and muscles. Superficially and to right side, fascial planes are disrupted and tissue appears more echogenic.

B, Detailed view of inflamed and edematous superficial tissues shows a mottled pattern of echogenicity with obliteration of normal fascial planes. Focal hypoechoic area suggests a swollen lymph node (*arrow*).

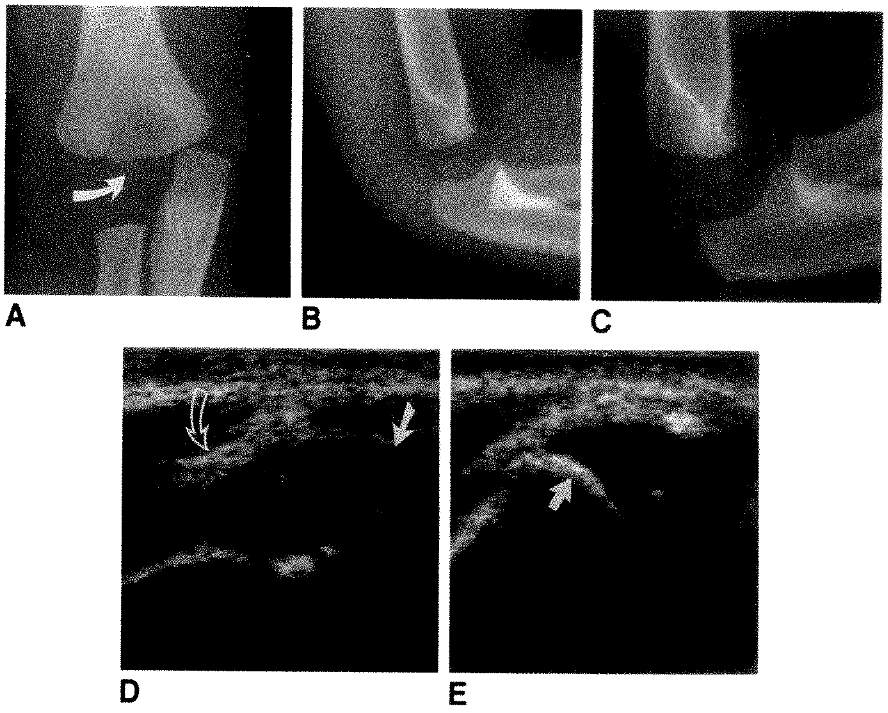

Fig. 5.—Radiographs and sonograms of 17-month-old boy with transphyseal fracture of distal humerus.

A, Frontal radiograph of forearm shows soft-tissue swelling around elbow and medial displacement of radius and ulna. Note how close secondary ossification center of capitellum (*arrow*) is to edge of metaphysis.

B and *C*, Lateral radiograph (*B*) shows mild posterior displacement of capitellum and extensive soft-tissue swelling posteriorly. Compare with normal opposite side (*C*).

D, Sagittal, posterior, midline sonogram of distal humerus shows complex fluid in olecranon fossa displacing fat pad (*open arrow*). Instead of normal trochlea, hypoechoic cartilage of capitellum (*solid arrow*) is seen and is displaced posteriorly.

E, Posterolateral sonogram after reduction shows capitellum back in its normal position. Physis (*arrow*) is slightly widened and more echogenic than it should be owing to a small amount of blood in fracture line.

time sonography was observed. Intraoperative real-time sonographic examination with the patient anesthetized can help the orthopedic surgeon understand the anatomic derangement and achieve optimal reduction without arthrography, which is invasive and increases the risk of infection. Similarly, other authors have found this technique useful in the diagnosis of epiphyseal fracture [3].

Joint Effusion

Although the fat-pad sign on radiographs is specific for effusion, sometimes it is difficult to detect because of difficulty in positioning a child who will not bend the elbow, or because there is so much soft-tissue swelling that the fat pads cannot be discerned. In these situations, sonography is an easy way to visualize an effusion and show its extent [4]. Figure 7 shows a large hemarthrosis in a 10-year-old boy who had sustained an avulsion fracture of the lateral epicondyle. Figure 8 shows a small effusion. Figure 9 shows a vascular malformation of the soft tissues, which on sonography did not involve the elbow joint.

In summary, as illustrated here, high-resolution sonography of the elbow in infants and children is helpful in those cases in which radiographs are either equivocal, inconclusive, or nonspecific, and in which depiction of the unossified cartilage and soft tissue will yield definitive diagnostic information.

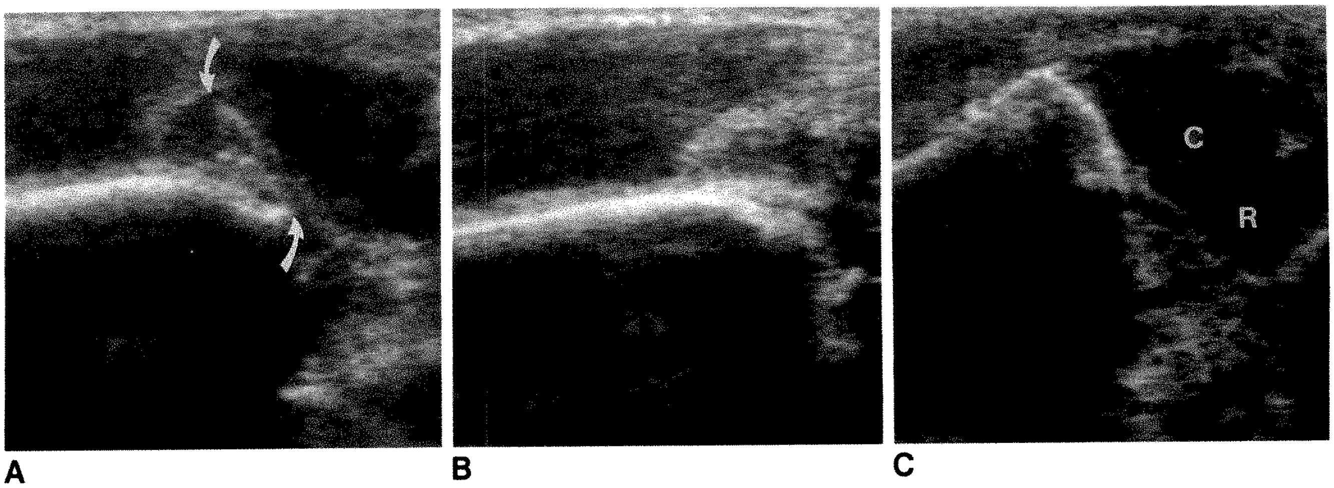

Fig. 6.—Sonograms of a newborn boy with transphyseal fracture of distal humerus.

A, Posterior, sagittal, midline image of distal humerus before reduction shows posterior displacement of hypoechoic epiphysis. Note extensive hyperechoic soft-tissue hematoma in and around end of bone. Malaligned fracture edges are indicated with *arrows*.

B, Posterior, sagittal midline view after reduction shows cartilage (trochlea) has returned to an almost normal position.

C, Posterolateral, sagittal image after reduction shows intact capitellum (C)–radial head (R) articulation. Distal humeral physis is markedly echogenic.

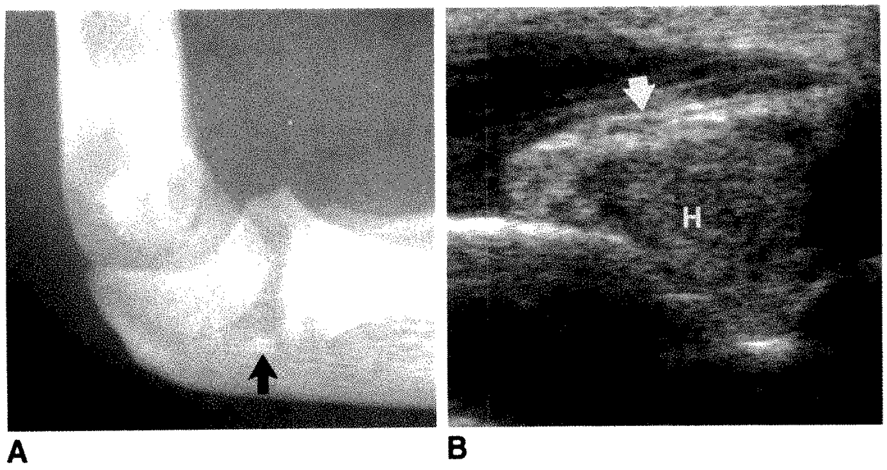

Fig. 7.—Radiograph and sonogram of 10-year-old boy with avulsion fracture and hemarthrosis.

A, Lateral radiograph shows displacement of anterior and posterior fat pads due to a large hemarthrosis. Note small, displaced bone fragment (*arrow*).

B, Posterior sagittal sonogram of distal humerus depicts echogenic fat pad (*arrow*) displaced out of olecranon fossa by a large, moderately echogenic hemarthrosis (H).

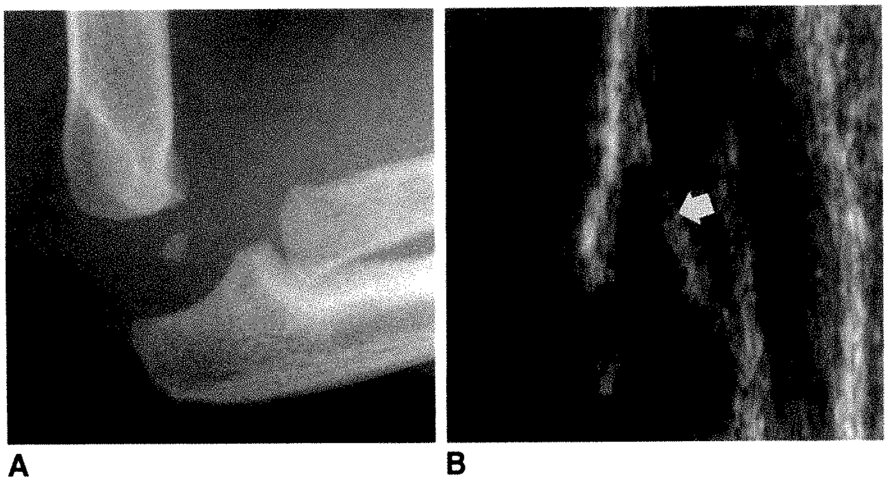

Fig. 8.—Radiograph and sonogram of 16-month-old boy with limited range of motion of elbow after falling.

A, Lateral radiograph of elbow shows mild displacement of fat pads. No fracture is seen.

B, Corresponding anterior sagittal sonogram of distal humerus shows a small effusion elevating anterior fat pad (*arrow*). Ossification center of capitellum lies deep within cartilage and lines up appropriately with shaft of humerus. Osseous-cartilaginous interface is intact.

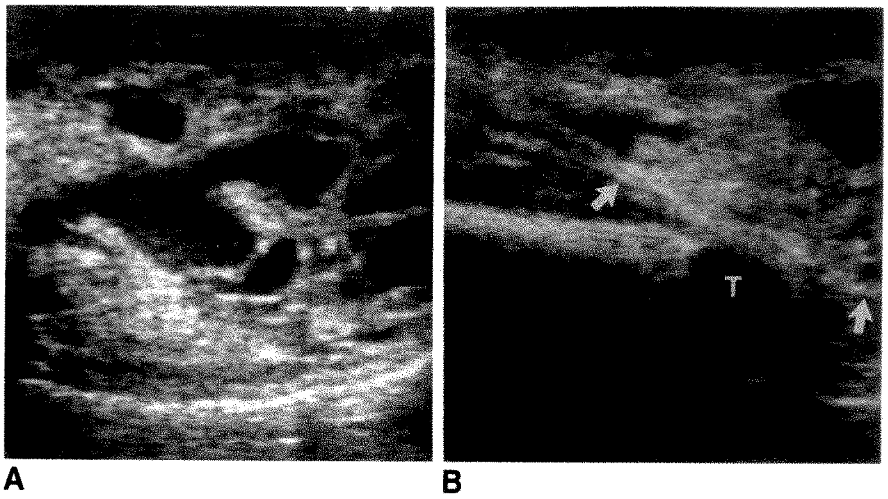

Fig. 9.—Sonograms of a 3-month-old boy with subcutaneous vascular malformation of the forearm and elbow.

***A,* Sagittal view shows mass comprising large and small vascular spaces with intervening echogenic tissue. Color Doppler flow sonogram (*not shown*) confirmed presence of venous flow.**

***B,* Anterior sagittal image of elbow shows sparing of periarticular structures, which lie deep to mass (*arrows*) and are neither infiltrated nor distorted by vascular malformation. (T = trochlea)**

REFERENCES

1. Barr LL, Babcock DS. Sonography of the normal elbow. *AJR* **1991**;157:793–798
2. Abiri MM, Kirpekar M, Ablow RC. Osteomyelitis: detection with US. *Radiology* **1989**;172:509–511
3. Dias JJ, Lamont AC, Jones JM. Ultrasonic diagnosis of neonatal separation of the distal humeral epiphysis. *J Bone Joint Surg* [Br] **1988**;70-B:825–828
4. Miles KA, Lamont AC. Ultrasonic demonstration of the elbow fat pads. *Clin Radiol* **1989**;40:602–604

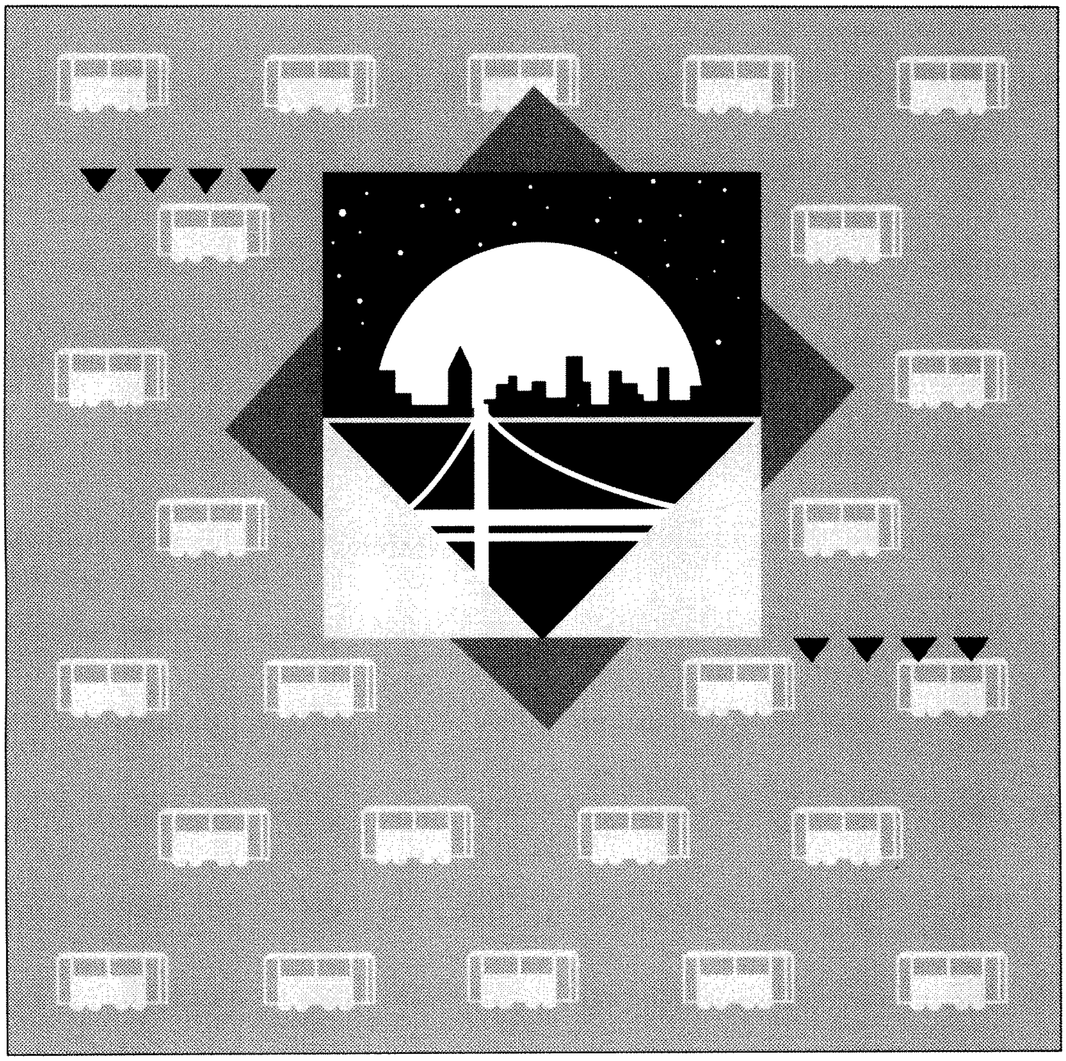

San Francisco

American Roentgen Ray Society

93rd Annual Meeting

April 25–30, 1993

San Francisco Marriott • San Francisco, CA

Case Report

Wilms' Tumor in a Patient with Beckwith-Wiedemann Syndrome: Onset Detected with 3-Month Serial Sonography

Matthew W. Andrews[1] and Eugenio G. Amparo

Beckwith-Wiedemann syndrome is characterized by a group of clinical abnormalities, the most salient being macroglossia, gigantism, and exomphalos. Childhood malignant tumors are a recognized association of Beckwith-Wiedemann syndrome, and Wilms' tumor, in particular, is a frequent occurrence.

An 18-month-old child with Beckwith-Wiedemann syndrome had a Wilms' tumor first detected with abdominal sonography, which had been performed every 3 months since birth for surveillance. This case demonstrates the value of sonographic abdominal surveillance in children with Beckwith-Wiedemann syndrome. We know of no other published reports of development of a Wilms' tumor in an interval as short as 3 months. Because the long-term survival of children with Beckwith-Wiedemann syndrome depends on early detection and treatment of tumors [1], we believe that these children should have abdominal sonographic surveillance at intervals of 3 months or less.

Case Report

Beckwith-Wiedemann syndrome was clinically diagnosed at birth in a male child on the basis of macroglossia, omphalocele, and large birth weight and height. Abdominal sonography at 3 months showed bilateral renal enlargement to greater than the 95th percentile for age without focal abnormalities. Sonographic examination of this patient's abdomen was performed at 3-month intervals. At 18 months, sonography showed a solid mass with a greatest diameter of 3.6 cm in the left kidney (Fig. 1B). The mass had not been present on a sonogram obtained 3 months earlier (Fig. 1A). Subsequent CT evaluation (Fig. 1C) showed that the mass was confined to the kidney, and no metastases were found. Surgery confirmed the abdominal CT findings, and a left-sided total nephrectomy was performed. Examination of the right kidney at surgery showed no focal lesions. Histopathologic studies showed that the lesion in the left kidney was a Wilms' tumor.

Discussion

The long-term survival of patients with Wilms' tumor that is diagnosed early and treated appropriately is good [1]. Early detection of Wilms' tumor, to which patients with Beckwith-Wiedemann syndrome are predisposed, is imperative for a favorable prognosis.

Beckwith-Wiedemann syndrome is a rare syndrome characterized by macroglossia, omphalocele, and splanchnomegaly (kidneys, liver, and spleen). Other associated features, including neonatal hypoglycemia, large birth weight, increased height at birth, hemihypertrophy, craniofacial dysmorphism, microcephaly, other abdominal wall abnormalities (such as umbilical hernia and diastasis of rectus muscles), and midgut malrotation, may be present [2]. The syndrome is caused by an unknown growth disorder resulting in organ hypertrophy and hyperplasia with resultant gigantism. It may exist in complete or incomplete forms that involve single or multiple organs of the whole body or one side of it.

Children with Beckwith-Wiedemann syndrome are predisposed to tumor formation because of focal or diffuse growth

---

Received February 27, 1992; accepted after revision April 10, 1992.

[1] Both authors: Department of Radiology, University of California Davis Medical Center, 2516 Stockton Blvd., TICON II Bldg., Sacramento, CA 95817. Address reprint requests to E. G. Amparo.

AJR 159:835–836, October 1992 0361–803X/92/1594–0835 © American Roentgen Ray Society

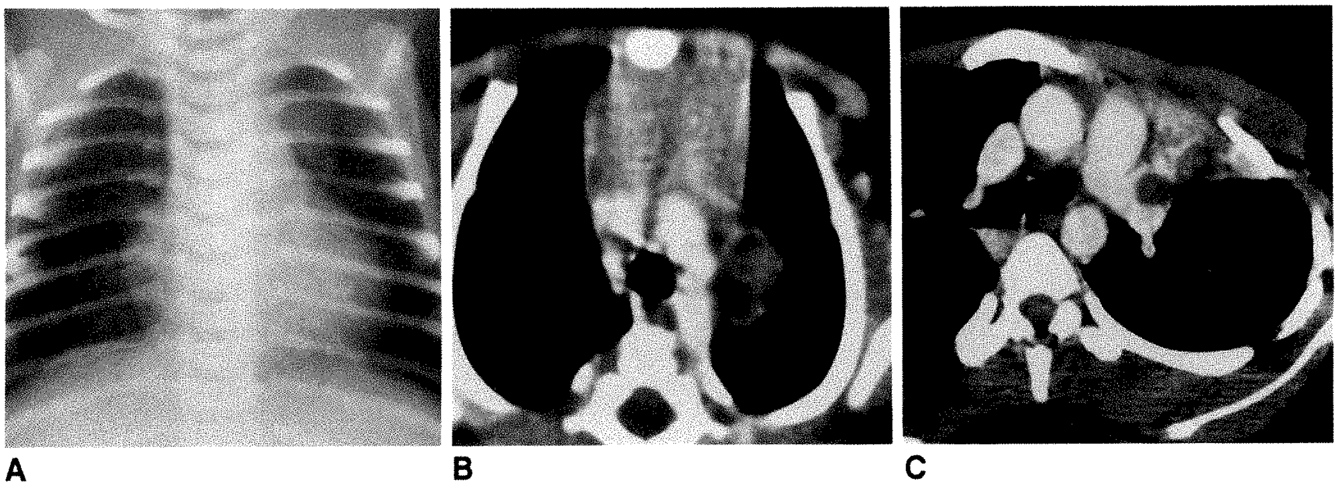

Fig. 1.—Child with Beckwith-Wiedemann syndrome.

***A*, Longitudinal sonogram of left kidney at age 15 months shows no lesion.**

***B*, Longitudinal sonogram of left kidney at age 18 months shows a 3.6 × 2.4 cm well-marginated, hyperechoic lesion (*arrow*) in middle of kidney.**

***C*, Contrast-enhanced CT scan through middle of left kidney at age 18 months shows a well-marginated mass (*arrow*) that is less dense than normal renal parenchyma.**

abnormalities and the associated cellular anaplasia that can accompany hypertrophy and hyperplasia. The prevalence of malignant tumor formation in patients with Beckwith-Wiedemann syndrome has been reported at 6–10% [3]. Most tumors are intraabdominal, most often retroperitoneal. Wilms' tumors, adrenal cortical carcinomas, and hepatoblastomas are the most common malignant tumors, in that order [4]. Risk increases significantly when hemihypertrophy is present [3], and patients with some of the manifestations of Beckwith-Wiedemann syndrome appear to have the same potential for tumor development as those with all of the signs and symptoms [5]. Other tumors reported include rhabdomyosarcoma, glioma, thoracic neural crest tumor, retroperitoneal ganglioneuroma, adrenal adenoma, cardiac hamartoma, cardiac myxoma, and carcinoid of the appendix [2, 5].

The age at which risk for neoplasia returns to close to normal has not been determined, but surveillance for tumor development has been suggested for patients with Beckwith-Wiedemann syndrome up to the age of 12 [3] and adolescence [6]. Most centers carry out surveillance sonography less often after the age of 6 years.

The appearance of Wilms' tumor during sonographic surveillance intervals of 9 and 5 months has been reported by Azouz et al. [3]. On the basis of their findings, they recommend sonography at intervals of 3 months. The appearance of a Wilms' tumor within a 3-month interval between sonograms in this case supports that protocol.

We believe that abdominal sonography should be performed at intervals of 3 months or less in patients with Beckwith-Wiedemann syndrome to detect early Wilms' tumors, thereby optimizing these patients' survival rates. This should form part of a tumor-screening protocol to detect early development of renal, hepatic, adrenal, and neural crest tumors.

REFERENCES

1. Snyder HM III, D'Angio GJ, Evans AE, Raney RB. Pediatric oncology. In: Walsh PC, Gittes RF, Perlmutter AD, Stamey TA, eds. *Campbell's urology*, 5th ed. Philadelphia: Saunders, **1986**:2244–2292
2. Sirinelli D, Silberman B, Baudon JJ, Sinnassamy P, Gruner M, Montagne JP. Beckwith-Wiedemann syndrome and neural crest tumors. *Pediatr Radiol* **1989**;19:242–245
3. Azouz EM, Larson EJ, Patel J, Gyepes MT. Beckwith-Wiedemann syndrome: development of nephroblastoma during the surveillance period. *Pediatr Radiol* **1990**;20:550–552
4. Tank ES, Kay R. Neoplasms associated with hemihypertrophy, Beckwith-Wiedemann syndrome and aniridia. *J Urol* **1980**;124:266–268
5. Sotelo-Avila C, Gonzalez-Crussi F, Fowler JW. Complete and incomplete forms of Beckwith-Wiedemann syndrome: their oncogenic potential. *J Pediatr* **1980**;96:47–50
6. Shah KJ. Beckwith-Wiedemann syndrome: role of ultrasound in its management. *Clin Radiol* **1983**;34:313–319

Case Report

Congenital Portohepatic Vein Fistula That Resolved Spontaneously in a Neonate

Andrew M. Lewis[1] and Norma M. Aquino[2]

Occasionally, reports of anomalous communications between the portal and systemic venous sytems have been published [1-7]. Of these, only two [2, 3] claim that the abnormality is congenital. The first series [2], which included a 53-year-old man, was published before the advent of modern diagnostic imaging. The second report [3] described this type of anomaly in a 50-year-old woman. No information is available about the natural course of these anomalies. To our knowledge, no report has been published of a congenital portosystemic communication that was diagnosed in a neonate on the basis of findings on duplex color Doppler imaging and was subsequently followed up. We report a portosystemic vein communication in a full-term neonate that was diagnosed by real-time sonography with duplex color Doppler imaging and that resolved spontaneously when the infant was 3 months old.

Case Report

A 2500-g female neonate twin born after 38 weeks' gestation was referred for abdominal sonography because of hyperbilirubinemia and possible sepsis. The delivery had been complicated by premature rupture of membranes. The Apgar scores were 3 at 1 min and 1 at 5 min. Initially, the hematocrit was 0.50 and the level of bilirubin was 0.4 mg/dl (6.8 μmol/l; normal 1.7–20.5 μmol/l). In the course of 1 week the hematocrit increased to 0.65, the bilirubin to 14.5 ml/dl (248 μmol/l), serum level of alanine aminotransferase to 58 U/l (normal, 1-36 U/l), and serum level of aspartate aminotransferase to 174 U/l (normal, 8-33 U/l). Tests for hepatitis B, cytomegalovirus, *Toxoplasma gondii*, rubella, and herpes simplex antigen were negative. Levels of galactose of uridyl transferase and D-L tyrosine were normal.

Initial diagnostic imaging consisted of a normal diisopropyliminodiacetic acid (DISIDA) scan to exclude biliary atresia. Real-time duplex color Doppler sonography showed an anechoic lesion in the anterior segment of the right lobe of the liver that was supplied by a branch of the right portal vein and drained by an enlarged branch of the right hepatic vein (Fig. 1A). Color flow study showed a mixture of blood flow with a to-and-fro movement (Fig. 1B). Doppler imaging with spectral wave analysis confirmed venous flow within the lesion (Fig. 1C). At this time, a technetium sulfur colloid liver spleen study was performed. The findings showed no evidence of portal hypertension or any other structural lesions of the liver or spleen. During the course of the next 4 weeks, the results of liver function tests returned to normal, and the patient was discharged with the diagnosis of idiopathic neonatal hepatitis. Follow-up duplex color Doppler imaging 3 months after discharge showed spontaneous resolution of the portohepatic vein communication (Fig. 1D).

Discussion

Abnormal vascular communications in the liver between the portal system and the hepatic venous drainage system are thought to be relatively rare [4]. Although it has been stated that most of these abnormal vascular communications either occur in patients with cirrhosis [5] or are congenital [6, 7], proof of the congenital nature is tenuous [3]. To our knowledge, this is the first report that describes duplex color Doppler imaging for diagnosis and follow-up of a congenital portohepatic venous fistula that resolved spontaneously.

The left portal vein normally communicates with the systemic venous system as the portal sinus in the fetus, and thus a communication between the left portal vein and the systemic venous system could represent persistence of this channel [8]. However, the right portal vein is not known to have a communication with the systemic venous drainage system. The right and left vitelline veins (embryologic portal

---

Received October 7, 1991; accepted after revision May 7, 1992.

[1] Department of Radiology, Nassau County Medical Center, East Meadow, NY 11554.
[2] Department of Radiology, Harlem Hospital Center, Columbia University College of Physicians and Surgeons, 360 Lenox Ave., New York, NY 10037.

AJR 159:837-838, October 1992 0361-803X/92/1594-0837 © American Roentgen Ray Society

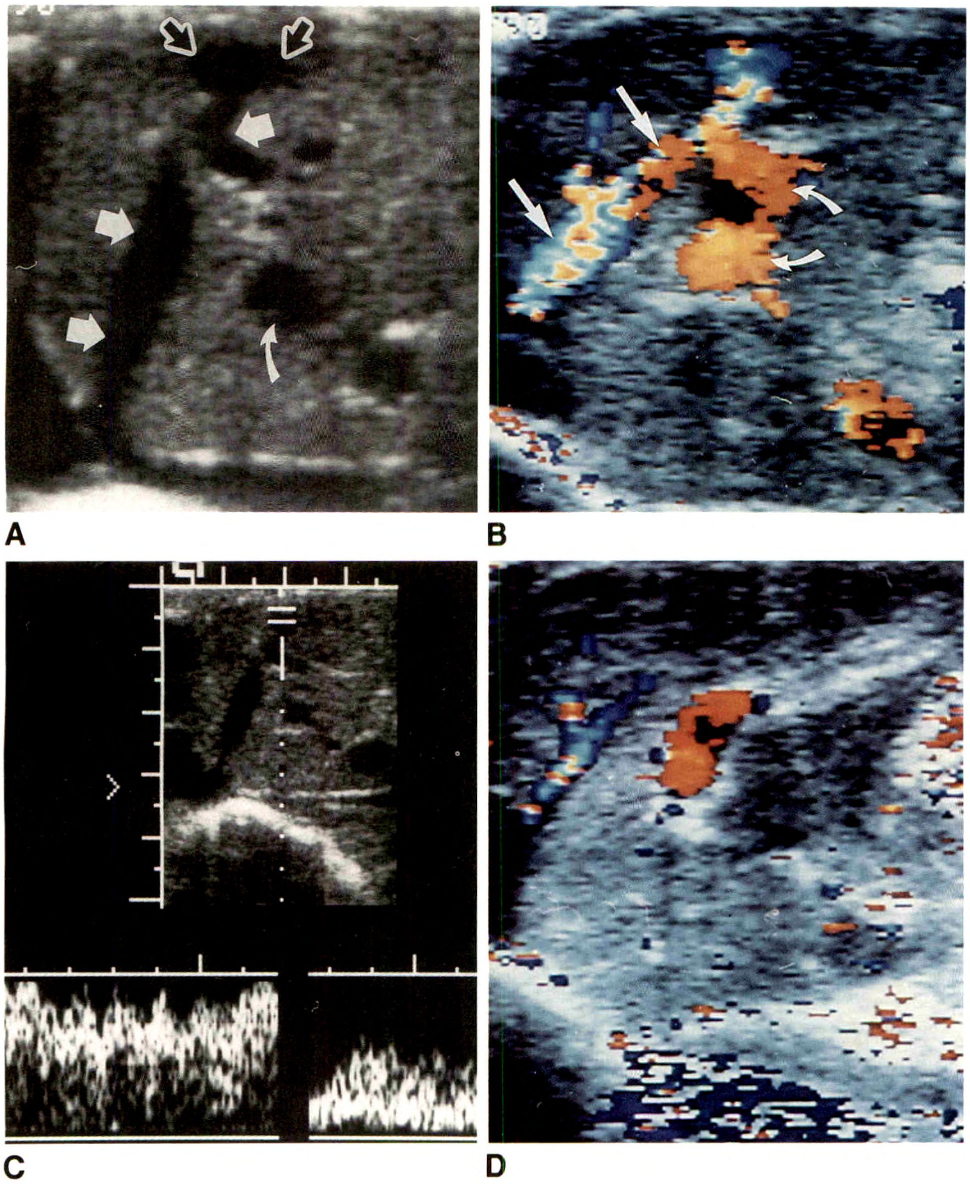

Fig. 1.—*A,* Sagittal sonogram of right lobe of liver shows "cystic"-appearing structure (*black arrows*) with tubular anechoic limbs (*straight white arrows*) just anterior to right portal vein branch (*curved arrow*).

B, Color Doppler sonogram shows vascular nature of structure with inflow (*straight arrows*) and outflow (*curved arrows*) components.

C, Duplex Doppler sonogram shows venous nature of structure.

D, Color Doppler sonogram reveals resolution of previously identified vascular abnormality.

veins) normally involute to form intrahepatic sinusoids, and thus partial persistence of the right vitelline (omphalomesenteric) vein could explain the communication between the right portal vein and the hepatic vein in our patient [3, 5, 7].

This portohepatic venous communication resolved spontaneously when the patient was 12 weeks old. The patient's clinical state became normal and presumably the global hepatic vascular state became normal also. These communications may be more common than previously realized, but they may not be seen later in life because they resolve spontaneously. With the advent of easy and noninvasive sonographic examination of the liver vasculature, more information on these and other congenital vascular anomalies will become available.

ACKNOWLEDGMENT

We thank June Marck for her assistance in the preparation of this manuscript.

REFERENCES

1. Doehner GA, Ruzicka FF Jr, Rousselot LM, Hoffman G. The portal venous system: on its pathological roentgen anatomy. *Radiology* **1956**;77:206–217
2. Raskin NH, Price JB, Fishman RA. Portal systemic encephalopathy due to congenital intrahepatic shunts. *N Engl J Med* **1964**;270:225–229
3. Wittich G, Jantsch M, Tscholakoff D. Congenital portosystemic shunt diagnosed by combined real-time and Doppler sonography. *J Ultrasound Med* **1985**;4:315–318
4. Park JM, Cha SM, Man JK, Man MC. Intrahepatic portosystemic venous shunt. *AJR* **1990**;155:527–528
5. Mori H, Hayashi K, Fukuda T, et al. Intrahepatic portosystemic venous shunt: occurrence in patients with and without liver cirrhosis. *AJR* **1986**;149:711–714
6. Chagnon SF, Vallee CA, Barge J, Chevalier LJ, LeGal J, Biery MV. Aneurysmal portohepatic venous fistula: report of two cases. *Radiology* **1986**;159:693–695
7. Ohnishi K, Saito M, Saito M, Terabayashi M, Okuda K. Hepatic encephalopathy associated with extensive portal-hepatic venous shunts: case report. *Am J Gastroenterol* **1985**;80:60–63
8. Arey LB. *Developmental anatomy.* Philadelphia: Saunders, **1974**

Case Report

Aneurysm of a Nonpatent Ductus Arteriosus in a Neonate: CT Findings

Thomas L. Slovis,[1] Manuel P. Meza,[1,2] Frederick E. Rector,[3] and Chung-Ho Chang[4,5]

The differential diagnosis of a middle mediastinal mass in a neonate or young infant includes a wide spectrum of entities: cystic hygroma, aberrant or abnormal vessels, ectopic thymus, duplication cyst, and enlarged lymph nodes. Abnormalities of the ductus arteriosus such as a large patent duct and aneurysms of the duct should be considered within the category of aberrant or abnormal vessels. Inasmuch as the ductal vessel may or may not be functional, enhancement on a CT scan is not mandatory for the diagnosis. We present a case of an aneurysm of a nonpatent ductus arteriosus in a neonate shown by CT.

Case Report

A full-term male neonate had mild respiratory distress at birth, without a history of perinatal asphyxia. A chest radiograph obtained 1 day after birth showed hyperexpansion of the lungs (Fig. 1A) and minimal opacities. A mass was noted in the aorticopulmonary window. The patient improved in the next 5 days and was sent home. A follow-up radiograph obtained 3 weeks later showed no change in the mass, and the infant was referred to Children's Hospital of Michigan for further workup. Dynamic contrast-enhanced CT scans showed a nonenhancing mass extending lateral to the aorta and located between the top of the aortic arch and above the left pulmonary artery—in the aorticopulmonary window (Figs. 1B and 1C). The preoperative differential diagnosis included bronchogenic cyst, foregut duplication cyst, and a complex adenomatoid malformation.

Left-sided lateral thoracotomy was performed and showed that the mass was a large (2 × 1 × 1 cm) aneurysm of the ductus arteriosus. The content of the mass was firm and not pulsatile. Both ends of the ductus were ligated, and the aneurysm was resected. Clot filled the entire mass. The gross pathologic specimen revealed a saccular structure with clot. Histologic examination showed marked irregular fibrous thickening of the intima of the saccular structure and focal disruption and thinning of the underlying muscle layers. Focal destruction of the internal elastic lamina, accompanied by fibrosis, extended to the adjacent muscle layers. No obvious cellular inflammation was seen. The infant was discharged 2 days after surgery and has remained well for more than 1 year.

Discussion

In the fetus, the ductus arteriosus (connecting the pulmonary artery and aorta) is frequently the size of the aorta. During the first 10–15 hr after birth, pulmonary arterial pressure decreases and muscles in the ductal wall contract, resulting in a decrease in the size of the duct [1]. Anatomic closure occurs during the next 2–3 weeks, with nonthrombotic obliteration originating on the pulmonary side. The end product is the ligamentum arteriosus.

In neonates, the ductus arteriosus is not usually seen on chest films unless superimposition of the patent ductus arteriosus and the pulmonary artery (the ductus bump) occurs [2].This may be seen as a mass on frontal radiographs obtained in the first 72 hr after birth but not on radiographs obtained later, because the ductus arteriosus decreases in size and is no longer superimposed on the pulmonary artery.

Received March 23, 1992; accepted after revision May 7, 1992.

[1] Department of Radiology, Children's Hospital of Michigan, 3901 Beaubien Ave., Detroit, MI 48201. Address reprint requests to T. L. Slovis.

[2] Present address: Department of Radiology, Children's Hospital of Pittsburgh, 3705 5th Ave. at De Soto, One Children's Plaza, Pittsburgh, PA 15213.

[3] Present address: Department of Surgery, Children's Hospital of Michigan, 3901 Beaubien Ave., Detroit, MI 48201.

[4] Present address: Department of Pathology, Children's Hospital of Michigan, 3901 Beaubien Ave., Detroit, MI 48201.

[5] Present address: Department of Pathology, William Beaumont Hospital, 3601 W. 13 Mile Rd., Royal Oak, MI 48072.

AJR **159:839–840, October 1992** 0361–803X/92/1594–0839 © American Roentgen Ray Society

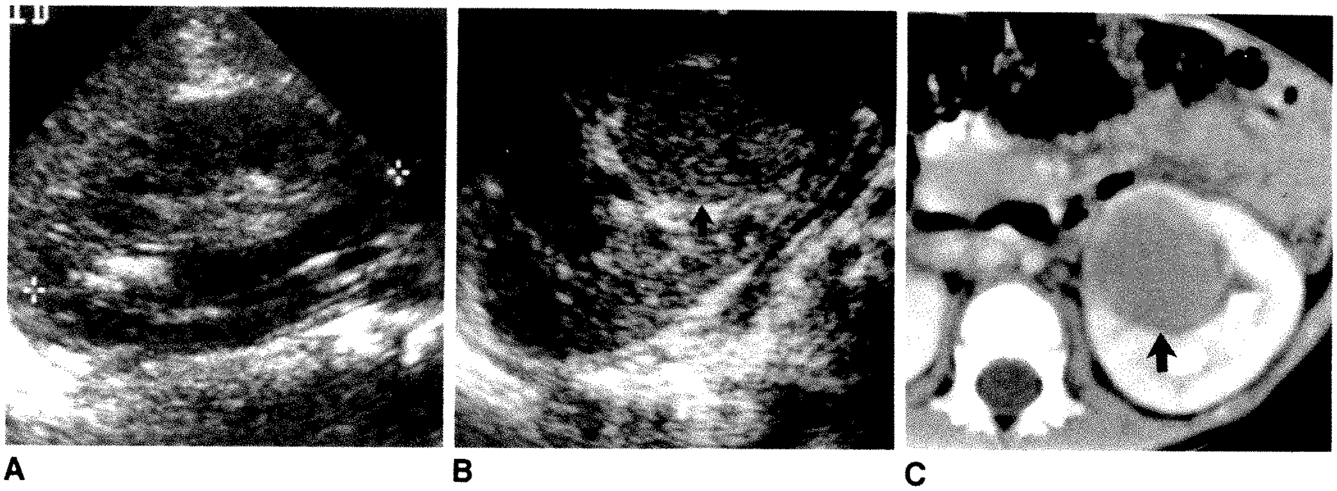

Fig. 1.—Nonpatent dissecting aneurysm of ductus arteriosus in a neonate.

***A*, Frontal radiograph obtained 1 day after birth shows mild hyperexpansion of lungs, increased markings, and a mass in aorticopulmonary window.**

***B* and *C*, Contrast-enhanced CT scans obtained 3 weeks after birth. Scan at level of aortic arch (*B*) shows a nonenhancing mass to left of aorta. Scan at level of pulmonary artery (*C*) shows nonenhancing mass is lateral to main pulmonary artery and anterior to left pulmonary artery.**

The pathogenesis of aneurysm of the ductus arteriosus is uncertain, although some relationship to neonatal hypoxemia has been suggested [3].The most logical theories are that (1) delay in closure of the aortic end of the ductus produces a diverticulum with continual exposure to systemic arterial pressures, causing myxoid degeneration and formation of the ductal aneurysm [1]; and (2) abnormal differentiation of the aortic wall, adjacent to the ductus arteriosus, promotes formation of an aneurysm [4]. A proposed anatomic classification of these aneurysms includes patent and nonpatent types of fusiform, tubular, and dissecting variants [5]. The prevalence of ductal aneurysm also is uncertain; in newborns, frequencies as high as eight aneurysms per 1000 autopsies have been reported [5]. More cases are now being discovered as, increasingly, diagnosis is based on findings on echocardiograms. In a significant number of cases the aneurysms resolve, with formation of a ligamentum arteriosum [5, 6]. Most infants with aneurysms of the ductus arteriosus are asymptomatic; however, fatal aneurysmal rupture, fatal dissection, thromboembolic phenomena with hypertension, and paralysis of the left side of the diaphragm and the left vocal cord have been reported [5, 7]. Many of the complications have occurred in adults.

Diagnosis of an aneurysm of the ductus arteriosus begins with the chest radiograph. The most important factor is the recognition of a mass, in a neonate or young infant, located in the aorticopulmonary window. The mass is convex to the left lung and is difficult to see on lateral radiographs. Echocardiography may show flow within the "cystic" mass if the aneurysm is patent. A CT scan will show the precise location of the mass, show if it is patent or nonpatent, and confirm its relationship to the vascular structures. It must be understood that a nonenhancing tubular mass in this location may be a nonpatent aneurysm of the ductus arteriosus. Although some have advocated observation of these masses in young infants, most often, as in our case, the mass is removed [5, 7].

The recognition of an aneurysm of the ductus arteriosus also should serve as a reminder that this condition is associated with coarctation of the aorta, aortic valvular disease, and Marfan syndrome [8].

REFERENCES

1. Kirks DR, McCook TA, Serwer GA, Oldham HN Jr. Aneurysm of the ductus arteriosus in the neonate. *AJR* **1980**;134:573-576
2. Berdon WE, Baker DH, James LS. The ductus bump: a transient physiologic mass in chest roentgenograms of newborn infants. *AJR* **1965**;95:91-98
3. Heikkinen ES, Simila S, Laitinen J, Larmi T. Infantile aneurysm of the ductus arteriosus. *Acta Paediatr Scand* **1974**;63:241-248
4. Bosman C, Leoncini B. On pathogenesis of a case of ductus arteriosus aneurysm. *Acta Cardiol* **1967**;22:279-288
5. Falcone MW, Perloff JK, Roberts W. Aneurysm of the nonpatent ductus arteriosus. *Am J Cardiol* **1972**;29:422-426
6. Malone PS, Cooper SG, Elliott M, Kiely EM, Spitz L. Aneurysm of the ductus arteriosus. *Arch Dis Child* **1989**;64:1386-1388
7. Morisot C, Dubos JP, Kacet N, Gremillet C, Remy-Jardin M, Lequien P. Neonatal hypertension and thrombosis of the ductus arteriosus. *Am J Perinatol* **1991**;8:77-79
8. Gillan JE, Costigan DC, Keeley FW, Rose V. Spontaneous dissecting aneurysm of the ductus arteriosus in an infant with Marfan syndrome. *J Pediatr* **1984**;105:952-955

Primary Cerebral Lymphoma in Patients with AIDS: MR Findings in 17 Cases

Yves-Sébastien Cordoliani[1]
Christian Derosier[2]
Christian Pharaboz[1]
Daniel Jeanbourquin[1]
Hubert Schill[2]
Guy Cosnard[1]

OBJECTIVE. The purpose of this study was to examine the MR imaging features of primary cerebral lymphoma in patients with AIDS. Knowledge of these findings may suggest the need for biopsy earlier in the course of the disease, avoiding the usual delay in empiric trials of antitoxoplasmosis treatment.

MATERIALS AND METHODS. We analyzed the MR features of biopsy-proved cerebral lymphoma in 17 patients with AIDS.

RESULTS. Typical MR findings were a single, large mass arising in the white matter and associated with moderate edema and mass effect; less often, primary cerebral lymphoma is an infiltrative periventricular lesion.

CONCLUSION. Familiarity with the MR features of cerebral lymphoma in patients with AIDS will aid in the early diagnosis of these lesions.

***AJR* 159:841–847, October 1992**

With the increasing prevalence of AIDS, primary cerebral lymphoma (PCL) is becoming a brain tumor of major importance because it occurs in about 2% of AIDS cases. PCL in patients with AIDS is almost always highly malignant and grows rapidly, hence the necessity of early diagnosis. As toxoplasmosis is the most common cerebral lesion found in these patients (30% of patients with AIDS in France [1]), empiric antitoxoplasmosis therapy is initiated when CT or MR imaging shows an enhancing lesion. Although the generalized use of the empiric antitoxoplasmosis treatment has undeniably been beneficial to most patients with toxoplasmosis, it has delayed the diagnosis in those patients with PCL. Therefore, we define certain MR imaging findings that suggest lymphoma in patients with AIDS so that the experimental antitoxoplasmosis treatment can be stopped and a stereotaxic biopsy can be done promptly.

Materials and Methods

Between January 1989 and December 1991, 17 PCLs were diagnosed among the AIDS patients referred to our institution for MR imaging, stereotaxic biopsy, or both. All patients except one were men between 27 and 46 years old (mean age, 33 years). All were examined with MR imaging (Signa 1.5 T, General Electric, Milwaukee, WI) before the biopsy. All examinations but one included one axial T2-weighted sequence, one axial T1-weighted sequence, one contrast-enhanced axial T1-weighted sequence, and a coronal T1-weighted sequence aiming to detect delayed lesion enhancement. In one patient (case 7), only the T1-weighted sequence was done after the injection of contrast material (gadolinium tetraazacyclododecane tetraacetic acid, Gd-DOTA, Dotarem, Guerbet Laboratories, Aulnay-sous-Bois, France).

The biopsies were performed under the Leksell or Fischer stereotaxic framework, after MR localization, with computer-assisted guidance of the needle's placement using a workstation (Sun Microsystems, Mountain View, CA) and specific software [2]. The patients came from various hospital departments in the Paris area and were admitted to the neurosurgery department for 48 hr, the time necessary for preoperative assessment, performance of the

Received February 5, 1992; accepted March 10, 1992.

Editor's note.—This article has been translated from the French and is reprinted with permission from *Journal de Radiologie*.

[1] Service d'Imagerie Médicale, Hôpital d'Instruction des Armées du Val-de-Grâce, 75230 Paris Cedex 05, France.

[2] Service de Biologie et Anatomie Pathologique, Hôpital d'Instruction des Armées du Val-de-Grâce, 75230 Paris Cedex 05, France.

0361-803X/92/1594-0841

TABLE 1: Clinical Data

Case No.	Age (yr)	Sex	Clinical Signs and Symptoms	Preexisting Toxoplasmosis
1	30	M	Seizure	Yes
2	29	M	Headaches	No
3	35	M	Seizure	Yes
4	33	M	Stupor, hemiparesis, aphasia	Yes
5	28	M	Hemiparesis	No
6	30	M	Stupor, seizure	Yes
7	36	M	Seizure	Yes
8	30	M	Hemiparesis	Yes
9	36	M	Loss of consciousness, hemiplegia	No
10	32	M	Stupor	No
11	41	M	Headaches	Yes
12	28	M	Seizures	No
13	27	F	Hemiparesis	No
14	46	M	Stupor	Yes
15	35	M	Hemiparesis	Yes
16	27	M	Hemiplegia	No
17	37	M	Seizures, aphasia	Yes

stereotaxic biopsy, and postbiopsy surveillance. The diagnosis of lymphoma was established histologically on average 3 days after the biopsy and was always confirmed later by immunohistochemistry.

The MR findings studied included the number and location of the lesions (white matter, gray nucleus, or junction of white matter and gray matter), their morphology, and the perilesional reaction. The morphologic analysis concerned the margins and the size of the mass, its signal (intensity of the signal compared with that of the gray matter, an increased signal on unenhanced T1-weighted images indicating the presence of methemoglobin), and the type of enhancement after injection of Gd-DOTA. The lesion's size was measured after injection of Gd-DOTA: the largest dimension for round lesions or the average of the largest dimension and the smallest dimension for oval lesions. Edema and mass effect were evaluated to determine the perilesional reaction. The edema was graded + (0–1 cm around the mass), ++ (1–2 cm), or +++ (>2 cm). The mass effect, rated more subjectively as nonexistent, moderate, or important, was related to the lesion's volume in order to determine if it was equal to, less than, or greater than the mass effect that would be expected for a lesion of that volume. Each case was reviewed by two experienced radiologists unaware of the final diagnosis, with the images interspersed with images from cases of cerebral toxoplasmosis. When the observers disagreed about whether the mass effect was appropriate for or too small for a lesion of that volume, the mass effect was considered appropriate for the volume in order to minimize the subjectivity of this nonquantifiable criterion.

Results

Clinical data are summarized in Table 1 and the MR imaging features are summarized in Table 2.

Number

The lymphoma sampled by biopsy was the only brain lesion visible in five cases. Among the 10 patients with a history of toxoplasmosis, five had lesions that were shown on successive examinations to regress during antitoxoplasmosis treat-

TABLE 2: Characteristics of the Lesions Shown on MR Images

Case No.	No. of Lesions[a]	Site[b]	Origin[c]	Diameter (cm)	Edema[d]	ME[e]	Outline	Intensity Relative to Gray Matter[f]		Doubling Time[g]	Enhancement	Visible Toxoplasmosis Sequelae
								T1	T2			
1	1	P	WM, paraventricular	3.5	++	=	Round	=	≠	?	Ring-shaped	Yes
2	1	F	WM, paraventricular	1.7	+	0	Oval	<	≠	13	Homogeneous	No
3	1	P	WM, paraventricular	4.2	+	=	Sinuous	>	≠	20	Peripheral	No
4	1	P	WM-GM junction	4.5	+++	=	Round	<	≠	?	Ring-shaped	Yes
5	2	P	WM, paraventricular	3.8	++	<	Sinuous	<	≠	10	Peripheral	No
6	1	P	WM-GM junction	3.4	++	<	Oval	>	<	?	Ring-shaped	Yes
7	4	F	WM, paraventricular	3.2	++	<	Sinuous	?	?	19	Peripheral	Yes
8	—[h]	PV	Periventricular	—	++	—	—	<	=	?	Peripheral	No
9	1	F-D	WM, paraventricular	5.2	++	<	Sinuous	<	<, ≠	?	Global heterogeneous	No
10	—	PV	Periventricular	—	++	—	—	<	<, ≠	?	Peripheral	No
11	1	O	WM-GM junction	2.0	++	=	Round	<	>, ≠	6	Homogeneous	Yes
12	2	F	WM-GM junction	2.5	++	<	Sinuous	<	>, ≠	9	Ring-shaped	No
13	2	P	WM, paraventricular	4.0	++	<	Round	=	>, ≠	?	Ring-shaped	No
14	1	NC	GN	2.0	+	=	Round	<	>, ≠	?	Ring-shaped	Yes
15	1	GP	GN	2.5	+	=	Round	<	<	21	Ring-shaped	No
16	1	P	WM, paraventricular	2.8	++	<	Round	>	<, ≠	14	Ring-shaped	No
17	2	T	WM-GM junction	4.5	+	<	Sinuous	<	<, ≠	11	Peripheral	Yes

[a] Number of visible lesions, with the exception of preexisting toxoplasmosis lesions.

[b] The site listed is the one that was the object of the stereotaxic biopsy. P = parietal lobe, F = frontal lobe, PV = periventricular, D = diencephalic, O = occipital lobe, NC = nucleus caudatus, GP = globus pallidus, T = temporal lobe.

[c] WM = white matter, GM = cortical gray matter, GN = gray nucleus.

[d] Grading of edema: +, <1 cm around the lesion; ++, 1–2 cm; +++, >2 cm.

[e] ME = mass effect: <, mass effect less than expected for volume of lesion; =, mass effect appropriate for volume of lesion; 0, absent.

[f] Signal intensity relative to gray matter on T1- and T2-weighted images: =, isointense; <, hypointense; >, hyperintense; ≠, heterogeneous with hyperintense foci.

[g] Time for tumor to double in volume expressed in days, calculated from the growth in diameter between two successive examinations. ? = not appreciable.

[h] Dashes indicate data that did not apply for the nontumorous periventricular forms.

ment, which confirmed that they were due to toxoplasmosis. Thus, in these patients, the PCL that was sampled by biopsy was associated with lesions that were sequelae of toxoplasmosis, but the PCL was presumed to be unifocal. In five cases, the PCL sampled by biopsy was accompanied by one or several other lesions presumed to be of the same nature (Fig. 1). On the basis of the imaging data, the multiple PCL location (i.e., these five cases and the two periventricular forms) represented, at most, only seven of 17 cases.

Site

About half of the lesions ($n = 8$) were located or had originated in the paraventricular white matter (Fig. 2). The other lesions were situated in the gray matter (two in a gray nucleus, Fig. 3), at the white matter–gray matter junction ($n = 5$, Fig. 4), or surrounding the ventricles (two periventricular forms, Fig. 5).

Size

Nine lesions had a diameter greater than 3 cm; in five cases, the diameter was 4 cm or more.

Morphology

On T1-weighted images, 13 lesions were isointense or hypointense with respect to the gray matter; that is, most of them were difficult to see within the perilesional edema; three were slightly more intense and visible in the edema. On T2-weighted images, all the lesions were isointense or hypointense with respect to the gray matter and easily visible in the increased signal of the perilesional edema (Figs. 3 and 4); most of the lesions were heterogeneous and included foci of increased signal. The contrast enhancement was global and homogeneous in two cases (Fig. 2); it was heterogeneous with peripheral predominance in the other cases. Among the

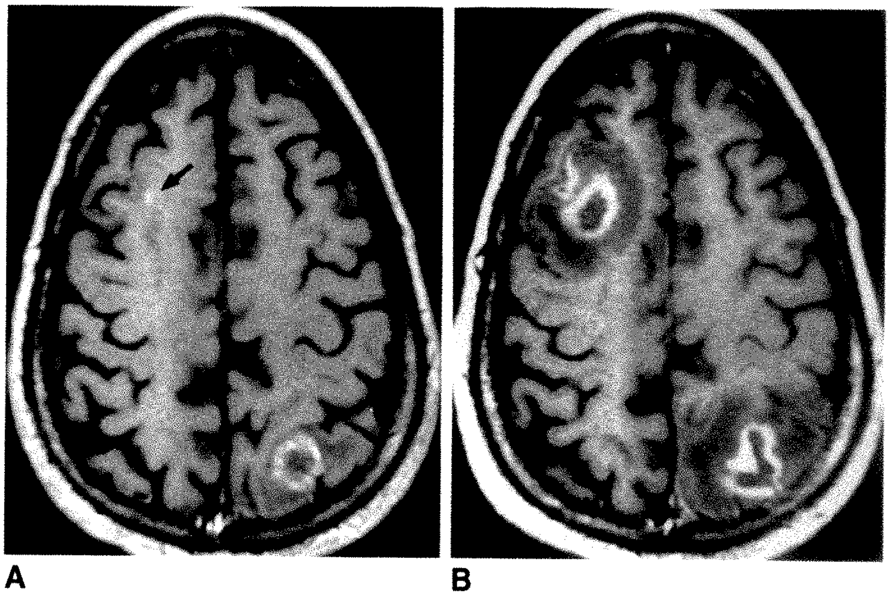

Fig. 1.—Lymphoma in two locations (case 12).
A, Contrast-enhanced axial MR image (SE 480/16) shows ring-shaped enhancement of round lesion in periphery of left parietal lobe and moderate edema and mass effect. Second lesion (*arrow*) is visible in frontal lobe.
B, Contrast-enhanced axial MR image (SE 480/16) after 3 weeks of antitoxoplasmosis treatment at the attack dose. Both lesions have grown, particularly lesion in right frontal lobe. Note irregular, sinuous margins of lesions.

2

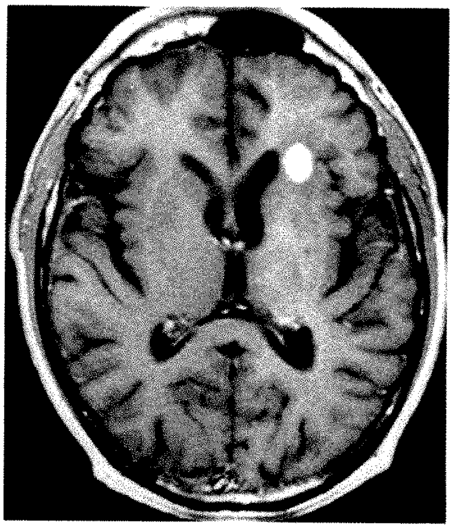

Fig. 2.—Lymphoma in paraventricular white matter (case 2). Contrast-enhanced axial MR image (SE 600/11) shows oval lesions whose center is located in anterior arm of left internal capsule, contiguous to frontal horn of lateral ventricle. Note homogeneous enhancement and absence of mass effect.

3

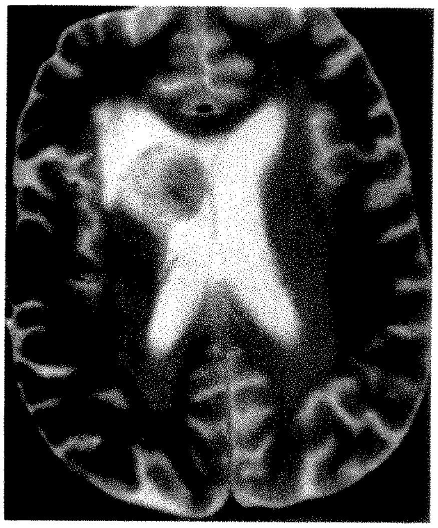

Fig. 3.—Lymphoma in a gray nucleus (case 14). Axial MR image (SE 2500/90) shows round mass in right caudate nucleus with heterogeneous signal, isointense with respect to gray matter with internal areas of increased signal, clearly visible between CSF of ventricles and edema.

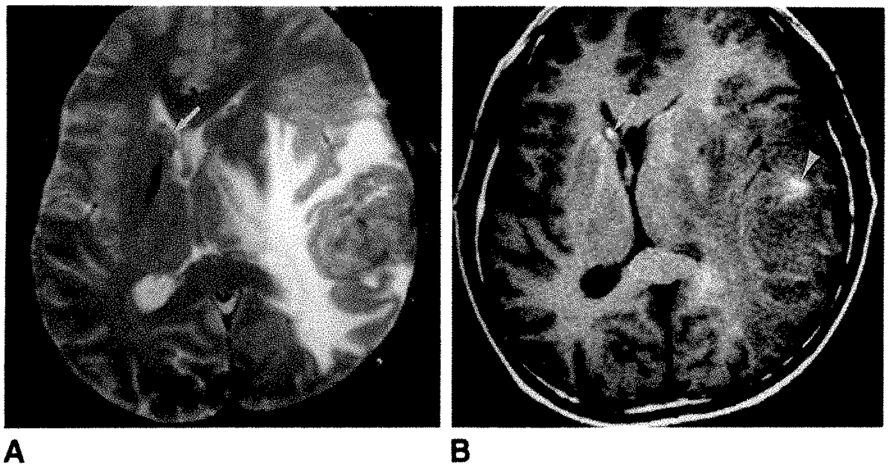

Fig. 4.—Lymphoma at junction of white and gray matter in patient with toxoplasmosis sequelae (case 4).

A, Axial MR image (SE 3000/90) shows large mass in left temporoparietal area with major edema and mass effect. Lesion (*arrow*) in right caudate nucleus is a sequela of toxoplasmosis.

B, Unenhanced axial MR image (SE 600/11) shows sequela of toxoplasmosis (*arrow*) in head of right caudate nucleus that has increased signal (due to hemoglobin). Main lesion also includes a small hemorrhagic focus (*arrowhead*).

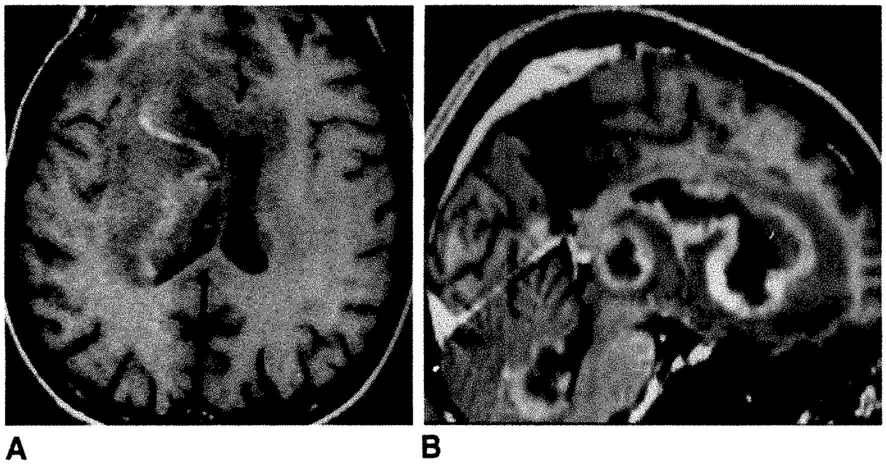

Fig. 5.—*A* and *B*, Periventricular lymphoma (case 8). Unenhanced axial MR image (*A*, SE 600/11) and oblique MR image (*B*) reconstructed on the basis of volume-acquisition data (2-mm slice thickness, 256 × 256 matrix, SPGR 24/2, 25° flip angle, Gd-DOTA injection) shows lymphoma infiltrating ventricular system in several places. Spontaneous focus of increased signal intensity on unenhanced T1-weighted image indicates a hemorrhage at edge of lesion (due to corticotherapy).

"tumoral" forms (excluding the two periventricular forms), nine were round or oval; six had irregular, sinuous margins (Fig. 1), corresponding to an infiltrating tumor. Two lesions had a focus of increased intensity on T1-weighted images, corresponding to a hemorrhagic zone (Figs. 4 and 5). Among the 10 patients with a history of toxoplasmosis, established by examinations that showed lesions regressing with antitoxoplasmosis treatment, four had one or several lesions containing hemoglobin degradation products (methemoglobin or hemosiderin, Fig. 4); three had foci of decreased signal intensity faintly enhanced by contrast injection; and three no longer had any detectable lesion.

Edema and Mass Effect

Both edema and mass effect were less than expected in slightly more than half the cases (nine cases, including the two periventricular lymphomas; Figs. 2 and 6). In the other cases, the edema and the mass effect were judged appropriate for the volume of the lesion.

Rate of Growth

The rate of growth could be measured by comparing successive images in nine cases. The time for the tumor to double in volume was between 6 and 21 days, with a mean of 13.6 days.

Discussion

PCLs occur in about 2% of AIDS cases, and in 0.6% of the cases PCL is the finding that indicates the patient has AIDS [3]. The progress made in the prevention of opportunistic diseases, especially pneumocystis pneumonia, and the systematic administration of azidothymidine (AZT) have significantly increased the life expectancy of these patients. This extended survival allows lymphomas to develop. In fact, it appears that the incidence of non-Hodgkin's lymphoma, in all locations, increases linearly with time from an immunodeficiency "threshold" of about 100 T4 lymphocytes per microliter. The risk of non-Hodgkin's lymphoma developing is about 30% in the 30 months after AZT treatment is started [4].

PCLs occurring in patients with AIDS are type B lymphomas, and they are almost always of high or intermediate malignancy according to the "working formulation for clinical usage" [5]. Hence, the tumors have a short doubling time. Three quarters of the patients die within 45 days after the appearance of the first clinical signs [6]. Radiotherapy, with or without chemotherapy, can prolong survival (4.5 months

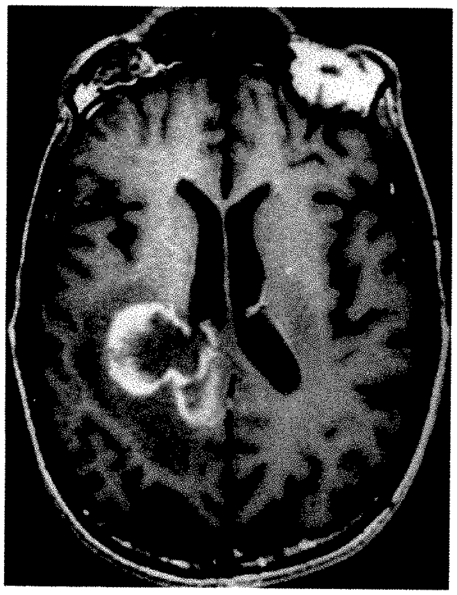

Fig. 6.—Moderate mass effect (case 5). Contrast-enhanced axial MR image (SE 480/16) shows that tumor, which originated in right semioval center, has infiltrated splenium of corpus callosum. Mass effect is very reduced, limited to amputation of occipital horn, without deviating ventricles with respect to median line despite greatness of lesion's diameter (nearly 4 cm).

on average for the patients treated [6]). Waiting 3 or 4 weeks to evaluate the efficacy of the antitoxoplasmosis treatment trials could be harmful for patients with PCL. Therefore, the diagnosis of lymphoma must be considered so that the delay in control of the disease after a trial antitoxoplasmosis treatment is started will be minimized. If the lesion is seen to grow within a short time after antitoxoplasmosis treatment is begun, stereotaxic biopsy must be done immediately.

Some MR imaging features suggest the diagnosis of lymphoma when a lesion enhances after the injection of contrast material. The features that are most evocative of PCL are the location in the deep white matter and the moderate edema and mass effect. The lymphoma can occur in the white matter or in the gray matter, but it is generally deep and near the midline, contiguous to the ventricualr system. The periventricular form, surrounding the ventricles on all or part of their contour, is highly specific and should suggest proceeding directly to stereotaxic biopsy [7]. The only disease that can mimic this appearance is cytomegalovirosis infection in its necrosing ependymitis form [8, 9]. In the tumoral (not periventricular) form, the site of the lesion is a good feature for discriminating lymphoma from toxoplasmosis if the lesion originated in the paraventricular white matter [10]; on the other hand, an origin in a gray nucleus or at the white matter–gray matter junction is ambiguous because these are the locations commonly seen in toxoplasmosis [11].

The second MR imaging feature that strongly suggests PCL is the moderate degree of the edema and mass effect. This feature was emphasized as early as the first PCL series (unrelated to AIDS) studied with CT [12] and then with MR [13]. The moderate edema and mass effect are due to the infiltrating nature of the lymphomatous proliferation. However, this feature cannot be objectively quantified and its recognition consequently depends on the radiologist's experience. In addition, it is inconstant (if we retain solely the obvious cases, we observe it only in somewhat over half our cases: nine times out of 17) but, when it is present, this feature has great diagnostic value.

The rapid growth of PCL (Fig. 1) accounts for the poor prognosis of the tumor [6]; however, the rapid growth can be used to shorten the time required to control the disease after the trial antitoxoplasmosis treatment is started. This delay, which comprises between 2 and 4 weeks, is needlessly long in cases of PCL. The short doubling time of the tumor makes it possible to show an objectively measurable increase in diameter within as brief a period as 8–10 days. This rapid growth and the infiltrating rather than space-occupying character of the lesion, reflected in the moderate mass effect, explain why PCL lesions are generally large when discovered. Therefore, a large lesion also suggests PCL [10]. A comparison between the diameters of the PCL lesions that we studied and the diameters of the toxoplasmosis lesions observed during the same period shows that the probability of PCL is very high for lesions 4 cm or greater in diameter (Fig. 7).

The number of lesion sites also allows discrimination of lymphoma from toxoplasmosis. PCL appears more often as a single lesion, whereas toxoplasmosis lesions usually are multiple. Although the data from the lymphoma series verified by autopsy indicate a higher proportion of multiple locations [14, 15], in the series verified by biopsy, the location detected in vivo often seems to be a single one [3, 16]. Ciricillo and Rosenblum [17], on the basis of a series of 159 lesions sampled by biopsy, of which 45 were lymphomas, concluded that a single lesion is four times as likely to be due to PCL than to toxoplasmosis [17]. On the other hand, Dina [7] counted only three solitary lesions in his 16-patient series, but he reported this discordance and nevertheless concluded that

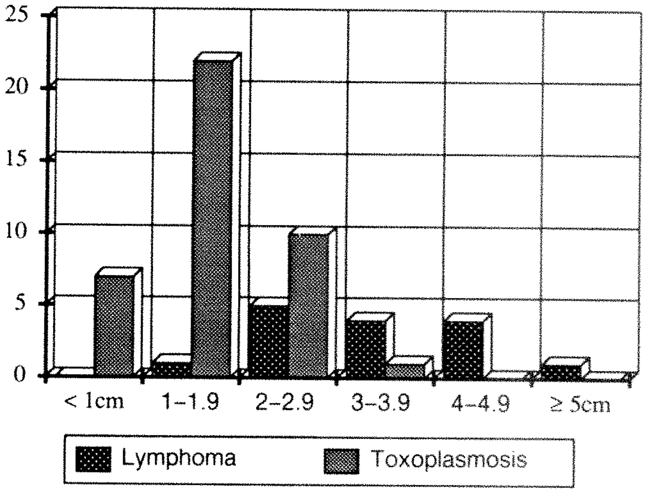

Fig. 7.—Comparison of size of primary cerebral lymphoma with maximum size of toxoplasmosis lesions observed during same period (40 cerebral lesions due to toxoplasmosis). At diameters of 4 cm or greater, probability of primary cerebral lymphoma is very high.

a single mass must be subjected to strict surveillance and should more readily prompt biopsy.

Preexisting toxoplasmosis lesions are very common, especially in France, where toxoplasmosis is more prevalent than in North America. Among the 17 patients in our series, 10 had a history of cerebral toxoplasmosis with lesions at variable stages (disappearance of lesions that were visible at earlier examinations, cicatricial lesions, or objective regression under treatment); all these patients were receiving antitoxoplasmosis treatment. Two of the lymphomas sampled had obviously undergone a secondary development near a lesion that was a sequela of toxoplasmosis. It should be noted that the location of both these cases (white matter–gray matter junction) was uncertain and that both had a significant mass effect. These observations and, more generally, the high number of associated toxoplasmosis lesions may suggest a possible predisposing role of *Toxoplasma* infection indirectly through local antigenic stimulations as was suggested for HIV infection and for other opportunistic infections [3].

The PCL's signal intensity on unenhanced T1-weighted images and on T2-weighted images is not a very useful diagnostic characteristic. The great majority of the lesions are difficult to see on T1-weighted images amid the edema and, on the contrary, have good contrast against this edema on T2-weighted images, but such is also the case for most toxoplasmosis lesions. One important point is the rarity of hemorrhage, to which MR imaging is very sensitive. Findings of hemorrhage are visualized, sometimes very early, in a large proportion of the toxoplasmosis lesions, whether they are being treated or are sequelae (about 60% among the toxoplasmosis cases imaged with MR in our department during the same period). On the other hand, PCL is seldom hemorrhagic (Fig. 4), unless the patient is treated with corticosteroids (Fig. 5) or irradiation (Fig. 8). Identification on MR images of hemoglobin degradation products is thus evidence against the diagnosis of PCL if the patient has not undergone corticotherapy.* All the lymphomas in our series showed contrast enhancement after injection of Gd-DOTA. Only twice was this enhancement global and homogeneous (Fig. 2); this type of enhancement, classic for the PCL of the nonimmunodeficient subject [12, 18], is in fact rare in patients with AIDS, in whom most lesions are enhanced at the periphery. Nevertheless, the homogeneous and intense enhancement of a lesion that is more than 2 cm in diameter should suggest lymphoma, because almost all toxoplasmosis lesions exhibit central necrosis from 1 to 2 cm in diameter.

The lesion's margin, demarcated by the injection of contrast material, is most often ring shaped and identical to most toxoplasmosis "abscesses." If it is irregular, sinuous, or even gyralike, then it is much more evocative of PCL [18].

Table 3 summarizes the main MR imaging features we found to be suggestive of PCL.

The superiority of MR imaging over CT for the diagnosis of PCL consists first of its better global sensitivity. It detects more lesions than does CT [10, 17, 19], especially in the posterior fossa, and can disclose associated abnormalities, such as those in the white matter (progressive multifocal leukoencephalitis or HIV encephalopathy), which are often not shown by CT. It provides better anatomic differentiation, allowing more precise localization of a lesion in relation to the various parenchymal components (white matter, gray matter, or gray nucleus) and the identification of periventricular extension [19], which represents an essential feature of the differential diagnosis between PCL and toxoplasmosis. In addition, MR imaging is more sensitive for the detection of hemoglobin

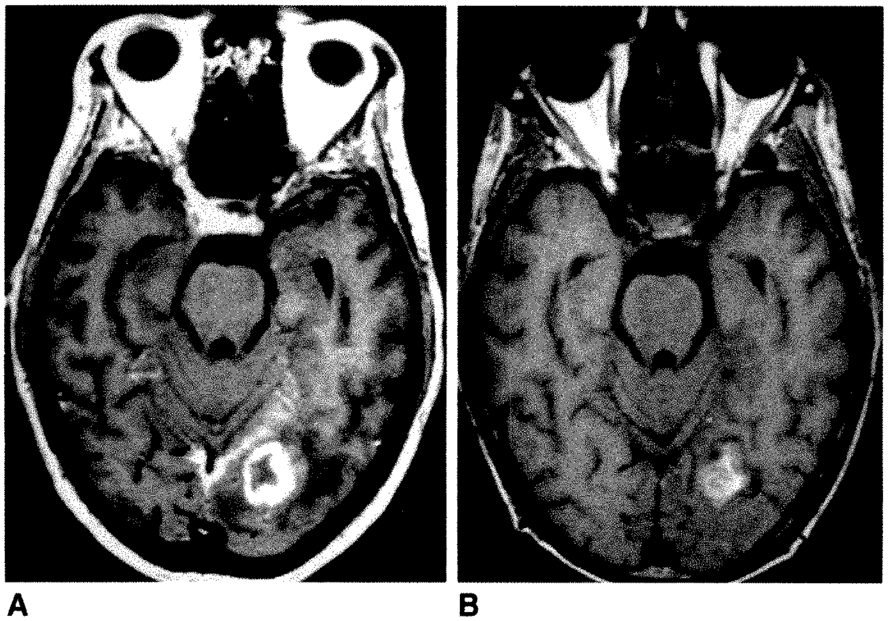

Fig. 8.—Hemorrhage after radiotherapy (case 11).

***A*, Contrast-enhanced axial MR image (SE 500/11) shows lymphoma in occipital lobe with enhancement at periphery.**

***B*, Unenhanced axial MR image (SE 480/16) 3 months after radiotherapy shows spontaneous focus of increased signal intensity on T1-weighted image, indicating global hemorrhage. Volume of lesion is stable, and edema and mass effect have disappeared.**

---

* In this regard, we must emphasize that corticotherapy should be avoided as soon as primary cerebral lymphoma is suspected, because it may halt growth of the lesion, even cause a transitory regression, which, on the one hand, falsifies the results of the empirical antitoxoplasmosis treatment and, on the other hand, can make the pathologic diagnosis difficult, indeed impossible, owing to the tumor necrosis.

TABLE 3: MR Imaging Findings Suggestive of Primary Cerebral Lymphoma

Finding	Degree
Periventricular form	++++
Tumor form	
Location in the paraventricular white matter	++
Edema and mass effect less than expected	++
Irregular, sinuous margins	+
Solitary lesion	+
Diameter greater than 3.5 cm	+
Homogeneous enhancement (if diameter ≥ 2 cm)	+

Note.—Degree of suggestiveness of finding (diagnostic probability) increases with the number of plus signs. Within tumor form, degree of suggestiveness is determined by adding the degrees for each of the six criteria noted.

degradation products, very often confirming the diagnosis of toxoplasmosis. In our department, where it is used for stereotaxic guidance, MR imaging provides data on volume acquisition with an isometric voxel, which allows great precision in determining the target and simulating the whole biopsy pathway [2], thus improving the safety of the stereotaxic biopsy.

In fact, the decisive factor in diagnosing PCL is the identification of growth of the lesion during antitoxoplasmosis treatment, which mandates a biopsy to obtain the histologic proof needed to choose the proper treatment (radiotherapy, sometimes in association with chemotherapy). With the use of the diagnostic criteria we have described, MR imaging early in the course of antitoxoplasmosis treatment (a 10-day period seems adequate to us) is sufficient to objectively show the lesion's growth in cases of PCL. Treatment is more effective when no time is lost before radiotherapy is started; indeed, the median survival of these patients increases significantly [3, 6, 15, 17].

The sensitivity of MR for the detection of the diffuse, endovascular form of PCL, formerly called diffuse angioendotheliomatosis [20], is poor. This form, discovered at autopsy, may not be visible on CT scans obtained before the patient's death [12, 21] or it may manifest only as diffuse ischemic lesions. Whatever the circumstances, these cases are exceptional, and to our knowledge, no cases of detection with MR imaging have been reported.

Conclusions

Recognition of the MR imaging findings that are suggestive of lymphoma elicits a prompt stereotaxic biopsy and shortens the delay in implementing effective treatment. MR imaging thus contributes to the increased survival of patients with lymphoma, and while a few months' increase in the survival of treated patients is short, it is significant relative to their overall life expectancy.

ACKNOWLEDGMENTS

The authors thank the physicians of the hospital departments that entrusted them with their patients for examination and/or stereotaxic biopsy. These are the infectious and tropical pathology departments, and the neurology and internal medicine departments of the following hospitals: Pitie-Salpetriere (Prof. Gentilini), Saint-Louis (Prof. Modai), Rothschild (Prof. Rozenbaum), Bicetre (Prof. Said), Broussais (Prof. Kazatchkine), and Avicenne (Prof. Modigliani).

REFERENCES

1. Direction Générale de la Santé. Surveillance du SIDA en France: situation au 31 décembre 1989. *Bull Epidémiol Hebd* **1990**;8:29–36
2. Derosier C, Cordoliani Y-S, Hor F, Schill H, Cosnard G. Stéréotaxie, IRM et console indépendante: 85 ponctions. *J Radiol* **1992**;73:103–108
3. Rosenblum ML, Levy RM, Bredesen DE, et al. Primary central nervous system lymphomas in patient with AIDS. *Ann Neurol* **1988**;23:S13–S16
4. Pluda JM, Yarchoan R, Jaffe LS, et al. Development of non-Hodgkins lymphoma in a cohort of patients with severe human immunodeficiency infection on long term antiretroviral therapy. *Ann Intern Med* **1990**;113:276–282
5. Ziegler JL, Beckstead JA, Volberding PA. Non-Hodgkin's lymphoma in 90 homosexual men: relation to generalized immunodeficiency syndrome. *N Engl J Med* **1984**;311:565–570
6. Baumgartner JE, Rachlin JR, Beckstead JH, et al. Primary central nervous system lymphomas: natural history and response to radiation therapy in 55 patients with AIDS. *J Neurosurg* **1990**;73:206–211
7. Dina TS. Primary central nervous system lymphoma versus toxoplasmosis in AIDS. *Radiology* **1991**;179:823–828
8. Post MJD, Hensley GT, Moskowitz LB, Fischl M. Cytomegalic inclusion virus encephalitis in patients with AIDS: CT, clinical and pathologic correlation. *AJNR* **1986**;7:275–280
9. Cordoliani Y-S, Pharaboz C, Jeanbourquin D, Le Gall R, Derosier C, Cosnard G. Imagerie par résonance magnétique des atteintes encéphaliques du SIDA. *Feuillets Radiol* **1991**;31:453–474
10. Kupfer MC, Zee CS, Colletti PM, Boswell WD, Rhodes R. MRI evaluation of AIDS-related encephalopathy: toxoplasmosis vs lymphoma. *Magn Reson Imaging* **1990**;8:51–57
11. Post MJD, Kursunoglu S, Hensley GT, Chan JC, Moskowitz LB, Hoffmann TA. Cranial CT in AIDS: spectrum of diseases and optimal contrast enhancement technique. *AJR* **1985**;145:929–940
12. Cellerier P, Chiras J, Gray F, Metzger J, Bories J. CT in primary lymphoma of the brain. *Neuroradiology* **1984**;26:485–492
13. Schwaighofer BW, Hesselink JR, Press GA, Wolf RL, Kealy ME, Berthoty D. Primary intracranial CNS lymphoma: MR manifestations. *AJNR* **1989**;10:725–729
14. Poon T, Matoso I, Tchertkoff V, Weitzner I Jr, Gade M. CT features of primary cerebral lymphoma in AIDS and non-AIDS patients. *J Comput Assist Tomogr* **1989**;13:6–9
15. So YT, Beckstead JG, Davis RL. Primary CNS lymphoma in AIDS: a clinical and pathological study. *Ann Neurol* **1986**;20:566–572
16. Goldstein JD, Zeifer B, Chao C, et al. CT appearance of primary CNS lymphoma in patients with acquired immunodeficiency syndrome. *J Comput Assist Tomogr* **1991**;15:39–44
17. Ciricillo SF, Rosenblum ML. Use of CT and MR imaging to distinguish intracranial lesions and to define the need for biopsy in AIDS patients. *J Neurosurg* **1990**;73:720–724
18. Lee YY, Bruner JM, Van Tassel P, Libshitz H. Primary central nervous system lymphoma: CT and pathologic correlation. *AJNR* **1986**;7:599–604
19. McKinstry CS. Intracranial malignant lymphoma. *J Neurosurg* **1987**;67:476–477
20. Hochberg FH, Miller DC. Primary central nervous system lymphoma. *J Neurosurg* **1988**;68:835–853
21. Levy RM, Rosenbloom S, Perrett LV. Neuroradiologic findings in AIDS: a review of 200 cases. *AJR* **1986**;147:977–983

RESIDENTS IN RADIOLOGY AWARDS

The American Roentgen Ray Society

sponsors the

1993 President's Award and the **Executive Council Awards**

RULES AND REGULATIONS

- Papers must be submitted on the clinical application of the discipline of radiology and radiological science.
- The event is open to residents in radiology and radiological sciences. If not the sole author, it is expected that the resident will have performed the majority of the work and be the senior author.
- The submitted manuscript should not exceed 5,000 words and 10 illustrations.
- The winners will be announced by March 16, 1993.
- The papers will be presented at the American Roentgen Ray Society 93rd Annual Scientific Meeting at the San Francisco Marriott, San Francisco, CA, April 25-30, 1993, and be submitted for publication to the *American Journal of Roentgenology.*
- Manuscripts will be returned to candidates not receiving awards.

AWARDS

- The winner of "The President's Award" will be presented a certificate and receive an honorarium of ***$2,000.***
- The two winners of "The Executive Council Award" will each receive a certificate and an honorarium of ***$1,000.***

DEADLINE

- Four copies of the paper and four packages of the illustrations should be submitted no later than **February 12, 1993** to:

Nancy O. Whitley, M.D.
Chairman, Committee on Education & Research
American Roentgen Ray Society
1891 Preston White Drive
Reston, Virginia 22091

Review Article

The Ostiomeatal Unit and Endoscopic Surgery: Anatomy, Variations, and Imaging Findings in Inflammatory Diseases

Fred J. Laine[1] and Wendy R. K. Smoker

Recent and ongoing advances made in endoscopic surgical techniques require the radiologist to understand the anatomy and pathophysiology of the paranasal sinuses and nasal passage. Endoscopy and CT are complementary procedures, and, as such, the normal anatomic relationships and their CT appearances need to be well understood in order for radiologists to offer continued support as consultants to their clinical colleagues. In this article, we review the pertinent anatomy of the lateral nasal wall and paranasal sinuses, discuss the most frequently encountered normal variations that may predispose a patient to inflammatory sinus disease, outline imaging protocols for evaluation of this region, and introduce the reader to current endoscopic surgical techniques. Last, the imaging findings in various inflammatory processes involving the sinuses, as well as the local and regional complications associated with paranasal sinus inflammatory diseases, are presented.

In our role as consultants, radiologists must keep abreast of clinical advances and be able to adapt imaging procedures as necessary to meet changing clinical demands. Advances in the understanding of mucociliary drainage patterns and the pathophysiology of paranasal sinus inflammatory disease, coupled with the availability of high-resolution CT and improvements in endoscopic instrumentation, have led to major changes in the surgical management of sinusitis. As a result, the radiologist must relearn the anatomy of nasal and paranasal structures, as well as the pathologic changes caused by diseases that affect this region, in order to correlate CT and endoscopic findings.

Normal Anatomy

The relationships between important bony and soft-tissue structures and sinus ostia can be more easily understood and interpreted on CT scans by first reviewing the anatomy of the lateral nasal wall and nasal septum.

Projecting from the lateral nasal wall are the inferior, middle, and superior turbinate bones (or conchae) (Fig. 1A). Occasionally, a supreme turbinate bone can be identified. Beneath each turbinate bone lies a respectively named meatus into which the various ostia drain (Fig. 1B).

The *inferior turbinate bone* is the largest of the three, under which lies the inferior meatus. The inferior meatus receives drainage from the nasolacrimal duct, which is typically seen only segmentally on axial scans. Occasionally, the duct can be followed from its origin in the inferomedial aspect of the orbit to its ostium in the anteroinferior aspect of the meatus, adjacent to the attachment of the inferior concha.

Under the *superior turbinate bone*, the smallest of the three, lies the superior meatus, through which posterior ethmoidal air cells drain via multiple ostia. This turbinate bone is identified on coronal images as a slender structure, suspended from the dome of the posterior aspect of the nose [1]. The *sphenoethmoidal recess*, draining the sphenoidal sinus through the sphenoidal ostium, lies posterosuperior to the superior turbinate bone, between the anterior wall of the sphenoidal sinus and the posterior wall of the ethmoidal sinus (Fig. 2). Lateral to the recess, the most posterior ethmoidal

---

Received November 8, 1991; accepted after revision April 16, 1992.

[1] Both authors: Department of Radiology, Medical College of Virginia Hospitals, MCV Station, Box 615, Richmond, VA 23298. Address reprint requests to F. J. Laine.

AJR 159:849–857, October 1992 0361–803X/92/1594–0849 © American Roentgen Ray Society

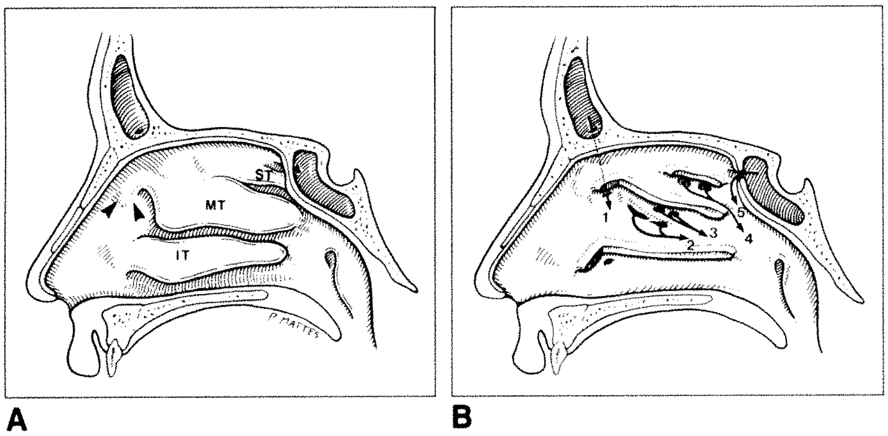

Fig. 1.—*A*, Line diagram of lateral nasal wall with intact turbinate bones. *Arrowheads* = agger nasi cells, IT = inferior turbinate bone, MT = middle turbinate bone, ST = superior turbinate bone.

B, Line diagram of lateral nasal wall with turbinate bones removed. *Arrows* = ostia and mucous flow patterns, 1 = drainage from frontal sinus, 2 = drainage from maxillary sinus, 3 = drainage from anterior and middle ethmoidal sinuses, 4 = drainage from posterior ethmoidal sinuses, 5 = drainage from sphenoidal sinus. 1, 2, and 3 drain to the middle meatus, whereas 4 and 5 drain through sphenoethmoidal recess to superior meatus.

air cell (cell of Onodi) and the sphenoidal sinus share a common wall, the sphenoethmoidal plate [2] (Fig. 2).

The *middle turbinate bone* covers the middle meatus, the most complex region of the lateral nasal wall. Near the superior attachment of the turbinate bone, a prominence of the lateral wall is produced by the *agger nasi* cells, the most anterior ethmoidal air cells (Fig. 1). Above these cells lies the *frontal recess*. The frontal sinus drains, via the frontonasal duct, agger nasi cells, and frontal recess, into the anterior aspect of the middle meatus, medial to the uncinate process, or directly into the ethmoidal infundibulum (Fig. 1B). The ethmoidal infundibulum is often continuous with the frontonasal duct.

The middle turbinate bone attaches to two areas of delicate bone, which can pose potential problems during endoscopic manipulation: the superior attachment to the delicate lateral aspect of the cribriform plate, and the lateral, intraethmoidal attachment, *basal (or ground) lamella*, to the thin lamina papyracea of the lateral ethmoidal wall (Fig. 3). Posteriorly, the basal lamella curves superiorly and becomes oriented in the coronal plane, behind the ethmoidal bulla, thereby separating the anterior and posterior ethmoidal air cells. Ethmoidal air cells located anterior to the basal lamella will drain into the middle meatus, whereas those cells located posterior to the basal lamella will drain into the superior meatus [2].

If the middle turbinate bone is removed, three prominent underlying structures are seen: the uncinate process anteriorly, the hiatus semilunaris, and the bulla ethmoidalis posteriorly. The *uncinate process*, a thin, hook-shaped, mucosa-covered bony prominence, originates anteriorly from the posteromedial border of the nasolacrimal duct. Almost parallel to the middle turbinate bone, it forms a free border that defines the anterior boundary of the hiatus semilunaris. On coronal CT, the uncinate process is easily detected as a superior extension of the medial maxillary sinus wall, forming the lateral wall of the middle meatus (Figs. 3 and 4). Lateral to the uncinate process lies the *infundibulum*, connecting the ostia of the maxillary and ethmoidal sinuses to the hiatus semilunaris (Figs. 3 and 4). Mucociliary drainage from the maxillary sinuses courses superiorly, through the ostia and posterior infundibulum to the hiatus semilunaris, and eventually into the middle meatus.

The *hiatus semilunaris* is bounded superiorly by the bulla ethmoidalis, laterally by the bony orbit, inferiorly by the uncinate process, and medially by the middle meatus. It accommodates multiple anterior ethmoidal ostia, and the single maxillary sinus ostium, to form the final segment of drainage from these sinuses. A superior extension of the hiatus semilunaris communicates with the sinus lateralis, the space between the posterior wall of the ethmoidal bulla and the basal lamella, providing drainage of this area and the middle ethmoidal air cells.

The *bulla ethmoidalis*, usually consisting of a single variable air cell, projects inferomedially over the hiatus semilunaris in a rounded fashion. The relationships of these three lateral wall structures are such that a channel is formed, linking the frontal, anterior and middle ethmoidal, and maxillary sinuses to the middle meatus. This connecting channel is collectively referred to as the ostiomeatal unit (OMU) (Figs. 3 and 4). In summary, mucociliary drainage of the sinuses eventually merges into two common pathways, allowing division into two anatomic and functional groups [2]. The first group (frontal, anterior ethmoidal, middle ethmoidal, and maxillary sinuses) drains into the middle meatus, around the ethmoidal bulla (the OMU) (Fig. 1B). This region is frequently involved by inflammatory disease. The second group (posterior ethmoidal and sphenoidal sinuses), draining into the sphenoethmoidal recess and superior meatus (Fig. 1B), is less frequently affected by inflammatory processes.

The nasal septum, easily identified on both axial and coronal CT, extends the entire length of the nasal cavity (Figs. 2 and 4). The anterior portion is composed of cartilage, whereas the posterior portion is osseous, formed mainly by the vomer and the perpendicular plate of the ethmoid bone. The interfrontal septum anteriorly and the intersphenoidal septum posteriorly do not always lie in the same plane as the nasal septum. This is an important anatomic consideration for endoscopic surgeons.

Two important anatomic relationships between the paranasal sinuses and adjacent structures must be mentioned. Awareness of the intimate relationship between the internal carotid artery and the sphenoidal sinus is important for understanding the potentially devastating complications of inflammatory disease or endoscopy (Fig. 2). Bulging of the

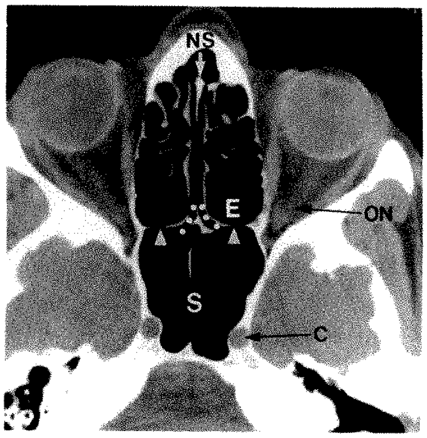

Fig. 2.—Axial CT scan obtained with intermediate windows shows sphenoethmoidal recesses (*white dots*) and proximity of carotid canals (C) to lateral wall of sphenoidal sinus (S). Note also proximity of optic nerve (ON) to posterior ethmoidal (E) and sphenoidal sinuses. NS = nasal septum, *arrowheads* = sphenoethmoidal plate.

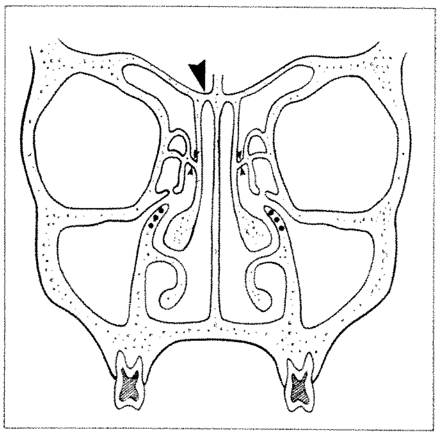

Fig. 3.—Line diagram of normal ostiomeatal unit. *Small arrowheads* = basal lamella, *large arrowhead* = cribriform plate, *dots* = uncinate process.

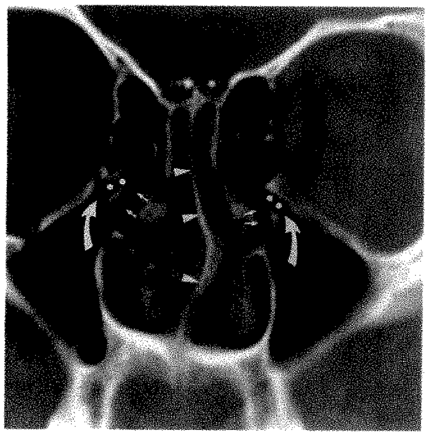

Fig. 4.—Coronal CT scan shows normal ostiomeatal unit. *Curved arrows* = maxillary ostium, *dots* = infundibulum, *straight arrows* = middle meatus, *arrowheads* = nasal septum.

carotid artery into the sphenoidal sinus is seen in 65–72% of patients [3-5]. The thin bone separating the artery from the sinus is less than 1 mm in 66% of patients, less than 0.5 mm in 88% of patients, and completely absent in 4–8% of cases [4, 5].

The location of the optic canal and nerve is an additional important anatomic consideration. Because of the location of the distal canal opening, in 75% of cases the nerve will be close to both the sphenoidal and ethmoidal sinuses [6] (Fig. 2). During its course, the optic nerve bulges into the superolateral sphenoidal sinus wall, forming the optic eminence. A thin bony partition is present in 70–78% of patients [5, 7], and complete bony dehiscence is present in 3.6–4% of cases [5, 8].

Anatomic Variations

The middle meatus and lateral nasal wall are subject to wide normal variations that must be distinguished from pathologic changes. These variations may, themselves, be the underlying cause of recurrent sinus disease. However, there is a lack of consensus among investigators with respect to the prevalence and clinical significance of these variations, as they have been encountered with similar frequency in patients being scanned for sinus-related problems, as well as those undergoing evaluation for non-sinus-related problems [9]. The more common variations can be divided into four groups, depending on the structures involved: middle turbinate bone, uncinate process, ethmoidal bulla, and nasal septum.

Middle Turbinate Variations

Concha bullosa.—The middle turbinate bone is usually a thin plate of bone. When this plate becomes pneumatized by extension of the anterior (55%) or posterior (45%) ethmoidal air cells, the air cell created is referred to as concha bullosa [9] (Fig. 5A). The reported prevalence of concha bullosa ranges from 4% to 80%, depending on criteria for pneumatization and differences in study populations. "True" concha bullosa (pneumatization of both the vertical lamellar and inferior bulbous portions) is reported in 4–15.7% of the population [9, 10]. If the definition is broadened to include any degree of middle turbinate pneumatization, the prevalence increases to 34% [11]. The highest prevalence (80%) is found in patients with chronic sinusitis [12]. For this reason, some suggest that concha bullosa may be a contributing factor in the pathogenesis of sinus inflammatory disease, although others do not share this view [9]. Stammberger and Wolf [13] and Lidov and Som [14] reported that concha bullosa can, when sufficiently large, produce signs and symptoms by encroaching on the infundibulum. Concha bullosa may also contain polyps, cysts, pyoceles, or mucoceles.

Paradoxically curved middle turbinate bone.—Normally, the convexity of the middle turbinate bone is directed medially, toward the nasal septum. When paradoxically curved, the convexity is directed laterally, toward the lateral sinus wall (Fig. 5B). A 26.1% prevalence of paradoxically curved middle turbinates has been reported [9]. Although no studies relate this variation to sinus disease, it is a presumed etiologic factor because of the deformity and obstruction or alteration of nasal passage air flow dynamics, especially when associated with other variations [13].

Uncinate Variations

Deviation of the uncinate tip.—The superior aspect of the uncinate tip may deviate laterally, medially, or anteriorly out of the meatus, appearing as a second middle turbinate bone [13, 15]. When deviated medially, it comes into contact with and compromises the middle meatus. When deviated laterally,

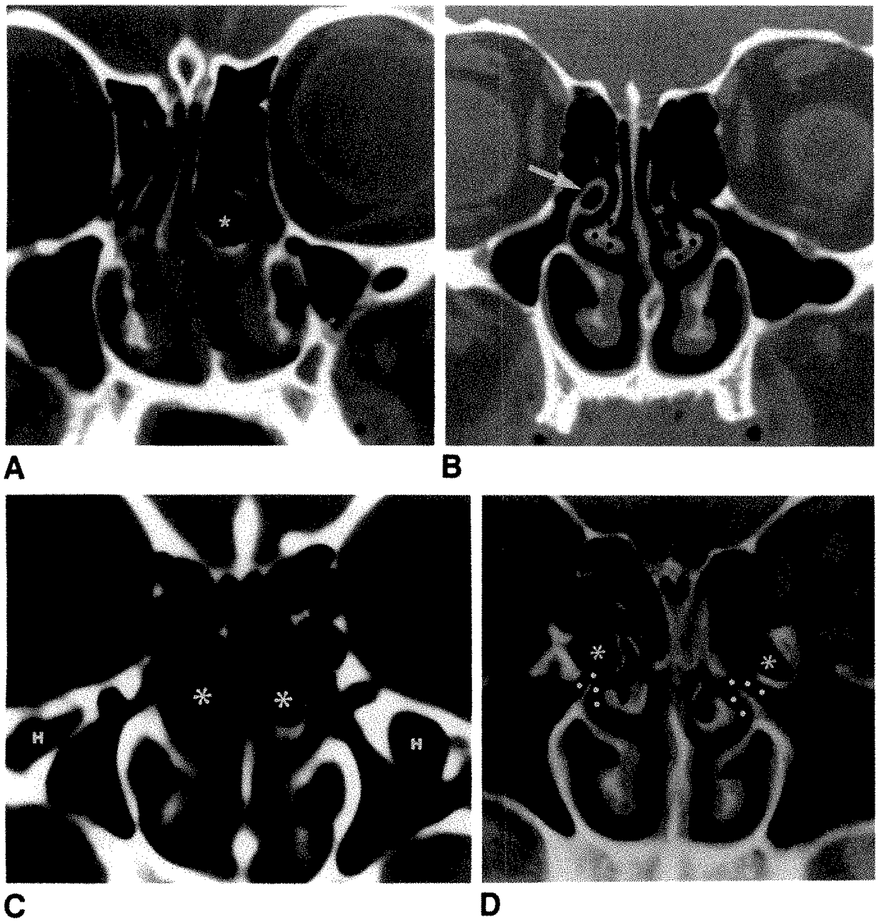

Fig. 5.—*A*, Coronal CT scan shows pneumatization of middle turbinate bones bilaterally (concha bullosa), much greater on left (*asterisk*) than on right. Also note nasal septal deviation, which narrows right middle meatus.

B, Coronal CT scan reveals paradoxically laterally curved middle turbinate bones bilaterally (*dots*). Also note pneumatization of right uncinate tip (*arrow*).

C, Coronal CT scan shows large Halle cells (H) projecting downward along roofs of maxillary sinuses. Concha bullosa is seen bilaterally (*asterisks*). Sinuses, at this time, are clear.

D, Coronal CT scan shows evidence of ethmoidal bullae (*asterisks*) bilaterally without evidence of associated sinus disease. Normal relationship to ostiomeatal unit (*dots*) is well visualized bilaterally.

it may encroach on the hiatus semilunaris and infundibulum, impeding drainage and ventilation of the anterior ethmoidal, frontal, and maxillary sinuses. The exact prevalence of these variations and their relation to sinus disease have not been determined.

Pneumatized uncinate tip (uncinate bulla).—The exact mechanism by which uncinate pneumatization (Fig. 5B) occurs is not known. It has been proposed that this process is due to growth of agger nasi cells into the most anterosuperior region of the uncinate process [9]. Studies reveal a prevalence of 0.4–2.5% [9]. This variation has been implicated in narrowing of the infundibulum, producing impaired sinus ventilation [16].

Ethmoidal Variations

Halle cells.—According to Kennedy and Zinreich [17], Halle cells, ethmoidal air cells that project inferiorly to the ethmoidal bulla into the floor of the orbit in the region of the maxillary sinus ostium, are encountered in 10% of the population (Fig. 5C). However, Bolger et al. [9] defined Halle cells as any air cells located beneath the ethmoidal bulla, lamina papyracea, or orbital floor. Using this criteria, they reported a prevalence of 45%. Although they found no significant difference in the prevalence of Halle cells between patients scanned for chronic sinus disease and patients scanned for nonsinus reasons, Stammberger and Wolf [13] consider the presence of these cells as another predisposing factor for recurrent maxillary sinusitis.

Large ethmoidal bulla.—The ethmoidal bulla can be so extensively pneumatized that it completely fills the sinus of the middle turbinate bone (Fig. 5D). Stammberger and Wolf [13] reported that an enlarged ethmoidal bulla may contribute to sinus disease by obstructing the infundibulum or middle meatus or by being primarily diseased and filled with pus, cysts, or polyps. The exact prevalence of an enlarged ethmoidal bulla is not known.

Agger nasi cells.—Agger nasi cells, the most constant ethmoidal air cells, lie below the frontal sinus, inferolateral to the lacrimal sinus, and represent pneumatization of the lacrimal bone by extension of the anterior ethmoidal cells [10]. They are located anterior and superior to the insertion of the middle turbinate bone, along the lateral nasal wall [13] (Fig. 1A). In anatomic dissection, the prevalence of the agger nasi cell varies from 10% [18] to 89% [19]. Because of their location near the lacrimal sac, involvement of these cells by sinus disease can lead to ocular symptoms. These cells may provide access to the frontal sinus and recess during endoscopy.

Nasal Septum Variations

Nasal septal deviation.—Normally, the structures that make up the nasal septum are aligned to form a straight wall, extending from the cribriform plate superiorly to the hard palate inferiorly (Fig. 4). At the junction of the nasal cartilage and vomer, acute bowing and deviation of the septum occur in 20% of the population [20]. When severe, the deviated septum may compress the middle turbinate bone laterally, narrowing the middle meatus and causing obstruction, secondary inflammation, and infection (Fig. 5A). When it is associated with swollen membranes, there is additional obstruction to the normal flow of mucus from the sinuses.

Imaging Techniques

Radiologic evaluation is directed toward assessing the patency of the maxillary sinus ostium, ethmoidal infundibulum, hiatus semilunaris, and middle meatus. Plain radiographs, widely available and inexpensive, provide insufficient detail to allow surgical planning. MR, with its excellent soft-tissue detail, does not adequately depict the osseous sinus walls and ostia. CT, because of its superb soft-tissue and bone detail, remains the best technique for evaluating the presence and extent of sinonasal disease before endoscopy.

The coronal plane provides the best demonstration of the OMU and simulates the plane seen by the endoscopist. For scanning, the patient is prone with the head hyperextended to ensure that free fluid layers along the maxillary sinus floor and does not "falsely" obliterate the OMU. Unenhanced 3- to 5-mm-thick contiguous slices are obtained. Although originally obtained with soft-tissue algorithms but filmed with soft-tissue and bone windows, our recent experience, as well as that of others [21], suggests that a single set of images obtained in bone algorithm and filmed with intermediate windows is sufficient in most instances. Contrast material, administered via a bolus drip technique, is used only when assessing for complications of inflammatory disease. Occasionally, extensive dental amalgams may require thin-section axial scanning with reformation in the coronal plane. Uncooperative patients and those who are unable to maintain their head in hyperextension can also be examined in the axial plane. Imaging is best performed *after* treatment of an acute process, so that areas of residual disease, most likely responsible for recurring problems, can be fully assessed [22, 23].

Endoscopic Surgery Techniques

Anterior rhinoscopy and indirect nasopharyngoscopy yield little information regarding the middle meatus and the OMU [24]. Paranasal sinus endoscopy now permits accurate, direct visualization of the entire nasal cavity, middle meatus, OMU, and sphenoethmoidal recess. It can be performed as a purely diagnostic procedure or as a therapeutic procedure (functional) to clear obstructed sinus ostia. "Functional" endoscopic sinus surgery is usually reserved for patients in whom medical management fails and who have OMU disease shown by CT and/or diagnostic endoscopy [23]. A fundamental knowledge of endoscopic techniques is necessary for meticulous CT evaluation.

For *diagnostic* endoscopy, a 4.0-mm, 0° and 30° illuminated endoscope or a 2.7-mm, 30° and 70° illuminated endoscope is used [24]. The endoscope is passed along the floor of the nose while the septum, inferior meatus and turbinate bone, middle turbinate bone, and nasopharynx are evaluated. The instrument is then rolled over the inferior turbinate bone into the posterior aspect of the middle meatus and drawn anteriorly as the ethmoidal bulla, hiatus semilunaris, and OMU are evaluated [24]. Cultures and mucosal biopsy specimens can be obtained, or antibiotics can be administered, if indicated.

Currently, two functional endoscopic surgical approaches are used [18, 25]. Both are based on the conjecture that once aeration of the sinuses is reestablished and normal drainage is restored, the mucosa will return to its prediseased state. The Wigand procedure, the more extensive and less commonly used of the two, begins posteriorly with a sphenoidotomy and proceeds anteriorly to the frontal recess. It involves a total sphenoethmoidectomy and a supramiddle turbinate antrostomy to create surgical drainage of the ipsilateral sinuses into the nose. The Messerklinger procedure begins at the ethmoidal bulla and moves anteriorly to the frontal recess or posteriorly to the posterior ethmoidal and sphenoidal sinuses, depending on the location of disease. This procedure, considered the true functional endoscopic surgical approach, relieves obstruction to the normal pathway of mucociliary drainage.

Advantages of functional endoscopic surgery over more conventional surgical techniques include (1) absence of skin or mucous membrane incisions and accompanying removal of intervening bone, (2) unparalleled visualization of the sinuses of the lateral nasal wall, (3) more accurate diagnosis of malformations or obstructing masses producing refractory sinusitis, and (4) precise localization and removal of the site of disease with mucosal preservation and restoration of normal mucociliary drainage [18]. Endoscopy is limited in its ability to show frontal sinuses and recesses, maxillary sinuses and ostia, ethmoidal bullae, and posterior ethmoidal and sphenoidal sinuses. CT is, therefore, a complementary procedure that ensures complete evaluation of changes caused by inflammatory paranasal sinus disease.

Inflammatory Sinus Diseases

Acute Sinusitis

Although occasionally due to a pure viral infection, acute sinusitis usually results from a bacterial superinfection, most commonly *Streptococcus pneumoniae*, *Haemophilus influenzae*, and *Staphylococcus aureus*. A single sinus is typically involved, usually a maxillary sinus. When the frontal, ethmoidal, or sphenoidal sinuses are independently or additionally acutely involved, risk of regional complications is increased, and aggressive treatment is required. The radiologic hallmark of acute sinusitis is the air-fluid level. Alternatively, CT findings may be limited to nonspecific, smooth or polypoid mucosal thickening. If the sinus ostium becomes obstructed, complete opacification may result.

Chronic Sinusitis

Chronic sinusitis is diagnosed clinically when the patient has either persistent inflammation or repeated bouts of acute inflammation. Anaerobes are more frequently implicated in chronic than in acute sinusitis [26]. CT may show mucosal thickening or opacification, but the hallmark of chronic sinusitis is osseous thickening of the sinus wall, representing remodeling and new bone formation in response to persistent inflammation [26] (Fig. 6). The prevalence of complications with chronic sinusitis is increased, including mucous retention cysts, polyps, and mucoceles. Although CT permits evaluation of the complications of chronic sinusitis, more importantly it shows the pathologic changes responsible for the chronic disease (e.g., obstructed ostium, apical tooth abscess). In addition to inflammatory disease, occasionally tumors may be responsible for recurrent disease. MR evaluation has been shown to be useful in this regard. Most sinus tumors, except neuromas and minor salivary gland tumors, are homogeneous and have intermediate signal intensity on T2-weighted images, as compared with the inhomogeneous high signal intensity of most inflammatory tissue [27].

Allergic Sinusitis

Allergic disease, a systemic process with a tendency for symmetric sinus involvement and pansinusitis [28], affects 10% of the population. CT often shows bilateral mucoperiosteal polypoid thickening of the sinus and turbinate membranes (Fig. 7). Air-fluid levels are typically absent unless associated acute bacterial superinfection occurs. Polypoid thickening is more often seen with allergic disease than with bacterial infection [29], resulting from persistent membrane hyperplasia.

Fungal Sinusitis

Although uncommon, a variety of fungal diseases involve the sinonasal cavities. *Mucor* and *Aspergillus*, both part of the normal respiratory flora, are the pathogens most commonly encountered. Although radiologically similar, they can frequently be differentiated clinically. Mucormycosis, an aggressive, highly invasive disease, occurs mainly in an immunocompromised or diabetic (50–75%) host. *Aspergillus*, however, can produce infection in otherwise healthy persons by colonization of a paranasal sinus. An allergic form of aspergillosis has also been described, associated with asthma and recurrent nasal polyps. Invasive aspergillosis occurs primarily in immunocompromised persons and progresses, like mucormycosis, to produce necrosis, vascular thrombosis, and intracranial extension. Initially, both cause nodular mucoperiosteal thickening, which eventually coalesces to opacify an entire sinus (Fig. 8). Multiple focal areas of bone destruction, occurring in later stages, may mimic an aggressive tumor. However, in contrast to tumors, areas of bone thickening and sclerosis may also be detected (Fig. 8). Regions of high density within the opacified sinus on CT are highly suggestive of fungal infection [30–33] (Fig. 8A). These dense concretions may be the result of the combination of metal ions and calcium salts known to occur in fungal mycetomas. Recent studies [32] suggest that MR may be more specific than CT for diagnosing fungal sinusitis. The presence of ferromagnetic metallic ions produces a hypointensity on T1- and T2-weighted images (Fig. 8C). In addition, MR more effectively shows the multiple intracranial complications of fungal diseases such as cavernous sinus thrombosis, arterial involvement, and skull base infection [34, 35].

Granulomatous Sinusitis

A variety of diseases can produce granulomatous changes in the sinonasal cavities. Actinomycosis, syphilis, tuberculosis, and sarcoidosis have all been reported [29], but Wegener's granulomatosis and midline granuloma are most familiar. Wegener's granulomatosis, a small-vessel necrotizing vasculitis, includes involvement of the sinuses, tracheobronchial tree, and kidneys. Midline granuloma, thought to be a lymphoreticular disease, has recently been described, and is being reported with increasing frequency in cocaine users [36]. Granulomatous diseases initially involve the nasal cavity and

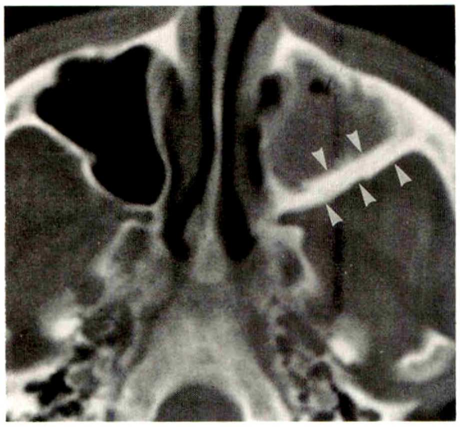
6

Fig. 6.—Chronic sinusitis. Axial CT scan shows total opacification of left maxillary sinus with marked thickening of lamina dura (*arrowheads*) compared with normal right sinus wall.

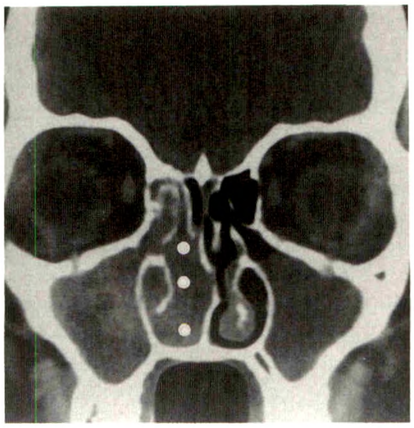
7

Fig. 7.—Polypoid disease. Coronal unenhanced CT scan shows complete opacification of right maxillary sinus with nearly complete opacification of left maxillary sinus. Mucosal thickening of turbinate bone and nasal passage (*dots*) contributes to obstruction. Biopsy revealed polypoid mucoperiosteal thickening.

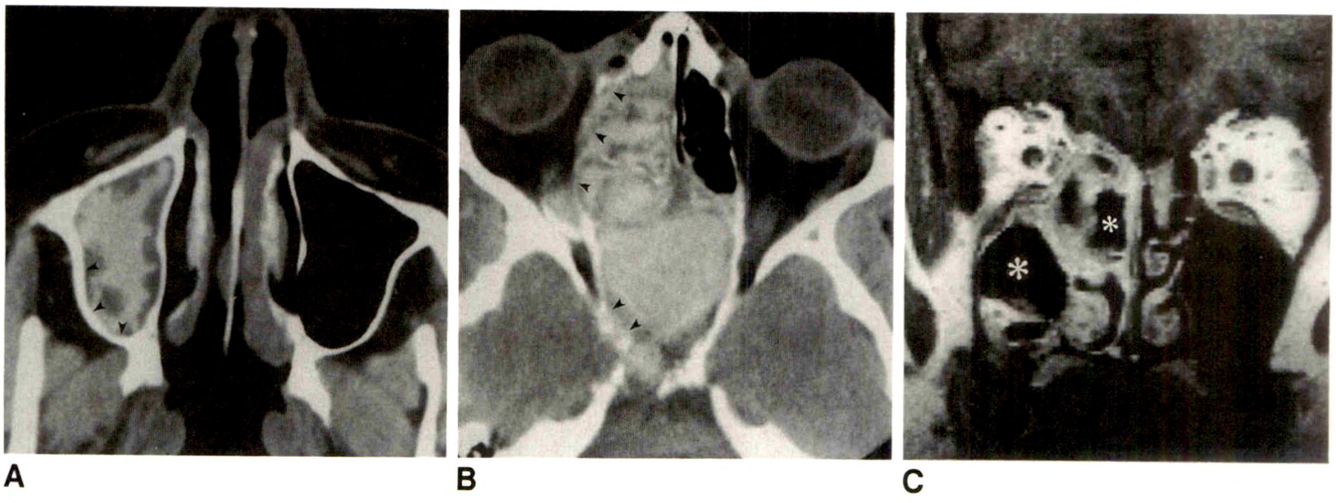

Fig. 8.—Fungal sinusitis.

A and *B*, Axial CT scans show soft tissue filling right maxillary, ethmoidal, and sphenoidal sinuses. "Lesion" is heterogeneous; increased density is suggestive of fungal infection with calcium and/or metals contained within mycetoma. Lamina dura of right maxillary sinus is slightly thickened compared with left, indicative of chronic disease (*arrowheads*, *A*). However, at higher level, there is evidence of sinus expansion and osseous destruction involving both right lateral ethmoidal wall and right posterolateral sphenoidal sinus wall (*arrowheads*, *B*).

C, Coronal contrast-enhanced T1-weighted MR image reveals heterogeneous enhancement of lesion. Areas of marked hypointensity (*asterisks*) represent signal void effects of calcium and metals contained within mycetoma. This appearance on MR images is highly suggestive of fungal disease.

Fig. 9.—Mucocele. Sagittal T1-weighted MR image shows a mass within frontal sinus that has expanded the sinus and is isointense with mucosal membranes.

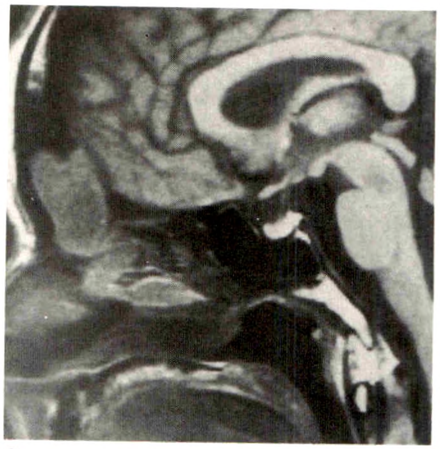

9

Fig. 10.—Mucocele. Coronal T1-weighted MR image shows mass occupying ethmoidal sinus with bony expansion of lateral walls. Mass is hyperintense relative to mucosal membranes and, when compared with mass seen in Fig. 9, exemplifies variable appearance of mucoceles on MR imaging.

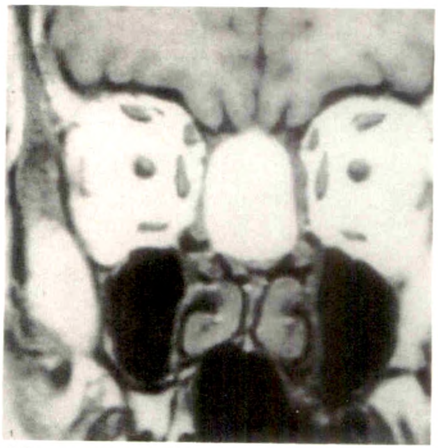

10

septum primarily and the paranasal sinuses secondarily [37]. Although Wegener's granulomatosis may cause extensive bone loss, without an associated mass [38], CT generally shows bulky, bilateral soft-tissue nodules lining the mucosa of the nasal cavity and septum. Advanced cases involve destruction of the cartilaginous nasal septum and osseous structures.

Local Complications of Sinusitis

Inflammatory polyp.—Mucous membrane hyperplasia from chronic inflammation is thought to be the underlying cause of inflammatory polyps. The hyperplasia is usually allergic in origin, most commonly located in the nasal cavity or maxillary sinus. CT typically shows a homogeneous soft-tissue mass. When severe, polyps may cause obstruction, leading to inspissated secretions and expansion of sinus walls. At this point, they may resemble tumors, and distinction on CT becomes difficult. As mentioned, MR has been shown to aid in this differential diagnosis [27].

Mucous retention cyst.—Mucous retention cyst, a benign lesion commonly occurring in the maxillary sinus floor, represents inflammatory obstruction of a seromucinous gland of the sinus mucosal lining. CT typically shows a homogeneous, dome-shaped, non–gravity-dependent soft-tissue mass with sharply defined margins.

Mucocele.—Mucoceles result from obstruction or septated sequestration of a portion of a sinus cavity. These collections result not only from inflammation but also from posttraumatic or neoplastic obstruction. The sinus fills with secretions, and eventually benign expansion occurs. Sixty percent of mucoceles occur in the frontal sinus, 30% in the ethmoidal sinus, and 10% in the maxillary sinus [37]. Sphenoidal mucoceles are rare. CT shows a low-density, nonenhancing mass that fills or expands the sinus. On both T1- and T2-weighted MR images the signal varies considerably, from hypointense to hyperintense depending on the concentration of water, protein, and mucus [39, 40] (Figs. 9 and 10). An enhancing rim with heterogeneous density suggests a mucopyocele, an infected mucocele [38, 41].

Regional Complications of Sinusitis

Regional complications may result from frontal, ethmoidal, or sphenoidal sinusitis. In particular, in one study, ethmoidal sinusitis was the cause of acute orbital inflammation in 75% of patients [42]. These infections may travel via an extensive system of valveless veins through the thin, occasionally dehiscent lamina papyracea. Orbital cellulitis, subperiosteal abscess, retrobulbar abscess, or optic neuritis may result. Distinction between postseptal abscess and cellulitis, usually possible on CT scans, is important, as treatment protocols will differ (Fig. 11). Cellulitis is characterized on CT by diffuse, homogeneously increased density and treated medically. On the other hand, abscesses characteristically have a central low-density area on CT and usually require both external ethmoidectomy and prolonged antibiotic therapy. Involvement of the intraconal space (orbital phlegmon) typically is manifested as an increased density of the retrobulbar fat ("dirty fat").

An additional complication of sinus inflammation is regional osteomyelitis, most commonly involving the frontal bone [26]. Infection can spread hematogenously, via diploic veins, or by direct extension. Extensive therapy is required. Frontal osteomyelitis, termed Pott's puffy tumor, causes lytic destruction of the frontal bone associated with an extracranial soft-tissue mass [43].

Intracranial Complications of Sinusitis

Intracranial complications of sinusitis, commonly due to extension of frontal, ethmoidal, or sphenoidal disease, include meningitis, subdural and epidural empyema, brain abscess, and venous sinus thrombosis. Spread of infection can occur along several routes: (1) hematogenous, (2) perineural, (3) retrograde thrombophlebitis, or (4) direct inoculation (trauma through an infected sinus) [26]. Complete head CT with contrast enhancement or MR examination is required when intracranial complications are suspected, as the infection may localize in areas distant from the primary infection.

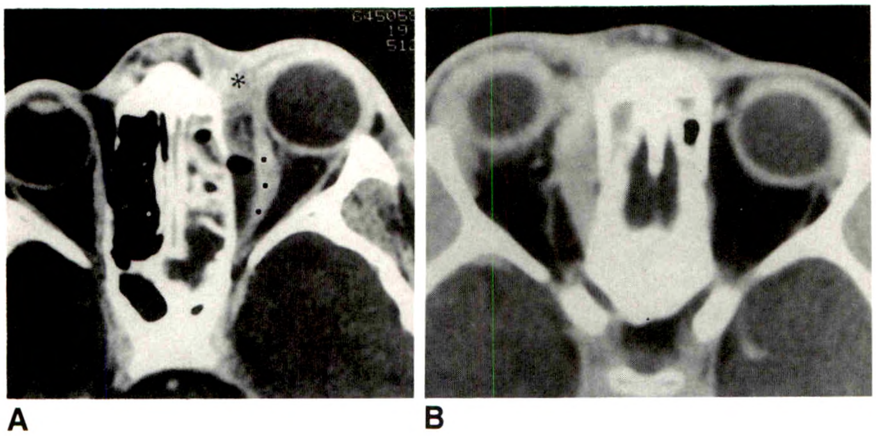

Fig. 11.—Orbital complications of inflammatory sinus disease.

A, Axial contrast-enhanced CT scan shows a hypointense postseptal collection containing air adjacent to opacified left ethmoidal air cells. This subperiosteal abscess required surgical intervention. Note marked edema of left medial rectus muscle (*dots*). Preseptal cellulitis (*asterisk*) and slight proptosis are also apparent.

B, Axial contrast-enhanced CT scan in a different patient shows homogeneously increased density involving both pre- and postseptal space of right orbit. There is also a suggestion of slight proptosis and cellulitis. This case resolved with medical management alone.

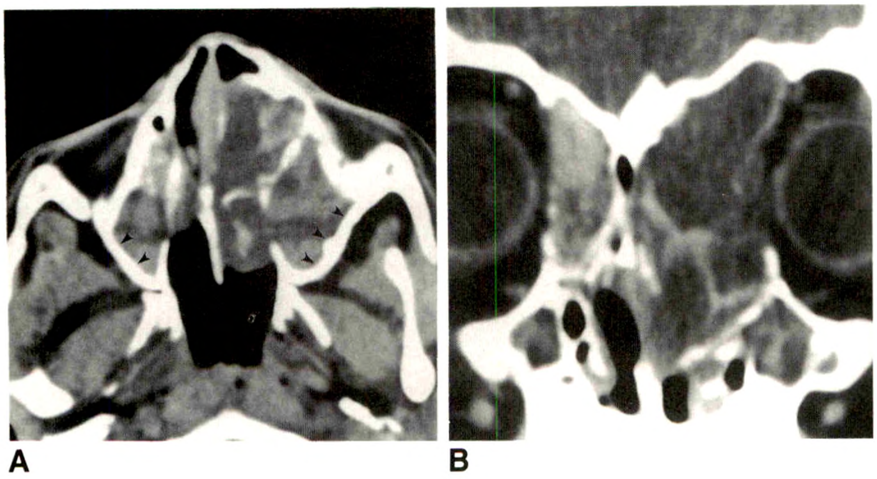

Fig. 12.—Cystic fibrosis.

A and B, Axial (A) and coronal (B) CT scans show heterogeneous, polypoid opacification of paranasal sinuses and nasal cavity. Thickening of maxillary sinus lamina dura indicates chronic, long-standing disease (*arrowheads*, A). There is pressure erosion of medial wall of left maxillary sinus and expansion of left nasal cavity. Ethmoidal sinuses are expanded bilaterally, left greater than right. Note pressure erosion of lamina paparycea in several areas bilaterally.

Syndromes

Systemic syndromes in which sinusitis is a component are infrequent but well described. The syndromes most frequently encountered are Kartagener's syndrome (immotile-cilia syndrome) and cystic fibrosis (mucoviscidosis). The primary defect in Kartagener's syndrome is a functionally inefficient central core of epithelial cell cilia that leads to inspissated sinus secretions [44]. Cystic fibrosis, on the other hand, is an inherited disorder involving a fundamental dysfunction of exocrine glands that results in the secretion of thick, tenacious mucus [45].

Although the causes of these syndromes differ, their CT appearances are similar. Almost universal opacification of all developed paranasal sinuses occurs. The secretions are frequently dense, reflecting the chronic inspissated state, with variable concentrations of mucoproteins and fluid. When the disease is long-standing or associated with polyps, sinus enlargement can occur, leading to bone remodeling and facial deformity (Fig. 12).

Summary

Endoscopic paranasal sinus surgery is consistently gaining momentum in the diagnosis and treatment of sinus disease. Otolaryngologists are now capable of visualizing and treating all sinus drainage passages on an outpatient basis. High-resolution CT has become an important complementary procedure to sinus endoscopy. The normal anatomy and variations of sinus structure, as well as pathologic appearances and complications of sinus disease, need to be well understood by the radiologist to provide optimal patient care.

REFERENCES

1. Wigand ME. *Endoscopic surgery of the paranasal sinuses and anterior skull base.* New York: Thieme, **1990**:18–41
2. Terrier F, Weber W, Ruefenacht D, Porcellini B. Anatomy of the ethmoid: CT, endoscopic, and macroscopic. *AJR* **1985**;144:493–500
3. Van Alyea OE. Sphenoid sinus. *Arch Otolaryngol Head Neck Surg* **1941**; 34:225–253
4. Renn WH, Rhoton AL Jr. Microsurgical anatomy of the sellar region. *J Neurosurg* **1975**;43:288–298
5. Fujii K, Chambers SM, Rhoton AL Jr. Neurovascular relationships of the sphenoid sinus: a microsurgical study. *J Neurosurg* **1979**;50:31–39
6. Ashikawa R. Most posterior paranasal sinus (with special reference to sphenoidal sinus). *Nippon Jibiinkoka Gakkai Kaiho* **1969**;10:762–770
7. Teatini G, Simonetti G, Salvolini U, et al. Computed tomography of the ethmoid labyrinth and adjacent structures. *Ann Otol Rhinol Laryngol* **1987**; 96:239–250
8. Maniscalo JE, Habal MB. Microanatomy of the optic canal. *J Neurosurg* **1978**;48:402–406
9. Bolger WE, Butzin CA, Parsons DS. Paranasal sinus bony anatomic variations and mucosal abnormalities: CT analysis for endoscopic sinus surgery. *Laryngoscope* **1991**;101:56–64
10. Ritter FR. *The paranasal sinuses: anatomy and surgical technique.* St. Louis: Mosby, **1973**:24–36
11. Zinreich SJ, Mattox DE, Kennedy DW, Chisholm HL, Diffley DM, Rosenbaum AE. Concha bullosa: CT evaluation. *J Comput Assist Tomogr* **1988**; 12:778–784
12. Goldman JL. *The principles and practice of rhinology: a text on the diseases and surgery of the nose and paranasal sinuses.* New York: Wiley, **1987**:405
13. Stammberger H, Wolf G. Headaches and sinus disease: the endoscopic approach. *Ann Otol Rhinol Laryngol Suppl* **1988**;97[134]:3–23
14. Lidov M, Som PM. Inflammatory disease involving a concha bullosa (enlarged pneumatized middle nasal turbinate): MR and CT appearance. *AJNR* **1990**;11:999–1001
15. Messerklinger W. *Endoscopy of the nose.* Baltimore: Urban & Schwarzenberg, **1978**:6–18
16. Zinreich SJ, Kennedy DW, Rosenbaum AE, Gayler BW, Kumar AJ, Stammberger H. Paranasal sinuses: CT imaging requirements for endoscopic surgery. *Radiology* **1987**;163:769–775
17. Kennedy DW, Zinreich SJ. Functional endoscopic approach to inflammatory sinus disease: current perspectives and technique modifications. *Am J Rhinol* **1988**;2:89–96
18. Schaefer SD, Manning S, Close LG. Endoscopic paranasal sinus surgery: indications and considerations. *Laryngoscope* **1989**;99:1–5
19. Van Alyea OE. Ethmoid labyrinth: anatomic study, with consideration of the clinical significance of its structural characteristics. *Arch Otolaryngol Head Neck Surg* **1939**;29:881–901
20. Blaugrund SM. The nasal septum and concha bullosa. *Otolaryngol Clin North Am* **1989**;22:291–306
21. Babbel R, Harnsberger HR, Nelson B, Sonkens J, Hunt S. Optimization of techniques in screening CT of the sinuses. *AJNR* **1991**;12:849–854
22. Rice DH. Basic surgical techniques and variations of endoscopic sinus surgery. *Otolaryngol Clin North Am* **1989**;22:713–722
23. Kennedy DW. Functional endoscopic sinus surgery. *Otolaryngol Head Neck Surg* **1985**;111:643–649
24. Gustafson RO, Kern EB. Office endoscopy: when, where, what, and how. *Otolaryngol Clin North Am* **1989**;22:683–688
25. Schaefer SD. Endoscopic total sphenoethmoidectomy. *Otolaryngol Clin North Am* **1989**;22:727–732
26. Weber AL. Inflammatory disease of the paranasal sinuses and mucoceles. *Otolaryngol Clin North Am* **1988**;21:421–437
27. Som PM, Shapiro MD, Biller HF, Sasaki C, Lawson W. Sinonasal tumors and inflammatory tissues: differentiation with MR imaging. *Radiology* **1988**; 167:803–808
28. Stahl RH. Allergic disorders of the nose and paranasal sinuses. *Otolaryngol Clin North Am* **1974**;7:703–718
29. Som PM. Sinonasal cavity. In: Som PM, Bergeron RT, eds. *Head and neck imaging*, 2nd ed., St. Louis: Mosby–Year Book, **1991**:114–128
30. Kopp W, Fotter R, Steiner H, Beaufort H, Stammberger H. Aspergillosis of the paranasal sinuses. *Radiology* **1985**;156:715–716
31. Kumazawa H, Zehm S, Nakamura A. CT findings of aspergillosis in the paranasal sinuses. *Arch Otolaryngol Head Neck Surg* **1987**;244:77–83
32. Zinreich SJ, Kennedy DW, Malat J, et al. Fungal sinusitis: diagnosis with CT and MR imaging. *Radiology* **1988**;169:439–444
33. Stammberger J, Jakse A, Beaufort F. Aspergillosis of the paranasal sinuses: X-ray diagnosis, histopathology and clinical aspects. *Ann Otol Rhinol Laryngol* **1984**;93:251–256
34. Yousem DM, Galetta SL, Gusnard DA, Goldberg HI. MR findings in rhinocerebral mucormycosis. *J Comput Assist Tomogr* **1989**;13:878–882
35. Press GA, Weindling SM, Hesselink JR, Ochi JW, Harris JP. Rhinocerebral mucormycosis: MR manifestations. *J Comput Assist Tomogr* **1988**;12: 744–749
36. Becker GD, Hill S. Midline granuloma due to illicit cocaine use. *Arch Otolaryngol Head Neck Surg* **1988**;114:90–91
37. Som PM. CT of the paranasal sinuses. *Neuroradiology* **1985**;27:189–201
38. Pollei S, Harnsberger HR. The radiologic evaluation of the sinonasal region. *Postgrad Radiol* **1989**;9:242–264
39. Dillon WP, Som PM, Fullerton GD. Hypointense MR signal in chronically inspissated sinonasal secretions. *Radiology* **1990**;174:73–78
40. Van Tassel P, Lee YY, Jing BS, Di Pena CA. Mucoceles of the paranasal sinuses: MR imaging with CT correlation. *AJNR* **1989**;10:607–612
41. Harnsberger HR, Osborn AG, Smoker WRK. CT in the evaluation of the normal and diseased paranasal sinuses. *Semin Ultrasound CT MR* **1986**; 7:68–90
42. Goodwin WJ Jr. Orbital complications of ethmoiditis. *Otolaryngol Clin North Am* **1985**;18:139–147
43. Wells RG, Sty JR, Landers AD. Radiological evaluation of Pott puffy tumor. *JAMA* **1986**;255:1331–1334
44. Afzelius BA. "Immotile-cilia" syndrome and ciliary abnormalities induced by infection and injury. *Am Rev Respir Dis* **1981**;124:107–109
45. Crockett DM, McGill TJ, Healy GB, Friedman EM, Salkeld LJ. Nasal and paranasal sinus surgery in children with cystic fibrosis. *Ann Otol Rhinol Laryngol* **1987**;96:367–372

Book Review

MRI of the Brain I. Non-Neoplastic Disease. Edited by William G. Bradley, Jr. and Michael Brant-Zawadzki. (One of 10 volumes in The Raven MRI Teaching File. Series editors: Robert B. Lufkin, William G. Bradley, Jr., and Michael Brant-Zawadzki.) New York: Raven, 254 pp., 1991. $60

This teaching file is a useful atlas that presents 101 cases of intracranial abnormalities diagnosed on the basis of MR findings. The book has a consistent format in which the MR images are presented along with a single sentence of history. The reader has the opportunity to inspect the images and offer a diagnosis before proceeding. Each case includes a summary of the imaging findings, presentation of the diagnosis, a discussion of the imaging approach used, and one to four references. This is clearly not intended to represent a comprehensive review of the literature. Instead, the authors have chosen references that summarize the important features of each case.

In keeping with the atlas format, the book has a large number of illustrations. In most cases, short TR, short TE, and long TR with long and short TE images are given for every lesion. The image quality is variable, ranging from adequate to excellent. The images are always of sufficient quality to display the important findings. This volume is confined to nonneoplastic diseases, so the emphasis on hemorrhagic and other vascular lesions is heavy. These represent the majority of the cases, and relatively little attention is devoted to topics such as radiation necrosis, developmental anomalies, anoxic injuries, and degenerative diseases.

This is a well done book, and many physicians should find it useful. I believe that it will be extremely valuable for radiology residents during their neuroradiology rotations. It will also be useful for residents who are reviewing for board examinations. However, for the last purpose, its value is primarily in the large number of images presented. The discussions are far too brief for this book to serve as a neuroradiology textbook. Residents in neurology and neurosurgery should find it an excellent, practical introduction to the appearance of common lesions on MR imaging. Inasmuch as the technical aspects of MR imaging are of little importance to residents in these fields, this atlas may be nearly ideal for their purposes. Radiologists in practice who have experience in neuroradiology or MR imaging will probably find this teaching file of limited value because of the abbreviated discussions and paucity of references. Perhaps a radiologist with experience in neuroradiology but who is new to MR might find the large number of carefully chosen and clearly labeled illustrations useful. Practicing radiologists with limited experience in neuroradiology but who find themselves occasionally interpreting brain MR studies may benefit from reviewing this text. Practicing neurologists and neurosurgeons may also find the large number of illustrations useful. Although the text has an unusually complete index for an atlas, the book is not intended as a reference source. It would serve as a convenient way to find several examples of the appearances of common lesions.

The authors of this text have well-deserved reputations as excellent educators, and the teaching file has the characteristics of a good review lecture. By radiologic standards, the book is a bargain at $60. The illustrations are clear, carefully chosen, and numerous. The emphasis is on common lesions and practical issues. The only drawback is that, having read through it once, most physicians will find little reason to use it again. For this reason, it may be a better choice for departmental or group libraries than for purchase by individuals.

David B. Hackney
Hospital of the University of Pennsylvania
Philadelphia, PA 19104

Pictorial Essay

Extrapineal Abnormalities of the Tectal Region: MR Imaging Findings

David P. Friedman[1]

This essay illustrates the imaging spectrum of extrapineal lesions that involve the tectal region, with emphasis on intrinsic tectal abnormalities. The superb sensitivity of MR and its multiplanar imaging capability permit unparalleled diagnostic accuracy in this region. The sagittal and axial planes are ideal for evaluating the tectum. CT remains important in the detection of acute hemorrhage and calcification. Grouping of abnormalities on the basis of anatomic boundaries (tectum, aqueduct, and quadrigeminal plate cistern) is useful in establishing the correct diagnosis.

A diverse group of lesions, many with characteristic MR imaging findings, can involve the tectal region of the brain (Fig. 1). The tectal region includes the tectum (quadrigeminal plate), cerebral aqueduct, quadrigeminal plate cistern, pineal gland, tentorial incisura, and deep cerebral veins. Although pineal masses (Fig. 2) are an important cause of tectal compression, their MR appearance is well described in the literature. Moreover, a comprehensive review of germ cell and pineal cell neoplasms would merit its own pictorial essay. The goal of this article is to provide a sound anatomic and radiologic basis for the evaluation of the less emphasized extrapineal tectal region abnormalities.

The tectum is the dorsal portion of the midbrain and is composed of the paired superior and inferior colliculi. The superior colliculi play an important role in the control of eye movements. The inferior colliculi serve as relay nuclei in transmitting auditory impulses to thalamic levels and are involved in acoustic reflexes. Parinaud's syndrome (conjugate paralysis of upward gaze) is the classic presentation of tectal dysfunction [1].

The diseases illustrated in this essay are grouped according to the following anatomic locations: tectum, aqueduct, and quadrigeminal plate cistern. The MR images are T1 weighted (383–750/11–39/1–4 [TR/TE/excitations]), T2 weighted (2000–3500/80–100/1), and proton-density weighted (2000–2717/30/1). They show representative examples of the range of diseases that can affect this small but vital area of the brain.

Intrinsic Tectal Lesions

Neoplastic

Tectal glioma.—These tumors (Figs. 3 and 4) enlarge the tectum and may completely obliterate the aqueduct. Gliomas of the midbrain often extend superiorly into the thalamus, whereas pontine gliomas tend to extend posteriorly or inferiorly. Hydrocephalus is uncommon in brainstem gliomas, except in those involving the tectum. The mass has low signal intensity on T1-weighted images and high signal intensity on T2-weighted images; enhancement is usually minimal or absent in small lesions.

Lymphoma.—Characteristic imaging findings of this tumor include solitary or multiple masses that involve the deep gray matter structures, periventricular region, and corpus callosum. Signal on T2-weighted MR images varies, but is most often isointense or hyperintense relative to that of gray matter;

Received February 12, 1992; accepted after revision March 23, 1992.

[1] Department of Radiology, Jefferson Medical College and Thomas Jefferson University Hospital, Room 1069, Main Bldg., 10th and Sansom Sts., Philadelphia, PA 19107. Address reprint requests to D. P. Friedman.

AJR 159:859–866, October 1992 0361–803X/92/1594–0859 © American Roentgen Ray Society

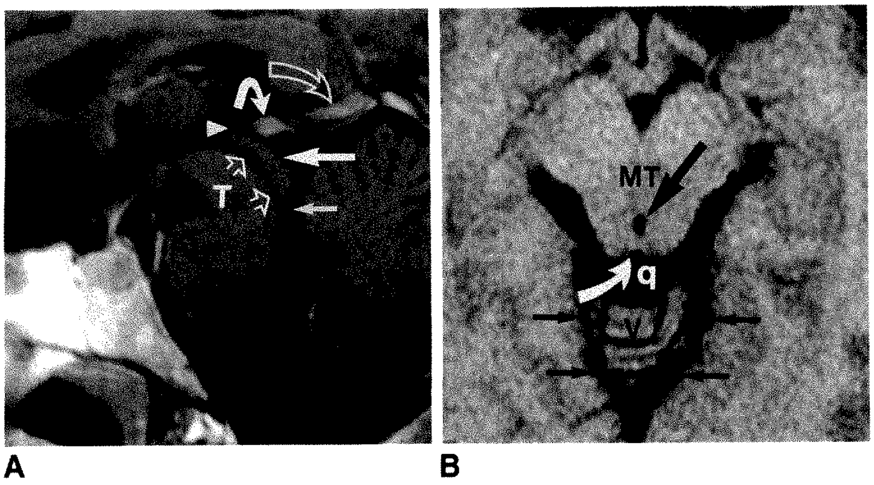

Fig. 1.—Normal anatomy.

A, Contrast-enhanced midline sagittal T1-weighted (500/12/4) MR image shows tectum (*long straight solid arrow*), tegmentum (T), aqueduct (*straight open arrows*), enhancing pineal gland (*curved solid arrow*), and vein of Galen (*curved open arrow*). Transition from mesencephalon to diencephalon is marked dorsally by posterior commissure (*arrowhead*). Transition from mesencephalon to pontine isthmus is marked dorsally by superior medullary velum (*short straight solid arrow*).

B, Axial T1-weighted (400/12/4) MR image shows midbrain tegmentum (MT), tectum (*curved arrow*), aqueduct (*long straight arrow*), quadrigeminal plate cistern (q), cerebellar vermis (v), and tentorial incisura (*short straight arrows*).

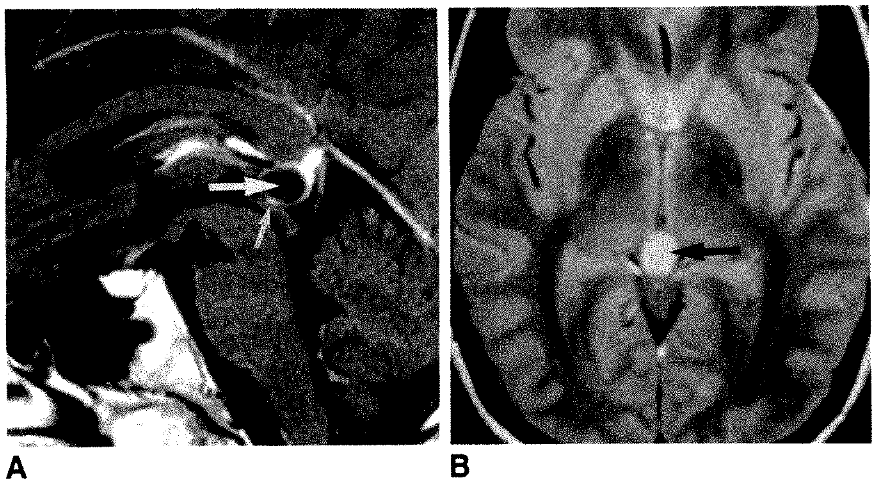

Fig. 2.—19-year-old woman with an incidental pineal cyst, unchanged during a 2-year interval.

A, Contrast-enhanced sagittal T1-weighted (500/12/4) MR image shows normally enhancing pineal gland stretched around CSF-intensity cyst (*large arrow*). Superior colliculus (*small arrow*) is compressed, but no hydrocephalus is present. Extraocular muscle movements were normal.

B, Axial proton density-weighted (2200/30/1) MR image shows a rounded lesion (*arrow*), moderately hyperintense relative to CSF, protruding into superior cerebellar cistern.

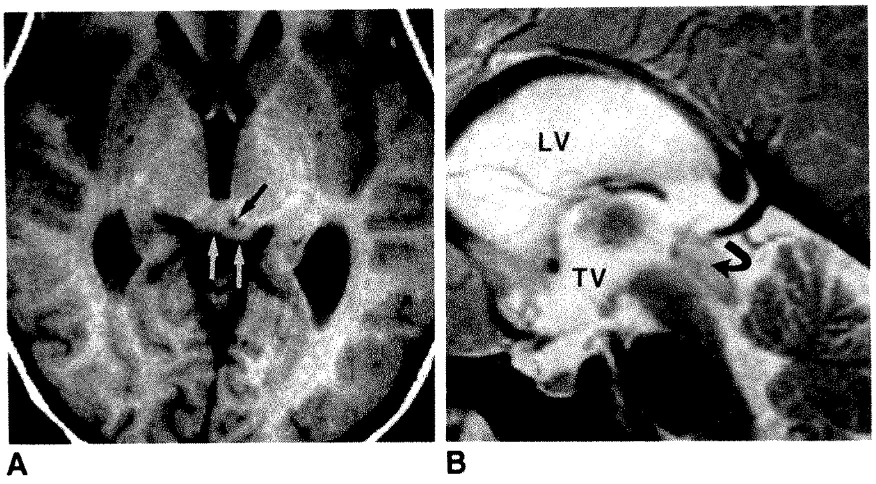

Fig. 3.—5-year-old autistic boy with presumed tectal glioma.

A, Axial T1-weighted (600/15/2) MR image shows enlargement and asymmetry of tectum (*white arrows*); aqueduct is displaced to left (*black arrow*). Lateral and third ventricles are dilated.

B, Sagittal T2-weighted (2650/80/1) MR image shows hyperintensity in thickened tectum (*arrow*). Superior and inferior colliculi cannot be separated from each other. Lateral (LV) and third (TV) ventricles are dilated.

isointensity may be seen in other hypercellular small-cell neoplasms. The extent of vasogenic edema is less than that seen with astrocytomas or metastases. Enhancement is generally uniform, although AIDS-associated CNS lymphoma commonly shows ring enhancement and extensive edema. Isolated infratentorial lymphoma (Fig. 5) is unusual.

Vascular

Occult cerebrovascular malformation.—Occult cerebrovascular malformations (Figs. 6 and 7), particularly cavernous angiomas, are frequently detected on MR images because of the presence of blood products. Asymptomatic occult cere-

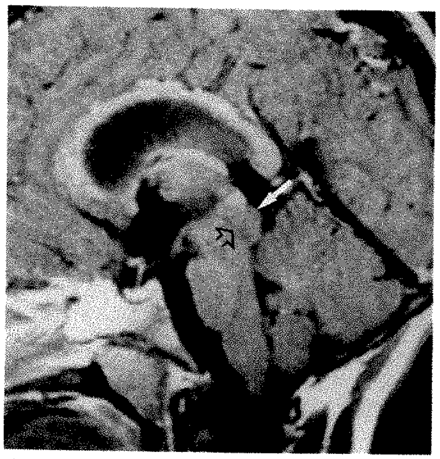

4

Fig. 4.—6-year-old boy with headaches and papilledema caused by presumed tectal glioma. Contrast-enhanced sagittal T1-weighted (600/20/2) MR image shows thickening of tectum (*solid arrow*) and obliteration of aqueduct (*open arrow*). Enhancement pattern is normal. Lateral and third ventricles are dilated. On T2-weighted images (*not shown*), lesion extended anteriorly and superiorly to involve tegmentum and thalami.

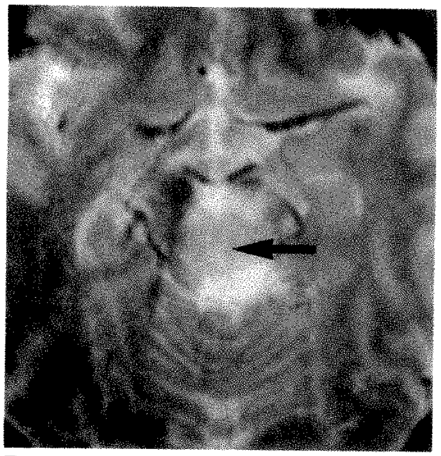

5

Fig. 5.—38-year-old HIV-negative woman with lethargy and cranial nerve palsies associated with biopsy-proved primary CNS lymphoma. Axial T2-weighted (2000/80/1) MR image shows a large, mildly hyperintense tectal and tegmental mass (*arrow*) with only mild surrounding edema. Enhancement was intense and uniform (*not shown*). A solitary, deep intraaxial mass with signal similar to that of brain should suggest diagnosis of lymphoma, especially if vasogenic edema is minimal.

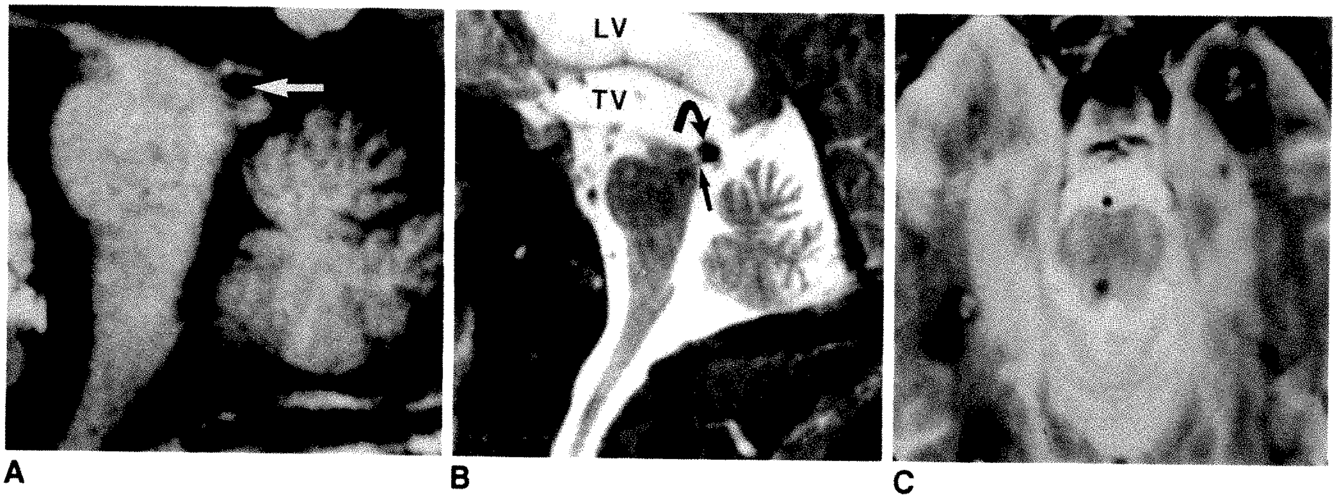

Fig. 6.—56-year-old man with headaches and multiple occult cerebrovascular malformations.

A, Sagittal T1-weighted (450/28/1) MR image shows a hypointense focus (*arrow*) in superior colliculus; aqueduct is poorly seen. Fourth ventricle appears normal.

B, Sagittal T2-weighted (3500/90/1) MR image shows "blooming" of hypointense focus (*curved arrow*), typical of chronic hemorrhage (hemosiderin). Aqueduct is obstructed (*straight arrow*). Lateral (LV) and third (TV) ventricles are dilated.

C, Axial T2-weighted (3500/90/1) MR image shows multiple hypointense foci, many with central hyperintensity (methemoglobin) typical of occult cerebrovascular malformations. There was no history of trauma; clinical and laboratory evaluations were normal.

brovascular malformations typically have central hyperintensity (methemoglobin), surrounded by a rim of hypointensity (hemosiderin). CT scans can show calcification. Tectal occult cerebrovascular malformations may result in obstructive hydrocephalus associated with aqueductal compression or scarring.

Mesencephalic arteriovenous malformation with associated vein of Galen aneurysm.—A vein of Galen aneurysm (Fig. 8) is a venous ectasia associated with markedly increased flow; the latter is usually caused by a deep-seated upper brainstem arteriovenous shunt draining either directly into the vein of Galen aneurysm or into a tributary of the vein of Galen. An associated obstruction of a dural sinus distal to the venous aneurysm is almost always present. Compression of the tectum and aqueduct can result in hydrocephalus. Perforating and/or circumflex mesencephalic arteries may be involved.

Ischemic disease.—The midbrain is supplied predominantly by mesencephalic branches of the posterior cerebral artery (interpeduncular perforating branches, peduncular branches, and circumflex mesencephalic branches). The circumflex mesencephalic arteries anastomose with small branches of the superior cerebellar artery in the region of the quadrigeminal plate, providing supply to the superior and inferior colliculi. Atherosclerotic disease may cause occlusion of these vessels and resultant infarction (Fig. 9).

Traumatic

Brainstem injury.—Diffuse axonal brainstem injury (Figs. 10 and 11) almost always occurs in the presence of similar lesions in the white matter and corpus callosum. The brainstem lesions are typically located in the dorsolateral portion

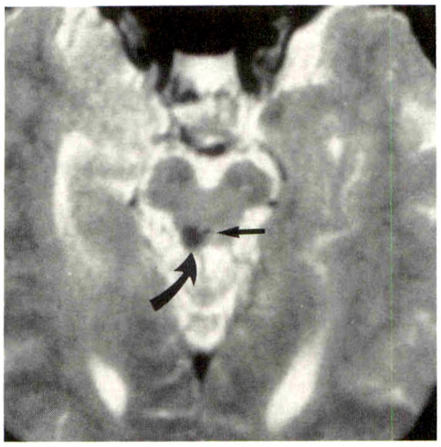

Fig. 7.—50-year-old man with incidental multiple occult cerebrovascular malformations. Axial T2-weighted (2400/80/1) MR image shows a hypointense lesion (*curved arrow*) in right inferior colliculus; aqueduct (*straight arrow*) is normal. Additional images showed multiple occult cerebrovascular malformations in cerebrum (*not shown*). Patient had no history of trauma; clinical and laboratory evaluations were normal.

of the upper pons and midbrain; they are often nonhemorrhagic. Hemorrhage in this location can also occur if the upper brainstem strikes the free edge of the tentorium; in this type of injury, the white matter and corpus callosum are not necessarily involved. Secondary (Duret) hemorrhages are usually located in the ventral and paramedian aspects of the upper pons and midbrain, with relative sparing of dorsolateral areas. CT is extremely sensitive in the detection of acute hemorrhage, whereas MR is superior in the subacute or chronic stage. On T2-weighted images, chronic shear injuries will appear hypointense because of hemosiderin; gliosis will appear hyperintense. Multiple occult cerebrovascular malformations and shear hemorrhages can have a similar appearance on MR; the clinical history and distribution of the lesions is helpful in their distinction.

Inflammatory

Multiple sclerosis.—Brainstem lesions (Fig. 12) may be seen in as many as 30% of patients with multiple sclerosis. Midbrain lesions can cause diplopia; an internuclear ophthalmoplegia results from involvement of the medial longitudinal fasciculus adjacent to the periaqueductal gray matter. Proton density–weighted images are excellent for distinguishing plaque from adjacent CSF. Wernicke's syndrome may also cause periaqueductal hyperintensity.

Cysticercosis.—Neurocysticercosis can be located in the parenchyma, subarachnoid space, or ventricular system. Depending on the stage of infection, edema, cysts, or calcifications may be seen. The brainstem can be involved (Fig. 13). The posterior fossa is the most common site of intraventricular cysts. A nonobstructing aqueductal cyst may cause hydrocephalus after treatment due to the inflammatory reaction incited by the dying cysticercus.

Degenerative

Progressive supranuclear palsy.—This neurodegenerative disease (Fig. 14) is seen in older patients. Clinical symptoms include axial rigidity, supranuclear ophthalmoplegia, and pseudobulbar palsy. The principal MR imaging abnormalities are found in the midbrain. As the superior colliculi are the subcortical region of oculomotor control, some patients with progressive supranuclear palsy have superior collicular focal

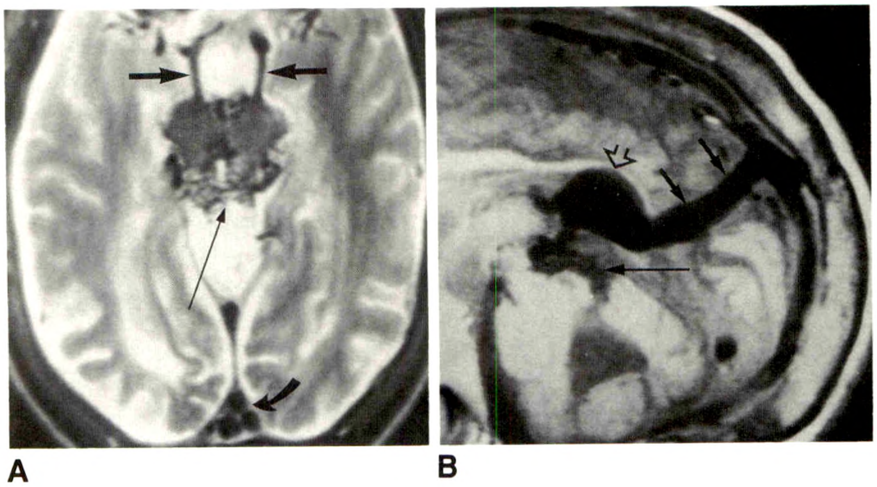

Fig. 8.—19-year-old man with mesencephalic arteriovenous malformation and vein of Galen aneurysm.

A, Axial T2-weighted (3500/80/1) MR image shows marked enlargement of posterior communicating arteries (*straight arrows*), large dorsally situated nidus in upper brainstem (*long thin arrow*), and enlarged draining veins (*curved arrow*).

B, Sagittal T1-weighted (700/34/1) MR image shows nidus (*long thin arrow*) protruding into quadrigeminal plate cistern, vein of Galen aneurysm (*open arrow*), and accessory falcial draining vein (*short arrows*). Straight sinus is absent.

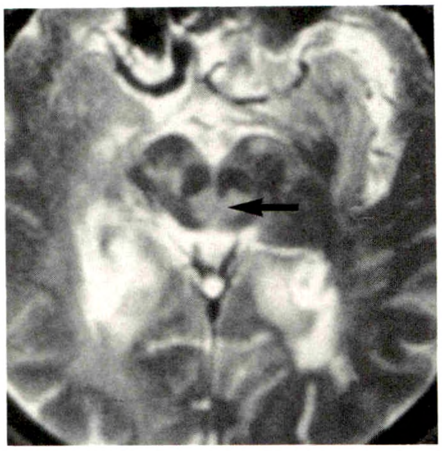

Fig. 9.—72-year-old hypertensive woman with severe vascular disease and multiple neurologic deficits. Axial T2-weighted (2467/90/1) MR image shows multiple areas of abnormal hyperintensity, particularly in dorsal midbrain (*arrow*), typical of ischemic disease/small-vessel infarction. Basilar artery was patent.

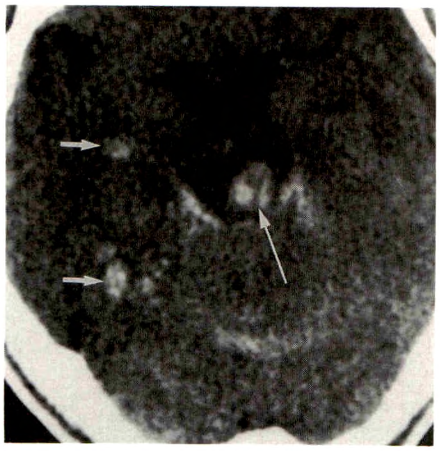

Fig. 10.—25-year-old man with severe head trauma and coma. Axial unenhanced CT scan shows hemorrhage in dorsal midbrain (*long arrow*) most consistent with axonal shear injury. Temporal lobe hemorrhages (*short arrows*) may represent contusions or shear injuries. Subarachnoid blood is present. More rostral levels showed multiple hemorrhages at gray-white interfaces and in corpus callosum.

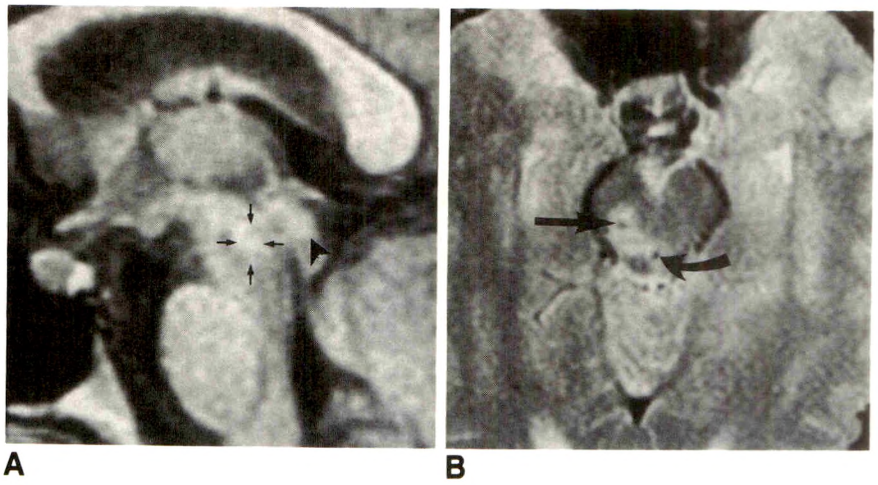

Fig. 11.—17-year-old man with severe head trauma and persistent coma despite normal findings on CT scan.

A, Sagittal T1-weighted (600/20/1) MR image obtained 4 days after injury shows small rounded areas of hyperintensity (intracellular methemoglobin) in tegmentum (*arrows*) and superior colliculus (*arrowhead*).

B, Axial T2-weighted (2182/80/1) MR image shows a focus (*straight arrow*) of hypointensity (deoxyhemoglobin) with surrounding hyperintensity (extracellular methemoglobin and edema) in right lateral tegmentum. Aqueduct (*curved arrow*) is patent. Additional shear injuries were present in supratentorial white matter.

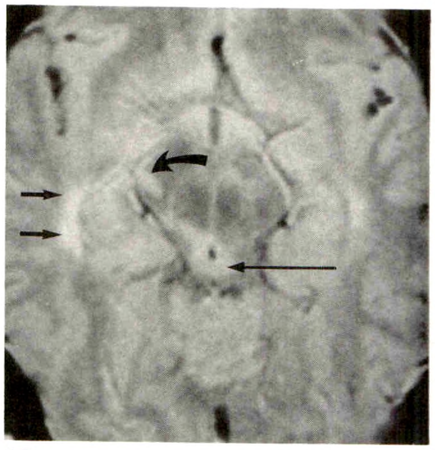

12

Fig. 12.—32-year-old man with diplopia and internuclear ophthalmoplegia due to clinically definite multiple sclerosis. Axial proton density–weighted (2000/30/1) MR image shows abnormally increased signal in tectum and periaqueductal gray matter (*long thin arrow*); additional plaques are present in right cerebral peduncle (*curved arrow*) and right temporal white matter (*straight arrows*).

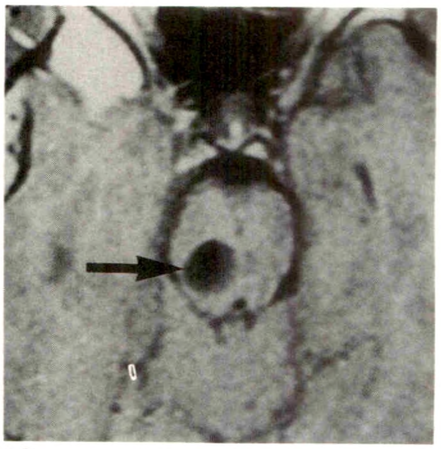

13

Fig. 13.—18-year-old man with cranial nerve palsies and presumed cysticercosis. Axial T1-weighted (700/20/2) MR image shows a cystic lesion (*arrow*) in right posterior midbrain. Additional lesions were seen in pons and cerebrum. There was no enhancement after contrast administration, and no calcification was seen on CT (*not shown*). The patient had previously traveled to Mexico, where cysticercosis is prevalent.

atrophy and/or hypointense signal on T2-weighted images. Hyperintense signal of the periaqueductal gray matter correlates with gliosis. The pars compacta of the substantia nigra may be narrowed.

Congenital

Chiari II malformation.—The tectum is abnormal in virtually all patients with Chiari II malformations (Fig. 15). The quadrigeminal plate is partially or completely fused. The midbrain is elongated caudally and posteriorly to overlie the midline cerebellum and pons; this results in a triangular ("beaked") appearance. The midbrain is distorted by dilated temporal horns and lateral extension of the cerebellum around the brainstem.

Aqueduct

Congenital aqueductal stenosis.—Patients with severe hydrocephalus generally have a stenosis in the proximal aqueduct, either at the level of the superior colliculi or at the entrance to the aqueduct immediately inferior to the posterior commissure. In patients with mild hydrocephalus, the level of the obstruction is often more distal. In distal aqueductal stenosis, the proximal aqueduct is dilated and the tectum is displaced posteriorly and stretched. An aqueductal web (Fig. 16) is a special form of aqueductal stenosis in which a small band of tissue is stretched across the distal aqueduct. Acquired aqueductal stenosis may develop as a complication of subarachnoid hemorrhage or infection.

Aqueductal tumors.—Primary neoplasms that fill the aqueduct rather than compress it are uncommon; differential con-

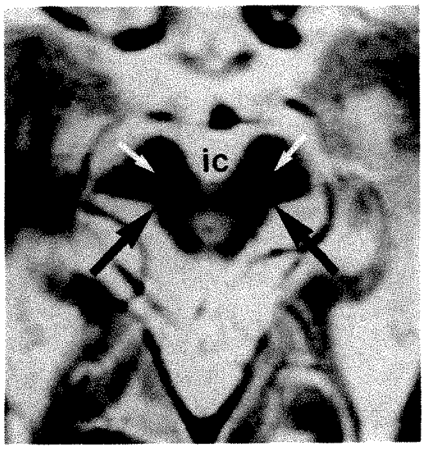

Fig. 14.—84-year-old woman with ophthalmoplegia and pseudobulbar palsy associated with progressive supranuclear palsy. Axial T2-weighted (2417/80/1) MR image shows midbrain atrophy (*black arrows*), with narrowing of the pars compacta (*white arrows*) and widening of interpeduncular cistern (ic).

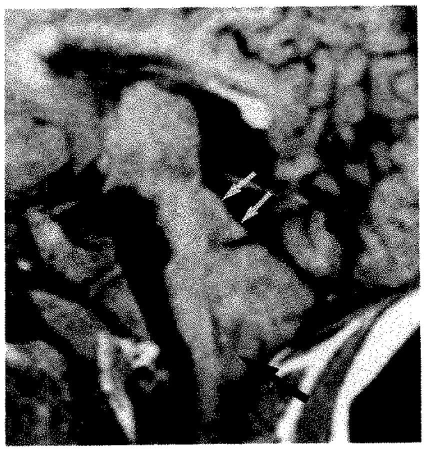

Fig. 15.—18-month-old boy with meningomyelocele and Chiari II malformation. Sagittal T1-weighted (500/16/1) MR image shows tonsillar ectopia (*black arrow*) and posteroinferior extension of beaked tectum (*white arrows*). There is fusion of colliculi and a triangular configuration of midbrain.

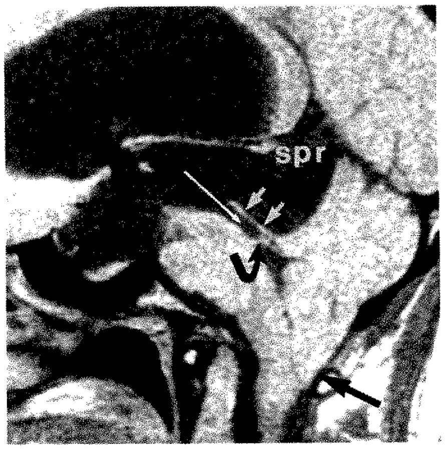

Fig. 16.—38-year-old woman with headaches and aqueductal web. Sagittal T1-weighted (750/25/2) MR image shows a distal aqueductal web (*curved arrow*), moderate dilatation of aqueduct (*long thin arrow*), and tonsillar herniation (*straight black arrow*). Tectum (*short white arrows*) is flattened by a hugely dilated suprapineal recess (spr). Fourth ventricle is normal in size.

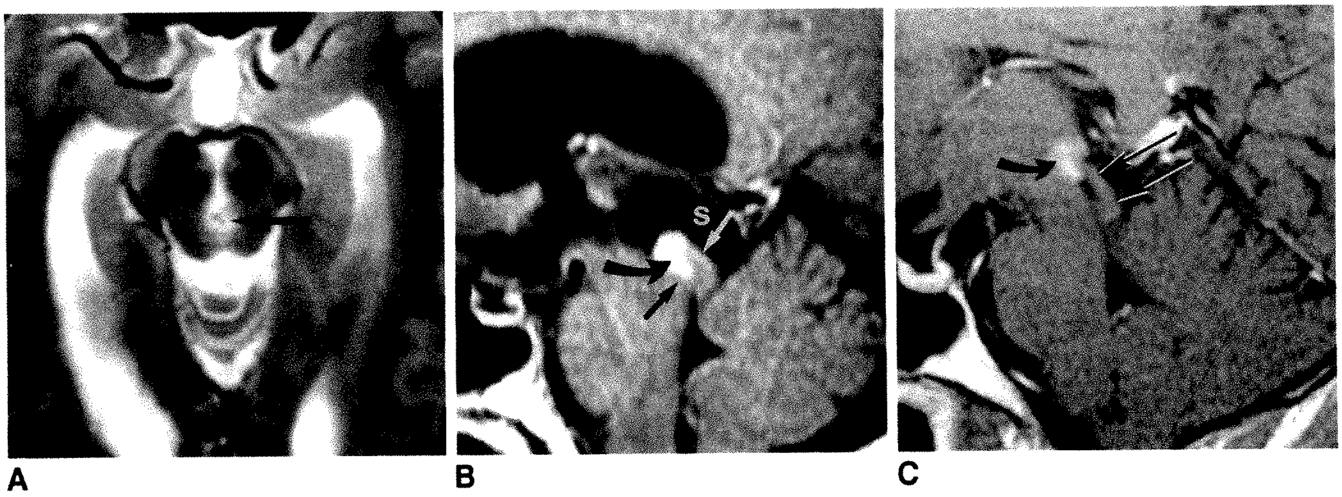

Fig. 17.—39-year-old man with headaches and papilledema associated with mass of upper aqueduct/posterior third ventricle. Differential diagnosis included ependymoma, subependymoma, and exophytic glioma.

A, Axial T2-weighted (2717/90/1) MR image shows a nodule (*arrow*), hypointense relative to CSF, in aqueduct. Nodule was markedly hyperintense relative to CSF on proton density-weighted MR image (*not shown*). Lateral and third ventricles are dilated.

B, Contrast-enhanced sagittal T1-weighted (700/23/2) MR image shows enhancement of aqueductal/posterior third ventricular mass (*curved arrow*). Tectum (*straight arrows*) is compressed and thickened by a dilated suprapineal recess (S).

C, Contrast-enhanced sagittal T1-weighted (500/12/2) MR image obtained 6 months after shunt placement. Mass (*curved arrow*) is unchanged in size. Hydrocephalus has resolved, and tectum (*straight arrows*) has returned to normal size.

siderations would include ependymoma, subependymoma, subependymal hamartoma, and exophytic astrocytoma (Fig. 17).

Hydrocephalus due to an aqueductal lesion may cause the tectum to appear short and thick. This is because of mass effect on the rostral aspect of the tectum by a dilated suprapineal recess (Fig. 17B). Distinction of compressed tectum from tectal astrocytoma can be difficult, particularly because astrocytomas in this region are generally low grade and small lesions often do not enhance. Return of the tectum to a normal thickness after shunting (Fig. 17C) is virtually diagnostic of a compressed tectum, whereas hyperintensity on T2-weighted images (Fig. 3B) indicates tumor.

Quadrigeminal Plate Cistern

Intracranial lipomas.—These lesions tend to occur in specific, characteristic locations within the brain. Truwit and

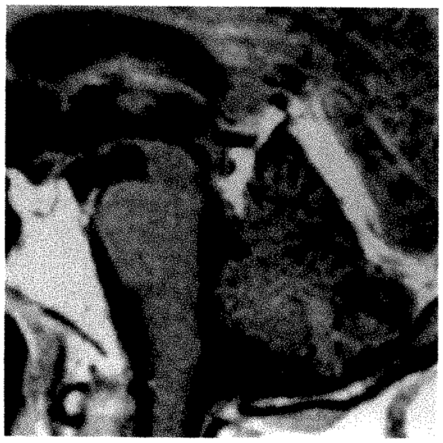

18

Fig. 18.—82-year-old woman with incidental dorsal mesencephalic lipoma. Contrast-enhanced sagittal T1-weighted (417/11/2) MR image shows relationship of hyperintense lipoma (*arrow*) to inferior colliculus (i), superior vermis, and superior medullary velum. Appearance was identical on unenhanced images.

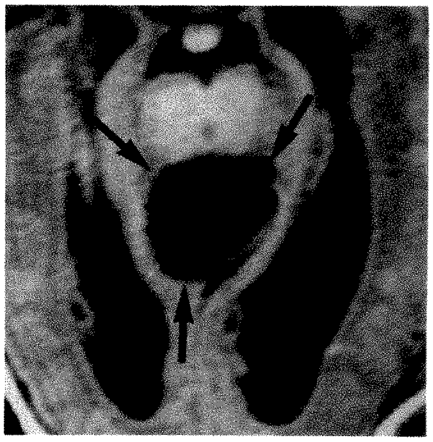

19

Fig. 19.—4-day-old girl with quadrigeminal plate arachnoid cyst. Axial T1-weighted (717/12/2) MR image shows a large rounded lesion (*arrows*), isointense with CSF, compressing tectum. Lateral ventricles are dilated.

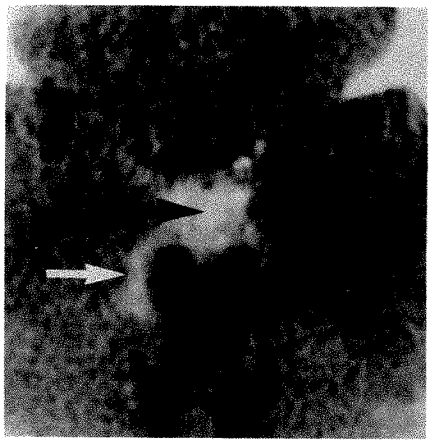

20

Fig. 20.—53-year-old man with explosive headache caused by nonaneurysmal perimesencephalic subarachnoid hemorrhage. Unenhanced axial CT scan shows subarachnoid hemorrhage in interpeduncular fossa (*black arrow*), with extension of blood into right ambient cistern (*white arrow*). No hemorrhage is present in sylvian fissures. Spinal fluid was positive for hemorrhage. Findings on three angiograms were normal.

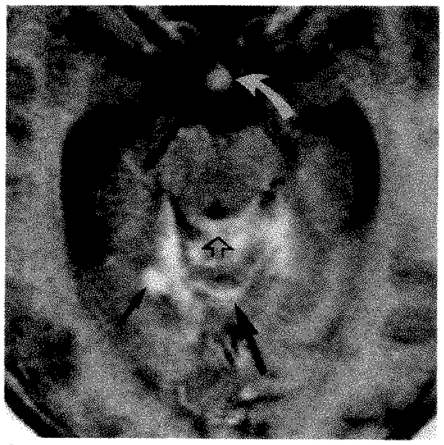

21

Fig. 21.—63-year-old woman with breast carcinoma and progressive confusion. Contrast-enhanced axial T1-weighted (383/11/2) MR image shows abnormal enhancement of quadrigeminal plate (*open arrow*) and cerebellar vermis (*long solid black arrow*) due to carcinomatous meningitis. Spinal fluid was positive for malignant cells. Enhancing metastases are also seen in right medial temporal lobe (*short solid black arrow*) and infundibulum (*white arrow*).

Barkovich [2] concluded that lipomas are congenital malformations that result from abnormal persistence and maldifferentiation of meninx primitiva during the development of the subarachnoid cisterns. The relationship of dorsal mesencephalic lipomas (Fig. 18) to the inferior colliculus is consistent. These lesions are hyperintense on T1-weighted images and isointense or hypointense on T2-weighted images. Vessels can be seen coursing through the lipoma, and a chemical-shift artifact is typically seen in the frequency-encoded direction.

Arachnoid cyst.—These lesions may be due to a congenital abnormality in the development of the arachnoid membrane or associated with an inflammatory reaction in the subarachnoid space. Quadrigeminal plate arachnoid cysts (Fig. 19) can cause hydrocephalus as a result of aqueductal compression. Arachnoid cysts are virtually isointense with CSF on all pulse sequences; calcification and enhancement are not seen in uncomplicated lesions.

Subarachnoid hemorrhage.—Blood in the quadrigeminal plate cistern is most often due to congenital aneurysm, arteriovenous malformation, or trauma. Rinkel et al. [3] recently reported a characteristic distribution of cisternal blood in patients with nonaneurysmal subarachnoid hemorrhage; on CT, the center of bleeding was located immediately anterior to the upper part of the brainstem (Fig. 20). Frank intraventricular hemorrhage was not found. Extension to the ambient cisterns was common, but the anterior interhemispheric and lateral sylvian fissures were never completely filled with blood. These authors concluded that the prognosis in this subset of patients is excellent, and the hemorrhage may represent a capillary or venous rupture. Their observations indicate the need for careful scrutiny of the extent of perimesencephalic subarachnoid hemorrhage.

Carcinomatous and inflammatory meningitis.—The quadrigeminal plate cistern may be affected by a variety of neoplastic and inflammatory processes. Breast carcinoma (Fig. 21), lung carcinoma, and melanoma frequently spread to the subarachnoid space. Infectious (e.g., tuberculosis, *Cryptococcus*) and noninfectious (e.g., sarcoid) types of granulomatous meningitis typically involve the basal cisterns. Gadopentetate dimeglumine-enhanced MR imaging is the most sensitive imaging technique available for detecting meningitis.

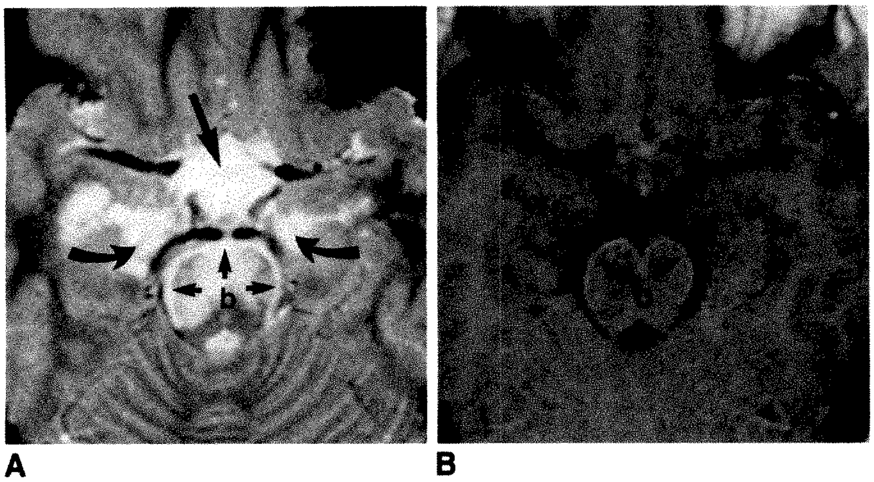

Fig. 22.—5-year-old girl with type 1 neurofibromatosis.

A, Axial T2-weighted (2600/90/1) MR image shows hyperintensity in optic chiasm (*long straight arrow*), optic radiations (*curved arrows*), and brainstem (b). A peripheral rim of hyperintensity (*short straight arrows*) surrounds brainstem.

B, Contrast-enhanced axial T1-weighted (416/12/2) MR image shows peripheral enhancement (*arrows*) of brainstem (b); more rostral level showed peripheral enhancement of optic chiasm glioma. This enhancement may represent arachnoidal hypertrophy.

Arachnoidal hypertrophy in neurofibromatosis.—Abnormal areas of parenchymal hyperintensity on T2-weighted images are common in patients with type 1 neurofibromatosis (Fig. 22). Peripheral enhancement of optic nerve gliomas associated with this disease may relate to the pathologic finding of marked arachnoidal hypertrophy surrounding the tumor [4]. It is possible that similar arachnoidal changes may occur in other areas of the brain because of the lesions of neurofibromatosis.

REFERENCES

1. Carpenter MB. *Core text of neuroanatomy*, 2nd ed. Baltimore: Williams & Wilkins, **1978**:141–163
2. Truwit CL, Barkovich AJ. Pathogenesis of intracranial lipoma: an MR study in 42 patients. *AJNR* **1990**;11:665–674
3. Rinkel GJE, Wijdicks EFM, Vermeulen M, et al. Nonaneurysmal perimesencephalic subarachnoid hemorrhage: CT and MR patterns that differ from aneurysmal rupture. *AJNR* **1991**;12:829–834
4. Byrd SE. Central nervous system manifestations of inherited syndromes. In: Atlas SW, ed. *Magnetic resonance imaging of the brain and spine*. New York: Raven, **1991**:539–566

Case Report

Intraocular Cryptococcosis: Imaging Findings

Woo Kyung Moon,[1] Moon Hee Han,[1] Chi Sung Song,[2] Kee Hyun Chang,[1] and Man Chung Han[1]

Cryptococcus neoformans is a yeastlike fungus of worldwide distribution that can infect healthy persons as well as those who are chronically ill or immunocompromised [1]. The lung, brain, and meninges are the most frequently involved areas in systemic cryptococcosis. Involvement of the eyes is relatively uncommon [2–5]. We report a case of intraocular cryptococcosis shown by sonography and confirmed after enucleation.

Case Report

A 31-year-old man had pain in the left eye and a cough for 2 months. He was an alcoholic and had been treated conservatively at a local clinic for a liver disease 3 months before admission, but the blurred vision and pain in the left eye became worse.

Sonography with an Aloka SSD 650 unit and a 7.5-MHz transducer showed a large echogenic mass located mainly in the anterior portion of the vitreous chamber of the left eye (Fig. 1A). The right eye was normal at that time. Chest CT scans showed scattered patchy infiltration in both lungs. Because of persistent severe pain in the eye, enucleation was performed. The mass was located at the anterior part of the vitreous body (Fig. 1B). It was irregularly shaped, pale yellow, and soft and friable. The retina was detached. Histological examination showed that the mass was composed of granulomatous inflammatory cells, including epithelioid cells, lymphocytes, plasma cells, a few multinucleated giant cells, and a few histiocytes. A few small yeastlike organisms were found, and silver stains showed that they were *C. neoformans*. A wedge biopsy of the lung lesion was done, but no organisms were seen in or cultured from the biopsy specimen.

One month after the enucleation, examination of the patient's remaining eye showed a lesion, thought to be caused by a fungus, at the posterior pole of the fundus. CT of the orbit (General Electric 9800 CT unit, 1-mm-thick slices) and sonography showed a small soft-tissue mass in the posterior part of the globe of the right eye (Figs. 1C and 1D). Findings on contrast-enhanced CT of the brain were normal. The patient was treated with IV flucytosine for 7 weeks, and his visual and chest signs and symptoms improved.

Discussion

C. neoformans is an encapsulated yeastlike ubiquitous fungus. The organism gains entrance to the human body through the respiratory tract [1, 2]. From an initial focus of infection in the lung, the organism can be disseminated hematogenously to other organs, with a special predilection for the CNS. Meningitis is the most frequent clinical CNS manifestation. Less commonly, the skin, genitourinary tract, lymph glands, viscera, bones, and eyes may be involved [2]. Ophthalmic complications such as papilledema, optic atrophy, and external ophthalmoplegias occur in 36–40% of cases of cryptococcal meningitis [3]; actual invasion of the intraocular structures by *C. neoformans* is less common. Chorioretinitis is the most frequently reported clinical ophthalmic manifestation [4]. Histologic examinations of cadaveric or enucleated eyes have shown choroiditis, neuroretinitis, invasion of the optic nerve, and diffuse intraocular cryptococcal infections [2–5].

Two theories exist about the origin of the ocular involvement in cryptococcosis. One possibility is direct spread from the CNS along the meninges to the optic nerve with subsequent intraocular proliferation. The other is hematogenous spread to the eye. This has been shown in mice experimentally infected intraperitoneally with *Cryptococcus* [6]. Of the

---

Received April 6, 1992; accepted after revision May 6, 1992.

[1] Department of Radiology, College of Medicine, Seoul National University Hospital, 28 Yongon-Dong, Chongno-Gu, Seoul 110-744, Republic of Korea. Address reprint requests to W. K. Moon.

[2] Department of Radiology, Seoul City Boramae Hospital, Sindaebang-Dong, Dongjak-Gu, Seoul, 156-012, Republic of Korea.

***AJR* 159:867–868, October 1992** 0361–803X/92/1594–0867 © American Roentgen Ray Society

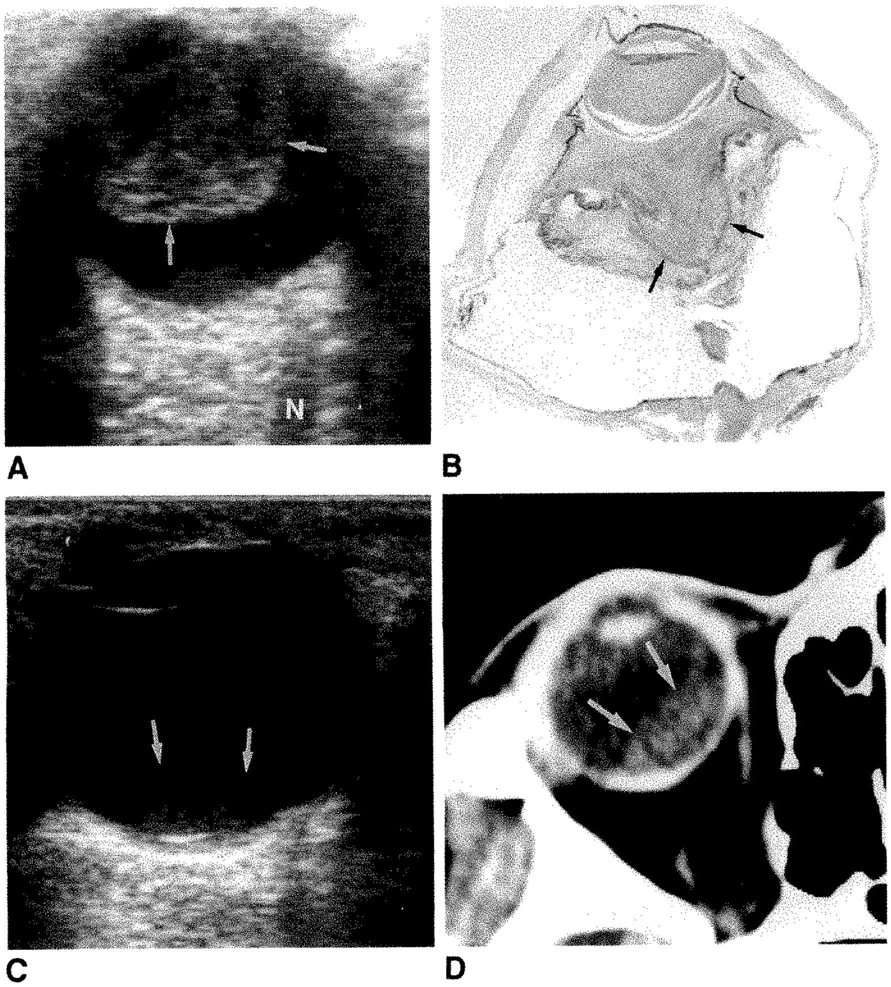

Fig. 1.—Intraocular cryptococcosis in a 31-year-old man.

A, **Sonogram of left eye shows well-marginated echogenic mass filling anterior part of vitreous chamber. Poorly defined echogenicity in posterior part of globe is probably due to retroretinal exudate. *Arrows* = detached retina, N = optic nerve.**

B, **Photomicrograph of sectioned left eye shows a soft, friable mass in anterior part of vitreous chamber. Histologic examination showed mass was an area of granulomatous inflammation with detached retina. *Arrows* = detached retina.**

C, **Sonogram of right eye obtained 1 month after enucleation of left eye shows a new echogenic nodular mass (*arrows*) in posterior part of globe.**

D, **CT scan obtained same day as C shows a soft-tissue mass (*arrows*) in posterior part of globe.**

22 reported cases of ocular cryptococcosis, six were not associated with CNS diseases [5]. In our case of endophthalmitis, we postulate hematogenous spread from the pulmonary infection.

To our knowledge, only one report of intraocular cryptococcosis that includes contact B-mode sonograms has been published in the English literature [4]. The sonograms showed a solid elevated echogenic lesion with a smooth anterior margin in the posterior pole, similar to the sonographic appearance of the lesion in the right eye in our patient. Inasmuch as *C. neoformans* has a marked predilection for neuronal tissues, it is logical to assume that the sensory retina is a preferred site for growth of these organisms and subsequent formation of a subretinal abscess and a granulomatous inflammatory mass. As the fungal infection progresses, retraction of the vitreous and detachment of the retina occur, with the mass occupying the anterior portion of the vitreous chamber.

The echogenic nodular mass visible on the sonogram or the increased density in the posterior part of the globe seen on CT were nonspecific radiologic findings. Many of the fungal diseases and so-called granulomatous infectious diseases, including tuberculosis, sarcoidosis, brucellosis, leprosy, and ocular toxocariasis, may undergo similar processes [7].

In neither our case nor the other reported cases of ocular cryptococcosis unaccompanied by meningitis has the diagnosis been established before enucleation. Our case further supports the importance of early diagnosis, especially when the vision of one eye is impaired and a similar inflammatory process seems to be occurring in the remaining eye. Proper treatment will prevent loss of vision and save lives.

REFERENCES

1. Fetter BF, Klintworth GK, Hendry WS. *Mycoses of the central nervous system.* Baltimore: Williams & Wilkins, **1967**:89–123
2. Bisseru B, Bajaj A, Carruthers RH, Chhabra HN. Pulmonary and bilateral retinochoroidal cryptococcosis. *Br J Ophthalmol* **1983**;67:157–161
3. Hiss PW, Shields JA, Augsburger JJ. Solitary retinovitral abscess as the initial manifestation of cryptococcosis. *Ophthalmology* **1988**;95:162–165
4. Sields JA, Wright DM, Augsburger JJ, Wolkowicz MI. Cryptococcal chorioretinitis. *Am J Ophthalmol* **1980**;89:210–218
5. Weis RF, Everett ED, Sprouse R, Elfervig JL. Endogeneous cryptococcal endophthalmitis. *South Med J* **1981**;74:482–483
6. Cordon PI, Terry SI, Falconer H. Cryptococcal eye disease. *Doc Ophthalmol* **1977**;44:49–55
7. Margo CE, Katz NNK, Wertz FD, Dorwart RH. Sclerosing endophthalmitis in children: computed tomography with histopathologic correlation. *J Pediatr Ophthalmol Strabismus* **1983**;20:180–184

The Cost-effectiveness of Replacing High-Osmolality with Low-Osmolality Contrast Media

J. Jaime Caro[1-3]
Evelinda Trindade[2]
Maurice McGregor[1,2]

OBJECTIVE. Our purpose was to assess the cost-effectiveness of substituting low-osmolality contrast media for high-osmolality media in noncardiac parenteral use in radiology.

MATERIALS AND METHODS. Estimates of effectiveness, taken as the reduction in risks of reactions affecting safety and comfort, were based on a recent meta-analysis of data published since 1980. Costs were those of the contrast medium and of treating reactions.

RESULTS. One hundred thousand uses of low-osmolality media instead of high-osmolality media would cost an additional $7.7 million. No deaths would be prevented, but there would be 80% fewer life-threatening events and 75% fewer minor reactions. Considering only life-threatening events, complete conversion to low-osmolality media costs $62,000 per event prevented. If only minor reactions are considered, this figure is $800 per event prevented. The cost-effectiveness of partial substitution of low-osmolality media in "high-risk" patients only cannot be estimated with confidence. With one set of assumptions, a 33% reduction in life-threatening reactions at a cost of $22,000 per event prevented is estimated. These estimates are insensitive to all inputs except the cost differential between high- and low-osmolality media: for every dollar decrease in cost differential per use, the cost per life-threatening event prevented drops by $790.

CONCLUSION. The allocation of limited resources requires the best available information on the relevant costs and benefits. A policy of substitution of low- for high-osmolality media will not influence mortality and will bring fairly small benefits at a considerable cost.

***AJR* 159:869-874, October 1992**

Awareness of limited health care resources increasingly forces decision makers to take into account the value and cost of contemplated health policies. The development of low-osmolality contrast media (LOM) for use in radiology has raised one such important issue in health policy; while the newer agents produce fewer adverse reactions than the older high-osmolality media (HOM), they also cost considerably more. Thus, the choice between these agents involves a trade-off between a higher risk of adverse reactions with the older media and increased costs with the newer media.

In order to judge whether the replacement of HOM by the safer but more expensive LOM is justified, those involved in the decision need to know what the costs of achieving any reductions in risk are, and how these compare with those for other technologies on which funds might be spent. Several economic analyses of the choice of contrast media have been published [1-5], but owing to outdated risk estimates, these are of limited use for making current policy decisions about the use of these agents.

For example, although a recent economic analysis [1] concluded that use of LOM would result in an increased ("incremental") cost of $65,000 per quality-adjusted life year (QALY), the authors acknowledged that their estimate of a 10-

Received January 21, 1992; accepted after revision April 28, 1992.

Presented in part at the annual meeting of the International Symposium on Technology Assessment in Health Care, Helsinki, June 1991.

This work was supported by the Conseil d'évaluation des technologies de la santé du Québec.

[1] Department of Medicine, Royal Victoria Hospital, McGill University, Montreal, Quebec H3A 1A1, Canada.

[2] Conseil d'évaluation des technologies de la santé du Québec, Tour de la Bourse, P.O. Box 215, Montreal, Quebec H4Z 1E3, Canada. Address reprint requests to M. McGregor.

[3] Medical Research International, 67 S. Bedford St., Burlington, MA 01803.

0361-803X/92/1594-0869
©American Roentgen Ray Society

fold reduction in the risk of death "is probably much greater than the true reduction in risk." Indeed, our recent estimates [6] indicate that the risk of death is not reduced with the use of LOM. Thus, the focus on years of life gained is inappropriate. Furthermore, apart from renal failure, none of the reactions to contrast media produce long-lasting effects in survivors, making quality adjustment of remaining life years unwarranted.

To remedy these problems, we carried out a cost-effectiveness analysis by using up-to-date risk estimates based on our previous meta-analysis [6] and cost estimates from the viewpoint of the insurer, either private or government-sponsored health care system. Intracardiac uses of contrast media were not considered because they carry very different risks.

Materials and Methods

Effectiveness Estimates

The effectiveness of using LOM instead of HOM was taken to be improvements in safety and comfort, since it is generally thought that image quality is the same with both [7-10] and LOM do not appear to have any adverse consequences relative to HOM use. Although more frequent strokes with LOM have been reported [11], the risk appears to be no higher now that awareness of the lower anticoagulant effect of LOM has led to changes in management [12, 13]. Similarly, a recent report indicates that with proper attention to phlebographic technique, the frequency of thrombosis of leg veins after phlebography is comparable with HOM and LOM [14].

Severe reactions affecting safety and milder reactions that affect only comfort were considered separately. Although safety of a contrast agent may be thought of only in terms of the resulting risk of death [5], here it is extended to include all severe reactions to contrast media, nonfatal as well as fatal. This was done because most severe reactions, despite usually being transient and resulting in full recovery, are potentially fatal, particularly if not treated promptly and appropriately.

The risks of severe reactions to parenteral use of HOM and the reductions in these risks by the use of LOM have been the subject of a recent meta-analysis [6]. In that study, all available original data on the subject reported between January 1, 1980, and December 31, 1989, were reviewed. Extension of that review to April 1, 1991, did not result in the inclusion of further data as no new reports met the inclusion criteria (provision of original data in sufficient detail regarding the occurrence of the adverse events of interest: at least 60 observations in noncomparative series, or at least 30 observations in each group in comparative studies). All reports were classified according to study design: randomized trials, nonrandomized studies with concurrent controls, nonrandomized studies with historical controls, and uncontrolled series. Reports were not excluded on the basis of the quality of the study design, but analyses of subsets of data according to study design were done. Data pertaining to patients explicitly identified by the authors as "high risk" were analyzed separately.

Data were abstracted on all fatal events and on all other events deemed by the original authors to be "severe." These reactions were anaphylaxis, severe hypotension or hypertension requiring urgent intervention, loss of consciousness, chest pain not rapidly responsive to nitrates, arrhythmia requiring urgent cardioversion or pacing, pulmonary edema, laryngeal edema or spasm, or bronchospasm sufficient to cause respiratory obstruction. For this analysis, all of these reactions were taken to be life-threatening, even though it is possible that some may not have been. In most reports, it is impossible to make this distinction. Permanent renal dysfunction requiring dialysis was not considered because data on this problem amount to only a few case reports. Studies of renal dysfunction after the use of contrast media have been concerned with transient small rises in serum levels of creatinine, a clinically insignificant event unlikely to have any implications for cost, or for the duration or quality of life.

Crude rates derived from all reports were used to estimate risks with HOM. The risk of severe reactions with the use of HOM was 157 per 100,000 uses (95% confidence interval, 144-172 per 100,000) (Table 1). The reduction in risk obtainable with LOM was estimated as the weighted average of the rate differences from all comparative studies, with the inverse of the corresponding variances as the weights. The use of LOM was estimated to reduce the risk of severe reactions by 80% (rate difference, 126 per 100,000; 95% confidence interval, 110-142 per 100,000). Considering only fatal reactions, the risk with the use of HOM was estimated as 0.9 per 100,000 uses (95% confidence interval, 0.3-2.6 per 100,000). Use of LOM did not appear to reduce this risk (rate difference, 0; 95% confidence interval, −1.2 to 1.2 per 100,000).

None of these estimates changed much if different subsets of studies were used as sources of data [6]. So few events occurred in randomized trials that if only these studies were used, the resulting confidence intervals were extremely wide and covered not only the best estimates, but their confidence intervals as well. For example, the reduction in risk of severe reactions with LOM is estimated from randomized trials to be 72%, but the confidence interval for the rate difference is −321 to 358 reactions prevented per 100,000 uses.

No attempt was made to meta-analyze data on the frequencies of events that have implications only for patients' comfort. Instead, the estimates obtained in a very large nonrandomized survey [15] were used. In this survey, the frequency of one or more transient symptoms (nausea, vomiting, heat sensation, itching, urticaria, flushing, hoarseness, vascular pain, transient chest pain, abdominal pain, palpitation, facial edema, rigor) was reported to be 12.44% after use of HOM and only 3.09% after use of LOM. The frequency of vomiting, estimated separately because it is a more objective event, was 1.8% with HOM and 0.4% with LOM. Delayed minor events such as skin rash, parotid swelling, and flulike symptoms appear to occur as often after use of LOM as after HOM [16] and thus were not considered in this report. Pain, which is frequent after peripheral intraarterial administration of HOM [17-19] and can be substantially reduced by use of LOM [18], was also not considered because the use of undiluted HOM for peripheral arterial injections is now rare.

The results of a large population survey [20] were used to obtain estimates of the increase in the risk of severe reactions in patients perceived to be at higher risk. In that study, 15% of recipients were

TABLE 1: Risks of Various Adverse Events with High-Osmolality Media and Reductions in These Risks Obtained by Conversion to Low-Osmolality Media

Event(s)	Risk or Reduction in Risk per 100,000 Uses (95% Confidence Interval)			
	Risk with High-Osmolality Media		Reduction in Risk with Low-Osmolality Media	
All severe[a]	157[b]	(144-172)	126	(110-142)
Fatal[a]	0.9	(0.3-2.6)	0	(−1.2-1.2)
All minor[c]	12,440	(12,284-12,599)	9350	(9171-9532)
Vomiting[c]	1,800	(1,719-1,884)	1473	(1400-1540)

[a] Based on [6], updated April 1, 1991.

[b] Best estimate.

[c] Based on [15].

thought to be at four times higher risk of severe reactions than the other 85%. This information was used to partition the average risk with HOM estimated in the meta-analysis by assuming that it was a weighted average of the risk in patients at higher risk and that of those at lower risk. Thus, in the estimated 15% higher risk patients, the risk of a severe reaction with HOM would be 432 per 100,000 uses, while in the other 85% of patients the risk would be 108 per 100,000. It was initially assumed that the 80% reduction in the risk provided by LOM use estimated in the meta-analysis [6] applied without modification to the higher risk patients.

Cost Estimates

Only direct costs to the system providing health care were considered. These were taken to be the costs of the contrast media and of managing reactions. These costs were not discounted because all the expenditures occur during, or immediately after, the use of contrast media. All costs are given in 1991 United States dollars except where specified.

The cost of one use of contrast medium depends on the volume used (including wastage) and the price of the medium per milliliter. The volume of contrast medium used varies with the type of investigation and with the user. In 29 articles reporting these data included in the meta-analysis of the risks [6], average volumes of use were 175 ml for angiography, 100 ml for CT, 60 ml for urography, and 100 ml for all other procedures. These amounts were used in this analysis (Table 2).

Prices also vary greatly, according to both the supplier and the user. In 1989, the price of 100 ml of HOM was reported to range in the United States from $10.81 to $13.63 and that of 100 ml of LOM from $87.00 to $105.81 [21]. For this analysis, based on the average list prices (1991) of American suppliers of contrast media, we estimated the cost of 100 ml of HOM as $14.59, that of 100 ml of high-iodine-content LOM as $95.34, and that of 100 ml of low-iodine-content LOM as $71.47.

To estimate the relative frequency of each procedure we used data from the province of Quebec, where in 1989, 17% of contrast procedures were angiographies and other intraarterial procedures, 47% were CT examinations, and 36% were urographies [22]. All other procedures constituted less than 1% of the total. About one third of angiographies were carried out with low-iodine-content media. Taking the estimate of volume used for each type of procedure, weighted by the proportion of each type of procedure, and multiplying by the corresponding estimated cost per milliliter of medium, yields an estimated average cost for use of LOM of $91.41 and for HOM of $14.36 (Table 2). This difference of $77.05 per use was varied from $50 to $150 in sensitivity analyses.

Contemporary estimates of the costs of managing severe reactions are not available in the literature. We therefore assumed, based on information from a university teaching hospital in Montreal, that all such events would lead to reinstallation of an IV infusion if one were not still in place and the use of atropine (average cost, $5). Further, it was assumed that consultation with a cardiologist or internist ($90) would be required in 10% of events, for an average added cost of $9. Finally, it was assumed that 2% of such reactions would require admission to an intensive care unit for an average stay of 1 day ($1300), for an average added cost of $26. Thus, averaged over all procedures, management of a severe reaction would cost approximately $40. In view of its implicit imprecision, this initial estimate was varied from $0 to $4000 in sensitivity analyses.

In spite of the best estimate not indicating any reduction in the risk of death with the use of LOM, the observed reduction in severe reactions suggests that with larger numbers of observations a difference in mortality might appear. Accordingly, it was assumed, for the purpose of sensitivity analyses, that LOM use might lead to some reduction in the risk of fatal reactions. The costs of managing fatal reactions were therefore also estimated. Although most deaths generate few such costs, others may take place only after a period in intensive care. Averaged over all deaths, it was assumed that the cost of managing a fatal event would amount to $600. A range of $0 to $6000 was used in sensitivity analyses.

It was assumed that no additional costs would be incurred with minor events affecting only comfort.

TABLE 2: Estimation of Average Cost per Use of Contrast Medium According to Osmolality

Type of Procedure	% of Use	Volume per Procedure (ml)	Price ($/ml)		Cost ($/Use)	
			HOM	LOM	HOM	LOM
Angiography	17	175	0.15	0.87	25.54	152.92
CT	47	100	0.15	0.95	14.59	95.34
Urography	36	60	0.15	0.95	8.76	57.20
Other	<1	100	0.15	0.95	14.59	95.34
Weighted average					14.36	91.41

Note.—HOM = high-osmolality media, LOM = low-osmolality media.

Cost-effectiveness Estimates

To depict the implications of replacing HOM with LOM for parenteral use, the reductions in reactions of each kind per 100,000 uses were derived and paired with the incremental costs of conversion. The cost-effectiveness ratio with respect to safety was first derived by taking a reduction in the risk of severe reactions as the sole benefit of LOM. Although the best estimate was that the frequency of deaths is not reduced with LOM use, a sensitivity analysis was done in which a cost-effectiveness ratio considering only fatal reactions was derived. For this purpose, the benefit was measured as the gain in life expectancy obtained by replacing HOM with LOM. Life expectancy was calculated as the product of the estimated average preprocedure life expectancy for the patients at issue and their probability of surviving the procedure given the type of contrast media used (the complement of the probability of dying as a result of the use of contrast media). With respect to comfort, a cost-effectiveness ratio considering only minor reactions was derived. No discounting was done because both the costs and the benefits take place immediately.

Extensive sensitivity analyses of all inputs were carried out. Apart from varying the cost estimates across the ranges stated above, the reductions in risk with LOM were varied across the range given by their 95% confidence interval. The cost-effectiveness ratios corresponding to complete elimination of each risk by LOM also were derived.

Results

Complete Substitution

The direct costs (those of the contrast medium and of management of ensuing adverse events) of 100,000 parenteral uses of HOM in general radiology are about $1.4 million. This number of uses would result in 157 severe reactions, approximately one of which would be fatal. In addition, 12,440 minor reactions would occur, 1800 of which would be episodes of vomiting. Use of LOM instead of HOM in all 100,000 instances would cost an additional $7.7 million. This expenditure would reduce the number of severe reactions to 31, a reduction of 80%. It would be unlikely, however, to reduce the frequency of fatal reactions. In addition, there would be 75% fewer minor reactions with 78% fewer episodes of vomiting.

The incremental cost of using LOM instead of HOM in all parenteral injections of contrast material is, therefore, $61,113 per severe reaction prevented. If only fatal reactions are considered, the replacement of HOM with LOM is clearly not cost-effective as no reduction in mortality is expected to follow.

There is no satisfactory method of combining, in a single index, the effects of LOM use on the risks of severe and of minor reactions. If the increase in safety is ignored and only reactions affecting comfort are considered, the cost per minor reaction avoided is $824. If only episodes of vomiting are considered, the cost per episode prevented is $5228.

The estimate of cost per severe reaction prevented depends on the degree of effectiveness of LOM in reducing this risk (Table 3). If the reduction in risk is only as much as the lower bound of its 95% confidence interval, the cost per severe reaction prevented rises to about $70,000. If the reduction in risk provided by LOM is as much as its upper 95% confidence bound, the cost per severe reaction prevented drops to about $54,000. To take an even more extreme case, if all risk were to be eliminated by an improved type of LOM, the cost would be about $49,000 per severe reaction prevented. In order to bring it below $10,000 per severe reaction prevented, the risk with HOM would have to be nearly fivefold higher than estimated here, and all of these reactions would have to be prevented by LOM.

Apart from the risk reduction with LOM use, the main determinant of cost-effectiveness is the difference in cost between the two types of contrast media. The cost per severe reaction prevented drops by about $790 for every dollar decrease in the difference in costs of the media per use. Thus, if the cost difference were $50 instead of the estimate of $77.05 used here, the cost per severe reaction prevented drops to about $40,000 (Table 3). If the cost difference were as high as $150, the cost per severe reaction prevented rises to nearly $120,000.

TABLE 3: Cost-effectiveness of Complete Conversion to Low-Osmolality Media

Estimate	Cost-effectiveness[a]
Risk reduction (per 100,000 uses)	
Best estimate (126)	61,113
Lower bound, 95% CI (110)	70,002
Upper bound, 95% CI (142)	54,227
Complete elimination (157)	49,046
Cost difference (LOM − HOM)/use	
Best estimate ($77.05)	61,113
Lower estimate ($50)	39,643
Upper estimate ($150)	119,108
Cost of managing reactions (per reaction)	
Best estimate ($40)	61,113
Lower estimate ($0)	61,153
Upper estimate ($4000)	57,153

Note.—CI = confidence interval, LOM = low-osmolality media, HOM = high-osmolality media.

[a] In U.S. dollars per life-threatening reaction prevented.

The cost difference depends on the volume of contrast medium used for each type of procedure, on the relative frequencies of the different types of procedures, and on the price per milliliter, quantities that vary with place and time. In Canada, for example, the average cost per 100 ml of high-iodine-content LOM is $70.23 (Can$84.28); of low-iodine-content LOM $62.82 (Can$73.39); and of HOM, $9.71 (Can$11.65). By using the same estimates of volumes used and of the distribution of procedures, the average cost of a use of LOM in Canada is $68.36 (Can$82.03) and of HOM, $9.55 (Can$11.46). With these estimates, which imply a cost differential between HOM and LOM of $58.81 per use, instead of $77.05 used in the main analysis, the additional cost of complete conversion to LOM in Canada would drop to $5.9 million (Can$7 million) per 100,000 uses, and, thus, the cost per severe reaction prevented would come down to about $47,000 (Can$56,000).

The cost-effectiveness of LOM use is insensitive to large alterations in the estimates of costs of managing adverse reactions. For example, a 100-fold increase in the cost of managing a life-threatening event, from $40 to $4000, produces only a 6% drop in the cost per severe reaction prevented, from $61,113 to $57,153 (Table 3).

It was estimated that no reduction in the risk of fatal events is provided by conversion to LOM. If, however, it was assumed that the risk with HOM is at the upper bound of the confidence interval, and that the reduction with LOM is also as high as the upper bound of its 95% confidence interval, 1.2 per 100,000, then the cost would be $6 million per death prevented (all other benefits ignored). Assuming an average life expectancy of 20 years in these patients, this would amount to about $300,000 per life year gained. To bring the cost per life year gained below $100,000, the risk associated with the use of HOM would have to be four times higher than the best estimate and LOM would have to eliminate this elevated risk completely.

The cost-effectiveness estimate pertaining to comfort does not change very much with changes in the assumptions regarding the inputs. For example, changing the risk reduction with LOM through the range given by its 95% confidence interval changes the cost per minor reaction prevented by only 2% either way.

Partial Substitution

As stated, there are insufficient data on which to base a firm estimate of the benefits of using LOM only in patients at higher risk. If it is assumed that 15% of patients are at an average fourfold higher risk of severe reactions (see Materials and Methods), substitution of LOM for HOM only in these patients would cost an additional $1.15 million and would prevent 52 reactions, at a cost of $22,187 per severe reaction prevented. On the basis of the five studies focusing on higher-risk patients [4, 20, 23–25], the risk with HOM is 376 per 100,000 and the risk reduction with LOM is 88%. Use of these estimates instead suggests that partial conversion to LOM would lead to 70 fewer reactions per 100,000 uses at a cost of $16,482 per severe reaction prevented. Even with these latter estimates that are more favorable to LOM, 80 life-threatening reactions would still occur in the 85,000 uses of HOM in low-risk patients, and seven such reactions would occur among the 15,000 uses of LOM in high-risk patients.

Discussion

In this analysis of parenteral uses of contrast medium, intracardiac use was excluded since the risks and the methodologic issues involved in this use of contrast material are quite different.

Although several different types of adverse reactions to contrast media can occur, we opted for a cost-effectiveness analysis instead of a cost-utility analysis because we thought that depiction of the reductions in risk for each type of reaction together with the attendant costs was more informative than bringing all of these to a single scale by arbitrary assignment of a "utility" to each type of reaction. All the events of concern lead either to rapid and complete resolution or to death, and, thus, there are no long-lasting effects on the quality of life of survivors. Thus, it is unwarranted, in this context, to measure the transient discomfort in question on a scale involving duration of life. Neither QALY [1] nor healthy-year equivalents [3] provides appropriate scales for this purpose.

The estimates of risks and of risk reductions used as inputs to this analysis are based on an exhaustive meta-analysis of recent literature. Although the use of such extensive data provides for quite precise estimates, it is possible that indiscriminate inclusion of studies may have introduced bias. The net effect of any such biases appears to be small, however, as the estimates based on more strictly selected subsets of studies, particularly those of randomized trials, are well within the 95% confidence intervals of the estimate used here [6]. This range of variation has been covered in sensitivity analyses. Similarly, although the use of a different subset of studies to estimate risk with HOM and risk reduction with LOM may have introduced bias, estimates made by using the same subset of studies are within the 95% confidence interval covered in sensitivity analyses.

Given the large variability in the determinants of the cost differential between HOM and LOM, the estimates made here will not correspond to actual differentials in all jurisdictions. The estimates of volume of use for different procedures are consistent, however, with estimates of use made at an academic hospital in Boston: 150 ml of contrast material injected for angiography, 60–100 ml for CT and urography, plus 15–25% wastage (Bettmann MA, personal communication); and at a university hospital in California: 150–250 ml for arteriography, 100–200 ml for CT, and 50 ml for urography, all including wastage (Smith DC, personal communication). The actual price paid may be lower than the list price by an amount that varies with time and place and is difficult to determine. Furthermore, any such savings are not necessarily applicable only to LOM, and, thus, the price differential between the types of media may be less affected by discounts. In any case, sensitivity analysis over a range wide enough to account for such variations in the cost differential was carried out.

The estimates of costs of managing adverse reactions were based on a very simplified conception of the course of these events. A more detailed accounting of the management of these reactions would not add greatly, however, as these costs have little impact on the cost-effectiveness estimates. Although the estimated costs of managing adverse reactions may underestimate costs in the United States as they are based on Canadian prices for resources consumed, they are within the ranges found in a 1988 American study of 405 reactions to contrast media [4].

The selective use of LOM in patients at higher risk of severe reactions has been frequently entertained [26–31], and strategies of partial substitution have been incorporated into formal guidelines issued by professional societies [32, 33]. Economic analysis of strategies of partial substitution is, for the reasons stated, fraught with difficulty. This analysis, based on plausible estimates, indicates that, although the selective use of LOM in higher risk cases is more cost-effective, such a policy would still fail to prevent most reactions.

On the basis of this analysis, it can be concluded that although the new agents do increase safety, the increase is small and the attendant costs considerable. Comparison of a policy of substitution of LOM for HOM with other contemplated health expenditures is difficult because no standards exist for measuring the attendant costs and benefits. Although some attempts have been made to use QALYs as a standard [34], this measure does not suit the nearly always sequelae-free reactions addressed here.

The objective of this study was to establish the economic implications of using LOM instead of HOM by using the best available contemporary estimates of the risks involved for the decision makers in question. How the information is used in any particular jurisdiction must also depend on resolution of the fiscal, political, and social considerations that pertain. Decisions regarding the use of LOM must turn on how much it is reasonable to pay in order to avoid how much risk or discomfort. On the basis of one author's estimate of use [20],complete substitution of HOM by LOM would increase health spending in the United States, where the cost difference is greater, by $770 million per year. In Quebec, where the cost difference is less, such a decision would increase the cost of health care by $12.8 million annually (Can$15 million).

In a jurisdiction such as a hospital in the Quebec health care system, where budgets are fixed, spending more on one item forces spending less on another. For example, in an average-sized academic hospital where the conversion from HOM to LOM might cost $700,000, it would be necessary to close two intensive care beds, each costing $1300 per day, or take some equivalent action to pay for the conversion.

Such a decision, made for economic rather than clinical reasons, is not one to be made by the individual radiologist acting independently. It is one to be made formally and openly by the responsible institution in the light of analyses such as this one and the advice of its own professional staff. Such a decision would, furthermore, have to be accompanied by clear, institutionally adopted guidelines for any use of LOM, together with acceptance by the institution of responsibility for all reactions resulting from HOM use undertaken within these guidelines.

It is to assist in the making of such decisions that these estimates have been provided. Clearly, the estimates are imperfect, and more accurate and specific information would be highly desirable. If and when such information becomes available, policies can be modified. Meanwhile, policy decisions must be made with the best available contemporary information.

REFERENCES

1. Goel V, Deber RB, Detsky AS. Nonionic contrast media: economic analysis and health policy development. *Can Med Assoc J* **1989**;140:389-395
2. Jacobson PD, Rosenquist CJ. The introduction of low-osmolar contrast agents in radiology: medical, economic, legal, and public policy issues. *JAMA* **1988**;280:1586-1592
3. Gafni A, Zylak CJ. Ionic versus nonionic contrat media: a burden or a bargain? *Can Med Assoc J* **1990**;143:475-478
4. Powe NR, Steinberg EP, Erickson JE, et al. Contrast medium-induced adverse reactions: economic outcome. *Radiology* **1988**;169:163-168
5. Sutherland JB, Huda W. Costs and benefits of low-osmolality contrast agents in radiology. *Can Assoc Radiol J* **1989**;40:18-21
6. Caro JJ, Trindade E, McGregor M. The risks of death and of severe nonfatal reactions with high- vs low-osmolality contrast media: a meta-analysis. *AJR* **1991**;156:825-832
7. Bryan RN, Miller SL, Roehm JOF Jr., Weatherall PT. Neuroangiography with iohexol. *AJNR* **1983**;4:344-346
8. Bettmann MA, Robbins A, Braun SD, Wetzner S, Dunnick NR, Finkelstein J. Contrast venography of the leg: diagnostic efficacy, tolerance, and complication rates with ionic and nonionic contrast media. *Radiolgoy* **1987**;165:113-116
9. Seyferth W, Dilbat G, Zeitler E. Efficacy and safety of digital subtraction angiography with special reference to contrast agents. *Cardiovasc Intervent Radiol* **1983**;6:265-270
10. Whitehouse GH, Snowdon SL. Metrizamide and iohexol in aortography for lower limb ischaemia: a comparative trial. *Acta Radiol Suppl* (Stockh) **1983**;366:164-165
11. Dawson P, Hewitt P, Mackie IJ, Machin SJ, Amin S, Bradshaw A. Contrast, coagulation, and fibrinolysis. *Invest Radiol* **1986**;21:248-252
12. Robertson HJF. Nonionic contrast media in radiology: procedural considerations. *Invest Radiol* **1988**;23[suppl 2]:S374-S377
13. Davidson CJ, Mark DB, Pieper KS, et al. Thrombotic and cardiovascular complications related to nonionic contrast media during cardiac catheterization: analysis of 8,517 patients. *Am J Cardiol* **1990**;65:1481-1484
14. Blumgart RL, Immelman EJ, Jeffery PC, Lipinski JK. Thrombotic side-effects of lower limb venography: the use of heparin-saline flush. *S Afr Med J* **1991**;79:88-89
15. Katayama H, Yamaguchi K, Kozuka T, Takashima T, Seez P, Matsuura K. Adverse reactions to ionic and nonionic contrast media: report of the Japanese Committee on the Safety of Contrast Media. *Radiology* **1990**;175:621-628
16. McCullough M, Davies P, Richardson R. A large trial of intravenous Conray 325 and Niopam 300 to assess immediate and delayed reactions. *Br J Radiol* **1989**;62:260-265
17. Nyman U, Nilsson P, Westergren A. Pain and hemodynamic effects in aortofemoral angiography: clinical comparison of iohexol, ioxaglate and metrizamide. *Acta Radiol Suppl* (Stockh) **1983**;366:S171-S172
18. Wolf GL. Adult peripheral angiography: results from four North American randomized clinical trials of ionic media versus iohexol. *Acta Radiol Suppl* (Stockh) **1983**;366:166-170
19. Zeitler E, Georgi-Tönnesen M, Hinski HG, Mader H, Richter E-I. *Angiography in lower extremities with new contrast media: review of double-blind studies.* Lyon, France: Springer-Verlag, **1982**:257-264
20. Palmer FJ. The RACR survey of intravenous contrast media reactions: final report. *Australas Radiol* **1988**;32:426-428
21. Anonymous. Low osmolality contrast agents. *Med Lett Drugs Ther* **1989**;31(801):87
22. Régie de l'assurance maladie du Québec. *Microfiches des actes diagnostiques et thérapeutiques payés aux professionels de la santé: 1989-1990.* Québec: Gouvernement du Québec, **1991**
23. Langer M, Behrends B, Langer R, Eichstadt H, Janicke UA. Tolerance of iopromide in angiography: a multicenter study. *Rofo Forstsch Geb Rontgenstr Neuen Bildgeb Verfahr* **1989**;128:61-66
24. Parfrey PS, Griffiths SM, Barret BJ, et al. Contrast material induced renal failure in patients with diabetes mellitus, renal insufficiency, or both. *N Engl J Med* **1989**;320:143-149
25. Lasser EC, Berry CC, Talner LB, et al. Pretreatment with corticosteroids to alleviate reactions to intravenous contrast material. *N Engl J Med* **1987**;317:845-849
26. Grainger RG. Annotation: radiological contrast media. *Clin Radiol* **1987**;38:3-5
27. Parfrey PS, Cramer BC, McManamon PJ. Should nonionic radiographic contrast media be given to all patients? *Can Med Assoc J* **1988**;138:497-500
28. McClennan BL. Ionic and nonionic iodinated contrast media: evolution and strategies for use. *AJR* **1990**;155:225-233
29. Bettmann MA. Guidelines for use of low-osmolality contrast agents. *Radiology* **1989**;172:901-903
30. Swanson DP, Thrall JH, Shetty PC. Evaluation of intravascular low-osmolality contrast agents. *Clin Pharm* **1986**;5:877-891
31. Wolf GL. Safer, more expensive iodinated contrast agents: how do we decide? *Radiology* **1986**;159:557-558
32. Mishkin MM, Edeiken J. Committee on Drugs and Contrast Media. The current efficacious use of water soluble contrast agents for intravascular injections. *ACR Bull* **1988**;44:9-10
33. Corporation Professionnelle des Médecins due Québec. *Guide to the use of low-osmolality media as contrast agents.* Montréal: Corporation Professionnelle des Médecins du Québec, **1988**:1-16
34. Dixon J, Welch HG. Priority setting: lessons from Oregon. *Lancet* **1991**;1:891-895

MR Lymphography with Iron Oxide Compound AMI-227: Studies in Ferrets with Filariasis

Tad Tanoura[1]
Michael Bernas[2]
Ammar Darkazanli[1]
Eric Elam[1]
Evan Unger[1]
Marlys H. Witte[2]
Allan Green[3]

OBJECTIVE. The purpose of this study was to assess the MR lymphographic potential of AMI-227 to reduce the signal intensity of hyperplastic inflammatory lymph nodes by using ferrets with filariasis as the animal model. Both interstitial and IV modes of administration were studied.

MATERIALS AND METHODS. Twelve ferrets were infected with the filaria *Brugia malayi* and six control ferrets were injected with superparamagnetic iron oxide AMI-227, either interstitially or IV. Signal intensities of the left popliteal lymph node, left hamstring muscle, and left inguinal fat were measured before, 48 hr after, and up to 138 days after contrast injection with the use of both spin-echo and gradient-echo techniques. The signal intensity data were statistically analyzed. The lymph nodes, liver, spleen, and lungs were studied with light and electron microscopy.

RESULTS. Forty-eight hours after the interstitial injection of AMI-227, the signal intensities of the ipsilateral popliteal nodes of the infected and control ferrets were significantly reduced ($p < .0005$) without significant changes in the signal intensities of the surrounding tissues on both spin-echo and gradient-echo MR images. No nodal signal reduction occurred with the IV route of injection in ferrets. Light microscopy revealed iron to be localized within nodal marginal zones exclusively. Lymphatic trunks were visualized after interstitial injection. Signal reduction persisted to our end point at 138 days.

CONCLUSION. AMI-227 shows regional specificity with significant enhancement of nodal structures and demonstrates potential as an interstitial MR lymphographic agent.

***AJR* 159:875-881, October 1992**

The radiographic techniques currently available for depicting the lymphatic system remain limited. Conventional oil contrast lymphography and radioisotopic lymphangioscintigraphy have well-known morbidities and limitations [1-4]. CT and MR are the imaging techniques now used most often for evaluating lymph nodes, especially in staging of cancer. In both, diseased lymph nodes are detected by their enlarged dimensions, but false negativity of normal-sized diseased nodes limits staging capabilities. Furthermore, MR differentiation of normal from diseased lymph nodes via signal-intensity characteristics is unreliable [5, 6].

Contrast enhancement of the lymphatic system with CT or MR would allow improvement in sensitivity for detecting lymph node abnormalities. Previous studies that used iron oxide compounds were able to distinguish normal from neoplastic nodes, but comparison with benign nodes (e.g., inflammatory) was not done [7]. Accordingly, we investigated contrast-enhanced MR imaging of the lymphatic system with superparamagnetic iron oxide AMI-227 in ferrets with filariasis, an established experimental counterpart of human inflammatory disease [4, 8-11]. We examined the potential of the superparamagnetic iron oxide AMI-227 to reduce the signal intensity of the hyperplastic nodes in our ferret model via interstitial and IV modes of administration.

Received December 11, 1991; accepted after revision April 5, 1992.

This work was supported in part by Advanced Magnetics, Cambridge, MA, and United Nations Development Programme/World Bank/World Health Organization special program 870051.

[1] Department of Radiology, The University of Arizona College of Medicine, 1501 N. Campbell Ave., Tucson, AZ 85724. Address reprint requests to E. Unger.

[2] Department of Surgery, The University of Arizona College of Medicine, Tucson, AZ 85724.

[3] Advanced Magnetics, Inc., 61 Mooney St., Cambridge, MA 02138.

0361-803X/92/1594-0875
© American Roentgen Ray Society

Materials and Methods

Contrast Agent

AMI-227 (Advanced Magnetics, Cambridge, MA) is a superparamagnetic dextran-coated iron oxide colloid with particles that range from 10 to 20 nm in diameter. Results of Sepharose 4B gel chromatography indicate an apparent mass of 800,000 daltons, and its magnetization curve and magnetic properties are similar to those of AMI-25 (Josephson L, Advanced Magnetics, personal communication) [12].

Animals

Eighteen male ferrets, *Mustela putorius furo* (Marshall Labs., University of Florida, Gainesville, FL), weighing 1.0–2.5 kg were studied. Twelve had been infected as previously described [8] by subcutaneous injection of 75 *Brugia malayi* larvae in both sides of the groin 2–9 months (mean, 5) earlier. Six uninfected ferrets were used for comparison images after injection with a neutral substance (RPMI culture media, Sigma, St. Louis, MO).

Under light anesthesia (five parts ketamine [Aveco, Fort Dodge, IA], 100 mg/ml, to one part acepromazine [Fermenta Animal Health Co., Kansas City, MO], 10 mg/ml, at 0.25 ml/kg intramuscularly), 13 (three control, 10 infected) ferrets received an intradermal injection of 0.5 mg Fe/kg AMI-227 in the dorsum of the left hind paw, while five (three control, two infected) received 0.2 mg Fe/kg. All ferrets were imaged before and 48 hr after contrast injection with spin-echo and gradient-echo sequences. Additionally, images were obtained at other times as noted below for specific protocols.

To confirm previously reported results, we studied six Sprague-Dawley male rats (Harlan Labs.) that weighed an average of 321 g. Two rats were intradermally injected with AMI-227 at 0.5 and 1.0 mg Fe/kg, while four others were injected IV as described below. Each rat was imaged before and 48 hr after injection with gradient-echo techniques, which produced the maximal magnetic susceptibility.

Anesthetized ferrets and rats were surgically explored immediately before euthanization at various times (0–177 days) after injection of AMI-227, as dictated by animal maintenance constraints. The anatomy of the peripheral lymphatic system was highlighted before dissection by injecting Evans blue dye (Sigma, at 50 mg/ml in phosphate buffered saline) intradermally into the hind paws 5 min before dissection. After euthanization, lymph node, liver, spleen, and lung samples were taken and processed with formalin for routine light microscopy. Additionally, sections of lymph nodes were processed for transmission electron microscopy.

In Vivo Imaging

A 0.5-T Toshiba MRT-50A magnet (Toshiba Corp., Gardena, CA) was used for imaging in vivo. Pulse sequences included the spin-

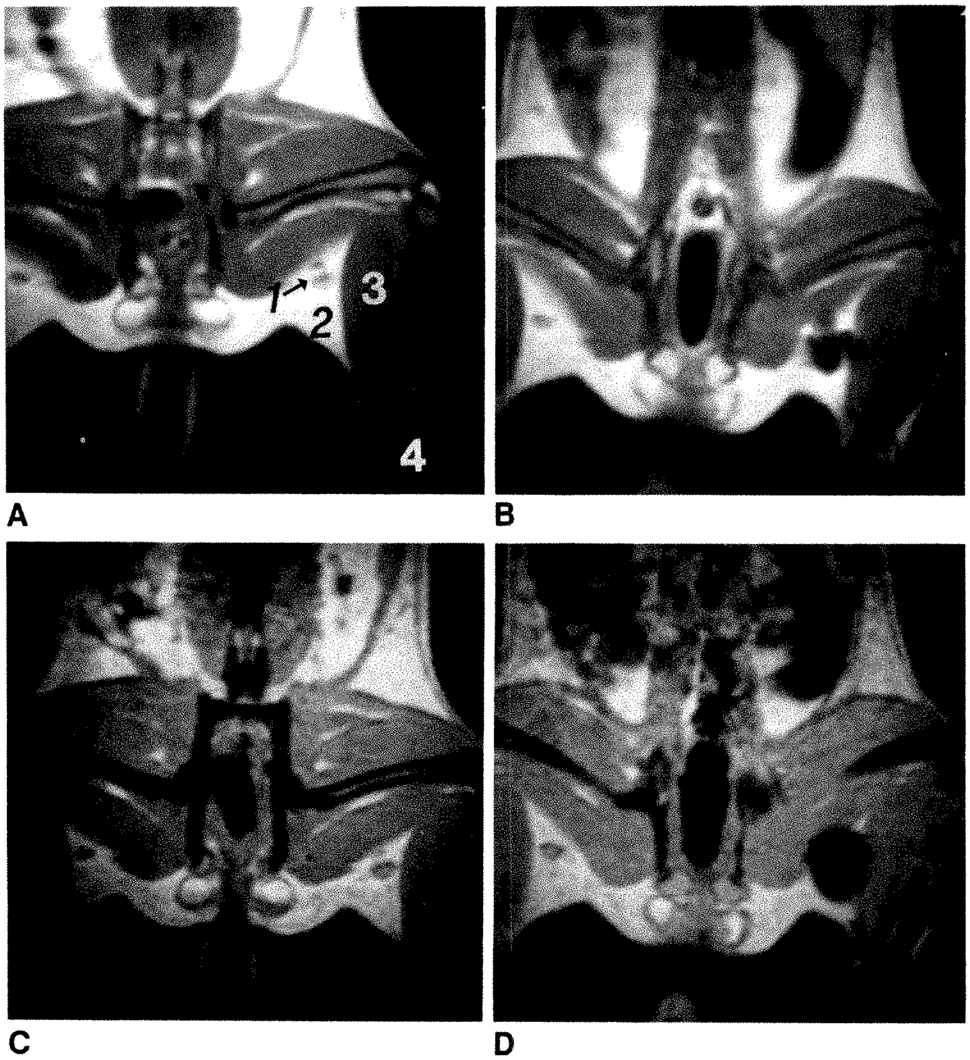

Fig. 1.—Spin-echo and gradient-echo MR images of a filarially infected ferret before (*A* and *C*) and after (*B* and *D*) interstitial injection of AMI-227 (0.5 mg Fe/kg) into left hind paw.

***A*, Unenhanced spin-echo image shows left popliteal lymph node (1), left inguinal fat (2), left hamstring muscle (3), and left hind paw (4).**

***B*, Spin-echo MR image 48 hr after contrast administration shows reduction in signal intensity of left popliteal lymph node. Reduced nodal intensity appears larger than actual nodal size because of magnetic susceptibility artifact caused by iron oxide agent. No change in signal intensity of adjacent inguinal fat or hamstring muscle is noted.**

***C*, Unenhanced gradient-echo image shows left popliteal node as a hypointense, oval structure embedded in surrounding inguinal fat.**

***D*, Gradient-echo image 48 hr after contrast administration shows reduction in signal about left popliteal node to be larger than on spin-echo images owing to enhanced magnetic susceptibility artifact. No change occurred in signal intensity of other two tissues.**

echo technique, 2000/30,60,90,120 (TR/TE), and the three-dimensional fast low-angle shot (FLASH) gradient field-echo technique, 34/14, with a 20° flip angle. The field of view was 20 cm (25 cm for IV injections), with a matrix size of 192 × 256 and two acquisitions for both techniques. Slice thickness for spin-echo images was 4 mm and for gradient-echo images, 1.3–1.5 mm. Dynamic "lymphangiomagnetograms" were taken within 15 min after contrast injection with the gradient-echo technique.

Signal Intensity Measurements After Interstitial Administration

Signal intensities of three different tissues (left popliteal lymph node, left inguinal fat, and left hamstring muscle) were measured with the area of the cursor (1.8 mm^2) before and 48 hr after intradermal injection of AMI-227 (0.5 mg Fe/kg) into the dorsum of the left hind paw. The latter two tissues (fat and muscle) were included to assess regional specificity of nodal enhancement by this route of administration. Data were analyzed by using the χ^2 statistical method.

Contrast Washout

Two infected ferrets and one uninfected (control) ferret were studied for contrast washout from the left popliteal node after interstitial injection of AMI-227. One infected and the uninfected ferret received the 0.5 mg Fe/kg dose into the left hind paw and were imaged with spin-echo and gradient-echo techniques before contrast administration and 48 hr and 8, 14, 30, 45, 85, and 138 days after injection. The second infected ferret received the 0.2 mg Fe/kg dose and was imaged with the same techniques 48 hr, 30 days, and 69 days after injection. The signal intensity of the left popliteal node was measured at each time interval by both spin-echo and gradient-echo techniques.

IV Route of Contrast Administration

Four ferrets (two infected and two uninfected) were studied for nodal signal reduction after IV administration of AMI-227 via cannulation cutdown of the left jugular vein. One infected and one uninfected ferret received a 2.0 mg Fe/kg dose; a third (infected), 4.0 mg Fe/kg; and a fourth (uninfected), 8.0 mg Fe/kg. Unenhanced spin-echo and gradient-echo images were obtained for all ferrets. Enhanced imaging for the 2.0 and 4.0 mg Fe/kg doses was done with spin-echo and gradient-echo techniques 48 hr after injection. The fourth ferret (8.0 mg Fe/kg dose) was serially imaged with spin-echo and gradient-echo sequences at 1, 2, 4, 8, 10, 24, and 48 hr after injection. Concomitant signal intensity was measured for the left popliteal lymph node, left hamstring muscle, and left inguinal fat at each time interval as above.

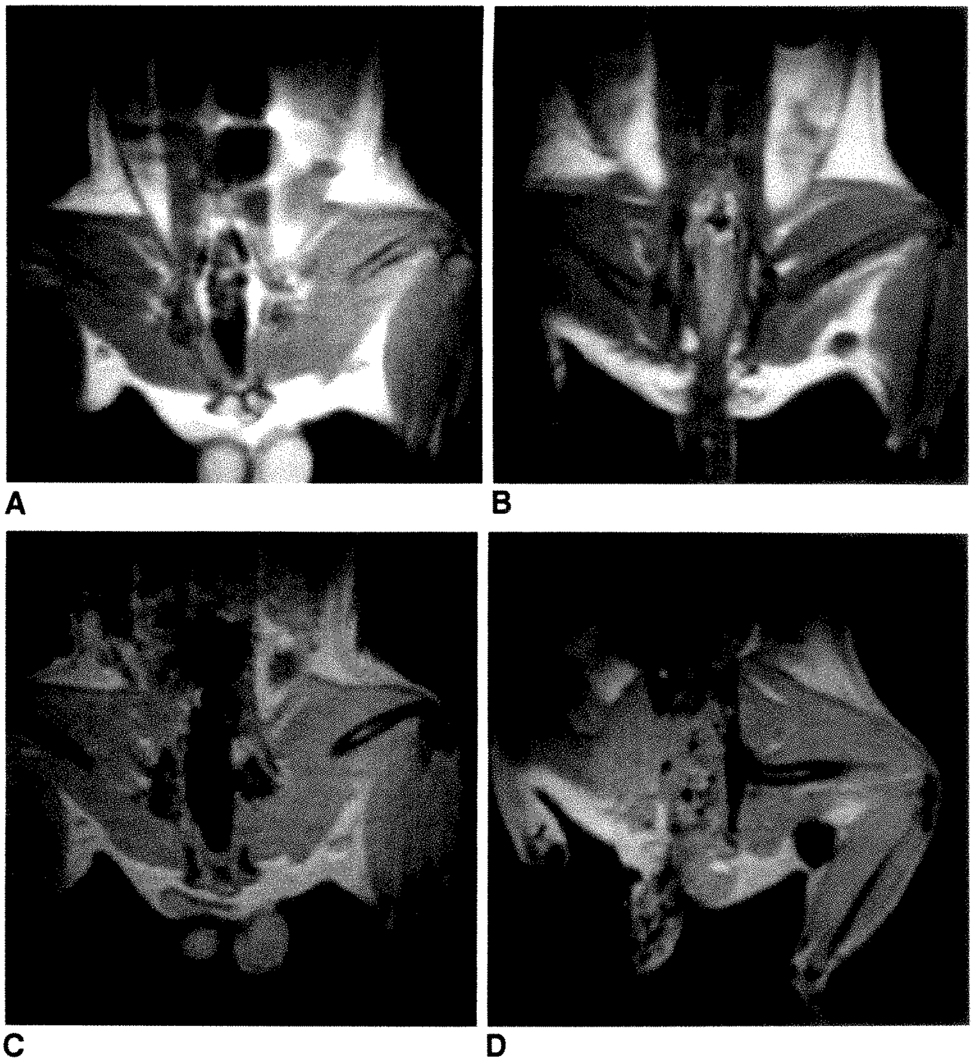

Fig. 2.—Spin-echo and gradient-echo MR images of a filarially infected ferret before (*A* and *C*) and after (*B* and *D*) interstitial injection of AMI-227 (0.2 mg Fe/kg) into left hind paw.

***A*, Unenhanced spin-echo image.**

***B*, Spin-echo image 48 hr after contrast administration. Area of signal reduction near left popliteal node is smaller than with higher dose of AMI-227 (see Fig. 1B).**

***C*, Unenhanced gradient-echo image.**

***D*, Gradient-echo image 48 hr after contrast administration. Again, area of signal reduction about left popliteal node is smaller than with higher dose (see Fig. 1D).**

Four Sprague-Dawley rats were injected IV with AMI-227. To be comprehensive in our modes of administration, the following IV injections were used. Two rats were injected via the tail vein, one with 1.7 mg Fe/kg and the other with 4.0 mg Fe/kg. A third received 4.0 mg Fe/kg via a cannula in the left jugular vein, whereas the fourth received 2.0 mg Fe/kg via injection of a vein in the foot.

Histopathologic Correlation

Specimens of liver, spleen, lungs, femoral nodes, and popliteal nodes from all ferrets were fixed in formalin and processed for light microscopy. Additionally, tissues were stained with Perls' Prussian blue to assess the tissue uptake of iron oxide.

Transmission electron microscopy of contrast-enhanced lymph node specimens also was done to evaluate the intracellular distribution of the electron-dense contrast agent.

TABLE 1: Signal Intensity Measurements of Selected Tissues

Imaging Sequence/ Tissue	Before Enhancement	48 Hr After Enhancement	Statistical Significance
Spin echo			
Node	460.5 ± 82.7	80.6 ± 45	$p < .0005$
Muscle	215.6 ± 69.6	275.3 ± 99.8	NS
Fat	731.2 ± 114.3	787.5 ± 120	NS
Gradient echo			
Node	126.2 ± 29.0	9.0 ± 5.3	$p < .0005$
Muscle	95.6 ± 25.9	129.4 ± 51.7	NS
Fat	187.7 ± 29.6	221.7 ± 38.9	NS

Note.—Mean signal intensities of three tissues on spin-echo and gradient-echo imaging of 12 ferrets (two controls, 10 infected) injected interstitially with AMI-227 (0.5 mg Fe/kg) into left hind paw. Spin-echo measurements are those for a 30-msec TE only, because later echoes (60, 90, and 120 msec) produced similar results (all significant signal reduction for node only). NS = not significant.

Results

On 0.5 mg Fe/kg unenhanced spin-echo images of the ferrets (Fig. 1A), the popliteal node was seen as a hypointense oval structure embedded in the left inguinal fat. Forty-eight hours after interstitial contrast injection, the signal intensity of the node was substantially reduced (Fig. 1B). Lower iron dosages decreased (Fig. 2), whereas gradient-echo images increased (Figs. 1D and 2D), the nodal dimension owing to magnetic susceptibility artifacts. The size of the lymph node with the lower dose more closely approximated the actual size of the lymph node at autopsy. No significant change was seen in the signal intensity of the left inguinal fat or hamstring muscle. These qualitative assessments were confirmed by significant ($p < .0005$) quantitative measurements of changes in signal intensity after AMI-227, which occurred only in lymph node and not in surrounding tissues (Table 1). No retroperitoneal nodes were identified consistently.

Signal reduction from popliteal nodes persisted for both the 0.5 and 0.2 mg Fe/kg doses at end points up to 138 days (Fig. 3), depending on the length of time that the animals remained alive after injection (range, 5–177 days).

Dilated lymphatics of a filarially infected ferret were visualized immediately after interstitial injection of 0.2 mg Fe/kg. These lymphatics originated from the popliteal node (Fig. 4A) and drained proximally into the femoral node (Figs. 4B–4D). At 48 hr after injection, these lymphatics were no longer seen. An uninfected ferret also exhibited hind-limb lymphatics (albeit much smaller) up to 2 hr after injection but not at 48 hr.

Histology of the infected popliteal nodes showed reactive hyperplasia associated with greatly dilated lymphatics. After interstitial contrast injection, significant iron staining by Prussian blue was noted exclusively in the marginal sinuses and not within germinal centers (Fig. 5B). Electron microscopy of the lymph node specimen after contrast injection showed iron oxide particles uniformly distributed throughout the macrophage cytoplasm and also aggregated within large phagosomes of the macrophage (Figs. 5C and 5D).

Prussian blue staining of iron in the liver of interstitially injected ferrets was distributed at control levels at 5 days and gradually became more intense up to our end point of 17 weeks. The staining was confined largely to the portal areas

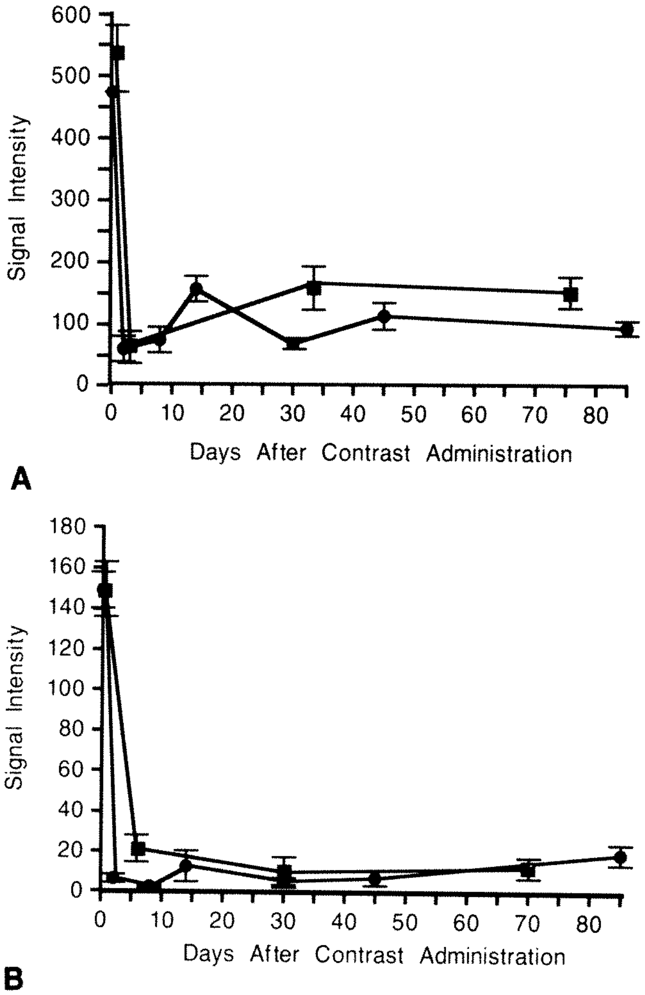

Fig. 3.—Persistence of signal reduction from left popliteal node after interstitial injection of two different doses of AMI-227.

***A*, Spin-echo signal intensity of left popliteal node vs time for 0.2 (*squares*) and 0.5 (*circles*) mg Fe/kg doses.**

***B*, Gradient-echo signal intensity of left popliteal node vs time for 0.2 (*squares*) and 0.5 (*circles*) mg Fe/kg doses. Note that decrease in signal intensity indicates greater contrast, which persists for 2 months.**

Fig. 4.—*A–D*, Gradient-echo MR lymphangiomagnetograms of a filarially infected ferret injected interstitially with AMI-227 (0.2 mg Fe/kg) into right hind paw show a tortuous dilated lymphatic vessel in right hind leg. MR images were obtained within 15 min of injection. Right lymphatic vessel (*solid arrows*) originates from right popliteal lymph node (*open arrow*, *A*), extends proximally (*A*), continues superiorly (*B*), and finally drains (*C* and *D*) into right femoral lymph node (*open arrow*, *D*). Signal reduction of contralateral (*left*) popliteal node is related to an earlier injection of AMI-227 into left hind paw.

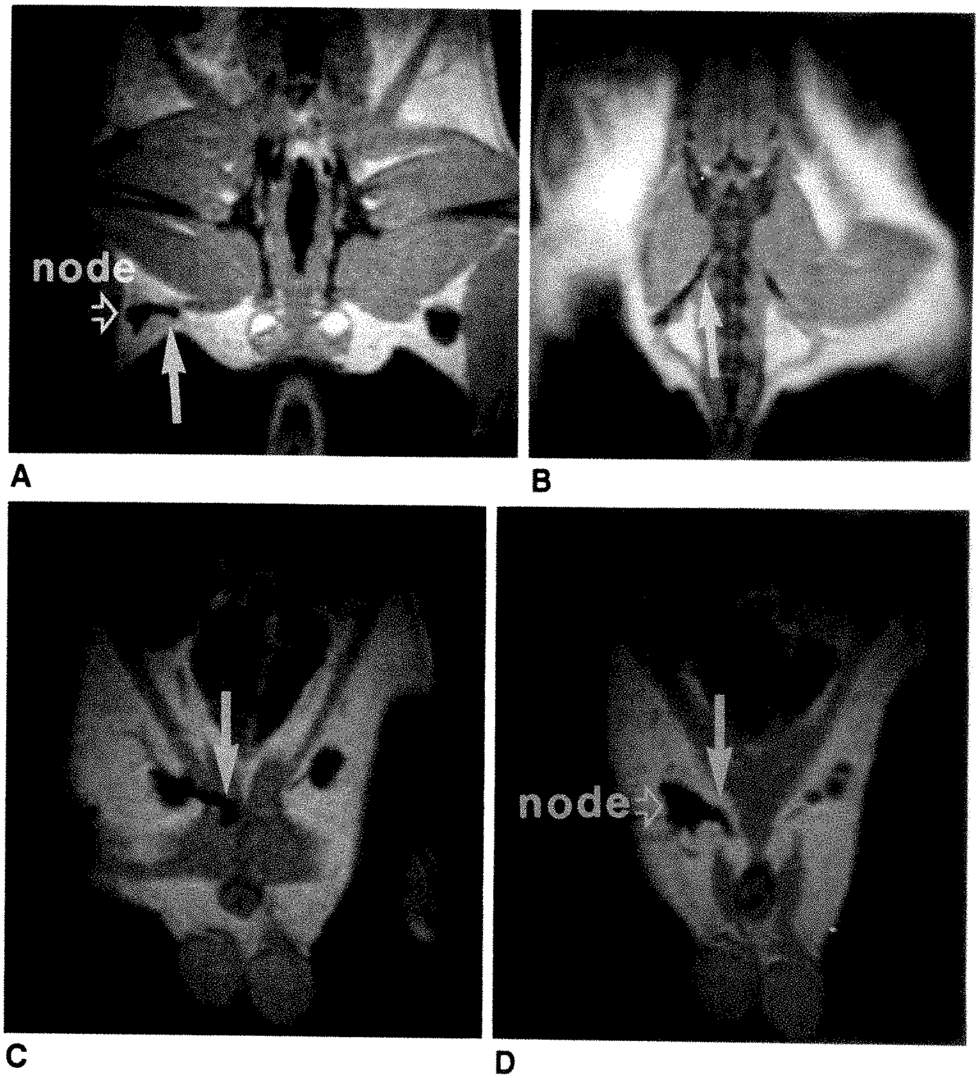

outlining the liver lobule. Similarly, the lung at 5 days showed no iron staining above normal, but staining gradually increased at our end point. The spleen did not show significant staining at 5 days or at the end point.

No ferret receiving IV injection of AMI-227 at low or high doses showed nodal signal reduction, although signal intensities of liver (185.7 before, 26.3 after; $p < .0005$), and to a lesser extent the spleen (131.7 before, 29.0 after; $p < .0005$), were reduced (Fig. 6). Rats, on the other hand, after IV injection show enhancement of lymph nodes as well as liver and spleen (data not shown). Prussian blue staining of tissues from IV-injected ferrets showed substantial staining of the liver, lung, and spleen while showing control levels for the node. Only the spleen showed a small reduction in staining over time.

When both MR signal intensity data and Prussian blue staining patterns of both interstitial and IV-injected ferrets were considered, no appreciable difference could be observed between the control and filiarially infected ferret groups. This demonstrates what we believe is no difference in the ability to distinguish benign hyperplastic nodes from normal nodes by signal-intensity reduction or iron uptake.

Discussion

This study shows that AMI-227 (iron oxide colloid) is a useful MR lymphographic agent when administered interstitially, as evidenced by reduction of the lymph node signal intensity (Fig. 1). Indeed, the AMI-227 uptake was not only lymphatic-specific when compared with surrounding tissues such as muscle, but also disappeared from the site of injection. Although there may be a magnetic susceptibility artifact (i.e., overestimation of the size of nodes leading to false positivity, Figs. 1 and 2), the phenomenon is dose-related and may be controllable by using lower iron oxide doses [13].

Weissleder et al. [7, 14] reported that interstitial administration of AMI-25 and/or IV injection of ultrasmall superparamagnetic iron oxide (USPIO) can be used to differentiate normal from tumor-involved nodes in rats by relaxivity measurements. However, inflammatory processes involving lymphatic tissues and the applicability of these techniques to animal species other than rats were not examined. With ferret filariasis, no notable difference in signal reduction was found between normal and inflamed (hyperplastic) nodes when using AMI-227, an iron oxide similar although not identical to AMI-

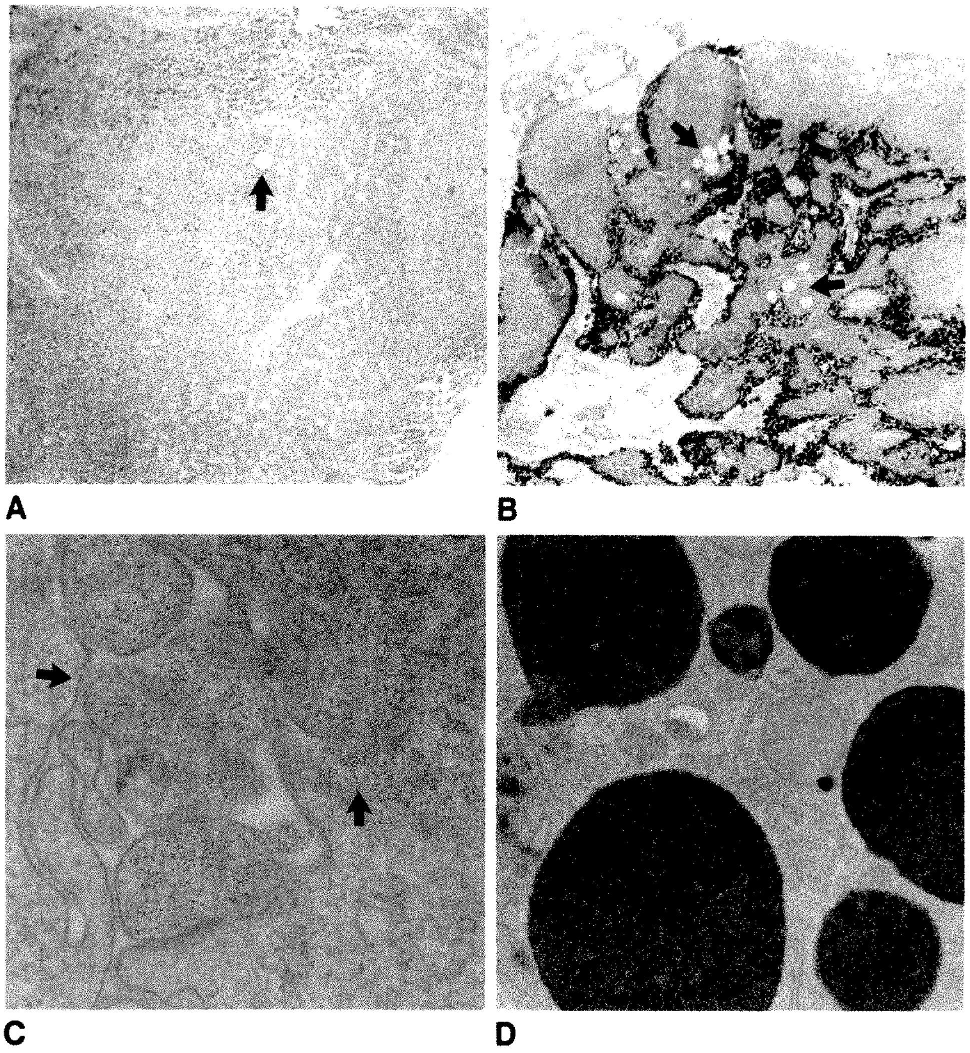

Fig. 5.—*A–D*, Photomicrographs (*A* and *B*) and electron micrographs (*C* and *D*) of left popliteal node of infected ferret before (*A*) and after (*B–D*) interstitial injection of AMI-227 (0.5 mg Fe/kg). Before enhancement (*A*, original magnification ×140), specimen shows no Prussian blue stain for iron. Seven days after contrast injection (*B*, original magnification ×70), nodal specimen shows prominent Prussian blue staining exclusively in marginal zones; no iron deposition is seen in follicles. In *A* and *B*, Swiss-cheese holes (*arrows*) in nodal tissue are from filarial worm migration. Electron micrographs of individual macrophages from popliteal node show iron oxide particles (*arrows*) distributed in a uniform and diffuse manner (*C*, original magnification ×76,325) and aggregated within phagosomes in cytoplasm (*D*, original magnification ×23,745).

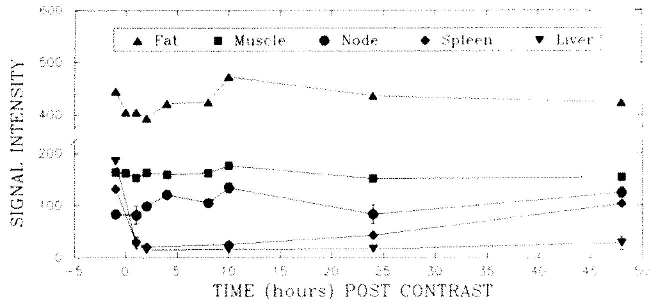

Fig. 6.—Signal intensity vs time for five tissues of uninfected (control) ferret injected IV with AMI-227 (8.0 mg Fe/kg). Note lack of signal reduction of node, fat, and muscle compared with dramatic signal reduction of liver and, to a lesser extent, spleen. (Note.—At most data points, error bars are smaller than the symbol.)

25 or USPIO. Both normal and inflamed lymph nodes exhibited dramatic signal reduction to a similar degree regardless of their size differences. In rats, on the other hand, interstitial (AMI-25) and IV (USPIO) administration has been shown not to alter the signal intensity of neoplastic nodes [7, 14]. Thus, under the right circumstances, neoplastic nodes (no reduction of signal intensity—data from Weissleder et al. [7]) may still be distinguishable from benign hyperplastic nodes (reduced signal intensity—data from this study) when using iron oxide–enhanced MR lymphography. This area, however, needs further investigation, particularly with the same animal model.

Consistent with current concepts of lymphatic physiology, interstitially injected iron oxide eventually reaches the bloodstream after traversing peripheral and central lymphatics to be cleared by the liver, spleen, and to a lesser extent, the lungs. As shown before [15], and in this study, iron is sequestered in macrophages and Kupffer cells of lymph nodes and the liver, respectively. How the particles arrive at these locations (whether predominantly free or cell-bound) is yet to be clarified.

Liver uptake of iron oxide was confirmed by Prussian blue staining. Iron deposition was greatest at the edge of the hepatic lobules, which conforms with the pattern of blood flow from the periphery toward the central lobular vein. Iron oxides trapped by the liver are biodegraded and incorporated into hemoglobin [16], but the kinetics of this process are unclear and most likely vary with particle size.

The pattern of iron deposition within lymph nodes also was distinctive, exclusively in macrophages within the marginal zones while sparing the lymphocyte-containing germinal centers. Two patterns of intracellular distribution of the iron oxides were seen on electron microscopy: uniform distribution of individual particles within the macrophage cytoplasm and large aggregates within phagosomes. Whereas the latter phenomenon suggests active uptake, the former is more consistent with pinocytosis and eventual release of particles into the cytoplasm from the primary phagosomes. Alternatively, passive uptake may occur at the macrophage surface membrane. Neither of these patterns was seen in control ferrets.

Uptake of iron was also seen in the other organs of the reticuloendothelial system, namely, the spleen and lungs. The spleen showed trapping in the red pulp, again presumably by macrophages and monocytes. In the lungs, iron deposits surrounded the pulmonary microvasculature and bronchi.

Signal reduction potential was not limited to lymph nodes with interstitial injection of AMI-227. Lymphatic channels also were visualized early. Although ferret filariasis exaggerates lymphatic dilatation, even small lymphatics were seen. An early image (within 15 min) after interstitial injection of iron oxide may screen for lymphatic obstruction, although the lymphangiomagnetographic effect thus far is at best transient.

Weissleder et al. [14] reported lymph node signal reduction after IV injection of USPIO in rats. We failed to demonstrate significant lymph node signal reduction in our ferret model after IV injection of AMI-227 despite a higher iron dose than that used with USPIO. However, nodal signal reduction was seen in our rats after IV injection of AMI-227. This discrepancy may relate to species differences or pharmacokinetic differences between AMI-227 and USPIO.

Delayed washout of AMI-227 from lymph nodes after interstitial injection may represent a potential drawback to the use of this imaging agent. Signal reduction is still detected in the lymph node several months after low-dose iron oxide administration. Weissleder et al. [14] observed that nodal signals returned to unenhanced values in rats 5 days after IV injection of USPIO when an intermediate dose of iron oxide was used. The reason for this discrepancy is unclear but may relate to the effective dose. After further research, the ultimate clinical dose is likely to be much smaller and may not exceed the capacity of the lymph node or reticuloendothelial system to process the iron oxide, and therefore would show a quicker clearance. Delayed washout is seen in both filarially infected and normal ferrets, although in the infected ferret, protracted disappearance may relate to peripheral lymph stasis. Thus, stagnant lymph may "trap" iron oxide but facilitate serial imaging and allow monitoring of progression or regression of lymph node disease without need for repeated contrast administration.

In summary, the iron oxide compound AMI-227 is potentially useful for MR lymphography. Image signal reduction is greatest in regional nodes after interstitial administration, but in the early phase, peripheral lymphatics also are seen. On the basis of previous work [7, 14] and this study, nodal inflammation may be distinguished from nodal neoplasia by comparing the degree of signal intensity reduction, but this area needs further investigation. The feasibility of signal reduction in lymph nodes by IV administration of iron oxide AMI-227 also needs further clarification, as a discrepancy was apparent between ferrets and rats. If iron oxide clearance can be augmented (or lower doses can be used), this superparamagnetic compound may prove a useful enhancer for MR imaging of the lymphatic system.

REFERENCES

1. Koehler PR. Complications of lymphography. *Lymphology* **1968**;1:117-120
2. Hessel SJ, Adams DF, Abrams HL. Complications of angiography. *Radiology* **1981**;138:273-281
3. Wallace S, Jing BS, Clouse ME, Harrison DA. *Lymphatic imaging: lymphography, computed tomography, and scintigraphy*, 2nd ed. Baltimore: Williams & Wilkins, **1985**
4. Witte M, McNeill G, Crandall C, et al. Whole body lymphangioscintigraphy in ferrets chronically infected with *Brugia malayi*. *Lymphology* **1988**;21:251-257
5. Dooms GC, Hricak H, Moseley ME, Bottles K, Fisher MR, Higgins CB. Characterization of lymphadenopathy by magnetic resonance relaxation times: preliminary results. *Radiology* **1985**;155:691-697
6. Bottomley PA, Hardy RE, Argersinger RE, Allen-Moore G. A review of 1H nuclear magnetic resonance relaxation in pathology: are T1 and T2 diagnostic? *Med Phys* **1987**;14:1-37
7. Weissleder R, Elizondo G, Josephson L, et al. Experimental lymph node metastasis: enhanced detection with MR lymphography. *Radiology* **1989**;171:835-839
8. Crandall RB, McGreevy PB, Connor DH, Crandall CA, Neelson JT, McCall JW. The ferret (*Mustela putorius furo*) as an experimental host for *Brugia malayi* and *Brugia pahangi*. *Am J Trop Med Hyg* **1982**;31:752-759
9. Crandall RB, Crandall CA, Nayar JK. Lymphatic filariasis in ferret. In: *Progress in lymphology XI*. New York: Elsevier, **1988**:675-677
10. Gooneratne BWN. *Lymphography: clinical and experimental*. London: Butterworths, **1974**:83-122
11. Case TC, Way D, Bernas M, et al. In vivo and in vitro microscopy of *Brugia malayi* life cycle in ferret lymphatic filariasis. *Clin Res* **1991**;39:60A
12. Josephson L, Lewis J, Jacobs P, Hahn P, Stark D. The effects of iron oxides on proton relaxivity. *Magn Reson Imaging* **1988**;6:647-653
13. Hamm B, Taupitz M, Hussmann P, Wagner S, Wolf K. MR lymphography with iron oxide particles: dose-response studies and pulse sequence optimization in rabbits. *AJR* **1992**;158:183-190
14. Weissleder R, Elizondo G, Wittenberg J, Lee A, Josephson L, Brady T. Ultrasmall superparamagnetic iron oxide: an intravenous contrast agent for assessing lymph nodes with MR imaging. *Radiology* **1990**;175:494-498
15. Pouliquen D, Le Jeune JJ, Perdrisot R, Ermias A, Jallet P. Iron oxide nanoparticles for use as an MRI contrast agent: pharmacokinetics and metabolism. *Magn Reson Imaging* **1991**;9:275-283
16. Weissleder R, Stark DD, Engelstad BL, et al. Superparamagnetic iron oxides: pharmacokinetics and toxicity. *AJR* **1989**;152:167-173

Memorial

Robert L. Scanlan, 1917-1991

Many, many radiologists of all ages will remember Bob Scanlan and what he gave them as a friend and as a teacher.

Robert L. Scanlan was born in Brooklyn, NY, on February 13, 1917. He graduated from Duke University in 1938 and from Columbia College of Physicians and Surgeons in 1942. The next year he did his internship at Philadelphia General Hospital. He then entered the army and requested that he be trained as a radiologist. In his own words, he was an "Arthur Murray taught me X-ray in a hurry" M.D. for 3 years during World War II. While in the army, he married Major Mary Christiansen (Chrissy), and then promptly shipped to Normandy, where radiologists were in short supply. After the war, he took 3 years formal residency training in radiology at the Mayo Clinic.

Bob's 45-year career in radiology was a rich blend of private practice and academics, with about a 50/50 split. He was director of three large private practice radiology groups, as well as associate professor of radiology at the Mayo Clinic and at the University of Southern California. Most recently, he was adjunct professor of radiology and chief of emergency radiology at the University of California, Los Angeles (UCLA), where he received two teaching awards. Bob was an ardent supporter of organized radiology. He attended the annual meetings of the Radiological Society of North America and the American Roentgen Ray Society every year from the time he was a resident until his retirement in 1987.

His publications and lectures covered a broad range of radiology subjects, including head and neck, neurologic, and gastrointestinal radiology; mammography; and equipment. Bob was intensely interested in patient care and in ways of improving it. He visited many departments all over the world, with an eye toward discovering the best way to provide radiology services. Every family vacation was combined with a trip to the local radiology department. In a lecture to residents at the Los Angeles Radiologic Society winter meeting in 1985 he said: "We all owe an enormous debt to our forebears and associates in medicine who worked hard and long to reach us and pull us up the ladder of knowledge for improvement in patient care. Therefore one should always do one's best to repay this debt to the best of their ability. Despite being in private practice much of my life, I always tried to have a clinical connection with a center of learning. I gave my share of papers on what I was doing and visited others to see what they were doing that would improve my practice. It was rewarding and I recommend it to you."

Bob was an extremely kind and gentle person. He occasionally, however, had a harsh word for hospital administration: "Administrators determine salary levels, dictate equipment and film quality without any medical idea of what must be done for optimal care, just what is cheapest. Many administrators do not understand that radiology is a major revenue-producing department that should be developed. Administrators seem to have lots of time to write, for example a 2½-page letter about the pigeons in the outside dining area at UCLA, threatening to arrest those suspected of feeding the birds."

He also said: "I have enjoyed the last 12 years at UCLA as much as anything in my life. I love the learning/teaching experience of such a place very much. However, I find the atmosphere of nonmedical domination frustrating, demeaning, and definitely interfering in the practice of radiology and I have the knobs on my liver to prove it. None of this, however, detracts from the joy of one-on-one teaching and learning at the view box and the assistance and advice of my colleagues."

Bob died at home in Ojai, CA, November 16, 1991, after a brief illness. He is survived by his wife, Chrissy; their children, Larry, Helen, Mick, Annie, and Janie; and 11 grandchildren. We all miss him very much.

Amy Thurmond Scanlan
Portland, OR 97201

Perspective

Canadian-Style Health Care: Implications for Radiologists

Richard L. Wesenberg[1]

The American free enterprise system of health care is in crisis. The Canadian Universal Health Care System (CUHCS) has been considered one of the practical alternatives to the American system gone awry. The misconceptions and myths about CUHCS need to be dispelled for radiologists, all physicians, and the general public in the United States. This article attempts to inform radiologists and allied workers in the field of diagnostic imaging about the advantages and disadvantages of CUHCS. It is not intended to promote the system.

The United States had a basically free enterprise system of health care until 1965 [1], when the U.S. Congress established the Medicare Program to provide health care for all persons over age 65, with a federal health insurance program financed through Social Security, and the Medicaid Program to provide medical care for the indigent via a federal-state program.

Legislators reasoned that most Americans would rely on private, voluntary health insurance. Twenty-six years later, however, this governmental attempt at limited national health coverage has been disastrous. Total health care expenditures have mushroomed from 6% of the gross national product to approximately 12%, an annual expenditure of over half a trillion dollars [1]. As expenditures have increased, coverage has decreased. Medicare now covers only approximately 40% of health care costs for the aged, and the states have drastically reduced Medicaid coverage. Thirty-seven million Americans (13% of the population) have no health insurance coverage [1], and an estimated 60 million are underinsured. Not surprisingly, the results of a 1991 Harris Poll [2] revealed 92% of Americans to be dissatisfied with the medical care system. In a 1992 Time-Cable News Network poll, 56% of Americans favored national health insurance over the current system.

Increasingly, there have been longing looks northward toward Canadian-style health care, a system heartily approved by the vast majority of Canadian citizens and the majority of physicians [1, 3-6]. Sixty-eight percent of Americans consider the Canadian health system superior [2, 3]. Philosophically, Canadians seem to have extended the guarantees contained in the American Bill of Rights that entitle citizens to "life, liberty, and the pursuit of happiness" to include "and universal access to adequate medical care" (contained in Canadian Health Care Act, 1971). Historically, the Canadian-style health care system began in 1961 in the province of Saskatchewan and by 1971 had been adopted by all the Canadian provinces.

Two medical myths of the Canadian health care system need to be dispelled: (1) Health care in Canada is *not* predominately governed and funded by the Canadian federal government. Rather, it is governed and funded by the provinces. The Canadian government provides funds to each of the Provincial Medicare Programs at approximately the 40% level with the proviso that the provincial health plans be accessible to all citizens, be comprehensive, be portable from province to province, and be publicly managed and administered. (2) The provincial medicare systems are *not* a socialized health service such as the British National Health Service (NHS). Rather, they are a form of health insurance. The conglomerate of these multiple provincial medicare insurance systems has been called the Canadian Health Care System. All residents of a particular province are required by law to purchase provincial medicare insurance (e.g., $52/month per family in the province of Alberta in 1991). If a resident is unable to pay the monthly fee, a short form and declaration appeal can be made, and if approved, the province then pays the insurance

---

Received December 16, 1991; accepted after revision April 16, 1992.

[1] Director of Diagnostic Imaging, Alberta Children's Hospital, and Professor of Radiology and Pediatrics, University of Calgary, Alberta, Canada (1980-1988). Present address: Department of Radiology, University of South Alabama, 2451 Fillingim St., Mobile, AL 36617. Address reprint requests to R. L. Wesenberg.

AJR 159:883-884, October 1992 0361-803X/92/1594-0883 © American Roentgen Ray Society

fee. The practical effect of this policy is that the entire population has health insurance coverage. The provincial insurance plan is the sole health insurance provider (with minor exceptions) and has major funding responsibilities for (1) hospitals—funded annually on the basis of a global budget and (2) physician services—paid for on the basis of fee-for-service. The latter fee is determined annually through negotiations between the provincial medical association and the provincial health care plan. Physicians thus remain independent, rather than being employees of the system (government) as in the British NHS. The Canadian Provincial Health Care System thus is politically and philosophically in the middle, between the British system on the left and the American system on the right. It is no panacea, but it works.

What are the implications for radiologists working in the "Canadian" health-care insurance system? University and academic radiologists commonly work for a salary that is negotiated with the department chairman, who negotiates for the university radiology group with the hospital administration. They in turn include radiology salary and all radiology department operational expenses in the global budget. Private radiologists may operate their own radiology offices, just as in the United States. In this case, the radiologists can bill for both the technical and professional components of the bill, which is charged to the provincial health care insurance system. There is a separate interventional procedure schedule that is billed at a significantly higher rate but with direct billing of the provincial health plan. In the system, the basic fee paid per examination is less than fees charged in the United States (e.g., for posteroanterior and lateral chest radiographs, the professional component was $6–$10 in 1991; Bullman D, Medicine Hat, Alberta, Canada, past president, Alberta Radiological Society, personal communication). However, all billing is to one insurer, which eliminates much of the bureaucratic work and expense of trying to collect from hundreds of different insurers. There are minimized accounts receivable, and as a general rule, the province does not "bounce" checks.

Private radiologists working in a hospital have the option of working for (1) an annually negotiated stipend, commonly with a provision to bill the health care plan separately for special procedures, or (2) a negotiated percentage of the gross billings to approximate the professional fees without having to send in charges on each patient (Canadian physicians consider this percentage arrangement "fee-for-service"), or (3) a straight fee-for-service for the professional component of the various examinations performed. The overall radiology fees are then buried by administration in the hospital global budget. Thus, most Canadian radiologists remain independent contractors. The overall fee schedule is negotiated annually between the provincial radiologic association and the provincial medical association. The latter then negotiates with the provincial health-care insurance agency. Fee alterations may come in the form of an overall percentage increase for each separate item in the radiology fee schedule or selected changes in the individual examinations or procedures. Fees may vary significantly among provinces. One province, Ontario, has even placed a cap on physicians' reimbursement [7]. The overall effect of this is to generate less personal income but involves less hassle for radiologists with insurance carriers and/or federal bureaucracy (the best guesstimate of the average annual private, full partner radiology compensation was approximately $255,000 to $300,000 in the province of Alberta in 1991; Bullman D, personal communication). Even by American standards, this would be enough to subsist on.

Disadvantages for radiologists of the Canadian-style health insurance system center on the system's tightly controlled expenditures [4, 6–8]. Anything perceived as "high tech" equipment, such as CT and MR imaging equipment, is deliberately delayed in funding approval. For instance, in 1991 the province of Alberta, one of Canada's wealthiest, had only two MR scanners for a population of 2 million [7]. The state of Alabama, with a population of 4 million, has 25 MR scanners (10 mobile vans) [9]. Access to MR imaging also is greatly restricted because only another specialist, *not* a general practitioner, can refer patients for MR imaging. Radiologists also may be affected by restrictions on hospitals' global budgets that delay replacement of old imaging equipment or result in deterioration of hospitals' physical plants, including radiology departments.

Physicians in Canada receive slightly less than their American counterparts [7]. Although Canadian radiology fees are lower per patient, volumes are higher than in the United States [7]. The cost of both malpractice insurance ($1722/year, 1991) and medical education is significantly less in Canada [7]. When these factors are considered, the Canadian radiologist has a marginal advantage over the American radiologist in gross income. However, income taxes generally are higher in Canada. The Canadian radiologist, along with his physician counterparts, is subject to being periodically "attacked" as earning too much money by provincial politicians. This is particularly tense during election campaigns. However, this pressure is probably no more intense than that experienced periodically by American radiologists and other physicians.

Although it is unlikely that a plan identical to the Canadian health care insurance plan, particularly as it relates to radiology, could function in the United States, an "Americanized" version of the Canadian health system merits consideration [10].

REFERENCES

1. Terris M. Lessons from Canad's health program. *J Public Health Policy* **1990**;11:151–160
2. Harris L. *The Harris Poll (#52): A 79–19 percent majority favors national health insurance for all.* New York: Louis Harris & Assoc., Dec. 22, 1991.
3. Woods D. Dissecting Canadian health care. *Pa Med* **1990**;6:40–43
4. Brown JS, Kimberly BP. The look north to the Canadian health care system: possible implications for otology and neurotology (editorial). *Am J Otol* **1991**;12:12(5)
5. Starfield B. Primary care and health: a cross-national comparison. *JAMA* **1991**;266:2268–2271
6. Enthoven A, Kronick R. A consumer-choice health plan for the 1990s. *N Engl J Med* **1989**;320:94–101
7. Orford RR. Reflections on the Canadian and American health-care systems. *Mayo Clin Proc* **1991**;66:203–206
8. Iglehart JK. Canada's health care system faces its problems. *N Engl J Med* **1990**; 322:562–568
9. State of Alabama, Office of Health Planning Data Bureau, Report SSE6. Montgomery, AL: State Office of Health Planning, **1990**
10. Himmelstein DU, Woolhandler S. A national health program for the United States. *N Engl J Med* **1989**; 320:102–108

Critical Performance Behaviors of Radiology Residents: Evaluation of Two Category Systems

Wilbur L. Smith[1]
Peggy S. Wood[2]
Elizabeth M. Altmaier[2]
Colleen O'Halloran[2]
E. A. Franken, Jr.[1]

OBJECTIVE. Previous research has suggested that certain behavioral aspects of job performance are critical for successful performance in a diagnostic radiology residency. We report two studies conducted to determine the long-term stability of critical performance behaviors for radiology residents and refine their definitions.

SUBJECTS AND METHODS. A trained psychology graduate student conducted critical incident interviews with 20 senior faculty in diagnostic radiology. From these interviews, the faculty generated 120 descriptions of exemplary or poor resident performance. These descriptors were then independently sorted by two radiologists into the previously defined categories of behaviors to evaluate consistency of the behaviors. As a second study, the 120 descriptors were sorted into an expanded behavioral definition system and the reproducibility, using the expanded system, was compared with the original results.

RESULTS. The interrater reliability for placing the current incidents in the originally described behavioral categories was good (Cohen's kappa 0.70). The overall distribution of incidents showed strong similarity to the original data. Sorting into the expanded categories improved the Cohen's kappa from 0.70 to 0.92, indicating that the expanded behavioral definitions improved reliability for categorizing a behavioral incident.

CONCLUSION. The critical behaviors necessary for successful performance in diagnostic radiology residency are stable over time. The expanded and refined system of definitions of these behaviors is more efficacious than the original system was.

***AJR* 159:885–888, October 1992**

The quality of radiology is largely influenced by the caliber of physicians entering the field. Criteria for selection of radiology residents are, therefore, of great importance to the profession. Our previous study showed that attitudes and behaviors, as well as cognitive abilities, are critical for success in a diagnostic radiology residency training program [1]. We identified six highly important and reproducible performance categories: knowledge, technical abilities, conscientiousness, curiosity, attitudes toward self, and interpersonal skills (Table 1). A subsequent study also found that a similar set of criteria was critical for successful residency performance at a number of other university-based diagnostic radiology residency programs [2]. More recent studies revealed that an instrument designed to measure these attitudes and behaviors had a high positive predictive value for residency performance and might be useful as a tool for selecting residents [3–5].

Several questions regarding the value of these findings remain: (1) Are these behavioral categories stable over time? (2) Could categories of behavioral descriptions be defined more accurately? In an attempt to answer these questions, we report two experiments: (1) a replication of the 1983 critical incident studies to test the long-term value of the previously defined categories of critical behavior of residents and (2) a refinement of two of the initial categories (conscientiousness and attitudes toward self) to discover if a further division of these categories would yield improved definition of important behaviors of radiology residents.

Received February 18, 1992; accepted after revision May 8, 1992.

[1] Department of Radiology, College of Medicine, The University of Iowa, Iowa City, IA 52242. Address reprint requests to W. L. Smith.

[2] Division of Psychological and Quantitative Foundations, College of Education, The University of Iowa, Iowa City, IA 52242.

0361-803X/92/1594-0885
© American Roentgen Ray Society

TABLE 1: Old Categories of Residents' Attitudes and Behavior

Category	Definition
Knowledge	Fundamental knowledge of general science and medicine as well as a thorough knowledge of the field
Technical skills and abilities	Manual skills and perceptual ability, ability to apply knowledge in assessing a situation or in making a differential diagnosis
Conscientiousness	Careful consideration of whole problem, willingness to exert effort and to spend time on a task, going beyond required minimum
Curiosity	Seeking knowledge because of intrinsic interest in radiology and/or science
Attitudes toward self	Decisive in work and secure in role of resident, confidently proceeds to implement choices appropriate to training level, recognition of one's limits
Interpersonal skills	Effective communication with other physicians and with allied health staff and patients

Subjects and Methods

The methods used for the current (1990) study replicated the methods used in the 1983 study. Twenty senior staff radiologists at the University of Iowa Hospitals and Clinics, Department of Radiology, served as subjects. Each was interviewed by one of two graduate students in counseling psychology who had been trained in the critical-incident technique. The structure of the interviews was identical to that described by Latham [6] and reported previously [1, 5]. Briefly, the radiologist (supervisor) was asked to give concrete examples of outstanding and poor behaviors of residents that they had encountered in the past year. Data from the interviews were recorded, and individual behaviors were transcribed onto index cards: 120 discrete behavioral incidents were generated by this process. Two radiologists then sorted these incidents into the six categories of behavior generated in the initial study [2] (Table 1).

In the second phase of the study, we added two new categories that were designed to define more precisely some areas of behaviors that were too broad in the original six-category discussion. These new categories were ethical judgments (most of which were previously sorted with conscientiousness) and "recognition of limits" and "interpersonal skills," which had been combined under the broad category of "attitude toward self." Definitions for the new scheme are given in Table 2.

The incidents generated by the radiology faculty were sorted into the new eight-category system by the same two radiologists who sorted the cards using the 1983 six-category system. The radiologists doing the resorting were not aware of the previous categorization of any of the critical incidents. For comparison, the same radiologists also sorted the 1983 incident cards into the new category system. Then the incidents generated in the present study were combined with the original incidents, and all of the incidents were sorted into the new category system in order to determine the utility of each individual category.

Results

Of the 120 descriptions of resident behavior, two were eliminated because the incidents either contained elements of two or more categories or were too vague. Of the remaining 118 incidents, the two physician raters agreed on category assignment 78% of the time. Interrater agreement was 0.70 when Cohen's kappa [7], an index that corrects for chance agreement, was used. The number and percentage of behaviors falling into each category for the current classification of incidents and the classification of the original incidents are shown in Table 3. These numbers represent the incidents that both raters placed within the same category.

The greatest percentage of incidents in both the current and previous study fell in the "conscientiousness" category. Twenty percent of the incidents were placed into the category of "interpersonal skills," defined as effective communication with other physicians and with allied health staff and patients. The category with the third highest percentage of incidents

TABLE 2: New Categories of Residents' Attitudes and Behavior

Category	Definition
Technical skills	Manual dexterity and visual perception ability
Knowledge	Fundamental knowledge of general science, medicine, and radiology; application of knowledge through synthesis of information from various sources
Confidence	Secure in role of resident, confidently implements choices appropriate to training level, appropriately assesses situations and prioritizes tasks to be completed
Recognition of limits	Appropriate use of help when knowledge or skills necessary to complete a procedure are lacking
Conscientiousness	Careful consideration of whole problem, willingness to exert effort and to spend time on a task, going beyond required minimum
Curiosity	Seeking knowledge because of intrinsic interest in radiology and/or science that goes beyond direct care of patients
Interpersonal skills	Ability to interact on both written and oral levels with patients, staff members, and clinicians
Ethical judgment	Integrity in practice; lack of willful actions, such as falsifying patient information or lying to cover up ignorance

TABLE 3: Stability of Categories

Category	No. (%) of Previous Incidents	No. (%) of Current Incidents
Technical skills	22 (17)	7 (8)
Knowledge	8 (6)	3 (3)
Attitudes toward self (confidence and recognition of limits)	18 (14)	13 (14)
Conscientiousness	51 (39)	43 (48)
Curiosity	16 (12)	6 (7)
Interpersonal skills	15 (12)	18 (20)

TABLE 4: Combined Critical Incidents Classified into New Categories

Category	No. (%)	Reallocation Index
Technical skills	33 (14)	0.79
Knowledge	17 (7)	0.65
Confidence	19 (8)	0.58
Recognition of limits	22 (9)	0.71
Conscientiousness	87 (36)	0.76
Curiosity	24 (10)	0.71
Interpersonal skills	35 (15)	0.69
Ethical judgment	3 (1)	0.75
Total	240	

(14%) was "attitudes toward self." The distributions of behaviors cited in the previous and current study are similar.

The two physician raters agreed on category assignment 94% of the time when sorting the incidents obtained in the present study into the expanded eight-category system. When Cohen's kappa [7] was used, interrater reliability was 0.92. When sorting the incidents from the previous study into the expanded category system, the two physician raters agreed on the category assignment 77% of the time, with a Cohen's kappa [7] reliability of 0.72. When the original and current incidents were combined, the interrater reliability was 86%. When Cohen's kappa [7] was used, interrater reliability was 0.82.

A reallocation index was computed for each category; this index is an evaluation of each category's utility (as opposed to κ, which is an evaluation of the whole system) [8]. The reallocation index is the ratio of the number of incidents both raters place in a category to the number that either alone places in a category. The improvement in reliability using the eight-item system showed that the eight-item system is more reliable than the earlier system and produces better agreement on the descriptions of behaviors (Table 4).

Discussion

In the 1983 study [2], five raters were able to reliably sort the critical incidents of residents' behavior into the six categories with an interrater agreement of 0.66. In the present study, the interrater reliability was 0.70. This strong degree of concurrence suggests that the 1983 categories still allow a reproducible classification of performance-related behavioral incidents and that behaviors deemed critical for successful resident behavior have not changed in 7 years.

Similar to our previous study, the categories that contained the largest number of incidents were conscientiousness, interpersonal skills, and attitudes toward self. These behaviors are often not systematically assessed in traditional resident selection, where knowledge-related categories (grades, standard test scores) are stressed [3]. The frequency of distribution of the categories in the present study was slightly different from the distribution of the categories in the original study. For example, in the original study, the category "attitudes toward self" contained a larger number of incidents than the category "interpersonal skills." In the present study, this relationship is reversed. However, the difference between the two distributions is quite small.

Knowledge and technical skills accounted for a small minority of the critical behaviors cited in both studies. This finding suggests that these factors are quite reliably preselected. Purely behavioral factors dominated the results in both studies, suggesting that the desired behaviors are uniform and the selection for these behaviors is nonuniform.

A new classification system with eight categories was proposed as a useful extension of the previous system. This new system was designed to assess ethical judgment as a separate behavior and to distinguish confidence from recognition of limits. In both studies, an occasional incident of unethical behavior was reported (i.e., dishonesty in practice, willful actions, such as falsifying patients' information or lying to cover up ignorance). These behaviors had been classified into conscientiousness in the original study; however, we believe that such incidents, although rare, are of significant importance and warrant a separate category. This category does not contain only negative behaviors. Given the complexity of medical practice, obviously positive ethical resolutions of dilemmas also could be described. Only a small minority (1%) of the incidents fit into the ethical behavior category, but these were of such gravity that they seemed to deserve special attention. For example, one incident dealt with a resident who failed to amend a report on a missed fracture of the cervical spine and then refused to acknowledge his responsibility for doing so.

In the expanded system, the single category of "attitudes toward self" was divided into two discrete categories: "recognition of limits" and "confidence." In this instance, the single category "attitudes toward self" appeared to be too general. In reviewing the incidents in which disagreement between raters occurred in the original study, it was clear that this category needed better definition. The efficacy of this action is reflected by the improved reliability of placing both the new and the old incidents in the new categories.

Although identification of these parameters of behavior is straightforward, their practical application is more difficult. Probably the most immediate benefit is a heightened awareness of the need to seek information regarding these parameters during the residency selection process. This may require reorientation of the selection process away from the traditional review of academically based criteria toward an open discussion of behaviors and behavior-modeling situations. At the University of Iowa radiology department, a graduate student in psychology interviews all resident applicants. We review their responses to a questionnaire regarding the eight categories of behavior. From 1983 to 1990, this process was considered part of a blind research study and was not used as a selection tool; however, we have recently begun using these data for selecting residents [3].

In summary, residents' behaviors deemed essential for successful residency performance were found to remain stable over time. In addition, expanding the original six-category behavioral descriptions into an eight-category system by clarifying the category of "attitudes toward self" and adding an ethical behavior category were found to be useful. It is imperative that radiology training programs continue to examine their criteria for selection of those physicians who will perpetuate the specialty. Behavior-based selection criteria offer an important means to improve the methods used to select radiology residents.

REFERENCES

1. Tarico VS, Smith WL, Altmaier EA, et al. Critical incident interviewing in the evaluation of resident performance. *Radiology* **1984**;152:327–329
2. Altmaier EM, Smith WL, Wood PS, et al. Cross-institutional stability of behavioral criteria desirable for success in radiology residency. *Invest Radiol* **1989**;24:249–251
3. Wood PS, Smith WL, Altmaier EM, et al. A prospective study of cognitive and noncognitive selection criteria as predictors of resident performance. *Invest Radiol* **1990**;25:855–859
4. Tarico VS, Altmaier EM, Smith WL, et al. An accomplishment interview for selection of radiology residents. *J Med Educ* **1986**;61:845–847
5. Tarico VS, Altmaier EM, Smith WL, et al. A resident perspective on the radiology residency: the critical incident technique. *Invest Radiol* **1986**;21:877–880
6. Latham GP, Wesley KN. *Increasing productivity through performance appraisal.* Reading, MA: Addison-Wesley, **1981**
7. Cohen J. A coefficient of agreement for nominal scales. *Educ Psychol Measurement* **1960**;46:142–146
8. Smith P, Kendall LM. Retranslation of expectations: an approach to the construction of unambiguous anchors for rating scales. *J Appl Psychol* **1963**;47:149–155

Radiology Outreach Foundation

The Radiology Outreach Foundation (ROF) is a nonprofit corporation whose goal is to help disadvantaged countries improve their health care by providing radiology equipment, books, consultation, education, and training to their practitioners. This assistance is on an application basis that is independent of political, ethnic, or religious orientation of the grantee. It depends on the need of the people and the ability of the ROF to meet that need. The ROF is approved by the U.S. Internal Revenue Service as a tax-exempt organization. It is endorsed by the following radiologic societies: American Association of Women Radiologists, American College of Radiology, American Roentgen Ray Society, Association of University Radiologists, Radiological Society of North America, Society of Chairmen of Academic Radiology Departments, Society for Pediatric Radiology, European Society of Pediatric Radiology.

All donations to the ROF are tax deductible. Persons who would like to contribute financially to the ROF, would be interested in being a visiting professor, would like to send books or journals to any of the institutions supported by the ROF, or would like further information about the ROF should write to Charles A. Gooding, M.D., President, Radiology Outreach Foundation, 3415 Sacramento St., San Francisco, CA 94118 USA.

Meeting News

The Fleischner Society 22nd Annual Symposium on Chest Disease: Scientific Session, May 1992

Elizabeth Whalen[1]

The Scientific Session of the 22nd Annual Symposium on Chest Disease presented by the Fleischner Society was held May 11-12, 1992, at the Château Laurier, Ottawa, Canada. The Fleischner Society is, by its own description, "an international fellowship of radiologists, physicians, and scientists dedicated to advancing knowledge of the normal and diseased chest, and fostering chest radiology as an art and a science." Preceding the Scientific Session, the annual Fleischner Society course was attended by a multidisciplinary group of participants and offered sessions that encompassed chest anatomy, pathology, physiology, and clinical management, as well as chest imaging. This course included plenary sessions, state-of-the-art sessions, lectures and refresher courses, focus sessions, "family feud" case presentations and film analyses, and the annual Fleischner Lecture.

However, the Fleischner Society annual course is not the subject of this report. The Scientific Session covered here—a session open only to members and to the winner of the annual Fleischner Memorial Award—followed the annual course and featured the presentation of the paper that won the award, along with presentations of papers by three new members of the society; also, members of the society presented 22 papers, including three case reports. Coverage of all the papers presented is impossible because of *AJR* page limitations; however, the following summary does include synopses of the award paper, the three presentations by new members, and eight of the other presentations. The descriptions of the talks will be categorized by general topic: specific lung diseases, MR imaging of the chest, and new technology and approaches in chest imaging.

Specific Lung Diseases

Solitary Pulmonary Nodules

Probability of Malignancy Based on Bayesian Analyses.—The winner of this year's Memorial Fleischner Award, Jud Gurney (Omaha, NB), presented a summary of a study by himself, J. McKay, and D. Lyddon on the likelihood of malignancy in solitary pulmonary nodules as calculated by using Bayesian analysis. Bayesian analysis is a technique that considers all radiologic and clinical findings. For solitary pulmonary nodules, these findings include the nodule's characteristics (e.g., calcification, growth, size, location, edge, and cavitation) and the patient's characteristics (e.g., age, smoking history, hemoptysis, and previous malignancy).

The purpose of the study was to investigate the use of Bayes' theorem to predict malignancy of solitary pulmonary nodules and to compare that prediction with the subjective evaluation by board-certified radiologists. First, the researchers derived the relevant likelihood ratios (which measure the degree of malignancy or benignity of a test result or clinical finding: likelihood ratio = [sensitivity]/[1 − specificity]). Likelihood ratios were derived from a literature review. To be included in the literature review, a study must have been published within the last 30 years (1962–1992), must have

---

[1] Contributing editor, *American Journal of Roentgenology*, Ste. 103, 2223 Avenida de la Playa, La Jolla, CA 92037.

Editor's note.—"Meeting News" articles report the highlights of important national radiology meetings. The articles will not undergo the peer review usually required of *AJR* publications, nor will they offer a critique of the information provided. The sole purpose of the series is to provide Journal readers with succinct, substantive, and accurate reviews of topics of current interest, written in a readable fashion and published promptly after the meeting.

AJR 159:889-895, October 1992 0361-803X/92/1594-0889 © American Roentgen Ray Society

included more than 100 nodules, and must have evaluated both benign and malignant nodules. Fifteen studies fulfilled all these criteria. Results from these studies were used to obtain likelihood ratios for radiologic and clinical characteristics. For example, two studies ($n = 903$) presented data on CT appearance of nodule edge (smooth, lobular, or irregular/spiculated); from that data, likelihood ratios were calculated, showing a likelihood ratio of 0.37 for smooth edges, 0.60 for lobular edges, and 5.77 for irregular/spiculated edges. Intuitively, a likelihood ratio less than one indicates a greater chance of benignity and a likelihood ratio greater than one indicates a greater chance for malignancy (test results with a likelihood ratio of exactly one do not change the pretest odds of malignancy; therefore, the data above translate into the qualitative statements that (1) smooth-edged nodules are more benign than those with lobular edges and (2) irregular/spiculated edges are highly associated with malignancy. Likelihood ratios were calculated for clinical and radiologic characteristics, the most malignant of which were as follows: size >3.0 cm (likelihood ratio = 10.03), irregular/spiculated edges on CT (5.77), hemoptysis (5.08), and previous malignancy (4.95).

Second, after the likelihood ratios were derived for use in Bayes' theorem, the researchers assessed the clinical and radiologic findings of 66 patients with solitary pulmonary nodules. Two groups assessed the data for probability of malignancy: (1) four expert academic radiologists (median experience, 24 years) used traditional methods of evaluation and (2) two observers (one academic radiologist and one resident-in-training) assessed the findings by using likelihood ratios. Of the 66 patients studied, 44 had malignant nodules (32 bronchogenic carcinoma, nine metastases, two carcinoid, and one bronchoalveolar cell cancer); 22 had benign nodules (nine confirmed benign by biopsy, nine by presence of a benign pattern of calcification and absence of growth, and four by absence of growth over a minimum of 2 years). Findings among the study population include the following differences between those with malignant and benign solitary pulmonary nodules: the average ages of the patients were 66 and 59 years, respectively, for those with malignant and benign nodules (not significantly different); percentages of smokers (or ex-smokers) were 57% and 37%, respectively; and the average sizes of nodules were 2.4 and 1.4 cm, respectively.

For evaluating malignancy in the 66 patients, the following images were available: 156 individual chest radiographs, 57 CT scans, three fluoro/tomograms, and seven reference phantom studies. On the basis of the radiographic findings, the four expert radiologists subjectively decided whether the nodules were benign or malignant. Then, the experts were asked to quantify (on a scale ranging from 1 to 100) their estimates as to whether the nodule identified was malignant. After this decision, the experts were provided with the patient's age and smoking history and were asked, "Does this change your decision?" If they answered "Yes," they made a new quantitative estimate about the probable malignancy of the nodule. For nodules that proved to be malignant, the average probability of malignancy given by the experts was 70%; for nodules that proved to be benign, the average probability of malignancy given by the experts was 18%.

Third, in the second method of assessment, two radiologists evaluated these same solitary pulmonary nodules by characterizing them according to radiologic and clinical findings. They then applied the previously derived likelihood ratios and Bayes' theorem to estimate the probability of malignancy.

Fourth, the accuracies of predictions of malignancy by the two groups were compared. The two readers who used Bayesian analysis more accurately assessed the probability of malignancy than did the four experts; the two also misclassified fewer nodules as benign (mean of six misclassifications vs mean of 16 misclassifications for the four experts).

These data indicate that likelihood ratios and the use of Bayes' theorem have potential for improving the accuracy of predicting the malignancy of solitary pulmonary nodules. Moreover, if radiologists provide a quantitative probability of malignancy (rather than using such terms as "most likely benign" or "possibly malignant"), physicians may better be able to determine the best course of patient care.

Fractal analysis of solitary pulmonary nodules.—John H. M. Austin (New York, NY) introduced his presentation as a "tool talk," saying that it looks like radiologists will be able to use fractal analysis based on thin-section CT to evaluate solitary pulmonary nodules, but this study is definitely a preliminary one. The word "fractal" is short for "fractional" and comes from the Latin "frangere" (meaning "to create irregular forms"). Fractals are irregularly shaped objects, and fractal geometry has been developed by Mandelbrot and others to study these objects. One example of a fractal is the island of Great Britain; to try to determine the length (L) of the entire coast of Great Britain, the equation in fractal geometry would be $L = N \times r$, where r = the length of one ruler unit and N = number of units. Note that the shorter the ruler length, the higher the result will be for the length of the coast, i.e., $N = f(r)$. This function is determined by the noninteger fractional dimension D, which is characteristic of the specific shape, and yields $L = k \times r^{1-D}$.

In this work, Dr. Austin and coresearchers (J. Chen, F. Czegledy, J. Katz, L. Boxt) examined 15 CT scans of nine solitary pulmonary nodules (parameters included the following: 1.5-cm slice thickness, 13-cm field of view, use of bone algorithm, 1:1 blow up, 14 × 17 in. film). After outlining the shape of the lesion onto tracing paper, the researchers digitized the image and, using a box-counting algorithm, calculated the fractional dimension, D. They found that they were able to assign to each image an individual D (mean $r = .996 \pm .001$); the lowest D (1.2346) was found for a smoothly rounded granuloma, and the highest D (1.4287) for a spiculated alveolar cell carcinoma.

These pilot results show the feasibility of using fractal analysis of the "coastline" of a solitary pulmonary nodule on CT images; however, the variability of the D of any individual nodule may prove to limit the usefulness of the analysis. Studies are needed to investigate possible correlates of the D of a tumor and clinical variables, e.g., prognosis.

Respiratory Distress Syndrome

Epithelial sodium transport in the developing lung: potential role in respiratory distress syndrome.—One of the new members of the society, Hugh O'Brodovich (Toronto, Canada) presented a hypothesis based on his work over the last 5-6 years: when neonates have inadequate lung epithelial sodium transport, this may be a *pathogenic* factor rather than a *complication* of respiratory distress syndrome. Fetal lungs are always filled with salt water at birth; abnormal clearance of this fluid leads to respiratory distress. Although fluid secretion promotes lung development, at some point secretion must be stopped and absorption started so that the formerly water-filled air space becomes an air-filled space for gas exchange. In a study using pregnant guinea pigs, Dr. O'Brodovich found that animals born with their lungs filled with the sodium transport blocker amiloride were blue and in respiratory distress; the degree to which fluid was blocked depended on the dose of amiloride. The experiment was repeated but sodium channel or other sodium transport blockers were given to some animals; respiratory distress was seen *only* in those neonates whose mothers received the specific sodium channel blocker, which confirmed that active sodium transport through sodium channels was a key to respiratory distress.

Observations from further animal experiments included the following: (1) fetal-derived alveolar epithelial cells were sodium-absorbing cells; (2) there are *some* high-amiloride affinity sodium channels, but there was evidence of additional members of the family of sodium channels; (3) each sodium channel has a "trap door" that opens and shuts, and its presence and characteristics can be determined by patch clamp electrophysiology; and (4) amiloride inhibits nonselective cation channels, which were found in fetal alveolar cells.

Surfactant is also an important factor in lung development. In neonates, immature surfactant and immature ion transport may cause premature respiratory distress syndrome, although Dr. O'Brodovich is not dismissing other possible mechanisms for this disease. However, he did stress that doctors should be aware that ion transport is important in lung disease and warrants further investigation. Other areas of future study in this area include regulation of sodium channels, RNA homology of sodium channels, the effects of C-section versus pelvic delivery on lung fluid, and lung repair mechanisms.

Use of nitric oxide to reduce pulmonary hypertension and improve gas exchange in severe adult respiratory disease syndrome.—Warren M. Zapol (Boston, MA) discussed a study in which he and his coworkers (R. Rossaint, K. Falke, Berlin, Germany) investigated using inhalation of nitric oxide to help patients with adult respiratory disease syndrome (ARDS) and pulmonary hypertension. Although nitric oxide has been considered a toxic substance, the researchers obtained positive results with tiny, nontoxic doses (<25 ppm, which Environmental Protection Agency regulations allow workers to breathe for 8 hr/day). Furthermore, because nitric oxide combines with hemoglobin 250 times faster than carbon monoxide, it is immediately inactivated by red cells, so no systemic effects occur. The researchers also hypothesized that inhalation of nitric oxide would be advantageous in comparison with other methods (e.g., IV prostacyclin) for reducing pulmonary hypertension in ARDS patients. For example, other methods (1) reduce both pulmonary and systemic pressure, whereas nitric oxide would only affect pulmonary pressure, and (2) dilate both shunt and normal regions, whereas nitric oxide would dilate normal regions but *reduce* shunt regions.

After Dr. Zapol and coworkers had performed successful preliminary studies in lambs (in which nitric oxide reduced experimentally induced pulmonary hypertension), nitric oxide was used in hypoxic human infants and it raised arterial oxygen tensions in some infants within minutes of inhalation. Their hypotheses were confirmed by the results of their studies in several ARDS patients with either chronic or acute pulmonary hypertension in which inhalation of nitric oxide (18 ppm) and IV prostacyclin (4 ng/kg/min) were used. Although pulmonary pressure was reduced significantly by both methods, systemic pressure was reduced significantly only by IV prostacyclin (from 86 ± 13 to 79 ± 19 mm Hg); the reduction in systemic pressure with nitric oxide was not statistically significant (from 85 ± 12 to 82 ± 13 mm Hg). The IV prostacyclin treatment resulted in dilatation of the shunting lung regions (Q_S/Q_T increased from 36% ± 15 to 45% ± 13); however, nitric oxide decreased the shunt blood flow significantly (Q_S/Q_T decreased from 36% ± 15 to 31% ± 14). Therefore, inhalation of nitric oxide by ARDS patients at a small, safe dose reduced pulmonary artery pressure without affecting systemic pressure and improved pulmonary gas exchange by redistributing blood flow away from shunting regions to normal regions. The safety of this dose of nitric oxide was shown by treatments in several patients who inhaled these low levels for up to 55 days with no systemic effects. In certain European medical centers, some ARDS patients with pulmonary hypertension are breathing nitric oxide daily. This innovative treatment of acute pulmonary hypertension in these patients offers improvement in overall patient care and an ability to improve matching of perfusion with ventilation.

Bacterial Colonization of Airways

The clinical relevance of bacterial colonization of airways was discussed by Adam Wanner (Miami, FL), a new member of the society, who acknowledged his coworkers, especially Y. Jackowski (recently deceased), as well as K. Kobayashi and S. Seibold. In the past, bacterial colonization has been considered irrelevant to a patient's prognosis. However, studies have found differences in the bacterial content of normal and diseased airways. Research conducted 20 years ago found that airways in normal subjects were 100% sterile; airways in viral pneumonia patients were 50% sterile, with 10% pathogens and 40% oropharyngeal commensals; airways in patients with noninfectious lung disorders were 35% sterile, with 50% pathogens and 15% oropharyngeal commensals; airways in patients with chronic obstructive pulmonary disease were 29% sterile, with 25% pathogens and 46% oropharyngeal commensals; airways in patients with aspiration pneumonia were 14% sterile, with 86% pathogens; and airways in patients with bacterial pneumonia were 8% sterile, with 92% pathogens. More recent research has shown that bacterial colonization may indeed cause damage to the airways.

These researchers based their study on the following hypothesis: If microorganisms were in the airway liquids, these microorganisms would not damage airway epithelium directly but would interact (through their soluble products) with phagocytes in the airway liquids, which would release toxic substances that would damage the airway epithelium. After considering various possible toxic substances that might be involved, these investigators chose toxic oxygen radicals as the focus of their study; ciliary activity was investigated as an expression of airway epithelial function.

Using a sheep model, Dr. Wanner and colleagues brushed the epithelium of the trachea; the brushed material was suspended in a chamber put under a microscope, by which procedure ciliary beat frequency (CBF) was measured. Several experiments were performed to determine the effects of bacterial products on the tracheal epithelium. They first observed that CBF was inhibited progressively with increasing concentrations of a cell-free supernatant of *Pseudomonas aeruginosa*; however, if they removed the neutrophils (i.e., if they only had macrophages and ciliated epithelial cells in the preparation), the bacterial supernatant was no longer capable of inhibiting ciliary activity, indicating that the inhibition is related to the neutrophils. They also found a dose-dependent ciliary inhibition caused by pyocyanin and 1-hydroxyphenazine (which are products of *P. aeruginosa*). The addition of an antioxidant markedly attenuated the ciliary inhibition, indicating that oxygen radicals are at least partly responsible for the inhibiting activity observed. Further experiments indicated that a protein kinase inhibitor can prevent ciliary inhibition induced by oxygen radicals, but only at certain doses (for example, H_2O_2 at concentrations of 10^{-6} M or lower will induce a CBF inhibition that is reversible by protein kinase inhibitors, but at a concentration of 10^{-5} M or higher will cause irreversible CBF inhibition because of the marked disruption of cells).

Dr. Wanner emphasized, in conclusion, that the bacteria that colonize lower airways may secrete toxins that can damage the epithelium and recommended that physicians reevaluate their views on the clinical relevance of bacterial colonization of airways in cases in which clinical evidence of infections is absent.

Asthma and Cystic Fibrosis

The relationship between response to a bronchodilator and bronchial hyperreactivity in children with asthma and cystic fibrosis was discussed by Victor Chernick (Manitoba, Winnipeg, Canada). Previously, the bronchodilator response indicative of asthma had been defined by a change of 15% or more in forced expiratory volume in 1 sec (FEV_1). Because this relationship had not yet been studied specifically in children, Dr. Chernick studied 50 children with asthma and 22 children with cystic fibrosis to investigate the relationship between the response to inhaled salbutamol and bronchial hyperactivity, which was assessed by determining what concentration of inhaled methacholine would decrease FEV_1 by 20% from baseline (PC_{20}).

In 50 children referred for confirmation of clinical suspicion of asthma and in 14 healthy control subjects, results of pulmonary function tests were within the normal range. On day 1 of the study, baseline pulmonary function tests were performed and the best score of three tries was recorded for each subject's FEV_1 and forced vital capacity. On day 2, the subjects were challenged with increasing doses of methacholine. The resulting reactions were categorized into four groups: 1 ($n = 12$), severe hyperreactivity, $PC_{20} \leq 0.25$ mg/ml in asthma patients; 2 ($n = 24$), moderate hyperreactivity, $PC_{20} = 0.26$ to 2.0 mg/ml in asthma patients; 3 ($n = 14$), mild hyperreactivity overlapping normal, $PC_{20} > 2.1$ in asthma patients; and 4 ($n = 14$), normal, $PC_{20} > 8.0$ in normal subjects. FEV_1 increased more than 6% in 58% of group 1, 29% of group 2, 7% of group 3, and 0% of group 4, indicating that a change in FEV_1 greater than 6% after bronchodilator is a specific (100%) but not sensitive (36%) test for bronchial hyperreactivity to methacholine in children with suspected asthma.

In the 22 children with cystic fibrosis, FEV_1 was 46–113% of normal; 11 of these patients had a history of allergy (seasonal rhinitis) and two had one parent each who had asthma. The same procedure was followed as described above to measure the change in FEV_1 after bronchodilator (salbutamol) and bronchial hyperreactivity (methacholine). However, results differed: an increase of more than 6% in FEV_1 was not only 100% specific for bronchial hyperreactivity but was also 83% sensitive for such hyperreactivity. A larger sample of children with cystic fibrosis is needed to confirm this relationship.

Dr. Chernick concluded that bronchial hyperreactivity to methacholine is probably present in children with suspected asthma or cystic fibrosis whose FEV_1 increases more than 6% after inhaled salbutamol. However, the sensitivity of the test is low in asthma patients, so it cannot be used in large population studies, and more patients with cystic fibrosis must be tested to confirm the results.

MR Imaging of the Chest

MR Evaluation of the Results of Conservative Therapy in Lung Cancer Patients

Michio Kono (Kobe, Japan), a new member and the first Japanese member of the Fleischer Society, presented a study of 52 lung cancer patients who had MR imaging studies for assessment of the effects of radiotherapy/chemotherapy treatment (coauthors: S. Adachi, M. Kusumoto, E. Sakai, M. Endo, K. Imanaka, M. Fujii, K. Yamasaki, E. Itouji). The three purposes of their study were as follows: to describe the gadolinium-enhanced MR appearance of lung cancer after conservative treatment, to use gadolinium-enhanced MR imaging to differentiate residual or recurrent tumor from radiation pneumonitis, and to evaluate by gadolinium-enhanced MR imaging the rate of reduction and necrosis resulting from radiotherapy/chemotherapy.

Before and after treatment, unenhanced and IV gadolinium-enhanced T1-weighted MR images were obtained in 52 patients (31 had squamous cell carcinoma, nine each had adenocarcinoma and small call carcinoma, and three had large cell carcinoma). Three patterns of tumor appearance were evident: homogeneous (which was seen after treatment in 13 squamous cell tumors, four adenocarcinomas, six small cell

AJR Subscription

AJR
American Journal of Roentgenology
Official Journal of the American Roentgen Ray Society

If you expect to use what you read
...Subscribe!

AJR is your best source for up-to-date coverage of clinical radiology. Our editors look for articles you can make use of in your daily work. That means lots of practical, pertinent information – the topics that interest you right now. Every month, you get original articles that are relevant to what you do. Plus time-saving review articles that bring together all the confusing or conflicting literature on a particular topic of interest and make sense of it for you. You also get case reports that help you reevaluate your own experience...technical reports that keep you on top of new techniques and give you clear pictures of the procedures used and the results obtained.

All this comes to you in one journal: **AJR**. Enter your subscription today.

Editor: Robert N. Berk, M.D., San Diego, California

YES, please start my subscription to AJR for

☐ 3 yrs. ☐ 2 yrs. ☐ 1 yr. ☐ Individual $125/yr ☐ In-training $25/yr* ☐ Institutional $135/yr

(Add $55 for postage outside the US; in Canada, also add 7% GST)

Payment options:

☐ Check enclosed (Payable to AJR)

☐ Bill me ☐ VISA ☐ MasterCard ☐ AmEx

Card # ______________________ Exp. Date ______________

Signature ______________________________

Name ______________________________

Address ______________________________

City/state/zip ______________________________

* Residents, fellows, interns...when requesting the in-training rate to which you are entitled for 3 years, please supply training status and name of institution. MD residents please add 5% state sales tax. Subscriptions outside the U.S. must be prepaid in U.S. dollars only. Airmail rates available on request.

• *Or call us FREE ... 1-800-638-6423 from anywhere in the U.S. or Canada* •

AJR Bound Volumes

Bound Volumes ... for current subscribers!

AJR
American Journal of Roentgenology
Official Journal of the American Roentgen Ray Society

Now you can get a year's worth of articles in bound volume form – so the information you need will be at your fingertips.

Bound volumes offer the timely coverage only a journal can provide – penetrating discussions of the topics that interest you most by the brightest names in the field – with all the durability and convenience of a hardcover edition. You'll have a year's worth of vital information all arranged and indexed in one sturdy source. And each carefully crafted volume will make a handsome addition to your permanent library.

Bound volumes are available for the current year only and are in addition to the regular subscription price. The 1992 Bound Volume will be mailed in early 1993.

Yes, send me the AJR, American Journal of Roentgenology 1992 Bound Volume at $97 ($112 outside the U.S.)

☐ Check enclosed *MD residents please add 5% sales tax.*

☐ Bill me ☐ VISA ☐ MasterCard ☐ AmEx

Card Number ______________________ Expiration ______________

Signature ______________________________

Name ______________________________

Address ______________________________

City/state/zip ______________________________

NO POSTAGE
NECESSARY
IF MAILED
IN THE
UNITED STATES

BUSINESS REPLY MAIL

FRIST CLASS PERMIT NO.724 BALTIMORE, MD

POSTAGE WILL BE PAID BY ADDRESSEE

Waverly Press
Attn: AJR
P.O. Box 23291
Baltimore, MD 21298-9533

NO POSTAGE
NECESSARY
IF MAILED
IN THE
UNITED STATES

BUSINESS REPLY MAIL

FRIST CLASS PERMIT NO.724 BALTIMORE, MD

POSTAGE WILL BE PAID BY ADDRESSEE

Waverly Press
Attn: AJR
P.O. Box 23291
Baltimore, MD 21298-9533

tumors, and one large cell tumor); mottled (which was seen after treatment in 10 squamous cell tumors, two adenocarcinomas, three small cell tumors, and one large cell tumor); and ringlike (which was seen after treatment in eight squamous cell carcinomas, three adenocarcinomas, no small cell carcinomas, and one large cell carcinoma).

After treatment, gadolinium-enhanced MR imaging showed that, in 15 of the 24 homogeneous tumors, tumor size was less than or equal to 50% of its pretreatment size; a lower rate of reduction was found in the other nine homogeneous tumors. For mottled tumors, after conservative treatment, only four of 16 lesions had decreased more than 50% in size, and for ringlike tumors, a reduction of 50% or more was found in only three of 12 cases. The significance of reduction of tumor size is shown by survival rates: of the patients with homogeneous tumors, those whose tumors had decreased in size more than 50% survived an average of 10.6 months, and those whose tumors had decreased in size less than 50% survived an average of 17.2 months. Of the patients with mottled tumors, those whose tumors had decreased in size more than 50% survived an average of 12.5 months, and those whose tumors had decreased in size less than 50% survived an average of 14.5 months. Finally, of the patients with ringlike tumors, those whose tumors had decreased in size more than 50% survived an average of 10.3 months, and those whose tumors had decreased in size less than 50% survived an average of 18.2 months. Therefore, this study showed that gadolinium-enhanced MR imaging had defined three lung tumor patterns and had shown the effects of conservative treatment on tumors with these patterns.

Radiation pneumonitis occurred in 13 of the 52 cases. In 8% of these cases, tumor enhanced more than the pneumonitis. In 23%, enhancement was equal, and in 69%, pneumonitis enhanced more than tumor. Moreover, on the gadolinium-enhanced MR images, viable tumor did enhance, necrotizing areas either did not enhance or showed delayed enhancement, and radiation pneumonitis showed remarkable enhancement. Thus, gadolinium-enhanced MR imaging did help differentiate recurrent tumor from radiation pneumonitis.

These researchers also performed MR spectroscopy on some of these patients for follow-up studies. MR spectroscopy may prove helpful in delineating even further the therapeutic effects of radiotherapy and chemotherapy on lung cancer.

MR Imaging in Venous Thromboembolic Disease

A prospective study of 61 consecutive patients referred for conventional venography was presented by H. Dirk Sostman (Durham, NC; coauthors: A. S. Evans, J. R. MacFall, T. K. F. Foo, J. F. Debatin, C. E. Spritzer, T. M. Grist). In these patients, both conventional venography and MR imaging were performed within 12 hr (mean, 2.6 hr). MR images were obtained first in 43% of cases, and conventional venograms were obtained first in 57% of cases. Results of all the imaging studies were interpreted blindly. If both MR imaging and conventional venography findings were positive, the result was considered a true positive; if both MR imaging and conventional venography findings were negative, the result was considered a true negative. In cases in which MR imaging results disagreed with those of conventional venography concerning thromboembolic disease in the calf and/or thigh, results from conventional venography were considered correct and MR imaging results were considered incorrect. However, in cases of pelvic vein disease, the correctness of discordant results was determined by direct puncture of femoral vein or follow-up.

As stated above, conventional venography was considered to be the gold standard for detecting thromboembolic disease in the thigh and calf veins. In thigh veins, MR imaging showed a sensitivity of 100% and a specificity of 100%. However, the values were somewhat lower for MR imaging in calf veins (sensitivity, 87%; specificity, 97%). In pelvic veins, the sensitivity of MR imaging was 100%; for conventional venography, sensitivities were 78% by direct puncture or 64% by follow-up confirmations. Specificity for pelvic vein disease was 100% for conventional venography; for MR imaging, specificities were 95% by direct puncture or 98% by follow-up confirmations. In summary, for assessing deep vein thrombosis, MR imaging is less sensitive than conventional venography in calf veins, equal to conventional venography in assessing disease in thigh veins, and more sensitive than conventional venography in assessing disease in the pelvic veins.

Dr. Sostman also discussed promising trends in the use of MR imaging of pulmonary circulation in the evaluation of pulmonary emboli. In one example, a three-dimensional MR data set from a dog model showed the advantage of the ability to change the plane and angle in order to examine different parts of the vessels. Possible new techniques encompass vascular imaging, thrombus imaging, two-dimensional and three-dimensional techniques, cine MR imaging, breathhold procedures, and black-blood methods.

Three-dimensional MR Tagging to Indicate Homogeneity of Left Ventricular Myocardial Strain

Elias A. Zerhouni (Baltimore, MD) and colleagues (E. McVeigh, C. Moore) used three-dimensional (3D) MR tagging to try to resolve a long-standing problem in cardiac physiology—that is, the inability to measure the deformation of the heart. In the study of an object such as the heart, which generates force, one needs to know its mechanical properties and to understand exactly its deformation. Because in traditional imaging methods, the heart moves through the imaging plane, the point-to-point deformation cannot be determined. To investigate whether left ventricular strain is temporally and spatially heterogeneous in the normal heart (as suggested by angiocardiographic, echocardiographic, and implanted bead studies), these researchers "tagged" the heart by labeling little planes in six directions (12 segments) and then examined the entire ventricle in three dimensions. After they had obtained all the MR images needed, they defined the volume elements in the computer and performed a complete finite strain analysis to study the strain in the radial, longitudinal, and circumferential directions and to therefore obtain a "map" of the deformation of the heart in all directions. A color scale was used for display, in which blue indicated the lowest amount of strain and yellow (red/yellow) the highest amount of strain.

By use of this method in 12 normal subjects, an enormous amount of heterogeneity of deformation was seen from the start (no stress, diastole) to strain (systole) of the heart cycle. The strain in the radial direction was very heterogeneous; however, the deformation was homogeneous in the longitudinal or circumferential directions. Moreover, despite the lack of change in total volume of the heart, changes were found in single-volume elements. Therefore, Dr. Zerhouni and colleagues concluded that the heterogeneity seen must be the result of an error introduced in the radial direction in measuring endocardial surface. When the error in the radial direction was corrected (i.e., when the volume was maintained), they found that the normal heart contracted homogeneously. This need for correction in the radial direction in assessing the heterogeneity of heart contraction indicates two things: tremendous uncertainty still exists as to the location of the endocardium on MR images, and the endocardium may move differently than does the rest of the heart.

New Technologies and Approaches in Chest Imaging

Dynamic, Ultrafast, High-Resolution CT of the Lung

A study of a new technique for diagnosing lung diseases characterized by airways obstruction and air trapping was described by W. Richard Webb (San Francisco, CA; coauthors, E. J. Stern, G. Gamsu). Dynamic, ultrafast high-resolution CT involves obtaining 10 100-msec high-resolution CT scans in 6 sec while the patient performs a forced vital capacity maneuver. The scans are evaluated qualitatively by viewing the scan sequence in the "movie mode," noting the lung-attenuation changes and volume changes during exhalation, and selecting for analysis regions of interest that appear to show air trapping. Quantitative evaluation includes time-attenuation curves, lung-attenuation values (in Hounsfield units) plotted vs time for selected regions of interest, and changes in lung attenuation from maximum inhalation to maximum exhalation.

Dynamic, ultrafast, high-resolution CT scans of the lung were obtained in 10 healthy, nonsmoking men with normal spirometry results. The increase in lung-attenuation values from maximum inhalation to maximum exhalation ranged from 84 to 372 H (average, 200 H). Also, with one exception in the normal subjects, the dependent lung showed a greater increase during exhalation than did the nondependent lung—this held true for all areas of the lung and for both prone and supine positions.

In patients with obstructive lung disease, studies with dynamic, ultrafast, high-resolution CT showed an increase in lung-attenuation values that averaged only about 50 H from maximum inhalation to maximum exhalation; moreover, in some patients, lung-attenuation values *decreased* from maximum inhalation to maximum exhalation. This technique detected air trapping in the lung that was as small as a secondary lobule, bronchial collapse associated with air trapping, and sometimes airways obstruction and air trapping in patients with normal pulmonary function tests.

On dynamic, ultrafast, high-resolution CT, normal lung had homogeneous parenchyma, homogeneous increase in attenuation with exhalation, and patent airways. In a patient with lymphangitic carcinomatosis, dynamic, ultrafast, high-resolution CT showed bronchial occlusion and subsegmental air trapping on exhalation. Dynamic, ultrafast, high-resolution CT showed secondary pulmonary lobular air trapping in patients with bronchiolitis obliterans, and it showed air trapping during exhalation in a patient with endobronchial metastasis. This new technique appears to be very promising, and issues still to be resolved include explanations for air trapping in normal subjects and for the decrease in lung-attenuation values on exhalation in some patients.

Thoracocardiography

Marvin A. Sackner (Miami Beach, FL; coauthors, K. E. Bloch, S. Jungoon) discussed the use of thoracocardiography for the noninvasive assessment of ventricular diastolic function and its respiratory variation. If an inductive plethysmographic transducer is placed around the rib cage below or near the ziphoid process, "little lumps" (cardiogenic oscillations) are shown on the respiratory curve; these cardiogenic oscillations, which have been known about for many years, constitute up to 4% of the total respiratory signal. Cardiogenic oscillations increased with inspiration (and decreased with expiration) if the transducer band was placed below the nipple line; the reverse was true (oscillations decreased with inspiration and increased with expiration) when the transducer band was placed below the xiphoid. These researchers therefore concluded that, by placing the band in different locations, they could judge whether they were measuring the volume of the left or right ventricle.

In 12 normal subjects, several measures of left ventricular function were obtained by use of thoracocardiography and then compared with the same measures as reported in the literature. For example, thoracocardiographic stroke volumes on inspiration and expiration of 1.0- and 1.5-l tidal volumes were compared with baseline stroke volumes of 0.5 l. At 1.5 l, stroke volume on inspiration was 84% of baseline, stroke volume on expiration was 126% of baseline, and average stroke volume was 103% of baseline. Also at 1.5-l tidal volumes, isovolumic relaxation time on inspiration was 77 msec; on expiration, 82 msec; and on average, 83 msec, all of which were comparable with measurements obtained by Doppler echo studies. Other measurements obtained by thoracocardiography were heart rate, early filling rate/atrial filling rate, early filling rate/stroke volume, and atrial filling rate/stroke volume. Moreover, imposed mechanical ventilation showed reversed respiratory amplitudes on thoracocardiography (e.g., with mechanical ventilation, the stroke volume of the left ventricle is greater on inspiration than on expiration). Dr. Sackner pointed out that, if such values can be obtained accurately by the noninvasive method of thoracocardiography, wedge pressure could be indirectly calculated and, in some cases, use of the Swan-Ganz catheter could therefore be avoided.

Finally, in 10 normal subjects, thoracocardiographic results were compared with those from an automatic edge detector echocardiographic device (HP-Somnos 1500). (Dr. Sackner noted that this part of the study took 1.5 days to perform and 3 months to analyze because of the difficulty of translating HP-Somnos data to analog values.) Stroke volumes found with the two methods were within 20% of each other, good agreement was found in both inspiratory and expiratory stroke volumes, the mean difference in isovolumic relaxation time between the two methods was only 2 msec, and the mean difference in peak and atrial filling rates between the two methods was zero.

These researchers concluded that thoracocardiography can measure the function of the right or left ventricle both accurately and noninvasively. Furthermore, they found that their normal values obtained by thoracocardiography for isovolumic relaxation time and early filling rate/atrial filling rate agreed closely with those published in the literature.

Dependence of Maximal Flow-Volume Curves on Time Course of Preceding Inspiration

A study on maximal expiratory flow-volume maneuvers was performed by E. D'Angelo (Milan, Italy), E. Prandi (Milan, Italy), and J. Milic-Emili (Montreal, Quebec, Canada) and presented to the society by Dr. Milic-Emili. Although the American Thoracic Society has provided guidelines for obtaining measures of peak expiratory flow and forced expiratory volume at 1 sec (FEV_1), no instructions are given concerning the inspiratory pattern *before* the forced expiration. Therefore, these researchers conducted a study in 13 naïve medical students in which volume was measured with body plethysmography and flow was measured at the mouth with a heated Fleisch pneumotachograph. Each subject performed forced expired vital capacity maneuvers after four different inspiratory maneuvers: 1, breathe in as fast as possible and then breathe out immediately and as quickly as possible; 2, breathe in as fast as possible, hold your breath for 5 sec, then breathe out quickly; 3, breathe in slowly, do not hold your breath, then breathe out quickly; and 4, breathe in slowly, hold your breath for 5 sec, then breathe out quickly.

In all subjects, the results of the test were similar: peak flow and FEV_1 were significantly higher with maneuver 1 than with any other inspiratory maneuver and were lowest with maneuvers 2 and 4. Similar differences were also seen in both $FEV_{0.25}$ and $FEV_{0.50}$ (forced expiratory volumes at 0.25 and 0.50 sec). Such results could be explained by a simple viscoelastic model of the respiratory system that was introduced 50 years ago.

The data provided by this study indicate that standardization of the forced vital capacity maneuver must take into account the pattern of the preceding inspiration. With such standardization, the measurements will be more reproducible and comparable than they are currently.

Forthcoming Articles

REVIEW ARTICLES

Evaluation of congenital heart disease using MR imaging: current and coming attractions. *Fellows KE, Weinberg PM, Baffa JM, Hoffman EA*

CT of the extraperitoneal space: normal anatomy and fluid collections. *Korobkin M, Silverman PM, Quint LE, Francis IR*

Color Doppler imaging of the hepatic vasculature. *Grant EG, Schiller VL, Millener P, et al.*

CARDIOPULMONARY RADIOLOGY

MR imaging of the lungs: value of short TE spin-echo pulse sequences. *Mayo JR, MacKay A, Müller NL*

Chronic hypersensitivity pneumonitis: CT diagnosis. *Buschman DL, Gamsu G, Waldron JA Jr, Klein JS, King TE*

Malignant pleural mesothelioma: value of CT and MR imaging to predict resectability. *Patz EF Jr, Shaffer K, Piwnica-Worms DR, et al.*

Pictorial essay. Radiographic appearance of bullet tracts in the lung. *George PY, Goodman P*

Case report. Bronchial stenosis due to endobronchial tuberculosis: successful treatment with self-expandable metallic stent. *Han JK, Im JG, Park JH, Han MC, Kim YW, Shim YS*

BREAST RADIOLOGY

Screening mammography in 350 women with breast implants: prevalence and findings of implant complications. *Destouet JM, Monsees BS, Oser RJ, Nemecek JR, Young VL, Pilgrim TK*

Commentary. Re: Screening mammography in 350 women with breast implants: prevalence and findings of implant complications. *Bassett LW, Brenner RJ*

GASTROINTESTINAL RADIOLOGY

Complications of continuous ambulatory peritoneal dialysis: evaluation with CT peritoneography. *Hollett MD, Marn CS, Ellis JH, Francis IR, Swartz RD*

Percutaneous obliteration of the cystic duct with Holmium:YAG laser: results of in vitro and animal experiments. *Girard MJ, Saini S, Mueller PR, et al.*

Percutaneous chemical gallbladder sclerosis after laser-induced cystic duct obliteration: results in an experimental model. *Girard MJ, Saini S, Mueller PR, et al.*

Gastric and duodenal obstruction in patients with cholangiocarcinoma in the porta hepatis: increased prevalence after radiation therapy. *Mogavero GT, Jones B, Cameron JL, Coleman J*

The distinction between benign and malignant liver tumors on sonography: value of a hypoechoic halo. *Wernecke K, Vassalo P, Bick U, Diederich S, Peters PE*

Pathologic explanation for hypoechoic halo seen on sonograms of malignant liver tumors: an in vitro correlative study. *Wernecke K, Henke L, Vassallo P, et al.*

Pictorial essay. Differential diagnosis of hyperintense liver lesions on T1-weighted MR images. *Lee MJ, Hahn PF, Saini S, Mueller PR*

Case report. Focal ischemic necrosis of the liver associated with cirrhosis: radiologic findings. *Fukui N, Kitagawa K, Matsui O, et al.*

GENITOURINARY RADIOLOGY

Retroperitoneal neurilemoma: CT and MR findings. *Kim SH, Choi BI, Han MC, Kim YI*

Case report. Transitional cell carcinoma of the renal pelvis associated with cyclophosphamide therapy. *Levine E*

Case report. Sonographic appearance of the torsion knot in spermatic cord torsion. *Maroto A, Serres X, Torrent N, Figueras M, Hoyo D, Velayos A*

MUSCULOSKELETAL RADIOLOGY

MR imaging of the quadriceps tendon: normal layered configuration and its importance in cases of tendon rupture. *Zeiss J, Saddemi SR, Ebraheim NA*

Case report. Mucormycosis osteomyelitis causing avascular necrosis of the cuboid bone: MR findings. *Chaudhuri R, McKeown B, Harrington D, Hay RJ, Bingham JB, Spencer JD*

Case report. Rapid growth of femoral herniation pit. *Crabbe JP, Martel W, Matthews LS*

NEURORADIOLOGY

Relapsing-remitting multiple sclerosis: sequential enhanced MR imaging vs clinical findings in determining disease activity. *Barkhof F, Scheltens P, Frequin STFM, et al.*

Evaluation of complex cystic masses of the brain: value of steady-state free-precession MR imaging. *Tien RD, MacFall J, Heinz R*

Predicting cerebral ischemia during carotid endarterectomy using cerebral angiography. *Schwartz RB, Jones KM, LeClercq GT, et al.*

Test to predict sequelae after permanent carotid occlusion: contrast MR imaging and HMPAO scintigraphy in conjunction with balloon test occlusion. *Simonson TM, Ryals TJ, Yuh WTC, Farrar GP, Rezai K, Hoffman HT*

Pictorial essay. MR imaging of clival and paraclival lesions. *Chaljub G, Van Fleet R, Guinto FC Jr, Crow WN, Martinez L, Kumar R*

Case report. Miliary tuberculosis involving the brain: MR findings. *Gee GT, Bazan C III, Jinkins JR*

VASCULAR RADIOLOGY

Femoral artery pseudoaneurysms: value of color Doppler sonography for predicting which ones will thrombose without treatment. *Paulson EK, Hertzberg BS, Paine SS, Carroll BA*

Closure of the ductus venosus in neonates: a color Doppler study. *Loberant N, Barak M, Gaitini D, Herskovits M, Ben-Elisha M, Roguin N*

Pictorial essay. Giant fistula between the right coronary artery and the left ventricle: diagnostic significance of right posterior oblique chest radiograph. *Takeda K, Okuda Y, Matsumura K, Sakuma H, Tagami T, Nakagawa T*

INTERVENTIONAL RADIOLOGY

Self-expanding metal stents for palliative treatment of malignant ureteral obstruction. *Lugmayr H, Pauer W*

Needle-tip localization during CT-guided abdominal biopsy: comparison of conventional and spiral CT. *Silverman SG, Bloom DA, Seltzer SE, Tempany CMC, Adams DF*

CONTRAST MATERIAL

Case report. Iodide mumps due to low-osmolality contrast material. *Berman HL, Delaney V*

DIGITAL RADIOLOGY

Digital archive center: implementation for a radiology department. *Wong AWK, Taira RK, Huang HK*

PERSPECTIVES

Capital planning in radiology. *Thrall JH*

Subspecialization and certification in radiology. *Margulis AR*

Letters

Red Arrows in Radiology

Radiologists must communicate their findings and interpretations to their medical colleagues. Many radiologic examinations, particularly in teaching hospitals, are reviewed a number of times after the initial interpretation: for consultations, conferences, teaching, and comparison with follow-up studies. The hard-copy images may be reviewed by the referring clinician or consultant with the assistance of a radiology resident, fellow, or staff member other than the person who originally interpreted the examination. This process can be time-consuming if the raw data, the images, must be examined de novo each time. Even if a printed report is at hand, it may be difficult to correlate the images with the radiologist's words.

With these problems in mind, we urge the liberal use of arrows or lines made with a red "china" crayon to show pertinent findings on images at the time the findings are first detected. This is true for plain radiographs, for example, to show subtle rib fractures, pulmonary nodules, skeletal metastases, and so forth. However, it is more important in conjunction with CT and MR studies, for which the examination of multiple scans or images, sometimes in excess of 100, is more time-consuming. Using red marks on sonograms is important because the location and orientation of the transducer during sonography may not be obvious, making interpretation difficult even for other radiologists. Pertinent findings can be indicated on selected digital images by red lines extending from the abnormality to the outer margin of the image frame. The selected frame could also be indicated by a red mark in the corner of the frame. Red arrows can even be helpful in reducing accidental omissions of significant findings at the time of initial interpretation, particularly when the study involves multiple films or multiple findings or the report is dictated some time after the initial viewing.

Another red-crayon time-saver is the routine numbering of each of the multiformatted images in a CT or MR examination. This can be done by the technologist or by the radiologist who previews the examination or at the time of the initial interpretation. Examinations usually consist of five to 10 films, each with 12 images, and numbering allows the images to be mounted correctly and expeditiously, even by a student or file clerk. Comparison with similarly numbered previous examinations is also expedited.

The marks are, of course, easily removable with thumb grease or a tissue. The crayon should be red, not black, to contrast with standard black-and-white radiologic images. This is particularly true now that most multiformatted digital images are printed on a black background. The lines should traverse a light area if possible. Red crayon marks thus represent a downstream saver of time and energy and provide a more focused learning experience for the secondary reviewers. We keep red crayons at all reading locations, and they can also be capped and carried by the radiologists.

Morris Simon
Ferris M. Hall
Beth Israel Hospital
Harvard Medical School
Boston, MA 02215

A Resident's Experience in the South Pacific

Occasionally, during conferences on sophisticated imaging of medical problems, I recollect my experience as an intern on an island in the South Pacific during June 1990. During my year as a transitional intern at the University of Hawaii, I volunteered to work in general surgery and medicine in a small hospital and clinic in the town of Koror in the Republic of Palau, an archipelago 3 hr by air from Guam. Five other physicians and I attended to the medical needs of 20,000 inhabitants and tourists.

The entire southwest Pacific has tremendous historical and geographic importance. Many of the islands from the Carolines to Palau and subsequently north to the Marianas mark the course of the territories captured during World War II and now under United States territorial control. The Republic of Palau is famous for its world-class scuba diving and for the battle of Pelilu, a remote southern island where the First Marine Corps Division fought against the entrenched Japanese forces in 1944.

The capital city of Koror has a 50-bed hospital, which is divided into male and female medicine and surgery suites. Most beds had mattresses, but only a few had linen. Paper towels did not exist. When a Western-trained physician arrives, he or she first notices the heat and humidity of the town and hospital and then becomes alarmed at the lack of supplies and equipment. The hospital had only one ventilator, which was kept in the operating room. When intubation was needed, the patient's family was required to provide ventilation via an "ambubag" until the patient was ready to be extubated. Shortages of antibiotics and other medicines are commonplace and force medical personnel to either improvise or begin their own rationing system.

Recent medical literature has addressed the problem of rationing medical services. This concept took on a new meaning during my stay at Palau. Shortages of beds frequently required a physician to decide, on the basis of prognosis, age, usefulness, and other factors, who should be admitted and who should be discharged. An example of such decision making occurred in the case of an elderly Palauan man who had fallen down a staircase. The patient had weakness and paresthesia of the right upper and lower extremities. The hospital had an old Korean X-ray machine that provided fair images; the patient's cervical spine was barely discernible and appeared to have a subluxation of C5 over C6. No Philadelphia collar or traction device was available in the hospital, so we used two sandbags to support the patient's head and instructed his family to carefully logroll him to avoid decubitus ulcers. Eventually, he regained some motor skills and was able to return to his village.

I am glad I had the opportunity to work in such an interesting setting. Practicing medicine in an underdeveloped region is a great experience for medical students, house staff, and attending physicians, and it provides valuable information and techniques to local physicians and health care personnel and great service to the local population. Sometimes, before taking a step forward in medicine, it is important to take one backward and relearn the role of physician.

Michael H. Wholey
The Johns Hopkins University
Baltimore, MD 21205

Faster Slide Photography

Although some departments use outside photography services to make slides from radiologic images for use at conferences, many departments still produce their own slides, particularly with respect to the new austerity imposed by diminishing reimbursements. With the proper equipment, making slides can be an efficient process.

In our experience, the least desirable aspect of using RPC film (Kodak, Rochester, NY 16450) to make slides from radiologic images is the 15- to 20-sec exposure time that is usually required. This problem can be eliminated by using a 10-bulb light box (model 186), which is available from S & S X-ray Company (Brooklyn, NY 11208). This light box can be positioned horizontally under a standard photography copy stand. The stands are available from camera shops; we are currently using a Kaiser RS1 (distributed by H. P. Marketing, Pinebrook, NJ 07058). With this light box, at f 2.8 aperture, with preloaded RPC film, we routinely use exposure times of 2 sec for CT scans and MR images. Although bulk load RPC film is also available, at a considerable savings per roll, we have found that the exposure time increases to 4 sec when bulk RPC is used. This reflects variation in the film, and each site should determine exact exposure times with its system.

In combining this system with one of the current autofocus, autowind cameras such as the Nikon 8008 (Nikon, Garden City, NY 12530) with a macrolens, the photography becomes much more efficient and borders on being enjoyable. One incidental note about the Nikon 8008: with the 60-mm macrolens, one-to-one reproduction is possible without use of extension pieces, which is quite useful when small sonograms are being photographed. A cable or remote electronic release is highly recommended to ensure stability of the camera during the exposure.

We hope this information will be of value to other readers who wish to expedite the transfer of images to slide format on RPC film.

Alexander C. Mamourian
Milton S. Hershey Medical Center
Hershey, PA 17033
Evan Fram
Barrow Neurologic Institute
Phoenix, AZ 85013

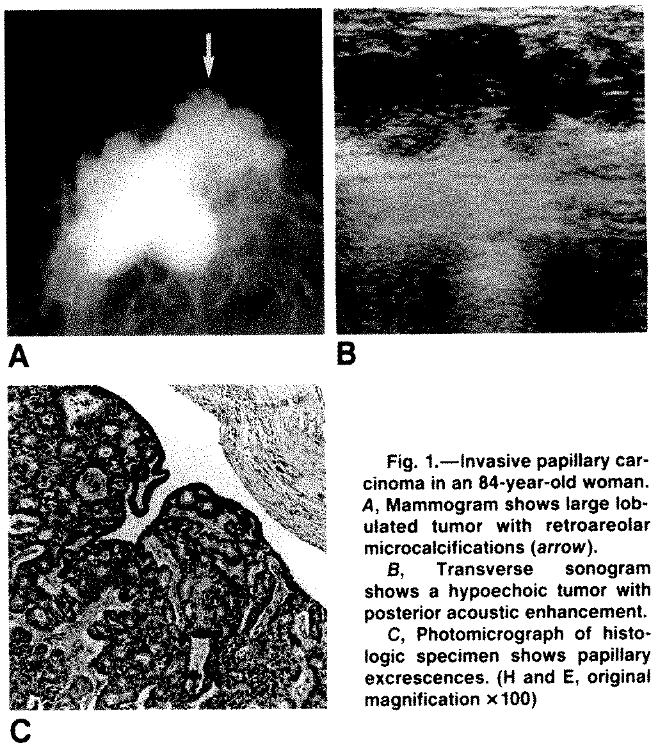

Fig. 1.—Invasive papillary carcinoma in an 84-year-old woman.
***A*, Mammogram shows large lobulated tumor with retroareolar microcalcifications (*arrow*).**
***B*, Transverse sonogram shows a hypoechoic tumor with posterior acoustic enhancement.**
***C*, Photomicrograph of histologic specimen shows papillary excrescences. (H and E, original magnification ×100)**

Invasive Papillary Carcinoma in Elderly Women: Sonographic and Mammographic Features

Invasive papillary carcinoma is a rare (1% prevalence) breast cancer [1]. It usually occurs in white, postmenopausal women and favors the upper quadrants of the breast. The prognosis is better than that for other breast cancers, including invasive ductal carcinoma and low-malignancy medullary carcinoma. Sonographic and mammographic findings in invasive papillary carcinoma have been described only recently [1, 2]. We report findings in two patients whose tumors contained microcalcifications.

The first patient was an 84-year-old white woman with a movable nontender mass in the upper outer quadrant of the left breast. The second patient was an 87-year-old white woman with a hard movable mass in the upper outer quadrant of the right breast. In both women, mammography showed a well-defined, lobulated, homogeneous opacity that followed the distribution of a duct. Mammograms showed rodlike calcifications (Le Gal type V) [3] (Fig. 1A) in the first patient and stippled areas of calcification (Le Gal type III) in the second patient. In both patients, sonograms showed a hypoechoic mass with lobulated margins and posterior enhancement (Fig. 1B). The first patient had a mastectomy, and the second patient underwent a fine-needle biopsy. Histologically, both tumors were composed of cystic structures with epithelial proliferations forming thin, short papillae (Fig. 1C). Columnar cells with eosinophilic cytoplasm were also present. Papillae formed irregular cavities containing cellular debris and concentric laminar microcalcifications.

Recently, Schneider [2] described the imaging features of four cases of invasive papillary carcinoma. Mammography showed lobulated tumors with well-defined margins. Mammographic findings were the same in our cases, except that our patients had calcifications.

R. Silva
F. Ferrozzi
C. Paties
and colleagues
Piacenza Hospital
29100 Piacenza, Italy

REFERENCES

1. Kline T, Kannan V. Papillary carcinoma of the breast. *Arch Pathol Lab Med* **1986**;110:189–191

2. Schneider JA. Invasive papillary breast carcinoma: mammographic and sonographic appearance. *Radiology* **1989**;171:377–379
3. Le Gal M, Durand JC, Laurent M, Pellier D. Conduite a tenir devant une mammographie revelatrice des microcalcification groupees sans palpable. *Nouv Presse Med* **1976**;5:1623–1627

Intramammary Lymph Node in the Lower Outer Quadrant Detected Mammographically

Intrammammary lymph nodes are frequently seen on mammograms, and accurate identification of these masslike densities prevents many unnecessary biopsies. Histologic detection of intramammary lymph nodes in all quadrants of the breast have been reported [1]; however, mammographic detection of lymph nodes in the inferior part of the breast (subareolar region) has not [2].

By definition, on both histologic preparations and mammograms, an intramammary lymph node must be surrounded by fibroglandular tissue [3]. Intramammary lymph nodes have a fairly characteristic appearance on mammograms. They are usually round, ovoid, or lobulated and have well-defined margins [2–4]. A lucent fatty center or hilar notch indicates that they are benign [2, 4].

When a lesion meets all these criteria and is located in the upper outer quadrant of the breast, no further evaluation is necessary. Reportedly, the upper outer quadrant is the only part of the breast in which intramammary lymph nodes are seen on mammograms, and such lymph nodes should not be considered related to a mass seen in any other section of the breast. In particular, it has been emphasized that intramammary lymph nodes are not seen in the lower quadrants of the breast [2]. We report a case of a pathologically proved intramammary lymph node in the subareolar area and below the midline of the breast that was detected mammographically.

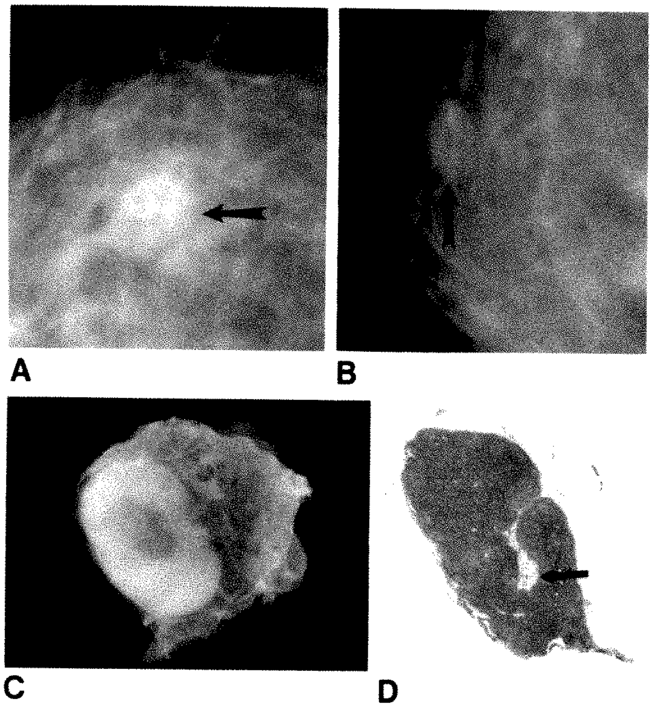

Fig. 1.—Intramammary lymph node in lower outer quadrant.
***A* and *B*, Craniocaudal (*A*) and oblique mediolateral (*B*) film-screen mammograms of left breast show a well-circumscribed mass (*arrow*) in lower outer quadrant.**
***C*, Specimen radiograph shows mass was completely excised. Doughnut shape and fatty center are indicative of a benign process.**
***D*, Low-power photomicrograph shows a lobulated lymph node with central fatty replacement (*arrow*), corresponding to mammographically detected central lucency.**

A 43-year-old woman was referred to our institution for evaluation of a mass in the lower outer quadrant of the left breast. The mass had been detected on a first-time screening mammogram. Oblique mediolateral and craniocaudal mammograms showed an ovoid medium-density mass 1.5 × 1.2 cm in the lower outer quadrant of the left breast (Figs. 1A and 1B). The mass had well-defined margins and a somewhat lucent center. The mass was not visualized on sonograms and therefore was thought to be solid. The mammographic appearance of the mass was consistent with that of a benign process, possibly an intramammary lymph node. However, because of the lesion's atypical location, a needle localization biopsy was performed.

The specimen radiograph showed a well-defined doughnut-shaped mass with a round lucent center (Fig. 1C). Histopathologic examination showed no tumor cells or areas of microcalcifications (Fig. 1D). The cellular characteristics were consistent with those of a lymph node surrounded by normal breast parenchyma, indicating an intramammary lymph node.

K. Kevin Shamlou
University of Florida College of Medicine
Gainesville, FL 32610-0374

REFERENCES

1. Eagan RL, McSweeny MB. Intramammary lymph nodes. *Cancer* **1983**;51:1838–1842
2. Kopans DB. *Breast imaging*. Philadelphia: Lippincott, **1989**:74–77, 105–106
3. Eagan RL. *Breast imaging, diagnosis and morphology of breast diseases*. Philadelphia: Lippincott, **1988**:313–323
4. de Paredes ES. *Atlas of film-screening mammography*. Baltimore: Urban and Schwarzenberg, **1989**:67

The Diseased Axillary Segment of the Lung: Characteristic Radiographic and Scintigraphic Appearance

The axillary segment of the lung has long been recognized as clinically important in pulmonary disease [1–3]. We saw a patient in whom disease involving the axillary segment had a characteristic radiographic and scintigraphic appearance. A 53-year-old woman had worsening right-sided pleuritic chest pain, nonproductive cough, fever, and elevated WBC count. Chest radiographs (Figs. 1A and 1B) showed a triangular, pleura-based opacity in the lateral right upper lobe of the lung, with its apex toward the hilum and its inferior margin formed by the horizontal and oblique fissures; its location corresponded to that of the axillary segment. Findings on lung scintigrams (Fig. 1C) were normal except for a perfusion defect the same size and in the same location as the opacity seen on radiographs. The imaging results indicated an intermediate probability for pulmonary embolus [4]. Because the clinical findings were not suggestive of pulmonary embolus and because no other perfusion deficits were found, the patient did not have pulmonary angiography. Heparin anticoagulation was discontinued, and the patient responded well to antibiotic therapy for pneumonia.

In a large study of segmental consolidations [3], 11% involved the lateral aspect of an upper lobe of the lung, most often an entire segment. Anatomically, the axillary segment is usually a subsegment of the anterior or posterior segment of the upper lobe. When supplied by a fourth segmental bronchus arising from the upper lobe bronchus, an axillary segment is a true bronchopulmonary segment; this variant occurs in 10–18% of the population [3].

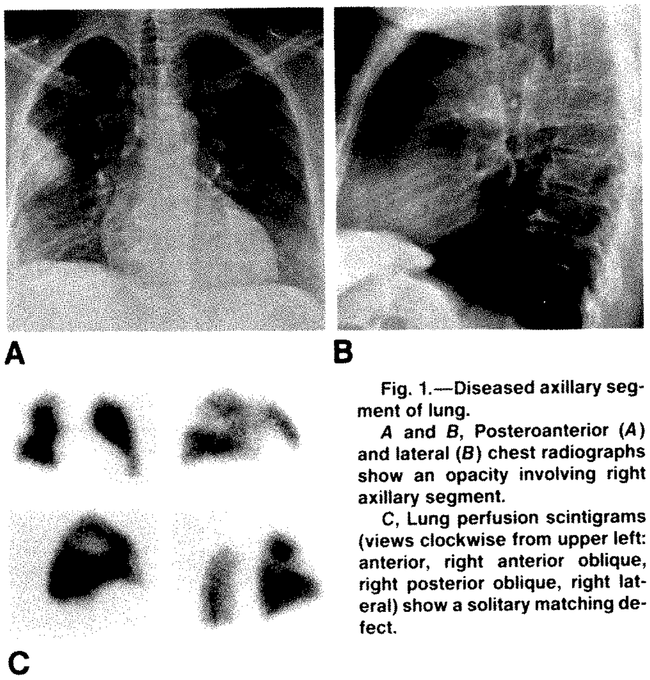

Fig. 1.—Diseased axillary segment of lung.

***A* and *B*, Posteroanterior (*A*) and lateral (*B*) chest radiographs show an opacity involving right axillary segment.**

***C*, Lung perfusion scintigrams (views clockwise from upper left: anterior, right anterior oblique, right posterior oblique, right lateral) show a solitary matching defect.**

In light of this distinction, we suggest that a solitary perfusion defect in the axillary region of the lung in the absence of a matching opacity seen on radiographs may create a challenging interpretative dilemma, because it will indicate a true segmental process in some patients. Such a finding would support an intermediate probability for pulmonary embolus and might lead to further invasive investigation. A subsegmental abnormality, however, is correlated with a low probability for pulmonary embolus [4].

Janine Slowinski
Stephen Bloom
Elizabeth Oates
New England Medical Center
Tufts University School of Medicine
Boston, MA 02111

REFERENCES

1. Felson B. *Chest roentgenology.* Philadelphia: Saunders, **1973**:150
2. Kassay D. Comments on some controversial questions of bronchial classification and nomenclature. *Dis Chest* **1961**;40:364–373
3. DiGuglielmo L, Bonomo B. The significance of the lateral subsegments of the lung in pulmonary disease: a review of 500 cases. *Acta Radiol* **1955**;44:217–229
4. PIOPED Investigators. Value of the ventilation/perfusion scan in acute pulmonary embolism. *JAMA* **1990**;263:2753–2759

Pneumomediastinum in an Unusual Location

Pneumomediastinum accounts for 2% of abnormalities on chest radiographs in children admitted to the hospital because of acute asthma [1]. This complication of asthma occurs mainly in children and occasionally in young adults. It is characterized by the presence of gas in mediastinal tissues outside the esophagus, tracheobronchial tree, or pericardium. Differentiating air surrounding the great vessels as pneumomediastinum or pneumopericardium can be difficult.

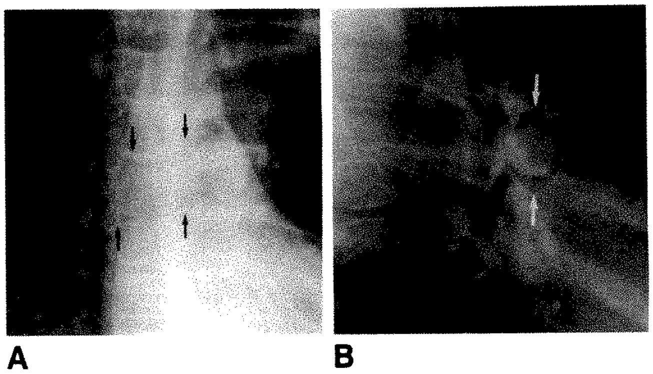

Fig. 1.—Pneumomediastinum in an unusual location in an 8-year-old boy with asthma.

***A*, Anteroposterior expiratory chest radiograph shows pericardial and mediastinal reflections (*arrows*) separated from pulmonary artery by a lucent band of air representing a pneumomediastinum.**

***B*, Lateral chest radiograph shows air (*arrows*) encircling right pulmonary artery.**

An 8-year-old boy with asthma had had wheezing, dyspnea, and nonproductive cough for 24 hr. The patient was hypoxic, and his condition was slow to improve despite multiple therapies. Inspiratory and expiratory anteroposterior and lateral chest radiographs obtained with the patient upright showed a collection of air in the mediastinum enveloping the right pulmonary artery (Fig. 1).

The cause of pulmonary interstitial emphysema may be related to rupture of a bleb, trauma, or a check valve. With a check valve, air under pressure is trapped behind plugs of mucus in the bronchioles. Subsequently, the alveolus ruptures, and air dissects into the perivascular sheaths. In nonpulmonary emphysema, air can dissect into the mediastinum from the retroperitoneal space or deep fascial planes of the neck or as a result of compromise of the esophagus, trachea, or bronchus. In a noted article, Macklin and Macklin [2] discussed the mechanism that produces pulmonary interstitial emphysema and the spread to the mediastinum. They proposed that a pressure gradient, existing between the periphery of the lung and hilus, causes air to dissect along the vascular sheath to the hilus.

Healey and Gibbon [3] have described the anatomic relationship of the pericardium and the great vessels. The inferior sac attaches to the diaphragm, and the superior sac is reflected onto the roots of the great vessels. The right pulmonary artery lies in the transverse sinus behind the aorta, pulmonary trunk, and superior vena cava and in front of the left atrium. The pericardium lines the transverse sinus and primarily abuts the ventral aspect of the right pulmonary artery. Extending from the anterosuperior to the posteroinferior surface, the pericardium covers up to three quarters of the surface of the right pulmonary artery, beginning near the origin of the artery and decreasing distally [4]. The air surrounding the right pulmonary artery is in the mediastinum and not the pericardium. Air surrounding a vessel can produce a target appearance or halo sign.

L. Mark Dean
St. Joseph Mercy Hospital
Pontiac, MI 48341
Lawrence R. Kuhns
Children's Hospital of Michigan
Detroit, MI 48201

REFERENCES

1. Gillies JD, Reed MH, Simmons FER. Radiographic findings in acute childhood asthma. *J Can Assoc Radiol* **1978**;29:28–33

2. Macklin MT, Macklin CC. Malignant interstitial emphysema of the lungs and mediastinum as an occult complication in many respiratory diseases and other conditions: an interpretation of the clinical literature in the light of laboratory experiment. *Medicine* **1944**;23:281-352
3. Healey JE Jr, Gibbon JH Jr. Intrapericardial anatomy in relation to pneumonectomy for pulmonary carcinoma. *J Thorac Surg* **1950**;19:864-873
4. Hollinshead WH. *Anatomy for surgeons: the thorax, abdomen and pelvis*, 2nd ed., vol. 2. New York: Harper and Row, **1971**:99-167

Duodenal Duplication Cyst in a 75-Year-Old Man

We present a rare case of duodenal duplication cyst in a 75-year-old man. Retrospective evaluation of CT scans suggested the diagnosis.

At the time of admission, the patient had had tarry stools for 1 day. He had nausea and loss of appetite but no other significant signs or symptoms. The results of a physical examination were unremarkable. The initial suggested diagnosis was bleeding in the upper gastrointestinal tract caused by recent use of a nonsteroidal antiinflammatory agent. Endoscopy showed a small lesion in the second or third portion of the duodenum that oozed bright red blood when touched. CT scans were obtained in order to investigate the possibility of an aortoduodenal fistula, and no oral contrast material was used. A low-attenuation collection was present in the transverse portion of the duodenum (Fig. 1A), but as no oral contrast material was used, the collection was mistakenly thought to represent intestinal fluid. The patient remained symptomatic, and endoscopy and an upper gastrointestinal series (Fig. 1B) showed a 2.5-cm polypoid submucosal lesion in the second to third portion of the duodenum. At surgery, a mobile submucosal mass was removed. Pathologic examination showed a duodenal duplication cyst.

Duodenal duplication cysts account for 4-12% of all intestinal duplications, and the prevalence is less than 1 in 100,000 births [1]. The cysts usually become apparent during infancy when they cause vomiting, palpable mass, and abdominal pain [2]. To date, the oldest patient in whom a duodenal duplication cyst has been found is a 73-year-old man [3]. Findings on barium study, sonography, and CT are rarely specific, and preoperative diagnosis is difficult. In one reported case [4], a duodenal duplication cyst containing enteroliths was diagnosed preoperatively on the basis of CT findings.

The CT finding of a structure within the lumen or close to the intestinal tract with an attenuation similar to that of fluid may aid in suggesting the diagnosis of duodenal duplication cyst preoperatively.

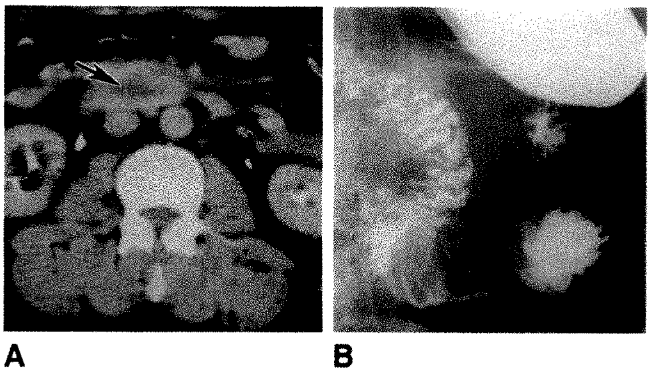

Fig. 1.—Duodenal duplication cyst in a 75-year-old man.

***A*, Axial CT scan shows a structure (*arrow*) within transverse duodenum that has an attenuation like that of fluid.**

***B*, Spot film obtained with patient prone during an upper gastrointestinal series shows submucosal mass lesion in third portion of duodenum.**

David A. Bader
Girish Tyagi
Douglas A. Burd
St. Vincent Hospital
Worcester, MA 01604

REFERENCES

1. Hocking M, Young DG. Duplications of the alimentary tract. *Br J Surg* **1981**;68:92-96
2. Leenders E, Osman M, Sukarochana K. Treatment of duodenal duplication with international review. *Am Surg* **1970**;36:368-371
3. Browning RW. Duodenal duplication. *Rev Surg* **1963**;20:226-229
4. Bar-Ziv J, Katz R, Nobel M, Antebi E. Duodenal duplication cyst with enteroliths: computed tomography and ultrasound diagnosis. *Gastrointest Radiol* **1989**;14:220-222

Polysplenia with Gastric Angiodysplasia

We describe a case of polysplenia associated with gastric angiodysplasia. As far as we know, the presence of this arteriovenous malformation of the stomach associated with polysplenia has not been previously described in the literature. An 18-year-old man was admitted to the hospital for evaluation of anemia. The results of routine studies for anemia were all normal. Abdominal CT showed a centrally located liver extending to both sides of the upper abdomen. The stomach was located on the right and had several splenic nodules along the greater curvature. Sections through the upper abdomen showed the inferior vena cava in the left paraaortic region, in a normal position on the right at the level of the renal hila (Fig. 1A). Results of gastroscopy were normal. Selective celiac trunk angiography showed a normal hepatic artery and a splenic artery coursing to the right supplying a cluster of splenic nodules in the right upper quadrant. Selective superior mesenteric angiography showed a second hepatic artery that arose from the superior mesenteric artery and had branches distributed symmetrically to both sides of the upper abdomen. Several gastric and duodenal arteries arising from the hepatic artery were distributed along the great curvature of the stomach, with an increased early and persistent venous drainage consistent with gastric angiodysplasia (Fig. 1B).

Polysplenia is an uncommon syndrome characterized by the presence of multiple spleens, abdominal heterotaxia, and vascular mal-

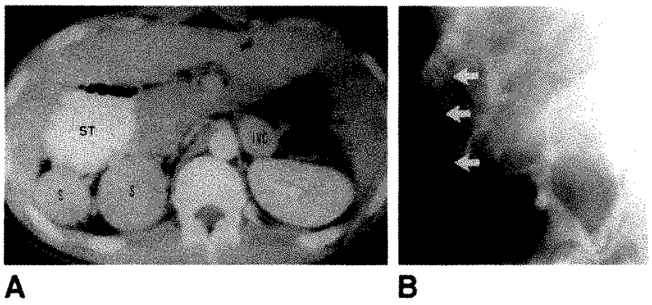

Fig. 1.—Polysplenia with gastric angiodysplasia in an 18-year-old man.

***A*, CT scan shows stomach (ST) on right side, centrally located liver, multiple splenic nodules (S) behind stomach, and inferior vena cava (IVC) on left side.**

***B*, Right gastric arteriogram, late arterial phase, shows dilated early draining veins (*arrows*).**

formations. The organs on the right side assume the morphology of their counterparts on the left side (bilateral left-sidedness) [1, 2]. CT can show the visceral and vascular anomalies present in this syndrome [2]. The absence of the hepatic segment of the inferior vena cava with azygous or hemiazygous continuation is the most frequent venous anomaly; it is found in 70-80% of patients with polysplenia. Other less frequently observed anomalies of the inferior vena cava are duplication of the vessel and location of the vessel on the left side [1, 2]. Selective visceral angiography is also a precise method for diagnosing this syndrome [1]. In our patient, angiograms showed the visceral and vascular anomalies and an early and persistent venous drainage with prominent dilated veins along the greater curvature of the stomach. Gastric angiodysplasia is a rare cause of gastrointestinal bleeding and can be easily missed on endoscopy. Angiography is the ideal method for diagnosing this arteriovenous malformation [3, 4].

Antonio Mariscal
Albert Salazar
Concha Sancho
Juan Mañá
Hospital de Bellvitge
Barcelona 08907, Spain

REFERENCES

1. Vaughan T, Hadwkins I, Elliott L. Diagnosis of polysplenia syndrome. *Radiology* **1971**;101:511-518
2. Vossenn P, Van Hedent E, Degryse H, Deschopper A. Computed tomography of the polysplenia syndrome in the adult. *Gastrointest Radiol* **1987**;12:209-211
3. Roberts L, Gold R, Routt W. Gastric angiodysplasia. *Radiology* **1981**;139:355-359
4. Tung K, Millar A. Gastric angiodysplasia: a missed cause of gastrointestinal bleeding. *Postgrad Med J* **1987**;63:865-866

Hydroxyapatite Pseudopodagra in Young Men

The most characteristic feature of acute calcific periarthritis of the first metatarsophalangeal joint (hydroxyapatite pseudopodagra) is the marked female predominance and the relatively young age of patients compared with those who have acute calcific periarthritis in general [1]. We report a case of hydroxyapatite pseudopodagra in a young man.

A 33-year-old man had had acute onset of pain, swelling, erythema, and restriction of movement of the right first metatarsophalangeal joint for 48 hr. The joint was swollen, erythematous, and warm. Blood leukocyte count, urate level, and erythrocyte sedimentation rate were normal. Radiographs of the right foot showed two large periarticular calcific deposits lateral to the sesamoids (Fig. 1) (the crystals were not analyzed). Radiographs of the shoulders were normal. The patient responded favorably to treatment with nonsteroidal antiinflammatory drugs over the next 8 days. Radiographs obtained 1 month after treatment showed complete resorption of the periarticular calcific deposit.

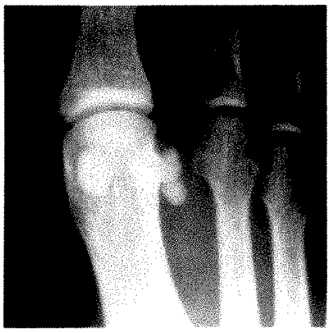

Fig. 1.—Hydroxyapatite pseudopodagra in a 33-year-old man. Radiograph shows two large periarticular calcific deposits lateral to right first metatarsophalangeal joint.

Twenty-six known cases of hydroxyapatite pseudopodagra, including the one presented here, have been described [2-4]. In the 21 fully documented cases (five were only mentioned in a large study on calcium hydroxyapatite crystal deposition disease [4]), 18 of the patients were female, with a mean age of 31.5 years (range, 12-53 years). In contrast, acute calcific periarthritis in general occurs equally in both sexes, and the patients are usually 40-60 years old [4, 5]. The most striking features in pseudopodagra are the periarticular calcific deposits seen on radiographs, the favorable course after treatment with nonsteroidal antiinflammatory drugs, and the complete resorption of the calcific deposit.

This increased frequency of hydroxyapatite pseudopodagra in women is probably due to underdiagnosis of the disorder in men. Indeed, when this clinical feature occurs in men, a presumptive diagnosis of gouty podagra is made without joint aspiration or radiographs, and the patients improve after treatment with colchicine or nonsteroidal antiinflammatory drugs.

Acute calcific periarthritis of the first metatarsophalangeal joint is undoubtedly an uncommon cause of pseudopodagra. However, lack of awareness of this condition can lead to delay in diagnosis, unnecessary laboratory tests, and inappropriate treatments. The disorder should be considered not only in young women but also in young men who have goutlike, acute monoarthritis of the first metatarsophalangeal joint. A systematic evaluation of radiographs would allow an estimation of the exact frequency of this disorder.

P. Goupille
J.-P. Valat
Trousseau Hospital
F37044 Tours, France

REFERENCES

1. Fam AG, Rubenstein J. Hydroxyapatite pseudopodagra: a syndrome of young women. *Arthritis Rheum* **1989**;32:741-747
2. Fam AG, Stein JL. Hydroxyapatite pseudopodagra in young women. *J Rheumatol* (in press)
3. Goupille P, Soutif D, Fouquet B, Amsallem G, Valat J-P. Hydroxyapatite pseudopodagra. *J Rheumatol* **1991**;18:786-787
4. Amor B, Chevrot A, Delbarre F. Le rhumatisme à hydroxyapatite (la maladie des calcifications tendineuses multiples). I. Etude clinique. *Rev Rhum* **1977**;44:301-308
5. Resnick D. Calcium hydroxyapatite crystal deposition disease. In: Resnick D, Niwayama G, eds. *Diagnosis of bone and joint disease*, 2nd ed. Philadelphia: Saunders, **1988:**1733-1769

Making an Impression in Interventional Radiology

Percutaneous techniques such as biopsy, nephrostomy, and abscess drainage are now common interventional radiologic procedures [1]. In each, the proposed skin puncture site is marked in some way before it is swabbed with an antiseptic solution and infiltrated with a local anesthetic. Several options for marking the skin are available. However, most have some disadvantages. Ballpoint pens function poorly on surfaces coated with gel for sonographic studies and are nonsterile. Marks made with skin-marker pens can be washed off with spirit-based antiseptic solutions [2]. Fingernails are of variable structural and hygienic quality and may be overly traumatic to the skin surface. The use of a needle cover (Fig. 1) to mark the puncture site has several advantages. The wider end of the cover has a flat face that when applied to the skin with minimum pressure will produce a ring-shaped indentation (Fig. 2A). This mark is not removed by washing and remains visible for 10-15 min, leaving plenty of time for

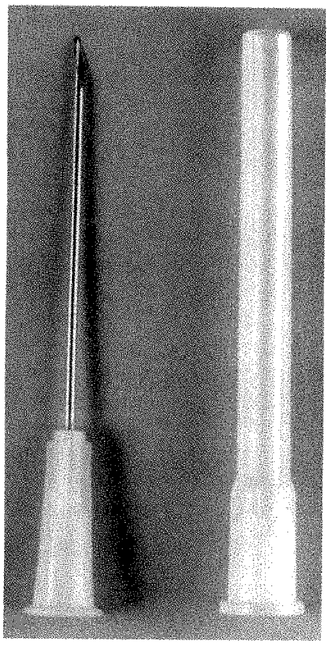

1

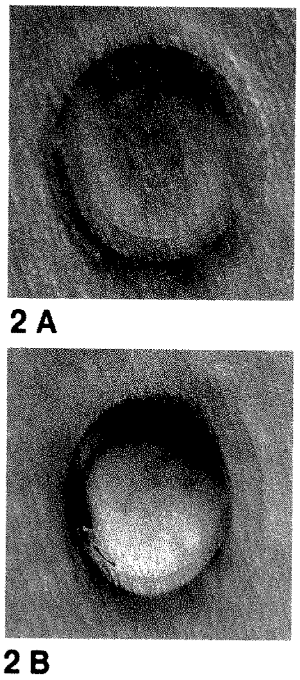

Fig. 1.—Microlance 2 needle and plastic needle guard (Becton-Dickinson, Dublin, Ireland).

Fig. 2.—*A*, Impression of needle guard on skin surface. Outer diameter of ring is 8 mm.

***B*, Appearance of skin surface after intradermal injection of local anesthetic into center of ring.**

preparation. The needle cover is usually packed sterile, so the proposed puncture site can be marked after the skin has been prepared with antiseptic, even if the skin surface is wet or greasy. A small intradermal injection of local anesthetic into the center of the ring tends to be retained, enhancing and prolonging the marking properties of the technique (Fig. 2B).

A. Coulthard
Newcastle General Hospital
Newcastle upon Tyne NE4 6BE
Tyne and Wear, United Kingdom

REFERENCES

1. Wilkins RA, Nunnerly HB, Allison DJ, et al. The expansion of interventional radiology: report of a survey conducted by the Royal College of Radiologists. *Clin Radiol* **1989**;40:457–462
2. Rafferty K, Glass RG. Making your mark in surgery. *Br J Surg* **1986**;73:609

Resolving Cerebral Hematoma Mimicking Cerebral Abscess

A 63-year-old woman had surgery because of a meningioma in the left parietal area. In the third postoperative week, the patient's general condition began to deteriorate. She had a low-grade fever and leukocytosis, and CT showed a hypodense mass 4 × 3 cm with prominent surrounding edema in the left parietal region. Marked ringlike enhancement was seen after the administration of IV contrast material (Figs. 1A and 1B). The suggested diagnosis was cerebral abscess. At surgery, an intracerebral hematoma was found. Postoperative CT indicated complete drainage of the hematoma and showed edema in the left parietal region (Fig. 1C).

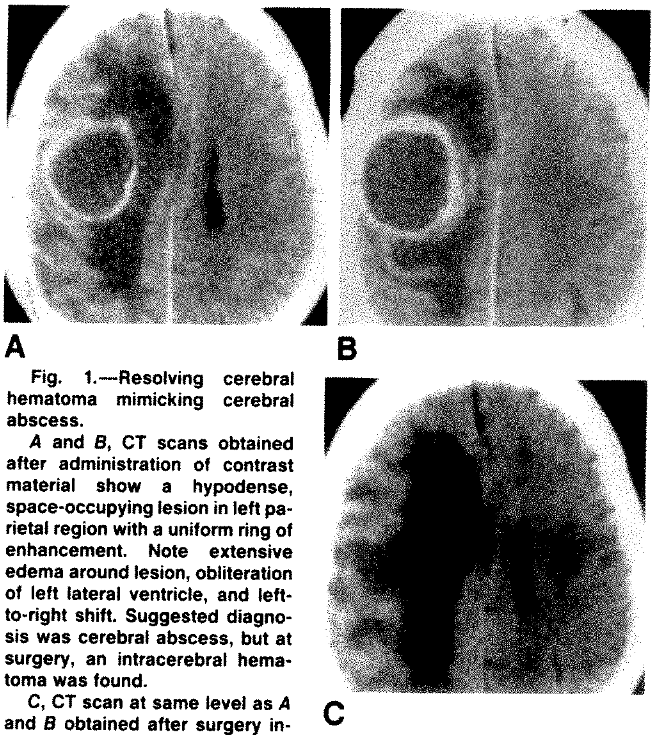

Fig. 1.—Resolving cerebral hematoma mimicking cerebral abscess.

***A* and *B*, CT scans obtained after administration of contrast material show a hypodense, space-occupying lesion in left parietal region with a uniform ring of enhancement. Note extensive edema around lesion, obliteration of left lateral ventricle, and left-to-right shift. Suggested diagnosis was cerebral abscess, but at surgery, an intracerebral hematoma was found.**

***C*, CT scan at same level as *A* and *B* obtained after surgery indicates complete drainage of hematoma.**

On CT, cerebral abscess appears as a hypodense mass, and a uniform ring of enhancement is seen after administration of contrast material. The abnormality is associated with considerable reactive edema and a suggestive clinical picture of fever and leukocytosis [1]. On the other hand, an acute intracerebral hematoma is hyperdense on CT and shows a decrease in peak density of approximately 1 H each day. Depending on its size, it becomes isodense in a matter of 9 days to 2 weeks and eventually becomes hypodense [2]. This is due to breakdown and absorption of hemoglobin. Pathologic examination shows ingrowth of capillary neovascularity at the margin of the hematoma [3] by the end of the first week. The ingrowth has an abnormal blood-brain barrier, and thus injected contrast material extravasates around the hematoma, causing ringlike enhancement. The CT appearance of the enhancing ring can easily be confused with that of a tumor (high-grade glioma or metastasis) or an abscess; however, lack of surrounding edema and mass effect, particularly during the hypodense phase, is strongly suggestive of an evolving hematoma [3]. In this case of resolving intracerebral hematoma, the presence of mass effect and surrounding edema, along with the clinical findings, were misleading.

S. Senaati
H. Caner
B. M. Oran
Hacettepe University School of Medicine
Ankara, Turkey

REFERENCES

1. Eisenberg RL. Clinical imaging. In: *An Atlas of differential diagnosis*. Rockville, MD: Aspen, **1988**:848–851
2. Dolinskas CA, Zimmerman RA, Bilanikk LT. A sign of subarachnoid bleeding on cranial computed tomograms of pediatric head trauma patients. *Radiology* **1978**;126:409–411
3. Zimmerman RA, Leeds ME, Naidich TP. Ring blush associated with intracerebral hematoma. *Radiology* **1977**;122:707–711

Intraspinal Enterogenous Cyst

We present the CT and MR findings in a patient with an intraspinal enterogenous cyst. An 18-year-old woman had a history of numbness in the right hemibody and weakness in the left arm. Cervical MR imaging showed an intradural extramedullary mass posterior to the C3–C4 disk space (Fig. 1A). The spinal cord was compressed and posteriorly displaced to the right. The mass itself had a signal like that of CSF on all pulse sequences. Subsequent CT showed no evidence of calcification, hemorrhage, or vertebral body abnormality. Shortly after the imaging studies, the patient had surgery, and the cystic mass was partially excised and marsupialized. Fluid from the cyst was clear, colorless, acellular, and sterile. The patient recovered completely and has been asymptomatic for 1 year.

Examination of the surgical specimen showed low cuboidal epithelium, and for that reason, samples were stained with PAS (Fig. 1B) and mucicarmine. These samples were markedly positive, confirming the diagnosis of enterogenous cyst and excluding an arachnoid cyst.

In the third week after conception, an embryo is a trilaminar structure, with endoderm in contact with the notochord. Subsequently, these structures separate, and the notochord is enveloped in mesodermal cells that eventually form vertebrae. Enteric cysts are thought to be caused by proliferation of embryonic endodermal remnants within the spinal canal that become adherent to the notochord and thus separated from the remainder of the endoderm in the third week of development [1].

Histologically, enterogenous cysts are characterized by cuboidal or columnar epithelium. The gut origin of this epithelium may not be apparent, and for that reason it is necessary to show that the cells stain positive with PAS or mucicarmine or contain carcinoembryonic antigen [2].

Only about half of enterogenous cysts are associated with vertebral anomalies, most commonly spina bifida occulta, hemivertebra, or blocked or fused vertebra. This is because the embryonic communication that existed between the spinal cord and the gut may become atretic and disappear completely or persist only as a fibrous tract. Nonetheless, if a canal or fissure is seen through a vertebral body in association with a cystic intraspinal mass, an enterogenous cyst is likely [2]. Arachnoid and enterogenous cysts have similar appearances, and in the absence of associated vertebral anomalies, the specific diagnosis is made on the basis of pathologic findings. Inflammatory cysts, such as those associated with cysticercosis, also should be included in the differential diagnosis, although the results of examination of CSF, clinical history, and lack of gadolinium enhancement on MR images usually indicate whether this possibility can be excluded.

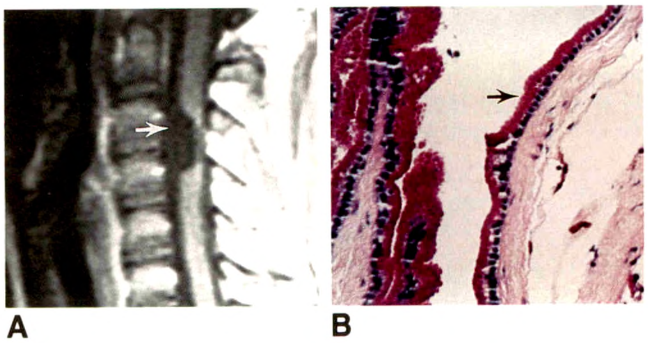

Fig. 1.—Intraspinal enterogenous cyst in an 18-year-old woman.

***A*, Sagittal T1-weighted (450/11, 1.5 T) MR image shows a mass (*arrow*) with a signal intensity like that of CSF anterior to spinal cord, which is compressed and displaced posteriorly.**

***B*, Photomicrograph of histologic specimen stained with PAS shows bright magenta epithelial cells (positive staining), which confirm endodermal derivation of this tissue and diagnosis of enterogenous cyst.**

Mark T. Yoshino
Thomas J. Meakem
Allan Hamilton
L. Philip Carter
University Hospital, University of Arizona
Tucson, AZ 85724

REFERENCES

1. Agnoli AL, Laun A, Schonmayr R. Enterogenous intraspinal cysts. *J Neurosurg* **1984**;61:834–840
2. Miyagi K, Mukawa J, Mekaru S, et al. Enterogenous cyst in the cervical spinal canal. *J Neurosurg* **1988**;68:292–296

Extramedullary Plasmacytoma Manifested as an Epidural Mass

We report the MR findings in a case of multiple myeloma that was manifested as an epidural mass. A 69-year-old man had had changes in mental status, generalized weakness, and worsening pain in the left hip for 2 months. At the time of admission, he had been unable to walk for 2 days. Six days after admission, acutely decreased motor function in the lower extremities and sensory loss below the T10 level developed. MR showed a large epidural process extending from C6 to T10, displacing the spinal cord anteriorly and encircling the cord at the inferior aspect, with cord compression at multiple levels. The epidural mass was isointense with the spinal cord on T1-weighted images and hyperintense on T2-weighted images and showed homogeneous enhancement with contrast material (Fig. 1). The C7 vertebral body had low signal on T1-weighted images and increased signal intensity on T2-weighted images. The rest of the visualized vertebral bodies were slightly inhomogeneous in signal intensity on T1- and T2-weighted images. Subsequent radiographs of the cervical, thoracic, and lumbar spine showed degenerative changes, and a skeletal survey showed no evidence of bone lesions. The patient had a T4 laminectomy and decompression. Pathologic findings were consistent with those of plasmacytoma. Subsequent bone marrow biopsy of the right posterior iliac crest showed 20% plasmacytosis of the marrow space, consistent with multiple myeloma.

Multiple myeloma is a malignant proliferation of plasma cells in the bone marrow, generally resulting in multiple osteolytic bone lesions. The classic triad of multiple myeloma is bone marrow plasmacytosis (>10%), lytic bone lesions, and monoclonal antibodies in the serum or urine. The diagnosis can be made in the absence of bone lesions if the plasmacytosis is associated with extramedullary (i.e., extraosseous) mass lesions.

To our knowledge, this is the first report of the MR appearance of an epidural plasmacytoma. The literature contains a number of reports of spinal cord compression in patients with multiple myeloma [1, 2]. However, these primarily involved the vertebral body, and plain radiographs and CT scans showed lytic bone lesions and bone expansion. Compression was diagnosed on the basis of myelographic findings, and no MR findings were reported. A more recent study [3] of the MR appearance of the spine in multiple myeloma found that in two patients, spinal cord compression was seen as localized edema in the cord. In these two, CT showed large focal lesions of the vertebral bodies that extended to the spinal canal. No mention was made of an epidural mass separate from the vertebral lesion. A case report in the Japanese literature [4] describes a patient with a

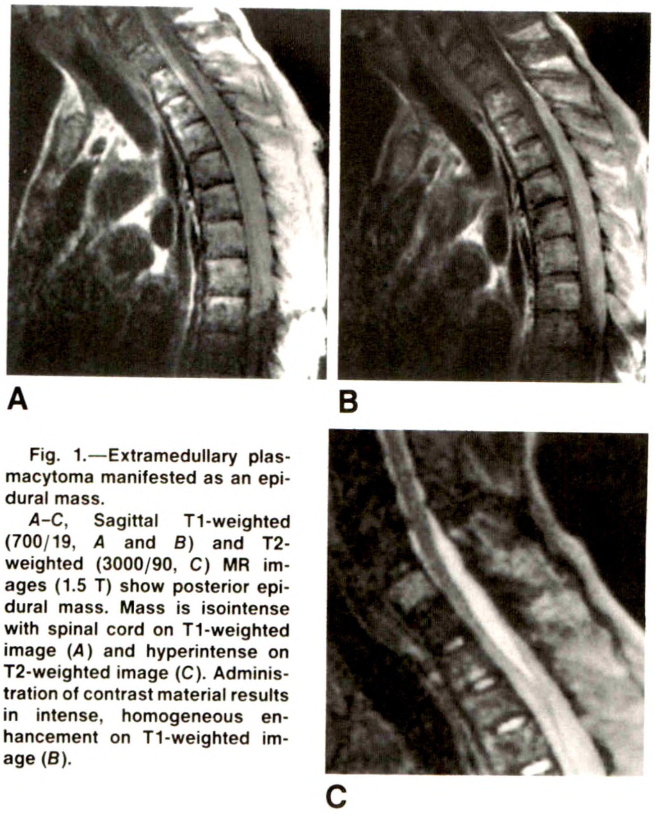

Fig. 1.—Extramedullary plasmacytoma manifested as an epidural mass.

***A–C,* Sagittal T1-weighted (700/19, *A* and *B*) and T2-weighted (3000/90, *C*) MR images (1.5 T) show posterior epidural mass. Mass is isointense with spinal cord on T1-weighted image (*A*) and hyperintense on T2-weighted image (*C*). Administration of contrast material results in intense, homogeneous enhancement on T1-weighted image (*B*).**

plasmacytoma that formed an epidural mass without involvement of an adjacent vertebral body. No abnormal bone changes in the spine were seen on plain radiographs or on CT scans. Again, no MR findings were reported.

Our case is unusual because the patient had an epidural mass that caused compression of the spinal cord. No evidence of bone involvement was seen on bone scintigrams or plain radiographs. MR images showed a vertebral body lesion with decreased signal on T1-weighted images and increased signal on T2-weighted images, reported to be typical of focal myeloma tissue replacing normal hematopoietic bone marrow. Nevertheless, this lesion was separate from and superior to the main epidural mass. The slight inhomogeneity of the vertebral bodies may represent diffuse involvement of the bone marrow with multiple myeloma or diffuse osteoporosis. The possibility of extramedullary plasmacytoma whether associated with plasmacytosis or not should be considered in the differential diagnosis of an epidural mass.

Francine M. Kim
Jordan Rosenblum
The University of Chicago
Chicago, IL 60637

REFERENCES

1. Camacho J, Arnalich F, Anciones B, et al. The spectrum of neurological manifestations in myeloma. *J Med* **1985**;16:597–611
2. Siegal T, Siegal T. Surgical decompression of anterior posterior malignant epidural tumors compressing the spinal cord: a prospective study. *Neurosurgery* **1985**;17:424–432
3. Ludwig H, Tscholakoff D, Neuhold A, Fruhwald F, Rasoul S, Fritz E. Magnetic resonance imaging of the spine in multiple myeloma. *Lancet* **1987**;2:364–366
4. Kato T, Nakagawa Y, Imamura H, et al. Extramedullary plasmacytoma forming a mass in the epidural space of the spinal cord: report of a case. *No Shinkei Geka* **1987**;15:213–218

Air Sinus in the Occipital Bone

A 39-year-old man was referred for evaluation of headaches. CT scans showed no intracranial pathologic changes. However, a low-density structure was seen in the left lateral portion (pars lateralis or exoccipital part) of the occipital bone. The structure had an attenuation value of approximately −600 Hu, compatible with the presence of air. This air cell had well-defined walls, was located in the vicinity of the foramen magnum medially, and extended to the occipitotemporal region laterally (to the petrooccipital fissure and the occipitomastoid suture). Anteromedially, it was bounded by the synchondrosis between the exoccipital and basioccipital portions of the occipital bone (Fig. 1).

Several facial and cranial bones contain air sinuses, including the maxillary, frontal, and sphenoidal sinuses and ethmoidal and mastoid air cells. These have access to atmospheric air through various thin connections, so they contain air under normal circumstances. To my knowledge, the air cell or sinus described here is the first example of such a structure seen at an unusual site, the occipital bone. This may be an isolated structure with air trapped tightly inside without being absorbed, or it may have a thin connection (undetectable with CT) with the left mastoid air cells, although these bones are separated by the occipitomastoid suture.

R. Nuri Sener
Hospital of Ege University
Bornova, Izmir, 35100, Turkey

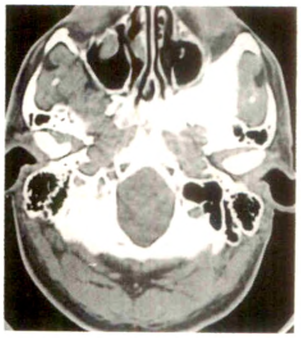

Fig. 1.—Axial CT scan (5-mm sections) through foramen magnum and pars lateralis (exoccipital part) of occipital bone shows normal pars lateralis on right and a 2.5 × 2.5 cm lobulated air cell on left. Air cell is localized between foramen magnum medially and occipitomastoid suture and petrooccipital fissure laterally and bounded anteromedially by synchondrosis between exoccipital and basioccipital parts of occipital bone. (This region corresponds to site of jugular tubercule of occipital bone). This air sinus could not be detected on any other CT sections, an indication that the sinus's depth was approximately 5 mm.

Micrencephalia Vera: CT Findings

A 6-month-old male neonate had left-sided otitis media. The patient was a full-term infant who might have been exposed to rubella virus during the first trimester of pregnancy. Physical examination showed severe developmental delay, spastic quadriparesis, deafness, and blindness. Head circumference was normal for the patient's age. CT showed large extraaxial fluid collections bilaterally, completely surrounding the brain (Fig. 1A). The brain was small but normally shaped. No ventricular dilatation was seen. The surface of the brain was somewhat smooth, suggesting pachygyria. Faint calcifications were present in the left cerebral hemisphere (Fig. 1B). The falx was intact. The cerebellum showed mild atrophy but was otherwise normal. After the CT study, the patient had placement of bilateral shunts to the peritoneum for drainage of CSF. One month later, follow-up CT showed that the sizes of the fluid collections were unchanged. The

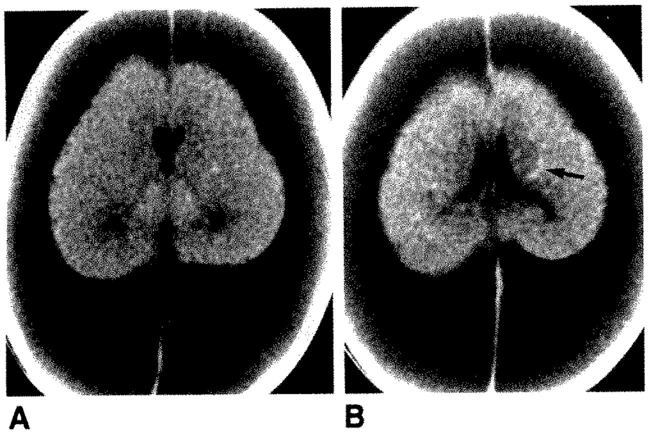

Fig. 1.—Micrencephalia vera.

A, Axial CT scan shows large bihemispheric extraaxial fluid collections. The brain is extremely small but of normal overall configuration, and no hydrocephalus is present. Cortex is smooth, suggesting pachygyria.

B, CT scan cephalad to *A* shows some faint intraparenchymal calcifications (*arrow*). Falx is well visualized.

patient died of pneumonia when he was 15 months old. An autopsy was not performed.

The imaging features in this case are compatible with those of micrencephalia vera. In this rare entity, the brain is formed but is markedly diminished in size. Although no clear explanation exists, the abnormality is thought to be associated with exhaustion of the germinal matrix zones. The injury takes places between the second and fifth month of intrauterine life, when neuronal proliferation, differentiation, and histogenesis are actively taking place. Rubella is a well-known cause of microcephaly. The mechanisms responsible include cytolysis and inhibition of mitoses of progenitor cells (located in the germinal matrix), giving rise to insufficient numbers of neurons and astroglia [1]. Oligodendrocytes may also be diminished in number, causing impaired myelination. Micrencephalia vera is not a destructive process, as shown by the normal configuration of the brain and absence of focal lesions in the patient described here.

To my knowledge, only one other case of micrencephalia vera has been described in the radiologic literature [2]. In that case, the head was small, and MR showed a very small brain with a smooth cortex. Although the findings were suggestive of lissencephaly, the thickness of the gray matter was diminished and not increased as expected with abnormal neuronal migration. In the case presented here, the head circumference was normal, probably because of the large underlying CSF spaces.

It is important to recognize micrencephalia vera and not confuse it with large subdural collections compressing the brain. Such confusion could lead to an erroneous diagnosis of trauma (including child abuse), which might have unjustified legal implications for the child's parents. Furthermore, treatment of these fluid collections may not be necessary, as the prognosis is poor.

Mauricio Castillo
University of North Carolina, School of Medicine
Chapel Hill, NC 27514

REFERENCES

1. Becker LE. Infections of the developing brain. *AJNR* **1992**;13:537–549
2. Barkovich AJ, Gressens P, Evrard P. Formation, maturation, and disorders of brain neocortex. *AJNR* **1992**;13:423–446

Letters are published at the discretion of the Editor and are subject to editing.

Letters to the Editor must not be more than two *double-spaced*, typewritten pages. One or two figures may be included. Abbreviations should not be used. Limit the number of authors to four, or we will list only the first three and add "and colleagues" to the end of the list. See Author Guidelines.

Material being submitted or published elsewhere should not be duplicated in letters, and authors of letters must disclose financial associations or other possible conflicts of interest.

Letters concerning a paper published in the *AJR* will be sent to the authors of the paper for a reply to be published in the same issue. Opinions expressed in the Letters to the Editor do not necessarily reflect the opinions of the Editor.

Review of Current Literature

Initials and addresses of corresponding authors are provided in parentheses for each article so that the reader can obtain reprints directly. Abstracts are printed verbatim from each journal.

Gastroenterology

The risk of upper gastrointestinal cancer in familial adenomatous polyposis. Offerhaus GJA, Giardiello FM, Krush AJ, et al. (GJAO, Dept. of Medicine, The Johns Hopkins University School of Medicine, Baltimore, MD 21205). *Gastroenterology* 102:1980–1982, 1992

Adenomas with potential for malignancy occur frequently in the upper gastrointestinal tract of patients with familial adenomatous polyposis. However, an assessment of relative risk of upper gastrointestinal cancer in patients with adenomatous polyposis has never been performed. Therefore, the incidence rate of upper gastrointestinal cancer in patients with familial adenomatous polyposis in The Johns Hopkins Registry was compared with the rate of the general population through person-year analysis with adjustment for demographics. There was an increased relative risk of duodenal adenocarcinoma (relative risk, 330.82; 95% confidence limits, 132.66 and 681.49; $P < 0.001$) and ampullary adenocarcinoma (relative risk, 123.72; 95% confidence limits, 33.65 and 316.72; $P < 0.001$). No significant increased risk was found for gastric or nonduodenal small intestinal cancer. These results indicate that periodic surveillance of the upper gastrointestinal tract for duodenal and periampullary cancer is needed in patients with familial adenomatous polyposis. Prophylactic duodenectomy is a consideration when large adenoma(s) with high-grade dysplasia are identified but awaits risk benefit analysis.

Reprinted with permission by the American Gastroenterological Association.

Histopathology of membranous obstruction of the inferior vena cava in the Budd–Chiari syndrome. Kage M, Arakawa M, Kojiro M, Okuda K (MK, First Department of Pathology, Kurume University School of Medicine, Kurume, Japan). *Gastroenterology* 102:2081–2090, 1992

It is generally believed that membranous obstruction of the inferior vena cava in the Budd–Chiari syndrome is caused by congenital malformation. However, it does not explain the late onset of the disease. In the current study, hepatic portion of the inferior vena cava and hepatic veins were studied in 17 autopsy cases of the Budd–Chiari syndrome, 16 of which had no demonstrable cause (idiopathic). A sufficient amount of vena cava tissue was available for evaluation in 15 cases. Nine had membranous obstruction, with thickness varying from 3 to 8 mm. Thrombus formation was recognized in 7 of 9 cases. Occlusion of hepatic vein orifices of varying degree was present in 8 cases. In these occluding lesions, the basic structure of the venous wall was maintained. The intima was transformed into a fibrous laminar structure, and organized thrombi of varying ages were recognized; they were a mixture of fresh thrombi, organized thrombi, fibrous tissues, recanalizations, and calcifications. It is concluded that in these cases of the Budd–Chiari syndrome, occluding and stenosing lesions in the inferior vena cava and hepatic veins were thrombosis and its sequelae. There was no indication of congenital malformation.

Reprinted with permission by the American Gastroenterological Association.

Digestive Diseases and Sciences

Normal 24-hr ambulatory esophageal pH values: influence of study center, pH electrode, age, and gender. Richter JE, Bradley LA, DeMeester TR, Wu WC (JER, Division of Gastroenterology, UAB Station, Birmingham, AL 35294). *Dig Dis Sci* 37(6):849–856, June 1992

Although the most sensitive and specific test for diagnosing gastroesophageal reflux disease, normal standards for prolonged esophageal pH monitoring are based on small sample sizes with questions raised about the effects of pH electrode, older age, gender, and methods of data analysis on pH variables. Recently three groups have established normal data bases using similar methodology. Multiple regression and nonparametric analyses showed that the values for the six traditional pH parameters were comparable across study centers. Therefore, the groups were combined for a total study population of 110 healthy subjects (47 men, 63 women, mean age 38 years with a range of 20–84 years). Further nonparametric analyses revealed the following: (1) type of pH electrode (antimony vs glass) is not significantly related to parameters of physiologic acid reflux; (2) age is not independently related to pH parameters; (3) men tend to have more physiologic reflux than women; and (4) older men tend to experience longer episodes of reflux than younger men and women. There was a significant effect of gender and a significant interaction between age and gender on the number of episodes >5 min ($P = 0.008$). Nearly significant differences were found for percentage of total acid exposure time ($P = 0.03$), total reflux episodes ($P = 0.02$), and the longest reflux episode ($P = 0.02$). We believe these normal esophageal pH values can be used confidently as standards in any laboratory, and consideration should be given to developing separate standards for men and women.

Gastrointestinal Endoscopy

Percutaneous endoscopic gastrostomy for decompression of the stomach and small bowel. Herman LL, Hoskins WJ, Shike M (MS, Memorial Sloan-Kettering Cancer Center, 1275 York Ave., New York, NY 10021). *Gastrointest Endosc* 38:314–318, 1992

Percutaneous endoscopic gastrostomies are used most commonly for enteral feeding. We report the use of such gastrostomies for decompression of the obstructed gastrointestinal tract. Percutaneous endoscopic gastrostomies were performed on 53 patients over a 2-

year period for gastrointestinal decompression because of gastric or small bowel obstruction. Forty-six patients had malignant obstruction from a primary abdominal or metastatic carcinoma and 7 patients had non-malignant obstruction or stasis. Gastrostomy for decompression was successful in 41 of 46 (89%) cases of malignant obstruction and in all 7 of the non-malignant cases. Tube utilization for decompression averaged 60 ± 91 days. A 28 F tube with a 4-inch perforated intragastric portion was fashioned to maximize drainage. This efficient decompression tube allowed oral intake of liquids and soft foods in 88% of patients. Complications, which occurred in 4%, included one case of fatal peritonitis and one case of cellulitis.

Incidence and risk factors for biliary and pancreatic stent migration. Johanson JF, Schmalz MJ, and Geenen JE (JEG, 1333 College Ave., Racine, WI 53403). *Gastrointest Endosc* 38:341–346, 1992

Endoprostheses are commonly used in the treatment of biliary and pancreatic disorders. The frequency of and potential risk factors for stent migration, however, remain largely unknown. From January 1986 to June 1990, 807 biliary and pancreatic stents were placed at our institution. Our study analyzed the occurrence of stent migration among the 589 stents for which follow-up data were available. Results demonstrated incidence rates of 4.9 and 5.9% for proximal (into the duct) and distal (out of the duct) biliary stent migration, respectively. Likewise, incidence rates of 5.2 and 7.5% were observed for proximal and distal pancreatic stent migration, respectively. Malignant strictures, larger diameter stents, and shorter stents were significantly associated with proximal biliary stent migration. Sphincter of Oddi dysfunction and longer stents were associated with proximal pancreatic stent migration. Migration of stents out of the common bile duct occurred more frequently in papillary stenosis. No other significant risk factors for distal migration were found. These results indicate that stent migration is an important complication. Multiple risk factors were associated with stent migration and need to be considered in the development of new stent types.

Clinical Orthopaedics and Related Research

Current assessment of spinal degenerative disease with magnetic resonance imaging. Ross JS, Modic MT (MTM, 9500 Euclid Ave., Cleveland, OH 44195-5103). *Clin Orthop* 279:68–81, June 1992

Radiography (plain roentgenography, myelography, computed tomography (CT), computed tomographic myelography) has been used to identify morphologic changes involving the various components of the diskovertebral unit. Added to this armamentarium of imaging techniques is magnetic resonance (MR) imaging, with its superior ability to define anatomy, its improved contrast sensitivity, and its potential to provide unique biochemical and physiologic information. The authors review the current use of MR imaging in defining degenerative changes in the spine, including the various patterns of herniation, annular tears, canal stenosis, and the use of gadolinium-diethylenetriaminepentaacetic acid for previously unoperated and operated patients. Prospective studies have compared surface-coil MR imaging, CT, and myelography in the evaluation of disk herniation and stenosis and found an 82.6% accuracy between MR imaging and surgical findings for the type and location of the disease. Recent experience with precontrast and postcontrast MR imaging in the postoperative lumbar spine indicated that it was 96% accurate in differentiating scar from disk in 44 patients at 50 reoperated levels. Three-dimensional imaging is, more and more, becoming an integral part of routine MR imaging. The theoretical and practical advantages of three-dimensional imaging are several and include a theoretical increase in the signal-to-noise ratio over two-dimensional imaging (by the square root of the number of partitions selected), the ability to obtain thin contiguous slices from the volume without the problem of cross-talk found in two-dimensional imaging, more accurate slice thickness than that achieved in two-dimensional imaging, and a reduction in susceptibility artifacts. Different three-dimensional techniques are capable of providing either high or low signal intensity cerebrospinal fluid (CSF), with excellent suppression of CSF pulsation artifacts. Certain sequences provide a high enough signal intensity that a computer algorithm may be used to display the CSF in a rotating three-dimensional manner, similar to a myelogram. This three-dimensional myelographic image has the potential of providing the clinician with a global assessment of the CSF spaces, an advantage previously lacking with other imaging techniques.

The Journal of Urology

Percutaneous reduction of cyst volume of polycystic kidney disease: effects on renal function. Higashihara E, Nutahara K, Minowada S, Homma Y, Aso Y (EH, Dept. of Urology, Faculty of Medicine, University of Tokyo, Tokyo, Japan). *J Urol* 147:1482–1484, June 1992

Percutaneous reduction of cyst volume was performed in 10 patients with autosomal dominant polycystic kidney disease and its effects on renal function were studied. Although creatinine clearance, urinary excretion of β2-microglobulin and N-acetyl-β-D-glucosaminidase, and renal uptake of ^{99m}technetium-dimercaptosuccinic acid did not change significantly, a transient increase in urinary protein and a decrease in inulin clearance were observed. Complications, such as hematuria, fever and decreases in hematocrit, were slight and transient in most patients. This procedure holds little promise for altering the course of polycystic kidney disease.

The Journal of Pediatrics

Magnetic resonance imaging in the diagnosis of growth hormone deficiency. Argyropoulou M, Perignon F, Brauner R, Brunelle F (RB, Paediatric Endocrinology Unit, Hôpital des Enfants Malades, 149 Rue de Sèvres, 75015 Paris, France). *J Pediatr* 120:886–891, 1992

Forty-six patients with idiopathic growth hormone deficiency were examined by magnetic resonance imaging at a mean (± SEM) age of 9 ± 1 years (range 15 days to 20 years). They were classified into two groups according to MRI images: group 1 ($n = 29$) had pituitary stalk interruption syndrome and group 2 ($n = 17$) had normal pituitary anatomy. All patients with pituitary stalk interruption had a pituitary height at <-2 SD for age; three had no visible anterior pituitary lobe. By contrast, the pituitary height was less than normal in only 10 patients (60%) with normal pituitary anatomy. Growth hormone deficiency was transient in one of the seven patients with normal pituitary anatomy and height. The group with pituitary stalk interruption had the first symptom of growth hormone deficiency at an earlier age (2.8 ± 0.6 vs 5.5 ± 1.2 years; $p < 0.001$), were of smaller stature (−4 ± 0.2 vs −3 ± 0.2 SD; $p < 0.01$) and had lower GH peak response to provocative testing (3 ± 0.4 vs 5 ± 0.5 ng/ml; $p < 0.001$) than did the group with normal pituitary anatomy. Their pituitary gland was also shorter (2.5 ± 0.2 vs 3.5 ± 0.2 mm; $p < 0.01$). All the patients with multiple pituitary deficiencies except one ($n = 19$) belonged to this group. One girl with pituitary stalk interruption and deficiencies in growth hormone and thyroid-stimulating hormone had advanced central precocious puberty. We conclude that the evaluation of the shape and height of the pituitary gland by MRI is an additional tool for the diagnosis of growth hormone deficiency. The presence of pituitary stalk interruption confirms this diagnosis and is predictive of multiple anterior pituitary deficiencies. The lack of a significant increase in perinatal abnormalities in this group and the association of pituitary stalk interruption with microphallus and with facial or sella abnormalities suggest that this appearance may have an early antenatal origin. The finding of a familial case of pituitary stalk interruption suggests a genetic origin.

Rate of bronchopulmonary dysplasia as a function of neonatal intensive care practices. Van Marter LJ, Pagano M, Allred EN, Leviton A, Kuban KCK (LJVM, Joint Program in Neonatology, Hunnewell 4, Children's Hospital, 300 Longwood Ave., Boston, MA 02115). *J Pediatr* 120:938–946, 1992

Some differences among neonatal intensive care units (NICUs) in incidence of bronchopulmonary dysplasia may reflect variations in medical care practices. After adjusting for differences in the inherent risk of bronchopulmonary dysplasia among 223 infants of less than 1751 gm birth weight who were admitted to three Harvard-affiliated NICUs, we used multivariate analysis to explore the extent to which medical care practices during the first days of life varied with the rate of bronchopulmonary dysplasia. In our analyses, variables were grouped by three major hypotheses: oxygen toxicity, barotrauma, and fluid overload. The NICU designated 1 (the one with the highest rate of bronchopulmonary dysplasia) used much higher than expected colloidal volumes during the first 4 days of life; in contrast, in the NICU designated 3 (the one with the lowest rate of bronchopulmonary dysplasia), infants consistently received lower than expected amounts of colloidal solution. Signs of patent ductus arteriosus were also much more frequent than expected during this time at NICU 1; rates were much lower than predicted at NICU 2 and were near predicted values at NICU 3. Maximum inspired oxygen fraction during the first 4 days varied significantly in a direction inconsistent with the oxygen toxicity hypothesis. Maximum arterial oxygen tension was significantly less than expected at the hospital with the lowest rate of bronchopulmonary dysplasia (NICU 3). None of six medical care practices indicating potential for barotrauma varied with NICU except for positive end-expiratory pressure, which varied in a direction suggesting a protective effect against bronchopulmonary dysplasia. These findings agree best with the hypothesis that differences in hydration during the first days of life account for some of the difference among NICUs in bronchopulmonary dysplasia occurrence.

The Journal of Nuclear Medicine

Comparison between thallium-201, technetium-99m-sestamibi and technetium-99m-teboroxime planar myocardial perfusion imaging in detection of coronary artery disease. Taillefer R, Lambert R, Essiambre R, Phaneuf DC, Léveillé J (RT, Département de Médecine Nucléaire, Hôtel-Dieu de Montréal, 3840 St-Urbain St., Montreal, Quebec, H2W 1T8, Canada). *J Nucl Med* 33:1091–1098, 1992

Technetium-99m-sestamibi (MIBI) and ^{99m}Tc-teboroxime (TEBO) are two new myocardial perfusion imaging agents. The purpose of this prospective study was to compare MIBI and TEBO to ^{201}Tl planar imaging. Eighteen patients with significant coronary artery disease on coronary angiogram were submitted to three treadmill stress tests performed within 3 mo and were imaged with the three radiopharmaceuticals as follows.

1. Tl: 2.2 mCi, immediate and delayed views (4 hr later, 8 min/view).
2. TEBO: 15–20 mCi at stress (1 min/view) and a second injection was repeated 4 hr later at rest (20–25 mCi).
3. MIBI: 15–18 mCi at stress (8 min/view) and 1–4 days later, 15–18 mCi at rest.

Patients achieved similar levels of exercise. A blinded reading was performed by three observers. The left ventricle was divided into three segments/view and ischemic/normal wall ratios were also determined. Segmental comparison showed an agreement in 85% (138/162) of the segments between Tl and TEBO, in 92% (149/162) between Tl and MIBI and in 84% (136/162) between MIBI and TEBO. Abnormal Tl, MIBI and TEBO studies were seen in 16 (89%), 16 (89%) and 15 (83%) patients, respectively, detecting 77, 75 and 65 abnormal segments. Ischemic-to-normal wall ratios were 0.75 ± 0.06, 0.73 ± 0.08 and 0.78 ± 0.08 for Tl, MIBI and TEBO, respectively. In conclusion, although the biologic characteristics of these agents are different, this study showed a good correlation between them in detection of significant coronary artery disease (high pretest likelihood population).

Radioiodine-131 therapy for well-differentiated thyroid cancer—a quantitative radiation dosimetric approach: outcome and validation in 85 patients. Maxon HR III, Englaro EE, Thomas SR, et al. (HRM, Director, Eugene L. Saenger Radioisotope Laboratory, University of Cincinnati Medical Center, 234 Goodman St., Cincinnati, OH 45267-0577). *J Nucl Med* 33:1132–1136, 1992

For almost five decades, ^{131}I treatment of thyroid cancer has been based empirically on administered activity rather than on actual radiation doses delivered. In 1983, we defined radiation dose thresholds for successful treatment. This report is concerned with the subsequent validation of those thresholds in 85 patients. The successful ablation of thyroid remnants occurred after a single initial ^{131}I administration in 84% of inpatients and in 79% of outpatients when treatment was standardized to a radiation dose of at least 30,000 cGy (rad). Administered activities low enough to permit outpatient therapy could be used in 47% of the patients. Lymph node metastases were treated successfully in 74% of patients with a single administration of ^{131}I calculated to deliver at least 8,500 cGy (rad). For athyrotic patients with nodal metastases only, success was achieved in 86% of patients at tumor doses of at least 14,000 cGy (rad). These success rates are equal to or better than those reported with empiric methods of ^{131}I administration. The individualized treatment planning selectively allocates hospitalization and higher exposures to ^{131}I to those patients who require them.

Gastrointestinal Radiology

Cytomegalovirus gastritis: protean radiologic features. Farman J, Lerner ME, Ng C, et al. (JF, Dept. of Radiology, M3-204, Columbia-Presbyterian Medical Center, New York, NY 10032-3284). *Gastrointest Radiol* 17:202–206, 1992

Infection with cytomegalovirus (CMV) is a major feature of acquired immunodeficiency syndrome (AIDS). Gastrointestinal involvement is being seen more frequently. Our collective experience involves nine patients with stomach involvement. Seven patients were intravenous drug abusers or homosexuals with AIDS. One developed CMV gastritis as a complication of leukemia and one patient was a West African with lymphoma and human immunodeficiency virus (HIV) infection. All our patients had biopsy-proven CMV inclusion bodies. The radiographic appearances varied widely. The findings included markedly thickened edematous folds, erosive gastritis with aphthous ulceration, and superficial and deep ulceration. One patient had deep ulceration with fistula formation. Computed tomographic (CT) scans confirmed the greatly thickened gastric wall and coarsened folds in two patients. Associated gastrointestinal infections included candida and herpes, and, in addition, pneumocystis carinii pneumonia (PCP) was present in two patients. CMV gastritis may mimic several other conditions including erosive gastritis, peptic ulceration, lymphoma, and carcinoma. It should be strongly considered in immunosuppressed patients.

Journal of Ultrasound Medicine

Normal and respiratory variations of the hepatic and portal venous duplex Doppler waveforms with simultaneous electrocardiographic correlation. Abu-Yousef M (MMA, Dept. of Radiology, The University of Iowa Hospitals and Clinics, Iowa City, IA 52242). *J Ultrasound Med* 11:263-268, June 1992

To understand hepatic vein (HV) and portal vein (PV) duplex waveforms and their normal and respiratory variations, HV and PV duplex sonography with simultaneous electrocardiography was performed on 11 volunteers. Absolute velocities of the waveforms' components and their ratios were determined at mid-inspiration, full inspiration, full expiration, and Valsalva maneuver. The normal HV waveform was variable in shape and component velocities and ratios but essentially consisted sequentially of (1) an antegrade systolic wave resulting from movement of the tricuspid annulus toward the cardiac apex and occurring shortly after QRS; (2) a retrograde v-wave resulting from atrial overfilling and occurring immediately after the T-wave; (3) an antegrade diastolic wave resulting from opening of the tricuspid valve and occurring shortly after the T-wave; and (4) a retrograde a-wave resulting from atrial contraction and occurring immediately after the P-wave. The ratio of the maximum systolic velocity to maximum diastolic velocity varied from 1.0 to 2.8 (mean 1.4). Systolic-to-diastolic ratio decreased during inspiration but was always greater than 0.6 and increased during expiration. The Valsalva maneuver diminished waveform pulsatility. PV waveforms were more triphasic than biphasic but less pulsatile, flow was totally antegrade, and respiratory changes were less remarkable than HV waveforms. All normal HV and most normal PV waveforms showed multiphasicity that corresponded to cyclic cardiac changes. The shapes of these waveforms were variable and were modified by respiratory movements.

Reprinted with permission by the American Institute of Ultrasound in Medicine.

News

Robert D. Moseley, Jr. Award

The National Council on Radiation Protection and Measurements (NCRP) is accepting applications for the Robert D. Moseley, Jr. Award in Radiation Protection in Medicine. The award honors the late Robert D. Moseley, Jr., a leader in radiology, who recognized the importance of having radiologists involved in radiation protection activities. The purpose of the award is to stimulate an interest, by young physicians or others in allied sciences, in radiation protection and measurement. The award will be made for an outstanding paper on radiation protection in medicine that has been published or accepted for publication in 1992. The paper will be judged on the basis of scientific merit, originality, and applicability to the field of radiation protection and measurement in the medical use of ionizing radiation. The awardee will receive $1000 and travel expenses to attend the NCRP annual meeting in Washington, DC, April 7–8, 1993. Applications will be accepted from an eligible author or from colleagues or others on behalf of an eligible author. The principal author of the paper must be in or have completed within the past 10 years an approved residency in diagnostic radiology, nuclear medicine, or radiation oncology or be otherwise qualified via postdoctoral experience in medical physics or radiobiology. The applicant must be a resident of the United States at the time of the submission and the Award. Applications, including a copy of the paper, should be submitted by Jan. 15, 1993, to the NCRP, Attn: Cindy L. O'Brien, 7910 Woodmont Ave., Ste. 800, Bethesda, MD 20814.

CT and MR Imaging of the Brain, Head, Neck, and Spine

The Dept. of Diagnostic Radiology, Rush-Presbyterian-St. Luke's Medical Center, will present its 19th annual course, Computed Tomography and Magnetic Resonance Imaging of the Brain, Head, Neck, and Spine, Oct. 15–16, at the Hyatt Suites Hotel, Chicago. Guest faculty: D. C. Harwood-Nash, V. M. Haughton, L. Heier, T. P. Naidich, A. G. Osborn, R. G. Ramsey, J. S. Ross, E. J. Russell, P. M. Som, and J. M. Taveras. Category 1 credit: 15 hr. Fee: $485. Information: Michael S. Huckman, M.D., Rush-Presbyterian-St. Luke's Medical Center, 1653 W. Congress Parkway, Chicago, IL 60612; (312) 942-5781.

Current Concepts of Magnetic Resonance

The Depts. of Radiology, Stanford University Medical Center and Duke University Medical Center, are sponsoring Current Concepts of Magnetic Resonance, Oct. 29–Nov. 1, at the Ritz-Carlton Resort Hotel, Laguna Niguel, CA. The course will present the physics of MR imaging and clinical examples. Program director: Gary H. Glover. Category 1 credit: 19.5 hr. Fee (through Oct. 3/after Oct. 3): Stanford alumni, $450/$450; physicians, $500/$550; residents, fellows, and technologists, $300/$350. Information: Dawne Ryals, Ryals and Associates, P. O. Box 1925, Roswell, GA 30077-1925, telephone: (404) 641-9773; fax: (404) 552-9859.

New Orleans Fall Radiology Conference

The Dept. of Radiology, Louisiana State University, School of Medicine, will present the New Orleans Fall Radiology Conference, Oct. 30–Nov. 1, at Le Meridien Hotel, New Orleans. The conference will focus on mammography and women's imaging, with special emphasis on sonography, MR imaging, and chest radiology. Category 1 credit: 19 hr. Fee: physicians, $465; residents (letter required), $295. Information: Dept. of Radiology, LSU School of Medicine, 1542 Tulane Ave., New Orleans, LA 70112; telephone: (504) 568-4647; fax: (504) 568-8955.

CT/MRI Head to Toe

The 11th annual course CT/MRI Head to Toe will be presented Dec. 14–19 at the Grand Hyatt New York, New York City. The course will present a practical update in CT and MR imaging. Workshops will cover diseases of the head, neck, sinuses, thorax, abdomen and pelvis, spine, and musculoskeletal system and relevant interventional techniques. Basic principles of technique and presentations of clinical case material will be included. The program will be given into two sections that can be taken independently or consecutively. Part A will cover chest and body CT and MR imaging. Part B will cover neuroradiology and CT and MR imaging of the spine, head, and neck. Category 1 credit: entire course, 41 hr; part A only, 22 hr; part B only, 19 hr. Fee: entire course, $750; part A only, $435; part B only, $375. Information: New York University, 550 First Ave., New York, NY 10016; telephone: (212) 263-5295; fax: (212) 263-5293.

Musculoskeletal MR Course

The Dept. of Radiology, University of California, San Diego School of Medicine, is sponsoring Musculoskeletal MR Course, Jan. 4–8, 1993, at the Ritz-Carlton Resort Hotel, Naples, FL. The course will cover diagnosis of musculoskeletal disorders. Emphasis will be on internal derangement of joints. Technical considerations, selection of pulse sequences, and optimization of imaging will be discussed.

Program directors: Donald L. Resnick and Mini N. Pathria. Category 1 credit: 25 hr (pending). Fee (through Dec. 14, 1992/after Dec. 14, 1992): physicians, $550/$595; residents, fellows, and technologists, $300/$345. Information: Dawne Ryals, Ryals and Associates, P. O. Box 1925, Roswell, GA 30077-1925, telephone: (404) 641-9773; fax: (404) 552-9859.

Society of Uroradiology Annual Meeting

The Society of Uroradiology will hold its annual meeting and postgraduate course, Imaging and Intervention of the Genitourinary Tract: The Cutting Edge, Jan. 9-15, 1993, at the Ritz-Carlton Resort Hotel, Naples, FL. The course will be a practical review of state-of-the-art imaging and interventional radiology of the genitourinary tract. Emphasis will be on the needs of practicing radiologists. Presentations will be clinically oriented and relevant to daily practice. Category 1 credit: 29 hr. Fee (through Dec. 26, 1992/after Dec. 26, 1992): physicians, $550/$595; residents, fellows, and technologists, $350/$395. Information: Dawne Ryals, Ryals and Associates, P. O. Box 1925, Roswell, GA 30077-1925, telephone: (404) 641-9773; fax: (404) 552-9859.

Interventional Radiology Update

The Dept. of Radiology, Stanford University Medical Center, is sponsoring Interventional Radiology Update, Jan. 16-17, 1993, at the Ritz-Carlton Resort Hotel, Laguna Niguel, CA. The course will review state-of-the-art interventional radiology. Topics to be covered include vascular stents, atherectomy, spiral CT angiography, inferior vena caval filters, TIPS, and percutaneous gastrostomy. Program chairman: Gary M. Glazer; program director, Michael Dake. Category 1 credit: 7.5 hr. Fee: Stanford alumni, $200; practicing physicians, $250; residents, fellows, and technologists, $150. Information: Dawne Ryals, Ryals and Associates, P. O. Box 1925, Roswell, GA 30077-1925, telephone: (404) 641-9773; fax: (404) 552-9859.

Neuroradiology Update

The Dept. of Radiology, Stanford University Medical Center, is sponsoring Neuroradiology Update, Jan. 18-20, 1993, at the Ritz-Carlton Resort Hotel, Laguna Niguel, CA. The course will be a review of state-of-the-art neuroradiology. Topics to be covered include temporal bone, sellar lesions, neck imaging, CNS infections, stroke, and cerebral MR angiography. Program chairman: Gary M. Glazer; program director, Barton Lane. Category 1 credit: 17.5 hr. Fee: Stanford alumni, $400; practicing physicians, $450; residents, fellows, and technologists, $300. Information: Dawne Ryals, Ryals and Associates, P. O. Box 1925, Roswell, GA 30077-1925, telephone: (404) 641-9773; fax: (404) 552-9859.

Breast Imaging Update

The Dept. of Radiology, Stanford University Medical Center, is sponsoring Breast Imaging Update, Jan. 21-24, 1993, at the Ritz-Carlton Resort Hotel, Laguna Niguel, CA. Topics to be covered in this review of state-of-the-art breast imaging will include risk factors for breast cancer, atypical hyperplasia, diagnosis of masses, needle localization techniques, implants, and breast sonography. Program chairman: Gary M. Glazer; program director: Debra M. Ikeda. Category 1 credit: 17.25 hr. Fee: Stanford alumni, $400; practicing physicians, $450; residents, fellows, and technologists, $300. Information: Dawne Ryals, Ryals and Associates, P. O. Box 1925, Roswell, GA 30077-1925; telephone: (404) 641-9773; fax: (404) 552-9859.

Breast Imaging Course

The Dept. of Radiology, University of Alabama at Birmingham, School of Medicine, is sponsoring the 3rd annual Breast Imaging Course, Jan. 25-28, 1993, at the Ritz-Carlton Resort Hotel, Naples, FL. The course will deal with pathologic, radiologic, and clinical considerations involved in the diagnosis and management of mammographically detected early breast cancer. A multidisciplinary approach will be used. Program director: Eva Rubin. Category 1 credit: 18 hr (pending). Fee (through Jan. 24, 1993/after Jan. 24, 1993): physicians, $500/$545; residents, fellows, technologists, $350/$395. Information: Dawne Ryals, Ryals and Associates, P. O. Box 1925, Roswell, GA 30077-1925; telephone: (404) 641-9773; fax: (404) 552-9859.

International Symposium on MR Imaging

The Dept. of Radiology, University of Munich, Munich, Germany; the Dept. of Diagnostic Radiology, National Institutes of Health, Bethesda, MD; and the Dept. of Radiology, University of California, San Francisco, CA, are organizing the 5th International Symposium on MR Imaging, MR '93, to be held Jan. 27-31, 1993, at the Congress center in Garmisch-Partenkirchen (Bavaria), Germany. Topics to be covered include the brain and spinal cord; thorax, abdomen, and pelvis; MR angiography; bones, joints, and soft tissues; contrast media; and works in progress. Simultaneous translation in English and German will be provided. Information: Prof. Dr. J. Lissner, Radiologische Klinik, Klinikum Grosshadern, Marchioninistr. 15, D-8000 München 70, Germany; telephone: (089) 7095 2750; fax: (089) 7095 8895.

Computed Body Tomography 1993—The Cutting Edge

The Johns Hopkins University School of Medicine is sponsoring Computed Body Tomography 1993—The Cutting Edge, Feb. 4-7, 1993, at the Peabody Orlando Hotel, Orlando, FL. The seminar will provide a comprehensive review of recent advances in CT of the chest and abdomen, including the spine; some correlations with MR imaging will be included. A series of 30-min lectures will concentrate on specific topics in detail. One-hour workshops will focus on problem-oriented topics, with emphasis on technique and differential diagnosis. Program directors: Elliot K. Fishman and Stanley S. Siegelman. Guest faculty: H. D. Curtin, N. R. Dunnick, W. D. Foley, P. R. Mueller, and S. S. Sagel. Category 1 credit: 22 hr. Fee: physicians, $525; residents, fellows, and technologists, $400 (letter required). Information: Program Coordinator, Johns Hopkins Medical Institutions, Office of Continuing Education, Turner Bldg., 720 Rutland Ave., Baltimore, MD 21205; (410) 955-2959.

U. B. C. Practical Radiology at Whistler

The 11th annual U. B. C. Practical Radiology at Whistler will be held Feb. 6-12, 1993, at the Chateau Whistler, Whistler/Blackcomb Mountain, B.C. The course will review established concepts in radiology and introduce new ones. Speakers will include T. Masaryk, D. Naidich, C. Higgins, B. Thompson, A. Moss, E. Stewart, P.

Freeney, and R. Baron. Category 1 credit: 20 hr. Fee: Can$525. Information: Dr. Peter L. Cooperberg, Dept. of Radiology, St. Paul's Hospital, 1081 Burrard Ave., Vancouver, B.C. V6Z 1Y6; or Diane Robert: telephone: (604) 631-5026; fax: (604) 631-5283.

Diagnostic Imaging Update

The Dept. of Radiology, Stanford University Medical Center, is sponsoring Diagnostic Imaging Update: Mammography, MRI, Body Imaging, Neuroradiology, Pediatrics, Feb. 15-19, 1993, at the Ritz-Carlton Resort Hotel, Palm Beach, FL. Topics to be discussed include MR and color Doppler imaging of the liver, mammography of microcalcifications, breast cancer missed on mammograms, pneumonia in children, MR imaging of stroke, MR angiography of carotid disease, and MR contrast agents. Program chairman: Gary M. Glazer; program director: R. Brooke Jeffrey, Jr. Category 1 credit: 23.75 hr. Fee (through Feb. 1, 1993/after Feb. 1, 1993): Stanford alumni, $500/$500; practicing physicians, $550/$595; residents, fellows, and technologists, $300/$345. Information: Dawne Ryals, Ryals and Associates, P. O. Box 1925, Roswell, GA 30077-1925, telephone: (404) 641-9773; fax: (404) 552-9859.

Sun Valley Imaging Meeting

The 9th annual Sun Valley Imaging Meeting will be held Feb. 20-27, 1993, at the Sun Valley Lodge, Sun Valley, ID. The course will review important aspects of body imaging and intervention and discuss the latest developments in these areas. Speakers will include P. Cooperberg, P. Harrison, B. Lentle, R. L. Baron, B. L. McClennan, P. H. Mueller, M. Rifkin, and S. Wilson. Category 1 credit: 20 hr. Fee: $525. Information: Dr. Peter Cooperberg, Box 285, 1027 Davie St., Vancouver, B.C. V6E 4L2; telephone: (604) 631-5026; fax: (604) 631-5283.

MRI Update 1993

The Medical College of Wisconsin will present the 8th in a series: MRI Update 1993: MR Imaging of the Head, Spine, and Musculoskeletal System, Feb. 22-26, 1993, at the La Quinta Golf and Tennis Resort, La Quinta, CA. The course will provide inclusive, detailed, up-to-date discussions of all important clinically proved MR imaging applications. Topics will include MR angiography, contrast media, and new musculoskeletal imaging applications. Detailed CNS and spinal anatomy with exclusive cryoanatomic sections will be featured. Program chairmen: Victor Haughton and Robert Quencer. Fee: through Dec. 31, 1992, $570; after Dec. 31, 1992, $620. Information: Marti Carter, CME, Inc., 11011 W. North Ave., Milwaukee, WI 53226; (414) 771-9520.

Diagnostic Imaging Update

The Dept. of Radiology, Stanford University Medical Center, is sponsoring Diagnostic Imaging Update, Feb. 22-26, 1993, at the Ritz-Carlton Resort Hotel, Kapalua Bay, Maui, HI. The course will review state-of-the-art body and neuroradiologic imaging. Topics will include MR angiography, fast-scan MR imaging, MR imaging of the liver, CT and MR imaging of lung cancer, adrenal imaging, and radiology of the esophagus and duodenum. Program chairman: Gary M. Glazer; program director, R. Brooke Jeffrey, Jr. Category 1 credit: pending. Fee (through Feb. 7, 1993/after Feb. 7, 1993): Stanford alumni, $500/$500; practicing physicians, $550/$595; residents, fellows, and technologists, $300/$345. Information: Dawne Ryals, Ryals and Associates, P. O. Box 1925, Roswell, GA 30077-1925, telephone: (404) 641-9773; fax: (404) 552-9859.

Magnetic Resonance Imaging

The University of Toronto is sponsoring Magnetic Resonance Imaging, Feb. 22-26, at the Ritz-Carlton Hotel, Naples, FL. The course will discuss the use of MR imaging as related to the evolution of new hardware. Program directors: David O. Davis, Edward Kassell, and Walter Kucharczyk. Category 1 credit: 21 hr (pending). Fee (through Feb. 1, 1993/after Feb. 1, 1993): physicians, $545/$595; residents, fellows, and technologists, $300/$345. Information: Dawne Ryals, Ryals and Associates, P. O. Box 1925, Roswell, GA 30077-1925; telephone: (404) 641-9773; fax: (404) 552-9859.

Positron Emission Tomography

The Division of Nuclear Medicine and Biophysics, University of California, Los Angeles, will present Positron Emission Tomography: Clinical Applications and Practical Considerations, Feb. 28-March 2, 1993, at Dana Point Resort, Dana Point, CA. Topics will include new clinical applications of positron emission tomography (PET) in oncology, neurology, and cardiology; competing imaging techniques (e.g., single-photon emission computed tomography, MR imaging, CT); lowering health care costs with PET; and patterns of reimbursement. Category 1 credit: 17.5 hr. Fee: physicians: through Jan. 24, 1993, $495; after Jan. 24, 1993, $595; fellows, residents, and technologists, $395. Information: Wendy Hagar; (310) 825-2724.

International Diagnostic Course in Davos

The 25th International Diagnostic Course in Davos will be held March 27-April 2, 1993, in Davos, Switzerland. The main topic will be the musculoskeletal system. Program directors: P. Braun and A. Rüttimann. Information: IDKD, Postfach 224, CH 8028 Zürich, Switzerland; telephone: 01 262.24.04; fax: 01 261.05.78.

CIRSE and SCVIR Annual Meeting

The annual meeting of the Cardiovascular and Interventional Radiological Society of Europe (CIRSE) and the Society of Cardiovascular and Interventional Radiology (SCVIR) of the United States will be held June 20-25, 1993, in Budapest, Hungary. Chairman: Laszlo Horvath. Information: CIRSE 93, P. O. Box 201, CH 8028, Zürich, Switzerland; telephone: 01 262.24.04; fax: 01 261.05.78.

The American Board of Radiology Examinations

Written examinations for the American Board of Radiology (ABR) are scheduled for Oct. 1-2, 1992, and Sept. 23-24, 1993. Oral examinations will be held at the Executive West Hotel in Louisville, KY, June 7-10, 1993. The ABR will accept applications for admission to the examinations after July 1, but not later than Sept. 30, in the year *preceding* the year in which the examination is to be taken. For application forms and further information: Office of the Executive Director, The American Board of Radiology, 2301 W. Big Beaver Rd., Ste. 625, Troy, MI 48084.

Meeting and Course Review

For the reader's convenience, a summary of upcoming meetings and courses is provided. Detailed listings are given in the *AJR* issue given in parentheses.

Visiting Fellowships in Interventional Radiology, times arranged, Baltimore (Sept)
Preceptorships in Ultrasound, times arranged, Baltimore (Sept)
Update in Film Screen Mammography, Sept. 30–Oct. 2, Richmond, VA (May)
Western Neuroradiological Society Annual Meeting, Oct. 1–4, San Francisco (July)
ARDMS Exam Preparation Courses, Ultrasound and Doppler Physics, Oct. 2–3, Chicago; **OB/GYN Ultrasound**, Oct. 4, Chicago; **Vascular Technology**, Oct. 4–5, Chicago (July)
Ultrasound Update: 1992, Oct. 3–4, Sacramento, CA (Sept)
MRI Visiting Fellowships at UCLA, Oct. 5–9 and Dec. 7–11, Los Angeles (Sept 1991)
International Symposium on Vena Cava Filters, Oct. 9–10, Poitiers, France (July)
Fall Foliage Imaging Seminar, Oct. 9–11, Burlington, VT (May)
International Body Imaging Congress, Oct. 10–17, Kona, HI (Aug)
MRI: Clinical State of the Art 1992, Oct. 12–14, New York City (Aug)
Practical Radiology, Oct 12–15, Charlottesville, VA (June)
AFIP Course on Radiologic-Pathologic Correlation, Oct. 12–16, Lake Buena Vista, FL (Sept)
Symposium on Cardiovascular and Interventional Radiology, Oct. 13–16, Boston (Aug)
Nuclear Cardiology Symposium and Workshop, Oct. 14–16, Milwaukee (June)
Progress in Magnetic Resonance, Oct. 15–17, Locarno, Switzerland (June)
Breast Cancer Diagnosis: State of the Art, Oct. 15–17, New York City (Aug)
Chest Imaging 1992, Oct. 16, Toronto (Aug)
Course on Prostate Ultrasound, Oct. 16–17, Albany, NY (June)
Michigan Fall Radiology Conference, Oct. 16–17, Birmingham, MI (July)
Pan-Philadelphia Neurosurgery Conference, Oct. 16–17, Philadelphia (Sept)
Practicum in Mammography for Technologists, beginning date, Oct 19, San Diego (May)
Breast Imaging Seminar, Oct. 19–21, New York City (July)
Computed Body Tomography for the Technologist, Oct. 22–25, Orlando, FL (Sept)
Society of Radiologists in Ultrasound Postgraduate Course, Oct. 23–25, Chicago (June)
Women's Health and Breast Cancer, Oct. 24, Sacramento, CA (Sept)
Musculoskeletal Imaging, Oct. 24–25, San Diego (July)
Interventional Neuroradiology, Oct. 24–25, Baltimore (Sept)
International Course on MR Imaging, Oct. 25–28, Riyadh, Kingdom of Saudi Arabia (March)
Mammographic Interpretation, Oct. 26–29, Boston (April)
Postgraduate Radiology Course, Oct. 26–30, San Diego (July)
Magnetic Resonance Imaging and CT Update, Oct. 26–30, Cambridge, MA (Aug)
Interventional Radiology Course, Oct. 30–Nov. 1, San Diego (Aug)
Postgraduate Radiology, Nov. 2–6, Naples, FL (Aug)
Dysphagia Research Society Inaugural Meeting, Nov. 6–8, Milwaukee (July)
Advanced Seminars in Diagnostic Imaging, Nov. 13–15, Laguna Niguel, CA (Aug)
Postgraduate Imaging Seminar, Dec. 28, 1992–Jan. 1, 1993, Maui, HI (Sept)
Holiday Imaging Update, Dec. 28, 1992–Jan. 1, 1993, Aspen, CO (Sept)
The Complete MRI Course, Jan. 4–8, 1993, Maui, HI (Sept)
Society of Gastrointestinal Radiologists Annual Meeting, Jan. 17–22, 1993, Scottsdale, AZ (Sept)

AJR carries announcements of courses, symposia, and meetings of interest to its readers if received a minimum of 5 months before the event. There is no charge; receipt of items by the *AJR* Editorial Office is not acknowledged. Submit items for publication typed double-spaced. Provide title, date, location, brief description, sponsor, course directors, fees, category I credit, and address and telephone number for additional information. Faculty from the host institution will not be listed. Guest faculty names will appear **only** if initials are provided. Mail news items to *AJR* Editorial Office, 2223 Avenida de la Playa, Suite 103, La Jolla, CA 92037-3218.

American Roentgen Ray Society:
Officers, Committees, and Membership Information

Officers

President: A. Everette James, Jr.
President-elect: Andrew K. Poznanski
1st Vice-president: George R. Leopold
2nd Vice-president: Ralph J. Alfidi
Secretary: Joseph T. Ferrucci, Jr.
Treasurer: Beverly P. Wood

Executive Council: R. J. Alfidi, R. N. Berk, M. P. Capp, W. J. Casarella, D. O. Davis, N. R. Dunnick, J. T. Ferrucci, Jr., A. E. James, Jr., J. A. Kirkpatrick, Jr., A. M. Landry, Jr., G. R. Leopold, J. E. Madewell, T. C. McLoud, A. A. Moss, A. K. Poznanski, R. J. Stanley, J H Thrall, N. O. Whitley, B. P. Wood, K. H. Vydareny, chair

Committees

Editoral Policy: R. N. Berk, E. Buonocore, M. M. Figley, R. G. Levitt, C. R. B. Merritt, K. Valji, W. J. Casarella, chair

Education and Research: G. M. Glazer, R. R. Hattery, C. B. Higgins, R. J. Stanley, W. M. Thompson, N. O. Whitley, chair

Finance and Budget: D. J. Anderson, R. K. Gedgaudas-McClees, J. E. Madewell, A. A. Moss, J. H. Thrall, chair

Nominating: M. P. Capp, C. A. Rohrmann, Jr., J. E. Madewell, chair

Publication: E. Buonocore, R. G. Levitt, C. R. B. Merritt, W. J. Casarella, chair

Membership: D. O. Davis, J. E. Madewell, T. C. McLoud, A. A. Moss, chair

Representatives to Other Organizations

American Board of Radiology: W. J. Casarella, J. A. Kirkpatrick, Jr., L. F. Rogers

American College of Radiology: J. E. Madewell, B. L. McClennan, R. J. Stanley, N. H. Messinger

American Medical Association: R. A. Gagliardi, delegate; R. G. Evens, alternate; K. L. Kidd, CPT Advisory Committee

American National Standards Institute: M. E. Haskin

National Council on Radiation Protection and Measurements: F. D. Miraldi, E. L. Saenger

Armed Forces Institute of Pathology: J. E. Madewell

Meeting Arrangements

Annual Meetings: April 25–30, 1993, Marriott San Francisco, San Francisco, CA; April 24–29, 1994, New Orleans Hilton, New Orleans, LA

Annual Meeting Committee: J. K. Crowe, N. R. Dunnick, R. R. Lukin, N. H. Messinger, R. J. Stanley, R. D. Steele, Jr., A. M. Landry, Jr., chair

Instructional Courses: B. L. McClennan, associate chair, R. J. Stanley, chair

Scientific Program: P. H. Arger, W. R. Brody, G. D. Fullerton, D. C. Kushner, W. M. Thompson, J. H. Thrall, A. K. Poznanski, chair

Scientific Exhibits: J. R. Haaga, D. S. Hartman, N. R. Dunnick, chair

ARRS Membership

An application form is printed in the January issue of the Journal. Qualified applicants will be admitted quarterly. Send completed forms to American Roentgen Ray Society, 1891 Preston White Dr., Reston, VA 22091. Active members are graduates of an approved medical or osteopathic school or hold an advanced degree in an allied science. They must practice radiology or work in an associated science in the United States or Canada and be certified by the American Board of Radiology, American Osteopathic Board of Radiology, or Royal College of Physicians of Canada or otherwise adequately document training and credentials. International members are foreign radiologists or scientists who are active in radiology or an allied science. Members-in-training are residents or fellows in radiology or postgraduate students in an allied science. Additional application forms can be obtained from the ARRS offices in Reston, VA.

Business Office

Paul R. Fullagar, Executive Director, American Roentgen Ray Society, 1891 Preston White Dr., Reston, VA 22091; (703) 648-8992; 1-800-438-2777.

Mark Your Calendar Now!

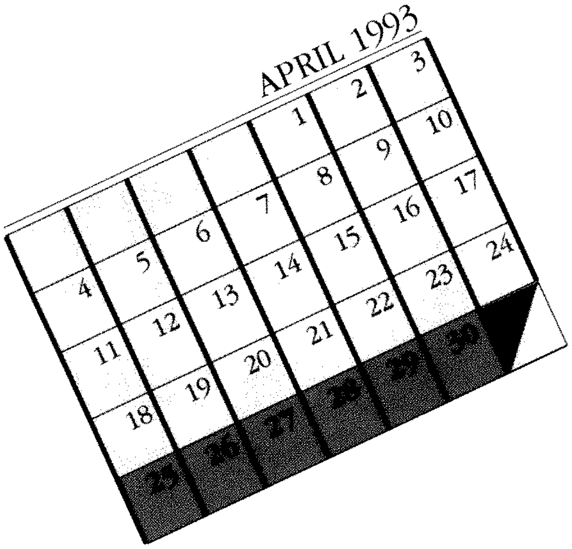

The American Roentgen Ray Society will return to San Francisco in 1993, and plans are already underway for what promises to be an educationally fulfilling and socially enjoyable week in the city by the bay. Look for the San Francisco logo in the next several issues of the *AJR* for updated meeting information.

Call for Papers

Abstracts of papers to be considered for the scientific program must be submitted by November 1, 1992. Abstract forms and instructions for submission are included in the July through October issues. The *AJR* has first rights to all papers accepted for presentation at the ARRS meeting.

Call for Scientific Exhibits

The deadline for submission of abstracts to be considered for scientific exhibits is November 1, 1992. Abstract forms and instructions for submission are included in the July through October issues.

Categorical Course

The topic of the 1993 Categorical Course is Ultrasound. A summary of topics and faculty for this course will appear in the February 1993 issue of the *AJR*.

Refresher Courses

Plans are underway to present at least 60 instructional courses on various topics of interest to the radiology community. A summary of these courses will be included in the February *AJR*. Early registration is strongly suggested, as these courses fill up quickly.

Residents' Award Papers

The society offers three cash awards for the best scientific papers prepared by residents in radiology. The President's Award has a cash prize of $2,000, and there are two Executive Council Awards with a cash prize of $1,000 each. The winners of these three awards are invited to present their papers during the opening ceremonies at the annual meeting. Papers must be submitted by February 12, 1993, for consideration in this competition. For additional information on these awards, contact the ARRS administrative offices at 1-800-438-2777.

Local Arrangements

The San Francisco area offers many opportunities for sightseeing, shopping and entertainment. Check the February *AJR* for detailed information on local tours developed especially for ARRS meeting attendees.

Registration and Hotel Reservations

All meeting activities will take place in the beautiful new San Francisco Marriott, centrally located on Market Street. The society has negotiated special room rates for meeting attendees, and the February *AJR* will contain meeting registration and hotel reservation forms. As in previous years, early registration is strongly suggested.

Travel

The society will make arrangements with United Airlines and a major car rental firm for preferred rates for meeting attendees. Taking advantage of these special rates benefits both you and the society – you save money on your reservations, and the society receives discounts to send staff and supplies to the meeting. Plan now to check the February issue of the *AJR* for details.

Classified Advertisements

Positions Available

GADSDEN RADIOLOGY ASSOCIATES is a 3-member radiology group seeking a fourth board-certified/eligible radiologist. Gadsden Radiology covers Baptist Memorial Hospital, a 250-bed hospital performing more that 55,000 radiologic exams/yr. All radiologic modalities are available, including state-of-the-art CT, SPECT, nuclear medicine, special procedures, and MRI. Gadsden Radiology Associates also covers their private office, imaging center, and a breast center. Teleradiography is used for call. Gadsden, AL, is a safe, clean city centrally located on the Coosa River approximately 1 hour from Birmingham, 90 Min. from Chattanooga, and 2 hours from Atlanta, GA. Salary and vacation are excellent. Health insurance and malpractice is paid. Interested candidates contact Homer A. Spencer, M.D., 401 Bay Street, Gadsden, AL 35999; (205) 543-3200, or fax (205) 546-7908. 7–1ap

BC/BE RADIOLOGIST—Busy clinic-and hospital-based practice is seeking to add additional BC/BE radiologists to its staff of 2 neuroradiologists and 7 general radiologists. Special skills or training in pediatrics, MRI, or nuclear medicine would be beneficial. Physician will join a 270-physician multispecialty group representing over 50 specialities. Fargo Clinic is affiliated with St. Luke's Hospitals, a 400-bed level III care center with a NACHRI designated Children's Hospital. Fargo-Moorhead is a tri-college community of 130,000 which supports an opera company, symphony, community theater, and various athletic events. Year-round recreational opportunities abound. Guaranteed first year salary and competitive compensatory arrangements are available. Respond to Kathleen Toft, Physician Recruitment Director, 737 Broadway, Fargo, ND 58123; (800) 437-4010, ext. 2151. 7–10xa

CENTRAL WISCONSIN—Established radiology group in independent practice is seeking 2 additional radiologists for growing practice in central Wisconsin. All imaging modalities. Competitive first yr salary with full partner status available second yr. Full benefits. Excellent schools, recreation, and quality of life. Contact David E. Enerson, M.D., 900 Illinois Ave., Stevens Point, WI 54481; (715) 346-5140 or Andrew M. Lucas, M.D., 410 Dewey St., Wisconsin Rapids, WI 54495-8080; (715) 423-6060. 10xa

MRI CLINICAL RESEARCH DIRECTOR—Roswell Park Cancer Institute is seeking an MRI clinical research director with interest in oncologic imaging. The radiology dept. includes a recently built GE MRI and research center linked with 2 new GE Hi-Light Advantage CT systems. This is part of an MRI, CT, SPECT Cancer Imaging and Research Center. PET collaboration with a nearby university is also possible. At this renowned comprehensive cancer center, opportunity for research and academic activity is outstanding. A faculty appointment will be at the School of Medicine and Biomedical Sciences, State University of New York at Buffalo, according to the level of professional qualifications. Please send CV to Andrew A. Gage, M.D., Deputy Institute Director, Roswell Park Cancer Institute, Elm and Carlton Streets, Buffalo, NY 14263. EOE M/F/H/V. 7–10ap

DIAGNOSTIC RADIOLOGY AND BREAST IMAGING—Roswell Park Cancer Institute is seeking board-certified radiologists with interests in oncologic and general radiology, CT/MRI, ultrasound, and breast imaging. The modernization of the entire Radiology and Nuclear Medicine Depts. includes a new multidisciplinary Breast Imaging Center, a new MRI Center, and new CT, ultrasound and flouroscopy suites. At this renowned comprehensive cancer center, opportunity for multimodality clinical diagnostic imaging, research and academic activity is outstanding. A faculty appointment will be at the School of Medicine and Biomedical Sciences, State University of New York, according to the level of professional qualifications. Please send CV to Andrew A. Gage, M.D., Deputy Institute Director, Roswell Park Cancer Institute, Elm and Carlton Streets, Buffalo, NY 14263. EOE M/F/H/V. 7–10ap

NEURORADIOLOGIST—Unique opportunity to join expanding N.Y.C. area practice. Board-certified radiologist with 2-yr fellowship in neuroradiology needed to head section of neuroradiology. This well-established university affiliated practice includes 9 board-certified radiologists practicing in a 487-bed teaching hospital and 2 private offices performing approximately 110,000 procedures/yr. State-of-the-art imaging equipment including 1.5-T GE Signa. Competitive salary leading to full equal partnership. Contact Jorge G. Pardes, M.D/William G. Wolff, M.D. Booth Memorial Medical Center; (718) 670-1594 or 1050. 7–10ap

FAIRBANKS, AK—Four diagnostic radiologists seek fifth partner for diversified practice including general radiology, ultrasound, nuclear medicine, MRI (GE 1.5-T), and CT (GE 9800). Hospital and office practice. Desirable life style advantages in a university town. Unlimited access to the outdoors. Excellent salary, benefits, retirement, and vacation. One yr to full partnership. Contact Douglas Hutchinson, M.D., 1919 Lathrop #5, Fairbanks, AK 99701; (907) 452-5092. 8–1ap

ISRAEL, DIAGNOSTIC RADIOLOGY—Opportunities for 3- to 4-wk or longer working vacations in a number of Israeli medical centers, on a volunteer basis. Positions varied, arrangements flexible. For information contact Jonathan H. Fish, M.D., 1844 San Miguel Dr., #302, Walnut Creek, CA 94596; (510) 947-0560. 8–10xa

SUPERB PARTNERSHIP POSITION IN LAS VEGAS—Rapidly expanding 7-member group practice covering 2 full-service imaging centers and a small hospital has an immediate opening. We are looking for an additional board-certified radiologist with an uncommon dedication to excellence in patient care. Our outpatient facilities include 2 MR, 2 CT, angio with a 4-bed recovery area, 5 ultrasound, 5 mammography, 3 SPECT, plus R&F. This is an excellent opportunity for a partnership position with a well-respected group in a growing community. Please send CV to Dr. Mark Winkler, SDMI, 2950 S. Maryland Pkwy., Las Vegas, NV 89109. 3–2ap

BOSTON—Expanding private-practice group. No night or evening call. Need experience in mammography. Great lifestyle. Salary leading to equal partnership. Send letter and CV to Box E49, *AJR* (see address this section). 5–10a

PARTNERSHIP POSITION IN PALM SPRINGS, CA—Well-established, 9-member group has openings for 2 board-certified radiologists. A physician with a strong background in MRI is sought as director of the section of MRI. The other position requires a physician with mammography experience to direct imaging in the breast health section of a new comprehensive cancer center. The group covers a 350-bed hospital and 2 offices in a desirable, rapidly expanding area of southern California. MRI facilities include 1.5-T Picker Vista HPQ with MRA package, ViStar imaging computer, and 1.5-T GE Signa. Other equipment includes 3 CT, a Cemax image processor, 2 Acuson color-flow Doppler ultrasound, 4 nuclear cameras including 2 SPECT, and all other diagnostic modalities. Ground has just been broken on a new 25,000 sq. ft. radiology wing, which will be furnished with state-of-the-art equipment. New trauma center, cancer center, and rehab hospital being built. Excellent compensation and benefits package leading to full partnership. Beaches and large-city amenities of Los Angeles only 2 hr away. Yr-round sunny weather. Ample free time to enjoy southern California and the unparalleled recreational opportunities offered by the resort community of Palm Springs. Direct inquiries to Curtis E. Manning, M.D., Desert Hospital, Dept. of Radiology, 1150 N. Indian Canyon Dr., Palm Springs, CA 92262. 10xa

COASTAL FLORIDA, IMMEDIATE OPENING FOR BC DIAGNOSTIC RADIOLOGIST to join 2-man group in single-site practice at well-equipped 110-bed hospital in small east coast community 60 miles from Orlando and Disney World. Relaxed practice includes all aspects of general radiology, including MRI. Excellent fringe benefits and early partnership. Contact Alan J. Stern, M.D. or Joseph E. Godard, M.D., P.O. Box 933, New Smyrna Beach, FL 32170; (904) 427-3401. 7–10ap

DIAGNOSTIC RADIOLOGIST, ABDOMINAL IMAGING—The University of Missouri– Columbia Hospital and Clinics is seeking a radiologist with expertise in abdominal imaging (GI, CT, ultrasound, and MRI). Board-certification required. Fellowship desirable. Tenure and non-tenure tracks available at assistant and associate professor levels. Address inquiries to Robert J. Churchill, M.D., Dept. of Radiology, University of Missouri—Columbia Hospital and Clinics, One Hospital Dr., Columbia, MO 65212. An equal opportunity/affirmative action employer. 5–10ap

TWO DIAGNOSTIC RADIOLOGISTS, WASHINGTON—Prominent, 100-physician multispecialty clinic in Pacific Northwest seeks both a diagnostic radiologist and an interventional radiologist. Interventional radiologist should have fellowship training and/or extensive experience in interventional radiology. Diagnostic radiologist should have general radiology experience to include all full-scope imaging services. Guaranteed salary and partnership track available. Excellent benefit package. Abundant 4-season recreational opportunities. Send CV to Fred Bockenstedt, M.D., P. O. Box 489, Wenatchee, WA 98807. 5–10ap

SAN ANTONIO, TEXAS—Large group covering multiple hospitals and outpatient facilities seeks radiologists with angiography skills. Send CV to Search Committee, M&S X-Ray Associates, P.O. Box 15920, San Antonio, TX 78212-9510. 7–12ap

SOUTH CENTRAL FLORIDA—Immediate opening for board-certified (or eligible with intention to certify), Florida licensed general diagnostic radiologist. Four radiologists are now covering 3 hospitals totaling 250 beds as well as private diagnostic office with mammography. Onsite MRI at 1 hospital and mobile unit at another. Expertise in all modalities including interventional and angiography. Competitive package including early partnership. Send CV to Lawrence S. Ross, M.D., Radiology Consultants, P.A., 114 Medical Center, Sebring, FL 33870. 10xa

CENTRAL NEW JERSEY, IMMEDIATE OPENING—Full-time and part-time radiologists with fellowship training or equivalent experience in vascular/interventional and/or in MR imaging to join 6-member group. Must be willing to do other aspects of diagnostic radiology, mammography, ultrasound, CT, and nuclear medicine. Practice includes a 340-bed community hospital, a private radiology office, and an MRI facility. Area is within a 10-mi. radius of Princeton and is near New York City and Philadelphia. Competitive salary, excellent benefits, and partnership opportunity. Send CV or call Margaret M. Beck, Business Manager, 2127 Hamilton Ave., Trenton, NJ 08619; (609) 587-9410. 10xa

DIAGNOSTIC RADIOLOGIST, NUCLEAR MEDICINE—500-bed hospital Midwest-based private practice radiology group seeking applications for a BE/BC radiologist with nuclear medicine competency and interest. Successful applicant will devote 50% of their time to nuclear medicine and remaining involved in diagnostic radiology. Nuclear medicine dept. utilizes state-of-the-art SPECT and planar equipment to support a wide range of imaging studies including nuclear cardiology. Equipment includes a majority of Siemens cameras and computers as well as a Trionix Triad camera. Imaging studies available include new heart agents and monoclonal antibodies. Excellent salary, benefits, retirement and vacation. Interested candidates should send CV and references to James E. Call, M.D., Radiology Nuclear Medicine, Inc., 622 Doctors Building, 4239 Farnam St., Omaha, NE 68131. 8–10ap

MUSCULOSKELETAL RADIOLOGIST—University of Arkansas for Medical Sciences, University Hospital, and McClellan Veterans Administration Hospital. This 14-person group in a large tertiary-care medical center seeks musculoskeletal radiologist. The 800-bed complex, receiving referrals from the entire state of Arkansas and from surrounding states, offers full service radiology depts., including digital fluoroscopy, nuclear medicine (with SPECT), Acuson ultrasound with color Doppler, GE 1.5-T MRI, and GE, Picker, and Phillips CT scanners. Position is for director of the musculoskeletal radiology division and includes musculoskeletal MR, CT, and interventional/biopsy cases, as well as 1 academic day per week. A 1- or 2-yr fellowship in musculoskeletal radiology is suggested; salary and academic intensity are negotiable. Little Rock is a medium-sized city in the foothills of the Ouachita Mountains with little traffic and clean air and water. Please send letters and CV to Richard E. Leithiser, Jr., M.D., Associate Professor of Radiology, University of Arkansas for Medical Sciences, 4301 West Markham, Little Rock, AR 72205. 8–10a

MAINE—BC/BE diagnostic radiologist with MRI and/or interventional skills. Join well-established multidimensional group. Associate leading to partnership. Competitive financial package. Family oriented small city. Business and cultural center. Major university. One hour to coast. Easy access to ski areas. Send CV to New England Health Search, 63 Forest Ave., Orono, ME 04473; (207) 866-5680. 10xa

PEDIATRIC RADIOLOGIST-CHILDREN'S HOSPITAL OF LOS ANGELES—Several faculty positions are available in pediatric radiology including ultrasound, MR, CT, and angiography/interventional radiology, and a position as a second pediatric neuroradiologist. CHLA is a 331-bed primary and tertiary-care hospital with pediatric and surgical programs. Faculty appointments are at the University of Southern California. The dept. is fully equipped with modern equipment including color Doppler ultrasound, CT, and a 1.5-T magnet. Approximately 100,000 radiologic studies are performed annually. Residency training and a fellowship training program are in place with an active teaching program. CHLA is a EOE/AA employer. For information write to Beverly P. Wood, M.D., Radiologist-in-Chief, Dept. of Radiology MS #81, Children's Hospital Los Angeles, 4650 Sunset Blvd., Los Angeles, CA 90027. 8–10a

DIAGNOSTIC RADIOLOGIST with skills in CT, MR, interventional, ultrasound, and nuclear medicine needed to join group of 8 board-certified radiologists. Growing practice in eastern Washington at a 228-bed hospital, a new multimodality imaging center and 1 private office. Potential for long-term practice is excellent. Top-notch school system, including 3 first-rate universities. Excellent hunting, fishing, boating and skiing. Contact Eric W. Koelsch, N. 5901 Lidgerwood, Ste. 18B, Spokane, WA 99207; (509) 487-1264. 8–1ap

VASCULAR/INTERVENTIONAL RADIOLOGIST—The University of Arizona Dept. of Radiology is recruiting a fellowship-trained vascular/interventional radiologist to join the faculty at the assistant associate professor level. Facilities at the University Hospital (300-bed) and Tucson Veteran's Hospital (300-bed) are state-of-the-art. Income is based on AAMC guidelines, but is negotiable. Contact Gerald D. Pond, M.D., Head, Section of Vascular and Interventional Radiology, University of Arizona Health Sciences Center, Tucson, AZ 85724; (602) 626-6794. Women and minorities are encouraged to apply. The University of Arizona is an EEO/AA employer. Applications will be accepted until position is filled. 10xa

NW ROCKY MOUNTAINS—Highly respected 8-person group with strong subspecialty interests seeks highly qualified radiologist. Fellowship or academic experience preferred. Body imaging/MRI or nuclear medicine with boards or ABR special competency strongly desired. Position includes all aspects of radiology. Practice is located in Boise, ID , which has many recreational and cultural amenities. Reply to Paul Traughber, M.D., or J. Tim Hall, M.D., Dept. of Radiology, St. Alphonsus Regional Medical Center, 1055 No. Curtis Rd., Boise, ID 83706; (208) 378-2161. 8–1a

EXCELLENT OPPORTUNITY FOR FULL-TIME BREAST IMAGING RADIOLOGIST—The Dept. of Diagnostic Radiology of Henry Ford Hospital in Detroit is seeking a board-certified radiologist with subspecialty training or expertise and experience in breast imaging. The Henry Ford Health System in the Metropolitan Detroit area performs over 35,000 mammograms annually. The Breast Imaging Division also performs breast sonography and fine needle aspiration cytology. We are a subspecialized dept. with large residency and fellowship programs, including mammography. There is opportunity for clinical research. Eligibility for or licensure by the State of Michigan is required. Please contact Murray Rebner, M.D., Director of Breast Imaging, Dept. of Diagnostic Radiology, Henry Ford Hospital, 2799 W. Grand Blvd., Detroit, MI 48202-2689; (313) 876-1331, fax (313) 876-9134. The Henry Ford Health System is an equal opportunity institution. 8–10 ap.

BC/BE DIAGNOSTIC RADIOLOGIST—Immediate opening with a well-established 12-person private hospital-based radiology group seeking diagnostic radiologist. Group is affiliated with 710-bed teaching medical center. Hospital is a tertiary referral center and a designated trauma center. Outstanding professional, financial and lifestyle opportunities with outstanding schools are available to qualified candidate. You may call Mariann Clark, Medical Search Consultant, at (800) 882-5911 or reply to Box 90 *AJR* (see address this section) 9–10a

OVERWORKED? Need a higher income and more vacation time? Tired of big city commuting and inner-city crime? Want a better quality of life but still want a professional challenge? We need a BC, capable, motivated radiologist qualified in all phases of diagnostic radiology but with special interest, ability and preferable fellowship training in MR to join a 7-member group of American trained, BC radiologists in 450-bed tertiary-care hospital, located in 125,000 populated city, 1 1/2 hrs from Pittsburgh and 3 1/2 hrs from DC and Baltimore. We do 100,000 exams/yr with state-of-the-art equipment. Generous starting salary and benefit package with complete and equal partnership to follow. If interested, send CV to Jon Abrahams, M.D., Chairman, Dept. of Radiology, Conemaugh Hospital, Johnstown, PA 15905; (814) 536-7226. 9–11ap

PART-TIME RADIOLOGIST—General diagnostic radiology; no call; no angiography; several half days per week; hours flexible; state-of-the-art-equipment; large community hospital, southern Chicago suburb. Interested individuals should contact Peter Kucharski, M.D., Dept. of Radiology, Ingalls Hospital, Harvey, IL 60426; (708) 333-2300, ext. 5600. 9–1lap.

EASTERN VIRGINIA—Position available for BC/BE diagnostic radiologist with interest/specialty training in body imaging and MR. Experience in all modalities needed and capability for basic angiography call. Practice includes full service regional medical center, multiple satellite offices, benefit package, and partnership tract. Location offers attractive climate and diversity for recreation. Send CV with initial correspondence to D. T. Bartol, M.D., Dept. of Radiology, Riverside Regional Medical Center, J. Clyde Morris Blvd., Newport News, VA 23601. 9–10ap.

FULL-TIME BC/BE DIAGNOSTIC RADIOLOGIST needed to replace retiring senior partner in a friendly, cooperative 4-man group in south-central Idaho. 165-bed hospital with GE Signa 1.5-T MR, GE 9800 quick CT, Acuson XP, and good technical staff. General radiology including angio, interventional, and nuclear medicine. Good income and vacation schedule 1 yr to partnership. Nice community with extensive nearby skiing, hunting, fishing, etc.,80 miles from Sun Valley, 4 hrs drive from Yellowstone. Send CV and references to Dr. Evan Thomas, Southern Idaho Radiology, P.O. Box AB, Twin Falls, Idaho 83303. 9–11ap

RESIDENT—Due to an unexpected vacancy, the University of Missouri-Kansas City will have an opening for a 2nd, 3rd, or 4th yr radiology resident, beginning January 2, 1993. The UMKC Radiology Residency program is an accredited program and has been in existence for approximately 7 yrs. Truman Medical Center - West is the primary teaching hospital for the program. Applicants must be eligible for Missouri licensure. Competitive salary and benefits. Please forward your CV and letter of interest to Kenneth Alfieri, M.D., Residency Program Director, Truman Medical Center, Dept. of Radiology, 2301 Holmes, Kansas City, MO 64108. 9–11a

NUCLEAR MEDICINE—RADIOLOGIST—CALIFORNIA—Immediate opening for diagnostic radiologist with nuclear medicine boards or special competency in growing private practice in the San Fernando Valley 20 minutes north of UCLA. Candidate to supervise growth of nuclear medicine dept. in addition to general diagnostic radiology work. Full partnership tract with excellent salary. Practice includes hospital and imaging centers. Group consists of young enthusiastic radiologists all with fellowship training. Equipment includes Sopha Spect nuclear, GE 1.5-T MRI with angio, 2 Acuson ultrasound, Siemens Angiostar specials, and 2 Picker 1200 CT scanners. Send CV to T. Sprague M.D., Holy Cross Medical Center, 15031 Rinaldi St., Mission Hills, CA 91345;.fax (818) 898-4451. 9–2ap

IMMEDIATE OPENING—BC/BE diagnostic radiologist to join 8 board certified radiologist incorporated practice covering 3 hospitals with approx. 700-beds and 100+ physician multispecialty clinic. All modalities represented. Must be willing to participate in all aspects of general radiology. Excellent fringe benefit package with competitive salary leading to early shareholder status at modest buy-in. Practice located in Arkansas River Valley. Excellent public and private schools. Send CV or contact June Martin, Business Manager, Radiology Services, P.A., P.O. Box 1827, Fort Smith, AR 72902; (501) 782-5035. 9–11ap

BEAUTIFUL COAST OF MAINE—Excellent opportunity for full-or part-time BC/BE radiologist to work with established radiologist in private practice. Pleasant community, yr-round recreational area, smog free, low crime environment. Fully accredited, multispecialty acute care hospital serving 25,000. All modalities of diagnostic radiology offered. Mobile nuclear medicine and MRI currently being pursued. Approximately 15,000 exams annually. Send CV to Executive Director, Waldo County General Hospital, P.O. Box 287, Belfast, ME 04915; (207) 338-2500. 9–11a

INTERVENTIONAL NEURORADIOLOGIST, COASTAL VIRGINIA—A 32-physician private radiology group which practices in 6 hospitals and several offices is seeking an interventional neuroradiologist who is eligible for senior membership in the American Society of Neuroradiology. The individual's clinical responsibilities would be primarily limited to a 644-bed tertiary-care center with level 1 trauma status. Diagnostic equipment includes 2 state-of-the-art Signa 1.5-T GE MR scanners (4.79 software and angio package), a DFP 60A bi-plane bi-digital 1024 matrix Toshiba DSA system (with digital stereo capabilities), and a Siemens DRH as well as a GE 9800 CT scanner. Some time would be spent at a 250-bed hospital with a Hitachi MRP-5000 0.2-T MR unit and a GE 9800 CT scanner with Hi-Light advantage software. Two (2) year fellowship trained neuroradiologists are already on staff. The practice is affiliated with a medical school and residency program which allows the pursuit of academic interests. The practice is located in a coastal resort area with a temperate climate and all water sports available. Interested persons should send a CV or contact Carl V. Bundschuh, M.D., Director of Neuroradiology and MRI, Medical Center Radiologists, Inc., 6161 Kempsville Circle, Ste. 330, Norfolk, VA 23502; (804) 466-0089. 10xa

MAMMOGRAPHER—Large private multi-hospital group in a coastal city of Virginia seeks a radiologist with special interests in all aspects of mammography. The practice includes a tertiary-care hospital which is affiliated with both a medical school and a radiology residency training program, thereby offering the benefits of both private practice and academics. The position would include directorship of future mammography clinics. Additional aptitude in other aspects of diagnostic radiology with specialized and/or fellowship training preferred. Interested applicants please send CV or inquiries to Medical Center Radiologists, Halifax Building, Ste. 330, 6161 Kempsville Circle, Norfolk, VA 23502; (804) 466-0089. 10xa

INTERVENTIONAL RADIOLOGIST—An opportunity exists for an interventionalist to join a group of 12 board-certified radiologists in their hospital and private practice. Position requires fellowship-trained interventionalist with an interest in diagnostic radiology. The practice is based in a 430-bed community hospital with 2 private offices and a hospital owned satellite facility. Services include 2 MRI units, 2 CT units, 2 SPECT cameras, and a new interventional suite with an established interventional practice. Bethlehem is 1 of 3 cities situated in the Lehigh Valley which is within close proximity of NY and Philadelphia. Contact G. Edward Streubert, M.D., Bethlehem Radiologists Associates, 95 Highland Ave., Ste. 105, Bethlehem, PA 18017. 4–12ap

SOUTHEAST PENNSYLVANIA/CENTRAL NEW JERSEY—Established state-of-the-art multi-hospital and private office practice seeks diagnostic radiologist with interest in all aspects of general radiology. Also seeks individual with subspecialty expertise in angio/interventional or nuclear medicine. Full or part time position. Excellent access to Philadelphia and NYC areas. Send CV to S. Meshkov, M.D., 838 W. State St., Trenton, NJ 08618. 9–11a

DIAGNOSTIC RADIOLOGIST, COASTAL DOWNEAST MAINE—We'd rather pay recruiting fee to you than to agency. Call for details. Opening for BC/BE radiologist at progressive small rural hospital; college community. Solid financial opportunity. Will tailor arrangements to fit candidate's desire. Contact administration, Down East Community Hospital, Machias, ME 04654; (207) 255-3356. 9–12ap

THE FALLON CLINIC—New England's most respected physician owned and directed multi-specialty group practice seeks 2 BC/BE diagnostic radiologists to join the dept. of 6 currently performing over 108,000 studies this year. Competence and interest in CT, ultrasound and mammography required. No night call. Excellent lifestyle, salary and benefits. Send CV to Stephen Patton, Recruitment Manager, 100 Central St., Worcester, MA 01608. 9–10a

IMMEDIATE OPENING FOR BC/BE DIAGNOSTIC RADIOLOGIST, NEW ENGLAND, to join a 6-member group, leading to partnership, in an active community, university-affiliated hospital. Over 100,000 exams/yr. Practice includes CT, ultrasound, nuclear medicine, MRI, angiography, and interventional. Locum needed in interval. Located in New England close to boating and skiing, 1 hr from Boston. Contact Allan M. Deutsch, M.D., Dept. of Radiology, The Miriam Hospital, 164 Summit Ave., Providence, RI 02906; (401) 331-8500, ext. 4400. 9–11ap

IMMEDIATE OPENING—The Dept. of Radiology at the University of Massachusetts Medical Center has a full-time position available in the musculoskeletal division at a rank and salary commensurate with experience. The medical center is a 370-bed university hospital and medical school located approximately 40 miles west of Boston. The dept. consists of 25 staff, 15 residents, and 24 fellows and does approximately 140,000 exams/yr. The dept is well-equipped with 2 GE 9800 HiLite CT scanners as well as 2 GE 1.5-T MRI scanners and a 2.0-T small-bore unit for animal research in a stand-alone facility. The hospital is a Level I trauma center maintaining a full-time trauma service and an active emergency room with an associated emergency medicine residency of approximately 36 residents. The hospital is serviced by a Life Flight helicopter. A strong interest in teaching and collaborative clinical research is desired. For further information contact Edward H. Smith, M.D. Professor and Chairman, Dept. of Radiology, University of Massachusetts Medical Center, 55 Lake Ave. North, Worcester, MA 01655; (508) 856-3253. UMMC is an equal opportunity/affirmative action employer. 10a

DIAGNOSTIC RADIOLOGIST—Yale University School of Medicine is seeking a board-certified radiologist with additional experience or training in body MRI/ultrasound/CT for full-time faculty position. Academic rank is at the level of assistant or associate professor, depending upon qualifications. Candidates must be United States Citizens or qualify as permanent residents in the United States. Please send CV and bibliography to Dr. Shirley McCarthy, M.D., Ph.D., Diagnostic Radiology, Yale University School of Medicine, 333 Cedar St., New Haven, CT 06510. Yale University is an equal opportunity/affirmative action employer applications from women and minority group members are encouraged. Application deadline is October 31, 1993. 10a

CHIEF, NEURORADIOLOGY ASSOCIATE PROFESSOR/PROFESSOR OF RADIOLOGY IN RESIDENCE UNIVERSITY OF CALIFORNIA, SAN FRANCISCO—The University of California, San Francisco (UCSF) is seeking a chief of neuroradiology. The candidate will be appointed at the level of associate professor or professor of radiology in residence depending on qualifications, and will also serve as Vice-Chairman of the Dept. of Radiology at UCSF. The chief of neuroradiology must have a demonstrated national research reputation in neuroradiology, be an excellent teacher, and be an experienced administrator who will supervise all clinical, teaching and research programs in neuroradiology at USCF and 3 other core affiliated teaching hospitals in San Francisco. The candidate would be board-certified by the American Board of Radiology and experienced in the performance and interpretation of CT scans, MR scans, myelograms, and angiographic procedures. The candidate must also hold a California Medical License. The University of California is an equal opportunity/affirmative action employer, minority groups, women, and handicapped individuals are encouraged to apply. Send CV to Roy L. Cordon, M.D. Chair, Search Committee, UCSF, Dept. of Radiology, San Francisco, CA 94143-0628. 10a

NASHVILLE, TENNESSEE—Fourteen-member group seeks 2 additional associates. One with MRI fellowship training who has interest in musculoskeletal imaging. Another with fellowship training willing to divide time between area of expertise and general radiology. Practice consists of 576-bed adult tertiary-care hospital and 2 outpatient offices. 192,000 exams last yr. All aspects of radiology currently in effect. Two new GE Signa MRIs; 2 new GE 9800 Advantage and 2 new 9800 quick highlite CTs. Start between now and July 1993. Contact Gary Bienvenu, M.D., 28 White Bridge Rd., Ste. 209, Nashville, TN 37205. 10a

STAFF POSITION/INTERVENTIONAL RADIOLOGY—Board-certified radiologist with fellowship training in vascular/interventional radiology for position to start as soon as possible. Academic rank is at the assistant or associate professor level depending on qualifications. This active clinical service (currently 3 staff, 3 fellows) performs an entire range of diagnostic and interventional procedures including embolization, angioplasty, atherectomy, stenting, infusion therapy, IVC filter placement, endourology, and biliary and abscess management. The interventional inpatient service admits 100 patients per yr, primarily for embolization and angioplasty. The interventional clinic evaluates referred patients with peripheral and renal vascular disease, and vascular malformations. Clinical and fundamental research interests are ongoing in atherectomy, embolization devices, new chemoperfusion catheters, endourology and endobiliary techniques. Please send applications with CV to Dr. Jeffrey Pollak, M.D., Section Chief or Robert I. White, Jr., M.D., Professor and Chair Dept. of Diagnostic Radiology, Yale University School of Medicine, 333 Cedar St., P.O. Box 3333, New Haven, CT 06510; (203) 785-4746; (203) 785-3024 fax. Yale University is an equal opportunity/affirmative action employer. Applications from women and minority group members are encouraged. Application deadline is October 31, 1992. 10a

DIAGNOSTIC RADIOLOGIST, to replace retiring partner in 2-person hospital based practice in Virginia. General radiology including angio, CT, ultrasound, SPECT and MR. Excellent income and early partnership. Very pleasant working environment in a rural hospital with a wide referral base. Great outdoor recreation area, within easy reach of large cities. Position available July '93. Address all inquiries to Jeff Beavers, M.D., 933 Pace Dr., South Hill, VA 23970. 10a

DIAGNOSTIC RADIOLOGIST WITH FELLOWSHIP TRAINING OR SPECIAL INTEREST/TRAINING—We are seeking board-certified individuals to add depth in certain areas of our practice. If you are currently looking for a change in employment, or if you will complete a fellowship or a residency with special interest/training in 1993 or 1994 in any of the following areas, please contact us, vascular interventional, musculoskeletal, ultrasound, neuroradiology. The group is based in Bloomington, Indiana, a beautiful big 10 university community of 50,000+ population, 1 hour from major metro area. Ten diagnostic radiologists servicing 2 hospitals, 1 outpatient center and other sites. Primary hospital has state-of-the-art equipment including 1.5-T MR. Send CV to, or contact, Phil Russell, P.O. Box 4366, Bloomington, IN 47402-4366; (812) 334-8948. 10–12ap

ULTRASOUND/CT/MRI—Opportunity for board-certified radiologist specializing in ultrasound, body CT, and body MRI to pursue academic career at the New York Hospital-Cornell Medical Center. Dept. provides state-of-the-art equipment, including Acuson and ATL ultrasound, GE 9800 CT, and GE Signa 1.5-T MR. Wide variety of ultrasound examinations include abdominal, OB/GYN, color Doppler, small parts, neonatal head, transvaginal, and transrectal. Prefer candidate with prior fellowship in sectional imaging or ultrasound. Responsibilities include clinical practice, teaching, and research. Position available 7-1-93. Please send CV to Elias Kazam, M.D., Dept. of Radiology, New York Hospital-Cornell Medical Center, 525 East 68th St., New York, NY 10021. 10–1a

BREAST IMAGING - THORACIC IMAGING AT YALE—Immediate opening for academically oriented radiologist with interest in mammography and thoracic radiology. Large screening and diagnostic program performing over 14,000/exams per yr. Mobile unit, mammography outpatient screening, stereotactic biopsy and ultrasound. Emphasis on quality assurance, auditing and computer applications in breast imaging. Strong clinical research collaboration with Yale Comprehensive Cancer Center and MRI. Thoracic imaging program offers integrated experience in conventional and cross-sectional techniques, including CT and MRI. Diffuse lung disease clinic offers research opportunities in high resolution CT. Access to interventional procedures and nuclear medicine. Yale University School of Medicine is an affirmative action/equal opportunity educator and employer. Applications from women and minority group members are encouraged. Qualified candidates send CV and contact Dr. Irena Tocino, Yale University School of Medicine, Dept. of Diagnostic Radiology, 333 Cedar St., New Haven, CT 06510. Application deadline is October 31. 1992. 10a

DIAGNOSTIC RADIOLOGIST, NEW MILFORD, CT—A third radiologist is sought for a busy, private practice located in one of the most beautiful areas of Connecticut. We provide the full range of diagnostic services for a modern, well-equipped, community hospital. Choice environment; excellent compensation. Send inquiries and CV to Jules White, M.D., New Milford Hospital, 21 Elm St., New Milford, CT 06776; (203) 355-2611, ext. 235. 10–1a

DIAGNOSTIC RADIOLOGIST for busy expanding 8 radiologist group in picturesque Gulf Coast community. Must have experience in all aspects of diagnostic radiology including angio/interventional/nuclear and MRI. Contact William Nyman, M.D., P.O. Box 1175, New Port Richey, FL 34656-1175. 1011a

WORK HARD AND PLAY HARD IN BEAUTIFUL SANTA FE, NM—Medical director position available at state-of-the-art outpatient imaging center with a 1.5-T Siemens SP MRI, DRH CT scanner, Acuson ultrasound, with R&F and mammography to fill in the gaps. Excellent salary and benefits for the individual willing to be proactive and competitive. Neuroradiologist with extensive MRI training MANDATORY. Call Jim Lester at (505) 983-9350 for more details or send CV to Santa Fe Imaging Center, 1640 Hospital Dr., Santa Fe, NM 87501. 10a

PART-TIME/LOCUM TENENS DIAGNOSTIC RADIOLOGIST NEAR NORTH CAROLINA COAST—High quality, amiable, hospital-based 2-man practice seeks well-trained BC/BE radiologist. Practice encompasses all imaging modalities but expertise in all modalities not required. Work schedule flexible. One hour to beautiful beaches. Send CV, inquiries to *AJR* Box # 101. (address this section) 10ax

PART-TIME PEDIATRIC/GENERAL RADIOLOGIST, CENTRAL MASSACHUSETTS—Radiologist sought with special competence in pediatric radiology to join an 11-member group. We serve a 550-bed medical center that includes the regional 40-bed neonatal intensive care unit. Position involves sharing general responsibilities including CT, ultrasound, and mammography. Part-time position may become full-time. Please send CV to Richard Danford, M.D., Worcester Radiologists, 121 Lincoln St., Worcester, MA 01605; (508) 753-8151. 10–12a

THE COMMONWEALTH OF THE NORTHERN MARIANAS ISLANDS located in the western Pacific is seeking a radiologist to join the staff of the modern 74-bed hospital. Facilities include flouroscopy, mammography, ultrasound, echocardiography and a CAT scanner will soon be added. Hospital staff includes 35 physicians with major specialities represented. Physician will be living on Saipan, an 89 square mile island with a population of 40,000 representing many ethnic groups, languages and cultures. Climate is always warm with temperatures in the 80's and occasional typhoons. There are many first class resorts and a variety of ocean sports available. Salary, benefits including free housing, hours and working conditions are favorable. Taxation lower than U.S. Transportation paid. Inquire, Jose Chong, Director, Dept. of Health and Environmental Services, Box 409 Commonwealth Health Center, Saipan, M.P. 96950; (670) 234-8930 fax. 10a

MINNESOTA—A 34-member multi-specialty group is seeking a BE/BC radiologist to join our expanding physician base. We offer an excellent first year guarantee, vacation, CME time, full health/dental, board study time, money purchase pension/profit sharing trust plans, and more. Beautiful lakes, unspoiled environment and 4 season recreation await you in Virginia, MN. For more information and a video call (800) 377-3290. 10–12ap

CT AND ULTRASOUND RADIOLOGIST—The Beth Israel Medical Center, Dept. of Radiology in New York City is seeking a BC diagnostic radiologist with expertise in CT and ultrasound. The newly renovated dept. of radiology has a staff of 20 full-time radiologists. An active clinical practice, a strong teaching program as well as stimulating research opportunities are available at this 874-bed teaching hospital affiliated with the Mount Sinai School of Medicine. In addition to clinical expertise, a strong interest and ability in teaching is required. Academic rank will be commensurate with candidates qualifications and experience. Excellent remuneration and benefits. Please send inquiries with a CV to Michael M. Abiri, M.D., Deputy Director, Dept. of Radiology, Beth Israel Medical Center, First Ave. at East 16th St., New York, NY 10003. An equal opportunity employer committed to a SMOKE-FREE environment. 10a

UCSD SCHOOL OF MEDICINE—The Dept. of Radiology is seeking a cardiovascular radiologist to participate in clinical, teaching, and research programs. Qualifications required: Board-eligibility/certification; California medical license; 1-yr fellowship in cardiovascular radiology or vascular/interventional radiology. Title Series: assistant/associate professor (in-residence or clinical series); level based on years experience; salary commensurate with rank and step of appointment based on the established salary schedule of the UCSD School of Medicine Faculty Compensation Plan. The University of California, San Diego is an equal opportunity/affirmative action employer. All CV's received prior to December 31, 1992 or thereafter until position is filled will be assured full consideration. Send to Joseph J. Bookstein, M.D., Professor of Radiology, Dept. of Radiology, UCSD Medical Center, 200 West Arbor Dr., San Diego, CA 92103-1990. 10a

DEPARTMENT HEAD, RADIOLOGY—The University of Arizona College of Medicine is seeking a highly qualified academic dept. head with demonstrated ability to provide leadership and management of the educational, research, and service programs of the dept. of radiology in Tucson, AZ. An M.D. degree (or equivalent) with board-certification is required. The dept. has 40 full-time faculty and 35 part-time and voluntary faculty located in Tucson and Phoenix. There are 25 residents and fellows in training. Administratively, the dept. is divided into 12 sections, representing the major subspecialty disciplines of radiology. Women and minorities are encouraged to apply for the Headship position. Applications should include a CV with the names and addresses of at least 3 references and mailed to, M.Wayne Heine, M.D., Professor and Head, OB/GYN, Chairman, Radiology Head Search Committee, University of Arizona College of Medicine, Administration, Rm. 2206 Searches & Reviews, Tucson, AZ 85724. The review of applications begin in November, 1992, and will continue until the position is filled. 10a

ASSISTANT PROFESSOR/ASSOCIATE PROFESSOR OF RADIOLOGY IN RESIDENCE, UNIVERSITY OF CALIFORNIA, SAN FRANCISCO—The Dept. of Radiology at the University of California, San Francisco (UCSF) is seeking to fill an open position for an assistant professor or associate professor of radiology in residence (depending on qualifications) to work in the Magnetic Resonance Science Center. The candidate will be expected to develop an independent research program in magnetic resonance imaging and spectroscopy as well as to provide technical support for Magnetic Resonance Science Center Investigators. Teaching responsibilities will include training of graduate students and fellows. The candidate must possess a Ph.D. degree in the physical or biomedical sciences and have experience in nuclear magnetic resonance imaging and spectroscopy, with demonstrated abilities in the creation of a new pulse program applicable to in vivo systems. The University of California is an equal opportunity/affirmative action employer. Minority groups, women and handicapped individuals are encouraged to apply. Send CV to Thomas F. Budinger, M.D., Ph.D., Chair Search Committee, UCSF, Dept. of Radiology, San Francisco, CA 94143-0628. 10a

EXCITING RADIOLOGIST OPPORTUNITIES NATIONWIDE!—Now is the time to make your move!

specialize in RADIOLOGY only, so we understand your needs. Positions from Sunbelt to Northern-most regions. Both salaried and private practice opportunities with top money offered. Utilizing the Snelling Search Computer Network. We know of the positions first and give you the inside tracks! Fax your CV to (214) 258-1092, or mail to Snelling Search Medical Group. 1303 Walnut Hill Lane, Ste. 103, Irving, TX 75038. For information on specific positions call toll free (800) 259-5973. Ask for Roman. 10xa

MIAMI VETERANS AFFAIRS MEDICAL CENTER is seeking staff radiologists for its teaching hospital affiliated with the University of Miami School of Medicine. Candidates must be board-certified or eligible, with education and experience in CT, MRI, and special procedures. Send CV to Personnel Service (05C3/Jean Little), VA Medical Center, 1201 NW 16th St. Miami, FL 33125, (305) 324-4455, Ext. 3617. VA is EOE. 10a

SUBSPECIALTY RADIOLOGY POSITIONS—An expanding 14-man subspecialized dept. has openings for fellowship-trained individuals in its section of cardiovascular and interventional radiology and in its body imaging section. A broad scope of angiographic procedures are currently performed by 2 full-time interventionists. Two well-equipped angiography suites are available and plans for expansion/updating are underway. An adjacent, fully staffed clinical office practice is available. Three full-time body imagers have 4 CT scanners, 7 ultrasound suites, and 2 MR scanners at their disposal. The full range of imaging procedures, including obstetrical ultrasound, are performed. Openings in other specialties are available locally as well. Physician couple applications are encouraged. Please send inquiries with CV to *AJR* Box 102 (address this section) EOE/AAM/F/H/V. 10a

RESEARCH ASSOCIATE—Position available to perform research projects in therapy vascular lesions of the brain and spinal cord. Position will microsurgically create experimental aneurysms in pigs and will then treat them with various embolic materials via transfemoral catheterization. Position requires M.D. or equivalent foreign degree with 2 yrs residency in radiology and 2 yrs of experience in a similar position. Knowledge of all necessary methods for animal research, specimen preparation, etc., and elementary knowledge in vascular surgery. Experience with diagnostic and interventional procedures in neurosurgical disorders and basic skills in the use of personal computers required. Starting salary will be $24,000. Submit CV to Georgia Dept. of Labor, 1275 Clarendon Ave., Avondale Estates, Georgia 30002, or to the nearest Georgia Job Placement Center. Job Order GA 5545038. 10a

INTERVENTIONAL RADIOLOGIST—Private multispecialty group of 125-physicians with University affiliation in Upper Midwest seeks second board-certified interventional radiologist. Excellent digital angiographic, CT and MR facilities. Superb cooperation with surgical staff. At least 50% interventional with option of some general and/or neuroradiology. Salary equals 90% of partners with full partnership in 1-2 yrs. City of 60,000 population with referral base of 300,000. Send CV to Gerald Smyser, M.D., The United Hospital, Box 6002, Grand Forks, ND 58206-6002; (800) 437-5375. 10–12ap

NEUROLOGICAL CLINIC IN BLACK HILLS OF SOUTH DAKOTA—Unusual opportunity for person interested in MRI practice in small private clinic with the best equipment available. Exceptional situation for one interested in slowing down and practicing in superb environment. MRI expertise is not as essential as is the desire for training. Position available now with compensation flexible and negotiable. Other fields of radiology of personal interest to applicant could be added. Contact J. D. Sabow, M.D., Neurologist, or Alan Baldwin, Director Imaging Services, 2805 5th St., Ste. 160, Rapid City, S.D. 57701; (605) 348-7560, fax (605) 348-6449. 10–11a

THE LOUISIANA STATE UNIVERSITY MEDICAL CENTER is actively seeking candidates for ultrasound/CT/MRI, bone, chest, nuclear medicine, GI, GU, neuroradiology, angiography/interventional, emergency room, pediatrics and mammography. We are expanding our dept. significantly, and are looking for enthusiastic individuals who want to develop a more expensive clinical practice, teaching program and research activities. A perfect opportunity to shape your own section. Applicants must be BE/BC and qualify for licensure in Louisiana. Salaries are competitive nationwide. The University is developing areas of special interest, including a multidisciplinary center for study of neurosciences and plans are underway to purchase all new state-of-the-art equipment. Enjoy the cultural and jazz music of New Orleans. The beaches of Northern Florida are only 3 1/2 hrs away. LSUMC is an AA/EOE. Send CV and 3 references to Jane Clayton, M.D., Acting Chairman, Dept. of Radiology, LSUMC, 1542 Tulane Ave., New Orleans, LA 70112; (504) 568-4647 or fax (504) 568-8955. 10–1a

UCSD SCHOOL OF MEDICINE—The Dept. of Radiology is seeking a diagnostic radiologist to participate in clinical service, medical student and resident teaching, and research projects in the subspecialty of osteoradiology. Qualifications required: Board-eligibility/certification; California medical license; 1-yr fellowship in osteoradiology; 1-yr experience including MRI in osteoradiology in an academic program is preferred. Title Series: assistant professor (in-residence or clinical series - not currently a tenure-track position); level based on years experience; salary commensurate with rank and step of appointment based on the established salary schedule of the UCSD School of Medicine Faculty Compensation Plan. The University of California, San Diego is an equal opportunity/affirmative action employer. All CV received prior to December 31, 1992 or thereafter until position is filled will be given full consideration. Send to Donald Resnick, M.D., Chief of Radiology, VA Medical Center, 3350 La Jolla Village Dr., San Diego, CA 92161. 10a

NEURORADIOLOGIST—A 25-person radiologic group in central New Jersey seeks a fourth neuroradiologist well-versed in all neuroimaging modalities and procedures. Senior member status eligibility in the ASNR is required. Practice includes 2,450-bed hospital, 3 offices, 3 MRI scanners, 5 CT scanners, a radiology residency, and medical student teaching. Send CV to Richard Feinstein, M.D., c/o Kathy McGrath, Radiology Group of New Brunswick, 230 Old Bridge Turnpike, South River, NJ 08882. 10-3a

Positions Desired

BOARD-CERTIFIED RADIOLOGIST with over 5 yrs post neurofellowship multimodality experience including over 12,000 CNS, body and extremity MRI examinations. Seeking private practice with opportunities in general radiology, MRI, CT and angio. Prefer locale offering wholesome environment for young children. Respond to Box 10 *AJR* (address this section) 10b

Fellowships and Residencies

FELLOWSHIP POSITION: WOMEN'S IMAGING —High-volume breast imaging (mammography, breast ultrasound, interventional procedures) and ultrasound with emphasis on obstetrical and gynecologic sonography. State-of-the-art mammographic and sonographic equipment including stereotactic table and digital capability. Using stereotactic, ultrasound, or mammographic guidance, all breast interventional procedures are performed, including fine needle and core biopsies, cyst aspirations, presurgical localizations, and galactography. Elective time in MRI, CT, and related clinical specialties (surgery, pathology, obstetrics-gynecology). One-year fellowship to start in July 1993. Fellows also have the opportunity to participate in teaching, conference presentations, and research projects, many of which culminate in publications. Inquiries should be addressed to Ellen B. Mendelson, M.D., Chief, Mammography and Women's Imaging, The Western Pennsylvania Hospital, 4800 Friendship Ave., Pittsburgh, PA 15224. 5-12c

ONCORADIOLOGY/MAMMOGRAPHY FELLOWSHIP—The Dept. of Radiology at the Dana-Farber Cancer Institute and Brigham and Women's Hospital, which are Harvard Medical School affiliates, offers a 1-yr fellowship position beginning July 1, 1993. All imaging modalities involved in the diagnosis, staging, and follow-up of patients with malignant disease are integrated into this program. An additional feature is a concentrated experience in the performance of interventional breast diagnostic procedures. Please contact Jack E. Meyer, M.D., Director of Diagnostic Radiology, Brigham and Women's Hospital and Dana-Farber Cancer Institute, 75 Francis St., Boston, MA 02115; (617) 732-6269. Brigham and Women's Hospital/Dana Farber Cancer Institute/Harvard Medical School is an affirmative action/equal opportunity educator and employer. 5-4c

FELLOWSHIP IN VASCULAR AND INTERVENTIONAL RADIOLOGY—The University of Arizona is sponsoring a 1-yr fellowship in vascular and interventional radiology beginning July 1, 1994. In-depth clinical experience and training in all aspects of interventional radiology will be offered. Facilities at the University Hospital (300-bed) and Tucson Veterans Hospital (300-bed) are state-of-the-art. Interested applicants should submit a current CV and 3 letters of recommendation (including one from their program director) to Gerald D. Pond, M.D., Head, Section of Vascular and Interventional Radiology, University of Arizona Health Sciences Center, Tucson, AZ 85724. For further information please contact Ruth Kneup at (602) 626-6794. 10xc

FELLOWSHIPS AT THOMAS JEFFERSON UNIVERSITY HOSPITAL—The Dept. of Radiology at Thomas Jefferson University Hospital in Philadelphia offers the following fellowship programs each yr: (1) Ultrasound/CT/MRI—Jefferson's ultrasound division is one of the largest in the world and performs all currently available exams, including obstetric, vascular, lithotripsy, invasive, and endoluminal. We also operate 4 GE 1.5-T MRI units and 3 CT scanners. Contact Barry Goldberg, M.D. regarding this program. (2) Cardiovascular/interventional—This division is housed in a new suite containing Philips angio units with DSA and performs the full range of vascular and nonvascular interventional procedures. Contact Geoffrey Gardiner, Jr., M.D. (3) Neuro/ENT radiology—very active clinical services supply a wealth of material to this division, which is housed in a neurosciences imaging center containing all imaging modalities. Contact Carlos Gonzales, M.D. (4) Breast imaging—Jefferson's new breast-imaging center performs approximately 85 studies/day including ultrasound and needle localizations. Contact Stephen Feig, M.D. (5) Chest—includes biopsies and CT. Contact Robert Steiner, M.D. (6) MRI—a dedicated body MRI program including excellent research opportunities in addition to a large clinical case load. Contact Donald Mitchell, M.D. (7) Ultrasound—a dedicated ultrasound program. Contact Barry Goldberg, M.D. (8) Musculoskeletal—includes MRI of the musculoskeletal system. Contact David Karasick, M.D. All program directors listed above can be contacted at the Dept. of Radiology, Thomas Jefferson University Hospital, Philadelphia, PA 19107. Jefferson is an equal opportunity/affirmative action employer. 10xc

VASCULAR/INTERVENTIONAL RADIOLOGY FELLOWSHIP—Temple University Hospital and School of Medicine has available a 1-yr fellowship beginning July 1, 1992. The candidate will have exposure to all areas of vascular and interventional radiology including noninvasive techniques and MRI/A. Applicants should contact, David S. Ball, D.O., Chief, Section of Vascular/Interventional Radiology, Dept. of Diagnostic Imaging, Temple University Hospital, 3401 N. Broad St., Philadelphia, PA 19140. Temple University Hospital and School of Medicine is an affirmative action/equal opportunity employer. 10xc

FELLOWSHIP POSITIONS—The Dept. of Radiology of the Brigham and Women's Hospital-Harvard Medical School has 1- or 2-yr fellowship positions in the following areas: (1) cardiovascular and interventional, (2) neuroradiology, (3) CT/ultrasound/MR/interventional, (4) oncoradiology, (5) chest, (6) bone, (7) nuclear medicine, and (8) computer science. For more information, please send CV specifying your area of interest to B. Leonard Holman, M.D., Chairman, Dept. of Radiology, Brigham and Women's Hospital, 75 Francis St., Boston, MA 02115. Harvard Medical School and Brigham and Women's Hospital are equal opportunity, affirmative action employers. 5-4c

FELLOWSHIPS AT ALBANY MEDICAL CENTER—The newly-renovated and equipped Dept. of Radiology at the Albany Medical College and Center in Albany, NY, offers the following fellowship positions each yr: (1) Abdominal Imaging—This fellowship encompasses all aspects of MRI, ultrasound, CT, and other advanced techniques in imaging the abdomen. Four state-of-the-art MRI and 4 CT scanners as well as 5 color Doppler ultrasound units are utilized daily. Contact James C. Peters, M.D. regarding this program. (2) Neuroradiology—This fellowship encompasses the full range of advanced neuro imaging including MRI, CT, angiography, and myelography. Contact William A. Wagle, M.D. (3) Angiography and interventional radiology—Three advanced angiographic suites are utilized daily for a full range of vascular and interventional procedures. Contact Mohammad S. Sarrafizadeh, M.D. All program directors listed above may be contacted at the Dept. of Radiology, A-113, Albany Medical Center, Albany, NY 12208; (518) 445-3277 or contact Matthew D. Rifkin, M.D., Chairman, Dept. of Radiology, A-113, at the above address. Albany Medical Center is an equal opportunity/affirmative action employer. 1-12c

FELLOWSHIP PROGRAM IN INTERVENTIONAL RADIOLOGY—The fellowship offered is a 1-yr training program in interventional radiology. A high volume of studies provides excellent experience for the fellowship training program. The 1-yr appointment is intensive, supervised, and allows for graded responsibility in performance and interpretation of studies including angioplasty, atherectomy, arterial and biliary stents, and all drainage procedures. The fellowship training involves performance of interventional procedures under sonographic and CT guidance as well as fluoroscopy. Inquiries should be addressed to Gordon K. McLean, M.D., Director, Interventional Radiology, The Western Pennsylvania Hospital, 4800 Friendship Ave., Pittsburgh, PA 15224. 5-12c

ACCREDITED FELLOWSHIPS IN PEDIATRIC RADIOLOGY AND PEDIATRIC NEURORADIOLOGY—Dept. of Radiology, Children's Hospital Medical Center, Cincinnati, OH, offers 1- or 2-yr accredited (Residency Review Committee for Radiology of ACGME) fellowships in pediatric radiology beginning July 1, 1994. A 1-yr pediatric neuroradiology fellowship program is also offered and may be taken separately or combined with 1 yr of adult neuroradiology fellowship at the University of Cincinnati Medical Center. Children's Hospital Medical Center (CHMC) is a 355-bed institution. The dept. performs over 105,000 radiological exams/yr in the largest children's hospital and ambulatory practice in the U.S. The dept. has 14 full-time faculty pediatric radiologists, 1 full-time research faculty, 7 fellows, and many resident trainees. Six pediatric radiology and 1 pediatric neuroradiology fellowship positions are available annually. Training includes all aspects of pediatric imaging neonatal radiology; neuroimaging; musculoskeletal radiology; cardiovascular and thoracic imaging; abdominal imaging; oncologic imaging; ultrasonography; nuclear medicine; computed tomography; MRI; and vascular/interventional procedures. The dept. has an active clinical service with state-of-the-art equipment as follows: digital fluoroscopy; Acuson and ATL ultrasound units with Doppler and color flow Doppler capabilities; planar SPECT gamma cameras; GE 9800 Quick CT scanner; 1.5-T GE MRI with spectroscopy, and cardiac catheterization/angiographic suite with digital vascular imaging. The fellowship provides a broad clinical experience in pediatric radiology as well as numerous opportunities to participate in both clinical and basic research. Candidates must be board-certified or board-qualified in diagnostic radiology and must obtain an Ohio medical license. Salary and fringe benefits are highly competitive. Applications are due prior to February 1993 with interviews scheduled during the fall and winter of 1992–93. There are numerous career opportunities in pediatric radiology and pediatric neuroradiology in both academic and private practice settings. To receive more information about the fellowships at CHMC or careers in pediatric radiology, please contact Director, Dept. of Radiology, Children's Hospital Medical Center, Cincinnati, OH 45229-2899; (513) 559-8058. Children's Hospital Medical Center and the University of Cincinnati College of Medicine are affirmative action/equal opportunity employers. 7–1cp

FELLOWSHIP IN PEDIATRIC RADIOLOGY—University of Arkansas for Medical Sciences offers a 1-yr fellowship in pediatric radiology at Arkansas Children's Hospital. Training includes all aspects of pediatric imaging including: plain films, digital fluoroscopy, neonatal radiology (ECMO); a very active neuroradiology service (GE 9800 Quick Highlight CT Scanner, GE 1.5-T MRI with MRA), nuclear medicine (with SPECT); interventional procedures; angiography; and state-of-the-art ultrasound with color flow Doppler. There is opportunity to participate in clinical or basic research if desired. Arkansas Children's Hospital is a 300-bed hospital which serves as the only pediatric tertiary referral care facility for the community. Little Rock/Central Arkansas provides ample recreational and cultural opportunities. UAMS is an equal opportunity employer. Please direct inquiries to Joanna Seibert, M.D., Director, Dept. of Radiology, Arkansas Children's Hospital, 800 Marshall St., Little Rock, AR 72202; (501) 320-1175. 10c

UNEXPECTED OPENING FOR FELLOWSHIP IN CARDIOVASCULAR-INTERVENTIONAL RADIOLOGY—Available July 1, 1992, 1-yr fellowship program is available at a 750-bed teaching hospital. Extensive clinical experience involving all aspects of cardiovascular imaging, interventional vascular, and nonvascular procedures. Availability for clinical or animal research. Send CV and inquiries to Oscar H. Gulierrez, M.D., Dept. of Radiology, Box 648, University of Rochester Medical Center, Rochester, NY 14642. AA/EO/M-F employer. 8–10c

IMAGING (ULTRASOUND, BODY CT, AND MRI) FELLOWSHIP TO BEGIN JULY 1993—The Dept. of Radiology at The Western Pennsylvania Hospital (a 578-bed advanced, tertiary-care teaching hospital), Pittsburgh, PA, offers a 1-yr imaging fellowship. The fellowship emphasizes diagnostic ultrasound with rotations in body magnetic resonance imaging and computed body tomography. Examinations in all areas of sonography are performed and include obstetrics and gynecology, vascular/Doppler, abdominal, prostate, pediatrics, breast, and small parts. State-of-the-art equipment in all areas of the dept. Fellows will participate in procedures guided by ultrasound and computed tomography. Fellows have ample opportunity to participate in conference presentations and research projects, many of which culminate in publications. Inquiries should be addressed to Marcela Bohm-Velez, M.D., Director of Imaging Fellowship Program, Dept. of Radiology, The Western Pennsylvania Hospital, 4800 Friendship Ave., Pittsburgh, PA 15224. 5–12c

CARDIAC IMAGING FELLOWSHIP (CLEVELAND CLINIC FOUNDATION)—The section of cardio-vascular imaging (division of radiology) announces to interested and qualified BC/BE radiologists a 2-yr cardiac imaging fellowship position (July 1, 1994 – June 30, 1996). This fellowship emphasizes integrated diagnostic imaging of acquired and congenital diseases of the heart and thoracic vasculature using non-invasive radiologic techniques (plain-film xray, CT, MRI, Nuclear Cardiology including PET) through a balance of practical clinical and research experiences. Research activities are complemented by lectures and technical assistance from the division's biostatistician. Didactic training both in cardiac catherterization/cine cardioangiographic interpretation and in performance/intepretation of echocardiography is coordinated with the dept. of cardiology for clinical and research cross-correlation. Direct all correspondences to Richard D. White, M.D. Head, Section of Cardio-Vascular Imaging, Division of Radiology L-10, Cleveland Clinic Foundation, 9500 Euclid Ave. Cleveland, OH, 44195; (216) 444-2740. 10–1c

NEURORADIOLOGY FELLOWSHIP—Two-yrs beginning July 1, 1993. Exposure to all aspects of clinical/academic neuroradiology including CT, MRI, interventional procedures, vascular ultrasonography and pediatric neuroradiology. Participation in research and teaching. Send cover letter, CV to Te-Hua Liu, M.D. Director, Neuroradiology Section, Dept. of Diagnostic Imaging, Temple University Hospital, 3401 N. Broad St., Philadelphia, PA 19140. Temple University Hospital is an affirmative action/equal opportunity employer. 10c

INTEGRATED CHEST RADIOLOGY FELLOWSHIP AT JOHNS HOPKINS UNIVERSITY HOSPITAL—The Dept. of Radiology, Division of Thoracic Imaging, Johns Hopkins University is offering a 1 or 2 yr academically-oriented fellowship in chest radiology. The fellowship offers an integrated experience in cross-sectional imaging including over 4,000 chest CT exams/yr and 1,000 thoracic MRI examinations. Strong research interests in high-resolution computed tomography, magnetic resonance imaging, and interventional thoracic radiology offer the potential candidate an exciting environment to work in. The fellowship is available starting July 1, 1993 or July 1, 1994. Contact Janet E. Kuhlman, M.D., Director of Chest Radiology, Dept. of Radiology, Johns Hopkins Hospital, Baltimore, MD 21287; (410) 955-4419. 10–1cp

FELLOWSHIP IN ABDOMINAL IMAGING AND INTERVENTIONS—The dept. of radiology, Massachusetts General Hospital and Harvard Medical School, offers a 2-yr fellowship in abdominal imaging and interventional radiology beginning July 1, 1994. Training covers all aspects of abdominal imaging (fluoroscopy, ultrasound, CT and MR) and nonvascular interventions in the GI/GU tract. Ample time is made available for both clinical and laboratory research in the above areas during the second year. Candidates should be ABR-eligible or certified. Address inquiries to Peter R. Mueller, M.D., or Nicholas Papanicolaou, M.D., Dept. of Radiology, Massachusetts General Hospital, Boston, MA 02114. An equal opportunity employer. 9–11c

FELLOWSHIP IN IMAGING/ANGIO-INTERVENTIONAL—A 1-yr fellowship program at Lehigh Valley Hospital in Allentown, PA. is available. LVH is a 514-bed acute care, university affiliated hospital. The fellowship program offers training in CT (head and body), ultrasound, MR, angiography, and interventional radiology. For further information contact Robert Kricun, M.D., Dept. of Radiology, Lehigh Valley Hospital, P.O. Box 689, Allentown, PA. 18105-1556. 10–12c

INTERVENTIONAL MAMMOGRAPHY AND BREAST IMAGING FELLOWSHIP—The University of Arizona is offering a flexible 1-yr fellowship in interventional mammography and breast imaging beginning July 1993. The section performs more than 14,000 mammograms per/yr and over 500 breast interventional procedures, including percutaneous stereotaxic breast needle biopsy, preoperative localizations, and galactography. Equipment includes 7 state-of-the-art mammographic units and 5 stereotaxic devices. The fellowship will include 20% academic/protected research time and up to 4 months could be spent in other areas of body imaging (CT, ultrasound, or MRI). We have an active research program including clinical, basic science and technology assessment/outcome analysis research related breast imaging. Other benefits include: relocation allowance, office space with computer, and funds to attend national meetings. No "night call" responsibilities. Salary $38,500. Must be BC/BE. Will need Arizona license upon arrival. For further information please contact, Laurie L. Fajardo, M.D., Director, Mammography and Breast Imaging, University of Arizona, 1501 N. Campbell Ave., Tucson, AZ 85724. Application deadline, January 31, 1993. The University of Arizona is an equal opportunity/affirmative action employer. 10–1a

MR FELLOWSHIPS, IMMEDIATE OPENINGS—The Dept. of Radiology, University of Rochester Medical Center MR fellowship offers a broad range of experience in both body and neuro MR. Associated imaging experience is available with CT. Research opportunities are available. Two 1.5-T G.E. Signa magnets with the latest software are in use and a third is being planned. Three CT units are in use. Eligible applicants must be board-certified or eligible for certification in diagnostic radiology and should be eligible for licensing in the state of New York. Contact Deborah Rubens, M.D., Dept. of Radiology, Box 648, University of Rochester Medical Center, Rochester, NY 14642; (716) 275-8365. EO/AA/M-F. 10–12c

FELLOWSHIPS - IMMEDIATE OPENINGS—The Dept. of Radiology, University of Rochester Medical Center, is offering fellowships in body imaging/interventional, neuroradiology, vascular/interventional radiology, and MR. Eligible applicants must be board-certified or eligible for certification is diagnostic radiology and should be eligible for licensing in the state of New York. Applicants should contact the program directors: MR and Body Imaging/Interventional, Deborah Rubens, M.D.; Neuroradiology, Leena Ketonen, M.D.; Vascular Interventional, Oscar Gutierrez M.D. Program directors can be contacted at the Dept. of Radiology, University of Rochester Medical Center, Box 648, 601 Elmwood Ave., Rochester, NY 14642; (716) 275-5200. EO/AA/M-F. 10–12c.

VASCULAR/INTERVENTIONAL RADIOLOGY FELLOWSHIP—Temple University Hospital and School of Medicine has available a 1-yr fellowship beginning July 1, 1993. The candidate will have exposure to all areas of vascular and interventional radiology including noninvasive techniques and MRI/A. Approximately 1100 procedures are performed annually including, vascular/non-vascular stents, TIPSS, transcatheter and percutaneous embolotherapy, extensive endourologic and biliary interventional procedures. Applicants should contact David S. Ball, D.O., Chief, Section of Vascular/Interventional Radiology, Dept. of Diagnostic Imaging, Temple University Hospital, 3401 N. Broad St., Philadelphia, PA 19140. Temple University Hospital and School of Medicine is an affirmative actions/equal opportunity employer. 10c

BODY IMAGING FELLOWSHIP—Opening for a 1-yr fellowship position is available starting July 1, 1993 at Beth Israel Medical Center, Dept. of Radiology in New York City. Beth Israel Medical Center is a nearly 1000-bed teaching hospital; affiliated with Mount Sinai School of Medicine. Fellowship offers extensive clinical training in ultrasound, CT and MRI on state-of-the-art equipment which includes 7 ultrasound units providing color flow Doppler, transvaginal and transrectal scanning, 2 GE 9200 CT scanners, and 1.5 GE Signa MRI. Experience offered in CT and ultrasound guided interventional procedures. Applicants must have completed an approved residency in diagnostic radiology for inquiries, please contact Helene Goldfarb, M.D., Beth Israel Medical Center, Dept. of Radiology, First Ave. at East 16th St., New York, NY 10003; (212) 420-4580. An equal opportunity employer committed to a SMOKE-FREE environment. 10a

PEDIATRIC RADIOLOGY CHILDREN'S HOSPITAL LOS ANGELES—Four fellowships annually in pediatric radiology with experience in general radiology, fluoroscopy, ultrasound, CT, MR, neuroradiology, angiography, interventional radiology, nuclear radiology and PET. Emphasis on clinical experience, education, and clinical research during training results in a comprehensive experience. One-yr fellowships are offered with an option of an additional year of specialized work. A specific fellowship in pediatric neuroradiology or special emphasis in angiography, interventional radiology is also available. Fellowship is ACGME accredited. CHLA is a 331-bed children's hospital servicing a community of 13 million. The dept. of radiology performs approximately 100,000 studies annually. All pediatric subspecialties are represented with centers in oncology, cardiopulmonary disease, neural sciences, and genetics established as part of the tertiary and quaternary mission of the hospital. Strong emphasis in teaching and training with 98 pediatric residents and over 100 fellows and Ph.D.'s in hospital. Research at the CHLA Research Institute. Ten diagnostic, 1 radiation oncology and 1 Ph.D., MR physics faculty are full time in radiology. Dept. is completely equipped with state-of-the-art equipment including a 1.5-T magnet, 3 ultrasound units with color Doppler, and SPECT. For more information contact Beverly P. Wood, M.D., Dept. of Radiology, Children's Hospital Los Angeles, 4650 Sunset Blvd., MS# 81, Los Angeles, CA 90054-0700; (213) 669-5686, fax (213) 666-4655. 10–12c

FELLOWSHIP IN ULTRASOUND AND BODY CT/MRI—One-yr fellowships in ultrasound and body CT/MRI beginning July 1, 1993 and July 1, 1994, are being offered by the New York Hospital-Cornell Medical Center. The dept. provides state-of-the-art equipment, including Acuson and ATL ultrasound, GE 9800 CT, and Ge Signa 1.5-T MR. Wide variety of ultrasound examinations include abdominal, OB/GYN, color Doppler, small parts, neonatal head, transvaginal, and transrectal. Applicants should be ABR eligible or certified. Send CV to Elias Kazam, M.D., Dept. of Radiology, New York Hospital-Cornell Medical Center, 525 East 68th St., New York, NY 10021. 10–1c

FELLOWSHIP IN VASCULAR/INTERVENTIONAL RADIOLOGY—The Yale University Dept. of Radiology has an unexpected opening for a third fellowship position starting July 1993. The section has an active clinical service performing a wide range of vascular and interventional procedures including: diagnostic angiography, angioplasty, stenting, atherectomy, infusion therapy, embolotherapy, IVC filter placement, and percutaneous renal, biliary, and abscess management. Additionally, there is an inpatient admitting service and clinic. The fellowship is for 1 yr. Please send CV and 3 letters of recommendation to Jeffrey Pollak, M.D., Section Chief, Dept. of Diagnostic Radiology, Yale University School of Medicine, 333 Cedar St., P.O. Box 3333, New Haven, CT 06501, (203) 785-4746, (203) 785-3024 fax. Yale University is an equal opportunity/affirmative action employer. Applications from women and minority group members are encouraged.

FELLOWSHIPS AT YALE UNIVERSITY—The Dept. of Radiology at Yale University School of Medicine offers the following fellowships: Body Cross-Sectional Imaging -- 3 positions, balanced CT/MRI/ultrasound, MRI focused, ultrasound focused. Contact John Pellerito, M.D. Thoracic Imaging, 1 position, includes mammography, lung biopsies, CT and MRI. Contact Anne Curtis, M.D. Neuroradiology 3 2-yr positions offered each year. Contact Gordon Sze, M.D. Vascular/Interventional -- 3 positions, contact Jeffrey Pollack, M.D. Interested applicants should send their CV and 3 letters of recommendation to the appropriate program director, at 333 Cedar St., New Haven, CT 06510. 10c

THE DEPARTMENT OF RADIOLOGY OF THE CHILDREN'S MEMORIAL HOSPITAL, CHICAGO, offers a fellowship in pediatric radiology beginning July 1, 1994. Children's Memorial is a 265-bed institution where approximately 95,000 radiological exams are done per yr by 13 attending radiologists. Rotations will include general radiology, ultrasound, computed tomography, nuclear medicine, MRI and neuroradiology. Requirements for fellowship include completion of a radiology residency and eligibility for IL licensure. Please send CV to Andrew K. Poznanski, M.D., Radiologist-in-Chief, Children's Memorial Hospital, 2300 Children's Plaza #9, Chicago, IL 60614. For inquiries, please call (312) 880-3520. 9-10c

Tutorials/Courses

KONA, HI 1992—Seventeenth Annual International Body Imaging Congress, Oct. 10–17. CME 1. Mauni Lani Bay Hotel. Contact Medical Seminars International, Inc., 18981 Ventura Blvd., Ste. 303, Tarzana, CA 91356; (818) 774-9077, fax (818) 774-0244. 5–10d

DIAGNOSTIC IMAGING IN ARUBA—The Dept. of Radiology, Cornell University Medical College and The New York Hospital will present the 18th annual postgraduate course, Diagnostic Imaging, January 31 – February 5, 1993 at the Hyatt Regency Hotel in Aruba. Category I credit: 30 hrs. Fee: Physicians, $495; residents, fellows and technologists $295. Information: Ms. Julia Anne Mala, Radiology, Cornell University Medical College, 1300 York Ave., New York, NY 10021; (212) 746-2522. 9–12d

CARIBBEAN CRUISE-BREAST IMAGING AT SEA—January 17–24, 1993. Presented by a renowned faculty member: Marc J. Homer, M.D. CME I application. Medical Seminars International, Inc., 18981 Ventura Blvd., Ste. 303, Tarzana, CA 91356: (818) 774-9077, fax (818) 774-0244. 9d

CARIBBEAN CRUISE-NEURO IMAGING/MRI AT SEA—January 10–17, 1993. Faculty: Hervey Segall, M.D. CME I application. Medical Seminar International, Inc., 18981 Ventura Blvd. Ste. 303, Tarzana, CA 91356: (818) 774-9077, fax (818) 774-0244. 9–12d

CARIBBEAN CRUISE-MRI AT SEA—January 24–31, 1993. Faculty: Barry S. Goldberg, M.D. CME I application. Medical Seminars International, Inc., 18981 Ventura Blvd., Ste. 303, Tarzana, CA 91356: (818) 774-9077, fax (818) 774-0244. 9–12d

No one ever said a lot of knowledge is a dangerous thing.

IN FACT, for radiologists, the only danger is not keeping up with what's new. **AJR: American Journal of Roentgenology** is your monthly guide to the latest advances, with articles that are timely, succinct, and relevant to daily practice.

AJR
American Journal of Roentgenology
Published monthly
Robert N. Berk, M.D., Editor
The University of California, San Diego

Call toll-free to order: **1-800-638-6423**
from anywhere in the U.S. or Canada.
Or clip and mail this coupon to
Waverly, Inc. ATTN: AJR

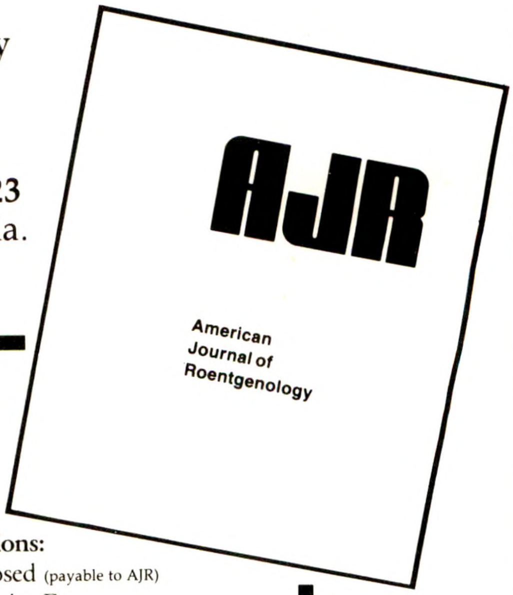

Subscribe to **AJR** now. (Current rates available for up to three years.)

☐ Individual $125/year
☐ Institutional $135/year
☐ In-training* $25/year
(Add $55/year outside the U.S.; in Canada, also add 7% GST.)
☐ 3 years ☐ 2 years ☐ 1 year

Maryland residents and 5% sales tax. Subscriptions outside the U.S. must be prepaid in U.S. dollars. Rates valid through October 31, 1992.

Name ____________
Address ____________
City/State/Zip ____________
*Please specify institution and training status ____________

AJR 1092

Payment Options:
☐ Check enclosed (payable to AJR)
☐ Bill me ☐ AmEx
☐ MasterCard ☐ VISA

Card # ____________ Exp. Date ______
Signature ____________

Return coupon to:
Waverly, Inc. ATTN: AJR
P.O. Box 23291, Baltimore, MD 21203–9990

AJR: AMERICAN JOURNAL OF ROENTGENOLOGY is the official journal of the American Roentgen Ray Society.

Final No.

Date Received

Tracking No.

Call for Scientific Exhibits

American Roentgen Ray Society
1993 Annual Meeting
April 25 – 30, 1993
San Francisco, CA

ADDRESS OF PRESENTING AUTHOR

Department

Institution

Street

City State Zip

Phone

Type title, authors, and abstract in the space provided below. (Instructions are on reverse side of this page.)

Select one category:

☐ Cardiovascular
☐ Neuroradiology
☐ Breast
☐ Bone
☐ Sonography
☐ Pediatric
☐ Gastrointestinal
☐ Nuclear medicine
☐ Genitourinary
☐ Medical physics
☐ Chest

What Type of Exhibit is Proposed? (Check one and fill in all appropriate blanks.)

_________ **Free-standing.** This is a self-contained display created in total by the exhibitor. It may be a fold-open unit, a unit shipped in cases and assembled on site, or a tabletop unit. Standard free-standing space is 10' x 10'. Indicate linear feet required_________.

_________ **Poster Board (Backboard panels).** Backboard panels are 4 x 8 ft. (1.2 x 2.5m). Number of panels required _________. If two panels are needed, there will be a ¼-in. frame separating the panels, thus requiring a separation in the presentation.

_________ **Viewbox.** Mounted materials (radiographs and other transparencies) for display on the society's illuminators. Each illuminator is 39.5 x 59.5 in. (100 x 151 cm). Number of illuminators required _______. Materials should not be glass mounted.

Instructions for Scientific Exhibit Abstracts

1. Type information single-spaced. Underline the name of the presenting author. Append as a last line of the abstract any research grant support, if applicable (e.g. Supported by USPHS Grant HE-80144). If the abstract is accepted, it will appear in the program book exactly as typed. Use the following format:

   MR IMAGING OF THE SPINE AND NECK
   F.S. Lau, M.D., A.N. Kirk, M.D., R.A. Beck, Ph.D.
   University of California, Bakersfield, Bakersfield, CA 92338

2. The abstract should be a brief paragraph that states the purpose, principal information and conclusions of the exhibit. Promissory statements are not acceptable. Brevity is desirable but not at the expense of specific information. Exhibits will be chosen on the basis of the quality of the abstract and exhibit space available. Poster board exhibits are encouraged as they do not require a viewbox or electricity.

3. The Scientific Exhibits Committee will grade each abstract and determine acceptance. Letters indicating acceptance or rejection will be mailed to all applicants in mid-January, together with meeting registration information. Exhibitors will receive instructions for exhibit preparation.

Deadline for submission of abstracts is November 1, 1992. Mail **one** copy of abstract to

N. Reed Dunnick, M.D.
Chairman, Scientific Exhibits Committee
c/o Susan Roberts, Projects Manager
American Roentgen Ray Society
1891 Preston White Drive
Reston, VA 22091

Although mail submission is preferable, abstracts will be accepted by fax at 703-264-8863. When faxing an application, **do not** mail a confirmation copy, as this results in unnecessary duplication of paper work.

Final No.

Call for Scientific Papers

Date Received

Tracking No.

American Roentgen Ray Society
1993 Annual Meeting
April 25 – 30, 1993
San Francisco, CA

ADDRESS OF PRESENTING AUTHOR

Department

Institution

Street

City State Zip

Phone

Type title, authors, and abstract in the space provided below. (Instructions are on reverse side of this page. Abstract should not exceed 300 words

Select one category: ☐ Angio/Interventional ☐ Breast ☐ Sonography ☐ CT ☐ Gastrointestinal Tract ☐ Genitourinary Tract
☐ Neuroradiology ☐ Skeletal ☐ Chest ☐ MR ☐ Pediatrics ☐ Medical Physics

Projection Requirements: ☐ 35mm– single or double (circle one) ☐ 16mm silent film ☐ VHS (1/2") ☐ VHS (3/4")

Has this been presented elsewhere? ☐ Yes ☐ No If yes, where?

Instructions for Scientific Paper Abstracts

1. Type information single-spaced. Underline the name of the presenting author. Append as a last line of the abstract any research grant support, if applicable (e.g. Supported by USPHS Grant HE-80144). If the abstract is accepted, it will appear in the program book exactly as typed. Use the following format:

   MR IMAGING OF THE SPINE AND NECK
   F.S. Lau, M.D., A.N. Kirk, M.D., R.A. Beck, Ph.D.
   University of California, Bakersfield, Bakersfield, CA 92338

2. Abstracts should include four paragraphs devoted sequentially to the following topics: (1) object or purpose of the study; (2) materials, methods and procedures; (3) results; and (4) significance of the results and conclusions. The text should not exceed 300 words. Specific data are essential. The abstract should be a succinct summary of work done rather than a promissory note.

3. The Scientific Program Committee will grade each abstract and determine acceptance. Letters indicating acceptance or rejection will be mailed to all applicants in mid-January, together with meeting registration information.

Deadline for submission of abstracts is November 1, 1992. Mail **one** copy of abstract to

ARRS President-Elect
c/o Susan Roberts, Projects Manager
American Roentgen Ray Society
1891 Preston White Drive
Reston, VA 22091

Although mail submission is preferable, abstracts will be accepted by fax at (703) 264-8863. When faxing an application, **do not** mail a confirmation copy, as this results in unnecessary duplication of paper work.

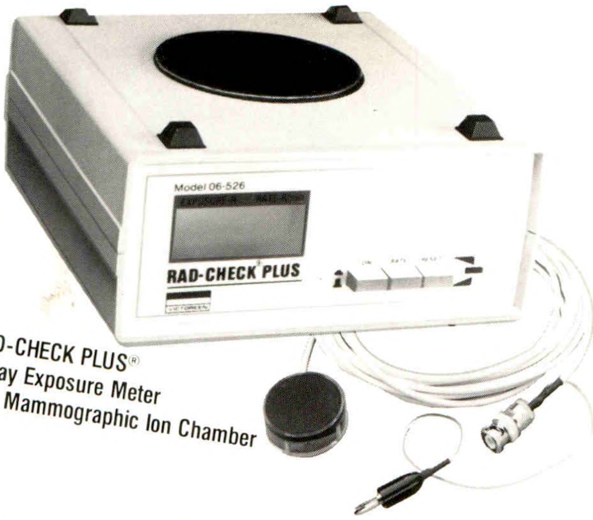

RAD-CHECK PLUS®
X-Ray Exposure Meter
with Mammographic Ion Chamber

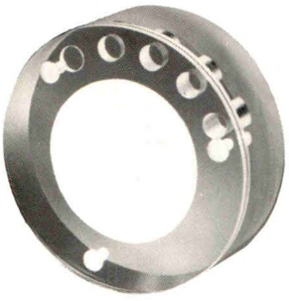

Mammographic
QC Phantoms

Hand-Held Dual-Color
Sensitometer

Comply with
ACR, JCAHO
and State
Mammographic
QC Requirements
Quickly, Easily,
Inexpensively!

Mammographic
Digital
kVp Meter

Hand-Held Digital
Clamshell Densitometer

Mammography
Focal Spot
Test Stand

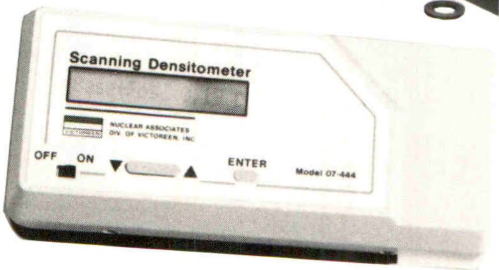

Hand-Held
MINISCAN
X-Ray Film
Processor
QC System

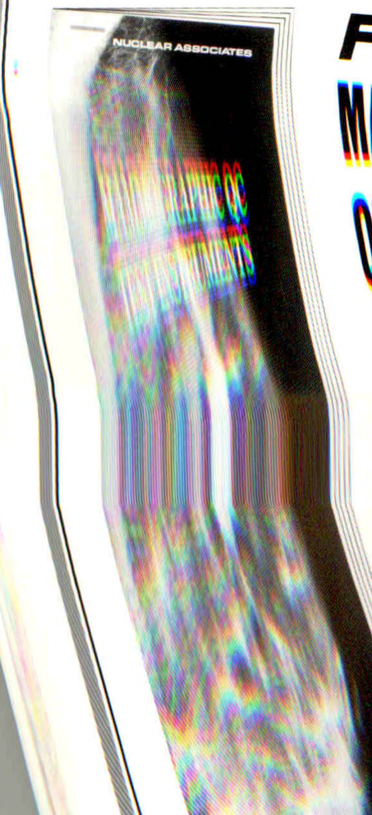

FREE
MAMMOGRAPHIC
QC CATALOG

Our extensive line of
mammographic QC test
instruments and accessories
will help you implement an
effective QC program in your
facility.

AX (516) 741-5414,

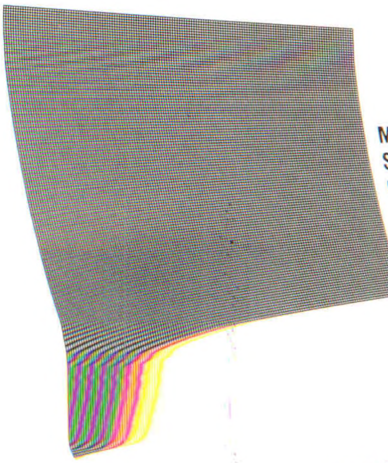

Mammographic
Screen-Film
Contact
Test Tool

NUCLEAR ASSOCIATES
Division of VICTOREEN, INC.
100 VOICE ROAD • P.O. BOX 349
CARLE PLACE, NY 11514-0349 U.S.A.
(516) 741-6360
FAX (516) 741-5414

VICTOREEN

©Victoreen, Inc.

Volume 159 **American Journal of Roentgenology** October 1992

CARDIOPULMONARY RADIOLOGY

695 **Diagnostic and therapeutic use of chest sonography: value in critically ill patients.** *Yu C-J, Yang P-C, Chang D-B, Luh K-T*
702 **Case report. Primary pulmonary artery sarcoma: diagnosis with CT, MR imaging, and transthoracic needle biopsy.** *Bressler EL, Nelson JM*
705 **Case report. Thoracic periaortic lymphoma mimicking aortic dissection.** *Kazerooni EA, Williams DM, Deeb GM*
708 **Case report. Development and resolution of systemic and coronary artery aneurysms in Kawasaki disease.** *Yacoe ME, Dake MD*

BREAST RADIOLOGY

711 **Ruptured gel-filled silicone breast implants: sonographic findings in 19 cases.** *Rosculet KA, Ikeda DM, Forrest ME, et al.*

GASTROINTESTINAL RADIOLOGY

717 **Review. CT of portal venous occlusion.** *Marn CS, Francis IR*
727 **Detection of malignant tumors in end-stage cirrhotic livers: efficacy of sonography as a screening technique.** *Dodd GD III, Miller WJ, Baron RL, Skolnick ML, Campbell WL*
735 **Differential diagnosis of hepatic tumors (hepatoma, hemangioma, and metastasis) with CT: value of two-phase incremental imaging.** *Honda H, Matsuura Y, Onitsuka H, et al.*
741 **Preoperative assessment of resectability of hepatic metastases from colonic carcinoma: CT portography vs sonography and dynamic CT.** *Soyer P, Levesque M, Elias D, Zeitoun G, Roche A*
745 **CT arterial portography: causes of technical failure and variable liver enhancement.** *Paulson EK, Baker ME, Hilleren DJ, et al.*
751 **Stent placement for benign pancreatic diseases: correlation between ERCP findings and clinical response.** *Gulliver DJ, Edmunds S, Baker ME, et al.*
757 **Pictorial essay. Regional lymph node metastases in carcinoma of the left side of the colon and rectum: CT demonstration.** *Granfield CAJ, Charnsangavej C, Dubrow RA, et al.*
762 **Technical note. Gadopentetate dimeglumine–barium paste for opacification of the esophageal lumen on MR images.** *Pavone P, Cardone GP, Cisternino S, Di Girolamo M, Aytan E, Passariello R*
765 **Case report. Intraluminal esophageal diverticulum caused by ingestion of acid.** *Plavsic BM, Robinson AE*
767 **Case report. Acute phlegmonous gastritis with mural abscess: CT diagnosis.** *Cruz FO, Soffia PS, Del Rio PM, Fava MP, Duarte IG*

GENITOURINARY RADIOLOGY

769 **Focal hyperdense areas in endometriomas: a characteristic finding on CT.** *Buy J-N, Ghossain MA, Mark AS, et al.*
773 **Color Doppler sonography of ureteral jets in normal volunteers: importance of the relative specific gravity of urine in the ureter and bladder.** *Baker SM, Middleton WD*
777 **Technical note. Percutaneous removal of a titanium Greenfield filter.** *Cynamon J, Bakal CW, Epstein SB, Gabelman G*

MUSCULOSKELETAL RADIOLOGY

779 **Review. MR imaging of the cervical spine: techniques for two- and three-dimensional imaging.** *Ross JS*
787 **MR imaging in the evaluation of SLAP injuries of the shoulder: findings in 10 patients.** *Cartland JP, Crues JV III, Stauffer A, Nottage W, Ryu RKN*
793 **Carpal tunnel syndrome: diagnosis with high-resolution sonography.** *Buchberger W, Judmaier W, Birbamer G, Lener M, Schmidauer C*
799 **Pictorial essay. Spondylolysis, spondylolisthesis, and associated nerve root entrapment in the lumbosacral spine: MR findings.** *Jinkins JR, Matthes JC, Sener RN, Venkatappan S, Rauch R*
805 **Pictorial essay. Lymphoma of bone, muscle, and skin: CT findings.** *Malloy PC, Fishman EK, Magid D*

PEDIATRIC RADIOLOGY

811 **Isolation of the fourth ventricle causing transtentorial herniation: neurosonographic findings in premature infants.** *Hall TR, Choi A, Schellinger D, Grant EG*
817 **MR angiography in children with cerebral neurovascular diseases: findings in 31 cases.** *Vogl TJ, Balzer JO, Stemmler J, Bergman C, Egger E, Lissner J*
825 **Sonographic diagnosis of intestinal malrotation in infants: importance of the relative positions of the superior mesenteric vein and artery.** *Weinberger E, Winters WD, Liddell RM, Rosenbaum DM, Krauter D*
829 **Pictorial essay. Sonography of the elbow in infants and children.** *Markowitz RI, Davidson RS, Harty MP, Bellah RD, Hubbard AM, Rosenberg HK*
835 **Case report. Wilms' tumor in a patient with Beckwith-Wiedemann syndrome: onset detected with 3-month serial sonography.** *Andrews MW, Amparo EG*
837 **Case report. Congenital portohepatic vein fistula that resolved spontaneously in a neonate.** *Lewis AM, Aquino NM*
839 **Case report. Aneurysm of a nonpatent ductus arteriosus in a neonate: CT findings.** *Slovis TL, Meza MP, Rector FE, Chang C-H*

NEURORADIOLOGY

841 **Primary cerebral lymphoma in patients with AIDS: MR findings in 17 cases.** *Cordoliani Y-S, Derosier C, Pharaboz C, Jeanbourquin D, Schill H, Cosnard G*
849 **Review. The ostiomeatal unit and endoscopic surgery: anatomy, variations, and imaging findings in inflammatory diseases.** *Laine FJ, Smoker WRK*
859 **Pictorial essay. Extrapineal abnormalities of the tectal region: MR imaging findings.** *Friedman DP*
867 **Case report. Intraocular cryptococcosis: imaging findings.** *Moon WK, Han MH, Song CS, Chang KH, Han MC*

CONTRAST MATERIAL

869 **The cost-effectiveness of replacing high-osmolality with low-osmolality contrast media.** *Caro JJ, Trindade E, McGregor M*
875 **MR lymphography with iron oxide compound AMI-227: studies in ferrets with filariasis.** *Tanoura T, Bernas M, Darkazanli A, et al.*

SOCIOECONOMIC ISSUES

883 **Perspective. Canadian-style health care: implications for radiologists.** *Wesenberg RL*

RESIDENT TEACHING

885 **Critical performance behaviors of radiology residents: evaluation of two category systems.** *Smith WL, Wood PS, Altmaier EM, O'Halloran C, Franken EA Jr*

MEETING NEWS

889 **Fleischner Society 22nd annual symposium on chest disease: scientific session, May 1992.** *Whalen E*

OTHER CONTENT

734 **History page.** *Nath H, Stanley RJ*
750 **Photo page.** *Anderson N*
756 **Radiologic-pathologic conference.** *Chew FS, Brown JH*
776 **Books received**
792 **List of book and videotape reviews**
816 **Photo page.** *Holman BL*
848 **ARRS 1993 residents' award papers information**
882 **Memorial. Robert L. Scanlan**
896 **Forthcoming articles**
897 **Letters**
907 **Review of current literature**
910 **News**
914 **American Roentgen Ray Society in**
915 **1993 ARRS meeting information**
916 **Classified advertisements**
A17 **Call for papers and exhib**
A2 **ARRS membership**
Guidelines for a
AJR busine

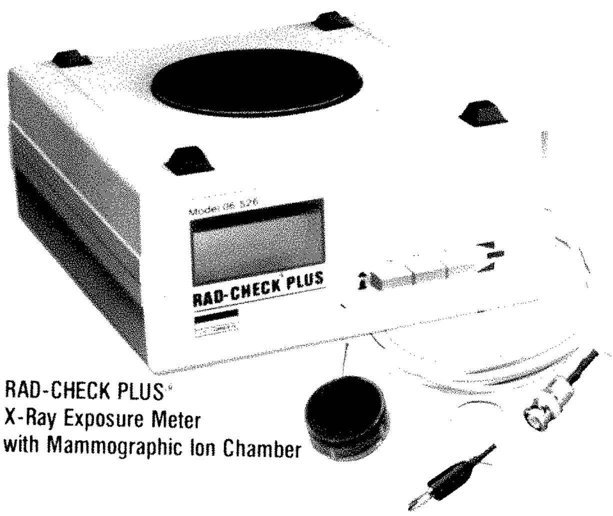

RAD-CHECK PLUS®
X-Ray Exposure Meter
with Mammographic Ion Chamber

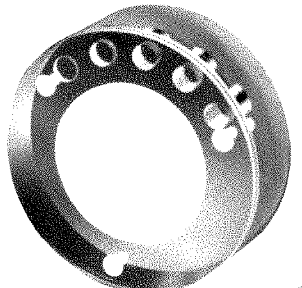

Mammographic
QC Phantoms

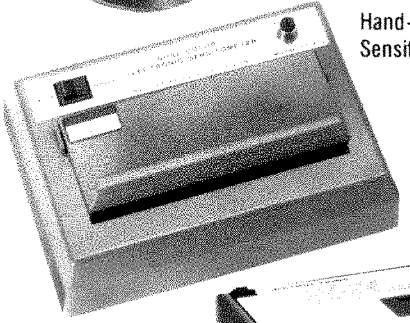

Hand-Held Dual-Color
Sensitometer

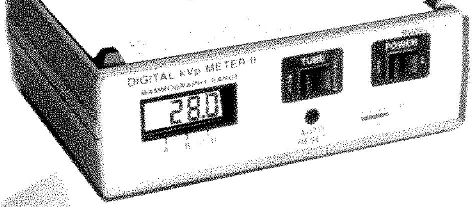

Mammographic
Digital
kVp Meter

Comply with ACR, JCAHO and State Mammographic QC Requirements Quickly, Easily, Inexpensively!

Hand-Held Digital
Clamshell Densitometer

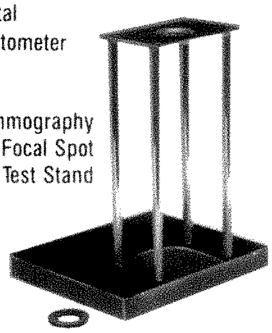

Mammography
Focal Spot
Test Stand

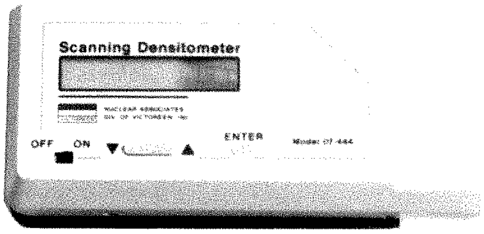

Hand-Held
MINISCAN
X-Ray Film
Processor
QC System

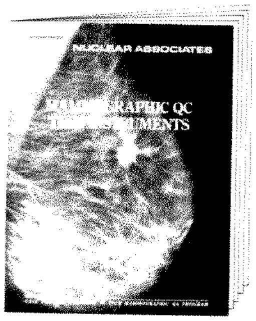

FREE
MAMMOGRAPHIC QC CATALOG

Our extensive line of mammographic QC test instruments and accessories will help you implement an effective QC program in your facility.

Phone (516) 741-6360, FAX (516) 741-5414, or write and request your FREE Mammographic Catalog MM-44

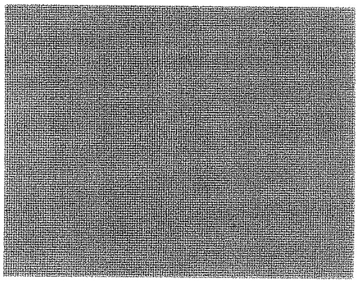

Mammographic
Screen-Film
Contact
Test Tool

NUCLEAR ASSOCIATES

VICTOREEN

Division of VICTOREEN, INC.
100 VOICE ROAD • P.O. BOX 349
CARLE PLACE, NY 11514-0349 U.S.A.
(516) 741-6360
FAX (516) 741-5414

Volume 159 **American Journal of Roentgenology** October 1992

CARDIOPULMONARY RADIOLOGY

695 **Diagnostic and therapeutic use of chest sonography: value in critically ill patients.** *Yu C-J, Yang P-C, Chang D-B, Luh K-T*
702 **Case report. Primary pulmonary artery sarcoma: diagnosis with CT, MR imaging, and transthoracic needle biopsy.** *Bressler EL, Nelson JM*
705 **Case report. Thoracic periaortic lymphoma mimicking aortic dissection.** *Kazerooni EA, Williams DM, Deeb GM*
708 **Case report. Development and resolution of systemic and coronary artery aneurysms in Kawasaki disease.** *Yacoe ME, Dake MD*

BREAST RADIOLOGY

711 **Ruptured gel-filled silicone breast implants: sonographic findings in 19 cases.** *Rosculet KA, Ikeda DM, Forrest ME, et al.*

GASTROINTESTINAL RADIOLOGY

717 **Review. CT of portal venous occlusion.** *Marn CS, Francis IR*
727 **Detection of malignant tumors in end-stage cirrhotic livers: efficacy of sonography as a screening technique.** *Dodd GD III, Miller WJ, Baron RL, Skolnick ML, Campbell WL*
735 **Differential diagnosis of hepatic tumors (hepatoma, hemangioma, and metastasis) with CT: value of two-phase incremental imaging.** *Honda H, Matsuura Y, Onitsuka H, et al.*
741 **Preoperative assessment of resectability of hepatic metastases from colonic carcinoma: CT portography vs sonography and dynamic CT.** *Soyer P, Levesque M, Elias D, Zeitoun G, Roche A*
745 **CT arterial portography: causes of technical failure and variable liver enhancement.** *Paulson EK, Baker ME, Hilleren DJ, et al.*
751 **Stent placement for benign pancreatic diseases: correlation between ERCP findings and clinical response.** *Gulliver DJ, Edmunds S, Baker ME, et al.*
757 **Pictorial essay. Regional lymph node metastases in carcinoma of the left side of the colon and rectum: CT demonstration.** *Granfield CAJ, Charnsangavej C, Dubrow RA, et al.*
762 **Technical note. Gadopentetate dimeglumine–barium paste for opacification of the esophageal lumen on MR images.** *Pavone P, Cardone GP, Cisternino S, Di Girolamo M, Aytan E, Passariello R*
765 **Case report. Intraluminal esophageal diverticulum caused by ingestion of acid.** *Plavsic BM, Robinson AE*
767 **Case report. Acute phlegmonous gastritis with mural abscess: CT diagnosis.** *Cruz FO, Soffia PS, Del Rio PM, Fava MP, Duarte IG*

GENITOURINARY RADIOLOGY

769 **Focal hyperdense areas in endometriomas: a characteristic finding on CT.** *Buy J-N, Ghossain MA, Mark AS, et al.*
773 **Color Doppler sonography of ureteral jets in normal volunteers: importance of the relative specific gravity of urine in the ureter and bladder.** *Baker SM, Middleton WD*
777 **Technical note. Percutaneous removal of a titanium Greenfield filter.** *Cynamon J, Bakal CW, Epstein SB, Gabelman G*

MUSCULOSKELETAL RADIOLOGY

779 **Review. MR imaging of the cervical spine: techniques for two- and three-dimensional imaging.** *Ross JS*
787 **MR imaging in the evaluation of SLAP injuries of the shoulder: findings in 10 patients.** *Cartland JP, Crues JV III, Stauffer A, Nottage W, Ryu RKN*
793 **Carpal tunnel syndrome: diagnosis with high-resolution sonography.** *Buchberger W, Judmaier W, Birbamer G, Lener M, Schmidauer C*
799 **Pictorial essay. Spondylolysis, spondylolisthesis, and associated nerve root entrapment in the lumbosacral spine: MR evaluation.** *Jinkins JR, Matthes JC, Sener RN, Venkatappan S, Rauch R*
805 **Pictorial essay. Lymphoma of bone, muscle, and skin: CT findings.** *Malloy PC, Fishman EK, Magid D*

PEDIATRIC RADIOLOGY

811 **Isolation of the fourth ventricle causing transtentorial herniation: neurosonographic findings in premature infants.** *Hall TR, Choi A, Schellinger D, Grant EG*
817 **MR angiography in children with cerebral neurovascular diseases: findings in 31 cases.** *Vogl TJ, Balzer JO, Stemmler J, Bergman C, Egger E, Lissner J*
825 **Sonographic diagnosis of intestinal malrotation in infants: importance of the relative positions of the superior mesenteric vein and artery.** *Weinberger E, Winters WD, Liddell RM, Rosenbaum DM, Krauter D*
829 **Pictorial essay. Sonography of the elbow in infants and children.** *Markowitz RI, Davidson RS, Harty MP, Bellah RD, Hubbard AM, Rosenberg HK*
835 **Case report. Wilms' tumor in a patient with Beckwith-Wiedemann syndrome: onset detected with 3-month serial sonography.** *Andrews MW, Amparo EG*
837 **Case report. Congenital portohepatic vein fistula that resolved spontaneously in a neonate.** *Lewis AM, Aquino NM*
839 **Case report. Aneurysm of a nonpatent ductus arteriosus in a neonate: CT findings.** *Slovis TL, Meza MP, Rector FE, Chang C-H*

NEURORADIOLOGY

841 **Primary cerebral lymphoma in patients with AIDS: MR findings in 17 cases.** *Cordoliani Y-S, Derosier C, Pharaboz C, Jeanbourquin D, Schill H, Cosnard G*
849 **Review. The ostiomeatal unit and endoscopic surgery: anatomy, variations, and imaging findings in inflammatory diseases.** *Laine FJ, Smoker WRK*
859 **Pictorial essay. Extrapineal abnormalities of the tectal region: MR imaging findings.** *Friedman DP*
867 **Case report. Intraocular cryptococcosis: imaging findings.** *Moon WK, Han MH, Song CS, Chang KH, Han MC*

CONTRAST MATERIAL

869 **The cost-effectiveness of replacing high-osmolality with low-osmolality contrast media.** *Caro JJ, Trindade E, McGregor M*
875 **MR lymphography with iron oxide compound AMI-227: studies in ferrets with filariasis.** *Tanoura T, Bernas M, Darkazanli A, et al.*

SOCIOECONOMIC ISSUES

883 **Perspective. Canadian-style health care: implications for radiologists.** *Wesenberg RL*

RESIDENT TEACHING

885 **Critical performance behaviors of radiology residents: evaluation of two category systems.** *Smith WL, Wood PS, Altmaier EM, O'Halloran C, Franken EA Jr*

MEETING NEWS

889 **Fleischner Society 22nd annual symposium on chest disease: scientific session, May 1992.** *Whalen E*

OTHER CONTENT

734 **History page.** *Nath H, Stanley RJ*
750 **Photo page.** *Anderson N*
756 **Radiologic-pathologic conference.** *Chew FS, Brown JH*
776 **Books received**
792 **List of book and videotape reviews**
816 **Photo page.** *Holman BL*
848 **ARRS 1993 residents' award papers information**
882 **Memorial. Robert L. Scanlan**
896 **Forthcoming articles**
897 **Letters**
907 **Review of current literature**
910 **News**
914 **American Roentgen Ray Society information**
915 **1993 ARRS meeting information**
916 **Classified advertisements**
Call for papers and exhibits for 1993 ARRS meeting
ARRS membership application
A17 **Guidelines for authors**
A2 ***AJR* business and subscriber information**